東京帝國大學

地震研究所彙報

第16號

昭和13年

BULLETIN
OF THE
EARTHQUAKE RESEARCH INSTITUTE
TOKYO IMPERIAL UNIVERSITY

Vol. XVI

1938

目　次

第 16 號

第1冊（昭和13年3月）

頁

1. 不連續性分散曲線を有するレーレー波の振幅（英文）…　妹澤克惟　1
2. 重力を受ける天體のプラスチツク釣合（英文）…………　妹澤克惟　金井清　7
3. 構造物震動の力學的制振器の模型實驗（不規則な振動）（英文）……………………………………　金井清　21
4. 五重塔の耐震性（第3報）（英文）…………………　妹澤克惟　金井清　30
5. 大島に於ける重力異常と鉛直線偏倚（英文）……………　武藤勝彦　39
6. 水準測量によるヂオイドの形の決定に就て（英文）……　武藤勝彦　60
7. 年平均潮位のフラクチユエーション（英文）……………　武藤勝彦　宮部直巳　70
8. 大島三原火山の地球物理學的研究（第3報）（英文）……　高橋龍太郎　永田武　平能金太郎　87
9. 淺間火山の磁氣測量（其の1）（英文）…………………　水上武　100
10. 草津白根火山の磁氣測量（其の1）（英文）………………　水上武　117
11. 發電機構に就いて（第5報）（英文）……………………　井上宇胤　125
12. 砂の中を傳播する彈性波の速度（英文）…………………　飯田汲事　131
13. 名古屋城天主閣の耐震性に就て（邦文）…………………　齋田時太郎　145
14. 朝鮮大同江に於ける彈性波式地下探査實施とその吟味（邦文）……………………………………　表俊一郎　155
15. 伊豆七島新島の火山（邦文）……………………………　津屋弘逵　171
16. 七島・マリアナ海嶺の地下構造に關する一解釋（英文）…　大塚彌之助　201
17. 千葉市西北郊登戸の地下水と震害（邦文）………………　吉村信吉　山本莊毅　212
18. 小串鑛山に於ける山崩の調査報告（英文）………………　高橋龍太郎　水上武　218

第2冊（昭和13年6月）

19. 彈性表面波の異常分散（英文）……………………… 妹澤克惟 225

20. 地球の液狀冷却時代に於ける重力的安定（英文）……… 妹澤克惟 金井清 234

21. 地球の冷却が重力の下にあるそのプラスチツク狀態に及ぼす影響（英文）……………… 妹澤克惟 金井清 244

22. 家屋の大黑柱又は類似部の耐震的效果（英文）………… 金井清 256

23. 重力と地下構造との關係（2）（英文）………………… 坪井忠二 淵田隆門 273

24. 地殼均衡說による地殼の厚さを求める簡單な方法（英文）……………… 坪井忠次 285

25. 火口周邊に於ける地磁氣偏角の異常分布（英文）……… 永田武 288

26. 臺灣中部の地殼變形（第1報）（英文）………………… 佐藤光之助 福永三郎 300

27. 彈性地殼內にある球狀震源より出る地震波（英文）…… 西村源六郎 高山威雄 317

28. 世界地震の季節的分布（英文）………………………… 山口生知 355

29. 筑波山に於ける土地傾斜變化の觀測（英文）…………… 萩原尊禮 366

30. 淺間火山の活動と地表傾斜變化（英文）……………… 水上武 372

31. 二三の土に於ける2種の粘性比とポアソン彈性比との關係（英文）……………… 飯田汲事 391

32. 支那震災の特異性と殘存する高塔より推定された其の震度に就て（邦文）……………… 齋田時太郎 407

33. 靜岡縣庵原郡東部の地質構造（邦文）………………… 大塚彌之助 415

34. 富士火山の地質學的並びに岩石學的研究（1）
1. 火御嶽の構造（邦文）……………… 津屋弘逵 452

35. 昭和13年1月12日，日ノ御崎沖地震調査報告（邦文）……………… 水上武 470

36. 岡山—厚狹間並に小松島—八幡濱間の水準改測結果（邦文）……………… 484

第3冊（昭和13年9月）

37. 周期的粘彈性波の走波距離についての減衰（英文）…… 妹澤克惟 金井清 491

38. 地殼內の不連續面に於ける境界波の生成（第1報）（英文）……………… 妹澤克惟 金井清 504

39. 地球の冷却が重力の下にあるそのプラスチツク狀態に及ぼす影響 II.（英文）……………… 妹澤克惟 金井清 527

40. 架構の立體的振動（英文）…………………… 金井清 538
41. 地磁氣異常と地下構造（英文）…………………… 永田武 550
42. 臺灣中部の地殼變形（第2報）（英文）…………………… 宮部直巳 福永三郎 佐藤光之助 578
43. 發震機構に就いて（第6報）（英文）…………………… 井上宇胤 597
44. 東京帝國大學構內に於ける地震動加速度の比較觀測（其の1）（邦文）…………………… 萩原尊禮 表俊一郎 632
45. 富士火山の地質學的並に岩石學的研究（II） 2. 青木原熔岩の分布と噴出中心（邦文）…………………… 津屋弘逵 638
46. 昭和13年5月9日及び15日の磐梯山麓川上溫泉附近に於ける山津浪並びに流下せる火山灰質土砂の二三の物理的性質（邦文）…………………… 飯田汲事 658

第4冊（昭和13年11月）

47. 彈性表面波の異常分散（第2報）（英文）…………………… 妹澤克惟 金井清 683
48. 粘性が地球の液狀冷却時代に於ける重力的安定に及ぼす影響（英文）…………………… 妹澤克惟 金井清 690
49. 筋違の耐震效果の理論（序報）（英文）…………………… 妹澤克惟 金井清 702
50. 三原火山の地球物理學的研究 昭和13年8月11日の小活動（英文）…………………… 永田武 714
51. 江東地域に於ける地盤沈下に就いて II.（邦文）…………………… 宮部直巳 721
52. 靜岡縣蒲原町の城山角閃石安山岩體中の斑晶配列方位とその地質學的解釋（英文）…………………… 大塚彌之助 猪俣眞三郎 757
53. 伊豆達磨火山に就いて（英文）…………………… 久野久 763
54. 昭和13年7月上旬の降雨による兵庫縣下の山崩（邦文）…………………… 宮部直巳 772
55. 筑波山山津浪調査報告（邦文）…………………… 萩原尊禮 779

Contents.

Vol. XVI.

Part 1.—March, 1938.

Page

1. K. **Sezawa**, Amplitudes of Rayleigh-waves with Discontinuities in their Dispersion Curves. (in English) 1
2. K. **Sezawa** and K. **Kanai**, The Plastic State of Certain Planets under Gravitational Forces. (in English) 7
3. K. **Kanai**, Model Experiments of a Dynamic Damper for Seismic Structural Vibration. Irregular Vibration. (in English) 21
4. K. **Sezawa** and K. **Kanai**, Studies on the Seismic Vibration of a Cozyûnotô. III. (in English) 39
5. K. **Muto**, Gravity Anomalies and Deviations of the Vertical in Izu-Osima. (in English) 39
6. K. **Muto**, The Possibility of Determining the Geoid by means of Levelling. (in English) 60
7. K. **Muto** and N. **Miyabe**, Studies in Fluctuations in the Heights of Yearly Mean Sea-levels. (in English) 70
8. R. **Takahasi**, T. **Nagata** and K. **Hirano**, Geophysical Studies of Volcano Mihara, Oosima Island. III. Microtremor Measurements in Oosima. (in English) 87
9. T. **Minakami**, Magnetic Surveys of Volcano Asama. (in English) 100
10. T. **Minakami**, Magnetic Surveys of Volcano Kusatu-Sirane. (in English) 117
11. W. **Inouye**, Notes on the Origin of Earthquakes. (in English) 125

12. K. IIDA, The Velocity of Elastic Waves in Sand. (in English) 131
13. T. SAITA, Vibrations of the Keep of Nagoya Castle due to Earthquake and Wind Pressure. (in Japanese) 145
14. S. OMOTE, Results of Seismic Prospecting at the Daidôkô River, Korea. (in Japanese) 155
15. H. TSUYA, Volcanoes of Nii-sima, One of the Seven Izu Islands. (in Japanese) 171
16. Y. OTUKA, A Geologic Interpretation on the Underground Structure of the Sititô-Mariana Island Arc in the Pacific Ocean. (in English) 201
17. S. YOSHIMURA and S. YAMAMOTO, The Underground Water in the Vicinity of Tiba City with Special Reference to Earthquake Damages. (in Japanese) 212
18. R. TAKAHASI and T. MINAKAMI, The Land-slide at the Ogusi Mine. (in English) 218

Part 2.—June, 1938.

19. K. SEZAWA, Anomalous Dispersion of Elastic Waves. (in English) 225
20. K. SEZAWA and K. KANAI, Gravitational Stability of the Earth at its Liquid Cooling Stage. (in English) 234
21. K. SEZAWA and K. KANAI, The Effect of Cooling on a Plastic Earth under Gravitational Forces. (in English) 244
22. K. KANAI, Aseismic Properties of a Daikoku-basira (Principal Column) or Similar Column in a Japanese Style House. (in English) 256
23. C. TSUBOI and T. FUCHIDA, Relation between Gravity Anomalies and the Corresponding Subterranean Mass Distribution. (II.) (in English) 273
24. C. TSUBOI, A Simple Method of Approximately Determining the Thickness of the Isostatic Earth's Crust. (in English) 285
25. T. NAGATA, Magnetic Anomalies around Volcanic Craters.

(in English) 288

26. M. HUKUNAGA and M. SATO, Crustal Deformations in Central Taiwan. (in English) 300

27. G. NISHIMURA and T. TAKAYAMA, Seismic Waves due to Tractions Applied to the Inner Surface of a Spherical Cavity in an Elastic Earth. (in English) 317

28. S. YAMAGUTI, Seasonal Distributions of Earthquakes in the World. (in English) 355

29. T. HAGIWARA, Observations of Changes in the Inclination on the Earth's Surface at Mt. Tukuba. (in English) 366

30. T. MINAKAMI, Explosive Activities of Volcano Asama and Tiltings of the Earth's Surface. (in English) 372

31. K. IIDA, Relation between the Normal-Tangential Viscosity Ratio and Poisson's Elasticity Ratio in Certain Soils. (in English) 391

32. T. SAITA, The Peculiarity of Chinese Earthquake Disasters and the Seismic Intensities as Deduced from Remaining Pagodas. (in Japanese) 407

33. Y. OTUKA, Geologic Structure of the Eastern Ibara District, Sizuoka Prefecture, Japan. (in Japanese) 415

34. H. TSUYA, Geological and Petrological Studies of Volcano Huzi (Fuji), I. 1. Geological structure of Komitake. (in Japanese) 452

35. T. MINAKAMI, The Hinomisaki-Oki Earthquake of January 12, 1938. (in Japanese) 470

36. Results of Recent Precise Levelling along the Lines; Okayama-Asa, and Komatuzima (or Tatue)-Yawatahama. (in Japanese) 484

Part. 3.—September, 1938.

37. K. SEZAWA and K. KANAI, Damping of Periodic Visco-Elastic Waves with Increase in Focal Distance. (in English) 491

38. K. SEZAWA and K. KANAI, The Formation of Boundary

Waves at the Surface of a Discontinuity within the Earth's Crust. I. (in English) 504

39. K. SEZAWA and K. KANAI, The Effect of Cooling on a Plastic Earth under Gravitational Forces. II. (in English) ... 527

40. K. KANAI, Three-dimensional Vibrations of a Framed Structure. I. (in English) 538

41. T. NAGATA, Magnetic Anomalies and the Corresponding Subterranean Mass Distribution. (in English) 550

42. N. MIYABE, M. HUKUNAGA and M. SATO, Crustal Deformations in Central Taiwan. Part 2. (in English) 578

43. W. INOUYE, Notes on the Origin of Earthquakes. (Sixth paper.) (in English) 597

44. T. HAGIWARA and S. OMOTE, Comparative Observations of the Acceleration of Earthquake Motions in the Compound of the Tokyo Imperial University. (Part I) (in Japanese)...... 632

45, H. TSUYA, Geological and Petrological Studies of Volcano Huzi (Fuji), II. 2. Distribution of the Aokiga-hara lava and its vent. (in Japanese) 638

46. K. IIDA, The Mud Flow that occurred near the Explosion-crater of Mt. Bandai on May 9 and 15, 1938, and some Physical Properties of Volcanic Mud. (in Japanese) 658

Part 4.—November, 1938.

47. K. SEZAWA and K. KANAI, Anomalous Dispersion of Elastic Surface Waves. II. (in English) 683

48. K. SEZAWA and K. KANAI, The Effect of Viscosity on the Gravitational Stability of the Earth at its Liquid Cooling Stage. (English) 690

49. K. SEZAWA and K. KANAI, Theory of the Aseismic Properties of the Brace Struts (Sudikai) in a Japanese-style Building. (Preliminary Notes). (in English) 702

50. T. NAGATA, Geophysical Studies of Mihara Volcano, Oosima

Island. IV. A Minor Activity of Volcano Mihara, August 11, 1938. (in Englsish) 714
51. N. MIYABE, Subsidence of the Earth's Surface in the Kôtô region, Tokyo. II. (in Japanese) 721
52. Y. OTUKA and S. INOMATA, Phenocryst distribution in the Siroyama hornblende andesite mass exposed near the town of Kanbara, Sizuoka prefecture, and its geologic interpretation. (in English) 757
53. H. KUNO, A Note on the Daruma Volcano, Izu, Japan. (in English) 763
54. N. MIYABE, The Landslides in Hyôgo Prefecture that accompanied the Heavy Rain of July 5, 1938. (in Japanese) 772
55. T. HAGIWARA, Mud Avalanche at Mt. Tukuba, Ibaraki Prefecture. (in Japanese) 779

1. *Amplitudes of Rayleigh-waves with Discontinuities in their Dispersion Curves.*

By Katsutada SEZAWA,

Earthquake Research Institute.

(Received Dec. 20, 1937.—Read Dec. 21, 1937.)

1. *Introduction.*

It was found in the previous paper[1] that the amplitude of Rayleigh-waves transmitted through a stratified layer is maximum for a certain ratio of wave length to thickness of the surface layer. It was furthermore ascertained that, although there are two peaks in the resonance curve of the waves, one of these peaks represents the prevalent oscillation in Rayleigh-waves, while the other concerns a mere resonance-like condition of bodily waves transmitted along the surface layer.

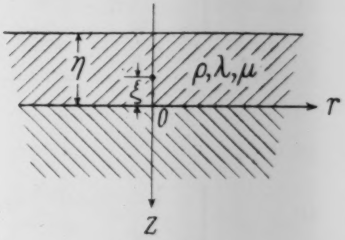

Fig. 1.

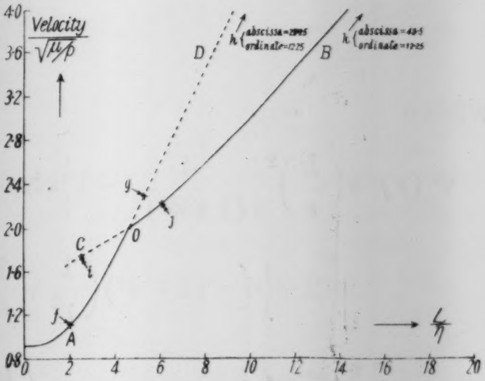

Fig. 2. Dispersion curves with discontinuity. Full and broken lines correspond to waves of the first and second sorts respectively.

The dispersion curves corresponding to the Rayleigh-waves now under consideration are of the type shown in Fig. 2, the two peaks of the resonance curve just mentioned belonging, as a matter of fact, to part AO of the first dispersion curve AOB and part OD of the second dispersion curve COD, respectively, the reason why the two peaks in question differing from each other in their qualities being therefore obvious. In the absence of numerical results for the amplitudes of waves corresponding to part OB of curve AOB or part CO of curve COD, it is not yet inadmissible to conceive of waves (surface waves as well as bodily waves) for a wide range of vibrational frequencies.2)

---

[1] K. SEZAWA and K. KANAI, "Relation between the Thickness of a Surface Layer and the Amplitudes of Dispersive Rayleigh-waves," *Bull. Earthq. Res. Inst.*, **15** (1937), 845~859.

It has already been found that the variation in the ratio of horizontal to vertical displacements of Rayleigh-waves3) is also discontinuous at the wave length that corresponds to discontinuity O in dispersion curve AOB. The present investigation shows that the values of the horizontal and vertical displacements themselves in the resonance curves are also discontinuous at the same wave-length.

2. *Method of calculation.*

We shall investigate the same problem as in the previous paper,4) all the conditions of the problem and the mathematical symbols being the same as those in that paper.

The final solutions are such that

$$u_{z=-\eta}=\left[\frac{1}{\sqrt{r\eta}}e^{i(\kappa r-\frac{\pi}{4}-pt)}\right]\frac{1}{\Phi'(\kappa)}\sqrt{\frac{2\pi}{\kappa\eta}\frac{k^2\eta}{h\gamma}}\left[\left\{\frac{2\gamma\delta}{1+\delta^2}\operatorname{sh}\delta\kappa\eta-\operatorname{sh}\gamma\kappa\eta\right\}\operatorname{ch}\gamma\kappa\xi\right.$$
$$\left.+\left\{\operatorname{ch}\gamma\kappa\eta-\frac{2}{1+\delta^2}\operatorname{ch}\delta\kappa\eta\right\}\operatorname{sh}\gamma\kappa\xi\right], \quad (1)$$

$$w_{z=-\eta}=\left[\frac{1}{\sqrt{r\eta}}e^{i(\kappa r+\frac{\pi}{4}-pt)}\right]\frac{1}{\Phi'(\kappa)}\sqrt{\frac{2\pi}{\kappa\eta}\frac{k^2\eta}{h}}\left[\left\{\frac{2}{1+\delta^2}\operatorname{ch}\gamma\kappa\eta-\operatorname{ch}\delta\kappa\eta\right\}\operatorname{ch}\gamma\kappa\xi\right.$$
$$\left.+\left\{\frac{1}{\gamma\delta}\operatorname{sh}\delta\kappa\eta-\frac{2}{1+\delta^2}\operatorname{sh}\gamma\kappa\eta\right\}\operatorname{sh}\gamma\kappa\xi\right], \quad (2)$$

where

$$\Phi'(\kappa)=\left(\frac{k}{\kappa}\right)^2\left\{\frac{4}{(1+\delta^2)^2}-1\right\}\operatorname{ch}\gamma\kappa\eta\operatorname{ch}\delta\kappa\eta$$
$$+2\gamma\delta\left\{4-(1+\delta^2)\left(\frac{1}{\gamma^2}+\frac{1}{\delta^2}\right)\right\}\left\{\frac{1}{4\gamma^2\delta^2}-\frac{1}{(1+\delta^2)^2}\right\}\operatorname{sh}\gamma\kappa\eta\operatorname{sh}\delta\kappa\eta$$
$$+\frac{\kappa\eta}{\delta}\left\{\frac{\left(\frac{h}{\kappa}\right)^2(1+\delta^2)}{2\gamma^2}-\frac{2\left(\frac{k}{\kappa}\right)^2}{1+\delta^2}\right\}\operatorname{ch}\gamma\kappa\eta\operatorname{sh}\delta\kappa\eta$$

---

2) The nature of discontinuity in dispersion curves is analogous to that of asymptotic lines as a limiting condition of hyperbolas.

3) K. SEZAWA and K. KANAI, "Discontinuity in Dispersion Curves of Rayleigh Waves," *Bull. Earthq. Res. Inst.*, **13** (1935), 245~250.

4) K. SEZAWA and K. KANAI, *loc. cit.* 1). It should be borne in mind that the condition of the source is such that the displacement at the same source is constant for any wave length.

$$+\frac{\kappa\eta}{\gamma}\left\{\frac{\left(\frac{k}{\kappa}\right)^2(1+\delta^2)}{2\delta^2}-\frac{2\left(\frac{h}{\kappa}\right)^2}{1+\delta^2}\right\}\mathrm{sh}\,\gamma\kappa\eta\;\mathrm{ch}\,\delta\kappa\eta, \qquad (3)$$

$$\gamma^2=1-\left(\frac{h}{\kappa}\right)^2, \qquad \delta^2=1-\left(\frac{k}{\kappa}\right)^2. \qquad (4)$$

Using these equations we obtained the values of u, w for part CO and part OB, the results of which, together with those in the preceding paper[5)], are given in Tables I, II, and plotted in Fig. 3, K in the tables and the figure denoting the value in every first pair of brackets in (1),(2).

Table I.

L/η	$\sqrt{\rho p^2/\mu f^2}$	u/K	$-w/K$	$-u/w$
1·00	0·9307	4·543	6·77	0·671
1·65	1·000	9·19	14·4	0·638
2·667	1·260	4·707	8·54	0·5513
3·12	1·414	1·826	3·505	0·521
3·96	1·732	1·964	4·265	0·4604
4·622	2·000	2·793	−1·613	——
4·949	2·05	2·751	−0·346	−7·95
6·095	2·236	2·817	−0·282	−9·99
7·295	2·45	2·551	−0·2113	−12·07

Table II.

L/η	$\sqrt{\rho p^2/\mu f^2}$	u/K	$-w/K$	$-u/w$
1·8615	1·644	1·5575	−0·889	−1·752
2 525	1·732	2·03	−0·6153	−3·3
3·885	1·898	2·598	−0·434	−5·988
5·333	2·298	8·208	22·57	0·3637
6·15	2·6458	14·27	43·06	0·3315
6·5	2·795	22·73	70·4	0·323
6·98	3 000	62·1	207·3	0·2996
8	3·44	4·582	18·07	0·2536
9	3·8730	3·056	12·67	0·2411

3. *Interpretation of the result for waves corresponding to the first dispersion curve.*

The condition of the present problem is such that the ratio of the elastic constant of the subjacent material to that of the surface layer is infinitely large. Comparing the dispersion curves of the present case with those for which the ratio in question is 5 or 20, it is possible to assume that the branch AOB in Fig. 2 represents the curve for the limiting condition of the first dispersion curve in general Rayleigh-waves.

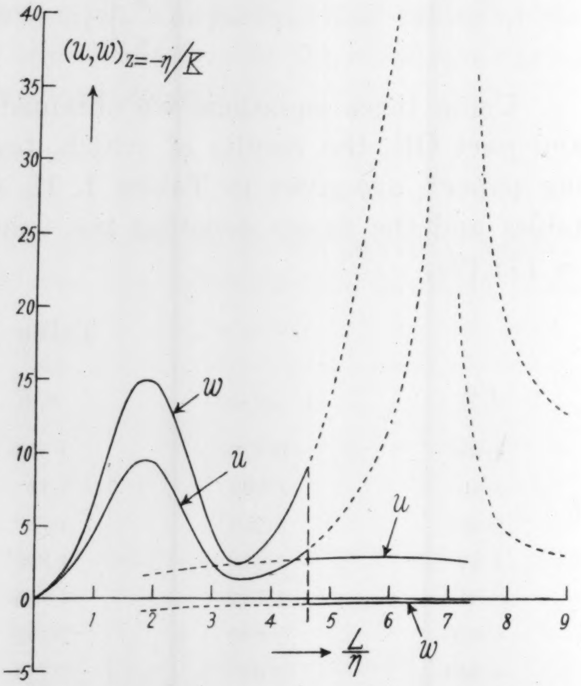

Fig. 3. Resonance curves of Rayleigh-waves with discontinuity in their dispersion curves. Full and broken lines correspond to waves of the first and second sorts respectively.

The values of horizontal and vertical displacements indicated by full lines in Fig. 3 or tabulated in Table I, correspond exactly to the first dispersion curve (Fig. 2). It will be seen that the variations in u as well as in w are both discontinuous at $L/\eta=4{\cdot}622$. While the vertical displacement is larger than the horizontal for $L/\eta<4{\cdot}622$, the reverse is the case for $L/\eta>4{\cdot}622$. At all events, the amplitude of Rayleigh-waves is maximum at $L/\eta=2$ as long as the first dispersion curve is concerned.

It is an important fact that, although u and $-w$ are in opposite sense for $L/\eta<4{\cdot}622$, both displacement components are of the same sign for $L/\eta>4{\cdot}622$, which indicates that, although the orbital motion of the surface for $L/\eta<4{\cdot}622$, is of the same sense as that in the usual Rayleigh-waves, the same motion for $L/\eta>4{\cdot}622$ is opposite to that of such waves (the usual Rayleigh-waves). But since the vertical displacement for $L/\eta>4{\cdot}622$ is practically zero, the actual displacement of Rayleigh-waves of such wave length would be mainly horizontal.

Although the ratio of horizontal to vertical components of displacements tends to infinity for $L/\eta\rightarrow\infty$, the respective components themselves also become zero at the same time.

4. *Interpretation of the result for waves corresponding to the second dispersion curve.*

With the same idea as in the preceding section, the branch COD in Fig. 2 represents the curve for the limiting condition of the second dispersion curve in general Rayleigh-waves. The values of the horizontal and vertical displacements, indicated by broken lines in Fig. 3, correspond exactly to the second dispersion curve (Fig. 2).

In this case, too, the variations in u as well as in w are both discontinuous at $L/\eta = 4{\cdot}622$. While the vertical displacement is less than the horizontal for $L/\eta < 4{\cdot}622$, the reverse is true for $L/\eta > 4{\cdot}622$, in which case the amplitude of the waves is infinitely large at $L/\eta \approx 7$. Since, nevertheless, it can hardly be assumed that the branch, COD, represents the resonance curve of the usual Rayleigh-waves, the infinitely large displacement just mentioned is rather of such a nature as to be a resonance-like condition of the bodily waves.

In this case, while the ratio of horizontal to vertical components of displacement tends to zero for L/η, the respective components themselves, on the other hand, become zero.

5. *Some remarks on seismic waves.*

Since the present problem concerns the case of a relatively large ratio of stiffness of the subjacent medium to that of the surface layer, the results apply to waves transmitted along a relatively shallow surface stratum, say, a few hundred meters thick, or even only a few meters thick. Since in such a case the ratio of wave length to thickness of the layer is so large that the relation $L/\eta > 4{\cdot}622$ holds, the surface displacement would then be mainly horizontal if the usual Rayleigh-waves were considered. If we were to take an earlier phase of the waves, then a transmission of bodily waves of large vertical displacement should be expected.

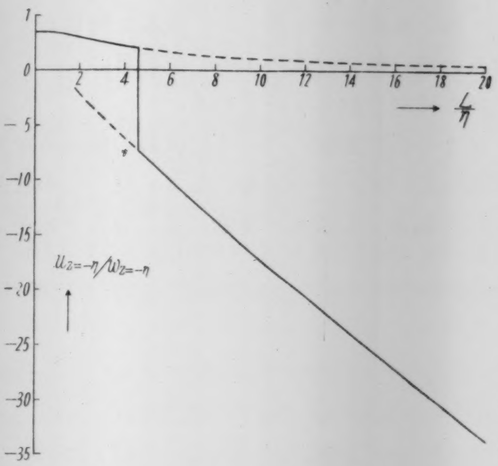

Fig. 4. Ratio of horizontal and vertical displacements. Full and broken lines correspond to the first and second sorts respectively.

At all events, our interest in the present problem is not in the transmission of waves in a layer of very small thickness, but rather in a possible existence of discontinuity in the dispersion curves of Rayleigh-waves.

Finally, with a view to confirming the nature of the present pro-

blem from a different point of view, we shall add curves showing the ratio of horizontal to vertical surface displacements for any wave length. The full and broken lines in Fig. 4 represent the respective cases corresponding to the first and second dispersion curves in Fig. 2.

In conclusion I wish to express my sincerest thank to Dr. K. KANAI, through whose assistance the investigation was successfully made.

1. 不連續性分散曲線を有するレーレー波の振幅

地震研究所 妹澤克惟

以前の報告で，地表層の彈性が下層のそれに比して著しく弱くなるとそれに傳はるレーレー波の分散曲線に不連續性が現はれる事を述べて置いた（之は實は双曲線の極限が漸近直線になることと多少 analogous である）. 之等に相當する水平，鉛直の振幅分布を出して見ると種々面白い事實のあることがわかつた.

第１の分散曲線について波長の短い所では，普通のレーレー波の場合と同じ位の水平，鉛直の振幅比があり，且つ $L/\eta=2$ 位の所で振幅が共振的に大きくなり，之が普通の意味に於けるレーレー波の卓越周期を與へる. 波長が相當長くなると殆ど水平の振幅のみとなる. 尙，面白い事は波長の短い所では波の orbit が普通のレーレー波の通りであるが，長い所では逆になり，水の波と同じ傾向を取るものである.

第２の分散曲線については波長の短い所が第１の分散曲線の波長の長い場合と同じ傾向を取り波長の長い所がその反對になる. 且つこの波長の長い所で固體波の共振の如き性質が存在する. 何れの場合にも波長が非常に長くなると水平，鉛直何れの振幅も零に近くなる.

2. *The Plastic State of Certain Planets under Gravitational Forces.*

By Katsutada SEZAWA and Kiyoshi KANAI,

Earthquake Research Institute.

(Read Oct. 19, 1937.—Received Dec. 20, 1937.)

1. *Introduction.*

It was found in the previous paper[1] that, although the Earth's shell, under gravitational forces, is in a plastic state, the same state has arised from such a dynamical condition that the horizontal compression greatly exceeds the vertical. The Earth being relatively large, it is scarcely possible to inquire into the critical condition at which the state of the crust changed from plastic to elastic, or *vice versa*, in the past, or will do so in the future. We shall now consider the cases of other planets of the solar system such as the Moon, Mercury, Mars, Venus, etc., from which it will be possible for us to obtain a criterion of the critical condition under consideration. Venus has almost the same size and mass as those of the Earth, whereas the Moon and Mercury are so small in these respects that they are likely to be elastic planets. The condition of Mars would appear to lie between the two just mentioned. From Jeffreys's paper[2] it appears that, although Venus and Mars have each a core, Mercury and the Moon have none; and neither in Mars under an alternative hypothesis also due to Jeffreys.

Our investigations thus far show that the question whether or not a planet has a core has greatly to do with the plasticity or otherwise of that planet.

We shall first discuss a multi-layered elastic planet, from which it will be possible to know the horizontal and vertical compressions that would exist in the crust of a planet were the same planet perfectly elastic. The second problem that will be examined is the possible state of the planet from the criterion of the plastic theory. Finally, the probability of an elastic layer at an intermediate depth within the shell of a planet having a liquid core will be investigated.

---

[1] K. SEZAWA and K. KANAI, "The Plastic State of the Earth under Gravitational Forces,"*Bull. Earthq. Res. Inst.*, **15** (1937), 878~887.

[2] H. JEFFREYS, "*M. N. R. A. S. Geophys. Suppl.*, **4** (1937), 50~60.

2. *The Moon and Mercury.*

Since, according to Jeffreys's idea, no outstanding mass discontinuity exists in the Moon or in Mercury, we shall assume that the respective ones of these two are uniform. From

$$V=\frac{4\pi\gamma}{r}\int_0^r \rho r'^2 dr' + 4\pi\gamma\int_r^\infty \rho r' dr', \tag{1}$$

we get

$$\frac{dp}{dr}=-\frac{\gamma M}{r^2}\rho,\quad M=\frac{4}{3}\pi\int_0^r \rho\, dr^3 \tag{2}$$

for any distribution of ρ with respect to r.

The equation of elastic equilibrium is

$$\frac{\partial p}{\partial r}+\frac{\partial}{\partial r}\left\{(\lambda+2\mu)\frac{\partial u}{\partial r}+2\lambda\frac{u}{r}\right\}+\frac{4\mu}{r}\left(\frac{\partial u}{\partial r}-\frac{u}{r}\right)=0\,, \tag{3}$$

where u is the radial displacement. If λ, μ, ρ were constant, we find from (2), (3) that

$$\frac{\partial^2 u}{\partial r^2}+\frac{2}{r}\frac{\partial u}{\partial r}-\frac{2u}{r^2}-\frac{1}{\lambda+2\mu}\frac{4}{3}\pi\gamma\rho^2 r=0\,, \tag{4}$$

the solution of which is

$$u=\frac{2}{15}\frac{\pi\gamma\rho^2 r^3}{(\lambda+2\mu)}+Br+\frac{C}{r^2}\,. \tag{5}$$

The corresponding stresses are

$$\left.\begin{aligned}\widehat{rr}&=\frac{2(5\lambda+6\mu)}{15(\lambda+2\mu)}\pi\gamma\rho^2 r^2+(3\lambda+2\mu)B\,,\\ \widehat{\theta\theta}=\widehat{\phi\phi}&=\frac{2(5\lambda+2\mu)}{15(\lambda+2\mu)}\pi\gamma\rho^2 r^2+(3\lambda+2\mu)B\,.\end{aligned}\right\} \tag{6}$$

From the boundary condition, $r=a$; $\widehat{rr}=0$, we get

$$B=-\frac{2(5\lambda+6\mu)}{15(3\lambda+2\mu)(\lambda+2\mu)}\pi\gamma\rho^2 a^2, \tag{7}$$

so that twice the maximum shear stress in the elastic condition is

$$\widehat{rr}-\widehat{\theta\theta}=\widehat{rr}-\widehat{\phi\phi}=\frac{8\mu\pi\gamma\rho^2 r^2}{15(\lambda+2\mu)}\,. \tag{8}$$

In the case of the Moon, $\rho=3{\cdot}334$, $a=1738$ km, $(\gamma=648{\cdot}10^{-10})$, so that we get

$$\widehat{rr}-\widehat{\theta\theta}=1{\cdot}206.10^{-6}\,\frac{\mu r^2}{\lambda+2\mu}\,.$$

If $\lambda=\mu$, the numerical values become

r(km)	1738	1500	1250	1000	750	500	250	0
$(\widehat{rr}-\widehat{\theta\theta})10^{-9}$(*C. G. S.*)	1·211	·903	·627	·402	·226	·101	·025	0

It will be seen that the values of $(\widehat{rr}-\widehat{\theta\theta})/2$ never exceed the plastic constants of the rocks usually met with in the Earth's crust. If the temperature of any part of the moon were not much higher than that within the surface crust of the Earth, the condition of the Moon would be perfectly elastic.

The radius of Mercury is about 2450 km. Assuming that its density is almost the same as that of the Earth, the numerical value of $(\widehat{rr}-\widehat{\theta\theta})$ in this case will be such that

r(km)	2450	2000	1738	……………	250	0
$(\widehat{rr}-\widehat{\theta\theta})10^{-9}$(*C. G. S.*)	2·410	1·607	1·211	……………	0·025	0

In this case, too, the planet is perfectly elastic, provided the temperature is less than that just mentioned.

3. *Mars, the Earth, and Venus treated as three-layered elastic planets.*

With Jeffreys's idea, we shall assume that both the Earth and Venus are three-layered planets. The gravity potentials in this case are then of the forms

$$\left.\begin{aligned}V_1&=\frac{4\pi\gamma}{3r}\left\{c^3(\rho_3-\rho_2)+b^3(\rho_2-\rho_1)\right\}+2\pi\gamma\rho_1\left(a^2-\frac{r^2}{3}\right),\\ V_2&=\frac{4\pi\gamma}{3r}c^3(\rho_3-\rho_2)+2\pi\gamma b^2(\rho_2-\rho_1)-\frac{2}{3}\pi\gamma r^2\rho_2+2\pi\gamma a^2\rho_1,\\ V_3&=2\pi\gamma c^2(\rho_3-\rho_2)-\frac{2}{3}\pi\gamma r^2\rho_3+2\pi\gamma b^2(\rho_2-\rho_1)+2\pi\gamma a^2\rho_1,\end{aligned}\right\}\qquad(9)$$

where a, b, c are the radii of the respective outer boundaries of the outermost layer, the intermediate shell, and the core, and ρ_1, ρ_2, ρ_3 the densities of the three parts under consideration.

The respective rates of the pressure change with radius for the three parts $a>r>b$, $b>r>c$, $c>r$ are then

$$\frac{\partial p}{\partial r}=-\frac{\xi_1}{r^2}-\eta_1 r,\quad \frac{\partial p}{\partial r}=-\frac{\xi_2}{r^2}-\eta_2 r,\quad \frac{\partial p}{\partial r}=-\eta_3 r, \tag{10}$$

where

$$\left.\begin{aligned} \xi_1&=\frac{4\pi\gamma}{3}\left\{c^3\rho_1(\rho_3-\rho_2)+b^3\rho_1(\rho_2-\rho_1)\right\},\quad \eta_1=\frac{4\pi}{3}\gamma\rho_1^2,\\ \xi_2&=\frac{4\pi\gamma}{3}c^3\rho_2(\rho_3-\rho_2),\quad \eta_2=\frac{4}{3}\pi\gamma\rho_2^2,\quad \eta_3=\frac{4}{3}\pi\gamma\rho_3^2. \end{aligned}\right\} 11$$

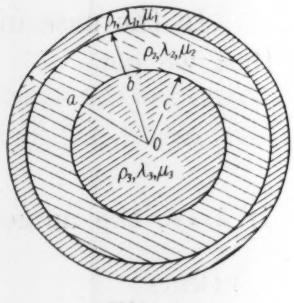
ρ_1, λ_1, μ_1
ρ_2, λ_2, μ_2
a
b
c
0
ρ_3, λ_3, μ_3

Fig. 1.

The equations of equilibrium and their solutions take the same forms as those in (3), (5) and also those shown in our previous paper. Although the substitution of the solutions in the boundary conditions in the previous paper was only approximate, it will here be made exact. The boundary conditions are such that

$$\left.\begin{aligned} r&=a;\quad \widehat{rr}_1=0,\\ r&=b;\quad u_1=u_2,\quad \widehat{rr}_1=\widehat{rr}_2,\\ r&=c;\quad u_2=u_3,\quad \widehat{rr}_2=\widehat{rr}_3. \end{aligned}\right\} \tag{12}$$

Substituting the general solutions in these expressions, we obtain twice the maximum shear stresses, as follows:

$$\left.\begin{aligned} \widehat{rr}_1-\widehat{\theta\theta}_1&=\frac{4\pi\gamma\rho_1^2\mu_1 r^2}{3(\lambda_1+2\mu_1)}\left[\frac{2}{5}+\left\{\frac{c^3(\rho_3-\rho_2)}{r^3\rho_1}+\frac{b^3(\rho_2-\rho_1)}{r^3\rho_1}\right\}-\frac{a^5C_1'}{r^5\eta_1}\right],\\ \widehat{rr}_2-\widehat{\theta\theta}_2&=\frac{4\pi\gamma\rho_2^2\mu_2 r^2}{3(\lambda_2+2\mu_2)}\left[\frac{2}{5}+\frac{c^3(\rho_3-\rho_2)}{r^3\rho_2}-\frac{a^5}{r^5}\left(\frac{\rho_1}{\rho_2}\right)^2\frac{C_2'}{\eta_1}\right],\\ \widehat{rr}_3-\widehat{\theta\theta}_3&=\frac{8\pi\gamma\rho_3^2\mu_3 r^2}{15(\lambda_3+2\mu_3)}, \end{aligned}\right\} \tag{13}$$

where

$$\begin{aligned} \frac{C_1'\Phi}{\eta_1}&=\frac{3\lambda_1}{2\mu_1}\left\{\left(1+\frac{4\mu_2}{3\lambda_1+2\mu_1}\right)\left(1-\frac{3\lambda_3+2\mu_3}{3\lambda_2+2\mu_2}\right)\right.\\ &\qquad\left.+\frac{4b^3\mu_2}{c^3(3\lambda_2+2\mu_2)}\left(1+\frac{3\lambda_3+2\mu_3}{4\mu_2}\right)\left(1-\frac{3\lambda_2+2\mu_2}{3\lambda_1+2\mu_1}\right)\right\}\kappa_1\\ &\quad-\frac{3b^2\mu_2}{5a^2\mu_1}\left\{\left(1-\frac{3\lambda_3+2\mu_3}{3\lambda_2+2\mu_2}\right)-\frac{b^3}{c^3}\left(1+\frac{3\lambda_3+2\mu_3}{4\mu_2}\right)\right\}\kappa_2\\ &\quad-\frac{3b^2(5\lambda_1+6\mu_1)}{20a^2\mu_1}\left\{\left(1-\frac{3\lambda_3+2\mu_3}{3\lambda_2+2\mu_2}\right)+\frac{4b^3\mu_2}{c^3(3\lambda_2+2\mu_2)}\left(1+\frac{3\lambda_3+2\mu_3}{4\mu_2}\right)\right\}\kappa_3 \end{aligned}$$

$$
\begin{aligned}
&+\frac{3c^2(\lambda_1+2\mu_1)(3\lambda_3+2\mu_3)}{20a^2\mu_1(\lambda_2+2\mu_2)}\left(1+\frac{4\mu_2}{3\lambda_2+2\mu_2}\right)\kappa_4\\
&\qquad\qquad-\frac{3c^2(\lambda_1+2\mu_1)(5\lambda_2+6\mu_2)}{20a^2\mu_1(\lambda_2+2\mu_2)}\left(1+\frac{4\mu_2}{3\lambda_2+2\mu_2}\right)\kappa_5\,,
\end{aligned}
$$

$$
\begin{aligned}
\frac{C_2'\Phi}{\eta_1}=&\frac{3\lambda_1(\lambda_2+2\mu_2)}{2\mu_1(\lambda_1+2\mu_1)}\left(1+\frac{4\mu_1}{3\lambda_1+2\mu_1}\right)\left(1-\frac{3\lambda_3+2\mu_3}{3\lambda_2+2\mu_2}\right)\kappa_1\\
&-\frac{3b^2(\lambda_2+2\mu_2)}{5a^2(\lambda_1+2\mu_1)}\left(1-\frac{b^3}{a^3}\right)\left(1-\frac{3\lambda_3+2\mu_3}{3\lambda_2+2\mu_2}\right)\kappa_2\\
&-\frac{3b^2(\lambda_2+2\mu_2)(5\lambda_1+6\mu_1)}{20a^2\mu_1(\lambda_1+2\mu_1)}\left(1-\frac{3\lambda_3+2\mu_3}{3\lambda_2+2\mu_2}\right)\left(1+\frac{4b^3\mu_1}{a^3(3\lambda_1+2\mu_1)}\right)\kappa_3\\
&+\frac{3c^2(3\lambda_3+2\mu_3)}{5a^2(3\lambda_2+2\mu_2)}\left\{\left(1+\frac{3\lambda_2+2\mu_2}{4\mu_1}\right)-\frac{b^3}{a^3}\left(1-\frac{3\lambda_2+2\mu_2}{3\lambda_1+2\mu_1}\right)\right\}\kappa_4\\
&-\frac{3c^2(5\lambda_2+6\mu_2)}{20a^2\mu_1}\left\{\left(1+\frac{4\mu_1}{3\lambda_2+2\mu_2}\right)-\frac{4b^3\mu_1}{a^3(3\lambda_2+2\mu_2)}\left(1-\frac{3\lambda_2+2\mu_2}{3\lambda_1+2\mu_1}\right)\right\}\kappa_5\,,
\end{aligned}
\tag{14}
$$

in which

$$
\begin{aligned}
\Phi=&-\left(1+\frac{4\mu_2}{3\lambda_1+2\mu_1}\right)\left(1-\frac{3\lambda_3+2\mu_3}{3\lambda_2+2\mu_2}\right)+\frac{a^3}{b^3}\left(1-\frac{\mu_2}{\mu_1}\right)\left(1-\frac{3\lambda_3+2\mu_3}{3\lambda_2+2\mu_2}\right)\\
&-\frac{4b^3\mu_2}{c^3(3\lambda_2+2\mu_2)}\left(1-\frac{3\lambda_2+2\mu_2}{3\lambda_1+2\mu_1}\right)\left(1+\frac{3\lambda_3+2\mu_3}{4\mu_2}\right)\\
&\qquad\qquad+\frac{a^3\mu_2}{c^3\mu_1}\left(1+\frac{3\lambda_3+2\mu_3}{4\mu_2}\right)\left(1+\frac{4\mu_1}{3\lambda_2+2\mu_2}\right),
\end{aligned}
\tag{15}
$$

$$
\begin{aligned}
\kappa_1&=\left\{\frac{c^3(\rho_3-\rho_2)}{a^3\rho_1}+\frac{b^3(\rho_2-\rho_1)}{a^3\rho_1}\right\}-\frac{5\lambda_1+6\mu_1}{10\lambda_1}\,,\\
\kappa_2&=-1+5\left\{\frac{c^3(\rho_3-\rho_2)}{b^3\rho_1}+\frac{\rho_2-\rho_1}{\rho_1}\right\}-\frac{5c^3\rho_2(\rho_3-\rho_2)(\lambda_1+2\mu_1)}{b^3\rho_1^2(\lambda_2+2\mu_2)}+\frac{\rho_2^2(\lambda_1+2\mu_1)}{\rho_1^2(\lambda_2+2\mu_2)}\,,\\
\kappa_3&=-1+\frac{10\lambda_1}{5\lambda_1+6\mu_1}\left\{\frac{c^3(\rho_3-\rho_2)}{b^3\rho_1}+\frac{\rho_2-\rho_1}{\rho_1}\right\}-\frac{10c^3\rho_2(\rho_3-\rho_2)\lambda_2(\lambda_1+2\mu_1)}{b^3\rho_1^2(5\lambda_1+6\mu_1)(\lambda_2+2\mu_2)}\\
&\qquad\qquad+\frac{\rho_2^2(\lambda_1+2\mu_1)(5\lambda_2+6\mu_2)}{\rho_1^2(5\lambda_1+6\mu_1)(\lambda_2+2\mu_2)}\,,\\
\kappa_4&=-\frac{\rho_2^2}{\rho_1^2}+\frac{5\rho_2(\rho_3-\rho_2)}{\rho_1^2}+\frac{\rho_3^2(\lambda_2+2\mu_2)}{\rho_1^2(\lambda_3+2\mu_3)}\,,\\
\kappa_5&=-\frac{\rho_2^2}{\rho_1^2}+\frac{10\rho_2(\rho_3-\rho_2)\lambda_2}{\rho_1^2(5\lambda_2+6\mu_2)}+\frac{\rho_3^2(\lambda_2+2\mu_2)(5\lambda_3+6\mu_3)}{\rho_1^2(5\lambda_2+6\mu_2)(\lambda_3+2\mu_3)}\,.
\end{aligned}
\tag{16}
$$

In the case of Mars (Mars I according to Jeffreys), the approximate values of the various constants are such that

$$a=3430\text{ km},\quad b=2040\text{ km},\quad c=1460\text{ km},$$

$$\rho_1=3{\cdot}50,\qquad \rho_2=4{\cdot}33,\qquad \rho_3=8{\cdot}46,$$

$$\lambda_1=\mu_1,\quad \lambda_2=\mu_2,\quad \mu_3=0\ \text{(incompressible core)},$$

$$\sqrt{\frac{\lambda_1+2\mu_1}{\rho_1}}=7\text{ km/s},\quad \sqrt{\frac{\lambda_2+2\mu_2}{\rho_2}}=12\text{ km/s},\quad \sqrt{\frac{\lambda_3}{\rho_3}}=9\text{ km/s},$$

so that

$$\rho_3-\rho_2=4{\cdot}13,\quad \rho_2-\rho_1=0{\cdot}83,$$

$$\left(\frac{c}{a}\right)^3=0{\cdot}0772,\quad \left(\frac{b}{a}\right)^3=0{\cdot}210,\quad \left(\frac{c}{b}\right)^3=0{\cdot}3665\,.$$

Using the expressions (13) we obtain

$$\widehat{rr}_1-\widehat{\theta\theta}_1=11{\cdot}09.10^9 r_1^2\left\{0{\cdot}4+1{\cdot}180\left(\frac{1{\cdot}46}{r_1}\right)^3+0{\cdot}2372\left(\frac{2{\cdot}04}{r_1}\right)^3+0{\cdot}161\left(\frac{3{\cdot}43}{r_1}\right)^5\right\},$$

$$\widehat{rr}_2-\widehat{\theta\theta}_2=16{\cdot}97.10^9 r_1^2\left\{0{\cdot}4+0{\cdot}954\left(\frac{1{\cdot}46}{r_1}\right)^3-0{\cdot}044\left(\frac{3{\cdot}43}{r_1}\right)^5\right\},$$

r_1 being radius in multiple of 1000 km from the centre of Mars.

In the case of the Earth we have constants

$$a=6350\text{ km},\quad b=5920\text{ km},\quad c=3480\text{ km},$$

$$\rho_1=3{\cdot}49,\qquad \rho_2=4{\cdot}85,\qquad \rho_3=10{\cdot}94,$$

$$\lambda_1=\mu_1,\quad \lambda_2=\mu_2,\quad \mu_3=0,$$

$$\sqrt{\frac{\lambda_1+2\mu_1}{\rho_1}}=7\text{ km/s},\quad \sqrt{\frac{\lambda_2+2\mu_2}{\rho_2}}=12\text{ km/s},\quad \sqrt{\frac{\lambda_3}{\rho_3}}=9\text{ km/s},$$

whence we get

$$\rho_3-\rho_2=6{\cdot}09,\quad \rho_2-\rho_1=1{\cdot}36,$$

$$\left(\frac{c}{a}\right)^3=0{\cdot}1646,\quad \left(\frac{b}{a}\right)^3=0{\cdot}81,\quad \left(\frac{c}{b}\right)^3=0{\cdot}203.$$

Using the expression (13) we obtain

$$\widehat{rr}_1-\widehat{\theta\theta}_1=11{\cdot}02.10^9 r_1^2\left\{0{\cdot}4+1{\cdot}745\left(\frac{3{\cdot}48}{r_1}\right)^3+0{\cdot}3897\left(\frac{5{\cdot}92}{r_1}\right)^3-0{\cdot}7702\left(\frac{6{\cdot}35}{r_1}\right)^5\right\},$$

$$\widehat{rr}_2-\widehat{\theta\theta}_2=21{\cdot}27.10^9 r_1^2\left\{0{\cdot}4+1{\cdot}255\left(\frac{3{\cdot}48}{r_1}\right)^3-0{\cdot}1195\left(\frac{6{\cdot}35}{r_1}\right)^5\right\}.$$

Twice the maximum shear stresses in elastic Mars and in the elastic Earth are plotted in Figs. 2, 3 in full lines.

It will be seen that the shear stress under consideration at any point in the Earth, and even in Mars, far exceeds the tenacities of the rocks composing the shell of the Earth, whence it follows that the rocky shells in both the Earth and Mars would be almost plastic.

It is odd that the maximum shear stresses in the second layer of the Earth and in both the rocky layers of Mars assume zero values at intermediate depths within the respective layers. In such parts of each shell as are shallower than the depth in question, the horizontal compression exceeds the vertical, whereas in the opposite part of the same shell, the vertical compression exceeds the horizontal. This results from the condition that the core of the planet is in a liquid state. Although the problem differs entirely from that of a thin shell, in a broad sense the thick shell in the present case still tends to bend. The surface where the maximum shear stress is zero may be called "the neutral surface of maximum shear stress". There is, however, a great difference between the present case in which there is high compression everywhere, and that of the bending of a plate, in which the fibre stress is zero on its neutral surface.

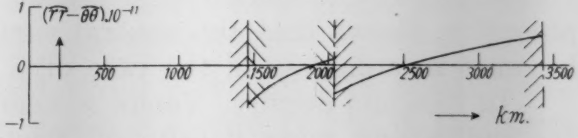

Fig. 2. Twice the maximum shear stress (C. G. S.) in the three-layered elastic Mars.

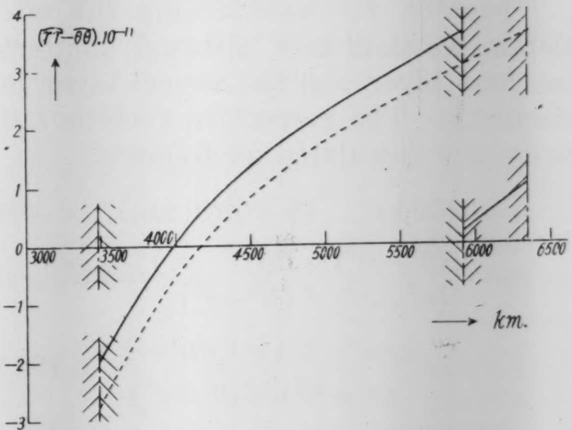

Fig. 3. Twice the maximum shear stress (C. G. S.) in the elastic Earth. Full and broken lines represent the three-layered Earth and the two-layered Earth respectively.

The maximum shear stress within the upper shell of the Earth is fairly small compared with that within the second layer—a fact that has an important bearing on the problem of compression in the superficial layer of the Earth. Even should there be a great horizontal compression in the crust, the effect of such compression on the surface would not be very great if soft soils lay on the very rigid base rocks, in which case the base rocks alone partake in the main resistance to compression.

It is a matter of importance whether or not, in the plastic state, the neutral surface of the maximum shear stress is affected. The mathematical calculation of a plastic problem, to which we shall come presently, shows that the neutral surface in the case of an elastic body becomes meaningless in the case of a plastic body.

In size and density, Venus is nearly the same as the Earth, namely, the radius and mean density of Venus differ from those of the Earth by only 0·8 percent and 2·4 percent respectively. The result for the Earth may therefore apply to Venus.

Finally, for ascertaining the effect of a soft upper layer on the Earth, we shall now, although indirectly, assume that the part including the first layer and the second layer is uniform in density as well as in elasticity. The respective (volume) means of the density and the elasticity are calculated as follows:

$$a=6350\text{ km},\quad (b=5920\text{ km}),\quad c=3480\text{ km},\quad \lambda_1=\mu_1,\quad \lambda_2=\mu_2,\quad \mu_3=0,$$

$$\rho=\frac{\rho_1(a^3-b^3)+\rho_2(b^3-c^3)}{(a^3-b^3)+(b^3-c^3)}=4{\cdot}538,\quad (\rho_1=3{\cdot}49,\quad \rho_2=4{\cdot}85),\quad \rho_3=10{\cdot}94,$$

$$\lambda=\mu=\frac{\lambda_1(a^3-b^3)+\lambda_2(b^3-c^3)}{(a^3-b^3)+(b^3-c^3)}=192{\cdot}8\ \text{(in km. gr. sec. unit)},$$

$$\sqrt{\frac{\lambda_1+2\mu_1}{\rho_1}}=7\text{ km/s},\quad \sqrt{\frac{\lambda_2+2\mu_2}{\rho_2}}=12\text{ km/s},\qquad \sqrt{\frac{\lambda_3}{\rho_3}}=9\text{ km/s},$$

so that we have

$$\rho_3-\rho_2=6{\cdot}402,\quad \rho_2-\rho_1=0,\quad \left(\frac{c}{a}\right)^3=0{\cdot}1646,\quad \left(\frac{b}{a}\right)^3=0{\cdot}81,\quad \left(\frac{c}{b}\right)^3=0{\cdot}203.$$

Substituting these values in the equations given for the case of a three-layered Earth, we finally get

$$\widehat{rr}_1-\widehat{\theta\theta}_1=18{\cdot}61.10^9 r_1^2\left\{0{\cdot}4+1{\cdot}41\left(\frac{3{\cdot}48}{r_1}\right)^3 -0{\cdot}1502\left(\frac{6{\cdot}35}{r_1}\right)^5\right\},$$

r_1 being the radius in multiple of 100 km from the Earth's centre; the result of the calculation is shown by a broken line in Fig. 3. It will be seen that although the distribution of maximum shear stress in the second layer does not differ greatly from that of the case of a three-layered Earth; the same stress at that part which corresponds to the original

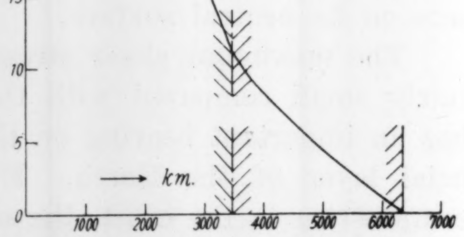

Fig. 4. Radial stress (C. G. S.) in the two-layered elastic Earth.

uppermost layer is increased to such an extent that its value is approximately equal to the greatest stress in the original second layer. The reason for the stress in the soft soil not being very great, even under a large horizontal compression, will now be obvious.

In order to compare the present result with that of a plastic body, the radial stress in the two-layered Earth is plotted in Fig. 4, the meaning of which will become apparent in a following section.

4. *The Earth and Venus treated as three- or two-layered plastic planets.*

The equations of equilibrium of the first and second shells and of the core are expressed by

$$\left.\begin{aligned} &-\frac{\xi_1}{r^2}-\eta_1 r+\frac{\partial \widehat{rr}_1}{\partial r}+\frac{2}{r}(\widehat{rr}_1-\widehat{\theta\theta}_1)=0,\\ &-\frac{\xi_2}{r^2}-\eta_2 r+\frac{\partial \widehat{rr}_1}{\partial r}+\frac{2}{r}(\widehat{rr}_2-\widehat{\theta\theta}_2)=0,\\ &-\eta_3 r+(\lambda_3+2\mu_3)\left(\frac{\partial^2 u_3}{\partial r^2}+\frac{2}{r}\frac{\partial u_3}{\partial r}-\frac{2u_3}{r^2}\right)=0. \end{aligned}\right\} \qquad (17)$$

The material in the core is incompressible, that is, it may be assumed to be elastic. The conditions of plasticity in the shells are such that

$$\widehat{rr}_1-\widehat{\theta\theta}_1=\pm 2k_1, \quad \widehat{rr}_2-\widehat{\theta\theta}_2=\pm 2k_2, \qquad (18)$$

so that the first and second equations in (17) reduce to

$$\left.\begin{aligned} &\widehat{rr}_1+4k_1\log r+\frac{\xi_1}{r}-\frac{\eta_1 r^2}{2}+I_1=0,\\ &\widehat{rr}_2+4k_2\log r+\frac{\xi_2}{r}-\frac{\eta_2 r^2}{2}+I_2=0. \end{aligned}\right\} \qquad (19)$$

The solutions are therefore

$$\left.\begin{aligned} &u_3=-\frac{\eta_3 r^3}{10(\lambda_3+2\mu_3)}+B_3 r, \quad \widehat{rr}_3=\frac{(5\lambda_3+6\mu_3)}{10(\lambda_3+2\mu_3)}\eta_3 r^2+(3\lambda_3+2\mu_3)B_3,\\ &\widehat{\theta\theta}_3=\widehat{\phi\phi}_3=\frac{(5\lambda_3+2\mu_3)}{10(\lambda_3+2\mu_3)}\eta_3 r^2+(3\lambda_3+2\mu_3)B_3. \end{aligned}\right\} \qquad (20)$$

The boundary conditions are such that

$$r=a;\ \widehat{rr}_1=0, \qquad r=b;\ \widehat{rr}_1=\widehat{rr}_2, \qquad r=c;\ \widehat{rr}_2=\widehat{rr}_3. \qquad (21)$$

Substituting (20) in these conditions, we get

$$\widehat{rr}_1=4k_1\log\frac{a}{r}+\frac{2\pi\gamma\rho_1^2a^2}{3}\left[\left(1-\frac{a}{r}\right)\left\{\left(\frac{c}{a}\right)^3\frac{\rho_3-\rho_2}{\rho_1}\right.\right.$$

$$\left.\left.+\left(\frac{b}{a}\right)^3\frac{\rho_2-\rho_1}{\rho_1}\right\}-\frac{1}{2}\left\{1-\left(\frac{r}{a}\right)^2\right\}\right],$$

$$\widehat{rr}_2=4k_1\log\frac{a}{b}+4k_2\log\frac{b}{r}+\frac{4\pi\gamma\rho_1^2a^2}{3}\left[\left(1-\frac{a}{b}\right)\left\{\left(\frac{c}{a}\right)^3\frac{\rho_3-\rho_2}{\rho_1}+\left(\frac{b}{a}\right)^3\frac{\rho_2-\rho_1}{\rho_1}\right\}\right.$$

$$\left.-\frac{1}{2}\left\{1-\left(\frac{b}{a}\right)^2\right\}\right]+\frac{4\pi\gamma\rho_2^2b^2}{3}\left[\left(1-\frac{b}{r}\right)\left(\frac{c}{b}\right)^3\frac{\rho_3-\rho_2}{\rho_2}-\frac{1}{2}\left\{1-\left(\frac{r}{b}\right)^2\right\}\right],$$

$$\widehat{rr}_3=4k_1\log\frac{a}{b}+4k_2\log\frac{b}{c}+\frac{4\pi\gamma\rho_1^2a^2}{3}\left[\left(1-\frac{a}{b}\right)\left\{\left(\frac{c}{a}\right)^3\frac{\rho_3-\rho_2}{\rho_1}+\left(\frac{b}{a}\right)^3\frac{\rho_2-\rho_1}{\rho_1}\right\}\right.$$

$$\left.-\frac{1}{2}\left\{1-\left(\frac{b}{a}\right)^2\right\}\right]+\frac{4\pi\gamma\rho_2^2b^2}{3}\left[\left(1-\frac{b}{c}\right)\left(\frac{c}{b}\right)^3\frac{\rho_3-\rho_2}{\rho_2}-\frac{1}{2}\left\{1-\left(\frac{c}{b}\right)^2\right\}\right]$$

$$-\frac{4\pi\gamma\rho_3^2c^2}{3}\,\frac{5\lambda_3+6\mu_3}{10(\lambda_3+2\mu_3)}\left\{1-\left(\frac{r}{c}\right)^2\right\}. \qquad (22)$$

These values together with $\widehat{\theta\theta}_1$, $\widehat{\theta\theta}_2$, $\widehat{\theta\theta}_3$, have already been shown previously.[3]

In the case of a single shell, we put

$$a=6350\text{ km},\quad c=3480\text{ km},\quad \rho\,(\text{volume mean of } \rho_1,\ \rho_2)=4{\cdot}538,$$
$$\rho_3=10{\cdot}94,\quad \rho_3-\rho=6{\cdot}402\cdots\cdots,\quad 2k_1=2k_2=5{\cdot}10^9\,(\text{C. G. S.}).$$

The radial stress is, therefore,

$$\widehat{rr}_1=\left[10\log\frac{a}{r}+2255\left\{-0{\cdot}2679-0{\cdot}2321\frac{a}{r}+0{\cdot}5\left(\frac{r}{a}\right)^2\right\}\right]10^9.$$

The horizontal stress is obtained by adding $2k_1$ to $\widehat{rr}_1$. The result of the calculation is indicated by a full line in Fig. 5.

If there are two outer shells, we put

$$a=6350\text{ km},\quad b=5920\text{ km},\quad c=3480\text{ km},$$
$$\rho_1=3{\cdot}49,\quad \rho_2=4{\cdot}85,\quad \rho_3=10{\cdot}94,$$
$$2k_1=5{\cdot}10^9,\quad 2k_2=5{\cdot}10^7,$$

from which we have

$$\widehat{rr}_1=\left[10\log\frac{6{\cdot}35}{r_1}+1333\left\{0{\cdot}1025-\frac{3{\cdot}826}{r_1}+0{\cdot}5\left(\frac{r_1}{6{\cdot}35}\right)^2\right\}\right]10^9,$$

$$\widehat{rr}_2=\left[-144+0{\cdot}1\log\frac{5{\cdot}92}{r_1}+2239\left\{-0{\cdot}2452-\frac{1{\cdot}509}{r_1}+0{\cdot}5\left(\frac{r_1}{5{\cdot}92}\right)^2\right\}\right]10^9,$$

---

3) K. SEZAWA and K. KANAI, *loc. cit.* 1).

r_1 being radius in multiple of 1000 km. The horizontal compression may be obtained by adding $\pm 2k_1$, $\pm 2k_2$ to $\widehat{rr}_1$, $\widehat{rr}_2$ respectively. The result of calculation is shown by the broken line in Fig. 5.

From Fig. 5 it will be seen that the results in both cases, the single outer layer and the double outer layer, do not differ greatly. Although the normal stresses increase with increase in depth, the effect of discontinuities in the respective layers is not marked. A comparison of the present result with that in Fig. 3 shows that the normal stress in the plastic condition does not much differ from that in the elastic condition. Since, nevertheless, the maximum shear stress participates only in the plastic deformation, it is quite irrelevant whether the normal stress in any case is very large or not.

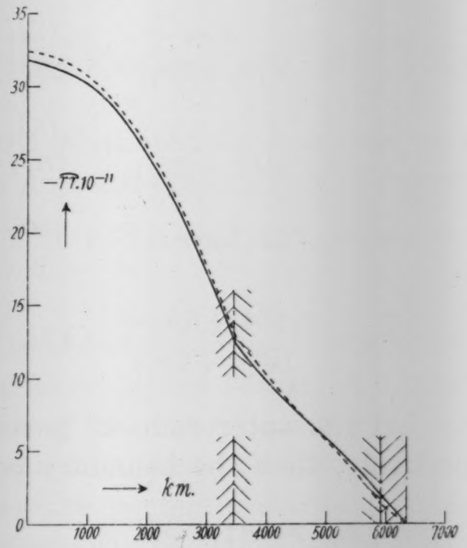

Fig. 5. Radial stress (C. G. S.) in the plastic Earth. Broken and full lines represent the three-layered Earth and the two-layered Earth respectively.

Whereas in the case of the elastic problem a neutral suface of maximum shear stress exists in some part of the rocky shell, in that of the plastic problem, on the other hand, no such surface can be found even should the boundary conditions for both cases be the same. It is, however, impossible for us to conclude that no neutral surface exists in the rocky shells of any planet. A criterion for this will be shown in the next section.

5. *The critical condition that a neutral surface of maximum shear stress exists within a plastic rocky shell.*

Referring to the sketch in Fig. 6, let I (ρ_1, k_1) and III (ρ_3, k_2) be the plastic parts in the rocky shell of a planet, between which is an elastic part II (ρ_2, λ_1, μ_1); the core, IV (ρ_4, λ_2, μ_2), being assumed to be elastic. The neutral surface of maximum shear stress, if existent, lies within the elastic layer II.

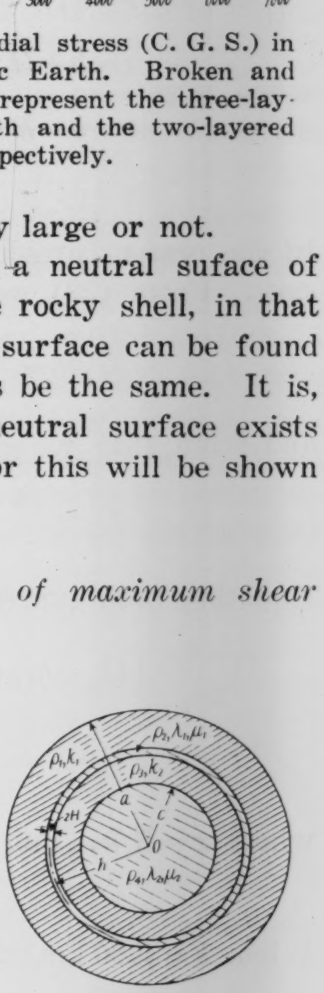

Fig. 6.

The stress conditions in I, II, III, IV are such that

$$\widehat{rr}_1 = -4k_1 \log r - \frac{\xi_1}{r} + \frac{\eta_1 r^2}{2} - I_1, \tag{23}$$

$$\left.\begin{aligned} \widehat{rr}_2 &= -\frac{\xi_2 \lambda_1}{r(\lambda_1 + 2\mu_1)} + \frac{\eta_2 (5\lambda_1 + 6\mu_1) r^2}{10(\lambda_1 + 2\mu_1)} + (3\lambda_1 + 2\mu_1) B_1 - \frac{4\mu_1 C_1}{r^3}, \\ \widehat{\theta\theta}_2 &= -\frac{\xi_2 (\lambda_1 + \mu_1)}{r(\lambda_1 + 2\mu_1)} + \frac{\eta_2 (5\lambda_1 + 2\mu_1) r^2}{10(\lambda_1 + 2\mu_1)} + (3\lambda_1 + 2\mu_1) B_1 + \frac{2\mu_1 C_1}{r^3}, \end{aligned}\right\} \tag{24}$$

$$\widehat{rr}_3 = -4k_2 \log r - \frac{\xi_3}{r} + \frac{\eta_3 r^2}{2} - I_2, \tag{25}$$

$$\widehat{rr}_4 = \frac{\eta_4 (5\lambda_2 + 6\mu_2) r^2}{10(\lambda_2 + 2\mu_2)} + (3\lambda_2 + 2\mu_2) B_2. \tag{26}$$

Let the outer radii of parts I, II, III, IV be a, $h+H$, $h-H$, c respectively, then the boundary conditions at these radii are

$$r = a; \qquad \widehat{rr}_1 = 0, \tag{27}$$

$$r = h+H; \qquad \widehat{rr}_1 = \widehat{rr}_2, \quad \widehat{rr}_2 - \widehat{\theta\theta}_2 = 2k_1, \qquad (28), (29)$$

$$r = h-H; \qquad \widehat{rr}_2 = \widehat{rr}_3, \quad \widehat{rr}_2 - \widehat{\theta\theta}_2 = -2k_2, \qquad (30), (31)$$

$$r = c; \qquad \widehat{rr}_3 = \widehat{rr}_4. \tag{32}$$

In the present problem the conditions, except (29), (31), are not necessary. From (29) we have

$$C_1 = -\frac{(h+H)^3 k_1}{3\mu_1} + \frac{(h+H)^2 \xi_2}{6(\lambda_1 + 2\mu_1)} + \frac{(h+H)^5 \eta_2}{15(\lambda_1 + 2\mu_1)}, \tag{33}$$

and from (31) we get

$$C_1 = \frac{(h-H)^3 k_2}{3\mu_1} + \frac{(h-H)^2 \xi_2}{6(\lambda_1 + 2\mu_1)} + \frac{(h-H)^5 \eta_2}{15(\lambda_1 + 2\mu_1)}. \tag{34}$$

Equating both expressions of C_1, we get the relation

$$\frac{\lambda_1 + 2\mu_1}{2\mu_1} \left\{ (k_2 - k_1)(1 + x^2) - (k_2 + k_1)(3x + x^3) \right\} \\ + \frac{5\xi_2}{h} x + \eta_2 h^2 (5x + 10x^3 + x^5) = 0, \tag{35}$$

where $x = H/h$. Put $\lambda_1 = \mu_1$. When $h = 5000$ km, there is no real x unless

$$2k > 2288.10^9 \text{ (C. G. S).}$$

When $h = 4200$ km, there is no real x unless

$$2k > 1973.10^9 \text{ (C. G .S.).}$$

When $h=3800$ km, there is no real x unless

$$2k > 1868.10^9 \text{ (C. G. S.)}.$$

These conditions apply to the case of the Earth or any other planet whose radius is nearly equal to, or greater than, that of the Earth.

It has now been ascertained that the plastic constant of the rocky shell would be exceptionally large were a neutral surface of maximum shear stress existent within the same shell.

6. *Concluding remarks.*

The object of the present paper is to ascertain the probable elastic and plastic states of the Earth in the past or in the future, for which purpose the conditions of various planets of the solar system were specially considered from both the plastic and the elastic theories.

Conditions in the Moon and Mercury are perfectly elastic provided the temperatures in them do not greatly exceed the temperature within the surface crust of the Earth.

If the Earth, Venus, and Mars are assumed to be elastic bodies and the maximum shear stresses in them are taken into consideration, the stresses in question exceed by far the tenacity of the rocks in the Earth's shell. In such conditions there would be neutral surfaces of maximum shear stress within the shell if the cores of these planets were fluid.

If these planets are assumed to be plastic, the neutral surface in question would not exist in their rocky shells. In order that such neutral surfaces may lie within plastic shells, the plastic constants of the rocks in the shells will have to be so large that it would scarcely be possible for such constants to be realized in the actual rocks known to us.

As a matter of fact, in every planet (or satellite) of the solar system investigated, the horizontal compression within the crust is invariably larger than the vertical, regardless of whether the condition of that crust is plastic or elastic.

2. 重力を受ける天體のプラスチック釣合

地震研究所 ｛妹澤克惟
　　　　　　｛金井清

この論文は地球の過去及び未來に於ける尤もらしいプラスチック的や彈性的の狀態について多少の推定を得る爲に試みた研究の經過を示すのであつて，その目的に向つて太陽系に於ける二三の星を態と選んで之について計算を試みたのである．

月や水星はその溫度が地球表面の岩石と同じやうな溫度でありさへすれば何れも彈性の狀態にあり得ることがわかつた．

火星，金星，地球等を假りに彈性的であると假定し，その最大剪應力を取つて見ると，それ等の剪應力は地球外殼の岩石のプラスチック限界よりも遙かに大きくなる．從つて何れもプラスチックならざるを得ない．但し，彈性的であると見る場合でも，核が流體的である爲に極大剪應力の neutral surface が外殼中に存在する．

之等の星がプラスチック性であるとして計算すると neutral surface は大體に於てあり得なくなり，强ひてこのやうな面を作る爲にはプラスチック値が非常に大きなものでなければならなくなる．

太陽系の何れの星（但しここに取扱つた所の）に於ても，それがプラスチック性であらうと彈性であらうと，岩石に働く水平方向の壓力が上下方向のそれよりも常に大きくなることには變りがないのである．

3. *Model Experiments of a Dynamic Damper for Seismic Structural Vibration. Irregular Vibration.*[*]

By Kiyoshi KANAI,

Earthquake Research Institute.

(Read Oct. 16, 1937.—Received Dec. 20, 1937.)

1. *Introduction.*

There are a number of artificial means of minimizing the effect of seismic structural vibrations. Although it is a well known fact that, if in an earthquake a structure were out of resonance and also resistive to that earthquake in non-resonance condition, the same structure would be almost earthquake-proof, since it is highly improbable that the vibration periods of the ground are invariably the same for any kind of earthquake, even in the same place, it is scarcely possible, however, that a structure just indicated would be the one to be commended. Even should there be some vibration periods peculiar to certain earthquakes, rigid possible structures are sometimes apt to be under resonance condition in seismic vibration, while flexible structures, on the other hand, are hardly resistive to statical forces. From these considerations, damping or dissipation assumes an important part of the vibrational condition. As to the dissipation of vibrational energy of a structure, having so often dealt with the subject, there is no need to recapitulate here about it. Although the inherent damping force in a structure increases with increase in vibrational frequency of that structure, the damping force under consideration, generally speaking, is insufficient to result any marked effects.

The vibration damper, already described in one of our Bulletins[1), 2)] is an artificial arrangement by which the damping force inherent in a structure manifests itself in a special effective way. It has been shown that the condition of an effective damper is such that the natural period of the damper is nearly equal to that of the main structure, and that the damping resistance to the relative movement of the damper part to the main structure is moderate (neither too large nor too small). It appears that in the case of the Gozyûnotô (Pagoda) the condition in question is partly satisfied. The apparent difference between the inner resistance of a structure in the usual sense and the resistance of the present dynamic damper arises from the condition whether the inertia force of the part in which there are relatively large movements is in a suitable state for resistance or not.

---

[*] The author made this investigation at Professor SEZAWA's proposal.

1) K. SEZAWA and K. KANAI, "A Method of Minimizing the Seismic Vibrations of a Structure," *Bull. Earthq. Res. Inst.*, **15** (1937), 21～32.

2) *Ditto*, "Model Experiment Confirmations of a Dynamic Method of Minimizing the Seismic Vibrations of a Structure," *Bull. Earthq. Res. Inst.*, **15** (1937), 598～613.

In previous model experiments of the dynamic damper, we examined the mere case of simple harmonic movements of the vibration table. Although oscillation of irregular type (repeated with a certain interval of time) is nothing more than a combination of different sinusoidal oscillations, at any rate from the theoretical point of view, yet in order to confirm this condition, we conducted model experiments so contrived that the movements of the vibration table were not simple harmonic.

2. *The forced experiments.*

The vibration table, the model structure, and the damper were the same as those used in the previous experiments. The amplitudes of the vibration table were adjusted by cam arrangement as shown in Fig. 1. The form of the cam C was such that two equal circles of 30 mm radius overlapped with their centres 1 mm apart and enveloped by two common tangent lines so as to form a bean-shaped plate, the centre of one of the original circles being the rotational axis. A pin P at the end of a horizontal oscillating rod R was placed in the circular groove encircling the cam; the clearance between the pin and the groove being less than 0·05 mm. The rod R was supported by two vertical swing levers Q, Q′ by means of ball bearings B_1, the swing levers themselves being also supported by ball bearings B_2; the lever Q′ is not shown in Fig. 1. Another horizontal rod pushing the vibration table was connected at its one end to any height in the lever Q′ in order to obtain various vibration amplitudes of the table.

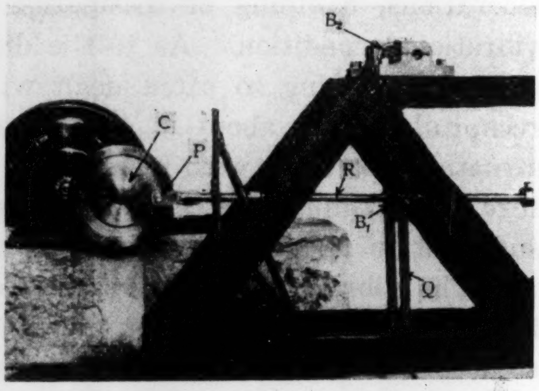

Fig. 1.

The mass M of the damper was of four kinds, as shown in Table I, whereas the area ratio of aperture-cylinder (the ratio of aperture area to sectional area of cylinder) in the damper was also of four kinds, as shown in Table II. Vibration experiments were made for almost all combinations of damper mass and aperture of damper piston, the elastic resistance of the damper being however kept constant throughout the experiments. The cases with which we experimented were AI, BII, BIII, BIV, CII, CIII, CIV, DIII.

Table I.

Case	A	B	C	D
M in gr.	450	1930	2445	3290
M/2 m	0·0475	0·201	0·256	0·344

Table II.

Case	I	II	III	IV
Area ratio of aperture-cylinder	0	0·000832	0·001728	0·00260

The period of free vibration of the structure without damper was 0·238 sec, which was nearly equal to the free vibration period 0·236 sec of the damper alone of Case B.

The original smoked records of the experiments were of the types shown in Figs. 2, 3, which correspond to Cases AI and CII. As will be seen presently, Case AI represents an undamped condition and Case CII a rather damped condition. The amplitudes of the respective floors and the damper relative to that of the vibration table were recorded without magnification. All the amplitudes of the respective floors and the damper as well as the corresponding vibration periods were read off from such records, and the ratios of these (relative) amplitudes to that of the table plotted in Figs. 4~11. These figures, as a matter of fact, represent the resonance curves. The ratios of $|y_1-y_0|/|y_0|$, $|y_2-y_0|/|y_0|$, $|\xi+y_2-y_0|/|y_0|$, namely, the ratios of the relative amplitudes of the first and second floors and the damper to that of the table are shown by chain, full, and broken lines respectively in the figures mentioned.

Figs. 2, 3 show that, although the movements of the vibration table were irregular, there were still two periodic oscillations peculiar to the table due to the cam arrangement, one of which was of half in period of the other, and of less amplitude. Such part of the vibration of the two floors and the damper that was forced with the quicker characteristic period in table movement, was recorded almost at the same time as that of the original movement in question, the other part of the same vibration that corresponded to the slower characteristic period in table movement was either in phase with, or in lag behind, the original movement according as the vibrational period was shorter or longer than the resonance period. The phase difference thus found for Cases BIII, CIII are shown by dotted lines in Figs. 5, 8; the positive and negative numbers corresponding to the vibrational conditions of the structure in phase with, and in lag behind, those of the table respectively. In other words, the numbers indicate the phase lag of the quicker oscillation in lag behind the slower one as represented by the fraction of the period of the latter.

3. *Results of forced vibration experiments.*

The general features of the effects of the vibration damper that were explained in the previous paper also manifested itself in the present experiments. Since in Case B, the natural period (0·236 sec) of the damper was approximately equal to that of the main structure (0·238 sec) without damper, the condition of the damper was theoretically the most favourable for effectiveness. In Case C, on the other hand, notwithstanding the somewhat different natural period (0·279 sec) of the damper, owing to the relatively larger damper mass, the damping effect of the forced vibration was more satisfactory than that of Case B. If

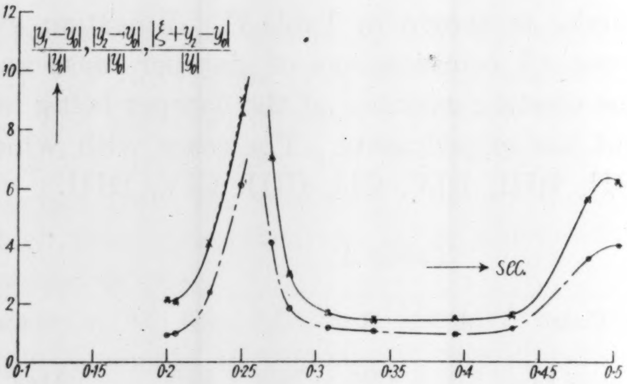

Fig. 4. AI.

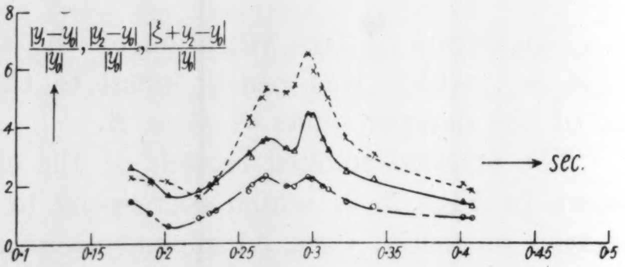

Fig. 5. BII.

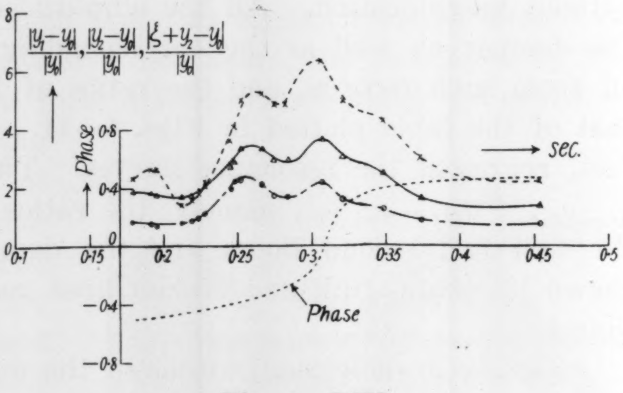

Fig. 6. BIII.

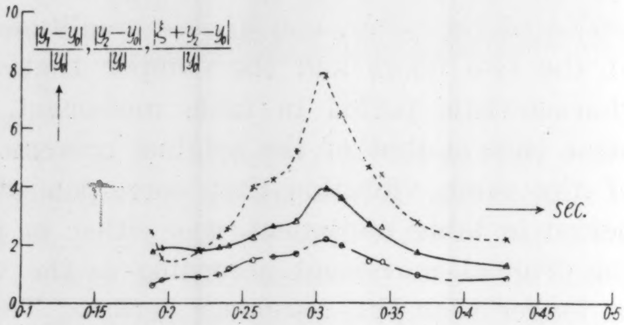

Fig. 7. BIV.

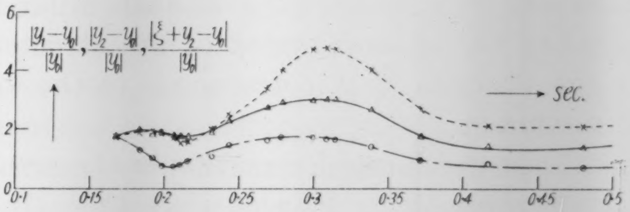

Fig. 8. CII.

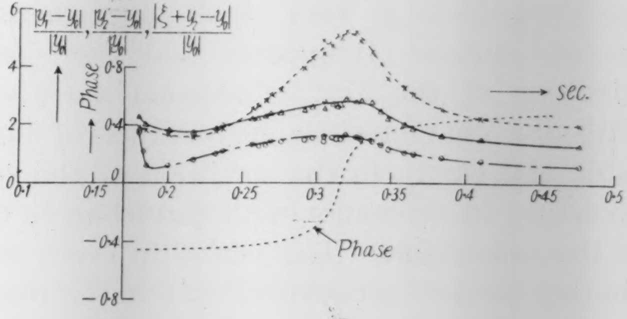

Fig. 9. CIII.

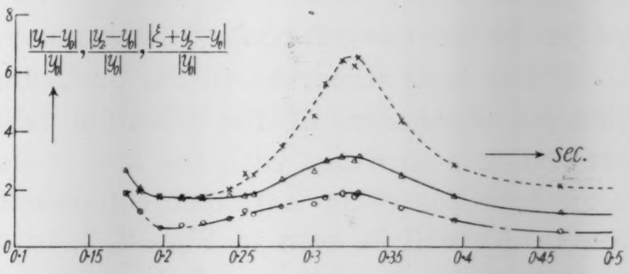

Fig. 10. CIV.

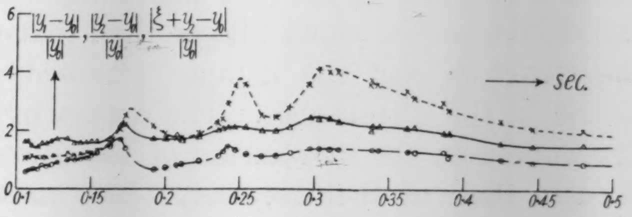

Fig. 11. DIV.

we had conducted model experiments of such a case of C as that in which the period of the damper and that of the structure were alike, a result with still better damping effect would have been possible.

The present experiment has shown that in the case of forced vibration not of simple harmonic type, the resonance amplitudes, even in undamped condition, are not exceptionally large. Whereas in the case of simple harmonic vibration the resonance amplitudes of both the second floor and the damper were more than twenty times that of the vibration table (Case AI of the previous paper[3]), in the case of vibration not of simple harmonic type, the same amplitudes were only about ten times that of the table (Case AI of the present paper), the reason of which is probably that the condition of the vibration structure in the latter case could not attain such a state of maximum work as in the case of usual resonance.

Although, as a matter of fact, the peak in the resonance curves in the case of the undamped condition is at the abscissa that corresponds to the natural period of the structure, in the damped condition

---

3) *loc. cit.*, 2), p 601.

there are two peaks lying at such different abscissae as do not correspond to the natural period of the structure, the ordinate of the curve at the abscissa that corresponds to the original resonance being then at minimum.

Since the damped condition in the present problem arose from coupled vibration, it is evident that there are usually two peaks in every resonance curve in such damped condition. On the other hand, in Case DIII, where vibration experiments were made for a wide range of frequencies, down to very small ones, there are several peaks in its resonance curves. It appears that these peaks correspond partly to the condition of the first vibrational mode of the structure in resonance with the characteristic disturbance of shorter period in the vibration table and partly to the condition of the second vibrational mode of the structure in resonance with disturbances of longer characteristic period in the same table. The peaks, in every resonance curve in Fig. 11, excepting the two pronounced ones in the range of relatively longer periods, represent the resonance conditions mentioned above. It should be borne in mind that the wide peak in every case of C is not well split into two peaks, owing probably to some special condition of the damper mass and in the damping force.

It has been remarked in the preceding section that even should the apparent movements of the vibration table be irregular, the structure vibrated in accordance with the law of forced vibration of simple harmonic type for every harmonic component in the irregular table movements. As will be seen in Figs. 2, 3, in vibrational frequencies near or less than that of resonance of the principal mode of the structure under disturbance of longer characteristic period, the same longer period only manifested itself in the floor and damper movements, whereas in vibrational frequencies much higher than that of the resonance above given, the structure and the damper vibrated with a quicker characteristic period in the disturbance. The feature of vibration here given was more pronounced in the movements of the second floor as also in the damper than in those of the first floor, which probably resulted from the effect of viscous damping mainly in the damper itself and also to a certain extent in the main structure. The phase difference between the structural vibration and the table movement also conformed well to the simple dynamic law as will be seen in the dotted line in Figs. 6, 9.

4. *Damping properties of the free vibrations of a structure provided with a dynamic damper.*

It has already been shown that, were the damper of the present type effective in the case of forced vibration, the free vibration of a structure with the same damper would also be damped very rapidly, as will be confirmed presently.

In the first place, the aperture of the damper piston was kept in condition III, namely the area ratio (0·001728) of the aperture-piston; and the damper mass was progressively increased to 450 gr, 1380 gr, 1710 gr, 1930 gr, 2258 gr, 2445 gr, 2665 gr, 2885 gr, 3290 gr, 4240 gr, and 5180 gr. The records of experiments of the principal free vibration are shown in Fig. 12, from which the damping coefficient f (sec^{-1}) in the expression e^{-ft} was calculated, the result being shown in Fig. 13. It will be seen that in this condition of the damper aperture and elasticity, Cases C and D were within the range of efficient condition.

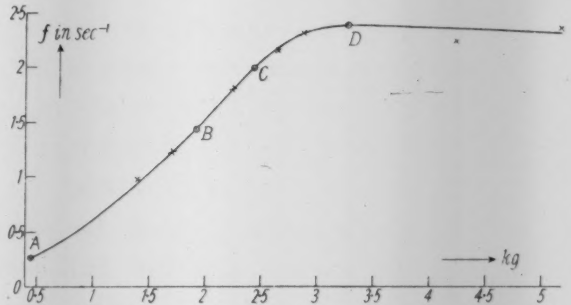

Fig. 13. Damping coefficient f in sec^{-1} for Case III.

In the second place, the damper mass was kept in condition C, and the ratio of aperture-piston was varied in such a range as 0·000462, 0·000832, 0·001728, 0·00260, 0·00389, 0·00989, 0·01980, 0·0560, 0·1011, and 0·1582. The damping coefficient f in sec^{-1} was again calculated from the records of experiments as shown in Fig. 14, and the result plotted in Fig. 15. This result tells us the fact that, since the f-value assumed its maximum at a certain range of ratio of aperture-piston, namely at the range near Case III or IV, moderate values of viscous resistance in the damper was sufficient for dampening the structural vibration. Neither a too large value nor a too small value of viscous force gave a satisfactory condition of the vibration damper.

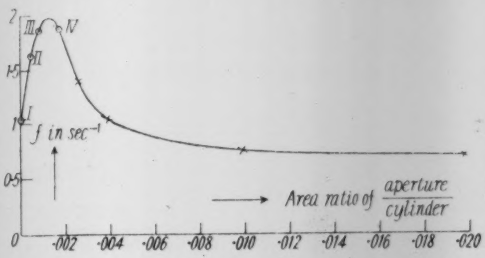

Fig. 15. Damping coefficient f in sec^{-1} for Case C.

Comparing the results of the free vibration tests as shown in Figs. 13, 15, with those of forced vibration tests as shown in Figs. 4∼11, it is possible to confirm what we have said, that the damping condition in free vibration fairly conformed to that under forced vibration, that is to say, an effective damper under forced vibration of a structure was also effective in damping its own free vibration. From this result it may be concluded that a dynamic damper would never give rise to any counter effect to a structure resulting from its oscillatory nature. Since, furthermore, the possible applicability of the damper, even in the case of irregular movements, has also been ascertained in the present paper, there only remains the question how such a sort of damper of relatively large mass could be used in an actual structure.

5. *The conditions of similitude for the damper and a full-scale structure.*

Although these conditions have already been explained in a previous paper,[4] we shall now make a few remarks concerning them.

There are two simple relations, the first being that the ratio of the damper mass to the structural mass must be the same for both the model and the full-scale structure and, the second, that the natural period of the structure must be nearly equal to that of the damper alone, for the model and the full-scale structure. Another important condition is that the ratio of the elastic stiffness in the damper to the product of viscous stiffness and natural frequency in the same damper shall be the same for the model and the full-scale structure. The last condition may be interpreted physically that the elastic resistance relative to the viscous resistance in the damper, both against the vibration of the structure, is invariably the same. All these conditions are mathematically expressed in equations (8), (9), (10), and (29) of our previous paper.[5]

6. *Concluding remarks.*

In the present paper we have ascertained experimentally the nature of our seismic vibration damper for the case of irregular vibration. The effectiveness of the same damper remains unchanged even in such irregular movements as just mentioned. It was also found that the vibrations of the structure are in accord with the law of forced vibrations of simple harmonic type, so that in the present experiments the respective harmonic components in the irregular disturbance separately gave rise to several simple vibrations of the structure, the dynamical relation of phase difference between the vibrating body and the periodic force being also well maintained.

The damping condition in forced vibration and that in free vibration agreed well with each other. Finally the conditions for similitude of models with actual structures and the use of the present damper in practice have been examined.

---

4), 5) *loc. cit.* 2), p. 610~612.

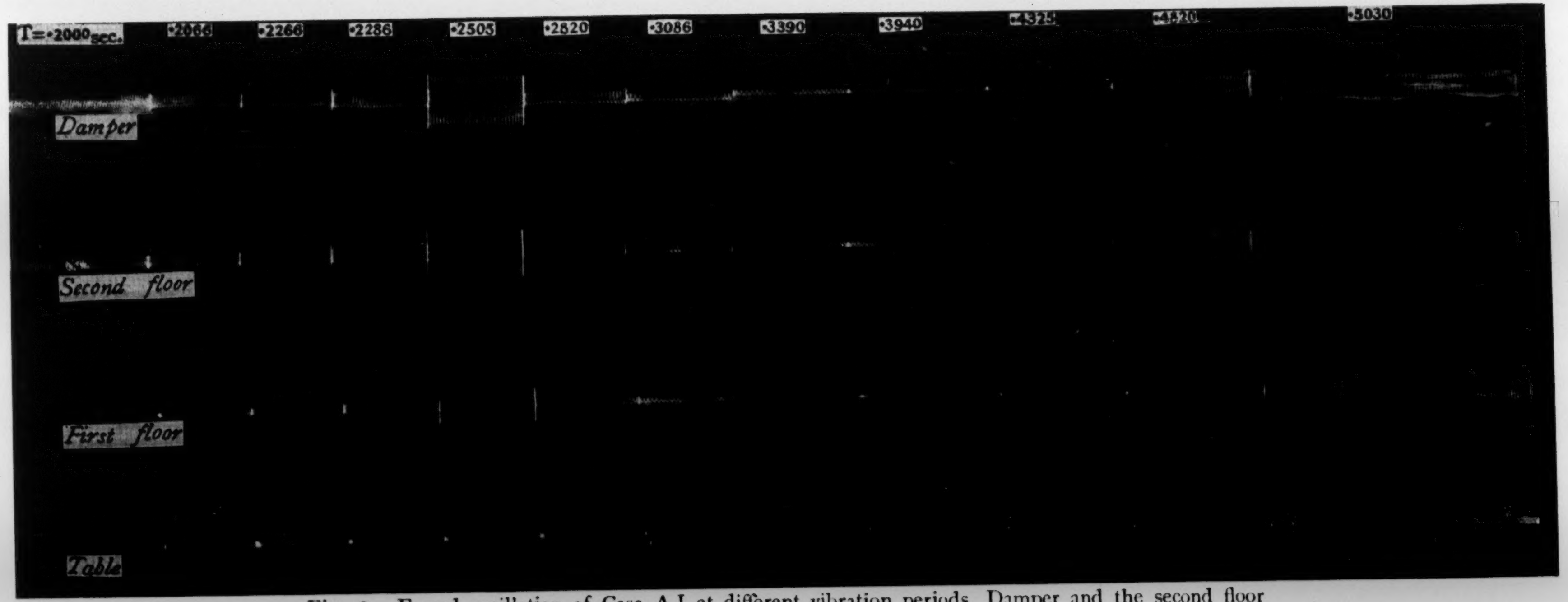

Fig. 2. Forced oscillation of Case A I at different vibration periods. Damper and the second floor vibrate with the same amplitude for any period. (Contraction $^1/_3$)

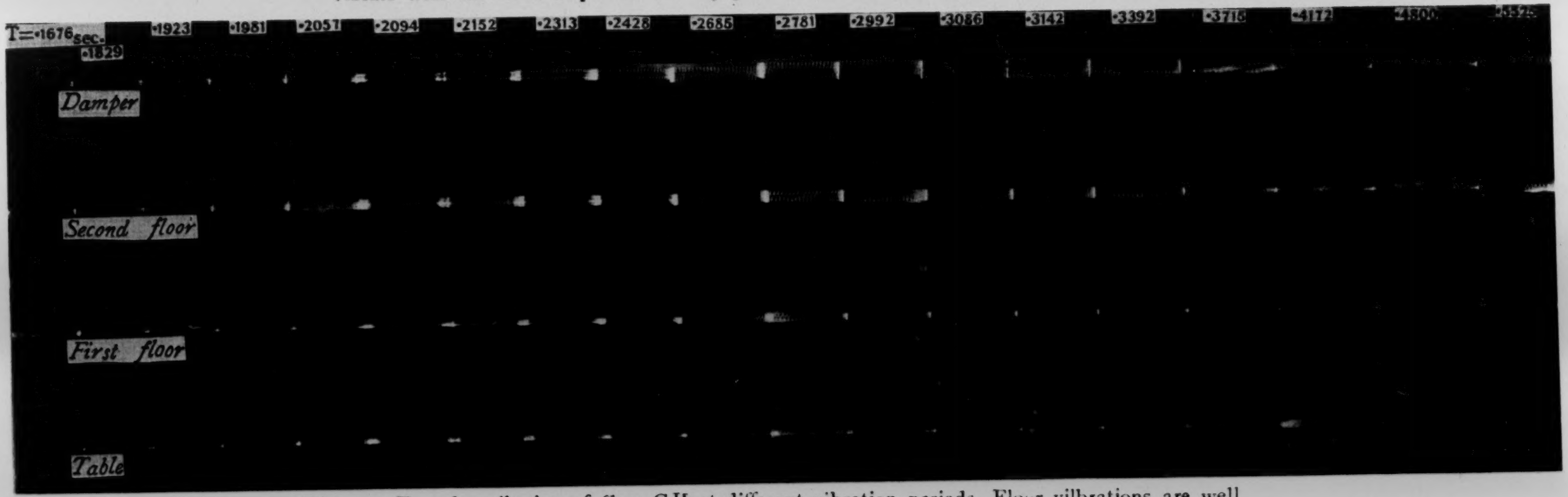

Fig. 3. Forced oscillation of Case C II at different vibration periods. Floor vibrations are well damped for any vibration period. (Contraction $^1/_3$)

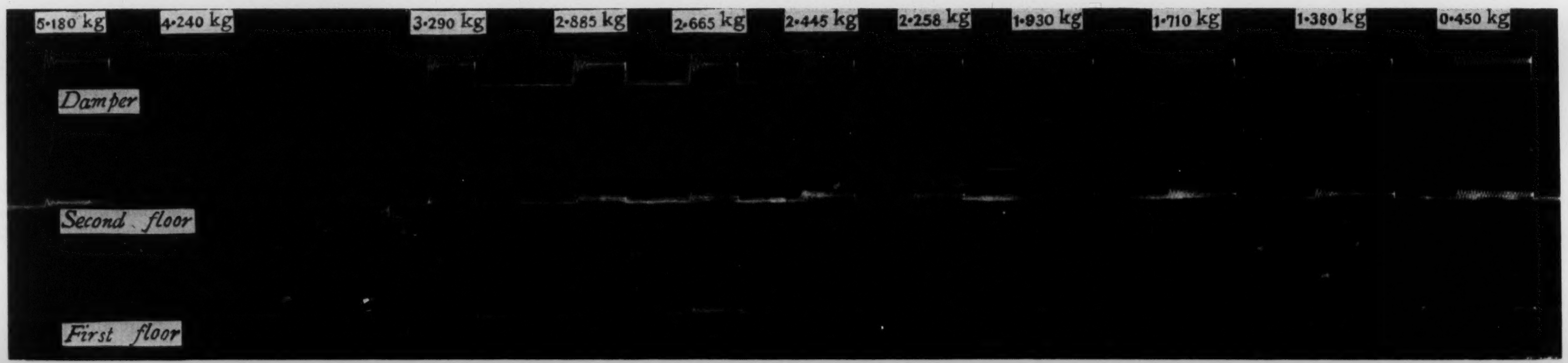

Fig. 12. Free vibration of Condition III for differerent damper masses. (Contraction $^1/_3$)

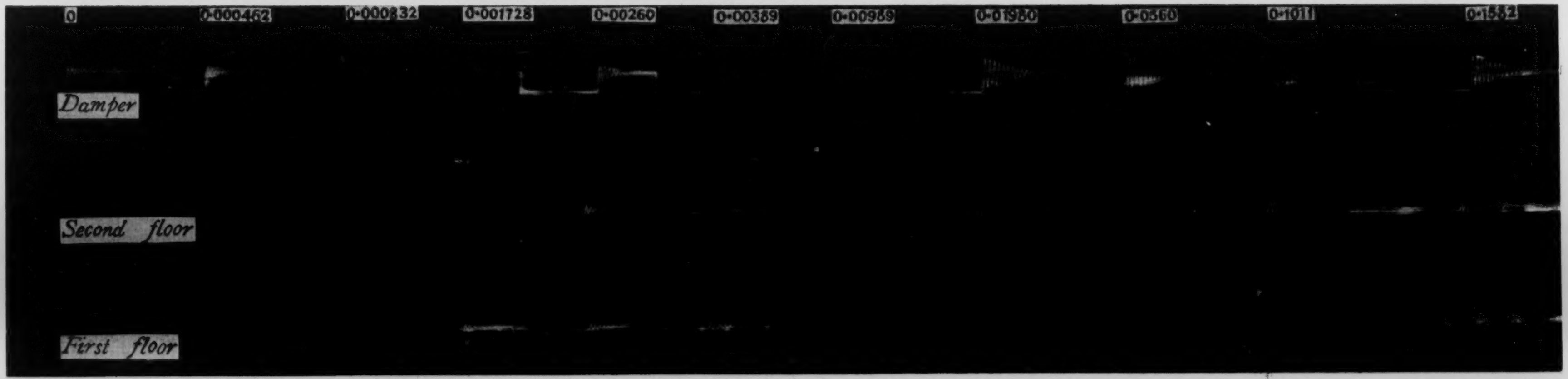

Fig. 14. Free vibration of Condition C for different damper apertures. (Contraction $^1/_3$)

In conclusion I wish to express my thanks to Professor SEZAWA for his kind advice, and also to the Council of the Japan Society of the Promotion of Scientific Research for aid received for conducting these experiments.

---

3. 構造物震動の力學的制振器の模型實驗（不規則な振動）

地震研究所　金井　清

この前に示した構造物震動の力學的制振法の模型實驗を繼續して試み，振動臺の運動がカム軸により不規則な振動になる場合を研究したのである．この場合でも力學的制振器の効果は依然としてよい傾向を示した．力學的制振器が强制振動に効果のあるときにはそれは自由振動に於ても同樣に効果のあることも同樣である．

振動臺の運動が不規則でも，構造及び制振器の模型の振動は原振動を正弦的振動に分解した各部分に對して力學が示す通りの(位相，振幅等に於て)强制振動をなすことがわかつたのである．尙，模型に對して注意すべき相似法則及び研究結果の實際問題に於ける應用性をも示して置いた．

終りに，この研究には妹澤教授を通して日本學術振興會の御援助を仰いだ所が多く茲に感謝する次第である．

4. *Studies on the Seismic Vibration of a Gozyûnotô. III.*

By Katsutada SEZAWA and Kiyoshi KANAI,

Earthquake Research Institute.

(Received Dec. 20, 1937.—Read Dec. 21, 1937.)

1. *Introduction.*

In the previous paper[1] we concluded that the aseismic properties of a gozyûnotô (pagoda) were mainly the result of Coulomb's damping in every columnar part between the roof truss parts. Since the structural members in the columnar part are connected by joggle joints, and not by simple slip joints, Coulomb's damping of vibration increases with increase in relative displacement, so that it is possible to put the damping force in the form

$$Fi(y_n - y_{n-1}), \tag{1}$$

but not

$$Fpi(y_n - y_{n-1}) \tag{2}$$

as in the case of viscous damping, nor

$$Fi \tag{3}$$

as in the case of constant damping for any amplitude including the motionless state. In the expressions (1) and (2), y_n, y_{n-1} represent the displacements of two adjacent roof truss parts, and p the vibrational frequency.

Although in the previous case, we did not specially refer to the effects of the inertia mass nor to the natural period of every part of the roof truss, three elements, namely, the elastic force, damping resistance, and the inertia force in every vibrational part, contribute, as a matter of fact, to the damping phenomena of the structure in seismic vibration, the reason of which is apparent from our investigation of the dynamic damper of structural vibrations. Since the case treated in the previous paper was one in which the mass, stiffness, and damping resistance are respectively the same for any part of the roof-truss, the damping condition of the gozyûnotô was naturally satisfied. Such resonance curves as those in Fig. 3 in the last paper[2] are scarcely obtainable in the usual structure, even were an artificial damper fitted.

---

[1] K. SEZAWA and K. KANAI, "Further Studies on the Seismic Vibrations of a Gozyûnotô", *Bull. Earthq. Res. Inst.*, **15** (1937), 33~40.

2. *Analysis of the quality of vibration damping in a gozyûnotô.*

It is extremely difficult to analyse the quality of damping in a gozyûnotô, assuming that every part of the roof truss is a special damping mass. Although it is possible for the solutions (7)~(12) in the previous paper[3] to be analytically correct, since those solutions are too complex to be of help in obtaining a comprehensive insight into the mechanism of the damping problem, we shall now suppose that only a mere part of the roof truss acts as a damper to the vibrations of all the remaining parts, making the problem a very idealized one.

Let us assume that the gozyûnotô vibrates as a whole with a shearing type of vibration, the equation of motion of the roof truss part being therefore

$$\frac{m}{l_1}\frac{\partial^2 y}{\partial t^2}=Ga\frac{\partial^2 y}{\partial x^2}, \qquad (4)$$

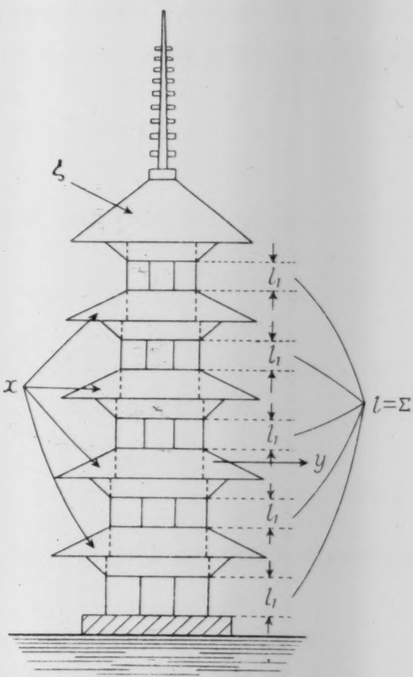

Fig. 1.

where y is the lateral deflection at the roof truss part x, a the area of columns of length l_1 at a section, m the mass to be concentrated at each part of the roof truss, and G the effective shear modulus. Since each elementary part of the structure never moves with a vibration of shearing type, but rather in flexural vibration type, we have, from our previous result,[4]

$$G=12{\cdot}4\frac{Ek^2}{l_1^2}. \qquad (5)$$

Writing $m/al_1=\rho$, (4) reduces to

$$\rho\frac{\partial^2 y}{\partial t^2}=G\frac{\partial^2 y}{\partial x^2}, \qquad (6)$$

the solution of which is

---

[2], [3] *loc. cit.*, 1).

[4] K. SEZAWA and K. KANAI, *Bull. Earthq. Res. Inst.*, **12** (1934), 819.

$$y=e^{ipt}\{Ae^{ifx}+Be^{-ifx}\}, \tag{7}$$

where

$$f=\sqrt{\rho p^2/G}. \tag{8}$$

Assuming that the restitutive force and Coulomb's damping of a special roof truss part (uppermost roof truss part including Kurin, that is, a central nine-ringed pinnacle, in the present case) for relative displacement ξ are

$$c\xi(=c\xi_0 e^{ipt}), \qquad \frac{\mu'}{p}\frac{\partial \xi}{\partial t}=(Fi\xi) \qquad (9),\ (10)$$

respectively, we find the boundary conditions to be

$$x=0; \qquad y=be^{ipt}, \tag{11}$$

$$x=l; \qquad Ga\frac{\partial y}{\partial x}-c\xi-\frac{\mu'}{p}\frac{\partial \xi}{\partial t}=0, \tag{12}$$

$$M\left(\frac{\partial^2 \xi}{\partial t^2}+\frac{\partial^2 y}{\partial t^2}\right)+c\xi+\frac{\mu'}{p}\frac{\partial \xi}{\partial t}=0, \tag{13}$$

corresponding to the seismic vibration of the ground,

$$be^{ipt}, \tag{11'}$$

where l is the effective height of the gozyûnotô.

Substituting (7) in (11)$\sim$(13), we get

$$A\Phi=be^{-ifl}\left[\left\{\frac{Ga}{lc}(fl)^2-\frac{\mu'}{c}fl-\frac{\rho al}{M}\right\}+i\left\{fl-\frac{\rho al}{M}\frac{\mu'}{c}\right\}\right], \tag{14}$$

$$B\Phi=be^{ifl}\left[\left\{\frac{Ga}{lc}(fl)^2+\frac{\mu'}{c}fl-\frac{\rho al}{M}\right\}-i\left\{fl+\frac{\rho al}{M}\frac{\mu'}{c}\right\}\right], \tag{15}$$

$$\xi_0\Phi=-2b\frac{Ga}{lc}(fl)^2, \tag{16}$$

$$\Phi=2\left[\left\{\frac{\rho al}{M}\left(\frac{M}{\rho al}\frac{Ga}{lc}(fl)^2-1\right)\cos fl+fl\sin fl\right\}\right.$$
$$\left.+i\frac{\mu'}{c}\left\{fl\sin fl-\frac{\rho al}{M}\cos fl\right\}\right], \tag{17}$$

so that the final solutions are such that

$$y_{x=l}=b\sqrt{\frac{R^2+S^2}{P^2+Q^2}}\cos\left(\mathrm{pt}-\tan^{-1}\frac{Q}{P}-\tan^{-1}\frac{S}{R}\right), \tag{18}$$

$$\xi=-b\frac{\frac{Ga}{lc}(fl)^2}{\sqrt{P^2+Q^2}}\cos\left(\mathrm{pt}-\tan^{-1}\frac{Q}{P}\right), \tag{19}$$

where

$$R=\frac{Ga}{lc}(fl)^2-\frac{\rho al}{M}, \qquad S=\frac{\rho al}{M}\frac{\mu'}{c}, \qquad (20),\ (21)$$

$$P=\left\{\frac{Ga}{lc}(fl)^2-\frac{\rho al}{M}\right\}\cos fl+fl\sin fl, \tag{22}$$

$$Q=\frac{\mu'}{c}\left\{fl\sin fl-\frac{\rho al}{M}\cos fl\right\}. \tag{23}$$

It will be seen that the vibration amplitudes of a gozyûnotô are functions of Ga/lc, $M/\rho al$, μ'/c, besides the frequency condition fl. Since

$$\frac{M}{\rho al}=\frac{\text{Damper mass}}{\text{Mass of main part}}, \tag{24}$$

$$\frac{\pi}{2}\sqrt{\frac{Ga}{lc}}\sqrt{\frac{M}{\rho al}}=\frac{\pi}{2}\sqrt{\frac{M}{c}}\sqrt{\frac{G}{\rho l^2}}=\frac{T_2}{T_1}$$

$$=\frac{\text{Natural period of damper part}}{\text{Natural period of main part}}, \tag{25}$$

it is possible to conclude that the ratio of the natural period of the so-called damper part (the uppermost roof truss part) to that of the main part and also the ratio of masses of both parts in question greatly participate in the vibration of the gozyûnotô.

The free vibration period of the main part of the gozyûnotô is obtained by putting the solution (7) in

$$x=0; \qquad y=0, \tag{26}$$

$$x=l; \qquad \frac{\partial y}{\partial x}=0, \tag{27}$$

from which the period of the free vibration becomes

$$T_1=\frac{2\pi}{p}=4\sqrt{\frac{\rho l^2}{G}}. \tag{28}$$

The free vibration of the uppermost roof truss part that is to be a damper is defined by

$$M\frac{d^2\xi}{dt^2}+\frac{\mu'}{p}\frac{d\xi}{dt}+c\xi=0, \tag{29}$$

from which the period of its natural vibration and the damping coefficient assume the forms

$$\frac{2\pi}{p}=2\pi\Big/\left\{\left(\frac{c}{M}\right)^2+\left(\frac{\mu'}{M}\right)^2\right\}^{\frac{1}{4}}\cos\left(\frac{1}{2}\tan^{-1}\frac{\mu'}{c}\right), \tag{30}$$

$$f=\left\{\left(\frac{c}{M}\right)^2+\left(\frac{\mu'}{M}\right)^2\right\}^{\frac{1}{4}}\sin\left(\frac{1}{2}\tan^{-1}\frac{\mu'}{c}\right). \tag{31}$$

When, specially, the period of the main structure is equal to that of the damper, we get

$$\frac{Ga}{lc}=\left(\frac{2}{\pi}\right)^2\frac{\rho al}{M}, \tag{32}$$

which is one of the efficient damping condition of the structure.

By using the above equations, it is possible to understand, mathematically, why a gozyûnotô resists seismic vibration.

3. *Some numerical examples, and the interpretation of the problem.*

It is uncertain whether or not the roof parts in an actual gozyûnotô are in the condition of the most favourable dynamic damper. Even an accurate observation of the seismic vibrations of a gozyûnotô would not give us the information.

From Omori's report,[5] the natural vibration period of a gozyûnotô is more than 1 sec, and the amplitude of the free vibration diminishes to about one-half its initial value after three or four cycles of vibrations. Although the damping coefficient of the free vibration of the whole gozyûnotô can be obtained by solving (17), since its treatment is extremely difficult, we performed a number of tentative calculation from Omori's data with repect to the free and forced vibration experiments of gozyûnotôs, after which we found that the following two examples represent the most probable condition of the actual towers, or at least a condition that is more favourable than what is actual.

(i) $$\frac{\rho al}{M}=5,\qquad \frac{T_2}{T_1}=1,\qquad \frac{\mu_1}{c}=0{\cdot}45; \tag{31}$$

---

[5] F. OMORI, *Bull. Earthq. Inst. Comm.*, **9** (1918~21), 110~150.

$$\text{(ii)} \qquad \frac{\rho a l}{M}=5, \qquad \frac{T_2}{T_1}=1{\cdot}370, \qquad \frac{\mu'}{c}=0{\cdot}45. \tag{32}$$

The resonance curves for the two cases are shown in Figs. 2, 3. The full and broken lines in these figures represent the displacement ratios of the uppermost point of the main part and the damper part to the ground vibration, namely $y_{x=l}/b$, ξ/b respectively, whereas the dotted lines indicate the phase difference between the displacement y at $x=l$ and the displacement ξ.

The solution (18) shows that the displacement y is independent of μ', provided

$$\left|\frac{\dfrac{Ga}{lc}(fl)^2-\dfrac{\rho a l}{M}}{\left\{\dfrac{Ga}{lc}(fl)^2-\dfrac{\rho a l}{M}\right\}\cos fl+fl\sin fl}\right|=\left|\frac{\dfrac{\rho a l}{M}}{fl\sin fl-\dfrac{\rho a l}{M}\cos fl}\right|. \tag{33}$$

This shows that the ordinates corresponding to the abscissae, for which (33) holds, are constant for any damping resistance of the damper part, unless the value Ga/lc, showing the frequency ratio for both parts, and $\rho a l/M$, showing the mass ratio for the same parts, were not changed. There are an infinite number of such points for a wide range of the vibrational frequencies. The same points for low vibrational frequencies are shown by the symbols K, K' in the figures ($fl=1{\cdot}191$, $1{\cdot}8523$, ……, in Fig. 2; $fl=1{\cdot}0241$, $1{\cdot}5859$, ……, in Fig. 3).

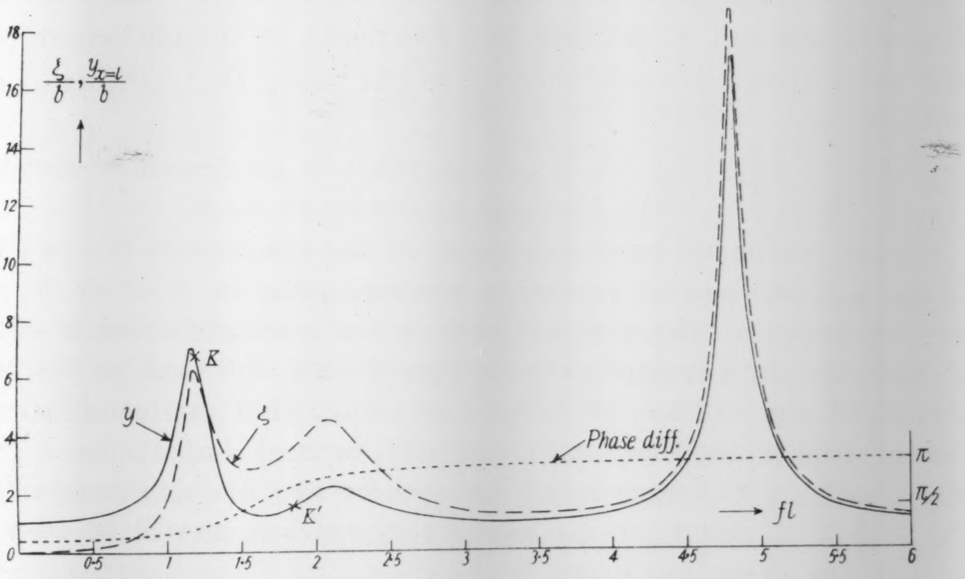

Fig. 2. Case (i), $\rho a l/M=5$, $\mu'/c=0{\cdot}45$, $T_2/T_1=1$; Full, broken, and dotted lines represent $y_{x=l}$, ξ, and phase difference respectively.

When the damping force μ' is infinitely large, the damper part is in a condition that is rigidly fixed to the main part, so that resonance curve that passes through K, K' has a peak, of infinite height, at $fl=\pi/2$; whereas when the damping force is zero, the damper part is connected to the main part only elastically, so that the resonance curve that passes through K, K' then has two peaks, of infinite height, nearly at the same abscissae corresponding to the peaks (left-hand two peaks) in the figures.

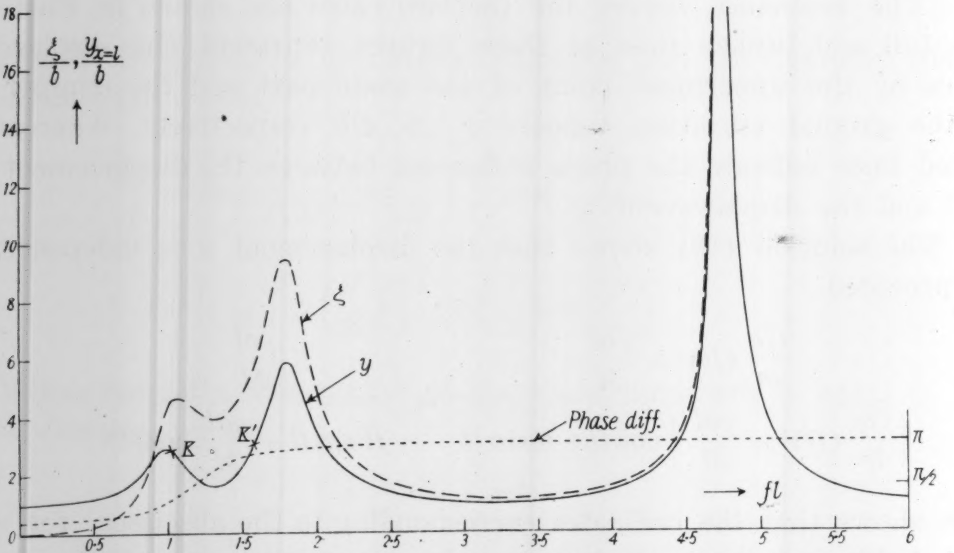

Fig. 3. Case (ii), $\rho al/M=5$, $\mu'/c=0{\cdot}45$ $T_2/T_1=1{\cdot}370$; Full, broken and dotted lines represent $y_{x=l}$, ξ, and phase difference respectively.

Whatever case may be, it is impossible to get resonance curves, the peaks of which are lower than the ordinates at K, K'.

Higher resonance conditions occur at the frequencies $fl=(n+1/2)\pi$. In Figs. 2, 3 the second resonance corresponding to $fl=3\pi/2$ is given. Since the action of the damper part on the main structure is effective only near the first resonance condition $fl=\pi/2$, the peak at $fl=3\pi/2$ is extremely sharp. It has often been remarked that mathematical sharp peaks at higher resonance are not of practical importance. In the actual condition of a gozyûnotô, since there are five damper parts, the peaks of higher resonance are never very marked, as will be seen from Fig. 3 in the preceding paper.[6]

---

[6] *loc. cit.* 1). It should be borne in mind that the condition of the problem in the present paper differs somewhat from that in the previous one. While in the previous case there was damping force in every columnar part, in the present case, on the other hand, no such force exists excepting in the part between the fourth and fifth roof truss parts, the result being such that the damping condition of the present case is effective for a moderate value of μ'/c.

Comparing the full lines with the chain or dotted lines in the resonance curves in Figs. 2, 3, it will be seen that the damping effect of the damper parts in a gozyûnotô is enormous.

It should be borne in mind that, as we have stated in the beginning of the last section, the damping condition here given is merely an idealized one. The result of the damping effect of the actual gozyunotô would be of the type shown in Fig. 3 in our previous paper.[7] Since in the previous case $F/Mg \ (=\mu'/Mg)=0{\cdot}2487\ \mathrm{cm}^{-1}$ and $M/c=0{\cdot}002052$ sec^2, it follows that $\mu'/c\{=(\mu'/Mg)(M/c)g\}=0{\cdot}2487.0{\cdot}002052.980\fallingdotseq 0{\cdot}50$, which is approximately the same as the value of $\mu'/c(=0{\cdot}450)$ in the present case. Although the ordinate at the peak in the resonance curve in the previous case was less than 2·5, the same ordinate in the present case is larger than 5, which shows that the damping condition in the actual gozyûnotô should be much more effective than that in the present idealized one.

In conclusion, we wish to express our thanks to the Council of the Japan Society of the Promotion of Scientific Research, with whose aid progress in the present investigation was considerably furthered.

4. 五重塔の耐震性(第3報)

地震研究所 {妹澤克惟
　　　　　 {金井清

五重塔の耐震性は各軸部に働く Coulomb 摩擦が大いに與ることをこの前述べて置いたが，その場合に僅かの摩擦力によつても可なりの効果があつたのである．之はよく考へて見るとその計算に於て順々の屋根及斗組の質量を一定にし且つ軸部の彈性及び摩擦力が夫々一定にしてあつたのであるから，しばしば述べたところの構造物の力學的制振器が幾つも組合つてをることを示すのである．殊に制振器はその質量が大きい程，且つその自己振動周期が主要構造部の周期に近い程効力が多いのであるから，この前の研究は單に摩擦力のみでなく，制振器の研究をなしてをつたことになるのである．

計算が相當複雜であつたから，力學的計算結果の何れの部分が制振器の作用をなしたのか判斷に苦しむのである．それで茲に一つの層の屋根例へば第５層（九輪を含み）を制振器と考へ，他の層は全部本構造と見做して計算を試みた．卽ち相當抽象的であつてこの前の計算よりも一層實際から離れてをるのである．

---

[7] *loc. cit.* 1).

その結果を見るさ摩擦力がこの前の場合さ殆ご同じであるのにも拘らず，効果は前のものよりも大分少な氣味である．制振器の質量は構造全體の質量の 1/5 位しかなく，從て効果が前のものよりも劣るのは當然な話である．それにしても共振曲線の峯は制振作用のないさきから見て非常に低くなつてをる．尙，構造物の第2次以上の共振に對しては殆ご制振作用を與へない．しかし高次の共振には種々の制振作用が働くから之は始めから問題さするに足らぬものである．このやうな高次のものでも，この前のやうに各屋根及斗組部分が制振器の作用を持つ場合にはやはり共振の峯がなくなるものである．

摩擦力の大きさは單に假定したのでなく，大森博士が試みた五重塔の振動實驗の自由振動及び強制振動の減衰率から推定したのである．複原力も振動周期から定めた．實際の五重塔に於ては，この前の報告や只今の研究結果程制振作用があるかごうかは各部の振動周期が同じかごうかわからぬ（之は實驗でも出し難い）だけそれだけ多少疑しいものである．しかし筆者等をして新に五重塔を設計せしめれば昔のものよりも一層耐震的の五重塔を作り得るさいふ考を持つ次第である．

Corrigenda to the authors's paper, "Vibrations of a Single-storied Framed Structure", published in the Bull. X (1932), Part 3, p. 767.

From the nature of longitudinal thrust in floor beams, the conditions (33), (44), (52) in the paper should be replaced by

$$\left.\begin{aligned} -E_1a_1k_1^2\left(\frac{d^3u_1}{dx_1^3}+\frac{d_3u_1'}{dx_1'^3}+\frac{d^3u_1''}{dx_1''^3}\right)&=2\rho_2a_2l_2p^2u_1, \\ u_1=u_1'&=u_1''. \end{aligned}\right\}$$

Since, nevertheless, the thrust in question is not large in such a particular problem as in the same paper, the numerical result obtained had no much error.

5. *Gravity Anomalies and Deviations of the Vertical in Izu-Osima.*

By Katuhiko MUTO,*

Military Land Survey.

(Read Oct. 19, 1937.—Received Dec. 20, 1937.)

During the period between Jan. 22 and March 2, 1937, the Military Land Survey conducted astronomical observations at Habu and Okada-mura, in Izu-Osima, as the result of which the meridian and prime vertical components of deviations of the verticals $\xi_{(G-A)}$ and $\eta_{(G-A)}$ at these places were found, as follows;

	$\xi_{(G-A)}$	$\eta_{(G-A)}$		$\xi_{(G-A)}$	$\eta_{(G-A)}$
Habu	$-11{\cdot}4''$	$-3{\cdot}9''$	Okada	$-28{\cdot}6''$	$+0{\cdot}8''$

The geodetic positions of these points were determined by tertiary triangulation with the standard datum of Tokyo as reference, the deviation of the vertical of which was assumed to be zero.

The astronomical longitudes and latitudes of the above mentioned places were determined by "the method of equal altitudes of different stars." The instrument used was Carl Bamberg's 21 cm Universal theodolite. The sensibility of the Talcott level is 1·8″ per 2 mm run, and that of the striding level 4·5″. For determining the time, the time signal of the Hunabasi Wireless Station was recorded by chronograph, and the pointing of the stars done by the key method.

The probable errors of astronomical observations are

at Habu	for longitude	$\pm 0{\cdot}240''$	at Okada	for longitude	$\pm 0{\cdot}195''$
	for latitude	$\pm 0{\cdot}117$		for latitude	$\pm 0{\cdot}174$

Position errors of observation points due to the triangulation may be ruled out, since it is very small (a few decimetres at most) compared with the astronomical results just mentioned. The deviations of the verticals obtained at Izu-Osima may be regarded as accurate, so far as precision of the astronomical work is concerned. The magnitude of deviation of the vertical measured in Izu-Osima is larger than those of other points in the inland. Large deviations of the verticals have also been noticed in Hawaii by the U. S. Coast and Geodetic Survey, their measurements being as follows.[1]

---

* Comm. by N. MIYABE.

[1] Coast and Geodetic Survey, U. S. A., *Spec. Publ. No.* 156 (1930).

Latitude stations

Kauai Island	
Waimea	−35·58″
Koloa	−44·28
Hanalei	+24·64
Oahu Island	
Kahuku	+24·52″
Honolulu	−25·55
Waikiki	−27·84
Maui Island	
Lahaina	− 9·81″
Haiku	+18·79
Pakaoao	−10·87″
Kaupo	−40·23
Hana	+11·80
Hawaii Island	
Kohala	+31·12″
Kawaihae	+ 0·20
Mauna Kea	− 0·13
Kalaieha	−12·17
Hilo	− 0·35
Kailua	−23·55
Ka Lae	−67·64

Longitude stations

Oahu Island	
Honolulu	+ 0·50″
Niu	−15·06″

On comparing the above mentioned values with those of Izu-Osima, the values of deviations of the verticals which we measured in Izu-Osima may be regarded as not being exceptionally large. A very remarkable point in which they differ from the Hawaiian values is that the sign of the ξ components of Izu-Osima is the same for both points, notwithstanding that Habu and Okada-mura are situated respectively at the southern and northern ends of the island, the great mass of Mihara Volcano lying between these stations.

Table I.

Station	Long. (E)	Lat. (N)	Height or Depth (in m)	g_0 (in gal)	$g_0-\gamma_0$ (in gal)
Hatizyōzima	139°50′	33°66′	64	979·765	+0·194
Kamakura	139 34	35 19	13	·783	+0·026
Osima	139 22	34 45	24	·862	+0·153
Odawara	139 9	35 15	65	·796	+0·044
Rendaizi	138 57	34 42	14	·812	+0·108
Numazu	138 52	35 5	7	·789	+0·051
Sizuoka	138 23	34 58	23	·760	+0·032
A	140 00·0	34 10·0	−1200	·800	+0·140
(1)	139 30·4	35 07·8	− 700	·752	+0·011
(3)	139 30	34 57	−1250	·758?	+0·032?
(2)	139 23·2	34 56·1	−1470	·749	+0·024
Z	139 14·7	33 38·2	− 790	·691	+0·076
B	138 45·8	33 00·6	−2500	·660	+0·097
P	138 30·2	34 15·2	−1570	·668	+0·001
S	137 56·8	33 36·0	−3700	·615	+0·003
T	137 27·7	33 00·8	−4100	·629	+0·066

In connection with the deviation of the vertical, gravity was measured at Izu-Osima and on the sea in the neighbourhood of Izu-Osima and other islands.

The values of the gravity anomaly $g_0-\gamma_0$ in the region under consideration are reproduced in Table I from Matuyama's report[2] and Tsuboi's book.[3]

In Table I, the values of the actual gravity g_0 are those reduced from observed values by applying the "free air" correction, while those of normal gravity γ_0 are those computed by Helmert's formula of 1901. In order to show the distribution of gravity anomalies, isanomaly lines are drawn from the data given in Table I, as shown in Fig. 1, the numerals affixed to the isanomaly lines designating the value of the anomaly in milligals.

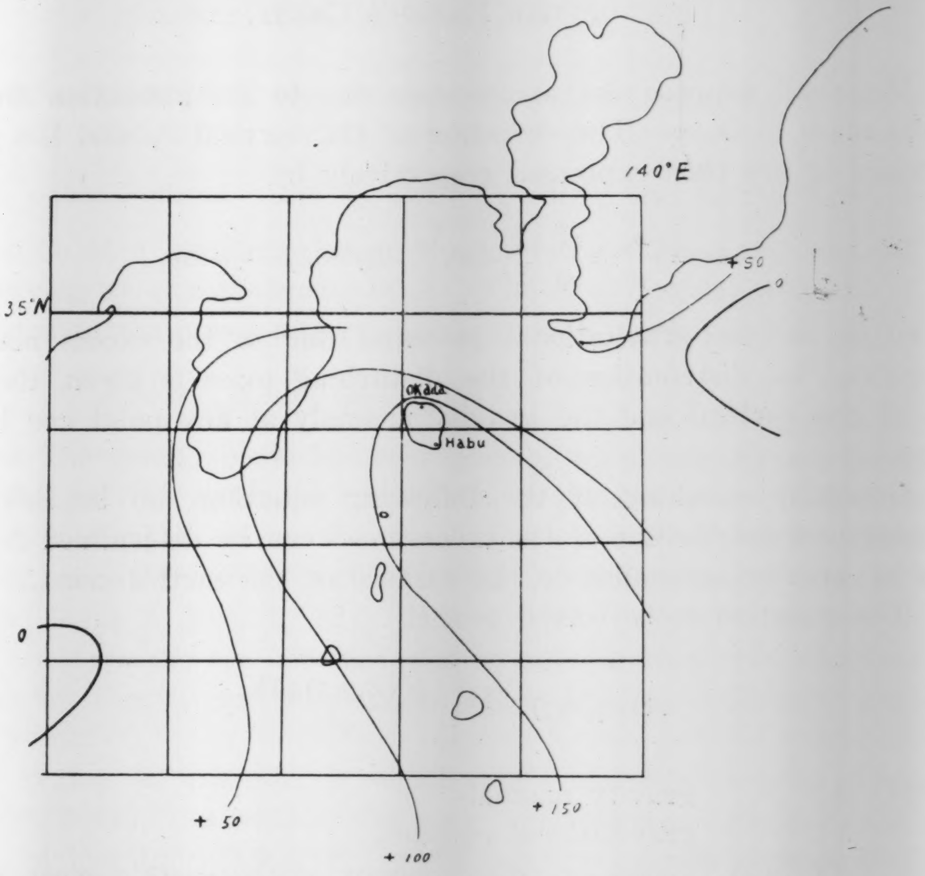

Fig. 1. Distribution of gravity anomalies in the neighbourfood of Izu-Osima.

In this paper the writer deals with the results of his studies with

---

2) M. MATUYAMA, "Gravity Survey by the Japanese Geodetic Commission since 1932."

3) C. TSUBOI, "Zyūryoku" (Gravity), Tokyo, 1936.

the object of ascertaining, under a certain likely assumption, the distribution of excess mass in the earth's crust (assuming that the earth's crust is in general homogeneous and of uniform density) that might admit of being estimated from the distribution of gravity anomaly on the surface of the earth. In doing so, the deviations of the verticals estimated from the mass distribution thus determined are compared with the actual values recently measured.

THE HORIZONTAL AND VERTICAL COMPONENTS OF THE ATTRACTION DUE TO THE EXCESS MASS OF THE EARTH'S CRUST.

We shall suppose the acceleration due to the attraction from the excess mass to be α. The deviation of the vertical $\delta\varphi$ and the gravity anomaly δg are then expressed respectively by

$$\delta\varphi=\frac{\alpha_x}{g}=\frac{1}{g}\frac{\partial}{\partial x}\delta w, \qquad \delta g=\alpha_z=\frac{\partial}{\partial z}\delta w,$$

where δw is the gravitational potential due to the excess mass. If, therefore, the distribution of the disturbing mass is given, the deviation of the vertical and the gravity anomaly at any point can be computed.

Generally speaking, if the following equation can be solved, the underground distribution of the excess mass can be determined from the data of gravity anomalies on the surface of the earth's crust.

The equation to be solved is then

$$A(x_1,\ y_1)=k^2\int_V \frac{\rho'(x,y,z)\,z\,dV}{r^3}, \qquad (1)$$

where A: gravity anomaly

k^2: gravitational constant

$\rho'(x,y,z)$: excess or defect density in the earth's crust, the last mentioned being assumed to be homogeneous.

$$r=\sqrt{(x-x_1)^2+(y-y_1)^2+z^2}.$$

In the above equation, the origin of the co-ordinates is taken at a point on the surface of the earth, and the positive direction of z is taken downwards. To solve mathematically the above equation is not easy.

If the distribution of the disturbing mass were estimated from geological investigations, and geometrically it is of simple form, the above equation could be easily solved and the density distribution responsible for the gravity anomalies determined.

The object of the present study is, however, to determine the density distribution that causes the gravity anomalies as deduced from the distribution of gravity anomalies on the surface of the earth, provided it is not so complex as to render virtually impossible a ready solution of the above equation.

METHOD OF DETERMINING THE DISTRIBUTION OF EXCESS MASS IN THE EARTH'S CRUST.

In order to simplify the problem to be treated here, the following method was used. The earth's crust was divided into a number of cubes of equal volume. Let $\alpha\rho' = k^2 \int \frac{\rho' z}{r^3} dV$ be the vertical component of attraction at a certain point on the surface of the earth caused by a cube having an excess density of ρ'. The total gravity anomaly A_p at point p due to the cubes under consideration is approximately given by

$$A_p = \alpha_{p.1}\rho'_1 + \alpha_{p.2}\rho'_2 + \alpha_{p.3}\rho'_3 + \dots\dots\dots\dots + \alpha_{p.i}\rho'_i. \qquad (2)$$

When the earth's crust in the region in which the surface distribution of the gravity anomalies are given, is divided into i cubic blocks, and, in each of these cubes the density is equal, the gravity anomaly at a point situated at the centre of the surface of each cube in the uppermost layer is given by (2). Hence, when $i = p$, simultaneous equations of the type (2) are obtained, and by solving them, the distribution of the excess density can be obtained. It is however still very difficult to solve them.

The region in question, in which the disturbing mass is supposed to be distributed, lies within the area enclosed by latitudes 35.3° *N*, 33·8° *N* and longitudes 138.5° *E*, 140° *E*, and to a depth of 90 km. The whole mass of the earth's crust is divided into 75 square blocks as shown in Figs. 1 and 2, the volume of each being $30 \times 30 \times 30$ km³. The density of each cube is assumed to be 0 or some constant which is common to all cubes.

To calculate numerically the vertical component of the attraction at a certain point (at the centre of the surface of the cube in the uppermost layer), each cube was subdivided into 27 smaller ones, all of the same volume, and the excess mass in each small cube supposed to be concentrated at its centre. The vertical components of the attraction due to each cubic mass for a point is then easily computed. In comparing these two calculated values of the vertical components of attraction, namely, the one that is calculated on the assumption that the excess mass is concentrated at the centre of each cubic block, and the other that is calculated on the assumption that the excess mass is distributed at the centre of the 27 smaller cubes composing the cubic block, we notice that the former is larger by several percent than the latter, although the difference is negligible within the limits of errors in the present discussion.

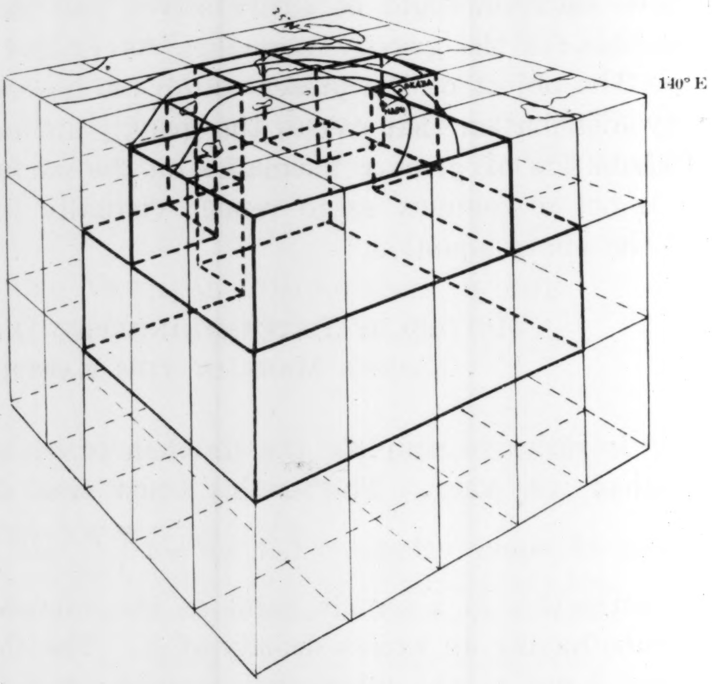

Fig. 2.

It may therefore be worth while to try to ascertain the extent to which the value of attraction at a point on the surface (calculated on the assumption that the excess mass is concentrated at the centre of the cubic block, just underneath the said point), deviates from that calculated on the assumption that the excess mass is distributed uniformly within the cubic block. For this purpose, we have used the following method.

Firstly, the vertical component of attraction at point p in Fig. 3 due to a cubic block and that of the same point due to the 27 smaller blocks are compared, the latter smaller blocks being formed by subdividing each side of the former block into 3 parts.

In calculating, the excess mass is treated as being concentrated at the centre of each of the cubic blocks. Let the length of a side and the excess density of the smaller block be $2a$ and ρ respectively. Then the gravity due to the mass of the larger block is $k^2 \times \rho \times 24a$, and that due to a cube consisting of 27 smaller blocks is $k^2 \times \rho \times 18{\cdot}584a$. The difference in gravity is $k^2 \times \rho \times 5{\cdot}416 \times a$. Similarly, the smaller cube just beneath the "point" mentioned, above the gravity at which is being sought, is subdivided

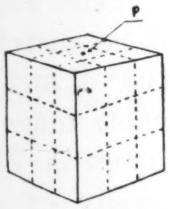

Fig. 3.

into 27 smaller square blocks, when the gravity thus calculated is found to be smaller by $k^2 \times \rho \times 5{\cdot}416a'$, where $a' = \frac{a}{3}$, than the larger block.

Since, in this case, the excess mass is 1/27 times that of the former case, the gravity thus calculated is smaller by $k^2 \times \rho \times 5{\cdot}416 \times a \times \frac{1}{3}$ than that calculated on the assumption that excess mass of the cube of $(6a)^3$ is concentrated at the center.

Thus by dividing the square block into a number of very small blocks, the value of gravity calculated approaches that which is obtained by integrating throughout the volume of the larger block. The correction for the gravity value calculated by the most simple method is therefore

$$C = \delta\left(1 + \frac{1}{3} + \frac{1}{3^2} + \frac{1}{3^3} + \ldots\ldots\ldots\ldots\right) = \delta \times \frac{3}{2}.$$

Since, in the present case, $\rho = 0{\cdot}1$ and $a = 5$ km, we have

$$\delta = 18{\cdot}1 \text{ (milligal)}.$$

The vertical components of attraction due to each cubic block at a point on the surface is shown in Table II, in which ρ' is taken as 1 for all cubes.

Table II.

Z in km	$X(Y)$ in km	0	30	60	90	120	150
	$Y(X)$ in km	$a\rho'$ in milligal					
$Z = 15$	0	528	72	11	4	2	1
	30		30	8	3	1	1
	60			4	2	1	1
	90				1	1	0
	120					1	0
	150						0
$Z = 45$	0	89	51	19	8	4	2
	30		34	15	7	4	2
	60			9	5	3	2
	90				3	2	1
	120					1	1
	150						1
$Z = 75$	0	32	26	15	8	5	3
	30		21	13	8	4	3
	60			9	6	4	3
	90				4	3	2
	120					2	2
	150						1

For convenience, the square blocks are designated by numbers as shown in Table III.

Table III.

upper layer

55	56	57	58	59
54	63	64	65	66
53	62	69	70	71
52	61	68	73	74
51	60	67	72	75

middle layer

30	31	32	33	34
29	38	39	40	41
28	37	44	45	46
27	36	43	48	49
26	35	42	47	50

lower layer

5	6	7	8	9
4	13	14	15	16
3	12	19	20	21
2	11	18	23	24
1	10	17	22	25

The gravity anomalies at the centres of the upper surfaces of cubes, numbers 61 to 65, 68 to 70 and 73 in Fig. 1, have been estimated, and the anomalies calculated for the above "points" with the aid of equation (2) and Table II, as shown in Table IV, in which ρ' is taken as 1, and in which the numerals in compartments show the values of $\alpha\rho'$ of the respective cubes for the point under consideration, the compartments being arranged as shown in Table III. The gravity anomalies were not calculated for points lying near the borders of the region under consideration, for which reason the value of attraction may not be correct as may be expected.

Taking the assumed value for the anomalies in density as being likely, the distribution of the excess mass, that satisfies the condition given by a series of equations, may be found by inspection, but in this

Table IV.

A_{69} = 140 mgal (upper)

4	8	11	8	4
8	30	72	30	8
11	72	528	72	11
8	30	72	30	8
4	8	11	8	4

A_{61} = 50 mgal (upper)

3	4	3	2	1
8	11	8	4	2
30	72	30	8	3
72	528	72	11	4
30	72	30	8	3

A_{69}=140 mgal (middle)

9	15	19	15	9
15	34	51	34	15
19	51	89	51	19
15	34	51	34	15
9	15	19	15	9

(lower)

9	13	15	13	9
13	21	26	21	13
15	26	32	26	15
13	21	26	21	13
9	13	15	13	9

A_{61}=50 mgal (middle)

7	8	7	5	3
15	19	15	9	5
34	51	34	15	7
51	89	51	19	8
34	51	34	15	7

(lower)

8	8	8	6	4
13	15	13	9	6
21	26	21	13	8
26	32	26	15	8
21	26	21	13	8

A_{62}=90 mgal (upper)

8	11	8	4	2
30	72	30	8	3
72	528	72	11	4
30	72	30	8	3
8	11	8	4	2

(middle)

15	19	15	9	5
34	51	34	15	7
51	89	51	19	8
34	51	34	15	7
15	19	15	9	5

(lower)

13	15	13	9	6
21	26	21	13	8
26	32	26	15	8
21	26	21	13	8
13	15	13	9	6

A_{63}=60 mgal (upper)

30	72	30	8	3
72	528	72	11	4
30	72	30	8	3
8	11	8	4	2
3	4	3	2	1

(middle)

34	51	34	15	7
51	89	51	19	8
34	51	34	15	7
15	19	15	9	5
7	8	7	5	3

(lower)

21	26	21	13	8
26	32	26	15	8
21	26	21	13	8
13	15	13	9	6
8	8	8	6	4

A_{68}=120 mgal (upper)

2	3	4	3	2
4	8	11	8	4
8	30	72	30	8
11	72	528	72	11
8	30	72	30	8

(middle)

5	7	8	7	5
9	15	19	15	9
15	34	51	34	15
19	51	89	51	19
15	34	51	34	15

(lower)

6	8	8	8	6
9	13	15	13	9
13	21	26	21	13
15	26	32	26	15
13	21	26	21	13

A_{73}=150 mgal (upper)

1	2	3	4	3
2	4	8	11	8
3	8	30	72	30
4	11	72	528	72
3	8	30	72	30

(middle)

3	5	7	8	7
5	9	15	19	15
7	15	34	51	34
8	19	51	89	51
7	15	34	51	34

A_{64}=100 mgal (upper)

8	30	72	30	8
11	72	528	72	11
8	30	72	30	8
4	8	11	8	4
2	3	4	3	2

(middle)

15	34	51	34	15
19	51	89	51	19
15	34	51	34	15
9	15	19	15	9
5	7	8	7	5

(lower)

13	21	26	21	13
15	26	32	26	15
13	21	26	21	13
9	13	15	13	9
6	8	8	8	5

A_{70}=150 mgal (upper)

2	4	8	11	8
3	8	30	72	30
4	11	72	528	72
3	8	30	72	30
2	4	8	11	8

(middle)

5	9	15	19	15
7	15	34	51	34
8	19	51	89	51
7	15	34	51	34
5	9	15	19	15

$A_{73}=150$ mgal (lower)

4	6	8	8	8
6	9	13	15	13
7	13	21	26	21
8	15	26	32	26
8	13	21	26	21

$A_{70}=150$ mgal (lower)

6	9	13	15	13
8	13	21	26	21
8	15	26	32	26
8	13	21	26	21
6	9	13	15	13

$A_{65}=70$ mgal

(upper)

3	8	30	72	30
4	11	72	528	72
3	8	30	72	30
2	4	8	11	8
1	2	3	4	3

(lower)

8	13	21	26	21
8	15	26	32	26
8	13	21	26	21
6	9	13	15	13
4	6	8	8	8

(middle)

7	15	34	51	34
8	19	51	89	51
7	15	34	51	34
5	9	15	19	15
3	5	7	8	7

paper the following method was used to ascertain the distribution of the excess mass.

The terms on the left-hand side of the equations (2), namely, A in Table IV, are reduced to a value common to all the equations, and the sum of $\alpha\rho'$ of successive compartments plotted against the number of cubes as abscissa, when all the values of $\sum\alpha\rho'$ corresponding to a certain point on the abscissa should either become equal to or $\frac{1}{\rho'}$ of the value on the left-hand side of the equations, ρ' being the same for every cubic block, as already assumed.

In the present problem, the numerical value on the left-hand side of the equation was reduced to 100 milligals and the value of ρ taken as 0·1. The results of the reduction are given in Table V, and the values of $\sum\alpha\rho'$ plotted as shown in Fig. 4.

Of the cubic blocks in the uppermost layer in Fig. 4. only the values of $\alpha\rho'$ due to the cubic blocks Nos. 62, 64 and 68 to 75 have been taken into consideration, because the values of $\alpha\rho'$ due to the other cubic blocks may obviously be rejected by inspection. For example, the observed gravity anomaly at the middle of the surface of block No.

60 is about 40 milligals, whereas the attraction at the same point due to cube No. 60 alone amounts to 53 milligals. In the writer's opinion

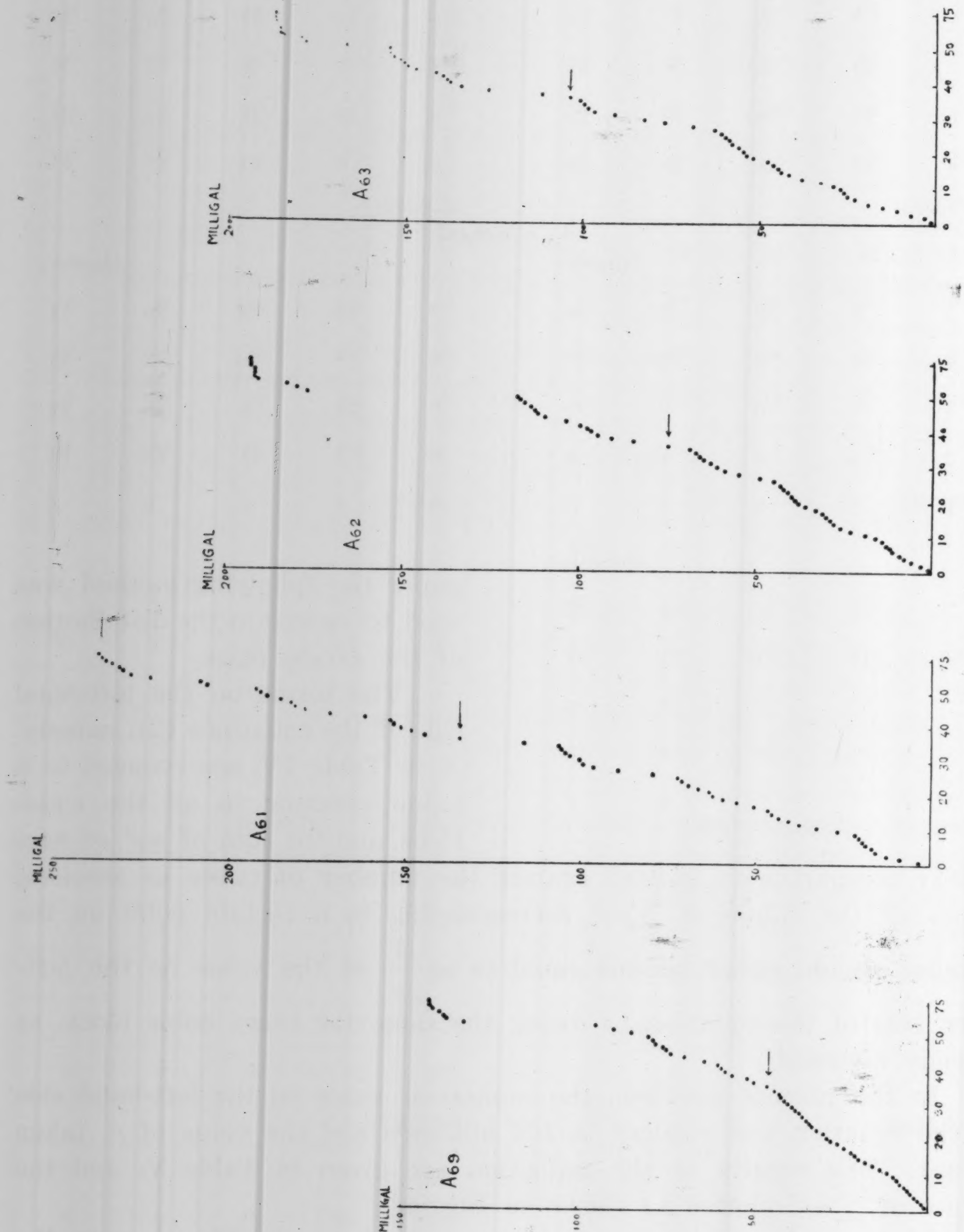

Fig. 4, 1.

this may show that there is no excess mass in the cubic block to cause any gravity anomaly on the surface of the earth.

It will be noticed that the sum of the $\alpha\rho'$ corresponding to cubes from No. 37 to No. 75 is almost the same in all the graphs. These

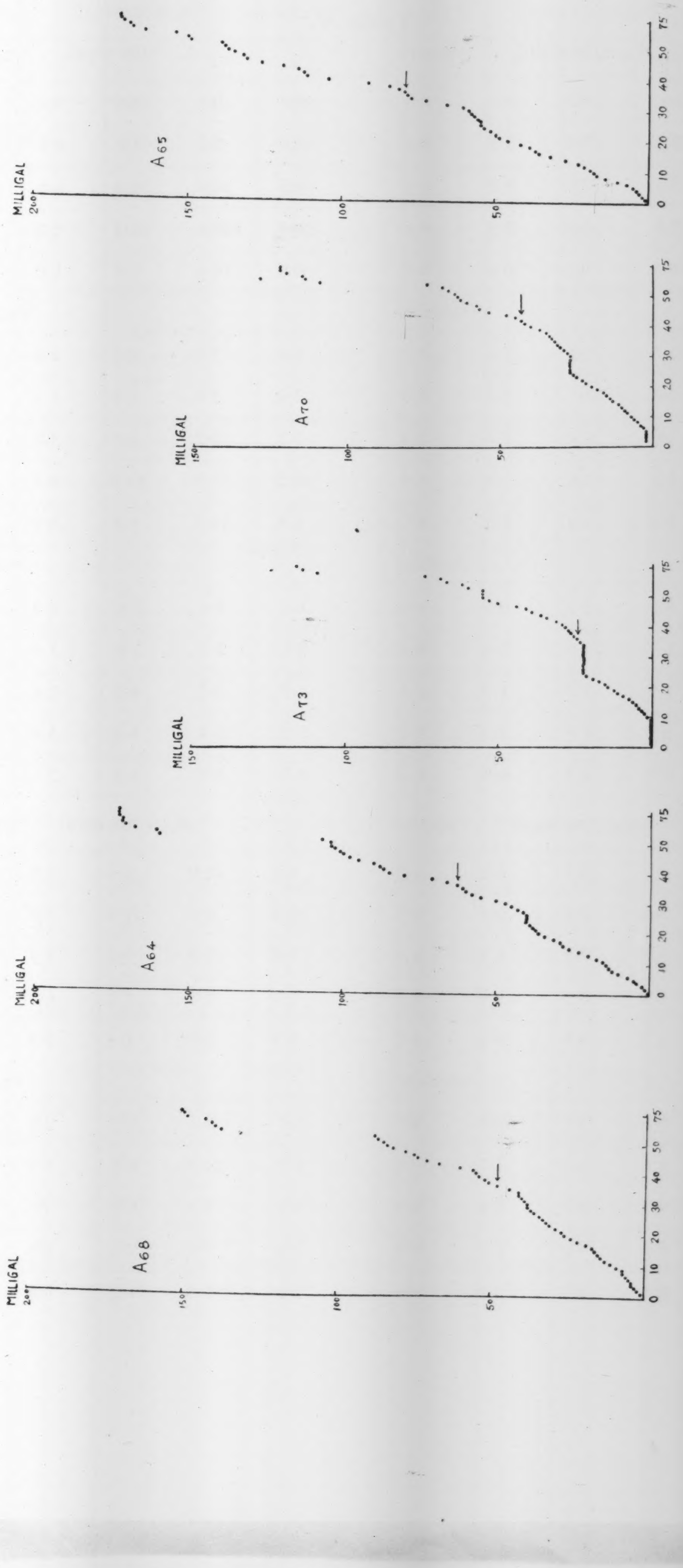

Fig. 4, 2.

Table V.

$A_{69}=100$ mgal (upper)

0·3	0·6	0·8	0·6	0·3
0·6	2·1	5·1	2·1	0·6
0·8	5·1	37·7	5·1	0·8
0·6	2·1	5·1	2·1	0·6
0·3	0·6	0·8	0·6	0·3

(middle)

0·6	1·1	1·4	1·1	0·6
1·1	2·4	3·6	2·4	1·1
1·4	3·6	6·4	3·6	1·4
1·1	2·4	3·6	2·4	1·1
0·6	1·1	1·4	1·1	0·6

(lower)

0·6	0·9	1·1	0·9	0·6
0·9	1·5	1·9	1·5	0·9
1·1	1·9	2·3	1·9	1·1
0·9	1·5	1·9	1·5	0·9
0·6	0·9	1·1	0·9	0·6

$A_{61}=100$ mgal (upper)

0·6	0·8	0·6	0·4	0·2
1·6	2·2	1·6	0·8	0·4
6·0	14·4	6·0	1·6	0·6
14·4	105·6	14·4	2·2	0·8
6·0	14·4	6·0	1·6	0·6

(middle)

1·4	1·6	1·4	1·0	0·6
3·0	3·8	3·0	1·8	1·0
6·8	10·2	6·8	3·0	1·4
10·2	17·8	10·2	3·8	1·6
6·8	10·2	6·8	3·0	1·4

(lower)

1·6	1·6	1·6	1·2	0·8
2·6	3·0	2·6	1·8	1·2
4·2	5·2	4·2	2·6	1·4
5·2	6·4	5·2	3·0	1·6
4·2	5·2	4·2	2·6	1·4

$A_{62}=100$ mgal (upper)

0·9	1·2	0·9	0·4	0·2
3·3	8·0	3·3	0·9	0·3
8·0	58·7	8·0	1·2	0·4
3·3	8·0	3·3	0·9	0·3
0·9	1·2	0·9	0·4	0·2

(middle)

1·7	2·1	1·7	1·0	0 6
3·8	5·7	3·8	1·7	0·8
5·7	9·9	5·7	2·1	0·9
3·8	5·7	3·8	1·7	0·8
1·7	2·1	1·7	1·0	0·6

$A_{63}=100$ mgal (upper)

5·0	12·0	5·0	1·3	0·5
12·0	8·8	12·0	1·8	0·7
5·0	12·0	5·0	1·3	0·5
1·3	1·8	1·3	0·7	0·3
0·5	0·7	0·5	0·3	0·2

(middle)

5·7	8·5	5·7	2·5	1·2
8·5	14·8	8·5	3·2	1·3
5·7	8·5	5·7	2·5	1·2
2·5	3·2	2·5	1·5	0·8
1·2	1·3	1·2	0·8	0·5

$A_{62}=100$ mgal (lower)

1·4	1·7	1·4	1·0	0·7
2·3	2·9	2·3	1·4	0·9
2·9	3·6	2·9	1·7	0·9
2·3	2·9	2·3	1·4	0·9
1·4	1·7	1·4	1·0	0·7

$A_{68}=100$ mgal (upper)

0·2	0·3	0·3	0·3	0·2
0·3	0·7	0·9	0·7	0·3
0·7	2·5	6·0	2·5	0·7
0·9	6·0	44·0	6·0	0·9
0·7	2·5	6·0	2·5	0·7

(middle)

0·4	0·6	0·7	0·6	0·4
0·8	1·3	1·6	1·3	0·8
1·3	2·8	4·3	2·8	1·3
1·6	4·3	7·4	4·3	1·6
1·3	2·8	4·3	2·8	1·3

(lower)

0·5	0·7	0·7	0·7	0·5
0·8	1·1	1·3	1·1	0·8
1·1	1·8	2·2	1·8	1·1
1·3	2·2	2·7	2·2	1·3
1·1	1·8	2·2	1·8	1·1

$A_{73}=100$ mgal (upper)

0·1	0·1	0·2	0·3	0·2
0·1	0·3	0·5	0·7	0·5
0·2	0·5	2·0	4·8	2.0
0·3	0·7	4·8	35·2	4·8
0·2	0·5	2·0	4·8	2·0

$A_{63}=100$ mgal (lower)

3·5	4·3	3·5	2·2	1·3
4·3	5·3	4·3	2·5	1·3
3·5	4·3	3·5	2·2	1·3
2·2	2·5	2·2	1·5	1·0
1·3	1·3	1·3	1·0	0·7

$A_{64}=100$ mgal (upper)

0·8	3·0	7·2	3·0	0·8
1·1	7·2	52·8	7·2	1·1
0·8	3·0	7·2	3·0	0·8
0·4	0·8	1·1	0·8	0·4
0·2	0·3	0·4	0·3	0·2

(middle)

1·5	3·4	5·1	3·4	1·5
1·9	5·1	8·9	5·1	1·9
1·5	3·4	5·1	3·4	1·5
0·9	1·5	1·9	1·5	0·9
0·5	0·7	0·8	0·7	0·5

(lower)

1·3	2·1	2·6	2·1	1·3
1·5	2·6	3·2	2·6	1·5
1·3	2·1	2·6	2·1	1·3
0·9	1·3	1·5	1·3	0·9
0·6	0·8	0·8	0·8	0·6

$A_{70}=100$ mgal (upper)

0·1	0·3	0·5	0·7	0·5
0·2	0·5	2·0	4·8	2·0
0·3	0·7	4·8	35·2	4·8
0·2	0·5	2·0	4·8	2·0
0·1	0·3	0·5	0·7	0·5

A_{73}=100 mgal (middle)

0·2	0·3	0·5	0·5	0·5
0·3	0·6	1·0	1·3	1·0
0·5	1·0	2·3	3·4	2·3
0·5	1·3	3·4	5·9	3·4
0·5	1·0	2·3	3·4	2·3

(lower)

0·3	0·4	0·5	0·5	0·5
0·4	0·6	0·9	1·0	0·9
0·5	0·9	1·4	1·7	1·4
0·5	1·0	1·7	2·1	1·7
0·5	0·9	1·4	1·7	1·4

A_{70}=100 mgal (middle)

0·3	0·6	1·0	1·3	1·0
0·5	1·0	2·3	3·4	2·3
0·5	1·3	3·4	5·9	3·4
0·5	1·0	2·3	3·4	2·3
0·3	0·6	1·0	1·3	1·0

(lower)

0·4	0·6	0·9	1·0	0·9
0·5	0·9	1·4	1·7	1·4
0·5	1·0	1·7	2·1	1·7
0·5	0·9	1·4	1·7	1·4
0·4	0·6	0·9	1·0	0·9

A_{65}=100 mgal

(upper)

0·4	1·1	4·3	10·3	4·3
0·6	1·6	10·3	75·4	10·3
0·4	1·1	4·3	10·3	4·3
0·3	0·6	1·1	1·6	1·1
0·1	0·3	0·4	0·6	0·4

(middle)

1·0	2·1	4·9	7·3	4·9
1·1	2·7	7·3	12·7	7·3
1·0	2·1	4·9	7·3	4·9
0·7	1·3	2·1	2·7	2·1
0·4	0·7	1·0	1·1	1·0

(lower)

1·1	1·9	3·0	3·7	3·0
1·1	2·1	3·7	4·6	3·7
1·1	1·9	3·0	3·7	3·0
0·9	1·3	1·9	2·1	1·9
0·6	0·9	1·1	1·1	1·1

cubes are numbered in Table VI, and the values of $\sum \alpha\rho'$ for points, summed over the interval corresponding to that mentioned above satisfy the respective equations fairly well as shown in Table VII.

Table VI.

		64		
	62	69	70	71
		68	73	74
			72	75

	38	39	40	41
	37	44	45	46
		43	48	49
		42	47	50

Table VII.

No. of cubes	Values of A in mgal		Differences
	Observed	Computed	
69	140	136	+ 4
61	50	51	− 1
62	90	105	−15
63	60	52	+ 8
68	120	125	− 5
64	100	110	−10
73	150	142	+ 8
70	150	137	+13
65	70	66	+ 4

As already mentioned, the value of ρ' was assumed to be 0·1. Since the equations are well satisfied with this value of ρ', this order of magnitude of the value of ρ' may be regarded as probable. The space which may be occupied by the excess mass obtained above is shown in Fig. 2, the boundary of which is drawn with thick lines. The width of the space occupied by the excess mass reaches 120 km and the depth at most 60 km.

Of course the distribution of the excess mass obtained above is only one of solutions obtained on the basis of the assumed uniform density. Actually, however, the density may be distributed irregularly, so that there may be several other ways in which the excess density in the earth's crust may be distributed, and which may satisfy the given mode in distribution of gravity anomaly. If, however, the deviations of the vertical computed by using the given mode of distribution of excess mass agree with the observed deviations, the distribution of the excess mass obtained above may become more likely.

DEVIATIONS OF THE VERTICALS IN IZU-OSIMA, COMPUTED AND OBSERVED.

The meridian and the prime vertical components of deviation of the vertical are given respectively by

$$\left.\begin{aligned}\xi&=\frac{1}{g}\frac{\partial}{\partial x}\delta w=\frac{k^2}{g}\int\frac{\rho' x}{r^3}dV\\ \eta&=\frac{1}{g}\frac{\partial}{\partial y}\delta w=\frac{k^2}{g}\int\frac{\rho' y}{r^3}dV\end{aligned}\right\}. \qquad (4)$$

The values of $\xi_{(G-A)}$ and $\eta_{(G-A)}$ due to the excess mass, the distribution of which has been given above, are shown in the following table together with the observed values.

	$\xi_{(G-A)}$			$\eta_{(G-A)}$		
	Computed	Observed	Difference	Computed	Observed	Difference
Habu	− 9·5″	−11·4″	+ 1·9″	−2·4″	−3·9″	+1·5″
Okada	−12·4	−28·6	+16·2	−4·0	+0·8	−4·8

The computed values of ξ's and η's given in the above table were integrated numerically in the same way as that used in computing the values of gravity anomalies given in Table II. Since the topographic correction is not likely to greatly affect the result, in determining the distribution of the excess mass in the earth's crust, this correction was not taken into consideration in reducing the observed gravity at Izu-Osima. But in discussing the deviation of the vertical at Izu-Osima, topographic correction may play an important part, for it is possible that the deviations of the vertical may be the result, chiefly, of the lateral force due to the attraction of the mass of the island, i.e., the mass of Mihara Volcano.

The topographic corrections for the deviations of the vertical due to the mass of Izu-Osima above sea level are computed by formulae (see Fig. 5)

$$\delta\varphi=\frac{k^2\rho d}{g}(\sin\alpha_{n+1}-\sin\alpha_n)\left\{ln\frac{a+r}{t}-1\right\}, \qquad (5a)$$

or

$$\delta\varphi=\frac{k^2\rho d}{g}(\sin\alpha_{n+1}-\sin\alpha_n)\left\{ln\frac{a_{m+1}+r_{m+1}}{a_m+r_m}\right\}, \qquad (5b)$$

the results being

	ξ	η
Habu	+7·5″	−5·1″
Okada	−7·2	+0·8

in which the mean density ρ of Izu-Osima is assumed to be 2·70. Applying this correction to the computed values of ξ's and η's, we have

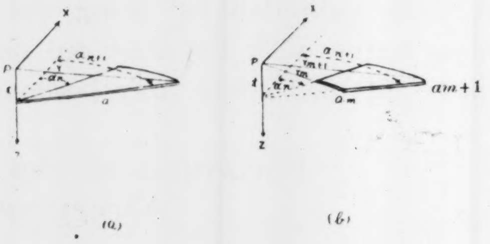

Fig. 5.

	$\xi_{(G-A)}$			$\eta_{(G-A)}$		
	Computed	Observed	Difference	Computed	Observed	Difference
Habu	− 2·0″	−11·4″	+9·4″	−7·5″	−3·9″	−3·6″
Okada	−19·6	−28·6	+9·0	−3·2	+0·8	−4·0

The meridian components of the deviations of the verticals computed differ by about 9″, and the prime vertical components by −4″. Many reasons could be invoked to explain the difference between the values computed and those observed, the most probable of which are

(i) The smallness of the width of the region under consideration.

(ii) The deviation of the vertical at the standard datum point at Tokyo.

(iii) The dimensions of the cubic blocks into which the earth's crust of the region under consideration were divided for convenience of calculation.

(iv) Unsuitableness of the formula for normal gravity in this region.

Cause (i) may be considered from a number of view points. For instance, the configuration of the isanomaly lines of gravity suggests that the excess mass may be present in that region which extends southward of the one under consideration. The fact that the computed gravity anomalies at points on the surfaces of cubic blocks No. 70 and 73 are smaller than those observed, suggest likewise.

As to cause (ii), it may be inferred that the deviations of the vertical at the standard datum point at Tokyo amounts to $-10{\cdot}0''$ in ξ and $6{\cdot}7''$ in η.[4]

The fact that the signs and approximate magnitudes of the value of (Obs.-Comp.) for Habu and Okada are equal in both ξ and η components, does not militate against the above inference.

We often hear that the distribution of g in Japan does not agree well with normal gravity. If we use another formula for normal gravity fitting well with the values of g in Japan,[5] the values of gravity anomalies will differ. The distribution of excess mass in the earth's crust, however, may not be much affected, seeing that it is determined from the distribution of gravity anomaly on the surface and from the configuration of the iso-Δg curves. The mode of distribution of Δg can not be greatly affected, even were the well fitting formula for the distribution of gravity in Japan used.

It may be worthy of note that, in drawing the isanomaly curves in the region under consideration, the value of gravity anomaly at Osima was not corrected. As a general rule, the value of gravity anomaly at a station in an oceanic island is very large, and this is the case with Osima. This fact is explained by considering the mass of the island to be the excess that is resting on the ocean bed, the last named consisting of sub-crustal rocks. So long as the ocean bed is considered to be in gravitational equilibrium, the excess mass of the island should cause an extraordinary anomaly in gravity in the region in the neighbourhood of Izu-Osima. As a matter of fact the value of gravity anomaly in Osima is very large, while on the ocean the value of gravity is also very large, it being of the same order as that of Osima. The large value of the gravity anomaly in oceanic islands was

---

4) Y. KAWAHATA, *Geopys. May.*, **10** (1936), 94.

5) C. TSUBOI, *Bull. Earthq. Res. Inst.*, **13** (1935), 554~557.

hitherto believed to be the effect of the excess mass of the island, but in the opinion of the writer, the large value of the gravity anomaly of the island of Osima is due not only to the excess mass of Mihara volcano alone, but is due largely to the effects of a still greater mass.

We also know that many earthquakes occur in the neighbourhood of this region, though not so frequently as in other regions of Japan. This may suggest that the earth's crust in this neighbourhood is not yet in (isostatic) equilibrium. From these facts, it is probable that the ocean bed in this neighbourhood is not in equilibrium, and that the mass of Osima is only an excess mass. This explains why, against usual practice, the value of gravity anomaly at Osima was not corrected.

SUMMARY

The result of the present study is summarized as follows:

The distribution of excess mass in the earth's crust in the region near Izu-Osima was determined by using the data of gravity anomalies on the surface of the earth.

In determining the distribution of the excess mass, we assumed, for convenience in calculation, that

(i) The earth's crust in the region under consideration is divided into 75 blocks or cubes; and that the excess mass that is responsible for the gravity anomalies on the surface of the earth is concentrated at the centre of each of such cubes.

(ii) The density of the excess mass ρ' was assumed to be 0·1 or zero.

After the distribution of excess mass was thus determined, the deviations of the verticals for the stations, Okada and Habu, were calculated, and the results compared with actual data, with satisfactory results.

It should be added, however, that the mode of distribution of the excess mass is not a unique solution.

5. 大島に於ける重力異常と鉛直線偏倚

陸地測量部　武藤勝彦

最近伊豆大島に於いて鉛直線偏倚を測つてみた結果.

波浮にて	南北成分 (G-A)	$-11{\cdot}4''$	東西成分 (G-A)	$-3{\cdot}9''$
岡田にて	〃	$-28{\cdot}6$	〃	$+0{\cdot}8$

なる値を得た. この程度の大いさの偏倚は特に重大視する程のものではないが, こゝに特異とすべき點は, 大島の北端岡田に於ても南端の波浮に於いても南北成分が共に符號が同一なる點である.

これは, 大島及びその南方海中に於ける重力異常の大なる事實と關聯してゐることと考へられる.

そこで, 大島を中心とする 150 km 平方の地域の地殼内に於ける過大質量分布の有樣をこの地域の地表面に於ける重力異常分布の狀況から決定することを試みた.

この問題は, 純數理的には解法を得ることが困難であるので, 數値計算法によることにした. それ故に求め得た一つの過大質量の分布樣式を決定し得たとしても, それが唯一解なりや否やを判定することは困難である.

筆者の採用した方法は次の如きものである. 問題の地域の地殼を若干個の正立方體部分に分け, その各立方體の中心に, その立方體内の過大質量が集中してゐるとし, 且つ, 少くとも立方體内では質量は一樣とする. その場合には一つの立方體の表面の中心點に於ける重力異常 Ap は,

$$Ap=\sum_i \alpha_{p.i}\rho_i$$

となる. こゝで更に ρ_i は一定の常數か 0 かであるとして, どれだけの立方體に過大質量があれば所與の重力異常分布を得るかを圖表計算的に求めたのである.

斯くして, 兎も角も, 求め得た結果は, 大體に於いて尤もらしいものである. 卽ちそれから計算される鉛直線偏倚と實測された鉛直線偏倚と比較しても大體合理的と解せられ, その他の諸種の事情環境とも排反しない.

6. *The Possibility of Determining the Geoid by means of Levelling.*

By Katuhiko MUTO,*

Military Land Survey.

(Read Oct. 19, 1937.—Received Dec. 20, 1937.)

1. We have two methods of determining the height of one triangulation point relative to another. While the relative height is measured by trigonometrical levelling, those of successive triangulation points are determined by measuring the zenith distances from one another. In the latter case, by correcting the deviation of the vertical for each point, the relative height thus determined will show the height referred to the ellipsoid. At the same time, the relative height can also be determined with spirit levels, the height thus obtained being that referred to the geoid.

The difference between the relative heights determined by these two methods is therefore the height of the geoid above the reference ellipsoid.

The reason the foregoing methods for determining the height of the geoid are considered impractical, is that the height of the geoid may be masked by the effects of atmospheric refraction.

The writer however found that these methods could be used for a certain place where the form of the geoid deviated markedly from the reference ellipsoid.

The writer's studies in these respects will now be described.

2. THE DIFFERENCE IN HEIGHT BETWEEN TWO TRIANGULATION POINTS DETERMINED BY TRIGONOMETRICAL LEVELLING, THE DEVIATION OF THE VERTICAL BEING TAKEN INTO CONSIDERATION[1].

To determine the relative height between triangulation points P_1 and P_2, the zenith distance of P_2, Z_{12}, from the zenith of P_1, and that of P_1, Z_{21}, from the zenith of P_2, are measured. When the two points P_1, P_2 are situated on different level surfaces above the reference ellipsoid, Z_{12} and Z_{21} are given by

---

* Comm. by N. MIYABE.

[1] F. R. HELMERT, *Höhere Geodäsie*, II, 574.

$$\left.\begin{aligned} Z_{12}&=Z'_{12}+\xi_1\cos a_{12}+\eta_1\sin a_{12}\\ Z_{21}&=Z'_{21}+\xi_2\cos a_{21}+\eta_2\sin a_{21},\end{aligned}\right\} \tag{1}$$

where

Z'_{12}, Z'_{21} = the observed values of the zenith distances, i. e., the zenith distances referred to the true vertical at each of the points, P_1 and P_2.

ξ_1, ξ_2 = the meridian components of the deviation of the vertical at P_1 and P_2 (Ast.—Geo.).

η_1, η_2 = the prime vertical components of the deviation of the vertical at P_1 and P_2 (Ast.—Geo.).

a_{12}, a_{21} = the azimuths of the sight lines $\overrightarrow{P_1\ P_2}$, $\overrightarrow{P_2\ P_1}$ referred to N.

When the triangulation points P_1, P_2 are sighted, the one from the other, the relative height h between P_1 and P_2 on the reference ellipsoid is given in terms of the observed zenith distances in the form

$$h=\mathfrak{H}_2-\mathfrak{H}_1=S_m\tan\frac{Z_{21}-Z_{12}}{2}+\frac{k_2-k_1}{4}\frac{S_m^2}{\rho_{12}}\sec^2\frac{Z_{21}-Z_{12}}{2}. \tag{2}$$

In the above formula (2),

$\mathfrak{H}_1$, $\mathfrak{H}_2$ = the heights of the triangulation points P_1, P_2 above the reference ellipsoid,

S_m $=S_0\left(1+\dfrac{\mathfrak{H}_1+\mathfrak{H}_2}{2\rho_{12}}\right)$, where S_0 is the horizontal distance between P_1 and P_2 measured on the surface of the reference ellipsoid.

ρ_{12} = the radius of curvature of the arc $\overset{\frown}{P_1\ P_2}$, the arc of the geodetic line on the reference ellipsoid joining the points at which the straight lines passing through P_1, P_2 normally intersect the surface of the ellipsoid.

k_1, k_2 = the coefficients of atmospheric refraction for the sight lines $\overrightarrow{P_1\ P_2}$ and $\overrightarrow{P_2\ P_1}$, which, for simplicity, are assumed to be equal, that is,

$$k_1=k_2,$$

whence we have from equation (2),

$$h=S_m\tan\frac{Z_{21}-Z_{12}}{2}, \tag{3}$$

$$\mathfrak{H}_2=\mathfrak{H}_1+S_m\tan\frac{Z_{21}-Z_{12}}{2}. \tag{4}$$

The height determined with the aid of equation (4) is that referred to the reference ellipsoid. Since the height measured by spirit levels is that referred to the geoid, by subtracting the height of the same triangulation point measured with spirit levels from the height thus determined, we get the height of the geoid above the reference ellipsoid.

Let N be the height of the geoid above the reference ellipsoid, and H the height of the triangulation point under consideration above the geoid, we then have

$$N=\mathfrak{H}-H. \tag{5}$$

3. THE RELATIVE HEIGHT MEASURED BY TRIGONOMETRICAL LEVELLING WITHOUT THE DEVIATION OF THE VERTICAL BEING TAKEN INTO CONSIDERATION[2].

If, in equation (1), the deviation of the vertical is excluded, the equation (3) becomes

$$h=S_m \tan\frac{Z'_{21}-Z'_{12}}{2}. \tag{6}$$

The relative height determined with equation (6) is that referred to the reference ellipsoid. The relative height determined by using the data of another pair of triangulation points is the relative height referred to another ellipsoid, although the orientation of the last-named differs

If, in such a case $\overrightarrow{P_1\ P_2}$ be denoted by S, the difference between the relative height referred to the ellipsoid and that referred to the geoid is given by

$$-\int\frac{\Lambda''}{\rho''}dS, \tag{7}$$

where Λ is the deviation of the vertical, the angle between the tangent of the level surface and that of the ellipsoid being measured counterclockwise with reference to the direction of the tangent of the level surface.

As to the pair of triangulation points for which the relative height is measured, we have

$$\Lambda_1+\Lambda_2=0. \tag{8}$$

If Λ is a linear function of S, as given by $\Lambda=\lambda+\lambda' S$, within the region between P_1 an P_2, the value of (7) becomes 0. Should, however, Λ be a function of S of a higher order, it usually does not become 0. For example, if Λ is $\lambda+\lambda'S+\lambda''S^2$, the result of integral (7) is $\frac{1}{6}\frac{\lambda''}{\rho''}S^3$.

---

[2] F. R. HELMERT, *Höhere Geodäsie*, II, 607.

In trigonometrical levelling of the Military Land Survey, the length of the sight line is about 4 km. For such a short distance the variation in Λ may be assumed to be a linear function of S, approximately, whence the integral

$$-\int\frac{\Lambda''}{\rho''}dS=h-(H_2-H_1)$$

may consequently be 0, i. e., the height measured by trigonometrical levelling excluding the deviation of the vertical, may be regarded as being equal to that measured by spirit levels, provided the distance between the triangulation points is sufficiently short.

4. NUMERICAL EXAMPLE.

In the trigomometrical levellings of the Military Land Survey, the height of the triangulation point is determined with reference to the height of a certain bench-mark on the precise level route, that part of the survey connecting the triangulation point with the bench-mark on the precise level route being carried out by means of second order levels. The heights of the surrounding triangulation points are then determined by means of equation (6).

Heights of triangulation points over wide areas are determined not only by trigonometrical levelling, but also by spirit levels.

The writer at first tried to determine the relative height between two triangulation points separated by a long distance, by using data already obtained by trigonometrical levelling.

Fig. 1 shows the distribution of triangulation points between Mitaka, west of Tokyo, and Hatukari-mura, about 30 km east of Kôhu. Table I gives the zenith distances Z_{12}, Z_{21}, the meridian and prime vertical components of the deviations of the verticals ξ, η, the direct azimuth of the sight line a, and the distances between successive points, in which the values of Z are those observed, while the values of ξ, η, and a have been estimated from Figs, 1, 2, 3. The relative height between these two triangulation points was determined by using the data of relative heights for successive triangulation points distributed between these two points, that were obtained by trigonometrical levelling.

In Table II, the numerals in column I are the heights determined with equation (3), for which the values of the deviation of the vertical were estimated from their geographical distribution as shown in

Figs. 2, 3 as mentioned above. The numerical values in column II are the heights determined with equation (6). As standard datum for the heights given in columns I, II, in Table II, the height of the point at Mitaka, which was obtained by second order levelling, was taken. The heights given in columns I, II are those determined by means of trigonometrical levelling with reference to the height of the triangulation point at Mitaka. The values of the height given in column III comprise several (marked *) that were determined by spirit levels, the others having been determined by trigonometrical levelling with reference to certain points whose heights are known.

The differences (I–III) are $N = \mathfrak{H} - H$, namely, the heights of the geoid above the reference ellipsoid; while the differences (II–III) are errors that may arise from observations, deviations from the assumption $k_1 = k_2$, etc.

The amount of error permitted in trigonometrical levelling by the Military Land Survey is so small that the discordance between the heights of a certain triangulation point determind by trigonometrical levelling from two other points should not exceed 20 cm. Seeing that the error here falls short of the said limit, the results of trigonometrical levelling for the triangulation points under consideration may be taken as being fairly precise.

Heretofore, the effect of atmospheric refraction was believed to be so

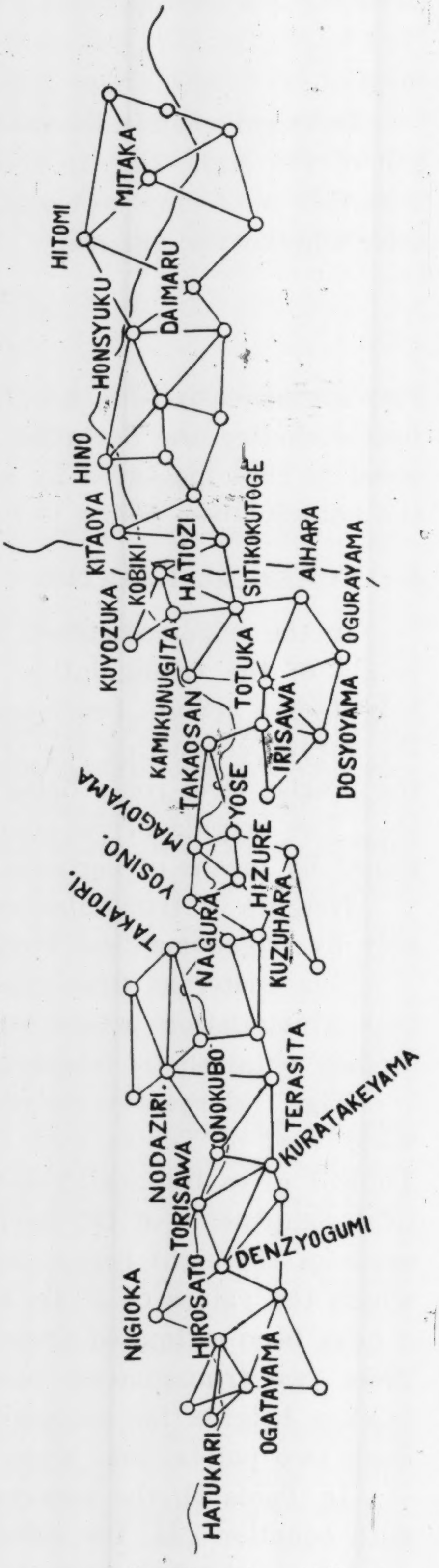
HITOMI
MITAKA
HONSYUKU
DAIMARU
HINO
KITAOYA
KOBIKI
HATIOZI
SITIKOKUTOGE
AIHARA
OGURAYAMA
KUYOZUKA
KAMIKUNUGITA
TOTUKA
DOSYOYAMA
IRISAWA
TAKAOSAN
YOSE
MAGOYAMA
YOSINO.
TAKATORI.
NAGURA
HIZURE
KUZUHARA
TERASITA
KURATAKEYAMA
NODAZIRI.
ONOKUBO
TORISAWA
DENZYOGUMI
NIGIOKA
HIROSATO
OGATAYAMA
HATUKARI

Fig. 4

TABLE I.

	Z_{12}			Z_{21}			ξ_{a-g}	η_{a-g}	α_{12}	log s
	°	′	″	°	′	″	″	″	°	
Mitaka	89	38	31	90	23	49	+0·4	+ 5·9	312	3,56254
Hitomi	89	28	52	90	33	43	+1·0	+ 4·0	110	3,64486
Daimaru	90	53	25	89	9	27	+1·5	+ 6·4	319	3,61428
Honsyuku	89	43	31	90	19	16	+2·2	+ 4·8	278	3,78317
Hino	89	34	55	90	26	44	+5·3	+ 4·0	255	3,51775
Kitaoya	89	28	40	90	32	57	+6·9	+ 4·0	218	3,49427
Kobiki	89	7	31	90	54	25	+7·4	+ 5·6	201	3,61440
Sitikokutoge	90	46	41	89	14	56	+7·7	+ 8·8	351	3,54323
Hatiozi	89	42	11	90	18	59	+8·0	+ 5·6	318	3,37492
Kuyozuka	88	8	39	91	52	55	+8·3	+ 4·0	205	3,50712
Kamikunugita	89	5	31	90	56	17	+8·1	+ 5·6	180	3,55294
Totuka	92	35	10	87	27	10	+7·8	+ 8·8	110	3,65909
Aiharamura	87	3	45	92	57	49	+7·2	+11·2	233	3,54364
Ogurayama	89	23	57	90	37	47	+7·3	+12·0	280	3,60504
Dosyoyama	87	55	1	92	6	21	+7·1	+10·4	9	3,45574
Irisawa	87	15	9	92	46	5	+7·5	+ 8·8	335	3,42958
Takaosan	92	38	16	87	23	50	+7·8	+ 6·0	250	3,63741
Yose	86	2	31	93	58	18	+7·0	+ 6·4	330	3,29564
Magoyama	93	35	29	86	25	33	+7·0	+ 4·8	212	3,42976
Hizuremura	87	20	38	92	40	42	+6·3	+ 6·4	335	3,45041
Yosinoeki	91	51	14	88	10	25	+6·8	+ 4·0	207	3,59758
Kuzuharamura	91	40	10	88	20	49	+6·3	+ 5·6	354	3,15776
Naguramura	87	11	54	92	49	34	+6·4	+ 4·8	350	3,44002
Takatoriyama	90	42	46	89	20	11	+6·6	+ 3·2	270	3,76294
Nodazirieki	84	50	50	95	11	37	+6·0	+ 2·4	189	3,70337
Terasitamura	94	17	43	85	44	41	+5·4	+ 4·8	302	3,65454
Onokubomura	80	11	15	99	50	24	+5·4	+ 3·2	190	3,43099
Kuratakeyama	98	21	3	81	40	53	+5·0	+ 4·0	328	3,58834
Torisawa	85	18	6	94	43	22	+5·1	+ 1·6	248	3,48503
Denzyogumi	89	25	43	90	35	56	+4·9	+ 1·6	319	3,58882
Nigiokamura	86	23	20	93	38	0	+5·0	+ 0·8	196	3,50128
Hirosatomura	80	21	10	99	40	16	+4·5	+ 0·8	240	3,43454
Ogatayama	99	53	19	80	7	52	+4·2	+ 0·8	315	3,39324
Hatukarimura							+4·2	+ 0·0		

great that it would practically be impossible[3] to determine the form of the geoid from levellings, but from data obtained by means of trigonometrical and spirit levels, the effect from this cause does not seem to be so serious as to prevent determination of the height of the geoi-

---

[3] F. R. HELMERT, *Höhere Geodäsie*, I, 521; II, 552.

TABLE II.

	I m	II m	III m	I-III m	II-III m
Mitaka	70·39 + 24·12	70·39	70·39*	0·00	0·00
Hitomi	94·51 + 41·56	94·42	94·42	+0·09	0·00
Daimaru	136·07 − 61·56	136·19	136·34	−0·27	−0·15
Honsyuku	74·51 + 31·66	74·56	74·73	−0·22	−0·17
Hino	106·17 + 24·92	106·10	106·41*	−0·24	−0·31
Kitaoya	131·09 + 29·31	131·00	131·09*	0·00	−0·09
Kobiki	160·40 + 64·19	160·32	160·27*	+0·13	+0·05
Sitikokutoge	224·59 − 46·72	224·21	224·24	+0·35	−0·03
Hatiozi	177·87 + 12·66	177·61	177·64	+0·23	−0·03
Kuyozuka	190·53 +105·51	190·32	190·24	+0·29	+0·08
Kamikunugita	296·04 + 57·42	295·15	295·18	+0·86	−0·03
Totuka	353·46 −204·64	352·74	352·72	+0·74	+0·02
Aiharamura	148·82 +180·48	148·28	148·28	+0·54	0·00
Ogurayama	329·30 + 43·47	328·50	328·44	+0·86	+0·06
Dosyoyama	372·77 +104·34	371·71	371·66	+1·11	+0·05
Irisawa	477·11 +129·49	476·15	476·10*	+1·01	+0·05
Takaosan	606·60 −198·41	605·68	605·66	+0·94	+0·02
Yose	408·19 +136·89	407·08	407·09*	+1·10	−0·01
Magoyama	545·08 −168.36	544·01	544·00	+1·08	+0·01
Hizuremura	376·78 +131·37	375·56	375·57	+1·21	−0·01
Yosinoeki	508·15 −126·94	507·02	507·01	+1·16	+0·01
Kuzuharamura	381·21 − 41·75	379·80	379·80	+1·41	0·00
Naguramura	339·46 +135·31	338·09	338·24	+1·22	−0·13

(to be continued.)

TABLE II. (*continued.*)

	I m	II m	III m	I-III m	II-III m
Takatoriyama	474·77 − 69·52	473·48	473·54	+1·23	−0·06
Nodazirieki	405·25 +457·49	403·85	403·94*	+1·31	−0·09
Terasitamura	862·74 −337·52	861·20	861·34	+1·40	−0·14
Onokubomura	525·31 +467·37	523·83	523·96*	+1·35	−0·13
Kuratakeyama	992·68 −568·76	991·10	991·18	+1·50	−0·08
Torisawa	423·92 +251·83	423·23	423·29	+0·64	−0·06
Denzyogumi	675·75 + 39·57	674·98	675·08	+0·67	−0·10
Nigiokamura	715·32 −201·21	714·56	714·71	+0·61	−0·15
Hirosatomura	514·11 +463·00	513·82	514·00*	+0·11	−0·18
Ogatayama	977·11 −430·81	976·66	976·93	+0·18	−0·27
Hatukarimura	546·30	546·01	546·22*	+0·08	−0·21

Heights given in this Table are those of the centre of the vertical circle of the theodolite at the stations.

The numerals with signs in column I denote the relative heights between the successive points.

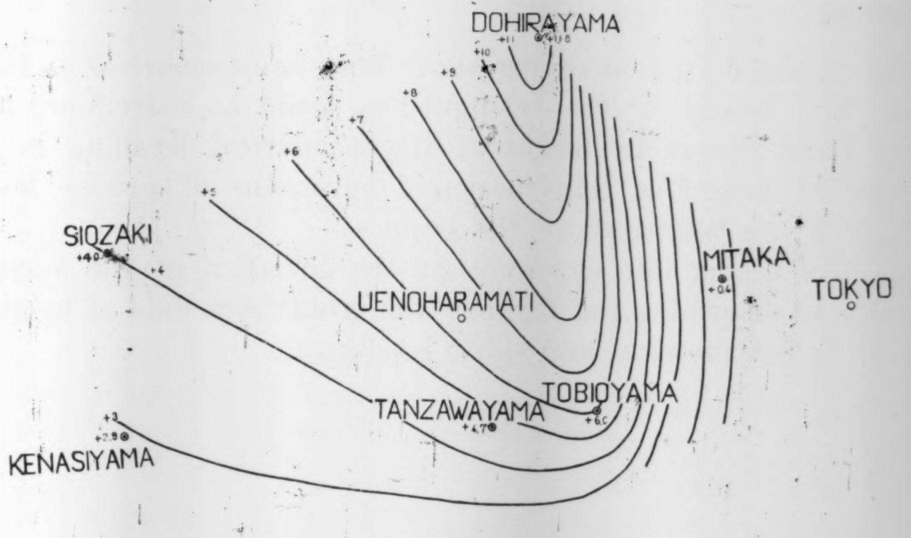
DOHIRAYAMA
+11
+11.8
+10
+9
+8
+7
+6
+5
SIOZAKI
+4.0
+4
UENOHARAMATI
MITAKA
+0.4
TOKYO
TOBIOYAMA
+6.0
TANZAWAYAMA
+4.7
+3
+2.9
KENASIYAMA

Fig. 2. Distribution of ξ.

dal surface above the surface of the reference ellipsoid. In fact, the result of III–I in Table I (see Fig. 4), agree well with the relative height of the geoidal surface in the region under consideration as obtained by Y. Kawahata[4], which were computed from astro-geodetic data.

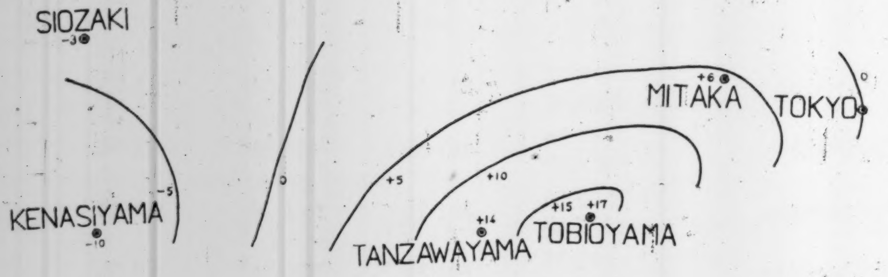

Fig. 3. Distribution of η.

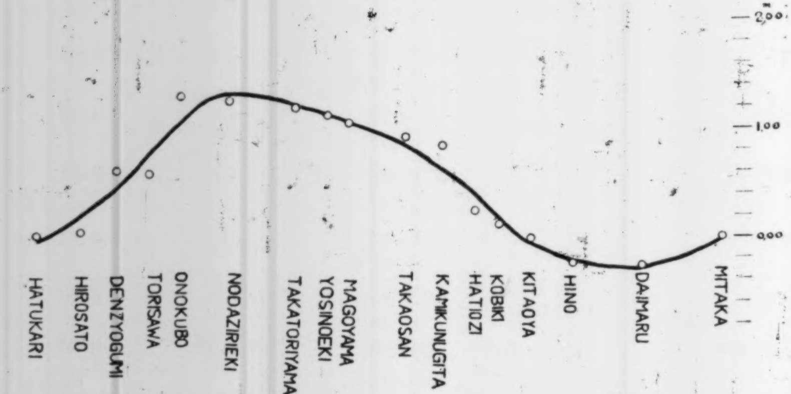

Fig. 4. Profile of Geoid.

5. RESUME.

The results of the foregoing study may be summarized as follows:

(i) The height of the triangulation point as determined by the Military Land Survey by means of trigonometrical levelling is of the same kind of height as that measured by means of precise levelling, that is, it is the height above the geoid.

(ii) By taking into consideration the deviation of the vertical, it is possible to determine the form of the geoid from data of heights obtained by trigonometrical and spirit levellings.

---

[4] Y. KAWAHATA, *Bull. Earthq. Res. Inst.*, **13** (1935), 78.

6. 水準測量によるヂオイドの形の決定に就て

陸地測量部 武藤勝彦

直接水準測量及び三角術的間接水準測量結果を比較して，基準楕圓體上ヂオイドの高さを決定し得る事は既に知られてゐるが，實際には視準時に於ける空氣中の光の屈折の影響が不明であるが爲に，かゝる方法によつてヂオイドの形を決定せんとする試みは未だ無いやうである．

筆者は，測量部の觀測値に就き，兩水準測量の結果を比較して見た處，視準線の長さが4km程度で天頂距離が兩點より相互に覘視されてゐる場合には，屈折系數 $k_1=k_2$ として，充分ヂオイドの高さを推算し得る見込のあることを知つた．この場合各點に於ける鉛直線偏倚は挿入法により求めた．

また測量部の間接水準測量による高さは，直接水準測量結果即ちヂオイド面からの高さと見倣して差支へない事が分つた．

7. *Studies in Fluctuations in the Heights of Yearly Mean Sea-levels.*

By Katuhiko MUTO and Naomi MIYABE,

Earthquake Research Institute.

(Read Nov. 16, 1937.—Received Dec. 20, 1937).

1. INTRODUCTION. Usually, the mean sea-level for a sufficiently long period at a mareograph station is taken as the standard datum of the height of land. The height of the sea-level, which is measured with reference to a rigidly fixed point on the land, varies secularly and periodically with time. The factors that cause the changes in the height of the sea-level are (i) astronomical disturbances, (ii) meteorological disturbances, and (iii) land deformations.

These factors that cause changes in the height of sea-level, especially, the astronomical and meteorological disturbances, are mostly periodic, i. e., the astronomical disturbances vary mostly with diurnal, semidiurnal, and fortnightly periods, and the meteorological disturbances with an approximate annual period. The effects of these regularly varying disturbances can therefore be eliminated by taking the yearly mean value of the sea-level.

The changes in the height of the yearly mean sea-level are therefore usually regarded as indicating the secular variation in the height of the land, i. e., crustal deformations.

From actual data, however, the yearly mean sea-level varies rather irregularly, so that it cannot be regarded as being due merely to upheaval and subsidence of the earth's crust.

On the other hand, astronomical disturbances of longer periods which may cause changes in the height of the yearly mean sea-level, for instance, those with periods of 9 years and 18·6 years, cannot be regarded as varying uniformly throughout the whole period; in other words, although the disturbing force due to astronomical bodies become equal after the lapse of 9 or 18.6 years, the variations in these disturbing forces cannot be expressed by simple sinusoidal functions of time. The same may also be said of meteorological disturbances; cyclones and other meteorological factors that affect the sea-level vary quite irregularly with time.1)

---

1) T. TERADA and S. YAMAGUTI, *Bull. Imp, Earthq. Inv. Comm.*, **9** (1928), 113.

Thus the yearly mean sea-level is disturbed in a marked manner by irregularly varying disturbances, so that these irregular variations in the height of the yearly mean sea-level cannot be attributed merely to crustal deformations.

In the present study, irregular variation in the heights of the yearly mean sea-level is believed to be due to irregular disturbances, both astronomical and meteorological. The effect of these irregular disturbance can be reduced by taking overlapping mean values over a number of years.

Of course, the crustal deformation may not only be chronic, but also acute, i. e., there may be quasi-periodic rise and subsidence of a part of the earth's crust with shorter periods, namely, periods of several years. Such fluctuations in land deformation cannot be separated from the irregular variations due to astronomical and meteorological disturbances. They can be discussed only when some accessory evidences are at hand, as will be dealt with later.

2. **Data of Yearly Mean Sea-Level.** This paper deals with data of the yearly mean sea-level for the following stations, for the periods mentioned below.

	Stations	Time intervals
(i)	Hosozima, Japan	1900∼1936[2]
(ii)	Frederikshavn, Denmark	1893∼1931[3]
(iii)	Fort Hamilton, New York, U. S. A.	1893∼1932[4]
(iv)	San Francisco, U. S. A.	1898∼1935[4]
(v)	Seattle, U. S. A.	1899∼1935[4]

Hosozima is in Kyûsyû, Japan, on the Pacific coast. The general course of the curve representing variations in the height of yearly mean sea-level at this station may be expressed approximately by

$$H_t = a + bt + ct^2,$$

where t is the number of years since 1900. The constants a, b, c in the above expression are determined by the method of least squares, and the deviations in actual height, H_a, from the calculated one, H_t, are obtained by

$$H_a - H_t = H_a - \{-35\cdot0 - 42\cdot3t - 9\cdot4t^2\} \quad \text{(mm)}.$$

Fredrikshavn is in Denmark. Egedar, in his paper,[3] gives the

---

2) Reports issued by the Military Land Survey.

3) J. Egedar, "*On the Determination of the normal height of the sea-level round the Danish coasts*", Copenhagen, 1933.

4) W. Bowie. *Spec. Publ. Coast and Geodetic Survey, U. S. A.* No. 207 (1936).

fluctuations in the heights of the yearly mean sea-levels for several other stations. As the curves of fluctuations in the heights of the yearly mean sea-levels of various stations in Denmark are very similar to one another, we take, for example, the data of Frederikshavn. These fluctuations are deviations from D. N. N. given in mm. The variation in the yearly mean sea-level at Frederikshavn may be given approximately by

$$H_t = a + bt.$$

In cases like the foregoing, in which the variation in the yearly mean sea-level can as a rule be expressed by a linear function of time, the constants can be determined by using the overlapping mean values, because this process does not affect the value of the constants a and b. The constants a and b thus determined are 2·5 mm and $-0{\cdot}16$ mm year respectively for Frederikshavn.

Similarly, for the secular variations in the heights of the yearly mean sea-levels at Fort Hamilton and San Francisco, the linear functions of t are

For Fort Hamilton $H_t = -7{\cdot}0 + 0{\cdot}4\,t$ (1/100 foot)
For San Francisco $H_t = -3{\cdot}5 + 0{\cdot}2\,t$ (1/100 foot)

As to the yearly mean sea-level of Seattle, no such secular variation as could be represented by a linear function of time is noticable.[5]

In determining therefore the constants a, b, etc. of the expressions for the secular variations in the yearly mean sea-level, we find that the values of b in the expressions for Japanese stations is much greater than those for European and American stations, which may be an indication that the crustal deformation is more marked in Japan than in Europe and America. We shall deal with this matter in a future paper.

3. FLUCTUATIONS IN HEIGHT OF THE YEARLY MEAN SEA-LEVEL. After the terms of the secular variations referred in the preceding paragraph have been eliminated, the residuals are treated statistically.

The fluctuations in the heights of the yearly mean sea-levels of the various stations cited above are shown in Figs. 1∼5. The curves in these figures will show that the yearly mean sea-levels appear to vary with periods amounting to several years. The mean period of the apparent periodic variation of the yearly mean sea-levels can be calculated by dividing the whole time interval, for which the yearly mean sea-levels are obtained, by the number of peaks in the respective

---

[5] The Data of fluctuations in the heights of the yearly mean sea-levels at various stations are given in a table in the appendix.

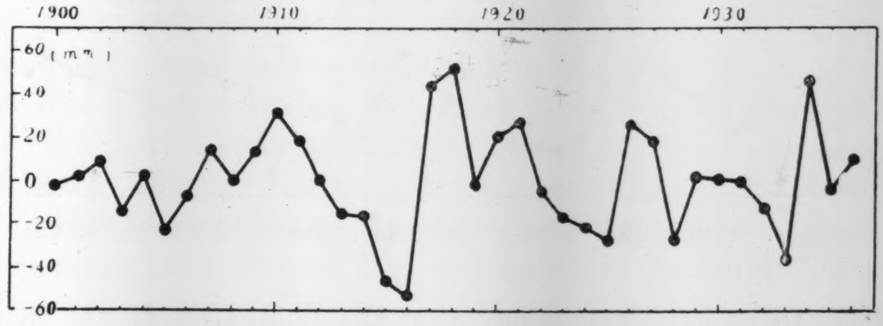

Fig. 1. Fluctuation in heights of yearly mean sea-level at Hosozima.

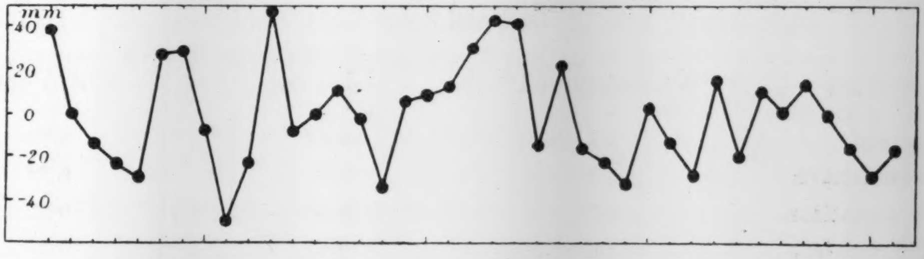

Fig. 2. Fluctuation in heights of yearly mean sea-level at Frederikshavn (Denmark).

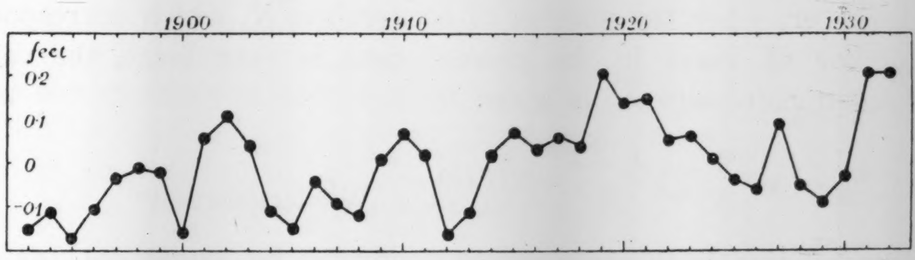

Fig. 3. Fluctuation in heights of yearly mean sea-level at Fort Hamilton (U. S. A.).

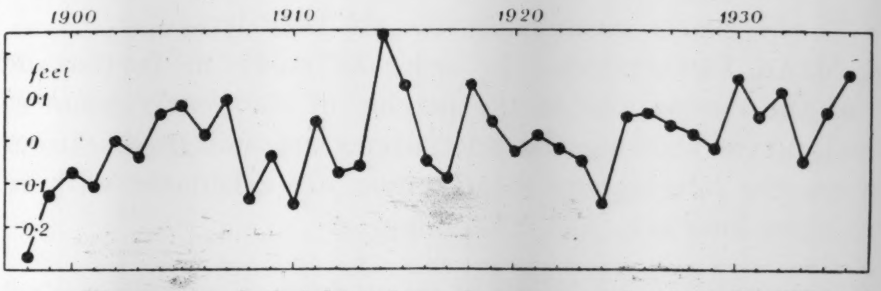

Fig. 4. Fluctuation in heights of yearly mean sea-level at San Francisco (U. S. A.).

curves. The results give the values of „Wiederkehrzeit".(6) The mean

---

6) Fürth. „*Schwankungserscheinungen in der Physik*". Leipzig, 1923.

periods thus calculated range, as shown in Table I, from 3 to 4, which is probably to be expected, seeing that the fluctuation in the heights of the yearly mean sea-levels is very irregular.[7]

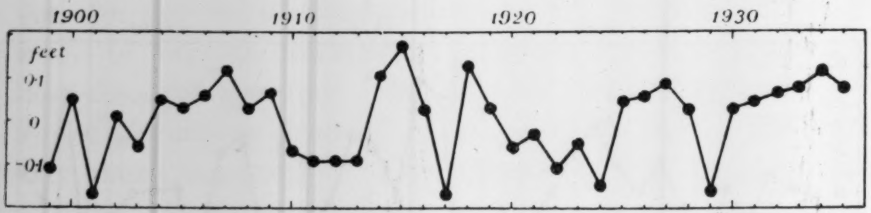

Fig. 5. Fluctuation in height of yearly mean sea-level at Seattle (U. S. A.).

TABLE I.

Station	"Wiederkehrzeit"	($\overline{\|\delta\|}$) cal	($\overline{\|\delta\|}$) obs
Hosozima	3·7	0·54	0·99
Frederikshavn	4·3	0·47	0·39
Fort Hamilton	3·7	0·54	0·52
San Francisco	3·0	0·67	0·37
Seattle	3·4	0·59	0·68

Moreover, when the number of occurrences N, which corresponds to the number of years in the present case, is very large, the value of „Schwankungsgrösse" $\overline{|\delta|}$ is given by

$$\overline{|\delta|} = \frac{1}{N} \sum \frac{\Delta_n - \overline{\Delta}}{\overline{\Delta}} = 2W(\delta) = \frac{2}{\text{„Wiederkehrzeit"}}.^{8)}$$

This relation is to some extent confirmed by actual data, as shown in Table I.

These facts agree with the conclusion that the fluctuations in the heights of the yearly mean sea-levels are very irregular.

4. ON MEAN DEVIATIONS. In order to study in further detail the nature of the fluctuations in the heights of the yearly mean sea-levels, the actual curves showing the fluctuations are smoothed. In smoothing the curves, the overlapping mean values are calculated with respect to different time intervals, i. e., the values of

---

7) The fluctuation in the heights of the yearly mean sea-levels may not be „Schwankungen mit Nachwirkung". The causes of the fluctuations, such as the number of cyclones per year, may be quite fortuitous.

8) In calculating „Schwankungsgrösse" from actual data, the deviations Δ_n are measured from the least value of the height of the yearly mean sea-level. The symbol $\overline{\Delta}$ designates the mean value of Δ_n.

$$\eta_i = \frac{\xi_{i-m}+\xi_{i-m+1}+\cdots+\xi_i+\xi_{i+1}+\cdots\cdots+\xi_{i+m}}{2m+1} \qquad \cdots\cdots\cdots\cdots(1)$$

are calculated, where ξ's are the amounts of deviations of the heights of the yearly mean sea-levels. The values of η_is are calculated for cases of $2m+1=3$, 4, 5, 6, 7, 8, 9 and 10.

For each smoothed curve, the mean deviation, i. e., the value of $|\overline{\eta}|$ are calculated and plotted against τ,[9] the time interval over which the overlapping mean values are calculated in smoothing the actual fluctuations, as shown in Figs. 8~12. As will be seen in these figures, the values of $|\overline{\eta}|$ decrease with increasing τ, which fact may be understood by studying the nature of the mean deviation.

Firstly, we consider the case in which the fluctuation ξ is given by the sum of the periodic functions, i. e..

$$\xi = \sum a_n \sin(nt+q_n)$$

Then the value of η is given by

$$\eta = \frac{1}{\tau}\int_{t-\frac{\tau}{2}}^{t+\frac{\tau}{2}} \sum a_n \sin(nt+q_n)\,dt.$$

Taking one of the components of η, we have

$$\eta_n = \frac{1}{\tau}\int_{t-\frac{\tau}{2}}^{t+\frac{\tau}{2}} a_n \sin(nt+q_n)\,dt.$$

$$= a_n \frac{\sin n\frac{\tau}{2}}{n\frac{\tau}{2}} \sin(nt+q_n)$$

Hence, the mean deviation is given by

$$|\overline{\eta_n}| = \frac{2}{\pi} a_n \left| \frac{\sin n\frac{\tau}{2}}{n\frac{\tau}{2}} \right| (\cos q_n - \sin q_n).$$

If we could put $q_n=0$,

---

[9] The time interval τ corresponds to $(2m+1)$ in equation (1).

$$|\eta_n| = \frac{2}{\pi} a_n \left| \frac{\sin n\frac{\tau}{2}}{n\frac{\tau}{2}} \right| .$$

If however the value of η consists of several components of periodic terms with different periods, it may be more convenient for the present discussion to take the standard deviations, i. e.,

$$\sqrt{\overline{\eta^2}} = \frac{1}{2} \sqrt{\sum a_n^2 \frac{1}{n} \left(\frac{\sin\frac{n\tau}{2}}{\frac{n\tau}{2}} \right)^2 }.$$

In Fig. 6, the variations in the values of $\left(\frac{\sin\frac{n\tau}{2}}{\frac{n\tau}{2}} \right)$ are plotted against $n\tau$ or $\frac{\tau}{T_n}$ where $n = \frac{2\pi}{T_n}$, from which it may be anticipated

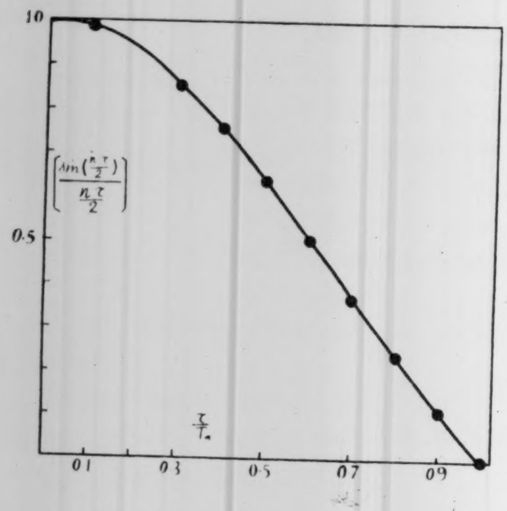

Fig. 6. Values of $\frac{\sin\frac{n\tau}{2}}{\frac{n\tau}{2}}$ plotted against $n\tau$, or $\frac{\tau}{T_n}$

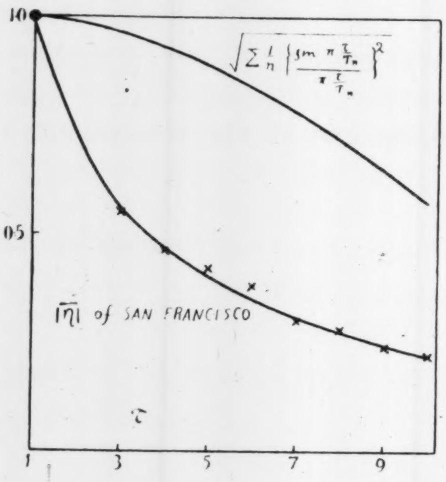

Fig. 7. The values of $\sqrt{\sum\frac{1}{n}\left\{\frac{\sin\frac{\pi\tau}{T_n}}{\frac{\pi\tau}{T_n}}\right\}^2}$ is compared with actual value of $|\eta|$ of San Francisco.

that the variation in $|\eta_n|$ with respect to $n\tau$ or $\frac{\tau}{T_n}$ cannot agree with the actual variation of $|\eta|$ with respect to τ. In Fig. 7, the curve of variation of an actual $|\eta|$ is compared with that of

$\sqrt{\frac{1}{n}\left(\frac{\sin\frac{n\tau}{2}}{\frac{n\tau}{2}}\right)^2}$, T_n being 12, 15, and 18 years, where $T_n = 2\frac{\pi}{n}$.

This discordance between the actual and the calculated mean deviations, based on the assumption that $\xi = \sum a_n \sin(nt + q_n)$, may become smaller if a sufficiently large number of terms are taken into consideration, in which case however the problem may be similar to that treated statistically. Since, on the other hand, the external disturbances are regarded as being quite irregular as already mentioned, the statistical treatment of the proposed problem may be considered reasonable, and the above mentioned deviations are therefore discussed from a statistical point of view.

Let the deviations ξ_i be

$$\xi_i = x_i - X, \quad \cdots\cdots\cdots\cdots\cdots\cdots \quad (2)$$

where the x_is are the actual values of the yearly mean sea-level, and X the mean value of an infinitely large number of x_is.

Assuming that the frequency distribution of ξ is given by Gauss's law, the probability that the mean value

$$s = \frac{1}{n+1}(\xi_1 + \xi_2 + \cdots\cdots + \xi_{n+1})$$

lies between s and $s + ds$ will be

$$Uds = (n+1)ds\left(\frac{K}{\pi}\right)^{\frac{n+1}{2}} \int_{-\infty}^{\infty} e^{-K\xi_1^2} e^{-K\xi_2^2} \cdots\cdots e^{-K\xi^2{}_{n+1}} d\xi_1,\ d\xi_2 \cdots\cdots d\xi_n.$$

Substituting ξ_{n+1} with $(n+1)s - \xi_1 - \xi_2 - \xi_3 - \cdots\cdots - \xi_n$, we have

$$I = \int_{-\infty}^{\infty} e^{-K\xi_1^2} \cdots\cdots d\xi_1 \cdots\cdots$$

$$= \int_{-\infty}^{\infty} e^{-K\xi n^2} d\xi_n \int_{-\infty}^{\infty} e^{-K\xi_{n-1}^2} d\xi_{n-1} \cdots\cdots \int_{-\infty}^{\infty} e^{-K\xi_1^2 - K\{(n+1)s - \xi_1 - \xi_2 \cdots\cdots\}^2} d\xi_1.$$

Therefore, the probability is given by

$$U = \sqrt{n+1}\sqrt{\frac{K}{\pi}}\, e^{-K(n+1)s^2}.$$

Next, we consider the summation

$$S=\sum_{i=0}^{\infty}\left\{\frac{x_i+x_{i+1}+\cdots\cdots+x_{i+n}}{n+1}-X\right\}$$

$$=\frac{1}{n+1}\sum_{i=0}^{\infty}\left\{\xi_i+\xi_{i+1}+\cdots\cdots+\xi_{i+n}\right\}.$$

The sum S is regarded as the sum of m terms of s, where $(n+1)s=\left|\sum_{K=0}^{\infty}\xi_{i+K}\right|$, i. e,

$$S=m.\,|s|.$$

The value of $\overline{|\eta|}$, which is the subject of our present investigation, is the given by

$$\overline{|\eta|}=\lim_{N\to\infty}\frac{S}{N}=\lim_{N=\infty}\frac{m\,|S|}{N}.$$

Since

$$\lim_{N\to\infty}\frac{m}{N}=U,$$

the value of $\overline{|\eta|}$ becomes

$$\overline{|\eta|}=2\sqrt{n+1}\sqrt{\frac{K}{\pi}}\int_0^{\infty}se^{-K(n+1)s^2}ds=\frac{1}{\sqrt{\pi}}\frac{1}{\sqrt{K(n+1)}}\quad\cdots\cdots\cdots(3)$$

in which $(n+1)$ corresponds to τ, the time interval of overlapping mean for smoothing the fluctuation curves.

The mean deviations $\overline{|\eta|}$ are thus shown as being dependent on the interval of time for the overlapping τ. The variations in the mean deviations $\overline{|\eta|}$ with respect to τ are as shown in Figs. 8∼12. The curves showing the variations in $\overline{|\eta|}$ are very similar to those which may be expected from equation (3). This fact may suggest that the disturbances that cause variations in the heights of the yearly mean sea-levels are not periodic, and occur fortuitously.

The mean error for the single value of the yearly mean sea-level is then given theoretically by

$$\text{Mean Error}=\frac{1}{\sqrt{2}}\cdot\frac{1}{K},$$

where K is the precision. Since K is connected with $\overline{|\eta|}$, the mean deviation, by the equation (3), the mean error will be

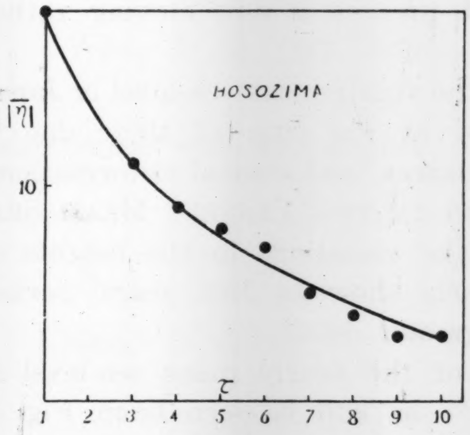

Fig. 8. Variation in $|\overline{\eta}|$ with respect to τ. (Hosozima.).

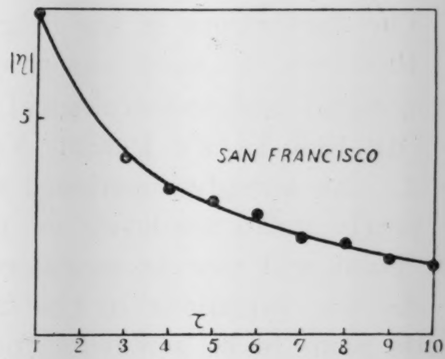

Fig. 11. Variation in $|\overline{\eta}|$ with respect to τ. (San Francisco.).

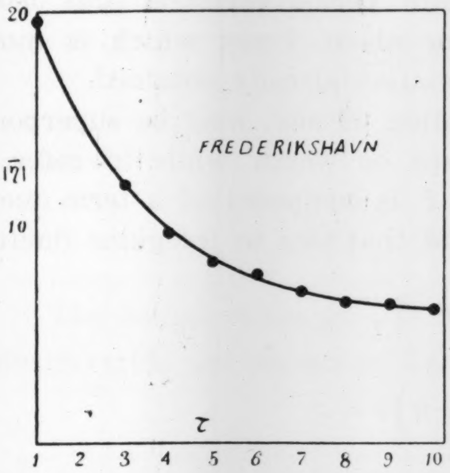

Fig. 9. Variation in $|\overline{\eta}|$ with respect to τ. (Frederikshavn.).

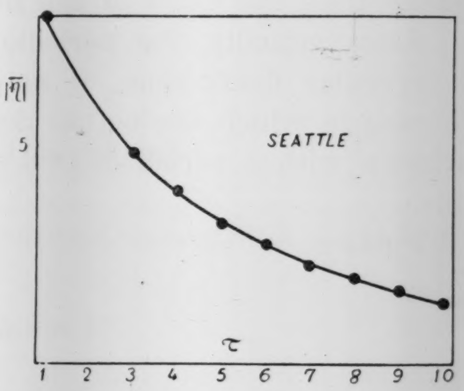

Fig. 12. Variation in $|\overline{\eta}|$ with respect to τ. (Seattle.).

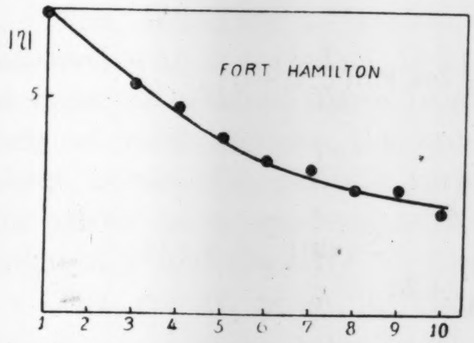

Fig. 10. Variation in $|\overline{\eta}|$ with respect to τ. (Fort Hamilton.).

$$\text{Mean Error}=\sqrt{\frac{\pi}{2}}\cdot|\overline{\eta}|.$$

Since the values of the mean deviations $|\overline{\eta}|$ for the case $\tau=1$ are about 20 mm, the yearly mean sea-level may be regarded as being variable within about 20 mm.

For the data of Japanese stations, however, the fluctuations in the height of the yearly mean sea-level with shorter periods may not be due merely to irregular meteorological and astronomical disturbances, seeing that earth's crust in Japan at present is now moving rather markedly in vertical directions.

The fluctuations in the height of the yearly mean sea-level in Japan are, therefore, in most cases, regarded as the sum of those due to astronomical and meteorological disturbances, and crustal deformations.

5. THE 18·6 YEAR'S PERIOD VARIATION IN THE YEARRLY MEAN SEA-LEVEL. As already mentioned in § 1, the variations in the heights of the yearly mean sea-levels do not clearly show an 18·6 years' period. This point will now be considered in greater detail.

As the variations in the heights of the yearly mean sea-level at Seattle seem to be somewhat periodic,[10] as will be seen from Fig. 5, the amplitude of the periodic variations with a period of 18·6 years was determined by using the data of Seattle by the method of least squares. The amplitude of the 18·6 years' period variation thus determined is about 2·3 units (1/100 foot) or about 7 mm which is much smaller than the value of the mean deviation already obtained.

Since, actually, the periodic fluctuation, if any, may be superposed by irregular fluctuations, it may perhaps be worth while to refer to the case in which the actual deviation ξ is composed of a term due to variation with a period of 18·6 years and that due to irregular fluctuations.

Putting

$$\xi_i = a\sin\left(\frac{2\pi}{T}t_i + q\right) + \varepsilon_i ,$$

where ε_i on the right-hand side of the equation is the term due to the irregular variations.

We calculate the mean value of

$$\xi_i^2 = a^2\sin^2\left(\frac{2\pi}{T}t_i + q\right) + \varepsilon_i^2 + 2a\varepsilon_i\sin\left(\frac{2\pi}{T}t_i + q\right),$$

i. e.,

$$\xi^2 = \frac{\Sigma\xi_i^2}{N} = a^2\frac{\sin^2\left(\frac{2\pi}{T}t_i + q\right)}{N} + \frac{\varepsilon_i^2}{N} + 2a\frac{\Sigma\varepsilon_i\sin\left(\frac{2\pi}{T}t_i + q\right)}{N}.$$

---

[10] Variations in the heights of the yearly mean sea-levels with long periods are not noticed in the data of other stations, which may be one of the evidences for the conclusion that variations in the heights of the yearly mean sea-levels with a period of 18·6 years are practically negligible.

When N is very large, the expression $\dfrac{\Sigma\sin^2\left(\frac{2\pi}{N}t_i+q\right)}{N}$ may be substituted with an integral

$$\frac{4}{T}\int_0^{\frac{T}{4}}\sin^2\left(\frac{2\pi}{T}t+q\right)dt.$$

Since

$$\frac{4}{T}\int_0^{\frac{T}{4}}\sin^2\left(\frac{2\pi}{T}t+q\right)dt=\frac{1}{2},$$

and

$$\left|\frac{\sum\varepsilon_i\sin\left(\frac{2\pi}{T}t+q\right)}{N}\right|\xrightarrow[N\to\infty]{}0,$$

we have

$$\xi^2=\frac{a^2}{2}+(\text{Standard deviation})^2$$

The actual values of $\sqrt{\overline{\xi^2}}$ for the various mareograph stations under consideration are shown in Table II.

TABLE II.

Station	Hosozima	Frederikshavn	Fort Hamilton	San Francisco	Seattle
$\sqrt{\overline{\xi^2}},_{\tau=3}$	14 (mm)	14·6 (mm)	6·38 ($\frac{1}{100}'$)	5·26 ($\frac{1}{100}'$)	5·84 ($\frac{1}{100}'$)

The amplitude of variations in the heights of the yearly mean sea-level with a period of 18·6 years is, if any, of the order of 7 mm at most, as obtained above from the data for Seattle. Since, from the data of most stations, the order of magnitude of the actual $\sqrt{\overline{\xi^2}}$ is about 20 mm, the periodic variations, i.e., variation in the heights of the yearly mean sea-level with a period of 18·6 years, can affect the value of $\overline{\xi^2}$ but slightly.

The results given in Table III below, suggests likewise. This Table gives the values of the ratios $\dfrac{\overline{|\xi|}}{\sqrt{\overline{\xi^2}}}$ for the various stations, which must be $\sqrt{\dfrac{2}{\pi}}=0{\cdot}8$, so that the fluctuations are quite fortuitous.

TABLE III.

Station	Hosozima	Frederikshavn	Fort Hamilton	San Francisco	Seattle
$\overline{\lvert\xi\rvert}/\sqrt{\overline{\xi^2}}$	0·78	0·81	0·78	0·83	0·84

6. CHANGES IN THE HEIGHT OF THE YEARLY MEAN SEA-LEVEL AT ABURATUBO. The Aburatubo mareograph station was levelled a number fo times since 1923 with reference to the standard datum point at Tokyo. An important point in our present study is that the changes in the height of the Aburatubo bench-mark do not agree well with those deduced from the data of the yearly mean sea-level for the same place.

In discussing fluctuations in the heights of the yearly mean sea-level at Aburatubo, data obtained before the earthquake of 1923 are excluded, because the land level underwent marked elevation at the time of the earthquake with the result that the reference surface for the sea-level has changed.

The data of the yearly mean sea-level and the vertical displacements of the bench-mark measured with reference to the standard datum point of Tokyo in 1930, 1934, and 1937 are given in Table IV.

TABLE IV.

Year	Y. M. Sea-level	Level (ref. Tokyo)	Year	Y. M. Sea-level	Level (ref. Tokyo)
1925	0 mm	0·0 mm	1931	− 7 mm	
1926	26		1932	−21	
1927	29		1933	−43	
1928	7		1934	−13	−81·4
1929	−10		1935	−62	
1930	−21	+ 1·7	1936	−53	−17·5

In Fig. 13, the deviations in the heights of the yearly mean sea-level, as measured from the yearl mean sea-level in 1925, together with the vertical displacements compared with the height measured in 1925 are plotted against the time by symbols ● and × respectively.

It is of course difficult to separate the term for fluctuation due to crustal deformation from that of fluctuations due to astronomical and meteorological disturbances in the data given above.

For trial, we shall assume that a smooth curve, joining the points representing the vertical displacements in Fig. 13, represents the change in the height of the land level at Aburatubo with respect to time, the reference being the standard datum point of Tokyo. Then the diffe-

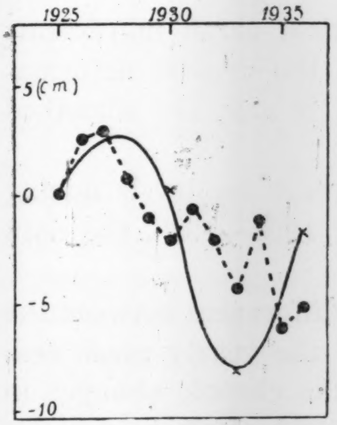

Fig. 13. Vertical displacement of the land at Aburatubo.
● : Deduced from mareogram data. × : Deduced from result of precise levels, referring to the standard datum point at Tokyo.

rences between the actual values of the yearly mean sea-level and those estimated from the hypothetical curve of the vertical displacements may be regarded as fluctuations due to astronomical and meteorological disturbances. In the case, the changes in the heights of the standard datum point, or those in the heights of the yearly mean sea-level at Tokyo may seriously affect the amplitude of the fluctuations.

The yearly mean sea-levels of Tokyo, the data of which are given in Table V together with the fluctuations in the heights of the yearly mean sea-level at Aburatubo, do not show any marked systematic variation.[11]

TABLE V.

(Y. M. Sea-level at Tokyo)

Year	Y. M. Sea-level	Year	Y. M. Sea-level
	m		m
1924	1·133	1930	1·132
1925	1·140	1831	1·143
1926	1·125	1932	1·139
1927	1·135	1933	1·147
1928	1·138	1934	1·170
1929	1·123	1935	1·208

TABLE VI.

Year	Fluctuations	Year	Fluctuations
1913	− 9 mm	1925	0 mm
1914	−13	1926	+ 8
1915	0	1927	+11
1916	−15	1928	−15
1917	25	1929	−27
1918	13	1930	−21
1919	8	1931	+20
1920	−36	1932	+55
1921	−17	1933	+40
1922	10	1934	+60
1923	12	1935	−12
1924	?	1936	−32

---

[11] The upheaval of the mean sea-level in 1934 and 1935 was somewhat remarkable, which however cannot be regarded as being due merely to depression of the land.

The curve in Fig. 13, showing the hypothetical earth movements at Aburatubo, may therefore show approximately the crustal deformation, although the fluctuations of shorter periods, if any, are smoothed out.

The fluctuations in the heights of the yearly mean sea-levels during 1925–1936 are slightly larger than those during 1900～1923, the data of which are given in Table VI.

The values given in the table above are the differences between the actual and the calculated values of the heights of the yearly mean sea-level. The general trend of the curve showing the chronic changes in the heights of the yearly mean sea-level during 1900～1923 is expressed by

$$H_t = 91{\cdot}3 - 136{\cdot}4t + 38{\cdot}5t^2 \quad \text{(mm)}.$$ [12]

from which the heights of the yearly mean sea-level were calculated and the results compared with the actual values.

The mean deviation in the heights of the yearly mean sea-level of Aburatubo during 1925～1936, given in Table V, is about 25 mm, which is slightly larger than those obtained for the foreign mareograph stations. This may partly be due to the assumption that the smooth curve in Fig. 13 represents the actual crustal deformation. If we were to take a more complex curve to represent the crustal deformation, the mean deviation could be made smaller so that it may more closely approach the ordinary value obtained above.

The fact that the durations of time for which the yearly mean sea-level are given was small, may also explain why the value of the mean deviation is slightly larger.

As found above, the fluctuations in the heights of the yearly mean sea-levels is about 20 mm on the average. Hence the discordance, amounting to about 20 mm, between the vertical displacements obtained by precise levelling and those deduced from data of the yearly mean sea-level, may sometimes be attributed to irregular fluctuations in the astronomical and meteorological disturbances.

In conclusion, the writers wish to express their sincere thanks to Dr. Tosio Uno for his numerous valuable suggestions. Their thanks are also due to Miss C. Setoyama for her assistance in calculating the numerical results in the tables given in this paper.

---

12) The constants in this formula were determined by the method of least squares.

APPENDIX TABLE.

Heights of Yearly Mean Sea-level.

Year A. D.	(Japan) Hosozima	(Denmark) Frederikshavn D. N. N.	(U. S. A.) Fort Hamilton	(U. S. A.) San Francisco	(U. S. A.) Seattle
1893		42 mm.	4·94 feet		
1894		3	4·98		
1895		−11	4·91		
1896		−20	4·99		
1897		−27	5·06		
1898		29	5·08	8·30 feet	
1899	m	30	5·07	8·44	3·94 feet
1900	2·557	− 5	5·93	8·50	4·10
1901	2·565	−48	5·16	8·46	3·88
1902	2·576	−21	5·20	8·57	4·06
1903	2·556	50	5·13	8·53	3·99
1904	2·577	− 7	4·98	8·63	4·10
1905	2·555	1	4·94	8·65	4·08
1906	2·574	12	5·05	8·58	4·11
1907	2·598	− 1	5·00	8·66	4·17
1908	2·587	−33	4·97	8·43	4·08
1909	2·603	8	5·10	8·53	4·12
1910	2·623	9	5·16	8·42	3·98
1911	2·612	14	5·11	8·61	3·96
1912	2·596	30	4·93	8·49	3·96
1913	2·583	44	4·98	8·51	3·96
1914	2·584	42	5·11	8·81	4·16
1915	2·555	−15	5·16	8·69	4·23
1916	2·550	21	5·12	8·52	4·08
1917	2·648	−17	5·15	8·48	3·88
1918	2·657	−24	5·13	8·70	4·18
1919	2·604	−34	5·30	8·61	4·08
1920	2·626	2	5·23	8·54	3·99
1921	2·633	−14	5·24	8·58	4·02
1922	2·602	−31	5·14	8·55	3·94
1923	2·590	13	5·15	8·52	4·00
1924	2·584	−22	5·10	8·42	3·90
1925	2·578	8	5·05	8·62	4·10
1926	2·632	− 1	5·03	8·63	4·11
1927	2·620	12	5·18	8·60	4·14
1928	2·577	2	5·04	8·58	4·08
1929	2·605	−13	5·00	8·55	3·89
1930	2·602	−26	5·06	8·72	4·08
1931	2·594	−14	5·30	8·62	4·10
1932	2·575		5·30	8·68	4·12
1933	2·560			8·52	4·13
1934	2·642			8·63	4·17
1935	2·582			8·72	4·13

7. 年平均潮位のフラクチュエーション

陸地測量部　武藤勝彦
地震研究所　宮部直巳

日本，アメリカ，デンマークの各地にある數個所の驗潮場につき，年平均潮位の變化を調べたその結果を概括すれば，

(i) 長期に亘る緩やかな變化——主として土地の變動と考へられる——の外に不規則な昇降運動が重つてゐる

(ii) この不規則な變動を起す原因として種々なものが考へられるが，其等を分離することは却々困難であるから，一先づ，一括して，時間的に不規則な分布をなす原因によつて生ずるものと考へる．何等か週期的な變化があるかにも思はれるので，色々の方法で檢したけれども，明瞭な週期的變化を取り出すことは出來なかつた．

(iii) 約 19 年を週期とする變動は，天文學的に豫期される所であるが，實際の資料から斯の如き週期を持つ變動を見出すことは困難である．

(iv) 油壺の驗潮記錄に表はれた所の土地の昇降と思はれるものと，東京を不動とした時の油壺の水準點の昇降との間には若干の不一致がある．これは，東京の基準點をそれだけ動かせば簡單に解消する．併し，不規則な原因による年平均潮位の變動があつて，20 mm 程度の範圍內で正しく年平均潮位を定めることは困難であるから，簡單に東京の基準點の高さを變更してよいか，否か再考の餘地がある．

尙，本文中，年平均潮位が單に不規則な原因によつて變化するとしたが，この點に關しては，野滿博士や，寺田，山口兩博士の研究等もある如く，幾分かは知られてゐる點もある．併し，實際の場合には，鹽分，溫度，海流，低氣壓等の 1~2 のもののみでは說明しきれないものがある．今後，尙，研究を進めるつもりである．

8. *Geophysical Studies of Volcano Mihara, Oosima Island. III.*

Microtremor Measurements in Oosima.

By Ryûtarô TAKAHASI, Takesi NAGATA, and
Kintarô HIRANO,

Earthquake Research Institute.

(Read Nov. 16, 1937.—Received Dec. 20, 1937.)

1. Introduction.

Although in the previous papers,[1] the writers stated that volcano Mihara[2] was calm then and likely to remain so for a while, rumblings, small explosions, and volcanic tremors never cease even in this calm period. For the purpose of recording the variations in the amplitude of the volcanic tremors, which serve as a measure of this volcano's activity, a microseismograph of magnification 400 was installed on February 1936, at Gozinka-tyaya,[3] on the western summit of the somma. Similar seismographs were installed later (August 1937) at Sendu,[4] the northern coast of Oosima, and at Sasikidi,[5] the south-eastern coast. Since then, continuous observations of the volcanic tremors and earthquakes were carried out by means of these seismographs.

The micro-tremors that were observed at Gozinka-tyaya were of the order of several microns in amplitude, without any marked correlation with the speed and direction of the wind. They vary incessantly in amplitude, no distinct regularity having been noticed in the manner of their growth and decay. These features, however, are those that are apparent in a period of calm, such as the present. In a more active period, the tremors may have very large amplitude, as has been reported by F. Omori[6]; or an intimate relation may be found to exist between their growth and decay and the activity of the volcano, as observed by K. Sassa[7] at Aso.

When F. Omori,[6] in 1912, observed micro-tremors at several points in Oosima, he found that the tremors east of Kagamihata,[8] the highest

---

1) *Bull. Earthq. Res, Inst.*, **15** (1937), 441, 1047.
2) 三原， 3) 御神火茶屋， 4) 泉津， 5) 差木地， 8) 鏡端.
6) *Rep. Earthq. Inv. Comm.*, No. 81, (1915).
7) *Mem. Coll. Sci. Kyôto Imp. Univ. Ser. A* **18** (1935), No. 5; **19** (1936), No. 1.

peak in the western somma, have larger amplitudes than those observed on the western slope of the central cone; also that the tremors at Motomura[9] are only one-third the amplitude of those observed at Kagamihata. The result was the same in the case of the tremors observed at Yuba,[10] the distance of which from Kagamihata is the same as that of Motomura. These results led him to conclude that the source of the tremors is not immediately beneath the crater, but at a point from 500 to 600 m beneath Kagamihata.

Since to ascertain the origin of the tremors is one of the pressing needs in the study of the volcano, the writers made observations of micro-tremors at 19 stations in Oosima, using a portable microseismograph of magnification 2000.

2. Instrument.

The seismograph used in these observations was the inverted pendulum seismograph[11] designed by M. Ishimoto. For portability, the oil damper used in the original pattern of this seismograph was replaced by an air damper. The improved pattern of this instrument is fitted also with a device for obtaining three changes in magnification, namely, 500, 1000, and 2000. When damped almost critically, the period of proper oscillations is 2·0 sec. Since none of the micro-tremors involved have periods exceeding a second, this seismograph is admirably suited for the present purpose. The records were obtained optically on bromide paper wound on a drum, revolving with sufficient uniformity, the length of the record always corresponding to 3 minutes within an error of 0·5 mm.

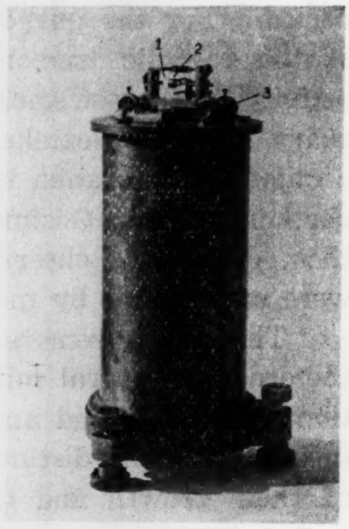

Fig. 1. Seismograph used in the present measurements.
1. Mirror
2. Roller
3. Air damper

It was therefore easy to measure the periods of the tremors with an accuracy of 0·01 sec. The bromide paper recorded for 3 minutes.

3. Stations and Observations.

Since the topography of the island made it impossible to distribute

---

9) 元村, 10) 湯場.
11) *Bull. Earthq. Res. Inst.*, **1** (1926), 1.

our 19 stations uniformly there, they were distributed as shown in Fig. 2, namely, 7 on the route from Motomura to the crater, 2 on the rim of the central cone, and the remaining 10 as uniformly as possible over the island.

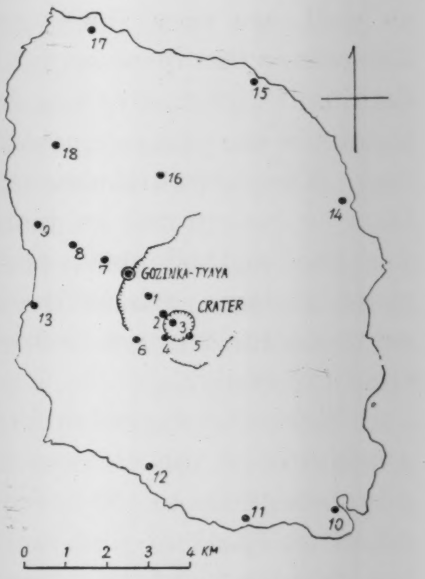

Fig. 2. Distribution of stations. Numerals indicate Station Nos.

The seismograph at every station was installed directly on the ground. To avoid the effect of winds, the observations were made at points as far as possible from big trees and houses. In the present measurements, only the horizontal component of the tremors was observed. Since for ease of transport, only one seismograph was used, the component *"station-crater"* was first observed, followed immediately by observations of the component perpendicular to it. Observation at a station usually consisted of taking two records for each of the two components. The instants of beginning and ending of a record were carefully noted for comparison with the continuous observations at Gozinka-tyaya.

The character of the tremors at Gozinka-tyaya was studied as the first step in this investigation, using two identical microseismographs at the same time. The two seismographs were installed in directions at right angles to each other. The combined horizontal motion of the ground thus obtained, which is shown in Fig. 3, is very irregular in shape, with no pronounced direction of oscillation; that is, when the oscillation is vigorous, the amplitude is large in all directions and *vice versa*. Moreover as plotted in the manner shown below, the growth and decay of the two components are nearly parallel as shown in Figs. 4a, 4b.

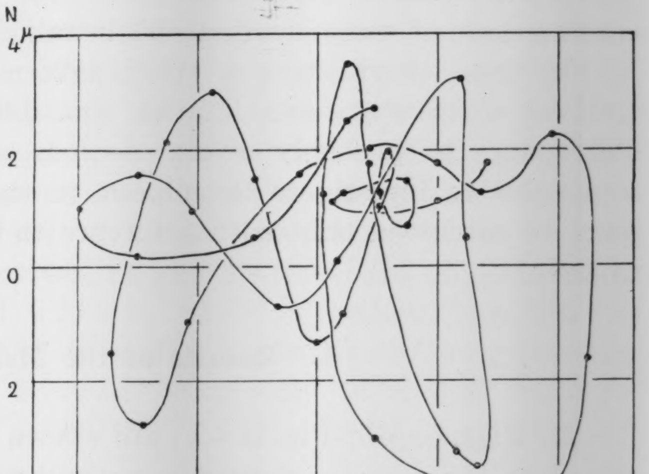

Fig. 3. The combined motion of the ground as observed at Gozinka-tyaya.

When this character of the oscillation of the tremors, as shown below, obtains at other stations as well, we may then ignore altogether the question of the dominant direction of the oscillations in the present investigation. The fact cited above may thus be interpreted as justifying the method used at the other stations, where the two components are not observed simultaneously.

Since the variation in the amplitude of the tremors usually amounts to 50 percent, when we speak of distribution, the amplitude of the tremors as measured at each station must be compared with simultaneous observations made at some standard station, for which we selected the microseismograph of magnification 400 installed at Gozinka-tyaya.

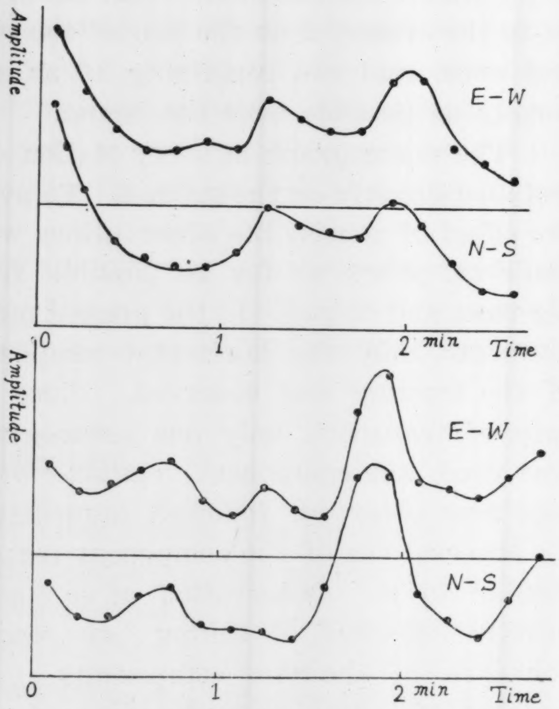

Figs. 4a, 4b. Parallelism in the growth and decay of the two horizontal components.

In these circumstances, strict agreement in time between the field stations and the standard station was difficult to attain, there being a discrepancy of probably several seconds, as the result of which it was impossible to investigate the phases, so that all the measured amplitude must be discussed only with reference to their mean values with regard to time.

4. Results of the Measurement.

In Figs. 5a∼5c Pl. III∼V, are shown a number of records thus obtained at the various stations. As will clearly be seen from these figures, some of the curves show merely simple harmonic oscillations of varying amplitudes, while others are composed of several harmonic oscillations of different periods, or are quite irregular.

There are at least three possible causes of these tremors. They are either propagated from a common source, or they are free oscillations of the superficial layer of the ground induced by the former cause; or they may be forced oscillations. Volcanicity is not necessarily the cause of these tremors; the sea waves and winds may induce these tremors exactly as in the case of common pulsations. Consequently, in order to determine the cause of the tremors, it is necessary to make simultaneous observations, using one vertical and two horizontal component seismographs. The relations between the phases of the oscillations will also have to be investigated at the different stations; that is, we must ascertain what sort of elastic waves the tremors consists of.

When tremors of a definite period appear at all the stations, we naturally conclude that they were propagated from a common source. With these meanings, we made the following frequency analysis. The time intervals between each successive instant $\dot{x}=0$, where x is the displacement, were read off from each record, and a frequency curve was drawn as shown in Fig. 6. According to necessity, the same process was repeated with the smoothed curves, in which the oscillations of shorter period were eliminated by joining the middle points of successive $\dot{x}=0$'s. The process then gives the oscillations of long periods.

A number of frequency curves thus obtained are shown in Fig. 6, a and b. If there are two curves in a diagram, they correspond to the original and the smoothed records respectively.

Fig. 7 shows the predominant periods at the various stations. As will be seen from this figure, oscillations of period 0·32∼0·30 sec. appear at all the stations, except one. Moreover, at such stations as No. 7 and No. 8, where the tremors have only a single period, the period is 0·32∼0·30 sec., without exception. It will also be noticed that, at the central cone, the tremor is composed of several oscillations of different periods, while at the slope of the somma the tremor is comparatively simple, although there are of course several exceptions to this rule. For example, at stations Nos. 14 and 15 there are oscillations of such short periods as 0·15 and 0·20 sec., while at stations, Nos. 10, 12, 13 (all coastal stations), we find irregular oscillations of long periods. These exceptional oscillations however occur only in one of the two components, as shown in Fig. 5, Pl. III∼V., whereas the oscillation of period 0·32∼0·30 sec. appears in both components.

From these facts, it may be said that tremors, which are composed of oscillations of different periods at the central cone, become simple oscillations with increased distance from the central cone, and again become irregular at the coast.

Since owing to a storm at the time, the measurement were made indoors at stations Nos. 14, 15, the short period oscillations observed there are probably those of the station houses. The irregular oscilla-

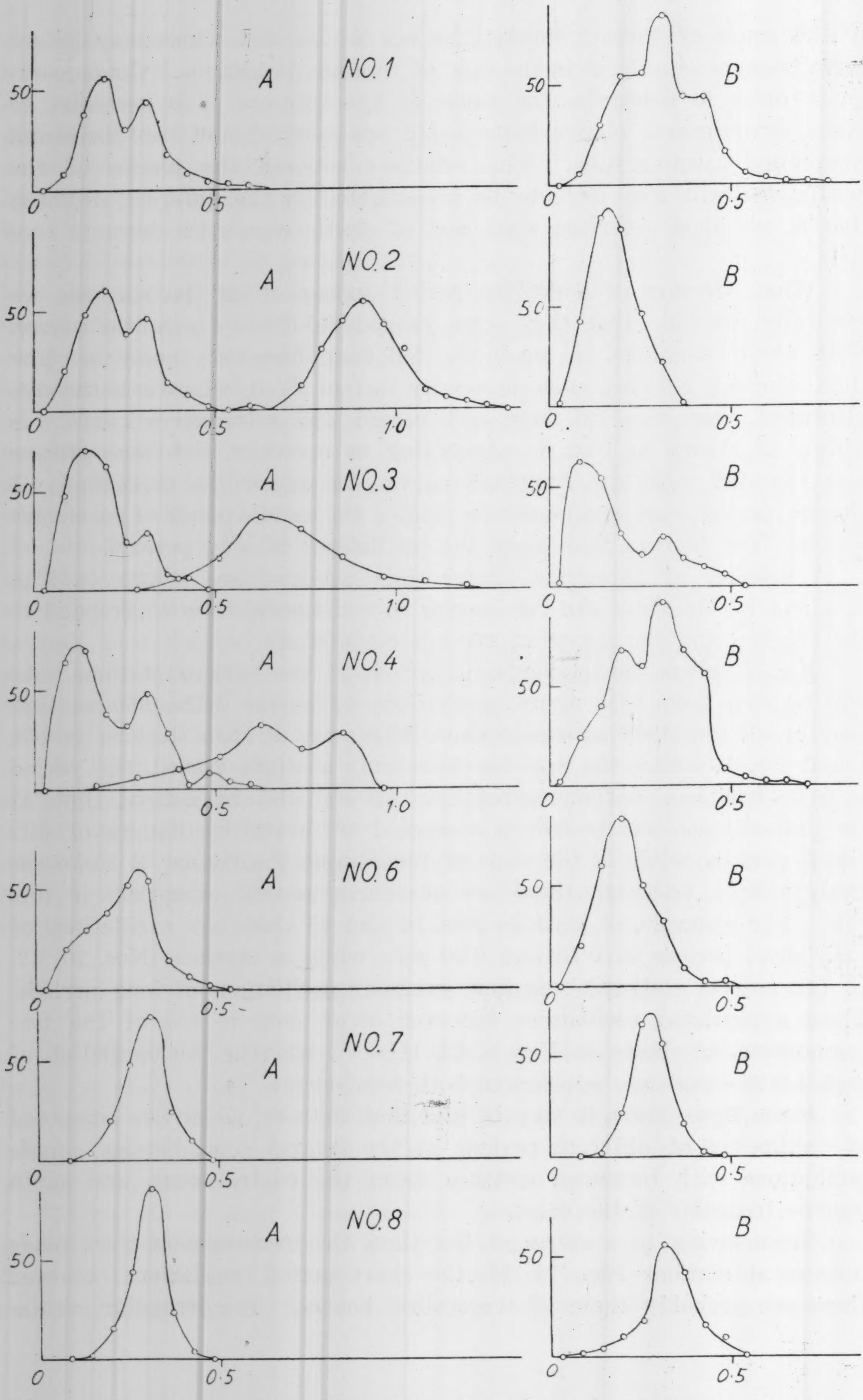

Fig. 6a. Frequency curves of the periods of tremors observed at the various stations. B. The component in the direction of the crater. A. The component that is perpendicular to B.

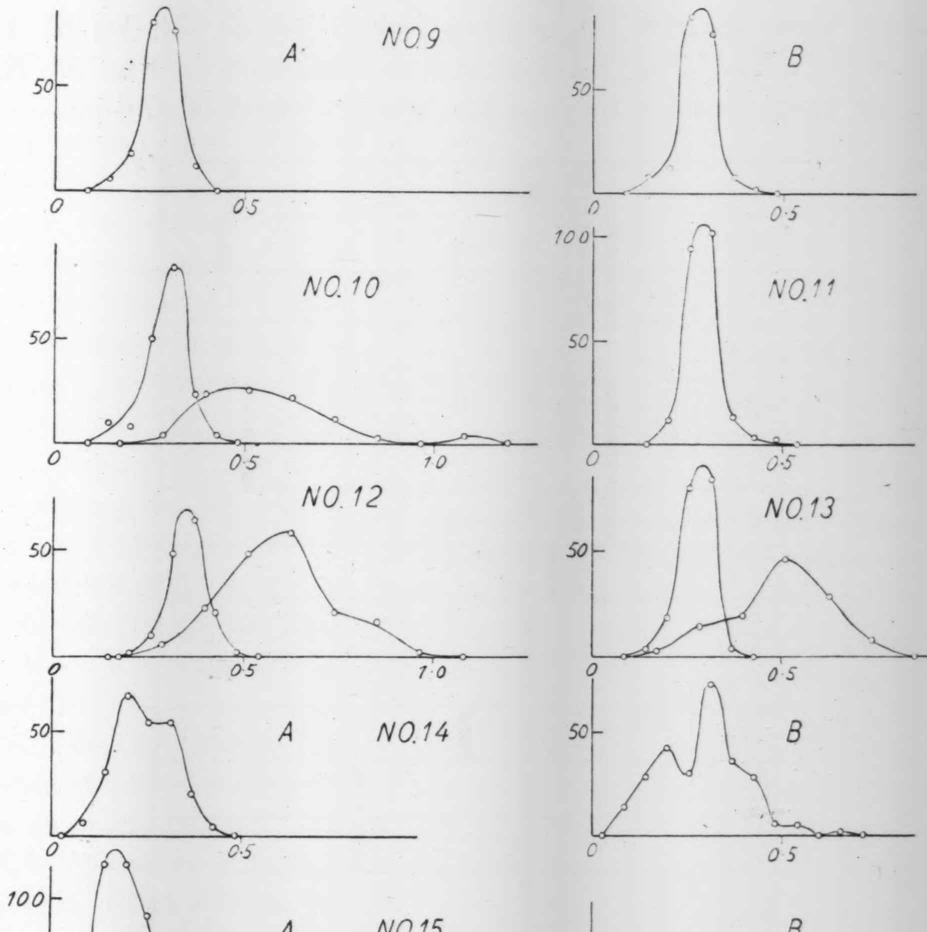

Fig. 6b. Frequency curves of the periods of tremors observed at the various stations. B. The component in the direction of the crater. A. The component that is perpendicular to B.

tions that were observed at stations Nos. 9, 10, 11, 12, 13, 16, 17 appeared only in the direction indicated by the bars in Fig. 8. Except No. 16, all these stations lie near the western coast of Oosima.

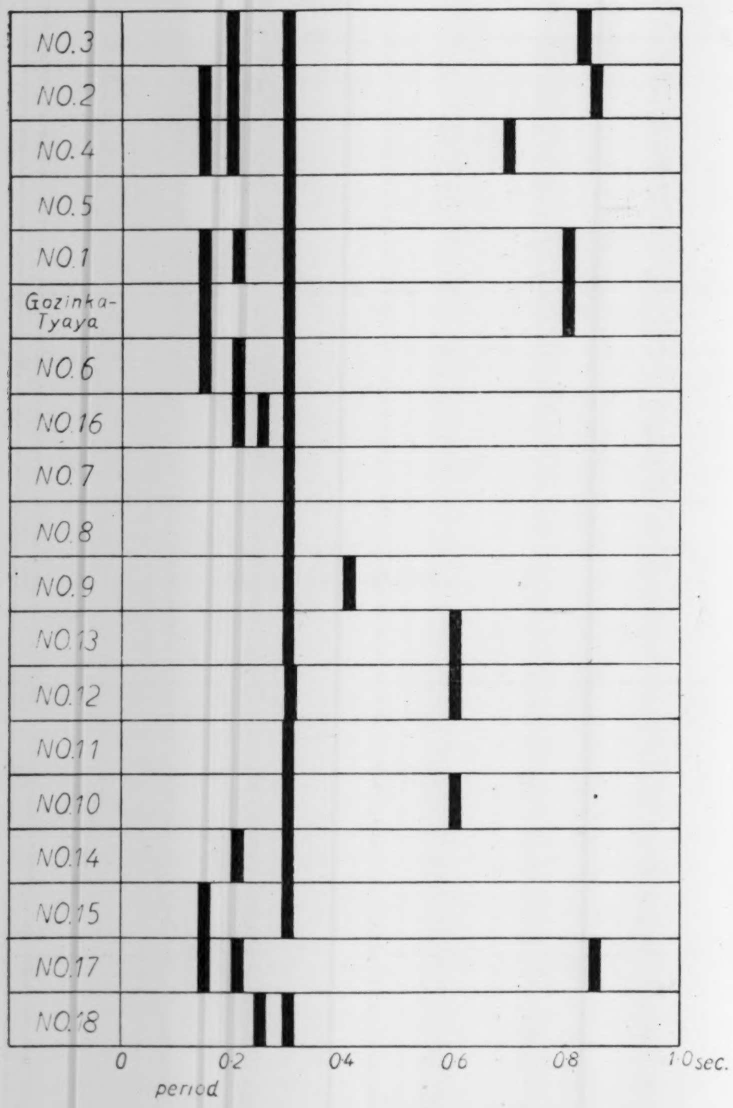

Fig. 7. Predominant periods at the 19 station.

Since during these measurements, the wind was blowing at the rate of 5～10 m/sec from the west, it is highly probable that these irregular oscillations are due to sea waves, although their mechanism of generation is not simple, seeing that they appear only in a direction parallel to the coast.

Since the tremors undergo incessant growth and decay, in order to ascertain the distribution of the amplitudes of the tremors in Oosima, the amplitude of the tremor must be compared with that of the tremor that is continuously observed at Gozinka-tyaya, the standard station. As already stated, this comparison is not one of phases. But since the period of growth and decay of the tremor is from 2 to 4 sec., we can take as a measure of variation in the amplitude of the tremors the curve obtained by plotting the maximum amplitude during the successive periods of growth and decay. The curve thus obtained may afford a means of comparing the field record with the standard at Gozinka-tyaya.

Actually, we plotted the maximum amplitudes for every 10 seconds against the time. As shown in Fig. 9, a and b, this simplified method yields practically the same result as the former, in which the maximum amplitude of each wave group was plotted. It is therefore sufficient for the present purpose.

The standard microseismograph installed at Gozinka-tyaya records only the component that is parallel to the direction of the crater. Since, however, the growth and decay of the tremor is practically the same for the two components that are perpendicular to each other, as already shown in Figs. 4, a and b, it will be quite in

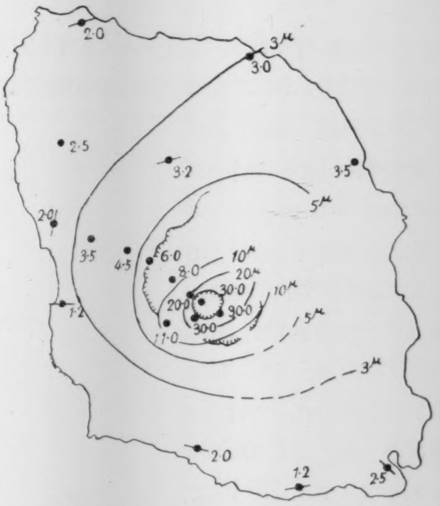

Fig. 8. Directions in which irregular oscillations appear and the distribution of the amplitudes of the tremors in Oosima.

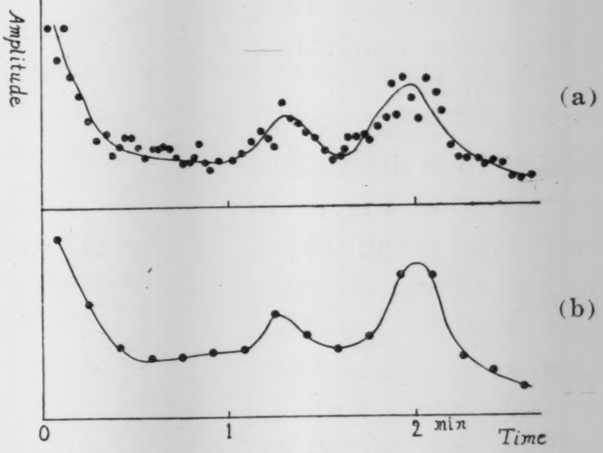

Fig. 9a. (a) Maximum amplitudes of successive wave groups.
(b) Maximum amplitudes every 10 sec.

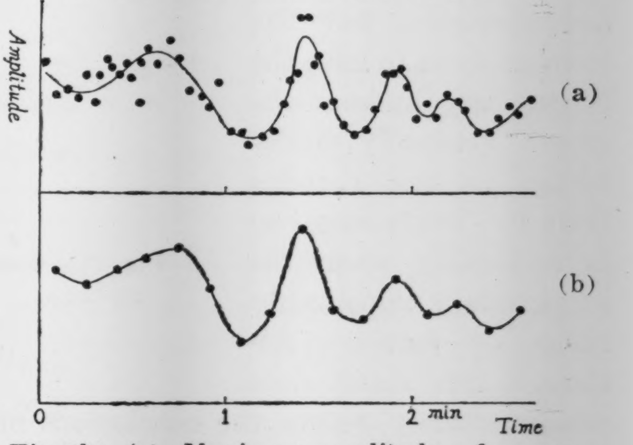

Fig. 9b. (a) Maximum amplitudes of successive wave groups.
(b) Maximum amplitudes every 10 sec.

order to compare the field observation made in an arbitrary direction with that by the standard seismograph installed in a particular direction.

If treated as described above, the tremors observed at some of the stations show, as in Fig. 10, nearly the same manner of growth and decay as those at the standard station, while those observed at other stations show, as in Fig. 11, no remarkable correlation. In the latter case, we took the ratio of the mean amplitudes for 3 minutes.

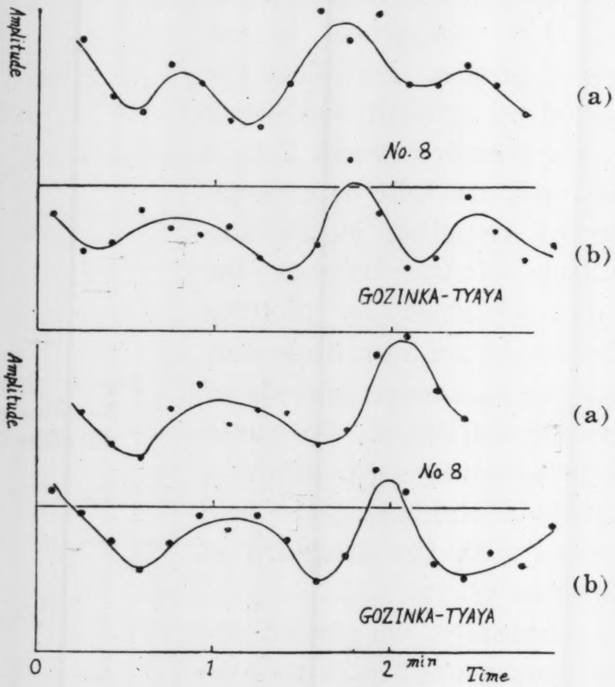

Fig. 10. Comparison of the field and standard stations.
(a) Field station.
(b) Standard station.

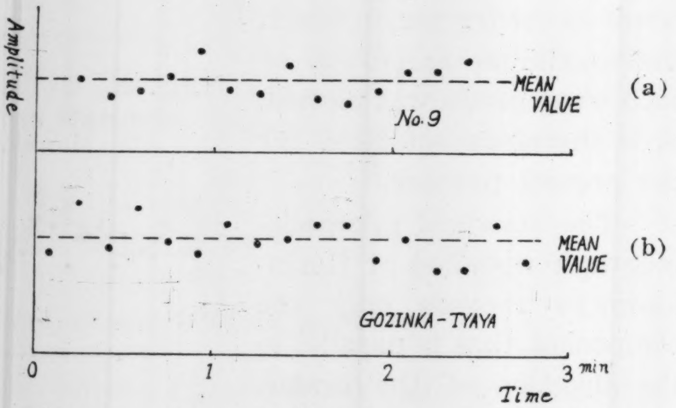

Fig. 11. Comparison of the standard and field stations.
(a) Field station.
(b) Standard station.

The amplitude of tremors thus determined are given in Fig. 8, in which the amplitude at Gozinka-tyaya, the standard station, has been taken as 5 μ. Since there are no more than 19 stations, we do not expect any conclusive results from the present measurements, but the tremors seem to have the largest amplitude at the crater, gradually diminishing as one recedes from it. There seems to be no locality where the amplitude is abnormally large or small. Although this result does not necessarily refute the conclusions of F. Omori, his conclusion is at least suspect, as his measurements were not made simultaneously.

The volcanic earthquakes that shake Oosima do not always originate from underneath the present crater. In the same way, during an active period of the volcano, the source of its tremors may be situated elsewhere than the present crater, so that we cannot reject Omori's conclusion *in toto*.

Judging from the present results, the sourse of the tremors seems to lie underneath the present crater, so that we have plotted the amplitudes of the tremor that were determined in the manner stated above against the distances of the respective stations from the crater. Fig. 12, thus obtained, seems to show a hyperbolic decrease of amplitude with distance.

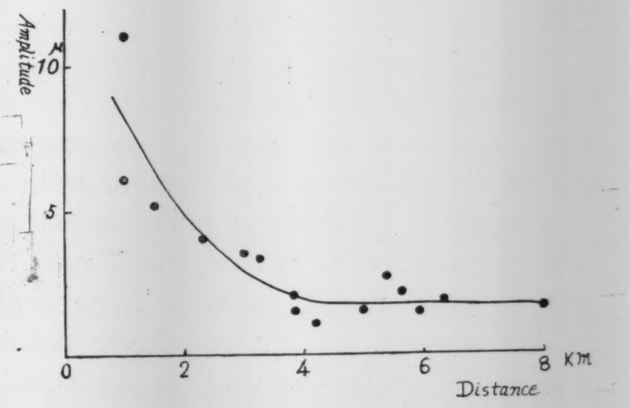

Fig. 12. Decrease in amplitude with increasing distance from the crater.

The manner in which the amplitude of the tremors diminishes with distance from the crater was carefully studied in detail, particularly with regard to the stations on the route from Motomura to the crater.

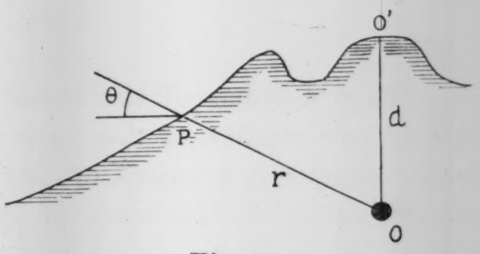

Fig. 13.

Assuming that the source of the tremors lies 400 m below the crater mouth, the measured amplitudes are inversely proportional to the hypocentral distance r of the stations, as shown in Fig. 14. Assuming now that a point sourse

$$A_0 e^{i\nu t}$$

is at the origin, the amplitude of the spherical waves that are propagated from it are given by

$$A = \frac{A_0}{4\pi r} e^{i\nu\left(t-\frac{r}{v}\right)},$$

where v is the velocity of the wave. Here amplitude A is inversely proportional to the distance r. In our case, the measured amplitude is not A, but is its horizontal component. This seems to support the idea

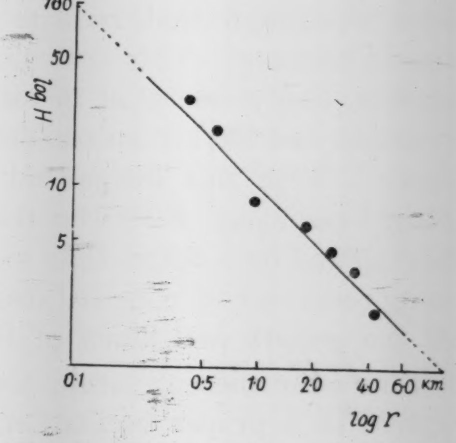

Fig. 14. Decrease in amplitude with hypocentral distance.

that the tremors observed by us are forced oscillation of the surface layer of the ground that is in turn induced by the primary wave propagated from the origin. The excited wave will then have an amplitude proportional to the exciting wave.

It is therefore very probable that the origin of the tremors is at the bottom of the present crater, or at a point 100 m below it, at the most, and that the tremor is generated by the same cause that causes the small explosions and rumblings at the crater bottom.

Another interesting phenomenon noticed in the course of the present measurements is that the tremor, which is nearly the same in amplitude with regard to both horizontal components at stations outside of the somma, has an amplitude nearly twice as large in direction towards the crater as that in direction perpendicular to the former at stations within the somma, especially on the central cone. We cannot tell from the present measurements, however, whether this phenomenon is due to some independent oscillation of the central cone, or to the gradual excitation of the transverse oscillation by the wave generated originally as a longitudinal wave from the crater bottom.

5. Conclusion.

These outlines of the nature of the tremors in Oosima are the result of our studies of the present measurements described above. Generally speaking, tremors of period 0·32∼0·30 sec. are generated at the crater bottom in the form of longitudinal waves, whence they are propagated to the whole island of Oosima.

In view of these charactistics of the tremors, we constructed a microseismograph that records directly the growth and decay of the volcanic tremors. This instrument is an inverted pendulum type seismograph, almost identical in form with those used in the present measurements, and having an oscillation period of 0·3 sec, but without any damper. With this instrument we hope to get a large magnification through resonance with the tremors. The record is made on smoked paper wound on a drum that revolves once a week. In Fig. 15, Pl. VI, is a reproduction of a record obtained by this seismograph, which shows well the growth and decay of the tremors.

Since our measurements were made with a portable microseismograph with a proper oscillation period of 2·0 sec., and since there are 3 station seismographs of magnification 400 and a proper oscillation period of 1·0 sec., the measurement are good only for waves with periods of less than 1·0 sec. We cannot, however, know anything about

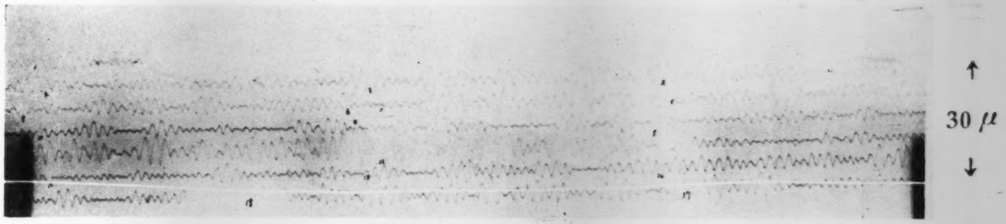

Gozinka-tyaya

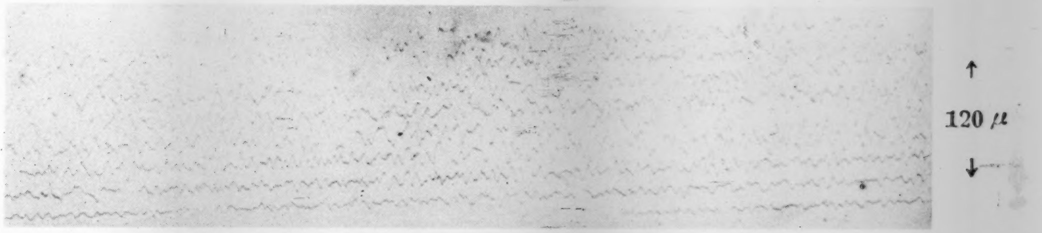

No. 3.

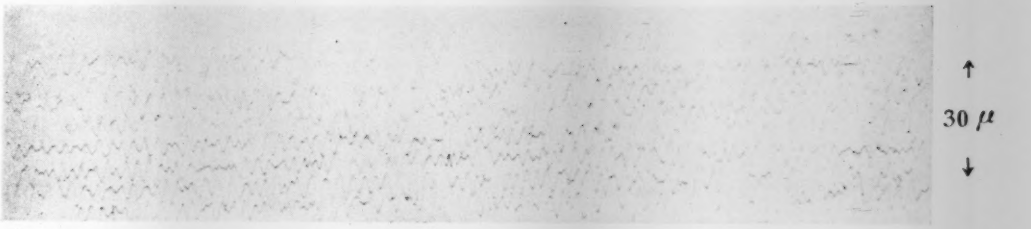

No. 6.

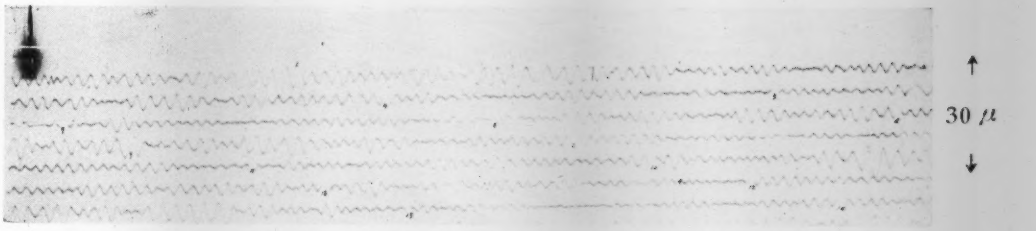

No. 7.

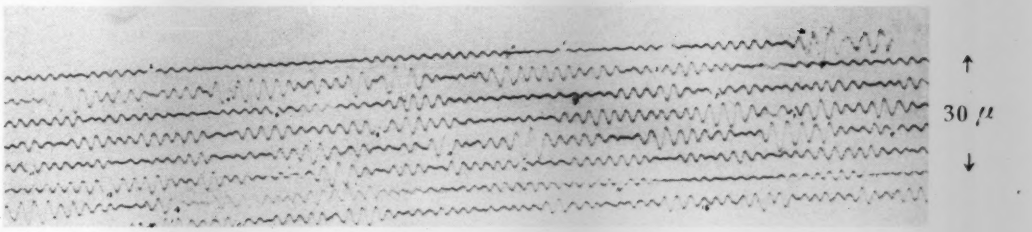

No. 8.

Fig. 5a. Records of tremors observed at the various stations. In the figure, 44 mm corresponds to 10 sec.

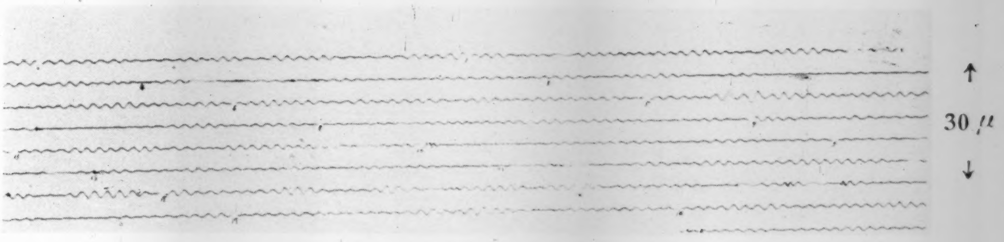

No. 9.

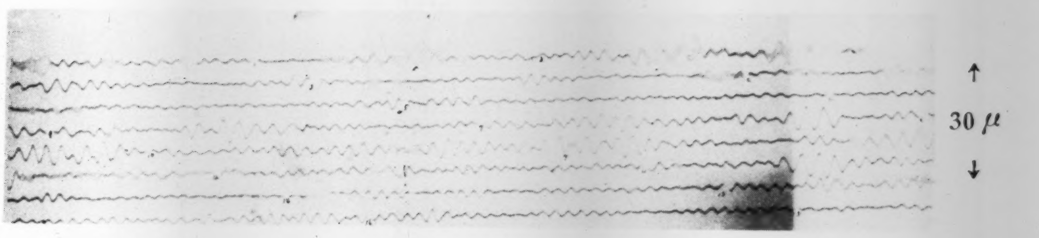

No. 10.

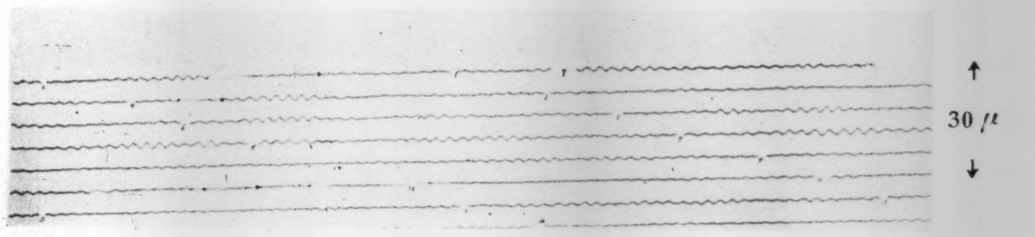

No. 11.

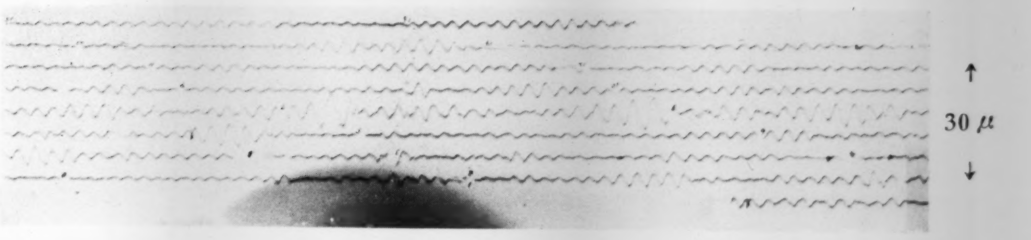

No. 12.

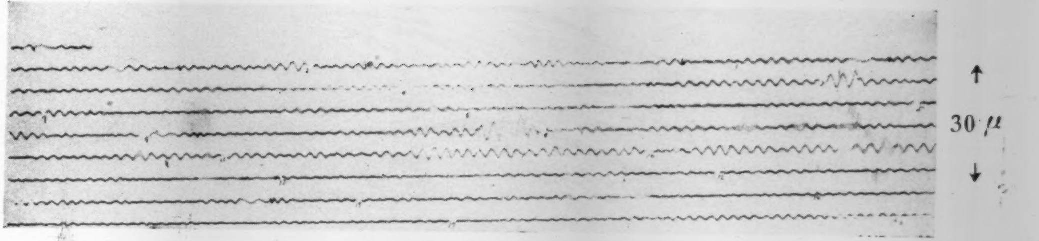

No. 13.

Fig. 5b. Ditto.

（震研彙報 第十六號 圖版 高橋・永田・平能）

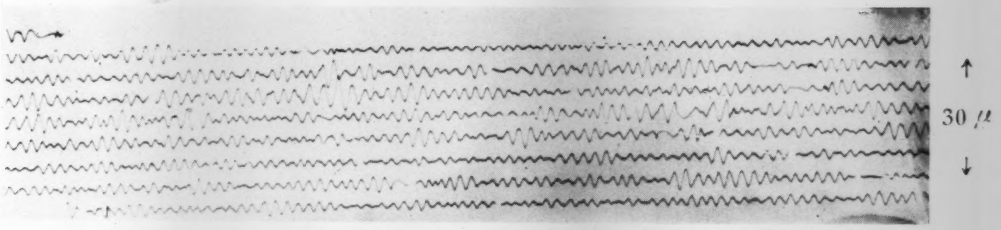

No. 14.

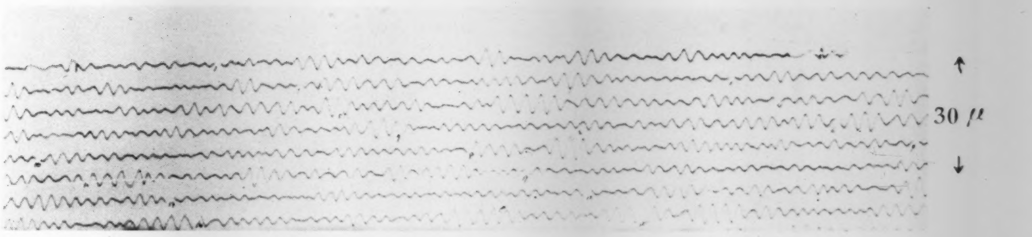

No. 15.

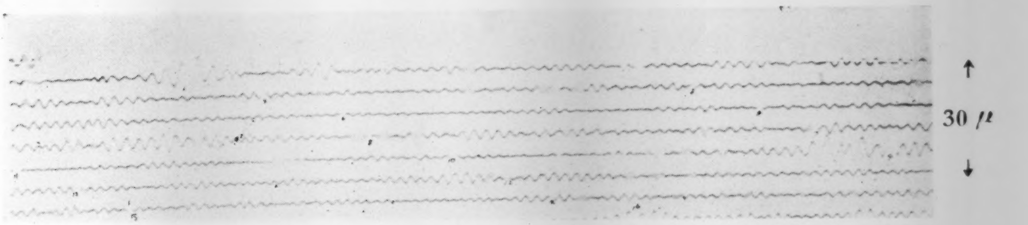

No. 16.

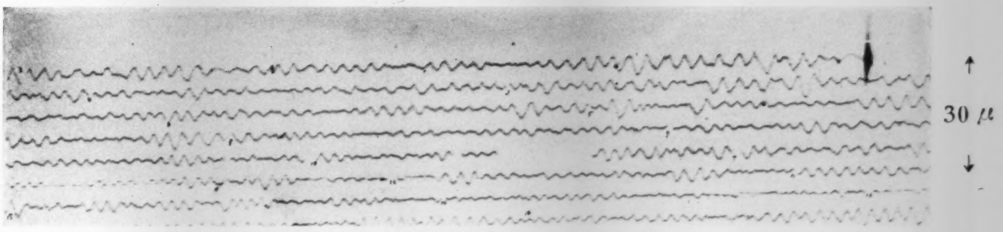

No. 18.

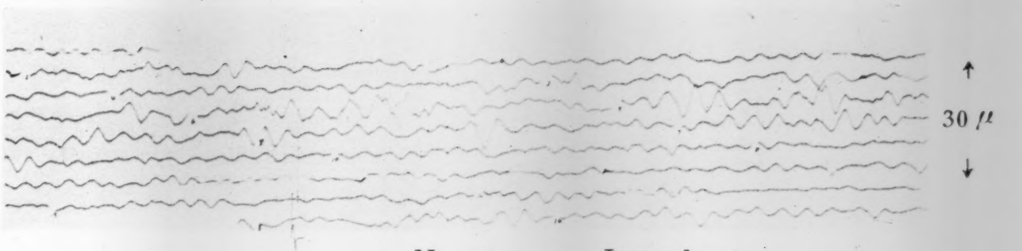

No. 10. Irregular type

Fig. 5c. Ditto.

（震研彙報 第十六號 圖版 高橋・永田・平能）

（震研彙報 第十六號 圖版 高橋・永田・平能）

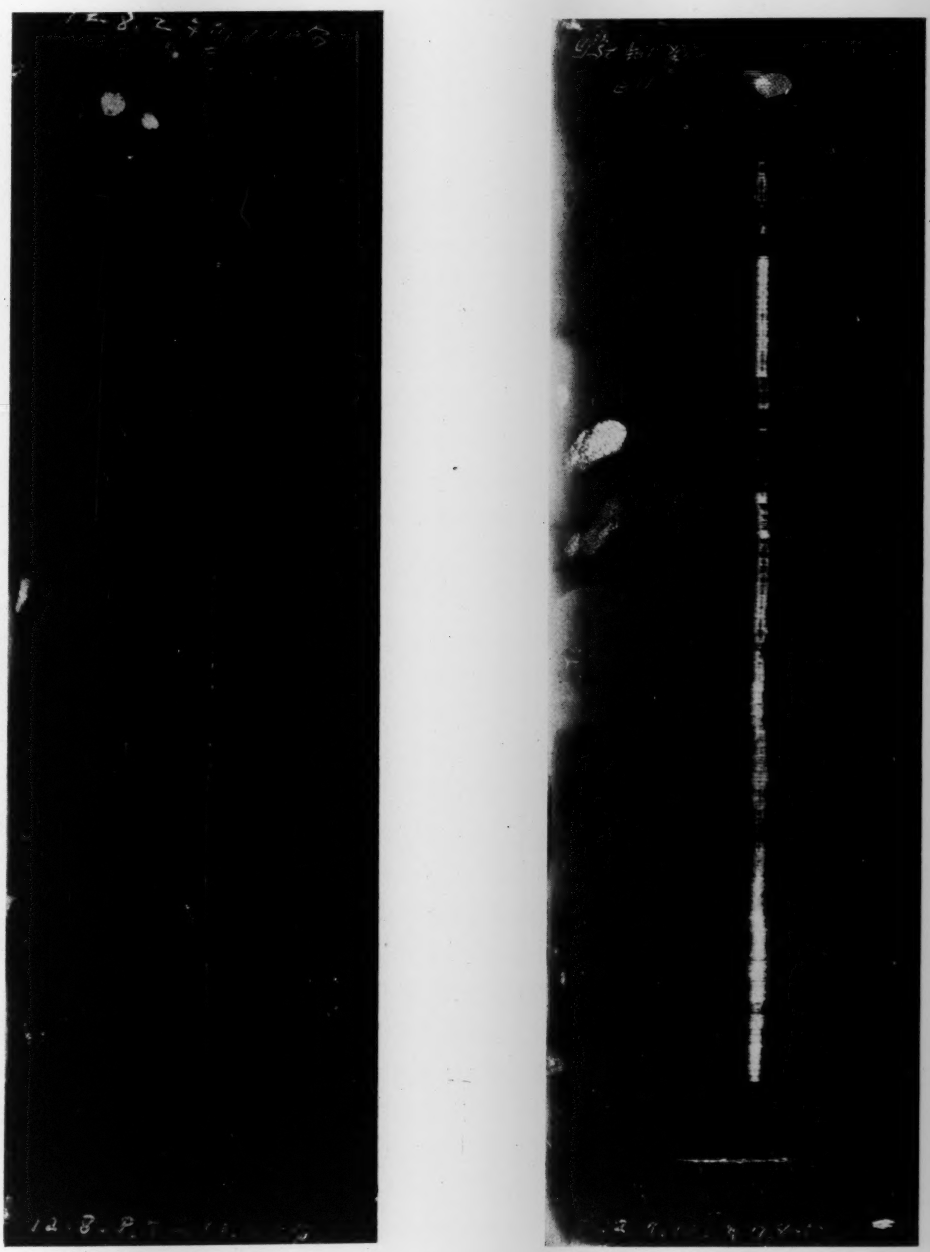

Fig. 15. Records obtained with the new seismograph which records direct on smoked paper the growth and decay of the tremors.

7

oscillations whose periods reach several seconds, which, since they were observed by K. Sassa at volcano Aso, we may expect also at Mihara when it is active. We may also expect surface waves of long period in the form of Love waves. As already stated, in order to increase our knowledge of the nature of the tremors to a further extent, measurements of the phase relations by rigidly controlled simultaneous observations are indispensable. We are now making preparations for solving these problems relating to the tremors in Oosima.

In conclusion, the writers wish to express their hearty thanks to the Hattori Hôkôkai, with the aid of whose grant the present measurements were made.

---

8. 大島三原火山の地球物理學的研究（第三報）

火山微動の測定

地震研究所　高橋龍太郎
永田　武
平能金太郎

倍率 2000 倍の逆立振子微動計を持ち廻つて，大島内に成る可く一樣になる樣に選定した十九の觀測點で微動の觀測を行つた，其の結果 2~3 の例外を除けば，微動は外輪山の内部では種々な周期から成る振動をしてゐるが，外輪山頂より外側では次第に單純な周期さなり，海岸に行くさ今度は不規則な振動が混る樣になる事が判つた．周期分析を行つた結果では 0·3 秒附近の周期の振動が湯場以外のごの觀測點にも現れる事が判つた．又各々の觀測點での微動の振幅を，西側外輪山の頂上にある御神火茶屋に据付けてある 400 倍微動計を基準さして調べて見るさ，微動の振幅は中央火口丘から離れるに從つて小さくなつて居り，其の減り方から考へて見るさ，微動は現在の火口底か或は其の直下 100 米以内の點から發生して居る周期 0·3 秒の衝擊に起されてゐる地表の二次的振動であるさ思はれる，

此の考に邪魔になる樣な，特に振幅の大きい點も特に小さい點もない．海岸での不規則な振動は多分海の波の爲に出來るものであらう．又中央火口丘での複雜な振動の原因，並に火口の方向の振幅が其れに直角な方向の振動よりも概して大きい事實は，中央火口丘の獨立の振動によるのであるか，又は火口底から出て來た波が途中で性質が變るのによるのか，只今の測つた結果だけでは判らない．

此の仕事は服部報公會から戴いた援助金で行つたもので，玆に同會に對し心からなる御禮を申上る次第である，

9. *Magnetic Surveys of Volcano Asama.*

By Takeshi MINAKAMI,

Earthquake Research Institute.

(Read Sept. 20, 1937.—Received Dec. 20, 1937.)

1. Introduction.

With the object of ascertaining the relations between volcanic activities in Japan and variations in the terrestrial magnetism that accompany these activities, S. T. Nakamura and Y. Kato made a study of the changes in the magnetic dip at the time of the activity of Volcano Komagadake[1], in Hokkaido, in 1929, the Sanriku earthquake in March, 1933, the Sizuoka earthquake[3] in July, 1934, the Yamato-Kawati[4] earthquake in January, 1936, and other activities of volcanoes and seismic zones, they found that the variations in the magnetic elements usually accompanied both these activities, and came to the conclusion that these magnetic variations that appeared in the neighbourhood of epicentres of earthquakes and in the case of volcanic activities are due to the heat changes in the disturbed crust caused by these activities. Quite recently, H. Hatakeyama[5] found the time variations in the magnetic quantities by comparing two series of results of magnetic surveys in Formosa, the one carried out in 1914 and 1924, and the other soon after the great earthquake on April 21, 1935, at the same stations as previously. He reported that these variations in terrestrial magnetism are distinctly related to crustal movement caused by the earthquakes just mentioned and the situation of the epicentre.

On the other hand, soon after the earthquake on Dec. 27, 1936, the epicentre of which was determined by T. Hagiwara[6] to be near Nii-Sima, T. Nagata[7] made magnetic dip surveys in the shaken regions, namely, Nii-Sima and Oo-Sima. After studying the previous surveys that had been made by S. Nakamura[8] in August, 1930, T. Nagata did not find any magnetic changes sufficiently marked to be put down as the result of the earthquake.

---

[1] S. T. NAKAMURA and Y. KATO, *Jap. Journ. Astr. Geophys.*, 12 *etc.*

[2] Y. KATO, *Disin*, (1935), 469, 529.

[3] Y. KATO reported at the annual seance of Physico-Mathematical Society of Japan in 1935, 1936.

[4] *loc. cit.*

[5] H. HATAKEYAMA, *Bull. Cent. Meteor. Obs. Jap.*, **6** (1937), 467.

[6] T. HAGIWARA, *Bull. Earthq. Res. Inst.*, **15** (1937), .

[7] T. NAGATA, *Bull. Earthq. Res. Inst.*, **15** (1937), 498.

In summarizing the results of magnetic measurements that have been made in connection with volcanic and seismic activities, it is clear that some of these activities were followed by no changes in terrestrial magnetism according to their magnitude of activities.

Some years ago, S. Nakamura[9] made magnetic dip surveys of Volcano Mihara, Oo-Sima island, while recently R. Takahasi and T. Nagata[10] carried out absolute measurements of the three components of terrestrial magnetism, namely, the declination, horizontal and vertical intensities, at the crater margin and at the base of Mihara. It would no doubt be interesting to study the variations in these magnetic quantities in view of the expected forthcoming activity of Volcano Mihara.

Although it is not difficult to imagine the existence of marked local anomalies in magnetism near the crater of an active volcano, T. Nagata[11] found that the eastward and westward anomalies in the magnetic declination at the margin of the crater of Mihara, as observed in Aug., 1937, as well as similar anomalies near the crater of Asama, as measured by T. Fukutomi[12] in 1930, are both separated by the N–S and E–W lines that intersect perpendicularly at almost the centre of each crater.

H. Nagaoka[13], who suspected that the magnetic variations that appear at the time of an explosion are rapid in character, made observations of the differentiated quantities of the vertical intensity of the terrestrial magnetism at Volcano Asama. With the results of these observations as basis, he studied the mechanism of occurence of the explosion and the underground structure near Asama, and at the same time, reported the existence of rapid changes of magnetic intensity at the time of explosions.

2. Present Surveys.

The present surveys of the magnetic dip at Volcano Asama were made with the object of obtaining an outline of the terrestrial magnetism of Asama as a whole to serve as the first step in the absolute measurements of the declination and the vertical and horizontal intensities to be shortly executed. Fortunately, we were able to use a dip circle, by courtesy of the Hydrographic Department, which had been tested in March, 1937, at the Magnetic Observatry, at Kakioka.

---

[8] S. Nakamura, *Disin* **6** (1934), 637.

[9] S. Nakamura, *loc. cit.*

[10] R. Takahasi and T. Nagata, *Bull. Earthq. Res. Inst.*, **15** (1937), 441.

[11] T. Nagata, *Disin* **9**, (1937).

[12] T. Fukutomi, *Disin* **2**, (1932).

[13] H. Nagaoka and T. Ikebe, *Proc. Imp. Acad. Tokyo*, **13** (1937) 30, 34, 62.

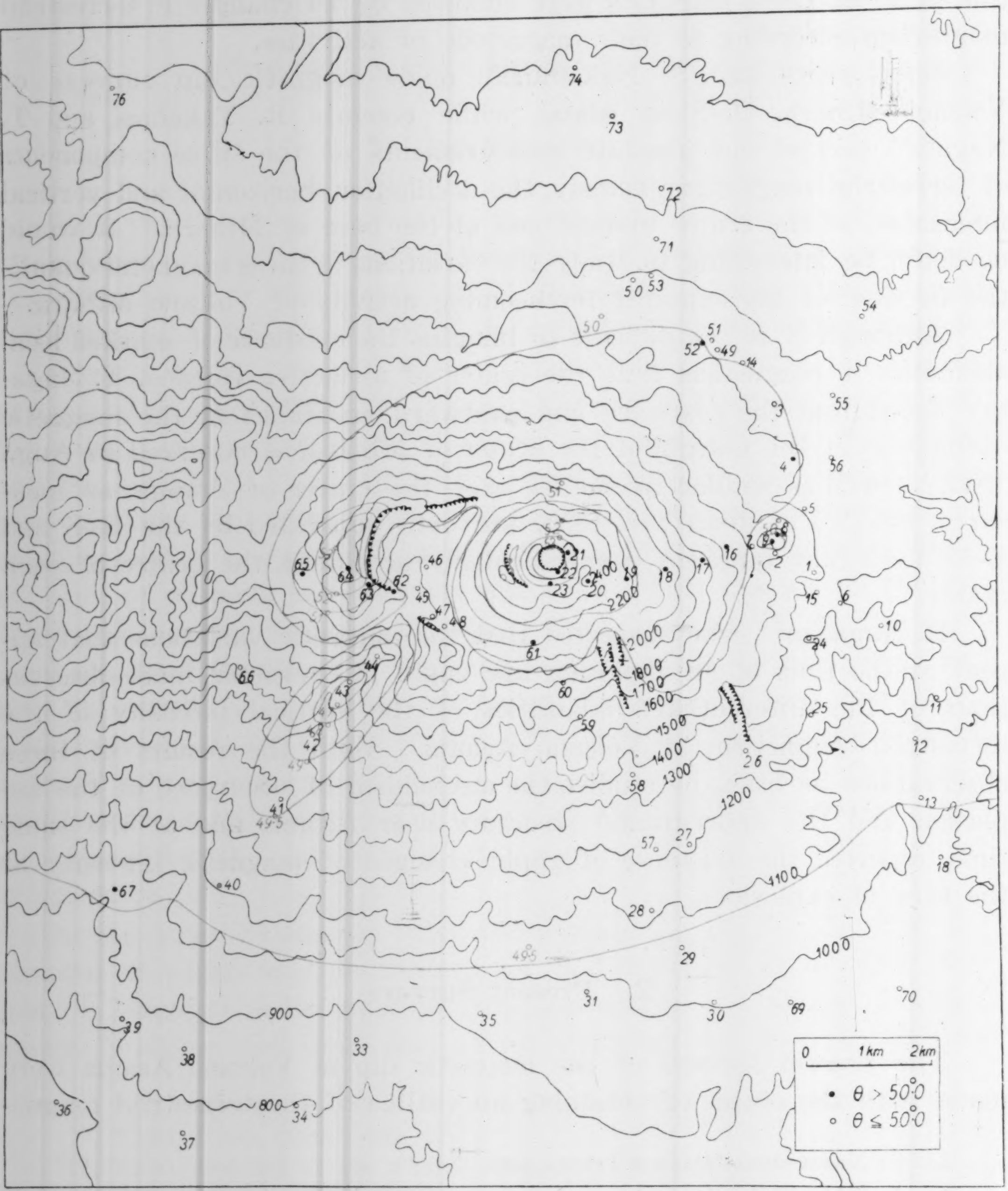
0 1km 2km
• θ > 50°0
◦ θ ≤ 50°0
2200
2000
1800
1700
1600
1500
1400
1300
1200
1100
1000
900
800
50°
49.5

Fig. 1. Isoclinic lines.

The present surveys were begun in May, 1937, and conducted at 76 stations until November, the same year. The results of these surveys of the magnetic dip form the subject of this paper, although these surveys are still being continued.

In Table I are given the latitudes and longitudes of the 76 stations, with their heights above sea level, and in Table II the dips and the dip anomalies (defined in following pages) and the dates and the times when the observations were made. The topography around the stations and the isoclinic lines are shown in Fig. 1. We find, first of all, that dip is intimately related to the topography. It will be seen from Fig. 1 that the dip generally increases with increase in the heights of the stations, although remarkably small dips are found for stations in the bottom of the ravine, notwithstanding the high altitudes of these stations above sea level. That is to say, the magnetic dip is affected distinctly by the gradient and the uneveness of the topography near the station. The contour lines at the principal mass of Volcano Asama are as a whole represented by closed curves—almost concentric circles with the crater as the center. Here the isoclinic lines also form closed curves approximately parallel to the contour lines. In order to show more clearly the corelation between dip and topography, the dips along

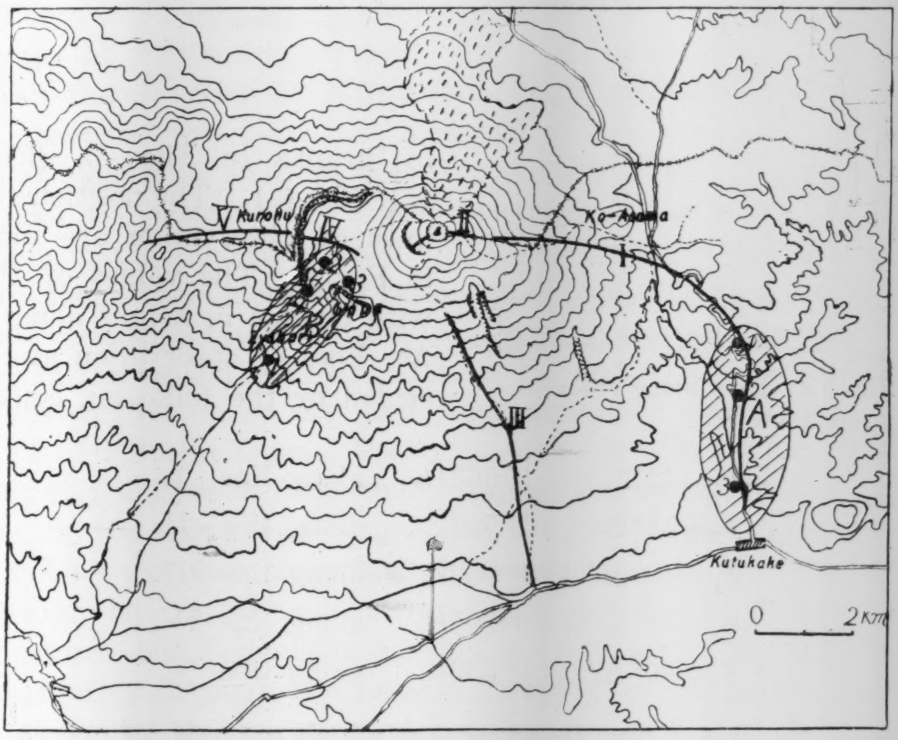

Fig. 2. Observation routes and regions A, B.

the lines of observation in radial directions from the summit to the foot of the volcano, and the heights of the stations above sea level are shown

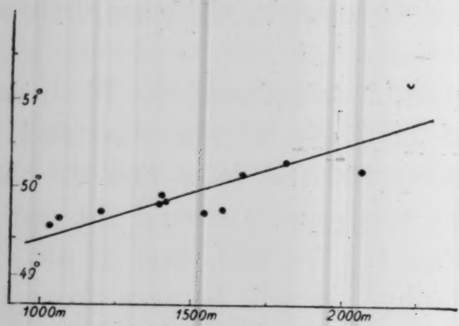

Fig. 3 a. Dips along observation route I.

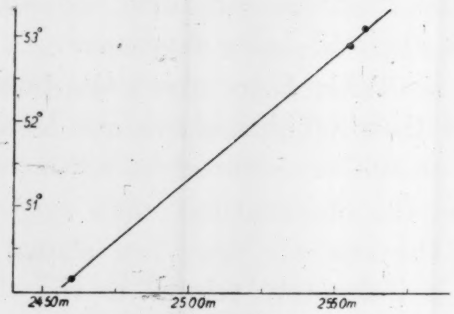

Fig. 3 b. Dips along observation route II.

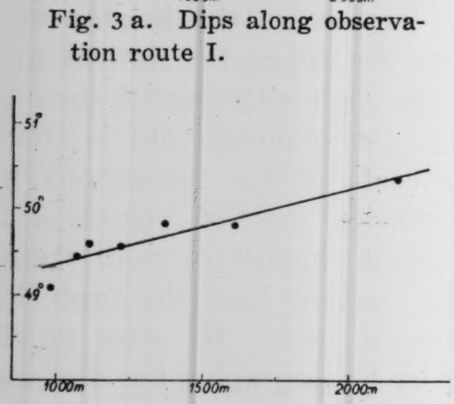

Fig. 3 c. Dips along observation route III.

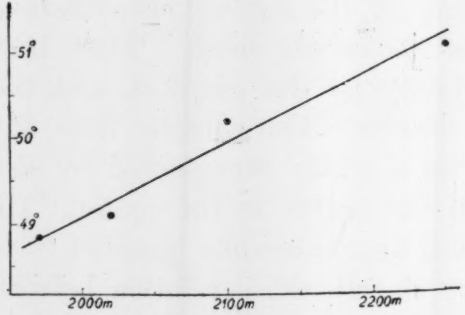

Fig. 3 d. Dips along observation route IV.

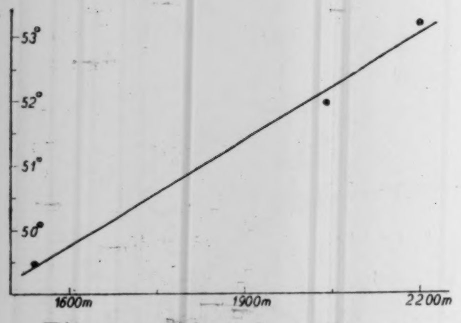

Fig. 3 e. Dips along observation route V.

by graphs in Figs. 3, (a), (b), (c), (d), (e). The positions of the lines of observation are indicated in Fig. 2. The values of the dip with change in height along every five lines of observation are represented by the following equations.

$$\theta_1 = 49°24'{\cdot}5 + 0'{\cdot}0631h \quad \text{along line I.}$$

$$\theta_2 = 51°21'{\cdot}1 + 1'{\cdot}787h \quad \text{along line II.}$$

$$\theta_3 = 49°30'{\cdot}9 + 0'{\cdot}053h \quad \text{along line III.}$$

$$\theta_4 = 48°59'{\cdot}3 + 0'{\cdot}605h \quad \text{along line IV.}$$

$$\theta_5 = 49°45'{\cdot}0 + 0'{\cdot}333h \quad \text{along line V.}$$

Along the line I and its extension which extends on over a simple topography from the S–E foot of the volcano, Kutukake, to the crater, the dips are better expressed by the quadratic equation

$$\theta = 49°19'{\cdot}7 + 0{\cdot}0464h + 0{\cdot}000049h^2,$$

where as the origin of h the lowest position of the lines of observation is taken, with the meter as unit. The increasing rates of dip along the various lines of observation markedly differ from one another, that is, the dip increases 6′·3, 178′·7, 5′·3, 60′·5, and 33′·3 with every 100 m increase in height.

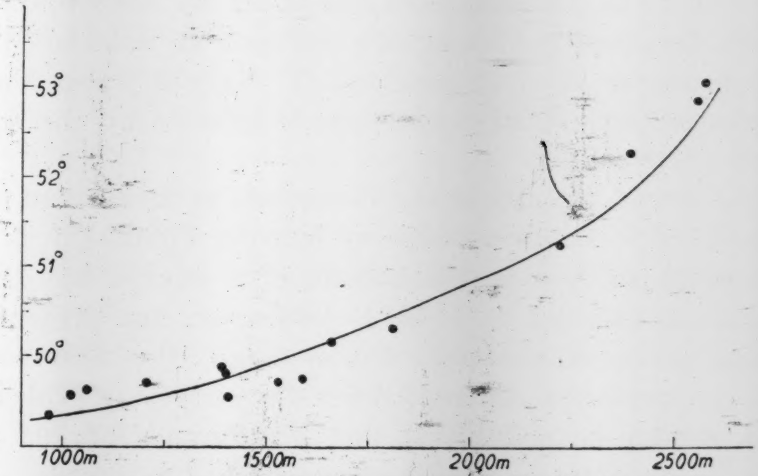

Fig. 4. Dips and heights above sea level along east route, from the foot of volcano to the summit.

There are many alternative explanations of these remarkable differences in the increasing rates of dip. Of these, the relative position between the direction of inclination of the mountain body, which is a huge magnetic mass, and the direction of the magnetic meridian, the steep and gentle inclinations according to the particular line of observation, and the concave or convex topography as a whole, all these differences in the conditions according to the lines passing through them, caused the various increasing rates. Moreover, line II is on the present central cone, lines I and III pass the slopes in an E–S directions from the crater in the second somma, and lines IV and V are on Kurohu-Yama, the first somma, in an east and west direction, respectively, from the summit of Kurohu-Yama. Owing to diversities in the magnetic permeability of the various lavas that compose the mountain, these local anomalies in the terrestrial magnetism are inevitable. The lava ejected does not always flow along the slope uniformly in all directions from the crater, but rather in a narrow belt as one usually sees on volcanoes; for example, the Temmei lava ran down the northern slope of Asama. Consequently, although the lines of observation are on the same mountain, owing to the varieties of lava ejected and to differences in the time they were ejected, the permeabilities of these lavas are not alike.

During the period from July 19 to July 27, 1937, the writer carried out similar surveys at Volcano Kusatu-Sirane, situated 25 km at Volcano

Asama. The result at the 8 stations on the margin of the crater of Kusatsu-Sirane show that the maximum, minimum, and mean values of dip were respectively 51°4′·3, 49°40′·7 and 50°19′·6, while at the 3 stations on the bottom of the crater the values of the dip were 49°17′·4, 49°7′·2, and 48°53′·5, the mean value being 49°6′·0. It was thus found that the former mean value exceeds the latter by 1°13′·6.

Moreover, the results of magnetic surveys at Volcano Mihara, Oosima island, made by R. Takahasi and T Nagata[14] also showed that the distribution of terrestrial magnetism is affected by the topography, which cannot be neglected.

Of the values of the dip at the 76 stations in the present survey, the maximum is 53°15′·5 on the summit of Kurohu-Yama, the first somma, and the minimum 46°29′·1 in the bottom of a ravine, the difference in the two values amounting to 6°46′·4. However, the present measurements do not cover Kengamine, Gippa-Yama, the first somma, and Amidagazyo, an explosion crater. When the survey of Volcano Asama is completed, it may be possibly to find a difference of 10° in the dip notwithstanding that the region is circumscribed to within a radius of 10 km only from the crater.

For convenience, the dip anomaly is expressed by

$$\theta_0=\frac{\Sigma\theta_i}{n}=49°40'{\cdot}8$$

$$\Delta\theta_i=\theta_i-\theta_0$$

$$n=76, \qquad i=1,\ 2,\ldots\ldots\ldots 76.$$

where,

θ_0 = mean value of dips at 76 stations,

θ_i = dip at each of the 76 stations,

n = total number of stations,

$\Delta\theta_i$ = dip anomaly.

It need hardly be said that the distributions of the dip anomaly as shown by means of iso-anomaly lines in Fig. 5, indicate the same tendency as those of the isoclinic lines. Generally speaking, however, the regions of positive and negative anomalies have been separeted by contour lines of 1400 metres, although there are regions of very large negative anomalies, notwithstanding that the regions are more than 1400 metres high, namely, the interiors of the first and the second sommas and the valley of the Zyabori river.

---

[14] R. TAKAHASI and T. NAGATA, *loc. cit.*

From the following quadratic equation which was obtained as the result of magnetic surveys of Japan made by the Hydrographic Department[15] in 1927, the value of the dip corresponding to the mean latitude and longitude of the 76 stations of Asama is given by

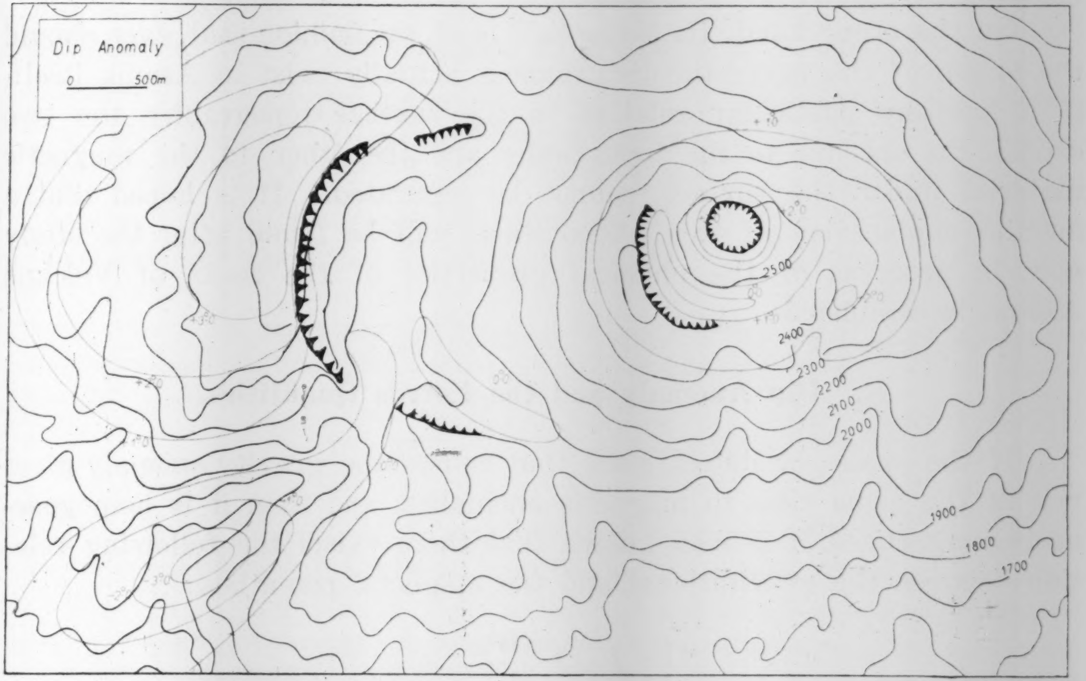

Fig. 5. Dip anomalies near the crater.

$$\theta_c = 34^\circ 4'\cdot 9 + 88'\cdot 61 \Delta\varphi - 3'\cdot 08 \Delta\lambda - 0'\cdot 768 \Delta\varphi^2 - 0'\cdot 2356 \Delta\varphi \Delta\lambda + 0'\cdot 1330 \Delta\lambda^2$$

$$\varphi_0 = \frac{\Sigma\varphi_i}{n}, \qquad \lambda_0 = \frac{\Sigma\varphi_i}{n}$$

$$\Delta\varphi = \varphi_0 - 25^\circ \qquad \Delta\lambda = \lambda_0 - 145^\circ \qquad \theta_0 - \theta_c = -16'\cdot 5$$

As the result of this, the calculated values of Volcanoes Asama and Sirane are 16′·5 and 18′·5 in excess of the mean observed values respectively. It is notable that the differences between the calculated and the observed mean values of the dip in the two volcanoes are very much smaller than the dip anomalies already referred to. It will be more logical to consider that the present surveys were conducted at a large number of stations regardless of whether they were situated on concave or convex topographies, with the result that the dip anomalies due to these complicated topographies have automatically cancelled one another. Consequently, the major part of the dip anomalies of Asama and Sirane is believed to be caused, not by the active volcanoes themselves nor by the presence of abnormal magnetic substances under the ground, but by the complex topography around the stations.

---

[15] *Bull. Hydrog. Dep.*, **8** (1936).

On the other hand, H. Nagaoka[16] is of the opinion that, even should the origin of the magnetic disturbances actually exist in Asama itself, if it has any particular relation to the surface topography, the two causes, the one due to the topography and the other to the magnetic material under the surface, cannot be separated. It is hoped that a definite explanation of this phenomenon will be found after the study now in progress of the physical properties of the rocks of Volcano Asama is completed.

3. Dip Anomaly and the Eötvös Quantities.

If the excess or defect mass that causes the gravity anomaly gives rise at the same time to magnetic anomalies, and then it is homogeneously magnetized, it is well known that there exists the following relation between the gravitational and the magnetic potentials:

$$P=J\frac{dW}{di}$$

P=the magnetic potential.
W=the gravitational potential.
J=intensity of magnetization.
i=direction of magnetization.

$$\frac{\partial P}{\partial x}=X, \qquad \frac{\partial P}{\partial y}=Y, \qquad \frac{\partial P}{\partial z}=Z, \tag{2}$$

where x, y, z are taken in the direction of magnetic north, magnetic east, and toward ground, and X, Y, Z are the two components of the horizontal intensity and the vertical intensity.

The three components of the normal values of the magnetic intensity at Asama, which are determined by the magnetic intensity distribution in Japan, as given by the Hydrographic Department, are represented by X_0, Y_0 and Z_0. At Asama the values of the dip are generally far larger than the dip anomaly, which enables us to make this calculation.

That is,

$$\frac{Z_0+Z}{\sqrt{(X_0+X)^2+(Y_0+Y)^2}}-\frac{Z_0}{\sqrt{X_0^2+Y_0^2}}\leqslant\frac{Z_0}{\sqrt{X_0^2+Y_0^2}}.$$

---

16) H. NAGAOKA, *loc. cit.*

Therefore, as already stated, for the present purpose, the calculated value of dip θ_c may be regarded as being to equal to the mean value of dip (θ_0), so that the dip anomaly $\varDelta\theta$ already mentioned, which is looked upon as due to the potential P, is expressed by the formula

$$\varDelta\theta=\frac{\sqrt{X_0^2+Y_0^2}\,Z-\sqrt{X^2+Y^2}\,Z_0}{\sqrt{X^2+Y^2}\{\sqrt{X_0^2+Y_0^2}+\sqrt{X^2+Y^2}\}}\times\frac{X_0^2+Y_0^2}{X_0^2+Y_0^2+Z_0^2} \qquad (3)$$

Formula (4) is the result of replacing X, Y, Z in formula (3) by the gravitational potential, W, namely,

$$\varDelta\theta=\frac{\dfrac{1}{G.f(s)}\cdot\left[\left\{\sqrt{X_0^2+Y_0^2}\left(\alpha\dfrac{\partial^2W}{\partial x\partial z}+\beta\dfrac{\partial^2W}{\partial y\partial z}+\gamma\dfrac{\partial^2W}{\partial z^2}\right)\right\}-Z_0\left\{\left(\alpha\dfrac{\partial^2W}{\partial x^2}+\beta\dfrac{\partial^2W}{\partial x\partial y}+\gamma\dfrac{\partial^2W}{\partial x\partial z}\right)^2+\left(\alpha\dfrac{\partial^2W}{\partial x\partial y}+\beta\dfrac{\partial^2W}{\partial y^2}+\gamma\dfrac{\partial^2W}{\partial y\partial z}\right)^2\right\}^{\frac{1}{2}}\right]}{\sqrt{X_0^2+Y_0^2}\left[\sqrt{X_0^2+Y_0^2}+\dfrac{1}{G.f(s)}\left\{\left(\alpha\dfrac{\partial^2W}{\partial x^2}+\beta\dfrac{\partial^2W}{\partial x\partial y}+\gamma\dfrac{\partial^2W}{\partial x\partial z}\right)^2+\left(\alpha\dfrac{\partial^2W}{\partial x\partial y}+\beta\dfrac{\partial^2W}{\partial y^2}+\gamma\dfrac{\partial^2W}{\partial y\partial z}\right)^2\right\}^{\frac{1}{2}}\right]}\times\cos^2\theta_0 \qquad (4)$$

where $G=$ gravity constant

$f(s)=$ density distribution

$$\sqrt{\frac{X_0^2+Y_0^2}{X_0^2+Y_0^2+Z_0^2}}=\cos\theta_0$$

and

$$\alpha=J\frac{\partial x}{\partial i},\qquad \beta=J\frac{\partial y}{\partial i},\qquad \gamma=J\frac{\partial z}{\partial i}.$$

Hence in formula (4), the intensity of magnetization was obtained experimentally and the density distribution, from the gravity surveys. Although there is no method of obtaining $\dfrac{\partial^2W}{\partial z^2}$ in the general case, if the problem is treated as a two dimensional one, all the Eötvös quantities required for the purpose are determined by torsion balance surveys. The results of the torsion balance surveys of Volcano Asama, in 1936, have been reported in the previous papers(17). The present magnetic surveys were conducted at the same 22 stations where the torsion balance surveys were made.

---

17) T. MINAKAMI, *Bull. Earthq. Res. Inst.*, **15** (1937), 50.

While study of the forthgoing two quantities, together with a comparison of the results, will be made on another occasion, in this paper the two kinds of quantities are compared only for the limited regions A, B as shown in Fig 6. A glance at these Figs. 6 and Table III will make clear the remarkable difference in the magnetic and gravitational characters of the two regions; that is, not only are the second derivatives of the gravitational potential and the dip anomalies at the three stations in region A almost similar to each other, but also the changes in dip anomalies in region A are parallel to those of the Eötvös quantities. On the other hand, these quantities in region B, at four stations, different much from each other and are distinctly larger than

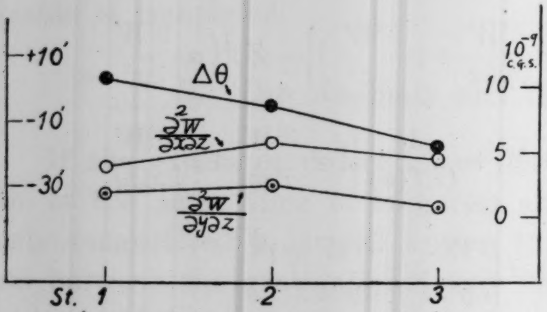

Fig. 6 a. Dip anomalies and Eötvös quantities in the region A.

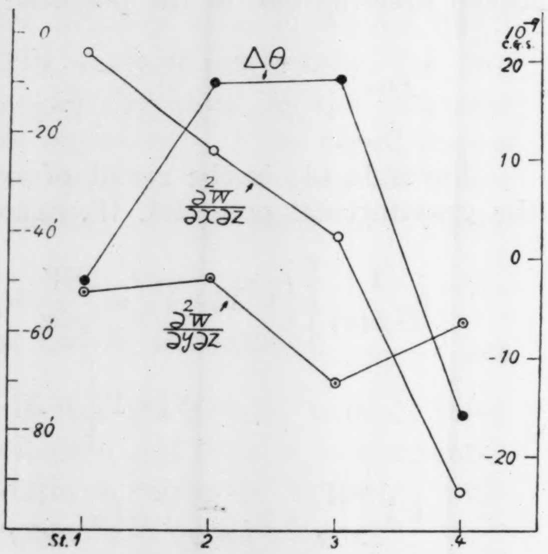

Fig. 6 b. Dip anomalies and Eötvös quantities in the region B.

Table III.

(a) (Observations in the A region)

Station	$\frac{\partial^2 W}{\partial x \partial z}$	$\frac{\partial^2 W}{\partial y \partial z}$	$\frac{\partial^2 W}{\partial y^2} - \frac{\partial^2 W}{\partial x^2}$	$2\frac{\partial^2 W}{\partial x \partial y}$	θ_i	$\Delta\theta_i$
Sengataki club	8·07	3·88	−12·22	0·35	49°43′·1	+ 3′·1
Sengataki lectur hall	11·79	5·13	− 8·98	−0·85	49°34′·8	.− 5′·5
Kutukake	9·91	1·48	−12·31	6·05	49°21′·2	−19′·1

(b) (Observations in the B region)

Station	$\frac{\partial^2 W}{\partial x \partial z}$	$\frac{\partial^2 W}{\partial y \partial z}$	$\frac{\partial^2 W}{\partial y^2} - \frac{\partial^2 W}{\partial x^2}$	$2\frac{\partial^2 W}{\partial x \partial y}$	θ_i	$\Delta\theta_i$
Asama-kan	20·91	− 7·17	−16·90	−1·61	48°50′·4	− 49′·9
Yunotaira	11·57	− 4·20	− 5·12	−0·44	49° 5′·5	− 10′·2
Tenguno-rozi	4·26	−25·06	− 9·20	2·82	49°28′·9	− 11′ 4
Yunotaira Obs.	−26·91	−14·91	−10·90	−1·33	48°23′·4	−1°16′·9

those of region A, but the similar tendency in both regions to parallelism of the magnetic anomalies and Eötvös quantities are obvious. Moreover, although region A has a very simple topography, region B has the most complicated topography in Volcano Asama, extending over Kurohu-Yama and Gippa-Yama, the first somma, and the deep valley of the Zyabori river, whereas the parallelism of the two kinds of quantities in the two regions A, B, is almost similar.

In order to further elucidate the gravitational and magnetic properties of Asama, it is hoped that it will be possible to measure the gravity $\left(\frac{\partial W}{\partial z}\right)$ and the other components of the terrestrial magnetism of Volcano Asama.

4. Accuracy of the Present Surveys.

It being known that according to the nature of the instrument, an error of one minute is unavoidable in the values indicated by the dip circle, every care was taken in the present surveys to reduce errors to the minimum, with which object, in the present surveys, the accuracy of observations were tested three times at the station near our Volcano Observatory.

The results of these tests made on October 15 are shown in Table IV, in which in the case of end A of a magnetized needle pointing N, the values of observation are represented in No. 1, 3, 5, 7, and in the case of the other end B magnetized to point N are shown in No. 2, 4, 6, 8. With the exception of the 6th value, the residuals in the same

Table IV.

No.	time	$\theta_i \pm \frac{m.g.\Delta l}{M} \cos\theta_i$	θ_i	$\theta_0 - \theta_i = \Delta\theta_i$
	h m			
1	13 13·0	50° 46′·9	49° 38′·0	−0′·4
2	13 26·0	48° 29′·0	49° 37′·9	−0′·5
3	13 32·0	50° 46′·7	49° 39′·1	+0′·7
4	13 39·5	48° 31′·4	49° 39′·2	+0′·8
5	13 50·0	50° 46′·8	49° 37′·7	−0′·7
6	14 00·0	48° 28′·5	49° 39′·5	+1′·1
7	14 8·0	50° 50′·5	49° 38′·1	−0′·3
8	14 16·0	48° 25′·6		

mean $\theta_0 = 49°38'{\cdot}4 \pm 0'{\cdot}4$

m; mass of needle. Δl; deviation of center of gravity.
g; acceleration of gravity. M; magnetic moment of needle.

table are less than one minute, and the probable error of the mean value is only ±0′·4. But, in the measurment of inversion once only, an error of observation of 1′ may be admissible.

Although the present surveys lasted a fairly long period of time, namely, during the period from May to November, 1937, no corrections of any kind have been made to present results, for the reason that the corrections were of such minute quantities as not to affect the results. On the other hand, one of our main objects is to know the extent to which volcanic activity causes variations in magnetism, when the results must be given the corrections due to daily variations, magnetic storm and the other causes. Moreover, whether or not the lava reservoir, as postulated by H. Nagaoka, really does exist in the neighbourhood of Asama, the distribution of time variations in terrestial magnetism which may be found by comparing the present results with those of observations repeated at intervals should throw some light on this problem.

5. Conclusion.

In this paper, the results are reported of magnetic dip surveys made at 76 stations around the crater of Asama, and it is pointed out that the magnetic dip is affected to a remarkable degree by the topography.

In conducting these surveys, it was fully realized that in observations of this kind, it it neccesary not only to execute the work as accurately as possible, but also, to have as many stations as possible in order to study the underground structure from measurments of gravity and of terrestrial magnetism.

As to the explanation of the dip anomaly, this is scarcely possible until the permeability of the lavas of Asama has been determined. Since the mountain consists of many kinds of lava and lavas that were ejected at various periods, it is natural to expect the presence of lavas of different permeabilities according to the part of Asama whence it is derived. On the other hand, the study of the permeability of Asama is related to the problem how lava of high temperature of about 1000°C at the time of ejection, came to be magnetized with its cooling.

For observing Volcano Asama, besides a variometer for the vertical intensity of magnetism designed by H. Nagaoka(18), at each of two stations, a declination-variometer also at each of the two stations, and a dip-variometer designed by T. Nagata(19) at one station were set up during the year.

---

18) H. NAGAOKA, *loc. cit.*

19) T. NAGATA, *Bull. Earthq. Res. Inst.*, **15** (1937), 185.

In conclusion, the writer wishes to express his hearty thanks to the Hydrographic Department for the loan of the dip circle and other courtesies shown. He also acknowledges his great indebtedness to the Foundation for the Promotion of Scientific and Industrial Research of Japan, with whose grant the present surveys were made possible.

Table I.

station	height	latitude	longitude	station	height	latitude	longitude
1	1405 m	36°24′14″	138°34′17″	34	790 m	36°19′19″	138°28′38″
2	1530	24′10″	34′50″	35		19′21″	24′39″
3	1392	25′25″	33′43″	36	810	19′19″	25′22″
4	1410	25′ 2″	34′ 8″	37	765	18′59″	27′26″
5	1400	24′33″	34′14″	38	855	19′49″	27′28″
6	1390	23′46″	34′32″	39	820	20′ 5″	26′46″
7	1590	24′17″	33′40″	40	1110	21′20″	28′ 3″
8	1655	24′25″	33′56″	41	1265	22′ 4″	28′27″
9	1630	24′19″	33′52″	42	1395	22′38″	28′47″
10	1400	23′36″	35′00″	43	1560	23′10″	29′39″
11	1205	22′52″	35′30″	44	1640	23′36″	29′57″
12	1060	22′26″	35′24″	45	2020	23′56″	29′59″
13	1020	21′42″	35′24″	46	2030	24′ 9″	30′ 5″
14	1370	25′38″	33′26″	47	1990	23′41″	30′ 7″
15	1375	23′53″	34′18″	48	2005	23′36″	30′13″
16	1660	24′17″	33′26″	49	1345	26′ 1″	33′ 6″
17	1810	24′ 6″	32′54″	50	1315	26′35″	32′17″
18	2060	24′ 2″	32′41″	51	1332	26′ 9″	33′10″
19	2220	23′54″	32′14″	52	1346	26′11″	32′56″
20	2390	24′ 2″	31′43″	53	1315	26′33″	32′30″
21	2560	24′24″	31′35″	54	1245	26′11″	34′42″
22	2555	24′ 7″	31′27″	55	1320	25′35″	34′26″
23	2485	24′ 1″	31′25″	56	1375	24′59″	34′26″
24	1310	23′25″	34′11″	57	1220	21′33″	32′30″
25	1290	22′46″	34′ 6″	58	1370	22′13″	32′19″
26	1250	21′25″	33′34″	59	1600	23′ 4″	31′51″
27	1215	21′47″	32′54″	60	1800	23′28″	31′40″
28	1110	21′ 2″	32′28″	61	2100	23′49″	31′13″
29	1065	20′54″	32′42″	62	2180	23′54″	29′47″
30	1012	20′21″	33′ 2″	63	2300	24′ 1″	29′23″
31	974	20′18″	31′51″	64	2160	23′ 3″	29′ 9″
32	935	20′ 8″	30′43″	65	1540	21′16″	27′17″
33	858	19′57″	29′25″	66	950	21′35″	26′46″

(to be continued.)

Table I. (*continued.*)

station	height	latitude	longitude	station	height	latitude	longitude
67	950 m	36°21′16″	138°26′46″	72	1175 m	36°27′30″	138°32′32″
68		21′35″	35′46″	73	1150	28′ 1″	32′ 8″
69	985	20′24″	35′ 1″	74	1110	28′32″	31′37″
70	955	26′39″	35′21″	75	1045	29′11″	30′56″
71	1255	25′13″	32′30″	76	1220	28′24″	26′48″

Table II.

station	date	time	dip (θ_i)	anomaly ($\Delta\theta_i$)
		h m		
1	June, 11	14 20	49° 31′·2	− 12′·7
2	〃	17 5	49° 40′·4	− 3′·5
3	〃 12	13 25	50° 17′·5	+ 33′·6
4	〃	14 54	50° 21′·5	+ 37′·6
5	〃	16 5	49° 32′·8	− 11′·1
6	〃	17 28	49° 54′·1	+ 10′·2
7	〃 14	11 55	49° 42′·6	− 1′·3
8	〃	13 17	50° 41′·5	+ 57′·6
9	〃	14 26	50° 1′·5	+ 17′·6
10	〃 18	9 45	49° 48′·5	+ 4′·6
11	〃	11 10	49° 43′·1	− 0′·8
12	〃	12 21	49° 39′·1	− 4′·8
13	〃	13 34	49° 34′·8	− 9′·1
14	〃	15 1	50° 36′·1	+ 52′·2
15	〃	17 10	49° 31′·6	− 12′·3
16	〃 19	9 29	50° 9′·6	+ 25′·7
17	〃	10 29	50° 17′·9	+ 34′·0
18	〃	11 37	50° 8′·7	+ 24′·8
19	〃	12 56	51° 14′·5	+1° 30′·6
20	〃	14 18	52° 20′·2	+2° 36′·3
21	〃	16 22	52° 53′·7	+3° 9′·8
22	〃	17 6	53° 5′·5	+3° 21′·6
23	〃 23	12 28	50° 9′·3	+ 25′·4
24	〃	13 52	49° 31′·4	− 12′·5
25	〃	14 54	49° 39′·9	− 4′·0
26	〃	16 4	49° 13′·7	− 30′·2
27	〃	17 5	49° 22′·7	− 21′·2
28	〃	18 8	49° 36′·4	− 7′·5
29	〃 24	9 22	49° 26′·8	− 17′·1

(*to be continued.*)

Table I1. (*continued.*)

station	date	time	dip (θ_i)	anomaly ($\Delta\theta_i$)
		h m		
30	June, 24	10 53	49° 3′·1	− 40′·8
31	″	12 28	49° 26′·8	− 17′·1
32	″	14 14	49° 34′·7	− 9′·2
33	″	15 55	48° 59′·5	− 44′·4
34	″	15 55	49° 36′·3	− 7′·6
35	″ 28	18 19	50° 4′·6	+ 20′·7
36	″	12 20	49° 33′·4	− 10′·5
37	″	14 3	49° 43′·4	− 0′·5
38	″	15 37	49° 57′·7	+ 3′·8
39	″	16 55	49° 29′·3	− 14′·6
40	″ 30	12 5	49° 31′·1	− 12′·8
41	″	13 36	49° 8′·0	− 35′·9
42	″	15 1	48° 50′ 4	− 53′·5
43	July, 1	16 0	46° 29′·1	−3° 14′·8
44	″	15 0	48° 23′·4	−1° 20′·5
45	″	8 35	49° 5′·5	− 38′·4
46	″	10 1	49° 55′·1	+ 7′·2
47	″	11 13	48° 51′·9	− 52′·0
48	″	12 0	49° 28′·9	− 15′·0
49	″ 8	13 53	49° 17′·8	− 26′·1
50	″	15 0	48° 34′·4	−1° 9′·5
51	″ 9	14 31	49° 19′·3	− 24′·6
52	″	16 1	50° 12′·5	+ 28′·6
53	″	15 36	50° 2′·3	+ 18′·4
54	″ 11	16 51	49° 50′·7	+ 6′·8
55	″	16 1	49° 23′·3	− 20′·6
56	″	15 10	49° 44′·8	+ 0′·9
57	Sept., 5	9 35	49° 33′·7	− 10′·2
58	″	10 35	49° 51′·2	+ 7′·3
59	″	12 3	49° 48′·6	+ 4′·7
60	″	13 51	49° 34′·2	− 9′·7
61	″	15 21	50° 20′·8	+ 36′·9
62	″ 6	8 30	50° 11′·3	+ 29′·4
63	″	11 4	51° 4′·9	+1° 21′·0
64	″	13 5	53° 15′·5	+3° 31′·6
65	″	14 20	51° 57′·0	+2° 13′·1
66	″	15 58	49° 28′·3	− 15′·6
67	″ 7	10 26	50° 38′·3	+ 54′·4
68	″ 14	12 47	49° 20′·4	− 23′·5

(*to be continued.*)

Table II. (*continued.*)

station	date	time	dip (θ_i)	anomaly ($\Delta\theta_i$)
		h m		
69	Sept., 14	13 25	49° 38′.3	− 5′·6
70	〃	14 34	49° 21′·2	− 22′·7
71	Nov., 7	10 11	49° 42′·7	− 1′·2
72	〃	11 5	50° 2′·2	+ 18′·3
73	〃	12 11	49° 30′·1	− 13′·8
74	〃	13 30	49° 37′·8	− 6′·1
75	〃	14 27	49° 52′·6	+ 8′·7
76	8	8 31	49° 59′·0	+ 15′·1

9. 淺間火山の磁氣測量(其の 1)

地震研究所 水上 武

淺間火山の火口を中心として，76點に於いて磁氣伏角の測定を行ひ地形の影響の著しい事を指摘した．尙又伏角の異常と重力偏差の關係を示し，兩者は略平行する事を示した．磁氣の他の成分の測定並に重力の測定を行ふと共に山體を形成する熔岩の物理的性質の究明は，今後の淺間火山の研究に於いて最も望ましいものの一つである．

今同，測定を施行するに當り，伏角計の使用を許可され，且種々便宜を與へられたる海軍水路部に對し，且又日本學術振興會の補助により，測定を行ひ得た事に對し共に，厚く感謝の意を表す．

10. *Magnetic Surveys of Volcano Kusatu-Sirane.*

By Takeshi MINAKAMI,

Earthquake Research Institute.

(Read Sept. 21, 1937.—Received Dec. 20, 1937.)

The Kusatu-Sirane volcano, Gumma prefecture, lies about 25 km from Asama, one of the most active volcanoes in Japan. Our Observatory of Volcano Asama, which is situated 4 km east of the crater of Asama, commands a view of the summit of Volcano Sirane, from which we may sometimes see the vapour issuing from Yugama, one of the craters on the summit of Volcano Sirane. The northern skirt of Asama and the southern foot of Sirane are bordered by the Agatuma river, the upper course of the Tone river, so that in some of the cliffs forming the banks of this river, one meets with layers of volcanic material traceable to these two volcanoes.

Although Volcano Sirane does not nowadays show any sign of activity, marked explosive activity manifested itself in October, 1932, on which occasion H. Tsuya,(1) notwithstanding the explosions near the crater, made personal observations and reported the results in the Bulletin.

In the volcanic phenomena displayed during explosions, the two volcanoes, Sirane and Asama, show a decided contrast. In the case of Asama, it is noticed that it throws out juvenile lava from the crater, and from the crater only, in the form of volcanic bombs and ash, while in the case of Sirane, it ejects ancient lava material that formed a part of the margin of the craterlets and fissures on the mountain slope, while no young lava are ejected from the crater nor from the fissures on the crater wall and the central cone. The history of volcanic activities of these two volcanoes shows that Asama enjoys a calm period almost regularly for 2 or 3 years after every similar period of continued activity, during which hundreds of explosions in all degrees of intensity occur, whereas of the activities of Volcano Sirane since historical times, we have only the following records.

---

1) H. TSUYA, *Bull. Earthq. Res. Inst.*, **11** (1933), 82.
Disin **4** (1932), (in Japanese).

(1) Aug. 6, 1882.

On the night of the 6th, an explosion in the interior of Yugama (water boiler) and its vicinity occurred with detonations and ejection of mud and ash, by which the trees and bushes on the peripheries and the margins of the craters, Yugama, Mizugama, and Karagama were completely destroyed. It is reported that as the result of this explosion, the water in Yugama rose in temperature and the water of Yumiike, a small crater lake, and of Mizugama exhibited changes in their chemical properties.

(2) July 8, 1897.

Since the latter part of May, detonations and earth-tremblings were noticed near the crater. They occurred in Yugama at the northeastern part of the center of the former explosion, with ejection of ash, which fell at Kusatu, distant 10 km E-SW from the crater.

July 31, 1897.

An explosion occurred in Yugama, ejecting numbers of large rocks about 160 kg to distances as 900 m. The activity lasted till Aug. 16, the same year.

(3) Oct. 1, 1900.

Activity reported, but without details.

(4) July 15, 1902.

The center of this activity was the northeastern part of Yumiike (see Fig. 1), instead of Yugama, the center of the former explosions, which was inactive and showed no signs out of the ordinary.

Aug. 20, 1902.

The second explosion occurred in the same part as the explosion of July 15, but less violently.

Sept. 4, 1902.

Explosions occurred near Yumiike and rained volcanic ash at Manza-Onsen, a hot spring, at its S-W foot, 3 km from the center of explosion.

Sept. 17, 1902.

An explosion occurred with detonations and ejection of rocks, and ashes which fell 2 km away. A column of black vapour shot up from the crater.

(5) Oct. 1905.

Explosions occurred in the hot-water pool in Yugama, and threw out large quantities of sulphur which fell into the Agatuma river.

(6) Jan. 22, 1925.

An explosion occurred in the northern part of Yugama, with ejection of rocks and ashes.

(7) Dec. 31, 1927.

Violent explosions occurred in the interior of Yugama and the southern slope of the present central cone. A remarkable phenomena accompanied the explosions in that the water in Yugama rose in temperature from 15°C to 24°C and its water level sank about 14 m.

(8) Oct. 1932.

On October 1, explosions occurred in the N-E part of the interior of the crater-wall of Yugama, and in the numerous fissures on the S-E slope of the central cone, that is, in a direction south of Yugama. This activity began 14h on October 1, and ended after the explosion at 9h on October 27, the same year. At the time of the first explosion, two workers in Yugama were killed and seven wounded by falling rocks.

As above described, the fact that the craterlets and fumaroles, that is, the centers of explosion, change with every volcanic activity, is one of the most outstanding characteristics of Volcano Sirane. In Fig. 1. are shown the movements of these centers of explosion.

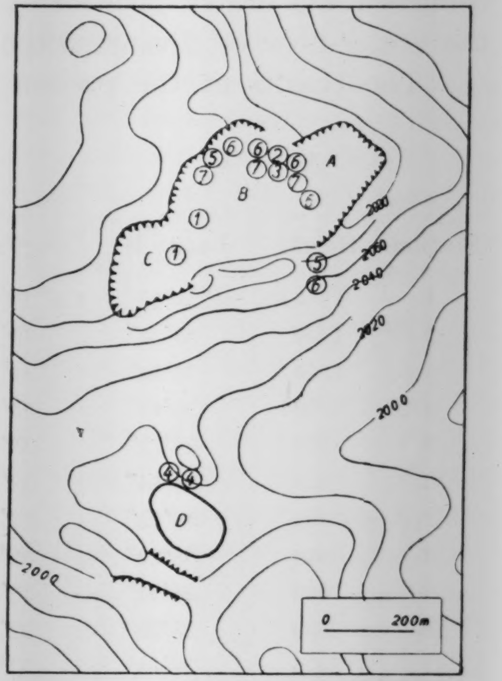

Fig. 1. Centers of explosions.

A; Mizugama. B; Yugama.
C; Karagama. D; Yumiike.
① Aug. 6, 1882.
② July 8, 1897.
③ Oct. 1, 1900.
④ July 15, 1902.
⑤ Jan. 22, 1925.
⑥ Dec. 31, 1927.
⑦ Oct. 30, 1932.

Dip Surveys.

Although geological and petrological studies of Volcano Kusatu-Sirane have been made by R. Ôhashi[2] and H. Tsuya,[3] nothing has yet been attempted from the geophysical point of view. Although as described above, the activity of Sirane is not so vioient as that of Asama, the study of the mechanism of explosion and the internal construction of volcanoes like that of Sirane is no less important and interesting than those of Asama. There is moreover the statement of the villagers of Asama and Sirane that the activities of the latter usually occurred when the former was inactive, so that, the existence of some geophysical relation between Asama and Sirane has to be considered. It is interesting to make clear the problem by the scientific method, seeing that the existence of some connections of lava-pits between Volcanoes Kilauea and Mauna-loa at Hawaii, is recognized by some volcanologists.

---

[2] R. Ôhashi, *Bull. Imp. Earthq. Invest. Comm.*, (1913), (in Japanese)

[3] H. Tsuya, *Bull. Earthq. Res. Inst.*, **12** (1933), 52.

As the first step in studying Sirane from the geophysical stand-point, the author carried out magnetic dip surveys at 40 stations within and at the circumference of the present crater, during the period between August 19 and 28, 1937. The instrument was a dip circle of the Hydrographic Department, which is the same instrument that was used at Asama. Although such a survey cannot be executed for the time being on the crater floor of Asama, it was done at three stations on the crater-floor of Sirane, without any difficulty.

The results of the present observations are given in Tables I, II, with the situations of the stations and the date and times of observation. The isoclinic lines near the crater, together with the contours, are given in Fig. 2, a glance at which shows the remarkable effects of

Table I.

Station	Height	Latitude	Longitude	Station	Height	Latitude	Longitude
1	1200 m	36°37′45″	138°35′48″	21	2150 m	36°38′87″	138°32′ 6″
2	1340	38′ 0″	35′ 6″	22	2120	38′34″	32′21″
3	1520	38′18″	34′11″	23	2080	38′25″	32′25″
4	1700	38′45″	33′37″	24	2090	37′22″	32′27″
5	1825	39′ 3″	33′ 9″	25	2040	37′47″	32′13″
6	2085	38′34″	32′31″	26	2050	38′42″	32′15″
7	2080	38′11″	32′ 9″	27	2090	38′29″	32′22″
8	2060	38′22″	32′ 8″	28	2010	38′45″	32′39″
9	2060	38′26″	32′17″	29	1930	38′50″	32′55″
10	2060	38′25″	32′15″	30	1850	38′52″	33′ 8″
11	2075	38′16″	32′19″	31	1760	38′22″	30′53″
12	2120	38′24″	32′11″	32	1940	38′19″	31′22″
13	2085	38′21″	32′25″	33	2040	38′14″	31′49″
14	2045	38′17″	32′15″	34	1740	38′18″	30′50″
15	2030	38′ 5″	32′10″	35	1835	39′ 7″	33′14″
16	1940	38′27″	32′55″	36	1980	37′11″	32′42″
17	1990	38′22″	32′54″	37	1950	37′48″	33′12″
18	2080	37′56″	32′18″	38	1860	37′14″	33′22″
19	2140	38′32″	32′ 1″	39	1470	37′32″	34′30″
20	2160	38′29″	31′53″	40	1300	37′12″	35′28″

Table II.

Station	Date	Time	Dip (θ_i)	Anomaly ($\Delta\theta_i$)
1	July, 19	$8^h 50^m$	49° 58′·3	+ 1′·5
2	〃	9 45	49° 59′·2	+ 2′·4
3	〃	10 49	50° 11′·1	+ 14′·3
4	〃	12 29	52° 23′·9	+2° 27′·1
5	〃	14 00	50° 12′·7	+ 15′·9
6	〃	15 21	50° 19′·0	+ 12′·2
7	July, 20	8 34	50° 2′·3	+ 5′·5
8	〃	9 14	49° 17′·4	− 39′·4
9	〃	10 4	49° 7′·2	− 49′·6
10	〃	11 10	48° 53′·5	−1° 3′·3
11	〃	12 43	50° 16′·3	+ 9′·5
12	〃	13 39	51° 4′·3	+1° 7′·5
13	July, 21	8 51	50° 7′·4	+ 10′·6
14	〃	9 40	49° 40′·3	− 16′·5
15	〃	10 28	49° 42′·9	− 13′·9
16	〃	12 6	49° 55′·1	− 1′·7
17	〃	13 10	50° 16′·3	+ 19′·5
18	〃	14 18	49° 55′·0	− 1′·8
19	July, 23	8 28	50° 55′·7	+ 58′·9
20	〃	9 17	50° 23′ 2	+ 26′·4
21	〃	10 1	50° 4′·9	+ 8′·1
22	〃	10 45	49° 40′·7	− 16′·1
23	July, 24	9 40	49° 53′·3	− 3′·5
24	〃	10 21	50° 29′·0	+ 32′·2
25	July, 23	12 58	49° 25′·6	− 31′·2
26	〃	13 44	48° 50′·3	−1° 6′·5
27	July, 24	9 00	50° 38′·1	+ 41′·3
28	〃	11 15	49° 52′·5	− 4′·3
29	〃	12 12	50° 24′·3	+ 27′·5
30	〃	12 53	50° 11′·1	+ 14′·3
31	July, 22	7 41	49° 15′·6	− 41′·2
32	〃	8 45	49° 36′·6	− 20′·2
33	〃	9 44	49° 34′·3	− 22′·5
34	〃	10 55	49° 21′·9	− 34′·9
35	July, 24	13 39	49° 46′·2	− 10′·6
36	July, 26	8 43	49° 59′·3	+ 2′·5
37	〃	9 39	49° 38′·3	− 18′·5
38	〃	10 41	49° 24′·4	− 32′·4
39	〃	11 19	49° 37′·3	− 19′·5
40	〃	12 22	49° 28′·4	− 28′·4

topography, while the values of the dip increase with the height of the station. In addition, the results of the present surveys show that the

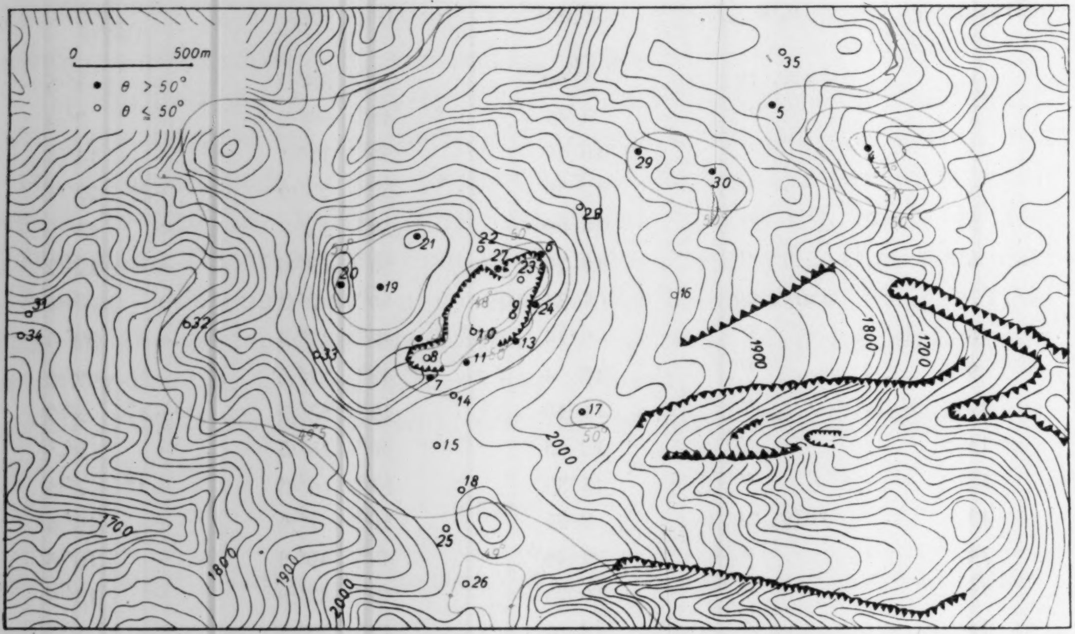

Fig. 2. Isoclinic lines.

values at stations situated higher than 2000 m above sea level, mostly exceed 50°, whereas the values on the crater-floor are very much smaller although their heights are more than 2000 m above sea level, being greatly affected by the abnormal topography. The dips at 11 stations situated on the crater floor and on the margin of the crater are connected with the heights of the stations with the following relations. (see Table III and Fig. 3.)

$$\theta'_0 = \frac{\Sigma\theta'_i}{n}, \qquad \Delta\theta'_i = \theta'_i - \theta'_0$$

$$h'_i = \frac{\Sigma h'_i}{n}, \qquad \Delta h'_i = h'_i - h'_0$$

$$\left(\begin{array}{l} n = 11 \\ i = 1,\ 2, \ldots\ldots 11 \end{array} \right.$$

where

θ'_i; dip at stations on the crater-floor and on the margins, of the crater-wall,

θ'_0; mean dip,

h'_i; height above sea level of the stations above mentioned,

h'_0; mean height.

Table III.

Station No.	Dip. (θ_i)	Height of Station (h_i)	$\varDelta\theta_i$	$\varDelta h_i$
6	50° 19′·0	2085 m	+18′·4	+10 m
7	50° 2′·3	2080	+ 1′·7	+ 5
8	49° 17′·4	2050	−43′·2	−25
9	49° 7′·2	2040	−53′·4	−35
10	48° 53′·5	2040	−67′·1	−35
11	50° 16′·3	2098	+15′·7	+ 3
12	51° 4′·3	2120	+63′·7	+45
13	50° 7′·4	2085	+ 6′·8	+10
23	49° 53′·3	2080	− 7′·3	− 5
24	50° 29′·0	2090	+28′·4	+15
27	50° 38′·1	2095	+37′·5	+20

mean $\theta_0=50°\ 0'{\cdot}6$ mean $h_0=2075$ m

In **Fig.** 3, the linear relation between $\varDelta\theta_i$ and $\varDelta h_i$ is that as seen at Asama.

Of the dips of 40 stations, the maximum and the minimum are 52° 23′·9 at station 4 at Yosinotaira and 48° 50′·3 at station 28 on the crater-floor. The mean dip of these 40 stations is as follows.

$$\theta_0=\frac{\Sigma\theta_i}{n}=49°\quad 56'{\cdot}8$$

$$\varphi_0=\frac{\Sigma\varphi_i}{n}=36°\quad 38'.1$$

$$\lambda_0=\frac{\Sigma\lambda_i}{n}=138°\quad 33'{\cdot}1$$

$$\left(\begin{array}{l} n=40 \\ i=1,\ldots\ldots 40 \end{array}\right.$$

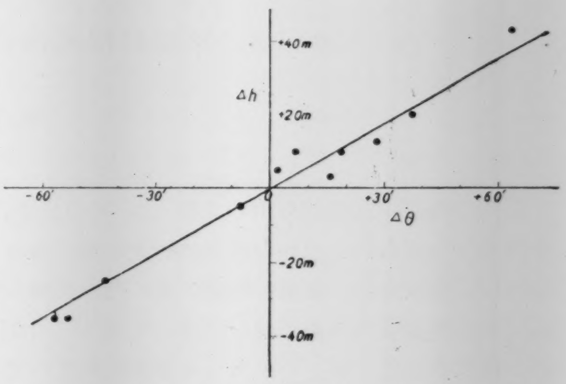

Fig. 3. Dip anomalies near the craters.

where φ_0, λ_0 are the mean latitude and longitude of the 40 stations. The value of the dip corresponding to the mean latitude and the longitude (φ_0, λ_0) calculated from the quadratic equation determined by the Hydrographic Department, is 50° 15′·3 The calculated value is 18′·5 in excess of the mean observed value, which tendency is the same as that at Asama.

$$\varDelta\theta_i=\theta_i-\theta_0$$

For our purpose, the remainders ($\varDelta\theta_i$) above defined are called here dip anomalies. From the distribution of these dip anomalies with reference to the topography, it is clear that there is an intimate corelation between the dip and the topography around the station, that is, the isoclinic lines and the iso-anomaly lines are parallel to the contour lines.

Although an outline of the magnetic character of Volcano Kusatu-Sirane has been obtained by the present surveys, one of our main objects was to bring out clearly the time variations in the magnetic changes that accompany volcanic activity, so that in order to facilitate resurveys, the stations where the present surveys were made have been marked by posts driven into the ground. It is hoped to repeat the magnetic surveys and other geophysical studies of Volcano Kusatu-Sirane.

In conclusion, the author wishes to express his hearty thanks to the Hydrographic Department for the loan of the dip circle. He also acknowlgdges his great indebtedness to the Foundation for the Promotion of Scientific and Industrial Research of Japan, with whose grant this study was made possible.

---

10. 草津白根火山の磁氣測量（其の 1）

地震研究所 水上武

草津白根火山は淺間火山の北約 25 粁の位置にあり，淺間火山に最も接近せる活火山である．今回草津白根火山の地球物理學的研究の第一歩さして，火口內外 40 點に於いて磁氣伏角の測定を行ひ，白根火山の磁氣の狀態，並に火山活動に伴ふ磁氣變化を明かにせんさ企てた．2, 3 年後或は火山活動後に再測し度いさ考へて居る．今回の測定を施行するに當り伏角計の使用を許可された海軍水路部に對し，尙又日本學術振興會の補助により測定を行ひ得た事に對し，共に厚く感謝の意を表す．

Station 5, Yosinotaira.

Station 8, Karagama.

Station 9, Yugama.

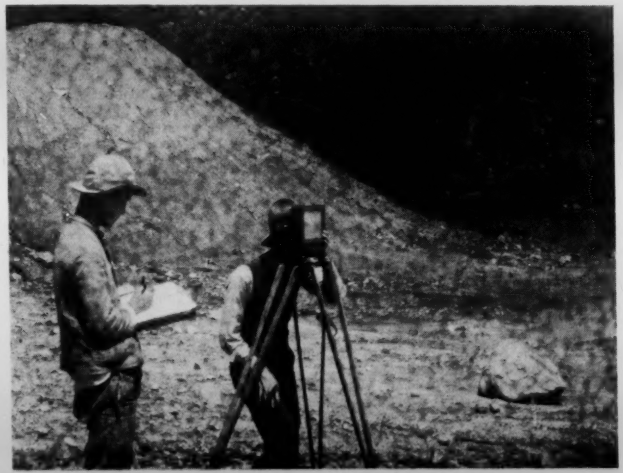

Station 10, Yugama.

（震研彙報　第十六號　圖版　水上）

11. Notes on the Origin of Earthquakes. (Fifth paper.)

By Win INOUYE,

Earthquake Research Institute.

(Read Dec. 22, 1937.—Received Jan. 6, 1938.)

1. Introduction.

In his previous paper⁽¹⁾ the writer discussed the conditions supposed to prevail within the seismic focus as based on observations so far made in connexion with the initial phase of seismic waves, and arrived at the conclusion that the maximum shear stresses, which might be constant within the seismic focus, reaches the limit of ultimate strength of the material immediately preceeding the earthquake.

In that paper, the writer treated the problem without taking into consideration the external and internal forces that bring about the earthquake.

In the following paragraphs, he attempts to make clear the forces that bring about the condition that the maximum shear stresses within the seismic focus are constant.

2. The Conical Type.

(a) It is supposed that the elastic body, which is stressed in one direction, has a spherical grain imbedded in it.

The problem has already been solved by Prof. K. SEZAWA and Dr. G. Nishimura.⁽²⁾

The boundary conditions, assuming the radius of the grain to be a, are

at $$r=\infty\,; \qquad \widehat{rr}=T\cos^2\theta, \qquad \widehat{\theta\theta}=T\sin^2\theta,$$

where T may be either uniform tension or uniform compression; and at $r=a$ the stresses and displacements are continuous.

The stresses in the internal portion are then expressed by

$r \leqq a$:

$$\widehat{rr'}=T\left[\frac{(\lambda+2\mu)}{(3\lambda+2\mu)}\,\frac{(3\lambda'+2\mu')}{(3\lambda'+2\mu'+4\mu)}+4\mu'\frac{D_1}{D}P_2(\cos\theta)\right],$$

---

1) Win INOUYE, *Bull. Earthq. Res. Inst.*, **15** (1937), 686.

2) K. SEZAWA and G. NISHIMURA, *Bull. Earthq. Res, Inst.*, **7** (1929), 389.

$$\widehat{\theta\theta'}=T\left[\frac{(\lambda+2\mu)}{(3\lambda+2\mu)}\,\frac{(3\lambda'+2\mu')}{(3\lambda'+2\mu'+4\mu)}+2\mu'\frac{D_1}{D}-4\mu'\frac{D_1}{D}P_2(\cos\theta)\right],$$

$$\widehat{\phi\phi'}=T\left[\frac{(\lambda+2\mu)}{(3\lambda+2\mu)}\,\frac{(3\lambda'+2\mu')}{(3\lambda'+2\mu'+4\mu)}+2\mu'\frac{D_1}{D}\right],$$

$$\widehat{r\theta'}=T\left[2\mu'\frac{D_1}{D}\,\frac{dP_2(\cos\theta)}{d\theta}\right],$$

where λ, μ are the elastic constants of the external medium and λ', μ' are those of the internal grain, while

$$D=\begin{vmatrix} \dfrac{\lambda'}{7}, & 4\mu', & -\dfrac{9\lambda+10\mu}{3}, & -24\mu \\ -\dfrac{8\lambda'+7\mu'}{21}, & 2\mu', & \dfrac{3\lambda+2\mu}{6}, & 8\mu \\ -\dfrac{\lambda'}{7\mu'}, & 2, & \dfrac{3\lambda+5\mu}{6\mu}, & 3 \\ -\dfrac{5\lambda'+7\mu'}{42\mu'}, & 1, & \dfrac{1}{6}, & -1 \end{vmatrix},$$

$$D_1=\begin{vmatrix} \dfrac{\lambda'}{7}, & \dfrac{2}{3}, & -\dfrac{9\lambda+10\mu}{3}, & -24\mu \\ -\dfrac{8\lambda'+7\mu'}{21}, & \dfrac{1}{3}, & \dfrac{3\lambda+2\mu}{6}, & 8\mu \\ -\dfrac{\lambda'}{7\mu'}, & \dfrac{1}{3\mu}, & \dfrac{3\lambda+5\mu}{6\mu}, & 3 \\ -\dfrac{5\lambda'+7\mu'}{42\mu'}, & \dfrac{1}{6\mu}, & \dfrac{1}{6}, & -1 \end{vmatrix}.$$

The maximum shear stress at any point is given by

$$\widehat{r\theta'}^2+\left(\frac{\widehat{rr'}-\widehat{\theta\theta'}}{2}\right)^2=T^2\left(3\mu'\frac{D_1}{D}\right)^2\equiv K^2.$$

Thus, in the spherical grain, the condition that the maximum shear stresses are constant is fulfilled.

As will be seen in the expressions of the stresses, there are two terms; the one which has no azimuthal differences, and the other which has azimuthal differences in the form $P_2(\cos\theta)$.

The former term, that is the $P_0(\cos\theta)$ term, makes the maximum shear stress zero. In other words, the $P_0(\cos\theta)$ term has no part in the value of the maximum shear stress at any point in the spherical grain.

The latter term, that is the $P_2(\cos\theta)$ term, is derived from the displacements, independent of dilatation (Δ) and rotation (ϖ); and it only satisfies the condition of the maximum shear stress. These facts were already noted in the previous paper.

(b) We next consider the stress distribution in the interior of a spherical inclusion in a gravitating semi-infinite elastic solid, assuming that the state of the gravitating semi-infinite medium is one of plane strain.

This problem has already been solved by Dr. G. Nishimura and Mr. T. Takayama.[3]

Let u, v be the components of displacement in the directions of radius r, co-latitude θ, and $\widehat{rr}$, $\widehat{\theta\theta}$, $\widehat{\phi\phi}$ the normal components of traction, $\widehat{r\theta}$ the shearing component of stress in the outer medium. And let u', v' be the radial and co-latitudinal components of displacement, and $\widehat{rr}'$, $\widehat{\theta\theta}'$, $\widehat{\phi\psi}'$ the normal components of stress, $\widehat{r\theta}'$ the shearing component of stress in the spherical inclusion, the radius of which is a.

The boundary conditions of the present problem are:

At $$r=a;\quad u=u',\quad v=v',\quad \widehat{rr}=\widehat{rr}',\quad \widehat{r\theta}=\widehat{r\theta}'.$$

Secondly, the displacement and the stress in the whole of the space in the medium far from that point where spherical inclusion is, are the same as those found in solving the problem relating to a gravitating semi-infinite elastic solid without any heterogeneous matter within it.

If we assume $\xi \gg a$, where ξ is the depth of the centre of the inclusion from the free surface, the stresses in the inclusion are given by

$r \leqq a$:—

$$\widehat{rr}'=\left(\lambda'+\frac{2\mu'}{3}\right)D_0P_0(\cos\theta)+4\mu'E_2P_2(\cos\theta)\,,$$

$$\widehat{\theta\theta}'=\left(\lambda'+\frac{2\mu'}{3}\right)D_0P_0(\cos\theta)+4\mu'E_2P_2(\cos\theta)+2\mu'E_2\frac{\partial^2P_2(\cos\theta)}{\partial\theta^2}\,,$$

$$\widehat{\phi\phi}'=\left(\lambda'+\frac{2\mu'}{3}\right)D_0P_0(\cos\theta)+4\mu'E_2P_2(\cos\theta)+2\mu'E_2\cot\theta\frac{\partial P_2(\cos\theta)}{\partial\theta}\,,$$

$$\widehat{r\theta}'=2\mu'E_2\frac{\partial P_2(\cos\theta)}{\partial\theta}\,,$$

---

[3] G. NISHIMURA and T. TAKAYAMA, *Bull. Earthq. Res. Inst.*, **11** (1933), 196.

where

$$D_0 = -\frac{3\rho g\xi}{(4\mu+3\lambda'+2\mu')},$$

$$E_2 = -\frac{5\rho g\xi\mu}{\{3\lambda(3\mu+2\mu')+2\mu(7\mu+8\mu')\}},$$

while λ, μ are the Lame's elastic constants in the outer medium, and λ', μ' those in the spherical inclusion,

ρ is the density of the outer medium, and

g is the acceleration due to gravity.

The $P_0(\cos\theta)$ term in the expressions of the stresses has no part in the value of the maximum shear stress at any point in the inclusion; while the $P_2(\cos\theta)$ term, which is derived from the displacements, independent of dilatation and rotation, satisfies the condition that the maximum shear stresses are constant throughout the inclusion.

Therefore, the maximum shear stress at any point in the spherical inclusion is given by

$$\widehat{r\theta}'^2 + \left(\frac{\widehat{rr}' - \widehat{\theta\theta}'}{2}\right)^2 = (\rho g\xi)^2\left(\frac{15\mu\mu'}{3\lambda(3\mu+2\mu')+2\mu(7\mu+8\mu')}\right)^2 = K^2 .$$

3. The Quadrand Type.

Now, we shall study the case where the elastic body that contains a spherical inclusion is subjected to a uniform simple shear.

The problem has already been solved by Dr. G. Nishimura.[4]

Let a be the radius of the spherical inclusion, λ', μ' the Lame's elastic constants, u', v', w' the components of displacement, and $\widehat{rr}'$, $\widehat{\theta\theta}'$, $\widehat{\phi\phi}'$, $\widehat{r\theta}'$, $\widehat{r\phi}'$, $\widehat{\theta\phi}'$ the components of stress in the inclusion, and let the symbols without dash represent those in the outer medium.

The boundary conditions are then as follows.

At $r=a$;

$$u=u', \qquad v=v', \qquad w=w',$$

$$\widehat{rr}=\widehat{rr}', \quad \widehat{r\theta}=\widehat{r\theta}', \quad \widehat{r\phi}=\widehat{r\phi}',$$

and at $r=\infty$;

$$\widehat{rr}=S\sin^2\theta\sin2\phi, \qquad \widehat{r\theta}=\frac{S}{2}\sin2\theta\sin2\phi,$$

$$\widehat{\theta\theta}=S\cos^2\theta\sin2\phi, \qquad \widehat{r\phi}=S\sin\theta\cos2\phi,$$

$$\widehat{\phi\phi}=-S\sin2\phi, \qquad \widehat{\theta\phi}=S\cos\theta\cos2\phi,$$

---

[4] G. NISHIMURA, *Kaheigakkaisi*, **25** (1931), 191.

where S is the shearing stress applied to the elastic body.

The stresses in the spherical inclusion are given by[5]

$r \leqq a$:—

$$\widehat{rr'} = 12\mu' E \sin^2\theta \sin 2\phi\,,$$

$$\widehat{\theta\theta'} = 12\mu' E \cos^2\theta \sin 2\phi\,,$$

$$\widehat{\phi\phi'} = -12\mu' E \sin 2\phi\,,$$

$$\widehat{r\theta'} = 6\mu' E \sin 2\theta \sin 2\phi\,,$$

$$\widehat{r\phi'} = 12\mu' E \sin\theta \cos 2\phi\,,$$

$$\widehat{\theta\phi'} = 12\mu' E \cos\theta \cos 2\phi\,,$$

where

$$E = \frac{5}{4}\,\frac{(\lambda+2\mu)\,S}{\{\mu(9\lambda+14\mu)+2\mu'(3\lambda+8\mu)\}}\,.$$

The stresses shown above are derived from the displacement that satisfies $\Delta=0$, $\varpi_r=0$, $\varpi_\theta=0$, and $\varpi_\phi=0$.

The maximum shearing stress at any point in the spherical inclusion is given by

$$\frac{1}{2}\left[\left(\frac{\widehat{rr'}-\widehat{\theta\theta'}}{2}\right)^2+\left(\frac{\widehat{\theta\theta'}-\widehat{\phi\phi'}}{2}\right)^2+\left(\frac{\widehat{\phi\phi'}-\widehat{rr'}}{2}\right)^2\right]$$
$$+\frac{3}{4}\left(\widehat{r\theta'}^2+\widehat{\theta\phi'}^2+\widehat{\phi r'}^2\right)=108\mu'^2E^2\equiv K^2\,.$$

The condition that the maximum shearing stress is constant throughout the spherical inclusion is now fulfilled.

4. Remarks.

In the preceeding two paragraphs, the writer studied the forces that bring about an earthquake and treated the problem according to the ordinary theory of elasticity. Nevertheless, the condition that the maximum shearing stress is constant throughout the seismic focus suggests that the seismic focus may be in a plastic state.

Thus, it seems to the writer that seismic waves may be generated as the result of changes in stress in the elastic medium about the seismic focus due to plastic yielding within the said seismic focus through the action of external forces.

As the external forces that are operating in the earth's crust, we may take the compressing stresses prevailing in the orogenic events, the forces due to gravity, and the forces operating from the magma reservoirs.

---

[5] The writer made some corrections in the calculations carried out by Dr. G. Nishimura.

The variations in temperature and the changes in the state of those substances that are within the seismic focus may play an important part in the plastic yielding within the seismic focus.

5. Summary.

The writer, after a study of the forces that bring about an earthquake, concludes that seismic waves may be generated as the result of changes in stress in the elastic medium about the seismic focus due to plastic yielding within the said focus under the action of certain external forces.

In concluding this short note, the writer's cordial thanks are due to Prof. Ch. Tsuboi and Dr. G. Nishimura for their encouragement and advices.

---

11. 發震機構に就いて（第5報）

地震研究所 井上 宇胤

第4報に於て初動の"壓し波""引き波"の地理的分布に二種類ある事から，地震の發生する直前に於ては震源の全域に亘り，最大剪應力が彈性の破壞限度に達してゐるのではないかと云ふ事を論じて居いた.

其の際には，所謂境界條件を問題にしなかつたので此の報告では外力を考へ境界條件を合してみた.

其の結果球狀の異物體を含む一樣な彈性體內に重力の作用して居る場合に於ても，一樣な壓縮力或は伸延力が作用した場合に於ても，或は又單純な剪應力が作用した場合に於ても其の異物體內では各點の最大剪應力が一定の値を取る事を知つた.

從つて此等の力が或る限度を越へ從つて異物體內の最大剪應力が彈性の破壞限度に達するか，或は又此等の力の作用下に於て異物體內の物理化學的條件の變化に依つて物質の彈性が減じ此の部が所謂可塑性變形をするならば，其の周圍の潭性體內の彈性應力が急激に變化して彈性波を生じ得るものと考へられる.

此の場合の異物體の占める部分が震源に相當しその附近より生ずる彈性波を地震波と考へて差支へない樣である.

12. *The Velocity of Elastic Waves in Sand.*

By Kumizi IIDA,

Earthquake Research Institute.

(Read Oct. 19, 1937.—Received Dec. 20, 1937.)

1. Introduction.

In our previous papers[1] we discussed the elastic properties of certain kinds of soil by subjecting them vibration. From our previous investigations[2] it was found that the elastic properties of soils differ with the kind of soil, the natural and the recomposed states, and the moisture content, etc. To apply our findings, not only to geophysical problems, such as the propagation of seismic waves, especially in the superficial layer of the earth's crust, but to civil engineering problems as well, it was found desirable to make further experiments with as large a variety of sands and soils as possible.

The object of this study is to ascertain the properties of sand in connexion with these subjects, and to develope the dynamics of granular substances like sand.

Some of the properties of sand have already been studied in Japan by T. Terada and N. Miyabe[3], namely the deformation of sand masses. They applied the results of their experiments to geophysical phenomena, such as chronic deformations of the earth's crust. Recently K. Takahasi[4], who studied the dynamical behaviour of a granular mass, found that there are two kinds of modes in the sand flow, similar to such natural phenomena as snow slides and land slides. In the field of civil engineering, some of the mechanical properties of sand such as porosity, shearing strength, etc. have received the attention of investigators[5], with the result that some of their mechanical properties are now fairly well known.

---

[1] M. ISHIMOTO and K. IIDA, *Bull. Earthq. Res. Inst.*, **14** (1936), 632; **15** (1937), 67.
K. IIDA, *Bull. Earthq. Res. Inst.*, **15** (1937), 828.

[2] M. ISHIMOTO and K. IIDA, *loc. cit.*, 1).

[3] T. TERADA and N. MIYABE, *Bull. Earthq. Res. Inst.*, **4** (1928), 33; **6** (1929), 109; **7** (1929), 65.
N. MIYABE, *Bull. Earthq. Res. Inst.*, **12** (1934), 195; **14** (1936), 553.

[4] K. TAKAHASI, *Geophys. Mag.*, **11** (1937), 165.

[5] T. WATANABE, *Bull. Geotechnical Committee, Government Railways*, **4** (1936), 176.
N. YAMAGUTI, *ibid.*, **4** (1936), 158, (in Japanese).
R. ONO and K. MANAI, *Journ. Civ. Eng. Soc.*, **22** (1936), 591, (in Japanese).

But as we are still ignorant how these substances will be affected by elastic waves, in the present experiments we first tried to subject sand to elastic waves in order to ascertain whether or not sand possesses any elastic properties, and also to know whether or not the relations between these properties and the kind of sand, its closeness of packing, and moisture content are similar to those ascertained for soils.

2. Mechanical Analysis of Sands.

Four kinds of sand were experimented with. These are shown in Fig. 1.

As the size of the sand grains has an important bearing upon its physical properties, we used sieves of Tyler's standard type as adopted by the U. S. Bureau of Standards. The experiments were conducted in the laboratory of the Geotechnical Committee, Government Railways of Japan. The methods of mechanical analysis are exactly the same as those described in Watanabe's paper[6]. The water is first removed from the sand, and the sand then passed through a series of Tyler's standard sieves mounted on a shaking machine and shaken for 15

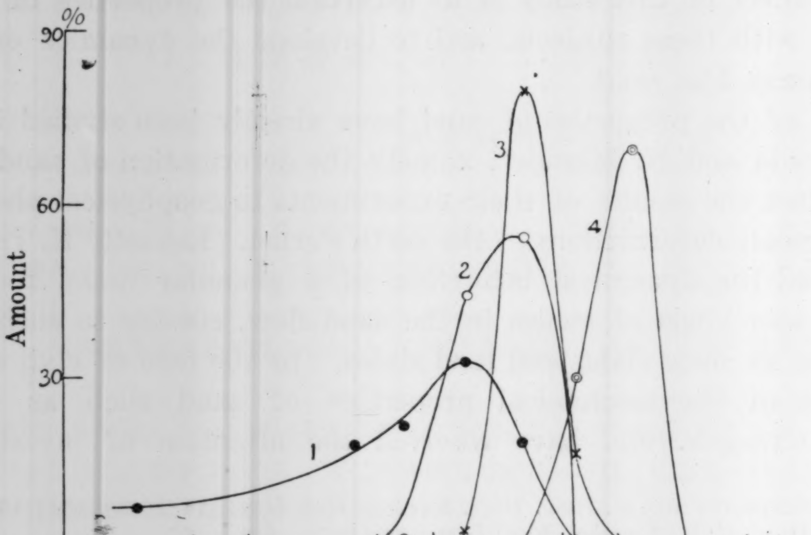

Fig. 2. Frequency curves of sizes of sand grains.
● Sand No. 1. ○ Sand No. 2.
× Sand No. 3. ◎ Sand No. 4.

---

[6] T. WATANABE, *loc. cit.*, 5).

Table I. Mechanical Analysis of Sand.

Kinds of sand No.	Mesh number (Tyler's standard sieves) 8 grain size 2·36 mm	14 grain size 1·17 mm	28 grain size 0·59 mm	48 grain size 0·30 mm	100 grain size 0·15 mm	200 grain size 0·07 mm	Silt grain size 0·07∼0·005 mm	Clay grain size 0·005∼0 mm	True density
	%	%	%	%	%	%	%	%	
1	0	0	1·08	18·70	32·98	21·58	18·22	7·44	2·825
2	0	0	0·02	54·36	44·02	1·58	0·02	0	2·732
3	0	0·08	16·92	79·96	3·04	0	0	0	2·660
4	0·16	69·84	29·98	0·02	0	0	0	0	2·746

minutes, so that the grains are duly separated. The results are shown in Table I and Fig. 2.

The resulting sand was then classified into four kinds, Nos. 1∼4, No. 1 being the finest and No. 4 the coarsest. As will be seen from the figure, the frequency curves of these sands differ. The frequency curves of Nos. 2, 3, 4 are sharp, while that of No. 1 is comparatively gentle. Upon classifying these sands according to their constituent minerals, No. 1 differs from the other three kinds in containing chiefly sediments derived from metallurgical slags, while the remainder are river sand containing chiefly quartz.

3. Variation in Sand Density with Moisture Content.

Since as already shown in Table I, the true densities of sand range from about 2·66 to 2·83, the differences between them are not great. At any rate, the density of sand No. 1 exceeds that of all the others, although their bulk densities vary with the water contained in them. Moreover the variations in densities seem to differ also with the kind of sand.

In order to observe the variation in sand density with moisture content, the specimens were first weighed in their moist state, after which they were gradually dried. We then measured their volumes and weighed them in their moist condition (weights of the sand grains and of the moisture),

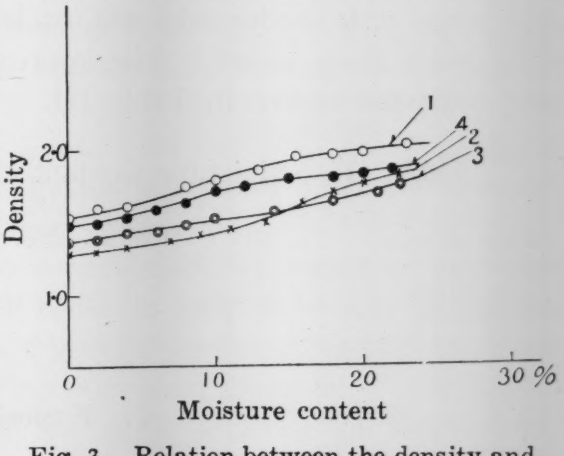

Fig. 3. Relation between the density and the moisture content. The numbers in the figure correspond to that of the kind of sand.

Table II. Bulk Density and Moisture Content of Sand.

Sand No. 1		Sand No. 2		Sand No. 3		Sand No. 4	
Moisture content	Density	Moisture content	Density	Moisture content	Density	Moisture content	Density
0	1·54	0	1·28	0	1·37	0	1·49
2·1	1·60	2·2	1·30	2·2	1·38	2·4	1·50
4·2	1·62	4·1	1·34	4·3	1·44	4·2	1·54
8·1	1·75	7·3	1·37	6·2	1·44	6·1	1·59
10·4	1·79	9·2	1·43	8·1	1·48	8·2	1·64
13·3	1·85	10·8	1·46	9·9	1·53	10·3	1·73
15·5	1·95	13·4	1·48	13·9	1·58	12·1	1·75
18·2	1·96	15·9	1·64	18·0	1·66	15·0	1·80
20·0	1·99	18·1	1·70	21·2	1·69	18·3	1·79
22·9	2·01	20·0	1·75	22·4	1·77	20·0	1·83
		22·4	1·81			22·0	1·84

and calculated their densities ρ from the ratio of their weights to their volumes. These are shown in Table II. The densities were plotted as ordinates and the moisture contents as abscissae, as shown in Fig. 3. As will be seen from this figure, the density seems slightly to increase with increase in moisture content. However it was found that when the moisture content exceeded 10 per cent, the density of No. 2 or 3 rapidly rose. This was more the case with No. 2 than any other. When the moisture content exceeded 16 per cent, the rise in density of No. 1 or 4 became almost constant.

As is well known, although it is possible to make a ball of sand only when it is moderately wet, it is impossible to do so when it contains much more water. The approximate moisture limits for making sand balls are shown in Table III.

Table III. Moisture Content that Sand Flow takes place.

Kind of sand	No. 1	No. 2	No. 3	No. 4
Moisture content	23·75%	24·6%	22·5%	9·9

4. Experiments.

(*a*) *Methods.* In the present experiments, both apparatus and methods were the same as those employed previously. The forms of the sand specimens were cylinders of initial heights of from 20 to 30 cm and the diameter about 5 cm.

With moderately wet sand, balls could be made, while with dry and very moist sand it could not be done, so that for the latter suitable devices for making the sand-cylinders had to be contrived. Since a receptacle in which to hold the sand is necessary, and since this receptacle must be of a substance that will not affect the properties of the sand in question, cellophane was selected to hold the sand. For reasons to be given later, the effect of the cellophane-tube holding the sand in the experiment is practically negligible. Thus in some cases of dry and very wet sands, we experimented with the sand packed in the cellophane-tube. In the case of moderately wet sand, we used brass moulds and packed the sands into them, and then extracted the sand-cylinder from the moulds.

These sand specimens were then set on the vibrating plate of our apparatus, a schematic diagram of which is shown in Fig. 4. In this figure *m* is a magnet, *M* a small lens mirror attached to pivot *P*. As already described in our previous papers, these serve to magnify the vibration amplitude of the top of the sand column. *V* is the vibrating plate for vibrating the specimen. Photographic records were made while applying forced transverse and longitudinal vibrations to the specimen up to the limit of vibration frequency. We could then find the resonance frequency of its vibration, after which we computed both the transverse and the longitudinal wave-velocities in the specimen.

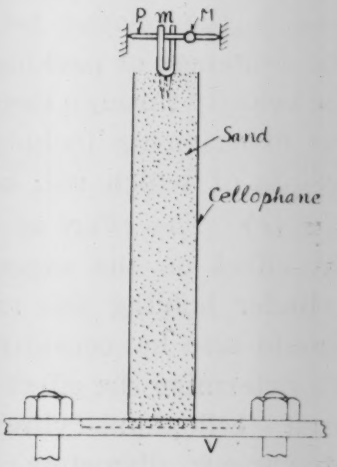

Fig. 4. Schematic diagram showing the arrangement of the longitudinal vibrating system.
P: pivot. *m*: magnet.
M: small lens mirror.
V: vibrating plate.

(*b*) *Methods of packing the sand.* As the closeness with which the sand grains are packed is an important factor in the propagation of elastic waves, the experiments were made with each of the sands both closely and loosely packed. In order to pack as closely as possible, the cylinder, which contained sand grains up to a height of 15 cm, was allowed to drop by withdrawing our hand from it.

Then as the cylinder droped the sand particles in the cylinder settled down, and the height of the sand-cylinder diminished with the number of times the cylinder was allowed to drop. The results of this treatment are shown in Fig. 5, in which the amounts of the fall in height are plotted against the number of times it was dropped. As will be seen from the figure, after it has been dropped five times, the height of the sand-cylinder becomes almost constant. To ensure densest packing, the same cylinder was also subjected to vibration, when its height diminished by about 1∼2 per cent. For example, in the case of dry sands, we investigated that the porosity of sand No. 3 varies from about 49 per cent to about 41 per cent, and that of sand No. 4 from about 46 per cent to about 40 per cent. To observe the relation between the denseness of packing and the velocity through the sand, the experiments included sand both closely and loosely packed, detailed results of which will be given later.

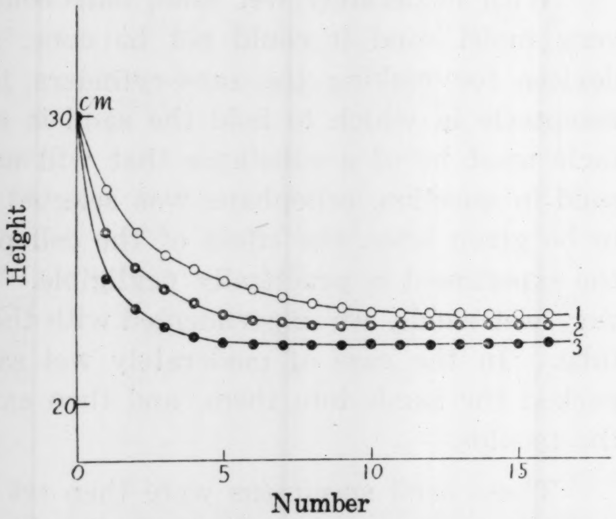

Fig. 5. Relation between the height of sand-cylinder and the number of times the cylinder was allowed to drop. 1, dry sand No. 1. 2, wet sand No. 2. 3, wet sand No. 4.

(*c*) *The effect of the cellophane boundary wall.* It is evident that the effect on the experiment of the boundary wall of the cellophane-cylinder holding the sand should also be considered. To determine the effect we used cellophane-cylinders of various diameters; as shown in Table IV. In Fig. 6, the curves showing the relation between the resonance frequency and the diameter are drawn for dry sand No. 4 and wet sand No. 2, the latter being considered from appearances to be in the fluid state. As will be seen from the curves in Fig. 6, the resonance frequencies of vibration are independent of the diameter of the cellophane-cylinder, from which it

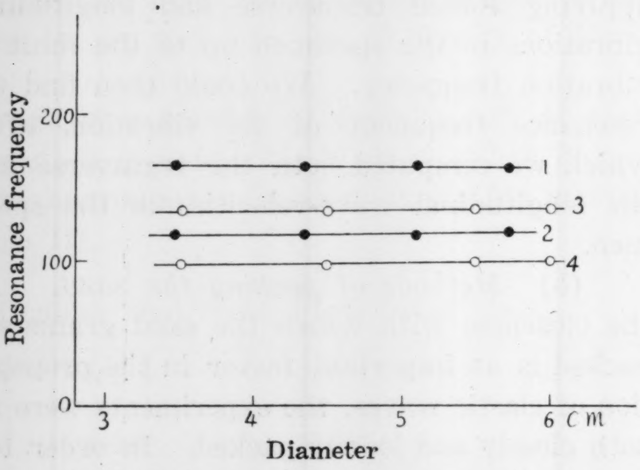

Fig. 6. Relation between the resonance frequency of vibration and the diameter of cellophane-cylinder.
● Dry sand No. 4. ○ Wet sand No. 2 with moisture content 19·4%. 1, 3 show the case of longitudinal vibration. 2, 4 show the case of transverse vibration.

Table IV. Resonance Frequencies and Diameters of Cellophane-cylinder.

(Nl: longitudinal resonance frequency; Nt: transverse resonance frequency.)

Sand No. 2			Sand No. 4		
Dia.	Nl	Nt	Dia.	Nl	Nt
3·52	135	98	3·47	166	118
4·49	134	97	4·34	166	118
5·49	136	100	5·10	165	119
6·00	136	100	5·72	164	120

will seem that the effect of the boundary wall is practically negligible so far as the present experiments are concerned. We may, therefore, extend the results of our experiment to the case of no boundary wall. We may say that the resonance frequencies obtained in our experiments are those of the sand column itself without the effect of the cellophane-boundary wall.

5. Results of the Experiments.

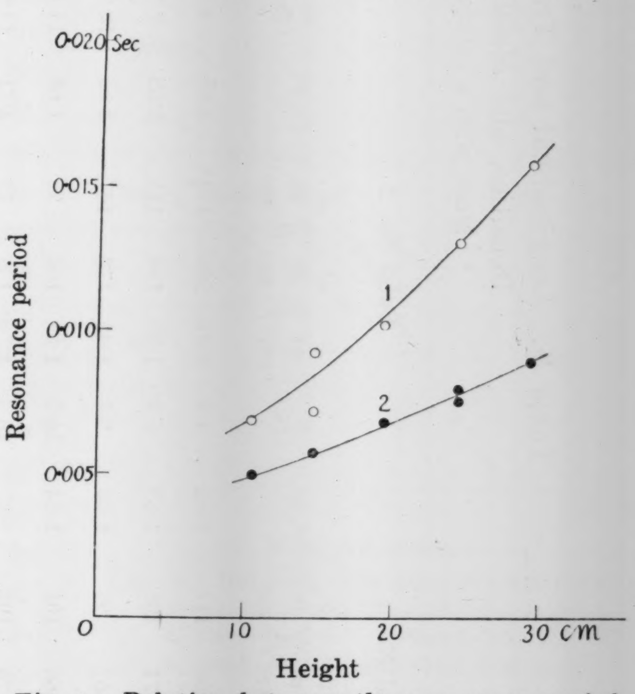

Fig. 7. Relation between the resonance period of vibration and the height of sand-cylinder. Specimen: wet sand No. 3, $w=14{\cdot}8\%$.
1, the case of torsional vibration.
2, the case of longitudinal vibration.

(*a*) *Determination of two kinds of wave-velocities.* With the same methods that were described in our previous papers, we determined two kinds of elastic wave-velocities: the longitudinal and the torsional. An example of a diagram showing the relation between the fundamental resonance periods T_l, T_t and the height of the sand column, h, may be seen in Fig. 7, in which the period, T_l or T_t is taken as ordinate and the height h as abscissa. The figures are the reducing curves, by which the two kinds of wave-velocities are determined. The values thus obtained in each kind of sand are shown in Table V. To observe the effect of moisture content on the physical properties

Table V. Longitudinal and Transverse Wave-velocities, Densities, and Moisture Content.

* Made with a cellophane-cylinder.

Sand No. 1					Sand No. 2					Sand No. 3					Sand No. 4				
w (%)	ρ $\left(\frac{\text{gr}}{\text{cm}^3}\right)$	V_l $\left(\frac{\text{m}}{\text{sec}}\right)$	V_t $\left(\frac{\text{m}}{\text{sec}}\right)$	V_l/V_t	w (%)	ρ $\left(\frac{\text{gr}}{\text{cm}^3}\right)$	V_l $\left(\frac{\text{m}}{\text{sec}}\right)$	V_t $\left(\frac{\text{m}}{\text{sec}}\right)$	V_l/V_t	w (%)	ρ $\left(\frac{\text{gr}}{\text{cm}^3}\right)$	V_l $\left(\frac{\text{m}}{\text{sec}}\right)$	V_t $\left(\frac{\text{m}}{\text{sec}}\right)$	V_l/V_t	w (%)	ρ $\left(\frac{\text{gr}}{\text{cm}^3}\right)$	V_l $\left(\frac{\text{m}}{\text{sec}}\right)$	V_t $\left(\frac{\text{m}}{\text{sec}}\right)$	V_l/V_t
0	1·76	200	117	1·71	1·9	1·30	202*	124*	1·63	4·1	1·43	180*	109*	1·65	0	1·49	163*	100*	1·63
3·1	1·78	171	105	1·63	6·0	1·35	190	115	1·65	7·2	1·46	170	103	1·65	2·1	1·50	160*	98*	1·63
5·3	1·79	162	99	1·64	9·9	1·45	178	107	1·66	10·9	1·56	148	89	1·66	4·2	1·54	148*	90*	1·64
8·2	1·80	166	101	1·64	14·2	1·59	160	95	1·68	14·0	1·58	135	81	1·67	6·9	1·59	140*	85*	1·65
10·6	1·83	170	102	1·67	18·3	1·70	136	79	1·71	14·8	1·60	133	78	1·71	9·8	1·72	120*	72*	1·67
11·7	1·86	161	96	1·68	20·0	1·75	130*	75*	1·73	17·0	1·63	116*	68*	1·71	12·3	1·74	117*	70*	1·67
14·5	1·89	143	83	1·72	21·8	1·77	140*	50*	2·80	20·1	1·67	96*	56*	1·71	13·9	1·76	100*	61*	1·61
17·6	1·92	94	54	1·74	24·0	1·80	147*	25*	5·88	22·9	1·78	92*	53*	1·74	18·0	1·79	80*	47*	1·70
19·3	1·99	95*	47*	2·02															
22·8	1·79	160*	12*	13·33															
24·0	1·70	200*	8*	25·00															

of sand, we plotted the wave-velocities obtained by the experiments against the moisture content, as shown in Figs. 8~9, in which we always took the moisture content as abscissa and the velocities as ordinate. In the experiments for determining these moisture relations, we sometimes used sand columns in the form of cellophane-cylinders and other times in the form of the sand-cylinder itself.

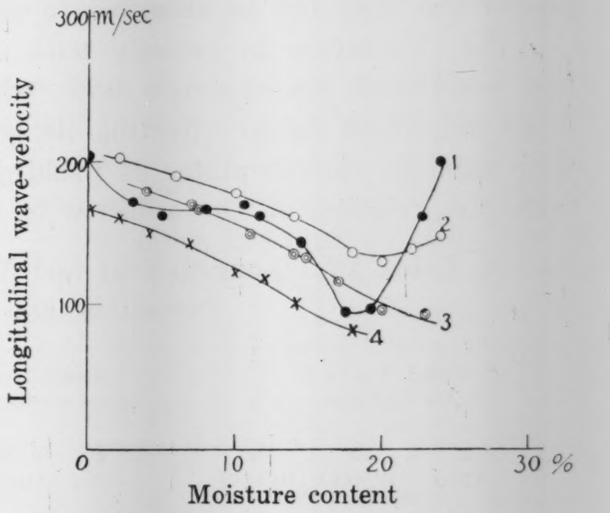

Fig. 8. Relation between the longitudinal wave-velocity and the moisture content.
1, sand No. 1. 2, sand No. 2.
3, sand No. 3. 4, sand No. 4.

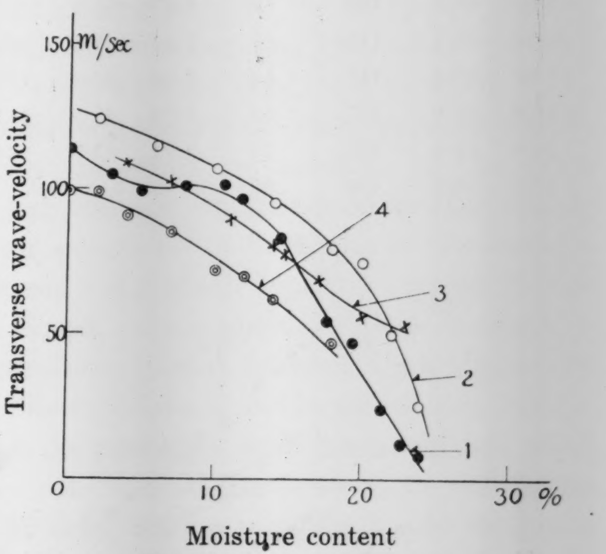

Fig. 9. Relation between the transverse wave-velocity and the moisture content.
1, sand No. 1. 2, sand No. 2.
3, sand No. 3. 4, sand No. 4.

As will be seen from these figures, the transverse wave-velocities, V_t, of these sands decrease somewhat rapidly with increase in moisture content, though the manner in which they do so differs with the particular kind of sand. Their longitudinal wave-velocities, V_l also decrease with increase in moisture content within the range of about 0~19 per cent of moisture, whereas those of sand Nos. 1 and 2 increase with moisture content below 19 per cent. Furthermore, in the case of sand No. 1, the relation between the longitudinal and the transverse wave-velocities and the moisture content fluctuated as shown in Figs. 8~9. As to the main reason for the fluctuation, it is believed that still finer grained particles or some adherent colloidal particles are introduced into the kind of sand, such as No. 1, and these adherent particles undoubtedly greatly affect its elastic properties. It seems that thixotropic phenomena may occur as the result of these colloidal particles. Further in the case of finer sands, such as Nos. 1 and 2, it was observed that their longitudinal wave-velocities seem to increase with increase in moisture content exceeded 20 per cent, while their transverse wave-velocities become too small for detection. These sands may be in the transition state from solid to liquid or to viscous fluid. Such phenomena may not be observed in coarse sand like No. 4.

(*b*) *Variation in velocity with denseness of packing.* Since as just mentioned, the closeness with which the sand grains are packed is an important factor affecting its elastic properties, we experimented with sand in various states of packings (Table VI). In order to determine the relation of the velocity to closeness of packing, we plotted the velocities as ordinates and the corresponding porosities of the sand as

Table VI. Longitudinal and Transverse Wave-velocities, Porosities, and Densities.

Sand No. 1 ($w=15\%$)				Sand No. 3 ($w=12\%$)				Sand No. 3 ($w=5\%$)			
ρ	P (%)	V_l (m/sec)	V_t (m/sec)	ρ	P (%)	V_l (m/sec)	V_t (m/sec)	ρ	P (%)	V_l (m/sec)	V_t (m/sec)
1·78	46·5	95	55	1·51	50·1	86	50	1·42	49·2	130	80
1·79	46·2	98	56	1·53	49·4	91	55	1·47	47·6	138	84
1·80	45·9	97	55	1·60	47·1	113	65	1·49	46·9	145	89
1·83	45·0	103	58	1·63	46·2	118	69	1·51	46·1	148	90
1·86	44·1	113	65	1·66	45·1	130	75	1·52	45·8	152	94
1·87	43·8	112	64	1·68	44·4	135	78	1·54	45·1	152	93
1·90	42·9	112	64	1·70	43·9	141	80	1·57	44·0	158	98
1·95	41·4	122	71	1·71	43·5	144	84	1·60	42·9	170	105
1·99	40·2	136	80								

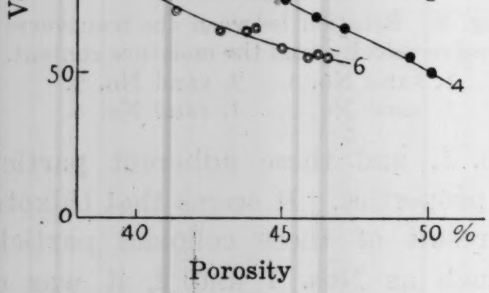

Fig. 10. Showing the relation of the velocity to closeness of packing.

● sand No. 3; moisture content $w=12\%$.

○ sand No. 3; $w=5\%$.

◎ sand No. 1; $w=15\%$.

1, 3, 5; the case of longitudinal vibration.

2, 4, 6; the case of torsional vibration.

abscissae, as shown in Fig. 10, in which porosity P, in percentage, is calculated from the true density and the bulk density, that is

$$P = 100 - \frac{\rho}{\rho_s}(100 - w), \tag{1}$$

where ρ_s is the true density, ρ the bulk density corresponding to the moisture content w per cent. As will be seen from Fig. 10, the velocities vary with the closeness of packing and seem to increase with diminishing porosity as a linear function of it. The curves of No. 1, 2, 3, 4, seen in the figure, are for the same kinds of sand as No. 3, and the curves of No. 5, 6 for the other kind of sand as No. 1. We see that the relations between the velocities and the porosities in the case of moist sand fluctuate somewhat more than those in the case of dry sand. We also noticed that this relation in the case of sand No. 1 fluctuates, which it seems, is partly due to its constituent particles, as already hinted.

6. Remarks.

As already explained in the preceding section, the elastic properties of sand are greatly affected by colloidal matters and the water contained in them. We noticed that in every kind of sand, the ratio of V_l/V_t increases with the moisture content, especially the finer grained sands, such as No. 1 and No. 2. When the moisture content in the finer grained sands, exceeds about 20 per cent, V_l increases somewhat rapidly, while V_t diminishes to such an extent as to be scarcely observable. When the water in sand is increased very much more, V_l seems to approach the velocity of sound in liquid. Consequently, sand in such a state behaves like a liquid. Therefore, it will be seen that there are two states in sand, according to their moisture contents. Since elastic waves propagate through sand, it is probably only natural that sand should possess elastic constants. It may be necessary to determine these elastic constants, although it may not be possible to do so from the theory of elasticity; its procedure will nevertheless be difficult in practice. It has never been shown that sand is fully governed by the condition required by the elastic theory. The assumption that the formulae of elastic theory can be applied to sand requires experimental justification. Although the exact mechanism by which the elastic waves propagate in sand seems to be still wrapped in mystery, we wished to know the elastic constants of sand from formulae similar to those of the elastic theory. We concluded, therebore, that the sand-cylinder

Table VII. E'. μ'. and σ'.

Sand No. 1				Sand No. 2				Sand No. 3				Sand No. 4			
w (%)	E' (c.g.s.)	μ' (c.g.s.)	σ'	w (%)	E' (c.g.s.)	μ' (c.g.s.)	σ'	w (%)	E' (c.g.s.)	μ' (c.g.s.)	σ'	w (%)	E' (c.g.s.)	μ' (c.g.s.)	σ'
0	$\times 10^8$ 7·04	$\times 10^8$ 2·41	0·46	1·9	$\times 10^8$ 5·25	$\times 10^8$ 2·00	0·31	4·1	$\times 10^8$ 4·64	$\times 10^8$ 1·70	0·36	0	$\times 10^8$ 3·96	$\times 10^8$ 1·49	0·33
3·1	5·20	1·96	0·33	6·0	4·88	1·79	0·36	7·2	4·22	1·55	0·36	2·1	3·84	1·44	0·33
5·3	4·69	1·75	0·34	9·9	4·59	1·66	0·38	10·9	3·42	1·24	0·38	4·2	3·38	1·25	0·35
8·2	4·96	1·83	0·36	14·2	4·07	1·44	0·41	14·0	2·88	1·04	0·38	6·9	3·12	1·15	0·36
10·6	5·29	1·90	0·39	18·3	3·14	1·07	0·47	14·8	2·83	0·97	0·46	9·8	2·48	0·89	0·39
11·7	4·82	1·72	0·40					17·0	2·19	0·76	0·44	12·3	2·38	0·85	0·40
14·5	3·86	1·32	0·46					20·1	1·54	0·52	0·48	13·9	1·76	0·66	0·33
17·6	1·68	0·56	0·49									18·0	1·15	0·39	0·47

would behave like an elastic solid, and assumed that the relations between the velocities and the elastic constants of sand at moisture content ranging from about 0 to 18 per cent are given by

$$\left.\begin{aligned} V_l=\sqrt{\frac{E'}{\rho}}, \quad V_t=\sqrt{\frac{\mu'}{\rho}}, \\ \sigma'=\frac{1}{2}\left(\frac{E'}{\mu'}-2\right), \end{aligned}\right\} \qquad (2)$$

where E', μ', σ' are the elastic constants similar to Young's modulus, modulus of rigidity, and Poisson's ratio respectively, and ρ the bulk density. The values derived from Table VI by equation (2) are given in Table VII.

The values for the coefficients, such as E', μ' obtained these methods are of the order of 10^8 in c.g.s. units at moisture content ranging from about 0 to about 10 per cent. These magnitudes are comparable with those of soils given by the foregoing investigations.

7. Summary and Conclusion.

We investigated the velocities of elastic waves in four kinds of sand. The relation between density and moisture content was also studied. The velocities of elastic waves in sand were obtained by means of the vibration method. Moreover, we succeeded in ascertaining the elastic wave-velocities of granular substances, such as sand, by using cellophane. It was ascertained that the elastic properties are greatly affected by the closeness of packing, the moisture content, and the presence of adherent colloidal particles in the sand. The velocities decrease with increase in moisture content or with increase in porosity. The transverse wave-velocities decrease somewhat rapidly with increase of moisture content, while the longitudinal wave-velocities of some sands increase with moisture content exceeded 19 per cent. We were thus able to observe the transitional state of sand from the ordinary solid state to the liquid state by virtue of the increasing water in the sand.

The velocities through the finer grained sands seem to be greater than those through the coarse grained sands.

Finally, the elastic constants of the sands were determined by the assumption that formulae similar to that of the elastic theory could be applied.

These studies on the properties of granular substances are being continued, and the results will be discussed a future issue of the Bul-

letin.

In conclusion, my sincerest thanks are due to Professor Mishio Ishimoto for his kind guidance and encouragement, and also to Dr. T. Watanabe, by whose kind guidance the mechanical analysis of the sands which were used in the present experiments was carried out.

---

12. 砂の中を傳播する彈性波の速度

地震研究所　飯田汲事

此の論文には砂の彈性的性質，特に砂の如き粒狀構造物體の中を傳播する彈性波の速度に就いて實驗した結果が述べてある．此の研究は今迄しばしば述べた如き物質の彈性的性質に對する研究の續きである．

實驗には粒徑の異つた4種類の砂を選んだ．今回の實驗方法は前回と全く同樣であり，且つ實驗物體もその形狀を圓壔形となした事は前回と同じである．砂の如き粒狀體の物體を圓壔形に作る場合には，砂が適度に濕つて居ればよいが，或程度以上に濕つて居る場合や全く乾燥して居る場合などに於ては砂を圓壔形にする事が出來ない．斯樣な場合にはセロフアン紙を用ひて圓壔を作りその中に砂を詰めて實驗を行つた．

實驗によつて得られた結果は土の場合と同じく，砂の彈性的性質は砂の種類，packing の狀態，含水量の如何によつて著しく支配される事である．而も含水量を徐々に增加すると含水率18～20% 位迄は縱波も橫波もその速度を減少するが，含水率 20% 以上になると橫波の速度は非常に小さなつて觀測されない程度となるに反し，縱波の速度は又再び大きくなる事が判明した．斯樣な狀態は多分液體の性質の表はれであると考へられる．又砂の彈性的性質は其の中に存在する粘着性のコロイド物質や，粒徑の極めて小さい物體によつて著しく影響を受ける．これは所謂 Thixotropy の樣な現象が表はれて居る爲ではないかと考へられる．又速度から普通の彈性式と同樣な式によつて砂の彈性係數を强いて求めると含水率 10% 位迄は土と同じやうに 10^8 (c.g.s) 程度のものが得られた．

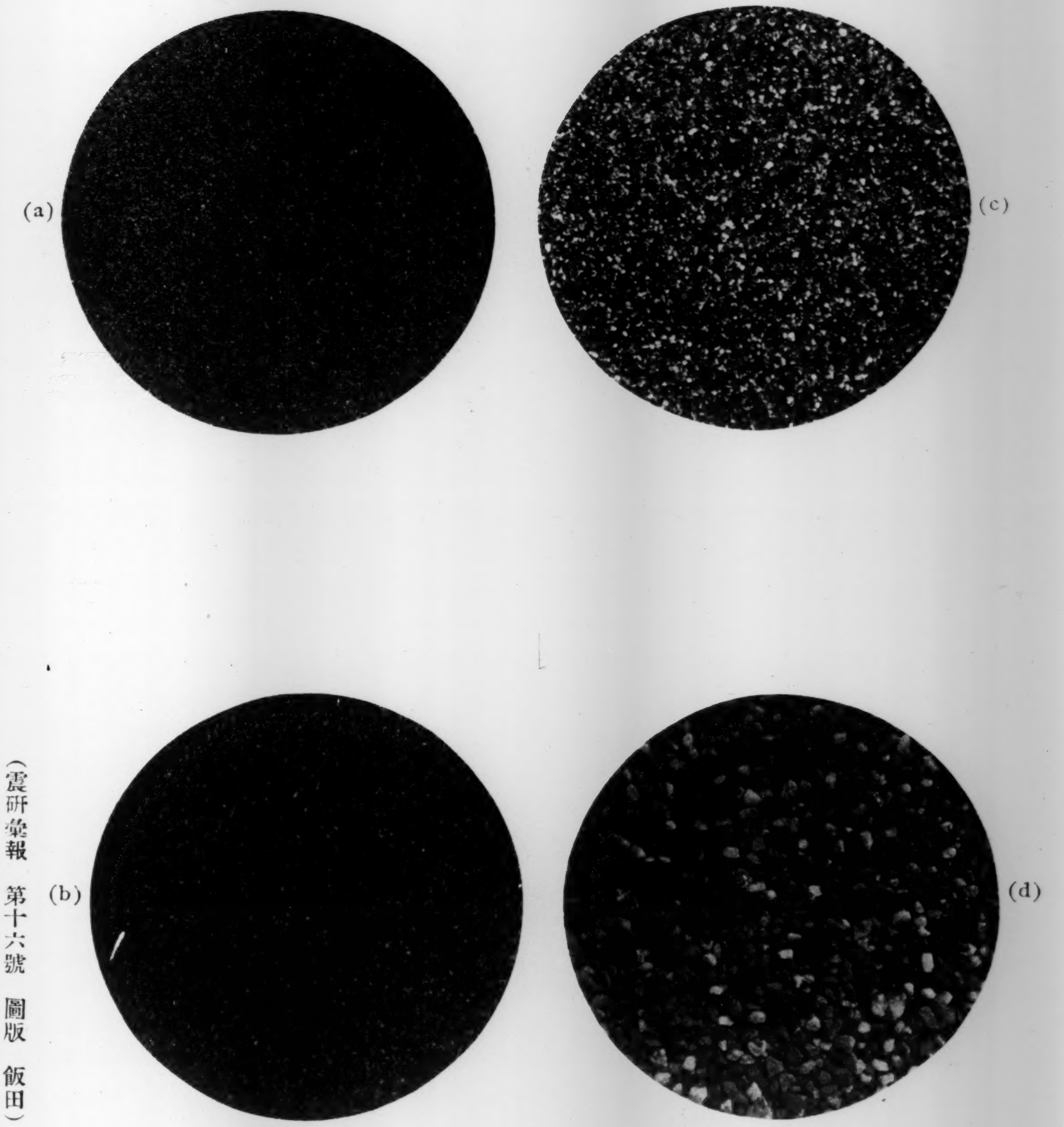

（震研彙報 第十六號 圖版 飯田）

Fig. 1. Photographs showing the grain size of sand specimens.

(a) Sand No. 1 (actual size). (b) Sand No. 2 (actual size).
(c) Sand No. 3 (actual size). (d) Sand No. 4 (actual size×1·3).

13.　名古屋城天守閣の耐震性に就て

地震研究所　齊田時太郎

(昭和12年5月18日發表——昭和12年12月20日受理)

緒言

わが國の建築史を顧みると，建築上に雄大な國民精神の發揮された時代が3回ある．即ち飛鳥，寧樂時代に於ける佛教建築の隆盛と，安土，桃山時代に於ける城郭建築の出現と，明治時代の歐米式建築の移植とである．いづれも國民の活動的精神は各方面に躍動し，對外的に雄飛し以て次の時代に於ける謂はゆる日本固有文化の建設時代の先驅となつてゐるのを見る．安土，桃山時代に著しく發達した城郭建築に於て安土城は織田信長の，大阪城は豐臣秀吉の氣宇の雄大さを表現してゐたのを文獻の上に尋ねることができるが，今日保存してゐないのは誠に遺憾の極みである．しかし名古屋，姫路城の如き豪華なものが今日保存されてゐるのは幸と言ふべきである．その他各所に保存されてゐるのは，これ等2城ほど豪華ではないが，いづれも，その白壁と石垣と濠の水のもつ魅力は郷土の華と稱してよい．

寫眞第1　名古屋城天守閣外觀

城郭建築の如き規模の大きい構造物は，既往の大地震に於て，どんなであつたか，また今後その保存上地震に對してどんな風に考へたらよいかが，豫て私の腦裡に潜んでゐた問題であつた．偶々，昭和12年3月中旬より名古屋市が博覽會を開催さるゝにあたり，東京帝國大學地震研究所より出品物の1として，地震計を送ることゝなつたので開會前に名古屋城の天守閣に据ゑつけ，風及び地震による振動を記錄せしめて，研究資料としたい旨を市當局に願ひ出でたところ，直に快諾を得且つ多大の援助をも賜り僅か1箇月間であつたが，振動を觀測することが出來た．本文はかゝる意圖に基いて，觀測された振動の結果より天守閣の耐震性に就て卑見を述べたものである．

城郭建築の震害一般

城郭建築に對する旣往の震災を大日本地震史料[1]に尋ねると，震害記錄が相當數多くある．卽ち石垣の崩壞，土壁の龜裂，剝落，建築物の損傷など記錄されてゐるが，注意してゐると城郭建築中，最も規模の大きい天守閣の震害は，他の城內建築物に比して著しく震害が輕微であるが常である．その1例として，寛文2年5月1日，（西曆1662年）山城，大和，河內，和泉，攝津，丹波，若狹，近江，美濃，伊勢，駿河，三河，信濃等の諸國地大に震ひ人畜屋舍の被害極めて夥し，とある廣範圍に亘る大地震に於て，その被害を記した元延實錄の1節に，龜山の城大破，膳所の城（筆者注，望湖城本多氏6萬石）天守閣ばかり殘れる由記載されてゐる．この天守閣及び城內の附屬建築物の構造狀態が明瞭でないから，何とも言へないが他の城郭建築の被害記錄に徵すと，いづれも天守閣の方が被害は輕微であると言へる．これは寺院建築の震害に於て佛殿庫裏等が全潰しても山門，五重塔が殆ど被害を受けずにゐるのと同樣である．要するに城郭及寺院建築は地震に對しても最も規模の大きい天守閣及山門，五重塔が安全であると言ふのが，經驗上の事實であると私は信ずる．この事實を世人は，これ等の建築物は特に地盤のよい所を選んで建てゝあるのを以てその說明となし，或は天守閣に就ては特に上層に至るに從ひ梁間桁行が縮小されて頂小底大の形體となり，垂直の動力的安定觀を與へる心理に基いて，地震動の如き水平方向の（震央附近の地動には垂直方向にも水平方向と略同等の加速度のあることが推定される）震動による振力に對しても，かゝる形體の構造物の安定を類推してゐる．この類推は煉瓦造煙突の頂小底大のもの，或は土堰堤の如き著しき安定觀を與へるものが震害を蒙つてゐるのを見れば，單に形體の安定觀より地震動の如き作用に對して，その安定を理解せんとするのが全く誤であるのが解る．しからば地盤のよいとは科學的に如何なることを意味するか，また天守閣，五重塔の如き大なるものが被害輕微で，同一地盤に在る寧ろ高さの低い佛殿，庫裏等の震害が著しいのは如何に解釋すべきか，これが私の當面の問題である．この問題解決のために名古屋城天守閣及びその地盤の振動狀態を調査したのである．天守閣と言ふても，その構造の細部に於て多少異つてゐるから，一々について調査してからでないと，一般的の結論を出すことは輕卒と思はれるが，私の旣往に於ける家屋の振動及び數多の震害調査の經驗によれば，木造である限り，いづれの天守閣についても振動上からは大差なく，また地盤については名古屋城の如き平地の場合を調査すれば一般に臺地，高地の謂はゆる地盤のよい所にある城郭の場

---

1) 震災豫防調査會報告第46號甲，乙.

合は容易に推定し得る．要するに今回の觀測の結果を以て一般性を把握したものと考へて大した誤はないと思ふが，なほ機會を得て各天守閣，五重塔，山門の如き建築物について調査を進めてみたいと願つてゐる．

名古屋城の遭遇した既往の大地震

名古屋城は慶長 16 年（西暦 1611 年）末略々竣工を見たものである．昭和 12 年を距ること 326 年前にあたる．その後この附近を襲ひ多大の被害を與へた地震を史料に尋ねると少くも 7 回はあつたやうである．卽ち發震年月日と被害區域とを示すと下の通りである．

1，寛文 2 年 5 月 1 日畿內，東海，東山兩道の一部
2，寶永 4 年 10 月 4 日東海，畿內，南海，東山，西海兩道の一部
3，文政 2 年 6 月 12 日美濃．伊勢附近
4，安政元年 6 月 15 日伊賀，伊勢附近
5，安政元年 11 月 4 日東海，東山，北陸道
6，安政 5 年 2 月 26 日飛彈，越中，越前
7，明治 24 年 10 月 28 日美濃，尾張及隣國

これ等の地震による震害記錄を史料に探ねるに，名古屋城の被害のことは更に見當らない．特記するほどの被害はなかつたと考へてよい．

名古屋城天守閣の修繕

地震史料の上に，天守閣の被害を知ることが出來なければ，修繕の年次と地震との關係の有無を調査するのも 1 の參考となる．名古屋市史によると，天守閣は建築後寛文 8 年まで 59 年間は無事であつたが，同年大破損あり寛文 9 年 3 月より修理に着手し，その後時々大小の修築をしたことがある．その年代を擧げると下の如くである．

貞享 2 年，寶永 6 年，享保 5 年，享保 10 年，享保 11 年，
享保 13 年，享保 15 年，享保 17 年，享保 19 年，享保 20 年，
元文 4 年，元文 5 年，寛保元年，寶暦 2 年，

修繕の原因は自然の腐朽及び狂ひ並に風害，震害によると考へられる．上記の各年代に如何なる修繕をなせるか只今の私にはその詳細を語ることが出來ないが，寶暦 2 年（西暦 1752 年）の修繕は大修繕であつたらしく，天守閣の石垣の組直し，土臺の不同沈下による軸部の狂ひの修築など施された．直接，地震による被害の修築と考へら

れるのは，寶永6年のものであるが，それとても同4年の大地震の翌々年になつての修繕であるから，該地震とは密接な關係があるらしく思はれない．もし地震によるとすれば數回に亘る地震で何時とはなしに，被害が蓄積したと考へられる．明治 24 年の濃美大地震に於ても大垣，犬山及び名古屋の天守閣は大なる被害を受けてゐない．要するに，この天守閣は直接地震で致命的の損傷を受けたことは無いと言へる．

名古屋城天守閣の概要

外觀は寫眞の如く全國天守閣中最も美しい形態を表はしてゐる．構造の概要は斷面略圖により知られるが，大さは名古屋市役所建築課の實測によれば大要下の通りである．

各階の高さ

地層 10 尺，初層 13 尺，第2層 22 尺5寸，第3層 24 尺7寸，第4層 22 尺 5 寸，第5層 13 尺．

棟上端まで地面（東側下足場附近）より約159尺．

	桁行（南北）	梁間	坪數
地層	尺 88·5	尺 77	194·130
初層	122	108	366·217
第2層	122	108	380·672
第3層	91	77	236·698
第4層	70	56	137·700
第5層	56	42	65·333

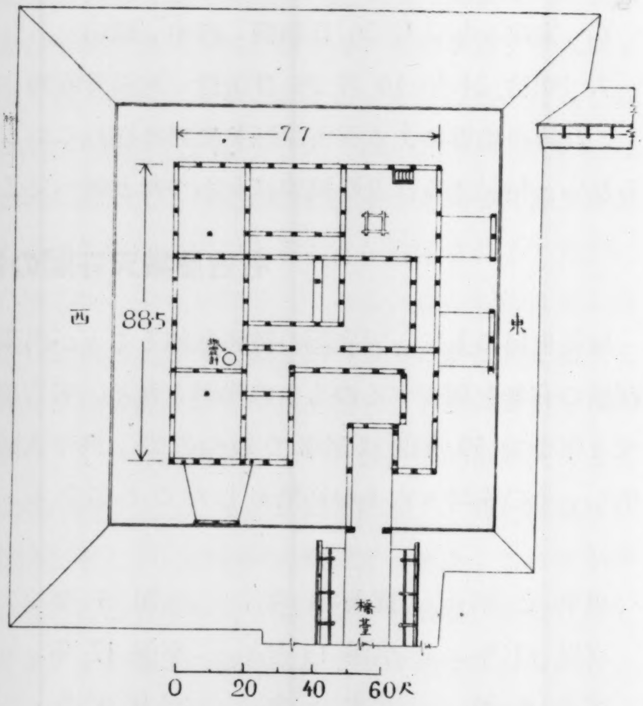

第1圖 名古屋城天守閣地層平面圖

天守閣の1間は略々今日の7尺となつてゐる．柱の大さは9寸乃至1尺4寸位の各種で，床板は7分乃至8分の厚さのものを使用してゐる．石垣は先づ地中に松材を敷き，その上に石を置いて築き上げたもので，地中に石垣の脚の埋ること約4尺で寶暦2年（創立後145年を經過す）の修理に，この松材は全く腐朽を免れて，もとのまゝであつたと言ふことである．斷面圖にて見られる通り初層と第2層の外側壁體の荷重は石垣にかゝり，天守閣軸部の

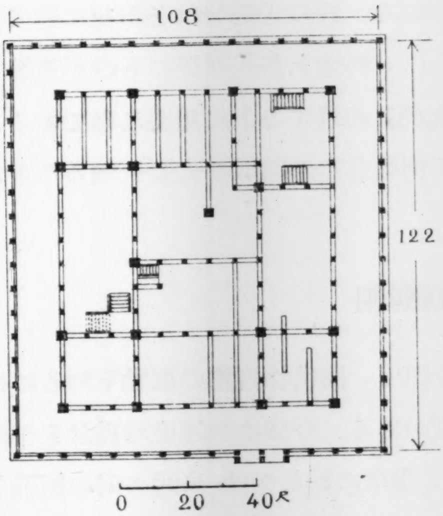
108
122
0
20
40尺

第2圖　名古屋城天守閣初層平面圖

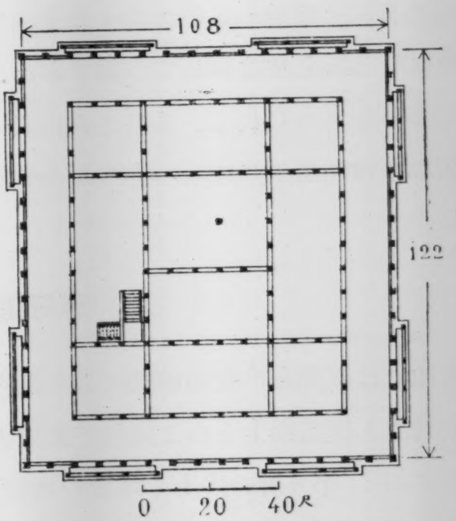
108
122
0
20
40尺

第3圖　名古屋城天守閣二層平面圖

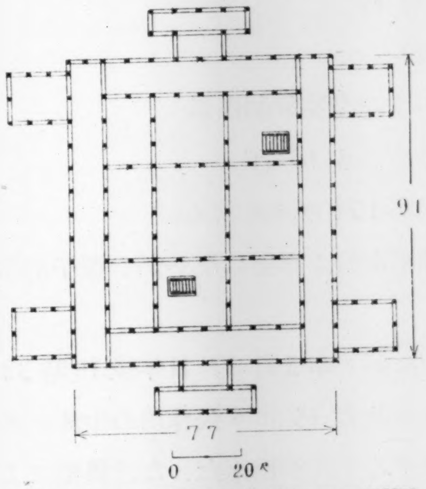

第4圖　名古屋城天守閣三層平面圖

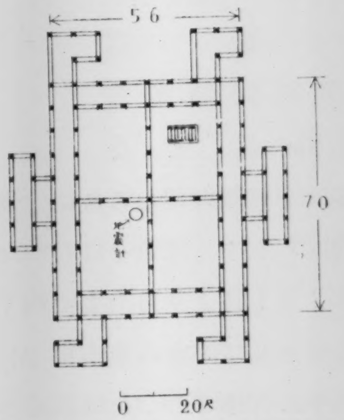

第5圖　名古屋城天守閣四層平面圖

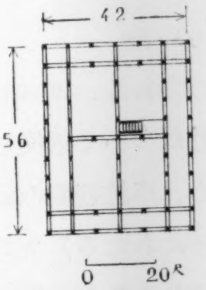

第6圖　名古屋城天守閣 五層平面圖

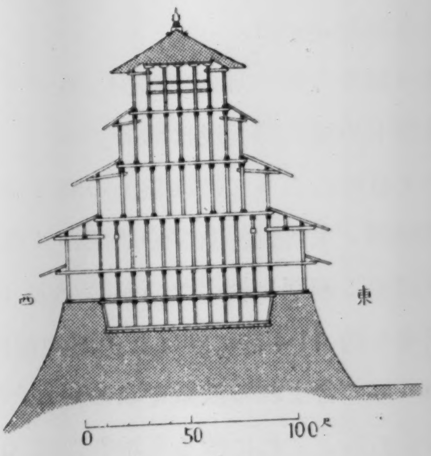

第7圖　名古屋城天守閣東西斷面略圖

主體の荷重は地層の基礎にかゝるやうになつてゐる. 柱の大部分は各階毎に建てられ2層に亙る通し柱は極めて小數である. 要するに，構造上各階單獨のものが重層となつてゐると考へられる. このことは天守閣の振動を理解する上に重要な點である. 平面圖は市役所建築課作製のものを多少省略して掲載したが間取の大要を知ることが出來る.

天守閣の振動觀測

大地には脈動及び交通機關による振動があるので，構造物自體の振動を知るには少く共地上と構造物上との2箇所で測定する必要がある. 今回は加速度地震計を平面圖に示す如く，第4層の床上と地層の地盤上との2箇所に据ゑつけ，東西方向の振動を記錄せしめる様にした. 地震計[1]の要素として重要なものを擧げると次の通りである.

振子の振動週期	0·115 秒
幾何倍率	213
制振器	ピストン型空氣制振器
記象紙回轉速度	1分につき 65 粍
地震計感度	1粍が 1·71 ガルに當る.

制振器は空氣制振器なる故に，溫度に對する補正を行ふ必要はないが，振子が常に臨界振動にあるやう注意をはらつた.

觀測は2月1日より月末まで約1箇月間であつたが，幸2月17日午後10時32分頃に名古屋市及び同市の東南東25キロ，岡崎市の北方15キロ矢作川の中流にある擧母町のみに有感であつた地震による震動を記錄することが出來た. なほ風壓による振動をも多數記錄した. それ等の記象は寫眞に示してある. 地震動記象より讀み取つた重な點を示せば，

第4層床の最大加速度は約 2·6 ガル　その週期 0·15 秒
地盤上の最大加速度は約 8 ガル　その週期 0·09 秒

で第4層床にありては地盤上の略3分の1に減少してゐるのである. 更に記象を初期微動部，主要動部及び終期部の3部分に分けて各々の波動について週期を讀みとつて卓越する週期を調べたのが第8,9,10,圖に示す曲線である. 卓越週期の讀取りには原記象を約11·4倍に延ばし各波の週期を0·1 mm（0·008秒にあたる）まで讀んで各0·1mm毎に含まれる波數を求め更にかくして得た波數の相隣れる數を平均して決定したのである. これに依ると地盤には0·09秒及び0·24秒の卓越週期があり第4層床に

---

[1] 石本巳四雄「地震とその研究」古今書院.

於ては0·16秒，0·33 秒及び風壓によるものから知られた1·12秒の3つあり，これが天守閣の自己振動週期であることは第11圖の共振曲線[1]から解る．

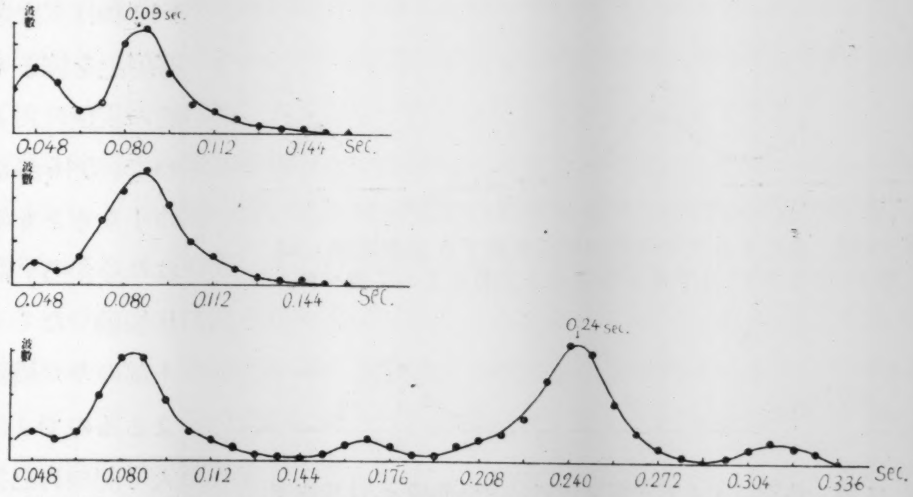

第8圖　地震による地盤に卓越する振動週期，上段は初期微動部，中段は主要動部，下段は終期部である．

風壓による振動として地震當日の午後6時頃の狀態をみると，瞬間風速の最大は15米秒，最小は4米秒で方向は西北西であつたと言ふことを愛知測候所の御好意により解つた．同測候所と天守閣とは約7キロを距たるが，これ等の數値を以て天守閣附近の値とするも差支あるまい．かゝる風壓による天守閣の卓越振動週期は第10圖に示す如くで加速度は，

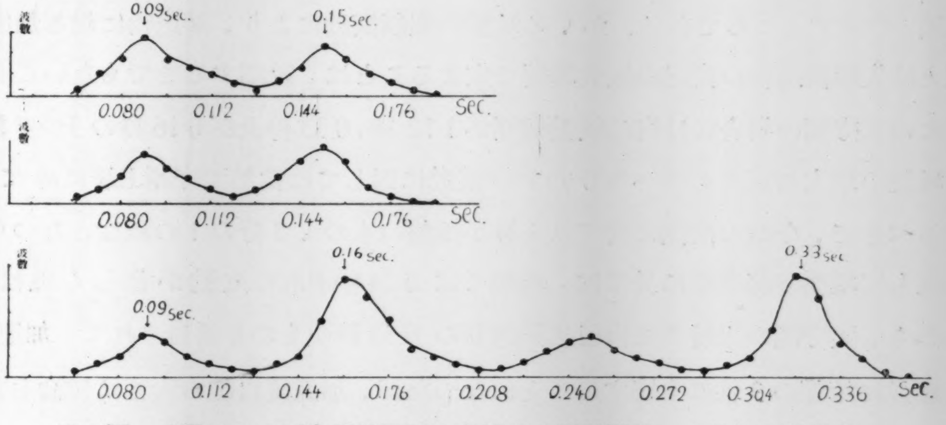

第9圖　地震による天守閣第四層に卓越する振動週期，上段は初期微動部，中段は主要動部，下段は終期部である．

瞬間風速 15 米秒のとき最大加速度 0·5 ガルその振動週期 1·12 秒．

瞬間風速 4 米秒のとき最大加速度 0·2 ガルその振動週期 0·16 秒と推定される．

---

[1] 齋田時太郎，鈴木正治「高層建築の地震動による振動」震研彙報，第14號第1冊

これに依つて見ると，風壓による振動週期には2つある卽ち1·12秒と0·16秒であるが，經驗によると1·12秒は天守閣の土臺附近を節とする全體の横振れによるもので，0·16秒は風壓の小なるときのみ現はれるから，高次の倍振動でなく天守閣上部のみの横振れによるもので，何れも天守閣の自己振動週期であることはその構造上容易に推定される．

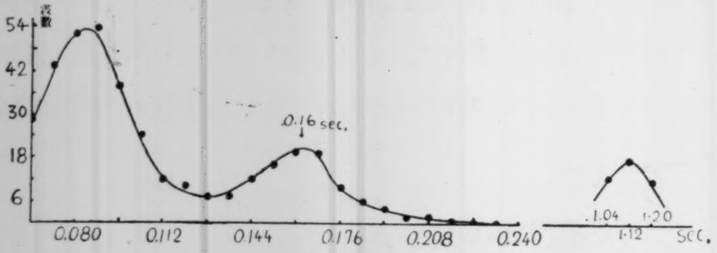

第10圖　風による天守閣第四層に卓越する振動週期，昭和12年2月17日午後6時頃の1分間をさつて調べた，

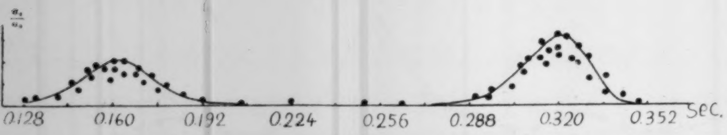

第11圖　地震による天守閣第四層の共振曲線 α_4 は第四層の，α_0 は地盤の振動加速度を示す．

今回の觀測せる地震は只1回であるが，上に述べたやうな卓越週期が地盤の固有週期で，地震により自己の週期にあたるところで，最大加速度を與へることは既往多數の觀測1)の示すところである．かゝる地盤の强制振動により，構造物に起る加速度と週期とは大體構造物の自己の振動週期で定まることは，說明するまでもないことである．この天守閣の場合には自己振動週期が1·12秒，0·33秒及び0·16秒の3つであるから，地盤の最大加速度を與へる0·09秒の波動に對しては當然天守閣上層に於て小さくなるべきで，今回の觀測に於ては上層が地盤のものゝ3分の1の程度となつた．これに反して地震の終期部に於ては，地盤では0·24秒附近の波動が著しく現はれてゐるから，天守閣の上層では自己振動週期の0·33秒のものを誘發されて，加速度は前とは逆に地盤の3倍にも達することになつたが，加速度自體の大さは勿論主要動の最初に現はれた最大加速度に比して，減少してゐることは寫眞にてみらるゝ通りである．

結　　言

從來地震に對して地盤のよい所と言ふのは略0·3秒以下の週期の所で，地盤の惡い所と言ふのは0·3秒以上就中0·7秒前後の週期の所にあたるのである．これは0·5秒

1）　齊田時太郎・鈴木正治「丸の內に於て觀測された地上及地下の地震動に就て」震研彙報，第12號第3册．

以上の自己週期をもつものが多い木造家屋の震害の著しいことから氣付いたのであるが，土藏造，煉瓦造，石造，鐵筋コンクリート造の如き低いもの，即ち自己の週期が木造家屋より遙に小なる構造物は，寧ろ地盤の硬い所で震害を著しく受けることは，關東大地震並に安政２年の江戸大地震の際東京市内の山手及び下町，江東方面に於ける被害について私が指摘1) する迄は一般に氣付かなかつた事實である．これによると，震害は地盤と構造物の性質とで相對的に定まるもので地盤のよし惡しは地盤固有のものでないことが解つた．古來城郭寺院の如き重要なる建築物が所謂地盤の硬い所に建てられてゐたゝめ高いものほど被害が輕微であつた事は上に述べた理由によることで，今回の觀測で實證された次第である．しかるに，從來の耐震工學で敎へる地震動の解釋では，最大加速度を與へる週期は１秒乃至 1·5 秒附近にあり，地盤の軟弱なところも硬い所も，その週期には大した相違はないが，振幅が軟弱地で著しく增大するので加速度は從て軟弱地で大きくなると言ふ風に考へてゐた．これは變位地震計から間接に求めた加速度と週期と，木造家屋の震害のみに注目しての結論であつて，構造様式の異なるものゝ震害を知らなかつた結果である．

今回の觀測の結果によれば名古屋城の如き平地に在る場合でさへ最大加速度を與へる地盤の週期が 0·24 秒程度以下であるから他の城郭の如く高地，臺地の硬い地盤に在るものは當然地震動に對して安全となるのである．高さの高い建物ほど上層で加速度が大きくなり從て振力の增大のため，その安定を保つことが不可能になりさうに考へるのが，從來の地震動の理解からすれば當然のことで，技術家及び一般の人々の常識となつてゐるが，わが國に於ける天守閣，五重塔の如き高層建築物が，地震に對して安全であるのは，地震動の最大加速度を與へる地盤の振動週期が，その地盤の自己振動週期にあり，しかも硬い地盤では 0·3 秒以下と言ふ値で，建物の自己週期に比し遙に小さな値であると言ふのが，主要な理由であると考へられる．

高層事務所建築に於ても，これと同様な結果を示してゐる　例へば 1906 年の米國桑港の大地震に於て，高さ 315尺 の當時最高の建物であつた，クラウス・スプレツケルビルディング2)（自己振動週期 2·32 秒及び 1·97 秒）が全く被害を受けなかつたので，技術界の注目するところとなり，又 1925 年の加州サンタバーバラの大地震及び 1933 年の加州ロングビーチ・ロスアンゼルス市の大地震に於ても，高層なものほど被害が輕少であつた．即ち建物は高い，規模の大きいものほど地震に對して安全であると言へる．特に地盤の硬い所であるならば一層振力を輕減することになる．

---

1)　齋田時太郎「耐震及び耐風家屋」防災科學の地震編，岩波書店．

2)　E. Hall「Vibrations of Buildings due to Street Traffic」Engineering News, v l. **68**, August **1**, 1912.

建築物に作物する振力は以上に說明した通り，構造物の大さ並に構造樣式と地盤の性質とで定まるのであるから，建築物の保存或は補强の意味で筋違，方杖等を施して建物の變形を少くしても，それが同時に耐震力を增加することになるとは言へない場合があるから注意すべきである．

筆を擱くにあたり今回の觀測のため種々便宜を御與へ下さつた名古屋市水道局擴張課の竹內英郎氏下水課長杉戶淸氏，及び土木部公園課長長野間守人氏，毎日の觀測に從事された水道局の後藤四郎氏柴田茂美氏，地震計据付のために出張された地震研究所の鈴木正治氏，地震計故障の時見て下さつたり地震及風速について御教示を賜つた愛知縣測候所長吉田余三男氏，天守閣建築について御教示を賜つた東京帝國大學工學部建築學敎室の木村貞吉氏の各位に深甚の謝意を表する次第である．

13. *Vibrations of the Keep of Nagoya Castle Due to Earthquake and Wind Pressure.*

By Tokitaro SAITA,

Earthquake Research Institute.

In our country great and tall wooden buildings are those of Buddhist temple and castle, namely—a five—storied pagoda, the great gate of a Buddhist temple and a keep. These buildings are well spoken of in safety against earthquake shocks while other low buildings are almost demolished. But there are no investigations about the safety againast earthquake shocks founded upon observations for these buildings.

The writer is at present engaged in observing the vibrations of a pagoda in Tokyo and its results are not yet ready for publication. This paper is of observations which have been done by the writer in the first place for the vibrations of the famous keep of Nagoya castle during earthquake and wind blows. From the observations the writer found that the acceleration at the upper floor of the keep is about 1/3 of the ground and the decrease of acceleration at upper floor depends on the relation between the natural period of the keep and the ground.

The writer is persuaded that the above statement is applicable to the fact that pagoda and other tall buildings are well proof against earthquake.

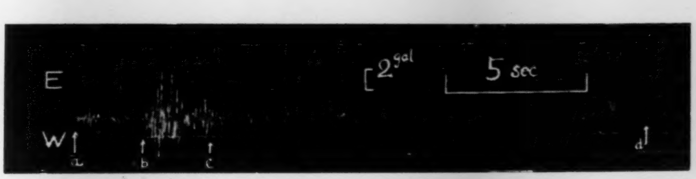

寫眞第 2　昭和12年2月17日午後10時32分頃の地震による天守閣第4層床の振動記錄 ab 間を初期微動部，bc 間を主要動部 cd 間を終期部とす（第8,9圖參照）.

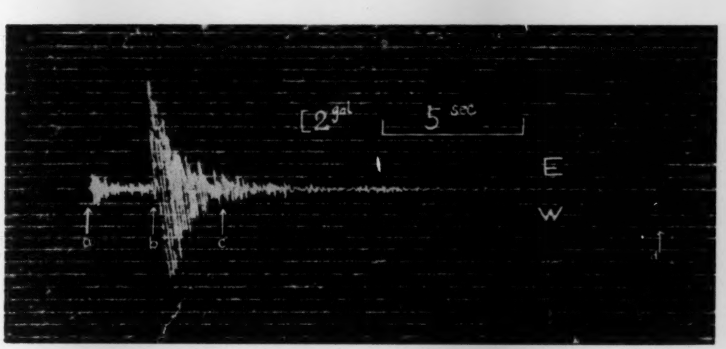

寫眞第 3　昭和12年2月17日午後10時32分頃の地震による天守閣地盤の振動記錄 ab 間を初期微動部，bc 間を主要動部 cd 間を終期部とす（第 8,9 圖參照）.

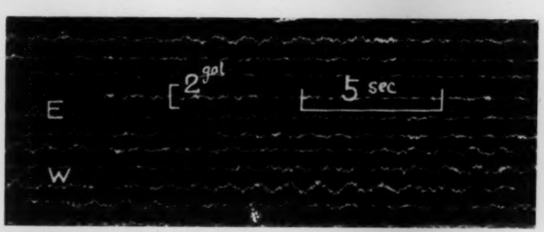

寫眞第 4　昭12和2年17月日午6後時頃の風による天守閣第4層床の振動記錄.

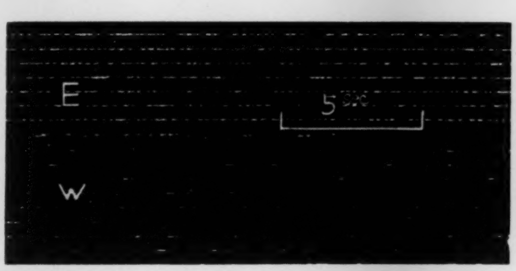

寫眞第 5　昭和12年2月17日午後6時頃の風による天守閣地盤の振動記錄（上層は振動せるも地盤は全く靜止せるを示す）.

（震研彙報　第十六號　圖版　齊田）

14.　朝鮮大同江に於ける彈性波式地下探査實施と其の吟味

地震研究所　表　俊　一　郎

（昭和12年11月16日發表——昭和12年12月20日受理）

1. 緒　言

朝鮮大同江に現在架設せられて居る京義線の鐵橋より約 40 米下流に新らしい鐵橋を架設する爲その場所に於ける岩盤の深さを知る事が必要であつた．此の深さを求むる目的を以て彈性波式地下探査を實施したので此所に其の結果を記述し，尙其の際，此の場合の如く河岸で實驗を行ふに當つては微動計を設置すべき場所について適當な考慮が拂はれねばならぬ事が分つたので其れについて二，三注意すべき點を付け加へる事とする．

實驗を行ひたる場所の平面圖は第 1 圖に示す如くである． 圖に見る如く河幅は約 1200 米位であるが，其の中央には膨大なる中の島（羊角島）が存在して居り實際に水の流れて居る部分は兩側の 400 米宛位の所である．従つて現在の鐵橋も此の部分にだけ架設せられて居り中央の中洲の所は築堤を築いて鐵道を布設してある．新鐵橋も之と同様に水の流れて居る部分にだけ架設せらるる豫定であるので地質調査も此の部分

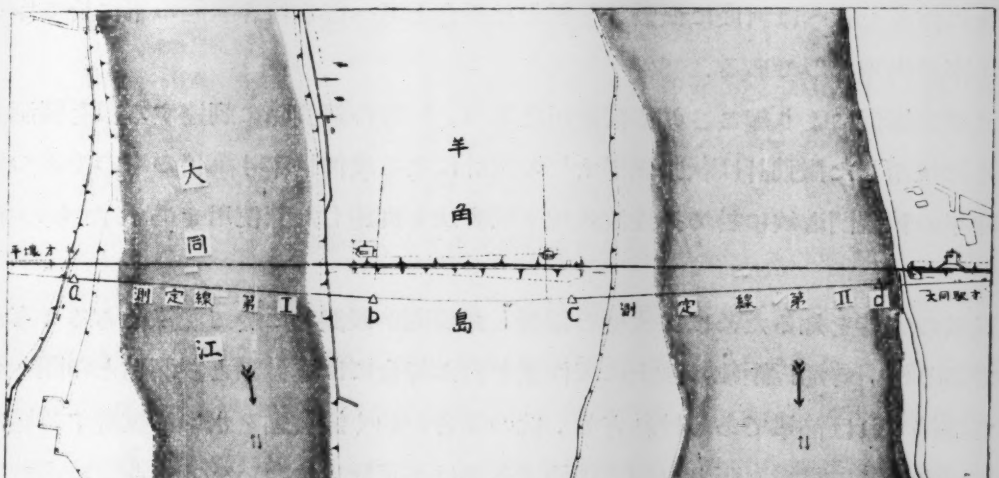

第 1 圖　地下探査實施地附近平面圖　△印微動計設置點

についてだけ行ふ事とした．從つて新鐵橋の中心線に沿つて圖の如く第 I 及び第 II の 2 本の測定線を選定し之等の測定線について地質斷面を求むる事とした．

2. 測定の方法

兩測定線はいづれも川を横斷して設定せられ大部分は水に浸されて居るので水中に設置する事の出來ぬ微動計を使用する以上，微動計を測線の兩端の岸の上に据ゑ爆發點を陸上又は水中にて順次移動せしめたのであつた．從つて微動計を設置する位置は成可く鐵橋の取り付けの近くに定めようとしたが道路，堤防等の位置により第 I 測定線にては堤防の內側の地點 a，及び羊角島側鐵橋取付け位置より 30 米左岸寄りの地點 b，第 II 測定線にては羊角島側鐵橋取付け位置より 20 米右岸寄りの地點 c 及び左岸鐵橋取付け位置より 50 米右岸寄りの地點 d としたのである．而して最後に述べた d 點は左岸鐵橋取付け位置の直下に大きな道路が在り人馬及び自動車等の通行の爲微動計を据ゑるに不適當であり且つ道路のすぐ下を川が洗つて居る等の理由により他の三地點の如く河岸に据ゑる事が不可能となり止むを得ず河岸より約 30 米程河の中へはいつた水中にコンクリートの臺を作り其の上に据ゑる事としたのであつた．幸ひ d 點附近の水深は極めて淺く干潮時に於ては 4～50 cm にすぎなかつたので，このあたりにては干滿の差は 2 m 僅りであつたにも拘らず 1 m 半程の高さの臺を作り干潮の前後に作業を行へば河底に微動計を据ゑた場合と考へ得る如き狀態の下に於て作業を行ふ事が出來たのである．

火藥の爆發により起こされる振動が之等 a，b 等の觀測點に到達するのを觀測するために使用した微動計は萩原理學士[1]の設計になる幾何倍率 4 萬倍のものであつて既に昨年の秋關門海峽に於て彈性波式地下探査法を實施した際使用せられたものである．

又波の走時を知るためには火藥の爆發した瞬間が觀測點に於て記錄せらるゝ事が必要であるが，普通近距離の陸上にて作業を行ふ場合には爆發點と觀測點との間を有線にて連絡すれば簡單であるけれども，此の場合の如く爆發點を水中に設置する樣な時には兩者の間に電線を張り有線で連絡する事は不可能ではないまでも非常に困難である．故にこの場合も關門海峽の場合と同樣兩者の間を無電で連絡する事とした[2]．卽ち發信機を船に積み，爆發點の移動と共に移動せしめ陸上觀測點には受信器を備へて爆發の前發せられる持續電波が爆發により中止せしめられる時刻を記錄する樣につく

---

[1] 萩原尊禮，彈性波式地下探査に使用せられる機器．物理地下探査 1 輯第 6 頁．

[2] 萩原尊禮，同　上．

られて居る．

観測點に於ける記録には以上二つの記録の他に時間の標準になるもの例へば 100 サイクルの音叉の振動が適當な方法で記録せらるゝ様にして置けば之等により各爆發毎の走時を測定することが出來る．

爆發點より観測點までの距離を知るためには陸上に据ゑた二つのトランシツトを用ひ交會法により爆發點の位置を定め之より距離を算出した．

3.　走時曲線の解析

斯くの如くして各測定線毎に 10 m～60 m の間距を置いて順次爆發を行ひ夫々の距離に應じそれに對應する走時を測定して第 1 表の如き結果を得た．之より走時曲線を作れば第 2 圖（第 I 測定線）及び第 3 圖（第 II 測定線）の如くなる．

第　1　表

測定線 I	a	距離	10	20	30	60	120	180	240	300	330 m			
		走時	3·3	3·8	4·7	6·2*	6·6	7·9	9·1	10·4	11·0×10^{-2}sec.			
	b	離距	6	16	26	40	60	66	96	126	186	246	306	366 m
		走時	2·8	3·8	4·6	4·9* 5·6 9·1	5·3* 7·1 13·1	5·4 7·6	5·1	5·7	7·2	8·2	9·4	11·6×10^{-2}sec.
測定線 II	c	距離	10	20	30	60	80	135	195	254	315	375	404	424 m
		走時	3·6	4·6	5·4	6·1	6·5	6·3	7·2	8·8	9·6	10·7	11·2	11·3×10^{-2}sec
	d	距離	9	17	29	72	139	194	254 m					
		走時	0·5	1·0	1·7	3·0	4·9	5·6	7·2×10^{-2}sec					

* 初動弱くして測定値稍確かならざるもの

速度の決定．四箇所の観測點の中 d 點を除く他の三點は陸上に設置せられ且つ陸上の部分は全て表土層を以て蓋はれて居るに反し河底の部分にては表面に土壌層が堆積して居ると考へ得べき所はなく少くとも測線の部分に就ては砂利層が川底に露出して居ると考へて過りでないと推察された．斯様な狀態の下に第 2, 3 圖に於て観測點 a, b 及び c の極近くに非常に遅い速度を與へる傾斜の小さい直線が現れて居り，而も河中に設置した観測點 d にては斯くの如き遅い速度を與へるものが現れて居らぬ事より之が表面土壌層の速度を與へるものなる事は明らかである．さてこの速度を決定するに観測點 a, c についてのものにては観測の材料不足で充分正確に定め得ないが，b の

観測にては 40 m, 60 m のものにつき初動より後に於て表面層を傳播し來りたる波によると思惟される相當明瞭な位相が見られるが故に，之等を用ひて 525m/sec なる値を以て表土層の速度と定めた.

表土層につゞいて之より速い速度を與へる傾きの直線が現れて居る. 而して之が表土層の下の砂利層の速度を與へるものである事は疑ひないが，a, b, c にて夫々 1130 m/sec，1240 m/sec，1130 m/sec と出て居るものが唯り d のみにて 1700 m/sec と出て居るのは一考を要する事である. 之を誤差であると考へる事が無理であるとすれば砂利層の上の表土層の厚さの變るため見掛の速度がかく異つて見えるものとするのが普通であるが此の場合 d にては河底に砂利層が露出して居ると考へるのであるから他の三ヶ所にては河岸に近づく程表土層の厚さが厚くならねばならぬ事となり，如何にも矛盾した結果を與へる. 故に今三つの觀測點 a, b, c 等は河岸より 5~60 m 陸地へ入つた所に設置せられ 1100~1200 m/sec の速度を與へて居るのは陸上の爆發點について，陸上の表土層下の砂利層を通過した波についての結果であつて，水中爆發を行ひ河底の砂利層を通過した波についての走時曲線は觀測點 d のもののみが與へて居る事を考へ砂利層は河底の部分と陸上の部分とでは其の組成に異る所があり從て其の中を通過する彈性波の速度も異るのであると考へる. 而して此等の走時曲線より

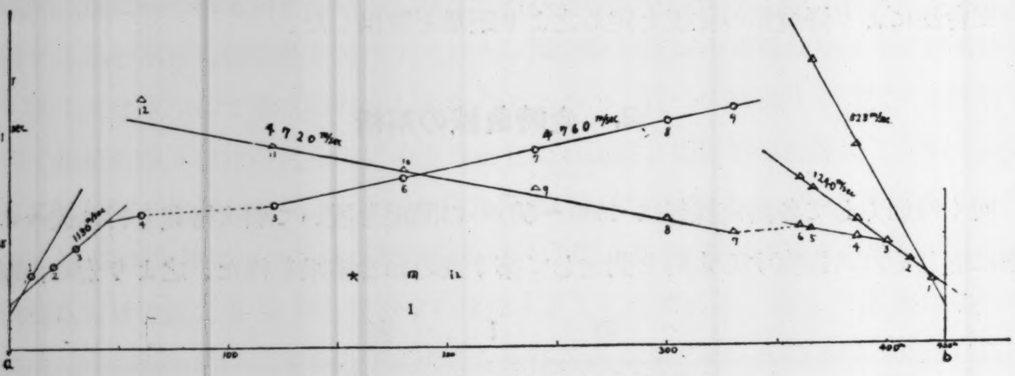

第2圖 第I測定線の走時曲線

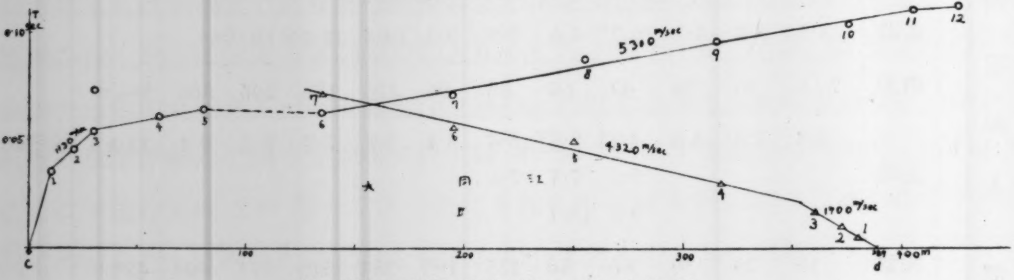

第3圖 第II測定線の走時曲線

河底の砂利層の速度 1700 m/sec

陸上の砂利層の速度 1130 m/sec

と定める事とする．而して此の實驗を行ひし場所にては地表面下30糎で地下水面に達する事を考へればかくの如き差が速度の上に現れるといふ事は單に水の存在の有無だけで說明する事は出來ない．

砂利層のBranchの次に更に早い速度を與へる直線が續く．之は砂利層の下の岩盤の速度を與へるものと考へる事が出來る．而して其の速度は第2圖觀測點a, bについては夫々4720 m/sec, 4760 m/sec 第3圖觀測點c, dについては夫々5300 m/sec, 4320 m/secとなつて居る．之は一見第I測定線の與へる岩盤の速度と第II測定線の與へる岩盤の速度とが異る如く思はるゝけれども次の如く考へれば互に矛盾するものではない事が分る．

今第II測定線に於て岩盤は觀測點cよりdへ向つて次第に淺くなつて居ると考へ，砂利層の平均の表面に對する岩盤の傾きをω，河底の砂利層と岩盤との間に於ける彈性波の臨界角をi，河底の砂利層に於ける彈性波の速度をV_2，岩盤に於ける波の見掛の速度の中速きものをV_{3+}遲きものをV_{3-}とすれば

$$V_{3+}=\frac{V_2}{sin(i-\omega)}$$

$$V_{3-}=\frac{V_2}{sin(i+\omega)}$$

なる關係より

$$i=20^0 50'$$

$$\omega=2^0 10'$$

となり眞の速度V_3は

$$V_3=\frac{V_2}{sin i}=4790\ \mathrm{m/sec}$$

と求める事が出來る．之は第I測定線より求められるものと略等しく之等を平均して

岩盤の速度 4770 m/sec

と定める．

各層の厚さの決定． 以上の如くして各層の中を傳播する彈性波の速度を決定し得た故之を用ひて各層の厚さを定める事が出來る．

先づ第I測定線に著いて表土層の厚さh_1は

a側にては $$h_1=\frac{8{\cdot}0}{2}\sqrt{\frac{1130-525}{1130+525}}=2{\cdot}4\ \mathrm{m}$$

b側にては $$h_1=\frac{8{\cdot}3}{2}\sqrt{\frac{1130-525}{1130+525}}=2{\cdot}5\ \mathrm{m}$$

となる．而して第2圖に於て測定點a_1が砂利層の直線の上に乘らないのはa_1の附近

にては表土層の厚さは上の如く公式より求めたる値よりは厚い爲である．而して其の厚さは測定點a_1が表土層の直線の上に乘る爲には 3·5 m 以上ならば如何程でもよいのであるが砂利層の深さ等を參照して觀測點及びa_1，點の下にては 4 m とし a_2～a_4 の部分にては上に得た値にダイナマイト埋塡の深さを加算して 3 m と定めた．次に b 側の觀測點の與へる砂利層の速度は 1130 m/sec より 110 m/sec 早いが故に表土層は河岸に近づく程薄くなつて居り正確には上の公式を用ひる事は出來ぬが其の補正量は小であるので第一近似として上の値を用ひて大差はない．之にもダイナマイト埋塡の深さを加算して 3 m と定める．砂利層の厚さ h_2 は a 側陸上部分の測定値 a_4 が記錄不明瞭のため，正確なりと保し難いが大體第1表の如き値であるとすればこの點を通り他の部分で定まる岩盤の速度を與へる直線と，砂利層の速度を與へる直線との交點より

$$h_2=\frac{43{\cdot}4}{2}\sqrt{\frac{4770-1130}{4770+1130}}-0{\cdot}5=16{\cdot}6\ \mathrm{m}$$

となる．右邊の第2項は表土層のあるための補正値である[1]

b 側陸上部分にても岩盤を通つてきた波の初動は可なり小さいが，やはり二つの直線の交點よりその深さを求めれば

$$h_2=\frac{27{\cdot}0}{2}\sqrt{\frac{4770-1130}{4770+1130}}-0{\cdot}5=10{\cdot}6\ \mathrm{m}$$

となる．第2項は補正値である．

河底部分の砂利層の厚さは，觀測點 b 附近には河底の砂利層と異る速度を持つ砂利層が存在して居たり又陸上の表土層の厚さも必ずしも一様でなかつたりするので公式に代入して簡單に求める事は出來ない．併し，各層の速度は分つて居て，各層間に於ける彈性波の臨界角は算出出來るから，適當の厚さを假定して波の經路を作圖し其の經路を進むに要する時間が測定より得られた走時と一致する如く砂利層の厚さを定むればよい．かくの如くして求めたものを圖示すれば第4圖の如くなる．砂利層の厚さは平均大體 20 m である．

第 II 測定線についても大體上と同様の事を行へばよい．c 側の表土層の厚さ

$$h_1=\frac{10{\cdot}8}{2}\sqrt{\frac{1130-525}{1130+525}}=3{\cdot}1\ \mathrm{m}$$

陸上表土層下の砂利層の厚さ

$$h_2=\frac{31{\cdot}6}{2}\sqrt{\frac{4770-1130}{4770+1130}}-0{\cdot}7=11{\cdot}7\ \mathrm{m}$$

---

(1) 例へば那須信治．地震計による地下探査法．岩波講座(地質)．

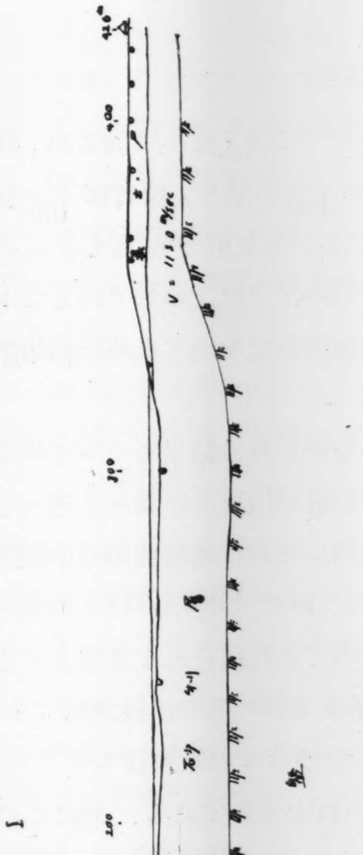
大 同 江
I
砂利層
岩盤
V = 1130m/sec
V = 1700m/sec
V = 1130m/sec
100
200
300
400
420m
+10m
0
-10m
-20m

第4圖 第I測定線斷面圖

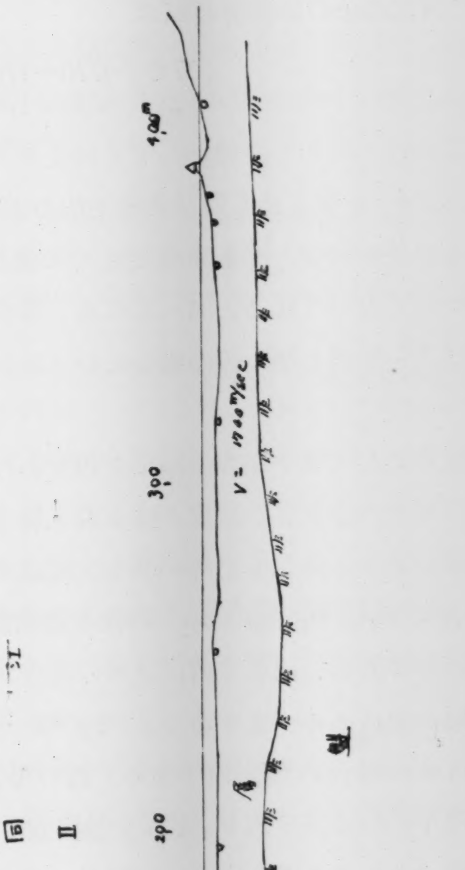
大 同 江
II
砂利層
岩盤
V = 1130m/sec
V = 1700m/sec
100
200
300
400m
+10m
0
-10m
-20m

第5圖 第II測定線斷面圖

△: 微動計設置點　表土層の速度 = 525m/sec

●: 爆發點　砂利層の速度 {(陸上) = 1130m/sec, (河底) = 1700m/sec}

岩盤の速度 = 4770m/sec

d 側にて河底部分の砂利層の厚さ

$$h_2=\frac{37{\cdot}0}{2}\sqrt{\frac{4770-1700}{4770+1700}}=12{\cdot}5\ \mathrm{m}$$

岩盤は既にのべた如く全體としてd側よりc側に向つて深くなつて居るが，測定値 c_7, d_6, 及 c_8, d_5 に見る如く前二者は平均の走時より $\frac{2}{100}$ 秒早く，後者は $\frac{3}{100}$ 秒遲くなつて居るが故に岩盤の形も亦爆發點 c_7 の箇所にては平均より 6 m 高く，c_8 の箇所にては 8 m 低くなつて居ると考へられる．岩盤の全體の深さは上の如くにして求めた砂利層の厚さを參照し第I線の場合にのべた如き數値計算をやつて求めた結果第5圖を得た．

以上の如くにして地下探査の結果を得たわけであるが，此の結果について最も注意すべき點は河底の砂利層の速度と陸上表土層下の砂利層の速度とが異ると考へて計算を行つた事である．而して之等が異ると結論するに致つたのは走時曲線の中觀測點 a, b, c 等に付て $\overline{a_2a_3}$, $\overline{b_2b_3b_4}$, $\overline{c_1c_2c_3}$ の枝と觀測點 d について $\overline{d_1d_2d_3}$ の枝との與へる傾きの差異のみである．而して眞に之等の速度が異るのであればそれを證據立てるものが走時曲線の中にあるべきである． その唯一の手懸りを與へるのは觀測點 b について距離 366 m の場合の測定値である．此の場合 b より 366 m の地點卽ち a より 60 m の點地の地下の形は測定値 b_{12} とは全然獨立に定められたものである．故にこの點の平均の直線 $\overline{b_7b_{11}}$ よりの Debiation が二つの砂利層の速度の相異に關係するのである．卽ち爆發點 b_{12} に於ける表土層の厚さ及砂利層の厚さを他の爆發點 b_{11}, b_{10} 等に於ける表土層及砂利層の厚さに較べれば（第4圖を參照して）下表の如くなる．

	b_{12}	b_{11}	b_{10}
表土層の厚さ	3 m	0 m	0 m
砂利層の厚さ	18·2 m	20·0 m	20·0 m

今爆發點 b_{12} の下の砂利層の速度は 1130 m/sec なるも爆發點 b_{11}, b_{10} 等の下に於ける砂利層の速度は分らないとし之を V とする．さうすると測定値 b_{12} の平均の値よりの Deviation 0·010 秒は b_{12} が 3 m の表土層を通る事による 0·0057 秒と b_{12} と b_{10} 等とが砂利層を通過するに要する時間の差との和に等しいはずである．

$$0{\cdot}0100=0{\cdot}00572+\left(\frac{18{\cdot}2}{1130}-\frac{20{\cdot}0}{V}\right)$$

故に $$V=1680\ \mathrm{m/sec}$$

となり河底の砂利層の速度として 1700 m/sec を用ひる事は不當ではない事が分る．

5. 吟味

斯の如く若し河底の砂利層の中を傳はる波の速度が陸上表土層下の砂利層の中を傳はるものより早いとすれば，上の例に於ける觀測點 d の如く之を水中に設置する等の事をなさなかつた場合には，他の觀測點 a, b, c 等に於けるが如く河底の砂利層の速度は他のものに隱されて見出されずに終る場合の生じ得る事は容易に想像される．從つて如何なる場所に微動計を設置すれば之を見逃す事がないかといふ問題は豫め吟味して置く事が必要である．

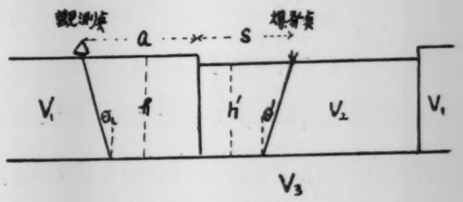

第　6　圖
V_1：陸上の砂利層の速度
V_2：河底の砂利層の速度
V_3：岩盤の速度
$V_1 < V_2 < {}_3V$

今第6圖の如き模型を考へる．中央の部分が河で其の下に V_2 なる傳播速度を有する砂利層が存在し之に續いて兩岸に V_1 なる傳播速度を有する砂利層があり其等の下に水平な岩盤が存在すると考へる．簡單のため陸上の砂利層の上には表土層は存在しないと考へる．今微動計を河岸より a なる距離の所に据ゑ爆發點を順次移動せしめた場合の走時を考へて見る．それには走時曲線に於て線の折れる點が如何に動いて行くかを見るのが最も便利であるが故に之を求める事とする．

例へば河岸よりの距離 Si なる點にて爆發を行ひたるとき，これによりて起こされたる彈性波が觀測點に到達する經路は一般に２つ考へられる．1つは直接波であつて之の走時を T_1 とすれば

$$T_1 = \frac{a}{V_1} + \frac{Si}{V_2}$$

である．他の一つは屈折波であつて之の走時を T_2 とすれば

$$T_2 = \frac{h}{\cos\theta}\,\frac{1}{V_1} + \frac{h'}{\cos\theta'}\,\frac{1}{V_2} + \frac{a+S-h\tan\theta-h'\tan\theta'}{V_3}$$

玆に

$$sin\theta = \frac{V_1}{V_3}$$

$$sin\theta' = \frac{V_2}{V_3}$$

走時曲線に於て Curve の折れる所とはこの２つの走時の等しい所であるからその點に於ける Si を So とすれば　$Si = So$　にては　$T_1 = T_2$

$$\frac{a}{V_1} + \frac{So}{V_2} = \frac{h}{\cos\theta}\,\frac{1}{V_1} + \frac{h'}{\cos\theta'}\,\frac{1}{V_2} + \frac{a+So-h\tan\theta-h'\tan\theta'}{V_3}$$

之より So を求むれば

$$So = \frac{V_3-V_2}{V_2V_3}\left(\frac{h\cos\theta}{V_1} + \frac{h'\cos\theta'}{V_2}\right) - \frac{V_2(V_3-V_1)}{V_1(V_3-V_2)}\,a$$

上の式に於て簡單のために　$h=h'$　と置き

又

$$V_3=\frac{1}{p}V_1$$

$$V_2=rV_1$$

と置けば

$$So=\frac{hr}{1-pr}\left(\sqrt{1-p^2}+\frac{\sqrt{1-p^2r^2}}{r}\right)-\frac{r(1-p)}{1-pr}a \qquad (1)$$

實際野外にて測定を行へば其の場合々々に應じて p, r 及 h の値は色々に變り得るが上に述べた大同江の場合に近い數値を之等の文字に與へた場合 a の値即ち微動計を設置する位置が移動する事により走時曲線が如何に變化するかをしらべる事とする.

$$p=1/4$$

$$r=1{\cdot}4$$

$$h=10\,\mathrm{m}$$

と假定すれば $V_2=1700$ m/sec のとき $V_1=1210$ m/sec, $V_3=4860$ m/sec となり大同江の場合と大體に於て似通つた數値となる. このとき微動計を河岸より 5 m, 10 m, 20 m, 及び 30 m の所に据ゑた場合それ等の走時曲線は第7圖に示す如くなる.

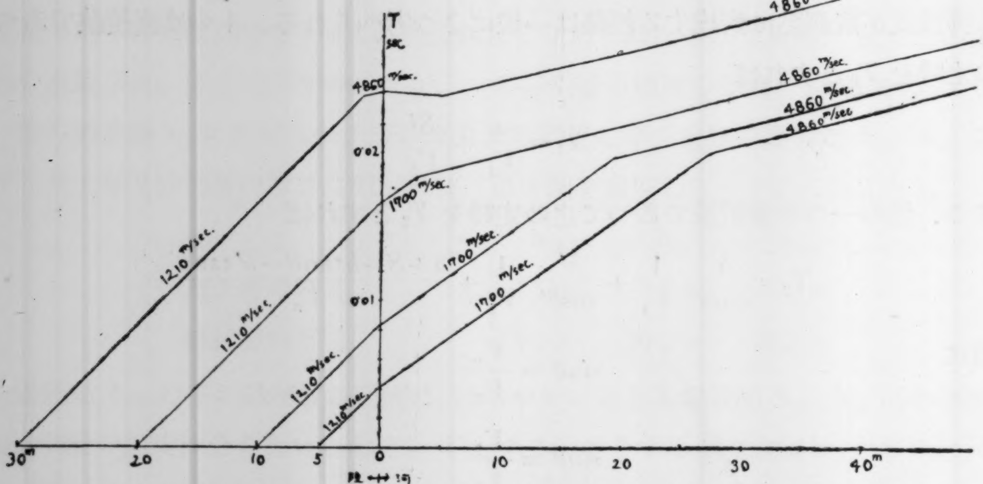

第7圖　$V_1=1210$ m/sec, $V_2=1700$ m/sec, $V_3=4860$ m/sec, $h=10$ m の場合, 河岸より 5m, 10m, 20m, 30m の所に微動計を設置せるさきの夫々の走時曲線

圖に於て横軸に距離 0 と書いた所が河岸であり之より右方は河, 左方は陸と考へる.

圖の如く岩盤が淺く僅か 10m 位しかない場合には微動計を河岸より僅々5米の所に据ゑても尙河底の砂利層の速度を見出す爲には爆發點を適當な位置に細い間隔で設けなければならぬ事が明らかである. 微動計を河岸より 10m の所に据ゑた場合は普

通の如く 10m の間隔で特に注意を拂はずに爆發點を設けて行つたのでは河底の砂利層の速度が見出される事は益々難かしくなる．若し河岸より 20m の所に微動計を据ゑたとすれば，初動の走時曲線だけから河底の砂利層の速度を見出す事は出來なくなり，河底の砂利層と陸上表土層下の砂利層との間に速度の相異の存在する事が氣付かれずに終る恐れがある．更に遠く例へば 30 米も河岸より隔りたる所にては尙更此の傾向は著しくなりも早如何にするも河底の砂利層に個有な速度を與へる傾は走時曲線の何所にも見出し得なくなる．而も此の形の走時曲線だけからでは河底の砂利層の速度を見決める事は出來ない．勿論丁度河岸の所で走時曲線の中岩盤の速度を與へる枝に段違ひは生じるけれども此の段違ひが生じたのは砂利層の速度が變つたが爲であるか又は岩盤の深さそれ自體が變つたが爲であるかを見分ける方法は此の走時曲線だけからは何等得られないからである．故に測定をなすに當つては微動計を設置する位置を充分注意し此の速度の差が存在する様な場所に於てはそれを區別する事の出來る様特別の注意が拂はれなければならぬ．尙微動計を非常に河岸近く据ゑた時に第7圖の5mの所から始まる走時曲線だけから陸上表土層下の砂利層の速度を見出す事は出來ないから別の方向に適當に短い補助の測線を設け之による走時曲線から其の速度を求むればよい．

大同江の調査を了りて後筆者はやはり朝鮮の大寧江といふ河に於て同じ様にして調査を行つたが此の際には

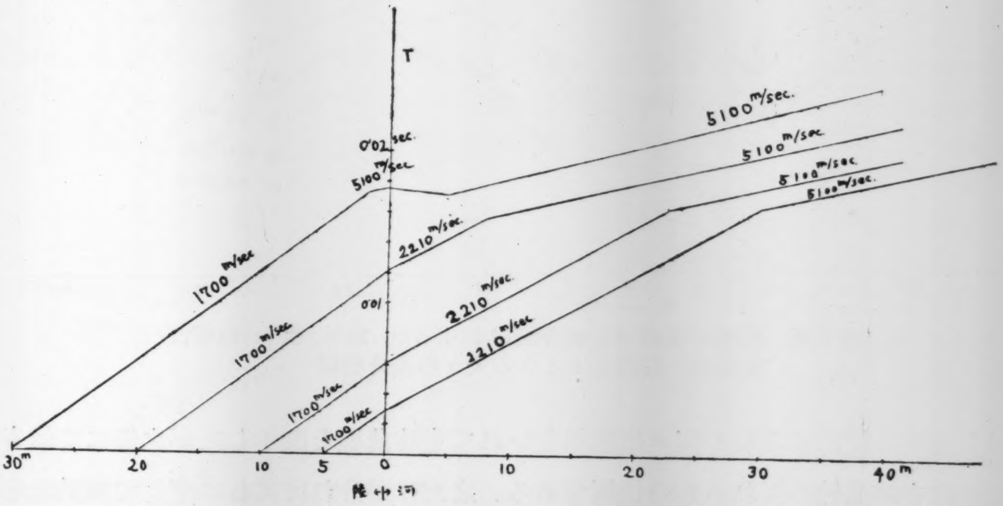

第8圖　$V_1=1700$ m/sec,　$V_2=2210$ m/sec,　$V_3=5100$ m/sec,　$h=10$ m　の場合，河岸より 5m, 10m, 20m, 30m の所に微動計を設置せるさきの夫々の走時曲線

陸上表土層下の砂利層の速度	1700 m/sec
河底の砂利層の速度	2210 m/sec
岩盤の速度	5000 m/sec

なる値を示した．之は先の(1)式に於て

$$p=1/3$$

$$r=1{\cdot}3$$

と置いた場合に近い．今 p, r を上の如く置き $V_1=1700$ m/sec, $h=10$ m と假定して第7圖と同じ様な曲線を畫けば第8圖の如くなる．

之に於ても微動計を置く位置が河岸よりあまり遠くなると河底の砂利層の速度を正確に決め得なくなる事第7圖に説明したと同様である．

以上の二つの圖は岩盤が水平なる場合に付てであるけれども次に之が傾斜して居る場合を考へる．岩盤が河の方へ向つて10°の傾斜角を以て傾いて居り丁度河岸の所で岩盤までの深さ 10 m で p, r, 及び V_2 等の數値は第7圖のものと同一なりと假定すれば其の時の走時曲線は第9圖の如くなる．

之に於ては微動計を置く位置が河岸より 20 米隔れば既に河底の砂利層の速度が走時曲線に現れて來なくなるのが見られる．

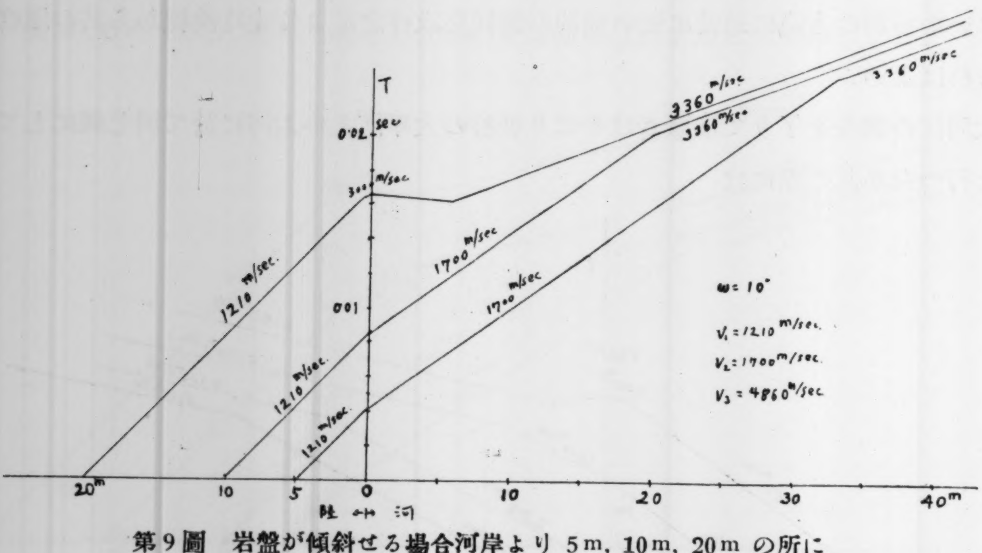

第9圖　岩盤が傾斜せる場合河岸より 5 m, 10 m, 20 m の所に微動計を設置せるときの夫々の走時曲線

以上說明に便にするため個々の數値をいれて走時曲線を圖示したが之等にて最も重要な所は走時曲線の折れる點の位置である．之だけが分れば其れに應じて微動計を設置すべき位置も定つてくる．故に豫め色々な場合を想像して走時曲線の折れる位置を求めて置く事も無駄ではないと思はれる．

先に書いた式(1)に於て今簡單のために $a=5$ m 卽ち微動計を最も河岸に近く置いた場合を考へる事とする．後の圖を見て明らかなる如く斯く河岸近く微動計を設置

しても尙 h が小なる場合には S_0 の値は甚だ小さくなり卽ち走時曲線に於て河底の砂利層に個有の傾きを與へる部分が非常に短くなり從つて河底の砂利層の速度が見出されずに終る恐れがあるから微動計を河岸より 20m も 30m も離して置く場合には充分注意を爲て居かなくてはならぬ.

(1) 式に於て $a=5$m 河底の砂利層の速度と陸上表土層下の砂利層の速度との比 r が 1·1, 1·3,（大寧江の場合）1·4（大同江の場合）, 及 1·6 等色々異る場合，表土層下の砂利層の速度と岩盤の速度との比 p 及び岩盤の深さ h が變るにつれ S_0 の値が如何に變るかは第10圖（A)~(D）に示す通りである.

之等の圖を用ひて豫め大體の見當を知る事が出來る．例へば大同江の如く

$$r=\frac{V_2}{V_1}=\frac{1700}{1130}\doteqdot 1\cdot4$$

$$p=\frac{V_1}{V_3}=\frac{1130}{4800}\doteqdot\frac{1}{4}$$

$$h\doteqdot 20\text{ m}$$

の場合第10圖（B）より $S_0\doteqdot 70$ m 卽ちたとへ微動計を河岸より 5m の所に据ゑても

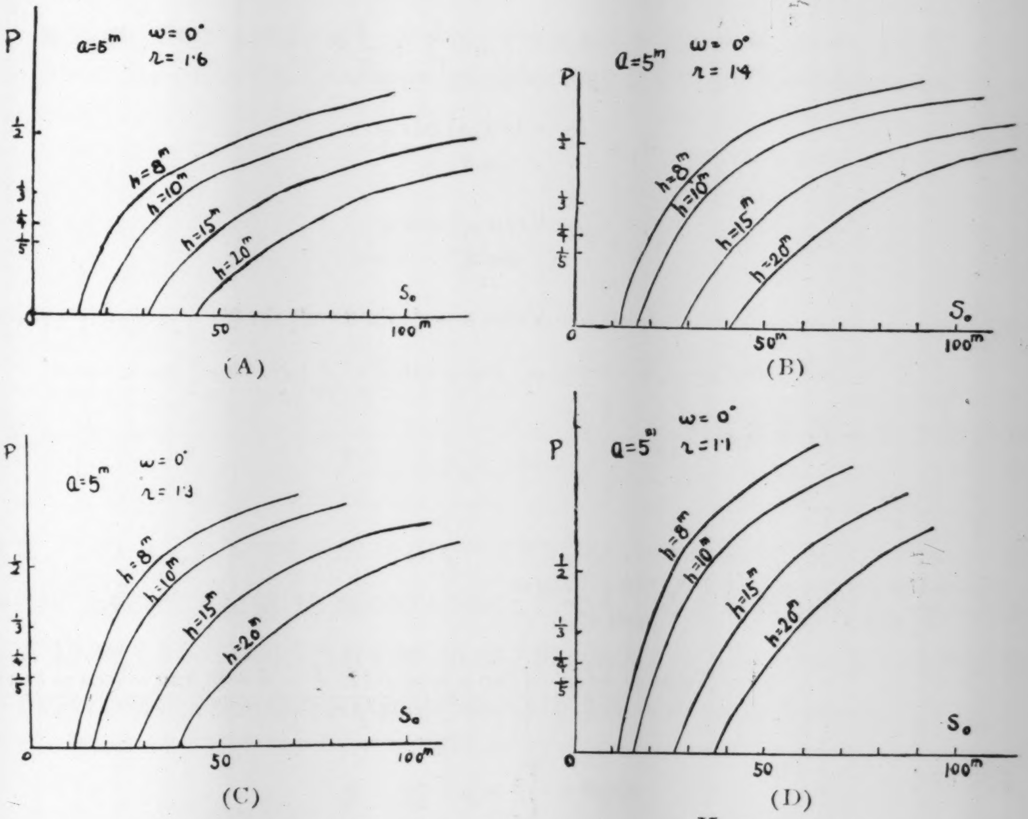

第10圖　$V_2=1\cdot6V_1$, $1\cdot4V_1$, $1\cdot3V_1$, $1\cdot1V_1$, のとき $\frac{V_1}{V_3}$ の變化に應じ走時曲線に於て V_2 を與ふべき部分の長さ

河底の砂利層個有の速度を與へる傾きを示す部分は走時曲線にては 70m しかない事を知る事が出來るのである．

併し一般に上の如く岩盤が水平である事は少く河の方へ深く傾斜して居る事が多い．故に此の様な場合に上の圖はどうなるかをしらべて置く事とする．

第 11 圖

V_1：陸上の砂利層の速度

V_2：河底の砂利層の速度

V_3：岩盤の速度

$V_1 < V_2 < V_3$

ω：岩盤が水平面となす傾きの角

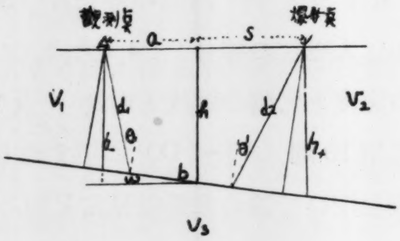

第 14 圖の如く岩盤が ω なる傾斜をなして居り丁度河岸での深さ h であつたとき水平な場合の如く S_0 を求める式を作る．今圖の如き符號を用ひる事とすれば，一般の式[1] を多少變形して直接波の走時 T_1 及屈折波の走時 T_2 は夫々次の如くなる．

$$T_1=\frac{a}{V_1}+\frac{S}{V_2}$$

$$T_2=\frac{d_1}{V_1}+\frac{d_2}{V_2}+\frac{b}{V_3}$$

玆に

$$d_1=\frac{(h-a\tan\omega)\cos\omega}{\cos\theta}$$

$$d_2=\frac{(h+S\tan\omega)\cos\omega}{\cos\theta'}$$

$$b=(a+S)\cos\omega-d_1\sin\theta-d_2\sin\theta'$$

$$=(a+S)\cos\omega-(h-a\tan\omega)\cos\omega\tan\theta-(h+S\tan\omega)\cos\omega\tan\theta'$$

$S=S_0$ にて $T_1=T_2$ とすれば

$$\frac{a}{V_1}+\frac{S_0}{V_2}$$

$$=\frac{(h-a\tan\omega)\cos\omega}{V_1\cos\theta}+\frac{(h+S_0\tan\omega)\cos\omega}{V_2\cos\theta'}$$

$$+\frac{(a+S)\cos\omega-(h-a\tan\omega)\cos\omega\tan\theta-(h+S_0\tan\omega)\cos\omega\tan\theta'}{V_3}$$

前の如く

$$\sin\theta=\frac{V_1}{V_3}=p$$

1）那須信治　前掲 第23頁

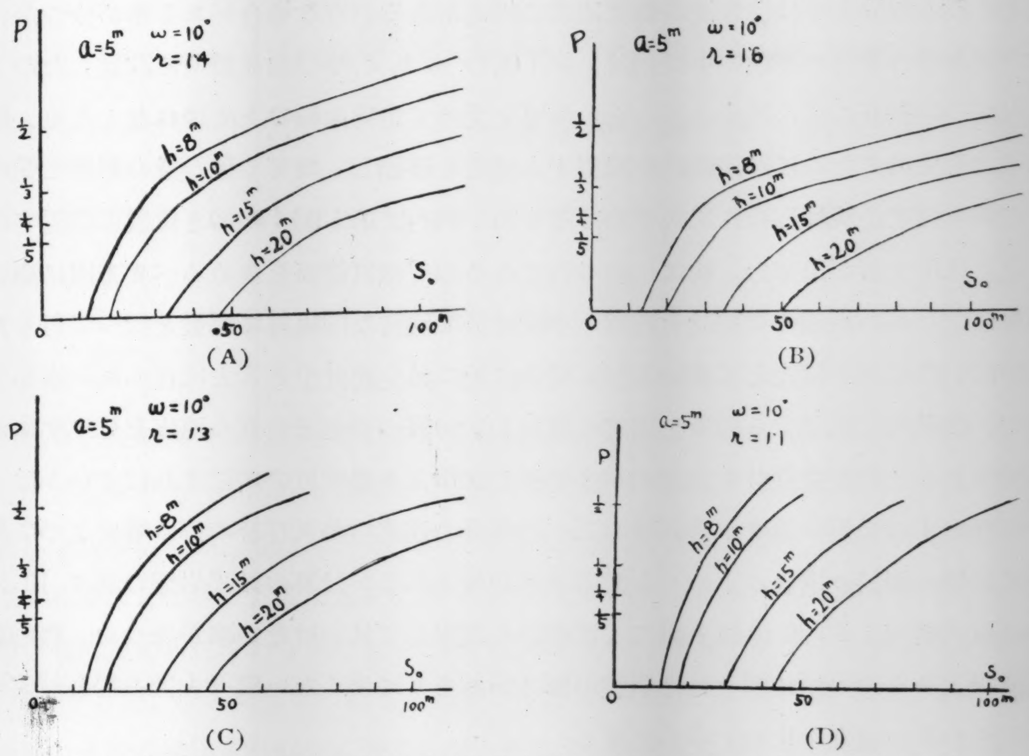

(A)　(B)

(C)　(D)

第12圖　岩盤が水平面に對し10^0の傾きを有する場合 $V_2=16\,V_1$, $1{\cdot}4\,V_1$, $1{\cdot}3\,V_1$, $1{\cdot}1\,V_1$のとき$\frac{V_1}{V_3}$の變化に應じ走時曲線に於てV_2を與るべき部分の長さ

$$\frac{V_2}{V_1}=r$$

$$\sin\theta'=\frac{V_2}{V_3}=rp$$

と置けば上の式は

$$S_0=\frac{h\left\{\cos\omega\sqrt{1-p^2}+\dfrac{\cos\omega\sqrt{1-r^2p^2}}{r}\right\}-a\left\{1-p\cos\omega+\sin\omega\sqrt{1-p^2}\right\}}{\dfrac{1}{r}-p\cos\omega-\dfrac{\sin\omega\sqrt{1-r^2p^2}}{r}}$$

となる．この a,p,r, 及び h に第10圖を作る際に用ひたと同様の數値をあてはめ，且つ$\omega=10^0$と假定すれば第 10 圖の時と同様にして S_0 の値を示す圖を求める事が出來る（第 12 圖 (A)～(D))．之等を第 10 圖と較べる事により $a=5$m ならば S_0 の値はかくの如く傾いて居た時の方が水平の場合よりも多少大であると云へる．

5. 結　　語

大同江の例に見る如く砂利層の中，水の流れて居る河底にある部分と陸上の表土層

の下にある部分とでは彈性波の傳播速度に相違があるやうな場合がある事が分つた．此の樣な場合筆者の實驗の中微動計を第1圖の a, b, c 等の如き箇所に設置したのでは河底の砂利層の眞の速度は他の層の影響を受けて走時曲線の上に現れなくなる．從つて之を見出すためには微動計を設置する位置を移動し，成可く他の層の影響を受けずに眞の速度が現れる樣に工夫せねばならぬ．例へば第1圖 d の如き位置に設置すれば之を見出す事が出來た．故に一般に行はれる如く地質斷面を求めるべき方向に測定線を設定し其の兩端に微動計を設置し中間に於て適當な間隔每に爆發を行つて行くだけでは，特に河を橫斷して實驗を行ふ場合に於ては，充分であるとは言へない事が分つた．微動計を設置する場所を適當に選定し，河底の砂利層の眞の速度を見出す事が必要である．此の微動計を設置すべき場所を河岸より幾米位の所にすればよいかは，砂利層の下の岩盤の速度，砂利層の二つの部分の速度の差及び層の厚さ等によつて異り又岩盤の傾斜の度合によつても變る事が想像されるが計算の結果岩盤の深さ 10 米の時は大體河より 20 米以上距てゝ微動計を設置してはいけない事が分つた．微動計を河岸より5米の所に据ゑれば岩盤の厚さがあまりに淺くない限り大抵の場合河底の砂利層の眞の速度を見出す事が出來る．

終りに臨み始終御懇篤な御指導を賜つた石本先生に厚く御禮を申上る次第である．

---

14. Results of Seismic Prospecting at the Daidôkô River, Korea.

By Syun'itiro, OMOTE,

Earthquake Research Institute.

With a view to ascertaining the depth of the bed rock under the Daidôkô River, last summer, seismic prospecting was resorted to.

High magnification seismographs were used. Wireless was availed of in timing the shots and communicating between shot-point and receivers.

The time-distance curves are shown in Figs. 2, 3 and the geological structures deduced from them in Figs. 4, 5. The depth of the bed rock was about 15～20 meters. The velocities found were as follows:

Through the superficial soil	525 m/sec.
Through the gravel layer underlying the superficial soil	1130 m/sec.
Through the gravel layer under the river	1700 m/sec.
Through the bed rock	4770 m/sec.

In prospecting of this kind, care must be taken not to overlook the velocity of the gravel layer under the river.

15. 伊豆七島新島の火山

地震研究所 津屋弘逵

(昭和12年2月16日發表——昭和12年12月20日受理)

緒言

昭和11年12月27日午前9時14分頃，伊豆七島中の新島附近に局部的の强震が起り，夫に因つて同島を初めとして附近の式根島及び利島に於いて多少の損害が生じた．之等の島々は何れも火山島で，特に新島は有史時代の噴火記錄を有し，從つて若し今回の地震が之等の島の何れかの火山の潜伏的活動に關係して起つたものとすれば，其關係を暗示する樣な現象が其火山の附近に現れ，或は地震に因る被害，地變等の分布に認められるかも知れないと考へられたので，昭和12年1月末より2月初めの約10日間，筆者は震災の最も甚しかつた新島の地震に因る地變を調査すると共に，同島の火山の構造を全般的に觀察した．其結果，今回の地震が新島の火山の潜伏火山活動或は同島の地下の地質構造に特に關係して起つた事を推定せしめる樣な現象は認められなかつた．今回の地震の規模，被害及び地變の程度，分布等は既に萩原，表兩學士[1]に依つて報告せられ，又松澤博士其他の諸氏[2]に依つても論ぜられてゐるから，玆では主として新島の火山の構造に就いて筆者の觀察し得た結果の大要を報告するに止める．

新島の地質

新島は北北東—南南西の方向に約11kmの長さと夫に直角の方向に最も廣い所で約2.5 kmの幅とを有する狹長な島で，地形的には宮塚山（海拔408 m）及び夫に接續する北部山地，向山（海拔283.4 m）及び夫に接續する南部山地，及び南北兩山地を連ねる本村の低地（海拔30〜60 m）の三部に分たれ（第1圖），地質的には島の北端近くの若鄉附近に見られる玄武岩質火山砂礫層を除けば，全島到る處流紋岩類の熔岩及び同質の火山灰砂層に依つて構成されてゐる．即ち，同島の南北兩山地は何れも流紋岩火山の集合してゐる部分である．此流紋岩火山の大多數は神津島の流紋岩火山と同

---

1) 萩原尊禮，表俊一郎，震研彙報，**15**（1937），561〜568.

2) 波江野清藏，河角廣，岸上冬彥，松澤武雄，鈴木武夫，吉山頁一，地震，**9**（1937），45〜55.

様に第四紀に噴出した新しい火山と考へられ，斯る新しい流紋岩火山は本邦に於いて極めて稀であるのみならず，世界に於いても比較的少數知られてゐるのみである．

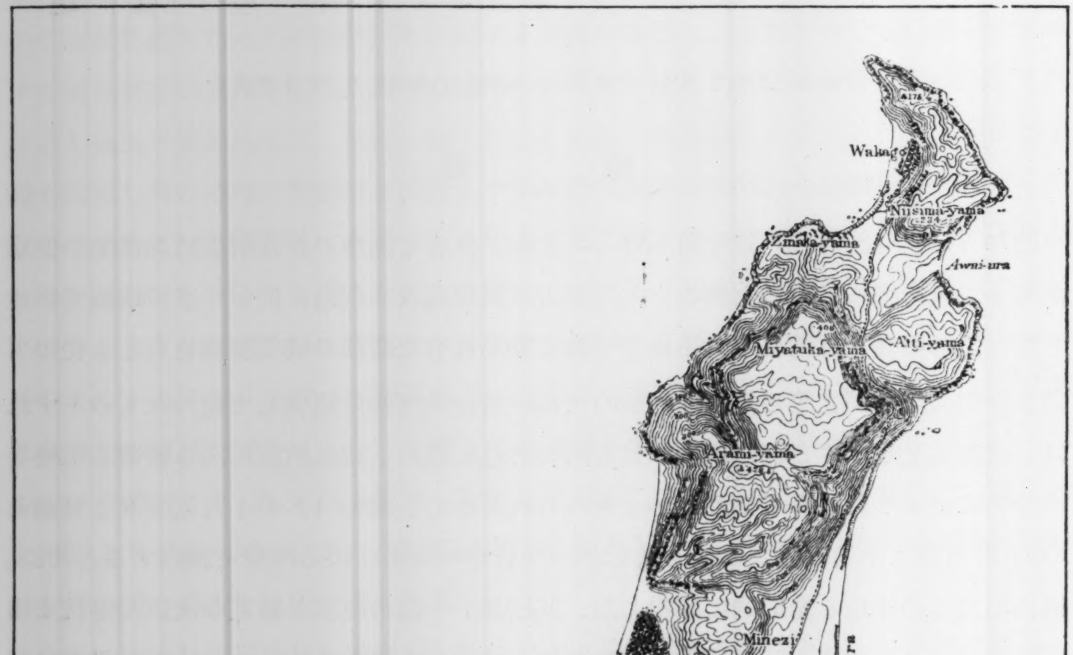

Wakago
Niisima-yama
Zinaka-yama
Awai-ura
Miyatuka-yama
Atti-yama
Arami-yama
Minezi
Honmura
Habusi-ura
Zinai-sima
Seto-yama
NII-SIMA
Mamasita-ura
Omine
Muko-yama
Marusima-yama
Kohama-ura
Nisi-ura
Haya-sima
SIKINE-SIMA
0
1000
2000
3000 m

第１圖　伊豆七島新島地形圖．

第 I 表

福地學士	辻村學士	
富士岩灰砂層	石山トロイデ	向山火山
白ママ層	大峰ホマーテ	
流紋岩類	白ママ層	
I．雲母流紋岩類	富士岩火山礫	
1，向山式熔岩	完全なるトロイデ…アツチ山	
2．淡井浦式熔岩	原形を有する流紋岩床	
3，羽伏浦式熔岩	新島山	
4，跡見ズノ澤式熔岩	宮塚山	
II．角閃石流紋岩類	早島	
5．地内島式熔岩	峰路	
6．若田式熔岩	最舊期流紋岩床	
7．堂丸式熔岩	地内島	
III．輝石流紋岩類	式根島	
8，西ノ浦式熔岩		
9．根武崎式熔岩		

新島は曾て故福地學士[3] 及び辻村學士[4] に依つて夫々地質學的及び地形學的に調査せられた．第 I 表は兩學士に依る新島の地質的及び地形的區分を示す．筆者も亦先に神津島火山[5] の構造及び岩石を研究するに當つて，兩三度新島の地形及び地質を觀察し，採集した數種の代表的岩石の岩石學的性質を檢べた事があるが，當時の觀察は主として福地，辻村兩學士の報告に從ひ，單に新島，神津島兩島の火山構造及び岩石を對比するに必要なる程度の局部的の結果を得たに過ぎなかつた．今回の調査の結果新島の地質區分に就いて從來の夫とは多少異なつた事實が判明した．即ち，同島の熔岩類及び堆積層は筆者の觀察に依れば舊より新に順次下記の如く區別される．

1．瀨戸山熔岩，峰路熔岩，及びヂナーカ山熔岩．
2．大三山凝灰岩及び同凝灰角礫岩層．
3．島分澤凝灰岩層．
4．赤崎ノ峯熔岩及び同灰砂層．
5．新島山熔岩及び丸嶋山熔岩．
6．若鄉玄武岩砂礫層．
7．宮塚山熔岩，同灰砂層，及び羽伏浦灰砂層．
8．淡井浦灰砂層．

---

3) 福地信世，**震像報告**，**39** (1902)，4～40.
4) 辻村太郎，前同，**89** (1918)，57～95.
5) H. TSUYA, *Bull. Earthq. Res. Inst.*, **7** (1929), 269～334.

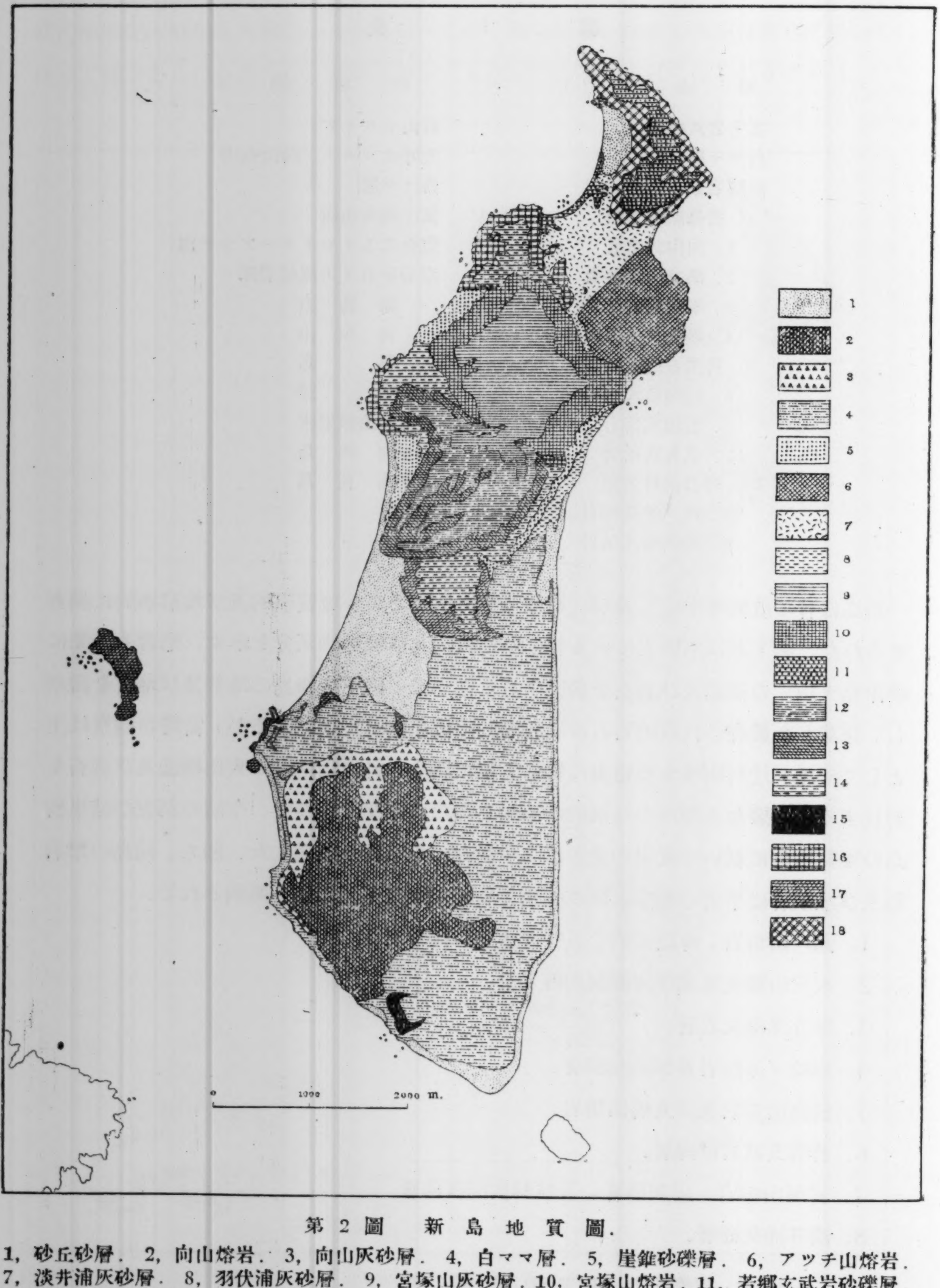
1
2
3
4
5
6
7
8
9
10
11
12
13
14
15
16
17
18
0
1000
2000 m.

第２圖　新島地質圖.

1，砂丘砂層．2，向山熔岩．3，向山灰砂層．4，白ママ層．5，崖錐砂礫層．6，アッチ山熔岩．7，淡井浦灰砂層．8，羽伏浦灰砂層．9，宮塚山灰砂層．10，宮塚山熔岩．11，若郷玄武岩砂礫層．12，赤崎ノ峯灰砂層．13，赤崎ノ峯熔岩．14，島分澤凝灰岩層．15，丸嶋山熔岩．16，ヂナーカ山熔岩．17，瀬戸山熔岩（峰路熔岩を含む）．18，新島山熔岩．

9．アツチ山熔岩．

10．白ママ層．

11．向山熔岩及び同灰砂層．

12．崖錐砂礫層．

13．砂丘砂層．

以上列擧した熔岩類及び堆積層の分布は第2圖の地質圖に示されてゐる通りである．次に之等に就いて其分布，構造，岩質等の大要を順次說明し新島の火山の構造を考察する．

1. 瀨戸山熔岩，峰路熔岩，及び チナーカ山熔岩．

新島の火山は現在の海水面下より聳えてゐるので，火山の所謂土臺と考へられる地層は島內の何處にも露出せず，玆に掲げた種類の熔岩床が，觀察される限りに於いて，同島に於ける最舊の地層を代表し，同島火山の最舊の噴出物である．何れも主として純白色乃至灰白色の浮石質角閃石流紋岩で，長石，石英，及び綠色角閃石の肉眼的斑晶を有する熔岩である．

瀨戸山熔岩は本村部落の南側に位する瀨戸山及び大三山（何れも海拔 120 m 內外）の最下部を構成する．大三山の西側の鳥島，鵜ノ根，黑根等の岩礁群に面する海崖の下部は此熔岩である．又，向山から本村前濱に抗火石採石を運搬する軌道に沿つて，瀨戸山の北東麓の二三ヶ處に同一熔岩が露出してゐる．鳥島及び鵜ノ根，黑根等の岩礁群も亦瀨戸山熔岩の一部である．大三山の西方に約 1 km の水道を距てゝ相對する地內島（長さ 1km, 幅 200 m, 高さ 76.6 m）は福地學士に依れば，角閃石流紋岩（地內島式熔岩）であつて，恐らく曾ては瀨戸山及び大三山の基部と共に一續きの熔岩

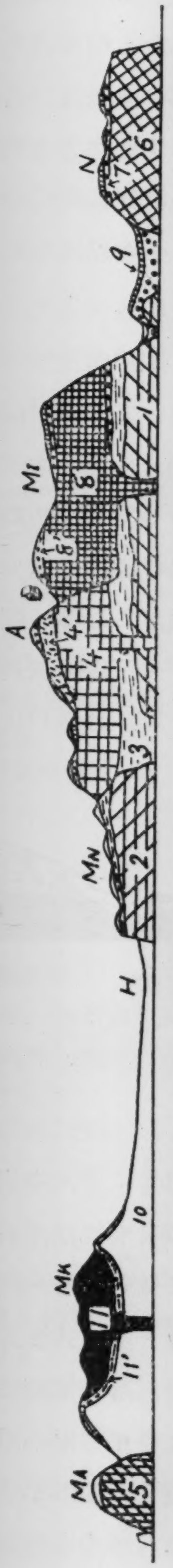

第3圖　新島の模式南北斷面圖．1，チナーカ山熔岩．2，峰路熔岩．3，島分澤凝灰岩層．4，赤崎ノ峯熔岩．4′，赤崎ノ峯灰砂層．5，丸嶋山熔岩．6，新島山熔岩．7，若鄉玄武岩砂礫層．8，宮塚山熔岩．8,′宮塚山灰砂層．9，淡井浦灰砂層．10，白ママ層．11,′向山灰砂層．11，向山熔岩．

N，新島山．MI，宮塚山．A，赤崎ノ峯．MN，峰路．H，本村低地．MK，向山．MA，丸嶋山．

床を形成し，其後の海蝕作用に依つて鳥島及び鵜ノ根，黒根其他の岩礁を殘して新島本島から切離されたものであろう．瀬戸山熔岩は地内島に於いては海面上 76.6 m に達し，大三山西側の海崖及び岩礁群に於いては海面上 20～50 m の高さに達してゐるから，其實際の厚さは之より更に大である．地形圖に示されてゐる樣に，瀬戸山，大三山，及び地内島の何れの部分にも一獨立火山としての形態が殘つてゐないから，此流紋岩の噴出の中心地點は明かでない．

瀬戸山熔岩は後に述べる大三山凝灰岩，同凝灰角礫岩，白ママ層等に依つて不整合に蔽はれてゐる．瀬戸山及び大三山の上部一帶は厚い白ママ層であつて，鳥島附近の間々下浦北端に於いては瀬戸山熔岩の上及び海蝕崖に白ママ層が直接接して堆積してゐる（圖版第1圖）．又，大三山南麓の溫泉場から黒根の船着場又は本村部落に至る通稱海岸道路に沿つた大三山の切取り面に於いては土壤化した瀬戸山熔岩が大三山凝灰岩及び同凝灰角礫岩層に依つて不整合に蔽はれ，更に後者が白ママ層に依つて不整合に蔽はれて露出してゐる（圖版第2圖及び第3圖）．第4圖は大三山西側の海岸附近の瀬戸山熔岩，大三山凝灰岩及び同凝灰角礫岩，及び白ママ層を示す模式斷面圖である．瀬戸山の北麓には瀬戸山熔岩の他に之と同じ岩質の浮石層が白ママ層の下に僅かながら露出してゐる所がある．又，間々下浦の南方に於いても白ママ層及び大三山凝灰角礫岩層に相當する角礫岩層に不整合に蔽はれて同樣の浮石層が殘つてゐる．從つて瀬戸山熔岩の噴出には浮石質火山砂礫の拋出が伴つたに相違ない．第5圖は間々下浦南方に於いて見られる角閃石流紋岩浮石層と之に不整合に接する大三山凝灰角礫岩層及び白ママ層との模式斷面圖である（圖版第17圖）．

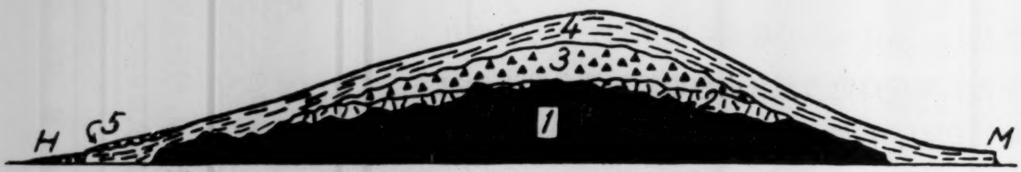

第4圖　大三山西部の模式南北斷面圖．

1，瀬戸山熔岩．2，大三山凝灰岩層．3，大三山凝灰角礫岩層．
4．白ママ層．5，砂丘砂層．H，本村前濱．M，間々下浦．

峰路熔岩は本村部落の東側の峰路と呼ばれる小丘（海拔約 150 m）の下部を構成してゐる．此小丘は略正方形の卓狀の臺地をなし，其北側は尙一段と高い赤崎峯及び宮塚山の山地に接續してゐるが，其他の三方向の山側は大部分絶壁を以つて外方の低地に臨んでゐて，辻村學士の指摘した樣に，獨立の一火山とも考へられる形態を示してゐる．此絶壁には峰路熔岩がよく露出し，少くとも 30～50 m の厚さを有し，其上部

は一樣に純白色乃至灰白色の浮石質であるが，下部には灰色で緻密な部分或は黑色乃至暗褐色で眞珠岩樣の割目を多く有する玻璃質の部分がある．

峰路熔岩は島分澤凝灰岩層及び白ママ層に蔽はれてゐて，熔岩の絶壁に取圍まれた峰路の頂上部一帶には之等の地層が相互に不整合に堆積してゐる．之等の地層は比較的軟弱で浸蝕され易く，大小の谷に依つて刻まれてゐる．峰路の頂上部の凹凸は斯樣な谷の發達に依つて生じた浸蝕地形であつて，峰路熔岩の表面の原地形ではない．後に述べる赤崎ノ峯，宮塚山，新島山等の頂上部の地形も同樣であつて，熔岩の表面の原地形を殘してゐるのはアツチ山及び向山のみである．第2圖の地質圖には峰路の頂

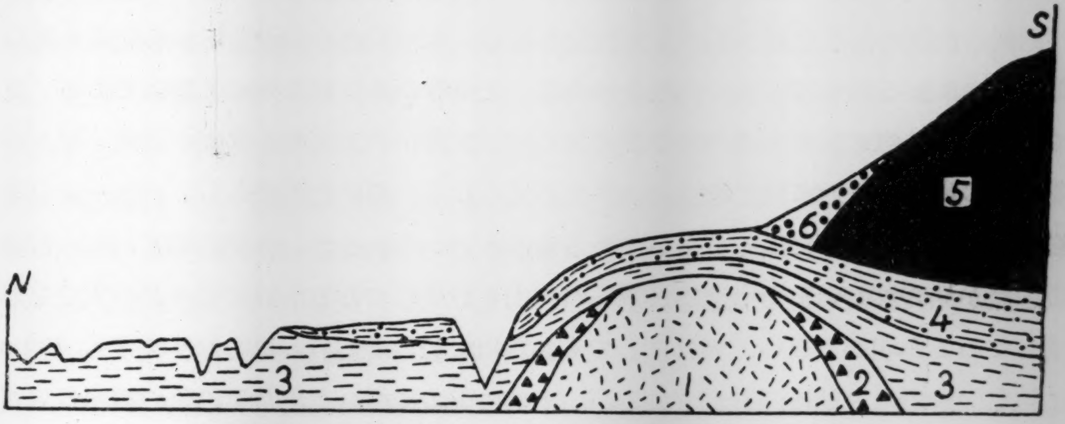

第5圖 (a) 向山西麓（間々下浦南部）の模式南北斷面圖．
1，角閃石流紋岩浮石層．2，大三山凝灰角礫岩層．3，白ママ層．
4，向山灰砂層．5，向山熔岩．6，向山熔岩崖錐堆積層．

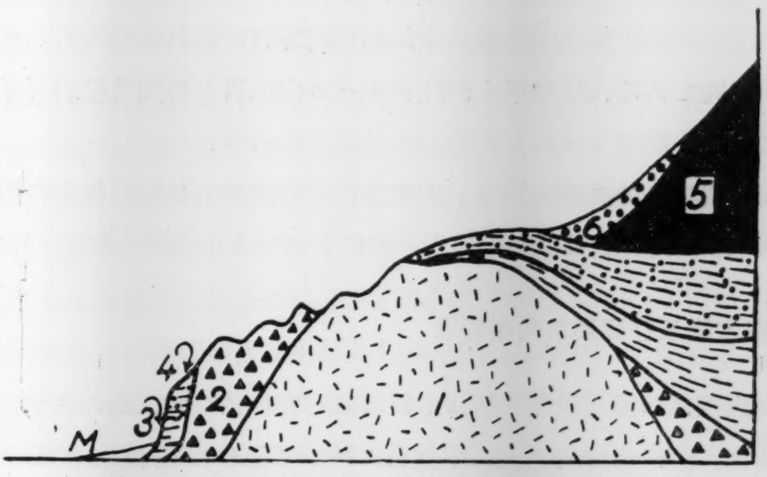

第5圖 (b) 向山西麓（間々下浦南部）の模式東西斷面圖．
1，角閃石流紋岩浮石層．2，大三山凝灰角礫岩層．3，白ママ層．
4，向山灰砂層．5，向山熔岩．6，向山熔岩崖錐堆積層．
M，間々下浦海岸．

上部に存在する白ママ層は省略されてゐる．峰路熔岩と瀬戸山熔岩とは顯微鏡的に全く同一の熔岩と見られるが，恐らく夫々の噴出孔を有する別の火山體であろう．

ヂナーカ山熔岩は宮塚山の北麓に接するヂナーカ山（海拔約170 m）の基部に代表的に露出してゐる．即，若郷前濱の南隅から堂丸崎を經て宮塚山の西麓アカマの海岸に至る間，ヂナーカ山を巡つて高さ100mに及ぶ海崖を形成してゐる熔岩は此熔岩である．ヂナーカ山の東側に於いては宮塚山から若郷に降る急峻な坂道の中途以下及び其兩側の山腹に同じ熔岩が點々と露出してゐる．本村前濱の北隅若田から北方に島分澤の出口に至る間の海崖及び其附近の高根，大磯等の岩礁群も亦同じ熔岩である．更に本村から若郷に至る本道の略中間に當つて，宮塚山の南東部と其南の赤崎ノ峯との間の澤の出口の附近に同じ熔岩の小露出が見られる．斯樣な露出から，ヂナーカ山熔岩は宮塚山火山の下に廣く分布してゐるものと考へられるが，各露出相互の間の實際の連絡が見られないから，之等が單一の火山を形成してゐるか或は夫々別の火山を形成してゐるか明かでない．何れにしても各露出に於ける熔岩の厚さは少くとも100 mに達し，熔岩の上部は浮石質であるが，下部に至るに從ひ灰色乃至黑色の緻密な岩質に移り變つてゐる．ヂナーカ山の北西岸の堂丸崎附近の熔岩には流理構造が見られ，又板狀或は柱狀の節理が發達してゐる．上部の浮石質の部分では瀬戸山熔岩及び峰路熔岩と同じく有色鑛物として角閃石の斑晶のみが現れてゐるが，下部の緻密な岩質の部分では此角閃石斑晶の縁の部分或は全部が單斜輝石に變じて角閃石の外形のみを止めてゐるのが普通である．福地學士が此ヂナーカ山熔岩を輝閃流紋岩（堂丸式熔岩）と呼んだのは恐らく斯樣な輝石を觀察した結果であろう．

ヂナーカ山熔岩は島分澤凝灰岩層，若郷玄武岩砂礫層，其他の後期の噴出物に蔽はれてゐるから，瀬戸山熔岩及び峰路熔岩と共に新島の火山活動の初期の噴出物である．

2. 大三山凝灰岩及び同凝灰角礫岩層．

大三山凝灰岩及び同凝灰角礫岩層は，既に述べた樣に，大三山の西側の海岸道路に沿つた切取り面に瀬戸山熔岩の上に不整合に載つて僅かに露出してゐる（圖版第2圖）．又，間々下浦の南方に於いて瀬戸山熔岩に伴ふ浮石層の上に之に相當する凝灰角礫岩層の小露出がある（第5圖及び圖版第17圖）．之等の他には，觀察した限りでは，新島内の何處にも同樣の地層は見出されなかつた．

第3圖又は圖版第2圖の露出に於いて，土壤化した瀬戸山熔岩の凹凸面上に50 cm内外の粘土層があり，其上に大三山凝灰岩層及び同凝灰角礫岩層が載つてゐる．大三山凝灰岩層は灰黃色の稍軟弱な地層で，微粒の凝灰岩の部分と其中に直徑5 cm内外

の火山岩片を含む凝灰角礫岩の部分とがある．凝灰岩は，顯微鏡觀察に依ると，變質した種々の火山岩の微粒と斜長石，單斜輝石，磁鐵鑛等の破片とから成る．火山岩の微粒の中には輝石安山岩，橄欖石玄武岩，角閃石・複輝石安山岩等が識別される．凝灰角礫岩中の角礫も亦之等の火山岩類である．

大三山凝灰岩層の上には更に明瞭な不整合關係をもつて大三山凝灰角礫岩層及び火山灰層が載つてゐる．此凝灰角礫岩層は 5 m 内外の厚さを有し，上に述べた凝灰岩層に伴ふ角礫岩とは稍趣を異にし，其中に角礫の他に直徑 10 cm 内外の圓礫を含んでゐる．之等の礫及び礫の間を充たす砂には，瀬戸山熔岩と同じ角閃石流紋岩の破片が見出されるが，其他に此島に於いては全く見られない岩石の礫が多量に含まれてゐる．卽，顯微鏡をもつて觀察し得たもののみでも，黑雲母花崗岩，黑雲母石英斑岩，變朽安山岩類，綠色凝灰岩，凝灰質頁岩，輝綠岩，角閃岩等が擧げられる．凝灰質頁岩の礫の中には多數の有孔虫化石を含むものがある．間々下浦の南方に露出する凝灰角礫岩も同樣に上に擧げた樣な種々の岩片を含んでゐる．

大三山凝灰岩及び同凝灰角礫岩層は共に白ママ層に依つて不整合に蔽はれてゐる．

大三山凝灰岩及び同凝灰角礫岩層は，以上の樣な構造から考へると，瀬戸山熔岩が噴出して或程度浸蝕されて後，其附近の流紋岩火山の活動が行はれてゐなかつた時期に其當時の陸上或は海岸近くに堆積した地層である．之等の地層を構成する物質は大部分現在の新島以外の地域から供給されたものに相違ないのであつて，凝灰角礫岩中の變朽安山岩類，綠色凝灰岩，有孔虫化石を含む凝灰質頁岩等は伊豆半島の各地に分布してゐる第三紀中新世を代表する地層を構成する岩石と全く同一である．此事實は新島の流紋岩火山の活動時代を定める上に役立つ一つの重要な材料であつて，此事實から，少くとも瀬戸山熔岩が噴出し，其後の流紋岩類が未だ噴出しない時代に，現在伊豆半島に見られる樣な中新世の地層が新島附近の陸上に在つて浸蝕されつつあつたと言ふ事が出來る．此時代に伊豆半島から新島附近まで陸地が續いてゐたかどうかは直ちに斷定されないが，伊豆半島の南端沖に在る神子元島及び神津島の南西 40 km の距離に在る錢洲礁の岩礁群が伊豆半島の第三紀層に相當する岩石から成立つてゐる事實は此種の第三紀層が伊豆半島から新島，神津島等の附近の現在の海底地域に迄擴がつてゐる事を示すものであろう．

3. 島分澤凝灰岩層.

島分澤凝灰岩層は宮塚山の南西麓の島分澤，佛ノホラ附近に最も代表的に發達してゐる地層であるが，峰路及びヂナーカ山に於いては夫々前に述べた角閃石流紋岩の熔

岩の上に載つて居り，峰路と宮塚山との間に位する赤崎ノ峯の東側の絶壁にも亦赤崎ノ峯熔岩の下に露出してゐる．

此凝灰岩層は極めて整然たる水平層理を示す地層で，島分澤に沿つた一露出に就いて見ると，厚さ約20 cmの赤褐色粘土層を最下として，よく固まつた凝灰岩，砂質凝灰岩，凝灰角礫岩等の互層より成り，50 m 以上の厚さに達し，若田から島分澤の出口迄の海岸に露出するヂナーカ山熔岩類の角閃石流紋岩熔岩及び其集塊岩の上に載つてゐる（圖版第5圖及び第6圖）．凝灰岩は流紋岩玻璃の他に長石，石英，角閃石，黑雲母，單斜輝石等の結晶片を含む．又，凝灰角礫岩中の礫は流紋岩と大三山凝灰角礫岩中に見出された様な第三紀火山岩類とである．

島分澤凝灰岩層は赤崎ノ峯熔岩，宮塚山熔岩，白ママ層等に依つて蔽はれてゐるが，此凝灰岩層と大三山凝灰岩及び同凝灰角礫岩層との直接の野外關係は明かでない．其構成物質から考へると，島分澤凝灰岩層は大三山凝灰角礫岩層に對比されるか或は後者より多少後期の堆積物であろう．

4. 赤崎ノ峯熔岩及び同灰砂層．

赤崎ノ峯熔岩は宮塚山と峰路との間に在る赤崎ノ峯，大峯，アラミ山（海拔 428.5 m）等の山地の主要部を構成する角閃石流紋岩熔岩である（圖版第4圖）．同山地の四周には此熔岩が至る所に絶壁をなして露出してゐるが，特に同山地の東西兩側の熔岩崖は著しい．即，本村から若郷に至る本道の略中央部の西側に，赤崎ノ峯の東側を限つて聳ゆる高さ約300 mの絶壁の中位に露出する熔岩，本村部落の北端のカサモリ稻荷祠附近を突端として北方及び東方に夫々アラミ山の西側及び南側を限つて絶壁をなす熔岩は何れも玆に言ふ赤崎ノ峯熔岩の一部である．

此熔岩は其噴出地點を明かに示さないが，熔岩の底面が赤崎ノ峯から南西方向に次第に低下し，本村部落北端附近では海面近くに達してゐる事實から，北東部に於いて噴出して南西方向に多少流れ下つた事が推定される．

赤崎ノ峯熔岩は150 m 內外の厚さを有し，其上部は灰白色，浮石質であるが，下部は暗灰色乃至黑色で，緻密で堅硬であるか或は眞珠岩狀の割目に富んで脆い．福地學士が若田式熔岩と稱して記載した熔岩は峰路の熔岩の大部分を含んでゐるが，赤崎ノ峯熔岩と峰路熔岩とは時代の異なつた別の噴出物である．赤崎ノ峯熔岩は石英，長石及び赤褐色の多色性の著しい角閃石斑晶を含み，此角閃石は時に一部或は全部單斜輝石に變じてゐる．

赤崎ノ峯熔岩の上には之と同じ岩質の浮石灰砂層が載り，赤崎ノ峯，大峯，アラミ

山等の上部に廣く分布してゐる．從つて，赤崎ノ峯熔岩の流出に次いで浮石質火山灰砂の噴出が行はれたと考へられる．

赤崎ノ峯熔岩及び同灰砂層は島分澤凝灰岩層の上に載り，宮塚山火山の噴出物及び白ママ層に依つて蔽はれてゐる．赤崎ノ峯熔岩と宮塚山熔岩とは島分澤に依つて距てられてゐるが，宮塚山灰砂層は島分澤上流の南側の赤崎ノ峯頂上部附近に於いて赤崎ノ峯灰砂層の上に不整合に載つてゐる．

5.　新島山熔岩及び丸嶋山熔岩．

新島山熔岩は新島の北端に近い若郷部落の背後に聳ゆる新島山（海拔 *234* m）の下部を構成する熔岩で，同山を取圍む北，東，南東の三方面の海崖及び若郷部落背後の絶壁に續いて露出し，海面上のみでも 100～150 m の厚さを有する（圖版第9圖）．其上部と下部とが相異なる岩質を示す事は他の熔岩の場合と同様である．下部には淡井浦の北隅の露出に見られる様に，集塊熔岩の狀態を示す所があり，又球顆狀構造を有する部分も少くない．此熔岩は長石，石英，黑雲母，角閃石等の斑晶を有する角閃石・黑雲母流紋岩で，稀に角閃石流紋岩の岩片を捕獲してゐる．角閃石斑晶は多くの場合一部或は全部單斜輝石に變化してゐる．

福地學士は此熔岩を頑火流紋岩（根武崎式熔岩）と稱し，新島に於いて最も舊い熔岩と見做したが，頑火流紋岩といふ名稱は適當でなく，最も舊い熔岩であるといふ事實も無い．新島山熔岩は後に述べる若郷玄武岩砂礫層及び淡井浦灰砂層に蔽はれてゐるから，之等の地層より確かに舊い．新島山熔岩とヂナーカ山熔岩との前後關係を示す直接に相接する露出は見られないが，上に述べた様に，前者は角閃石流紋岩の破片を捕獲してゐるから，角閃石流紋岩熔岩より後期の噴出物に相違ない．新島山熔岩と其南方に夫々の火山を形成する宮塚山熔岩及びアツチ山熔岩との直接に相接してゐる露出も見られないが，新島山熔岩は若郷玄武岩砂礫層及び淡井浦灰砂層より舊期の噴出物であり，宮塚山熔岩及びアツチ山熔岩は若郷玄武岩砂礫層より後期の噴出物であるから，兩者の前後關係は自ら明白である．從つて，新島山の角閃石・黑雲母流紋岩はヂナーカ山其他の角閃石流紋岩類の噴出期と宮塚山，アツチ山等の黑雲母流紋岩類の噴出期との中間の一時代に噴出した熔岩で，恐らく夫自身の噴出中心を有する一火山であろう．然し，現在の新島山の形態からは此火山の生成當初の大いさ並びに噴出中心を知る事は出來ない．

丸嶋山熔岩は新島の南端に近く，向山火山の南麓に小突起をなす丸嶋山又は丸山（海拔約 *230* m）を構成し，此山の北，西，南の三方面の絶壁に高さ 150 m 内外の熔

岩崖をなして露出してゐる（圖版第8圖）．山の頂上部及び東側は白ママ層に蔽はれ，白ママ層の噴出中心である大峯火山に接續してゐる．北，西，南の三面の熔岩崖の麓にも，白ママ層が熔岩壁に接して殘つてゐるのであつて，曾て丸嶋山熔岩の山體が白ママ層の下に埋もれてゐた事を示す．

丸嶋山を取圍む絶壁に露出する熔岩の上部は灰白色浮石質であるが，中部以下は板狀節理と柱狀節理とを有し，灰色緻密石質であるか或は眞珠岩樣割目を多く有する黒曜石質で，集塊岩狀を呈する部分もある．山の西側の絶壁には明瞭な流理構造が見られ，山體の中心部に當る所には殆ど垂直の流理，外側に當る所には中心部に向つて約60° の傾斜を示す流理が發達し，同熔岩が一の熔岩圓頂丘の構造を有する事を示してゐる．

丸嶋山熔岩は上に述べた新島山熔岩と同じく，長石，石英，黒雲母，角閃石等の斑晶を含む角閃石・黒雲母流紋岩で，角閃石斑晶の一部或は全部は單斜輝石に變化してゐる．丸嶋山熔岩は白ママ層より舊く，從つて向山熔岩より舊い事勿論である．恐らく丸嶋山熔岩と新島山熔岩とは略同期の噴出物で，夫々別の噴出中心を有する火山體であろう．

福地學士は丸嶋山の大部分を向山熔岩と見做し，丸嶋山の東南麓海岸近くに露出する熔岩の一部を輝石流紋岩（西ノ浦式熔岩）と稱して區別してゐるが，向山熔岩は丸嶋山に迄擴がつてゐるのでなく，丸嶋山に露出する熔岩は一續きの角閃石・黒雲母流紋岩である．又，同學士は丸嶋山の南麓の稍東方に於いて白ママ層の下に輝雲流紋岩（跡見ズノ澤式熔岩）の露出を記載してゐるが，之は白ママ層の下に埋もれてゐる丸嶋山熔岩の大きい岩塊を誤認したものと思はれる．

新島南端の神渡鼻の沖に在る早嶋は一枚の熔岩より成る小島であるが，此熔岩は如何なる種類に屬するか未だ明かでない．

6. 若郷玄武岩砂礫層.

若郷玄武岩砂礫層は新島山頂上の平坦部及び若郷部落南方の臺地の下部を構成する地層で，若郷前濱の南半の臺地を削つて出來た海蝕崖及び若郷部落背後に聳ゆる新島山熔岩の絶壁の上端によく露出してゐる（圖版第9圖）．又，同じ地層はヂナーカ山の頂上部にも見出されるが、宮塚山及びアツチ山の上には全く存在しない．

此地層は厚い所で約 50 m の厚さを有し，略水平の層理を示し，主として暗灰色の玄武岩砂礫及び火山灰より成り，少量の流紋岩礫を雜へてゐる．玄武岩砂礫は稍鑛滓狀で，殆ど斑晶の無い單斜輝石・橄欖石・亞灰長石玄武岩である．玄武岩礫には流紋

岩の小片を捕獲してゐるものがある．此地層の中に雜つてゐる流紋岩の礫は角閃石流紋岩及び角閃石・黑雲母流紋岩で，ヂナーカ山熔岩，新島山熔岩等の如く此地層の堆積前に既に噴出してゐた種類に屬する流紋岩である．

若郷玄武岩砂礫層がヂナーカ山熔岩及び新島山熔岩より新しい事は前者が後者の上に載つてゐる事實から疑ひない．若郷前濱の南端ではヂナーカ山熔岩の海蝕崖の前面に玄武岩砂礫層が附着して居り，曾て此海蝕崖が 30 m 或は夫以上の高さまで玄武岩砂礫層に依つて埋められてゐた事を示してゐる（圖版第 7 圖）．前濱の北端では新島山熔岩の海蝕崖と玄武岩砂礫層との間に同様の關係が認められる．

玄武岩砂礫層が流紋岩熔岩に依つて蔽はれてゐる事を示す露出は見られないが，新島山の頂上部及び若郷部落南方の臺地上に於いて玄武岩砂礫層は淡井浦灰砂層に蔽はれ，又後に述べる様に，玄武岩砂礫層に蔽はれてゐない宮塚山熔岩及びアツチ山熔岩が共に多數の玄武岩礫を捕獲してゐる事實は玄武岩砂礫層が淡井浦灰砂層，宮塚山熔岩，アツチ山熔岩等より舊い事を示すものである．

若郷玄武岩砂礫層は玄武岩火山の噴出物が直接堆積した地層で，玄武岩火山に前以つて存在してゐた玄武岩が浸蝕されて二次的に堆積したものではない．又，此地層は若郷の低地のみならず新島山及びヂナーカ山の上にも存在し，且つ新島山熔岩及びヂナーカ山熔岩の海蝕崖に接して堆積してゐるから，陸上堆積物と考へなければならぬ．此地層に材料を供給した玄武岩火山の中心が何處に在るかは興味ある問題であつて，I. Friedlaender[6] は新島の北方 3 km の距離に在る鵜渡根島に之を求め，辻村學士は宮塚山の北東麓卽ち若郷部落から本村に至る道路を南方へ 1·5 km 程行つた所の路傍に見られる小凹地を其噴火口であろうと推定した．若郷玄武岩砂礫層中の玄武岩は鵜渡根島の玄武岩に岩石學的には可なりよく似てゐるが，前者が鵜渡根島火山から供給されたとは考へられない．若郷前濱に露出する玄武岩砂礫層は北から南へ多少厚さを增し，且つ中に含む砂礫の大いさを增してゐる様であるから，其噴出點は南方に在るものと考へられる．又，同層中には流紋岩の岩片のみならず，斯る岩片を捕獲する玄武岩礫が見出されるから，同層を構成する玄武岩砂礫の噴出は流紋岩の地域を破つて行はれたに相違ない．辻村學士に依つて指摘された宮塚山北東麓の窪地は東西，南北の直徑夫々約 100 m，200 m の楕圓形をなし，西側の宮塚山の絕壁と東側の高さ 30 m 內外（窪地の中央底部から）の半月狀に連なる尾根に依つて圍まれてゐる（圖版第 11 圖）．此尾根の外側は北方に漸次低くなつて若郷部落南方の臺地面に續いて

---

6) I. FRIEDLAENDER, *Mitteil. d. Deutch. Gesell. f. Natur-u. Volkerkunde Ostasiens*, **12** (1909), 76.

ゐるが，其內側は外側より急傾斜を以つて窪地の底の平坦地に降り，噴火孔跡たる地形を示してゐる．窪地の內部及び東壁の外側は一帶に流紋岩灰砂層（淡井浦灰砂層）に依つて蔽はれてゐるが，其西壁をなす宮塚山の絶壁の下部及び東壁の一部にはヂナーカ山熔岩が露出する．玄武岩砂礫層は窪地の北壁の上部に露出し，宮塚山の絶壁の中部にもヂナーカ山熔岩と宮塚山熔岩との間に挾まれて同層らしい地層が遠望される．斯樣な事實から，此窪地は玄武岩砂礫を噴出した噴火口の跡の一部と推定されるのであつて，ヂナーカ山熔岩より成る地面に火山爆發が起り，其部分のヂナーカ山熔岩を破壞して噴火孔を開き，此噴火孔から噴出した玄武岩砂礫が多少の流紋岩の岩片を伴つて噴火孔附近の低地及び其當時既に存在したヂナーカ山，新島山等の上に堆積して若鄉玄武岩砂礫層を形成したが，其後宮塚山及びアツチ山の噴出によつて，玄武岩噴火孔は其噴出物の下に埋まり，玄武岩砂礫層も若鄉部落背後の絶壁，前濱の海蝕崖等に主として露出するのみとなつたと考へられる．

7. 宮塚山熔岩，同灰砂層，及び羽伏浦灰砂層．

宮塚山熔岩は新島北部山地の中央部に聳ゆる宮塚山（海拔 408 m）の主要部を構成し，南側の赤崎ノ峯に接續する一部分を除いて，同山の四周の山腹に絶壁をなして露出してゐる（圖版第11圖）．卽，宮塚山の西側は島分澤を南限とし，西海岸アカマ及び佛ノホラに臨んで，高さ 350 m に達する絶壁をなし，其上部約 150 m は宮塚山熔岩の熔岩崖で，夫より下部は宮塚山熔岩の崖錐堆積層と島分澤凝灰岩層，ヂナーカ山熔岩等とである．又，宮塚山の北東側及び南東側は夫々ヘイノ平（宮塚山とアツチ山との間の低地）及び羽伏浦に臨んで，高さ 300 m に達する宮塚山熔岩の絶壁である．北東側と南東側との連なる部分は東方に稍突出した尾根をなし，此部分に於いては宮塚山熔岩は海濱迄續き，更にミクツ根の岩礁に露れてゐる．昭和 11 年 12 月 27 日の新島地震の際，宮塚山の熔岩崖は各處に於いて著しい崖崩れを起したのであつて，同地震後通行不能となつた本村，若鄉間の本道の七曲りの嶮は宮塚山の熔岩崖の東方に突出した部分を越ゆる處である．

宮塚山熔岩は 300 m 以上の厚さを有し，他の熔岩と同樣に，其上部と下部とは色，組織等を夫々異にしてゐるが，一樣に石英，長石，及び黑雲母の斑晶を有する黑雲母流紋岩である．宮塚山の西側の熔岩崖には著しい流理構造が認められる．此熔岩は夫自體一火山を構成するもので，其噴出地點は，地形的には確められないが，此山の略中央に在ると考へられる．福地學士は宮塚山の熔岩を羽伏浦式熔岩と淡井浦式熔岩とに區別し，之等を共にアツチ山を構成する熔岩に續くと考へてゐる．然し，宮塚山と

アツチ山とは何れも同種の黑雲母流紋岩熔岩に依つて構成されてはゐるが，構造上夫々全く別の火山である．

宮塚山熔岩がヂナーカ山熔岩及び島分澤凝灰岩層より新しい事は宮塚山の北側及び西側の絕壁下に於いて前者が後者の上に載つてゐる事實に依つて明かである．宮塚山熔岩と赤崎ノ峯熔岩との直接に接觸する露出は認められなかつたが，次に述べる宮塚山灰砂層が赤崎ノ峯の上に分布してゐるから，宮塚山熔岩は赤崎ノ峯熔岩より新期の噴出物であるに相違ない．宮塚山北東側の絕壁に於いては，既に述べた樣に，宮塚山熔岩とヂナーカ山熔岩との間に若郷玄武岩砂礫層が介在してゐる樣に見られる．此關係は十分確められないが，宮塚山熔岩は若郷玄武岩砂礫層に含まれる玄武岩と全く同種の單斜輝石・橄欖石玄武岩の破片を捕獲してゐるのであつて，宮塚山東麓の七曲り附近に露出する熔岩中に斯る岩片が屢々見出される．從つて，宮塚山熔岩は若郷玄武岩砂礫層よりも新期の噴出物と考へられる．福地學士が羽伏浦式熔岩中に見出し，輝綠小紋岩といふ名稱の下に記載してゐる捕虜岩は恐らく玆に述べる宮塚山熔岩中の單斜輝石・橄欖石玄武岩と同一であろう．顯微鏡で檢べると，此玄武岩の斑晶及び石基に見られる單斜輝石は屢々其一部或は全部が角閃石に變化してゐる．斯樣な變化は神津島の流紋岩中の鹽基性捕虜岩に見られ，又後に述べるアツチ山熔岩中の玄武岩捕虜岩にも見られるのであつて，玄武岩の樣な鹽基性火山岩が流紋岩の樣な酸性火山岩の熔岩に捕獲せられた場合に，捕虜岩中の結晶と母岩の岩漿との間に起る化學反應の一結果を示すものである．

宮塚山熔岩とアツチ山熔岩とは羽伏浦の北方ミクツ根附近の海岸に於いて接觸して居るらしいが，此接觸部の兩者の關係を確める事は出來なかつた．又，宮塚山とアツチ山との間の低地ヘイノ平は淡井浦灰砂層に依つて蔽はれ，此兩火山の熔岩の接觸關係を不明にしてゐる．然し，宮塚山頂上の北部には淡井浦灰砂層と考へられる地層が認められるから，宮塚山熔岩はアツチ山熔岩より舊期の噴出物であろう．

宮塚山灰砂層は宮塚山熔岩を蔽ひ，宮塚山の頂上部に數十米の厚さを以つて堆積してゐる地層で，主として黑雲母流紋岩の浮石及び火山灰砂より成り，其他に變質した玄武岩質岩石の砂礫を雜へ，明かな層理を示してゐる．赤崎ノ峯の頂上部に於いて，此地層は赤崎ノ峯灰砂層の上に不整合に載り，白ママ層に依つて不整合に蔽はれて居り，宮塚山頂上の北部に於いては同地層は淡井浦灰砂層に依つて不整合に蔽はれてゐる．從つて，宮塚山灰砂層は宮塚山熔岩と略同期で，後者の流出に伴つて噴出した浮石，火山灰砂等が堆積して生じた地層と考へられる．

羽伏浦灰砂層は新島の東岸羽伏浦の北部約 1.5 km の間の海岸に沿つて，高さ 20 m

内外の海崖を形成してゐる地層で（圖版第10圖），主として宮塚山熔岩と同質の火山灰砂及び熔岩塊から成つてゐるが，上に述べた宮塚山灰砂層の如く浮石質でなく，成層狀態も之に比して粗雜である．此地層の發達してゐる處は丁度宮塚山の南東側の絕壁の下に當たり，絕壁の直下には崖錐層が分布してゐるから，羽伏浦灰砂層も或は此崖錐層の一部分であるかも知れない．羽伏浦灰砂層と羽伏浦の南部に發達する白ママ層とは夫々明かに區別せらるべき地層で，兩者は羽伏浦の海底電信線陸上場附近を境としてゐるが，其境は砂丘に蔽はれて明かでない．

8. 淡井浦灰砂層．

淡井浦灰砂層は新島山，宮塚山，及びアツチ山に取圍まれた若郷部落南方の臺地を蔽ひ，新島山とアツチ山との間の海岸淡井浦に沿つて最もよく露出してゐる．此地層は明瞭なる層理を示し，淡井浦に於いては海面上約 15 m の厚さを有し，主として黑雲母流紋岩の砂礫及び火山灰によつて構成されてゐるが，其他に玄武岩の砂礫，玄武岩捕虜岩を有する流紋岩塊等を含み，又下部には角閃石流紋岩，第三紀火山岩等の破片を含んでゐる．

淡井浦灰砂層は宮塚山頂上の北部にて宮塚山灰砂層を蔽ひ，新島山の頂上部にては若郷玄武岩砂礫層を蔽つてゐる．若郷玄武岩砂礫層と淡井浦灰砂層との關係は若郷前濱の南部に於いても明瞭に認められる（圖版第9圖）．淡井浦の南隅に於いては淡井浦灰砂層がアツチ山熔岩に蔽はれ（圖版第12圖），其北隅に於いては前者が新島山熔岩の海蝕崖に接してゐる狀態が見られる．淡井浦に若郷玄武岩砂礫層が露れてゐないのは，淡井浦灰砂層の堆積前に此方面に分布してゐた若郷玄武岩砂礫層が海蝕に依つて島內深く取去られ，其跡に淡井浦灰砂層が堆積したためと考へられる．淡井浦から西方へ約 500 m 行くと，若郷部落南方の臺地の上に登らんとする處に一段の段丘崖狀の地形が略南北に連なつてゐる事が氣付かれる．此地形は若郷前濱に現在見られる樣な玄武岩砂礫層の海蝕崖が此處に於いて淡井浦灰砂層の下に埋まつてゐる事を示すものであらう．第6圖は此關係を模式的に示す斷面圖である．若郷前濱方面の玄武岩砂礫層も曾ては淡井浦灰砂層の下に全く埋まつてゐたであらうが，强い西風及び夫に因

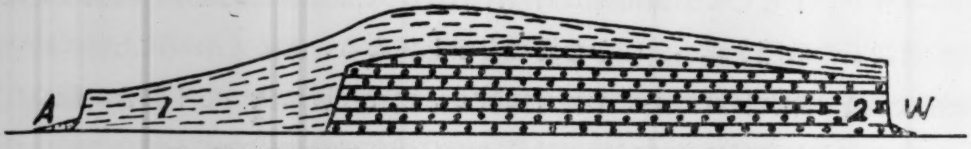

第6圖　若郷前濱（W）と淡井浦との間の模式東西斷面圖．
1，淡井浦灰砂層．2，若郷玄武岩砂礫層．

つて起る波浪の浸蝕作用が前濱の海岸線を漸次後退せしめたため，此處には玄武岩砂礫層が淡井浦灰砂層と共に再び海蝕崖をなして露れたものと考へられる．

淡井浦灰砂層は宮塚山熔岩及び同灰砂層より新期の噴出物であるが，アツチ山熔岩には蔽はれてゐるから，此熔岩に先立つて噴出した火山灰砂の堆積して生じた地層であるに相違ない．

9. アツチ山熔岩.

アツチ山熔岩は宮塚山の北東麓に接するアツチ山（海拔約 230 m）を構成する黑雲母流紋岩である．此山は其東側の山麓部を海蝕に依つて多少削り取られてゐるが，平面的に略圓形をなし，35° 内外の急傾斜の山腹と略平坦な頂上部とを有し，殆ど完全な熔岩圓頂丘の地形的特徴を示してゐる．熔岩は火山灰砂に蔽はれず，此山の至る處に塊狀熔岩として露出し，淡井浦の南方の海蝕崖に於いては淡井浦灰砂層の上に載つてゐる狀態が認められる．從つて，アツチ山は一種の黑雲母流紋岩熔岩から成る獨立の一火山で，新島の北部山地の中で最も新しい．

アツチ山熔岩は灰白色浮石質で，長石，石英，黑雲母等の斑晶を含み，岩石學的には後に述べる向山熔岩に類似してゐる．又，此熔岩は宮塚山熔岩と同樣に單斜輝石・橄欖石玄武岩を捕虜岩として多量に含んでゐるのであつて，灰白色の流紋岩中に黑色の玄武岩が點々として散在してゐる狀態は淡井浦の南方の海蝕崖或はヘイノ平附近のアツチ山熔岩の露出によく見られる（圖版第 13 圖）． 福地學士が淡井浦式熔岩中に見出し，閃綠小紋岩として記載してゐる岩石は此捕虜岩の一種である．アツチ山熔岩中の捕虜岩は宮塚山熔岩中の捕虜岩に比較して稍著しい變質作用を受けてゐる事が多い．即，比較的大きい捕虜岩には多くの場合明瞭に玄武岩の構造が殘されてゐるが，直徑 5 cm 内外或は夫以下の捕虜岩には元來の玄武岩の構造が全く消滅して斜長石，角閃石，磁鐵鑛等の集合體に變化してゐる事が少くない．然しかゝる場合にも，玄武岩中の元來の斑晶と見られる斜長石，單斜輝石，橄欖石等が夫々其緣の部分のみ變化して殘つてゐる事が普通である．何れにしても，斯樣な捕虜岩は流紋岩の岩漿中で晶出した鑛物の分結物ではなく，母岩たる流紋岩が噴出する際，其噴出地點附近に既に存在してゐた玄武岩が破碎せられ，流紋岩熔岩に捕獲せられた岩片に相違ない．

10. 白ママ層.

白ママ層は新島の海岸に沿つて，方言にて "ママ" と稱する斷崖を構成する地層に對して福地學士に依つて與へられた名稱である．而して，同學士は白ママ層を二種類

に分かち，其一種類を流紋岩熔岩の流出する前後に噴出した火山灰砂の堆積した地層，他の種類を流紋岩の破碎して生じた砂の堆積した地層とした．從つて同學士のいふ白ママ層は新島に於ける流紋岩質の火山灰砂層及び流紋岩の破碎して堆積した二次的堆積層を凡て含んでゐる．筆者の白ママ層と稱する地層は大峯圓錐丘（辻村學士の所謂“大峯ホマーテ”）の噴火に際して噴出した火山灰砂の堆積した地層で，大峯圓錐丘及び本村低地に廣く分布し，新島の南東岸の羽伏浦及び西ノ浦，南西岸の間々下浦及び小濱浦等に海蝕崖をなして露出してゐる．又既に述べた樣に，白ママ層は瀨戶山，峰路，赤崎ノ峯等の舊火山體の上にも分布してゐるが，大三山凝灰岩層，島分澤凝灰岩層等は勿論，赤崎ノ峯灰砂層，宮塚山灰砂層，淡井浦灰砂層等からも嚴密に區別さるべき地層である．

白ママ層は羽伏浦の北方の海底電信線陸上地附近に於いては海面上僅かに5m内外の低い崖をなし，砂丘に依つて大部分蔽はれてゐるが，此海岸に沿つて南方に行くに從つて次第に其海面上の厚さを增し，本村低地中央部の東に當る海岸にて 50m 内外となり，尙南に進むに從つて更に厚さを增し，大峯の東側カンメガモリに於いて高さ 200m に達する大斷崖を形成してゐる（圖版第14圖）．此斷崖下の海岸を更に南に進めば，西ノ浦の海岸に沿つて丸嶋山の南麓小濱ノ浦附近に至る迄，白ママ層は再び 50m 内外の厚さに減じてゐる（圖版第8圖）．間々下浦に沿つて斷崖をなす白ママ層は海面上の厚さ約 40m である（圖版第1圖及第17圖）．

辻村學士は向山南方の近海に曾て一火山が存在し，此火山から噴出した火山灰砂が堆積して白ママ層を形成し，其後同層の上に大峯圓錐丘が建設されたと考へてゐる．筆者がカンメガモリの斷崖を觀察した結果では，白ママ層と大峯圓錐丘を構成してゐる地層との間に構造上の相違は認められず，兩層を構成する主要物質は岩石學的に全く同一の黑雲母流紋岩の浮石質灰砂である．從つて，白ママ層と大峯圓錐丘を構成する灰砂層とは別物ではなく，大峯圓錐丘火山の噴火に依る全部一續きの噴出物と考へられる．

大峯圓錐丘は新島の南部山地を代表する向山火山の一部で，向山熔岩の噴出に先立つて，火山灰砂の噴出に依つて形成された一火山體である．其西半部は向山熔岩の噴出に際して破壞され，或は同熔岩の下に埋まつてしまつたが，東半部は殆ど完全に殘されてゐるのであつて，向山の東側に半圓形に連なる大峯（海拔 300·7m）及びナカ山（海拔約 290m）の尾根は此圓錐丘の頂上部を截る火口壁の上緣に相當する．圓錐丘の東側は殆ど頂上近くまでカンメガモリの大斷崖に依つて切斷されてゐるが，北東側及び南東側は完全な圓錐面を保ち，頂上から海拔 100m 内外の高さの山麓に至る

迄約35°の傾斜を以つて下り，此處から急に傾斜を減じて，夫々本村の低地及びハバタの低地の地表面に續いてゐる．火口の內部は向山熔岩に埋められ，火口の元の大いさは判明しない．然し火口壁と向山熔岩との間に殘されてゐる新月形の窪地は二重火山に於ける火口原に相當して大峯の頂上から約 100 m の深さに達してゐる．斯樣な窪地は大峯の頂上から南西に突出する短い尾根を境として南北兩側に在り，從つて辻村學士の注意した樣に，大峯圓錐丘の頂上火口は二個或は夫以上の噴火口に分れてゐたに相違ない．圓錐丘の南側には丸嶋山の北麓を巡つて小濱浦に通ずる深い澤があり，此澤の上部は大峯圓錐丘の南側を馬蹄形に抉つて，一噴火口の跡らしい地形を示してゐる．

白ママ層は，大峯圓錐丘と其山麓の低地とに於いて區別なく，何處も主として次に述べる向山熔岩と同じ黑雲母流紋岩に屬する白色浮石質の火山灰砂，火山礫，熔岩塊及び灰色緻密質或は黑曜石質の熔岩砂礫に依つて構成され，其他に舊期の流紋岩類の破片，變朽安山岩其他の第三紀岩と考へられる岩片等を雜へてゐる．之等の從屬的及び偶然的に拋出された岩片は白ママ層の下部に比較的多く見出される．丸嶋山の南東側の熔岩崖の下部に接して堆積してゐる白ママ層の下部には丸嶋山熔岩の大小の岩塊が埋もれてゐる．此岩塊は白ママ層の堆積しつゝあつた時に，丸嶋山の熔岩崖から落ちて白ママ層中に雜つたものと考へられる．

白ママ層は全體として下部に大きい礫及び岩塊を比較的多く含んでゐるが，上下部を通じて微細な火山灰砂の層と粗大な火山砂礫の層との互層である（圖版第15圖）．層理は此地層の露出に接近して見ると寧ろ不分明であるが，多少離れて見ると明瞭であつて，大峯圓錐丘の山腹に於いては圓錐丘の表面に平行な傾斜を示し，其他の部分に於いては殆ど水平で多少の波狀屈曲を示すに過ぎない．然し，水平層の間には處々に不規則な僞層及びレンズ層が挾まつてゐる．

羽伏浦に沿つて南下すると，白ママ層の層理が初め殆ど水平で，大峯圓錐丘に近付くに從つて同層の上部の層理が次第に大峯圓錐丘の斜面に平行に移り變る狀態が見られる．カンメガモリの大斷崖の上部は大峯圓錐丘の圓錐面を南北方向の略垂直の一平面で截つた斷面であつて，双曲線狀の層理を示してゐる．此斷崖の下部の海面上約 50 m の間は海岸に沿つた南北の斷面には殆ど水平の層理を示してゐるが，同斷崖を刻む櫛齒狀の溝の側壁を見ると，地層が東方へ多少傾斜してゐる事が知られる．此部分は大峯圓錐丘が現在の大いさに迄發達してゐなかつた時代に堆積したのであつて，宛も現在の大圓錐丘の山麓から距つた低地の白ママ層と同樣の堆積狀態を示してゐるものと考へられる．

白ママ層は，既に述べた様に，瀬戸山及び大三山の大部分を蔽ひ，瀬戸山熔岩及び大三山凝灰角礫岩層の上に不整合に載つてゐる．又，峰路に於いては峰路熔岩及び島分澤凝灰岩層を，赤崎ノ峯に於いては赤崎ノ峯熔岩及び赤崎ノ峯灰砂層を不整合に蔽つてゐる．峰路及び赤崎ノ峯の白ママ層は瀬戸山及び大三山の同層に比較して遙かに薄く，しかも峰路から赤崎ノ峯に至るに從つて次第に薄くなり，赤崎ノ峯の北部及び宮塚山本體の上には分布してゐない．向山の南西海岸に沿つて丸嶋山の南西麓小濱浦から鼻戸崎（アカグヨリ）附近迄の間には，白ママ層は向山熔岩及び同灰砂層の下に露出し，鼻戸崎の北方に於いて，間々下浦の白ママ層に連なる．

要するに，白ママ層は瀬戸山，大三山等を初め新島北部の山地が既に形成された後に，大峯圓錐丘の現在の位置を中心として活動し始めた火山の噴出物を代表する．瀬戸山，丸嶋山等が恐らく淺い海に依つて北部山地から距てられた島であつた時代に，此火山は海中火山として生れ，其噴出物を以つて次第に附近の淺海を埋め，やがて海上に其姿を現し，更に其噴出物を以つて北部山地と丸嶋山，瀬戸山等とを陸續きにし遂に現在の大峯圓錐丘に迄成長したと考へられる．從つて，此火山の初期の噴出物の一部は海中堆積層として存在してゐるであろうが，少くとも現在新島上に露出してゐる白ママ層の大部分は，辻村學士が述べてゐる様に，陸上に堆積した噴出物と考へなければならない．

11.　向山熔岩及び同灰砂層．

向山熔岩及び同灰砂層は上に述べた白ママ層と共に向山複合火山（辻村學士の所謂″向山ホマトロイデ″）を構成する．白ママ層が此火山の外輪山に相當する大峯圓錐丘及び其外域の低地を構成するのに對し，向山熔岩及び同灰砂層は中央火口丘に相當する向山圓頂丘（辻村學士の所謂″石山トロイデ″）を構成する噴出物である．

向山は其一部なる丹後山（海拔 283·4 m）及び石山（海拔　234·8 m）と共に大峯圓錐丘の頂上部から西方に間々下浦及び瀬戸山南麓附近に迄連なつてゐる．此山の東側は頂上部に於いて直接に大峯圓錐丘の頂上部に續いてゐるが，南西側は小濱浦と間々下浦との間の海岸に臨んで殆ど絶壁をなし，北側は瀬戸山及び大三山の南麓の低地に臨んで35° 内外の傾斜面を形成する．山の頂上部は臺地狀に擴がり，神津島天上山の頂上に類似して，大小の窪地と丘陵との相交錯する複雑な地形を示し，大體三部に分たれる．卽，南部の丹後山と呼ばれてゐる部分は北西一南東方向に長い四條の平行の丘陵及び之等の丘陵の間の窪地から成り，東部の向山本體は北東一南西方向に長い三條の丘陵，大峯圓錐丘の火口壁に沿つて連なる丘陵，及び之等の丘陵の間の窪地から

成り，西半部の石山と呼ばれる部分は丹後山及び向山本體から北西方に連なる數條の丘陵及び窪地から成つてゐる（第7圖）．各丘陵の最高點と窪地の最低點との高低差は一般に 50 m 以下である．斯様な地形は浸蝕作用の結果ではなく，向山の頂上部一帶を構成する向山熔岩の噴出當時の熔岩表面の地形を殆ど其儘示してゐるものと考へられる．

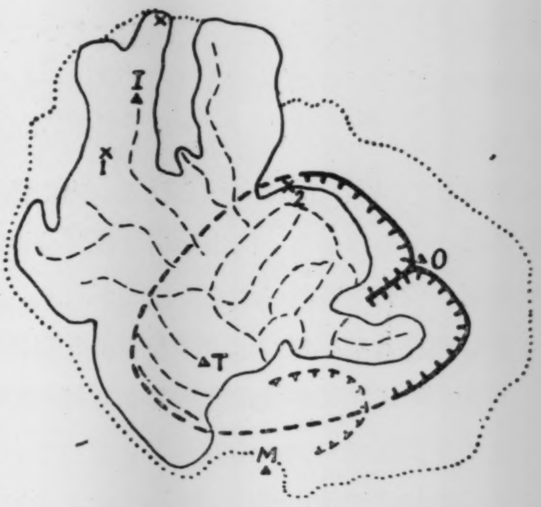

第7圖　向山火山頂上部の地形．

O，大峯（300·7 m）．T，丹後山（283·4 m）．I，石山（234·8 m）．M，丸嶋山．1，石山石切場．2，五右衛門石切場．

點線：向山火山外郭（低地の白ママ層を除く）．
細い實線：向山熔岩外郭
細い破線：向山熔岩表面の丘陵線．
太い破線：大峯圓錐丘火口壁の推定部．

向山熔岩は向山の頂上部の至る處に露出してゐる．其表面部は大小の岩塊の集合となつて塊狀熔岩の形態を示してゐるが，其內部は，南西岸に臨む斷崖或は石切場の露出に見られる様に，一續きの熔岩床である．此熔岩は石英，長石，及び黑雲母の斑晶を含む黑雲母流紋岩であつて，純白色乃至灰白色の浮石質の部分は極めて加工され易く，抗火石と呼ばれて盛んに採掘されてゐる．向山の頂上部一帶に露出する熔岩は大部分浮石質であるが，石山の石切場附近の熔岩が最も標式的の浮石質流紋岩で，恐らく最も良質の抗火石と考へられる．向山本體の五右衛門石切場附近の熔岩は灰白色で，比較的氣泡の少ない浮石質流紋岩であり，丹後山附近に露出する熔岩の一部は暗灰色乃至黑色で，眞珠岩様の割目に富む玻璃質流紋岩或は黑曜石質流紋岩である．小濱浦と間々下浦との間の斷崖に露出する熔岩も亦玻璃質で，眞珠岩様の割目に富み，暗灰色，黑色，或は赤褐色の外觀を示してゐる．

小濱浦と間々下浦との間の斷崖に於いて見られる様に，向山熔岩は最も厚い處で，200 m 內外の厚さを有する．熔岩の噴出地點は明かでないが，上に述べた様な向山頂上部に於いて見られる熔岩表面の地形的並びに岩質的變化の狀態から，丹後山附近に在る様に察せられる．丹後山附近に於いて噴出した向山熔岩は先づ北東方向に擴がつて大峯圓錐丘の噴火口の東方內壁に衝突し，此內壁との間に新月形の窪地を殘して停止し，次いで瀨戸山及び大三山の南麓の低地に向つて北西方向に擴がつたものであろう．向山熔岩が大峯圓錐丘の火口壁に接して停滯し，又前者が後者の上を越して北西

方向に擴がつてゐる狀態は大峯最高點の北西方五右衞門石切場附近に於いて最も明瞭に觀察される．北西方向に擴がつた向山熔岩の一部は，本村部落から溫泉場に通ずる自動車道路の中途，採石事務所附近に於いて見られる樣に，瀨戶山南麓の海拔約 40 m の低地に迄達してゐる．

向山の頂上部の凹凸地形は向山熔岩の噴出當時の粘稠度と熔岩下の地形とに主として支配されて出來た樣に考へられる．向山熔岩の下には大峯圓錐丘の西半部が埋まつてゐるはずであるから，向山熔岩は此部分の地形に支配されて擴がつたに相違ない．向山熔岩の噴出する前に恐らく爆發が起り，大峯圓錐丘の西半部は之に依つて多少破壞され，現在其東半部の示す樣な完全な圓錐形の地形を保つてはゐなかつたであろうが，丹後山附近及び丹後山北西部から五右衞門石切場附近に至る間の熔岩地形は其熔岩下に大峯圓錐丘の夫々南西部及び北西部が埋まつてゐる事を示すものの樣である．卽，向山熔岩は丹後山附近に於いては大峯圓錐丘の噴火口の南西壁を埋め，此火口壁と同方向なる北西—南東方向に長い丘陵及び窪地を形成し，丹後山北西部から五右衞門石切場附近に至る間に於いては大峯圓錐丘の噴火口の北西壁を埋め，同樣に之と同方向なる北東—南西方向の丘陵及び窪地を形成したと考へられる．此考へが正しいとすれば，大峯圓錐丘の噴火口は向山熔岩の噴出前には全體として略圓形で，約 2 km の直徑を有してゐたに相違ない．而して，向山熔岩の東半部（丹後山及び向山本體）は此噴火口の內部と南西壁及び北西壁の上とを占め，西半部（石山）は大峯圓錐丘の北西外側を占めてゐるのである．從つて，向山熔岩は全體としては一の完全な熔岩圓頂丘でなく，大峯圓錐丘の噴火口の南西部から噴出して此噴火口の內部に滿ちると共に一部分は熔岩流として噴火口の北西壁を越へて北西方の低地に流れ出したと考へられる．

向山灰砂層は向山熔岩の北西部外緣の急斜面に主として露出し，向山熔岩と同種の浮石質火山灰砂，火山礫，熔岩塊等から成つてゐる．向山熔岩の斷崖の下には一般に同熔岩の破碎した砂礫及び岩塊が堆積して崖錐を形成してゐるが，向山灰砂層は此崖錐層とは異なつて，向山熔岩に蔽はれてゐる火山噴出物である．向山灰砂層と白ママ層とは其構成物の岩質上からは殆ど區別され難いが，間々下浦の南方斷崖に於いて，前者が後者の上に載り，明瞭な不整合を以つて境されてゐる關係が認められる（第5圖及び圖版第17圖）．又，第8圖に示す樣に五右衞門石切場附近に於いて，向山灰砂層が大峯圓錐丘を構成する白ママ層の上に不整合に載つてゐる．從つて，向山灰砂層は大峯圓錐丘が形成されて後，向山熔岩の噴出する前の噴出物で，恐らく向山熔岩の噴出直前に爆發的噴火が起り，其際拋出された火山灰砂が堆積して生じたものであろ

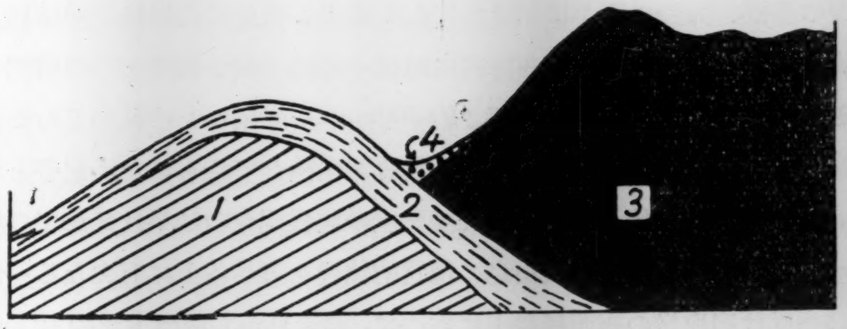

第8圖　向山五右衞門石切場附近の模式南北斷面圖.
1，白ママ層（大峯圓錐丘）．2，向山灰砂層．
3，向山熔岩．4，向山熔岩崖錐堆積層．

う．第2圖の地質圖には大峯圓錐丘上に分布する向山灰砂層は省略されてゐる．

12. 崖錐砂礫層.

崖錐砂礫層は急峻な熔岩崖から崩壞した砂礫及び岩塊の堆積した地層で，第2圖には赤崎ノ峯及び宮塚山の東西兩熔岩崖の下に見られる此種の地層が示されてゐるのみであるが，尙此他の各處にも發達してゐる．

13. 砂丘砂層.

砂丘砂層は本村及び若鄉の低地に分布する砂層で，主として流紋岩類の破碎して生じた石英，長石，黑雲母，磁鐵鑛，其他の有色鑛物の砂粒，及び玻璃の破片を含んでゐる．新島に於いては一年中を通じて西風が優れてゐるから，砂丘砂層は若鄉及び本村の西海岸に沿つて特に發達し，東海岸に於いては羽伏浦北方の海底電信線陸上場附近に見られるのみである．若鄉低地の砂丘砂層は前濱海岸から新島山の西側斷崖の直下迄分布してゐる．本村の砂丘砂層は前濱南部に於いては瀨戶山及び大三山の北西麓一帶を蔽ひ，前濱北部に於いては峰路の西側斷崖の直下に達し，峰路と瀨戶山との間の低地に於いては前濱海岸から1km 餘の內陸に迄擴がつてゐる．本村部落の東端附近の砂丘砂層は約 6m の厚さを有し，耕作に適せず，畑は之を取除いて〃トチ〃（白ママ層）の上に作られると云ふ．

新島火山の發育史

新島の火山の構造及び其數個の火山の相互の地質的關係は以上の地質說明を以つて大體了解されるので，之に基いて新島の火山の發育史を要約して述べれば次の如くである．

新島火山の基盤．海圖に明かに示されてゐる様に，新島は式根島，神津島，恩走島等の流紋岩火山島と共に北東—南西方向に竝ぶ一島列（故小藤博士6) の所謂 "神津島火山脈"）を形成し，同方向に連なる深さ約 200m の一海嶺の上に載つてゐる．辻村學士は此海嶺を一弱線に沿つて噴出した火山物質が堆積して造られた隆起帶と考へたのであるが，新野學士8) に依つて行はれた錢州礁の底質調査の結果は此海嶺の地質及び成因を考へ，新島其他の流紋岩火山島の地質的位置を考へる上に有力なる一資料を提供した．錢州礁は同海嶺の南西延長上に在つて，神津島から南西方に約 40 km 距たり，從來は一般に夫が新島—神津島島列の延長上に在る事實から之等の島々と同様に流紋岩の岩礁であろうと想像されてゐた．筆者は曾て恩走島及びサツパン島の岩礁群を調査した際に之を確めようと企てて荒天のため果さず，其後新野學士の錢州漁礁調査の機會に，同漁礁の中央部に當たる錢州岩礁の岩石の採集を同學士に依頼した．而して此調査に依つて錢州漁礁の底質と共に錢州岩礁の地質が明かにされ，同岩礁が從來想像してゐた様な流紋岩でない事が確められた．新野學士に依ると，錢州岩礁は東西に約 200 m 離れて相對立する 2 個の尖岩と之等から約 2·5 km 南西方に距たる數個の岩礁群とから成り，何れも海面上僅かに數米突出し，岩礁群中の一岩礁が南東に緩傾斜を以つて上下に相重なる熔岩と集塊岩とから成る外，凡て集塊岩である．同學士の好意に依つて筆者の得た岩石標本は熔岩の岩片 3 個と集塊岩の岩片 7 個とであるが，何れも淡綠灰色乃至淡青灰色を帶び，緻密堅硬なる斑狀岩で，肉眼で見ると，變質した斜長石の多量の白い斑晶と黃鐵鑛の微粒とを含んでゐる．其薄片を顯微鏡で觀察すると，熔岩及び集塊岩は何れも一部分曹長石化した斜長石斑晶，綠泥石化した輝石斑晶，及び粒狀化した石基から成り，黃鐵鑛其他の鐵鑛物に依つて鑛染され，伊豆半島の中新世の火山岩類中に最も多い變朽安山岩と全く同一の性質を有する．更に新野學士に依ると，錢州岩礁の周圍の海底は海面下 120 m より淺い廣大な平坦面で，其處には基盤岩石が露出し或は極めて良好に水蝕された礫が分布してゐる．而して，此礫の少數は石灰藻及び造礁珊瑚であるが，其他の多數は錢州岩礁の岩石と同質である．

以上の事實の他に，神津島に於いては秩父山灰砂層及び白ママ層が伊豆半島の第三紀火山岩類に類似する岩片を含み，其北岸の海面近くには下田の萬藏山の岩石と殆ど同質の加里流紋岩が僅かに露出し，新島に於いては大三山凝灰岩及び同凝灰角礫岩層が第三紀岩類の水蝕された圓礫を多數に含み，其他の流紋岩灰砂層も亦第三紀火山岩類の破片を伴つてゐる．之等の事實は新島，神津島等の流紋岩火山島の基盤となつて

---

7) B. KOTO, *Jour. Fac. Sci. Imp. Univ. Tokyo*, **3** (1934), 205.

8) 新野弘，地學雜誌，**47** (1935), 590.

ゐる海嶺が大部分伊豆半島の中新統に相當する第三紀層に依つて構成されてゐる事を示すものである．而も，錢州礁附近の120m或は夫以上の深さの海底に分布してゐる圓礫は斯る深い海底に於いては形成され難く，陸上或は海岸近くに於いて形成されたと考へられるから，此圓礫の載つてゐる海嶺は且て廣い陸地の一部或は幾つかの島として海面上に現れてゐて，其後海水面に相對的に現在の位置に沈降したに相違ない．新島，式根島，神津島等に就いて見ても，之等の島々は最近に至つて或は數米程度隆起⁹⁾したかもしれないが，其火山噴出物は大部分陸上に堆積したものであり，全體としては反つて餘程沈降してゐる様に考へられる．然し，白ママ層を初め，淡井浦層，若鄉玄武岩砂礫層，島分澤凝灰岩層等の少くとも平坦地に堆積してゐる部分は何れも殆ど水平的の層理を示してゐるから，新島の沈降が事實あつたとすれば，夫は島全體としての略一様な沈降であつて，所謂地塊運動に伴つた傾動的の沈降ではない．

新島の若鄉玄武岩砂礫層は，少くとも觀察された範圍内に於いては，同島及び神津島の流紋岩灰砂層中に見出される様な第三紀岩類の破片を伴つてゐない．大島火山の玄武岩砂礫層中にも同火山の基盤に由來すると考へられる様な偶然的抛出物の存在する事は記載されず，¹⁰⁾ 筆者の觀察した限り，三宅島の玄武岩砂礫層中にも亦斯る抛出物は見出されない．御藏島の海岸には玄武岩礫に雜つて，花崗岩質の礫が見出されるが，此花崗岩質礫は曾て南洋方面から人工的に運搬されたものと云はれてゐる．然し之等の事實は第三紀層或は其他の所謂大陸的の基盤岩類が新島の北端附近から北東方の玄武岩火山島を含む地域に缺けてゐて，新島及び其南西方の流紋岩火山島を含む地域にのみ存在する事を必ずしも示すものではない．流紋岩火山は玄武岩火山に比較して地表に近い地殼內に其岩漿溜を有し，極めて爆發的の噴火を屢々行つたがために，其噴出物中に基盤岩の破片を多く伴つてゐるとも考へられる．斯る見方の何れが事實に近いかは現在に於いては斷定出來ない．

以上に述べた種々の事實を綜合して考へると，新島火山は神津島火山と同様に其基盤を成す第三紀層が旣に地殼運動に因つて變位し且つ浸蝕作用を受けた後に形成されたに相違ない．之等の火山島の流紋岩類の大部分が大島，三宅島等の玄武岩類と同様に新期（第四紀）の噴出物であるといふ事は最初に辻村學士に依り，次に坪井博士に依つて，地形學的及び地質學的に論ぜられたのであるが，筆者の旣に發表した神津島火山の研究及び今回の新島調査の結果に依つて益々裏書きされたのである．

新島火山の噴出順序．新島火山の構造及び其噴出物の岩石學的類別は神津島火山の

---

9) 福富孝治，地震，**10**（1938），1〜4.

10) S. Tsuboi, *Jour. Col. Sci., Imp. Univ. Tokyo, Art* 6，**43**（1920），96.

夫等に比較して一層簡單であつて，大別すれば次の如くである．

(火山單位)	(岩型)
1　最舊期火山群	角閃石流紋岩．
2．赤崎ノ峯火山	角閃石流紋岩．
3．新島山火山及び丸嶋山火山	角閃石・黒雲母流紋岩．
4．若郷玄武岩火山	單斜輝石・橄欖石玄武岩．
5．宮塚山火山	黒雲母流紋岩．
6．アッチ山火山	黒雲母流紋岩．
7．向山火山	黒雲母流紋岩．

新島に現在露出してゐる限りに於いて，最も舊い火山噴出物は瀬戸山熔岩，峰路熔岩，ヂナーカ山熔岩等の角閃石流紋岩類である．之等の熔岩は恐らく夫々別個の火山を構成するものであろうが，各火山の相互の新舊順序及び噴出中心が明かでないから，玆では最舊期火山群として一括される．此火山群は，假りに海底火山として生れたものとしても，次期の火山が活動を始める前に，少くとも其頂上部を既に其當時の海面上に現し，幾つかの相接近した火山島として存在してゐたに相違ない．大三山凝灰岩，同凝灰角礫岩層，及び島分澤凝灰岩層は最舊期火山群の少くとも一部分が海面上に在つて，陸上浸蝕作用を受けてゐた時代に，其陸上に堆積した火山噴出物である．之等の地層は何れも角閃石流紋岩火山の噴火に由來するものであるが，其火山が何れであるか未だ確められない．島分澤凝灰岩層中に多少見出される黒雲母が初生的の火山噴出物であるとすれば，此地層の堆積當時既に角閃石の他に黒雲母をも含んだ流紋岩の火山が活動してゐたと考へられる．

島分澤凝灰岩層の堆積に次いで，赤崎ノ峯火山が峰路熔岩とヂナーカ山熔岩との夫々の火山體の中間に，角閃石流紋岩の熔岩と火山灰砂とを以つて形成された．此火山の活動時代には若郷の南部から宮塚山の下を經て峰路に至る地域は一續きの陸地に成つてゐたに相違ない．

角閃石流紋岩の噴出は赤崎ノ峯火山の活動を以つて終り，次いで角閃石・黒雲母流紋岩の噴出時代となり，北部には新島山火山が，南部には丸嶋山火山が形成された．丸嶋山火山は恐らく最初には海中火山として活動を始めたのであろうが，後に向山火山が活動を始める頃には，一の火山島として當時の海面上に現れてゐたと考へられる．新島山火山はヂナーカ山熔岩を以つて代表される角閃石流紋岩火山の一部を破つて熔岩を噴出し，當時既に後者と陸續きの火山になつてゐた．

新島山火山の活動に次いで，若郷玄武岩火山がヂナーカ山熔岩を破つて活動を開始した．此火山の噴出中心は現在宮塚山の北東麓に淺い窪地として殘る噴火口である．

此噴火口から噴出した單斜輝石・橄欖石玄武岩の砂礫は新島山，ヂナーカ山等の熔岩を蔽ひ，又之等の火山の間の低地に厚く堆積して，現在の若郷玄武岩砂礫層を形成した．其當時，若郷前濱及び淡井浦方面の低地には，此地層は現在よりも遙かに廣く分布してゐたであらうが，其後の海蝕作用に依つて，現在の分布を示すに至つたと考へられる．然し，峰路，赤崎ノ峯，瀬戸山等新島南半の舊火山體の上には此玄武岩砂礫層が全く見出されないから，若郷玄武岩火山の爆發的噴火は新島の北部にのみ影響を及ぼした比較的小規模の活動であつたに相違ない．

若郷玄武岩火山の活動に次いで，黑雲母流紋岩の噴出期となり，宮塚山火山及びアツチ山火山が相次いで形成された．當時赤崎ノ峯火山の北隣にはヂナーカ山熔岩，島分澤凝灰岩層，若郷玄武岩火山の南半部等から成る低い山地が在り，此處に噴出した黑雲母流紋岩の熔岩及び火山灰砂は此山地の大部分を蔽つて，新島に於いて赤崎ノ峯火山に次いで高い宮塚山火山を構成した．宮塚山火山の北東麓に於いて，其後再び黑雲母流紋岩の噴出が起り，先づ若郷玄武岩火山の東側の一部を破つて噴出した火山灰砂は淡井浦灰砂層として堆積し，次いで噴出した熔岩がアツチ山熔岩丘を形成した．

以上數次の火山活動の結果，新島の北部は現在見られる地形と略同様の山地となり，夫自身一の島として存在し，瀬戸山及び丸嶋山は恐らく淺い海に依つて此島から距てられ，夫々別個の火山島として海面上に現れてゐたと考へられる．

新島北部に於ける火山活動はアツチ山熔岩の噴出を以つて終り，次いで丸嶋山火山の北方の其當時の海中に向山火山が活動を始め，黑雲母流紋岩の火山灰砂及び熔岩を順次噴出した．先づ烈しい爆發的噴火が起り，白ママ層に依つて代表される火山灰砂が噴出し，噴火口附近の海底に堆積した．噴火が進むに從つて，此地層は漸次厚さを增し，遂に海面上に現れ，北部山地と瀬戸山，丸嶋山等とを陸續きとし，其後更に此陸地となつた低地に堆積したのみならず瀬戸山，峰路，赤崎ノ峯等の山頂部をも厚く蔽つた．又此火山が陸上火山になつて後，噴出した火山灰砂は其噴火口の周圍に特に多く堆積し，遂に大峯圓錐丘を形成するに至つた．白ママ層が次第に厚さを增して海面上に現れるや否や，其陸地の內部に於いては更に引續いて噴出した火山灰砂に依つて益々厚さを增したに相違ないが，海に接してゐた部分には海蝕作用が働き始め，白ママ層の陸地を次第に削り取り，羽伏浦及び間々下浦に現在見られる様な斷崖を形成したと考へられる．

大峯圓錐丘の形成時代の末期の噴火は初期の夫に比較して劣勢で，遂に一時靜穩に歸するに至つたが，其後再び此圓錐丘の頂上部に爆發的噴火が始まり，火山灰砂を噴出すると共に圓錐丘の西部を破壞し，向山灰砂層を堆積せしめた．此爆發的噴火に引

續いて向山熔岩が噴出し，大峯圓錐丘の噴火口を埋め，更に其西側の火口壁を越へて西北方に溢出し瀬戸山の南麓附近に迄擴がつた．

以上述べた様に，新島の噴火は最舊期火山群に始まり，赤崎ノ峯，丸嶋山，新島山宮塚山，アツチ山等の諸火山を經て，向山火山に終り，玆に現在の新島複合火山島を形成した．之等の火山は相互の間に構造上何等の主從的關係を示さず，夫々獨立の火山として順次既存の火山の隣接地域に噴出し，隣接した火山の一部が相互に重なり合つてゐるに過ぎない．各火山自體の地形或は構造には，新島の地下の何か特別の地質構造の影響に依つて現れたと考へられる様な特徴は認められない．又，各火山の配列は噴出地點が順次規則正しく或地點から一方的或は多方的に移動した事を示してゐない．然し，新島の火山全體としては島の長軸の方向，卽，新島，式根島，神津島及び恩走島を含む北東—南西方向の一帶上に配列し，此流紋岩火山島列の生成に關係ある火山構造線が新島の地下に存在し，略此線に沿つて各火山が噴出した事を示してゐる．

新島の南方に位する式根島は，福地學士に依ると，大部分黑雲母流紋岩熔岩で，辻村學士に依ると，新島附近の最舊期流紋岩床の一である．筆者は未だ此島を觀察してゐないが，若し夫が黑雲母流紋岩熔岩であるとすれば，新島の熔岩の規則正しい噴出順序から考へて，其噴出は古くとも宮塚山火山の噴出時代の前後と推定される．

有史時代の噴火．新島の有史時代の噴火の記錄と見られてゐるのは三代實錄，日本紀略，及び扶桑略記に載つてゐる仁和2年5月24日（西曆886）の噴火記事で，中村博士11）に依つて初めて引照され，故大森博士12）に依つて日本噴火誌中に採錄されてゐる．此記事は簡單で，噴火の起つた位置，噴火の規模等を詳しく記錄してゐないが，辻村學士及び坪井博士が既に論じた様に，恐らく新島の最新の火山である向山火山の噴火を指すものであろう．續日本後紀に載つてゐる神津島の承和5年7月5日（西曆838）の噴火の記事は新島の噴火の記事よりも詳しく，同島の最新の火山である天上山火山の噴火である事をよく傳へてゐる．要するに，新島は神津島と同様に地質學的及地形學的に見て新期の火山島であるのみでなく，有史時代にも神津島の噴火に後れる事僅に48年にして噴火し，黑雲母流紋岩の火山灰砂及び熔岩を噴出して構造的及び岩石學的に神津島の天上山火山に極めてよく類似する複合火山向山を形成したのである．

新島地震に因る地變

昭和11年12月27日に起つた新島地震に因つて生じた地變の中で，地震直後に

11）　中村清二　震豫報告，**79**（1915），42.

12）　大森房吉　震豫報告，**86**（1918），109.

直接觀察される事の出來たものは崖崩れと地割れとである．

崖崩れは新島の各火山の周圍に發達する斷崖及び急傾斜の山腹の各處に起つた．新島山の西側及び南側の熔岩崖は約7個處に於いて著しく崩壞し，新島山熔岩の巨塊が崖下の低地に多數轉落した．特に若鄉前濱の北端の新島山熔岩崖に起つた崖崩れは熔岩の巨塊及び砂礫を海中に迄押出してゐて，地震當時此海岸にゐた若鄉部落民の一人を生埋めにした．アツチ山の山腹は比較的緩傾斜で，著しい崖崩れを起さず，同山の北西山腹及び淡井浦に面する海崖に小規模の崩壞が認められたのみであつた．宮塚山の崖崩れは新島の中に於いて最も大規模で，且つ最も多數であつた．卽，同山の東，北，及び西側の斷崖は殆ど連續的に崖崩れを起し，至る處に於いて高さ 200 m に達する熔岩の絕壁の殆ど上端近くから崩壞してゐる．本村，若鄉間の本道は此崖崩れのために宮塚山東麓の七曲り及び宮塚山とアツチ山との間の峠附近に於いて崩落した宮塚山熔岩の巨塊及び砂礫の下に埋められた．又，宮塚山の南西麓アジヤ山（島分澤の北側）の崩壞に依つて本村部落民の一人が生埋めにされた．赤崎ノ峯火山の東側の熔岩崖には約4個處に著しい崖崩れがあり，同火山の西側の本村前濱北部に面する熔岩崖にも數個處に小規模の崩壞があつた．若鄉部落は以前には本村部落の北端附近に在つたのであるが，其附近の熔岩崖の崖崩れが劇しいために約 50 年前に現在の位置に移つたと云はれてゐる．峰路の東，南及び西側の熔岩崖には合計7個處餘りの小規模の崖崩れが見られた．向山火山に於いては羽伏浦，西ノ浦，及び間々下浦に沿つて白ママ層の斷崖が各處に於いて崩壞したが，向山熔岩は南西海岸に面する絕壁を除けば殆ど崖崩れを起さなかつた．石山及び五右衞門石切場は多少崩壞したが，地震當時は其從業員の休憩時間に丁度當つてゐたため被害者が生じなかつたと云ふ．

地割れは各火山の頂上部の平坦地には殆ど無く，本村及び若鄉の低地の主として道路上に現れ，多くの場合道路の方向に走つてゐた．本村低地の地割れは白ママ層及び砂丘砂層中に現れ，若鄉低地の地割れは淡井浦灰砂層及び砂丘砂層中に現れたのであつて，熔岩中の地割れは一も認められなかつた．

以上述べた崖崩れ及び地割れは何れも各火山の地形に現れてゐる特種な條件に支配されて生じた表面的の地變で，火山の內部構造或は火山地下の地質構造の表現であると考へられる樣な特質は個々の崖崩れ或は地割れには勿論，之等の分布の上にも亦認められなかつた．松澤博士等に依ると，淡井浦の西方に於いて崖或は土堤に直接關係してゐないと考へられる地割群が N 30°E～S 30°W の方向に 400～500 m の長さの間に現れた． 此地域には淡井浦灰砂層が分布し，特に際立つた斷崖は發達してゐないが，既に述べた樣に，比較的急傾斜を以つて東方に降る一帶が略南北に連なり，淡

井浦灰砂層の下に若郷玄武岩砂礫層の斷崖が埋もれてゐると推定されるから（第 6 圖），上述の地割群は恐らく此斷崖上に當る地表に現れたものであろう．

要するに，今回の新島の地質調査及び地變調査の結果のみでは，新島地震の原因が新島の地質構造或は火山活動に直接關係してゐるか否かを判定する事が出來なかつた．

---

15. *Volcanoes of Nii-sima, One of the Seven Izu Islands.*

By Hiromichi Tsuya,

Earthquake Research Institute.

Nii-sima, situated about 40 km SW. of Volcano O-sima, in 34°23′N. and 139°15′E., is a volcanic island measuring about 11 km in a N.-S. direction and 2.5 km E.-W. It consists, like Kozu-sima, of several Quaternary liparitic volcanoes, besides the ruin of a basaltic volcano, of which the Mukoyama volcano in the southern part of the island is the youngest as well as the largest. The rocks constituting the liparitic volcanoes are grouped under three main headings——hornblende-plagioliparite, hornblende-biotite-plagioliparite, and biotite-plagioliparite——in order of eruption. Thus the structural scheme of the island, together with the rock-types represented may be summarized as follows:

1. Lavas forming the lowest visible part of Nii-sima (*hornblende-plagioliparite*)	Seto-yama lava. Minezi lava. Zinaka-yama lava.
Daisan-yama tuff and tuff-breccia (juvenile ejecta: *hornblende-plagioliparite*).	
Simawaké-zawa tuff (juvenile ejecta: *hornblende-plagioliparite*).	
2. Akasakino-miné volcano (*hornblende-plagioliparite*)	Akasakino-miné lava. Akasakino-miné ejecta bed.
3. Niisima-yama volcano (*hornblende-biotite-plagioliparite*)	Niisima-yama lava.
Marusima-yama volcano (*hornblende-biotite-plagioliparite*)	Marusima-yama lava.
4. Wakagō basaltic volcano (*augite-olivine-bytownite-basalt*)	Wakagō basaltic ejecta bed.
5. Miyatuka-yama volcano (*biotite-plagioliparite*)	Habusi-ura ejecta bed. Miyatuka-yama lava. Miyatuka-yama ejecta bed.
6. Atti-yama volcano (*biotite-plagioliparite*)	Awai-ura ejecta bed. Atti-yama lava.
7. Mukō-yama volcano (*biotite-plagioliparite*)	Siromama bed (Ōmine pumice-cone). Mukō-yama ejecta bed. Mukō-yama lava.

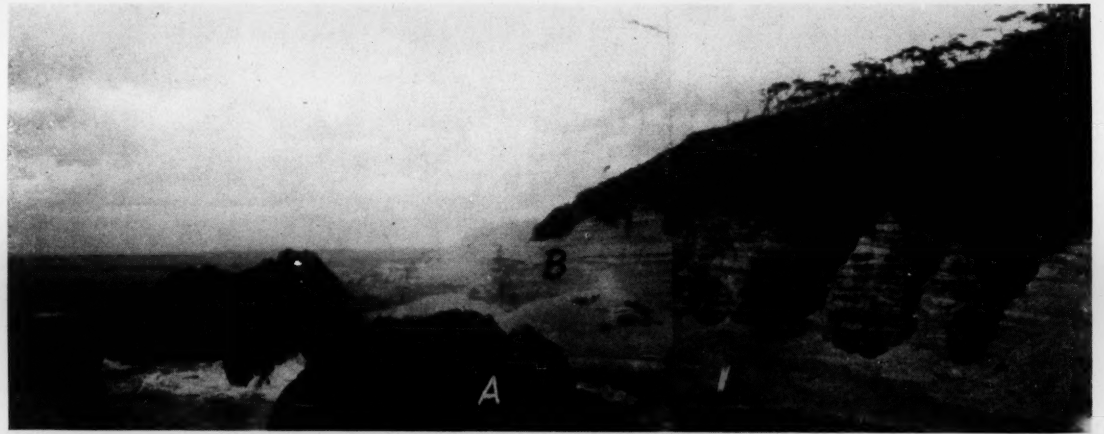

第１圖　大三山西側の海岸．Ａ，瀬戸山熔岩．Ｂ，白ママ層．
白ママ層の崖の下の崖錐は地震に因つて崩れ落ちたるもの．

（震研彙報　第十六號　圖版　津屋）

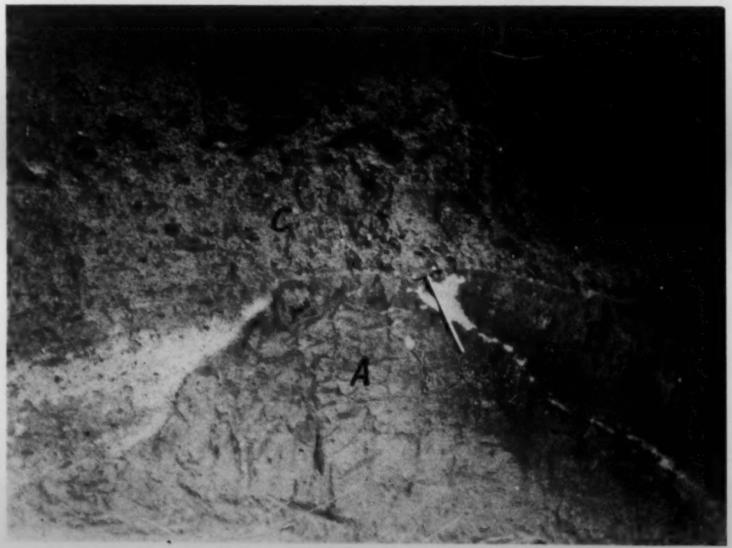

第２圖　Ａ，土壤化した瀬戸山熔岩．Ｂ，大三山凝灰岩層．
Ｃ，大三山凝灰角礫岩層．
（大三山西側道路の切割りの露出）．

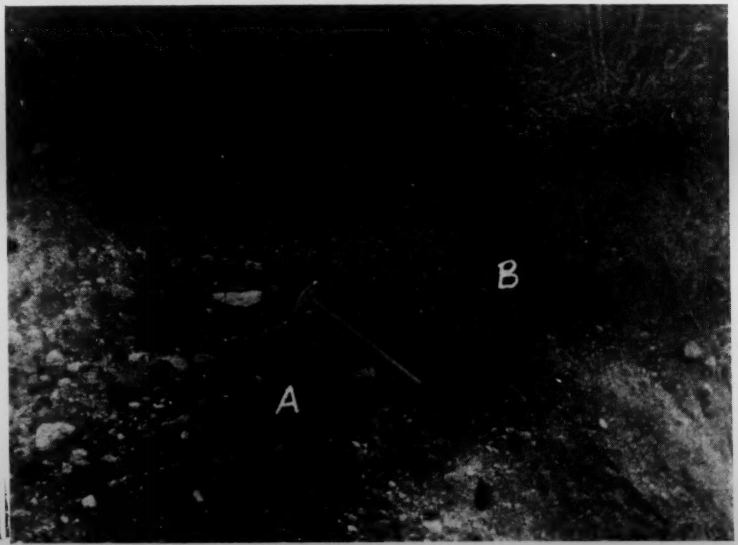

第３圖　Ａ，大三山凝灰角礫岩層．Ｂ，白ママ層，
（大三山南西側道路の切割りの露出）．

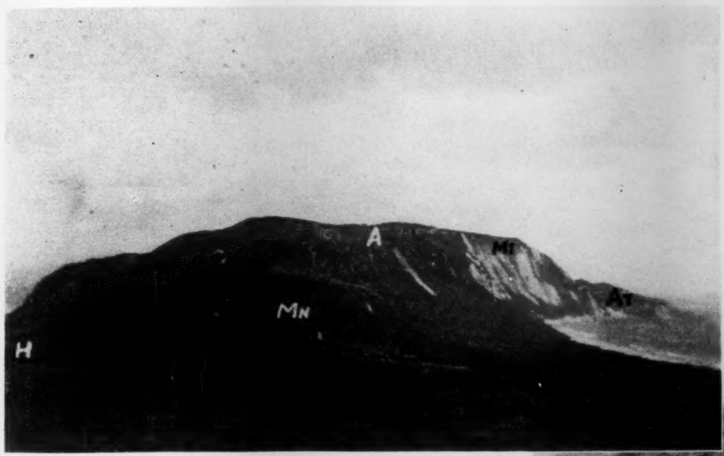

第4圖　H，本村部落．MN，峯路．
A，赤崎ノ峯．MI，宮塚山．
AT，アッチ山．
（向山五右衞門石切場から
北方山地を望む）

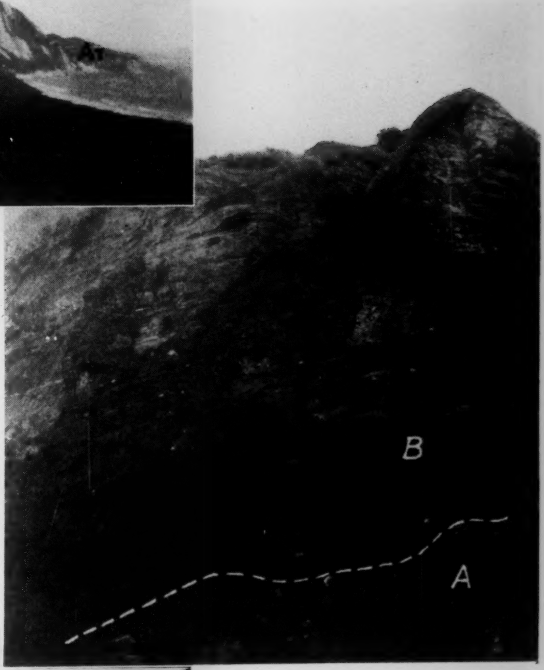

第6圖　A，島分澤凝灰
岩層．B，宮塚山熔岩
南西側斷崖．
（第5圖さ同處）．

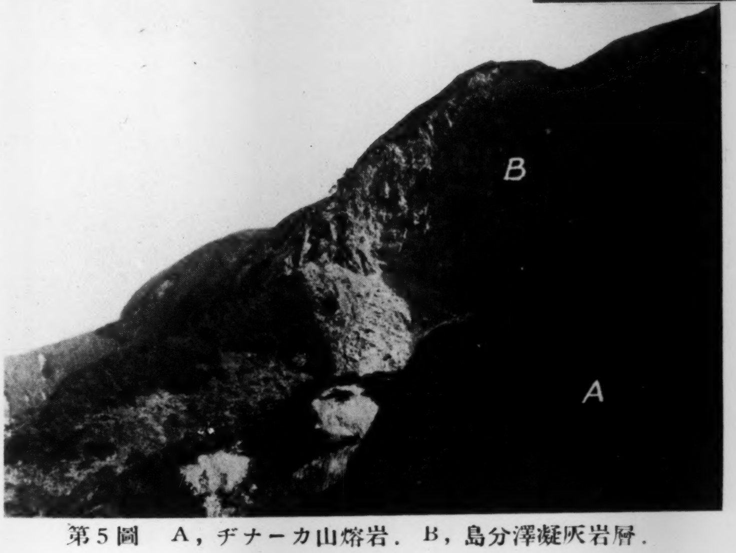

第5圖　A，チナーカ山熔岩．B，島分澤凝灰岩層．
（島分澤南側大磯海岸附近）．

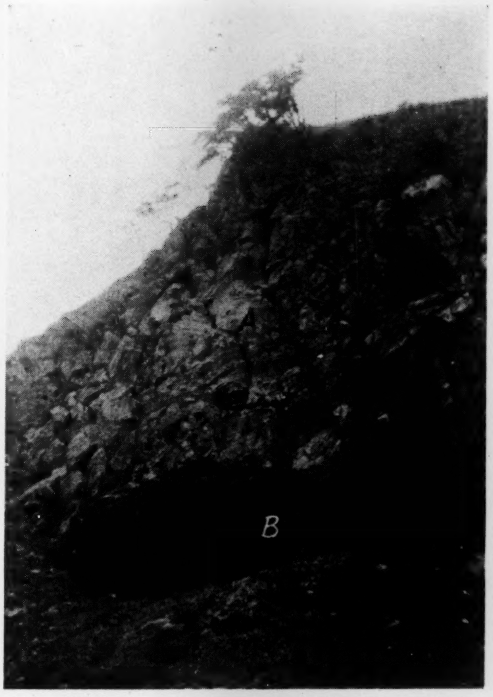

第7圖　A，ヂナーカ山熔岩．B，若郷玄武岩砂礫層．（Aの斷崖の前面に接する）．（若郷前濱南端）．

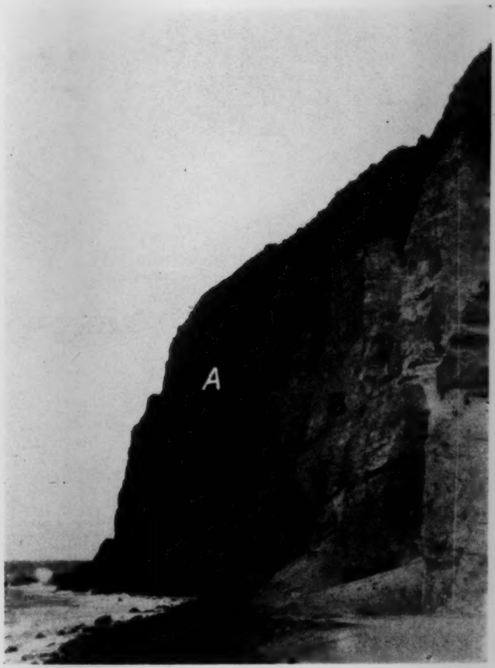

第8圖　A，丸嶋山熔岩．B，白ママ層．（丸嶋山南側海岸）．

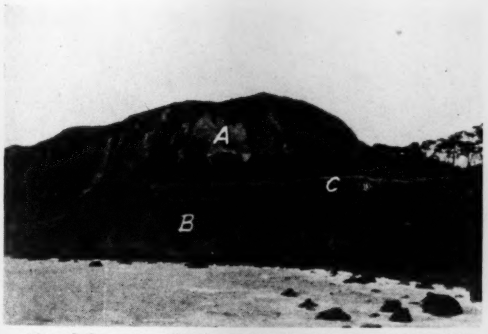

第9圖　A，新島山熔岩（地震に因る崖崩れ多し）．B，若郷玄武岩砂礫層．C，淡井浦灰砂層．

（若郷前濱南端から北東方に新島山を望む）．

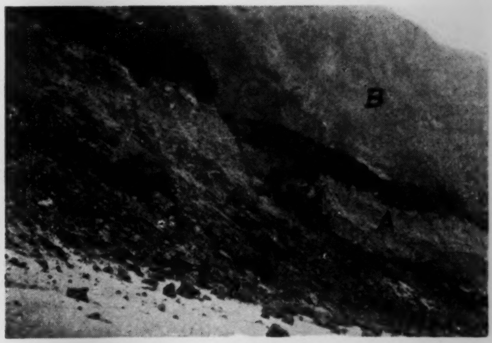

第10圖　A，羽伏浦灰砂層（地震に因る崖崩れ多し）．B，宮塚山熔岩崖．（羽伏浦北部）．

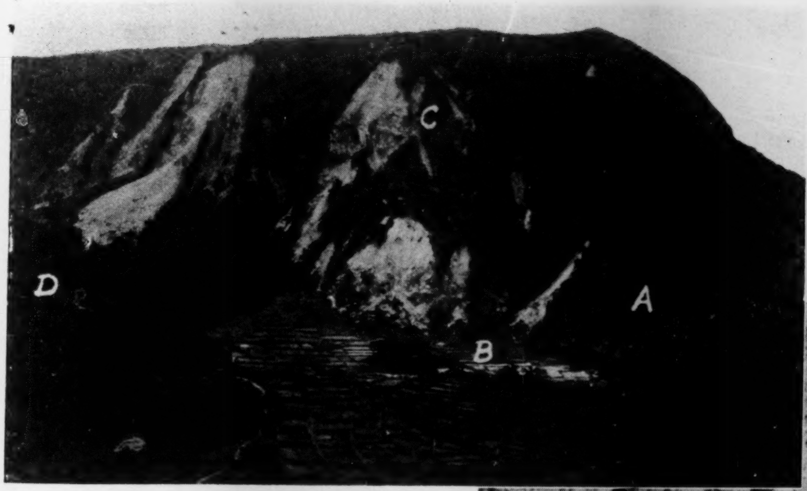

第11圖　A，ヂナーカ山熔岩．B，若郷玄武岩砂礫層の噴出地點さ推定される窪地．C，宮塚山熔岩（地震に因る崖崩れ多し）．D，アツチ山熔岩．

（新島山から南方に宮塚山を望む）．

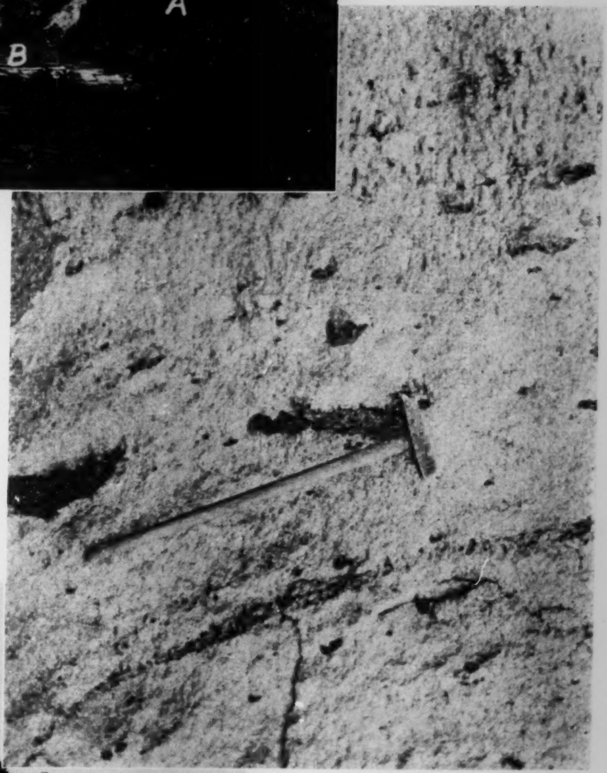

第13圖　淡井浦熔岩中の玄武岩捕虜岩．（淡井浦）．

第12圖　A，淡井浦灰砂層．B，アツチ山熔岩．（淡井浦南端）．

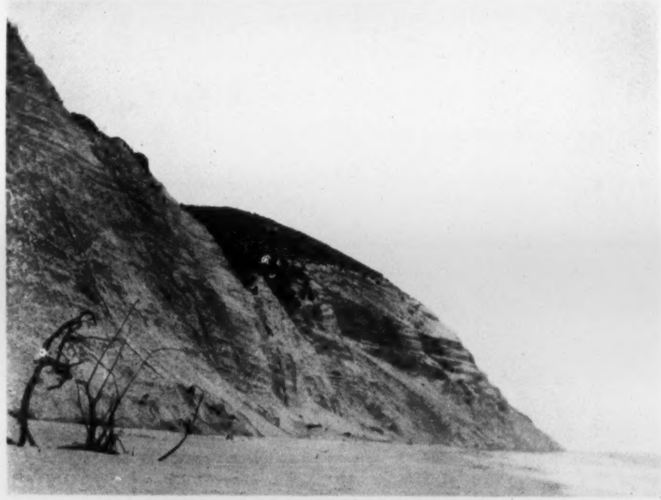

→ 第 14 圖　白ママ層
（大峯圓錐丘東側カンメガモリの斷崖）.
（西浦海岸）.

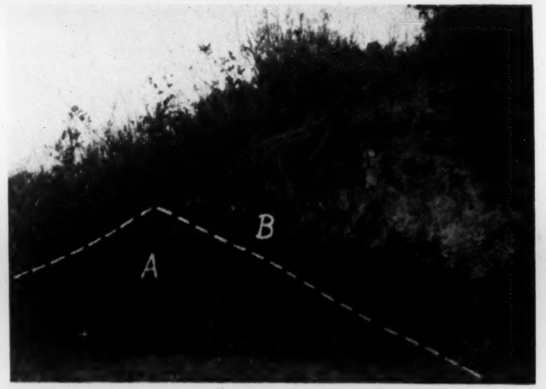

第 16 圖　A，白ママ層．B，向山灰砂層．
（向山五右衛門石切場附近）.

第 15 圖　白ママ層の細部．
（間々下浦）.

（震研彙報　第十六號　圖版　津屋）

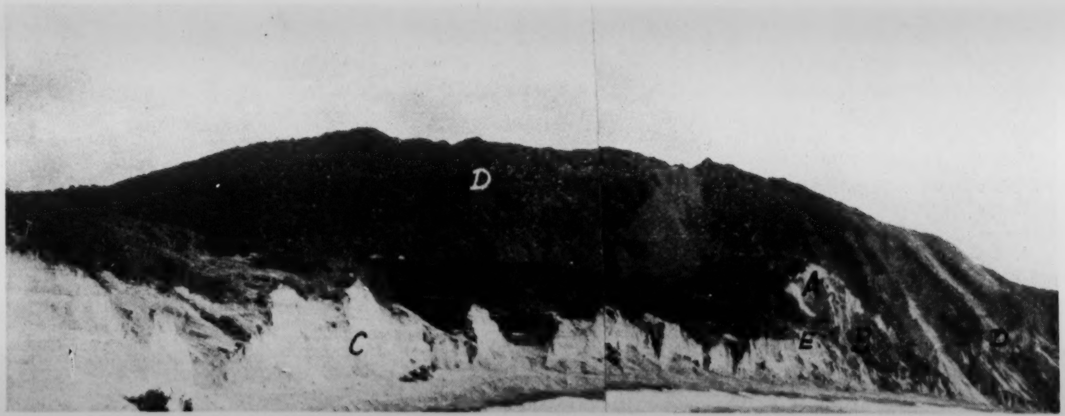

第 17 圖　A，角閃石流紋岩浮石層．B，大三山凝灰角礫岩層．C，白ママ層．D，向山熔岩．E，向山灰砂層．（間々下浦島ケ島から南東方に向山を望む）.

16. *A Geologic Interpretation on the Underground Structure of the Sititô-Mariana Island Arc in the Pacific Ocean.*

By Yanosuke OTUKA,

Earthquake Research Institute, Tokyo Imperial University.

(Read Dec. 21, 1937.—Received Dec. 21, 1937.)

In connection with the subject of the permanency of the ocean and Wegener's theory of drifting continents, many theories have been advanced regarding the geology of the ocean floor and its internal structure, for the apparent reason that they do not lend themselves so readily to survey as is the case on land. For example, there are a number of theories regarding the floor of the northern Pacific ocean. Notwithstanding the present obstacle, many geological and geophysical facts concerning the northern Pacific ocean have been brought to light by Japanese scientists, and the need for a new hypothesis on this part of the ocean has been felt in view of these new scientific results. In this paper the writer proposes a new geologic hypothesis of the underground structure of the Sititô-Mariana submarine ridge and the Japan trench considered from these new scientific results.

The Sititô-Mariana group of islands, together with the submarine ridge, which is a large, long bulge of the sea floor, branches off from the central part of the Japanese main island arc toward the southern part of the north Pacific Ocean.

In 1937, the Imperial Japanese Naval Hydrographic Office[1] published a bathymetric chart of the northern Pacific, which latter was recently resounded. This has greatly advanced our knowledge of the bottom topography of this ocean. According to this chart (Fig. 1), the deep Japan trench, which runs from the eastern coast of the Tisima island arc to the southern coast of the Caroline islands through the east coast of the Northeast Japan and the east coast of the Sititô-Mariana group, which is given in great detail, is narrower than before; that is, it is only about 200 km wide and has many deeps which exceed 8000 m. West of this trench, at its northern part, there is a large long, narrow bulge, where the Tisima island arc lies, and

---

[1] *Bathymetric chart of the sea near Japan, Imp. Jap. Nav. Hydr. Off.* (1937).

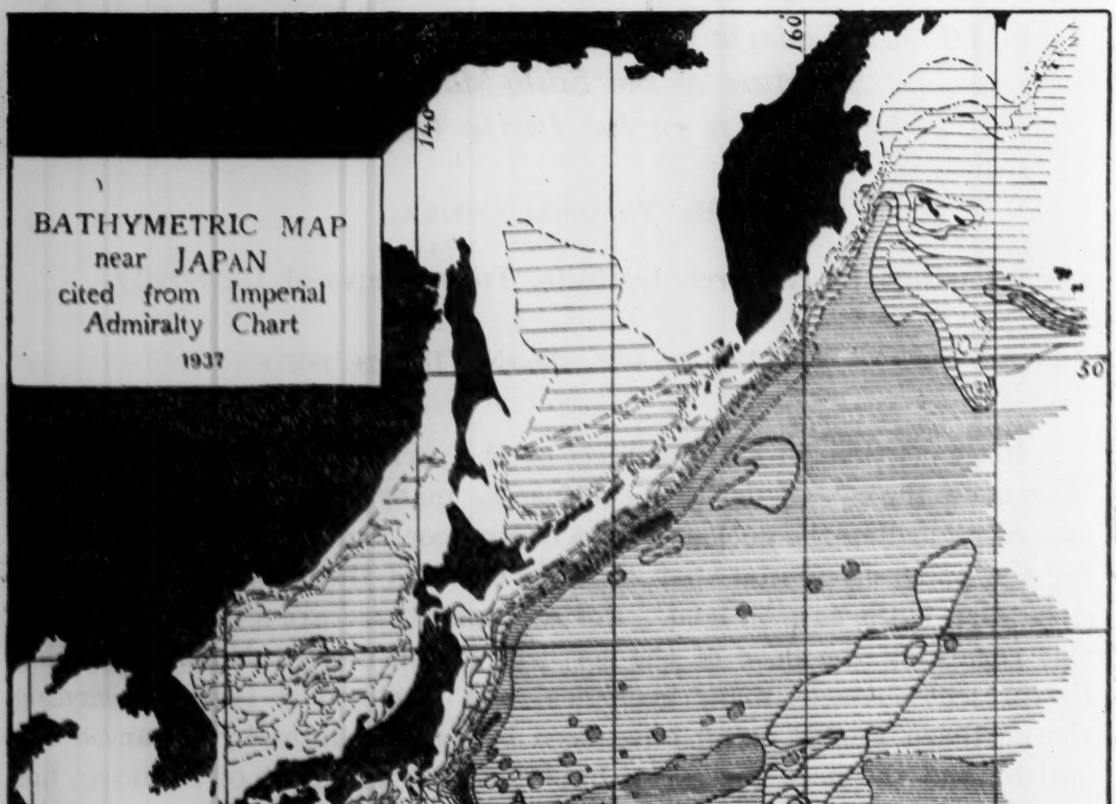
BATHYMETRIC MAP
near JAPAN
cited from Imperial
Admiralty Chart
1937
140
160
50
30
10
A
B
C
D
E
0
1000
2000
3000
4000
5000
6000
7000
8000

Fig. 1.

at its central part a similar bulge where the Hokkaidô and Northeast Japan lie. On its southern part, we have the Sititô-Mariana island arc and the submarine ridge, both of which are situated west of the Japan trench. Consequently, if profiles perpendicular to the general trend of the trench are taken across the trench and the bulge, these profiles will show similar forms no matter where they are taken, as shown in Fig. 2, except near the central part of the Japanese island arc and Hokkaidô. Since this is characteristic of any profile as just mentioned, if the sea-level were neglected, the profiles near Tisima, those near Northeast Japan, and those near the Sititô-Mariana island arc and submarine ridge, may be regarded as being the same as those taken on the land part of Northeast Japan, at any rate from the megamorphological view point.

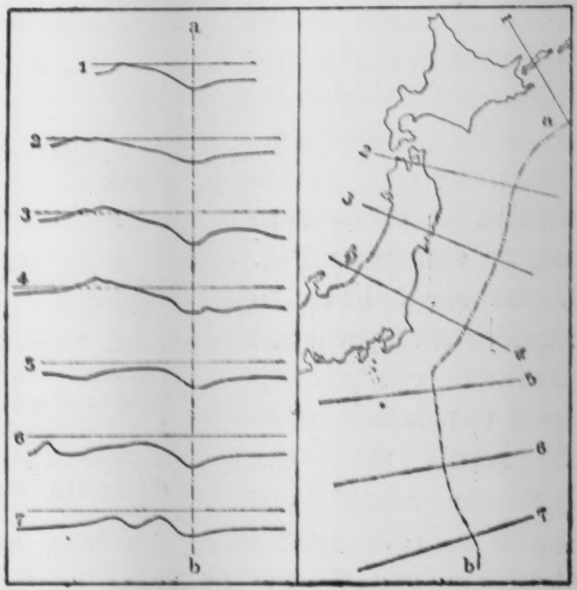

Fig. 2. Profiles perpendicular to the general trend of the Japan trench (ab). Vertical scale: horizontal scale=13: 1

Recently R. Tayama[2] made a morphological study of the coastal terraces that are developed on the coral islands of the Sititô-Mariana island arc, and concluded that they were Cainozoic upwarps of this island arc. According to him, the Mariana island arc generally has its convex side eastward in plan and is asymmetrically upwarped in elevation perpendicular to the general trend of the island arc. In this asymmetric upwarping, the east wing of this upwarping has steepened since the Pliocene age, while the slope of the west one has been lowered, as if the east wing were dragged downward by the subsidence of the submarine trench.

In other words the Sititô-Mariana island arc and submarine ridge may be a large upwarping zone of the earth's surface, and the Japan trench a deepening zone.

The writer[3] once criticized Prof. H. Yabe's paper and opinion ex-

---

2) R. TAYAMA, *Sci. Rep. Tôhoku Imp. Univ. in Japanese Language*, **28** (1937).

3) Y. OTUKA, *Jour. Geol. Soc. Tokyo (now Japan)*, **37** (1930), 439, pp. 175~178.

pressed that the Japanese island arc may be an upwarped zone. According to H. Yabe[4], who studied the submarine topography around the Japanese island arc, the higher terrace (his terrace "*T*" = (*PN*) in Fig. 3) on the land part corresponds to the deeper submarine terrace, and the lower (his "*M*" = (*T*) in Fig. 3) to the shallower one. If this inference is correct, to unite these contemporaneous two-levelled terraces into one, as shown in Fig. 3, we shall have to consider an upwarped surface containing these two levels, with the result that the Japanese island arc has to be upwarped along its long axis (as shown in Fig. 3) to explain the distribution of these contemporaneous two-levelled terraces, similar to the Sititô-Mariana island arc and submarine ridge.

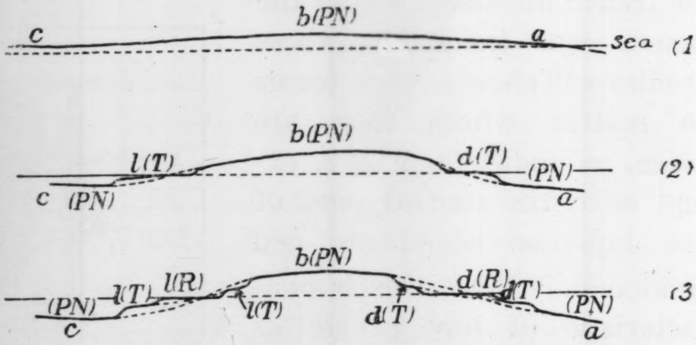

Fig. 3. Correlation of the terraces above and below the sea-level. Line abc in (1) (2) (3) shows the land surface during the latest Pliocene; full line *l* (*T*) & *d* (*T*) in (2) show the new erosion and sedimentation surfaces during Pleistocene; *l* (*R*) & *d* (*R*) are those during Holocene.

For this reason, the writer is not prevented by any morphological objections, generally speaking, from assuming the upwarping of the island arc and the downwarping of the submarine trench during the Quaternary age.

Recently C. Tsuboi[5] has called attention to the upwarping of the ground over which pass the bench marks across the island arc. It will not be surprising if this upwarp of the island arc generally agrees with the results of the precise levelling.

Geologically, the Sititô-Mariana island arc mainly consists of Cainozoic pyroclastics and volcanic rocks. Most of the islands on the submarine ridge are volcanic; while in the submarine trench no volcanic evidences have yet been found. The basal complex of these Cainozoic rocks are crystalline schist and some plutonic rocks which are exposed only on the island of Yap, but no pre-Tertiary sedimentary rocks are found on these islands.

According to R. Tayama[6], the schistosity of the crystalline schist

---

4) H. YABE, *Proc. Imp. Acad.*, **5** (1929), 9, p. 167.

5) C. TSUBOI, *Jap. Jour. Astr. Geophys*, **10** (1933), pp. 117~125.

6) R. TAYAMA, *Sci. Rep. Tôhoku Imp. Univ. in Jap. Language*, **19** (1935).

exposed on the island of Yap runs parallel to the long axis of the island, that is, the trend of the basal structure is almost parallel to the general trend of the southern part of the Sititô-Mariana submarine ridge and island arc.

Recently T. Tomita[7] summarized the preceding authours' views on the alkali rocks and published a map showing the distribution of the Tertiary alkali and alkalicalc effusive rocks in the world, as partly shown in Fig. 4. Although the distribution map contains certain hypothetical boundary lines, in connexion with the two kinds of rocks, it was an epoch making map of the kind.

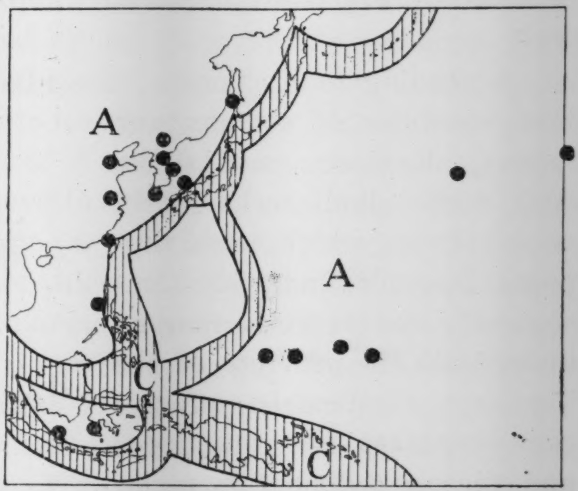

Fig. 4. Map showing the distribution of the Neogene effusive alkali rock (A) and alkalicalc rock (C) in the northern Pacific (Mainly after T. Tomita and M. Yosii.)

According to this map, although the effusive rocks of the Sititô-Mariana island arc are alkalicalcic, those of the eastern Caroline islands are alkalic. Since then M. Yosii[8] and H. Tsuya[9], who studied the distribution of the Cainozoic effusive rocks of the northern Pacific, have filled in the results in Tomita's map just mentioned. The boundary between the province of the Mariana alkalicalc rock and that of the east Caroline alkali rock is the deep submarine trench (Nero deep) southeast of the Mariana islands.

As seen in the chart (Fig. 1), the islands of Truck, Panope, and Kusai which belong to the east Caroline alkali rock province, are a group of isolated islands in which we find no characteristic features of the island arc nor those of a chain of submarine ridges as seen in the Sititô-Mariana group. Since according to Tomita's map (Fig. 4), the province of the alkalicalc effusive rock comes closely within the Tertiary tectogenetic zone of the world, a number of investigators have attempted to explain the origin of the alkalicalcic rock by means of the tectonic conditions prevailing in this zone. T. Tomita, in summarizing the views of previous writers on the origin of the alkali rock, conclu-

---

7) T. TOMITA, *Jour. Geol. Soc. Jap.*, **39** (1932), p. 613; pp. 684∼687.

8) M. YOSII, *Sci. Rep. Tohoku Imp. Univ. in Japanese Language*, **17** (1935).

9) H. TSUYA's papers on the Sititô-Mariana published in these Bulletins.

des that the common interpretation is that the magma from which the alkali rock is derived may have effused through largh fissures from great depths in the earth's crust.

N. L. Bowen[10] fully discussed the influences of magma affected by the aluminous and siliceous sedimentary rocks, and noted that the increase in mass in anorthite (plagioclase) promotes the crystallization of rhombic pyroxene, which two minerals are common in alkalicalcic rock.

According to T. Tomita, the alkalicalcic effusive rocks often contain xenoliths of sedimentary rocks (aluminous and siliceous), while alkali rocks rarely contain them, which, if so, supports Bowen's findings. Consequently the original magma underneath the province of the Tertiary alkalicalcic effusive rock captures the aluminous and siliceous sedimentary rocks, which change the chemical composition of the magma. The extent to which this has occurred may be considerable.

As mentioned already, similar occurrences underneath the Sititô-Mariana submarine ridge may also have been considerable.

M. Matuyama[11] has measured the gravity anomalies on the Japan trench, using V. Meinesz's method, from a submarine of the Imperial Japanese Navy. The results of $(g_0-\gamma_0)$ are given, in the reports of the International Union of Geodesy and Geophysics.

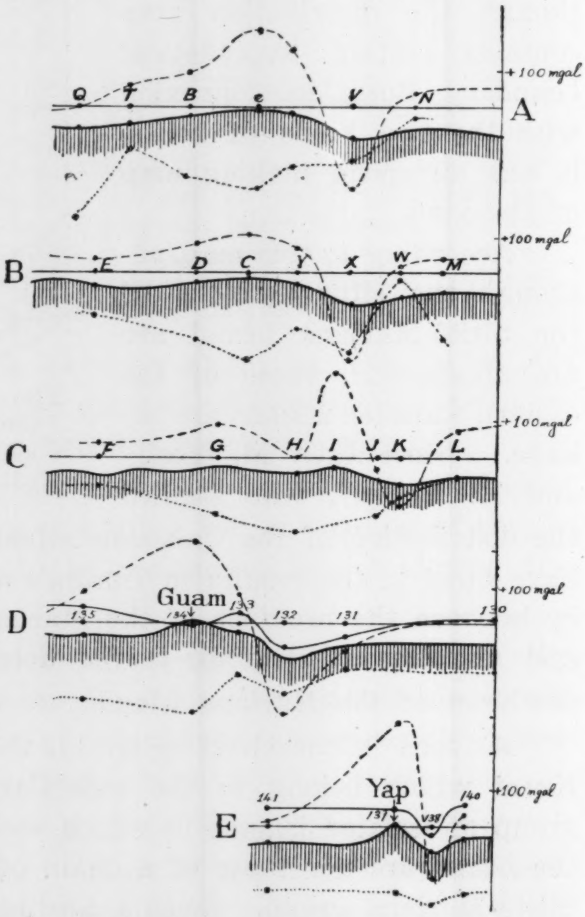

Fig. 5. Gravity anomaly (dash line) and isostatic anomaly (full line) on the line A···E in Fig. 1. (After M. Matuyama and V. Meinesz).

According to this report, the zone of negative gravity anomaly, generally speaking, falls on the Japan trench, and that of large positive gravity anomaly on the Sititô-Mariana island arc and submarine ridge as shown in A, B, C in Fig. 5.

---

[10] N. L. BOWEN, *The Evolution of Igneous Rocks*, (Princeton), (1928).

[11] M. MATUYAMA, *I. U. Geod. Geophys., 6th Conf.*, (1935), *Japan Rep.* 2.

Bofore this investigation of M. Matuyama, V. Meinesz[12] measured the gravity anomaly near the islands of Yap and Guam, and calculated the regional isostatic gravity anomaly in this region (as shown in D, E in Fig 5), according to whose results, there is a characteristic distribution of isostatic anomaly similar to that of the gravity anomaly near the Sititô island arc reported by M. Matuyama. Although Matuyama's results have not been checked by Bouguer's and other corrections, judging from the topographic features and V. Meinesz's results of isostatic anomalies on the islands of Yap and Guam, the writer believes with the reference of isostatic condition that a relatively thick layer of material of low specific gravity (e. g. sedimentary rocks) lies below the submarine trench, material of high specific gravity lies relatively near the land surface of the submarine ridge and island arc.

Recently, a number of the deep-focus earthquakes that have occurred near Japan have been studied by K. Wadati[13], T. Ito[14], and S. Yamaguti[15]. Some of them originate 700 km below the earth's surface. According to these studies, some of these deep-focus earthquakes are distribute and parallel to the Sititô-Mariana island arc from Vladiovostock to the Mariana island arc. According to E. Tam[16] and E. F. Bellamy[17], the origins of shallow-focus earthquakes in this region are densely distributed in a similar manner to these of deep focus.

In Fig. 6b, the deep-focus earthquake origins are projected on a plane perpendicular to the general trend of the Japan trench, from which it will be seen that the origins of these earthquakes are distributed close to and parallel to inclined plane (dip about 30°, 45° & 60° west) which intersects with the land surface along the west margin of the Japan trench.

It may be inferred from the distribution of these origins, that they are closely related to the bulge and trench shown in Fig. 2.

Since the thickness of the earth's crust traversed by many earthquake waves is believed to be about 50~60 km, most of the deep focus earthquakes must have originated in the basaltic layer below the earth's

---

[12] V. Meinesz, *Gravity expeditions at Sea.* II. Delft (1934).

[13] K. Wadati, *Geophys. Mag.*, **8** (1935), pp. 303~325.

[14] T. Itô, *Jap. Jour. Astr. Geophys.*, **11** (1934), 2.

[15] S. Yamaguti, *Earthq. Res. Inst. Imp. Univ. Tokyô*, **15** (1937), pp. 170~177.

[16] E. Tam, *Zeitschr. Geophys*, **4**, 7/8.

[17] E. F. Bellamy, *Index Epicentr*, 1913~1930.

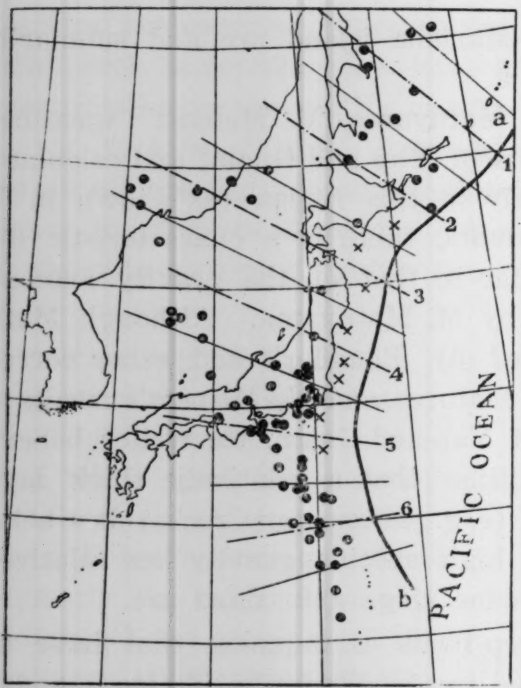

Fig. 6a shows the projection of origins of deep-focus earthquake (black circle) and the locality densely distributed by the origins of shallow-focus earthquake (cross). "ab" is the general trend of the Japan trench. Numerals show the number of segments almost equally divided by the vertical plane perpendicular to the general trend of the Japan trench.

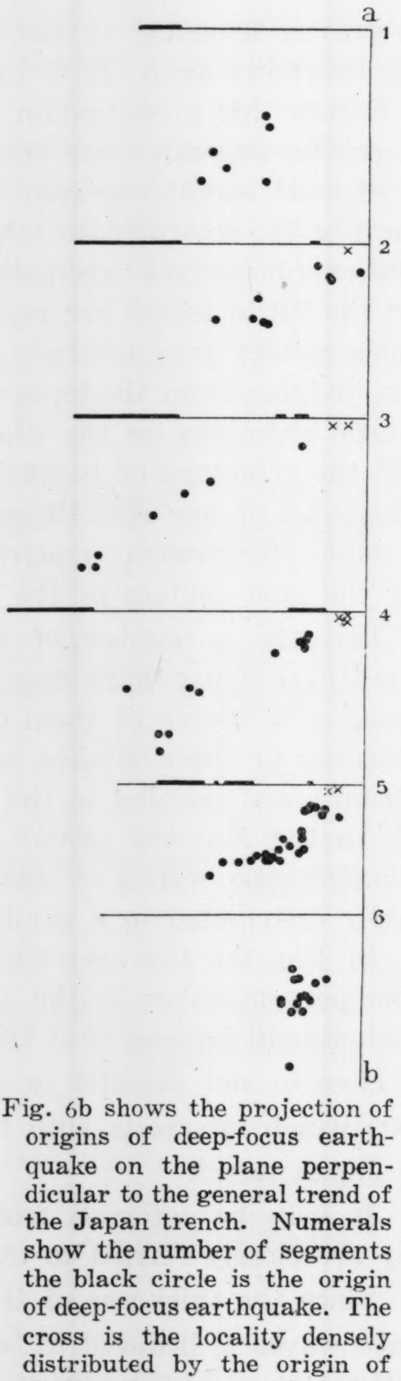

Fig. 6b shows the projection of origins of deep-focus earthquake on the plane perpendicular to the general trend of the Japan trench. Numerals show the number of segments the black circle is the origin of deep-focus earthquake. The cross is the locality densely distributed by the origin of shallow-focus earthquake. Vertical scale horizontal scale =1:1.

crust of sial, a number of the geologic phenomena witnessed on the Sititô-Mariana ridge and trench must be considered with reference to the peculiar conditions obtaining in this basaltic layer.

Petrologists and geophysicists believe the basaltic layer below the earth's crust or sial to be composed of ultrabasic or alkalic basaltic magma, which is plastic and in a semi-solid state under very high pressure and temperature.

As to the sort of disturbance that probably occurred in this basaltic layer, T. Ogawa[18] has advanced the opinion that, "since the pressure increases with depth, the subcrustal layer may be in a highly plastic and solid-like condition although it is heated to a very high temperature. The process by which the disturbances travel from the interior of such plastic and solid-like matter to the surface may be the result of local changes in the pressure, which by disturbing the equilibrium of the basaltic layer, induce liquifaction and gasification of the subcrustal material under high pressure and temperature. Such liquified or gasified subcrustal material may ascend to the upper zone of low pressure from the lower zone of high pressure." If this explanation is true, this upward movement of material may, on the one hand, push the earth's crust upward, and on the other hand, iuduce downward movement of the neighbouring subcrustal layer to fill the space left by the upheaved part. This downward movement of the subcrustal layer drags the crustal part adhering to the subcrustal material owing to the high viscosity of the latter.

---

[18] T. OGAWA, *New Interpretation of Geologic Phenomena* (地質現象の新解釋), (1929), pp. 364～366.

By this movement, the upheaved subcrustal material dissolves the xenoliths of the crustal part.

M. Ishimoto[19], in referring to the recent studies of H. Kawasumi, expressed the opinion that an earthquake is not necessary to explain the breaking of an elastic body, but that it may be explained by a mere change of pressure in an inclosed cavity. If his view is correct, deep-focus earthquakes might easily occur from mere change in pressure in the subcrustal layer mentioned above.

In the foregoing, the writer has enumerated and described the characteristic features of the Sititô-Mariana region, based on his geomorphological, geological, and geophysical studies of this island group.

The new interpretation of the Sititô-Mariana island arc and submarine ridge are schematically shown in Fig. 7.

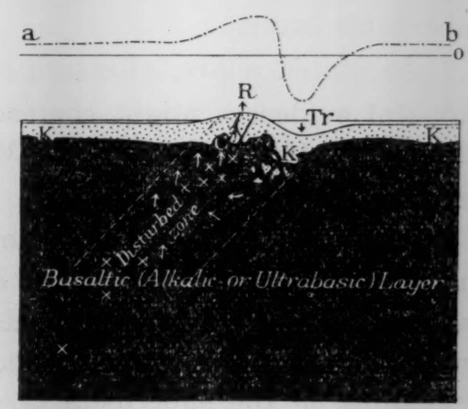

Fig. 7. Schmatic diagram showing the interpretation on the underground structure of the Sititô-Mariana submarine ridge and the Japan trench. ab=gravity anomaly or isostatic anomaly. R=submarine ridge. Tr=submarine ridge. K=earth's crust. C=alkalicalcic molten rock.

There is a basaltic (alkalic or ultrabasic) layer under the earth's crustal layer. But local changes in pressure occurred at depths of less than about 700 km below the landsurface within the zone that dips about 45° NW and intersects the landsurface with the general trend of the northwest margin of the Japan trench.

---

[19] M. Ishimoto, *Disin*, 9 (1937), 10.

This local change in the pressure causes the highly viscous and semisolid state of the basaltic layer to become more fluid. The fluidified material moves from the lower horizon to the upper. This movement is accompanied by crustal upwarpings and volcanic activities on the earth's surface. This upward escape of fluidified material is compensated by the downward movement of the adjacent subcrustal material by a convexion like flow. The subcrustal material adheres to the aluminous and siliceous crustal part by virtue of its high viscosity, and drags it downward by the downward movement as mentioned above.

With this adhesion of the aluminous and siliceous crustal part to the subcrustal material, the chemical composition of the basaltic magma may change to an alkalicalcic one, which latter is a characteristic feature of the composition of the Sititô-Mariana islands.

Geophysically the mass defect on the Japan trench and the mass excess on the island arc and submarine ridge may prove to be the upward movement of the fluidified heavy subcrustal material which pushes up earth's crust and sometimes extrudes from it, while the downward drag of the light crustal part which deeply embeds into the subcrustal layer.

As stated above, although no geomorphological geological, nor geophysical evidences might contradict this new interpretation of the interior structure of the Sititô-Mariana island arc, it is not free from certain assumptions.

Although this interpretation presumes that the tectogenetic zone merely indicates an abnormal condition of the subcrustal layer in the earth's crust, a study of the history of the life cycle of this zone may conduce to a more concrete understanding of the abnormal conditions prevailing in the subcrustal layer. It is hoped that a more concrete knowledge of magmatic differentiation and the physical nature of the original magma will confirm this interpretation. These studies constitute not only the fundamental problems of crustal movement but also the fundamental problem of the origin of earthquakes.

The writer in his studies of the Tertiary geologic structure of Northeastern Japan, seeks a fundamental cause of the crustal movements that occurred during the Tertiary period, and is desirous of applying this new interpretation to the Tertiary tectonic history of northeastern Japan, and in doing so, considers the Sititô-Mariana island arc and trench as a youthful stage in the growth of the tectogenetic zone.

In conclusion, the writer wishes to express his sincere thanks to Prof. H. Yabe, Prof. M. Ishimoto, Prof. S. Tsuboi, Prof. C. Tsuboi, Dr. T. Tomita, and H. Kuno for their valuable discussions with him on this new interpretation.

---

16. 七島・マリアナ海嶺の地下構造に關する一解釋

地震研究所 **大塚彌之助**

七島・マリアナ海嶺の地下の地質構造に關して，その海底地形・段丘・地質・岩石・重力・地震等の知られた事實から推定して，一つの地質學的解釋を述べた．

17. 千葉市西北郊登戸の地下水と震害

東京文理科大學地理學教室 {吉村信吉* 山本莊毅}

著者等は昭和 10 年4月 28～29 日千葉市西北郊下總臺地の堀井 110 につき研究を行ひ，別文に發表した.[1] その論文を取纒中に特異の地下水の分布狀態と大正 12 年9月1日の關東地震當時の震害地との間に密接な關係のあることを著者の1人山本が氣付いた．概略は一昨年の地震研究所談話會に於て發表したが，石本所長の御奬めによつて改めて發表することとする．千葉市附近の地質構造について敎示された內務省土木試驗所の高田昭技師にも感謝の意を表する．

登戸附近の地形及地質

詳細は前記論文に讓り大體だけを述べやう．登戸は千葉市の西北郊の下總臺地上を占めてゐる（第1圖）．その附近は 15～20 m の小起伏の臺地をなし，東京灣に對しては急な海蝕崖で終るが，南方千葉市に向つては緩斜してゐる．登戸附近は海岸附近と東方吾妻臺方面との高まりの間にあつて緩斜した凹地をなしてゐる．これよりも北方に多い砂丘は登戸附近に迄延び，臺地上の低い丘と介在する淺い凹地との錯綜した地形を作つてゐる．

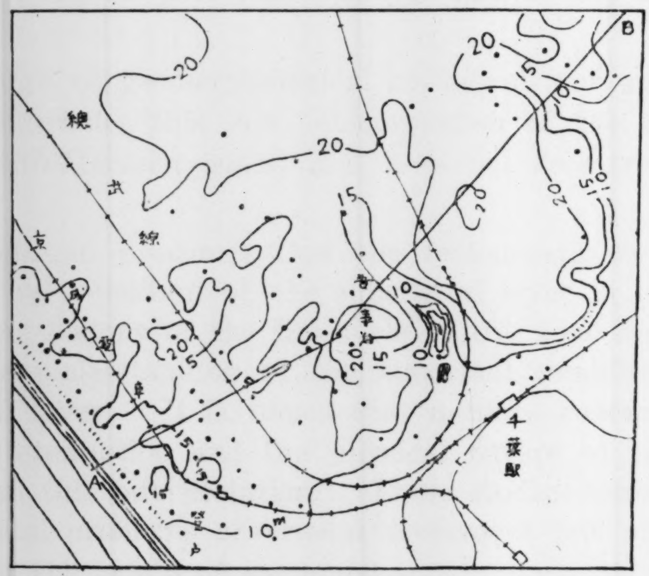

第1圖　千葉市北郊臺地の地形（高度 m, 點は調査地點）

千葉市附近に於ける數個所の試錐によると本問題には直接關係はないが，地下 150 m 附近迄に帶水層となる三

---

* 石本巳四雄紹介．

1) 吉村信吉，山本莊毅 1936：千葉市西北郊下總臺地の地下水．陸水學雜誌 6 74—84.

つの粘土層があり，その間は砂層で充される．粘土層の走向は下總臺地一般の地層と同じやうに東北より西南で，西北に緩斜してゐる．最上位の粘土層は海面下約 45m（臺地面下約 60～70 m）にあり，厚い砂層に被はれてゐるが，砂層の下部は稍粘土質である.²⁾ 以下述べるのは皆この砂層又はそれよりも上の地層である．（第2圖）

上記の厚い**砂層**の表面は海面上 10～13 m にあるが，上部は幾分粘土質となり，その厚さは 3 m 位である．

砂質粘土層の表面は大體現在の地表面の様に登戸より東西兩側に向ひ高くなり登戸附近に粘土層の谷がある．粘土層は 1m 以内の厚さで多少硬いので中井戸の底岩と云はれてゐる．幾分砂質ではあるが部分的に後述の中水の不透水層をなし震害に關係して重要なものである．

ローム層　粘土層の上を被ひ厚さは登戸附近では 1～2 m であるが，兩側では數mに及ぶ．下部は粘土質となりヘナと呼ばれる．

砂層　砂丘をなすもので所々ローム層を 2～3 m の厚さに被つてゐるが，凹地帶には缺いてゐる．

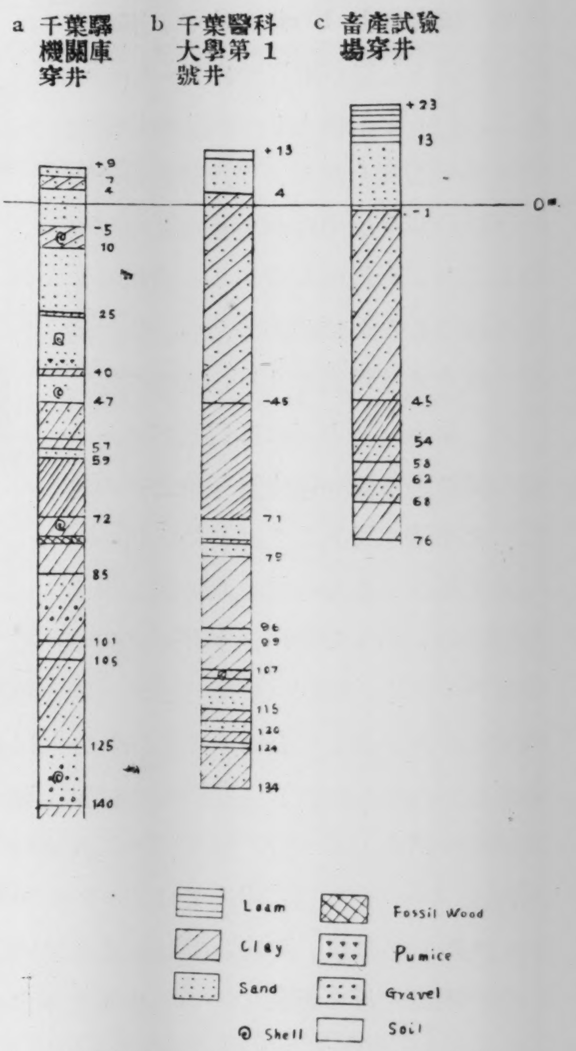
a 千葉驛機關庫穿井
b 千葉醫科大學第1號井
c 畜產試驗場穿井
+9
7
4
-5
10
25
40
47
57
59
72
85
101
105
125
140
+13
4
-45
71
79
96
99
107
115
120
124
134
+23
13
-1
45
54
58
62
68
76
0ᵐ
Loam
Clay
Sand
Shell
Fossil Wood
Pumice
Gravel
Soil

第2圖　千葉市附近地質柱狀斷面圖
（試錐による）
a は第1圖千葉驛附近，b，c は圖より南の臺地上にある

京成登戸驛より吾妻臺に至る井戸（第1圖）の側壁で觀察した層序は第3圖のやうで，前述のやうに登戸附近で粘土層等は低下してゐるのが分る．

登戸附近の地下水

登戸附近の淺所の地下水は次の二つになる

---

2)　この附近の地質は次の報文參照．
三土知芳 1935：千葉地質圖幅說明書．pp. 25.

I　本水　　海面下 30 m の最上位の粘土層を不透水層として厚い砂層中に帶水するもので，地下水面の高さは臺地の西北部では海面上 10 m 内外で，漸次南に向ひ低下し登戸附近では 4〜6 m である．3 m を最低として西方海岸附近では 6 m 迄高くなる．登戸附近の水面の谷狀の窪みは深所の不透水層の影響であるか，附近に人家が多く盛に揚水する爲であるかは明かでない．登戸附近では本水は地表下 10 m 以深にある．

II　中水　　上記の砂質及びローム層の間にある薄い粘土層（中井戸の底岩）を不透水層とし上部の粘土質ローム層に帶水するもので本水に對し中水と呼ばれ，かゝる井戸を本井戸に對し中井戸と云ふ．範圍は極限され總武線の線路を胴として蝶翅のやうに 600×300 m の地域にのみ分布してゐる．それ以外の所にも粘土層は續いてゐるが觀測當時には殆ど帶水してゐなかつた．上記のやうに粘土層は砂質で薄くよい不透水層ではないから，谷底狀に凹んでゐる登戸附近以外には常時帶水しないのであらう．中水の地下水面は海面上 13m より登戸附近では 8〜9 m である．地表面下の深さはその左翅部では 3 m 内外であるが，右翅及び胴に當る登戸附近では 1〜2 m に過ぎない．

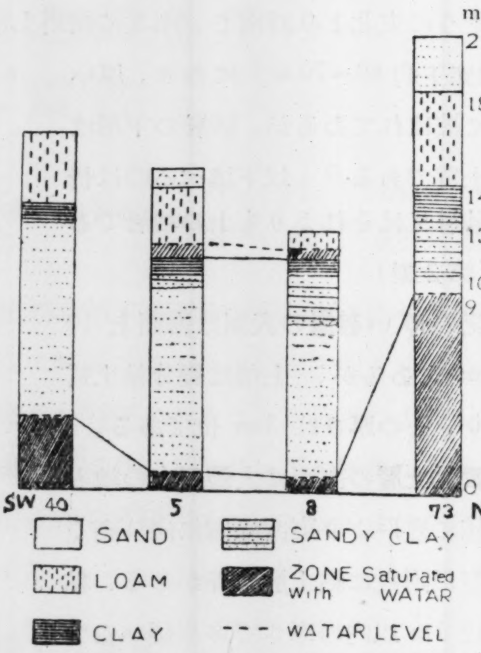
m
21
18.4
14.8
13
10
9
0
SW 40
5
8
73 NE
SAND
SANDY CLAY
LOAM
ZONE Saturated With WATAR
CLAY
WATAR LEVEL

第3圖　第1圖 A B 間の地質斷面

登戸附近を通る斷面について中水及本水の帶水狀態は第4圖のやうである．一番下の線は井戸の底の位置を示すが，こゝに不透水層があるのではなく，本水は海面下迄

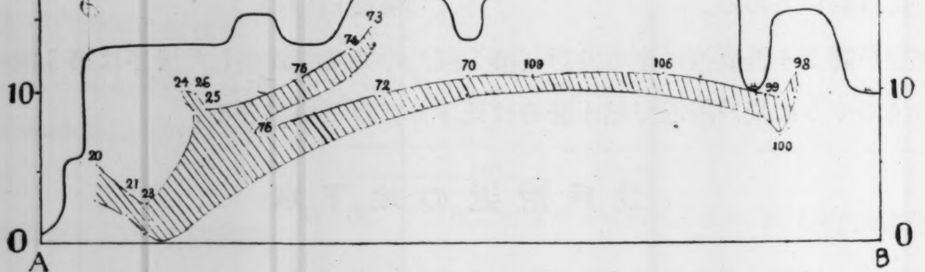
20m
10
0
A
20m
10
0
B
20
21
23
24
26
25
76
78
74
73
72
70
109
106
99
98
100

第4圖　A B の斷面

の砂層を充してゐることは勿論である．中水は登戸附近にのみ存在し，登戸附近では本水，中水面共に低下してゐる．登戸附近の 2，3 の井では本水と中水とが一つの井戸の中で相接し滯水が 5 m にも達してゐる．井戸掘の話では中水を得る目的で掘穿中底岩を掘抜き本水と接したのであると云ふ．

上記のやうに登戸附近には蝶翅狀に極めて淺い特殊な中水が存在してゐるが，この外登戸附近の地下水面の淺いことを裏書し，關係のある事項を列擧すると，

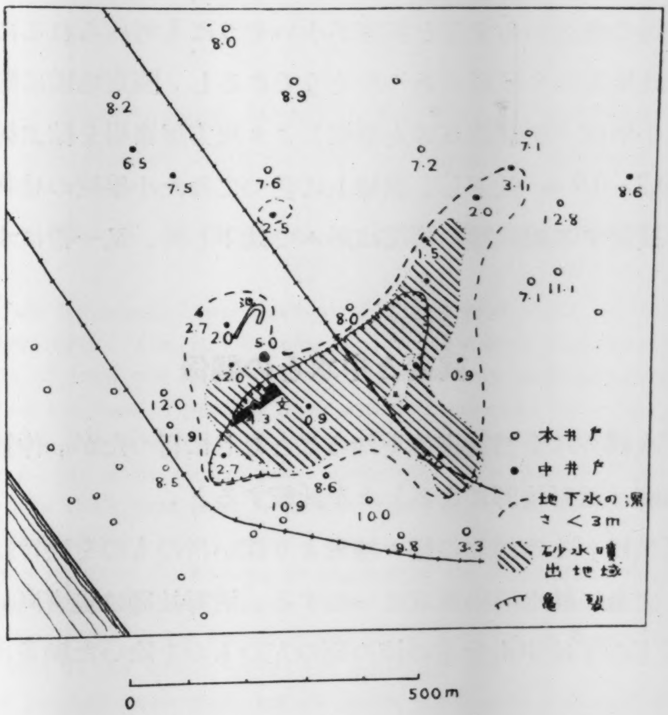
8·0
8·9
8·2
6·5
7·5
7·6
7·2
7·1
3·1
8·6
2·0
12·8
2·5
1·5
11·1
7·1
池
2·7
2·0
5·0
8·0
0·9
2·0
文
3
0·9
12·0
11·9
2·7
8·5
8·6
10·9
10·0
9·8
3·3
○ 本井戸
● 中井戸
地下水の深さ < 3m
▨ 砂水噴出地域
亀裂
0
500m

第 5 圖　登戸附近の中水區域と震災時の亀裂並に砂水噴出地域との關係（數字は地下水面の深さ）

1 豪雨後登戸附近には臺地上であるにも關らず相當深く雨水が湛水し，平時でも泥濘がひどい．

2 臺地上であるにも關らず人工的の池があり，1 萬分地形圖を見ると小面積ではあるが以前水田があつた．

3 屠畜場，養豚場其他通常低濕地にある建物が存在する．家屋も一般に沖積地に於けるやうな貧弱なものが多い．土地が低濕で地價が廉いので生活程度の低い人々の住宅地となるからであらう．

登戸附近の震害

關東地震に際し清野技師3) の調査によると千葉市附近では

（1）登戸附近　（2）千葉驛及綿打池附近　（3）出洲及寒川埋立地

の三個所に震害が著しかつたと云ふ.（3）は海岸の埋立地であるから暫く措く.（2）は恐く登戸附近と同じやうな原因（後述）に基くらしいが，この方面は調査しなかつたから觸れない.

登戸は臺地面又はそれを薄く削つた谷の上にあり，沖積地の上に發達してゐる千葉市自身よりも普通の概念からすると震害が小いやうにも考へられるにも關らず，土地の人によると安政地震にも激震があつたそうであるし，關東地震に際しては地域の西端千葉市立第四小學校（現淑徳高等女學校）より東方屠畜場を結ぶ線に龜裂を生じそれより南部は 0.3～0.9 m 低下し，裂罅上に當つてゐた小學校の建物の大部分は全壞し，陷沒區域を横斷する總武線の築堤は所々で低下した．又一帶に水と共に砂を噴出したと云ふ.

震害と中水との關係

本地域の地下水調査は全然震害等を知ることなしに行つたが，作製した中水の分布區域と震害分布圖（清野技師による）とを比較すると，

1 中水分布區域は，その西北の稍々地表より深い所のものを除けば（大體地表面下3 m 以内の線）完全に砂水湧出區域に一致する．清野技師は震害區域が丁字狀であると形容されたが丁の字は中水分布の蝶の翅の左のものを除いた胴並に右翅の部に相當する.

2 龜裂の位置は中水の北限線と一致する.

3 最も震害が甚しく龜裂が澤山出來た舊小學校附近は中水までの深さが最も淺く，本水とも接し帶水が最も厚い所に當つてゐる.

前述のやうに登戸附近には地質の差又は斷層等は認められないから，これから見て登戸附近の震害の著しかつたのは地下水が淺い所にあり，水で飽和された土層が地震動の週期を變へさせたものであらう.4) 龜裂を生じたり砂水を湧出したりするのは地下水面の淺い河原等で强震の度に報告されてゐた所である．本地域のやうな臺地上での砂水の噴出は不思議のやうであるが登戸には河原のやうに淺所に地下水や砂層があ

---

3) 清野信雄 1925：千葉市附近地震調査報文．地質調査所特別報告 **2**，171—185.

4) 水で飽和された土の震動に關しては石本博士の研究がある，
石本巳四雄，飯田汲事：地震研究所彙報 **14**（1936），632，**15**（1937），67.

るから矛盾なく解釋されると思ふ.

結　　　言

終に一言するならば本地域は最近著しく發展して住宅地となつて來たから今後もしも强震があつたならば前述の如き地災のみならず建物にも深甚な影響があらう．今後の震害輕減の爲にも地震動の實測に基く研究が望ましいと思ふ.

---

17. The Underground Water in the Vicinity of Tiba City with Special Reference to Earthquake Damages.

By S. YOSHIMURA and S. YAMAMOTO.

The writers made hydrological investigations of 110 drilled wells in the vicinity of Tiba City on Apr. 28/29, 1935. The region being surveyed by them is diluvial hill which consists of alternative strata of loam and sand. At the bottom of very shallow valley in the neighbourhood of Nobuto, there is a zone of perched water which is sustained on a thin sandy clay stratum between loam (upper) and sand (lower) layers. The depth of underground water table below the ground is only 1—2 m at its central part, while that of surrounding district whose ground water is contained in a thick sand layer is no less than 8 m. The surface of the perched water zone is muddy on rainy days.

According to the report of N. Kiyono, an engineer of the Imperial Geological Survey, there were serious earthquake damages near Nobuto at the time of severe Kwanto Earthquake on Sept. 1, 1923. The ground in the valley was depressed being bordered by a number of cracks. Sand and water were ejected on the surface within the depressed area.

The region of perched water and that of severe earthquake damages which were studied independently by different investigators are coincided very closely. It is probable that the perched water near the land surface may make some influences upon the period of seismic waves to accelerate the earthquake damages at that district.

18. *The Land-slide at the Ogusi Mine.*

By Ryûtarô TAKAHASI and Takesi MINAKAMI,

Earthquake Research Institute.

(Read Nov. 16, 1937.—Recieved Dec. 20, 1937.)

Introduction. On Nov. 11, 1937, the radio broadcasted that a serious land-slide had occurred at the Ogusi[1] mine in Gumma[2] Prefecture, burying alive over 300 miners, and totally destroying the mine. With a view to making investigations, the writer left Tokyo the following day (Nov. 12) for the scene of the disaster.

Ogusi is a sulpher mine in Tumagoi[3] Village, Aduma[4] District, Gumma Prefecture, although it spreads also into Nagano[5] Prefecture. It is 20 km distant from the volcano Kusatu-sirané[6], and 17 km from the town of Susaka[7], Nagano Prefecture. A cable-way for hauling the refined sulpher and other loads operates between this mine and Susaka. The location of the mine may be seen in Fig. 1.

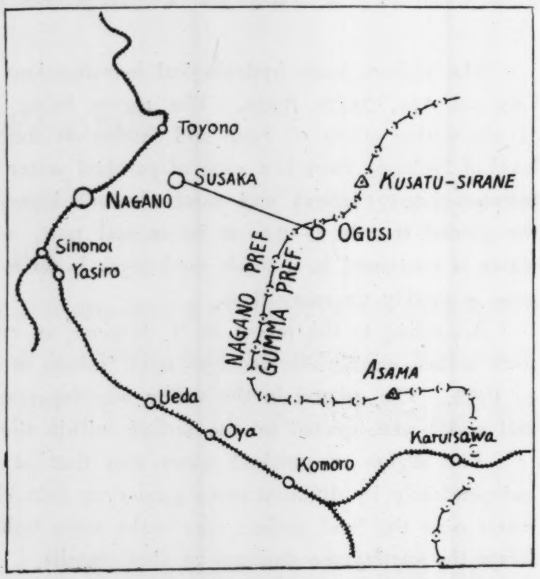

Fig. 1. Location of the Ogusi mine.

Topography and Geology. The topography of the mine and vicinity is shown in Fig. 2. To the west of the mine, beyond the the valley of the Aka-gawa[8], rise Donabé-yama[9] and Habudaké[10], and to the north we see soaring high a ridge consisting of the Kenasi Pass[11], and the two peaks, Ogusi-daké[12] and Omesi-daké[13]. These mountain ranges divide the prefectures of Gumma and Nagano. The eastern side of the mine is bounded by a small ridge called Myôzin-daké[14], which extends southward from Ogusi-daké. The southern side of the mine opens out into a broad expanse, looking towards volcano Asama far beyond the valley of the Aduma-gawa[15]. According to T. Matumoto[16], the large semi-circular depression surrounded by the mountain ridges just mentioned is an old explosion crater, but it is now so dissected that its original form is not apparent. North of the mine, on the way to the summit of Ogusi-daké, there is a small semi-circular depression fringed by a cliff several meters high, as shown in Fig. 3, (Plate XV). The slope is gentle in this depression, but it steepens downward to the scene of the present land-slide, and again forms a fan of gentle slope at the lower reaches, until it eventually ends in the valley of the Aka-gawa.

---

[1] 小串 [2] 群馬 [3] 嬬戀 [4] 吾妻 [5] 長野 [6] 草津白根 [7] 須坂 [8] 赤川 [9] 土鍋山 [10] 破風岳 [11] 無毛峠 [12] 小串岳 [13] 御飯岳 [14] 明神岳 [15] 吾妻川

[16] Graduate thesis.

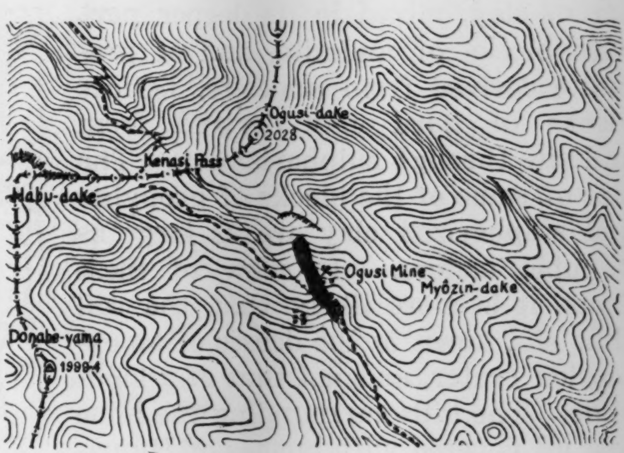

Fig. 2. Topography of the mine and vicinity.

There is little evidence to show whether this depression is a small explosion crater that formed secondarily in the great explosion crater mentioned above, or whether it is the remains of an old land-slide that occurred in the great explosion crater. In view, however, of the fact that the soil is thin on the east, north, and west sides of the depression, while it is very thick in the depression itself as well as on its south side, and also that the base rock, the lavas of volcano Omesi-daké, are scooped out at the depression and its lower reaches, it would seem more reasonable to regard the depression as a small explosion crater. A small trace of lava effusion on the east side of the depression, which was found by S. Watase(17) of the Geological Survey, seems to support this interpretation. The matter that slid down in the present land-slide consequently seems to be the old ejecta from this explosion crater.

A rough idea of the geology of this region, as investigated by T. Matumoto, is given in Fig. 4. The lava of Omesi-daké, denoted by *A* in the figure, which is a two-pyroxene andesite intercalated by tuff, forms the base rock of this region, as one finds in the valley of the Aka-gawa as well as in the bottom of the explosion craters. The present sulpher bed of the Ogusi mine was deposited in this tuff through the hydro-thermal action of volcanic gas and water. Another lava that flowed from Omesi-daké, denoted by *B* in Fig. 4, is a gray two-pyroxene andesite, completely overlying lava *A*.

---

17) Read before the investigation committee of the present land-slide, held on Nov. 25, at the Patent Bureau, under the auspice of the Department of Commerce.

The soil that forms the bulk of the land-slide is a brown, rather porous clay, mixed in its deeper part with blocks of andesite, and of propylite derived from andesite, besides blocks of hard clay derived from andesite through sulpherization. The size of some of the blocks of propylite and sulpherized clay are as large as 2 cubic meters. In view of these facts, it is more likely that the soil that slid down is the debris of an explosion crater, and not that of a land-slide. The hills surrounding the mine are all covered with bushes of Kuma-zasa (*Bambusa veitchii*), with scarcely any other noticeable vegetation.

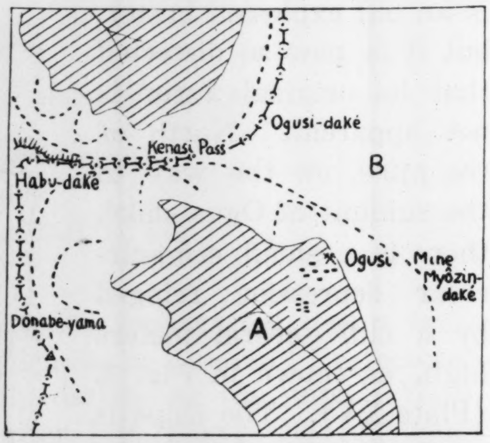

Fig. 4. Geological map of the mine and vicinity. Semi-circles in dotted line show the explosion craters.

The sulpher bed of the Ogusi mine, which is situated as shown in Fig. 5, is a disc-shaped deposit inclined to the east, with its only outcrop at the point marked *A*. Of the four adits, which are separated by heights of 18 m, the one from the other, only the second, third, and fourth are being worked. The first adit, which is the highest of all, is used for hauling in the sand for packing up the excavated galleries. As this mine has a very poor water supply, the dry packing system is in vogue.

The land-slide. The land-slide occurred at 15 h 32 m, Nov. 11 at the slope immediately north of the area, where are situated all the important parts of the mine, such as the refineries, office, school, miner's dormitories, and other buildings, all crowded together. The soil that broke loose crushed nearly all of them, buried them under the debris, and killed a large number of the miners.

The volume of the soil that broke loose is estimated at 140,000 cubic meters. The damage caused by this land-slide, as investigated by the police of both Nagano and Gumma, amounted to

Persons killed	234,	
〃 severely wounded	12,	
〃 wounded	20.	

But when reckoned by the number of families,

Families buried	120,	
〃 burnt out	38,	
〃 intact	12.	
Buildings buried	30	of which 46 were dwellings
〃 burnt	25	and 9 were warehouses etc.
〃 intact	4	

The four buildings that remained are two miner's dormitories and two refineries. The total population of the mine at the time was 1090. The damage caused by this land-slide is estimated at ¥ 300,000.

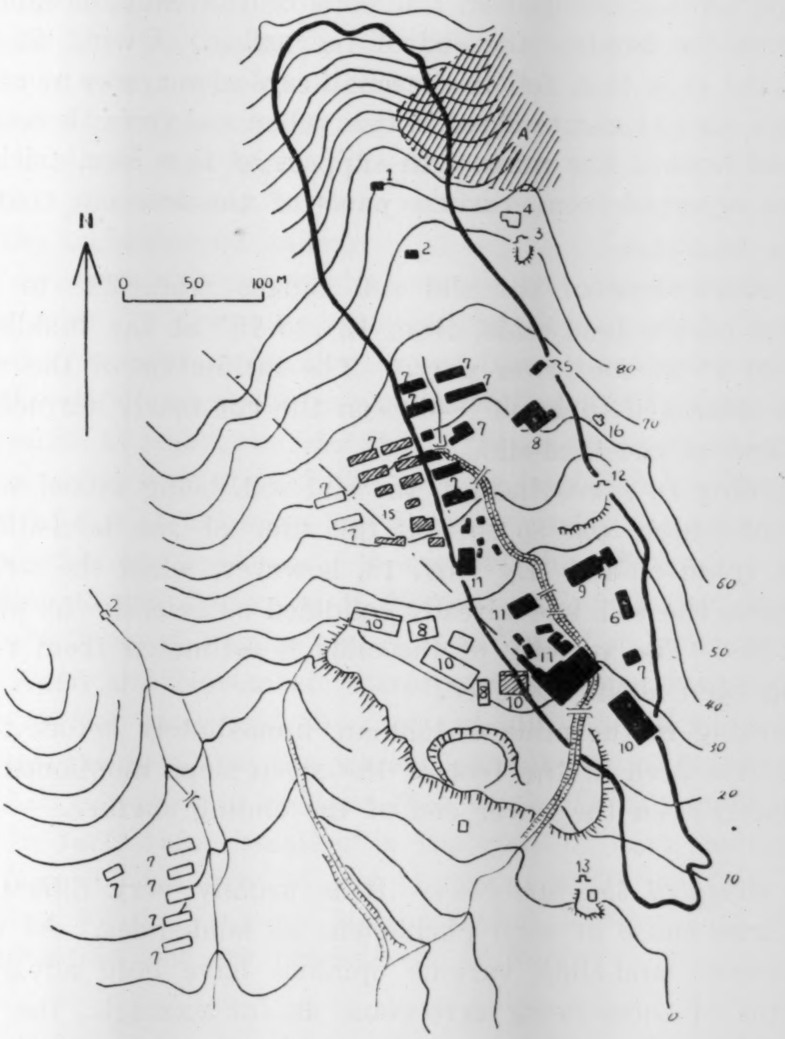

Fig. 5. Topography of the present land-slide. Contour lines drawn every 10 m. The thick closed curve in the figure gives an outline of the land-slide. Buildings painted black were destroyed; the hatched ones, burnt. The shaded area at the upper right corner shows the location of the ore deposit. *A*, the out-crop.

1. Powder magazine.
2. Water tank.
3. First adit.
4. Engine room for packing the galleries with sand.
5. Second adit.
6. School.
7. Miner's dormitories.
8. Ore storehouses.
9. Office.
10. Refineries.
11. Storehouse, etc.
12. Third adit.
13. Fourth adit.

A detailed topography of the scene of the present land-slide will be found in Fig. 5, which, before the event, was a shollow valley dug in the steep slope already mentioned, the slope of the valley-bottom gradually easing from the head to the end of the valley. Owing to these topographies, the rain that fell in the small explosion crater mentioned above might have always accumulated in this valley and from thence seeped into the ground toward the mine. In support of this idea, trickling water have been reported from various parts of the new cut that was opened by the land-slide.

The mean slope of the slid soil ranges from 28° to 30° at the upper part of the land slide, from 12° to 15° at the middle part, and from 5° to 7° at the lower part. The inclination of the sliding surface was measured to be $50^\circ \sim 60^\circ$ on the cut newly formed at the uppermost end of the land-slide.

According to eye-witnesses, the slid soil, being mixed with a large quantity of water, was so soft at the time of the land-slide that one could not tread on it. By Nov. 13, however, when the writer arrived at the mine, the soil had already solidified sufficiently to permit walking over it. The velocity of the slide is estimated from various data as having been about 10 m/sec.

According to the mine watchman, immediately before the event, a red band was seen at the foot of the steep slope mentioned above. He had probably seen the lower end of the sliding surface.

The cause of the land-slide. It is usually very difficult to ascertain the true cause of such phenomena as land-slides. As to the cause of the present land-slide, various opinions have been advanced by the press, some of them being erroneous, as for example, the one that it was caused by the explosion of the powder magazine of the mine.

This powder magazine, which, at the time of the land-slide, was at the middle of the steep slope mentioned above, contained 3100 kg of dynamite. After the land-slide, the powder magazine was found half destroyed at a lower level of the slope in the middle part of the slid soil, where half the quantity of the dynamite originally stored was found on the soil. the remaining half being probably embedded in the debris.

Since the mine is in a volcanic region and is very near the water divide already mentioned, the water supply is very meagre. For household and other uses, the water that trickled out from the slope behind the mine was allowed to collect into ditches, whence it was led by pipes to a concrete tank of 56 cubic meter capacity, situated at the foot of the steep slope mentioned above.

Water leaking from this tank is believed by some to have caused the present land-slide, but seeing that the tank was at the lower end of the sliding surface of the land-slide, this opinion cannot be correct.

It is said that in the spring of 1937, the ground in the neighbourhood of the powder magazine subsided in the form of a funnel, 3 m in diameter and 2 m deep. According to another report, the date of this subsidence is placed in August. The depression was however immediately repaired. The locality of this subsidence corresponds to the SW corner of the underground gallery.

Since, owing to the poor water supply, the dry packing system is used in this mine for preventing the ceilings from caving in, as already stated, cases of imperfect packing are at times inevitable, with the result that the earth overlying the galleries is liable to cave in, so that it is not possible to reject the idea that some unknown subsidence of the earth had in some way started the present land-slide. The fact that the ore bed of the Ogusi mine lies partially under the area where the present land-slide occurred seems to support this opinion.

According to the studies of K. Nakamura[18], in Japan, especially in the two prefectures of Nagano and Niigata[19], land-slides occur most frequently in April and November, corresponding respectively to the times of melting of the snow and the frequent autumn-end rains. In these circumstances, the idea that the present land-slide is intimately related to the rains that fell prior to the land-slide in the Ogusi region, is highly probable. In fact, rainy weather is reported to have continued from Oct. 29 to Nov. 9. On Nov. 10 and 11, the weather was fine.

According to the Nagano Meteorological Observatory, the annual and daily precipitations are respectively as follows:

Precipitation observed at Nagano.

Year	Annual total	November				
		7	8	9	10	11
1930	1062 mm	0 mm	0 mm	9·2 mm	0 mm	0·7 mm
31	941	0·3	0	0	0	0
32	1047	7·7	2·2	0	0	0
33	866	0	0	0·1	0	0
34	920	3·0	0	0·2	0	2·3
35	928	0	0	0	0	2·0
36	1063	14·7	2·1	0	0	0
37	1042*	0·2	14·9	12·5	0·2	0

* Up to the end of October.

---

18) *The land-slide*, 1933, (in Japanese).

19) 新潟.

Seeing that the loosend soil was almost saturated with water, there is no doubt that water, probably rain, was the cause.

It is difficult, however, to explain just how the rains caused the land-slide, seeing that rain had frequently been experienced up to the time of the disaster. Perhaps some unknown invisible change of state, such as the formation of cracks due to subsidence of the earth, progress of sulpherization or weathering of the soil, or changes in the inclination of the earth due to crustal movement, had cooperated with the rain.

In this connection, we might mention here the eruption on Nov. 27 of Kusatu-sirané, an active volcano lying only 20 km distant from this mine. Seeing that a volcanic eruption is often preceded by changes in the inclination of the surface of the earth around the volcano, as observed at Asama[20] and Kilauea[21], it is highly probable that this eruption of Kusatu-siraé brought about changes in the inclination of the earth around the mine, which in turn caused a sudden change in the distribution of the water soaked in the soil, resulting eventually in a land-slide.

In conclusion, the writers wish to express their thanks to the authorities of the mine, the police authorities of Nagano and Gumma, and the members of the Mining Inspection Office for numerous facilities extended to them in the course of their investigation.

---

18. 小串鑛山に於ける山崩の調査報告

地震研究所 {高橋龍太郎
水上武

小串鑛山は群馬，長野兩縣の縣境にある硫黄鑛山である．昭和 12 年 11 月 11 日，此の鑛山に山崩が起つて，鑛山の諸施設の大部分が破壞され，270 名餘の死傷者を生じた．

本報文には此の山崩の狀況及び此の山崩の原因さなり得る種々の現象に對する考察を述べた．此の山崩の原因を確かめる事は出來なかつたが，山崩前に降り續いた降雨さ密接な關係があるのではないかさ思はれる．

---

[20] R. Takahasi, *Bull. Earthq. Res. Inst.*, **11** (1933), 25.
T. Minakaki, *ibid.*, **13** (1935), 629.
R. Takahasi and T. Minakami, *ibid.*, **15** (1937), 463.

[21] T. A. Jaggar and H. Finch, *Bull. Seis. Soc. Amer.*, **19** (1929), 38.

（震研彙報 第十六號 圖版 高橋・水上）

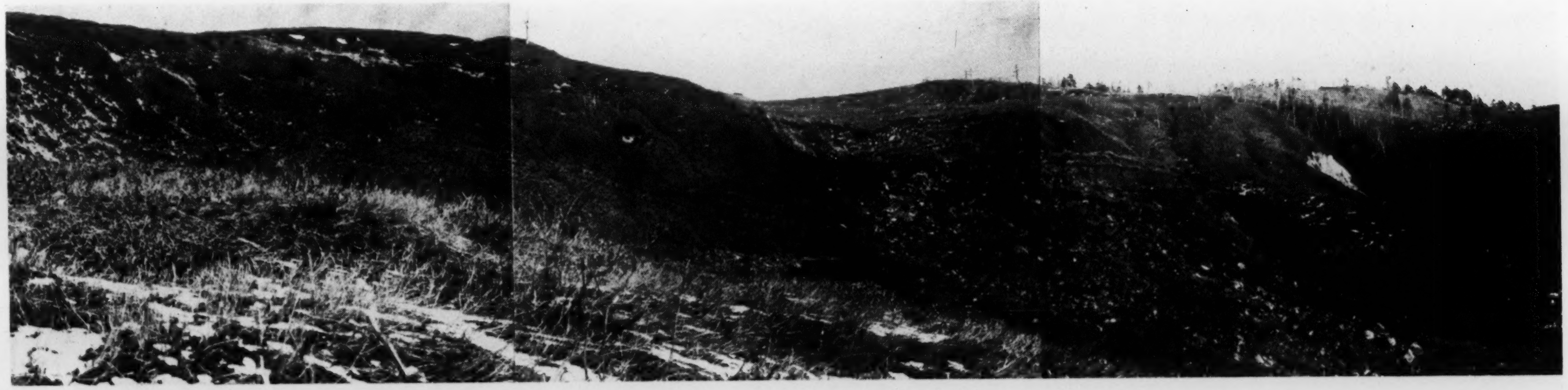

Fig. 3. The upper part of the land-slide

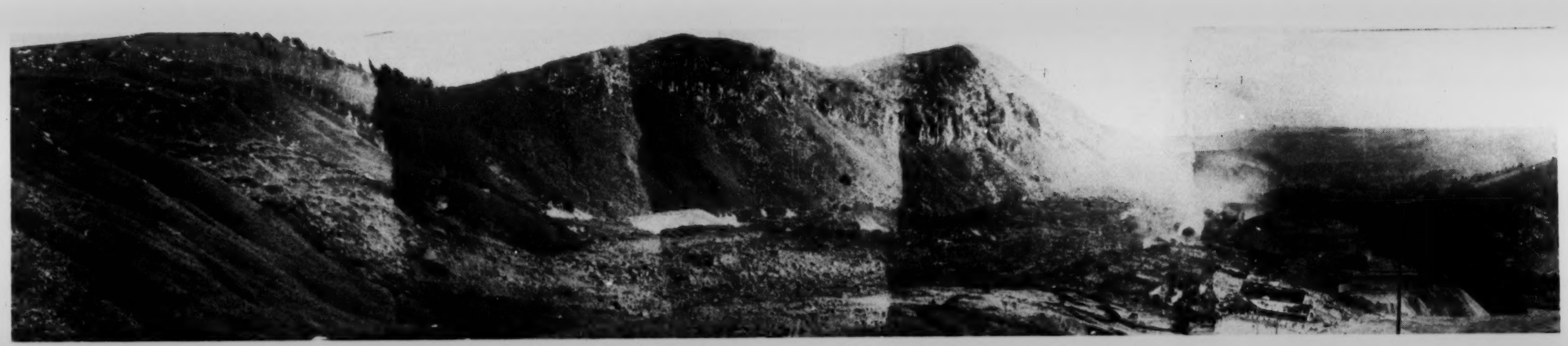

Fig. 6. General view of the land-slide.

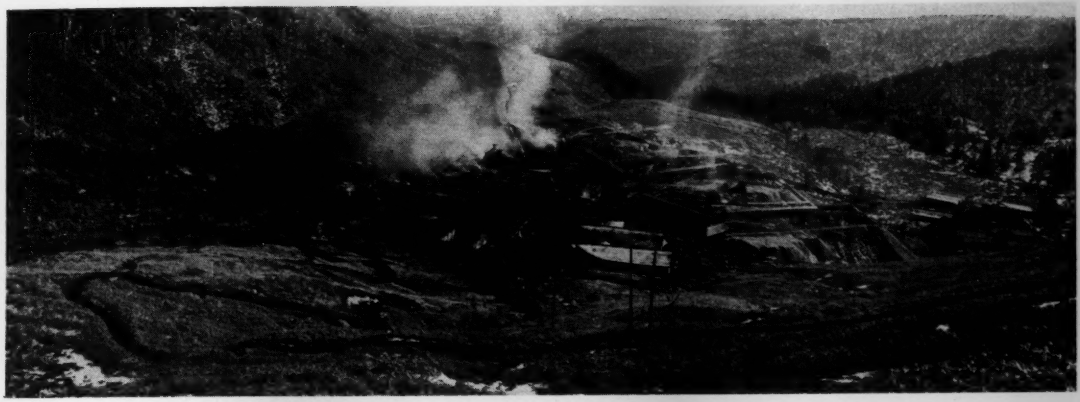

Fig. 7. The lower part of the land-slide.

（震研彙報 第十六號 圖版 高橋・水上）

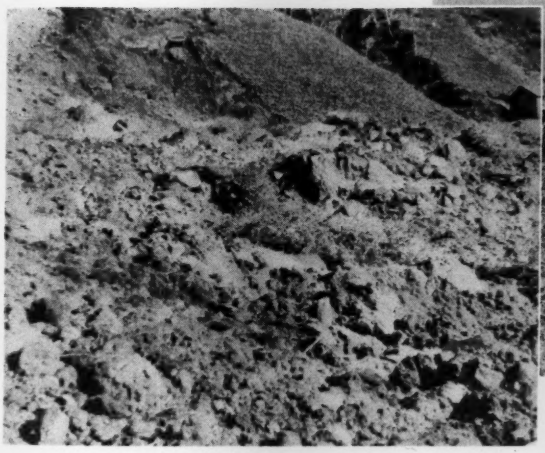

Fig. 8. Character of the loosend soil.

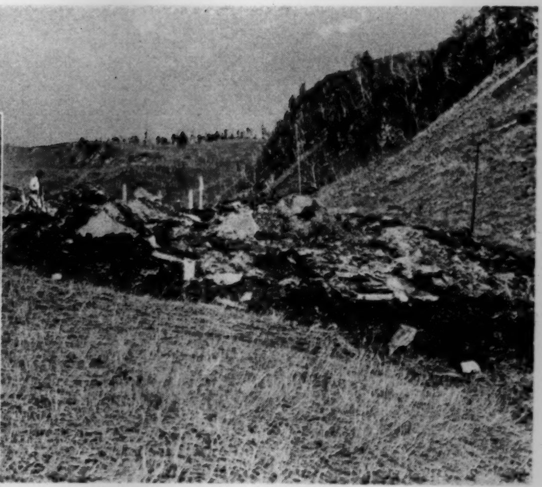

Fig. 9. The lowest end of the land-slide.

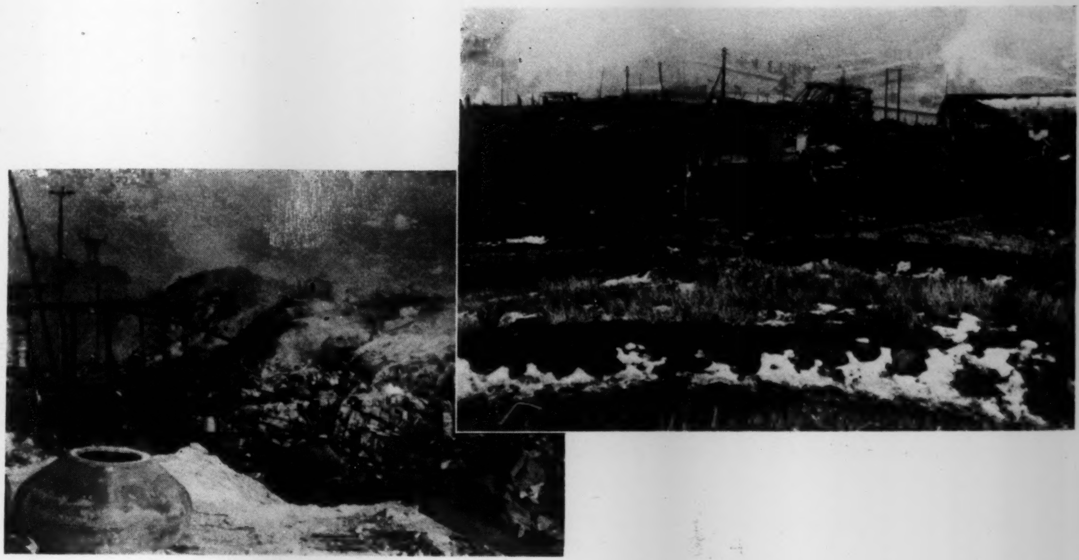

Fig. 10. Views of the general destruction.

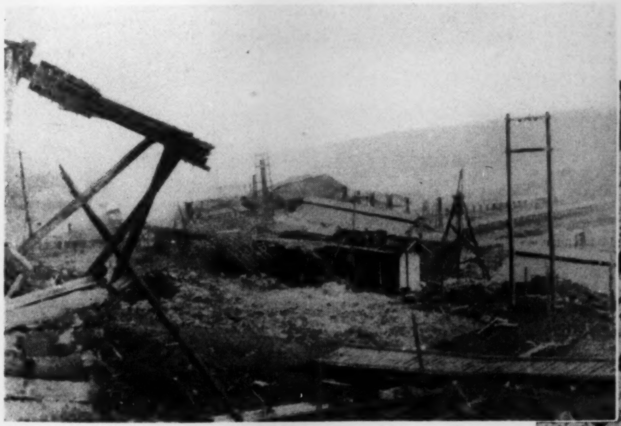

Fig. 11. View of the destruction.

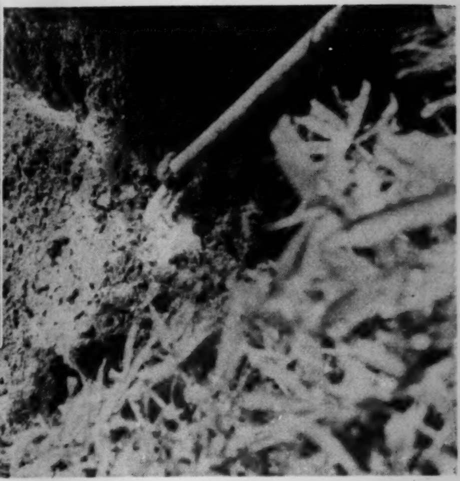

Fig. 12. Remains of the pipe that formerly conveyed water to the tank.

19. *Anomalous Dispersion of Elastic Surface Waves.*

By Katsutada SEZAWA,

Earthquake Research Institute.

(Read Jan. 18, 1938.—Received March 22, 1938.)

1. *Introduction.*

The propagational velocity of elastic surface waves, whether Rayleigh-waves or Love-waves, that are transmitted on a stratified surface, generally increases with increase in wave-length, its nature therefore being similar to that of normal dispersion in the case of problems in optics.[1] The condition implied in the case of elastic surface waves is however such that the velocity of bodily waves in the surface layer is invariably less than that in the subjacent medium. If, on the other hand, the condition in question were reversed, propagation of surface waves would probably be impossible in the majority of cases.

The present investigation shows that even should the velocity of bodily waves in the surface layer be higher than that in the subjacent medium (density of the surface layer being less than that of the subjacent layer), it is possible for Rayleigh-type waves to be transmitted for a certain range of wave-length. Since moreover velocity of propagation of the surface waves now under consideration diminishes with increase in wave-length, the nature of dispersion is quite anomalous. Although the idea of the probable existence of such waves occurred to me about ten years ago when I was studying the dispersion of Rayleigh-waves, having even gone as far as to present a few results of the investigation at one of the meetings of the Institute, yet owing to there being certain uncertainties about my numerical calculations, I refrained from publishing any part of it. Now that with the kind aid of Dr. Kanai, the investigation has progressed favourably, I shall deal with the results in this paper.

2. *Love-waves.*

Let the densities and the rigidities of the surface layer and the subjacent medium be ρ', μ'; ρ, μ respectively, the thickness of the layer being H. In order that the Love-type movements shall be surface waves, the displacements in the surface layer and the subjacent medium must assume the forms

---

[1] K. SEZAWA, *Bull. Earthq. Res. Inst.*, **3** (1927), 1.

$$v' = (Ae^{s'y} + Be^{-s'y})\cos(pt+fx), \qquad (1)$$

$$v = Ce^{sy}\cos(pt+fx), \qquad (2)$$

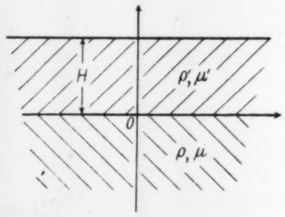

Fig. 1.

where

$$s'^2 = f^2 - \kappa'^2, \quad \kappa'^2 = \rho' p^2/\mu',$$
$$s^2 = f^2 - \kappa^2, \quad \kappa^2 = \rho p^2/\mu. \qquad (3)$$

Substituting (1), (2) in the boundary conditions

$$y=0; \qquad v'=v, \qquad \mu'\frac{\partial v'}{\partial y} = \mu\frac{\partial v}{\partial y}, \qquad (4)$$

$$y=H; \qquad \mu'\frac{\partial v'}{\partial y} = 0, \qquad (5)$$

we get the relation

$$\tanh s'H = -\frac{\mu s}{\mu' s'}, \qquad (6)$$

from which it is possible to find the velocity of propagation of the Love-waves.

The problem will now be confined to the case in which, from the condition of the present investigation, $\rho'/\mu' < \rho/\mu$, whence $\kappa'^2 < \kappa^2$, so that from (3), $s'^2 > s^2$. Since s is real, s' is also real: s can never be negative. The relation (6) therefore does not hold. It follows then that were neither s nor s' a complex quantity, Love-waves cannot exist in the layer in the condition assumed.

We shall next suppose the case in which either s or s' is a complex quantity. Writing, generally, $s = a+ib$, $s' = a'+ib'$, we get from (6) the relations

$$\left.\begin{aligned} \frac{\sinh 2a'}{\cosh 2a' + \cos 2b'} &= \frac{\mu(aa' + bb')}{\mu'\,(a'^2 + b'^2)}, \\ \frac{\sinh 2b'}{\cosh 2a + \cos 2b'} &= \frac{\mu(ab' - a'b)}{\mu'\,(a'^2 + b'^2)}. \end{aligned}\right\} \qquad (7)$$

Writing, on the other hand, $\kappa = \kappa_1 + i\kappa_2$, $\kappa' = \kappa_1' + i\kappa_2'$, and comparing with (3), we find that

$$\left.\begin{aligned} a^2 - b^2 &= f^2 - \kappa_1^2 + \kappa_2^2, & ab &= -\kappa_1\kappa_2, \\ a'^2 - b'^2 &= f^2 - \kappa_1'^2 + \kappa_2'^2, & a'b' &= -\kappa_1'\kappa_2', \end{aligned}\right\} \qquad (8)$$

from which the values of a, b, a', b' are determined. This shows that for stationary waves to exist, either a or b (and similarly either a' or b') vanishes. The complex values of s and s' cannot possibly exist.

Generally speaking, were the velocity of propagation of transverse waves in the surface layer higher than that in the subjacent medium, Love-waves do not exist. The nature of the dispersion of the possible Love-waves is thus normal as usually considered. It appears that even in the case of a doubly stratified layer[2), 3)], the possible Love-waves exhibit, as a matter of fact, the nature of normal dispersion.

3. *Rayleigh-waves.*

Let the densities and the elastic constants of the layer and the subjacent medium be ρ', λ', μ'; ρ, λ, μ (Fig. 2) respectively. The equation necessary for obtaining the velocity of transmission is expressed by a determinant of the form

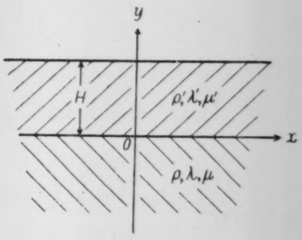

Fig. 2.

$$\begin{vmatrix} -\frac{(f^2-s'^2)}{k'^2}Y_2, & 2\frac{\mu' ifs'}{\mu k'^2}Y_1, & 0, & -2\frac{\mu' ifs'}{\mu k'^2}, & 0, & \frac{s'f}{k'^2} \\ -\frac{(f^2-s'^2)}{k'^2}Y_1, & -2\frac{\mu' ifs'}{\mu k'^2}Y_2, & \frac{\mu'(f^2-s'^2)}{\mu k'^2}, & 0, & \frac{if^2}{k'^2}, & 0 \\ 2\frac{ifr'}{h'^2}X_1, & \left(2\frac{\mu' r'^2}{\mu h'^2}-\frac{\lambda'}{\mu}\right)X_2, & -\frac{\mu' 2ifr'}{\mu h'^2}, & 0, & \frac{r'f}{h'^2}, & 0 \\ 2\frac{ifr'}{h^2}X_2, & \left(2\frac{\mu' r'^2}{\mu h'^2}-\frac{\lambda'}{\mu}\right)X_1, & 0, & \left(\frac{\lambda'}{\mu}-2\frac{\mu' r'^2}{\mu h'^2}\right), & 0, & -\frac{if^2}{h'^2} \\ 0, & 0, & -\frac{(f^2+s^2)}{k^2}, & 2\frac{ifs}{k^2}, & -\frac{if^2}{k^2}, & -\frac{sf}{k^2} \\ 0, & 0, & -\frac{2ifr}{h^2}, & \left(2\frac{r^2}{h^2}-\frac{\lambda}{\mu}\right), & -\frac{rf}{h^2}, & \frac{if^2}{h^2} \end{vmatrix} = 0, \quad (9)$$

where $X_1=\cosh r'H$, $X_2=\sinh r'H$, $Y_1=\cos s'H$, $Y_2=\sin s'H$. This reduces to[4)]

---

2) T. MATUZAWA, *Proc. Phys.-Math. Soc., Japan*, [iii], **10** (1928), 25~33.

3) R. STONELEY and E. TILLOTSON, *M.N.R.A.S. Geophys. Suppl.*, **1** (1928).

4) K. SEZAWA and K. KANAI, *Bull. Earthq. Res. Inst.*, **13** (1935), 238.

$$\frac{4r's'}{f^2}\left(2-\frac{k'^2}{f^2}\right)\eta-\frac{r's'}{f^2}\left\{4\vartheta+\left(2-\frac{k'^2}{f^2}\right)^2\zeta\right\}\cosh r'H\cos s'H$$

$$+\frac{r'}{f}\varphi\left\{\frac{4rs'^2}{f^3}+\frac{s}{f}\left(2-\frac{k'^2}{f^2}\right)^2\right\}\cosh r'H\sin s'H$$

$$+\frac{s'}{f}\varphi\left\{-\frac{4sr'^2}{f^3}+\frac{r}{f}\left(2-\frac{k'^2}{f^2}\right)^2\right\}\sinh r'H\cos s'H$$

$$+\left\{-\frac{4r'^2s'^2}{f^4}\zeta+\left(2-\frac{k'^2}{f^2}\right)^2\vartheta\right\}\sinh r'H\sin s'H=0, \qquad (10)$$

where

$$\left.\begin{aligned}
&\varphi=\frac{\mu'k^2k'^2}{\mu f^4},\quad \zeta=\frac{4rs}{f^2}\left(\frac{\mu'}{\mu}-1\right)^2-\alpha^2,\quad \eta=\frac{2rs}{f^2}\left(\frac{\mu'}{\mu}-1\right)\beta-\alpha\gamma,\\
&\vartheta=\frac{rs}{f^2}\beta^2-\gamma^2,\quad \alpha=\frac{2\mu'}{\mu}-\left(2-\frac{k^2}{f^2}\right),\quad \beta=\frac{\mu'}{\mu}\left(2-\frac{k'^2}{f^2}\right)-2,\\
&\gamma=\frac{\mu'}{\mu}\left(2-\frac{k'^2}{f^2}\right)-\left(2-\frac{k^2}{f^2}\right),\\
&r^2=f^2-h^2,\quad s^2=f^2-k^2,\quad r'^2=f^2-h'^2,\quad s'^2=k'^2-f^2,\\
&h^2=\rho p^2/(\lambda+2\mu),\quad h'^2=\rho' p^2/(\lambda'+2\mu'),\quad k^2=\rho p^2/\mu,\quad k'^2=\rho' p^2/\mu'.
\end{aligned}\right\} \qquad (11)$$

In this case, too, the condition of the problem is that the velocity of longitudinal waves (or transverse waves) in the surface layer is higher than that of the longitudinal waves (or transverse waves) in the subjacent medium, so that the relation

$$\left(\frac{k}{f}\right)^2>\left\{\begin{matrix}\left(\frac{h}{f}\right)^2>\left(\frac{k'}{f}\right)^2\\ \left(\frac{k'}{f}\right)^2>\left(\frac{h}{f}\right)^2\end{matrix}\right\}>\left(\frac{h'}{f}\right)^2 \qquad (12)$$

must exist.

(i) If $(k/f)^2<1$; we have $(r/f)^2>0$, $(s/f)^2>0$, $(r'/f)^2>0$, $(s'/f)^2<0$. The expression (10) is then soluble without using complex values for the quantities given in the same expression. The reason why complex values do not fit the problem is the same as that in the case of Love-waves. The relations $(r/f)^2>0$, $(s/f)^2>0$, show the condition that energy of the waves is accumulated near the surface. There is then every likelihood of Rayleigh-type waves being transmitted in the present case.

(ii) If $(k/f)^2>1>\{(k'/f)^2,\ (h/f)^2\}$; then $(r/f)^2>0$, $(s/f)^2<0$, $(r'/f)^2>0$, $(s'/f)^2<0$. The expression (10) then becomes complex owing to (11). These relations show at the same time that the waves are not of surface type. Transmission of Rayleigh-waves is not possible in the present case.

(iii) If $(k'/f)^2>1>(h/f)^2$; then $(r/f)^2>0$, $(s/f)^2<0$, $(r'/f)^2>0$, $(s'/f)^2>0$. In this case, too, the expression (10) becomes complex and the waves are not of surface type owing to the relation $(s/f)^2<0$. There are no Rayleigh-waves in the present case.

(iv) If $(h/f)^2>1>(k'/f)^2$; then $(r/f)^2<0$, $(s/f)^2<0$, $(r'/f)^2>0$, $(s'/f)^2<0$. The relations $(r/f)^2<0$, $(s/f)^2<0$ make the expression (10) complex and at the same time prevent the waves from being of surface type, it being therefore impossible for Rayleigh-waves to exist.

(v) If $\{(h/f)^2,\ (k'/f)^2\}>1>(h'/f)^2$; then $(r/f)^2<0$, $(s/f)^2<0$, $(r'/f)^2>0$, $(s'/f)^2>0$. The relations $(r/f)^2<0$, $(s/f)^2<0$ make the expression (10) complex and they also show that the waves are not of surface type. No Rayleigh wave exists in this case.

(vi) Finally, if $(h'/f)^2>1$; then $(r/f)^2<0$, $(s/f)^2<0$, $(r'/f)^2<0$, $(s'/f)^2>0$. The relations $(r/f)^2<0$, $(s/f)^2<0$, $(r'/f)^2<0$ make the expression (10) complex. We see also from $(r/f)^2<0$, $(s/f)^2<0$, that the waves are not of surface type, it being therefore impossible for Rayleigh waves to exist.

From these conditions it will be seen that, even should there be Rayleigh-waves, their possible velocities are of the range $1>(k/f)^2$. The group velocity, also increasing with decrease in wave length, may however be greater than $\sqrt{\rho/\mu}$ for smaller wave length.

It is a special feature in the dispersion of the present kind that the propagational velocity is never greater than the velocity of transverse waves in the superficial layer nor that in the subjacent medium.

As an example we shall take the case $\rho'/\rho=1/2$, $\lambda=\mu$, $\lambda'=\mu'$, $\lambda=\lambda'$, and solve the velocity equation (10), its treatment being naturally to use a trial and error method. The results of calculation are shown in Table I and Fig. 3.

Table I.

$\sqrt{\rho p^2/\mu f^2}$	1·000	0·980	0·950	0·930	0·9194
fH	1·351	0·763	0·332	0·1075	0
L/H	4·650	8·240	18·91	58·50	∞

The result of calculation shows that Rayleigh-type waves are possible for the range $L/H=4{\cdot}650\sim\infty$, and that the velocity of propagation decreases with increase in wave length; and, furthermore, that for such wave length as $L/H<4{\cdot}650$, no surface wave exists. Dispersion of the waves is therefore anomalous.

It is possible to get a dispersion curve for every case of stratification that is subjected to the conditions $(k/f)^2>(k'/f)^2$, $(h/f)^2>(h'/f)^2$. Although the dispersion curve for any case in question is anomalous, the value of L/H corresponding to the lower critical of the dispersion curve increases with increase in the ratios $(k/f)^2\big/(k'/f)^2$, $(h/f)^2\big/(h'/f)^2$.

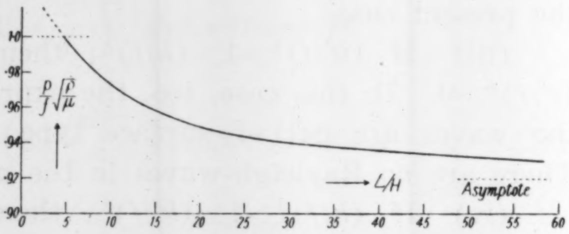

Fig. 3.

4. *Amplitude distribution of Rayleigh-waves in the media of transmission.*

With a view to knowing the distribution of amplitudes of Rayleigh-waves whose dispersion is anomalous, we examined the expressions for displacements, its horizontal and vertical components within the stratum and in the subjacent medium being written[5]

$$\begin{aligned}u'_y=-\frac{s'}{f}\Bigg[&-\Big(\frac{k'^2}{f^2}-2\Big)\eta\sin ir'(H-y)-\frac{2ir's'}{f^2}\eta\sin s'(H-y)\\&+\frac{ir's}{f^2}\varphi\Big\{\Big(\frac{k'^2}{f^2}-2\Big)\cos ir'H\cos s'y+2\cos s'H\cos ir'y\Big\}\\&+\frac{ir's}{f^2}\zeta\Big\{\Big(\frac{k'^2}{f^2}-2\Big)\cos ir'H\sin s'y+2\sin s'H\cos ir'y\Big\}\\&-\frac{rs'}{f^2}\varphi\Big\{2\sin s'H\sin ir'y+\Big(\frac{k'^2}{f^2}-2\Big)\sin ir'H\sin s'y\Big\}\\&+\vartheta\Big\{\Big(\frac{k'^2}{f^2}-2\Big)\sin ir'H\cos s'y+2\cos s'H\sin ir'y\Big\}\Bigg],\end{aligned}\qquad(13)$$

$$\begin{aligned}v'_y=i\Bigg[&\frac{ir's'}{f^2}\eta\Big\{\Big(\frac{k'^2}{f^2}-2\Big)\cos ir'(H-y)-2\cos s'(H-y)\Big\}\\&+\frac{s'}{f}\varphi\Big\{\frac{r}{f}\Big(\frac{k'^2}{f^2}-2\Big)\sin ir'H\cos s'y+\frac{2r'^2s}{f^3}\cos s'H\sin ir'y\Big\}\end{aligned}$$

---

5) K. SEZAWA and K. KANAI, *Bull. Earthq. Res. Inst.*, **13** (1935), 240.

$$+\left\{\frac{2r'^2s'^2}{f^4}\zeta\sin s'H\sin ir'y+\left(\frac{k'^2}{f^2}-2\right)\vartheta\sin ir'H\sin s'y\right\}$$

$$+\frac{ir's'}{f^2}\left\{2\vartheta\cos s'H\cos ir'y-\left(\frac{k'^2}{f^2}-2\right)\zeta\cos ir'H\cos s'y\right\}$$

$$-\frac{ir'}{f}\varphi\left\{\frac{2rs'^2}{f^3}\sin s'H\cos ir'y-\frac{s}{f}\left(\frac{k'^2}{f^2}-2\right)\cos ir'H\sin s'y\right\}\Bigg], \tag{14}$$

$$u=\frac{i\mu's'k'^2}{\mu f^3}\left[Pe^{ry}+\frac{s}{f}Qe^{sy}\right], \tag{15}$$

$$v=-\frac{\mu's'k'^2}{\mu f^3}\left[\frac{r}{f}Pe^{ry}+Qe^{sy}\right], \tag{16}$$

where

$$\left.\begin{aligned}P=&\frac{2sr'}{f^2}\beta\cos s'H+\frac{2r's'}{f^2}\alpha\sin s'H\\&-\frac{2sr'}{f^2}\left(2-\frac{k'^2}{f^2}\right)\left(\frac{\mu'}{\mu}-1\right)\cosh r'H+\left(2-\frac{k'^2}{f^2}\right)\gamma\sinh r'H,\\Q=&-\frac{2r'}{f}\gamma\cos s'H-\frac{4rr's'}{f^3}\left(\frac{\mu'}{\mu}-1\right)\sin s'H\\&+\frac{r'}{f}\left(2-\frac{k'^2}{f^2}\right)\alpha\cosh r'H-\frac{r}{f}\left(2-\frac{k'^2}{f^2}\right)\beta\sinh r'H.\end{aligned}\right\} \tag{17}$$

The distribution of horizontal and vertical displacements at different depths for two cases, namely (i) $\sqrt{\rho p^2/\mu f^2}=0{\cdot}980$, $L/H=8{\cdot}24$ and (ii) $\sqrt{\rho p^2/\mu f^2}=0{\cdot}930$, $L/H=58{\cdot}50$, are shown in Figs. 4, 5.

These results show that while, for shorter waves, the amplitudes converge fairly sharply with depth, for longer waves, on the other hand, the convergency is very gradual. In any case, there is a nodal point in the horizontal component of displacement, whereas none exists in the vertical component. It appears that the ratio of horizontal to vertical displacements on the free surface is nearly 2/3 in the present condition of the problem. At all events, these features are quite similar to those in the case of Rayleigh-waves transmitted on a semi-infinite body or even in certain special cases of waves of normal dispersion.

The special feature in amplitude distribution in the present condition of the problem would be the relatively large horizontal displacement near the boundary between the stratum and the subjacent medium, which results from the accumulation of the vibrational energy of the waves in the said boundary.

5. *Concluding remarks.*

From mathematical calculation we found that, while the dispersion of Love-waves is normal, the dispersion of Rayleigh-waves in certain special conditions of stratification is anomalous. It is possible for this condition to exist for a certain range of lengths of waves that are transmitted through such a surface layer that the velocity of bodily waves in the same layer is higher than that in the subjacent medium.

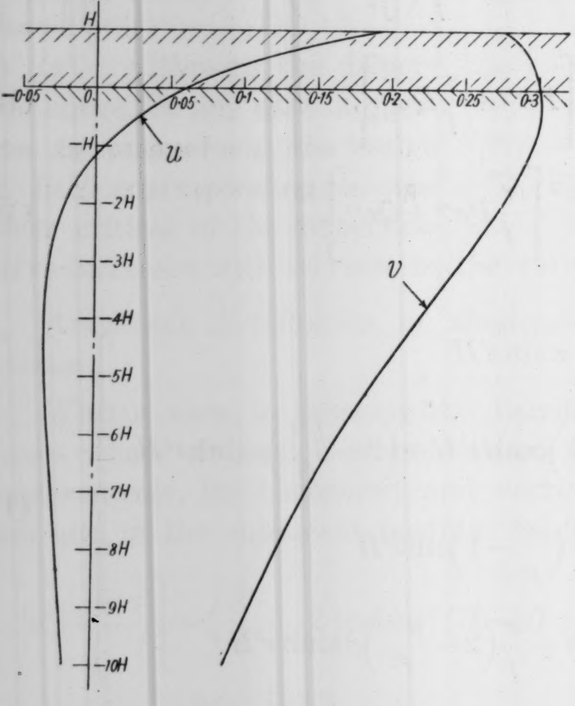

Fig. 4. $\sqrt{\rho p^2/\mu f}=0{\cdot}980$, L/H=8·24.

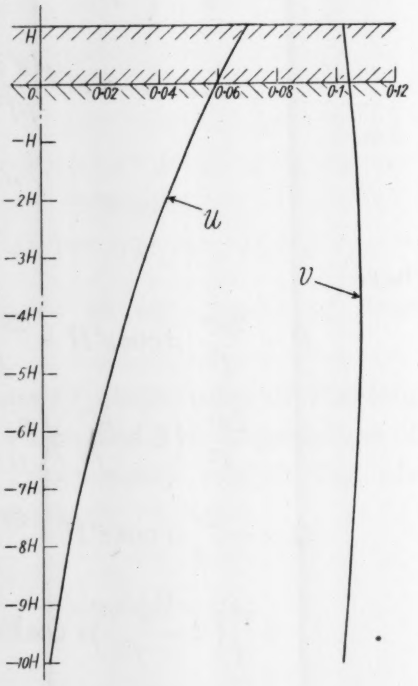

Fig. 5. $\sqrt{\rho p^2/\mu f}=0{\cdot}930$, $L/H=58{\cdot}5$.

It is a special feature in the dispersion of the present kind that the propagational velocity of the surface waves is greater than neither the velocity of transverse waves in the superficial layer nor that in the subjacent medium. Excepting a few conditions, the distribution of displacements with depth does not greatly differ from that of the usual Rayleigh-waves.

In conclusion I wish to express my sincerest thank to Dr. K. Kanai, with whose kind aid the investigation was brought to a successful close.

19. 彈性表面波の異常分數

地震研究所 妹澤克惟

表面層の物質の密度が下層のそれよりも少い場合は實際問題さして寧ろ多いかも知れぬ．このやうな場合に彈性波の異常分散さいふ事が問題になり得るのである．

數學的研究により，ラブ波の分散は常にノーマルであるけれごも，或特別の場合のレーレー波の分散は異常であるこさがわかつた．このやうな異常分散の狀態は地表層中の固體波の速度が下層のそれよりも速いさきに起り得るのである．しかしあまり短い波はこの場合に存在し得ないものである．尙，この場合に於けるレーレー波の速度が，地表層の橫波の速度及び地中層の橫波の速度の何れよりも低いさいふ事は極めて特別な性質である．異常分散をなす場合の波動振幅の地中に於ける分布は，一二の特別の條件，卽ち兩層の境界附近の振幅が比較的に大きいさいふこさ以外は，ノーマル分散の場合さ大して違はぬものである．

---

20. *Gravitational Stability of the Earth at its Liquid Cooling Stage.*

By Katsutada SEZAWA and Kiyoshi KANAI.

Earthquake Research Institute.

(Read. Feb. 15, 1938.—Received March 22, 1938.)

1. *Introduction.*

It would seem that when the primitive Earth was already at the liquid stage, that part near its surface cooled more rapidly than the inner part, with the result that even in the uniform condition of a liquid, the mass density would vary with depth. If, in such a condition, the mass in the superficial layer were denser than that in the subjacent layer, the denser mass would sink in consequence of the gravitational instability of the liquid Earth.

Although the gravitational instability of liquid layers with plane boundaries has already been shown by Lord Kelvin[1] and others, the same problem for the case of a liquid sphere, so far as we know, has not yet been discussed, although the tidal equilibrium of an elastic Earth covered with water has been dealt with by Street[2], which problem, however, lies outside the scope of the present investigation.

We shall first treat of the gravitational potential of the two-layered liquid Earth in a deformed condition, the result of which will next be applied to a small oscillation of the same Earth. It is possible to assume that in a relatively later stage of the liquid Earth, the effect of rotation on its stability is negligible, the undisturbed form of the Earth being therefore spherical. Although our final aim is to find the gravitational stability of a general heterogeneous Earth, since the case of the simplest possible condition still represents the characteristic feature of the problem, we shall consider the two-layered Earth just mentioned.

2. *Gravitational potential.*

Let r, θ, ϕ be the coordinates of a point P with respect to the centre of a sphere; the gravitational potential of the same point is then expressed by

---

[1] LORD KELVIN, *Papers*, 4; H. LAMB, *Hydrodynamics*, § 267.

[2] R. O. STREET, *M. N. R. A. S. Geophys. Suppl.*, 1 (1925), 292~306.

$$V=-\gamma\int_0^\infty dr_1\int_0^{2\pi}d\phi_1\int_{-1}^{1}\frac{\rho r_1^2 d\mu_1}{\sqrt{r^2-2rr_1\cos\zeta+r_1^2}},\tag{1}$$

where

$$\begin{aligned}\cos\zeta&=\cos\theta\cos\theta_1+\sin\theta\sin\theta_1\cos(\phi-\phi_1)\\&=\mu\mu_1+\sqrt{1-\mu^2}\sqrt{1-\mu_1^2}\cos(\phi-\phi_1),\end{aligned}\tag{2}$$

ρ is the density of mass at r_1, θ_1, ϕ_1, and γ the gravitational potential. It is well known that

$$\left.\begin{aligned}\frac{1}{\sqrt{r^2-2rr_1\cos\zeta+r_1^2}}&=\frac{1}{r}\sum_{n=0}^{\infty}\left(\frac{r_1}{r}\right)^n P_n(\cos\zeta),\qquad (r>r_1)\\&=\frac{1}{r_1}\sum_{n=0}^{\infty}\left(\frac{r}{r_1}\right)^n P_n(\cos\zeta).\qquad (r<r_1)\end{aligned}\right\}\tag{3}$$

We shall now consider a spherical body of two layers, the respective outer radii of which are a, b, the densities of the two parts being ρ_1, ρ_2 respectively. It is possible to assume that, generally, in a slightly deformed condition, the radii a, b become $a+\delta$, $b+\varepsilon$, so that the thicknesses δ, ε are ideally constant on the respective spherical surfaces, whereas the increased density between a and $a+\delta$ and that between b and $b+\varepsilon$ vary from point to point on each spherical surface. The gravitational potentials within the outer and inner layers then assume the forms

$$\begin{aligned}V_1=&-\gamma\int_0^b dr_1\int_0^{2\pi}d\phi_1\int_{-1}^{1}\frac{1}{r}\sum_{n=0}^{\infty}\left(\frac{r_1}{r}\right)^n P_n(\cos\zeta)\rho_2 r_1^2 d\mu_1\\&\qquad-\gamma\int_b^{b+\varepsilon} dr_1\int_0^{2\pi}d\phi_1\int_{-1}^{1}\frac{1}{r}\sum_{n=0}^{\infty}\left(\frac{r_1}{r}\right)^n P_n(\cos\zeta)\rho_2' r_1^2 d\mu_1\\&-\gamma\int_b^r dr_1\int_0^{2\pi}d\phi_1\int_{-1}^{1}\frac{1}{r}\sum_{n=0}^{\infty}\left(\frac{r_1}{r}\right)^n P_n(\cos\zeta)\rho_1(r) r_1^2 d\mu_1\\&\qquad-\gamma\int_r^a dr_1\int_0^{2\pi}d\phi_1\int_{-1}^{1}\frac{1}{r_1}\sum_{n=0}^{\infty}\left(\frac{r}{r_1}\right)^n P_n(\cos\zeta)\rho_1(r) r_1^2 d\mu_1\\&\qquad-\gamma\int_a^{a+\delta} dr_1\int_0^{2\pi}d\phi_1\int_{-1}^{1}\frac{1}{r_1}\sum_{n=0}^{\infty}\left(\frac{r}{r_1}\right)^n P_n(\cos\zeta)\rho_1' r_1^2 d\mu_1,\end{aligned}\tag{4}$$

$$V_2=-\gamma\int_0^r dr_1\int_0^{2\pi}d\phi_1\int_{-1}^{1}\frac{1}{r}\sum_{n=0}^{\infty}\left(\frac{r_1}{r}\right)^n P_n(\cos\zeta)\rho_2(r) r_1^2 d\mu_1$$

$$-\gamma\int_r^b dr_1\int_0^{2\pi} d\phi_1\int_{-1}^1 \frac{1}{r_1}\sum_{n=0}^{\infty}\left(\frac{r}{r_1}\right)^n P_n(\cos\zeta)\rho_2(r)r_1^2d\mu_1$$

$$-\gamma\int_b^{b+\varepsilon} dr_1\int_0^{2\pi} d\phi_1\int_{-1}^1 \frac{1}{r_1}\sum_{n=0}^{\infty}\left(\frac{r}{r_1}\right)^n P_n(\cos\zeta)\rho_2'r_1^2d\mu_1$$

$$-\gamma\int_b^a dr_1\int_0^{2\pi} d\phi_1\int_{-1}^1 \frac{1}{r_1}\sum_{n=0}^{\infty}\left(\frac{r}{r_1}\right)^n P_n(\cos\zeta)\rho_1(r)r_1^2d\mu_1$$

$$-\gamma\int_a^{a+\delta} dr_1\int_0^{2\pi} d\phi_1\int_{-1}^1 \frac{1}{r_1}\sum_{n=0}^{\infty}\left(\frac{r}{r_1}\right)^n P_n(\cos\zeta)\rho_1'r_1^2d\mu_1. \tag{5}$$

If the deformation, particularly, is of the type of spherical harmonics, we put

$$\left.\begin{aligned}\rho_1' &= cP_n^m(\cos\theta_1)\cos m\phi_1(=cS_n(\mu_1,\varphi_1)),\\ \rho_2' &= eP_n^m(\cos\theta_1)\cos m\phi_1(=eS_n(\mu_1,\varphi_1)),\end{aligned}\right\} \tag{6}$$

where c, e are constants determined from other conditions. If the actual displacements of the boundaries $r=a$, $r=b$ be η, ξ, then we have

$$\rho_1'\delta=\rho_1\xi, \qquad \rho_2'\varepsilon=(\rho_2-\rho_1)\eta. \tag{7}$$

Substituting (6), (7) in (4), (5) and using the relations

$$\int_{-1}^1\int_0^{2\pi} S_mS_nd\mu_1d\phi_1=0 \quad (m\gtrless n);$$

$$\int_{-1}^1\int_0^{2\pi} P_n(\cos\zeta)S_n(\mu_1,\phi_1)d\mu_1d\phi_1=\frac{4\pi}{2n+1}S_n(\mu,\phi), \tag{8}$$

we get

$$\left.\begin{aligned}V_1 &= -4\pi\gamma\left[\frac{\rho_2b^3}{3r}+\frac{eS_n\varepsilon b^{n+2}}{(2n+1)r^{n+1}}+\frac{\rho_1(r^3-b^3)}{3r}+\frac{\rho_1(a^2-r^2)}{2}+\frac{r^ncS_n\delta a^{1-n}}{2n+1}\right],\\ V_2 &= -4\pi\gamma\left[\frac{\rho_2r^2}{3}+\frac{\rho_2(b^2-r^2)}{2}+\frac{r^neS_n\varepsilon b^{1-n}}{2n+1}+\frac{\rho_1(a^2-b^2)}{2}+\frac{r^ncS_n\delta a^{1-n}}{2n+1}\right],\end{aligned}\right\} \tag{9}$$

where

$$eS_n\varepsilon=(\rho_2-\rho_1)\eta_n, \qquad cS_n\delta=\rho_1\xi_n. \tag{10}$$

3. *Hydrodynamical condition for small oscillations.*

Let ϕ_n, ϕ_n' be the potential functions of the hydrodynamical conditions of the outer and the inner layers respectively. The equations of incompressible fluid

$$\Gamma^2\phi_n=0, \qquad \Gamma^2\phi_n'=0 \tag{11}$$

give the solutions

$$\left.\begin{aligned} \phi_n&=S_n\left(Ar^n+\frac{B}{r^{n+1}}\right)e^{i\sigma_n t}, \\ \phi_n'&=S_nEr^ne^{i\sigma_n t}. \end{aligned}\right\} \tag{12}$$

Let ξ_n, η_n be the normal displacements of the boundaries $r=a$, $r=b$; then there exist the kinematical relations

$$\frac{\partial\xi_n}{\partial t}=-\frac{\partial\phi_n}{\partial r}, \qquad \frac{\partial\eta_n}{\partial t}=-\frac{\partial\phi_n'}{\partial r}. \tag{13}$$

On the other hand, Bernoulli's equation

$$\frac{p}{\rho_1}=\frac{\partial\phi_n}{\partial t}-V_{r=a}+\text{const.} \tag{14}$$

shows that

$$\frac{\partial\phi_n}{\partial t}=\text{variable part of }[V_{I,\,r=a}] \tag{15}$$

on the free surface on which p is constant. Since at the boundary $r=b$, the pressure, p, of the outer liquid and that, p', of the inner one satisfy

$$p=p', \tag{16}$$

we have

$$\rho_1\frac{\partial\phi_n}{\partial t}=\rho_2\frac{\partial\phi_n'}{\partial t}+V_I(\rho_1-\rho_2), \tag{17}$$

where the variable parts only of V_I are taken into account. Another condition on the boundary, $r=b$, is

$$\frac{\partial\phi_n}{\partial r}=\frac{\partial\phi_n'}{\partial r}. \tag{18}$$

Solving (15), (17), (18), it is possible to find the condition of the vibratory motion of the problem.[3]

4. *Solution of the problem.*

Write

$$\xi_n=PS_ne^{i\sigma t}, \qquad \eta_n=QS_ne^{i\sigma t}; \tag{19}$$

---

[3] The condition of no relative slide of the liquids along the boundary between them is not satisfied; this can be allowed as in the hydrodynamical problem in two-dimensions.

then, from the first of (13),

$$P=\frac{1}{i\sigma}\left\{-na^{n-1}A+(n+1)a^{-(n+2)}B\right\}. \tag{20}$$

From (15)

$$i\sigma\left\{a^nA+a^{-(n+1)}B\right\}=4\pi\gamma\left[\frac{(\rho_1-\rho_2)Qb^{n+2}}{(2n+1)a^{n+1}}+P\left\{\frac{b^3(\rho_2-\rho_1)}{3a^2}-\frac{\rho_1 a}{2n+1}+\frac{\rho_1 a}{3}\right\}\right]. \tag{21}$$

From the second of (13)

$$Q=-\frac{nb^{n-1}}{i\sigma}E, \tag{22}$$

so that from (18), (22)

$$A-\frac{(n+1)b^{-(2n+1)}}{n}B-E=0. \tag{23}$$

The variable part of V_1 at $r=b+\eta_n$ is

$$4\pi\gamma\left[\frac{b\eta_n}{3(2n+1)}\left\{3\rho_1+2\rho_2(n-1)\right\}-\frac{\rho_1 b^n a^{1-n}\xi_n}{2n+1}\right]. \tag{24}$$

(17) gives

$$A+b^{-(2n+1)}B-\frac{\rho_2}{\rho_1}E+\frac{4\pi\gamma(\rho_1-\rho_2)}{i\sigma\rho_1}\left[\frac{\rho_1 a^{1-n}}{2n+1}P-\frac{b^{1-n}\{3\rho_1+2\rho_2(n-1)\}}{3(2n+1)}Q\right]=0. \tag{25}$$

In these treatments, small quantities of the first order in the expansions of $(a+\xi_n)^\alpha$ and $(b+\eta_n)^\beta$ have been taken into account.

The frequency equation of the vibratory motion is expressed by

$$\begin{aligned}
&\frac{n(n+1)}{2n+1}\left(1-\frac{\rho_2}{\rho_1}\right)\left\{1-\left(\frac{b}{a}\right)^{2n+1}\right\}\left[\left\{\frac{1}{2n+1}-\frac{1}{3}\right.\right.\\
&\qquad\left.\left.+\frac{1}{3}\left(1-\frac{\rho_2}{\rho_1}\right)\left(\frac{b}{a}\right)^3\right\}\left\{1+\frac{2\rho_2(n-1)}{3\rho_1}\right\}-\frac{1}{2n+1}\left(1-\frac{\rho_2}{\rho_1}\right)\left(\frac{b}{a}\right)^{2n+1}\right]\\
&\qquad+\left(\frac{\sigma^2}{4\pi\gamma\rho_1}\right)\left[(2n+1)\left\{\frac{1}{2n+1}-\frac{1}{3}+\frac{1}{3}\left(1-\frac{\rho_2}{\rho_1}\right)\left(\frac{b}{a}\right)^3\right.\right.\\
&\qquad\left.-\frac{1}{2n+1}\left(1-\frac{\rho_2}{\rho_1}\right)\left(\frac{b}{a}\right)^{2n+1}\right\}+(n+1)\left\{\left(\frac{b}{a}\right)^{2n+1}-1\right\}.
\end{aligned}$$

$$\cdot\left(1-\frac{\rho_2}{\rho_1}\right)\left\{\frac{1}{3}\left(1-\frac{\rho_2}{\rho_1}\right)\left(\frac{b}{a}\right)^3-\frac{1}{3}\right\}$$

$$+\frac{2\rho_2(n-1)n}{3\rho_1(2n+1)}\left(1-\frac{\rho_2}{\rho_1}\right)\left\{\frac{n+1}{n}+\left(\frac{b}{a}\right)^{2n+1}\right\}\Bigg]$$

$$+\left(\frac{\sigma^2}{4\pi\gamma\rho_1}\right)^2\left[\frac{2n+1}{n}-\left(1-\frac{\rho_2}{\rho_1}\right)\left\{\frac{n+1}{n}+\left(\frac{b}{a}\right)^{2n+1}\right\}\right]=0\,, \tag{26}$$

where σ is the circular frequency and n the order of the spherical harmonic showing the mode of vibration.

In the special case, if $\rho_1=\rho_2$, (26) transforms to

$$\frac{\sigma^2}{4\pi\gamma\rho_1}=\frac{2n(n-1)}{3(2n+1)}\,, \tag{27}$$

which is the frequency equation in the case of a uniform sphere[4]. The same condition may also be obtained by putting $b=a$ in (26).

Should the wave length of the vibration be very small, n tends to ∞, when the equation (26) is decomposed into two expressions, namely,

$$\left.\begin{aligned}\frac{\sigma^2}{4\pi\gamma\rho_1}&=\frac{n}{3}\left\{1-\left(\frac{b}{a}\right)^3\left(1-\frac{\rho_2}{\rho_1}\right)\right\},\\ \frac{\sigma^2}{4\pi\gamma\rho_1}&=\frac{n\rho_2(\rho_2-\rho_1)}{3\rho_1(\rho_1+\rho_2)}\,.\end{aligned}\right\} \tag{28}$$

To interpret the meanings of the respective expressions in (28), we treat them as follows. If we put $B\to 0$, $Q\to 0$ in the expressions (20), (21), we get the final solution

$$\frac{\sigma^2}{4\pi\gamma\rho_1}=\frac{n}{3}\left\{1-\left(\frac{b}{a}\right)^3\left(1-\frac{\rho_2}{\rho_1}\right)\right\}, \tag{29}$$

whereas if we put $A\to 0$, $P\to 0$ in (22), (23), (25), we finally obtain

$$\frac{\sigma^2}{4\pi\gamma\rho_1}=\frac{n\rho_2(\rho_2-\rho_1)}{3\rho_1(\rho_1+\rho_2)}\,. \tag{30}$$

These results show that the first equation of (28) corresponds to the vibration of the liquid sphere merely near its free surface, and the second to the vibration of the same sphere merely near the boundary of the two liquids.

Lamb and Kelvin[5] showed that the waves transmitted along a plane boundary between two liquids of densities ρ_1, ρ_2 have the frequency equation

---

[4] H. LAMB: *Hydrodynamics*, § 262.

[5] *loc. cit.* 1).

$$\sigma^2=\frac{\rho_2-\rho_1}{\rho_2+\rho_1}gk, \tag{31}$$

where $2\pi/k=$wave length. Since $k=n/a'$ (if $n\rightarrow\infty$) and $g=(4/3)\pi\gamma a'\rho_2$, where a' is the effective radius of the Earth, we have from (31)

$$\frac{\sigma^2}{4\pi\gamma\rho_1}=\frac{n\rho_2(\rho_2-\rho_1)}{3\rho_1(\rho_2+\rho_1)}. \tag{32}$$

The second equation of (28) therefore represents waves that are independent of the outer free surface.

Lamb[6] also treated the case of an ocean of any uniform depth, covering a spherical rigid nucleous, his formula being

$$\sigma^2=\frac{n(n+1)\left\{\left(\frac{a}{b}\right)^n-\left(\frac{b}{a}\right)^{n+1}\right\}}{(n+1)\left(\frac{a}{b}\right)^n+n\left(\frac{b}{a}\right)^{n+1}}\left(1-\frac{3}{2n+1}\frac{\rho_1}{\rho_0}\right)\frac{g}{a}, \tag{33}$$

where ρ_0 is mean density, and

$$g=\left(\frac{4}{3}\right)\pi\gamma a\rho_0, \qquad \rho_0=\rho_1\left\{1-\left(\frac{b}{a}\right)^3\left(1-\frac{\rho_2}{\rho_1}\right)\right\}.$$

When $n\rightarrow\infty$, (33) reduces to

$$\sigma^2=\frac{4}{3}\pi n\gamma\rho_1\left\{1-\left(\frac{b}{a}\right)^3\left(1-\frac{\rho_2}{\rho}\right)\right\}, \tag{34}$$

which is of the same form as the first equation of (28). Notwithstanding the rigid condition of the inner sphere in Lamb's case, since the deformation near the inner sphere does not affect the condition of $r=a$, his problem in such a condition can be reduced to ours.

5. *Numerical calculation and interpretation of the result.*

With a view to confirming the nature of the problem, we calculated the frequencies for $n=1$, 2, 3, 4, and various ratios of ρ_2/ρ_1, the thickness H $(=a-b)$ being kept at $H=0$, $H=200$ km and, $H=300$ km. The results of calculation are shown in Figs. 1, 2, 3, 4 ($H=0$: chain line, $H=200$ km: broken line, $H=300$ km: full line).

It will be seen that there are, for any case, two vibrational frequencies. Whereas one of them is real for all cases, the other becomes

---

[6] H. LAMB: *Hydrodynamics*, 264.

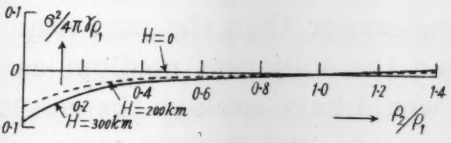

Fig. 1. $n=1$.

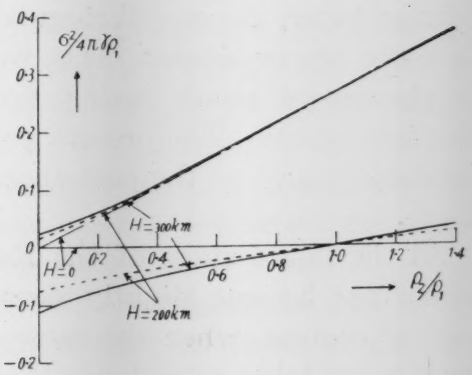

Fig. 2. $n=2$.

imaginary for the condition $\rho_2/\rho_1 > 1$. The imaginary frequency corresponds to the unstable vibration, that is to say, the configuration of every point diverges without limit. It should be borne in mind, however, that the divergent instability is unaffected by the presence of damping or dissipative resistance.

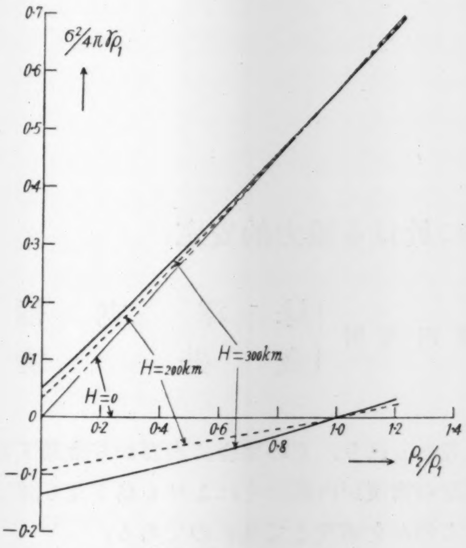

Fig. 3. $n=3$.

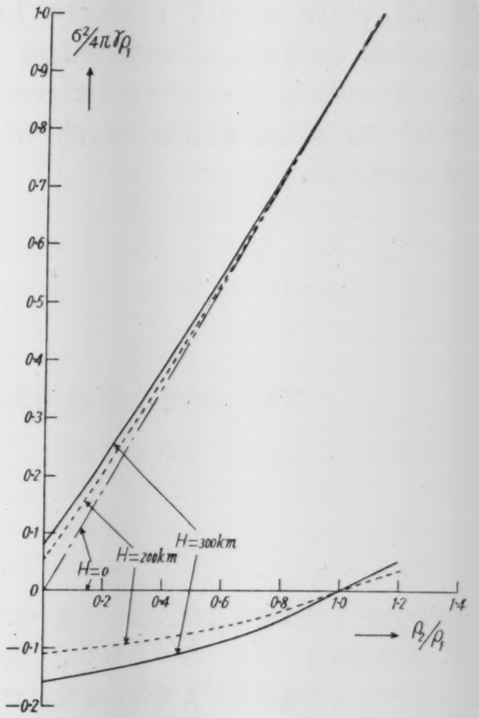

Fig. 4. $n=4$.

The vibration whose frequency is always real, corresponds to the disturbance whose energy mostly accumulates near the outer free surface of the sphere, whereas the vibration whose frequency becomes imaginary for $\rho_2/\rho_1 > 0$, relates to the waves whose energy accumulates near the boundary of the two liquids.

At any rate, if the liquid of the outer layer is denser than that of the inner layer, the equilibrium is physically unstable, in consequence of which the upper denser mass would submerge in the lower medium. The phenomena result mainly from the existence of the boundary between two layers. The present condition is independent of the modes of deformation, such as the pear-shaped, ellipsoidal, tetrahedral, hexahedral, and etc.

At the liquid stage of the Earth, no sooner than the part near the free surface became slightly denser than the subjacent medium as the result of cooling, when the same part would have sunk as the result of a certain unstable condition. If, however, the sunken mass were small, owing to the thermal nature of materials, the condition of cooling and that of density would have been soon altered; the unstable state once attained would have been rapidly altered to a stable one. If, on the other hand, the sunken mass were of such large dimensions as those specified by $n=1, 2, 3$ in the present mathematical notations, the thermal modification of the material state being then almost impossible, the unstable state would scarcely have been altered; a pear-shaped, an ellipsoidal, or even a tetrahedral deformation in the past liquid stage of the Earth is therefore extremely probable. We have, however, at present no good criterion showing which one of these modes is the most unstable.

---

20. 地球の液狀冷却時代に於ける重力的安定

地震研究所 {妹澤克惟
金井清

地球の液狀時代は相當長期に涉つて續いたものと考へられる．その場合に表面から冷却するために，地球の物質がたとへ均一であつても表面の部分の密度が內部のそれよりも高くなる譯である．このやうな狀態に於ける重力的安定が如何なるものかを研究して見たのである．

この目的に向つて密度の異なる二層から成る球體の重力的の振動問題を計算する．均一の球形液體の場合や球形固體の上に均一厚の液の層のある場合は既に取扱れてをるが，二層の液の場合は不思議にも未だ手がつけられてをらぬ．但し只今の場合でも地球の同轉の影響は見逃してある．

小變形をなした場合の重力及び流體力學を取扱ひ，自己振動數の式を作つた．このやうにして出る振動數は２種存在し，その一方は主として自由な表面の振動に關係する變形であり，他は主として二液の境界面の振動に關係する變形であることがわかる．始めの方の振動は如何なる密度の割合でも安定であるけれども，後の方の振動は表面層の密度が內部のそれよりも高くなると必

ず不安定になることがわかつた．この不安定は自己振動が如何なる調和型であつても變りがないのである．但し實際問題として振動型の次數の高いもの，換言すれば不安定となつて移動する部分の容積が小さなもの程，不安定となつて沈下する部分の溫度及び密度等の物理的狀態が直ちに變化し，不安定が不安定でなくなる筈である．之に反して振動型の次數が低いもの，換言すれば不安定となつて移動する部分の容積が大きなものでは，その移動によつて溫度及び密度の物理的狀態がそれ程急激には變らぬ譯である．故に次數の低い $n=1, 2, 3$ 等の變形の痕跡が比較的後迄も認められる筈であるといふ事はいひ得るのである．

計算上の問題であるが，只今の一般の振動數の式に於て n の次數を非常に高くすると，振動型が自由表面にのみ關係する振動數の式と，二液の境にのみ關係する振動數の式とに分解できる．前者は剛い核のある大洋の振動數の式と一致し，後者は二液間に平面の境のある場合のその境界重力波の振動數の式に一致することが確められる．

21. *The Effect of Cooling on a Plastic Earth under Gravitational Forces.*

By Katsutada SEZAWA and Kiyoshi KANAI,

Earthquake Research Institute.

(Read March 15, 1938.—Received March 22, 1938.)

1. *Introduction.*

It appears to be generally held that in the earlier stage of secular cooling of the solid Earth, the superficial layer of the Earth tended to contract, forming tension cracks within the layer, while in the later stage the substratum contracted more rapidly than the superficial layer, thereby causing wrinkling of the Earth's surface. This problem has been theoretically discussed by Davison,[1] Darwin,[2] and Jeffreys.[3] On the other hand, we have shown that it is possible for the Earth's crust to be subjected to such horizontal compression as to exceed the vertical compression,[4] thus providing an alternative explanation of the wrinkled state of the surface. We shall now ascertain the extent to which the cooling of any special layer affects the plastic condition of the Earth under gravitational forces.

We shall first discuss the case in which a subjacent layer of uniform thickness is cooled, and then deal with the case in which the superficial layer is cooled, the remaining part of the Earth in every case retaining its original temperature, after which the mathematical expressions for the case of more complex distribution of the cooling will be discussed.

Although the plastic condition will differ more or less with the kind of plastic theory applied, since the difference is qualitatively imperceptible, we have used the maximum shear stress theory as we did in our previous papers. The present treatment shows that, whereas in the case of problems concerning a purely plastic Earth, the uniform cooling of any layer has no effect on the condition of the Earth, in the case of such problems concerning a plastic Earth as treated in the manner of elasticity the cooling under consideration slightly affects the condition of that Earth. In any case the Earth should be compressible even in a statical state. Since from Jeffreys's paper,[5] it appears that the Earth is in a statically compressed state, our idea cannot be very farfetched.

---

[1] C. DAVISON, *Phil. Trans. Roy. Soc.*, **178** (1887), 231~241.

[2] G. H. DARWIN, *ibid.*, 242~250.

[3] H. JEFFREYS, *The Earth*, Chap. 10; *M. N. R. A. S. Geophys. Suppl.*, **3** (1937), 53~59.

[4] K. SEZAWA, *Bull. Earthq. Res. Inst.*, **15** (1937), 878~887.

2. *Cooling of a substratum, the plasticity problem being treated in the manner of elasticity.*

Let a, b, c be the radii of the respective outer boundaries of the superficial layer, substratum, and inner layer, and ρ_1, ρ_2, ρ_3 and λ_1, μ_1, λ_2, μ_2, λ_3, μ_3 the densities and the elastic constants of the three parts under consideration. Let also θ be the temperature rise of the substratum. Then, the equations of equilibrium of the respective layers are written

$$\left.\begin{aligned}
&-\frac{\xi_1}{r^2}-\eta_1 r+(\lambda_1+2\mu_1)\left(\frac{\partial^2 u_1}{\partial r^2}+\frac{2}{r}\frac{\partial u_1}{\partial r}-\frac{2u_1}{r^2}\right)=0,\\
&-\frac{\xi_2}{r^2}-\eta_2 r+(\lambda_2+2\mu_2)\left(\frac{\partial^2 u_2}{\partial r^2}+\frac{2}{r}\frac{\partial u_2}{\partial r}-\frac{2u_2}{r^2}\right)-\beta_2\frac{\partial\theta_2}{\partial r}=0,\\
&-\eta_3 r+(\lambda_3+2\mu_3)\left(\frac{\partial^2 u_3}{\partial r^2}+\frac{2}{r}\frac{\partial u_3}{\partial r}-\frac{2u_3}{r^2}\right)=0,
\end{aligned}\right\}\tag{1}$$

where $\beta_2=(\lambda_2+2\mu_2/3)q$; $\lambda_2+2\mu_2/3$, q being modulus of compression and volume expansion coefficient respectively. When $\partial\theta_2/\partial r=0$, the solutions of (1) are

$$\left.\begin{aligned}
u_1&=-\frac{\xi_1}{2(\lambda_1+2\mu_1)}+\frac{\eta_1 r^3}{10(\lambda_1+2\mu_1)}+B_1 r+\frac{C_1}{r^2},\\
u_2&=-\frac{\xi_2}{2(\lambda_2+2\mu_2)}+\frac{\eta_2 r^3}{10(\lambda_2+2\mu_2)}+B_2 r+\frac{C_2}{r^2},\\
u_3&=\frac{\eta_3 r^3}{10(\lambda_3+2\mu_3)}+B_3 r.
\end{aligned}\right\}\tag{2}$$

The stresses of the respective layers are denoted by

$$\left.\begin{aligned}
\widehat{rr}_1&=-\frac{\lambda_1\xi_1}{r(\lambda_1+2\mu_1)}+\frac{(5\lambda_1+6\mu_1)}{10(\lambda_1+2\mu_1)}\eta_1 r^2+(3\lambda_1+2\mu_1)B_1-\frac{4\mu_1}{r^3}C_1,\\
\widehat{rr}_2&=-\frac{\lambda_2\xi_2}{r(\lambda_2+2\mu_2)}+\frac{5\lambda_2+6\mu_2}{10(\lambda_2+2\mu_2)}\eta_2 r^2+(3\lambda_2+2\mu_2)B_2-\frac{4\mu_2}{{}^3r}C_2-\beta_2\theta_2,
\end{aligned}\right\}\tag{3}$$

---

[5] H. JEFFREYS, *M.N.R.A.S. Geophys. Suppl.*, **4** (1937), 50~60.

$$\left.\widehat{rr}_3=\frac{5\lambda_3+6\mu_3}{10(\lambda_3+2\mu_3)}\eta_3r^2+(3\lambda_3+2\mu_3)B_3,\quad\right\}$$

$$\left.\begin{aligned}
\widehat{\theta\theta}_1&=\widehat{\phi\phi}_1=-\frac{\lambda_1+\mu_1}{\lambda_1+2\mu_1}\frac{\xi_1}{r}+\frac{5\lambda_1+2\mu_1}{10(\lambda_1+2\mu_1)}\eta_1r^2+(3\lambda_1+2\mu_1)B_1+2\mu_1\frac{C_1}{r^3},\\
\widehat{\theta\theta}_2&=\widehat{\phi\phi}_2=-\frac{\lambda_2+\mu_2}{\lambda_2+2\mu_2}\frac{\xi_2}{r}+\frac{5\lambda_2+2\mu_2}{10(\lambda_2+2\mu_2)}\eta_2r^2+(3\lambda_2+2\mu_2)B_2+2\mu_2\frac{C_2}{r^3}-\beta_2\theta_2,\\
\widehat{\theta\theta}_3&=\widehat{\phi\phi}_3=\frac{5\lambda_3+2\mu_3}{10(\lambda_3+2\mu_3)}\eta_3r^2+(3\lambda_3+2\mu_3)B_3.
\end{aligned}\right\}\tag{4}$$

ξ_1, ξ_2, η_1, η_2, η_3 are such that

$$\left.\begin{aligned}
&\xi_1=\frac{4\pi\gamma}{3}\Big\{c^3\rho_1(\rho_3-\rho_2)+b^3\rho_1(\rho_2-\rho_1)\Big\},\quad \xi_2=\frac{4\pi\gamma}{3}c^3\rho_2(\rho_3-\rho_2),\\
&\eta_1=\frac{4\pi\gamma}{3}\rho_1^2,\quad \eta_2=\frac{4\pi\gamma}{3}\rho_2^2,\quad \eta_3=\frac{4\pi\gamma}{3}\rho_3^2,
\end{aligned}\right\}\tag{5}$$

γ being gravitational constant. From the boundary conditions

$$\left.\begin{aligned}
r&=a; &\widehat{rr}_1&=0,\\
r&=b; &\widehat{rr}_1&=\widehat{rr}_2,\quad u_1=u_2,\\
r&=c; &\widehat{rr}_2&=\widehat{rr}_3,\quad u_2=u_3,
\end{aligned}\right\}\tag{6}$$

we get

$$\begin{aligned}
\frac{B_1\Phi}{\eta_1}=\frac{-2c^2\mu_2}{5(\lambda_1+2\mu_1)(3\lambda_2+2\mu_2)}&\Bigg[\frac{5}{2}\left(\frac{a}{b}\right)^3\left(\frac{a}{c}\right)^2\frac{\lambda_1(3\lambda_2+2\mu_2)}{\mu_1(3\lambda_1+2\mu_1)}\\
&\cdot\left\{\left(1-\frac{\mu_1}{\mu_2}\right)\left(1-\frac{3\lambda_3+2\mu_3}{3\lambda_2+2\mu_2}\right)-\left(\frac{b}{c}\right)^3\left(1+\frac{4\mu_1}{3\lambda_2+2\mu_2}\right)\left(1+\frac{3\lambda_3+2\mu_3}{4\mu_2}\right)\right\}\kappa_1\\
&+\left(\frac{b}{c}\right)^2\frac{3\lambda_2+2\mu_2}{3\lambda_1+2\mu_1}\left\{\left(1-\frac{3\lambda_3+2\mu_3}{3\lambda_2+2\mu_2}\right)-\left(\frac{b}{c}\right)^3\left(1+\frac{3\lambda_3+2\mu_3}{4\mu_2}\right)\right\}\kappa_2\\
&+\left(\frac{b}{c}\right)^2\frac{5\lambda_1+6\mu_1}{3\lambda_1+2\mu_1}\left\{\frac{3\lambda_2+2\mu_2}{4\mu_2}\left(1-\frac{3\lambda_3+2\mu_3}{3\lambda_2+2\mu_2}\right)+\left(\frac{b}{c}\right)^3\left(1+\frac{3\lambda_3+2\mu_3}{4\mu_2}\right)\right\}\kappa_3\\
&-\frac{(\lambda_1+2\mu_1)(3\lambda_3+2\mu_3)}{(3\lambda_1+2\mu_1)(\lambda_2+2\mu_2)}\left(1+\frac{3\lambda_2+2\mu_2}{4\mu_2}\right)\left\{\kappa_4-\frac{5\lambda_2+6\mu_2}{3\lambda_3+2\mu_3}\kappa_5\right\}\Bigg],
\end{aligned}\tag{7}$$

$$
\begin{aligned}
\frac{C_1\Phi}{\eta_1} = \frac{a^3c^2}{10(\lambda_1+2\mu_1)}\Bigg[&\frac{5}{2}\left(\frac{a}{c}\right)^2\frac{\lambda_1}{\mu_1}\Big\{\left(1+\frac{4\mu_2}{3\lambda_1+2\mu_1}\right)\left(1-\frac{3\lambda_3+2\mu_3}{3\lambda_2+2\mu_2}\right)\\
&+\left(\frac{b}{c}\right)^3\frac{4\mu_2}{3\lambda_2+2\mu_2}\left(1-\frac{3\lambda_2+2\mu_2}{3\lambda_1+2\mu_1}\right)\left(1+\frac{3\lambda_3+2\mu_3}{4\mu_2}\right)\Big\}\kappa_1\\
&-\left(\frac{b}{c}\right)^2\frac{\mu_2}{\mu_1}\Big\{\left(1-\frac{3\lambda_3+2\mu_3}{3\lambda_2+2\mu_2}\right)-\left(\frac{b}{c}\right)^3\left(1+\frac{3\lambda_3+2\mu_3}{4\mu_2}\right)\Big\}\kappa_2\\
&-\left(\frac{b}{c}\right)^2\frac{5\lambda_1+6\mu_1}{4\mu_1}\Big\{\left(1-\frac{3\lambda_3+2\mu_3}{3\lambda_2+2\mu_2}\right)+\left(\frac{b}{c}\right)^3\frac{4\mu_2}{3\lambda_2+2\mu_2}\left(1+\frac{3\lambda_3+2\mu_3}{4\mu_2}\right)\Big\}\kappa_3\\
&+\frac{(\lambda_1+2\mu_1)(3\lambda_3+2\mu_3)}{4\mu_1(\lambda_2+2\mu_2)}\left(1+\frac{4\mu_2}{3\lambda_2+2\mu_2}\right)\left\{\kappa_4-\frac{5\lambda_2+6\mu_2}{3\lambda_3+2\mu_3}\kappa_5\right\}\Bigg],
\end{aligned}
\tag{8}
$$

$$
\begin{aligned}
\frac{B_2\Phi}{\eta_1} = \frac{2c^2\mu_2}{5(\lambda_1+2\mu_1)(3\lambda_2+2\mu_2)}\Bigg[&\frac{5}{2}\left(\frac{a}{c}\right)^5\frac{\lambda_1}{\mu_1}\left(1+\frac{4\mu_1}{3\lambda_1+2\mu_1}\right)\left(1+\frac{3\lambda_3+2\mu_3}{4\mu_2}\right)\kappa_1\\
&+\left(\frac{b}{c}\right)^5\left(1+\frac{3\lambda_3+2\mu_3}{4\mu_2}\right)\left\{1-\left(\frac{a}{b}\right)^3\right\}\kappa_2\\
&-\left(\frac{b}{c}\right)^5\frac{5\lambda_1+6\mu_1}{4\mu_1}\left(1+\frac{3\lambda_3+2\mu_3}{4\mu_2}\right)\left\{\frac{4\mu_1}{3\lambda_1+2\mu_1}+\left(\frac{a}{b}\right)^3\right\}\kappa_3\\
&+\frac{(\lambda_1+2\mu_1)(3\lambda_3+2\mu_3)}{4\mu_2(\lambda_2+2\mu_2)}\Big\{\left(1+\frac{4\mu_2}{3\lambda_1+2\mu_1}\right)\\
&\qquad-\left(\frac{a}{b}\right)^3\left(1-\frac{\mu_2}{\mu_1}\right)\Big\}\left\{\kappa_4-\frac{5\lambda_2+6\mu_2}{3\lambda_3+2\mu_3}\kappa_5\right\}\Bigg],
\end{aligned}
\tag{9}
$$

$$
\begin{aligned}
\frac{C_2\Phi}{\eta_1} = \frac{b^5}{10(\lambda_2+2\mu_2)}\Bigg[&\frac{5}{2}\left(\frac{a}{b}\right)^5\frac{\lambda_1(\lambda_2+2\mu_2)}{\mu_1(\lambda_1+2\mu_1)}\left(1+\frac{4\mu_1}{3\lambda_1+2\mu_1}\right)\left(1-\frac{3\lambda_3+2\mu_3}{3\lambda_2+2\mu_2}\right)\kappa_1\\
&+\frac{\lambda_2+2\mu_2}{\lambda_1+2\mu_1}\left(1-\frac{3\lambda_3+2\mu_3}{3\lambda_2+2\mu_2}\right)\left\{1-\left(\frac{a}{b}\right)^3\right\}\kappa_2\\
&-\frac{(5\lambda_1+6\mu_1)(\lambda_2+2\mu_2)}{4\mu_1(\lambda_1+2\mu_1)}\left(1-\frac{3\lambda_3+2\mu_3}{3\lambda_2+2\mu_2}\right)\left\{\frac{4\mu_1}{3\lambda_1+2\mu_1}+\left(\frac{a}{b}\right)^3\right\}\kappa_3\\
&-\left(\frac{c}{b}\right)^2\frac{3\lambda_3+2\mu_3}{3\lambda_2+2\mu_2}\Big\{\left(1-\frac{3\lambda_2+2\mu_2}{3\lambda_1+2\mu_1}\right)\\
&\qquad-\left(\frac{a}{b}\right)^3\left(1+\frac{3\lambda_2+2\mu_2}{4\mu_1}\right)\Big\}\left\{\kappa_4-\frac{5\lambda_2+6\mu_2}{3\lambda_3+2\mu_3}\kappa_5\right\}\Bigg],
\end{aligned}
\tag{10}
$$

$$\begin{aligned}\frac{B_3\Phi}{\eta_1}=\frac{2c^2\mu_2}{5(\lambda_1+2\mu_1)(3\lambda_2+2\mu_2)}&\Bigg[10\left(\frac{a}{c}\right)^5\frac{\lambda_1}{4\mu_1}\left(1+\frac{4\mu_1}{3\lambda_1+2\mu_1}\right)\left(1+\frac{3\lambda_2+2\mu_2}{4\mu_2}\right)\kappa_1\\&+\left(\frac{b}{c}\right)^5\left(1+\frac{3\lambda_2+2\mu_2}{4\mu_2}\right)\left\{1-\left(\frac{a}{b}\right)^3\right\}\kappa_2\\&-\left(\frac{b}{c}\right)^5\frac{5\lambda_1+6\mu_1}{4\mu_1}\left(1+\frac{3\lambda_2+2\mu_2}{4\mu_2}\right)\left\{\frac{4\mu_1}{3\lambda_1+2\mu_1}+\left(\frac{a}{b}\right)^3\right\}\kappa_3\\&+\frac{(\lambda_1+2\mu_1)(3\lambda_2+2\mu_2)}{4\mu_1(\lambda_2+2\mu_2)}\Bigg\{\frac{\mu_1}{\mu_2}\left(1+\frac{4\mu_2}{3\lambda_1+2\mu_1}\right)+\left(\frac{a}{b}\right)^3\left(1-\frac{\mu_1}{\mu_2}\right)\\&-\left(\frac{a}{c}\right)^3\left(1+\frac{4\mu_1}{3\lambda_2+2\mu_2}\right)+\left(\frac{b}{c}\right)^3\frac{4\mu_1}{3\lambda_2+2\mu_2}\left(1-\frac{3\lambda_2+2\mu_2}{3\lambda_1+2\mu_1}\right)\Bigg\}\kappa_4\\&-\frac{(\lambda_1+2\mu_1)(5\lambda_2+6\mu_2)}{4\mu_1(\lambda_2+2\mu_2)}\Bigg\{\frac{\mu_1}{\mu_2}\left(1+\frac{4\mu_2}{3\lambda_1+2\mu_1}\right)+\left(\frac{a}{b}\right)^3\left(1-\frac{\mu_1}{\mu_2}\right)\\&+\left(\frac{a}{c}\right)^3\frac{3\lambda_2+2\mu_2}{4\mu_2}\left(1+\frac{4\mu_1}{3\lambda_2+2\mu_2}\right)-\left(\frac{b}{c}\right)^3\frac{\mu_1}{\mu_2}\left(1-\frac{3\lambda_2+2\mu_2}{3\lambda_1+2\mu_1}\right)\Bigg\}\kappa_5\Bigg],\end{aligned}\tag{11}$$

$$\begin{aligned}\Phi=&-\left(1+\frac{4\mu_2}{3\lambda_1+2\mu_1}\right)\left(1-\frac{3\lambda_3+2\mu_3}{3\lambda_2+2\mu_2}\right)+\left(\frac{a}{b}\right)^3\left(1-\frac{\mu_2}{\mu_1}\right)\left(1-\frac{3\lambda_3+2\mu_3}{3\lambda_2+2\mu_2}\right)\\&+\left(\frac{a}{c}\right)^3\frac{\mu_2}{\mu_1}\left(1+\frac{3\lambda_3+2\mu_3}{4\mu_2}\right)\left(1+\frac{4\mu_1}{3\lambda_2+2\mu_2}\right)\\&-\left(\frac{b}{c}\right)^3\frac{4\mu_2}{3\lambda_2+2\mu_2}\left(1-\frac{3\lambda_2+2\mu_2}{3\lambda_1+2\mu_1}\right)\left(1+\frac{3\lambda_3+2\mu_3}{4\mu_2}\right),\end{aligned}\tag{12}$$

where

$$\kappa_1=\left(\frac{c}{a}\right)^3\frac{\rho_3-\rho_2}{\rho_1}+\left(\frac{b}{a}\right)^3\frac{\rho_2-\rho_1}{\rho_1}-\frac{5\lambda_1+6\mu_1}{10\lambda_1},\tag{13}$$

$$\begin{aligned}\kappa_2=&-1+5\left(\frac{c}{b}\right)^3\frac{\rho_3-\rho_2}{\rho_1}+\frac{5(\rho_2-\rho_1)}{\rho_1}\\&-5\left(\frac{c}{b}\right)^3\frac{\rho_2(\rho_3-\rho_2)}{\rho_1^2}\frac{\lambda_1+2\mu_1}{\lambda_2+2\mu_2}+\left(\frac{\rho_2}{\rho_1}\right)^2\frac{\lambda_1+2\mu_1}{\lambda_2+2\mu_2},\end{aligned}\tag{14}$$

$$\kappa_3=-1+\frac{10\lambda_1}{5\lambda_1+6\mu_1}\left\{\left(\frac{c}{b}\right)^3\frac{\rho_3-\rho_2}{\rho_1}+\frac{\rho_2-\rho_1}{\rho_1}\right\}$$

$$-10\left(\frac{c}{b}\right)^3\frac{\rho_2(\rho_3-\rho_2)}{\rho_1^2}\frac{\lambda_2(\lambda_1+2\mu_1)}{(5\lambda_1+6\mu_1)(\lambda_2+2\mu_2)}$$

$$+\left(\frac{\rho_2}{\rho_1}\right)^2\frac{(\lambda_1+2\mu_1)(5\lambda_2+6\mu_2)}{(5\lambda_1+6\mu_1)(\lambda_2+2\mu_2)}-\frac{30\beta_2\theta_2}{4\pi\gamma\rho_1^2b^2}\frac{\lambda_1+2\mu_1}{5\lambda_1+6\mu_1}, \quad (15)$$

$$\kappa_4=-\left(\frac{\rho_2}{\rho_1}\right)^2+\frac{5\rho_2(\rho_3-\rho_2)}{\rho_1^2}+\left(\frac{\rho_3}{\rho_1}\right)^2\frac{\lambda_2+2\mu_2}{\lambda_3+2\mu_3}, \quad (16)$$

$$\kappa_5=-\left(\frac{\rho_2}{\rho_1}\right)^2+\frac{10\rho_2(\rho_3-\rho_2)}{\rho_1^2}\frac{\lambda_2}{(5\lambda_2+6\mu_2)}+\left(\frac{\rho_3}{\rho_1}\right)^2\frac{(\lambda_2+2\mu_2)(5\lambda_3+6\mu_3)}{(5\lambda_2+6\mu_2)(\lambda_3+2\mu_3)}$$

$$+\frac{30\beta_2\theta_2}{4\pi\gamma\rho_1^2c^2}\frac{\lambda_2+2\mu_2}{5\lambda_2+6\mu_2}. \quad (17)$$

Substituting the values of these constants in (3), (4), it is possible to get the principal stresses within the Earth. The plastic stresses are equal to the maximum shear stresses, namely,

$$\frac{\widehat{rr}_1-\widehat{\theta\theta}_1}{2}, \quad \frac{\widehat{rr}_2-\widehat{\theta\theta}_2}{2}, \quad \frac{\widehat{rr}_3-\widehat{\theta\theta}_3}{2}. \quad (18)$$

Comparing (3), (4), (7) ~ (18), it will be seen that, were the materials incompressible, that is, $\lambda/\mu=\infty$, the maximum shear stresses $(\widehat{rr}_1-\widehat{\theta\theta}_1)/2$, $(\widehat{rr}_2-\widehat{\theta\theta}_2)/2$, $(\widehat{rr}_3-\widehat{\theta\theta}_3)/2$ would assume zero value, the value of the coefficient β_2 being invariably finite from the thermal nature of the problem. In such a case the horizontal forces $\widehat{\theta\theta}_1$, $\widehat{\phi\phi}_1$ on the free surface $r=a$ are also zero since $\widehat{rr}_1$ on the same surface is zero. We are ascertaining the stress condition of the solid Earth with reference to the state of the liquid Earth, the gravitational conditions for both cases being approximately the same.

Let the thicknesses of the surface layer and the subjacent layer be 100 km and 300 km respectively; then $a=6350$ km, $b=6250$ km, and $c=5950$ km. From the ideas of Jeffreys[6] and others it appears that the temperature fall of the second layer is of the order of 2000° since the Earth solidified, that is to say, a volume contraction of 5 per cent. Assume that the temperature fall of the second layer relative to that of the neighbouring layers is 700°C and $q=3.0\cdot 8.10^{-4}$, $k=\lambda+(2/3)\mu=10^{12}$ (C.G.S.), $\rho_1=\rho_2=3{\cdot}49$, $\rho_3=4{\cdot}85$, $\lambda_1=\mu_1=\lambda_2=\mu_2=\lambda_3=\mu_3\equiv\lambda\equiv\mu$. Then $\theta=-700$°C, $\beta=0{\cdot}24.10^8$. Using these values, we calculated the distribution of $(\widehat{rr}-\widehat{\theta\theta})/2$; the results being shown by full lines in Fig. 1.

---

[6] H. **Jeffreys**, *loc. cit.* 3).

For comparison, the distribution for the case of no temperature fall is shown by a broken line in the same figure. The values of $\widehat{rr}$ for the respective cases are shown in Fig. 2.

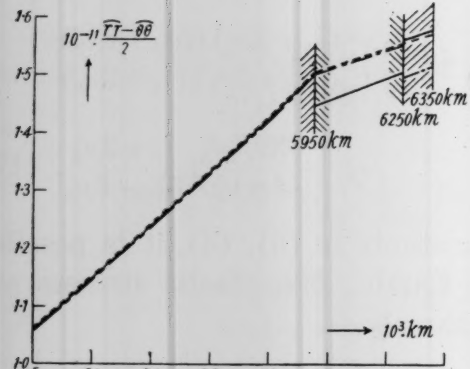

Fig. 1.

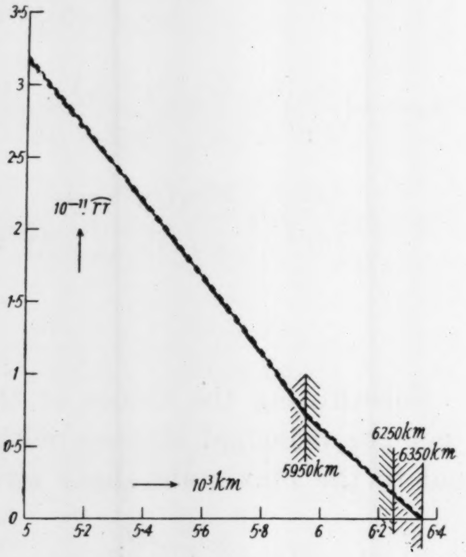

Fig. 2.

It will be seen that the effect of cooling on the plastic state under gravitational forces is negligible in $(\widehat{rr}-\widehat{\theta\theta})/2$ as well as in $\widehat{rr}$.

3. *Cooling of a surface stratum, the plasticity problem being treated in the manner of elasticity.*

Let the temperature rise of a superficial stratum be θ_1, the temperature of the second layer retaining its original value. The equations of equilibrium are then of the forms

$$\left.\begin{aligned}
&-\frac{\xi_1}{r^2}-\eta_1 r+(\lambda_1+2\mu_1)\left(\frac{\partial^2 u_1}{\partial r^2}+\frac{2}{r}\frac{\partial u_1}{\partial r}-\frac{2u_1}{r^2}\right)-\beta_1\frac{\partial\theta_1}{\partial r}=0,\\
&-\frac{\xi_2}{r^2}-\eta_2 r+(\lambda_2+2\mu_2)\left(\frac{\partial^2 u_2}{\partial r^2}+\frac{2}{r}\frac{\partial u_2}{\partial r}-\frac{2u_2}{r^2}\right)=0,\\
&-\eta_3 r+(\lambda_3+2\mu_3)\left(\frac{\partial^2 u_3}{\partial r^2}+\frac{2}{r}\frac{\partial u_3}{\partial r}-\frac{2u_3}{r^2}\right)=0.
\end{aligned}\right\} \qquad (19)^{7)}$$

When $\partial\beta_1/\partial\theta_1=0$, the expressions for the displacements are the same as those in (2), whereas the stresses of the respective layers are expressed by

---

7) The simultaneous equations of the second and third expressions in (19) are not particularly important except for comparison with the preceding section.

$$\left.\begin{aligned}
\widehat{rr}_1&=-\frac{\lambda_1\xi_1}{r(\lambda_1+2\mu_1)}+\frac{5\lambda_1+6\mu_1}{10(\lambda_1+2\mu_1)}\eta_1r^2+(3\lambda_1+2\mu_1)B_1-\frac{4\mu_1}{r^3}C_1-\beta_1\theta_1,\\
\widehat{rr}_2&=-\frac{\lambda_2\xi_2}{r(\lambda_2+2\mu_2)}+\frac{5\lambda_2+6\mu_2}{10(\lambda_2+2\mu_2)}\eta_2r^2+(3\lambda_2+2\mu_2)B_2-\frac{4\mu_2}{r^3}C_2,\\
\widehat{rr}_3&=\frac{5\lambda_3+6\mu_3}{10(\lambda_3+2\mu_3)}\eta_3r^2+(3\lambda_3+2\mu_3)B_3.
\end{aligned}\right\}\quad(20)$$

$$\left.\begin{aligned}
\widehat{\theta\theta}_1=\widehat{\phi\phi}_1&=-\frac{\lambda_1+\mu_1}{\lambda_1+2\mu_1}\frac{\xi_1}{r}+\frac{5\lambda_1+2\mu_1}{10(\lambda_1+2\mu_1)}\eta_1r^2+(3\lambda_1+2\mu_1)B_1+2\mu_1\frac{C_1}{r^3}-\beta_1\theta_1,\\
\widehat{\theta\theta}_2=\widehat{\phi\phi}_2&=-\frac{\lambda_2+\mu_2}{\lambda_2+2\mu_2}\frac{\xi_2}{r}+\frac{5\lambda_2+2\mu_2}{10(\lambda_2+2\mu_2)}\eta_2r^2+(3\lambda_2+2\mu_2)B_2+2\mu_2\frac{C_2}{r^3},\\
\widehat{\theta\theta}_3=\widehat{\phi\phi}_3&=\frac{5\lambda_3+2\mu_3}{10(\lambda_3+2\mu_3)}\eta_3r^2+(3\lambda_3+2\mu_3)B_3,
\end{aligned}\right\}$$

$$(21)$$

where $\beta_1=(\lambda_1+2\mu_1/3)q$. Using the boundary conditions (6), we find the values of the constants κ_1, κ_2, κ_3, κ_4, κ_5 in the expressions of B_1, C_1, B_2, C_2, B_3 in (7)$\sim$(11), the results being shown below.

$$\kappa_1=\left\{\left(\frac{c}{a}\right)^3\frac{\rho_3-\rho_2}{\rho_1}+\left(\frac{b}{a}\right)^3\frac{\rho_2-\rho_1}{\rho_1}\right\}-\frac{5\lambda_1+6\mu_1}{10\lambda_1}+\frac{3\beta_1\theta_1}{4\pi\gamma\rho_1^2a^2}\frac{(\lambda_1+2\mu_1)}{\lambda_1},\tag{22}$$

$$\begin{aligned}\kappa_2=-1+5\left(\frac{c}{b}\right)^3\frac{\rho_3-\rho_2}{\rho_1}+\frac{5(\rho_2-\rho_1)}{\rho_1}\\
-5\left(\frac{c}{b}\right)^3\frac{\rho_2(\rho_3-\rho_2)}{\rho_1^2}\frac{\lambda_1+2\mu_1}{\lambda_2+2\mu_2}+\left(\frac{\rho_2}{\rho_1}\right)^2\frac{\lambda_1+2\mu_1}{\lambda_2+2\mu_2},\end{aligned}\tag{23}$$

$$\begin{aligned}\kappa_3=-1+\frac{10\lambda_1}{5\lambda_1+6\mu_1}\left\{\left(\frac{c}{b}\right)^3\frac{\rho_3-\rho_2}{\rho_1}+\frac{\rho_2-\rho_1}{\rho_1}\right\}\\
-10\left(\frac{c}{b}\right)^3\frac{\rho_2(\rho_3-\rho_2)}{\rho_1^2}\frac{\lambda_2(\lambda_1+2\mu_1)}{(5\lambda_1+6\mu_1)(\lambda_2+2\mu_2)}\\
+\left(\frac{\rho_2}{\rho_1}\right)^2\frac{(\lambda_1+2\mu_1)(5\lambda_2+6\mu_2)}{(5\lambda_1+6\mu_1)(\lambda_2+2\mu_2)}+\frac{15\beta_1\theta_1}{2\pi\gamma\rho_1^2b^2}\frac{\lambda_1+2\mu_1}{5\lambda_1+6\mu_1},\end{aligned}\tag{24}$$

$$\kappa_4=-\left(\frac{\rho_2}{\rho_1}\right)^2+\frac{5\rho_2(\rho_3-\rho_2)}{\rho_1^2}+\left(\frac{\rho_3}{\rho_1}\right)^2\frac{\lambda_2+2\mu_2}{\lambda_3+2\mu_3},\tag{25}$$

$$\kappa_5=-\left(\frac{\rho_2}{\rho_1}\right)^2+\frac{10\rho_2(\rho_3-\rho_2)}{\rho_1^2}\frac{\lambda_2}{5\lambda_2+6\mu_2}+\left(\frac{\rho_3}{\rho_1}\right)^2\frac{(\lambda_2+2\mu_2)(5\lambda_3+6\mu_3)}{(5\lambda_2+6\mu_2)(\lambda_3+2\mu_3)}. \tag{26}$$

Assume that the temperature fall of the surface layer relative to that of the neighbouring layer is 700°C, all other conditions being the same as those in the preceding section. The results of calculation are shown by chain-lines in Figs. 1, 2. It will be seen that in this case, too, the effect of cooling on the plasticity problem is negligible.

4. *Cooling of strata, the plasticity problem being treated in the manner of pure plasticity.*

The equations of equilibrium in this case are expressed by

$$\left.\begin{aligned}&-\frac{\xi_1}{r^2}-\eta_1 r+\frac{\partial\widehat{rr}_1}{\partial r}+\frac{2}{r}(\widehat{rr}_1-\widehat{\theta\theta}_1)-\beta_1\frac{\partial\theta_1}{\partial r}=0,\\&-\frac{\xi_2}{r^2}-\eta_2 r+\frac{\partial\widehat{rr}_2}{\partial r}+\frac{2}{r}(\widehat{rr}_2-\widehat{\theta\theta}_2)-\beta_2\frac{\partial\theta_2}{\partial r}=0,\\&-\eta_3 r+\frac{\partial\widehat{rr}_3}{\partial r}+\frac{2}{r}(\widehat{rr}_3-\widehat{\theta\theta}_3)=0,\end{aligned}\right\} \tag{27}$$

the conditions of plasticity being of the forms

$$\widehat{rr}_1-\widehat{\theta\theta}_1=\pm 2k_1,\quad \widehat{rr}_2-\widehat{\theta\theta}_2=\pm 2k_2,\quad \widehat{rr}_3-\widehat{\theta\theta}_3=\pm 2k_3. \tag{28}$$

The solutions of (26) are therefore of the types

$$\left.\begin{aligned}&\widehat{rr}_1+4k_1\log r+\frac{\xi_1}{r}+\frac{\eta_1 r^2}{2}+I_1+\beta_1\theta_1=0,\\&\widehat{rr}_2+4k_2\log r+\frac{\xi_2}{r}+\frac{\eta_2 r^2}{2}+I_2+\beta_2\theta_2=0,\\&\widehat{rr}_3+4k_3\log r+\frac{\eta_3 r^2}{2}+I_3=0.\end{aligned}\right\} \tag{29}$$

If we write

$$I_1+\beta_1\theta_1=I_1',\quad I_2+\beta_2\theta_2=I_2', \tag{30}$$

and put the solutions in the boundary conditions

$$r=a;\ \widehat{rr}_1=0,\quad r=b;\ \widehat{rr}_1=\widehat{rr}_2,\quad r=c;\ \widehat{rr}_2=\widehat{rr}_3, \tag{31}$$

it is possible to make the solutions fit the present problem. From the nature of the problem the solutions are the same whatever may be the forms of

$$I_1+\beta_1\theta_1, \qquad I_2+\beta_2\theta_2.$$

The temperature fall of any layer has no effect on the plasticity condition, not at any rate from the present criterion of plasticity.

5. *Cooling, the distribution of which with radius is irregular.*

Let us assume for simplicity that the density and elasticity are uniform throughout the Earth, the temperature rise being distributed in the manner

$$\theta=f\,(r). \tag{32}$$

The equation of equilibrium in the manner of elasticity, then, is of the form

$$-\gamma r+(\lambda+2\mu)\left(\frac{\partial^2 u}{\partial r^2}+\frac{2}{r}\frac{\partial u}{\partial r}-\frac{2u}{r^2}\right)-\beta f'(r)=0. \tag{33}$$

The radial displacement is thus

$$u=\frac{\gamma r^3}{10\,(\lambda+2\mu)}+Br+\frac{C}{r^2}+\frac{\beta/(\lambda+2\mu)}{D^2+\dfrac{2}{r}D-\dfrac{2}{r^2}}\,f'(r), \tag{34}$$

D being operator in r. The stresses are of the forms

$$\left.\begin{aligned}\widehat{rr}&=\lambda\left(\frac{\partial u}{\partial r}+\frac{2u}{r}\right)+2\mu\frac{\partial u}{\partial r}-\beta f\,(r)\ ,\\ \widehat{\theta\theta}=\widehat{\phi\phi}&=\lambda\left(\frac{\partial u}{\partial r}+\frac{2u}{r}\right)+2\mu\frac{u}{r}-\beta f\,(r)\ .\end{aligned}\right\} \tag{35}$$

Using the boundary condition

$$r=a\ ; \qquad \widehat{rr}=0, \tag{36}$$

it is possible to determine B, C. In this case the plastic stress and normal stresses are affected by $f(r)$, the numerical determination of which will be reserved for future study. From the results in the preceding section, the influence of the temperature fall would be trifling.

In the case of a purely plasticity problem, the equation of equilibrium is

$$-\gamma r+\frac{\partial\widehat{rr}}{\partial r}+\frac{2}{r}(\widehat{rr}-\widehat{\theta\theta})-\beta f'(r)=0, \tag{37}$$

with a plastic condition

$$\widehat{rr}-\widehat{\theta\theta}=\pm 2k, \tag{38}$$

so that

$$\left.\begin{aligned}\widehat{rr}&=4k\log\frac{a}{r}-\frac{\eta}{2}(a^2-r^2)+\beta\Big\{f(a)-f(r)\Big\},\\ \widehat{\theta\theta}&=4k\log\frac{a}{r}-\frac{\eta}{2}(a^2-r^2)+\beta\Big\{f(a)-f(r)\Big\}-2k.\end{aligned}\right\}\tag{39}$$

Although in this case, the plastic stress

$$\frac{\widehat{rr}-\widehat{\theta\theta}}{2}\tag{40}$$

is independent of temperature fall, the normal stresses $\widehat{rr}$, $\widehat{\theta\theta}$ at a certain depth are affected, though probably only very slightly, by the temperature fall under consideration.

6. *Concluding remarks.*

We have ascertained that the effect of cooling of any layer on the plastic deformation of the Earth under gravitational forces is not very marked, even should the accounted temperature fall be that of the Earth after solidification. Whereas in the case of treatments like elasticity, the correction due to temperature fall on the plastic behaviour is extremely small, in the case of pure plasticity treatments, there is no need for temperature correction, not, at any rate, from such criterion of plasticity as concerns the maximum shear stress.

It has been shown that the horizontal compression in the surface crust of the Earth is the result of the usual gravitational forces, the effect of temperature fall of the substratum being negligible compared with the gravitational action. The crack-forming condition in the early stage of the solid Earth can never be large compared with the compression due to gravity. It should, however, be borne in mind that our theory assumes that the Earth is compressible even in the statical state. If, on the other hand, the Earth is incompressible in the statical state, shear stresses at any part of the Earth are zero so that there is no plastic stress; and also no horizontal compression exists, particularly, on the free surface of the Earth. It is possible that, in the earliest stage of the Earth's solidification, the Earth was incompressible; the mechanical condition on the surface would have been under temperature stress, in which case the explanation of the tension cracks in the superficial layer of the Earth might then be quite simple.

21. 地球の冷却が重力の下にあるそのプラスチック状態に及ぼす影響

地震研究所 {妹澤克惟
金井清

地球が固體化してからの初期の狀態では表面の薄い層が冷却によつて收縮して表面層に機械的作用を及ぼし，次の時期には第２の層がよく冷却する爲にその結果として表面層を水平に壓縮し從て地表の皺が生じたといふ理論は相當に信用されてをるやうである。我々が最近出したところの，地球の殼が壓縮性である以上は重力の爲に地殼内に剪斷應力(プラスチック應力)を生じ，且つ地表層が水平に壓され得るといふ理論と兩立することになるから，重力と冷却とが同時に存在する場合に何れがよくきくかを確めて見たのである。

地球の第２層又は第１層が殘りの層に比較して700°Cだけ餘計に冷却したとして計算して見ると，冷却の爲のプラスチックの應力が重力のそれに比して著しく小さいことがわかつたのである。故に地表に働く大體の横壓力は重力の作用の結果としてよいと考へられる。

只今の理論は地球が壓縮性であるとするとき成り立ち得るのであつて，非壓縮性であるとすると地殼内のプラスチック應力や表面の横壓力は全然存在しない事になる。しかし Jeffreys が最近研究したところによると地球はその核部に到る迄も普通の Poisson 比が示す程度近くに壓縮されてをるやうであるから，只今の議論は相當正しいものと見てよい。しかし地球が固體化した極く初期にだけ非壓縮性であつたとすると地表の引張りの割目を説明し得るから更に好都合かも知れぬ。

---

22. *Aseismic Properties of a Daikoku-basira (Principal Column) or Similar Column in a Japanese Style House.*

By Kiyoshi KANAI,

Earthquake Research Institute.

(Read Feb. 15, and March 15, 1938.-Received March 22, 1938.)

1. *Introduction.*

Almost at the centre, in houses of old Japanese style, there is a column (sometimes two) called *daikoku-basira* (principal column). The peculiarity of such a column(1) is that its diameter is much larger than that of any other column in the same building. Whereas in an oridinary dwelling house of past centuries, either of military family or of farmer class, there is only one principal column, in a palace or a temple there are usually two principal columns (not called daikoku-basira in this case). Although the special column now under consideration originally used to support the heavy weight of the roof or to batten horizontal members in every floor, the same column in the course of time tended to serve more of a decorative purpose than utility, and eventually lost its structural meaning. But, it came to be known that a house with this special column, even though its object was no more than for decoration, actually resisted wind and seismic forces. Although the resistance to such horizontal forces may depend on the structural condition of the column, since no satisfactory theory with respect to the problem has yet been offered, it would scarcely be possible to conclude that this thick column, to all apparent purposes for decoration only, is meaningless from the structural point of view. Mathematical investigations show that, even though the connection between this column and the horizontal members be fairly weak, the former still contributes greatly to the resistance of a building to seismic forces.

The general requirement for a high-class house of Japanese style is that it should have as far few walls as possible, the reason originally being probably ventilation during the hot weather. If, therefore, a strong extra thick column or any substitute for it were used in houses, such as just mentioned, it should be possible to render the house aseismic

---

1) From T. KAN's paper (*Jour. Arch.*, **47** (1933), 29) it appears that its quality is also better than that of any other column.

to a certain extent, even though it may be wall-less.

It is a common sense reasoning in engineering that all members in a structure should be distributed as uniformly as possible, it appearing therefore that the idea of daikoku-basira contradicts with the common sense under consideration.

There is the fact that in a strong earthquake, some houses rotated about their extra thick columns with but little structural failure. Although from this consideration it may be advisable to solve the case of a three-dimensional framed structure, namely, the case of space lattice, yet owing to the extreme complexity of the problem, it will be discussed two-dimensionally, certain special points only being treated three-dimensionally.

2. *A single-storied house, the problem being two-dimensional.*

To ascertain the aseismic properties of the daikoku-basira (extra thick column), it is advisable to consider the case of a finite number of columns. We have, thus, taken the case of seven columns, the middle one of which is the extra-thick column. Let the stiffness of the thick column, that of each of all the other ordinary columns, and that of the floor be E_0I_0, EI, $E'I'$ respectively. Let also the inertia mass at the panel point corresponding to the top of the thick column and that at every remaining panel point be m_0, m respectively. The column height and the length of every span are shown in the sketch.

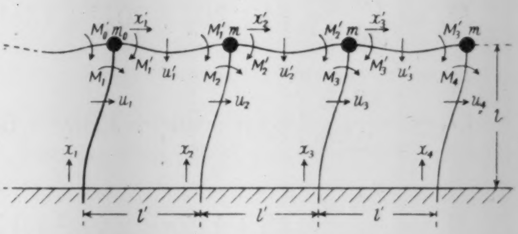

Fig. 1.

The expressions of vibratory motion for the columns and the floors are of the types

$$\left.\begin{aligned} u_s &= (A_s + B_s x_s + C_s x_s^2 + D_s x_s^3)e^{ipt}, \\ u'_s &= (A'_s + B'_s x'_s + C'_s x'^2_s + D'_s x'^3_s)e^{ipt}. \end{aligned}\right\} \qquad (1)$$

The boundary conditions are such that

$$x_s = 0; \qquad u_s = be^{ipt}, \quad \frac{du_s}{dx_s} = 0, \qquad (2),\ (3)$$

$$x_1 = l,\ x'_1 = 0; \qquad M_1 - 2M'_1 = 0, \quad u'_1 = 0, \quad \frac{du_1}{dx_1} = \frac{du'_1}{dx'_1}, \qquad (4),\ (5),\ (6)$$

$$x_2 = l,\ x'_1 = l',\ x'_2 = 0; \qquad M_2 + M'_1 - M'_2 = 0, \qquad (7)$$

$$u'_1 = u'_2 = 0, \quad \frac{du_2}{dx_2} = \frac{du'_1}{dx'_1} = \frac{du'_2}{dx'_2}, \qquad (8),\ (9)$$

$$x_3=l,\ x'_2=l',\ x'_3=0; \qquad M_3+M'_2-M'_3=0, \tag{10}$$

$$u'_2=u'_3=0, \quad \frac{du_3}{dx_3}=\frac{du'_2}{dx'_2}=\frac{du'_3}{dx'_3}, \qquad (11),\ (12)$$

$$x_4=l,\ x'_3=l'; \quad M_4+M'_3=0, \quad u'_3=0, \quad \frac{du_4}{dx_4}=\frac{du'_3}{dx'_3}, \qquad (13),\ (14),\ (15)$$

$$x_s=l; \qquad u_1=u_2=u_3=u_4, \tag{16}$$

$$-\left\{E_0I_0\frac{d^3u_1}{dx_1^3}+2EI\left(\frac{d^3u_2}{dx_2^3}+\frac{d^3u_3}{dx_3^3}+\frac{d^3u_4}{dx_4^3}\right)\right\}=(m_0+6m)p^2u_1. \tag{17}$$

Substituting expressions of types (1) in (2)$\sim$(17), we get

$$C_1=-\frac{3\gamma b}{l^2\Phi}\left\{\eta_0(4+20\eta+30\eta^2+13\eta^3)+\eta(20+86\eta+114\eta^2+45\eta^3)\right\},$$

$$D_1=\frac{\gamma b}{l^3\Phi}\left\{\eta_0(4+20\eta+30\eta^2+13\eta^3)+2\eta(22+91\eta+117\eta^2+45\eta^3)\right\},$$

$$C_2=-\frac{3\gamma b}{2l^2\Phi}\left\{\eta_0(8+64\eta+120\eta^2+59\eta^3)+2\eta(8+56\eta+96\eta^2+45\eta^3)\right\},$$

$$D_2=\frac{\gamma b}{2l^3\Phi}\left\{\eta_0(8+112\eta+240\eta^2+125\eta^3)+4\eta(4+46\eta+90\eta^2+45\eta^3)\right\},$$

$$C_3=-\frac{\gamma b}{l^2\Phi}\left\{\eta_0(12+96\eta+171\eta^2+75\eta^3)+3\eta(8+62\eta+105\eta^2+45\eta^3)\right\},$$

$$D_3=\frac{\gamma b}{l^3\Phi}\left\{\eta_0(4+56\eta+111\eta^2+49\eta^3)+\eta(8+110\eta+207\eta^2+90\eta^3)\right\},$$

$$C_4=-\frac{3\gamma b}{2l^2\Phi}\left\{\eta_0(8+52\eta+96\eta^2+53\eta^3)+2\eta(8+50\eta+87\eta^2+45\eta^3)\right\},$$

$$D_4=\frac{\gamma b}{2l^3\Phi}\left\{\eta_0(8+76\eta+168\eta^2+107\eta^3)+2\eta(8+74\eta+153\eta^2+90\eta^3)\right\}, \tag{18}$$

where

$$\begin{aligned}\Phi=\gamma&\left\{2\eta_0(4+20\eta+30\eta^2+13\eta^3)+\eta(16+76\eta+108\eta^2+45\eta^3)\right\}\\ &-6\left\{\eta_0^2(4+20\eta+30\eta^2+13\eta^3)+2\eta_0(12+172\eta+406\eta^2+282\eta^3+45\eta^4)\right.\\ &\left.\qquad+12\eta(4+46\eta+90\eta^2+45\eta^3)\right\},\end{aligned} \tag{19}$$

$$\eta=\frac{E'I'l}{EIl'},\quad \eta_0=\frac{E_0I_0}{EI},\quad \gamma=\frac{(m_0+6m)\,p^2l^3}{EI}. \tag{20}$$

$\Phi=0$ is the frequency equation of the natural vibration.

The foregoing results may be obtained by the slope-deflection method, namely, if the deflections, slopes, shearing forces, and bending moments at the two ends of a member of span l and stiffness EI be u_A, u_B, θ_A, θ_B, F_A, F_B, M_A, M_B respectively, then the resultant of the moments at every panel point is zero and the resultant shearing forces for all the columns on that floor are equal to the sum of the (horizontal) inertia forces at all the panel points. The mathematical conditions are as follows:

$$M_A=\frac{2EI}{l}\left\{2\theta_A+\theta_B+\frac{3(u_A-u_B)}{l}\right\},\quad M_B=\frac{2EI}{l}\left\{\theta_A+2\theta_B+\frac{3(u_A-u_B)}{l}\right\},$$

$$-F_A=F_B=-\frac{6EI}{l^2}\left\{\theta_A+\theta_B+\frac{2(u_A-u_B)}{l}\right\},$$

$$\begin{aligned}&\textstyle\sum M \text{ at every panel point } =0\ ,\\ &\textstyle\sum F \text{ for all columns } =P.\end{aligned} \tag{21}$$

The bending moments, shearing force, and inertia at every panel point are expressed by

$$\left.\begin{aligned}\text{I}:\quad &M_1=\frac{2E_0I_0}{l}\left(2\theta_1-\frac{3u_1}{l}+\frac{3b}{l}\right),\quad M_1'=M_1''=\frac{2E'I'}{l'}(2\theta_1+\theta_2),\\ &-F_1=-\frac{6E_0I_0}{l^2}\left(\theta_1-\frac{2u_1}{l}+\frac{2b}{l}\right),\quad P=-m\,p^2u_1,\end{aligned}\right\} \tag{22}$$

$$\left.\begin{aligned}\text{II}:\quad &M_2=\frac{2EI}{l}\left(2\theta_2-\frac{2u_2}{l}+\frac{3b}{l}\right),\quad M_2'=\frac{2E'I'}{l'}(\theta_1+2\theta_2),\\ &M_2''=\frac{2E'I'}{l'}(2\theta_2+\theta_3),\\ &-F_2=-\frac{6EI}{l^2}\left(\theta_2-\frac{2u_2}{l}+\frac{2b}{l}\right),\quad P=-mp^2u_2,\end{aligned}\right\} \tag{23}$$

$$\left.\begin{aligned}\text{III}:\quad &M_3=\frac{2EI}{l}\left(2\theta_3-\frac{3u_3}{l}+\frac{3b}{l}\right),\quad M_3'=\frac{2E'I'}{l'}(\theta_2+2\theta_3),\\ &M_3''=\frac{2E'I'}{l'}(2\theta_3+\theta_4),\end{aligned}\right\} \tag{24}$$

$$\left.\begin{aligned}&-F_3=-\frac{6EI}{l^2}\left(\theta_3-\frac{2u_3}{l}+\frac{2b}{l}\right),\quad P=-mp^2u_3,\\[2ex]\text{VI:}\quad &M_4=\frac{2EI}{l}\left(2\theta_4-\frac{2u_4}{l}+\frac{3b}{l}\right),\quad M'_4=\frac{2E'I'}{l'}(\theta_3+2\theta_4),\\&-F_4=-\frac{6EI}{l^2}\left(\theta_4-\frac{2u_4}{l}+\frac{2b}{l}\right),\quad P=-mp^2u_4.\end{aligned}\right\}\tag{25}$$

From the conditions (22) ~ (25) and the relations

$$\left.\begin{aligned}&\sum M \text{ at every panel point }=0,\quad \sum F \text{ for all columns }=\sum P,\\&u_1=u_2=u_3=u_4,\end{aligned}\right\}\tag{26}$$

we get the same solutions as in (18)—(19).

As examples, we shall take four cases of $E'I'/EI$, namely, $E'I'/EI=0$, 1, 10, and ∞. The vibrational frequencies of every case for different ratios of E_0I_0/EI are shown in Fig. 2. From this figure it will be seen that for every case of floor stiffness, a small increase in stiffness in the extra-thick column fairly increases the natural frequency of the building. The same figure also shows that in the case of extremely large stiffness of the thick column, considerable increase in floor stiffness is not yet sufficient for the building to acquire a sensible increase in its natural vibrations. This shows also how efficiently the thick column serves in rendering a house rigid. It is well-known that, other conditions being the same, increase in natural frequency affords good resistance to seismic vibrations in every condition (except the resonance condition) and also to wind forces. The damping forces (except dissipation) usually increase with increase in the natural frequency of a structure.

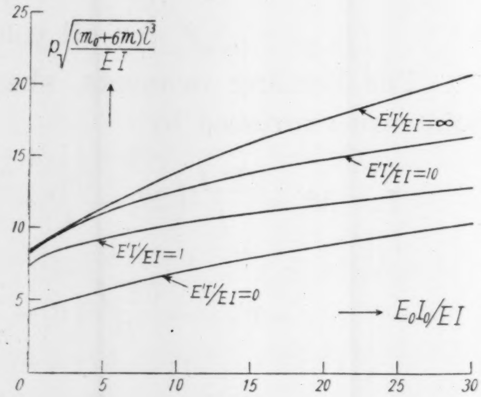

Fig. 2.

We shall next ascertain the amplitudes of the floor (roof) for different vibrational frequencies, including the resonance condition. Since in the present case no damping nor dissipative property is taken into account, it is impossible to obtain the general features of the problem resulting from the structure thus stiffened; it still shows that the more the house is stiffened the greater the increase of such a range of frequencies that the amplitudes of the floor (roof) are not specially large (see Figs. 3, 4, 5, 6).

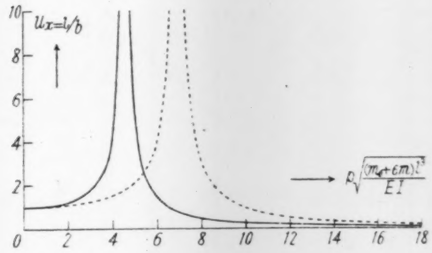

Fig. 3. $E'I'/EI=0$. Full and broken lines represent $E_0I_0/EI=1$, 10 respectively.

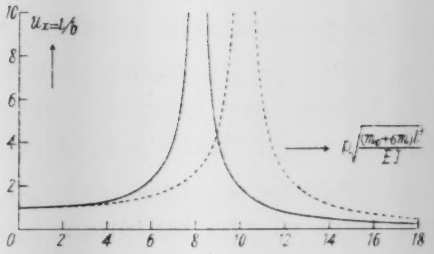

Fig. 4. $E'I'/EI=1$. Full and broken lines represent $E_0I_0/EI=1$, 10 respectively.

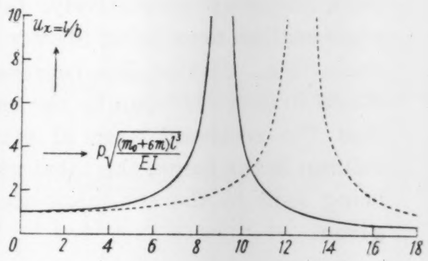

Fig. 5. $E'I'/EI=10$. Full and broken lines represent $E_0I_0/EI=1$, 10 respectively.

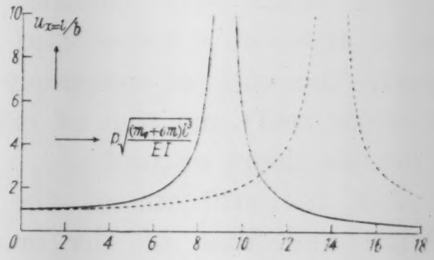

Fig. 6. $E'I'/EI=\infty$. Full and broken lines represent $E_0I_0/EI=1$, 10 respectively.

With a view to ascertaining the extent to which the stresses in columns are reduced by the addition of the extra-thick column, we shall let the abscissa of Fig. 7 represent the ratio of the diameter (z_0) of the thick column to that (z) of the ordinary columns. With increase in diameter of the thick-column, the stresses in the ordinary columns enormously diminish, and even the stress in the thick column itself (for the range $E_0I_0/EI>1$) also decreases. In these conditions, owing to the larger diameter of the thick column, the total area (a_0+6a) of cross sections of all the columns gradually increases, as shown by the chain-line in the figure. If we increase the area of every column without any special increase in the area of the thick column, the stresses in every column then decrease in the manner shown by the dotted line in the figure. The stresses in this condition are much greater than the stresses in the ordinary columns, and still somewhat higher than that in the thick column in the case just mentioned.

In an actual case, if the thick column were of some material other than wood say steel, in built-up form or in reinforced concrete, the stresses in the thick column would not necessarily be small; the aseismic properties of the thick column would then be particularly marked at the same time. It is highly commended that hotels and similar house of Japanese style have special columns (steel-framed, if possible) in some inner part of the building.

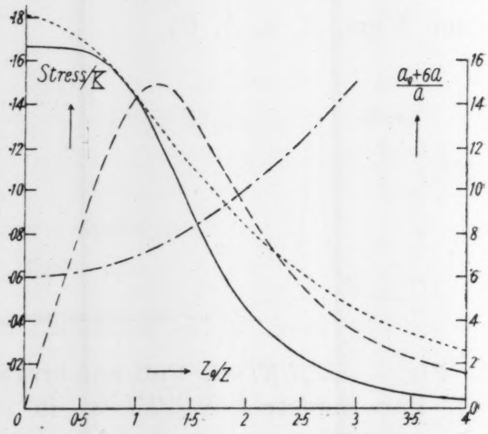

Fig. 7. Full and broken lines represent stresses in ordinary and thick columns respectively, total cross section area being shown by chain line. Dotted line represent stress in every column in the case that the sectional area of every column is the same, the total area being kept in the condition above given.

3. *Special cases of a two-storied buildings, the problem being two-dimensional.*

We shall next consider some special cases of a two-storied house, namely the case of extremely rigid floors (or roof) and that of extremely flexible floors or roof.

Let the stiffness of the thick column and that of the oridinary columns below the first floor and those below the roof be E_0I_0, EI; $E_0'I_0'$, $E'I'$ respectively. Let also the masses concentrated on the panel points corresponding to the tops of the respective columns just mentioned be m_0, m; m_0', m' respectively. If the deflections of the thick column and the oridinary columns, below the first floor and below the roof are u_1; u_2, ……, u_7; u_1'; u_2', ……, u_7', then the expressions for the vibrations of columns have the same forms as those in (1), and the boundary conditions are such that, s being 1, 2, ……, 7,

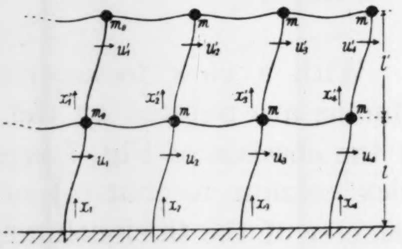

Fig. 8.

$$x_s=0; \qquad u_s=b\cos pt, \quad \frac{\partial u_s}{\partial x_s}=0, \qquad (27),\ (28)$$

$$x_s=l,\ x_s'=0; \qquad u_s=u_s', \quad u_1=u_2=\cdots\cdots=u_s=\cdots\cdots=u_7, \qquad (29),\ (30)$$

$$-\left\{E_0I_0\frac{\partial^3 u_1}{\partial x_1^3}+2EI\left(\frac{\partial^3 u_2}{\partial x_2^3}+\frac{\partial^3 u_3}{\partial x_3^3}+\frac{\partial^3 u_4}{\partial x_4^3}\right)\right\}$$

$$+\left\{E_0'I_0'\frac{\partial^3 u_1'}{\partial x_1'^3}+2E'I'\left(\frac{\partial^3 u_2'}{\partial x_2'^3}+\frac{\partial^3 u_3'}{\partial x_3'^3}+\frac{\partial^3 u_4'}{\partial x_4'^3}\right)\right\}-(m_0+6m)p^2u_1=0, \qquad (31)$$

$$\left.\begin{aligned}&\frac{\partial u_s}{\partial x_s}=\frac{\partial u'_s}{\partial x'_s}=0 \text{ for the case of extremely rigid floors,}\\ &\frac{\partial u_s}{\partial x_s}=\frac{\partial u'_s}{\partial x'_s}, \quad EI\frac{\partial^2 u_s}{\partial x_s^2}=E'I'\frac{\partial^2 u'_s}{\partial x'^2_s}\\ &\qquad\qquad \text{for the case of extremely flexible floors,}\end{aligned}\right\} \quad (32),\ (33)$$

$$x'_1=l'; \qquad u'_1=u'_2=\cdots\cdots=u'_s=\cdots\cdots=u'_7, \tag{34}$$

$$-\left\{E'_0I'_0\frac{\partial^3 u'_1}{\partial x'^3_1}+2E'I'\left(\frac{\partial^3 u'_2}{\partial x'^3_2}+\frac{\partial^3 u'_3}{\partial x'^3_3}+\frac{\partial^3 u'_4}{\partial x'^3_4}\right)\right\}-(m'_0+6m')p^2u'_1=0, \tag{35}$$

$$\left.\begin{aligned}&\frac{\partial u'_s}{\partial x'_s}=0 \text{ for the case of extremely rigid floors,}\\ &E'I'\frac{\partial^2 u'_s}{\partial x'^2_s}=0 \text{ for the case of extremely flexible floors.}\end{aligned}\right\} \tag{36}$$

Substituting expressions of types (1) in (27) ~ (36), we get
(i) for the case of extremely rigid floors,

$$\begin{aligned}u=be^{ipt}\Bigg\{1-\frac{1}{\Phi}\Big[\xi^3\gamma_1\Big\{\gamma_2-12(\eta_4+6)\Big\}\\ -12\gamma_2(\eta_2+6\eta_3)\Big]\Big\{3\Big(\frac{x}{l}\Big)^2-2\Big(\frac{x}{l}\Big)^3\Big\}\Bigg\},\\ u'=be^{ipt}\Bigg\{1-\frac{1}{\Phi}\Big[\xi^3\gamma_1\Big\{\gamma_2-12(\eta_4+6)\Big\}-12\gamma_2(\eta_2+6\eta_3)\Big]\\ +\frac{12}{\Phi}\xi^3\gamma_2(\eta_1+6)\Big\{3\Big(\frac{x'}{l'}\Big)^3-2\Big(\frac{x'}{l'}\Big)^3\Big\}\Bigg\},\end{aligned} \tag{37}$$

where

$$\Phi=\xi^3\Big\{\gamma_1-12(\eta_1+6)\Big\}\Big\{\gamma_2-12(\eta_4+6)\Big\}-12\gamma_2(\eta_2+6\eta_3), \tag{38}$$

$$\begin{gathered}\eta_1=\frac{E_0I_0}{EI}, \quad \eta_2=\frac{E'_0I'_0}{EI}, \quad \eta_3=\frac{E'I'}{EI}, \quad \eta_4=\frac{E'_0I'_0}{E'I'},\\ \gamma_1=\frac{(m_0+6m)p^2l^3}{EI}, \quad \gamma_2=\frac{(m'_0+6m')p^2l'^3}{E'I'}, \quad \xi=\frac{l'}{l},\end{gathered} \tag{39}$$

$\Phi=0$ being the frequency equation of natural vibrations;
(ii) for the case of extremely flexible floors,

$$
\begin{aligned}
u = be^{ipt}\Bigg\{ 1 + 3\xi\Big[& \xi^2\gamma_1\gamma_2(3\eta_3+2\xi) - 6\gamma_1(\eta_4+6) \\
& - 6\eta_3\gamma_2\Big\{\xi(\eta_1+6) + (\eta_4+6)\Big\}\Big]\frac{1}{\Phi}\left(\frac{x}{l}\right)^2 \\
& + 2\xi\Big[3\eta_3\gamma_2(\eta_4+6) + 3\gamma_1(\eta_4+6) - \xi^2\gamma_1\gamma_2(3\eta_3+\xi)\Big]\frac{1}{\Phi}\left(\frac{x}{l}\right)^3\Bigg\}, \\
u' = be^{ipt}\Bigg\{ 1 + \frac{\xi}{\Phi}\Big[& \xi^2\gamma_1\gamma_2(3\eta_3+4\xi) - 12\gamma_1(\eta_4+6) \\
& - 6\eta_3\gamma_2\Big\{3\xi(\eta_1+6) + 2(\eta_4+6)\Big\}\Big] + 6\xi^2\Big[\xi^3\gamma_1\gamma_2 - 3\gamma_1(\eta_4+6) \\
& - 3\eta_3\gamma_2\Big\{2\xi(\eta_1+6) + (\eta_4+6)\Big\}\Big]\frac{1}{\Phi}\left(\frac{x'}{l'}\right) \\
& - 9\xi^4\gamma_2\Big\{\xi\gamma_1 + 2(\eta_1+6)\Big\}\frac{1}{\Phi}\left(\frac{x'}{l'}\right)^2 + 3\xi^4\gamma_2\Big\{\xi\gamma_1 + 2(\eta_1+6)\Big\}\frac{1}{\Phi}\left(\frac{x'}{l'}\right)^3\Bigg\},
\end{aligned}
\tag{40}
$$

where

$$
\begin{aligned}
\Phi = & \Big\{\xi\gamma_1 + 2(\eta_4+6)\Big\}\Big[18(\eta_4+6) - 3\xi\gamma_2\Big\{\eta_3(1+3\xi) + 2\xi^2\Big\}\Big] \\
& - \Big[6(\eta_4+6) - \xi\gamma_2\Big\{3\eta_3(1+2\xi) + 2\xi^2\Big\}\Big]\Big[\xi\Big\{6(\eta_1+6) + \gamma_1\Big\} + 6(\eta_4+6)\Big],
\end{aligned}
\tag{41}
$$

$$
\eta_1 = \frac{E_0I_0}{EI}, \quad \eta_2 = \frac{E_0'I_0'}{EI}, \quad \eta_3 = \frac{E'I'}{EI}, \quad \eta_4 = \frac{E_0'I_0'}{E'I'},
$$

$$
\gamma_1 = \frac{(m_0+6m)p^2l^3}{EI}, \quad \gamma_2 = \frac{(m_0'+6m')\,p^2l'^3}{E'I'}, \quad \xi = \frac{l'}{l}. \tag{42}
$$

In the special condition wherein $\xi=1$, $\eta_1=\eta_2=\eta_4\equiv\eta$, $\eta_3=1$, $\gamma_1=\gamma_2\equiv\gamma$, we get the frequency equations (i), (ii) below.

(i) $$\gamma^2 - 36\gamma(\eta+6) + 144(\eta+6)^2 = 0,$$

so that $$\gamma = (\eta+6)[4{\cdot}584,\ 31{\cdot}416], \tag{43}$$

(ii) $$7\gamma^2 - 108(\eta+6)\gamma + 36(\eta+6)^2 = 0,$$

so that $$\gamma = (\eta+6)[0{\cdot}341,\ 15{\cdot}088]. \tag{44}$$

The results of calculations for various ratios of E_0I_0/EI are shown in Fig. 9. It will be seen that, even in the case of a two-storied house, the presence of a thick-column increases the vibrational frequency of that house. Although the absolute frequencies of the fundamental vibrations are very low compared with those in the case of a one-storied house, the rate of increase in frequency with increase in the stiffness of the thick column is the same as that in the one-storied house under consideration.

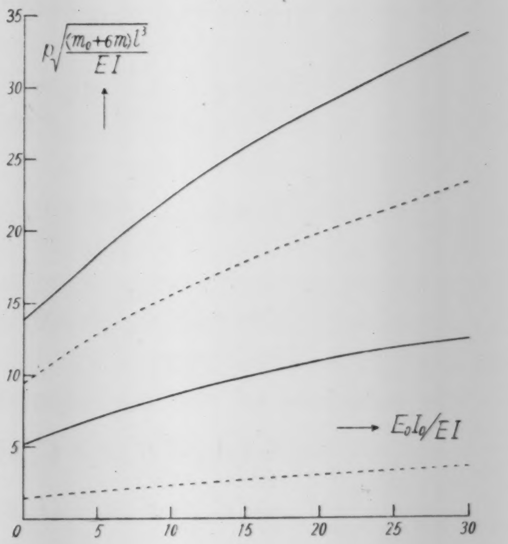

Fig. 9. Full and broken lines represent the cases of rigid floors and flexible floors respectively. There are two vibrational frequencies (fundamental and second) in every case.

4. *The problem of a space-latticed framed structure (solid Rahmen) in connection with an extra thick column.*

It is well known that the problem of space-latticed framed structure is extremely difficult. Although Reissner,[2] Prager,[3] Ban,[4] Takimoto,[5] Waltking,[6] Hohenemser,[7] Reinitzhuber,[8] and others have studied this problem, there seems little chance of their results being are used in the case of vibration problems, whereas in some cases it is even impossible to apply them to practical cases. Notwithstanding the complexity of the problem, since the principle of its dynamical conditions is rather simple, we shall discuss the problem from the elementary stage of its treatment.

Referring to Fig. 10, inertia masses, m_0, m, m, m, are concentrated at panel points, $0_1'$, $0_2'$, $0_3'$, $0_4'$. The bending stiffnesses and the torsional stiffnesses of the members $0_10_1'$; $0_20_2'$, $0_30_3'$, $0_40_4'$; $0_1'0_2'$, $0_2'0_3'$, $0_3'0_4'$, $0_4'0_1'$ are E_0I_0, EI, $E'I'$ respectively.

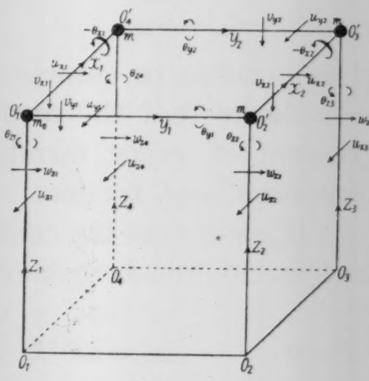

Fig. 10.

---

[2] H. REISSNER, *Zeits. Bauwesen*, **8** (1903), 135~162.

[3] W. PRAGER, *Z. techn. Phys.*, **10** (1929), 275~280.

[4] S. BAN, *Jour. Arch., Japan*, **44** (1930), 75~118.

[5] G. TAKIMOTO, *ditto*, **45** (1931), 743~771.

[6] F. W. WALTKING, *Ing. Arch.*, **2** (1931), 247~274.

[7] K. HOHENEMSER und W. PRAGER, *Dynamik d. Stabwerke* (Berlin, 1933).

[8] REINITZHUBER, *Ing. Arch.*, **8** (1937) 349~363.

Since the vibratory equations of every member in bending as well as in torsion are of the types

$$\left.\begin{array}{llll} \dfrac{\partial^4 u_{zs}}{\partial z_s^4}=0, & \dfrac{\partial^4 w_{zs}}{\partial z_s^4}=0, & \dfrac{\partial^2 \theta_{zs}}{\partial z_s^2}=0, & [s=1,\ 2,\ 3,\ 4] \\[2ex] \dfrac{\partial^4 u_{ys}}{\partial y_s^4}=0, & \dfrac{\partial^4 v_{ys}}{\partial y_s^4}=0, & \dfrac{\partial^2 \theta_{ys}}{\partial y_s^2}=0, & [s=1,\ 2] \\[2ex] \dfrac{\partial^4 u_{xs}}{\partial x_s^4}=0, & \dfrac{\partial^4 v_{xs}}{\partial x_s^4}=0, & \dfrac{\partial^2 \theta_{xs}}{\partial x_s^2}=0, & [s=1,\ 2] \end{array}\right\} \qquad (45)$$

the solutions of the corresponding equations have the forms

$$\left.\begin{array}{l} u_{zs}=(A_{zs}+B_{zs}z_s+C_{zs}z_s^2+D_{zs}z_s^3)e^{ipt}, \\ w_{zs}=(E_{zs}+F_{zs}z_s+G_{zs}z_s^2+H_{zs}z_s^3)e^{ipt}, \\ \theta_{zs}=\alpha_{zs}+\beta_{zs}z_s, \end{array}\right\} [s=1,\ 2,\ 3,\ 4] \qquad (46)$$

$$\left.\begin{array}{l} u_{ys}=(A_{ys}+B_{ys}y_s+C_{ys}y_s^2+D_{ys}y_s^3)e^{ipt}, \\ v_{ys}=(P_{ys}+Q_{ys}y_s+R_{ys}y_s^2+S_{ys}y_s^3)e^{ipt}, \\ \theta_{ys}=\alpha_{ys}+\beta_{ys}y_s, \end{array}\right\} [s=1,\ 2] \qquad (47)$$

$$\left.\begin{array}{l} u_{xs}=(A_{xs}+B_{xs}x_s+C_{xs}x_s^2+D_{xs}x_s^3)e^{ipt}, \\ v_{xs}=(P_{xs}+Q_{xs}x_s+R_{xs}x_s^2+S_{xs}x_s^3)e^{ipt}, \\ \theta_{xs}=\alpha_{xs}+\beta_{xs}x_s. \end{array}\right\} [s=1,\ 2] \qquad (48)$$

It is possible to assume that the lengthwise stiffness of every member is so large that the member cannot elongate or contract. The possible freedom of every member is therefore bendings in two perpendicular directions, and torsion.

If we choose the components of displacements in the senses as shown in Fig. 10, the boundary conditions assume the forms

$$z_s=0; \qquad u_{zs}=ae^{ipt}, \quad w_{zs}=be^{ipt}, \quad \frac{du_{zs}}{dz_s}=0, \quad \frac{dw_{zs}}{dz_s}=0, \quad \theta_{zs}=0,$$

$$[s=1,\ 2,\ 3,\ 4] \quad (49),\ (50),\ (51),\ (52)$$

$$z_1=l,\ y_1=0,\ x_1=0; \qquad v_{y_1}=0, \quad v_{x_1}=0, \quad u_{z_1}=u_{y_1}, \quad w_{z_1}=u_{x_1},$$

$$(53),\ (54),\ (55),\ (56)$$

$$\frac{dw_{z_1}}{dz_1}=\frac{dv_{y_1}}{dv_1}=\theta_{x_1}, \quad \frac{du_{y_1}}{dy_1}=\frac{du_{x_1}}{dx_1}=-\theta_{z_1}, \quad -\frac{dv_{x_1}}{dx_1}=\frac{du_{z_1}}{dz_1}=\theta_{y_1},$$

$$(57),\ (58),\ (59)$$

$$-E_0I_0\frac{d^2w_{z_1}}{dz_1^2}+E'I'\frac{d^2v_{y_1}}{dy_1^2}+G'J'\frac{d\theta_{x_1}}{dx_1}=0, \tag{60}$$

$$E'I'\frac{d^2u_{y_1}}{dy_1^2}+E'I'\frac{d^2u_{x_1}}{dx_1^2}+G_0J_0\frac{d\theta_{z_1}}{dz_1}=0, \tag{61}$$

$$-E'I'\frac{d^2v_{x_1}}{dx_1^2}-E_0I_0\frac{d^2u_{z_1}}{dz_1^2}+G'J'\frac{d\theta_{y_1}}{dy_1}=0, \tag{62}$$

$z_2=l,\ y_1=l',\ x_2=0;\qquad v_{y_1}=0,\quad v_{x_2}=0,\quad u_{z_2}=u_{y_1},\quad w_{z_2}=u_{x_2},$
(63), (64), (65), (66)

$$\frac{dw_{z_2}}{dz_2}=\frac{dv_{y_1}}{dy_1}=\theta_{x_2},\quad \frac{du_{y_1}}{dy_1}=\frac{du_{x_2}}{dx_2}=-\theta_{z_2},\quad -\frac{dv_{x_2}}{dx_2}=\frac{du_{z_2}}{dz_2}=\theta_{y_1},$$
(67), (68), (69)

$$-EI\frac{d^2w_{z_2}}{dz_2^2}-E'I'\frac{d^2v_{y_1}}{dy_1^2}+G'J'\frac{d\theta_{x_2}}{dx_2}=0, \tag{70}$$

$$-E'I'\frac{d^2u_{y_1}}{dy_1^2}+E'I'\frac{d^2u_{x_2}}{dx_2^2}+GJ\frac{d\theta_{z_2}}{dz_2}=0, \tag{71}$$

$$E'I'\frac{d^2v_{x_2}}{dx_2^2}+EI\frac{d^2u_{z_2}}{dz_2^2}+G'J'\frac{d\theta_{y_1}}{dy_1}=0, \tag{72}$$

$z_3=l,\ y_2=l',\ x_2=l';\qquad v_{y_2}=0,\quad v_{x_2}=0,\quad u_{z_3}=u_{y_2},\quad w_{z_3}=u_{x_2},$
(73), (74), (75), (76)

$$\frac{dw_{z_3}}{dz_3}=\frac{dv_{y_2}}{dy_2}=\theta_{x_2},\quad \frac{du_{y_2}}{dy_2}=\frac{du_{x_2}}{dx_2}=-\theta_{z_3},\quad -\frac{dv_{x_2}}{dx_2}=\frac{du_{z_3}}{dz_3}=\theta_{y_2},$$
(77), (78), (79)

$$EI\frac{d^2w_{z_3}}{dz_3^2}+E'I'\frac{d^2v_{y_2}}{dy_2^2}+G'J'\frac{d\theta_{x_2}}{dx_2}=0, \tag{80}$$

$$-E'I'\frac{d^2u_{y_2}}{dy_2^2}-E'I'\frac{d^2u_{x_2}}{dx_2^2}+GJ\frac{d\theta_{z_3}}{dz_3}=0, \tag{81}$$

$$-E'I'\frac{d^2v_{x_2}}{dx_2^2}+EI\frac{d^2u_{z_3}}{dz_3^2}+G'J'\frac{d\theta_{y_2}}{dy_2}=0, \tag{82}$$

$z_4=l,\ y_2=0,\ x_1=l';\qquad v_{y_2}=0,\quad v_{x_1}=0,\quad u_{z_4}=u_{y_2},\quad w_{z_4}=u_{x_1},$
(83), (84), (85), (86)

$$\frac{dw_{z_4}}{dz_4}=\frac{dv_{y_2}}{dy_2}=\theta_{x_1},\quad \frac{du_{y_2}}{dy_2}=\frac{du_{x_1}}{dx_1}=-\theta_{z_4},\quad -\frac{dv_{x_1}}{dx_1}=\frac{du_{z_4}}{dz_4}=\theta_{y_2}, \qquad (87),\ (88),\ (89)$$

$$EI\frac{d^2w_{z_4}}{dz_4^2}-E'I'\frac{d^2v_{y_2}}{dy_2^2}+G'J'\frac{d\theta_{x_1}}{dx_1}=0, \qquad (90)$$

$$E'I'\frac{d^2u_{y_2}}{dy_2^2}-E'I'\frac{d^2u_{x_1}}{dx_1^2}+GJ\frac{d\theta_{z_4}}{dz_4}=0, \qquad (91)$$

$$E'I'\frac{d^2v_{x_1}}{dx_1^2}-EI\frac{d^2u_{z_4}}{dz_4^2}+G'J'\frac{d\theta_{y_2}}{dy_2}=0, \qquad (92)$$

$$z_1=z_4=l,\ y_1=y_2=0; \qquad u_{z_1}=u_{z_4}, \qquad (93)$$

$$-E_0I_0\frac{d^3u_{z_1}}{dz_1^3}-EI\frac{d^3u_{z_4}}{dz_4^3}+E'I'\frac{d^3u_{y_1}}{dy_1^3}+E'I'\frac{d^3u_{y_2}}{dy_2^3}=m_0p^2u_{z_1}+mp^2u_{z_4}, \qquad (94)$$

$$z_2=z_3=l,\ y_1=y_2=l; \qquad u_{z_2}=u_{z_3}, \qquad (95)$$

$$-EI\frac{d^3u_{z_2}}{dz_2^3}-EI\frac{d^3u_{z_3}}{dz_3^3}-E'I'\frac{d^3u_{y}}{dy_1^3}-E'I'\frac{d^3u_{y_2}}{dy_2^3}=mp^2u_{z_2}+mp^2u_{z_3}, \qquad (96)$$

$$z_1=z_2=l,\ x_1=x_2=0; \qquad w_{z_1}=w_{z_2}, \qquad (97)$$

$$-E_0I_0\frac{d^3w_{z_1}}{dz_1^3}-EI\frac{d^3w_{z_2}}{dz_2^3}+E'I'\frac{d^3u_{x_1}}{dx_1^3}+E'I'\frac{d^3u_{x_2}}{dx_2^3}=m_0p^2w_{z_1}+mp^2w_{z_2}, \qquad (98)$$

$$z_3=z_4=l,\ x_1=x_2=l; \qquad w_{z_3}=w_{z_4}, \qquad (99)$$

$$-EI\frac{d^3w_{z_3}}{dz_3^3}-EI\frac{d^3w_{z_4}}{dz_4^3}-E'I'\frac{d^3u_{x_1}}{dx_1^3}-E'I'\frac{d^3u_{x_2}}{dx_2^3}=mp^2w_{z_3}+mp^2w_{z_4}. \qquad (100)$$

Substituting (49) ~ (100) in (46) ~ (48), and eliminating constants, it is possible to get the frequency equations, and then to find the expressions of the displacements of every member. There are, however, 80 constants to be determined. We shall eliminate 63 of these constants, when the following 17 relations then hold. Although it is possible to eliminate more constants and thus reduce the number of the relations even down to 4, since the resulting relations take very complex forms, nothing is gained by doing so.

$$(6\eta+2\zeta_1)X-2\eta Y+2\eta l'^3D_{x_2}+(6\eta+\zeta_1)l'^3D_{y_2}-(4\eta+\zeta_1)l'B_{y_2}=0, \qquad (101)$$

$$2\eta X-2(3\eta+\zeta_0)Y-(6\eta+\zeta_0)l'^3D_{x_1}-2\eta l'^3D_{y_1}+(4\eta+\zeta_0)l'B_{y_2}=0, \qquad (102)$$

$$2\eta X+2(\eta+\zeta_0)Y+(5\eta+\zeta_0)l'^3D_{x_1}-\eta l'^3D_{x_2}+3\eta l'^3D_{y_1}$$

$$+\eta l'^3 D_{y_2} - (4\eta+\zeta_0) l' B_{y_2} = 0, \qquad (103)$$

$$2(2\eta+\zeta_1)X - 2(2\eta+\zeta_0+\zeta_1)Y - (4\eta+\zeta_0)l'^3 D_{x_1} - (4\eta+\zeta_1)l'^3 D_{x_2}$$
$$-6\eta l'^3 D_{y_1} + (2\eta+\zeta_1)l'^3 D_{y_2} + (\zeta_0-\zeta_1)l' B_{y_2} = 0, \qquad (104)$$

$$2\eta X + 2\eta Y - 2\eta l'^3 D_{x_1} - 2\eta l'^3 D_{y_2} - (4\eta+\zeta_1) l' B_{y_2} = 0, \qquad (105)$$

where

$$X = l^2 C_{z_3} + l^3 D_{z_3} - l^2 C_{z_4} - l^3 D_{z_4}, \quad Y = l^2 G_{z_3} + l^3 H_{z_3} - l^2 G_{z_2} - l^3 H_{z_2}, \qquad (106)$$

$$(4\eta_0+4\eta+\zeta) l D_{z_1} - \zeta l D_{z_2} - 2\zeta C_{z_3} - 2\zeta l D_{z_3} + 2(\eta_0+6\eta+\zeta) C_{z_4}$$
$$-2(\eta_0+7\eta+\zeta) l D_{z_4} = 0, \qquad (107)$$

$$2\zeta l D_{z_1} - 2(3\eta+\zeta+4) l D_{z_2} - 2(6\eta+\zeta+1) C_{z_3} - (12\eta+\zeta-2) l D_{z_3}$$
$$+2\zeta C_{z_4} + \zeta l D_{z_4} = 0, \qquad (108)$$

$$(4\eta_0+3\eta) l D_{z_1} + (3\eta+4) l D_{z_2} + (6\eta+1) C_{z_3} + (6\eta-1) l D_{z_3}$$
$$+ (2\eta_0+6\eta-1) C_{z_4} + (2\eta_0+6\eta-3) l D_{z_4} = 0, \qquad (109)$$

$$\zeta l D_{z_1} - (4\eta+\zeta+4) l D_{z_2} - 2(6\eta+\zeta+1) C_{z_3} - 2(7\eta+\zeta+1) l D_{z_3}$$
$$+2\zeta C_{z_4} + 2\zeta l D_{z_4} = 0, \qquad (110)$$

$$6\eta_0 l^3 D_{z_1} + 6 l^3 D_{z_2} + 2\gamma l^2 C_{z_3} + 2(\gamma+3) l^3 D_{z_3} + (\gamma_0+\gamma) l^2 C_{z_4}$$
$$+ (\gamma_0+\gamma+6) l^3 D_{z_4} = -a(3\gamma+\gamma_0), \qquad (111)$$

$$3 l^3 D_{z_2} + \gamma l^2 C_{z_3} + (\gamma+3) l^3 D_{z_3} + 3\eta\xi^2 l'^3 D_{y_1} + 3\eta\xi^2 l'^3 D_{y_2} = -\gamma a, \qquad (112)$$

$$3 l^3 H_{z_4} + \gamma l^2 G_{z_3} + (\gamma+3) l^3 H_{z_3} + 3\eta\xi^2 l'^3 D_{x_1} + 3\eta\xi^2 l'^3 D_{x_2} = -\gamma b, \qquad (113)$$

where

$$\left.\begin{array}{l} \eta = \dfrac{E'I'l}{EIl'}, \quad \eta_0 = \dfrac{E_0 I_0}{EI}, \quad \zeta = \dfrac{G'J'l}{EIl'}, \quad \zeta_0 = \dfrac{G_0 J_0}{EI}, \quad \zeta_1 = \dfrac{GJ}{EI}, \\ \xi = \dfrac{l}{l'}, \quad \gamma = \dfrac{mp^2 l^3}{EI}, \quad \gamma_0 = \dfrac{m_0 p^2 l^3}{EI}. \end{array}\right\} \qquad (114)$$

(I) Now, solving (101)~(105), it is possible to determine D_{x_1}, D_{x_2}, D_{y_1}, D_{y_2}, as functions of C_{z_3}, D_{z_3}, C_{z_4}, D_{z_4}, G_{z_3}, H_{z_3}, G_{z_2}, H_{z_2}.

(II) On the other hand, (107)~(111) render six relations representing D_{z_2}, C_{z_3}, D_{z_3}, C_{z_4}, D_{z_4} in terms of D_{z_1}, a.

(III) Judging from some of boundary conditions, it is possible to understand that the mutual relations between H_{z_4}, G_{z_3}, H_{z_3}, G_{z_2}, H_{z_2}, H_{z_1}, b are quite similar to those between D_{z_2}, C_{z_3}, D_{z_3}, C_{z_4}, D_{z_4}, D_{z_1}, a; from which it is very simple to represent H_{z_4}, G_{z_3}, H_{z_3}, G_{z_2}, H_{z_2} in terms of H_{z_1}, b.

Substituting three kinds of relations, (I), (II), (III), in (112), (113), we finally get mere two relations representing D_{z_1}, H_{z_1} in terms of a, b. The denominator of either one of D_{z_1} or H_{z_1} then determined corresponds to the frequency equation of the natural vibration of the structure.

Other constants can be determined from above results in successive calculations.

We shall calculate six cases, of E_0I_0/EI, namely, $E_0I_0/EI=0$, 1, 3, 10, 20, 100; the relations $m_0=m$, $l=l'$, $E'I'=EI=G'J'=GJ$, $E_0I_0=G_0J_0$ being kept costant. The frequency equations then become

(i) $E_0I_0/EI=0$; $43008\gamma^2-1567744\gamma+7709184=0$,
$43008\gamma^2-594016\gamma+1762488=0$,
(ii) $E_0I_0/EI=1$; $(13\gamma-285)^2-144^2=0$, $(5\gamma-42)^2=0$,
(iii) $E_0I_0/EI=3$; $228072\gamma^2-10549792\gamma+85605948=0$,
$228072\gamma^2-5652640\gamma+33055740=0$,
(iv) $E_0I_0/EI=10$; $(19412\gamma^2-928170\gamma+8706429)^2$
$-(197496\gamma-3265002)^2=0$,
(v) $E_0I_0/EI=20$; $(2372316\gamma^2-150533310\gamma+1649095272)^2$
$-(23429628\gamma-566649351)^2=0$,
(vi) $E_0I_0/EI=100$; $(1781136\gamma^2-326221506\gamma+5161564296)^2$
$-(16916688\gamma-1566296109)^2=0$.

There are four vibrational frequencies in every case. Although it is possible for four vibrational frequancies to exist even in Case (ii), owing to the nature of the symmetry, mere three frequencies exist in this case.

The vibrational frequencies thus found are

(i); 4·322, 5·865, 9·5, 30·63,
(ii); $\gamma=8{\cdot}4$, 8·4, 10·846, 33,
(iii); $\gamma=9{\cdot}5$, 10·5, 15·3, 35·77,
(iv); $\gamma=10{\cdot}19$, 14·03, 27·45, 43·8,
(v); $\gamma=10{\cdot}63$, 16·46, 42·97, 56·9,
(vi); $\gamma=12{\cdot}58$, 22·13, 161·1, 170·5.

The first and second frequencies of case (i), (ii), or (iii) correspond to the mode of vibration parallel to every diagonal of the square formed by the horizontal members, the third frequency to the mode of rotary vibration, and the fourth frequency to the vibration, according to which every diagonal of the square elongates and contracts alternately. In other words, for the first, second and third frequencies, the square just mentioned remains nearly in its original form, whereas for the fourth frequency at any instant is deformed into a rhombic shape.

The third and the fourth frequencies of cases (iv), (v), or (vi) roughly correspond to the third and the fourth frequencies of the first and the second of cases (i), (ii), or (iii); but, other two vibrations of cases (iv), (v), (vi) are in much more coupled conditions.

It will be seen that in the present case, the first and second frequencies are very low, regardless of whether the thick column (daikoku-basira) is very stiff or not, which arises from the condition that there is no diagonal member in the plane of the square formed by the horizontal members. It is evident that some diagonal members should be fitted within the square formed by the horizontal members to render the condition of the thick column effective. Since, in an actual problem, however, it is by no means difficult to place diagonal members in the plane of any floor, the use of the thick column in palace or hotel types of buildings is quite practicable. The mathematical solution of such a case is reserved for next study.

It is obvious that if the thick column is near the centre of the building, its aseismic properties are almost the same as those in the case of a two-dimensional problem. It appears that even in the event that the thick column is at some distance from the centre of the building, its aseismic properties are still fairly satisfactory, details of which, however, will be shown in a forthcoming paper.

5. *Concluding remarks.*

From mathematical calculations we found that the use of a principal column, that is, a daikoku-basira (extra thick column) is to be recommended in Japanese style structures of a palace or hotel style, provided that the floor and the roof are made rigid, particularly in their diagonal directions. The column need not necessarily be of wood, but may, instead, be of built-up form in steel or of reinforced concrete, the building in which case, could be as nearly wall-less.

The present investigation was made at Professor SEZAWA's suggestion in connection with his other research work as member of the Investigation Committee for Earthquake-proof Construction, of the Japan Society of the Promotion of Scientific Research, to whom I wish to express my sincerest thank for his kind advices.

Note. While the importance of this problem in connection with Japanese style buildings is admittedly great, its solution is so difficult that as many as 80 constants have to be eliminated from a like number of conditions. Dr. Kanai, in my opinion,

being the person most fitted for attacking the problem, I requested him to do so. The foregoing result, probably, is only preliminary, in which case it is hoped that the work will be continued with success.

Finally, I wish to express my warmest thanks to the Council of the Japan Society for the Promotion of Scientific Research for aid received in a series of investigation of which this is a part.

K. SEZAWA.

22. 家屋の大黒柱又は類似部の耐震的効果

地震研究所 **金井 清**

日本式の御殿風の家や旅館等では壁をなるべく用ひない方が望ましい．古い家屋に用ひられた大黒柱の考を今少しく活用する道はないものかと，この研究を試みたのである．數理的計算を試みたところが，家屋の斜の方向の剛性をよくしさへすれば，大黒柱の効果が發揮することがわかつた．但し効果といふのは材料を經濟的に考へた場合の効果であつて，全柱をそれぞれ大黒柱の如くすれば尙更よいのにきまつてをる．實際問題として大黒柱は必しも木材でなくてもよろしく，場合によつては鐵組立材又は鐵筋コンクリートで作ればー層効果がある譯である．尙この考は構造物の材料をなるべく均等に分布しようといふ工學的常識とはむしろ逆の傾向にあるのである．床面に斜材のないときの立體架構の場合を計算して見ると，大黒柱が家の隅にあり且つ斜材がない爲に極めて低い振動數の自己振動のあることがわかつた．卽ち斜材の必要な事がよく知られる．この立體架構の問題は面白いけれども甚だ複雜であり，今後も研究を續ける積りである．

註――家屋の大黒柱の問題は日本式の家屋に極めて大切なのにも拘らず，その一般的の理論計算は甚だ複雜である．之の解決には金井氏が最適任と考へて之を取扱つて貰つたのである．

只今の問題に限らずこの連續の研究には日本學術振興會の御援助に負ふ所が多く玆に厚く感謝する次第である（妹澤克惟）

23. *Relation between Gravity Anomalies and the Corresponding Subterranean Mass Distribution. (II.)*

By Chûji TSUBOI and Takato FUCHIDA.

Earthquake Research Institute.

(Read Nov. 16, 1937.—Received March 20, 1938.)

In our earlier papers[1], methods were given by means of which subterranean mass distributions could be determined "directly" from the corresponding gravity anomalies observed along the earth's surface. In developing the methods, it was assumed (1) that the mass is distributed on a single horizontal subterranean plane, and (2) that it varies in one direction only but not in direction perpendicular to it. Although several interesting distributions of gravity anomalies, such as those observed in Japan, the Dutch East Indies and in the African Rift Valleys, could be discussed by means of these "two-dimensional" methods, it is desirable to extend their scope, so that they could be applied to any "three-dimensional" distribution of gravity anomalies as well, which extension can be effected by means of the potential theory, as will presently be shown.

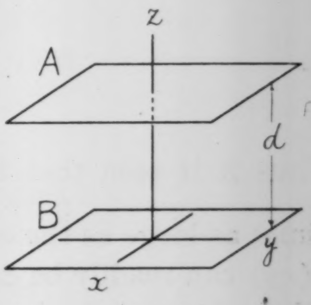

Fig. 1.

Let A in Fig. 1 be the plane of the earth's surface the gravity anomalies $\Delta g(xy)$ along which are known from point to point, and B another plane, which is at depth d from the surface, and on which are distributed surface densities $\rho(xy)$ that are responsible for these gravity anomalies. The potential of attraction U due to $\rho(xy)$ is the solution of Laplace' sequation,

$$\frac{\partial^2 U}{\partial x^2}+\frac{\partial^2 U}{\partial y^2}+\frac{\partial^2 U}{\partial z^2}=0. \tag{1}$$

which assumes the form

$$U=\sum\sum A_{mn}\genfrac{}{}{0pt}{}{\sin mx}{\cos mx}\genfrac{}{}{0pt}{}{\sin ny}{\cos ny}\,e^{-\sqrt{m^2+n^2}z}. \tag{2}$$

The boundary condition at the subterranean surface is

$$-\left(\frac{\partial U}{\partial z}\right)_{z=0}=2\pi k^2\rho(xy). \tag{3}$$

---

1) C. TSUBOI and T. FUCHIDA; *Bull. Earthq. Res. Inst.*, **15** (1937), 636; 650.

If

$$\rho(xy)=\sum\sum B_{mn}\begin{matrix}\sin mx & \sin ny\\ \cos mx & \cos ny\end{matrix}, \tag{4}$$

it follows from the boundary condition (3) that

$$\sqrt{m^2+n^2}\,A_{mn}=2\pi k^2\,B_{mn}\,. \tag{5}$$

On the other hand, we are given the gravity anomalies $\Delta g(xy)$ along the earth's surface,

$$\Delta g(xy)=\sum\sum C_{mn}\begin{matrix}\sin mx & \sin ny\\ \cos mx & \cos ny\end{matrix}. \tag{6}$$

Since

$$-\left(\frac{\partial U}{\partial z}\right)_{z=d}=\Delta g(xy)\,, \tag{7}$$

it follows that

$$\sqrt{m^2+n^2}\,A_{mn}e^{-\sqrt{m^2+n^2}\,d}=C_{mn}\,. \tag{8}$$

Combining (8) and (5), we get

$$2\pi k^2\,B_{mn}e^{-\sqrt{m^2+n^2}\,d}=C_{mn}\,, \tag{9}$$

or

$$B_{mn}=\frac{C_{mn}}{2\pi k^2}e^{\sqrt{m^2+n^2}\,d}\,. \tag{9'}$$

Thus it is seen that the Fourier coefficients of $\rho\ (xy)$ are $\dfrac{1}{2\pi k^2}e^{\sqrt{m^2+n^2}\,d}$ times as large as the corresponding ones of $\Delta g(xy)$. From these results, $\rho(xy)$ can readily be calculated from $\Delta g(xy)$, provided d is known from other data or is reasonably assumed. The procedure is to develop $\Delta g(xy)$ into a double Fourier series, then to multiply each coefficient by the corresponding $\dfrac{1}{2\pi k^2}e^{\sqrt{m^2+n^2}\,d}$ and, lastly, to sum up the new series.

If it is more convenient to solve Laplace's equation in cylindrical co-ordinates,

$$\frac{\partial^2 U}{\partial r^2}+\frac{1}{r}\frac{\partial U}{\partial r}+\frac{1}{r^2}\frac{\partial^2 U}{\partial \theta^2}+\frac{\partial^2 U}{\partial z^2}=0\,, \tag{10}$$

the solution for which is

$$U=\sum\sum A_{m\alpha}J_m(\alpha r)\begin{matrix}\sin m\theta\\ \cos m\theta\end{matrix}\;e^{-\alpha z}\,, \tag{11}$$

the boundary condition then at the subterranean surface is, as before, namely,

$$-\left(\frac{\partial U}{\partial z}\right)_{z=0}=2\pi k^2\rho\,(r\theta)\,. \tag{12}$$

If

$$\rho(r\theta)=\sum\sum B_{m\alpha}J_m(\alpha r)\,\frac{\sin m\theta}{\cos m\theta}\,, \tag{13}$$

it follows from the boundary condition (12) that

$$\alpha A_{m\alpha}=2\pi k^2\,B_{m\alpha}\,. \tag{14}$$

On the other hand, we are given the gravity anomalies $\Delta g(r\theta)$ along the earth's surface,

$$\Delta g(r\theta)=\sum\sum C_{m\alpha}J_m(\alpha r)\,\frac{\sin m\theta}{\cos m\theta}\,. \tag{15}$$

Since

$$-\left(\frac{\partial U}{\partial z}\right)_{z=d}=\Delta g(r\theta)\,, \tag{16}$$

it follows that

$$\alpha A_{m\alpha}e^{-\alpha z}=C_{m\alpha}. \tag{17}$$

Combining (17) and (14), we get

$$2\pi k^2 B_{m\alpha}e^{-\alpha z}=C_{m\alpha}\,, \tag{18}$$

or

$$B_{m\alpha}=\frac{C_{m\alpha}}{2\pi k^2}\,e^{\alpha z}\,. \tag{18'}$$

Should Laplace's equation in spherical co-ordinates

$$\frac{1}{r^2}\left\{\frac{\partial\left(r^2\dfrac{\partial U}{\partial r}\right)}{\partial r}+\frac{1}{\sin\theta}\,\frac{\partial\left(\sin\theta\dfrac{\partial U}{\partial\theta}\right)}{\partial\theta}+\frac{1}{\sin^2\theta}\,\frac{\partial^2 U}{\partial\varphi^2}\right\}=0\,, \tag{19}$$

have to be solved, the solution then takes the form

$$U=\sum\frac{(a-d)^{m+1}}{r^{m+1}}\,A_m Y_m(\mu\varphi)\,, \tag{20}$$

outside the spherical surface $r=a-d$ on which the subterranean mass is distributed, and

$$U'=\sum\frac{r^m}{(a-d)^m}\,A'_m Y_m\,(\mu\varphi), \tag{21}$$

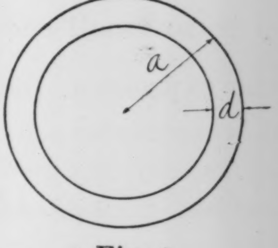

Fig. 2.

within the same surface, where μ is the cosine of co-latitude, φ, the azimuth, and Y_m, the surface spherical harmonics of m-th order. As the potential must be continuous across $r=a-d$, it must be

$$A'_m=A_m. \tag{22}$$

Another condition at $r=a-d$ is

$$-\left(\frac{\partial U}{\partial r}\right)_{a-d}+\left(\frac{\partial U'}{\partial r}\right)_{a-d}=4\pi k^2\rho\,(\mu\varphi). \tag{23}$$

If

$$\rho\,(\mu\varphi)=\sum B_m Y_m\,(\mu\varphi)\,, \tag{24}$$

it follows from the conditions (22) and (23) that

$$\sum\left\{\frac{(m+1)A_m}{a-d}Y_m(\mu\varphi)+\frac{mA_m}{a-d}Y_m(\mu\varphi)\right\}=4\pi k^2\sum B_m Y_m(\mu\varphi)\,, \tag{25}$$

or

$$\frac{2m+1}{a-d}A_m=4\pi k^2 B_m. \tag{26}$$

On the other hand, we are given the gravity anomalies along the earth's surface $r=a$,

$$\Delta g\,(\mu\varphi)=\sum C_m Y_m\,(\mu\varphi). \tag{27}$$

Since

$$-\left(\frac{\partial U}{\partial r}\right)_{r=a}=\Delta g\,(\mu\varphi)\,, \tag{28}$$

it follows that

$$\frac{(m+1)\,(a-d)^{m+1}}{a^{m+2}}A_m=C_m\,. \tag{29}$$

Combining (29) and (26), we get

$$C_m=4\pi k^2\frac{(m+1)\,(a-d)^{m+2}}{(2m+1)a^{m+2}}B_m\,, \tag{30}$$

or

$$B_m=\frac{1}{4\pi k^2}\,\frac{(2m+1)a^{m+2}}{(m+1)\,(a-d)^{m+2}}C_m\,. \tag{30'}$$

If a is so small compared with d that $\left(\frac{d}{a}\right)^2$ may be neglected against 1, the expression (30) or (30′) reduces to

$$C_m=4\pi k^2\frac{(m+1)}{(2m+1)}\left\{1-(m+2)\frac{d}{a}\right\}B_m\,, \tag{31}$$

or

$$B_m=\frac{1}{4\pi k^2}\,\frac{(2m+1)}{(m+1)}\left\{1+(m+2)\frac{d}{a}\right\}C_m. \tag{31'}$$

In all the foregoing cases, the mass has been assumed to be concentrated over a sphere of constant depth. If, as in Pratt's theory of isostasy, the mass is distributed uniformly within a thickness D, relations between B_m and C_m can be derived by means of calculations similar to the foregoing ones.

From the methods just described, the subterranean mass distribution may be determined "directly" from the corresponding gravity anomalies along the earth's surface, or the latter from the former, provided we assume that the mass is distributed over a surface of constant prescribed depth. Applications of the double Fourier or other expansions in these problems lead to the implication that the same distributions of gravity anomaly and those of subterranean mass are repeated periodically also beyond the area in which they are expressed in these expansions. Although this implication is evidently not actually the case, results obtained on this assumption do not much differ from the actual, seeing that any mass which is the difference of the actual and hypothetical periodic density distributions beyond this range will not cause any large gravity in the area in question.

In what follows, a few examples will be given of the application of the above methods. In the first example, we calculate the gravities due to the masses which, as in Fig. 3, are distributed in the form of a checkered pattern. If the area bounded by the thick lines be taken as the fundamental unit, which corresponds to 2π, then $\rho\,(xy)$ is expressed by

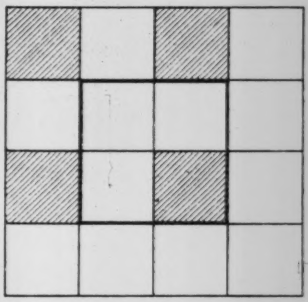

Fig. 3.

$$\rho(xy)=\sum\sum\left\{\frac{1}{2}-\frac{2}{\pi}\frac{1}{2m+1}\sin(2m+1)x\right\}$$
$$\times\left\{\frac{1}{2}-\frac{2}{\pi}\frac{1}{2n+1}\sin(2n+1)y\right\}. \tag{32}$$

If the masses are at depth π, then the gravities due to $\rho\,(xy)$ are given by

$$\Delta g(xy)=2\pi k^2\sum\sum\left\{\frac{1}{2}-\frac{2}{\pi}\frac{1}{2m+1}\sin(2m+1)x\right\}$$
$$\times\left\{\frac{1}{2}-\frac{2}{\pi}\frac{1}{2n+1}\sin(2n+1)y\right\}e^{-\sqrt{m^2+n^2}\,\pi}. \tag{33}$$

Fig. 4 shows the lines of equal $\Delta g(xy)$ within the fundamental unit calculated by means of this expression. Fig. 5 shows the lines of equal $\Delta g(xy)$ due to the rectangular mass that is placed at depth π, and which is shown by the shaded square inside it. The gravity values due to any subterranean mass that may be regarded as being composed of these small squares may be calculated by superposing the results shown in Fig. 5. Thus Fig. 6 shows the gravity values due to an L-shaped

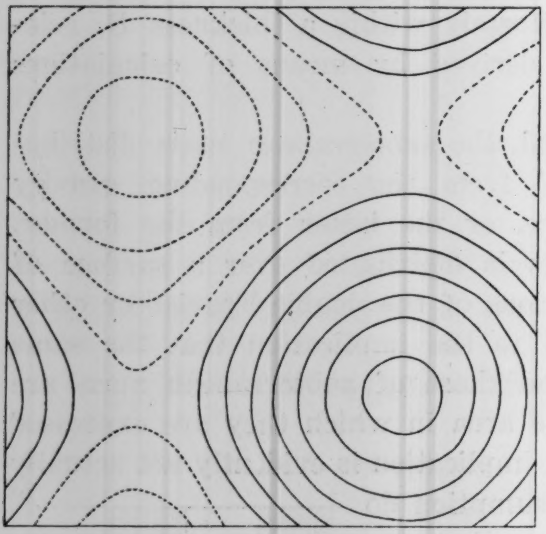

Fig. 4.

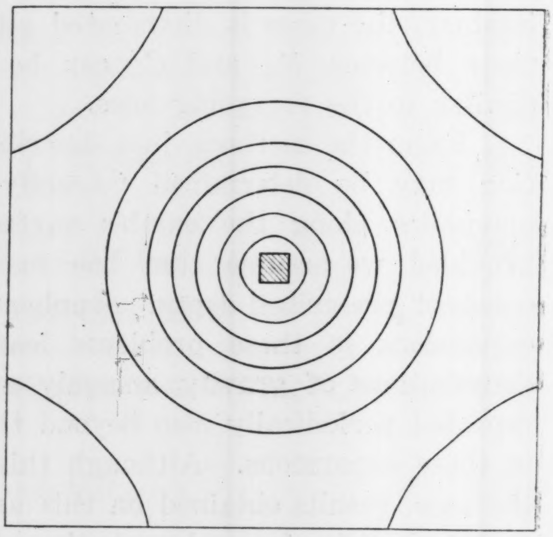

Fig. 5.

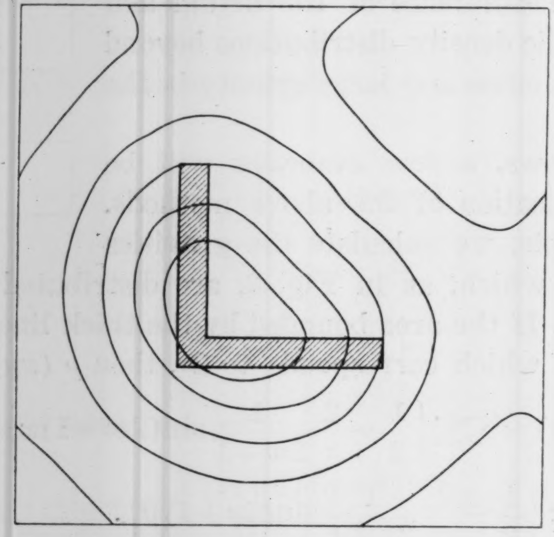

Fig. 6.

mass placed at depth π.

We might add that the following simple method is sometimes useful in finding an approximate distribution of gravity anomalies due to subterranean mass of any shape with constant density. As in Fig. 7, a plate of milk-white glass is illuminated uniformly from below and on the plate is placed a sheet of black paper, from which the shape of the mass to be studied is cut out. A photogra-

Fig. 7.

Fig. 8.

phic paper is placed at a certain distance above the glass plate. The intensity of illumination at any point on the photographic paper is proportional to $\int \frac{1}{r^2} \cos\theta \, dS$, which is also proportional to the gravity at the same point due to the mass of the same shape. Although the blackning of the photographic paper is not proportional to the illumination owing to its sensitivity characteristic, the blackning will approximately indicate the distributions of the gravity values. Fig. 9 shows the blacknings due to an L-shaped cut made on photographic papers placed at various distances above it, therefore indicating approximately the corresponding gravity values due to the mass of the same shape.

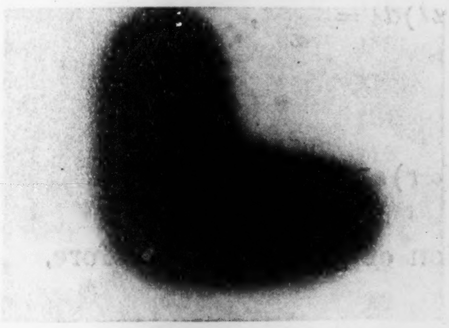
Fig. 9—a.

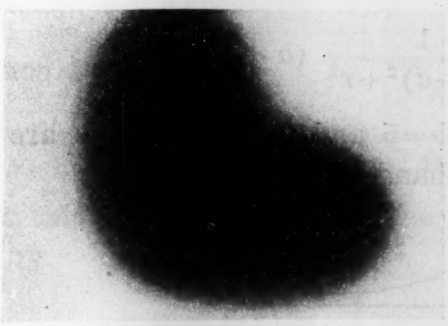
Fig. 9—b.

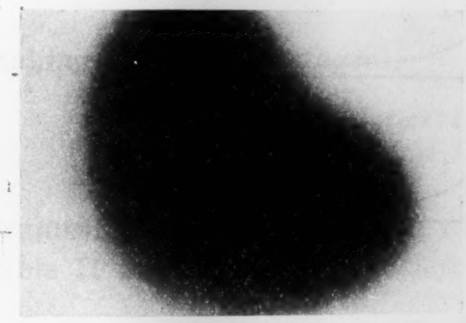
Fig. 9—c.

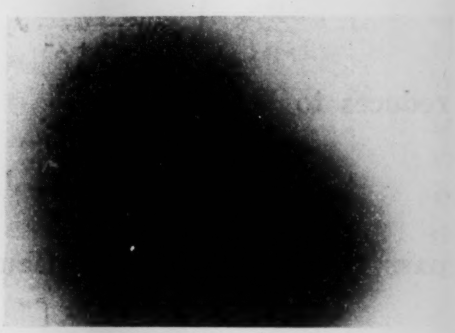
Fig. 9—d.

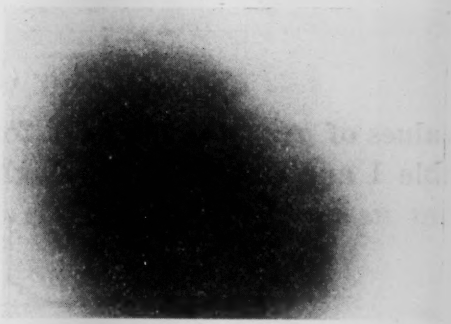
Fig. 9—e.

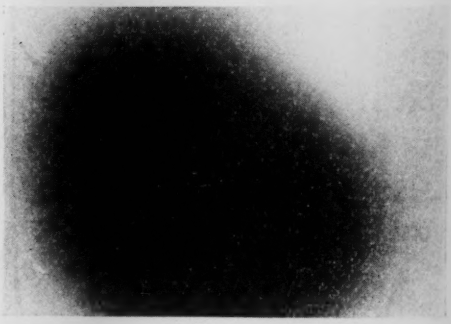
Fig. 9—f.

The next problem is to find the subterranean mass that will cause the gravity values,

$$g(r)=\frac{1}{\sqrt{b^2+r^2}}\,. \tag{34}$$

This expression can be expanded in Bessel functions namely,

$$g(r)=\int_0^\infty\int_0^\infty \frac{1}{\sqrt{b^2+\lambda^2}}J_0(\alpha r)J_0(\alpha\lambda)\,\alpha\lambda\, d\alpha d\lambda. \tag{35}$$

Since

$$\int_0^\infty \frac{\lambda}{\sqrt{b^2+\lambda^2}}J_0(\alpha\lambda)\,d\lambda=\frac{e^{-b\alpha}}{\alpha}\,, \tag{36}$$

(35) reduces to

$$g(r)=\int_0^\infty J_0(\alpha r)\,e^{-b\alpha}d\alpha. \tag{37}$$

The mass that causes this distribution of gravity is therefore,

$$\begin{aligned}\rho(r)&=\frac{1}{2\pi k^2}\int_0^\infty J_0(\alpha r)\,e^{-(b-d)\alpha}d\alpha.\\ &=\frac{1}{2\pi k^2}\,\frac{1}{\sqrt{(b-d)^2+r^2}}\ (b<d).\end{aligned} \tag{38}$$

The values of $g(r)$ and $2\pi k^2\rho(r)$ for $b=5$ and for various d's are given in Table I and plotted on the right-hand side of Fig. 10.

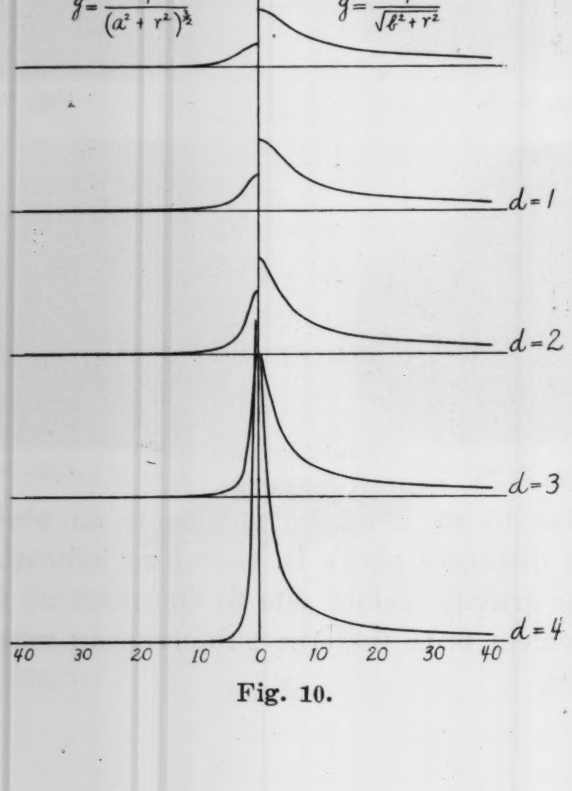

Fig. 10.

Table I.

r	$g(r)$	$2\pi k^2\rho(r)$			
		$d=1$	$d=2$	$d=3$	$d=4$
0	0·200	0·250	0·333	0·500	1·000
1	0·196	240	316	446	709
2	0·186	224	277	353	446
3	0·172	200	236	277	316
4	0·156	177	200	224	243
5	0·141	156	172	186	196
6	0·128	139	149	158	164
7	0·116	124	131	137	141
8	0·106	112	117	121	124
9	0·097	102	105	108	110
10	0·089	93	96	98	100
15	0·063	64	65	66	67
20	0·048	49	49	50	50
30	0·033	33	33	33	33
40	0·025	25	25	25	25

Should

$$g(r)=\frac{1}{(a^2+r^2)^{3/2}}, \tag{39}$$

similar calculations show that the corresponding subterranean mass is given by

$$\rho(r)=\frac{1}{2\pi k^2}\,\frac{(a-d)}{\left\{r^2+(a-d)^2\right\}^{3/2}}, \tag{40}$$

by making use of the integral,

$$\int_0^\infty \frac{J_0(\alpha\lambda)\lambda}{(a^2+\lambda^2)^{3/2}}\,\alpha\lambda=\frac{e^{-a\alpha}}{\alpha}\,. \tag{41}$$

The values of $g(r)$ and $2\pi k^2\rho(r)$ for $a=5$ and for various d's are given in Table II and plotted on the left-hand side of Fig. 10.

Table II.

r	$g(r)$	$2\pi k^2\rho(r)$			
		$d=1$	$d=2$	$d=3$	$d=4$
0	0·00800	0·01250	0·02222	0·05000	0·20000

(to be continued.)

Table II. *(Continued)*

r	$g\ (r)$	$2\pi k^2\rho(r)$			
		$d=1$	$d=2$	$d=3$	$d=4$
1	754	1144	1902	3559	7143
2	639	896	1275	1765	1780
3	505	640	787	850	634
4	382	442	480	448	286
5	283	305	303	256	151
6	210	214	199	158	89
7	157	153	136	104	43
8	119	112	97	71	38
9	92	84	70	51	27
10	72	64	53	38	20
15	25	22	17	12	6
20	11	10	8	5	3
30	4	3	2	2	1
40	2	1	1	1	1

Both deviation of the vertical and undulation of the geoid could be discussed similarly. If

$$U=\sum\sum A_{mn}\begin{matrix}\sin mx & \sin ny\\ \cos mx & \cos ny\end{matrix}\; e^{-\sqrt{m^2+n^2}\,d}, \tag{42}$$

the components of attraction in x- and y-directions are given by

$$\begin{aligned}X=-\frac{\partial U}{\partial x}&=\mp\sum\sum mA_{mn}\begin{matrix}\cos mx & \sin ny\\ \sin mx & \cos ny\end{matrix}\; e^{-\sqrt{m^2+n^2}\,d}\\ &=\mp\sum\sum 2\pi k^2\frac{m}{\sqrt{m^2+n^2}}B_{mn}\begin{matrix}\cos mx & \sin ny\\ \sin mx & \cos ny\end{matrix}\; e^{-\sqrt{m^2+n^2}\,d}\\ &=\mp\sum\sum\frac{m}{\sqrt{m^2+n^2}}C_{mn}\begin{matrix}\cos mx & \sin ny\\ \sin mx & \cos ny\end{matrix},\end{aligned} \tag{43}$$

and

$$\begin{aligned}Y=-\frac{\partial U}{\partial y}&=\mp\sum\sum nA_{mn}\begin{matrix}\sin mx & \cos ny\\ \cos mx & \sin ny\end{matrix}\; e^{-\sqrt{m^2+n^2}\,d}\\ &=\mp\sum\sum 2\pi k^2\frac{n}{\sqrt{m^2+n^2}}B_{mn}\begin{matrix}\sin mx & \cos ny\\ \cos mx & \sin ny\end{matrix}\; e^{-\sqrt{m^2+n^2}\,d}\\ &=\mp\sum\sum\frac{n}{\sqrt{m^2+n^2}}C_{mn}\begin{matrix}\sin mx & \cos ny\\ \cos mx & \sin ny\end{matrix}.\end{aligned} \tag{44}$$

The deviation of the vertical is therefore,

$$\theta_x=\frac{X}{g}=\mp\sum\sum\frac{2\pi k^2}{g}\frac{m}{\sqrt{m^2+n^2}}B_{mn}\begin{matrix}\cos mx\ \sin ny\\ \sin mx\ \cos ny\end{matrix}\ e^{-\sqrt{m^2+n^2}\,d}$$

$$=\mp\sum\sum\frac{m}{g\sqrt{m^2+n^2}}C_{mn}\begin{matrix}\cos mx\ \sin ny\\ \sin mx\ \cos ny\end{matrix}, \qquad (45)$$

and

$$\theta_y=\frac{Y}{g}=\mp\sum\sum\frac{2\pi k^2}{g}\frac{n}{\sqrt{m^2+n^2}}B_{mn}\begin{matrix}\sin mx\ \cos ny\\ \cos mx\ \sin ny\end{matrix}\ e^{-\sqrt{m^2+n^2}\,d}$$

$$=\mp\sum\sum\frac{n}{g\sqrt{m^2+n^2}}C_{mn}\begin{matrix}\sin mx\ \cos ny\\ \cos mx\ \sin ny\end{matrix}. \qquad (46)$$

The height of the geoid $h(xy)$ with respect to $h(x_0y_0)$ is, therefore, given by

$$h(xy)=\left[\int_{x_0}^{x}\theta_x dx\right]_{y=y_0}+\left[\int_{y_0}^{y}\theta_y dy\right]_{x=x}$$

$$=\frac{2\pi k^2}{g}\sum\sum\frac{B_{mn}}{\sqrt{m^2+n^2}}e^{-\sqrt{m^2+n^2}\,d}\left\{\begin{matrix}\sin mx\ \sin ny\\ \cos mx\ \cos ny\end{matrix}-\begin{matrix}\sin mx_0\ \sin ny_0\\ \cos mx_0\ \cos ny_0\end{matrix}\right\}$$

$$=\frac{1}{g}\sum\sum\frac{C_{mn}}{\sqrt{m^2+n^2}}\left\{\begin{matrix}\sin mx\ \sin ny\\ \cos mx\ \cos ny\end{matrix}-\begin{matrix}\sin mx_0\ \sin ny_0\\ \cos mx_0\ \cos ny_0\end{matrix}\right\} \qquad (47)$$

The results of applying the foregoing methods to actual gravity fields now in progress will be published later.

In conclusion, the writers wish to express their thanks to Dr. T. Yamanouchi and to Mr. G. Nishimura for valuable advices given them in connection with this study.

23. 重力と地下構造との關係 (2)

地震研究所 坪井忠二
地震研究所 淵田隆門

曩に我々は同一の表題で二次元の問題を取扱つたが，本文はそれを一般化して三次元の問題を取扱つたものである．地下構造をすべて一定の深さの面上に凝縮してあるものと假定することによつて，之を各種の調和函數で展開した場合に，その係數と重力の同じ展開による係數との關係を求める事が出來た．この關係を利用して任意の重力分布からそれに相當する地下構造を求めることが出來る．

---

24. *A Simple Method of Approximately Determining the Thickness of the Isostatic Earth's Crust.*

By Chûji Tsuboi.

Earthquake Research Institute.

(Read Dec. 22, 1937.—Received March 20, 1938.)

Notwithstanding the importance to geophysics of determining the most probable thickness of the isostatic earth's crust in various parts of the world, the studies that have been made of this subject so far are unfortunately very few, the main reason for which is that, in order to do so, laborious numerical calculations are required, particularly, as the determination usually depends on the trial and error method, namely, by adopting various thicknesses for the isostatic earth's crust and deciding on the one that gives the smallest sum of the squares of isostatic gravity anomalies. Provided no great accuracy is required, the method now to be proposed, which is a direct method, should be useful in rapid estimations of the thickness.

Let the surface topography of the area in question be expressed in a double Fourier series, such as,

$$h(xy)=\sum\sum H_{mn}\begin{matrix}\sin mx\sin ny\\ \cos mx\cos ny,\end{matrix}\tag{1}$$

and the Bouguer anomalies in the same area by

$$\Delta g(xy)=\sum\sum B_{mn}\begin{matrix}\sin mx\sin ny\\ \cos mx\cos ny.\end{matrix}\tag{2}$$

According to Airy isostasy, the load of the surface mass $\rho h(xy)$ is compensated at a certain depth by $-\rho h$. If, for simplicity, the subterranean mass were here assumed to be concentrated on a single horizontal surface of depth d, the Bouguer anomalies as the result of this mass would be given by

$$\begin{aligned}\Delta g(xy)&=-\sum\sum 2\pi k^2\rho h(xy)e^{-\sqrt{m^2+n^2}d}\\ &=-\sum\sum 2\pi k^2\rho H_{mn}\begin{matrix}\sin mx\sin ny\\ \cos mx\cos ny\end{matrix}\,e^{-\sqrt{m^2+n^2}d}.\end{aligned}\tag{3}$$

Should the perfect isostatic conditions prevail, the expression (2) and

(3) must be identical, whence

$$B_{mn} = -2\pi k^2 \rho H_{mn}\, e^{-\sqrt{m^2+n^2}\,d},$$

or

$$d = -\frac{1}{\sqrt{m^2+n^2}} \ln\left(-\frac{B_{mn}}{2\pi k^2 \rho H_{mn}}\right). \tag{4}$$

This is the expression with which the value of d can be calculated directly from the surface gravities and topographies. In order that d should have a reasonable value, the algebraic signs of B_{mn} and H_{mn} must differ and B_{mn} must be less than $2\pi k^2 \rho H_{mn}$, at least for the lower orders. Otherwise it will lead to the conclusion that the area is in condition far removed from that of the isostasy. The value of d calculated in this way gives the probable depth at which the compensating masses are distributed. In order to get the thickness of the isostatic earth's crust D, which corresponds to zero height, the thickness t of the mass compensating the constant term of the topography H_{00} must be subtracted from d. Thus we get

$$D = -\frac{1}{\sqrt{m^2+n^2}} \ln\left(-\frac{B_{mn}}{2\pi k^2 \rho H_{mn}}\right) - \frac{B_{00}}{2\pi k^2 (\rho' - \rho)}, \tag{5}$$

where ρ' and ρ are densities of the subcrustal and crustal materials respectively.

Were the distributions of gravity and topography "two-dimensional", matters would indeed be simplified. Putting $m=0$ in (5), we get

$$D = -\frac{1}{n} \ln\left(-\frac{B_n}{2\pi k^2 \rho H_n}\right) - \frac{B_0}{2\pi k^2 (\rho' - \rho)}. \tag{6}$$

Several tests made by applying the foregoing methods to actual problems showed them to be fairly satisfactory.

24. 地殼均衡說による地殼の厚さを求める簡單な方法

地震研究所 坪井 忠二

或る一定の區域の地形を

$$h(xy)=\sum\sum H_{mn}\begin{matrix}\sin mx\sin ny\\ \cos mx\cos ny\end{matrix}$$

さし，ブーゲー異常を

$$\varDelta g(xy)=\sum\sum B_{mn}\begin{matrix}\sin mx\sin ny\\ \cos mx\cos ny\end{matrix}$$

さすれば，エアリー説による地殼の厚さは

$$D=-\frac{1}{\sqrt{m^2+n^2}}\ln\left(-\frac{B_{mn}}{2\pi k^2\rho H_{mn}}\right)-\frac{B_{00}}{2\pi k^2(\rho'-\rho)}$$

で與へられる。

25. *Magnetic Anomalies around Volcanic Craters.*

By Takesi NAGATA,

Earthquake Research Institute.

(Read Jan. 18, and Mar. 16, 1938—Received Mar. 22, 1938.)

1. Introduction

With the object to study the variations in the earth's magnetic field that accompany volcanic activities, R. Takahasi and the writer⁽¹⁾ observed, in September 1936, the three components of the earth's magnetic field at 12 stations around Volcano Mihara. These surveys indicated that the earth's magnetic field in the island showed an anomalous distribution, almost equal to the magnetic field due to a bar magnet placed in the centre of the volcano, coaxially with the normal magnetic meridian.⁽²⁾

A number of papers have been published by investigators on the subjects of magnetic anomalies in volcanic regions, of which those of C. Maurain and his collaboraters⁽³⁾, particularly are replete with many interesting results, and contain numerous useful suggestions in connexion with these studies. A number of papers have also appeared in Japan, among which may be mentioned Tanakadate's surveys⁽⁴⁾ on Mt. Huzi (Fuji) and Mt. Asama, and the very recent one of Hatakeyama⁽⁵⁾ on Mt. Daitô in Formosa, and that of Yoda⁽⁶⁾ on Mt. Mayu in Kyûsyû. The topographies of these mountains are so complex that these authors did not calculate the magnetization of the rocks composing these mountains. They merely compared the observed magnetic anomalies with the field due to a bar magnet of sufficient intensity, of suitable dimensions, and in the right direction.

The writer, however, calculated the mean susceptibility of the rocks composing the Volcanoes Mihara and Asama from observations of magnetic declinations at 20 stations distributed almost equidistantly around

---

1) R. TAKAHASI and T. NAGATA, *Bull. Earthq. Res. Inst.*, **15** (1937), 441.

2) 〃 , *Zisin*, **9** (1937), 431, (in Japanese).

3) For example, *Ann. Phys. Globe*, **15** (1937).

4) A. TANAKADATE, *Jour. Coll. Sci. Tokyo*, **2** (1889). T.S.B.K., **2** (1904), 149, 405.

5) H. HATAKEYAMA, *Bull. Cent. Meteoro. Obs. Japan*, Vol. VI, No. 2 (1937).

6) W. YODA, *Read at the annual meeting of Nippon-Tikyū-Buturi-Gakkai* (Geoph-ysical Society of Japan) (May, 1937).

the crater of Volcano Mihara and from similar observations carried out by T. Fukutomi[7] around the crater of Volcano Asama.

2. Method of observation

A compass transit was used in the present survey. Although this instrument is not accurate, errors of several minutes in observation of the magnetic meridian being inevitable, it suited our purposes, seeing that the magnitude of the anomalies in question for both volcanoes amounted to several degrees. The observations were made as follows: Upon measuring from station A angle α between the magnetic meridian and the direction of straight line AB, and then conversely angle β from station B, as shown in Fig. 1, the difference between α and β is that of the magnetic declinations at A and B. That is,

$$\alpha-\beta=\delta_A-\delta_B,$$

where δ_A and δ_B are declinations at A and B respectively. The positions of the stations were determined trigonometrically, the same transit being used. Repeating the operation successively at 20 stations, we traversed around the crater. To attain maximum accuracy, the traverses were conducted not only between adjoining stations, but also with as varying a combination of stations as possible. In determining α or β, we took the mean value of eight readings of an observed value at one station, the mean errors of one reading of the azimuth of the magnetic compass and also of the transit being 5′ and 30″ respectively. The closing errors were 15′ and 2·0′ in the magnetic and trigonometric traverses respectively; which errors are negligible considering the observation mentioned in the next paragraph.

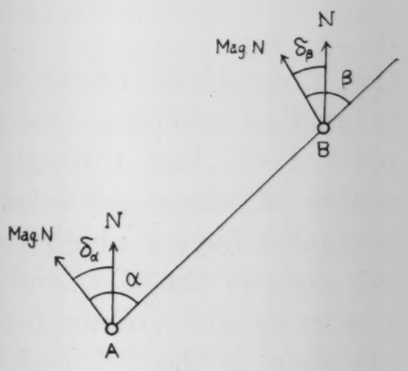

Fig. 1.

3. Results of observations

The distribution of the twenty stations and the results of observations are shown in Fig. 2 and in Table I. In this table, the numerals in the column entitled "Anomaly of declination" are deviations from the mean value of the observed declinations at twenty stations, the (+) and (−) signs referring to the westerly and easterly deviations respectively. As shown in Fig. 2, the anomalies in magnetic declina-

---

7) T. FUKUTOMI, *Zisin*, **2** (1930), 641 (In Japanese).

Table I.

Azimuth φ	Anomaly in Declination δ	φ	δ
12°	−1° 23′	186°	+2° 35′
40	0 00	200	−0 20
58	+5 20	232	+2 20
75	+5 00	255	+0 40
92	+1 40	277	−1 20
112	−1 10	290	−1 30
123	−0 20	310	−7 20
135	−1 30	328	−3 40
152	−1 40	348	−2 15
170	+3 10		

tion around the crater are distributed in quadrants, divided by the magnetic meridian and the magnetic E–W line through the centre of the crater; i.e. the anomalies have a plus (westerly) sign in the SW and NE quadrants, and a minus (easterly) sign in the SE and NW quadrants. Very similar results were obtained in the case of Volcano Asama in the course of observations carried out by T. Fukutomi in 1930, as shown in Fig. 3. The relations between the magnitude of the anomaly and the azimuths of stations from the centre of the crater are shown in Figs. 4, 5. Comparing these two figures, we see that, although there are certain differences in the details, the general tendencies are very similar in the two cases.

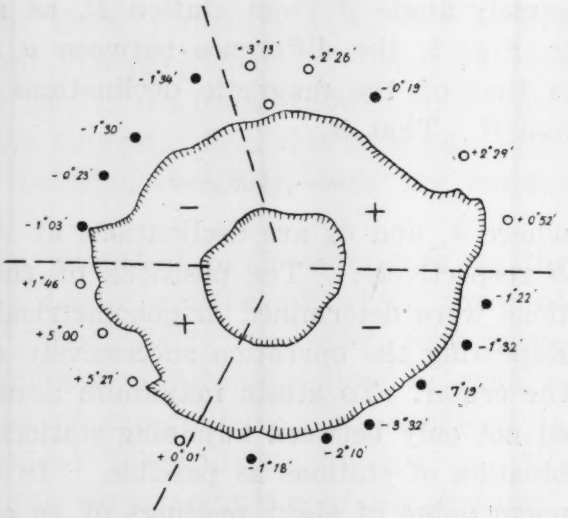

Fig. 2. Distribution of anomaly in declination around the crater of Mt. Mihara.

○ Westerly anomaly
● Easterly 〃

In both cases, the magnitude of the anomaly on the magnetic southern side is larger than that on the northern side, i.e. the anomaly around the crater may be expressed not only with second harmonics but also with a superposed curve of the first and second harmonics of the azimuthal angle from the centre of the crater.

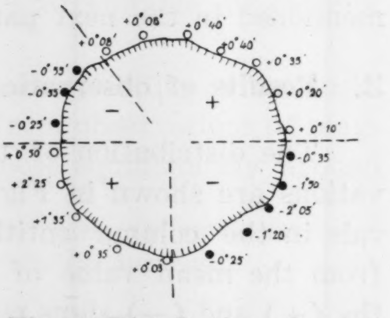

Fig 3. Distribution of anomaly in declination around the crater of Mt. Asama (Observed by T. Fukutomi).

If now we let the direction of magnetic south from the centre of the crater be the zero line, and let the azimuthal angle as measured clockwise from the zero line be φ, then the anomaly in declinations δ and φ may be approximately expressed by the equation,

$$\mathrm{tg}\,\delta = A\sin\varphi + B\sin 2\varphi + C \qquad (1).$$

Assuming that relation (1) holds for both volcanoes, Asama and Mihara, the constant, A, B, C are determined from the observed values with the aid of least squares, as follows,

$$\left.\begin{aligned}(\mathrm{tg}\,\delta)_{\text{Asama}} &= 0{\cdot}0133\sin\varphi + 0{\cdot}0221\sin 2\varphi + 0{\cdot}0017\\ (\mathrm{tg}\,\delta)_{\text{Mihara}} &= 0{\cdot}0283\sin\varphi + 0{\cdot}0468\sin 2\varphi + 0{\cdot}0002\end{aligned}\right\} \qquad (2).$$

The relations expressed by equations (2) are graphed in Figs. 4 and 5 in full lines.

These anomalies just mentioned are believed to be due to singularities in the topography of the crater. Considering that the distributions of these anomalies are nearly symmetrical with the magnetic meridian, they are probably due to induced magnetism in the rocks with large magnetic susceptibility around the crater. If this assumption holds in our case, the susceptibility may be calculated from our observed data. Here we shall estimate the extent of the susceptibility by roughly approximating the shape of the crater. We could assume that the crater is a circular hole of cylindrical form, of depth d and radius l, on the plane surface of a semi-infinite body of susceptibility K, as shown in Fig. 6. The magnetic anomaly due to the presence of

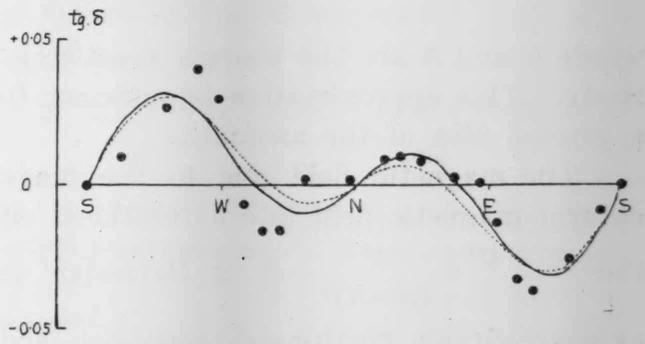

Fig. 4. The observed and theoretical distribution of anomaly in declination around the crater of Mt. Asama.
Full line = observed. Dotted line = theoretical.

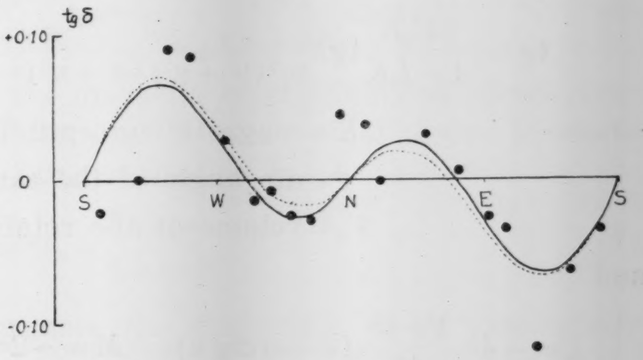

Fig. 5. The observed and theoretical distributions of anomaly in declination around the crater of Mt. Mihara.
Full line = observed. Dotted line = theoretical.

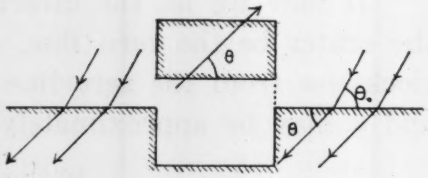

Fig. 6.

this hole is exactly the same as that due to a body having the same dimensions and the same position as this hole, and having the same susceptibility as the surrounding medium, but magnetized inversely to the earth's normal magnetic field in that region, for if there were no hole, the magnetic field on the surface should be quite uniform.

We shall, therefore, estimate the value of the magnetic anomaly due to the body just mentioned. For simplifying the mathematics, it is assumed that the body is a rotational ellipsoid, the axis of which is vertical, and satisfying the condition

$$\frac{4\pi}{3}ab^2 = V_0 = \pi l^2 d,$$

where a and b are the shorter (vertical) and the longer radii respectively. This approximation is sufficient for the present in order to get a general idea of the anomaly.

The magnetic field due to the magetism induced by the earth's natural magnetic field into a rotational ellipsoid, expressed by the equation $\frac{x^2+y^2}{b^2}+\frac{z^2}{(a-h)^2}=1$ in Cartesian coodinates, where the x, y, z axes are drawn northward, eastward, and downward respectively, has been caluculated by J. Koenigsberger[8], according to whom, the magnitude of declination of the magnetic anomaly on the earth's surface ($z=0$ plane) is expressed by the equation,

$$\operatorname{tg}\delta = \frac{3V_0K}{1-LK}\operatorname{tg}\theta\frac{yh}{m^2(b^2+n^2)(a^2+n^2)^{\frac{1}{2}}} - \frac{4V_0K}{1-MK}\frac{xy(a^2+n^2)^{\frac{1}{2}}}{m^2(b^2+n^2)^2} \qquad (3),$$

where K = magnetic susceptibility,

θ = dip angle of the earth's field,

V_0 = volume of the rotational ellipsoid,

and

$$L = -4\pi\frac{1+u^2}{u^3}(u - \operatorname{arctg} u), \quad M = -2\pi\frac{1+u^2}{u^3}\operatorname{arctg}\left(u - \frac{u}{1+u^2}\right),$$

$$u = \frac{\sqrt{b^2-a^2}}{a},$$

---

8) J. Königsberger, *Gerl. Beitr. Geophys.*, **19** (1928), 241.

$$m^4=(h^2+x^2+y^2)^2+(b^2-a^2)\Big[(b^2-a^2)-2(x^2+y^2-h^2)\Big],$$

$$n^2=\frac{1}{2}(h^2+x^2+y^2-b^2-a^2+m^2).$$

Assuming that the formula (3) is applicable to our cases, we shall estimate the susceptibility of the rocks composing the volcanoes Asama and Mihara.

(i) Asama

In the case of Volcano Asama, the magnitudes of a, b, h are taken as follows:

$$a=h=100\ \mathrm{m}$$
$$b=170\ \mathrm{m}.$$

As our stations are distributed almost in a circle with its centre on the centre of the crater, as shown in Fig. 3, we take

$$x=-r\cos\varphi,\quad y=-r\sin\varphi \tag{4},$$

where the positive sense of φ is taken clockwise, when equation (3) becomes

$$-\mathrm{tg}\,\delta=\frac{3V_0K}{1-KL}\mathrm{tg}\,\theta\frac{ar}{m^2(b^2+n^2)(a^2+n^2)^{\frac{1}{2}}}\sin\varphi$$
$$+\frac{2V_0K}{1-KM}\frac{(a^2+n^2)^{\frac{1}{2}}r^2}{m^2(b^2+n^2)^2}\sin 2\varphi \tag{5}.$$

If we take approximately $r=200$ m, we get

$$-\mathrm{tg}\,\delta=K\left(\frac{1{\cdot}59}{1+4{\cdot}7K}\mathrm{tg}\,\theta\sin\varphi+\frac{1{\cdot}40}{1+5{\cdot}0K}\sin 2\varphi\right) \tag{6}.$$

It is not possible to get the magnetic susceptibility K direct from equation (6), seeing that the dip angle θ is not equal to the dip θ_0 on the earth's surface, θ and θ_0 being related as in

$$\cot\theta_0=\frac{\cot\theta}{1+4\pi K} \tag{7}.$$

We shall accordingly estimate the magnitude of K successively. First, instead of (6), we take

$$-\mathrm{tg}\,\delta=K'(1{\cdot}6\,\mathrm{tg}\,\theta_0\sin\varphi+1{\cdot}4\sin 2\varphi) \tag{8}.$$

Since, according to T. Minakami[9], the mean value of the dip in the vicinity of the crater of Volcano Asama is 50°, we take

---

[9] T. MINAKAMI, *Bull. Earthq. Res. Inst.*, **16** (1938), 100.

$$\mathrm{tg}\,\theta_0=\mathrm{tg}\,50^\circ=1{\cdot}2.$$

Comparing eq (8) with eq (2), we have

$$K'=0{\cdot}012 \qquad (9).$$

In this comparison, the sign of the right side of eq (8) should be reversed since the direction of magnetization of our model is exactly opposite to that of the natural field, as mentioned in the beginning of this paragraph. From (7) and (9) we get $\mathrm{tg}\,\theta=1{\cdot}0$,

whence $$\mathrm{tg}\,\delta=K\left(\frac{1{\cdot}6}{1+4{\cdot}7\,K}\sin\varphi+\frac{1{\cdot}4}{1+5{\cdot}0\,K}\sin 24\varphi\right) \qquad (10).$$

Comparing eq (9) with eq (2), we have

$$K=0{\cdot}011$$

$$(\mathrm{tg}\,\delta)_{\mathrm{Asama}}=0{\cdot}019\sin\varphi+0{\cdot}017\sin 2\varphi.$$

The relation between δ and φ shown in eq (11) is graphed with dotted lines in Fig. 4.

(ii) Mihara

In this case, taking the constants a, b, h, r to be

$$a=h=35\ \mathrm{m}$$

$$b=r=500\ \mathrm{m},$$

we get

$$-\mathrm{tg}\,\delta=\frac{3V_0K}{1-KL}\,\mathrm{tg}\,\theta\,\frac{\sqrt{a^2+ab}}{2ab(a+b)^2}\sin\varphi+\frac{V_0K}{1-KM}\,\frac{\sqrt{a^2+ab}}{ab(a+b)^2}\sin 2\varphi$$

$$=K\left(\frac{1{\cdot}5}{1+11{\cdot}0K}\,\mathrm{tg}\,\theta\sin\varphi+\frac{1{\cdot}0}{1+0{\cdot}7K}\sin 2\varphi\right) \qquad (12).$$

Taking $\theta_0=50^\circ$[10], we get eq (13) from eq (12), with the same successive method used in the case of Asama,

$$-\mathrm{tg}\,\delta=\frac{1{\cdot}3K}{1+11{\cdot}0K}\sin\varphi+\frac{K}{1+0{\cdot}7K}\sin 2\varphi.$$

Comparing eq (13) with eq (2), we have

$$\left.\begin{aligned}K&=0{\cdot}038\\ \mathrm{tg}\,\delta&=0{\cdot}036\sin\varphi+0{\cdot}038\sin 2\varphi\end{aligned}\right\} \qquad (14).$$

(iii) Effect of the present pit in the case of Mihara

---

[10] R. TAKAHASI *and* T. NAGATA, *loc. cit.*

In the preceding calculations the effect of the presence of the pit was neglected. We, now, estimate approximately the extent of the effect, assuming that it is almost the same as that due to a sphere having suitable dimensions and position. The declination on the plane surface $z=0$ due to the induced magnetism of a sphere is expressed by the relation,

$$\left.\begin{aligned} \mathrm{tg}\,\delta' &= \frac{3V_0K}{1+\frac{4\pi}{3}K}\frac{y}{R^5}(h\,\mathrm{tg}\,\theta-x) \\ R^2 &= x^2+y^2+h^2=r^2+h^2 \end{aligned}\right\} \qquad (14),$$

in the same coordinates and notations as used in cases (i) and (ii). Modifying eq (14) in exactly the same way as in the above case, we get

$$-\mathrm{tg}\,\delta' = \frac{3V_0K}{1+\frac{4\pi}{3}K}\frac{r}{R^5}\left(h\,\mathrm{tg}\,\theta\sin\varphi+\frac{r}{2}\sin 2\varphi\right) \qquad (15).$$

Taking the constants R, h, and the radius of the sphere ρ as

$$R=500\text{ m},\quad h=200\text{ m},\quad \rho=120\text{ m},$$

we get

$$-\mathrm{tg}\,\delta' = \frac{K}{1+4{\cdot}2K}(0.048\,\mathrm{tg}\,\theta\sin\varphi+0{\cdot}061\sin 2\varphi) \qquad (16).$$

Inserting the values of K and $\mathrm{tg}\,\theta$ obtained in case (ii) in eq (16) we get,

$$-\mathrm{tg}\,\delta' = 0{\cdot}0012\sin\varphi+0{\cdot}0020\sin 2\varphi \qquad (17).$$

Adding eq (17) to eq (14), as $\delta \ll 1$, and $\delta' \ll 1$,

$$\left.\begin{aligned} (\mathrm{tg}\,\delta_0)_{\text{Mihara}} &\doteqdot \mathrm{tg}\,\delta+\mathrm{tg}\,\delta' = 0{\cdot}037\sin\varphi+0{\cdot}040\sin 2\varphi \\ K &= 0{\cdot}038 \end{aligned}\right\} \qquad (18).$$

The relation between δ_0 and φ shown in eq (18) is graphed with dotted lines in Fig. 5.

4. Discussion of results

From Figs. 6, 7, we see that, barring the slight discrepancy in them, the general tendencies in both the theoretical and the analysis curves, are similar. This shows that the anomalous distribution of magnetic declinations is mainly due to the anomalous topography of the crater, and that the earth's magnetic field induces magnetism in the rocks around the crater; at any rate the direction of its magnetization is parallel to the present magnetic field. Upon going strictly into details, however, we notice that there is some discrepancy in the ratio of the coefficient of $\sin\varphi$ to that of $\sin 2\varphi$ in both the theoretical and analysis curves; that is, the ratio in the theoretical result is larger than that in the results obtained by analysing the observed data. Seeing that the coefficient of $\sin\varphi$ in the theoretical formula contains $\mathrm{tg}\,\theta$, and assuming that the discrepancy is due to the difference between the dip-angles of magnetization of the rocks and of the earth's magnetic field, we get the following relation from (2) and (6) and from (2) and (12),

$$\mathrm{tg}\,\theta \fallingdotseq 0{\cdot}54, \quad \theta = 28{\cdot}5^\circ \quad \text{for Asama,}$$

$$\mathrm{tg}\,\theta \fallingdotseq 0{\cdot}46, \quad \theta = 24{\cdot}5^\circ \quad \text{for Mihara.}$$

Inserting the values of this $\mathrm{tg}\,\theta$ in formulae (6), (12), we get the same results as the observed values. The discrepancy, however, could be also due to our assuming the shape of the crater to be a rotational ellipsoid, since only a slight difference between the shape of the actual crater and the model affects the result not a little, particularly as our observations were made near the edge of the crater.

The magnetic susceptibilities of the andesite of Asama and the basalt of Mihara seem to be somewhat larger than the values determind experimentally by a number of investigators[11]. These problems will be discussed after the completion of our experiments on the magnetic properties of the rocks of Volcanoes Asama and Mihara.

5. Appendix

In the above calculations, the form of the crater was assumed to be a rotational ellipsoid, under which assumption, however, there seem to be some discrepancies in the details between the theoretical results and the observed data.

We shall now take more suitable assumption for the form of crater, although the consequent calculations will not be mathematically elegant.

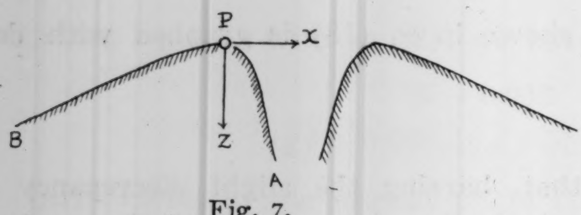

Fig. 7.

---

[11] For example, *Handb. d. Exp. phys.*, 3 *Teil.* (1930), pp. 28∼31.

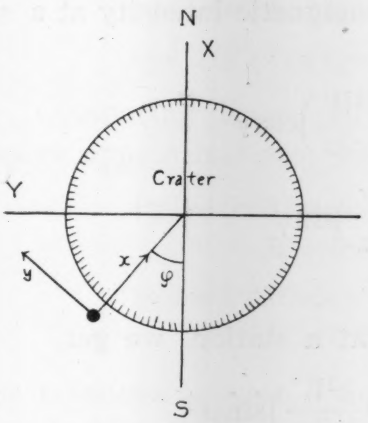

Fig. 8.

Fig. 7 shows the vertical section through the centre of the crater, the topography around which is assumed to be quite symmetric. In Fig. 7, we assume that magnetic anomaly at every observing station P is due to the presence of a mass A–P–B, which continues infinitely in a direction perpendicular to the paper. In Fig. 8, the circle represents the boundary of the crater. Coordinate systems (XYZ) and (xyz) are taken as shown in the figure. If H_0 and Z_0 denote the horizontal and vertical components of the normal earth's magnetic field respectively, then the x, y, and z-components of the field x_0, y_0, and z_0 are

$$x_0 = H_0 \cos\varphi, \quad y_0 = H_0 \sin\varphi, \quad z_0 = Z_0 \qquad (1).$$

And the three components of the magnetic anomaly due to the presence of mass A–P–B at observing station P are

$$\left.\begin{aligned} \Delta x &= KH_0\left(\cos\varphi \frac{\partial^2 W}{\partial x^2} + \frac{Z_0}{H_0} \frac{\partial^2 W}{\partial x \partial z}\right) \\ \Delta y &= 0 \\ \Delta z &= KH_0\left(\cos\varphi \frac{\partial^2 W}{\partial x \partial z} - \frac{Z_0}{H_0} \frac{\partial^2 W}{\partial x^2}\right) \end{aligned}\right\} \qquad (2),$$

where K is the magnetic susceptibility of the rocks composing the mass, and W the gravitational potential due to the mass. The three components of the total magnetic field at station P, therefore, are

$$\left.\begin{aligned} x = x_0 + \Delta x &= H_0 \cos\varphi + KH_0\left(\cos\varphi \frac{\partial^2 W}{\partial x^2} + \frac{Z_0}{H_0} \frac{\partial^2 W}{\partial x \partial z}\right) \\ y = y_0 \quad &= H_0 \sin\varphi \\ z = z_0 + \Delta z &= Z_0 + KH_0\left(\cos\varphi \frac{\partial^2 W}{\partial x \partial z} - \frac{Z_0}{H_0} \frac{\partial^2 W}{\partial x^2}\right) \end{aligned}\right\} \qquad (3).$$

Since transformations of these values from the (xyz) coordinate system to the (XYZ) coordinate system give the relations,

$$\left.\begin{aligned} X &= x\cos\varphi + y\sin\varphi \\ Y &= -x\sin\varphi + y\cos\varphi \\ Z &= z \end{aligned}\right\} \qquad (4),$$

the north and west components of the total magnetic intensity at a station become

$$\left.\begin{aligned} X &= H_0 + H_0 K\left(\cos\varphi \frac{\partial^2 W}{\partial x^2} + \mathrm{tg}\,\theta \frac{\partial^2 W}{\partial x \partial z}\right)\cos\varphi \\ Y &= -KH_0\left(\cos\varphi \frac{\partial^2 W}{\partial x^2} + \mathrm{tg}\,\theta \frac{\partial^2 W}{\partial x \partial z}\right)\sin\varphi \end{aligned}\right\} \qquad (5),$$

where θ is the dip angle, i.e. $\mathrm{tg}\,\theta = Z_0/H_0$.

If δ denotes the anomaly in declination at a station, we get,

$$\mathrm{tg}\,\delta = Y/X = \frac{-KH_0\left(\cos\varphi \dfrac{\partial^2 W}{\partial x^2} + \mathrm{tg}\,\theta \dfrac{\partial^2 W}{\partial x \partial z}\right)\sin\varphi}{H_0 + H_0 K\left(\cos\varphi \dfrac{\partial^2 W}{\partial x^2} + \mathrm{tg}\,\theta \dfrac{\partial^2 W}{\partial x \partial z}\right)\cos\varphi}$$

$$\fallingdotseq -K\left(\frac{\partial^2 W}{\partial x \partial z}\,\mathrm{tg}\,\theta \cdot \sin\varphi + \frac{1}{2}\frac{\partial^2 W}{\partial x^2}\sin 2\varphi\right) \qquad (6).$$

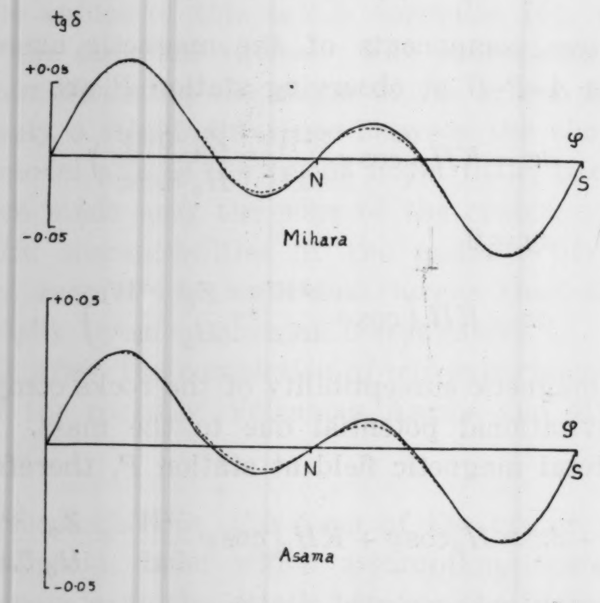

Fig. 9. The observed and theoretical distributions of anomaly in declination around the craters.
Full lines = observed. Dotted lines = theoretical (§ 5).

This relation agrees with the empirical formula (2) in § 3. Calculating with the aid of numerical integration, the values of $\dfrac{\partial^2 W}{\partial x^2}$ and $\dfrac{\partial^2 W}{\partial x \partial z}$ due to mass A–P–B, the form of which in the cases of Volcanoes Asama and Mihara, is the mean value of the topography around the crater, we obtain

$$\operatorname{tg}\delta = K(2{\cdot}41\operatorname{tg}\theta\sin\varphi + 3{\cdot}26\sin 2\varphi)\cdots\cdots\cdots\cdots\text{Mihara},$$

$$\operatorname{tg}\delta = K(2{\cdot}54\operatorname{tg}\theta\sin\varphi + 3{\cdot}05\sin 2\varphi)\cdots\cdots\cdots\cdots\text{Asama}.$$

Comparing these relations with eq (2) in § 3 by means of successive approximations, we get

$$\left.\begin{aligned} \operatorname{tg}\delta &= 0{\cdot}031\sin\varphi + 0{\cdot}043\sin 2\varphi. \;\cdots\cdots\cdots\cdots\text{Mihara},\\ K &= 0{\cdot}013.\\ \operatorname{tg}\delta &= 0{\cdot}015\sin\varphi + 0{\cdot}017\sin 2\varphi. \;\cdots\cdots\cdots\cdots\text{Asama}\\ K &= 0{\cdot}0055. \end{aligned}\right\} \quad (7).$$

The relations between δ and φ shown in eq (7) are graphed with dotted lines in Fig. 9.

These results seem to be more reliable than the values obtained by calculating with the assumption of the presence of a negative mass having the form of a rotational-ellisoid.

In conclusion, the writer wishes to express his sincere thanks to Prof. M. Ishimoto and Dr. R. Takahasi for their encouragement in the course of this study. His cordial thanks are also due to Dr. Ch. Tsuboi for his interest in the present work. The writer also wishes to express his hearty thanks to the Hattori-Hokokai, with the aid of whose grant the present study was made.

---

25. 火口周邊に於ける地磁氣偏角の異常分布

地震研究所　永田　武

三原火山の火口周邊に於ける地磁氣偏角の異常量の分布を測定した結果，火口附近の特異な地形の影響によつて，一つの規則だつた分布をしてゐる事を知つた．此の測定結果は，福富理學士等による淺間火山の火口周邊に於ける同様の測定の結果と全く一致する．偏角異常量を δ とし，各測點の火口中心より，磁氣南を0にとる方位角を φ とすれば δ の分布は次式で表はされる．

$$\operatorname{tg}\delta = A\sin\varphi + B\sin 2\varphi.$$

此の分布は火口附近の岩石に Induce された磁氣に因ると考へて説明出來る事を示し，且つ三原及び淺間兩火山の場合に於ける平均帶磁率を求めた．火口の地形に對しては，二つの理想的な場合，卽ち一つは火口の形を廻轉楕圓體で近似した場合，他の一つは，各測點に於いては地形を二次元的分布として取扱ふ場合に就いて行つた．何れによつても，分布の形式は説明出來るし，又三原山の玄武岩の帶磁率は淺間山の安山岩の 2·5 倍乃至 3 倍位になる．然し後の場合の近似の方が實際により近い結果を得たと思はれる．

此の研究は，服部報公會より高橋助教授及び筆者に與へられた三原火山研究費の一部で行はれたものであつて，此處に同會に對して厚く感謝の意を表する．

26. *Crustal Deformations in Central Taiwan.*
(*Part 1*)

By Mituo HUKUNAGA and Mitunosuke SATO,*

Seismological Institute.

(Read Dec. 21, 1937. Received March 20, 1938.)

I. Introduction.

The destructive earthquake that shook the central part of Taiwan on April 21, 1935, was accompanied by marked crustal deformations. Associated with this earthquake, there appeared two faults, the Siko fault and the Tonsikyaku fault, their locations being shown in Fig. 1. After the earthquake, extensive relevellings and re-triangulations were made by the Military Land Survey over such regions as where the earth's crust was supposed to have been disturbed by the earthquake. These re-surveys showed that horizontal and vertical displacements of triangulation points and bench-marks had occurred since the last surveys were made. It is believed that they are mostly associated with the earthquake just mentioned.[1] The horizontal displacements of the triangulation points and the vertical displacements of the bench-marks thus obtained are shown respectively by arraws and numerals against the corresponding points in Figs. 1 and 2.

In this paper, the writers discuss the crustal deformations on the basis of the above-mentioned data.

II. Horizontal Deformations.

1. Method of calculating the horizontal strains.

In calculating the horizontal strains, the following method was used. If we let u and v be the x- and y-components of the horizontal displacement of a triangulation point, referred to certain rectangular coordinates x and y, then the components of horizontal strain are given by proper combinations of the values of $\frac{\partial u}{\partial x}$, $\frac{\partial u}{\partial y}$, $\frac{\partial v}{\partial x}$, and $\frac{\partial v}{\partial y}$. In calculating the values of $\frac{\partial u}{\partial x}$, $\frac{\partial u}{\partial y}$, etc., by the method proposed by T. Terada and N. Miyabe,[2] u and v are assumed to be linear functions of x and y, given in the form

---

* Comm. by N. Miyabe.

[1] The data of horizontal displacements of triangulation points and the vertical displacements of the bench-marks are given in Bull. Earthq. Res. Inst., Suppl. Vol. **3** (1936), 216~227.

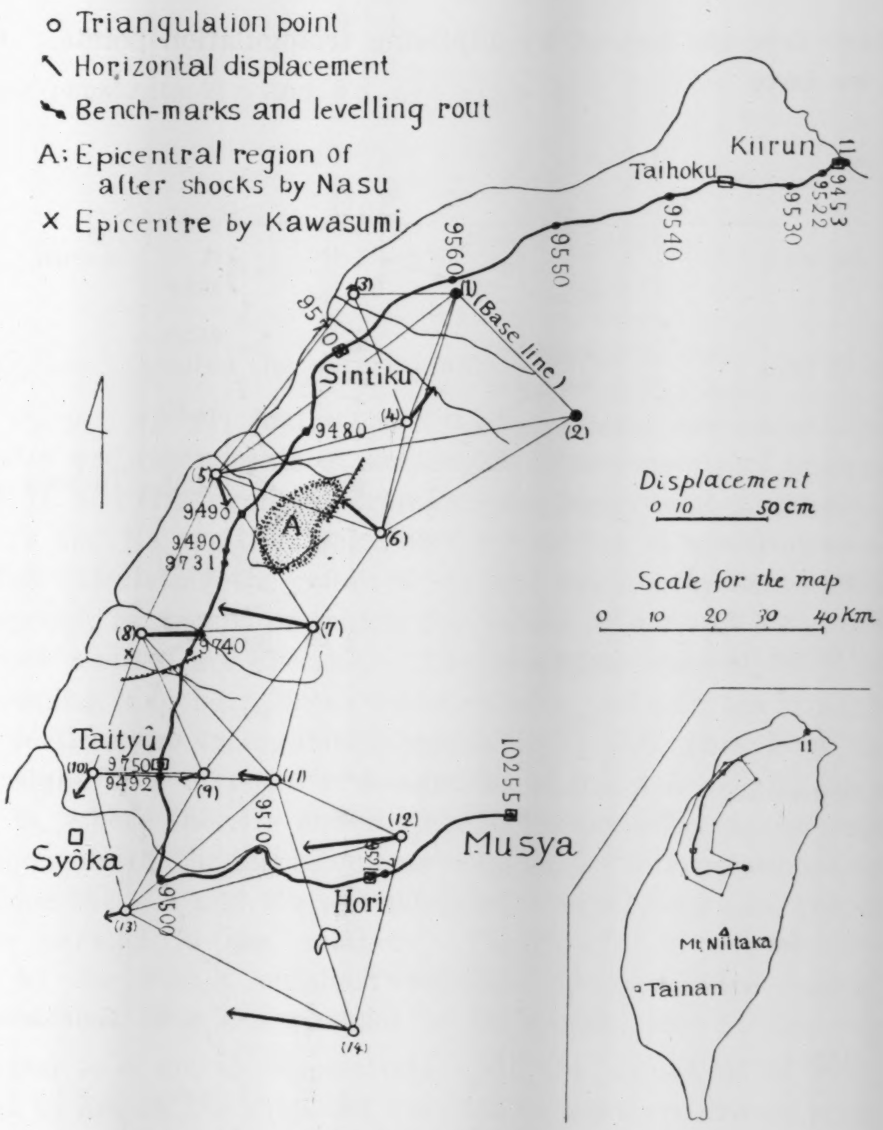

o Triangulation point
Horizontal displacement
Bench-marks and levelling rout
A: Epicentral region of after shocks by Nasu
× Epicentre by Kawasumi
Kiirun
Taihoku
11
9453
9522
9530
9540
9550
9560
(1) (Base line)
(2)
(3)
9570
Sintiku
(4)
9480
(5)
9493
A
(6)
9490
9731
(7)
(8)
9740
Taityû
(10)
9750
9492
(9)
(11)
10255
(12)
Musya
Syôka
9510
9521
Hori
(13)
9500
(14)
Displacement
0 10 50 cm
Scale for the map
0 10 20 30 40 Km
11
Mt. Niitaka
Tainan

Fig. 1.

---

[2] T. Terada and N. Miyabe, *Bull. Earthq. Res. Inst.*, 7 (1929), 223.

$$u = ax + by + c,$$
$$v = a'x + b'y + c',$$

within each triangle formed by adjoining triangulation points. Consequently we have

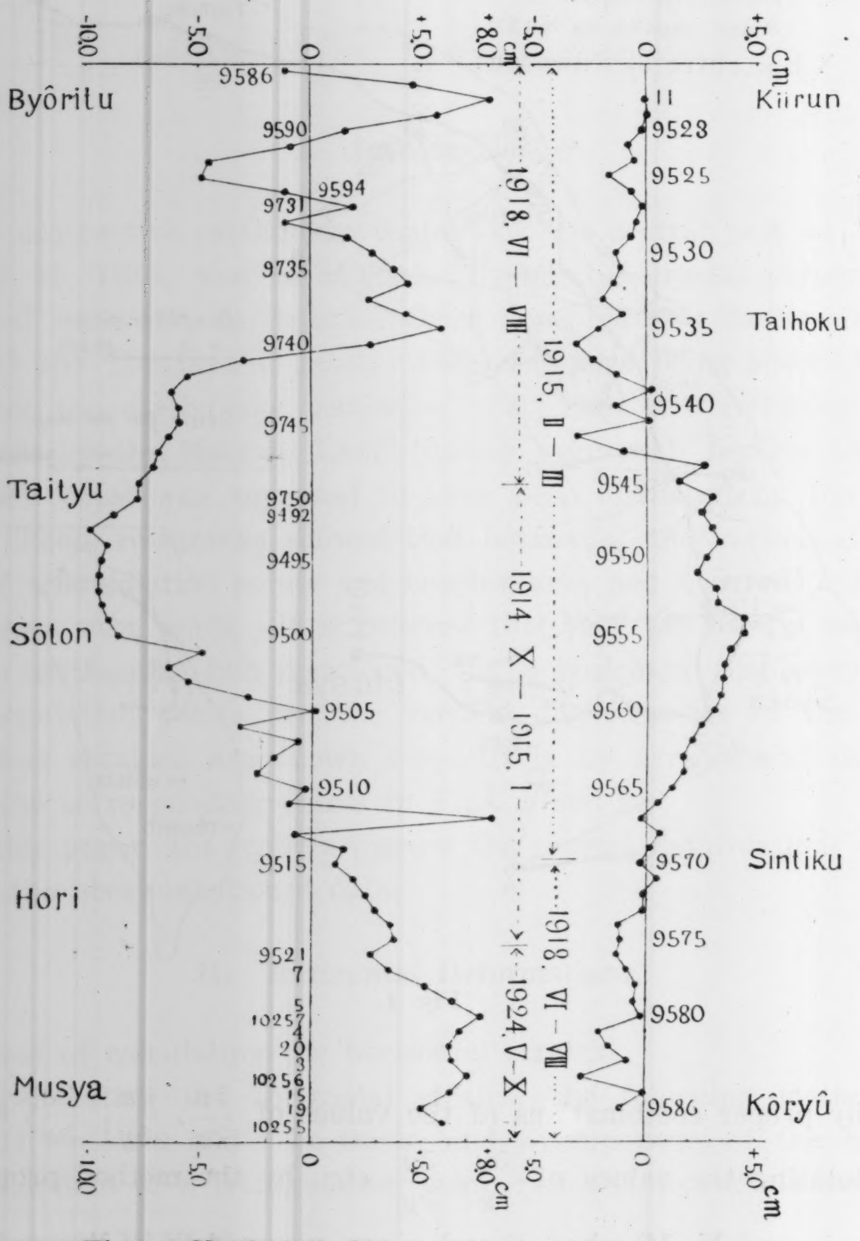

Fig. 2. Vertical displacements of bench-marks along the levelling routes.

$$\left.\begin{aligned}\frac{\partial u}{\partial x}&=a\\[1em] \frac{\partial u}{\partial y}&=b\end{aligned}\right\}\qquad\qquad \left.\begin{aligned}\frac{\partial v}{\partial x}&=a'\\[1em] \frac{\partial v}{\partial y}&=b'\end{aligned}\right\}$$

The four constants, a's and b's, are given by

$$\left.\begin{aligned}a&=\frac{|uy|}{|xy|}\\[1em] b&=\frac{|xu|}{|xy|}\end{aligned}\right\}\qquad\qquad \left.\begin{aligned}a'&=\frac{|vy|}{xy|}\\[1em] b'&=\frac{|xv|}{|xy|}\end{aligned}\right\}$$

in which $|uy|$ denotes the determinant $\begin{vmatrix} u_2-u_1 & y_2-y_1 \\ u_3-u_1 & y_3-y_1 \end{vmatrix}$ and so on, and x_1, y_1; x_2, y_2; x_3, y_3; and u_1, v_1; u_2, v_2; u_3, v_3; are respectively the coordinates and components of horizontal displacements of triangulation points I, II, and III, forming a triangle. In the present study, the values of the a's and b's are thus calculated by solving a simultaneous equation. For calculating the values of a's and b's, a graphical method was also proposed, by means of which the values of a's and b's obtained by the former method are checked. The graphical method is as follows:

Assuming u to be a linear function of x and y in the triangle having as vertices the triangulation points I, II, III (See Fig. 3a), we have straight lines of equal u denoted by A_0B_0, A_1B_1, A_2B_2, as shown in Fig. 3*a*, where the A's and B's are corresponding to the values of the components of the displacements obtained by interpolation (See Fig. 3b). Since the A's and B's are taken with equal intervals, the contour lines are parallel to one another. The length of a part of a line parallel to the x-axis, obtained between the successive contor lines, say α, and that of a line parallel to the y-axis, say β, are inversely proportional to a and b respectively. If the values of α and β are measured in km on the map and the contour lines are drawn with intervals of 1 cm, we have

$$\begin{aligned}\alpha&=\frac{1}{a}\times10^{-5} \qquad & a&=\frac{\partial u}{\partial x}=\frac{1}{\alpha}\times10^{-5}\\[1em] \beta&=\frac{1}{b}\times10^{-5} \qquad & b&=\frac{\partial u}{\partial y}=\frac{1}{\beta}\times10^{-5}\end{aligned}\left.\vphantom{\begin{aligned}a\\[1em]b\\[1em]c\end{aligned}}\right\}.$$

The values op a' and b' may also be obtained in a similar way by using the data of v's. The theoretical basis of this graphical method of calculation however is the same as that of the analytical method previously mentioned.

The values of a's and b's are thus calculated and, by combining

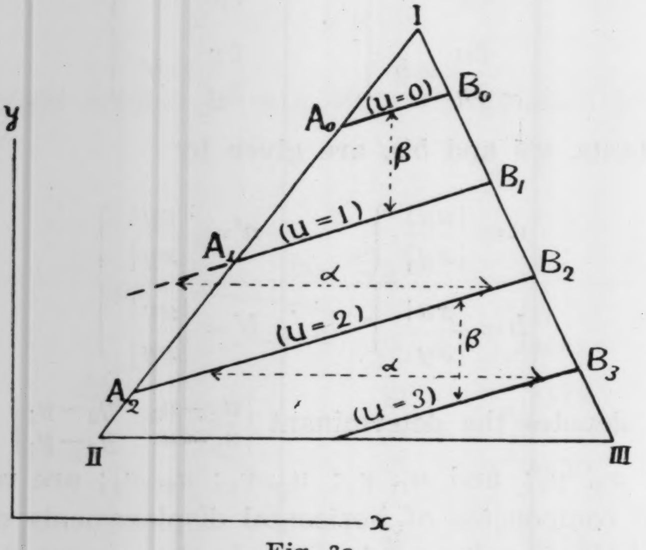
I
B_0
A_0
$(u=0)$
β
B_1
$(u=1)$
A_1
α
B_2
$(u=2)$
β
α
B_3
A_2
$(u=3)$
II
III
y
x

Fig. 3a.

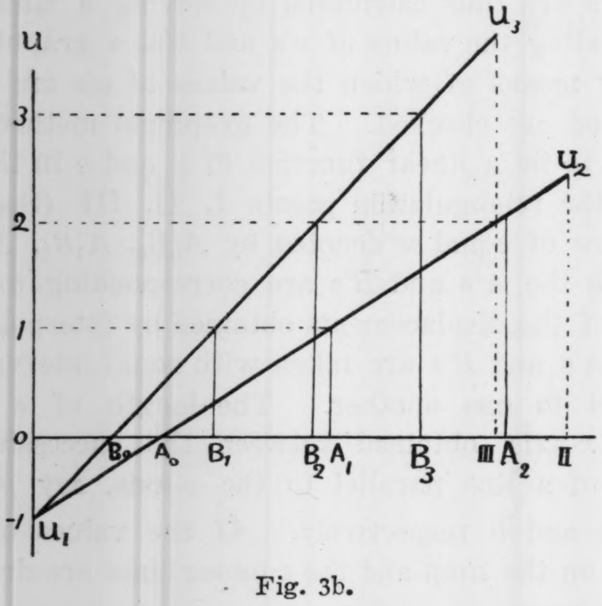
u
u_3
3
u_2
2
1
0
-1
u_1
B_0
A_0
B_1
B_2
A_1
B_3
III
A_2
II

Fig. 3b.

these values in various ways, the following strain components are obtained:

rotation $\omega=\frac{1}{2}(b-a')$

dilatation $\varDelta=a+b'$

shear $S=\frac{1}{2}(a'+b)$

maximum shear $S_m=\sqrt{(a'+b)^2+(a-b')^2}$

principal axes of strains $\gamma_{\frac{1}{2}} = \Delta \pm S_m$

their directions $\tan 2\theta_{\frac{1}{2}} = \dfrac{a'+b}{a-b'}$

In this study, the strain components are calculated by using the the data of horizontal displacements of the primary triangulation points reproduced in Table I, the results being given in Table II. The distribution of dilatation, rotation, shear, and principal strains are shown in Figs. 4~7, in which the numerical values of the strain components are set down at the approximate centres of the corresponding triangles.

Table I.

Triangulation point	u eastward displacement (m)	v northward displacement (m)	Triangulation point	u eastward displacement (m)	v northward displacement (m)
1	0·00	0·00	8	+0·26	+0·01
2	0·00	0·00	9	−0·13	−0·02
3	−0·01	+0·02	10	−0·07	−0·12
4	+0·13	+0·17	11	−0·17	+0·03
5	+0·04	−0·14	12	−0·45	−0·05
6	−0·26	+0·20	13	−0·10	−0·04
7	−0·43	+0·07	14	−0·57	+0·08

Table II.

		ω in 10^{-6} +, counter-clockwise	Δ in 10^{-6}	S_m in 10^{-6}	γ_1 in 10^{-6}	γ_2 in 10^{-6}	θ_1, referred to E., measured counter-clockwise
(1)	1—2—5	+ 1·4	+ 1·4	3·1	+ 4·5	− 1·7	73° 40′
(2)	1—2—6	− 4·6	+ 1·8	9·3	+11·1	− 7·5	1 45
(3)	1—3—4	+ 2·6	− 6·4	10·9	+ 4·5	−17·3	−20 50
(4)	1—3—5	+ 0·3	+ 7·0	6·6	+13·6	+ 0·4	16 30
(5)	1—4—5	+11·1	− 7·1	19·2	+12·1	−26·3	20 50
(6)	1—5—6	+ 0·9	−16·2	19·1	+ 2·9	−35·3	46 10
(7)	2—5—6	− 6·6	−23·1	29·1	+ 6·0	−52·2	30 10
(8)	3—4—5	+ 8·1	+ 2·1	9·8	+11·9	− 7·7	21 50
(9)	4—5—6	− 4·8	− 7·4	33·4	+26·0	−40·8	44 20
(10)	5—6—7	− 0·6	− 6·4	28·6	+22·2	−35·0	50 55
(11)	5—7—8	− 0·1	−33·1	20·6	−12·5	−53·7	72 35
(12)	7—8—9	− 1·5	−24·4	29·6	+ 5·2	−54·0	82 40
(13)	7—8—11	+ 3·3	−25·1	27·2	+ 2·1	−52·3	−87 50
(14)	8—9—10	− 4·4	+ 0·1	21·8	+21·9	−21·7	54 50
(15)	8—9—13	− 4·0	−17·8	21·8	+ 4·0	−39·6	78 5
(16)	8—10—11	− 4·5	+ 0·6	21·2	+21·8	−20·6	54 30
(17)	8—11—13	− 3·0	−10·0	15·7	+ 5·7	−25·7	69 50
(18)	9—10—13	+ 2·7	− 5·7	6·5	+ 0·8	−12·2	50 55
(19)	10—11—13	+ 2·4	− 5·9	5·9	+ 0·1	−11·8	51 20
(20)	11—12—13	− 4·8	− 5·8	16·7	+10·9	−22·5	79 30
(21)	11—12—14	− 5·7	−14·3	8·8	− 5·5	−23·1	88 0
(22)	11—13—14	− 1·7	− 9·8	13·6	+ 3·8	−23·4	66 40
(23)	12—13—14	− 2·3	−14·1	9·0	− 5·1	−23·1	65 40

(2) Geographical distributions of horizontal strains.

From the geographical distributions given in Figs. 4~7, we notice the following points.

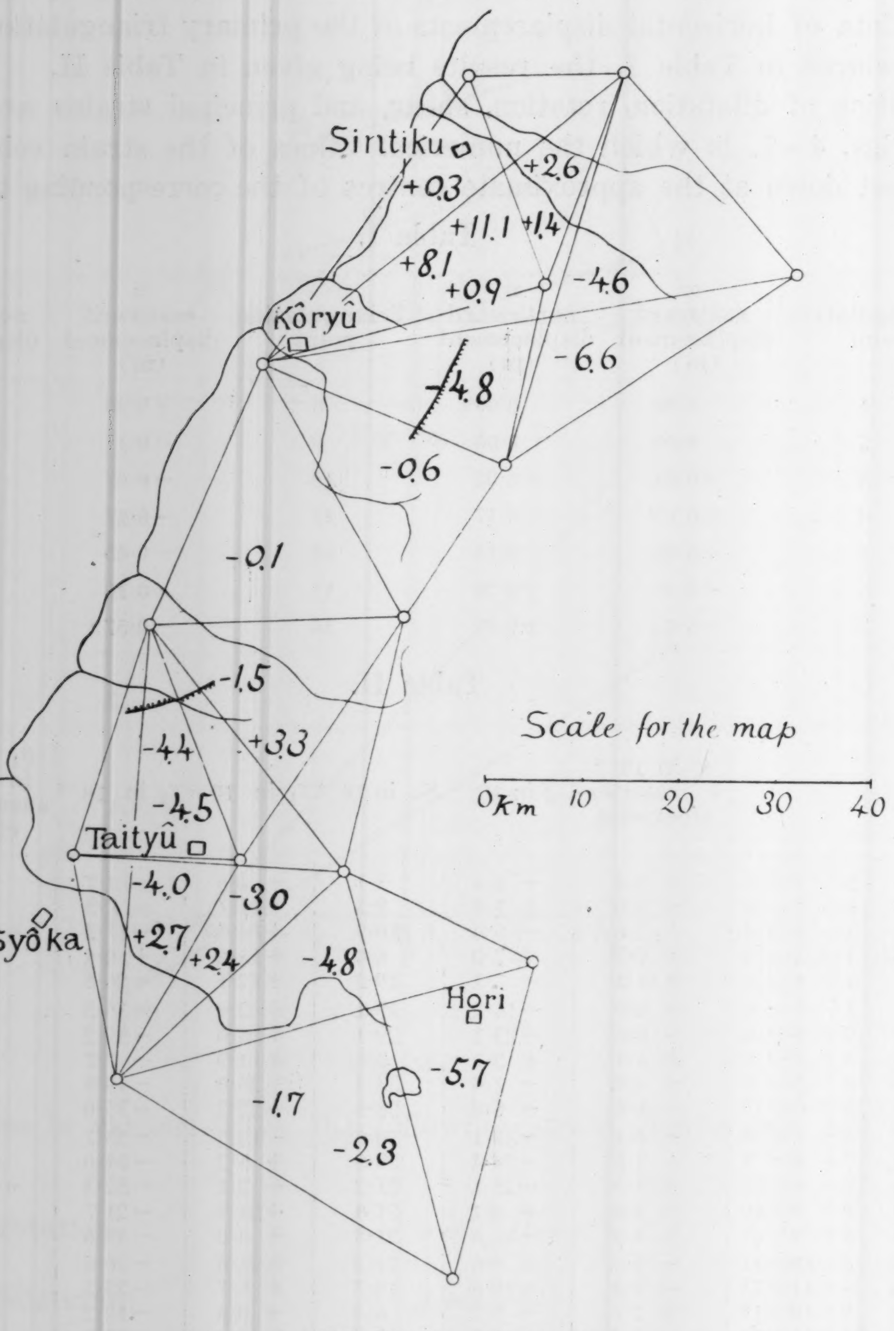
Sintiku
+0.3
+2.6
+11.1
+1.4
+8.1
+0.9
-4.6
Kôryû
-6.6
-4.8
-0.6
-0.1
-1.5
-4.4
+3.3
-4.5
Taityû
-4.0
-3.0
Syôka
+2.7
+2.4
-4.8
Hori
-5.7
-1.7
-2.3
Scale for the map
0 Km
10
20
30
40

Fig. 4. Distribution of rotation.

a) From the distribution of rotational deformation shown in Fig. 4, it is noticed that, with minor exceptions, the rotational deformation is negative, i.e. the sense of rotation is clockwise, its magnitude being of the order of 10^{-6}.

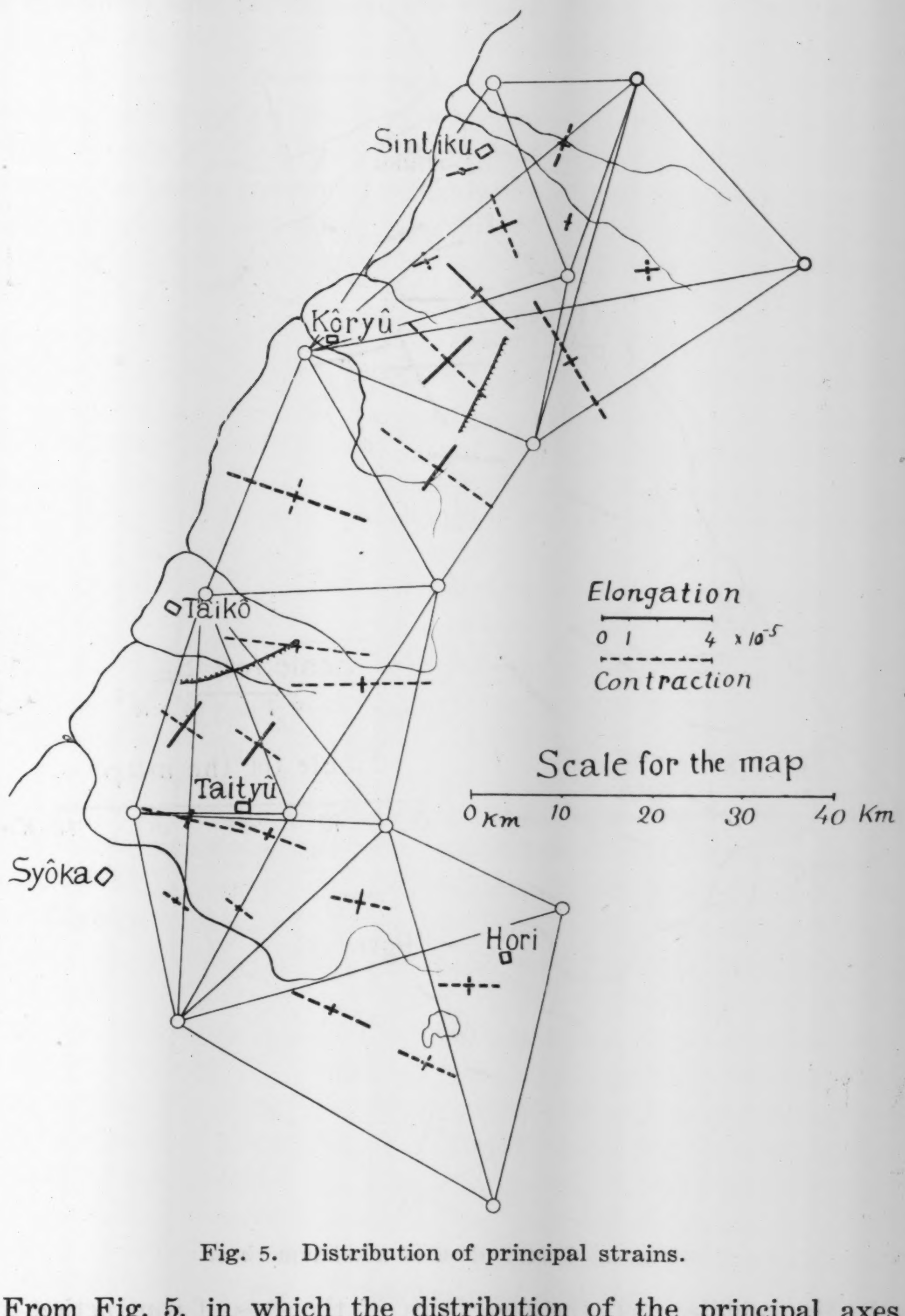
Sintiku
Kôryû
Taikô
Taityû
Syôka
Hori
Elongation
0 1 4 ×10⁻⁵
Contraction
Scale for the map
0 Km 10 20 30 40 Km

Fig. 5. Distribution of principal strains.

b) From Fig. 5, in which the distribution of the principal axes of strain ellipses are shown, it may be suggested that the region under consideration could be divided tentatively into three parts, namely, the middle part where crustal deformation was most conspicuous, and the northern and the southern parts where the earth's crust was not so disturbed as in the middle part.

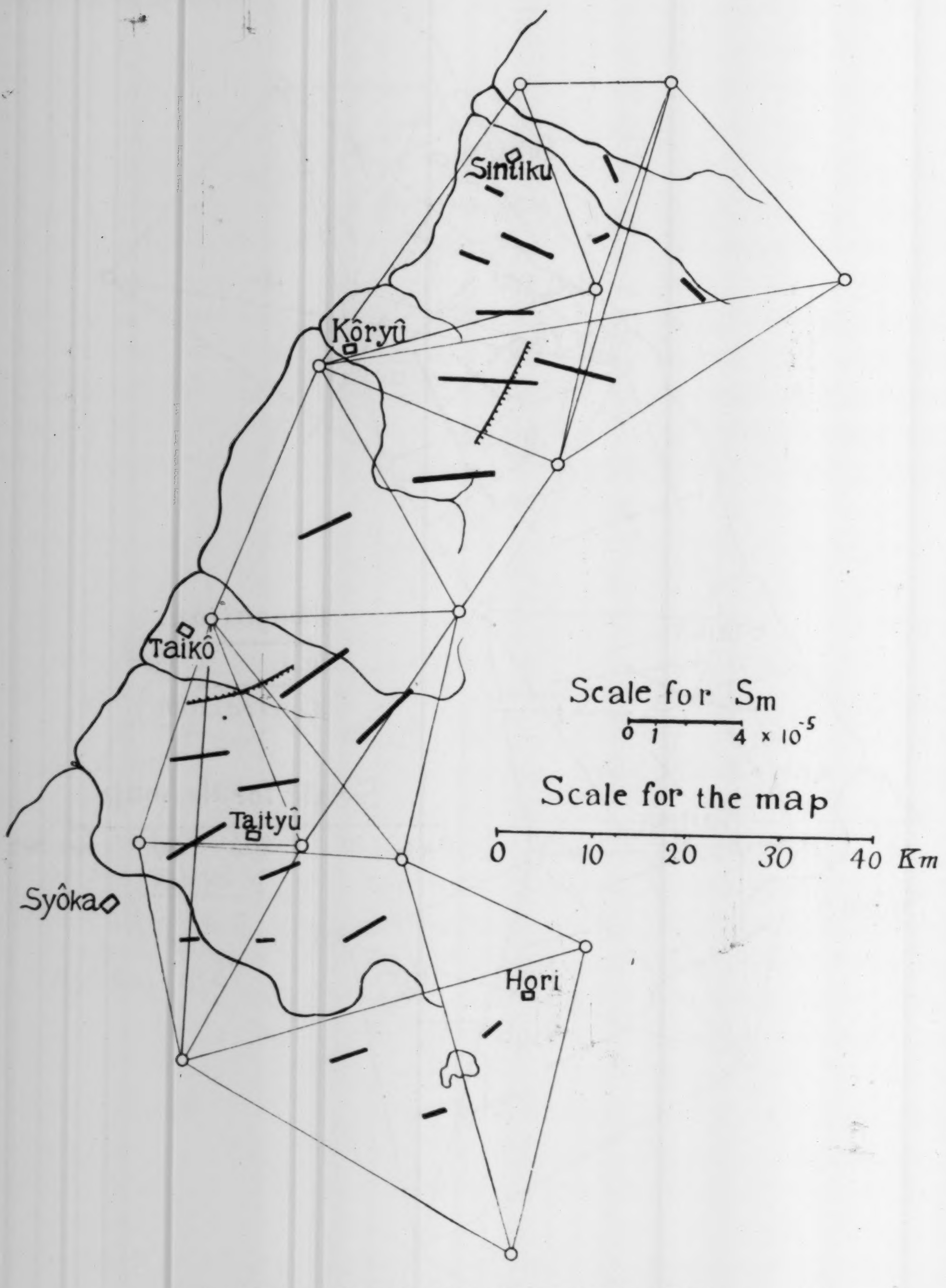
Sintiku
Kôryû
Taikô
Taityû
Syôka
Hori
Scale for Sm
0 1 4 × 10⁻⁵
Scale for the map
0 10 20 30 40 Km

Fig. 6. Distribution of maximum shear.

In the middle part, the directions of the axes of contraction of the principal strains are approximately perpendicular to the general trend of the Siko fault, its magnitude being of the order of 10^{-5}. In the other parts, the magnitudes of elongation and contraction are decidedly small compared with those of the middle part.

c) It will be noticed from Fig. 7, in which the distribution of dilatation is shown, that throughout the region under consideration, the sign of dilatation is on the whole negative, its magnitude being of the order of 10^{-6} -10^{-5}.

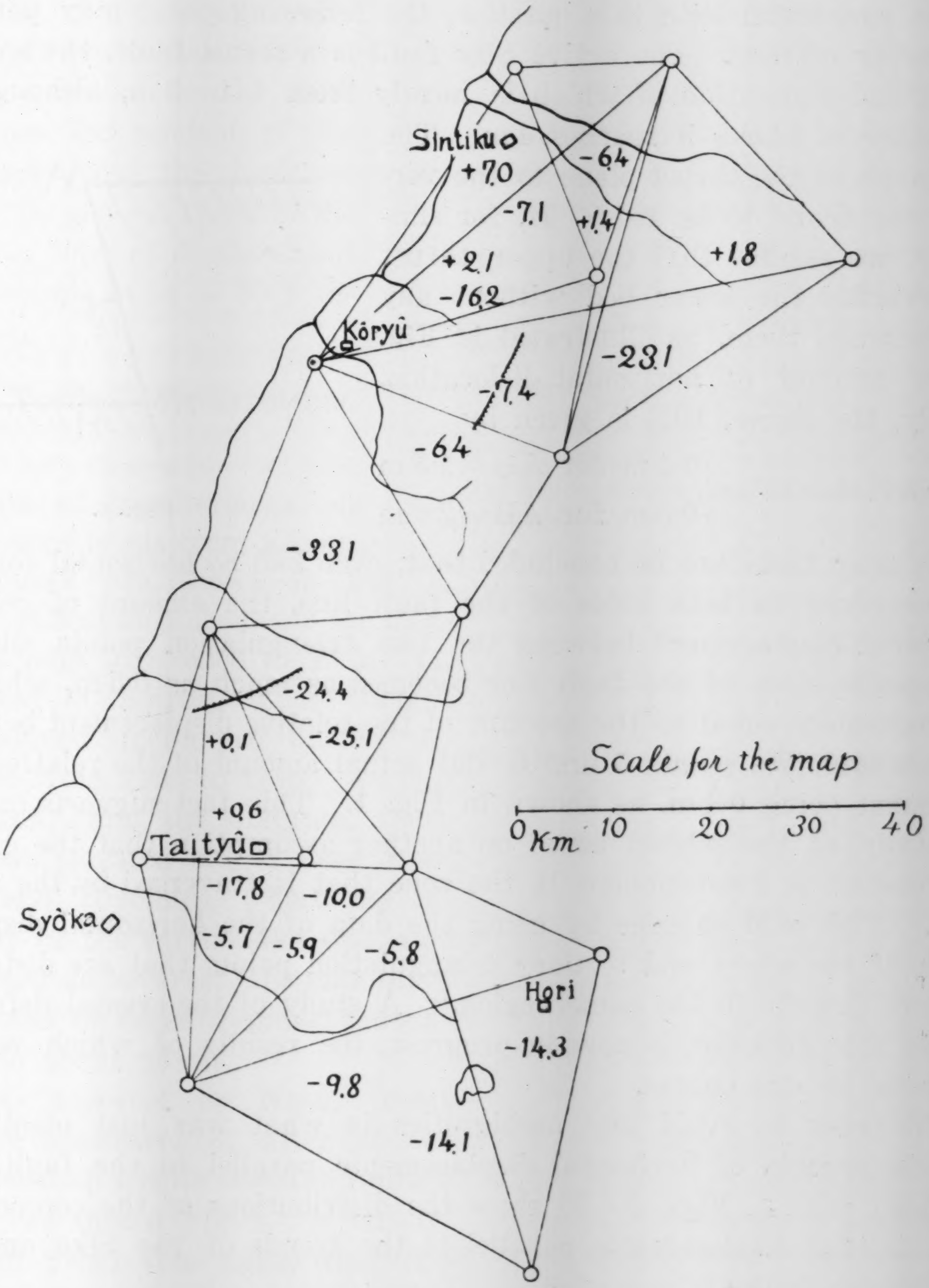
Sintiku
+7.0
-6.4
-7.1
+1.4
+1.8
+2.1
-16.2
Kôryû
-23.1
-7.4
-6.4
-33.1
-24.4
+0.1
-25.1
Scale for the map
0 Km 10 20 30 40
+0.6
Taityû
-17.8
-10.0
Syôka
-5.7
-5.9
-5.8
Hori
-14.3
-9.8
-14.1

Fig. 7. Distribution of dilatation.

d) In the above calculation it was assumed that in each of the triangular areas, the horizontal displacements are linear and are continuous functions of x and y. It may however be questioned whether this assumption is valid, especially in discussing crustal deformation in regions traversed by active faults.

In connection with this question, the following point may perhaps be worthy of note. The active Siko fault is a thrust fault, the amount of vertical dislocation of which is mostly from 1 to 2 m, although in a number of places it reaches 4 m. The inclination of the thrust plane to the vertical was found to be 15°.[3] If, for simplicity, we assume that the upper thrust bed overlies the lower bed without any gap between them, as illustrated in Fig. 8, the amount of horizontal dislocation, namely, the heave, BH, is given by

$$BH = AH \cdot \tan 15° = \begin{cases} 0{\cdot}4\text{ m for } AH = 1{\cdot}5\text{ m} \\ 0{\cdot}5\text{ m for } AH = 2{\cdot}0\text{ m} \end{cases}$$

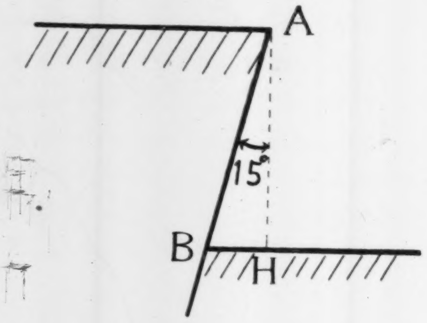

Fig. 8.

It may therefore be concluded that, even had no horizontal contraction occurred on both sides of the fault line, the amount of relative horizontal displacement between the two triangulation points situated on opposite sides of the fault line becomes as much as 0·5 m, which is approximately equal to the amount of the relative displacement between the triangulation points 5 and 6, thd actual amount of the relative displacement being 0·4 m. as shown in Fig. 1. This fact suggests making a restudy of the subject based on another assumption that the crustal deformation is discontinuous in the zone that is traversed by the active fault. This will be done by using the data of the horizontal displacements of secondary and tertiary triangulation points that are distributed more densely in the same region.[4] A study of the crustal deformation in this direction is now in progress, the results of which will be published in due course.

e) In order to avoid any ambiguities in what was just mentioned, the components of horizontal displacements parallel to the fault lines are dealt with. Figs. 9~10 show the distributions of the components of horizontal displacements parallel to the trends of the Siko and the Tonsikyaku faults.

A glance at Fig. 9 will show that the amount of the component of displacement at any triangulation point on the west side of the Siko fault is equal to that of the triangulation points situated on the east side of the fault. In Fig. 10 it is pointed out that, in the eastern part of the Tonsikyaku fault, the components of horizontal displacements parallel to the fault line are independent of the distance from the fault, so that the general trend of the contour lines of displacement components is in a N–S direction.

---

[3] Y. OTUKA, *Bull. Eartq. Res. Inst., Suppl.* Vol. **3** (1936). 22~74 (Japanese)

[4] The data are published by the Military Land Survey (1937).

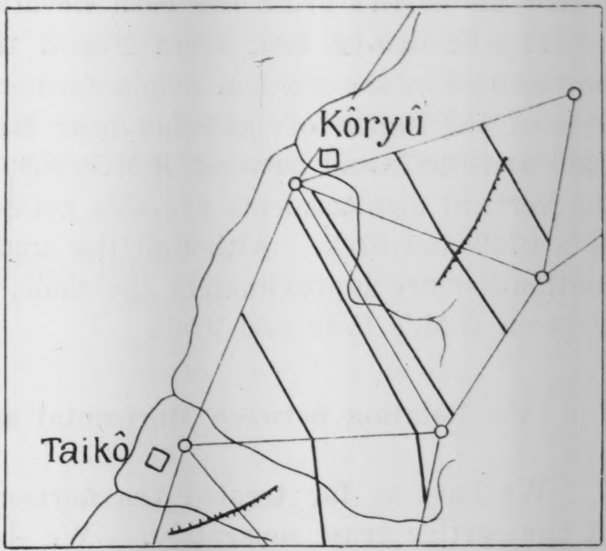

Fig. 9. Distribution of components of horizontal displacements parallel to the trend of Siko fault.

III. Vertical Displacements.

The changes in the heights of bench-marks on the line of levels from Kiirun to Musya are shown in Fig. 2. The vertical displacements are measured with reference to B. M. 11, situated at Kiirun, whose height is assumed unchanged during the period from 1915 to 1936. As will be seen from the diagram, there are two elevated bulges near Byōritu and Toyohara, where the intensity of the earthquake was also reported as severest, the maximum elevation in these regions amounting to about 80 cm.

As reported by Nasu,[5] most of the epicentres of after shocks are located within certain limited areas, as shown Fig. 1. It will be noticed from this figure that the region where the epicentres of the after-shocks are concentrated is very close to the elevated region, a fact that agrees with the general tendency pointed out by Ishimoto[6] that

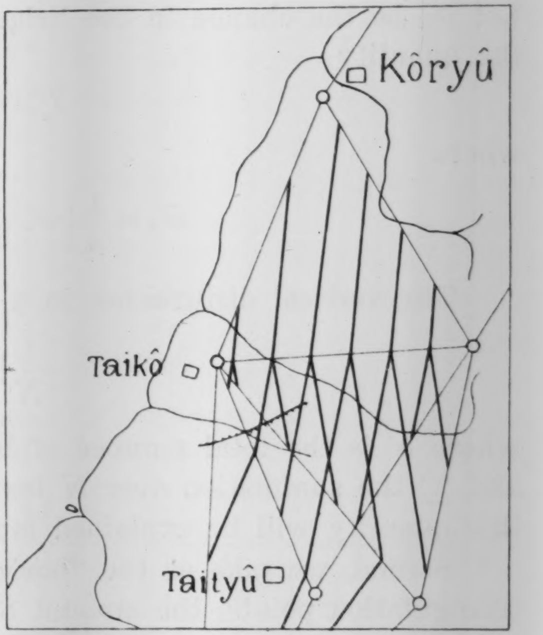

Fig. 10. Distribution of components of horizontal displacements parallel to the trend of the Tonsikyaku fault.

---

[5] N. NASU, *Bull. Earthq. Res. Inst., Suppl.* Vol. **3** (1936), 75. (in Japanese)
[6] M. ISHIMOTO, *Zisin,* Vol. **9** (1937), 108. (in Japanese)

the epicentres of after-shocks distribute themselves mostly in regions-where the earth's crust has been elevated.

It will also be seen from Fig. 2 that there are remarkable discontinuities in the vertical displacements at the northern and southern ends of the region of up-bulge near Byōritu, namely, between B.M.'s 9586 and 9987, and between B.M.'s 9589 and 9592. Discontinuities in the vertical displacements are also noticed near Naiho-syō, between B. M.'s 9740 and 9742. Although the amount of dislocation at these discontinuities are approximately the same, an active fault was found only between B.M.'s 9740 and 9742.

IV. Relation between Horizontal and Vertical Displacements.

We have so far treated the horizontal and vertical displacements of the earth's crust separately. We shall now deal with the relation between the two components, the horizontal and vertical earth movements. We first introduce the quantity "local disturbance of vertical displacements", or, shortly, vertical disturbances, defined as follows. Let w_n be the change in the height of the n-th bench-mark, and take the quantity

$$\delta_n = w_n - \overline{w}_n,$$

where

$$\overline{w}_n = \frac{1}{4}\left\{w_{n-1} + 2w_n + w_{n+1}\right\}.$$

The vertical disturbance in a certain region is then expressed by

$$\frac{1}{N}\left|\sum \delta_n\right|,$$

where N is the total number of bench-marks in the region in queastion and $\sum$ the summation over N bench-marks. The physical meaning of this quantity will be explained later.

Second, we take as the "horizontal disturbance" between any two triangulation points, the amount of elongation or contraction in length in the direction of the line joining the two triangulation points, namely, the quantity denoted by $|\delta l|/l$, where l is the length of the line joining the triangulation points and δl the variation in its direction.

In comparing the vertical disturbance with the horizontal disturbance just defined, the values of $\frac{1}{N}\sum|\delta_n|$ are calculated for parts of the line of levels approximately parallel to the line joining the two triangulation points. The values of $\frac{1}{N}\sum|\delta_n|$ are thus calculated for six parts of the line of levels under consideration, the results being given in Table III, together with the values of the horizontal disturbances. In Fig. 11, the vertical disturbance for various parts of the line of levels thus calculated are plotted against the corresponding horizontal disturbance.

Table III.

No.	Triangulation points	l in km	Δl in cm	$\frac{\Delta l}{l}$ in 10^{-6}	Bench-marks	N	$\sum\|\delta\|$ in mm	$\frac{1}{N}\sum\|\delta\|$ in mm
I	1~ 3	15	+0	+0·0	9560~9567	8	8·5	11
II	3~ 5	32	+11	+3·4	9568~9586	19	87·0	44
III	5~ 8	27	−20	−7·4	9587~9739	16	108·5	68
IV	8~10	23	+22	+9·6	9740~9493	13	33·4	26
V	9~13	20	+0	+0·0	9494~9500	7	4·2	6
VI	13~12	40	−35	−8·8	9501~4	25	192·3	77

As will be seen from this figure, the horizontal disturbances and the vertical disturbances are in approximate linear relation, and the former is large when the latter is large. There is a point (IV) in the diagram of Fig. 11 which deviates considerably from the approximate linear relation. This shows the relation between the two sorts of disturbances for the part of the line that crosses the Siko fault.

It is of course a question whether the linear relation mentioned above has really any physical significace. However, if the linear relation mentioned above really exists, the following may be one of the explanations for it.

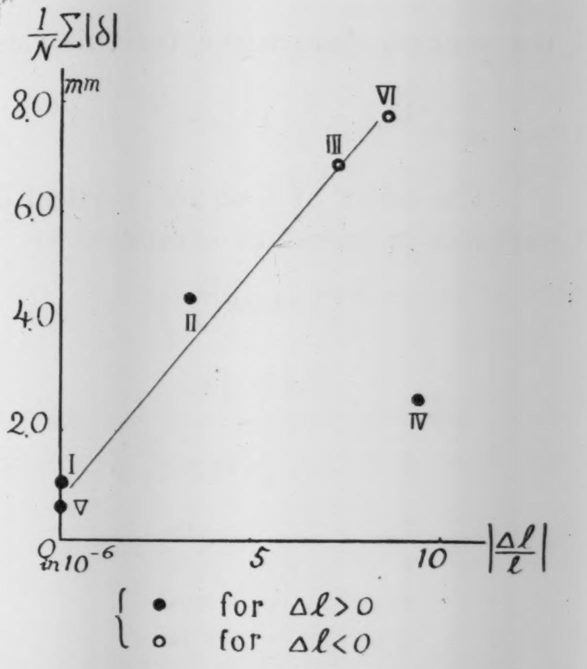

Fig. 11. Relation between horizontal and vertical disturbances.

Consider an extreme case in which the vertical displacements are expressed by a circular function of the number of the bench-marks, n, namely,

$$w_n = A\sin\left(\frac{2\pi}{\lambda}\cdot n+\alpha\right), \qquad (\lambda \geqq 2, \quad n=1,\ 2,\cdots\cdots N)$$

we have

$$\overline{w}_n = \frac{1}{2}\left(1+\cos\frac{2\pi}{\lambda}\right)w_n,$$

$$\delta_n = \frac{1}{2}\left(1-\cos\frac{2\pi}{\lambda}\right)w_n,$$

and

$$\frac{1}{N}\sum|\delta_n| = \frac{1}{2N}\left(1-\cos\frac{2\pi}{\lambda}\right)\cdot\sum|w_n|.$$

And since

$$\sum|w_n| = A\cdot\sum_{n=1}^{N}\left|\sin\left(\frac{2\pi}{\lambda}n+\alpha\right)\right|$$

$$\fallingdotseq A\ \frac{2N}{\lambda}\int_0^{\frac{\pi}{2}}\sin x dx$$

$$= A\cdot\frac{2N}{\lambda},$$

the vertical disturbance for this case is given by

$$\frac{1}{N}\sum|\delta_n| = \frac{1}{\lambda}\left(1-\cos\frac{2\pi}{\lambda}\right)\cdot A.$$

The effect of λ on the vertical disturbance is therefore expressed by

$$\frac{1}{\lambda}\left(1-\cos\frac{2\pi}{\lambda}\right).$$

Table IV.

λ	$\frac{1}{\lambda}\left(1-\cos\frac{2\pi}{\lambda}\right)$.
2	1·00
3	0·50
4	0·25
5	0·14
6	0·08
7	0·06
8	0·04

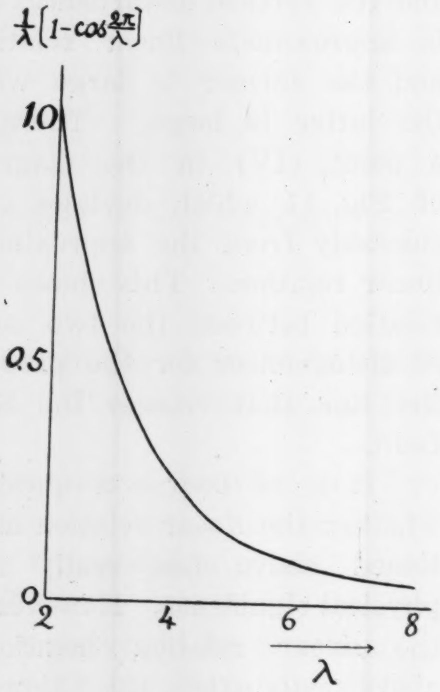

Fig. 12.

In Table IV, will be found the amount of $\frac{1}{\lambda}\left(1-\cos\frac{2\pi}{\lambda}\right)$ for various values of λ. The function

$\frac{1}{\lambda}\left(1-\cos\frac{2\pi}{\lambda}\right)$ is plotted against λ as shown in Fig. 12.

As shown in Fig. 12, the amount of $\frac{1}{\lambda}\left(1-\cos\frac{2V}{\lambda}\right)$, consequently $\frac{1}{N}\sum|\delta_n|$ in this extreme case, decreases rapidly with increasing λ.

Should the foregoing consideration for the extreme case be applied in explaining the actual deformation, it is possible to conclude from the linear relation between the horizontal and the vertical disturbances, as shown in Fig. 12, that, except for the region traversed by active faults, the greater the horizontal disturbances, the smaller the value of λ, as in the case of wave-length when the amplitude of fluctuation in vertical or horizontal disturbance is kept constant. Should, in this case, the wave-length of the assumed wavy deformation be constant, the amplitude would naturally become greater.

V. Summary.

The results of the present study are summarized as follows;

(1) From the results of re-triangulation of the primary triangulation points in the central part of Taiwan, where the destructive earthquake of 1935 occurred, the horizontal strain components are calculated for each triangle having three adjoining triangulation points at their vertices. The geographical distribution of rotation, dilatation, shear, maximum shear, as well as the principal strains, are shown.

(2) The mode of deformation is discussed on the basis of two different assumptions. The one that the deformation is continuous in the zone of active faults and the other that the deformation is discontinuous there.

(3) In that region where the epicentres of the after-shocks were concentrated, the earth's crust was elevated in a marked manner, as it had already done in other districts.

(3) A linear relation between the horizontal and the vertical disturbances was noticed, and its physical meaning considered.

In conclusion, the writers wish to express their sincere thanks to Professor Sakuhei Fujiwhara for his suggesting the subject for study, and to Doctor Naomi Miyabe for much information and kind guidance received throughout the course of this study.

26. 臺灣中部の地殼變形（第一報）

地震學教室 佐藤光之助
福永三郎

昭和 10 年 4 月 21 日の臺中新竹烈震後行はれた復舊測量に依つて地震前後數年間に於ける地殼變動が明らかにされた．本論文はそれを取扱つたものである．今回は一等三角點と一等水準點との變動に就いて論ずるに止めた．水平の歪の計算に當つては二つの別な方法を取つた．第一は各三角內で變移が連續であると假定して行つたもので，その結果は第 4 圖～第 7 圖に示してある．紙湖斷層附近では，それに垂直な縮みが大きく，屯子脚斷層附近ではそれに略平行な縮みが大きい．垂直變動については紙湖斷層の西側に二つの隆起部分が有り，而もそれが餘震の頻發地域に近接してゐる事が著しい．最後に垂直變動と水平變動とを併せ考へて見た．卽ち數學的に假りに定義した「水平の disturbance」と「垂直の disturbance」とを色々の地域に就いて比較した所，兩者の間に稍明瞭な關係を得たので之に對する物理的解釋を述べておいた．

終りに，本研究は筆者等後期學生の演習問題として藤原先生から戴き，專ら宮部先生の御懇切な御指導の下に行はれたものである事を記して兩先生に厚く御禮を申し上げます．

27. *Seismic Waves due to Tractions Applied to the Inner Surface of a Spherical Cavity in an Elastic Earth.*

By Genrokuro NISHIMURA and Takeo TAKAYAMA,

Earthquake Research Institute.

(Received March 20, 1938.)

1. In the present paper, which is a continuation of the previous one[1], we shall, with the aid of numerous figures, deal with wave-phenomena in the following two cases; [1] that in which the inner surface of a spherical cavity in an elastic earth is subjected to normal traction of shock type, [2] that in which the inner surface of the cavity is subjected to a shearing force of the same type.

2. Now let the boundary-conditions on the inner surface of a spherical cavity in an elastic earth be expressed as follows[2]:

When $t \geqq 0$,

$$\widehat{rr}_{r=a} = -P\frac{t}{t_m}\exp\{1-t/t_m\}, \qquad \widehat{r\theta}_{r=a} = \widehat{r\phi}_{r=a} = 0,$$

and when $t \leqq 0$,

$$\left.\widehat{rr}_{r=a} = \widehat{r\theta}_{r=a} = \widehat{r\phi}_{r=a} = 0. \right\} \tag{1}$$

Then the radial vibrations of a particle in the earth due to the longitudinal wave that issues from the cavity are expressed by

$$\begin{aligned} u = \frac{aP}{\mu}\left(\frac{a}{r}\right)\Bigg[& \frac{\alpha(V/v)^3}{\sqrt{1-(V/v)^2}} \frac{\{4\alpha-4(V/v)^2-\alpha^2\}}{\{4(V/v)^2-4(V/v)^2\alpha+\alpha^2\}^2} \cdot \\ & \cdot \exp\{1-2(V/v)^2\tau\} \cdot \sin\left\{2(V/v)\sqrt{1-(V/v)^2}\tau\right\} \\ & + \frac{\alpha(V/v)^2\{\alpha^2-4(V/v)^2\}}{\{4(V/v)^2-4(V/v)^2\alpha+\alpha^2\}^2}\exp\{1-2(V/v)^2\tau\} \cdot \\ & \cdot \cos\left\{2(V/v)\sqrt{1-(V/v)^2}\tau\right\} \end{aligned}$$

---

[1] G. NISHIMURA, *Bull. Earthq. Res. Inst.*, **15** (1937), 614~635.

[2] The meanigs of the notations used in the present paper are explained in the previous paper. G. NISHIMURA, *loc. cit.*

$$+\frac{\alpha(V/v)^2\{4(V/v)^2-\alpha^2\}}{\{4(V/v)^2-4(V/v)^2\alpha+\alpha^2\}^2}\exp\{1-\alpha\tau\}$$

$$\left.-\frac{\alpha^2(V/v)^2}{\{4(V/v)^2-4(V/v)^2\alpha+\alpha^2\}}\tau\exp\{1-\alpha\tau\}\right]$$

$$+\frac{aP}{\mu}\left(\frac{a}{r}\right)^2\left[\frac{\alpha(V/v)}{2\sqrt{1-(V/v)^2}}\frac{\{\alpha^2-4(V/v)^2\alpha-4(V/v)^2\}+8(V/v)^4}{\{4(V/v)^2-4(V/v)^2\alpha+\alpha^2\}^2}\cdot\right.$$

$$\cdot\exp\{1-2(V/v)^2\tau\}\sin\left\{2(V/v)\sqrt{1-(V/v)^2}\tau\right\}$$

$$+\frac{2(V/v)^2\alpha\{2(V/v)^2-\alpha\}}{\{4(V/v)^2-4(V/v)^2\alpha+\alpha^2\}^2}\exp\{1-2(V/v)^2\tau\}\cdot$$

$$\cdot\cos\left\{2(V/v)\sqrt{1-(V/v)^2}\tau\right\}$$

$$+\frac{2(V/v)^2\alpha\{\alpha-2(V/v)^2\}}{\{4(V/v)^2-4(V/v)^2\alpha+\alpha^2\}^2}\exp\{1-\alpha\tau\}$$

$$\left.+\frac{\alpha(V/v)^2}{\{4(V/v)^2-4(V/v)^2\alpha+\alpha^2\}}\tau\exp\{1-\alpha\tau\}\right], \qquad (2)$$

where

$$\alpha=\frac{a}{t_m v},\quad \tau=\frac{v}{a}\left(t-\frac{r-a}{v}\right),\quad v=\sqrt{\frac{\lambda+2\mu}{\rho}},\quad V=\sqrt{\frac{\mu}{\rho}}. \qquad (3)$$

Expression (2) may easily be deduced from expression (12) of the previous paper(3). It may be seen from expression (2) that the longitudinal waves generated by a normal (perpendicular) force of shock type (1) are of three kinds; [1] waves of the same time-variation as the force applied to the cavity, [2] waves of sinusoidal time-variation, and [3] other waves with an aperiodic damping time-variation that are set up in order to satisfy the initial conditions on the boundary of the cavity. For ease of reference, we shall refer to the first, second, and third kinds of waves as FORCED, FREE(4) and COMPLEMENTARY WAVES. In other words,

the waves that emanate from the cavity =
the forced waves + the free waves
+ the complementary waves. (4)

---

3) G. NISHIMURA, *loc. cit.*

4) Naturally, both the periods and the damping ratio of the free waves, which are respectively expressed by $\frac{\pi}{(V/v)\sqrt{1-(V/v)^2}}\frac{a}{v}$, $e^{\pi\frac{(V/v)}{\sqrt{1-(V/v)^2}}}$ in the present case, do not depend on the mode of time-variation in the stress applied to the inner surface of the cavity, although their intensities depend entirely on it. H. KAWASUMI and R. YOSHIYAMA. *Disin*, **7** (1935), 367.

The respective amplitudes of these three kinds of waves are functions of the value of $a/(t_m v)$, which we may call the rapidity of the stress applied to the cavity. We notice from expression (2) that when $a/(t_m v) \rightarrow 0$, only the following forced waves issue from the cavity:

$$u=\frac{1}{4}\frac{aP}{\mu}\left(\frac{a}{r}\right)^2\frac{1}{t_m}\left(t-\frac{r-a}{v}\right)\exp\left\{1-\frac{1}{t_m}\left(t-\frac{r-a}{v}\right)\right\},$$

of which the amplitudes are proportional to the square of the inverse ratio of the distance from the centre of the cavity—a fact which shows that the wave-phenomena occur when $a/(t_m v) \rightarrow 0$, is likely to be the same as in the statical problem.

Since the damping ratio σ_f[5] of the free wave is give by $e^{\pi\sqrt{1-2\sigma}}$, when Poisson's ratio becomes 0·50, σ_f becomes unity. If therefore, we hypothetically suppose that the value of the Poisson ratio of the material changes temporally from the normal value[6] to a value near 0·50 on and near the earthquake origin only at the instant the seismic waves emanate from the origin, it will be seen that even if one shock were applied to the earthquake origin, the seismic waves emanating from that origin would consist of many regular trains of oscillatory waves, the damping ratio of which is nearly unity.

To get the nature of the wave-motion of particles that are some distance away from the cavity, we obtain from expression (2) the following approximate expression for longitudinal waves:

$$u_{r\rightarrow\infty} \simeq u_{\text{free}} + u_{\text{forced}} + u_{\text{complementary}}, \tag{5}$$

where u_{free}, u_{forced}, and $u_{\text{complementary}}$ are respectively the free, forced, and complementary waves that emanate from the cavity, and which are expressed by

$$u_{\text{free}}=\frac{aP}{\mu}\left(\frac{a}{r}\right)\left[\frac{\alpha(V/v)^3}{\sqrt{1-(V/v)^2}}\cdot\right.$$
$$\cdot\frac{\{4\alpha-4(V/v)^2-\alpha^2\}}{\{4(V/v)^2-4(V/v)^2\alpha+\alpha^2\}^2}\exp\{1-2(V/v)^2\tau\}\cdot$$
$$\cdot\sin\left\{2(V/v)\sqrt{1-(V/v)^2}\tau\right\}$$

---

5) See foot note 4).

6) In the earth's cruts, the normal value of Poisson's ratio is assumed to be nearly 0·25.

$$\left.\begin{aligned} &+\frac{\alpha(V/v)^2\{\alpha^2-4(V/v)^2\}}{\{4(V/v)^2-4(V/v)^2\alpha+\alpha^2\}^2}\exp\{1-2(V/v)^2\tau\}\cdot \\ &\qquad\cdot\cos\left\{2(V/v)\sqrt{1-(V/v)^2}\tau\right\}\Bigg], && \text{(a)} \\ &u_{\text{forced}}=-\frac{aP}{\mu}\left(\frac{a}{r}\right)\frac{\alpha^2(V/v)^2}{\{4(V/v)^2-4(V/v)^2\alpha+\alpha^2\}}\tau\exp\{1-\alpha\tau\}, && \text{(b)} \\ &u_{\text{complementary}}=\frac{aP}{\mu}\left(\frac{a}{r}\right)\frac{\alpha(V/v)^2\{4(V/v)^2-\alpha^2\}}{\{4(V/v)^2-4(V/v)^2\alpha+\alpha^2\}^2}\exp\{1-\alpha\tau\}\cdot && \text{(c)} \end{aligned}\right\} \quad (6)$$

From expression (5), we obtain Figs. 1~12, in which are shown the radial vibrations of particles for various values of $a/(t_m v)$ in the elastic earth, the Poisson ratio of which is 1/4. From Figs. 1~12, we see that when rapidity $a/(t_m v)$ becomes large, the oscillatory nature of the wave-motion of the particle increases, and it will be seen, besides, that both the amplitudes and the apparent periods in a state of initial motion, as well as the apparent damping ratios of the radial vibrations of par-

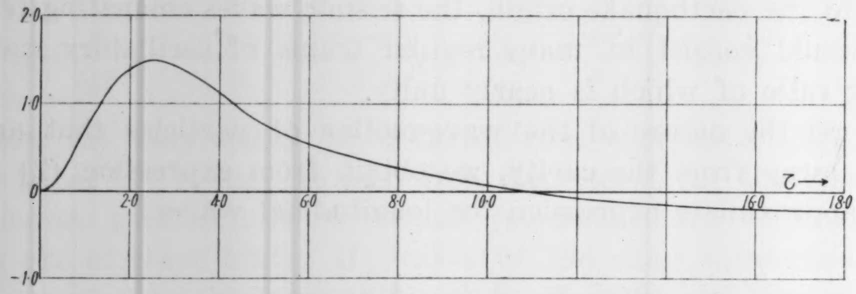

Fig. 1. $\frac{a}{t_m v}=0{\cdot}10$. The unit of the vertical scale$=\frac{u_{r\to\infty}}{aP/\mu\cdot(a/r)}$.

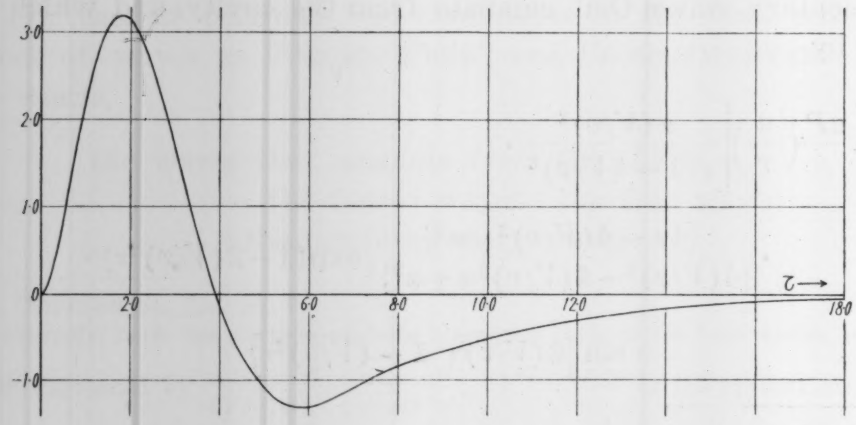

Fig. 2. $\frac{a}{t_m v}=0{\cdot}4$. The unit of the vertical scale$=\frac{u_{r\to\infty}}{aP/\mu\cdot(a/r)}$.

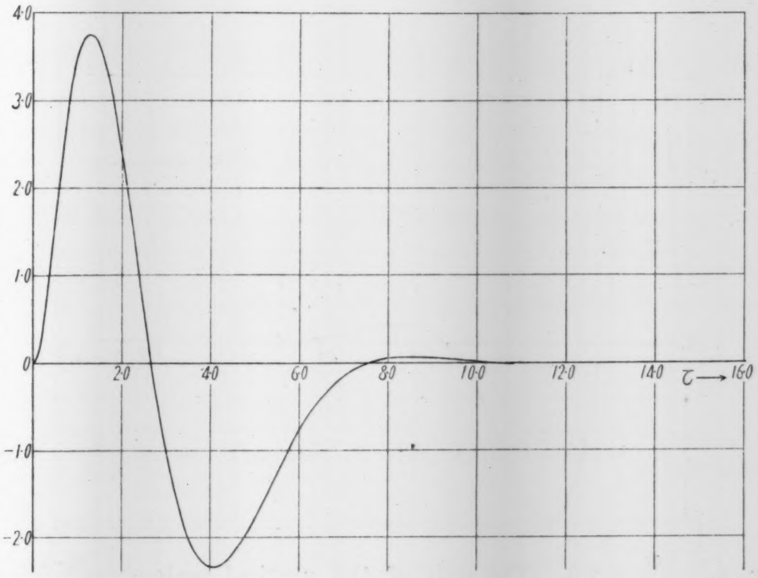

Fig. 3. $\frac{a}{t_m v}=1{\cdot}0$. The unit of the vertical scale$=\frac{u_{r\to\infty}}{aP/\mu\cdot(a/r)}$.

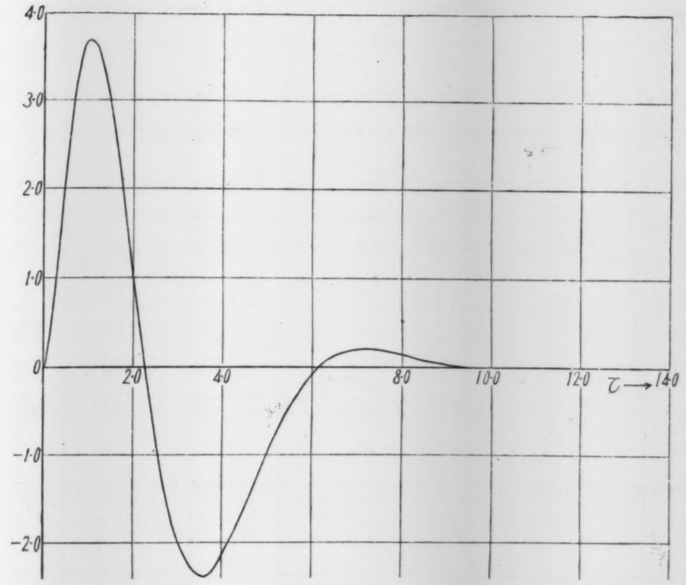

Fig. 4. $\frac{a}{t_m v}=1{\cdot}5$. The unit of the vertical scale$=\frac{u_{r\to\infty}}{aP/\mu\cdot(a/r)}$.

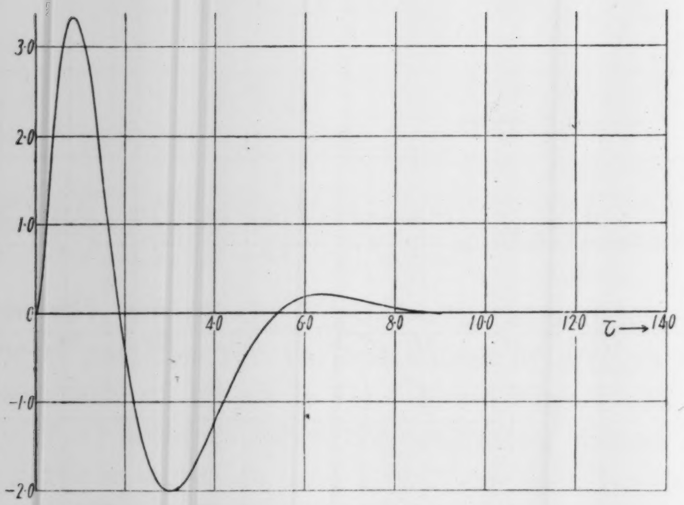

Fig. 5. $\dfrac{a}{t_m v}=2\cdot0$. The unit of the vertical scale$=\dfrac{u_{r\to\infty}}{aP/\mu\cdot(a/r)}$.

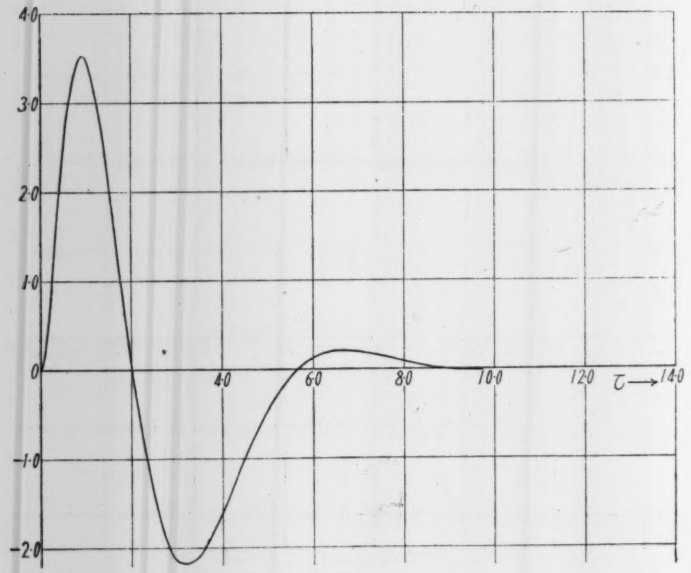

Fig. 6. $\dfrac{a}{t_m v}=2\cdot4$. The unit of the vertical scale$=\dfrac{u_{r\to\infty}}{aP/\mu\cdot(a/r)}$.

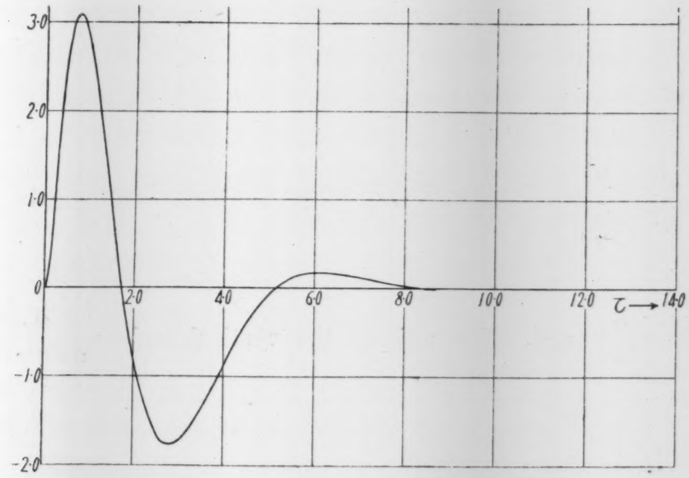

Fig. 7. $\frac{a}{t_m v}=3\cdot0$. The nnit of the vertical scale$=\frac{u_{r\to\infty}}{aP/\mu\cdot(a/r)}$.

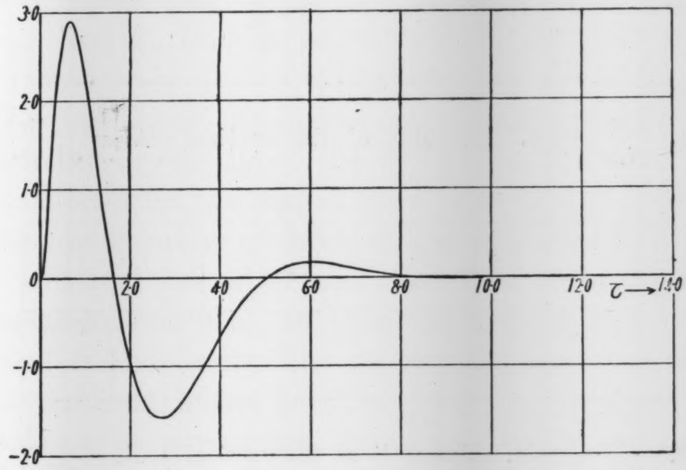

Fig. 8. $\frac{a}{t_m v}=3\cdot5$. The unit of the vertical scale$=\frac{u_{r\to\infty}}{aP/\mu\cdot(a/r)}$.

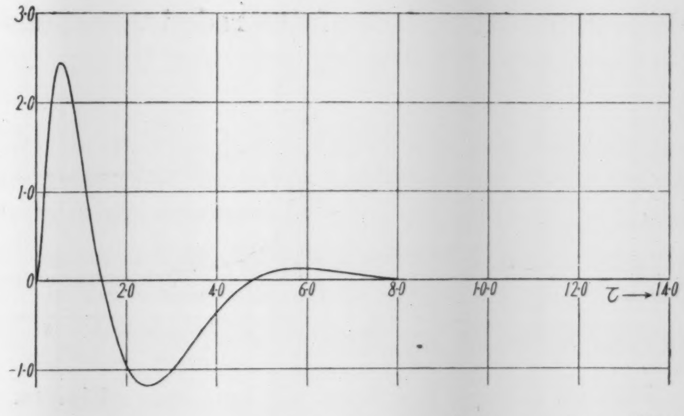

Fig. 9. $\frac{a}{t_m v}=5\cdot0$. The unit of the vertical scale$=\frac{u_{\cdot\to\infty}}{aP/\mu\cdot(a\ r)}$.

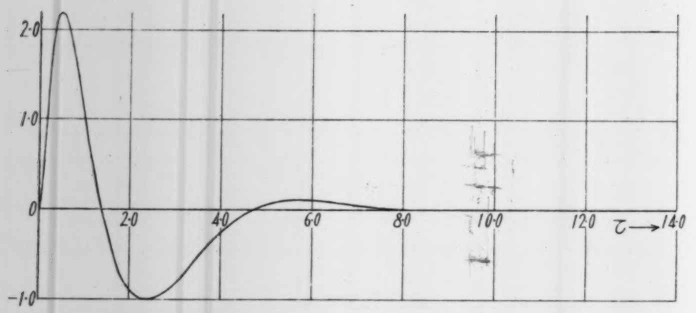

Fig. 10. $\frac{a}{t_m v}=6\cdot0$. The unit of the vertical scale$=\frac{u_{r\to\infty}}{aP/\mu\cdot(a/r)}$.

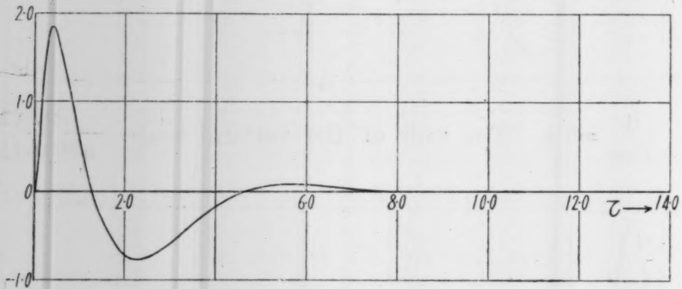

Fig. 11. $\frac{a}{t_m v}=8\cdot0$. The unit of the vertical scale$=\frac{u_{r\to\infty}}{aP/\mu\cdot(a/r)}$.

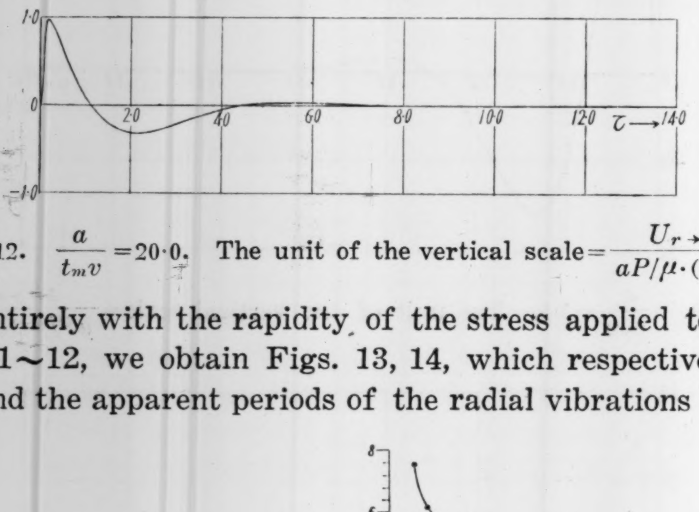

Fig. 12. $\frac{a}{t_m v}=20\cdot0$. The unit of the vertical scale$=\frac{U_{r\to\infty}}{aP/\mu\cdot(a/r)}$.

ticles, vary entirely with the rapidity of the stress applied to the cavity. Using Figs. 1∼12, we obtain Figs. 13, 14, which respectively show the amplitudes and the apparent periods of the radial vibrations in a state of

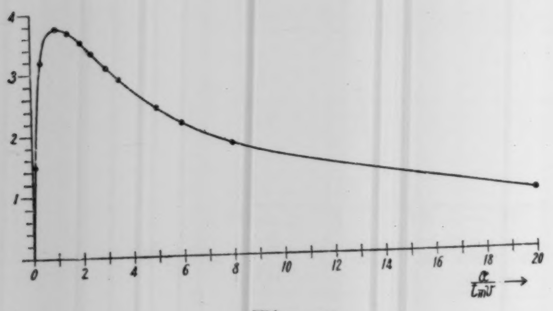

Fig. 13.

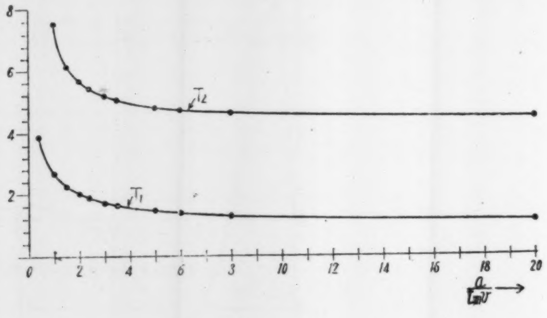

Fig. 14.

initial motion, the abscissae in these Figs. being the value of $a/(t_m v)$.

It will be seen from Fig. 13 that the amplitude of initial motion of a particle due to the longitudinal wave becomes maximum when $a/(t_m v) \doteqdot 1$, and also that when $a/(t_m v)$ becomes nil or increases infinitely, it becomes nil or very small respectively. It is not easy to understand the reason for the maximum amplitude of the initial wave-motion's occurring when $a/(t_m v) \doteqdot 1$, although the reason for the spectrum-like nature of the amplitude of wave-motion, as shown in Fig. 13, will be understood by calculating the kinetic energy as the result of the applied stress on the inner surface of the cavity. A spectrum-like nature of vibration-amplitude in a state of initial motion, as shown in Fig. 13, is also conceived for the case of a steady state[7], in which an infinite train of harmonic forced waves emanates from a spherical cavity as the result of the normal pressure of simple-harmonic time-variations applied to its inner surface, although such free and complementary waves as mentioned in the present paper do not actually issue from it.

Curves T_1 and T_2 in Fig. 14, which are obtained by using Figs. 1~12, show respectively the duration of time from the beginning of vibration to the time when the displacement-amplitude first becomes nil, and those from the beginning of the motion to the time when the displacement becomes nil for the second time. For ease of reference, we shall refer to the former duration of time as the apparent half-period and the latter as the apparent period of vibration in a state of initial motion.

It will be seen from Fig. 14 that the greater the rapidity of the pressure applied to the cavity, the shorter the apparent period of radial vibration in a state of initial motion. As in the case of an infinite train of forced waves emanating from the cavity owing to the pressure of simple-harmonic time-variation applied to its inner surface, the apparent period of the forced wave contained in expression (6)b is the linear function of the rapidity of the applied pressure. The fact that the relation between the apparent period of the initial motion and the rapidity of the applied pressure, as will be seen from Fig. 14, is not

---

7) When $\widehat{rr}_{r=a} = -Pe^{i\frac{2\pi}{T}}$ and $\widehat{r\theta}_{r=a} = \widehat{r\phi} = 0$, the radial vibrations of particles that are some distance away from the cavity and which are due to the longitudinal forced waves issuing from it, are expressed by

$$u_{r\to\infty} \approx \frac{Pa}{\mu}\left(\frac{a}{r}\right)\frac{\sqrt{16\alpha^4 + 4\alpha^2\{1-\alpha^2(v/V)^2\}^2}}{4[4\alpha^2+\{1-\alpha^2(v/V)^2\}^2]}\, e^{i\left\{2\pi\left(\frac{t}{T}-\frac{r-a}{L}\right)+\tan^{-1}\zeta\right\}},$$

where $\alpha = \pi\frac{a}{L}$, $\zeta = (2\alpha)/\{1-\alpha^2(v/V)^2\}$, L = the wave-length of the forced wave. From this expression, it will be seen that the amplitude becomes maximum when $L/a = 1{\cdot}0$, and that the vibration-amplitudes of the particles exhibit a spectrum-like nature with variations in the value of L/a.

so simple as in the case of the forced wave, is mainly owing to the existence of both free and complementary waves in addition to the forced wave. As will be seen from Fig. 14, even if should rapidity of the applied pressure become very pronounced, the apparent period of the initial motion does not become so markedly small.

3. The wave-motions of particles that lie some distance away from a spherical cavity in an elastic earth have already been discussed for the case when the normal stress $\widehat{rr}$ on the inner surface of the cavity has co-latitudinal and azimuthal distributions, like $\widehat{rr}_{r=a}=-f(t)\sin 2\theta\cdot\cos\phi$, and the shearing stresses on this surface ($\widehat{r\theta}_{r=a}$, $\widehat{r\phi}_{r=a}$) are zero. Now let the time-factor $f(t)$ in expressions[8] (26)$\sim$(32), which are obtained in the case when Poisson's ratio $=1/4$, in the previous paper, be as follows:

$$\left.\begin{array}{lll} \text{When} & t\geqq 0, & f(t)=t/t_m\cdot\exp\{1-t/t_m\}\,, \\ \text{and when} & t\leqq 0, & f(t)=0, \end{array}\right\} \tag{7}$$

as in Art. 2. Then the radial, co-latitudinal and azimuthal components of displacement u_1, v_3, w_3, which are some distance away from the cavity, are expressed by

$$\left.\begin{array}{ll} u_1\approx-\dfrac{1}{6\pi}\dfrac{V^2vP}{\mu a^3}\dfrac{1}{r}\sin 2\theta\cos\cdot X\Big(t-\dfrac{1}{v}(r-a)\Big), & \text{(a)} \\ v_3\approx\dfrac{1}{3\pi}\dfrac{v^4P}{\mu Va^3}\dfrac{1}{r}\cos 2\theta\cos\theta\cdot Y\Big(t-\dfrac{1}{V}(r-a)\Big), & \text{(b)} \\ w_3\approx-\dfrac{1}{3\pi}\dfrac{v^4P}{\mu Va^3}\dfrac{1}{r}\cos\theta\sin\phi\cdot Y\Big(t-\dfrac{1}{V}(r-a)\Big), & \text{(c)} \end{array}\right\} \tag{8}$$

where

$$X\Big(t-\frac{1}{v}(r-a)\Big)=\frac{1}{t_m}\int_{-\infty}^{\infty}\frac{P'(p)}{\psi'(p)}\frac{e^{1-ip\left\{t-\frac{1}{v}(r-a)\right\}}}{\Big(p-i\dfrac{1}{t_m}\Big)^2}\,dp, \tag{9}$$

$$Y\Big(t-\frac{1}{V}(r-a)\Big)=\frac{1}{t_m}\int_{-\infty}^{\infty}\frac{T'(p)}{\psi'(p)}\frac{e^{1-ip\left\{t-\frac{1}{V}(r-a)\right\}}}{\Big(p-i\dfrac{1}{t_m}\Big)^2}\,dp, \tag{10}$$

and

---

[8] G. NISHIMURA, *loc. cit.*

$$P'(p) = -i\left(\frac{1}{V}\right)^4 a^4p^5 - 5\left(\frac{1}{V}\right)^3 a^3p^4 - i21\left(\frac{1}{V}\right)a^2p^3 + 48\left(\frac{1}{V}\right)ap^2 - i48p, \quad (11)$$

$$T'(p) = 2\left(\frac{1}{v}\right)^3 a^3p^4 - i10\left(\frac{1}{v}\right)^2 a^2p^3 - 24\left(\frac{1}{v}\right)ap^2 + i24p, \quad (12)$$

$$\psi'(p) = (p+a_1)(p+a_2)(p+a_3)(p+a_4)(p+a_5)(p+a_6), \quad (13)$$

$$\left.\begin{array}{lll} a_1 = (\alpha_1 - i\beta_1)\dfrac{v}{a}, & a_2 = -(\alpha_1 + i\beta_1)\dfrac{v}{a}, & a_3 = (\alpha_2 - i\beta_2)\dfrac{v}{a}, \\ a_4 = -(\alpha_2 + i\beta_2)\dfrac{v}{a}, & a_5 = (\alpha_3 - i\beta_3)\dfrac{v}{a}, & a_6 = -(\alpha_3 + i\beta_3)\dfrac{v}{a}, \\ \alpha_1 = 0{\cdot}83199, & \alpha_2 = 2{\cdot}416332, & \alpha_3 = 0{\cdot}600844, \\ \beta_1 = 2{\cdot}10618, & \beta_2 = 1{\cdot}040118, & \beta_3 = 0{\cdot}463744. \end{array}\right\} \quad (14)^{9)}$$

where u_1, expressed by (8)a, corresponds to the longitudinal waves with velocity v; and where v_3, w_3 as expressed by (8)b, (8)c are due to the transversal waves with propagational velocity V, these two kinds of waves being of course propagated from the cavity as the result of the tractions applied. For evaluating the integrals (9), (10), as in the previous paper[10)], we expand the integrants in expressions (9), (10) in partial fractions as in the following way:

$$\frac{P'(p)\,e^{1-ip\left\{\frac{1}{v}(r-a)\right\}}}{\psi'(p)\left(p-i\dfrac{1}{t_m}\right)^2} = \left\{\frac{A_1}{(p+a_1)} + \frac{A_2}{(p+a_2)} + \frac{A_3}{(p+a_3)} + \frac{A_4}{(p+a_4)} + \frac{A_5}{(p+a_5)} + \frac{A_6}{(p+a_6)} + \frac{A_7}{\left(p-i\dfrac{1}{t_m}\right)^2} + \frac{A_8}{\left(p-i\dfrac{1}{t_m}\right)}\right\} e^{1-ip\left\{t-\frac{1}{v}(r-a)\right\}}, \quad (15)$$

$$\frac{T'(p)\,e^{1-ip\left\{t-\frac{1}{V}(r-a)\right\}}}{\psi'(p)\left(p-i\dfrac{1}{t_m}\right)^2} = \left\{\frac{B_1}{(p+a_1)} + \frac{B_2}{(p+a_2)} + \frac{B_3}{(p+a_3)} + \frac{B_4}{(p+a_4)} + \frac{B_5}{(p+a_5)} + \frac{B_6}{(p+a_6)} + \frac{B_7}{\left(p-i\dfrac{1}{t_m}\right)^2} + \frac{B_8}{\left(p-i\dfrac{1}{t_m}\right)}\right\} e^{1-ip\left\{t-\frac{1}{V}(r-a)\right\}}, \quad (16)$$

---

9) H. KAWASUMI and R. YOSHIYAMA, *loc. cit.*
G. NISHIMURA, *loc. cit.*, p. 624.

10) G. NISHIMURA, *loc. cit.*, p. 625∼626.

where the values A_1, A_2, A_3, A_4, A_5, A_6, A_7, A_8, B_1, B_2, B_3, B_4, B_5, B_6, B_7, B_8 are certain functions of the rapidity of the applied pressure $a/(t_m v)$. They are calculated for various values of $a/(t_m v)$ as in Tables I ~ II.

Table I.

$\frac{a}{t_m v}$	$\frac{A_1}{\left(\frac{a}{v}\right)^6}$	$\frac{A_2}{\left(\frac{a}{v}\right)^6}$	$\frac{A_3}{\left(\frac{a}{v}\right)^6}$	$\frac{A_4}{\left(\frac{a}{v}\right)^6}$	$\frac{A_5}{\left(\frac{a}{v}\right)^6}$	$\frac{A_6}{\left(\frac{a}{v}\right)^6}$	$\frac{A_7}{\left(\frac{a}{v}\right)^5}$	$\frac{A_8}{\left(\frac{a}{v}\right)^6}$
0·1	$1{\cdot}40366$ $+i0{\cdot}09897$	$-1{\cdot}40366$ $+i0{\cdot}09897$	$-0{\cdot}33440$ $-i0{\cdot}14897$	$0{\cdot}33440$ $-i0{\cdot}14897$	$-0{\cdot}09606$ $-i1{\cdot}34530$	$0{\cdot}09606$ $-i1{\cdot}34530$	$-0{\cdot}25755$	$2{\cdot}79060$
0·4	$1{\cdot}83968$ $-i0{\cdot}09349$	$-1{\cdot}83968$ $-i0{\cdot}09349$	$-0{\cdot}38639$ $-i0{\cdot}07628$	$0{\cdot}38639$ $-i0{\cdot}07628$	$-1{\cdot}48102$ $-i1{\cdot}06214$	$1{\cdot}48102$ $-i1{\cdot}06214$	$-1{\cdot}13793$	$2{\cdot}46382$
1·5	$3{\cdot}24787$ $-i5{\cdot}35551$	$-3{\cdot}24787$ $-i5{\cdot}35551$	$-0{\cdot}31132$ $+i0{\cdot}26177$	$0{\cdot}31132$ $+i0{\cdot}26177$	$0{\cdot}05050$ $+i0{\cdot}46096$	$-0{\cdot}05050$ $+i0{\cdot}46096$	$-3{\cdot}72826$	$9{\cdot}26556$
1·8	$-0{\cdot}07871$ $-i8{\cdot}44732$	$0{\cdot}07871$ $-i8{\cdot}44732$	$-0{\cdot}22840$ $+i0{\cdot}30791$	$0{\cdot}22840$ $+i0{\cdot}30791$	$0{\cdot}09597$ $+i0{\cdot}29464$	$-0{\cdot}09597$ $+i0{\cdot}29464$	$-7{\cdot}54750$	$15{\cdot}68953$
2·0	$-5{\cdot}54331$ $-i9{\cdot}43054$	$5{\cdot}54331$ $-i9{\cdot}43054$	$-0{\cdot}10839$ $+i0{\cdot}34356$	$0{\cdot}10839$ $+i0{\cdot}34356$	$0{\cdot}10177$ $+i0{\cdot}21575$	$-0{\cdot}10177$ $+i0{\cdot}21575$	$-12{\cdot}95040$	$17{\cdot}74247$
2·4	$-8{\cdot}39114$ $-i1{\cdot}50698$	$8{\cdot}39114$ $-i1{\cdot}50698$	$-0{\cdot}07065$ $+i0{\cdot}31223$	$0{\cdot}07065$ $+i0{\cdot}31223$	$0{\cdot}08576$ $+i0{\cdot}13732$	$-0{\cdot}08576$ $+i0{\cdot}13732$	$-14{\cdot}69639$	$2{\cdot}11488$
3·0	$-3{\cdot}14629$ $+i3{\cdot}14862$	$3{\cdot}14629$ $+i3{\cdot}14862$	$0{\cdot}02921$ $+i0{\cdot}25255$	$-0{\cdot}02921$ $+i0{\cdot}25255$	$0{\cdot}06271$ $+i0{\cdot}07524$	$-0{\cdot}06271$ $+i0{\cdot}07524$	$-12{\cdot}01904$	$-6{\cdot}95280$
3·5	$-0{\cdot}89240$ $+i2{\cdot}35562$	$0{\cdot}89240$ $+i2{\cdot}35562$	$0{\cdot}06920$ $+i0{\cdot}19508$	$-0{\cdot}06920$ $+i0{\cdot}19508$	$0{\cdot}04831$ $+i0{\cdot}04990$	$-0{\cdot}04831$ $+i0{\cdot}04990$	$-8{\cdot}92184$	$-5{\cdot}20118$
4·0	$-0{\cdot}17598$ $+i1{\cdot}54125$	$0{\cdot}17598$ $+i1{\cdot}54125$	$0{\cdot}08442$ $+i0{\cdot}14590$	$-0{\cdot}08442$ $+i0{\cdot}14590$	$0{\cdot}03793$ $+i0{\cdot}03516$	$-0{\cdot}03793$ $+i0{\cdot}03516$	$-6{\cdot}7827$	$-3{\cdot}44459$
5·0	$0{\cdot}11247$ $+i0{\cdot}72339$	$-0{\cdot}11247$ $+i0{\cdot}72339$	$0{\cdot}08188$ $+i0{\cdot}07984$	$-0{\cdot}08188$ $+i0{\cdot}07984$	$0{\cdot}02483$ $+i0{\cdot}01984$	$-0{\cdot}02483$ $+i0{\cdot}01984$	$-4{\cdot}38625$	$-1{\cdot}64611$
6·0	$0{\cdot}12099$ $+i0{\cdot}40079$	$-0{\cdot}12099$ $+i0{\cdot}40079$	$0{\cdot}06747$ $+i0{\cdot}04456$	$-0{\cdot}06747$ $+i0{\cdot}04456$	$0{\cdot}01738$ $+i0{\cdot}01259$	$-0{\cdot}01738$ $+i0{\cdot}01259$	$-3{\cdot}15434$	$-0{\cdot}91586$
8·0	$0{\cdot}07875$ $+i0{\cdot}16999$	$-0{\cdot}07875$ $+i0{\cdot}16999$	$0{\cdot}04266$ $+i0{\cdot}01535$	$-0{\cdot}04266$ $+i0{\cdot}01535$	$0{\cdot}00980$ $+i0{\cdot}00629$	$-0{\cdot}00980$ $+i0{\cdot}00629$	$-1{\cdot}96319$	$-0{\cdot}38325$
15·0	$0{\cdot}02195$ $+i0{\cdot}03318$	$-0{\cdot}02195$ $+i0{\cdot}03318$	$0{\cdot}01225$ $+i0{\cdot}00022$	$-0{\cdot}01225$ $+i0{\cdot}00022$	$0{\cdot}00277$ $+i0{\cdot}00147$	$-0{\cdot}00277$ $+i0{\cdot}00147$	$-0{\cdot}80560$	$-0{\cdot}06975$
20·0	$0{\cdot}01204$ $+i0{\cdot}01682$	$-0{\cdot}01204$ $+i0{\cdot}01682$	$0{\cdot}00672$ $-i0{\cdot}00047$	$-0{\cdot}00672$ $-i0{\cdot}00047$	$0{\cdot}00155$ $+i0{\cdot}00079$	$-0{\cdot}00155$ $+i0{\cdot}00079$	$-0{\cdot}56080$	$-0{\cdot}03429$

Table II.

$\frac{a}{t_m v}$	$\frac{B_1}{\left(\frac{a}{v}\right)^6}$	$\frac{B_2}{\left(\frac{a}{v}\right)^6}$	$\frac{B_3}{\left(\frac{a}{v}\right)^6}$	$\frac{B_4}{\left(\frac{a}{v}\right)^6}$	$\frac{B_5}{\left(\frac{a}{v}\right)^6}$	$\frac{B_6}{\left(\frac{a}{v}\right)^6}$	$\frac{B_7}{\left(\frac{a}{v}\right)^5}$	$\frac{B_8}{\left(\frac{a}{v}\right)^6}$
0·1	$0{\cdot}071886$ $+i0{\cdot}01371$	$-0{\cdot}071886$ $+i0{\cdot}01371$	$-0{\cdot}01253$ $-i0{\cdot}02953$	$0{\cdot}01253$ $-i0{\cdot}02953$	$-0{\cdot}42945$ $+i0{\cdot}81951$	$0{\cdot}42945$ $+i0{\cdot}81951$	$0{\cdot}13871$	$-1{\cdot}60737$
0·4	$0{\cdot}09565$ $+i0{\cdot}00639$	$-0{\cdot}09565$ $+i0{\cdot}00639$	$-0{\cdot}02019$ $-i0{\cdot}02798$	$0{\cdot}02019$ $-i0{\cdot}02798$	$0{\cdot}48074$ $+i1{\cdot}15415$	$-0{\cdot}48074$ $+i1{\cdot}18415$	$0{\cdot}77245$	$-2{\cdot}26511$
1·5	$0{\cdot}20051$ $-i0{\cdot}25696$	$-0{\cdot}20051$ $-i0{\cdot}25696$	$-0{\cdot}03559$ $-i0{\cdot}00184$	$0{\cdot}03559$ $-i0{\cdot}00184$	$0{\cdot}13689$ $-i0{\cdot}28716$	$-0{\cdot}13689$ $-i0{\cdot}28716$	$0{\cdot}61148$	$1{\cdot}09191$

(to be continued.)

Table II. (*continued.*)

	$\dfrac{B_1}{\left(\frac{a}{v}\right)^6}$	$\dfrac{B_2}{\left(\frac{a}{v}\right)^6}$	$\dfrac{B_3}{\left(\frac{a}{v}\right)^6}$	$\dfrac{B_4}{\left(\frac{a}{v}\right)^6}$	$\dfrac{B_5}{\left(\frac{a}{v}\right)^6}$	$\dfrac{B_6}{\left(\frac{a}{v}\right)^6}$	$\dfrac{B_7}{\left(\frac{a}{v}\right)^5}$	$\dfrac{B_8}{\left(\frac{a}{v}\right)^6}$
2·0	−0·16529 −*i*0·46241	0.16529 −*i*0·46241	−0·03018 +*i*0·01028	0·03018 +*i*0·01028	0·02334 −*i*0·16612	−0·02334 −*i*0·16612	−0·00032	1·23650
2·4	−0·42452 −*i*0·12907	0·42452 −*i*0·12907	−0·02319 +*i*0·01578	0 02319 +*i*0·01578	−0·00048 −*i*0·11105	0·00048 −*i*0·11105	−0·35601	0·44868
3·0	−0·18180 +*i*0·14353	0·18180 +*i*0 14358	−0 01322 +*i*0·01792	0·01322 +*i*0·01792	−0·00943 −*i*0·06652	0·00943 −*i*0·06652	−0·36713	−0·18984
3·5	−0·06049 +*i*0·11628	0 06049 +*i*0·11628	−0·00723 +*i*0·01663	0·00723 +*i*0·01663	−0·01018 −*i*0·04655	0·01018 −*i*0·04655	−0·27112	−0·17272
5·0	0·00140 +*i*0 03807	−0·00140 +*i*0·03807	0·00047 +*i*0·01001	−0·00047 +*i*0·01001	−0·00733 −*i*0·02054	0·00733 −*i*0·02054	−0·11750	−0·05509
6·0	0·00381 +*i*0·02145	−0·00381 +*i*0·02145	0·00166 +*i*0·00689	−0·00166 +*i*0·00689	−0·00560 −*i*0·01362	0·00560 −*i*0·01362	−0·07698	−0·02944
8·0	0·00303 +*i*0·00927	−0·00303 +*i*0·00927	0·00182 +*i*0·00353	−0·00182 +*i*0·00353	−0·00345 −*i*0·00720	0·00345 −*i*0·00720	−0·04018	−0·01119
15·0	0·00105 +*i*0·00174	−0·00105 +*i*0·00174	0·00078 +*i*0·00078	−0·00078 +*i*0·00078	−0·00108 −*i*0·00180	0·00108 −*i*0·00180	−0·01023	−0·00145
20·0	0·00053 +*i*0·00094	−0·00053 +*i*0·00094	0·00046 +*i*0·00137	−0·00046 +*i*0·00037	−0·00062 −*i*0·00102	0·00062 −*i*0·00102	−0·00556	−0·00059

Hence, by using relations (15), (16), it may be possible to evaluate the integrals (9), (10) by Cauchy's residue method. Then, after the necessary mathematical treatment, the wave-motions of particles that are some distance away from the cavity, owing to the longitudinal and transversal waves emanating from it, are expressed by

$$u_1 = u_{\text{free}} + u_{\text{forced}} + u_{\text{complementary}}, \tag{17}$$

$$v_3 = v_{\text{free}} + v_{\text{forced}} + v_{\text{complementary}}, \tag{18}$$

$$w_3 = w_{\text{free}} + w_{\text{forced}} + w_{\text{complementary}}, \tag{19}$$

where

$$\left.\begin{aligned}
u_{\text{free}} &\approx -\frac{Pa}{27\mu}\left(\frac{a}{r}\right)\sin 2\theta\cos\phi\Big[\xi_1\exp\{-\beta_1\tau\}\sin(\alpha_1\tau+k_1)\\
&\qquad +\xi_2\exp\{-\beta_2\tau\}\sin(\alpha_2\tau+k_2)\\
&\qquad +\xi_3\exp\{-\beta_3\tau\}\sin(\alpha_3\tau+k_3)\Big], && \text{(a)}\\
u_{\text{forced}} &\approx -\frac{Pa}{27\mu}\left(\frac{a}{r}\right)\sin 2\theta\cos\phi\Big[\xi_4\tau\exp\{-\zeta\tau\}\Big], && \text{(b)}\\
u_{\text{complementary}} &\approx -\frac{Pa}{27\mu}\left(\frac{a}{r}\right)\sin 2\theta\cos\phi\Big[\xi_5\exp\{-\zeta\tau\}\Big], && \text{(c)}
\end{aligned}\right\} \tag{20}$$

$$\left.\begin{aligned}
v_{\text{free}} &\approx \frac{Pa}{27\mu}\left(\frac{a}{r}\right)\cos 2\theta \cos\phi \Big[\xi_1' \exp\{-\beta_1\tau'\} \sin(\alpha_1\tau' + k_1') \\
&\qquad + \xi_2' \exp\{-\beta_2\tau'\} \sin(\alpha_2\tau' + k_2') \\
&\qquad + \xi_2' \exp\{-\beta_3\tau'\} \sin(\alpha_2\tau' + k_3') \Big], && \text{(a)} \\
v_{\text{forced}} &\approx \frac{Pa}{27\mu}\left(\frac{a}{r}\right)\cos 2\theta \cos\phi \Big[\xi_4' \tau' \exp\{-\zeta\tau'\} \Big], && \text{(b)} \\
v_{\text{complementary}} &\approx \frac{Pa}{27\mu}\left(\frac{a}{r}\right)\cos 2\theta \cos\phi \Big[\xi_5' \exp\{-\zeta\tau'\} \Big], && \text{(c)}
\end{aligned}\right\} \quad (21)$$

$$\left.\begin{aligned}
w_{\text{free}} &\approx \frac{Pa}{27\mu}\left(\frac{a}{r}\right)\cos\theta \sin\phi \Big[\xi_1' \exp\{-\beta_1\tau'\} \sin(\alpha_1\tau' + k_1') \\
&\qquad + \xi_2' \exp\{-\beta_2\tau'\} \sin(\alpha_2\tau' + k_2') \\
&\qquad + \xi_3' \exp\{-\beta_3\tau'\} \sin(\alpha_3\tau' + k_3') \Big], && \text{(a)} \\
w_{\text{forced}} &\approx \frac{Pa}{27\mu}\left(\frac{a}{r}\right)\cos\theta \sin\phi \Big[\xi_4' \tau' \exp\{-\zeta\tau'\} \Big], && \text{(b)} \\
w_{\text{complementary}} &\approx \frac{Pa}{27\mu}\left(\frac{a}{r}\right)\cos\theta \sin\phi \Big[\xi_5' \exp\{-\zeta\tau'\} \Big]. && \text{(c)}
\end{aligned}\right\} \quad (22)$$

In expressions (20), (21), (22),

$$\tau = \frac{v}{a}\left\{t - \frac{1}{v}(r-a)\right\}, \quad \tau' = \frac{v}{a}\left\{t - \frac{1}{V}(r-a)\right\}, \quad \zeta = \frac{a}{t_m v},$$

and the values α_1, α_2, α_3, β_1, β_2, β_3 are shown by (14). The valves ξ_1, ξ_2, ξ_3, ξ_4, ξ_5, ξ_1', ξ_2', ξ_3', ξ_4', ξ_5', k_1, k_2, k_3, k_1', k_2', k_3' are certain functions of $a/(t_m v)$, being numerically calculated for various values of $a/(t_m v)$, as shown in Tables III, IV.

Table III.

$a/(t_m v)$	ξ_1	ξ_2	ξ_3	ξ_4	ξ_5	k_1	k_2	k_3
0·1	−0·7650	0·1990	0·7340	−0·0700	0·7586	−0·0704	−0·4193	−1·500
0·4	−4·006	0·8566	3·962	−1·237	2·6789	0·0501	−1·950	−0·622
1·5	−51·091	3·320	−3·784	−15·20	37·780	1·0258	0·699	−1·462
2·0	118·942	3·918	−2·596	−70·406	96·459	−1·0398	1·2652	−1·130
2·4	111·246	4·176	−2·112	−95·878	13·797	−0·1773	1·3483	−1·015
3·0	72·594	4·142	−1·597	−98·014	−56·699	0·786	−1·4555	−0·876
3·5	47·932	−3·941	−1·322	−84·883	−49·485	1·2086	−1·230	−0.802
5·0	−19·898	−3·110	−0·858	−59·616	−22·373	−1·417	−0·773	−0·674
6·0	−13·654	−2·638	−0·700	−51·447	−14·937	−1·278	−0·584	−0·627
8·0	−8·148	−1·972	−0·5066	−42·692	−8·334	−1·137	−0·346	−0·571
15·0	−3·246	−0·9990	−0·2560	−32·848	−2·844	−0·986	−0·018	−0·488
20·0	−2·248	−0·7328	−0·189	−30·488	−1·864	−0·950	−0·070	−0·471

Table IV.

$a/(t_m v)$	ξ'_1	ξ'_2	ξ'_3	ξ'_4	ξ'_5	k'_1	k'_2	k'_3
0·1	−0·4134	0·1812	5·224	0·3920	−4·5395	−0·188	−1·170	1·0872
0·4	−2·160	0·802	−28·242	8·722	−25·588	−0·067	−0·946	−1·1762
1·5	−27·596	3·017	−26·942	25·904	46·256	0·908	−0·052	1·126
2·0	55·474	3·600	−18·952	−0·0181	69·843	−1·228	0·328	1·431
2·4	60·148	3·803	15·056	−24·130	30·412	−0·295	0·597	−1·567
3·0	39·246	3·774	11·387	−31·106	−16·084	0·6681	0·935	−1·430
3·5	25·918	3·588	9·422	−26·800	−17·073	1·091	1·161	−1·356
5·0	−10·760	−2·830	6·160	−16·592	−7·779	−1·534	−1·523	−1·228
6·0	−7·383	−2·402	4·985	−13·045	−4·989	−1·395	−1·334	−1·181
8·0	−4·406	−1·794	3·606	−9·078	−2·528	−1·255	−1·095	−1·124
15·0	−1·720	−0·932	1·7792	−4·334	−0·614	−1·029	−0·785	−1·029
20·0	−1·220	−0·6676	1·3488	−3.140	−0·3333	−1·06	−0·68	−1·025

As in Art. 2, expressions (17)$\sim$(19) show that the longitudinal and transversal waves are of three kinds, namely, [1] free waves expressed by (20)a, (21)a, (22)a, [2] forced waves given by (20)b, (21)b, (22)b, and [3] complementary waves shown by (20)c, (21)c, (22)c. Naturally, the amplitudes of these three kinds of waves and also their phase-differences become certain functions of the rapidity of the pressure applied to the inner surface of the cavity. It will be seen, therefore, that the amplitudes of wave-motion of the particles that lie some distance away from the cavity vary with the rapidity of the applied pressure, and the apparent periods[11] of vibrations of the same particles in a state of initial motion also become certain functions of the value of $a/(t_m v)$. By using expressions (17)$\sim$(19), we obtained Figs. 15$\sim$27, in which are shown the radial, the co-latitudinal, and the azimuthal vibrations (u_1, v_3, w_3) of the particles due to the longitudinal and the transversal waves issuing from the cavity for various rapidities of the pressure applied. The units of the vertical scales in Figs. 15$\sim$27 are taken as $\frac{Pa}{27\mu}\left(\frac{a}{r}\right)\sin 2\theta\cos\phi$, $\frac{Pa}{27\mu}\left(\frac{a}{r}\right)\cdot\cos 2\theta\cos\phi$, and $\frac{Pa}{27\mu}\left(\frac{a}{r}\right)\cos\theta\sin\phi$ for u_1, v_3, and w_3 respectively. It will be noticed from Figs. 15$\sim$27 that the vibrations of particles, lying some distance away from the cavity, are of damped oscillations, which are the resultant oscillations obtained by adding the free, the forced, and the complementary waves. The maximum amplitudes of vibration due to the longitudinal waves are usually smaller than those due to the transversal waves, and the apparent periods of vibration in a state of initial mtion due to the former waves are shorter than those due to the latter.

---

[11] See p. 325 for definition of the apparent period of vibration of particle in a state of initial motion.

The curves U_1, V_3, and W_3 in Fig. 28, which are derived from

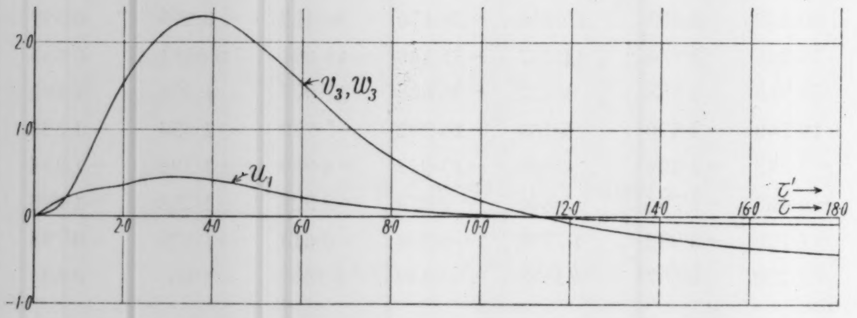

Fig. 15. $\dfrac{a}{t_m v} = 0{\cdot}10$.

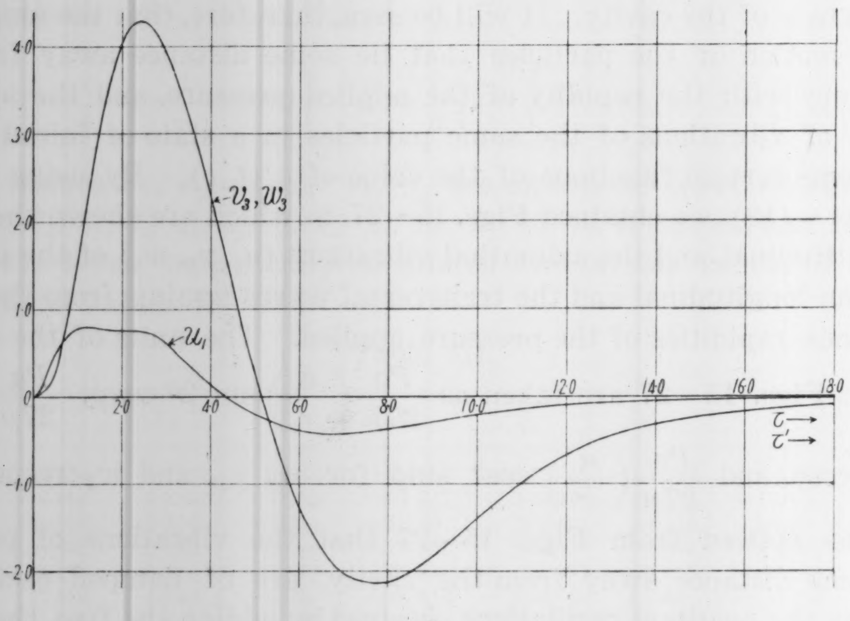

Fig. 16. $\dfrac{a}{t_m v} = 0{\cdot}40$.

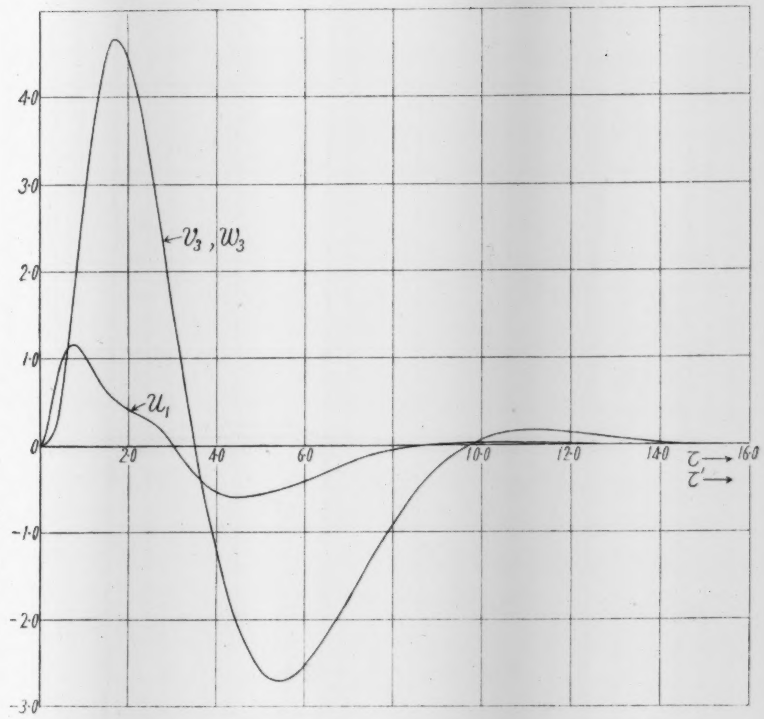

Fig. 17. $\frac{a}{t_m v} = 1{\cdot}0$.

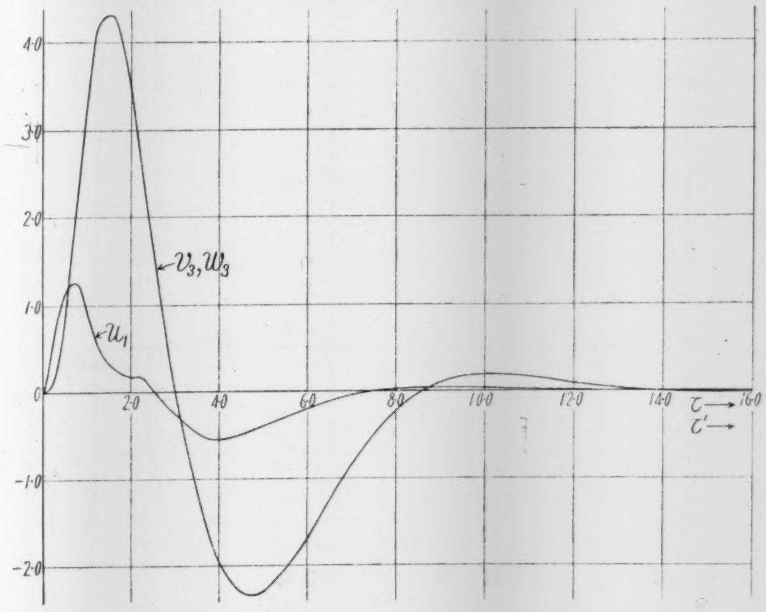

Fig. 18. $\frac{a}{t_m v} = 1{\cdot}5$.

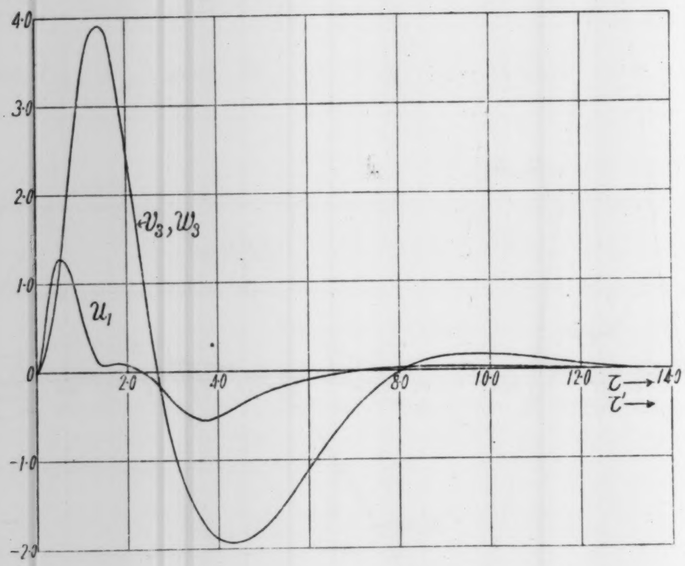

Fig. 19. $\frac{a}{t_m v} = 2\cdot0.$

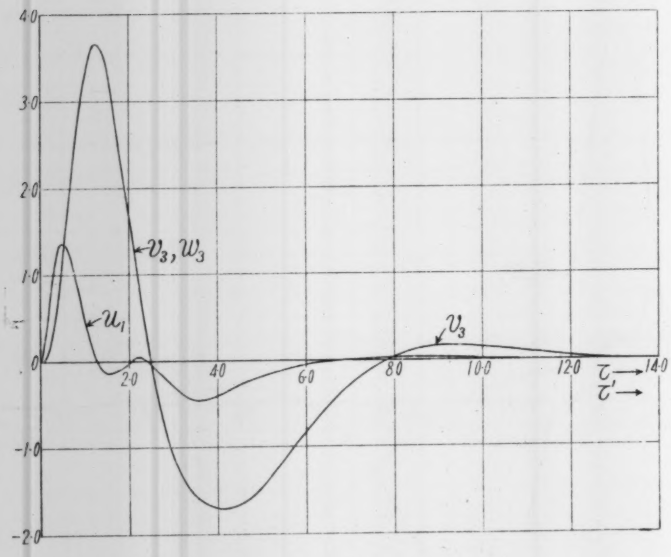

Fig. 20. $\frac{a}{t_m v} = 2\cdot4.$

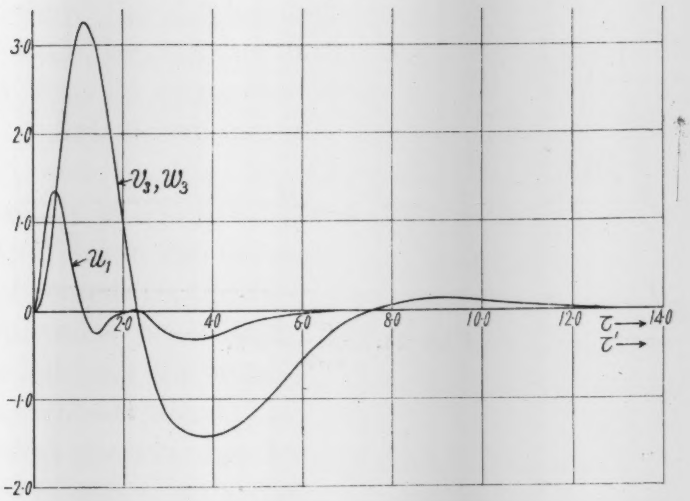

Fig. 21. $\frac{a}{t_m v} = 3{\cdot}0$.

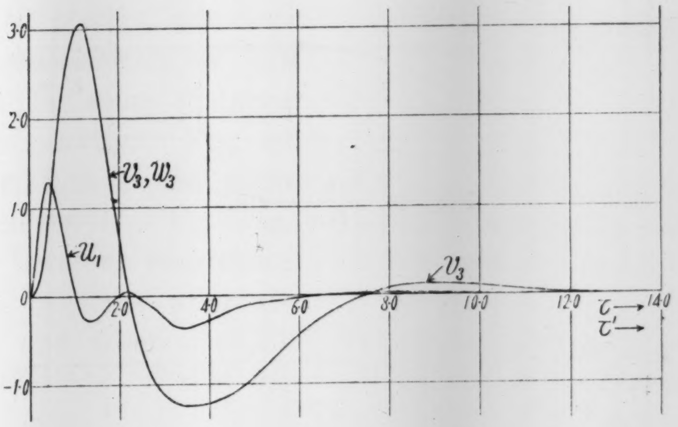

Fig. 22. $\frac{a}{t_m v} = 3{\cdot}5$.

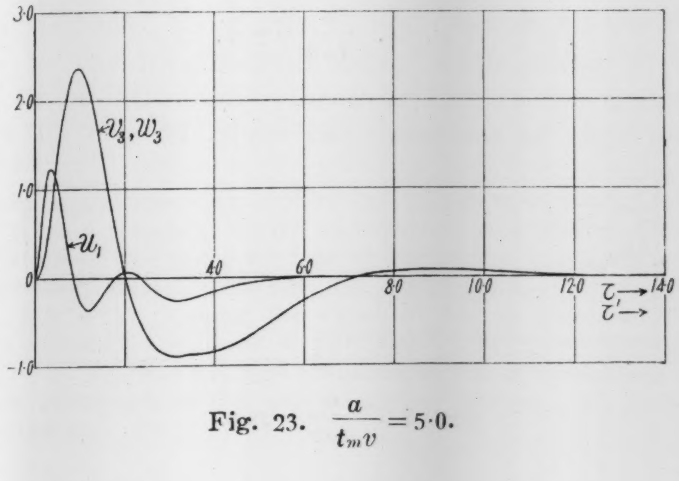

Fig. 23. $\frac{a}{t_m v} = 5{\cdot}0$.

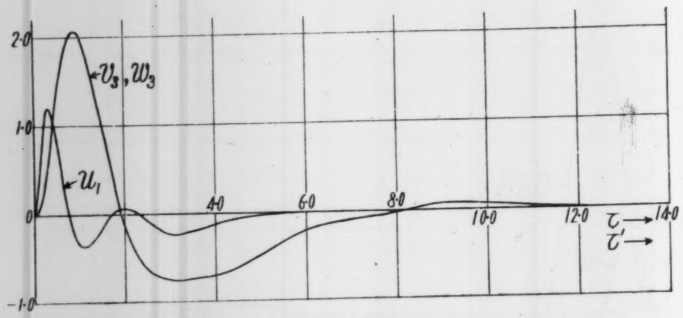

Fig. 24. $\frac{a}{t_m v} = 6\cdot0.$

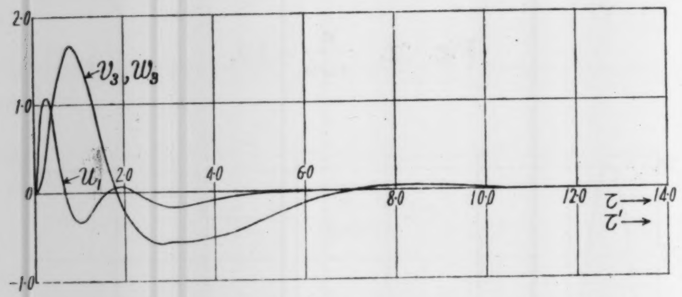

Fig. 25. $\frac{a}{t_m v} = 8\cdot0.$

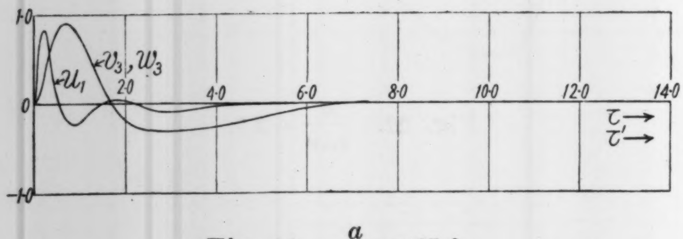

Fig. 26. $\frac{a}{t_m v} = 15\cdot0.$

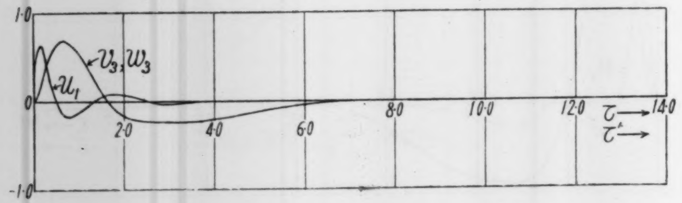

Fig. 27. $\frac{a}{t_m v} = 20\cdot0.$

Figs. 15~27, show the displacement-amplitudes of vibration of particles in a state of initial motion due to the longitudinal and transversal waves, the absissa in Fig. 28 being the value of the rapidity of the pressure applied. As in Art. 2, we can also see the spectrum-like nature of the two curves U_1 and V_3, Fig. 28, although the variation in the former curve with rapidity is less pronounced than in that of the latter, whence it will be seen that when the value $a/(t_m v)$ greatly exceeds 20, the displacement-amplitudes due to both waves will be nil, and the maximum displacement-amplitude in a state of initial motion due to the transversal wave will be smaller than those due to the longitudinal wave. Since when $a/(t_m v)$ becomes zero, the problem becomes one of statics, we cannot see any wave-motion of the particles that lie some distance away from the cavity. Fig. 29 shows the variation in the ratio of the two curves U_1, V_3, Fig. 28; the ratio becomes maximum when $a/(t_m v)$ becomes approximately unity, and when $a/(t_m v)$ greatly exceeds 20, it will be smaller than unity.

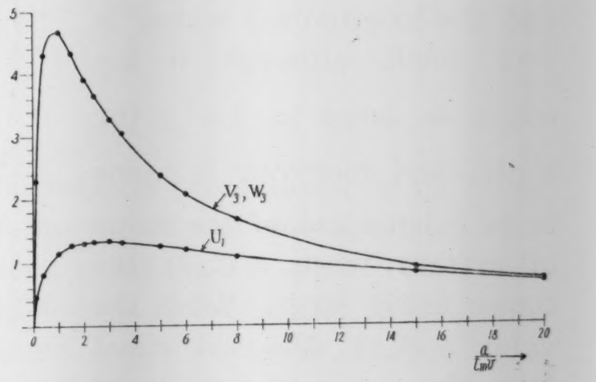

Fig. 28.

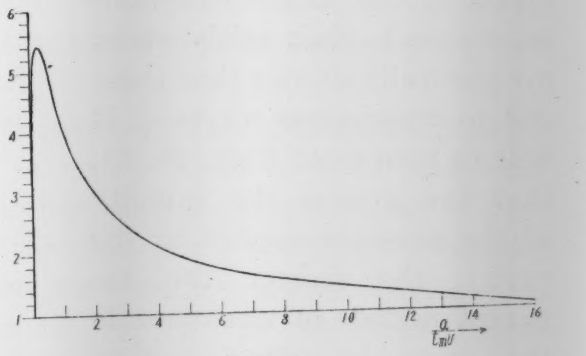

Fig. 29.

Curves T_1 and T_1', Fig. 30, which are derived from Figs. 15~27, show the durations of time from the beginning of the vibration until we come to the first nil of the displacement-amplitude; the curve T_1 corresponds to the case of radial vibrations due to the longitudinal wave, while curve T_1' is the case of the azimuthal or co-latitudinal vibrations due to the transversal waves. Curves T_2 and T_2', Fig. 31, show the durations of time from the begin-

---

12) H. Honda and others have studied the vibration of particle due to the forced wave emanating from a spherical cavity in the stationary state for the case when the the pressure-variation on the inner surface of the cavity has the same space-distribution as in the present article, although the time-factor of the applied pressure is simple-harmonic, like e^{ipt}. Taking the value of L/a as abscissa, they obtained the ratio-curve of the vibration-amplitude of particles, lying some distance away from the cavity, and due to the longitudinal and transversal waves emanating from it. Their study, however, is restricted to the case of forced waves. H. Honda, T. Miura, *Kensin-Zihô*, **10** (1937).

ning of the vibration to the time when the second nil of the displacement-amplitude occurs, the two corresponding respectively to the vibrations due to the longitudinal and the transversal waves. It will be seen from Figs. 30, 31, that when $a/(t_m v)$ is small, the difference between the apparent periods of the respective vibrations in their initial states due to the transversal and the longitudinal waves is very small, although it becomes as large as $1{\cdot}2\frac{v}{a}t$ (or $6\frac{v}{a}t$), and moreover it seems to be independent of the value of $a/(t_m v)$ when $a/(t_m v)$ becomes fairly large. When the value $a/(t_m v)$ does not equal zero, the apparent periods of vibration due to the longitudinal waves, in their initial state, are generally shorter than those due to transversal waves. It will be seen from Figs. 30, 31, that the greater the rapidity of the pressure applied to the cavity, the shorter the apparent periods of vibrations in the state of initial motion. Even if the rapidity $a/(t_m v)$ becomes very large, neither seem to vary so much as the period of vibration due to forced waves as in Art. 2. The fact that the relation between both the apparent periods and the rapidity of the applied pressure is not so simple as in the case of forced waves, is obviously due to the presence of both free and initial waves in addition to the forced wave, as will be seen from expressions (20), (21), (22).

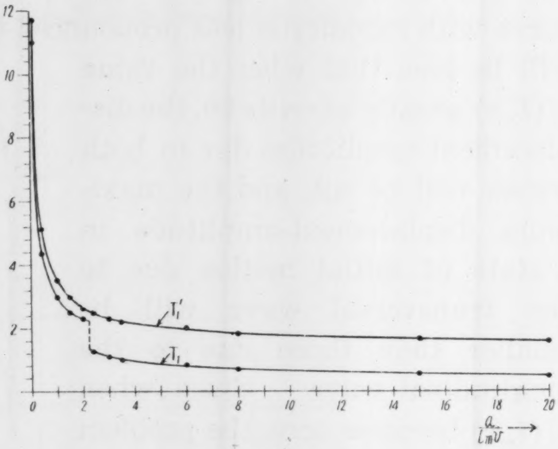

Fig. 30.

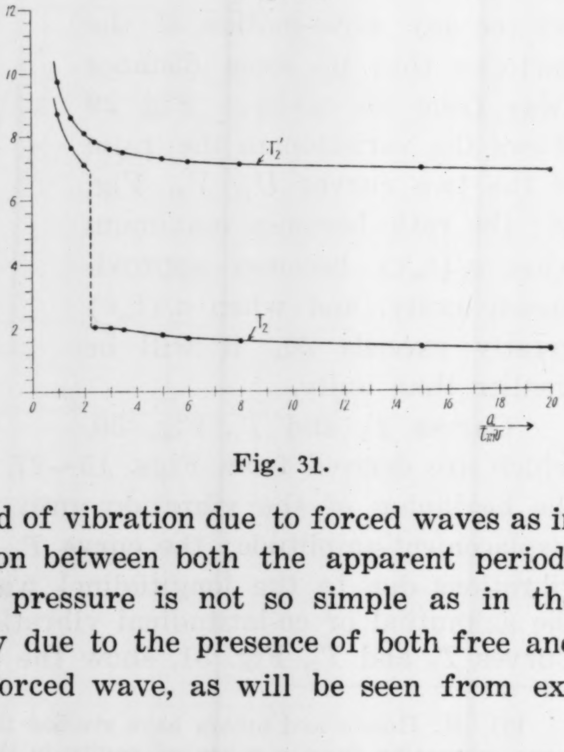

Fig. 31.

Now, from Fig. 30, we can easily obtain the curve T_s/T_p in Fig. 32, which shows the ratio of the apparent half-period of vibration T_s due to transversal waves to T_p due to the longitudinal waves. The ratio T_s/T_p, which is slightly larger than unity when the rapidity is small, becomes from 2·0 to 3·0 even if it becomes fairly large. Letting both the wave-lengths of the longitudinal and the transversal waves in the state of their initial motions be L_p, L_s respectively, we obtain the relations,

$$L_p = vT_p, \quad L_s = VT_s,$$

where v, V are the velocities of both waves, so that when Poisson's ratio is 1/4,

$$L_s/L_p = (1/1{\cdot}732)\ (T_s/T_p).$$

The ratio L_s/L_p for the present case is also shown in Fig. 32, which ratio is proportional to the value of T_s/T_p, and is certain function of the rapidity of the applied stress. It is remarkable that the ratio L_s/L_p, which is less than unity when the rapidity is small, is from 1·0 to 2·0 even if $a/(t_m v)$ be fairly large. By using the curves of the apparent periods shown in Fig. 31, it may be possible to obtain the curves T_s/T_p, L_s/L_p, like those in Fig. 32, although the qualitative character of the two ratios T_s/T_p, L_s/L_p relating to variation in the value $a/(t_m v)$ do not differ much from those shown in Fig. 32.

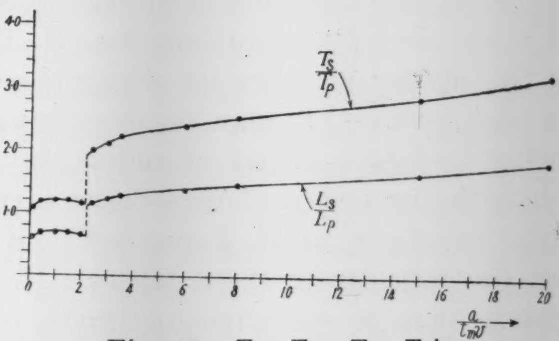

Fig. 32. $T_p = T_1$, $T_s = T_1'$.

By studying the deep-focus earthquake of Feb. 20, 1931, T. Ishikawa[13] found that the ratio T_s/T_p is nearly equal to 1·77, and that $L_s = L_p$ for that earthquake, and further that the displacement of particles near the earthquake-origin in the case of a deep-focus earthquake is usually quicker than that in the case of a shallow earthquake. From Fig. 32, we can see that when the rapidity of the applied pressure is fairly large, the ratios T_s/T_p, L_s/L_p are respectively 2, 1·2, the two values being of the same order as those of Ishikawa. So that it may be in order to conclude that the seismic waves, in the case of deep-focus earthquake, may be propagated from a cavity, the inner surface of which is subjected to a pressure of shock type, as assumed in the present Article.

The writers regret here that the theoretical results thus obtained of the periods of vibration due to the longitudinal and the transversal waves are not strictly borne out by seismometrical studies of actual earthquakes, and they fervently hope that experimenters will not be long in verifying their theoretical results with the aid of seismometrical results with actual deep-focus earthquakes; for to use the data of deep-focus earthquakes may not only be more reasonable, but is more convenient than to use the data of shallow earthquakes.

---

[13] T. Ishikawa *Jour., Met. Soc., Japan,* **10** (1932), 252.

Applying their mathematical results to seismometrical observations of seven deep-focus earthquakes, H. Honda[14] and T. Miura found that in the matter of vibration-amplitudes of the initial motion due to both *P*- and *S*-waves, it may be more consistent with the facts of seismometry to take a cavity of radius, say, $9 \sim 11$ km as a model in connexion with the origin of deep-focus earthquakes rather than to assume a point as origin, as H. Kawasumi, and W. Inouye[15] have already pointed out theoretically in their papers. H. Honda[16] found, moreover, that the distributions of vibration-amplitudes of the initial-motion on the earth's surface due to the *P*- and *S*-waves in the case of certain deep-focus earthquakes, are fairly consistent with the theoretical distribution of vibration-amplitudes obtained by him under the assumption that the forced waves emerge from a cavity, to which inner surface the following stresses are applied:

$$\widehat{rr}_{r=a} = F \sin 2\theta \cos\phi \cdot \sin pt, \quad \widehat{r\theta}_{r=a} = \widehat{r\phi}_{r=a} = 0,$$

in which the surface-distributions are the same as those in the present Article, although the time-factor differs from expression (7) assumed in this paper. Therefore, assuming the deep-focus earthquakes examined by H. Honda to be generated by a pressure with the time-variation expressed by (7), we obtain the values of $a/(t_m v)$ for earthquakes Nos. 1, 2, as shown in the seventh column in Table V[17]. (The period of earthquake No. 1 was obtained by H. Honda, and that of No. 2 by H. Morita.) As the ordinates of the curve, Fig. 29, were obtained experimentally by Honda, we easily obtain the values $a/(t_m v)$ of the abscissa

Table V.

No.	time of occurrence	Hypocenter		focal-depth	period of *P*-wave	Amplitude factor of *P*-wave	$\frac{a}{t_m v}$	$\frac{v}{a}t$
		longitude	Latitude					
1	June, 3, 1929	137·2°	34·3°	320 km	3·5 sec	$4{\cdot}95 \times 10^5$cm^2	2·2	2·04 or 7
2	June, 30, 1931	136·5°	34·2°	360 km	2·5 sec	$1{\cdot}54 \times 10^5$cm^2	3·0	2

---

[14] H. Honda, and T. Miura, *loc. cit.*

[15] H. Kawasumi and R. Yoshiyama, *loc, cit.* W. Inouye, *Bull. Earthq. Res. Inst.*, **14** (1936), 582; **15** (1937), 90.

[16] H. Honda, *Geophy. Mag.*, **8** (1934), 153.

[17] Since the periods of the *P*-wave of the other five earthquakes (No. 3~7) are not given in Honda's paper, we shall reserve our discussion of them for an other occasion.

in Fig. 29, as shown in Table V. Therefore, from Fig. 31, we obtain the values vt/a, which give the apparent periods of the initial motion due to the longitudinal waves in the cases of $a/(t_m v)=2{\cdot}2$, $a/(t_m v)=3{\cdot}0$, as shown in the eighth column in Table V, and by using the velocity of the longitudinal wave, which is 8·8 km/sec, as assumed by Honda, we obtain the dimensions of the cavities, namely, for earthquake No. 1, $a=15{\cdot}8$ or 4·4 km, and for earthquake No. 2, $a=11$ km. These dimensions, however, differ somewhat from those given by Honda[18]. Next, by equating both the theoretical and experimental amplitudes of the initial-motions for the respective cases in which $a/(t_m v)=2{\cdot}2$, 3·0, we get the equations, $1{\cdot}32\ P_m a^2/(27\mu)=4{\cdot}94\times10^5\,\mathrm{cm}^2$ for earthquake No. 1, and $1{\cdot}34\ P_m a^2/(27\mu)=1{\cdot}54\times10^5\,\mathrm{cm}^2$ for earthquake No. 2. The values of the left-hand terms of both equations are obtained from ordinates of the curve U_1 in Fig. 28; and those of the right-hand terms are shown in the sixth column of Table V. Then, assuming $\mu=8{\cdot}4\times10^{11}$ dynes/cm^{-2}, we obtain $P_m=3{\cdot}4\times10^6$ or $4{\cdot}4\times10^7$ dynes/cm^2 for earthquake No. 1, and $P_m=2{\cdot}1\times10^6$ dynes/cm^2 for earthquake No. 2. Lastly, the values t_m for both earthquakes No. 1 and No. 2 are easily calculated by using the values of a, v, namely, $t_m=0{\cdot}818$ or 0·227 sec for earthquake No. 1, and $t_m=0{\cdot}416$ sec. for earthquake No. 2.

In other words, we have found it possible to make the results of seismometrical observations of deep-earthquake No. 1, which particularly concerns both vibration-amplitude and direction of motion of the particles on the earth's surface in the state of their initial motions due to both P- and S-waves, consistent with the results that were obtained by a mathematical study of the same earthquake wherein the following reasonable assumptions were made, namely, that seismic waves, both longitudinal and transversal, emanate from a cavity, the radius of which is 15·8 or 4·4 km, at a depth of 320 km from the earth's surface as the result of pressure applied normal to its inner surface. This pressure, which has a distribution of $P_2^1(\cos\theta)\cdot\cos\phi$ on the inner surface of the cavity, reaches maximum $P_m=4{\cdot}4\times10^7$ dyne/cm^2 at $t_m=0{\cdot}8$ or 0·2 sec., after its variation begins, which accords with the time-variation expressed by $\dfrac{t}{t_m}\exp\{1-t/t_m\}$. It is also possible to explain the mechanism of occurrence of earthquake No. 2, which explanation harmonizes with experimental results, the following data being assumed:

Focal depth $=360$ km, $a=11$ km, $P_m=2{\cdot}1\times10^6$ dynes/cm^2,
$t_m=0{\cdot}4$ sec.

---

[18] The dimensions obtained by Honda are 11 km and 9 km for earthquakes Nos. 1, 2 respectively. H. HONDA and T. MIURA, *loc. cit.*

To summarize, we have obtained from the present calculations, the following facts which in no way conflict with the results of seismometrical observations, namely, that certain deep-focus earthquakes result from pressure of shock-type, which acts on the inner surface of a spherical cavity in the earth, and of which the time when its maximum occurs is less than one second. The dimension of the spherical cavity range from a few tens of kilometers to a few kilometers, the distance of its center from the earth's surface being a few hundred kilometers.

Since from the data given by Honda and others, it is not possible to know the apparent vibration-periods of particles due to the transversal (S-) wave, should both the apparent periods of vibrations in the condition of initial motion due to P-and S-waves determined experimentally for the various kinds of deep-earthquakes, then by assuming a more favourable time-variation in the traction applied to the cavity, it may be possible to trace more accurately the mechanism of deep-earthquake occurrence. As already discussed, we hope that experimenters will do all in their power to determine these periods to enable not only an understanding of the mechanism of earthquake occurrence, but also to give us an idea of the exact nature of seismic waves in the earth's crust.

In concluding Art. 3, the writers shall enumerate some of the ideas that they have on the question of the origin of earthquakes. As is well known, when a great earthquake occurs, the epicentral region of the earth's crust is subjected to severe seismal vibrations, mainly as the result of seismic wave-energy propagated from the earthquake origin, causing permanent crustal deformations in the region affected, accompanied sometimes with considerable dislocations. If we assume the necessity of invoking a mechanical force to explain the origin of earthquakes with all its attendant phenomena, for example, the wave-motions of particles in the earth, crustal deformations, ground cracks, dislocations, etc., it is possible to roughly calculate the energy of an earthquake in the earth, the crust of which is composed of plastico-elastic material. For example, by applying a force of a certain magnitude at the origin of an earthquake, some energy may be imparted to the earth's crust. A part of the work thus done by the force may be consumed in straining the earth's plastic crust, which is irreversible, and the remainder of the work may be stored as elastic strain energy. The former strain may appear as crustal deformations of permanet set, while the latter strain energy may be transformed into surface energy as the result of the occurrence of earthquake cracks, besides changing into seismic wave-energy at the instant of the earthquake. In other words,

$$\text{The work done by force}\left[\begin{array}{l}\text{Straining the plastic earth—Crustal deformation of permant set.}\\ \text{Elastic strain energy}\left[\begin{array}{l}\text{Surface energy of crack.}\\ \text{Seismic wave-energy.}\end{array}\right.\end{array}\right.$$

The work consumed in crustal deformation may be roughly calculated by modifying the theory[19] obtained by one of the present writers, and the surface energy due to the appearance of earthquake cracks in the earth's crust may also be calculated by suitably assuming the area of cracks, the wave-energy being assumed from the theory given in this paper.

4. When the stresses on the inner surface of a spherical cavity in an elastic earth are expressed by co-latitudinal and azimuthal distributions, such as

$$\left.\begin{aligned} \widehat{rr}_{r=a}&=0,\\ \widehat{r\theta}_{r=a}&=f(t)\cos 2\theta\cos\phi,\\ \widehat{r\phi}_{r=a}&=-f(t)\cos\theta\sin\phi, \end{aligned}\right\} \tag{23}$$

then the diverging waves that emanate from the cavity become two bodily waves, the longitudinal and transversal, as in the case of Art. 3, and the particles that are some distance away from the cavity assume the following vibrational motions of the radial, co-latitudinal, and azimuthal displacements (u_1, v_3, w_3) in the elastic earth, the Poisson ratio of which is 1/4:

$$u_1 \approx -\frac{3}{\pi}\frac{V^6}{\mu v a^3}\frac{1}{r}\int_{-\infty}^{\infty} K'(p)\frac{P''(p)e^{ip\left\{t-\frac{1}{v}(r-a)\right\}}}{\psi'(p)}\sin 2\theta\cos\phi\, dp, \tag{24}$$

$$v_3 \approx -\frac{1}{2\pi}\frac{V^3 v^2}{\mu a^3}\frac{1}{r}\int_{-\infty}^{\infty} K'(p)\frac{Q''(p)e^{ip\left\{t-\frac{1}{V}(r-a)\right\}}}{\psi'(p)}\cos 2\theta\cos\phi\, dp, \tag{25}$$

$$w_3 \approx \frac{1}{2\pi}\frac{V^3 v^2}{\mu a^3}\frac{1}{r}\int_{-\infty}^{\infty} K'(p)\frac{Q''(p)e^{ip\left\{t-\frac{1}{V}(r-a)\right\}}}{\psi'(p)}\cos\theta\sin\phi\, dp, \tag{26}$$

where

$$K'(p)=\int_{-\infty}^{\infty} f(\lambda)e^{-ip\lambda}d\lambda, \tag{27}$$

---

[19] G. NISHIMURA, *Bull. Earthq. Res. Inst.*, **12** (1934), 368~401.

$$P''(p) = -\left(\frac{a}{V}\right)^3 p^4 + i5\left(\frac{a}{V}\right)^2 p^3 + 12\left(\frac{a}{V}\right)p^2 - i12p, \tag{28}$$

$$Q''(p) = -i3\left(\frac{a}{v}\right)^4 p^5 - 13\left(\frac{a}{v}\right)^3 p^4 + i37\left(\frac{a}{v}\right)^2 p^3 + 72\left(\frac{a}{v}\right)p^2 - i72p, \tag{29}$$

and $\psi'(p)$ has the the same expressision as (13) in Art. 3. As in the case of Art. 3, the amplitudes of the co-latitudinal and the azimuthal components of displacements of the longitudinal wave are less than the radial component of displacement (u_1) of that wave, and those of the radial component of displacement due to the transversal wave are also less than those of the co-latitudinal and the azimuthal components of displacements (v_3, w_3) due to the same wave. We, therefore, ignore these small displacements in studying the wave-motions of particles that are some distance away from the cavity.

By letting the time-factor $f(t)$ be

$$\left.\begin{array}{ll} & f(t) = T\dfrac{t}{t_m}\exp\{1-t/t_m\}, \\ \text{when } t \geqq 0, \text{ and} & f(t) = 0, \end{array}\right\} \tag{30}$$

when $t \leqq 0$, we obtain the following expression of displacement from expressions (24), (25), (26):

$$u_1 \approx \frac{3}{\pi}\frac{V^6}{\mu v a^3} T\frac{1}{r}\sin 2\theta\cos\phi \cdot X'\left\{t - \frac{1}{v}(r-a)\right\}, \tag{31}$$

$$v_3 \approx \frac{1}{2\pi}\frac{V^3 v^2}{\mu a^3} T\frac{1}{r}\cos 2\theta\cos\phi \cdot Y'\left\{t - \frac{1}{V}(r-a)\right\}, \tag{32}$$

$$w_3 \approx \frac{-1}{2\pi}\frac{V^3 v^2}{\mu a^3} T\frac{1}{r}\cos\theta\sin\phi \cdot Y'\left\{t - \frac{1}{V}(r-a)\right\}, \tag{33}$$

where

$$X'\left\{t - \frac{1}{v}(r-a)\right\} = \frac{1}{t_m}\int_{-\infty}^{\infty} \frac{P''(p)}{\psi'(p)} \frac{e^{1-ip\left\{t-\frac{1}{v}(r-a)\right\}}}{\left\{p - i\dfrac{1}{t_m}\right\}^2} dp, \tag{34}$$

$$Y'\left\{t - \frac{1}{V}(r-a)\right\} = \frac{1}{t_m}\int_{-\infty}^{\infty} \frac{Q''(p)}{\psi'(p)} \frac{e^{1-ip\left\{t-\frac{1}{V}(r-a)\right\}}}{\left\{p - i\dfrac{1}{t_m}\right\}^2} dp. \tag{35}$$

Applying the same method as in Art. 3, we expand the integrants of the integrals (34), (35) for evaluating these integrals, as follows:

$$\frac{P''(p)e^{1-ip\left\{t-\frac{1}{v}(r-a)\right\}}}{\psi'(p)\cdot\left(p-i\dfrac{1}{t_m}\right)^2}=\left\{\frac{C_1}{(p+a_1)}+\frac{C_2}{(p+a_2)}+\frac{C_3}{(p+a_3)}\right.$$
$$+\frac{C_4}{(p+a_4)}+\frac{C_5}{(p+a_5)}+\frac{C_6}{(p+a_6)}$$
$$\left.+\frac{C_7}{\left(p-i\dfrac{1}{t_m}\right)^2}+\frac{C_8}{\left(p-i\dfrac{1}{t_m}\right)}\right\}e^{1-ip\left\{t-\frac{1}{v}(r-a)\right\}}, \tag{36}$$

$$\frac{Q''(p)e^{1-ip\left\{t-\frac{1}{V}(r-a)\right\}}}{\psi'(p)\cdot\left(p-i\dfrac{1}{t_m}\right)^2}=\left\{\frac{D_1}{(p+a_1)}+\frac{D_2}{(p+a_2)}+\frac{D_3}{(p+a_3)}\right.$$
$$+\frac{D_4}{(p+a_4)}+\frac{D_5}{(p+a_5)}+\frac{D_6}{(p+a_6)}$$
$$\left.+\frac{D_7}{\left(p-i\dfrac{1}{t_m}\right)^2}+\frac{D_8}{\left(p-i\dfrac{1}{t_m}\right)}\right\}e^{1-ip\left\{t-\frac{1}{V}(r-a)\right\}}. \tag{37}$$

Table VI.

$\frac{a}{t_m v}$	$\frac{C_1}{\left(\frac{a}{v}\right)^6}$	$\frac{C_2}{\left(\frac{a}{v}\right)^6}$	$\frac{C_3}{\left(\frac{a}{v}\right)^6}$	$\frac{C_4}{\left(\frac{a}{v}\right)^6}$	$\frac{C_5}{\left(\frac{a}{v}\right)^6}$	$\frac{C_6}{\left(\frac{a}{v}\right)^6}$	$\frac{C_7}{\left(\frac{a}{v}\right)^5}$	$\frac{C_8}{\left(\frac{a}{v}\right)^6}$
0·1	−0·23588 +i0·01092	0·23588 +i0·01092	0·12073 −i0·02616	−0·12073 −i0·02616	−0·00642 −i0·33298	0·00642 −i0·33298	−0·06435	0·69644
0·4	−0.30480 +i0·05150	0·30480 +i0·05150	0·12040 −i0·05622	−0·12040 −i0·05622	−0·35168 −i0·28097	0·35168 −i0·28097	−0·27999	0·57139
1·0	−0·4957 +i0·3036	0·4957 +i0·3036	0·0859 −i0·1123	0·0859 −i0·1132	−0·1380 +i0·2124	0·1380 +i0·2124	−0·1405	−0·8058
1·5	−0·43676 +i0·95603	0·43676 +i0·95603	0·03259 −i0·13331	−0·03259 −i0·13331	0·00654 +i0·11434	−0·00654 +i0·11434	0·48329	−1·87412
2·0	1·0790 +i1·4831	−1·0790 +i1·4831	−0·0273 −i0·1253	0·0273 −i0·1253	0·0209 +i0·0577	−0·0209 +i0·0577	2·0668	−2·8311
3·0	0·46295 −i0·58624	−0·46295 −i0·58624	−0·05827 −i0·06293	0·0527 −i0·06293	0·01450 +i0·01937	−0·01450 +i0·01937	1·70255	1·25960
5·0	−0·03286 −i0·11837	0·03286 −i0·11837	−0·03820 −i0·00542	0·03820 −i0·00542	0·00587 +i0·00521	−0·00587 +i0·00521	0·44850	0·23717
8·0	−0·01645 −i0·02679	0·01645 −i0·02679	−0·01467 +i0·00432	0·01467 +i0·00432	0·00234 +i0·00167	−0·00234 +i0·00167	0·13499	0·04160
11·0	−0·00851 −i0·01108	0·00851 −i0·01108	−0·00702 +i0·00361	0·00702 +i0·00361	0·00124 +i0·00075	−0·00124 +i0·00075	0·06267	0·01343
15·0	−0·00458 −i0·00489	0·00458 −i0·00489	−0·00341 +i0·00231	0·00341 +i0·00231	0·00068 +i0·00062	−0·00068 +i0·00026	0·03059	0·00463

Table VII.

$\frac{a}{t_m v}$	$\frac{D_1}{\left(\frac{a}{v}\right)^6}$	$\frac{D_2}{\left(\frac{a}{v}\right)^6}$	$\frac{D_3}{\left(\frac{a}{v}\right)^6}$	$\frac{D_4}{\left(\frac{a}{v}\right)^6}$	$\frac{D_5}{\left(\frac{a}{v}\right)^6}$	$\frac{D_6}{\left(\frac{a}{v}\right)^6}$	$\frac{D_7}{\left(\frac{a}{v}\right)^6}$	$\frac{D_3}{\left(\frac{a}{v}\right)^8}$
0·1	0·14692 $+i$0·01071	−0·14692 $+i$0·01071	−0·11152 $+i$0·06657	0·11152 $-i$0·06657	1·39651 $-i$2·36155	−1·39651 $-i$2·36155	−0·41652	4·83483
0·4	0·19364 $-i$0·01007	−0·19364 $-i$0·01007	−0·13288 $-i$0·04295	0·13288 $-i$0·04295	−1·24767 $-i$3·49078	1·24767 $-i$3·49078	−2·35363	7·08760
1·0	0·3294 $-i$0·1516	−0·3294 $-i$0·1516	−0·1473 $+i$0·0253	0·1473 $+i$0·0253	−1·8870 $+i$0·8910	1·8870 $+i$0·8910	−3·7206	−1·5294
1·5	0·34097 $-i$0·5602	−0·34097 $-i$0·56022	−0·12073 $+i$0·07904	−0·12073 $+i$0·17904	−0·44914 $+i$0·82948	0·44914 $+i$0·82948	−3·02683	−0·69660
2·0	−0·8241 $-i$1·1659	0·8241 $-i$1·1659	−0·0559 $+i$0·1124	0·0559 $+i$0·1124	−0·0935 $+i$0·4861	0·0935 $+i$0·4861	−3·7109	1·1349
3·0	−0·33001 $+i$0·32916	0·33001 $+i$0·32916	0·00039 $+i$0·09019	0·00039 $+i$0·09019	0·01779 $+i$0·19842	−0·01779 $+i$0·19842	−2·47810	−1·23555
5·0	0·01168 $+i$0·07574	−0·01168 $+i$0·07574	0·02547 $+i$0·03159	−0·02547 $+i$0·09019	0·01856 $+i$0·06193	−0·01856 $+i$0·06193	−1·08562	−0·33853
8·0	0·00820 $+i$0·01782	−0·00820 $+i$0·01782	0·01438 $+i$0·00720	−0·01438 $+i$0·00720	0·00912 $+i$0.02185	−0·00912 $+i$0·02185	−0·54558	−0·09375
15·0	0·00210 $+i$0·00358	−0·00210 $+i$0·00358	0·00429 $+i$0·00057	−0·00429 $+i$0·00057	0·00292 $+i$0·00561	−0·00292 $+i$0·00561	−0·24388	−0·01954

The values $C_1 \sim C_8$, $D_1 \sim D_8$, thus obtained, which become certain functions of $a/(t_m v)$, are numerically calculated for various values of $a/(t_m v)$, as shown in Tables VI, VII. Then, by using (36), (37), we obtain the following expressions for thc wave-motions of particles that are some distance away from the cavity, from expressions (31) ∼ (33), by applying Cauchy's residue methode on (34), (35):

$$u_1 = u_{\text{free}} + u_{\text{forced}} + u_{\text{complementary}}, \tag{38}$$

$$v_3 = v_{\text{free}} + v_{\text{forced}} + v_{\text{complementary}}, \tag{39}$$

$$w_3 = w_{\text{free}} + w_{\text{forced}} + w_{\text{complementary}}, \tag{40}$$

where

$$\left.\begin{aligned} u_{\text{free}} &\approx \frac{Ta}{27\mu}\left(\frac{a}{r}\right)\sin 2\theta\cos\phi\Big[\eta_1 \exp\{-\beta_1\tau\}\sin(\alpha_1\tau+\kappa_1) \\ &\qquad +\eta_2\exp\{-\beta_2\tau\}\sin(\alpha_2\tau+\kappa_2) \\ &\qquad +\eta_3\exp\{-\beta_3\tau\}\sin(\alpha_3\tau+\kappa_3)\Big], && \text{(a)} \\ u_{\text{forced}} &\approx \frac{Ta}{27\mu}\left(\frac{a}{r}\right)\sin 2\theta\cos\phi\Big[\eta_4\tau\exp\{-\zeta\tau\}\Big], && \text{(b)} \\ u_{\text{complementary}} &\approx \frac{Ta}{27\mu}\left(\frac{a}{r}\right)\sin 2\theta\cos\phi\Big[\eta_5\exp\{-\zeta\tau\}\Big], && \text{(c)} \end{aligned}\right\} \tag{41}$$

$$\left.\begin{aligned}
v_{\text{free}} &\approx \frac{Ta}{27\mu}\left(\frac{a}{r}\right)\cos 2\theta\cos\phi\Big[\eta_1'\exp\{-\beta_1\tau'\}\sin(\alpha_1\tau'+\kappa_1') \\
&\qquad +\eta_2'\exp\{-\beta_2\tau'\}\sin(\alpha_2\tau'+\kappa_2') \\
&\qquad +\eta_3'\exp\{-\beta_3\tau'\}\sin(\alpha_3\tau'+\kappa_3')\Big], && \text{(a)} \\
v_{\text{forced}} &\approx \frac{Ta}{27\mu}\left(\frac{a}{r}\right)\cos 2\theta\cos\phi\Big[\eta_4'\tau'\exp\{-\zeta\tau'\}\Big], && \text{(b)} \\
v_{\text{complementary}} &\approx \frac{Ta}{27\mu}\left(\frac{a}{r}\right)\cos 2\theta\cos\phi\Big[\eta_5'\exp\{-\zeta\tau'\}\Big], && \text{(c)}
\end{aligned}\right\} \quad (42)$$

$$\left.\begin{aligned}
w_{\text{free}} &\approx \frac{Ta}{27\mu}\left(\frac{a}{r}\right)\cos\theta\sin\phi\Big[\eta_1'\exp\{-\beta_1\tau'\}\sin(\alpha_1\tau'+\kappa_1') \\
&\qquad +\eta_2'\exp\{-\beta_2\tau'\}\sin(\alpha_2\tau'+\kappa_2') \\
&\qquad +\eta_3'\exp\{-\beta_3\tau'\}\sin(\alpha_3\tau'+\kappa_3')\Big], && \text{(a)} \\
w_{\text{forced}} &\approx \frac{Ta}{27\mu}\left(\frac{a}{r}\right)\cos\theta\sin\phi\Big[\eta_4'\tau'\exp\{-\zeta\tau'\}\Big], && \text{(b)} \\
w_{\text{complementary}} &\approx \frac{Ta}{27\mu}\left(\frac{a}{r}\right)\cos\theta\sin\phi\Big[\eta_5'\exp\{-\zeta\tau'\}\Big], && \text{(c)}
\end{aligned}\right\} \quad (43)$$

in which τ, τ', ζ, α_1, α_2, α_3, β_1, β_2, β_3 have the same values as in Art. 3, which are obviously independent of the time-variations in the applied pressure. $\eta_1\sim\eta_5$, $\eta_1'\sim\eta_5'$, $\kappa_1\sim\kappa_3$, $\kappa_1'\sim\kappa_3'$ are also certain functions of the rapidity of the applied shearing stress, being calculated numerically for various values of $a/(t_m v)$ as shown in Tables VIII, IX.

As in Arts. 2, 3, the longitudinal wave u_1 expressed by (38) and the transversal waves v_3, w_3 expressed by (39), (40) are respectively

Table VIII.

$\zeta\,(=a/(t_m v))$	η_1	η_2	η_3	η_4	η_5	κ_1	κ_2	κ_3
0·1	0·1226	−0·0642	0·1728	−0·0167	0·1808	0·046	0·214	−1·552
0·4	0·6420	−0·2726	0·9358	−0·2907	0·5933	0·167	0·437	−0·674
1·0	3·018	−0·7382	1·3166	−0·3647	−2·092	0·550	0·922	0·995
1·5	8·192	−1·0684	−0·8900	1·882	−7·297	1·142	1·331	−1·514
2·0	−19·552	1·3322	−0·6376	10·730	−14·698	−0·942	−1·3565	−1·223
3·0	−11·650	1·3364	−0·3784	13·259	9·809	−0·9025	−0·823	−0·929
5·0	3·190	1·0020	−0·2024	5·821	3·079	−1·30	−0·14	−0·72
8·0	1·3082	0·6354	−0·1204	2·803	0·8639	−1·018	0·285	−0·638
11·0	0·7990	0·4507	−0·0828	1·789	0·3835	−0·916	0·475	−0·544
15·0	0·5218	0·3208	−0·0568	1·191	0·1803	−0·818	0·595	−0·365

Table IX.

$\zeta\,(=a/(t_m v))$	η_1'	η_2'	η_3'	η_4'	η_5'	κ_6'	κ_2'	κ_3'
0·1	−0·066	0·0584	−1·2334	−0·0936	1·087	−0·0728	−0·538	1·037
0·4	−0·3488	0·2512	6·668	−2·116	6·373	0·0519	−0·313	−1·2276
1·0	−1·632	0·6780	9·388	−8·364	−3·438	0·431	0·170	0·441
1·5	−4 424	0·9738	6·366	−10·206	−2·349	1·024	0·580	1·0746
2·0	12·840	1·1294	4·452	−16·684	5·103	−0·956	1·109	1·381
3·0	6·284	1·2162	−2·684	−16·712	−8·332	0·784	1·566	−1·481
5·0	−1·622	−0·9130	−1·4524	−12·202	−3·807	−1·418	−0·892	−1·280
8·0	−0·706	−0·5784	−0·8524	−9·812	−1·686	−1·139	−0·464	−1·176
15·0	−0·2798	−0·2920	−0·429	−8·224	−0·659	−1·040	−0·130	−1·091

composed of three kinds of waves; [1] the forced waves expressed by (41)b, (42)b, (43)b, [2] the free waves given by (41)a, (42)a, (43)a, and [3] the complementary waves expressed by (41)c, (42)c, (43)c. The vibrations of particles due to the free waves (41)a, (42)a, (43)a, which are of damped waves, are the resultants obtained by superposing three kinds of damped oscillations with their respective damping ratios $e^{\pi\beta_1/\alpha_1}$, $e^{\pi\beta_2/\alpha_2}$, $e^{\pi\beta_3/\alpha_3}$, and also with the respective free periods $2\pi\dfrac{a}{\alpha_1 v}$, $2\pi\dfrac{a}{\alpha_3 v}$, $2\pi\dfrac{a}{\alpha_3 v}$.

In order to find the nature of the oscillatory vibrations of the particles that lie some distance away from the cavity due to waves (38)～(40), we obtained Figs. 33～41 for various values of $a/(t_m v)$. The units of the vertical scales in Fig. 33～41 are taken as $\dfrac{Ta}{27\mu}\left(\dfrac{a}{r}\right)$.

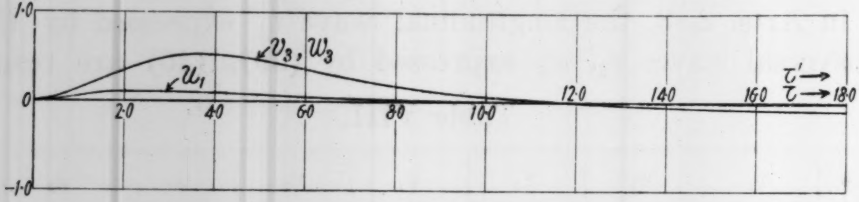

Fig. 33. $\dfrac{a}{t_m v} = 0·1.$

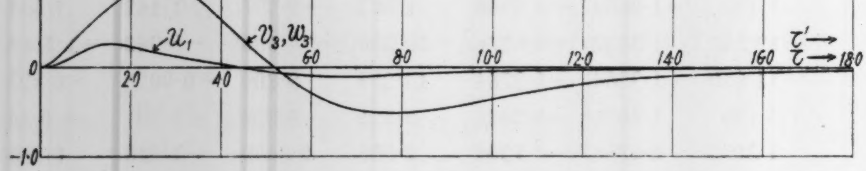

Fig. 34. $\dfrac{a}{t_m v} = 0·4.$

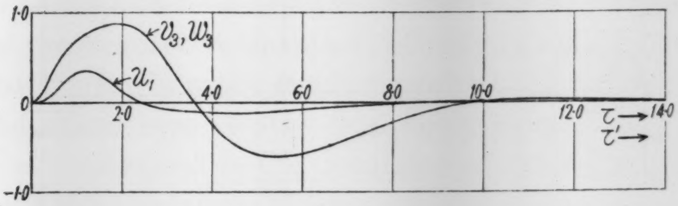

Fig. 35. $\dfrac{a}{t_m v} = \mathbf{1 \cdot 0}.$

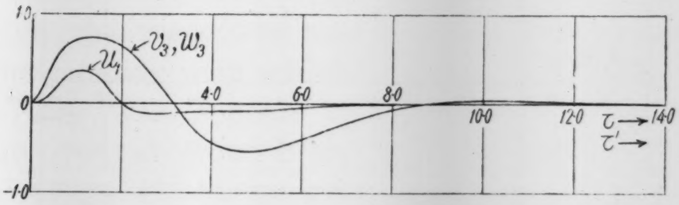

Fig. 36. $\dfrac{a}{t_m v} = \mathbf{1 \cdot 5}.$

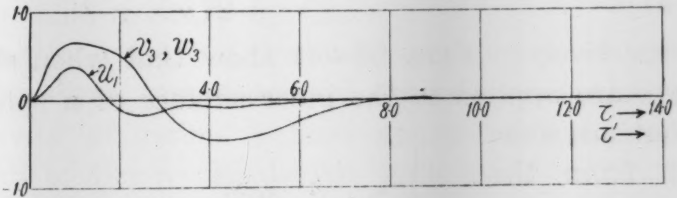

Fig. 37. $\dfrac{a}{t_m v} = \mathbf{2 \cdot 0}.$

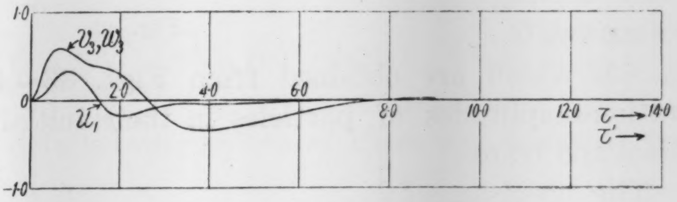

Fig. 38. $\dfrac{a}{t_m v} = \mathbf{1 \cdot 00}.$

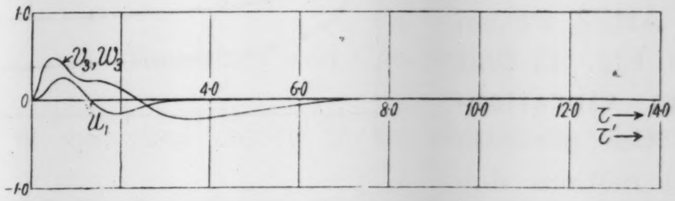

Fig. 39. $\dfrac{a}{t_m v} = \mathbf{5 \cdot 0}.$

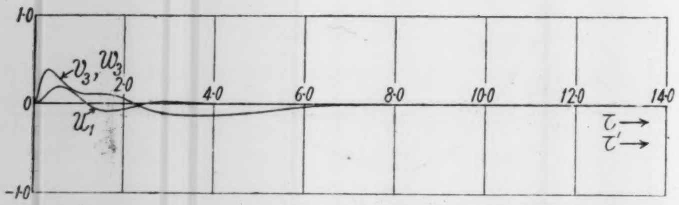

Fig. 40. $\frac{a}{t_m v} = 8{\cdot}0.$

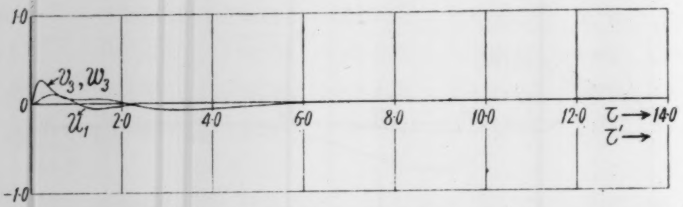

Fig. 41. $\frac{a}{t_m v} = 15{\cdot}0.$

sin 2θ cosϕ, $\frac{Ta}{27\mu}\left(\frac{a}{r}\right)$ cos 2θ cosϕ, and $\frac{Ta}{27\mu}\left(\frac{a}{r}\right)$ cosθ sinϕ for u_1, v_3, and w_3 respectively. Figs. 33~41 show that when shearing force of the shock type are applied to the inner surface of a spherical cavity, the particles that are some distance away from the cavity assume the character of damped oscillations due to the longitudinal and transversal waves leaving the cavity. The curves U_1, V_3, W_3 in Fig. 42, which are obtained from Figs. 33~41, show the respective vibration-amplitudes of particles in their initial motions due to the longitudinal and transversal waves. The abscissa of Fig. 42 shows the value of the rapidity of the shearing stresses applied to the cavity. As in Art. 3, we can also see from Fig. 42 that the maximum vibration-amplitudes of the particles in their initial motions due to the transversal waves are generally larger than those due to the longitudinal waves, their resonance-

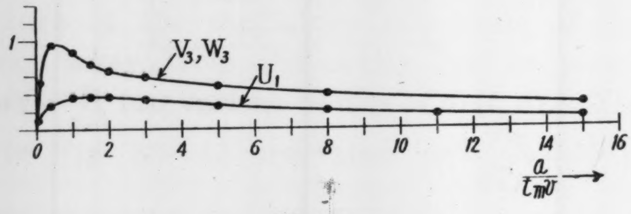

Fig. 42.

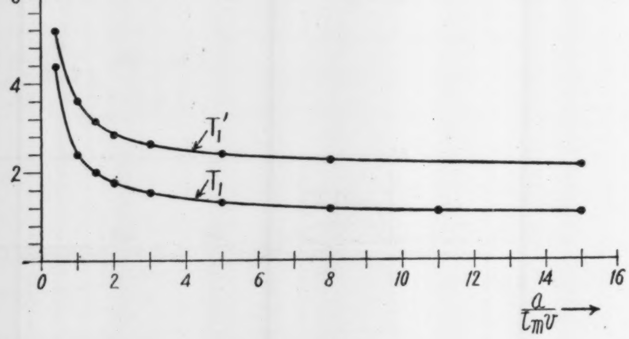

Fig. 43.

like characters being also seen from these two curves. The curves T_1, T_1' in Fig. 43 show the respective durations of time from the beginning of the vibration to the time when the displacement of the particles due to both longitudinal and transversal waves first becomes nil, and the curves T_2 and T_2' in Fig. 44 correspond to the durations of time from the beginning of the vibrations to the time when the displacement of the same particles due to the same respective waves becomes nil for the second time. Figs. 43, 44, in which the respective abscissae show the rapididy with which the shearing force was applied to tne cavity, are derived from Figs. 33~41. From Figs. 43, 44, we get an idea again of the nature of the apparent vibration-periods of the particles as in Figs. 30, 31 in Art. 3.

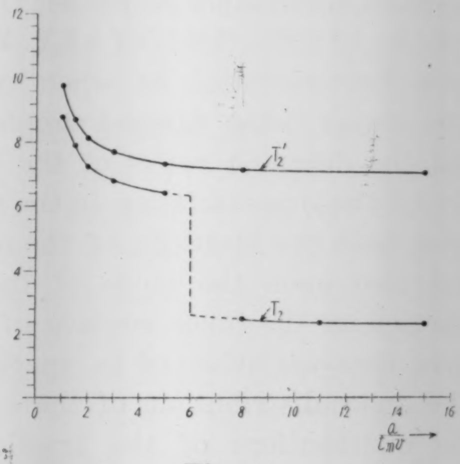

Fig. 44.

5. We may be able to study by the same method as in Arts. 3, 4, the wave-phenomena in cases where the normal and the shear components of stresses on the inner surface of a spherical cavity of radius a have space-distributions expressed by Zonal-harmonics of the second degree, such as

$$\widehat{rr}_{r=a}=P\frac{t}{t_m}\exp\{1-t/t_m\}\,P_2(\cos\theta),\quad \widehat{r\theta}_{r=a}=0, \tag{44}$$

or

$$\widehat{rr}_{r=a}=0,\quad \widehat{r\theta}_{r=a}=T\frac{t}{t_m}\exp\{1-t/t_m\}\,\frac{\partial P_2(\cos\theta)}{\partial\theta}, \tag{45}$$

although our detailed discussions of them are reserved for another occasion.[20]

The writers express their thanks to Professor Katsutada Sezawa for his encouragement and valuable advices.

Summary and Conclusion.

Assuming a spherical cavity in an elastic earth, we studied the vibrational motions of particles, lying some distance away from the cavity, caused by elastic waves propagated from it for the case in which the tractions that are applied to its inner surface are of the shock type. The elastic waves due to tractions of shock type are usually longitudinal and transversal bodily waves, both of which are composed of three kinds of waves; [1] FORCED WAVES, [2] FREE WAVES, and [3] COMPLEMENTARY WAVES. The forced waves have the same time-variation as when tractions are applied to the cavity, the free waves being damped simple-harmonic time-variations. The periods and the damping ratios of the free waves are independent of the manner of the time-variation in the traction applied to the cavity, but depend upon both the elasticity of the medium and the dimension of the cavity, and also upon the mode of the intensity-distributions of the applied traction on the inner surface of the cavity. The complementary waves have time-variations of an aperiodic decaying character, like $exp\{-\alpha\tau\}$. The space-distributions of these three kinds of waves are determined by the distributions of the tractions applied to the inner surface of the cavity, and their amplitudes at any point in the medium are certain functions of the rapidity of the applied tractions.

---

[20] A paper on the mathematical results for the case in which the boundary conditions are expressed by (44) was read at the 131st Local Meeting of the Earthq. Res. Inst., (Nov. 16, 1397).

The particles that are some distance away from the cavity, are usually damped vibrations as the result of longitudinal and transversal waves that issue from the cavity, both being the resultants obtained by superposing these free, forced, and complementary waves. Now the respective amplitudes of the co-latitudinal and azimuthal components of displacements of the propagated longitudinal wave are less than the radial component of displacement of that wave when the distance from the center of the cavity becomes very large, and those of the radial displacement due to the propagated transversal wave are less than those of the co-latitudinal and azimuthal components of displacement due to the same wave when the distance from the cavity is very great. These small quantities of displacements may therefore be disregarded in studying the wave-motions of particles that are some distance away from the cavity; in other words, the longitudinal waves that emerge from the cavity excite only the radial vibrations of the particles that are some distance away from the cavity, while the transversal waves excite only the co-latitudinal and azimuthal vibrations of the same particles.

When the distance from the center of the cavity is very great, the apparent period of the longitudinal wave in a state of initial motion is usually shorter than that of the transversal wave, the two periods being certain functions of the rapidity of the stress applied to the cavity, although the difference between them becomes nearly constant, notwithstanding the rapidity of the applied stress when it exceeds a certain value. The more rapid the applied stress on the cavity, the shorter the two apparent periods, which, however, do not vary so much as the period of the forced wave. The reason that the relation between the apparent periods and the rapidity with which the stress is applied is not so simple as in the case of the forced wave, is the existence of both the free and complementary waves in addition to the forced wave.

The amplitudes of vibration of the particles that are some distance away from the cavity, which vibrations are due to the longitudinal and transversal waves issuing from the cavity, are also certain functions of the rapidity of the applied stress, showing a spectrum-like character in its variations. Generally speaking, for a certain range of the rapidity of the applied stress, the amplitudes due to longitudinal waves are smaller than those due to transversal waves. When the rapidity becomes very large, the amplitudes due to the transversal wave may become smaller than those due to the longitudinal wave.

The mathematical results shown in this paper have not been verified with seismometrical data on an actual earthquake, the mechanism of occurrence of certain deep-earthquake being merely discussed by using both the experimental results obtained by H. Honda, as already mentioned, and the present theoretical results obtained by us, to which have added a brief outline of our ideas on earthquake origin.

The present paper concerns only wave-phenomena that occur at places some distance away from the cavity, reserving for a future occasion our studies of phenomena that occur near the cavity for the case when the inner surface of the cavity is subjected to tractions of shock-type as assumed in Arts. 3, 4.

27. 彈性地殼內にある球狀震源より出る地震波

地震研究所 {西村源六郎
高山威雄

著者の一人西村は以前に彈性地殼內に球狀空窩が存在してゐると假定し，その空窩內面に衝擊型の壓力が作用した時に發生する地震波を研究して置いた.1) 本論文はその延長と見るべきものであるが，計算結果を多數の圖面に示めし，地震波生成に關して相當面白いと思はれる結果を得る事が出來た．卽ち振動性 P 波 S 波の生成，それ等の初動の週期，振幅，或は波長に關して彈性波動學論的に興味あるのみならず，實驗上或は驗震學的に得た事實を說明するに大切な理論的結果を得た.

尙これは實驗的に證明されるかも知れないが，震源より出る地震波は，P 波 S 波何れにせよこれを解析すれば，强制波，自由波及び初期波の三種より成立つてゐる事が解かつたのであるがこれも研究結果の一つである．若し實驗的にこの强制波を取出す事が出來れば，震源での力の變り方が明かにされ，發震機構の研究を一步進める事が出來るのである.

---

1) 西村源六郎, 地震研究所彙報 15 (昭和 12 年), 3 號.

28. *Seasonal Distributions of Earthquakes in the World.*

By Seiti YAMAGUTI,

Earthquake Research Institute.

(Read Dec. 21, 1937.—Received March 20, 1938.)

The "Index Catalogue of Epicentres for 1913–1930" recently compiled by E. F. Bellamy which contains the times of occurrence, and the co-ordinates of epicentres, of 6738 earthquakes that occurred in the world during the said period, is a storehouse of valuable material from which reliable statistics can be made relating to the occurrences of earthquakes. Although the seasonal distributions of earthquakes have been the subject of many classical studies, it may not be profitless to discuss this problem with the newly arranged materials in view.

By plotting the epicentres on maps separately, for each month, it became clear that the geographical distributions of earthquakes differ from month to month. The maps were divided into compartments by parallel latitudes and longitudes, which were drawn for every 30 degrees,

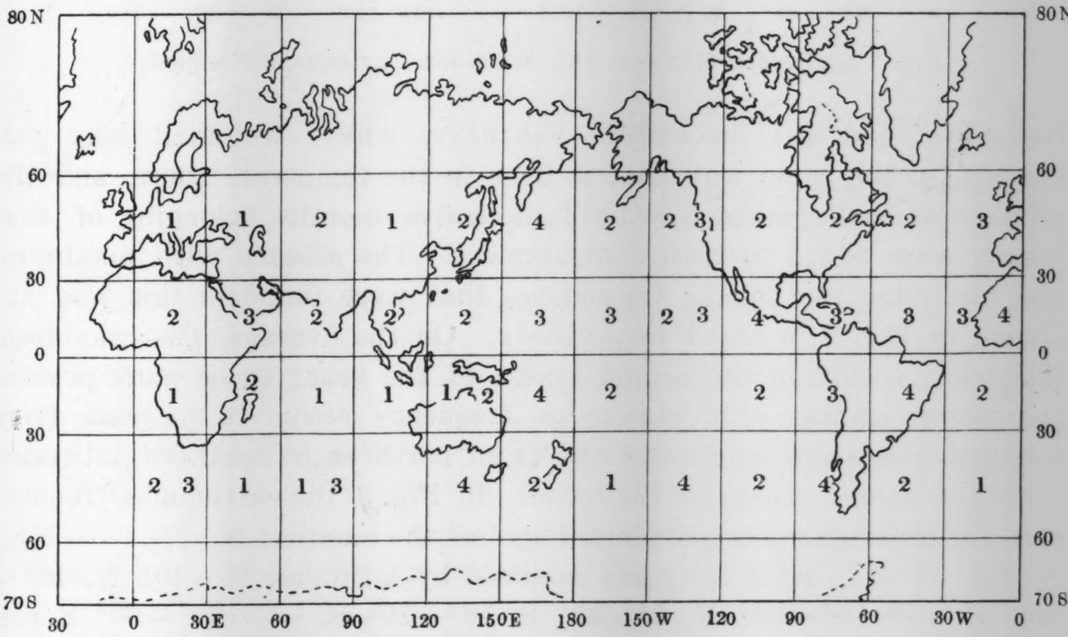
80 N
60
30
0
30
60
70 S
30
0
30E
60
90
120
150E
180
150W
120
90
60
30W
0
1 1 2 1 2 4 2 2 3 2 2 2 3
2 3 2 2 2 3 3 2 3 4 3 3 3 4
1 2 1 1 1 2 4 2 2 3 4 2
2 3 1 1 3 4 2 1 4 2 4 2 1

Fig. 1 *a*. Season Number with Maximum Earthquake Frequency.
1: March~May, 2: June~Aug., 3: Sept.~Nov., 4: Dec.~Feb.

and the number of earthquakes that fell into each compartment a month was counted. In order to see the changes in earthquake frequencies for varions times of the year, the 12 months were divided into four groups, viz. (1) March∼May, (2) June∼August, (3) September∼November and (4) December∼February, which we shall here call seasons, in the same way that is done in the temperate zones, and the number of earthquakes for the 3 successive months belonging of that season were added to each compartment. The seasons with maximum and minimum earthquake frequencies that were found in this way are shown in Fig. 1, *a* and *b* respectively. On the average, the maximum frequency occurs in the second season of the year; to be more precise, the season number with maximum frequency seems to increase from western to eastern longitudes and from northern to southern latitudes, with the second season as the mean. In Fig. 3, the earthquake frequencies for different zones are plotted against the months: N_1, N_2, …… $N_{7\sim9}$, S_1, S_2, …… $S_{5\sim9}$ being the zones bounded by latitudes, 0°∼10° N, 10°∼20° N, …… 70°∼90° N, 0°∼10° S, 10°∼20° S, …… 50°∼90° S respectively. In Fig. 4, the earthquake frequencies for the four quadrants are also plotted against the months. In every figure, the thick lines indicate overlapping means. What is remarkable is that the curves for the NE and NW quadrants are approximately opposite in phase.

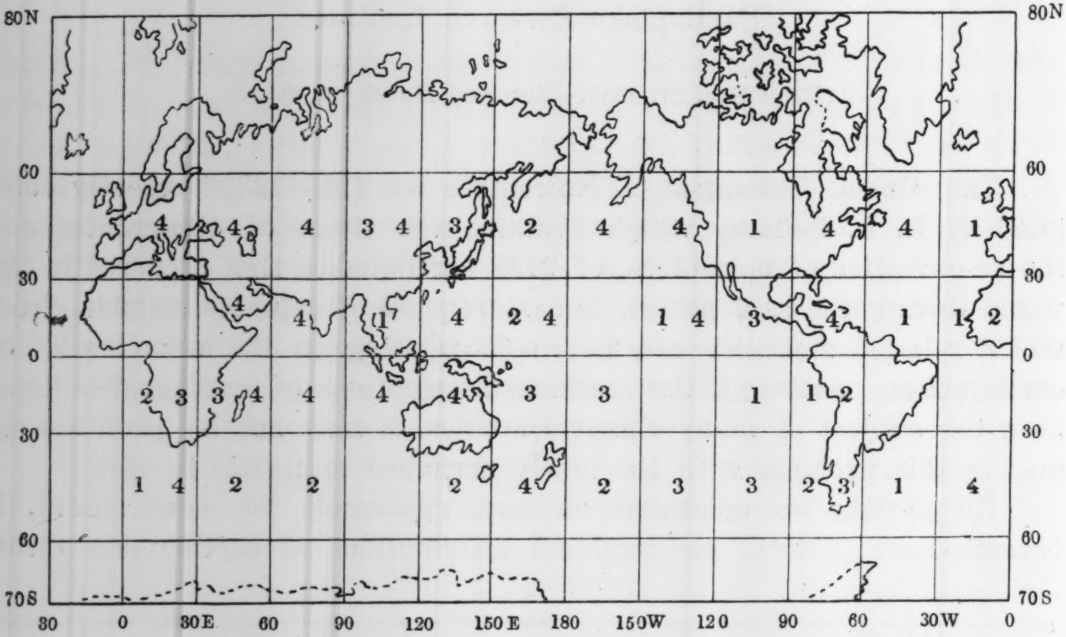

Fig. 1 *b*. Season Number with Minimum Earthquake Frequency.

In order to get results that are likely to prove of more geophysical

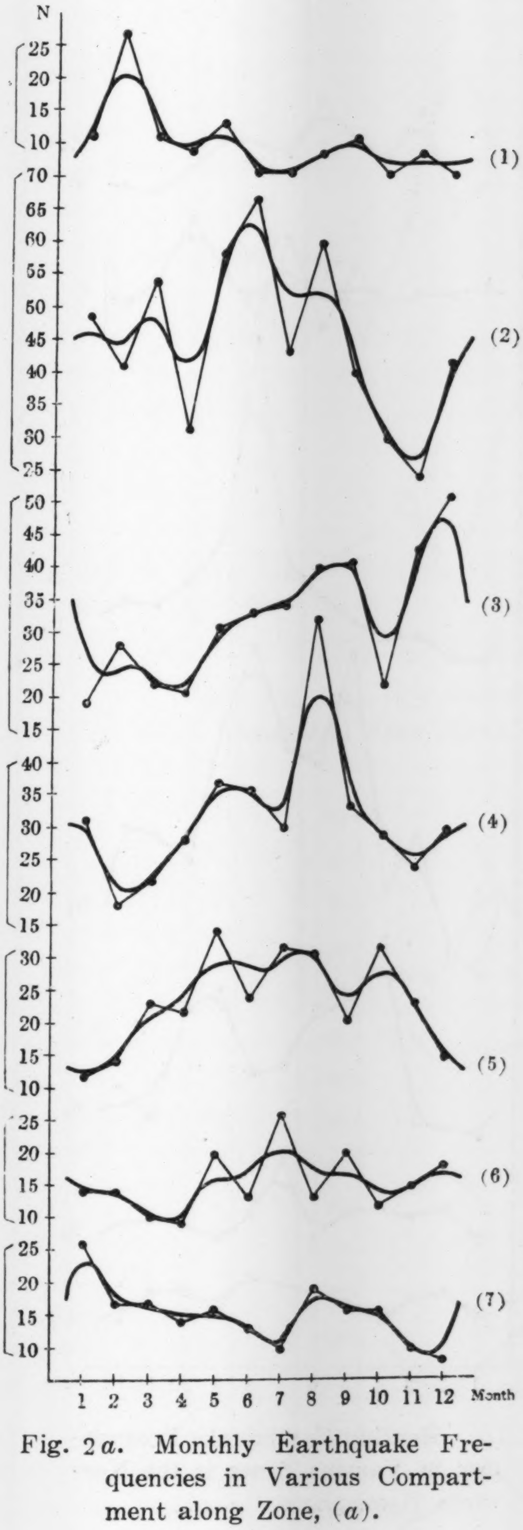

Fig. 2*a*. Monthly Earthquake Frequencies in Various Compartment along Zone, (*a*).

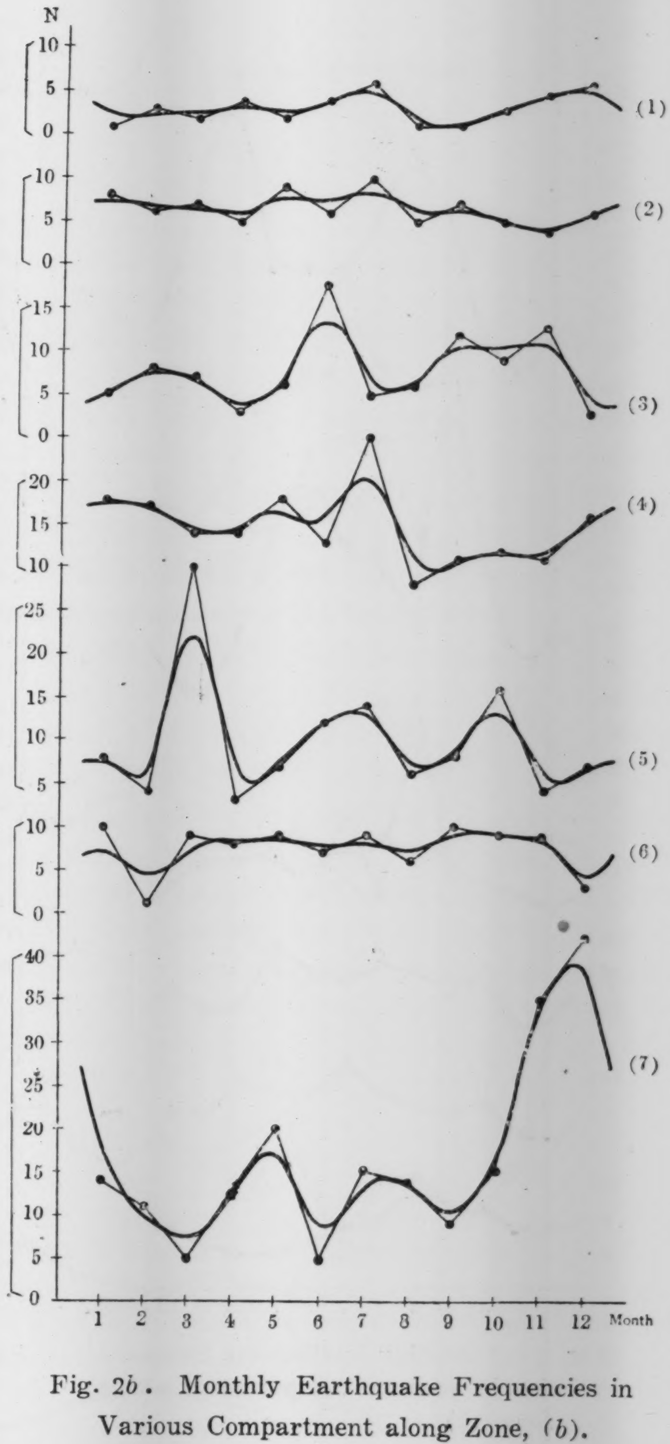

Fig. 2*b*. Monthly Earthquake Frequencies in Various Compartment along Zone, (*b*).

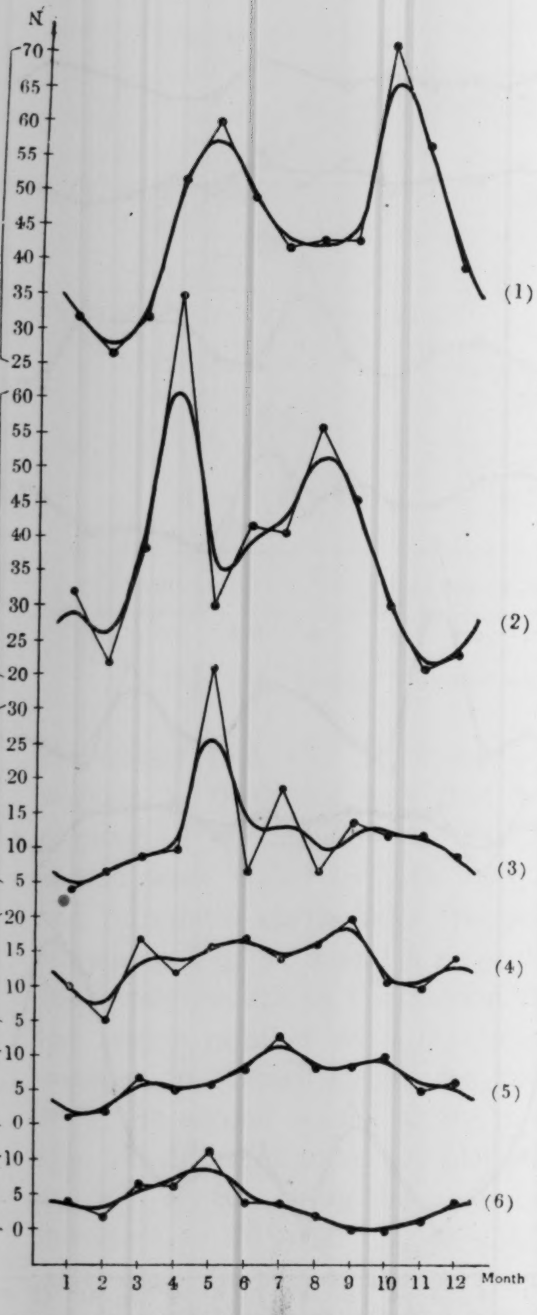

Fig. 2 *c*. Monthly Earthquake Frequencies in Various Compartment along Zone, (*c*).

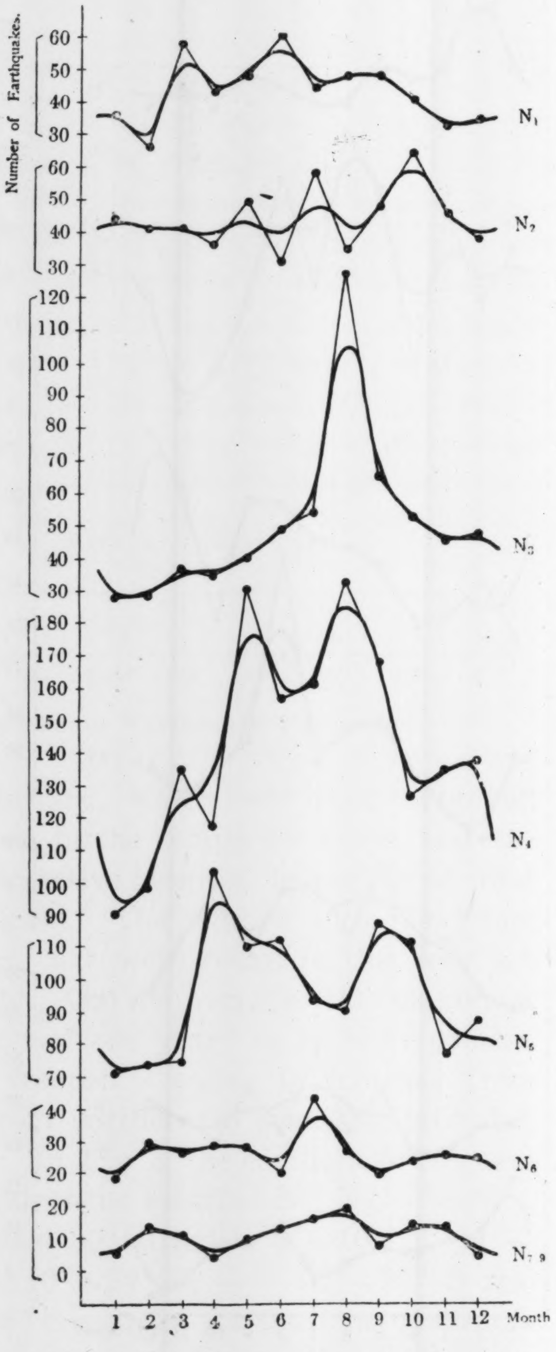

Fig. 3 *a*. Monthly Earthquake Frequencies in Various Zones in the Northern Hemisphere.

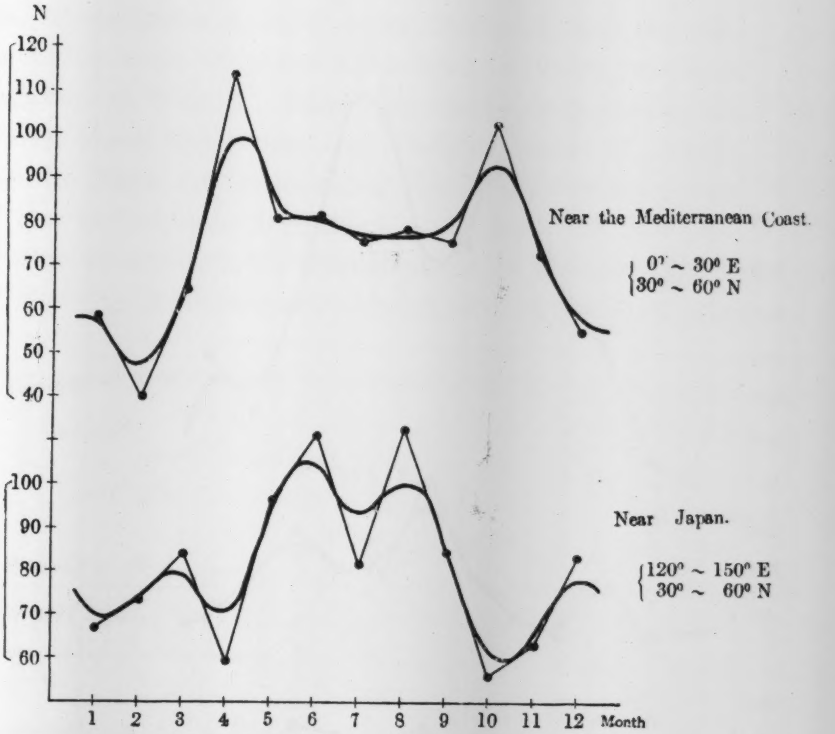

Fig. 2 *d*. Monthly Earthquake Frequencies along the Mediterranean Coast and Near Japan.

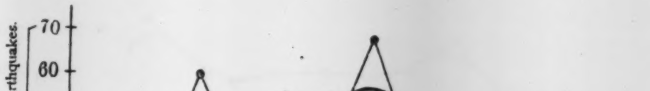

Fig. 3 *b*. Monthly Earthquake Frequencies in Vavious Zones in the Southern Hemisphere.

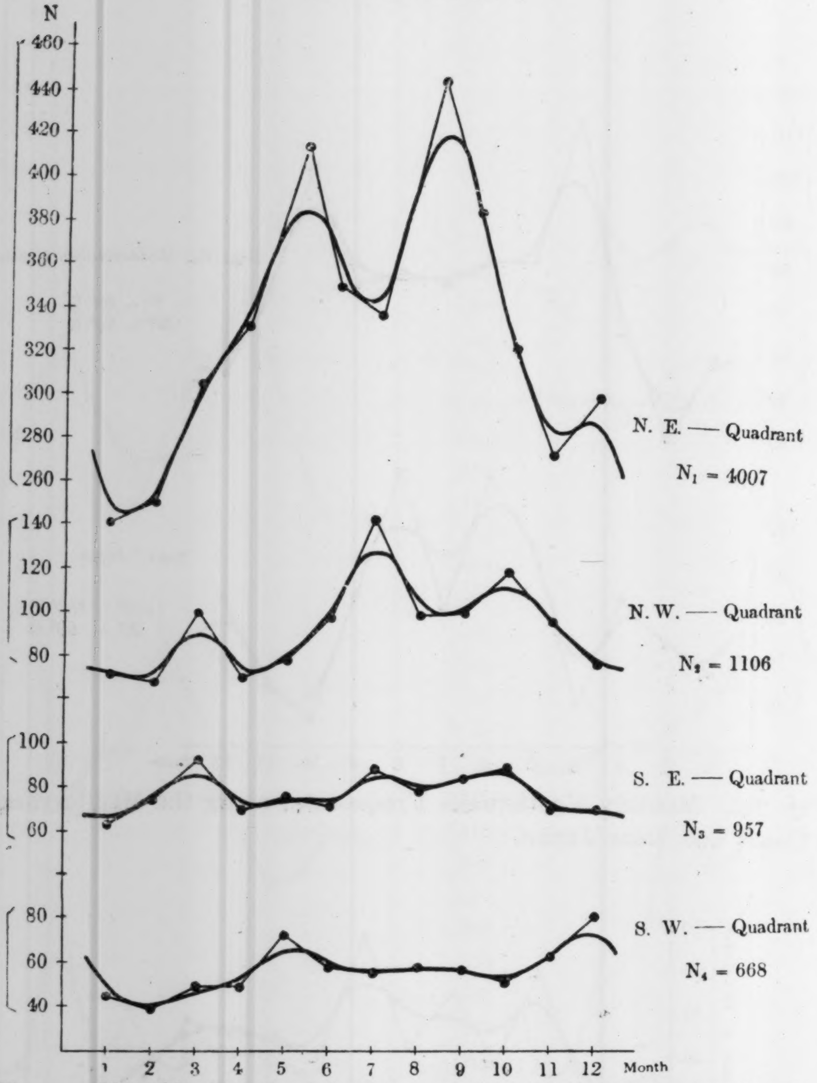

Fig. 4. Monthly Earthquake Frequencies in the Four Quadrants.

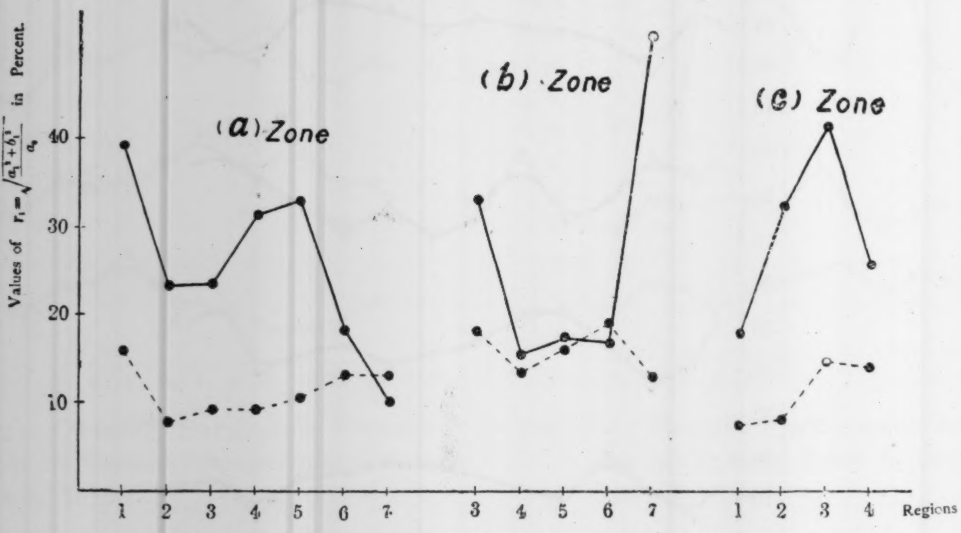

Fig. 5. Amplitudes of the Annual Term (Full Line) and Corresponding Expectancy (Dotted Line).

significance, three zones *a*, *b*, *c* were taken along the three principal earthquake belts, each of these zone being divided into several compartments as shown in Fig. 8. Zone (*a*) runs along Japan, the Philippines, and Australia, Zone (*b*) along the Pacific coast of North and South America, while Zone (*c*) runs along the Mediterranean coast of Eurasia. In Fig. 2. the earthquake frequencies for each of the small compartments are plotted against the months. It is notable that the curves for Japan and for the Mediterranean coast are opposite in phase.

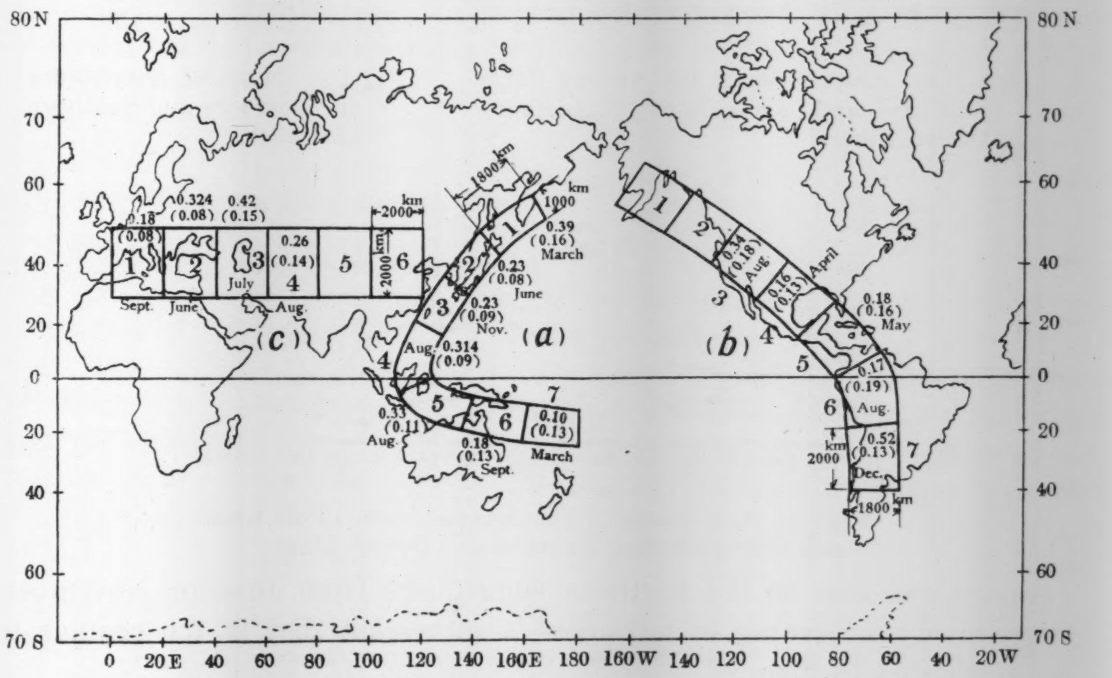
80 N
70
60
40
20
0
20
40
60
70 S
0
20E
40
60
80
100
120
140
160E
180
160W
140
120
100
80
60
40
20W
(c)
1
2
3
4
5
6
0.18
(0.08)
Sept.
0.324
(0.08)
June
0.42
(0.15)
July
0.26
(0.14)
Aug.
km
2000
km
2000
(a)
1800 km
1000 km
0.39
(0.16)
March
0.23
(0.08)
June
0.23
(0.09)
Nov.
Aug.
0.314
(0.09)
0.33
(0.11)
Aug.
0.18
(0.13)
Sept.
7
0.10
(0.13)
March
(b)
0.34
(0.18)
Aug.
0.16
(0.13)
April
0.18
(0.16)
May
0.17
(0.19)
Aug.
0.52
(0.13)
Dec.
km
2000
1800 km

Fig. 8. Divisions of Compartments, Month with Maximum Earthquake Frequency, Amplitude of Annual Term, Expectancy (Bracket).

In order to get more concrete results, Fourier's analysis was resorted to in arriving at the annual distributions of earthquake frequencies. Given 12 values, of monthly frequencies, the Fourier coefficients a_0 $a_1 \cdots\cdots a_6$, $b_1 \cdots\cdots b_5$ for the annual distribution were determined in the usual way. From the values found, the relative amplitude of the annual term ($r_1=\sqrt{a_1^2+b_1^2}\big/a_0$) and the phase of maximum, $\varepsilon=\tan^{-1}\dfrac{b_1}{a_1}$ were calculated and plotted in Figs. 5, 6, 7. To enable a comparison of these values with what may be expected as the result of fortuitous happenings, the expectancy of the annual amplitude $r=\sqrt{\dfrac{\pi}{N}}$ is also shown by the dotted lines in Fig. 5, where N is the number of earthquakes taken in the calculation. In the same figure, the months with maximum earthquake frequencies are also indicated. The times of maximum

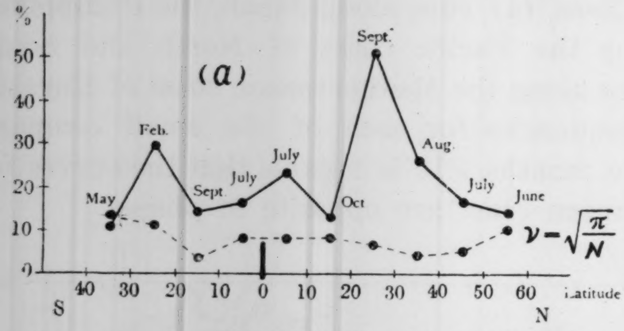

Fig. 6 *a*. Amplitudes of the Annual Term (Full Line) and Corresponding Expectancy (Dotted Line).

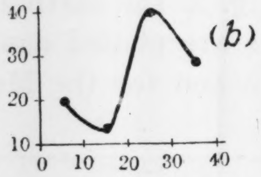

Fig 6 *b*. Mean of Amplitudes for Northern and Southern Latitudes.

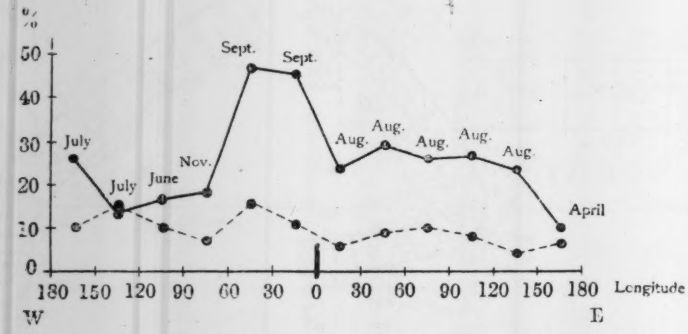

Fig. 7. Amplitudes of the Annual Term (Full Line) and Corresponding Expectancy (Dotted Line).

frequency change in the northern hemisphere from June to November, successively, according to latitudes– a succession that is too regular to be attributed to chance.

It is also noteworthy that, whereas the maximum in September takes place in N_3–zone, in February it does so in the S_3–zone, a difference of about half a year separating them.

The amplitudes of the annual term differ considerably with the particular compartments. They are large along the Mediterranean Sea, Japan, the Philippines; and also along the southern Pacific coast of South America where the amplitude exceeds four times the expectancy.

The coefficients for the higher harmonics were similarly calculated, the values $r_n = \sqrt{a_n^2+b_n^2}/a_0$ of which will be found in Tables I and II. Certain periods seem to predominate in certain compartments, although whether this fact has any real physical meaning or not is not clear.

In conclusion, I wish to express my best thanks to Dr. C. Tsuboi, who has given me many useful suggestions in the course of these studies.

Table I. For 3 Principal Earthquake Zones.

(*a*) Earthquake Zone, through Japan, the Philippines, and Australia.

Regions	Coefficients in Fourier's Harmonic Analysis.												$r_n=\frac{\sqrt{a_n^2+b_n^2}}{a_0}$					$\nu=\sqrt{\frac{\pi}{N}}$
	a_0	a_1	a_2	a_3	a_4	a_5	a_6	b_1	b_2	b_3	b_4	b_5	r_1	r_2	r_3	r_4	r_5	
(1)	10·3	1·4	- 2·7	- 2·5	- 1·8	1·05	0·17	3·8	2·3	1·5	- 3·75	- 2·3	0·39	0·34	0·28	0·40	0·25	0·16
(2)	44·8	-10·0	3·4	- 0·83	5·9	- 1·65	0·33	2·98	7·1	4·2	- 4·5	8·2	0·23	0·18	0·10	0·17	0·19	0·08
(3)	32·1	1·7	4·8	4·8	4·6	2·5	0·40	- 7·3	0·55	- 1·3	- 6·6	- 3·5	0·23	0·15	0·16	0·25	0·13	0·09
(4)	31·9	- 6·6	-20·0	6·7	18·7	- 3·1	2·4	- 7·6	3·75	4·2	- 3·75	6·3	0·31	0·64	0·25	0·60	0·22	0·09
(5)	23·6	- 6·5	- 0·7	- 0·3	- 2·8	2·4	- 0·6	- 4·3	- 3·2	- 1·8	- 0·6	3·5	0·33	0·14	0·08	0·12	0·18	0·11
(6)	15·3	- 1·3	2·4	0·2	- 0·1	3·6	- 2·2	- 2·5	1·6	0·5	- 0·15	- 1·97	0·18	0·19	0·04	0·01	0·27	0·13
(7)	15·2	0·61	- 2·34	- 0·83	- 1·67	- 2·28	- 0·67	1·4	2·3	3·5	0·6	2·6	0·10	0·22	0·24	0·12	0·23	0·13

(*b*) Earthquake Zone, Through North America, Central America, and South America.

Regions	Coefficients in Fourier's Harmonic Analysis.												$r_{,}=\frac{\sqrt{a_n^2+{}_n^2}}{a_0}$					$\nu=\sqrt{\frac{\pi}{N}}$
	a_0	a_1	a_2	a_3	a_4	a_5	a_6	b_1	b_2	b_3	b_4	b_5	r_1	r_2	r_3	r_4	r_5	
(3)	7·9	- 1·73	0·58	- 3·83	2·08	- 1·94	- 0·08	- 1·99	- 1·01	- 0·33	- 1·59	- 0·84	0·34	0·15	0·49	0·33	0·27	0·18
(4)	14·8	- 0·93	2·42	- 0·67	- 1·25	3·1	- 1·42	2·09	1·87	- 0·5	2·16	- 1·09	0·16	0·21	0·06	0·17	0·22	0·13
(5)	9·9	- 1·22	- 5·58	- 2·67	7·08	1·38	- 1·92	1·25	0·29	- 4·17	2·89	5·58	0·18	0·56	0·50	0·77	0·58	0·16
(6)	7·5	- 0·86	- 0·42	0·0	- 0·25	- 1·15	- 1·83	- 0·95	- 1·3	0·33	1·59	0·78	0·17	0·18	0·04	0·21	0·19	0·19
(7)	16·5	8·1	8·1	6·33	- 1·25	4·07	0·17	- 2·72	- 4·18	- 2·0	- 3·32	- 1·28	0·52	0·55	0·40	0·22	0·26	0·13

(*c*) Earthquake Zone, Through the Coast of the Mediterranean Sea.

Regions	Coefficients in Fourier's Harmonic Analysis.												$r_n=\frac{\sqrt{a_n^2+b_n^2}}{a_0}$					$\nu=\sqrt{\frac{\pi}{N}}$
	a_0	a_1	a_2	a_3	a_4	a_5	a_6	b_1	b_2	b_3	b_4	b_5	r_1	r_2	r_3	r_4	r_5	
(1)	45·6	- 3·3	-13·9	- 2·2	11·1	0·47	1·25	- 7·5	-13·8	0·67	1·45	2·6	0·18	0·43	0·05	0·25	0·06	0·08
(2)	3·8	-12·3	- 8·1	1·0	- 0·75	- 7·2	3·3	0·25	- 0·73	1·3	7·1	- 2·9	0·32	0·21	0·27	0·19	0·20	0·08
(3)	12·2	- 5·1	1·8	0·0	- 2·4	6·1	- 3·5	- 0·37	- 4·8	2·3	- 2·5	0·2	0·42	0·42	0·19	0·28	0·50	0·15
(4)	13·4	- 3·03	- 0·42	1·67	3·59	- 0·14	- 1·08	- 1·78	- 0·58	0·83	0·0	1·11	0·26	0·05	0·14	0·27	0·08	0·14

Table II. For Various Latitude Zones, and Various Longitude Sectors.

(a) Latitude Zones.

Zones	Coefficients in Foulier's Harmonic Analysis.												$r_n=\frac{\sqrt{a_n^2+b_n^2}}{a_0}$					$\nu=\sqrt{\frac{\pi}{N}}$
	a_0	a_1	a_2	a_3	a_4	a_5	a_6	b_1	b_2	b_3	b_4	b_5	r_1	r_2	r_3	r_4	r_5	
N_1	43·7	-9·9	-1·58	-0·17	7·08	-2·95	-1·17	-1.03	-1·3	-0·5	1·3	5·03	0·23	0·05	0·01	0·17	0·13	0·08
N_2	44·6	1·37	-1·58	-4·5	-4·58	7·14	-3·42	-5·32	-2·72	-1·0	4·46	1·32	0·12	0·07	0·11	0·14	0·16	0·08
N_3	50·8	-10·2	-7·42	13·3	-1·25	-4·13	5·92	-23·9	9·68	-0·5	-10·5	9·46	0·51	0·24	0·26	0·21	6·20	0·07
N_4	141·5	-27·8	3·08	9·5	7·91	8·84	-5·08	-23·2	-2·43	3·0	-19·2	9·66	0·26	0·03	0·07	0·15	0·09	0·04
N_5	96·1	-15·3	1·83	2·33	-3·67	0·52	5·42	-5·07	-15·0	8·83	8·34	-7·09	0·17	0·16	0·10	0·09	0·07	0·05
N_6	26·2	-3·68	0·25	1·0	-3·92	4·68	-0·5	0·57	1·59	-4·66	0·43	-1·74	0·14	0·06	0·18	0·15	0·19	0·10
$N_{7\sim9}$	11·0	-2·24	-0·75	-1·83	-1·75	0·07	0·5	-2·84	1·59	-2·84	-2·16	1·5	0·33	0·16	0·31	0·25	0·14	0·15
S_1	45·8	-7·1	-0·5	-0·83	0·5	4·43	-6·25	-2·3	-2·02	-7·0	1·45	2·3	0·16	0·05	0·15	0·03	0·11	0·08
S_2	29·1	-1·52	-0·75	-0·17	0·42	-1·81	-0·25	-3·72	3·9	4·0	-0·14	3·22	0·14	0·14	0·14	0·02	0·13	0·03
S_3	20·5	4·75	3·33	0·17	-1·0	3·59	0·67	3·7	-0·87	2·17	-4·9	1·97	0·29	0·17	0·11	0·24	0·20	0·11
S_4	16·3	-1·08	2·84	4·83	4·0	3·25	0·92	1·47	-4·04	2·0	2·02	0·03	0·11	0·30	0·32	0·28	0·20	0·13
$S_{5\sim9}$	14·7	-1·78	0·25	0·67	2·08	3·12	0·92	-1·77	1·3	-1·5	0·14	2·26	0·17	0·09	0·11	0·14	0·26	0·13

(b) Sectors Bounded by Longitudes.

Sectors	Coefficients in Foulier's Harmonic Analysis.												$r_n=\frac{\sqrt{a_n^2+b_n^2}}{a_0}$					$\nu=\sqrt{\frac{\pi}{N}}$
	a_0	a_1	a_2	a_3	a_4	a_5	a_6	b_1	b_2	b_3	b_4	b_5	r_1	r_2	r_3	r_4	r_5	
E_1	65	-12·7	-5·58	4·83	-4·92	-5·16	16·4	-8·22	-16·3	-0·33	10·5	1·88	0·23	0·27	0·08	0·19	0·09	0·06
E_2	34·1	-8·64	-4·75	1·5	-2·58	6·63	-3·25	-5·0	-6·5	9·0	-0·14	2·5	0·29	0·24	0·27	0·08	0·21	0·09
E_3	24·7	-5·63	8·66	0·67	-7·83	4·46	-2·0	-3·24	-1·16	-3·33	1·45	3·4	0·26	0·35	0·14	0·32	0·23	0·10
E_4	40·4	-8·56	-2·0	9·17	2·84	4·38	-0·25	-6·58	2·88	0·33	-3·75	6·41	0·27	0·09	0·23	0·12	0·19	0·08
E_5	176	-33·7	-1·17	8·5	13·0	-6·83	2·66	-22·1	12·5	1·83	-22·6	16·9	0·23	0·07	0·05	0·15	0·10	0·04
E_6	48	-0·37	-3·08	-3·33	-1·75	0·21	-2·67	4·6	5·06	5·5	-6·21	-2·6	0·10	0·12	0·13	0·13	0·05	0·07
W_1	23·2	-2·72	-3·25	0·33	-0·92	1·88	2·5	-10·1	1·3	-1·33	-2·45	1·75	0·45	0·15	0·06	0·11	0·11	0·11
W_2	10·1	-0·13	-1·25	2·17	0·92	2·47	-0·25	-4·69	1·59	-2·0	1·01	-1·81	0·47	0·20	0·29	0·14	0·30	0·16
W_3	45·6	6·02	0·92	-0·83	3·42	6·32	-5·42	-5·78	-3·02	-7·66	1·58	4·62	0·18	0·07	0·17	0·08	0·17	0·08
W_4	25·5	-3·78	5·83	-3·33	2·5	-0·89	-1·83	2·16	2·9	-1·0	1·17	-0·16	0·17	0·26	0·14	0·11	0·04	0·10
W_5	12	-1·41	2·34	-2·84	0·0	-0·26	-0·83	-0·74	-0·58	-2·83	0·58	0·41	0·13	0·20	0·33	0·05	0·04	0·15
W_6	27	-6·83	4·08	-0·67	-0·25	2·99	0·67	-1·39	-2·45	-2·33	2·45	0·06	0·26	0·18	0·09	0·09	0·11	0·10

28. 世界地震の季節的分布

地震研究所 山口生知

1913年から1930年に至る滿18年間に世界中に起つた6738個の主なる地震に就いて其地方的並に季節的分布を調べて見た。

其結果或る特定の場所に於いては或る季節に地震の起る回數が非常に多く，又或る他の特定の場所に於いては地震の起る回數が少ないと云ふことは面白いことゝ思ふ。殊に南緯北緯共20° から 30° の間の所に地震回數の最大があり，而も北半球に於いては九月に，南半球に於いては約半年の差を有する二月に最大回數を有すると云ふことは著しい事實であつて，之には何か或る物理的意義の存在することを暗示するものと思はれる。

概して世界中を通じて夏季に地震回數の最大になる傾向が見受けられる。

又各地に於ける地震回數の月々の分布を見ると日本附近に起る地震と地中海沿岸に起る地震とは位相が反對であり，又全世界を四つの象限に分けると北東の象限と北西の象限に起る地震とは位相が互に反對である傾向を認める

各地の地震を夫々十二ケ月に分けて調和分析を試ると，場所に依つては一年週期の外に，半年週期及び三ケ月週期の目立つ場所も有る樣に思はれる。これは更に將來の研究を待つことにしたいと思ふ。

29. *Observations of Changes in the Inclination of the Earth's Surface at Mt. Tukuba.*

By Takahiro HAGIWARA,

Earthquake Research Institute.

(Read Feb. 15, 1938.—Received March 20, 1938.)

The observations of changes in the inclination of the earth's surface at Mt. Tukuba, where a branch of our Institute is situated, were made during 1927—1931 with Ishimoto all-silica clinographs, installed in a windowless stone house built on a natural granite foundation. Several papers on this subject have already been published by W. Inouye, according to which, the changes in inclination are very large, the daily variations in inclination amounting to 1″ of arc, and the secular changes to a few seconds of arc. It seems to be a phenomenon largely due to changes in temperature, but further investigations are needed. Although the all-silica clinograph is scarcely affectted direct by changes in temperature, it is likely to be affected by changes in inclination of the surface ground caused by fluctuations in temperature due to sunshine and by changes in temperature of the air, etc.. The changes in inclination that we wish to assertain are not such phenomena but changes of more geophysical significance.

For reducing such temperature effects, a gallery 1 m wide and 2 m high was bored in partially weathered granite, forming a ridge of the mountain on which our branch Institute stands. A boring was made horizontally for a distance of about 25 m from the entrance, and a chamber excavated at the end of the gallery where a faily fresh granite appeared. To avoid the flow of air, doors were placed in number of places. The plan of the gallery is shown in Fig. 1. For ease of reference we shall call this room "*A*".

Continuous observations in room "*A*" were begun in October, 1935. Later, other clinographs were installed at the place near the entrance marked "*B*" in the figure, and comparative observations were made since November, 1936. In room "*A*", the changes in inclination were, as expected, so small that the sensibility of the instruments were in-

---

1) W. INOUYE, *Bull. Earth. Res. Inst.*, **8** (1930), 346; **10** (1932), 130; **11** (1933), 693.

creased so that 1 mm on the record shall correspond to an inclination of about 0·01″ of arc.

This paper is a preliminary report of these observations.

Daily variation. In room "*A*", the magnitute of the daily veriation in inclination was of the order of 0·01″ of arc, while in room "*B*" it was of the order of 0·05″ of arc, as shown in reproductions of the records in Fig. 4. In room "*A*", the dairy variations have two maximum values in the E–W component and one in the N–S component, while in room "*B*", the variations have one maximum value in each component. The mean daily variations in rooms "*A*" and "*B*" are shown vectorially in Fig. 2. The variations in rooms "*A*" and "*B*" differ not only in their quantities but also in their types.

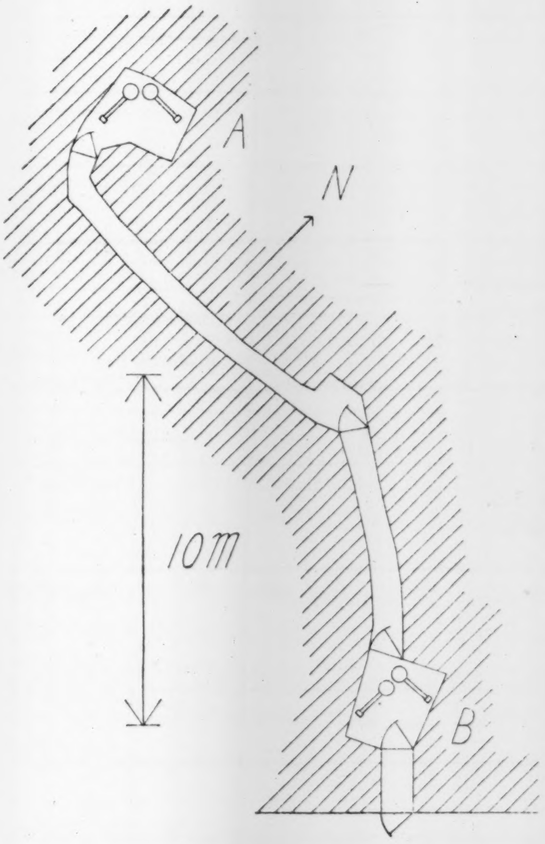

Fig. 1. The plan of the gallery.

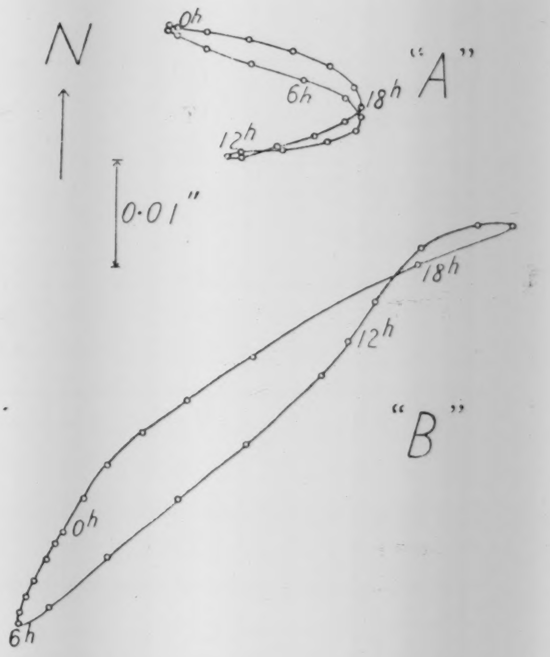

Fig. 2. The mean daily variations.

No daily variations with respect to the lunar period could be detected. The variations due to lunar attraction are expected to be of the order of 0·01″ of arc, but they could not be detected in the present observations.

Secular variations. The secular variations in inclination are shown in Fig. 3, in which the mean value for each day is plotted. The variations in room "*B*" are large compared to that in room "*A*". However,

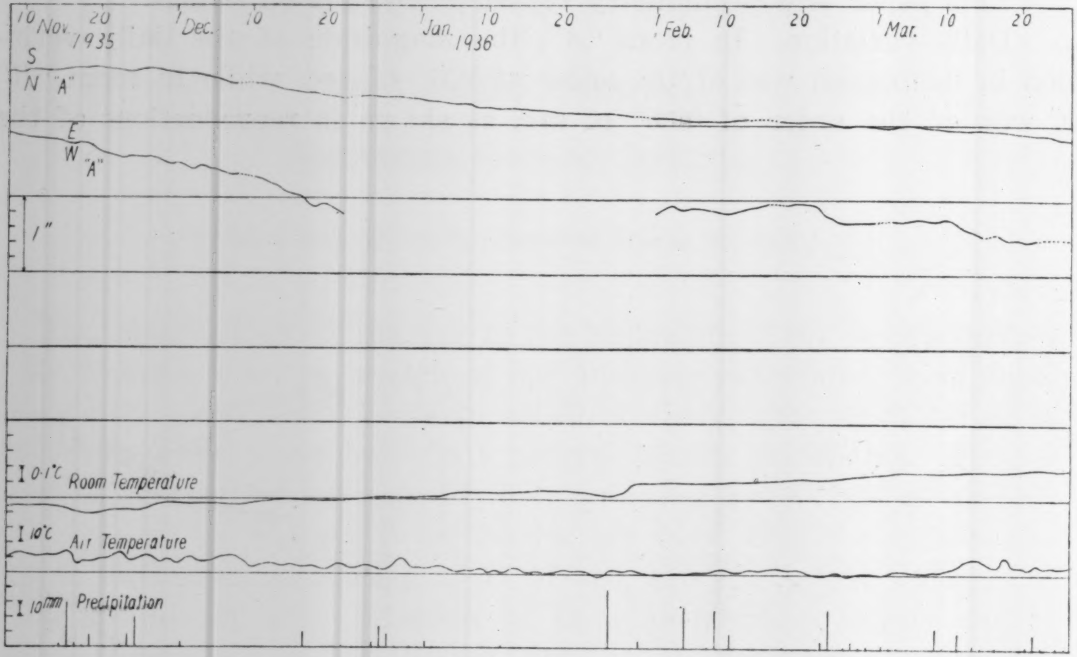

Fig. 3 a.

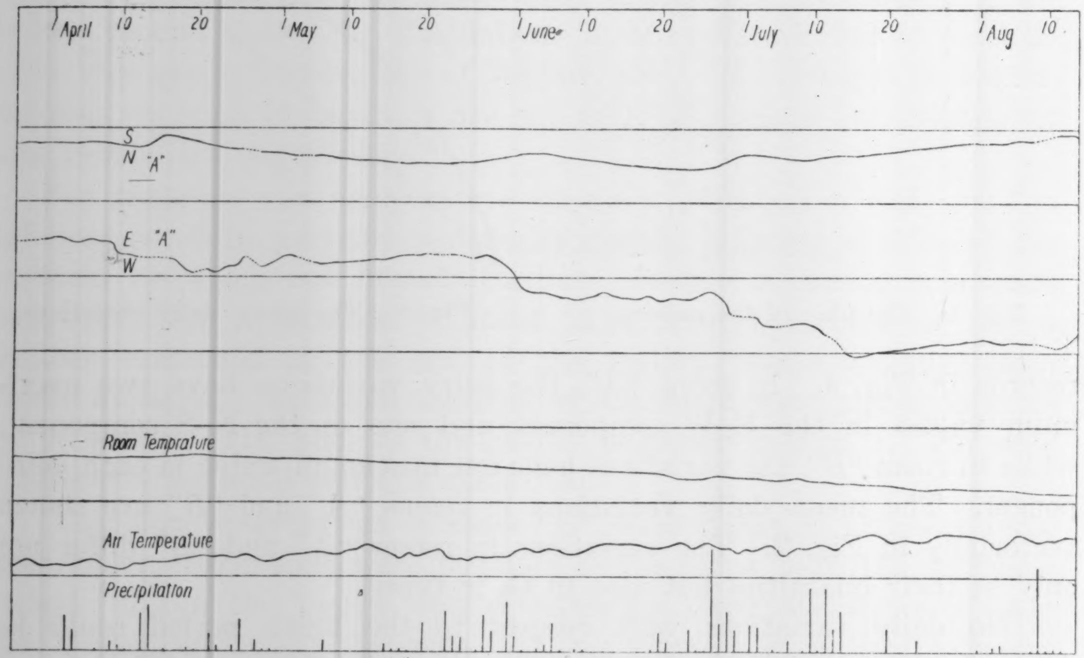

Fig. 3 b.

no correlation between them is evident. For comparison, the temperature of the open air, the temperature of room "*A*" (which were read off from a Beckmann thermometer), and the precipitation are also plotted in the figure, from which it will be seen that the annual variation and

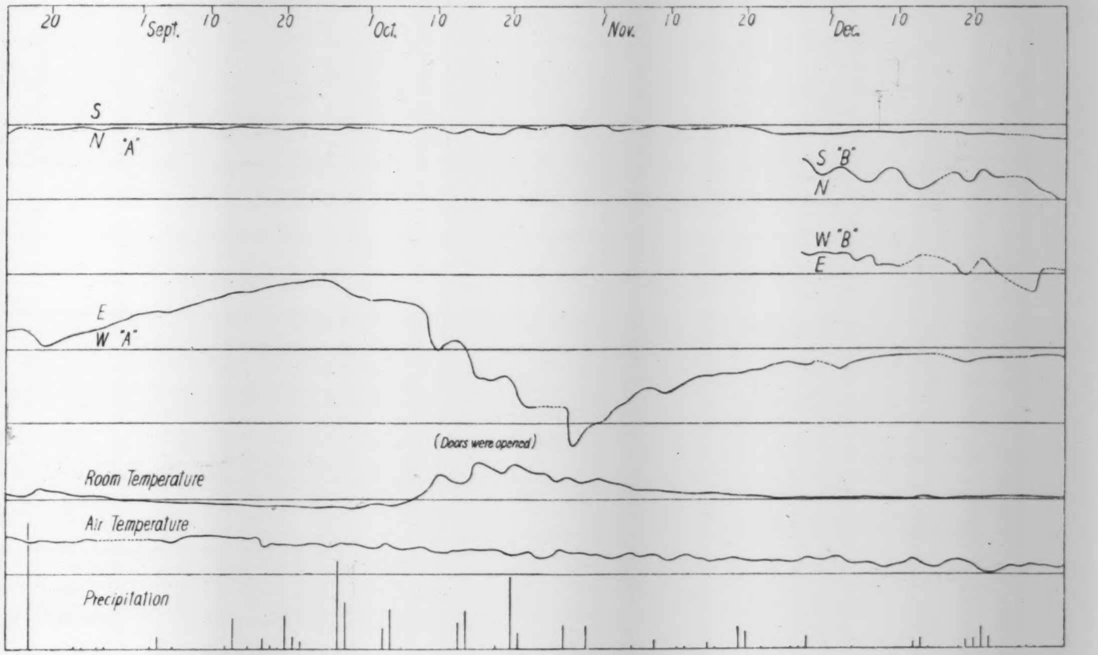

Fig. 3 c.

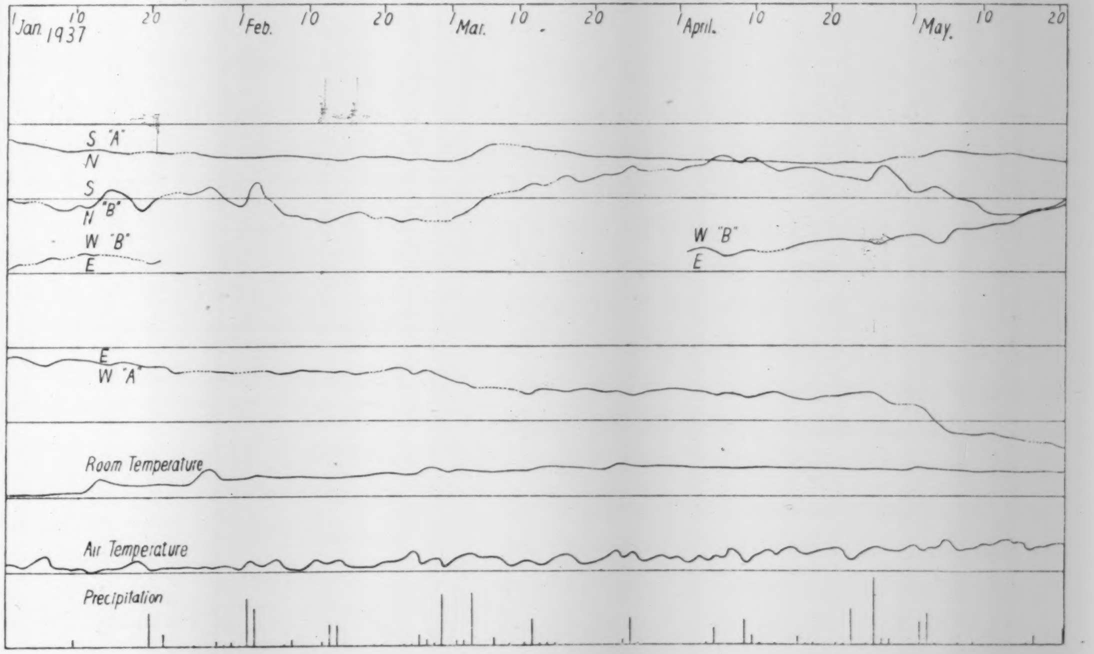

Fig. 3 d.

the large irregular variations in room "*A*" are intimately related to the variations in room temperature. It was thought that the underground water might in some way affect the temperature underground, and consequently the temperature of the observation room, but the figures do not show any such relationship between them.

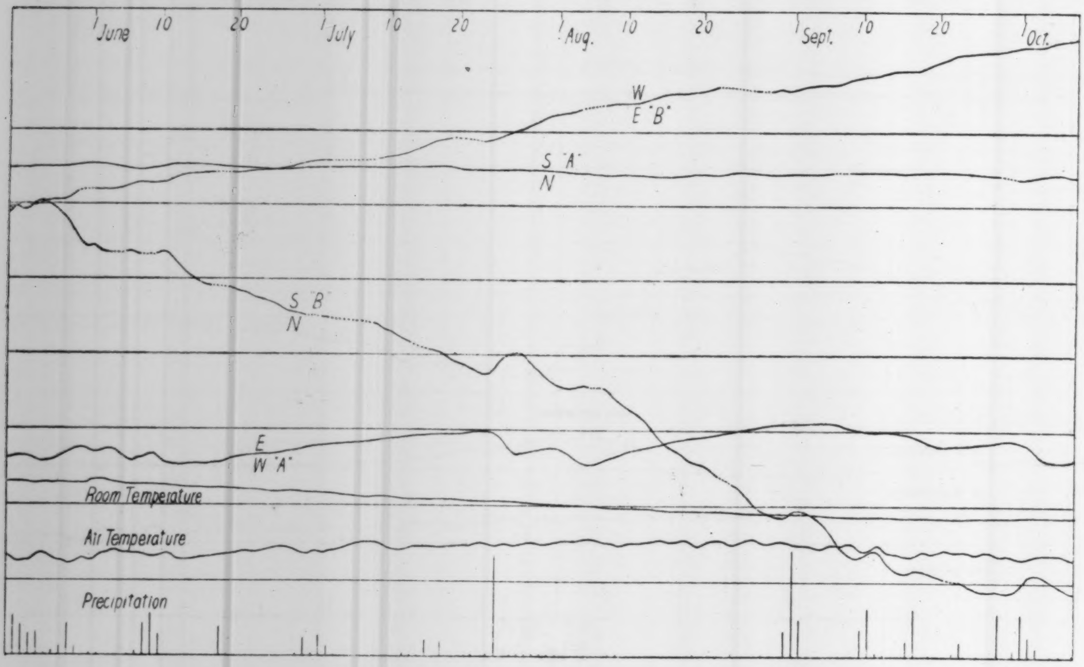

Fig. 3 e.

Remarks. The fact that the changes in inclination in rooms "*A*" and "*B*" differ entirely from each other show that measurements of changes in inclination of the earth's surface is a very difficult matter. The changes in inclination are disturbed by irregular changes due to changes in temperature, while relationship between them is in most cases very complicated. We cannot find a simple relation by means of which we could devise ways of eliminating their effects. It is not evident which part of the changes is due to temperature and which part to geophysical causes. So far as our knowledge goes, no such comparative observation has yet been made elsewhere. In the cases of such

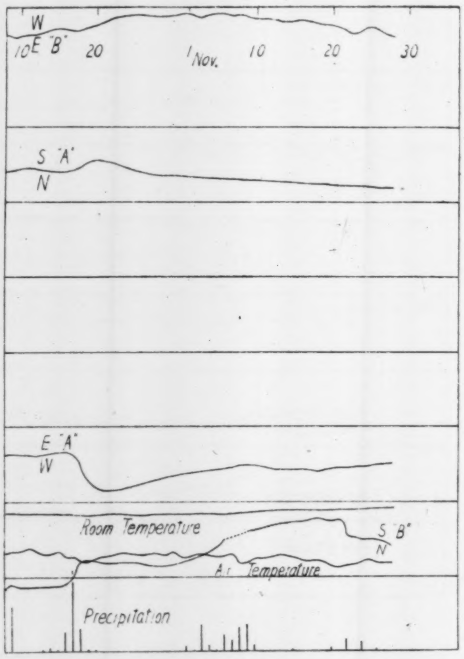

Fig 3 f.

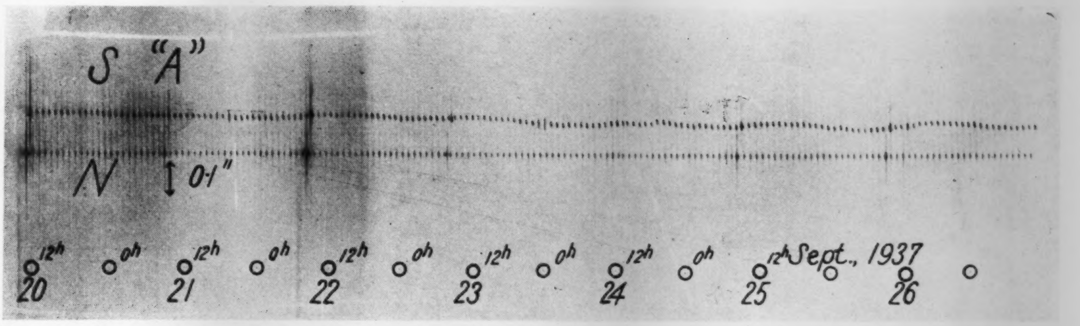

Fig. 4 a.

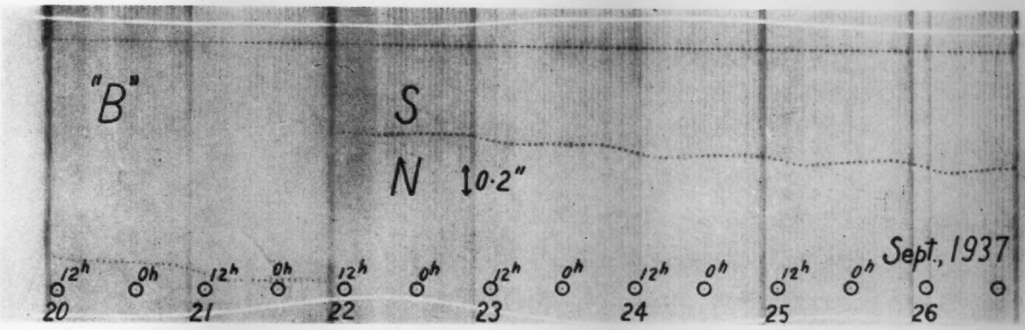

Fig. 4 b.

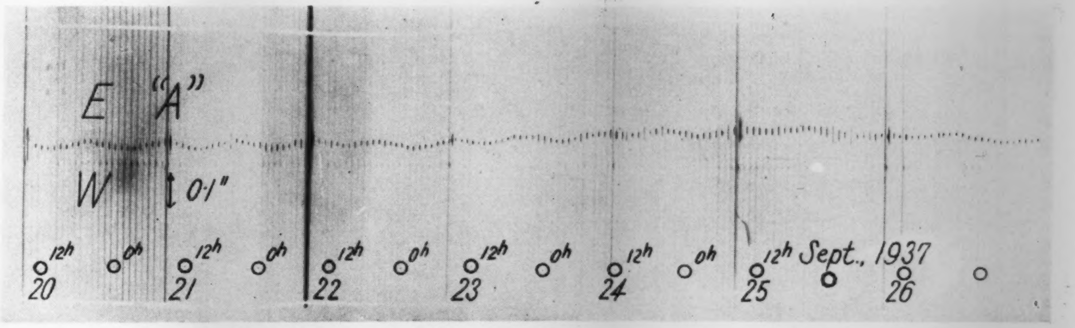

Fig. 4 c.

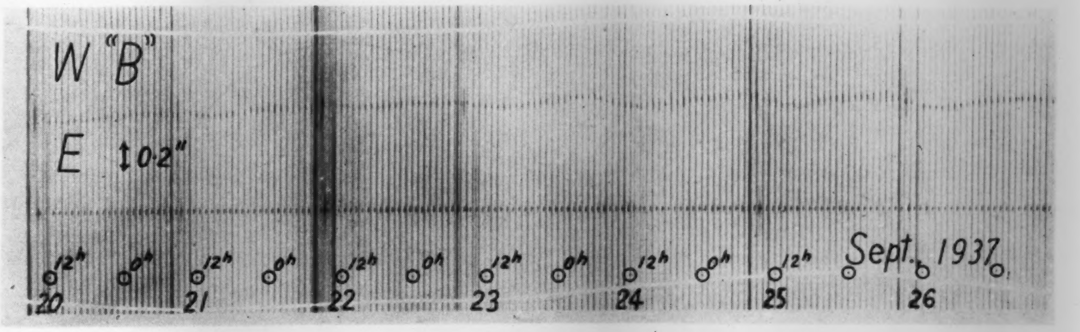

Fig. 4 d.

（震研彙報 第十六號 圖版 萩原）

phenomena, observations at only one place cannot give such macroscopic changes as, for instance, changes in inclination of the *earth's crust*, which question, needless to say, cannot be answered positively from the present observations alone, although it is an important problem worth investigating. This report is preliminary, and does not solve the problem mentioned. The solution will have to await further investigations.

---

29. 筑波山に於ける土地傾斜變化の觀測

地震研究所 萩原尊禮

筑波山腹にある地震研究所支所に於て昭和2年以來約4年に亘つて行はれたシリカ傾斜計に依る土地傾斜變化の觀測結果は井上理學士に依つて屢々報告せられた． 此の觀測は自然岩（花崗岩）の一部を切取つて其の上に建てられた抗火石造建物の內部に於て行はれたものである． 從つて氣溫變化の影響を免れ難く，傾斜の日變化の量は1秒角にも達し，永久變化は年數秒角乃至十數秒角にも達した．

其後，氣溫變化の直接間接の影響から免れるため同支所裏手の急斜面に深さ20米餘の橫坑を穿ち其の最奧に觀測室を設けることを試みた． 橫坑は花崗岩の風化部分を掘進み，餘り風化の進んで居ない部分に行き當つた所に觀測室を設けたのである． 觀測室の溫度變化を防ぐため橫坑の數箇所に扉を仕切り外部との空氣の流通を遮斷した． 觀測室の1日中の溫度變化は極めて少く0·01°C程度と思はれる． 年變化は約0·3°Cである． 傾斜觀測は昭和10年10月より開始された． 又昭和11年11月より比較のため橫坑の入口に近い場所にも傾斜計を設置し親測を續行して居る． 假に橫坑の奧の觀測室をA，入口に近い觀測室をBと名付ける．

A觀測室に於ては傾斜日變化は0·01″程度であるが，B觀測室に於ては0·05″程度に達する． 年變化及び永久變化もB觀測室の方がA觀測室に比較して遙かに大い． 卽ち地表近い程日變化年變化のみならず永久變化の量も大である． 然も量のみならず其の傾斜方向もAとBとは一般に共通では無い． 斯樣に傾斜變化が僅か20餘米を距てた兩觀測室に於て全く異つた形態を示すと云ふことは，此の變化が極めて局部的のものであつて廣範圍に亘つて起つた變化では無いことを示すことになる． 然し乍ら我々の知らんとする土地傾斜變化は斯樣な局部的變化ではなく，地球物理學的に重要性のあるところの，より廣範圍に亘つて一樣に現るべき變化である．

斯樣な比較觀測は從來行はれて居ないが，今回の樣な現象が若し他の何處に於ても起ると考へたなら單に1箇所の觀測のみを以てして地殼の傾斜と云ふが如き Macroscopic のものを代表させることは出來なくなるであらう． 勿論今回の觀測のみを以て斯樣な事實を斷定することは出來ないが，將來充分に吟味されて然るべき問題と思はれる． 本文は事實を報告して一つの問題を提出するに止まり其の解決は今後の研究を待つものである．

30. Explosive Activities of Volcano Asama and Tiltings of the Earth's Surface.

By Takeshi MINAKAMI.

Earthquake Research Institute.

(Read March 15, 1938—Received March 22, 1938)

1. Introduction.

It is well known that in some of the world's volcanoes, tiltings of the ground near them constitute one of the most general and remarkable of volcanic phenomena. In observatories on these volcanoes, changes in the inclination of the earth's surface are measured with numerous types of horizontal pendulums. The Hawaiian Volcano Observatory(1) makes use of the two components of a Bosch-Omori seismograph for the purpose, while the Aso Volcano Observatory,(2) uses a horizontal pendulum apparatus of Rebeur's type. At our Asama Volcano Observatory,(3) tiltings of the ground are recorded optically by means of a pair of Ishimoto clinographs constructed of fused silica, which is scaresly affected by changes in air temperature.

This paper summarizes the remarkable changes in tilts observed during the period from January, 1934, to December, 1937.

2. Tiltings during Inactive and Active Periods of the Volcano.

It is resonable to expect from the results of precise levellings that have been done in certain volcanic regions that tilts of the ground near an active volcano, such as Asama, even during the peaceful stage of the volcano, will amount as a rule to a much larger quantity compared with tilts in other regions, whence it follows that a comparison of the tilts of a volcano during its active and quiescent stages ought to be of help in elucidating certain volcanic phenomena and in understanding of the structure of the volcano. Although the year 1934 was a peaceful one for Asama, the year 1935, 1936, and 1937 were those of violent explosion.

---

1) T. A. JAGGAR and R. H. FINCH, *Bull. Seis. Soc. Amer.* **19** (1929), 38.

2) K. SASSA, *Mem. Coll. Sci. Kyoto Imp. Uni.*, **19** (1936), 11.

3) R. TAKAHASI and T. MINAKAMI, *Bull. Earthq. Res. Inst.*, **15** (1937), 463.

Roughly speaking, the cycle of Asama's activities seems to be about five or six years.

The tilt curves in Fig. 1. of the two components, E–W and S–N, in 1934, the calm periods of the volcano, indicate that the seasonal changes in tilts during the winter season from October to April have a range of about four seconds of arc, their periods being less than seven days. The seasonal variations in the summer season the period from May to September are distinctly small compared with the former, namely, only one second in maximum amplitude and three or five days in their periods. The daily variation in the tilting moreover is less than one second throughout the year. Although there is practically no correlation between tilt and air temperature, either daily or seasonally, it is probable that the seasonal variations in the winter are due to the effects of the earth's surface being frozen.

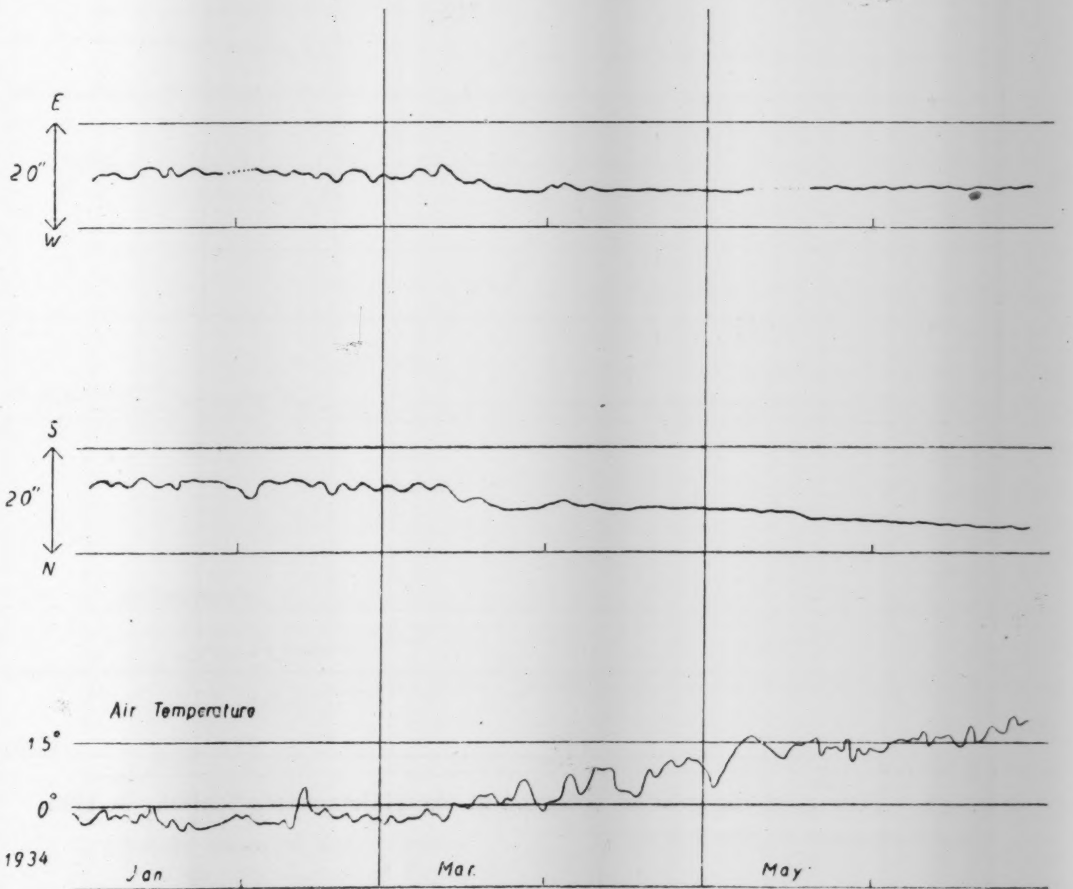

Fig. 1 a. Tilting of the ground observed at the Nakanosawa Station, in 1934. (Inactive stage of the volcano.)
(The direction of tilt-curves is the one of depression of the ground.)

The present activities, which began with the violent explosion on April 20, 1935, and ended with a still more violent one on April 16, 1937, which latter was the largest scale explosion since 1920, comprise about three hundred explosions of various degrees of intensity.

The ground tilts during these activities of the volcano in 1935, 1936, and 1937 are indicated by graphs in Fig. 2, 3, 4, with the air temperature at noon each day, and the comparatively severe explosions that occured in the intervals.

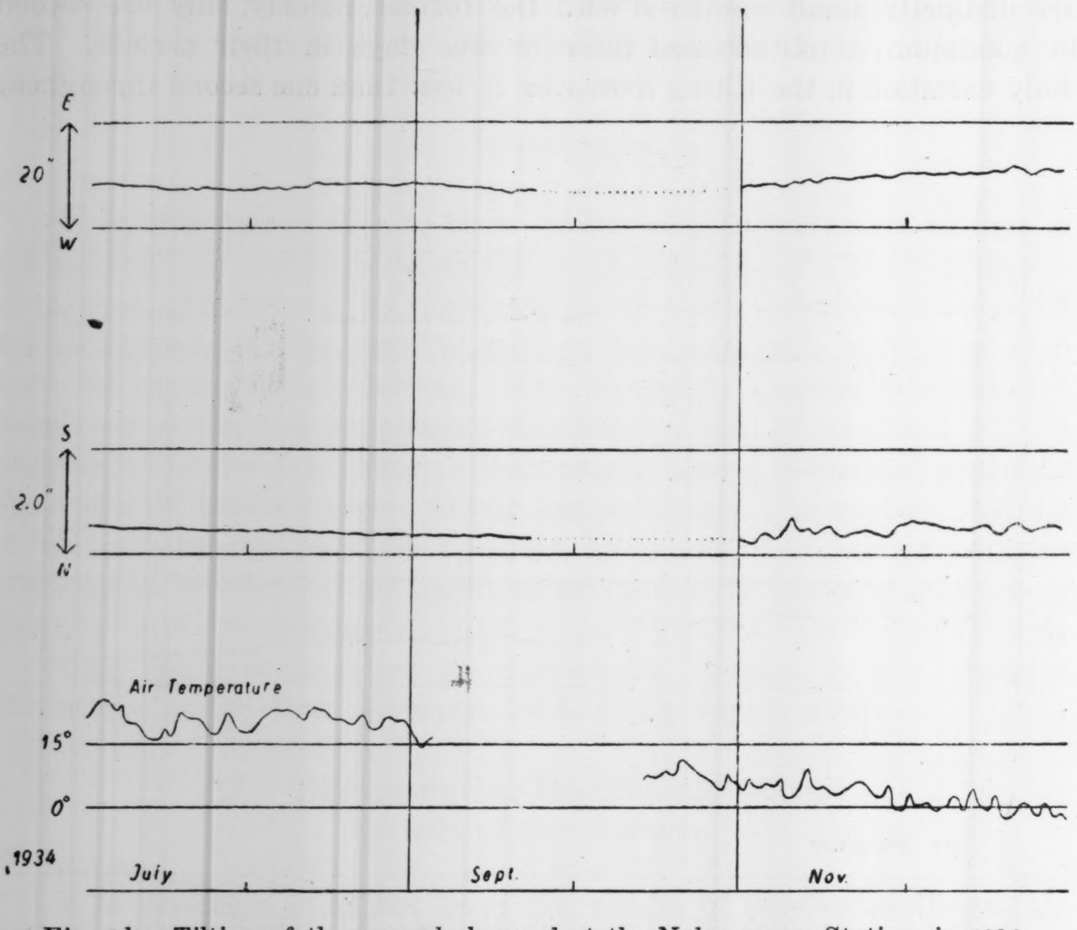

Fig. 1b. Tilting of the ground observed at the Nakanosawa Station, in 1934. (Inactive stage of the volcano.)

The marked tiltings that preceeded the present activities began on February, 15, 1935, and in the middle of April increased to 30 seconds of arc in a NE direction. Strictly speaking, this tilting which began with a SE direction on February 15, amounted to 24 seconds eastward and 23 seconds southward on March 31, after which the two components of tilts changed their directions, and continued to tilt. However, the ground did not show any marked tilting after May. It returned to the original positions prior to occurence of the conspicuous tilts.

The unusual changes in the inclination of the ground which began to appear since the begining of 1936, consisted of to and fro tilts within a range less than ten seconds of arc and with various periods not exceeding twenty days. These tilts have characteristics indicating that they differ distinctly from the previous conspicuous tilts of March and April, 1935; they also differ from the seasonal change during the calm period of 1934. No doubt, they are volcanic origin. From the later part of March to the end of June, 1936, the ground continued gradually to incline with long periods. During August and September of the same year, as

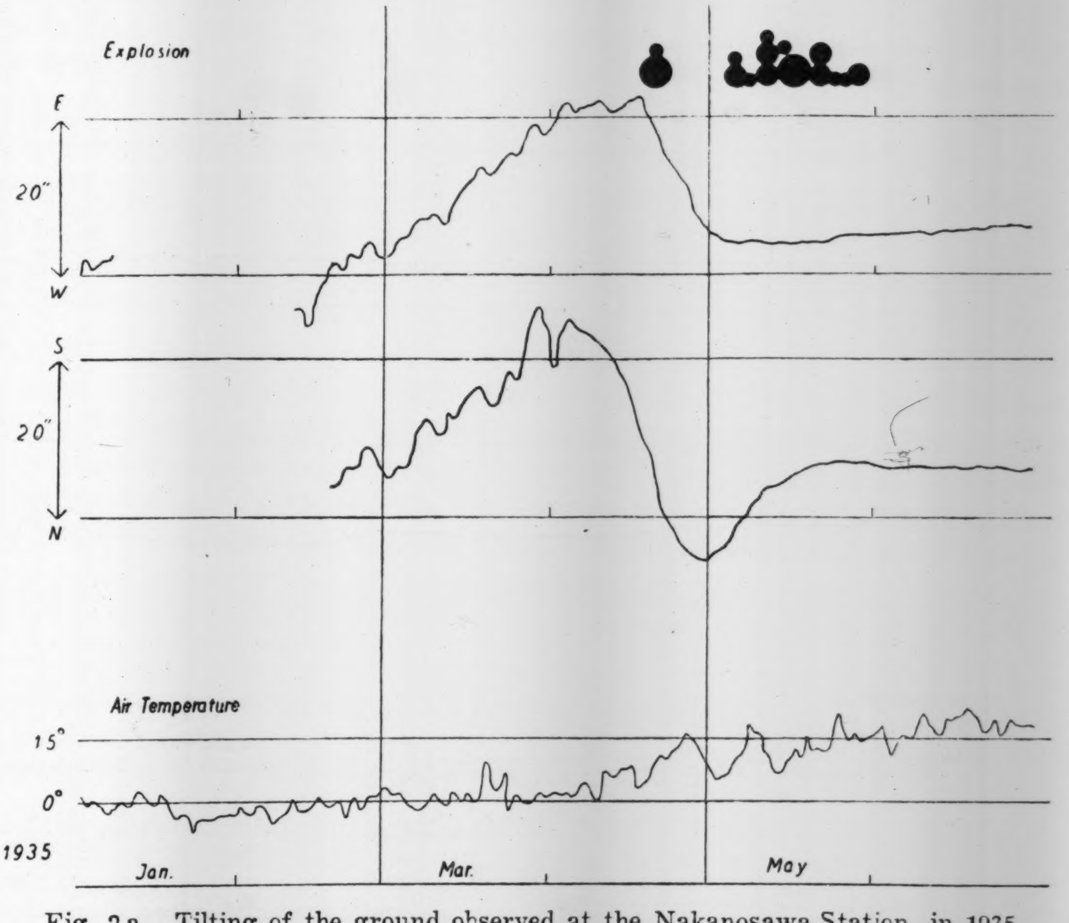

Fig. 2a. Tilting of the ground observed at the Nakanosawa Station, in 1935. (Active stage of the volcano.)

● Explosion of Class A
● ,, ,, B (Defined in the previous paper.*)
• ,, ,, C

---

* T. MINAKAMI, *Bull, Earthq. Res. Inst.*, **13** (1935), 629.

in the interval between June and December, 1935, notwithstanding the active stage, changes in inclination did not appeared. Toward late October 1936, and after, the clinographs recorded tiltings that might have been related more or less to the volcano. Since the begining of 1937, the earth's surface began to incline in a northerly direction until March 26, when it amounted to 23 seconds of arc. Although on that day, the ground changed its direction of tilt, to E–S, it changed again on April 12 to W–N. On April 16, four days after the change in direction of the tilting of the ground, there was a severe explosion of the volcano. At the time of this severe explosion on April, 1937, about 10^6 tons of young lava were ejected from the crater in the form of volcanic bombs and ash. The clinographs both before and after this explosion recorded very striking tilts of the ground with the great speed of a daily rate of 5 seconds, which finally on May, amounted to as much as 42 seconds in the E–W component and 40 seconds in the other component all in the course of

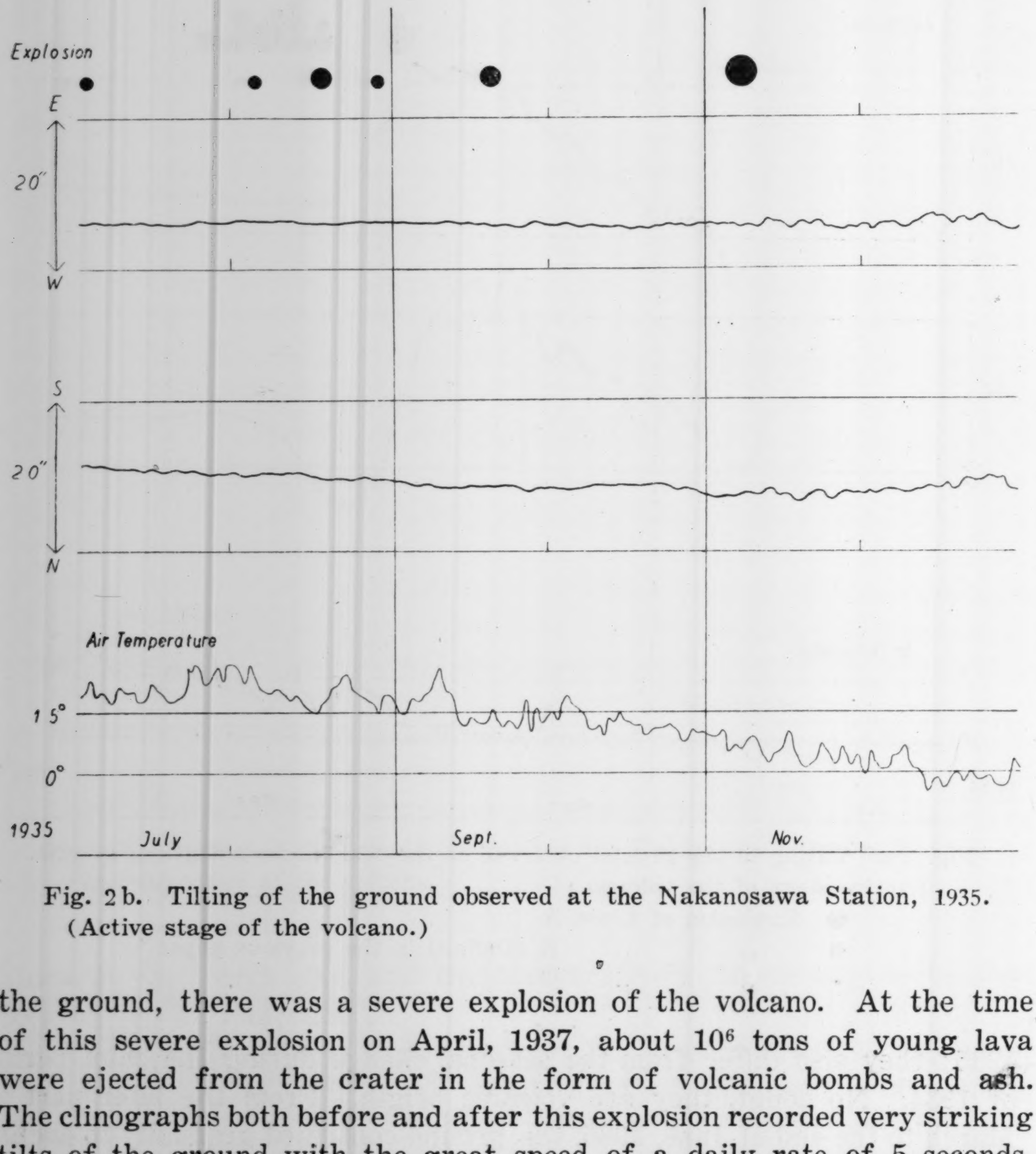

Fig. 2b. Tilting of the ground observed at the Nakanosawa Station, 1935. (Active stage of the volcano.)

three months. It would seem resonable to expect that displacement of lava on such a large scale with consequent marked change in loading might cause serious changes in the inclination of the ground. These remarkable tilts and this severe explosion formed the climax in the present cycle of activities.

In the beginning of 1936, another station of Asama was erected on the great lava flow, of the Tenmei era, the Oni-Osi-Dasi, on the northern slope of the volcano, in which a pair of the same type of clinographs as used in the other station was set up, and measurments of changes in the inclination begun. The tilt curves in 1937 at the new station are shown in Fig. 5. these curves, show tilts in a S–N direction from the beginning of 1937. On February 6, the tilt changed its direction to south, and on March 3, it returned to its former direction. Althuogh on March 18, the accumulation of tilt amounted to 40 seconds, it continued in the same direction without stopping, but inclined at a less rapid rate. On

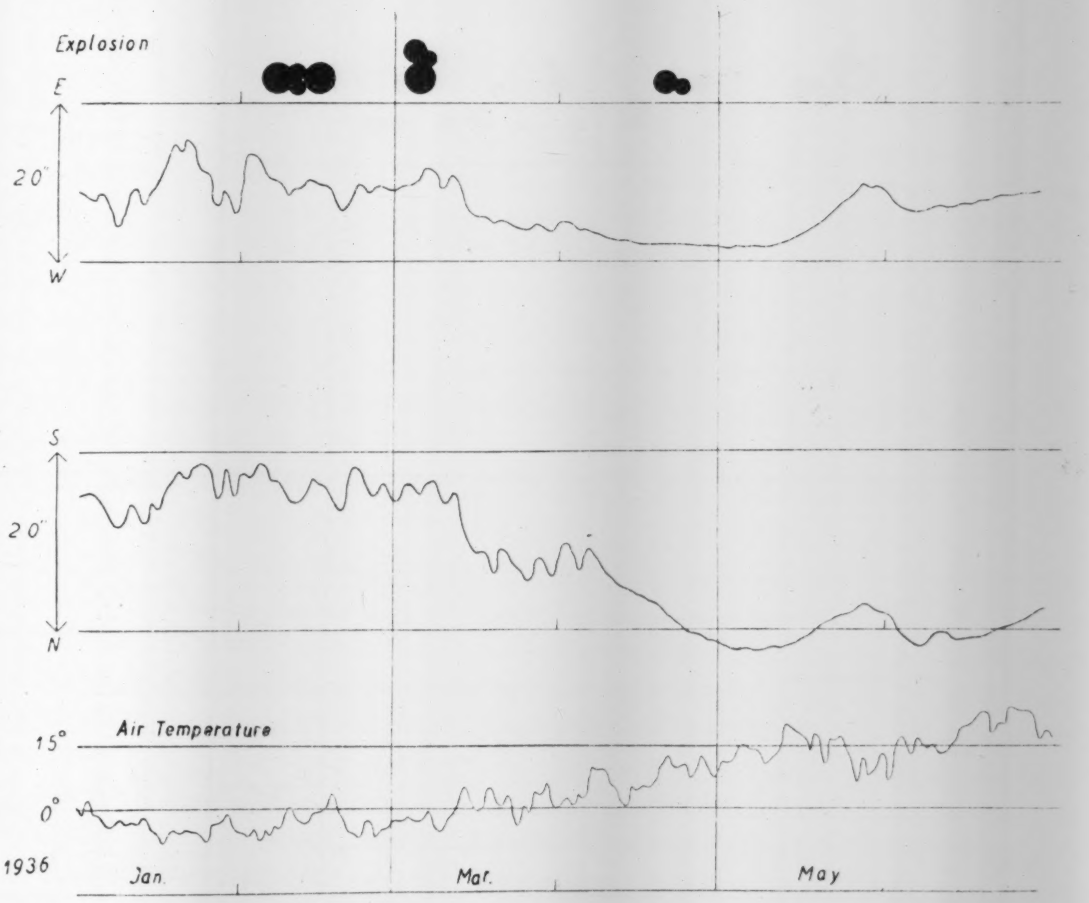

Fig. 3a. Tilting of the ground observed at the Nakanosawa Station, 1936. (Active stage of the volcano.)

the other hand, the clinograph of the other conponent recorded during that time only small changes in tilt. After May, 1937, tilting of the groung ceased at both the Nakanosawa station and the Oni–Osi-Dasi station.

As will be seen from these tilt curves, the remarkable variations during the active stage of the volcano differ entirely from the seasonal and daily changes, and the other changes that occur when the volcano is quiet.

The two tilt curves recorded by the N–S and E–W components at the Nakanosawa station correspond each other not only in the large variations caused by volcanic activity, but also in the small fluctuations of tilt due to seasonal and the other causes.

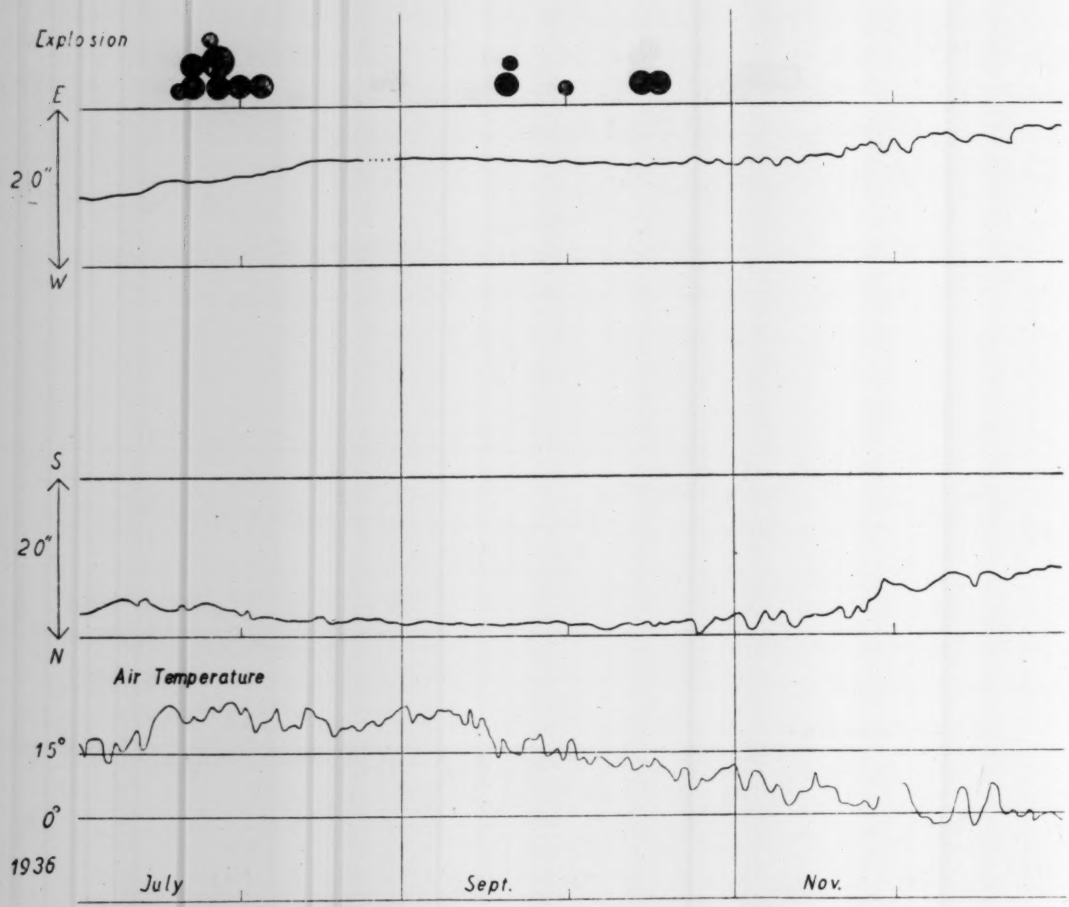

Fig. 3 b. Tilting of the ground observed at the Nakanosawa Station, 1936. (Active stage of the volcano.)

Comparing the tilt curves of March, April, and May, 1937, at the above two stations, it is clear that, although these changes in inclination at the two stations do not agree, not only in the amounts, but also in the direction of tilt, these remarkable tilts at the time of the severe explosion on April 16 were recorded at the two stations at almost the same time, whence it may be resonable to suspect that such volcanic phenomena as the remarkable ground tilts of 1935 and 1937, and the swarms of explosion are geophysically connected and have the same origin. Moreover, the time relation between the occurences of explosions and the remarkable tilts show that the latter are more clearly related to the occurence of explosion swarms, that is, to the beginning of the cycle of activities, than to the occurence of the individual explosion.

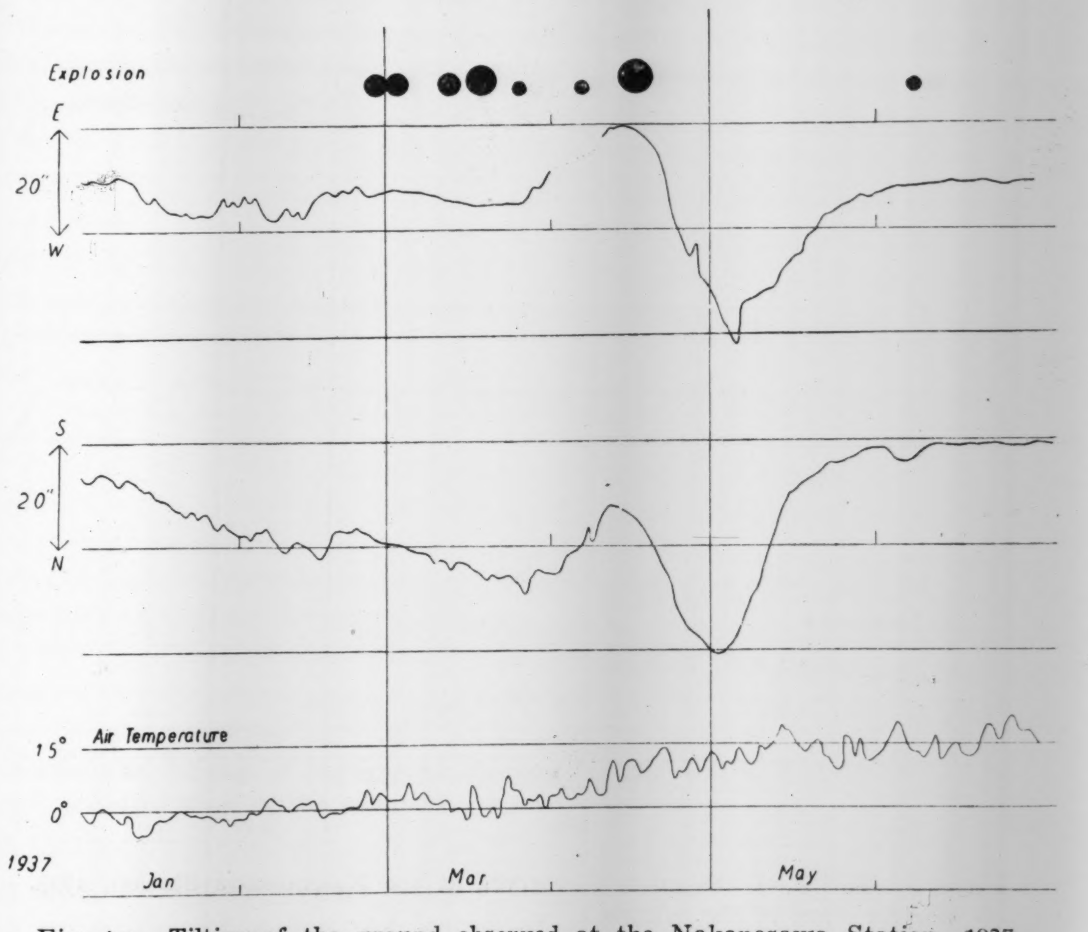

Fig. 4 a. Tilting of the ground observed at the Nakanosawa Station, 1937. (Active stage of the volcano.)

3. Vector Diagram of Tilts.

In Fig. 6, 7, 8, 9 and 10, vector diagrams of the tilts for each year are shown together with those for the violent explosions, in which the directions of the vector coincide with those for the depression of the ground.

The vector diagram for 1934, gives the annual variation in the tilts during the calm stage of the volcano, in which the locus of the tilts is almost an ellipse. On the other hand, the vector diagrams at the Nakanosawa station for 1935, 1936, and 1937, show also an approximate ellipse, of which the longer radius points NW. Although these vector diagrams of tilts include the annual variation, etc., their principal parts are the tilts due to volcanic causes. It may be pointed out that the shapes of these vectors of the annual variation in the calm stage and the remarkable tilts of volcanic origin resemble each other, from which it may be suspected that the two kinds of tilt are affected, primarily, by some force having the property of moving in certain restricted directions more readily than in others. Recently, A. E. Jones⁽⁴⁾ reported that the results of tilt-observations and topographical surveys made near the crater

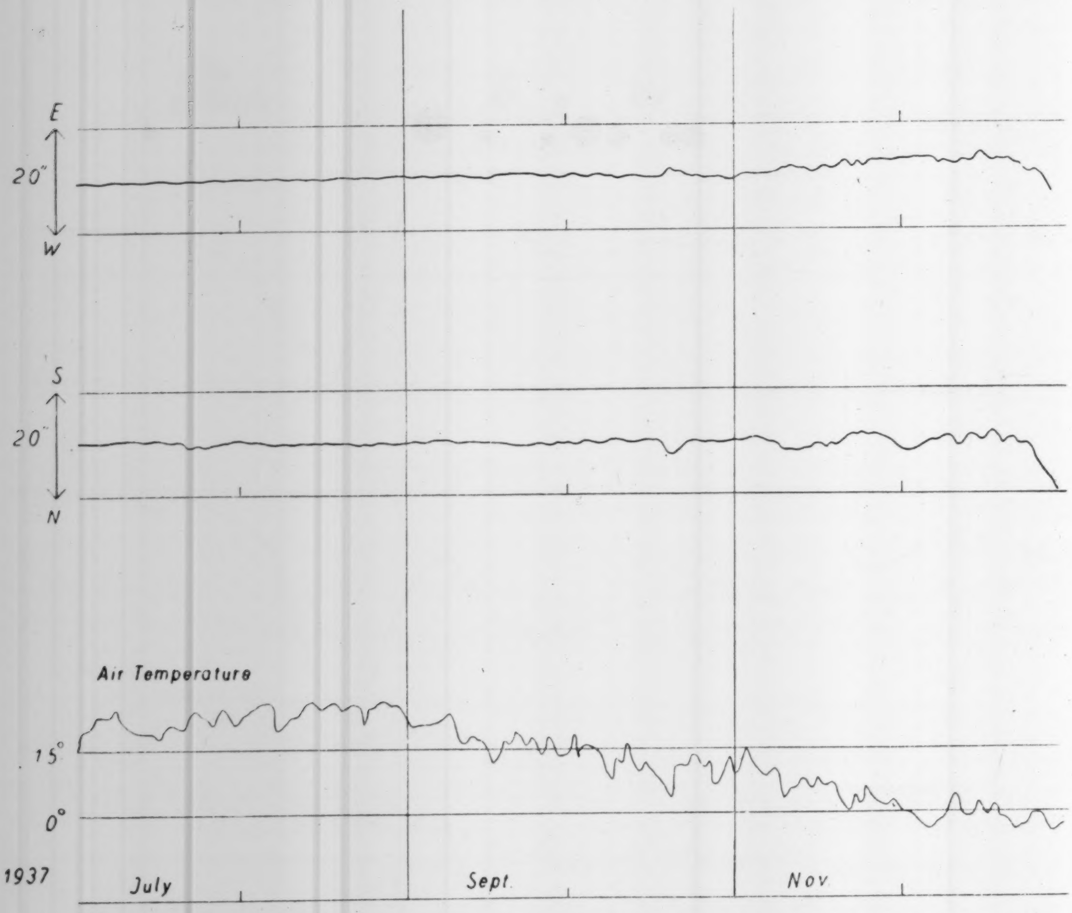

Fig. 4 b. Tilting of the ground observed at the Nakanosawa Station, 1937. (Active stage of the volcano.)

---

4) A. E. JONES, *Bull. Seis. Soc. Amer.*, **27** (1937), 113.

of Volcano Kilauea, are satisfactorily explained by assuming the formation of blocks.

As already mentioned, if we pay attention only to the large changes in the inclinations in the vector diagrams, ignoring the small fluctuations in tilts, the annual change and the tilts of volcanic origin are represented by an ellipse, of which the length of the longer radius is nearly twice that of the shorter. Moreover, the longer radii of these ellipses point in a direction almost N 30° W.

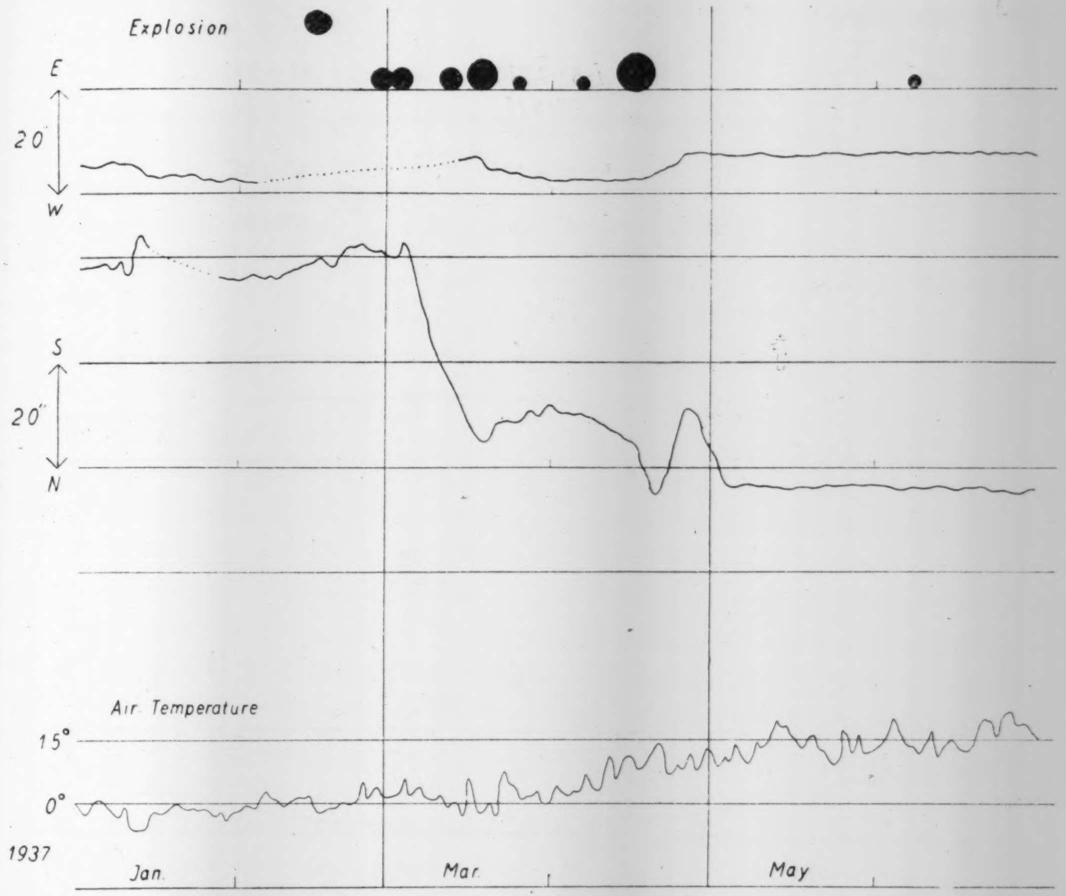

Fig. 5a. Tilting of the ground observed at the Oni-osi-dasi Station, 1937. (Active stage of the volcano.)

	Longer diameter	Shorter diameter	Direction of the longer radius
1934	11″·5	5″·7	31°
1935	32″·0	14″·0	27°
1936	25″·5	13″·0	31°
1937	46″·0	22″·0	37°

4. Secular Variations in Tilt.

In addition to changes in inclination due to the various origins above mentioned, there is the secular variation, as shown in Fig. 11. The secular variation as observed at the Nakanosawa station for the past four years were

1934	8″·7 N	1″·5 E
1935	5″·3 N	2″·3 E
1936	7″·2 N	7″·2 E
1937	3″·5 N	4″·1 W
Total	24″·7 N	6″·9 E

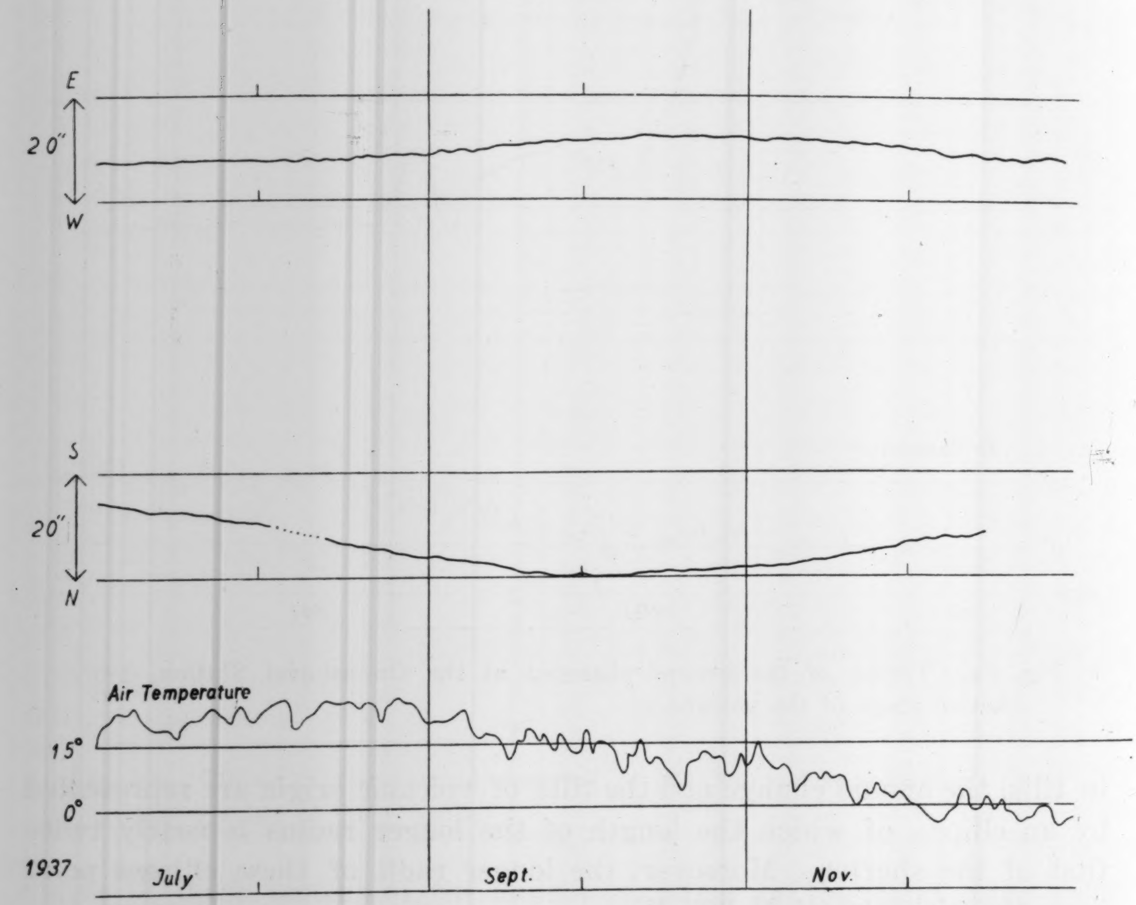

Fig. 5 b. Tilting of the ground observed at the Oni-osi-dasi Station, in 1937. (Active stage of the volcano.)

These secular variation have been continuing to incline to the north with a mean annual rate of about 6 seconds and to the east with a rate of about 1·5 seconds, although these annual rates are small compared with the accumulations of tilts during the active stages.

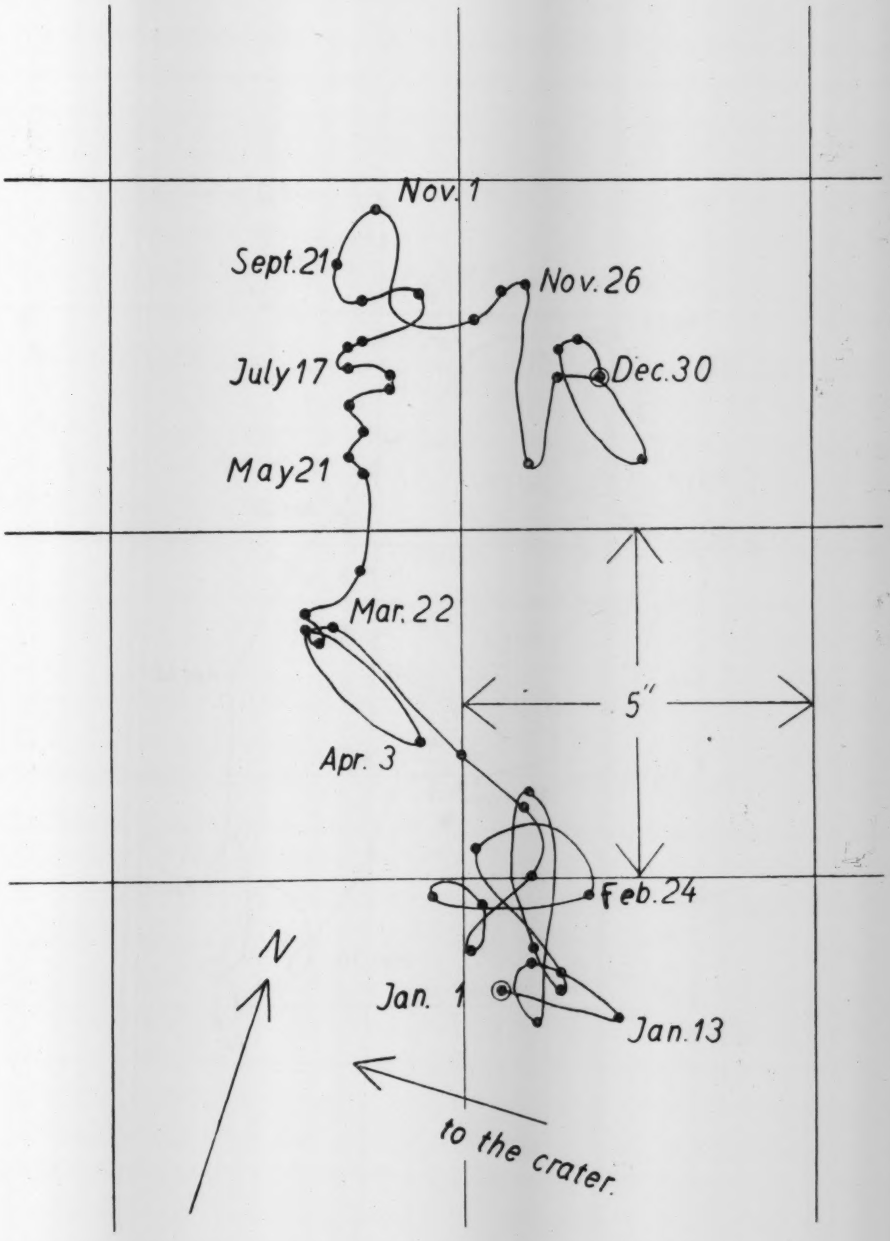

Fig. 6. Vector Diagram of Tilt during 1934. (at Nakanosawa.)
(The direction of vector is the one of depression of the ground.)

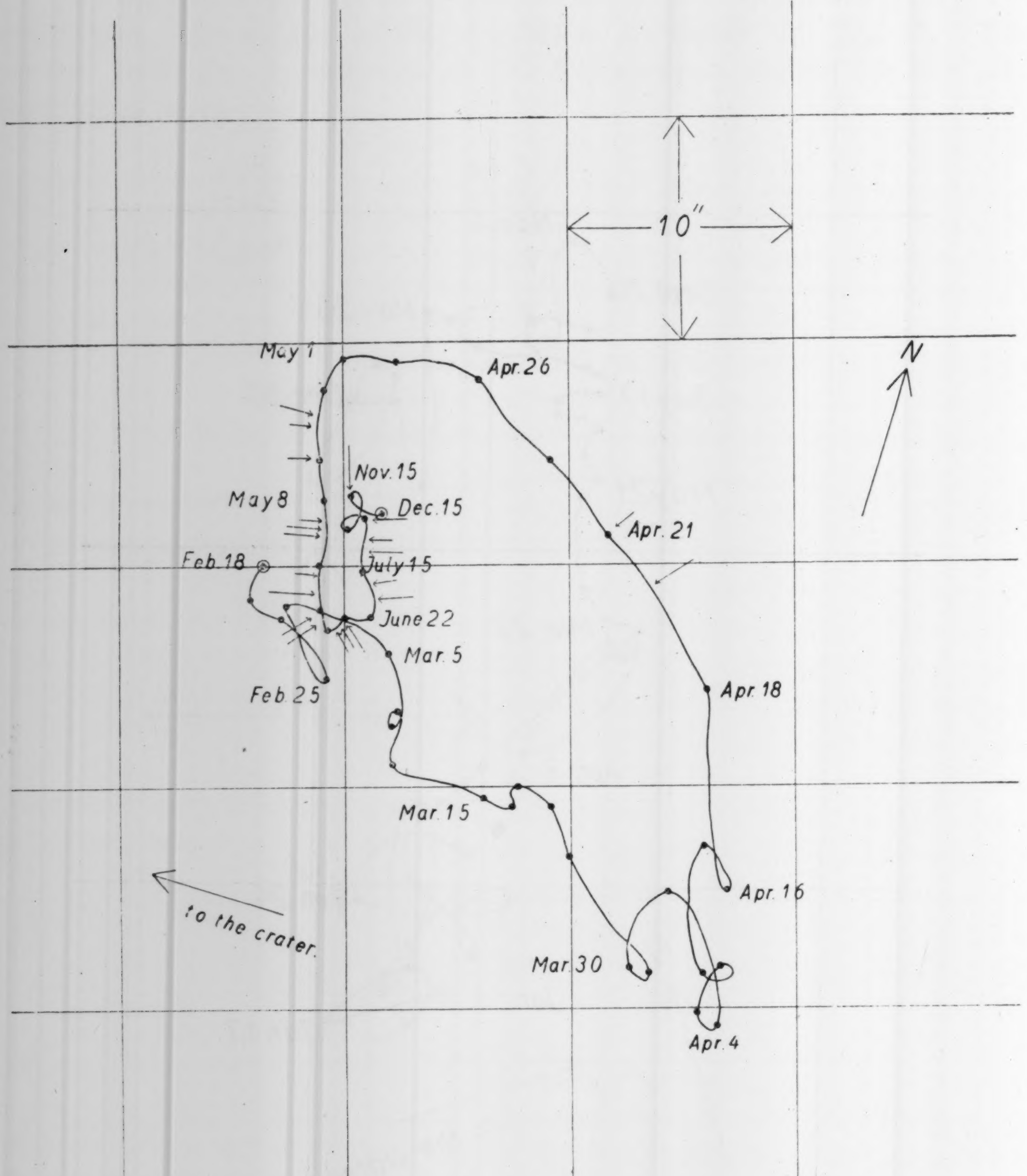

Fig. 7. Vector diagram during 1935. (at Nakanosawa.)

⟶ Explosion of Class A.
→ ,, ,, ,, B.
→ ,, ,, ,, C.
(Defined in the previous paper.)

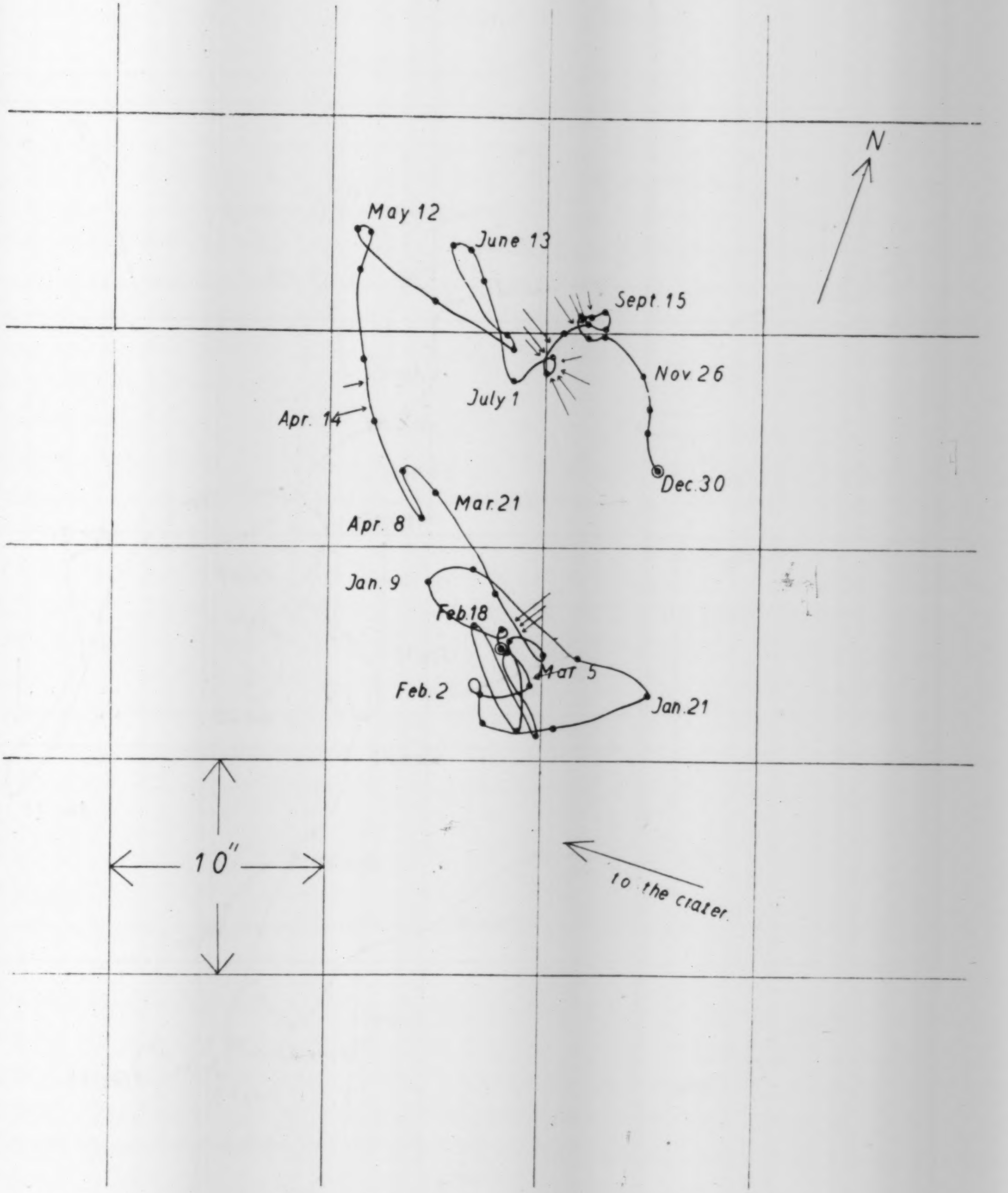

Fig. 8. Vector diagram during 1936. (at Nakanosawa.)

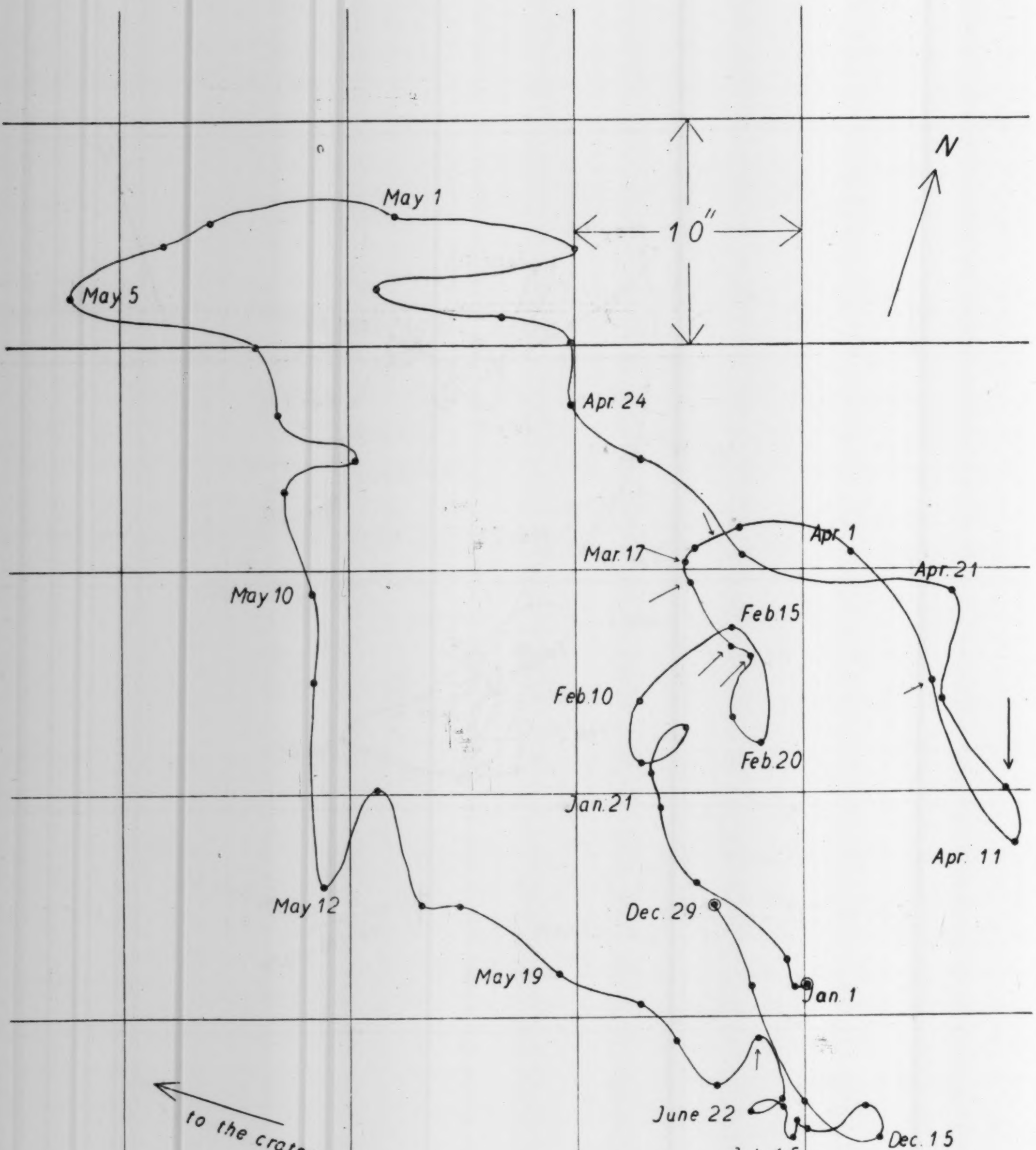

Fig. 9. Vector diagram during 1937. (at Nakanosawa.)

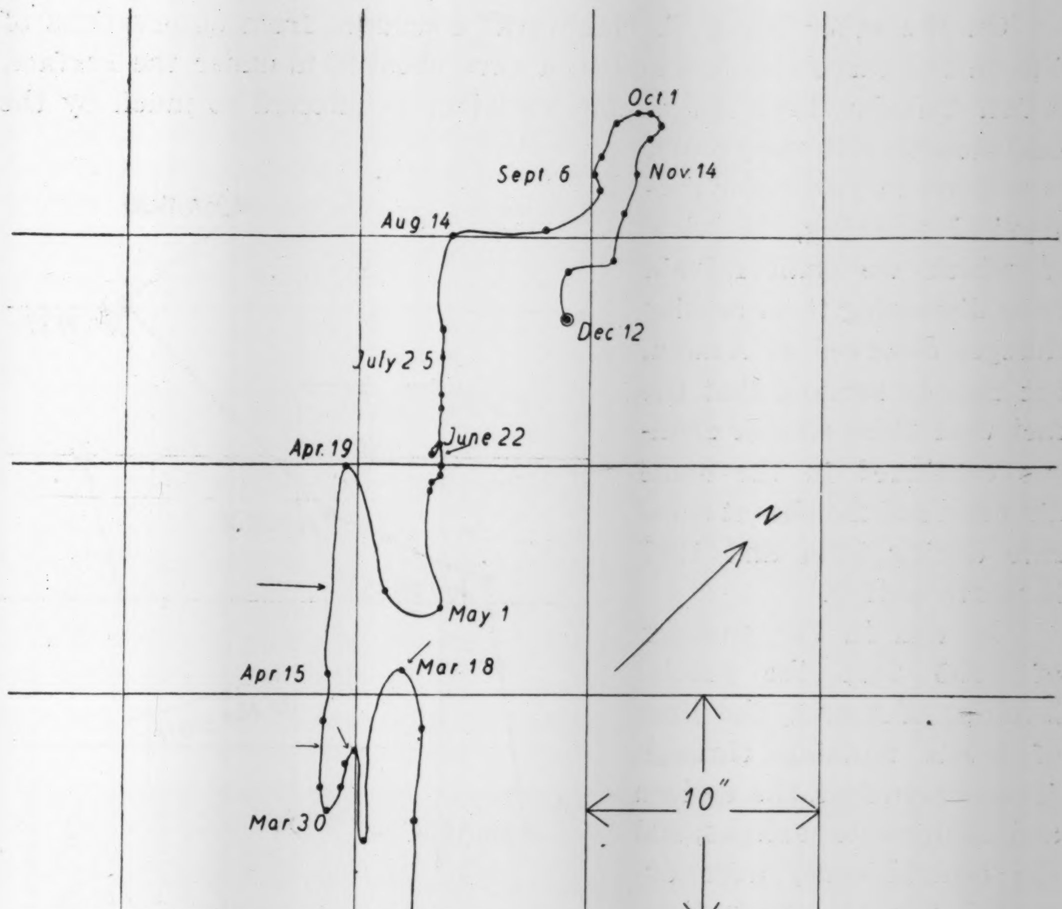

Fig. 10. Vector diagram during 1937. (at Oni-Osi-Dasi.)

On the other hand, T. Hagiwara[5] concludes from observations of tilts on the earth's surface and in a cave about 20 m under the surface, at Mt. Tukuba, that the secular variation is affected so much by the local structure of the ground as to have no particular geophysical meaning, in view of which we shall refrain from discussing these secular changes observed at Asama, but merely remark that the fact that these secular changes continued in the same direction and the almost same rate during 1934 and 1937 is worth noting.

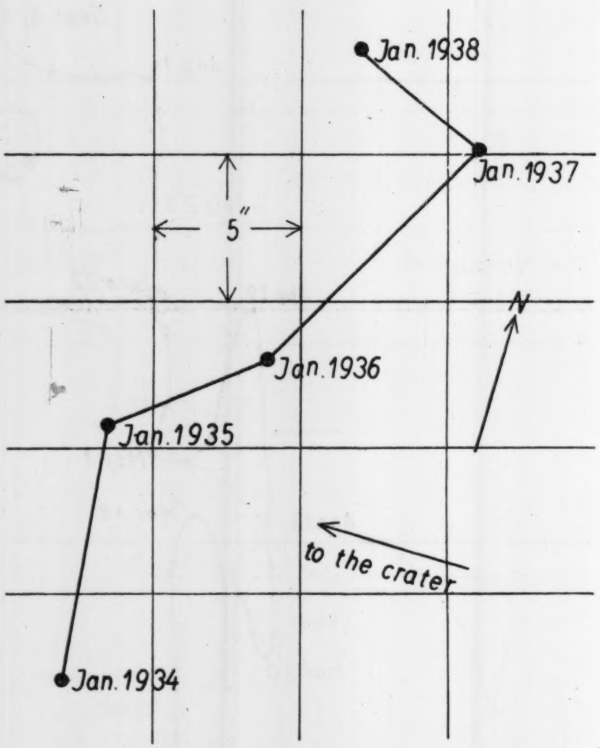

Fig. 11. Secular variation of tilt during 1934 and 1937. (at Nakanosawa.)

It was in the summer of 1935 that the precise levelling of Asama, the lines of levels running through its southern foot, the eastern and southwestern slopes, and the central cone, were executed for the first time. At the same time, the writer[6] made observations of the zenith distance between the bench mark in the grounds of our observatory and the one imbedded in the central cone, the object being to ascertain the relative height changes in the two positions. From these observations, it was made clear that the angle of elevation between the two bench marks diminished 23″·4 ± 3″·5 during the interval between October, 1934, and April 26, 1935. These values however do not agree with the results of tilt-observations made during the same interval. This negative result suggests that the central cone may deform independently of the movements of the block, on which the bench mark at our observatory and the Nakanosawa station are situated. On the other hand, according to the geological survey of Asama by H. Tsuya,[7] the lava flow on which the clinographs are set, does not extend to the central cone, which geological fact supports the view that the deformations of the ground in the two

---

5) T. HAGIWARA, *Bull. Earthq. Res. Inst.*, **16** (1938), .
6) T. MINAKAMI, *Bull. Earthq. Res. Inst.*, **14** (1936), 222.
7) H. TSUYA, *Bull. Earthq. Res. Inst.*, **11** (1933), 575.

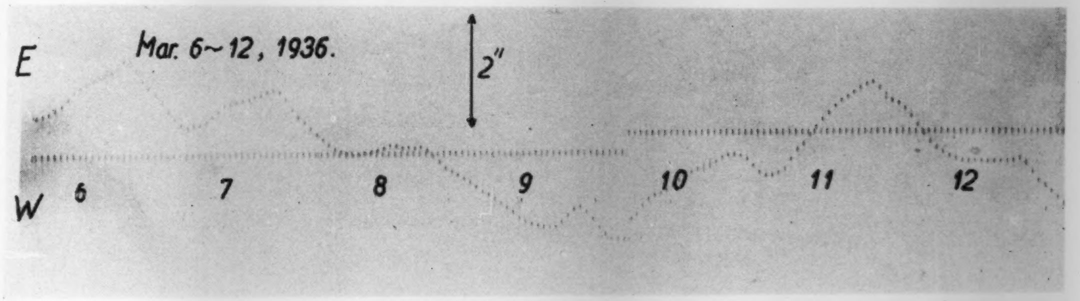

(12)

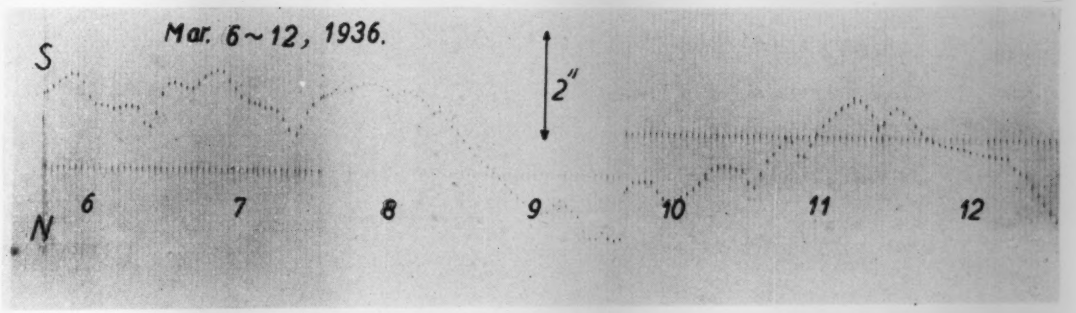

(13)

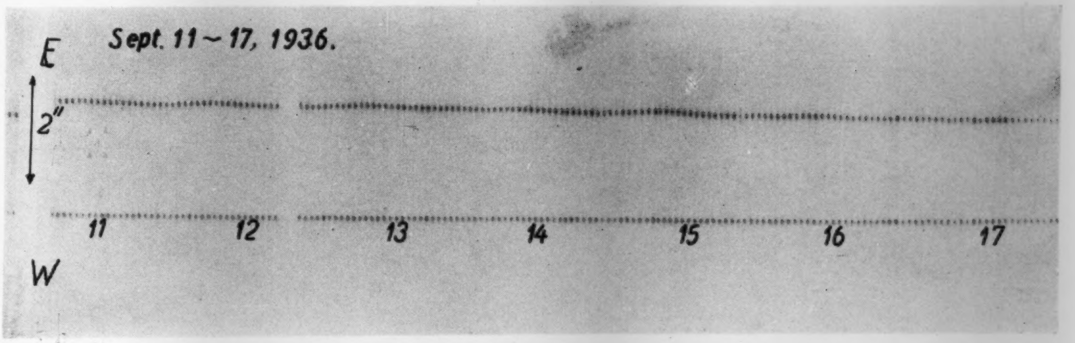

(14)

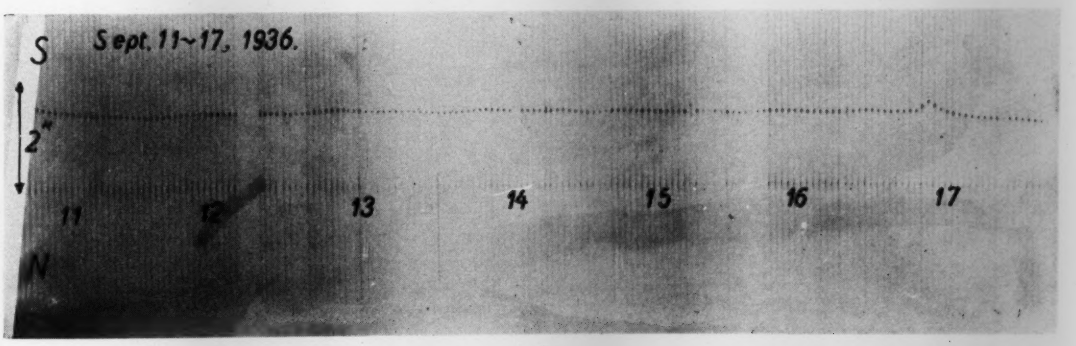

(15)

Fig. 12, 13, 14, 15. Records of Clinographs at the Nakanosawa Station.

（震研彙報　第十六號　圖版　水上）

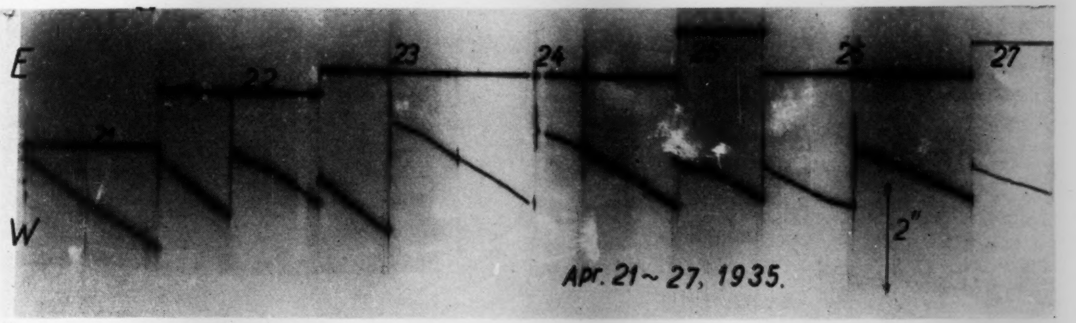

(16)

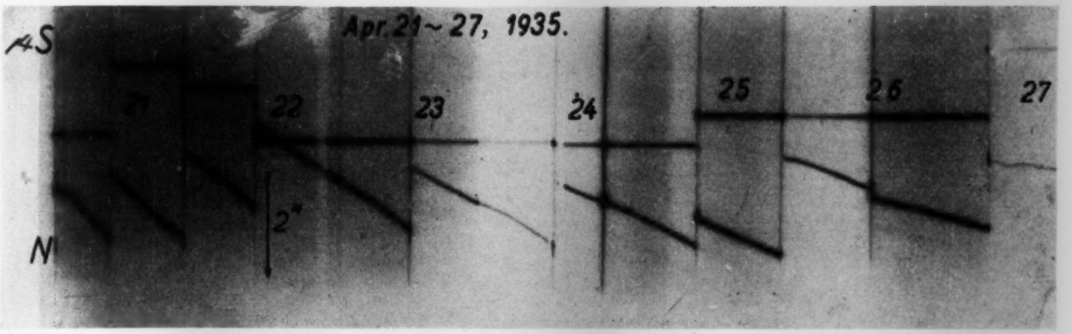

(17)

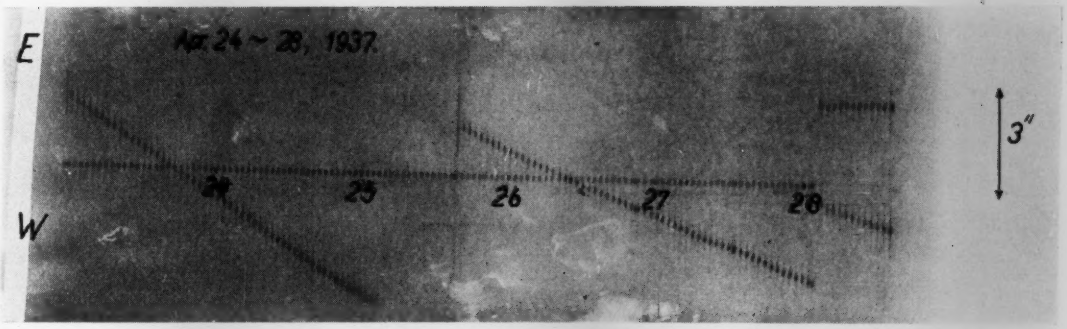

(18)

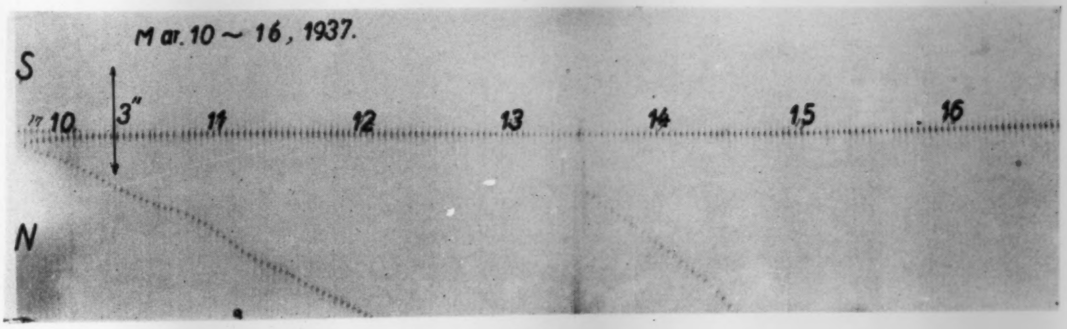

(19)

Fig. 16, 17, 18. Records of Clinographs at the Nakanosawa Station.
Fig. 19. Records of Clinographs at the Oni-osi-dasi Station.

（震研彙報 第十六號 圖版 水上）

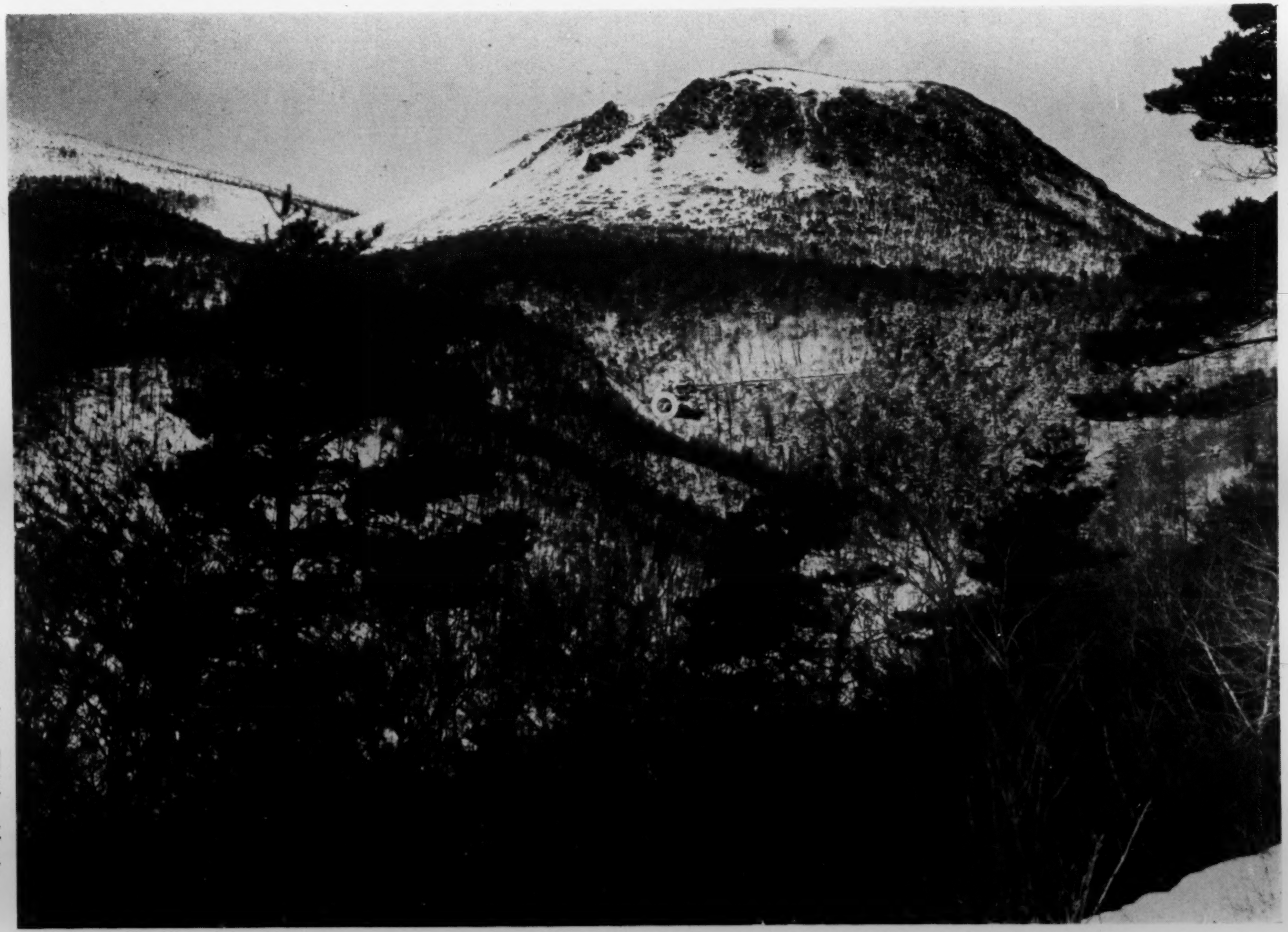

Fig. 20. The Nakanosawa Station and Parasitic Volcano Ko-Aioma, (4 km east from the Crater.) ○ clinographs setting.

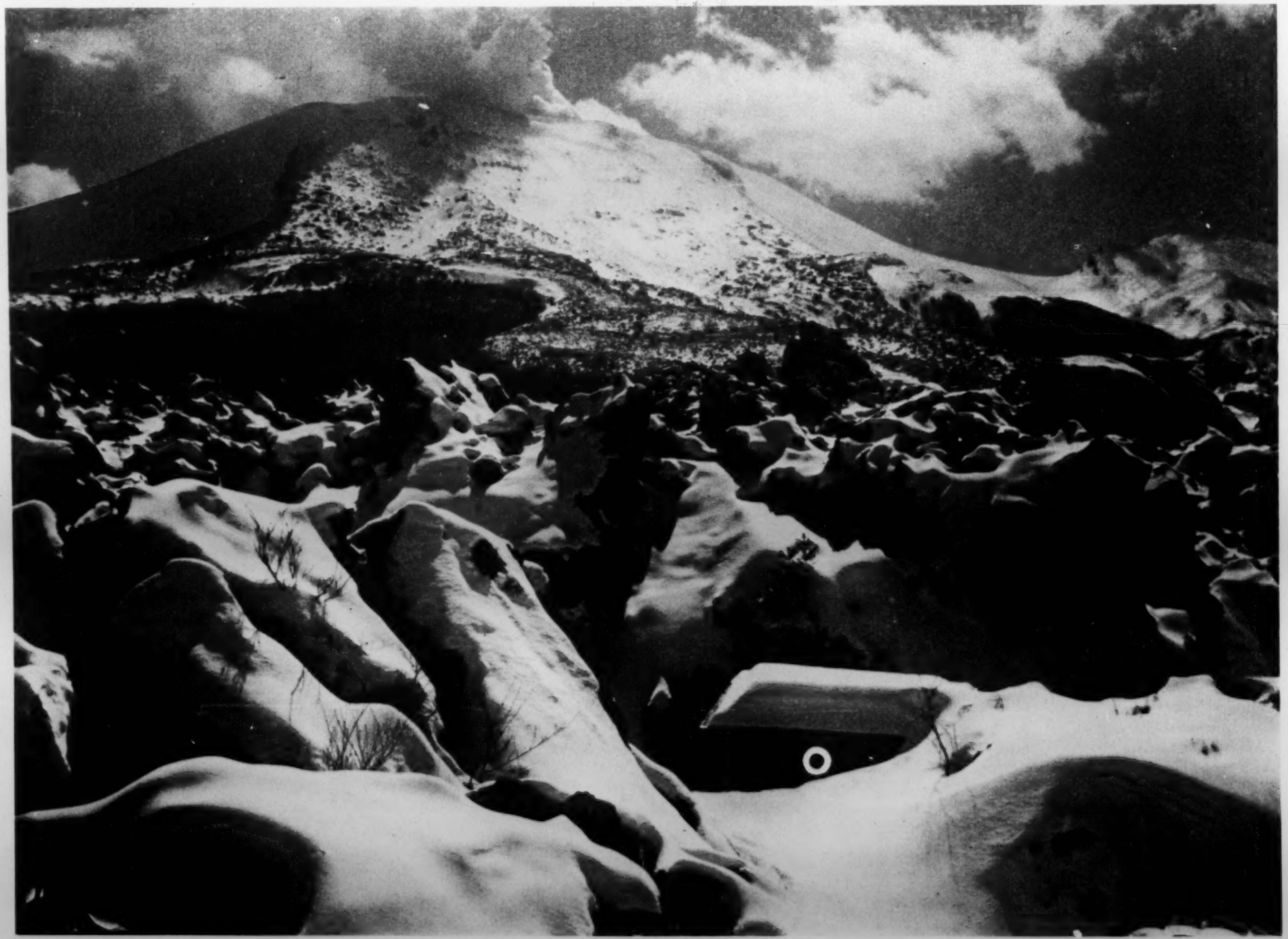

（震研彙報 第十六號 圖版 水上）

Fig. 21. The Oni-osi-dasi Station and the Lava Flow of the Temmei era (4 km north from the Crater.) ○ clinographs setting.

positions of the volcano just mentioned are independent of each other.

5. Conclusion.

The results of tilt-observations made during the period from 1934 to 1937, that is, during the active and inactive stages of Volcano Asama are reported in this paper. The marked changes in the inclination of the ground during the active stage of the volcano clearly differ from the seasonal and other variations that occur during the calm stages. Tilting on a large scale began about two months preceding the explosive activity which began on April 20, 1935, suggesting the possibility of forecasting coming activities.

In conclusion, the writer wishes to express his cordial thanks to Professor M. Ishimoto for his encouragement in the course of this study. He also acknowledges his great indebtedness to the Foundation for the Promotion of Scientific and Industrial Research of Japan, with whose grant this study was made possible.

---

30. 淺間火山の活動と地表傾斜變化

地震研究所　水上　武

昭和9年1月より昭和12年12月に至る4ケ年の淺間火山に於ける傾斜觀測の結果を綜合して報告せるものである。

昭和9年の火山の平穩期と10，11，12年に亘る活動期との傾斜變化とを比較し，著しい相異の存在する事を示し，特に昭和10年2月より4月に亘つて現はれた傾斜及び昭和12年3月から5月に現はれたものは夫々30″及び40″に達し，何れも火山活動に關係して現はれた山體の傾斜變化である。此等の異常傾斜は北西方向が沈降し，略隋圓を畫いて再び元の位置に復する方向に起つてゐるが，その傾斜運動の形狀は平穩期に於ける年變化のそれと甚だ類似して居る。

又鬼押出に於ける昭和12年2月より5月に亘る傾斜變化は約60″に達して居る。この傾斜と中の澤に於ける觀測とを比較するに，量に於いてのみならず，その方向が必ずしも一致して居ないが，出現の時期は略一致して居る。

一方，昭和9年7月より10月に亘る三角術的水準測量と昭和10年5月に於けるものと比較から得た相對的水準變化と傾斜觀測結果とは一致して居ない。是等の事實からも傾斜變化及び地形變動を獨立に行ひ得る幾つかの小地塊より火山が構成されて居る事を示すものと考へられる。

永年變化は過去４ケ年間年平均約６″の割で北西へ向ふ傾斜を示して居る。この變化は火山活動に際して現れた異常傾斜に比して小いものであり，且萩原理學士が指摘せる如き局部的のものを含むと考へられる。然し是等の永年變化がどの程度の地域が共通の傾斜を示して居るかは，精密水準測量の再測により明かとなる可能性がある。

最後に，淺間火山に於ける傾斜變化の研究は，日本學術振興會の補助に負ふ所多く，こゝに厚く感謝の意を表す。又冬期間の困難な觀測を繼續するに當り助力された，内堀，河合，及び内嶋の三氏に感謝の意を表し度い。

31. *Relation between the Normal-Tangential Viscosity Ratio and Poisson's Elasticity Ratio in Certain Soils.*

By Kumizi IIDA,

Earthquake Research Institute.

(Read March 15, 1938.—Received March 20, 1938.)

1. Introduction.

In our previous papers[1] we discussed the elastic properties of certain kinds of soil exhibited by subjecting them to vibration. As already explained, the principal object of our experiments was to impart various vibration frequencies to the foot of the soil specimen where it touches the vibrating plate, and thus ascertain the fundamental resonance frequency, after which its elastic constants were computed. In order to determine the velocity of elastic waves in the soil specimen, a diagram was constructed, in which the fundamental resonance periods obtained from our experiments were plotted as ordinate, and the various heights of the same soil specimen as abscissa. Seeing that the curves showing these relations do not pass through the coordinate origin, we concluded that these results are due to the solid viscosity of the soil.

We therefore formulated equations of motion for the longitudinal and the torsional wave in the soil column with the assumption that the stresses in the soil specimen could be regarded as having been derived from the ordinary elastic stresses due to Hooke's law plus the viscous stresses, namely,

$$\rho\frac{\partial^2 w}{\partial t^2}=E\frac{\partial^2 w}{\partial z^2}+\gamma_l\frac{\partial^3 w}{\partial z^2\partial t}, \tag{1}$$

$$\rho\frac{\partial^2 u}{\partial t^2}=\mu\frac{\partial^2 u}{\partial z^2}+\gamma_t\frac{\partial^3 u}{\partial z^2\partial t}, \tag{2}$$

where w is the displacement in the direction of z, u the displacement in the direction of x (Fig. 1), ρ the density, t the time; E, μ Young's modulus and modulus of rigidity respectively, and γ_l, γ_t the normal and tan-

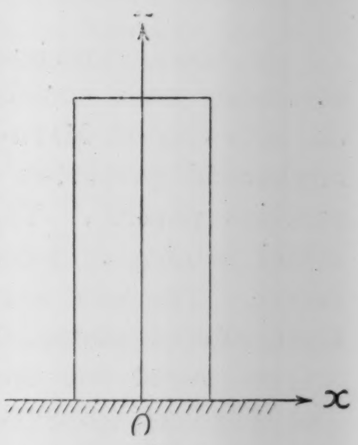

Fig. 1.

---

[1] M. ISHIMOTO and K. IIDA, "Determination of Elastic Constants of Soils by means of Vibration Methods," *Bull. Earthq. Res. Inst.*, **14** (1936), 632; **15** (1937), 67.

gential solid viscosity coefficients respectively.

As already shown in our previous papers[2], the longitudinal and the torsional fundamental resonance periods, T_l and T_t, are given by

$$T_l = \frac{4h}{\sqrt{\dfrac{E}{\rho} - \dfrac{\pi^2 \gamma_l^2}{16\rho^2 h^2}}}, \tag{3}$$

$$T_t = \frac{4h}{\sqrt{\dfrac{\mu}{\rho} - \dfrac{\pi^2 \gamma_t^2}{16\rho^2 h^2}}}. \tag{4}$$

With these equations it is possible to determine the elastic constants E, μ and the solid viscosity coefficients γ_l, γ_t. Although we have already pointed out that the ratio of γ_l to γ_t thus obtained seems to diminish with increase in water content, we did not prove the accuracy of these quantities, so that it was found desirable to make further experiments in order to ascertain these relations. On the other hand, it is yet unknown whether or not the normal-tangential viscosity ratio, namely, γ_l/γ_t, might correspond to Poisson's elasticity ratio.

The objects of our experiments were to ascertain the nature of soil with reference to its elastic and viscous properties, for which purpose we studied not only the relations between the ratio γ_l to γ_t and the water content of the soil, but also the relations of the ratio γ_l to γ_t and Poisson's elasticity ratio.

2. Soil Specimens.

In these experiments we used the same kinds of soil as those previously used, namely, the loam at Hongô (Imperial University) and the silty-clay at Maru-no-uti in Tôkyô. The original conditions and the mechanical properties of these soils are similar to those described in previous papers[3]. The forms of the soil specimens were cylinders of initial heights of from 20 to 30 cm, with a diameter of about 5 cm as before. The soils were tested in their natural state, and sometimes in their altered state. The water contents were altered by leaving the original moist soil specimen to dry under ordinary room temperature. The physical properties in question were studied for the foregoing variety of conditions.

---

[2] M. ISHIMOTO and K. IIDA, *loc. cit.*

[3] *loc. cit.*

3. Experiments.

In the present experiments, both apparatuses and methods were the same as those employed previously. When a soil specimen becomes hard through loss of its water, it is difficult to observe the resonance frequencies of the higher orders within the limit of our scope of experiment, because of the increase in fundamental resonance frequency, for which reason it was not possible for us to investigate the properties of each soil for water contents other than those coming within the scope of this paper. The diagram showing the relations between the fundamental resonance period T_l or T_t and the height h of the soil specimens are shown in Figs. 2 and 3, in which the period T_l or T_t is taken as ordinate and the height h as abscissa.

In the present case, we determined both elastic constants E, μ, and solid viscosity coefficients γ_l, γ_t by means of the method of least squares with the aid of equations (3) and (4), into which we put the experimental values, such as T_l, T_t, corresponding to each height h. We then computed the longitudinal and the transverse wave-velocities V_l, V_t in the soil specimen by means of the following relations: $V_l=\sqrt{\dfrac{E}{\rho}}$, $V_t=\sqrt{\dfrac{\mu}{\rho}}$. All the values thus obtained are shown in Tables I, II, from which it will be seen that the probable errors in these values range from about 2 per cent to 20 per cent. The resonance periods, however, were determined with an accuracy of from 1 to 2 per cent.

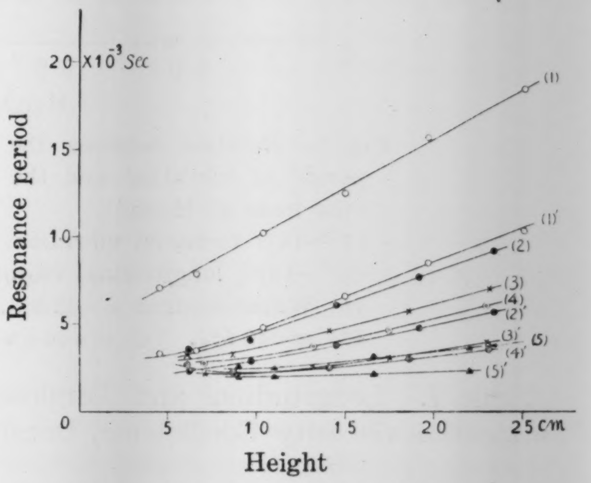

Fig. 2. Relation between the fundamental resonance period of vibration and the height of soil specimen (the silty-clay at Maru-no-uti).

(1)∼(5): torsional vibration.
(1)'∼(5)': longitudinal vibration.
(1) Water content $w=48{\cdot}5\%$.
(2) $w=42{\cdot}3\%$. (3) $w=39{\cdot}5\%$.
(4) $w=37{\cdot}4\%$. (5) $w=31{\cdot}5\%$.

It is possible to get from Tables I, II several diagrams representing the relations between the elastic constants and the solid viscosity coefficients and the water contents.

These diagrams are shown in Figs. 4∼8, in which the abscissa al-

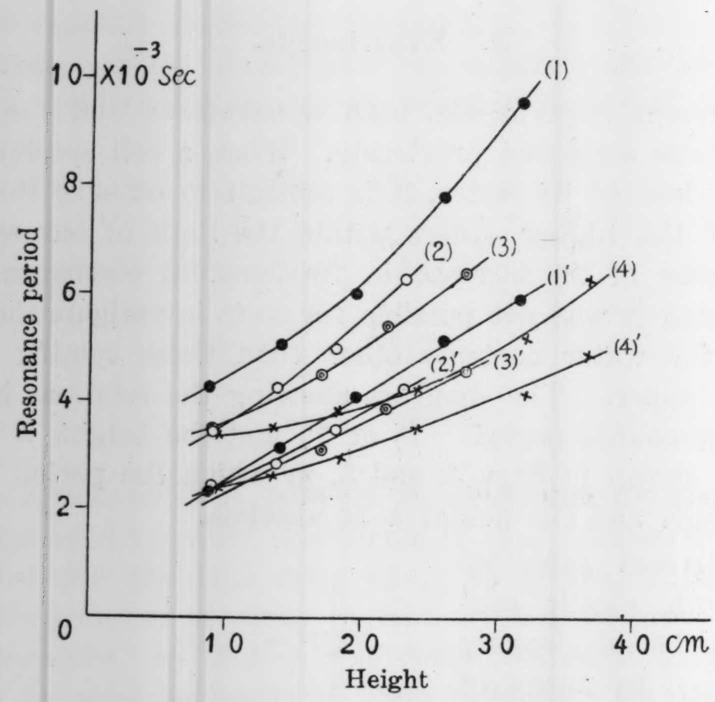

Fig. 3. Relation between the fundamental resonance period of vibration and the height of soil specimen (the loam at Hongô).
(1)∼(4): torsional vibration.
(1)′∼(4)′: longitudinal vibration.
(1) Water content $w=48{\cdot}0\%$. (2) $w=46{\cdot}2\%$.
(3) $w=43{\cdot}6\%$. (4) $w=40{\cdot}0\%$.

Table I. Longitudinal and Torsional Wave-Velocities, Normal and Tangential viscosity Coefficients, Density, and Water Content of Soils.

Kind of soil	No.	Water cont. w (%)	Density ρ	V_l (m/sec)	V_t (m/sec)	γ_l	γ_t	$\frac{V_l}{V_t}$
						$\times 10^5$	$\times 10^5$	
Silty-clay (Maru-no-uti)	1	51·0	1·46	63·6± 4·5	37·2± 3·0	0·359±0·010	0·212±0·009	1·709
	2	48·5	1·50	96·1± 6·1	56·0± 7·6	0·569±0·016	0·398±0·012	1·716
	3	42·3	1·56	167·6±23·1	103·8±22·5	1·576±0·045	0·921±0·044	1·615
	4	39·5	1·63	240·1±13·2	151·5± 8·7	3·182±0·053	1·760±0·035	1·585
	5	37·4	1·56	251·0±21·6	157·1± 8·6	3·065±0·633	1·368±0·025	1·597
	6	31·5	1·59	377·6±33·8	246·7± 6·1	6·600±0·891	2·890±0·325	1·531
	7*	47·9	1·49	34·5± 2·2	20·0± 1·5	0·396±0·015	0·212±0·011	1·729
Loam (Hongô)	1	53·5	1·31	185·3±10·1	110·0± 9·3	1·764±0·180	0·877±0·092	1·684
	2	48·0	1·24	217·0±19·6	134·2±13·6	3·525±0·450	1·481±0·104	1·617
	3	46·2	1·19	233·0± 9·1	149·0±21·0	3·750±0·256	1·585±0·121	1·564
	4	43·6	1·16	247·6± 8·0	162·0± 5·1	4·090±0·088	1·736±0·056	1·528
	5	40·0	1·09	299·8±20·9	198·5±19·5	4·760±0·490	2·155±0·362	1·510

Table II. Elastic Constants, γ_l/γ_t, and E/μ of Soils.

Kind of soil	No.	Young's modulus E (c. g. s.)	Rigidity μ (c. g. s.)	Poisson's ratio σ	λ (c.g.s.)	$\frac{\gamma_l}{\gamma_t}$	$\frac{E}{\mu}$
		$\times 10^8$	$\times 10^8$		$\times 10^8$		
Silty-clay (Maru-no-uti)	1	0·590±0·009	0·202±0·006	0·46±0·04	2·324	1·689±0·085	2·920±0·097
	2	1·385±0·012	0·470±0·015	0·47±0·02	7·369	1·708±0·065	2·944±0·037
	3	4·382±0·046	1·681±0·045	0·30±0·04	2·521	1·713±0·093	2·607±0·074
	4	9·400±0·264	3·741±0·174	0·26±0·06	4·053	1·808±0·047	2·511±0·136
	5	9·826±0·432	3·850±0·017	0·27±0·05	4·520	2·240±0·454	2·550±0·112
	6	22·670±0·676	9·677±0·121	0·17±0·04	4·984	2·280±0·400	2·344±0·075
	7*	0·176±0·004	0·055±0·003	0·49±0·03	2·911	1·866±0·121	2·991±0·051
Loam (Hongô)	1	4·498±0·202	1·585±0·018	0·42±0·06	8·321	2·012±0·294	2·836±0·131
	2	5·839±0·391	2·233±0·027	0·31±0·08	3·643	2·331±0·344	2·614±0·177
	3	6·460±0·184	2·642±0·042	0·22±0·04	2·076	2·366±0·242	2·445±0·079
	4	7·112±0·159	3·044±0·101	0·17±0·04	1·568	2·356±0·091	2·336±0·093
	5	9·800±0·419	4·295±0·389	0·14±0·02	1·670	2·209±0·434	2·281±0·228

* The original moist soil (No. 2) was tested in its altered state of packing.

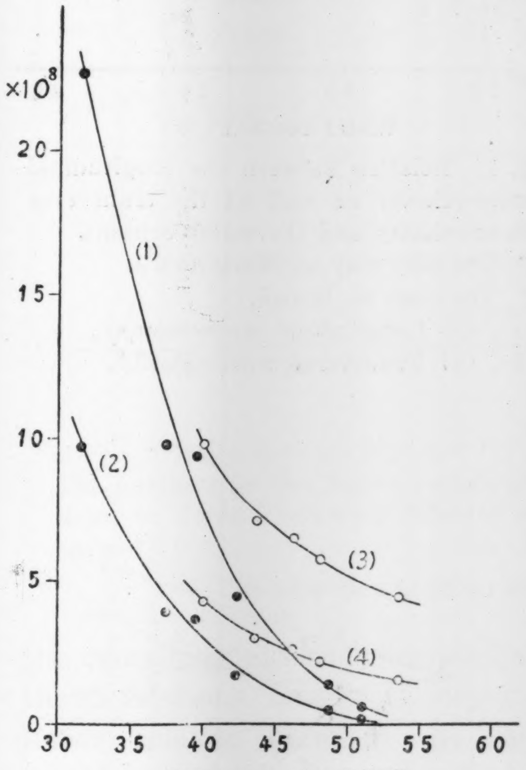

Fig. 4. Showing that the elastic constants diminish with increase in water content.

(1), (3): Young's modulus E.

(2), (4): modulus of rigidity μ.

Ordinate: E or μ.

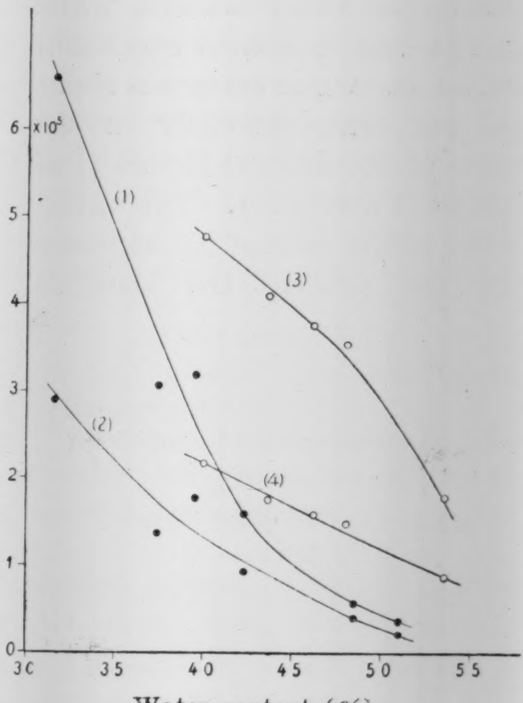

Fig. 5. Showing that the solid viscosity coefficients diminish with increase in water content.

(1), (3): normal viscosity γ_l.

(2), (4): tangential viscosity γ_t.

Ordinate: γ_l or γ_t.

• The silty-clay at Maru-no-uti. ○ The loam at Hongô.

ways represents the water content and the ordinate one kind of the following values, namely, the wave-velocities; the elastic constants E and μ; σ; the normal and tangential viscosity coefficients γ_l and γ_t; the ratio of γ_l to γ_t; and the ratio of E to μ.

The relations between any one of V_l, V_t, E, μ, σ, γ_l, γ_t and the water content are similar to those previously obtained, that is, the terms V_l, V_t, E, μ, γ_l, γ_t all somewhat rapidly diminish with increase in water content, σ or E/μ increasing with increase in water content, while γ_l/γ_t seems to become maximum when the water content is about 45 per cent, especially in the case of the loam at Hongô (Imperial University). The variations in the ratio of γ_l/γ_t to water in the case of the loam at

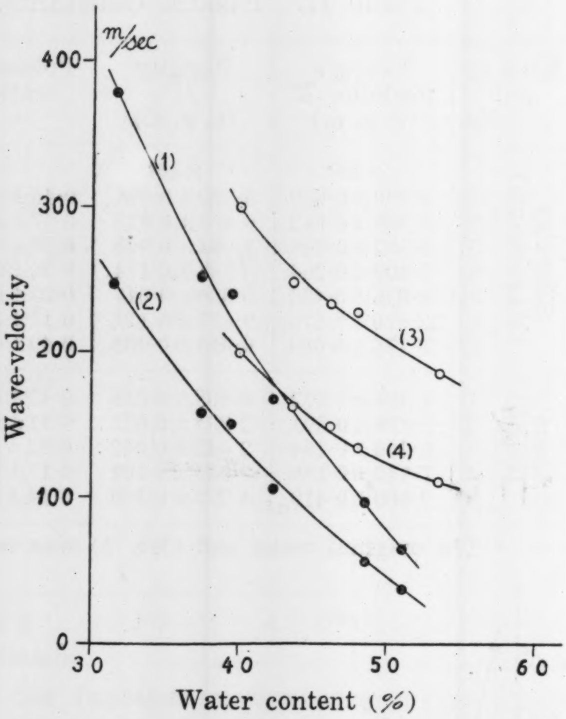

Fig. 6. Relation between the longitudinal wave-velocity as well as the transverse wave-velocity and the water content.
• The silty-clay at Maru-no-uti.
° The loam at Hongô.
(1), (3) Longitudinal wave-velocity.
(2), (4) Transverse wave-velocity.

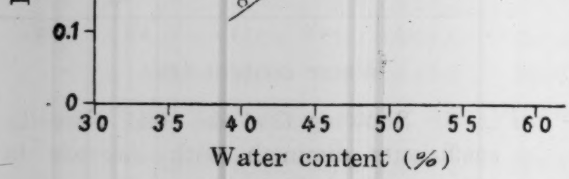

Fig. 7. Showing that Poisson's ratios increase with increase in water content. Ordinate: Poisson's ratio.

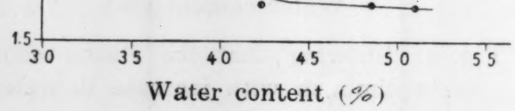

Fig. 8. Relation between the water content and E/μ as well as γ_l/γ_t.
Ordinate: E/μ or γ_l/γ_t.
(1), (3): E/μ. (2), (4): γ_l/γ_t.

• The silty-clay at Maru-no-uti. ° The loam at Hongô.

Hongô are smaller than in the silty-clay at Maru-no-uti, so far as the present experiments are concerned.

In order to know the possible relation between E/μ and γ_l/γ_t, we plotted E/μ against γ_l/γ_t for every case of water content as shown in Fig. 9, from which we found the relation in question within a certain range of water content. As will be seen from Fig. 9, the white circles 3, 4, 5 and the black circle 6 fall on a part of such a straight line as represented by $\gamma_l/\gamma_t = E/\mu$, while the white circle 2 and the black circle 5 fall on a part of the curve represented by $\gamma_l/\gamma_t = 1/3 \cdot (E/\mu)^2$, the remaining circles lying similarly on other curves. We shall discuss these relations later. If, experimentally, there were always such a linear relation between γ_l/γ_t and E/μ for certain water content, it would be possible to assume that the relation is of the form

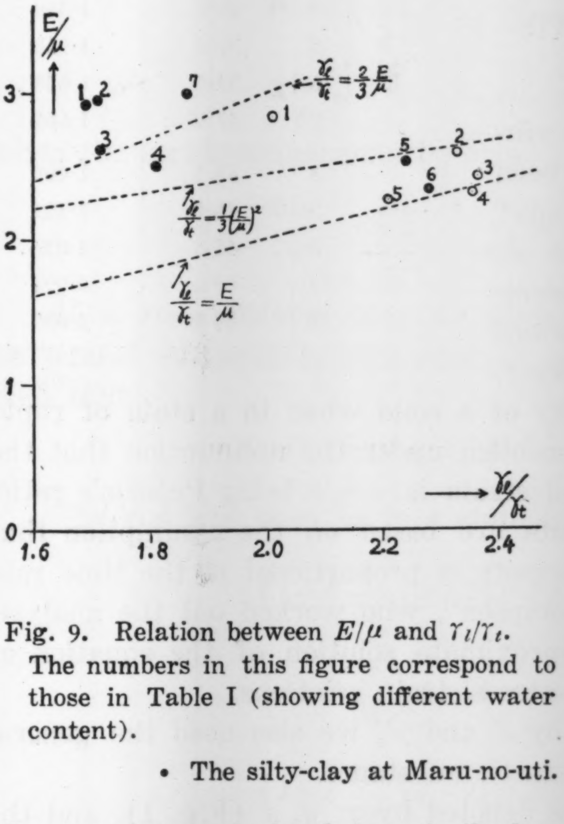

Fig. 9. Relation between E/μ and γ_l/γ_t. The numbers in this figure correspond to those in Table I (showing different water content).

• The silty-clay at Maru-no-uti.

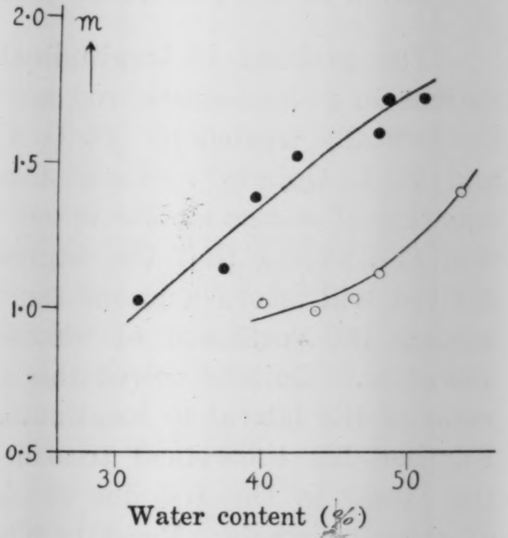

Fig. 10. Relation between m and the water content. m assumes a decreasingly smaller value with decrease in water content.

∘ The loam at Hongô.

$$\frac{E}{\mu} = m\frac{\gamma_l}{\gamma_t},$$

where m is a constant depending on the water content.

The values of m may be determined from the experimental result as shown in Table I. The values of m thus determined (Table III) are plotted against the water content (Fig. 10), which shows that the greater the increase of water in the soil the larger the value of m.

We are also going to determine viscous coefficients λ' and μ'[4] analogous to Lamé constants λ and μ in the case of elasticity. For this purpose we use equations of motion having the same form as those of (1) and (2) from the generalized stress-strain relations in a visco-elastic body.

Table II. The Value of m and Water Content of Soils.

Kind of soil	No.	Water content w (%)	m
Silty-clay (Maru-no-uti)	1	51·0	1·729
	2	48·5	1·723
	3	42·3	1·521
	4	39·5	1·388
	5	37·4	1·138
	6	31·5	1·028
	7*	47·9	1·602
Loam (Hongô)	1	53·5	1·409
	2	48·0	1·121
	3	46·2	1·033
	4	43·6	0·991
	5	40·0	1·032

4. Longitudinal and Torsional Vibration of a Visco-elastic Rod.

The problem of longitudinal vibrations in a visco-elastic rod has been theoretically treated by W. G. Cady[5] and S. L. Quimby[6]. Cady used an equation of motion similar to our equation (1), adding that the expressions derived will afford a means for determining the coefficient of viscosity of a solid when in a state of rapid vibration. Quimby solved this problem under the assumption that the ratio of the lateral to longitudinal strain is $-\sigma$, σ being Poisson's ratio. Further, his theoretical treatments are based on the assumption that the stress in the rod due to viscosity is proportional to the time rate of shearing strain. Recently Thompson[4], who worked out the analysis of this problem, obtained an approximate solution of the equation of motion derived from the general stress-strain relations.

In order to express γ_l or γ_t by λ' and μ', we also used the general stress-strain relations of a visco-elastic substance.

The directions of the axes are denoted by x, y, z (Fig. 1), and the components of displacement by u, v, w. The equation of motion then becomes

$$\rho\frac{\partial^2 w}{\partial t^2}=\frac{\partial \widehat{xz}}{\partial x}+\frac{\partial \widehat{yz}}{\partial y}+\frac{\partial \widehat{zz}}{\partial z}\,. \tag{5}$$

As is generally known, the stress-components are given by the equations[8]

---

[4] K. SEZAWA had already used these coefficients in his study on waves in visco-elastic solid bodies. *Bull. Earthq. Res. Inst.*, **3** (1927), 43.

[5] W. G. CADY, *Phys. Rev.*, **15** (1920), 146; **19** (1922), 1.

[6] S. L. QUIMBY, *Phys. Rev.*, **25** (1925), 558.

[7] J. H. C. THOMPSON, *Phil. Tran. Roy. Soc.*, **231** (1933), 339.

$$\widehat{xx}=\left(\lambda+\lambda'\frac{\partial}{\partial t}\right)\Delta+2\left(\mu+\mu'\frac{\partial}{\partial t}\right)e_{xx}\,, \tag{6}$$

$$\widehat{yy}=\left(\lambda+\lambda'\frac{\partial}{\partial t}\right)\Delta+2\left(\mu+\mu'\frac{\partial}{\partial t}\right)e_{yy}\,, \tag{7}$$

$$\widehat{zz}=\left(\lambda+\lambda'\frac{\partial}{\partial t}\right)\Delta+2\left(\mu+\mu'\frac{\partial}{\partial t}\right)e_{zz}\,, \tag{8}$$

$$\widehat{yz}=2\left(\mu+\mu'\frac{\partial}{\partial t}\right)e_{yz}\,, \quad \text{etc.,} \tag{9}$$

$$\Delta=e_{xx}+e_{yy}+e_{zz}\,, \tag{10}$$

when the strain-components become

$$e_{xx}=\frac{\partial u}{\partial x}\,, \quad \text{etc.,} \qquad e_{yz}=\frac{1}{2}\left(\frac{\partial w}{\partial y}+\frac{\partial v}{\partial z}\right), \quad \text{etc.}$$

If a rod, uniform over its plane ends, and free from traction on its lateral surfaces, is subjected to $\widehat{zz}$, it will be in a state of stress, such that

$$\widehat{xx}=\widehat{yy}=\widehat{xy}=\widehat{zx}=\widehat{yz}=0. \tag{11}$$

The rod will then be in a state of strain, such that

$$\left(\lambda+\lambda'\frac{\partial}{\partial t}\right)\Delta+2\left(\mu+\mu'\frac{\partial}{\partial t}\right)e_{xx}=0\,, \tag{12}$$

$$\left(\lambda+\lambda'\frac{\partial}{\partial t}\right)\Delta+2\left(\mu+\mu'\frac{\partial}{\partial t}\right)e_{yy}=0\,, \tag{13}$$

$$\left(\lambda+\lambda'\frac{\partial}{\partial t}\right)\Delta+2\left(\mu+\mu'\frac{\partial}{\partial t}\right)e_{zz}=\widehat{zz}\,. \tag{14}$$

Substituting (12) in (13), we obtain

$$\left(\mu+\mu'\frac{\partial}{\partial t}\right)e_{xx}=\left(\mu+\mu'\frac{\partial}{\partial t}\right)e_{yy}\,. \tag{15}$$

Adding (12), (13), to (14), we obtain

$$\widehat{zz}=\left\{(3\lambda+2\mu)+(3\lambda'+2\mu')\frac{\partial}{\partial t}\right\}\Delta\,, \tag{16}$$

whence

---

[8] K. **SEZAWA**, *loc. cit.*, 4)

$$\left(\lambda+\lambda'\frac{\partial}{\partial t}\right)\widehat{zz}=\left\{(3\lambda+2\mu)+(3\lambda'+2\mu')\frac{\partial}{\partial t}\right\}\left(\lambda+\lambda'\frac{\partial}{\partial t}\right)\Delta . \tag{17}$$

Substituting (12), (13) in (17), we obtain

$$\left(\lambda+\lambda'\frac{\partial}{\partial t}\right)\widehat{zz}=-2\left(\mu+\mu'\frac{\partial}{\partial t}\right)\left\{(3\lambda+2\mu)+(3\lambda'+2\mu')\frac{\partial}{\partial t}\right\}e_{xx}, \tag{18}$$

$$\left(\lambda+\lambda'\frac{\partial}{\partial t}\right)\widehat{zz}=-2\left(\mu+\mu'\frac{\partial}{\partial t}\right)\left\{(3\lambda+2\mu)+(3\lambda'+2\mu')\frac{\partial}{\partial t}\right\}e_{yy}. \tag{19}$$

By means of the same operation as (17), we get

$$2\left(\mu+\mu'\frac{\partial}{\partial t}\right)\widehat{zz}=2\left(\mu+\mu'\frac{\partial}{\partial t}\right)\left\{(3\lambda+2\mu)+(3\lambda'+2\mu')\frac{\partial}{\partial t}\right\}\Delta . \tag{20}$$

Adding (18), (19) to (20), we obtain

$$\left\{\lambda+\mu+(\lambda'+\mu')\frac{\partial}{\partial t}\right\}\widehat{zz}=\left(\mu+\mu'\frac{\partial}{\partial t}\right)\left\{(3\lambda+2\mu)+(3\lambda'+2\mu')\frac{\partial}{\partial t}\right\}e_{zz}. \tag{21}$$

Thus the equation of motion, namely, equation (5), becomes

$$\rho\left\{(\lambda+\mu)+(\lambda'+\mu')\frac{\partial}{\partial t}\right\}\frac{\partial^2 w}{\partial t^2}=\left(\mu+\mu'\frac{\partial}{\partial t}\right)\left\{(3\lambda+2\mu)+(3\lambda'+2\mu')\frac{\partial}{\partial t}\right\}\frac{\partial^2 w}{\partial z^2}. \quad (22)^{9)}$$

The solution of the equation (22) is of the form

$$w=Ae^{ifz}e^{pt},$$

or

$$w=(A\cos fz+B\sin fz)e^{pt}, \tag{23}$$

where p is the root of the equation,

$$\rho\left\{(\lambda+\mu)+(\lambda'+\mu')p\right\}p^2+f^2(\mu+\mu'p)\left\{(3\lambda+2\mu)+(3\lambda'+2\mu')p\right\}=0 . \tag{24}$$

We shall determine the constants A and B in (23) under the condition, such that

$$\left.\begin{aligned} w&=0 , &&\text{at} \quad z=0 ,\\ \frac{\partial w}{\partial z}&=0 , &&\text{at} \quad z=h , \end{aligned}\right\} \tag{25}$$

where h is the height of the rod. We then obtain

$$A=0 , \qquad f=\frac{\pi}{2h}(2r-1), \qquad r=1, 2, 3, \ldots\ldots . \tag{26}$$

Thus we have the solution of (22) for $r=1$, namely,

---

9) J. H. C. **THOMPSON** got the same expression in a like manner. *loc. cit.*, 7)

$$w=\sin\frac{\pi}{2h}z\sum_{i=1}^{3}A_i e^{p_i t},$$

where p_i is the root of (24) when $r=1$.

We can solve mathematically the equation (24), but owing to the complexity of its solution, it is difficult to discuss the nature of the vibration of a rod so that we have to resort to the method of physics. Thompson shows that one of the roots is always large, provided that μ/μ' and λ/λ' are large, while the other two roots may be small if the height of the rod is large.

Since the value of μ/μ' of soil is of the order of 10^4, and the height of soil specimen is of the order of 30 cm, we may suppose, according to Thompson's results, that one of the roots is large and the other small. We may then put (24) approximately in a form such that

$$\rho p^2+f^2\frac{\mu(3\lambda+2\mu)}{\lambda+\mu}(1+\nu p)=0\,, \tag{27}$$

where,

$$\nu=\frac{\lambda\mu\left(\frac{\lambda'}{\lambda}-\frac{\mu'}{\mu}\right)+\frac{\mu'}{\mu}(\lambda+\mu)\,(3\lambda+2\mu)}{(\lambda+\mu)\,(3\lambda+2\mu)}\,, \tag{28}$$

whence the equation of motion becomes approximately

$$\left.\begin{aligned}\rho\frac{\partial^2 w}{\partial t^2}&=E\left(1+\nu\frac{\partial}{\partial t}\right)\frac{\partial^2 w}{\partial z^2}\,,\\ \text{where,}\qquad E&=\frac{\mu(3\lambda+2\mu)}{\lambda+\mu}\,.\end{aligned}\right\} \tag{29}$$

This equation is of the same form as equation (1), by comparing which with (1), we obtain

$$\begin{aligned}\gamma_l&=E\nu\\ &=\mu\left\{\lambda\mu\left(\frac{\lambda'}{\lambda}-\frac{\mu'}{\mu}\right)+\frac{\mu'}{\mu}(\lambda+\mu)\,(3\lambda+2\mu)\right\}\frac{1}{(\lambda+\mu)^2}\,.\end{aligned} \tag{30}$$

In the case of the torsional vibration of a visco-elastic rod, the stress-components are given by

$$\left.\begin{gathered}\widehat{xx}=\widehat{yy}=\widehat{zz}=\widehat{xy}=0\,,\\ \widehat{yz}=x\left(\mu+\mu'\frac{\partial}{\partial t}\right)\frac{\partial u}{\partial z}\,,\quad \widehat{zx}=-y\left(\mu+\mu'\frac{\partial}{\partial t}\right)\frac{\partial u}{\partial z}\,,\end{gathered}\right\} \tag{31}$$

whence the equation of motion is given by

$$\rho\frac{\partial^2 u}{\partial t^2}=\left(\mu+\mu'\frac{\partial}{\partial t}\right)\frac{\partial^2 u}{\partial z^2}\,. \tag{32}$$

Thus we obtain the relation between γ_t and μ' by comparing (32) with (2), that is

$$\lambda_t=\mu'. \tag{33}$$

5. The Ratio of γ_l to γ_t.

We can obtain the ratio of γ_l to γ_t from equation (30) and (31).

$$\frac{\gamma_l}{\gamma_t}=\frac{\lambda\mu\left(\frac{\lambda'}{\lambda}-\frac{\mu'}{\mu}\right)+\frac{\mu'}{\mu}(\lambda+\mu)(3\lambda+2\mu)}{\frac{\mu'}{\mu}(\lambda+\mu)^2}\,. \tag{34}$$

Table IV. λ'/μ', n, and Water Content of Soils.

Kind of soil	No.	Water content w(%)	$\frac{\lambda'}{\mu'}$	n
Silty-clay (Maru-no-uti)	1	51·0	−180·78±20·12	−15·73
	2	48·5	−327·77±30·56	−20·90
	3	42·3	−4·08± 0·31	−2·72
	4	39·5	−2·59± 0·23	−2·39
	5	37·4	−0·29± 0·09	−0·25
	6	31·5	0·37± 0·12	0·72
	7*	47·9	−2762·5±293·1	−56·4
Loam (Hongô)	1	53·5	−26·95± 3·86	−5·15
	2	48·0	−0·33± 0·18	−0.20
	3	46·2	0·53± 0·21	0·68
	4	43·6	0·56± 0·18	1·09
	5	40·0	0·25± 0·10	0.64

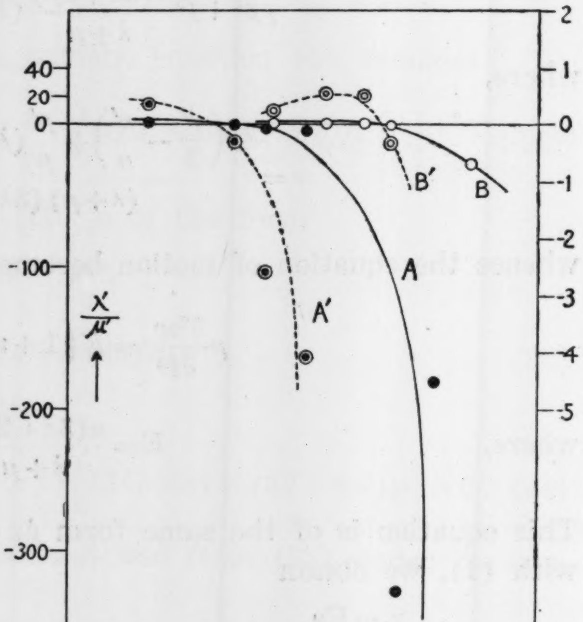

Fig. 11. Relation between λ'/μ' and the water content. λ'/μ' tends to assume a negatively greater value with increase in water content.
The ordinates of curves A, B are shown in the left-hand side scale; those of A′ and B′ in the right-hand side scale.
A: The silty-clay at Maru-no-uti.
B: The loam at Hongô.

Since the values of γ_l/γ_t are found experimentally, we can determine, by means of equation (34), the viscous coefficient λ' and also the value of λ'/μ' for various water contents, the results being shown in Table IV. The relations between λ'/μ' and the water content thus found are shown in Fig. 11, λ'/μ', the water content being taken as ordinate and abscissa. As will be seen from this figure, λ'/μ' assumes an increasingly larger negative value with increase in water content. In the case of the silty-clay at Maru-no-uti, if its water content w is less than about 36 per cent, $\lambda'/\mu' > 0$, and if its water content is about 36 per cent, $\lambda'/\mu' = 0$. In the case of the loam at Hongô, if w is larger than about 47 per cent, $\lambda'/\mu' < 0$, and if w is less than about 47 per cent, $\lambda'/\mu' > 0$.

Hence the stress behaviour in the soil due to viscosity obeys the law of compressible or incompressible viscous fluid, in agreement with water content in the soils.

It would, moreover, be interesting to consider special cases of the equation (34).

(a) If $\lambda'/\mu' = \lambda/\mu$, from (34), we obtain

$$\frac{\lambda_l}{\gamma_t} = \frac{E}{\mu}. \tag{35}$$

This relation corresponds to $m=1$ in the empirical formula shown in Section 3, such as $\dfrac{E}{\mu} = m\dfrac{\gamma_l}{\gamma_t}$.

(b) If $\lambda' + \dfrac{2}{3}\mu' = 0$, as in hydrodynamics, then (34) becomes

$$\frac{\gamma_l}{\gamma_t} = \frac{1}{3}\left(\frac{E}{\mu}\right)^2. \tag{36}$$

(c) If Quimby's equations are satisfied, the following relation can be obtained. Since Quimby's equation[10] of motion is

$$\rho\frac{\partial^2 w}{\partial t^2} = E\frac{\partial^2 w}{\partial z^2} + \frac{4}{3}(1+\sigma)\mu'\frac{\partial^3 w}{\partial z^2 \partial t},$$

γ_l can be obtained. Therefore the ratio of γ_l to γ_t becomes

$$\frac{\gamma_l}{\gamma_t} = \frac{2}{3}\frac{E}{\mu}. \tag{37}$$

(d) If $\dfrac{\lambda'}{\lambda} = n\dfrac{\mu'}{\mu}$,

then (34) becomes

$$\frac{\gamma_l}{\gamma_t} = 2\left\{\sigma(1-2\sigma)(n-1) + (1+\sigma)\right\}. \tag{38}$$

---

[10] S. L. Quimby, *loc. cit.*, 6)

These relations we have investigated experimentally, with results as shown in Figs. 11∼13. As already described in Section 3, soil seems to be in a state represented by relations, such as (a), (b), (c) respectively for certain ranges of water content. In other words, soil may be regarded as changing with decrease in water content from the state expressed by (c) to that of (b), and even to that of (a). It will thus be noticed from these relations that, with increase in water content, the soil will approach the condition of a viscous fluid.

Since the cases (a), (b), (c), may be included in the cases of (d), we specially studied the nature of n obtained from the relation of (d) by introducing our experimental results. We plotted the values of n (Table IV) against the water content as shown in Fig. 12, from which we found that the value of n assumes an increasingly larger negative value with increase in water content. In the case of the silty-clay at Maru-no-uti, if the water content w is less than 36 per cent, $n > 0$, whereas if the water content w is larger than 36 per cent, $n < 0$. Such a condition also held in the case of the loam at Hongô. If w is smaller than 47 per cent, $n > 0$, whereas if w is larger than about 47 per cent, $n < 0$. Thus there must be such a case as $n = 0$. The water content in question differs with the kind of soil, namely, the content is about 47∼48 per cent for loam, and about 36∼38 per cent for silty-clay.

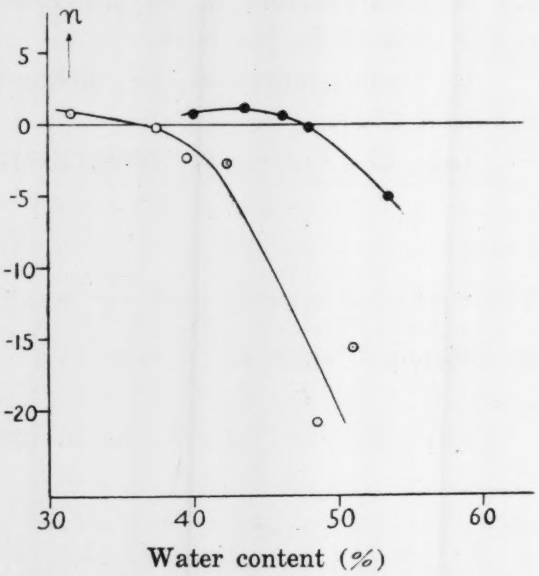

Fig. 12. Relation between n and the water content. n tends to assume a negatively greater value with increase in water content.

○ The silty-clay at Maru-no-uti.

● The loam at Hongô.

Hence when the water content increases, the soil behaves as a viscous fluid.

6. Summary and Conclusion.

In this paper, the writer discussed the experimental results in connection with the elastic properties and the solid viscosity of certain kinds of soil.

The relations between their properties and the water content are investigated. The elastic constants and solid viscosity coefficients diminish somewhat rapidly with increase in water content, as before.

The Poisson's ratios of these soils increase with increase in water content; the variation in which is the same as that previously described.

The ratio of γ_l to γ_t seems to be maximum at a certain water content. In the case of the loam at Hongô, the variation in the ratio of γ_l/γ_t to water, so far as the present experiments are concerned, is smaller than that of the silty-clay at Maru-no-uti.

The relations between the ratio of γ_l to γ_t and that of E to μ are investigated.

The value of m obtained under the assumption $\frac{E}{\mu}=m\frac{\gamma_l}{\gamma_t}$, varies with the water content, the greater the increase of water in the soil the larger the value of m.

The viscous coefficients λ' and μ' similar to both Lamé elastic constants λ, μ are determined by means of an approximate solution derived from the generalized stress-strain relations in a visco-elastic body.

The relations between λ'/μ' and the water content are investigated. λ'/μ' assumes an increasingly larger negative value with increase in water content. In the case of the silty-clay at Maru-no-uti, if its water content is about 36 per cent, $\lambda'/\mu'=0$. In the case of the loam at Hongô, if its water content is about 47 per cent, $\lambda'/\mu'=0$. It was ascertained that in the case of water contents exceeding these values, the soils behave like a viscous fluid. It is supposed that λ'/μ' may assume an increasingly larger positive value with decrease in water content below the values in question, and the state of the soils may then approach to that of a solid.

The relations between the ratios of γ_l/γ_t and E/μ obtained in our experiments are investigated in the following three cases.

(a) If $\frac{\lambda'}{\mu'}=n\frac{\lambda}{\mu}$, then $\frac{\gamma_l}{\gamma_t}=2\left\{\sigma(1-2\sigma)(n-1)+(1+\sigma)\right\}$.

(b) If $\lambda'+\frac{2}{3}\mu'=0$, then $\frac{\gamma_l}{\gamma_t}=\frac{1}{3}\left(\frac{E}{\mu}\right)^2$.

(c) If Quimby's equation holds,

then
$$\frac{\gamma_l}{\gamma_t}=\frac{2}{3}\frac{E}{\mu}.$$

We observed that, from our experimental results, these relations seem to be approximately satisfied with different conditions of water contents. In the case of the loam at Hongô, we obtained $\frac{\gamma_l}{\gamma_t}\approx\frac{E}{\mu}$ for a water content ranging from about 40 per cent to 46 per cent, with

$\frac{\gamma_l}{\gamma_t}\approx\frac{2}{3}\frac{E}{\mu}$ for a water content of 54 per cent, and $\frac{\gamma_l}{\gamma_t}\approx\frac{1}{3}\left(\frac{E}{\mu}\right)^2$ for a water content of 48 per cent. In the case of the silty-clay at Maru-no-uti, $\frac{\gamma_l}{\gamma_t}\approx\frac{E}{\mu}$ at about 32 per cent, $\frac{\gamma_l}{\gamma_t}\approx\frac{1}{3}\left(\frac{E}{\mu}\right)^2$ for a water content ranging from about 37 per cent to 40 per cent, $\frac{\gamma_l}{\gamma_t}\approx\frac{2}{3}\frac{E}{\mu}$ at about 42 per cent. Since the water content exceeded nearly 42 per cent, these simple relations do not hold.

The relations between n in the conditions of (a) and the water content are investigated. In the case of the silty-clay at Maru-no-uti, if the water content w is less than 36 per cent, $n>0$, while if w is greater than about 36 per cent, $n<0$. In the case of the loam at Hongô, if w is smaller than 47 per cent, $n>0$, while if w is greater than about 47 per cent, $n<0$. It was thus ascertained that these water relations differ with the kind of soil.

From the fact that n assumes an increasingly larger negative value with increase in water content, it was concluded that the condition of the soil approaches that of a viscous fluid.

It was ascertained that the stress behaviour in the soil due to viscosity obeys the law of compressible or incompressible viscous fluid, in agreement with different water content in the soils.

In conclusion, the writer wishes to express his sincerest thanks to Professor Katsutada Sezawa for his kind advices and critiques, and to Drs. C. Tsuboi, H. Kawasumi, and G. Nishimura for their valuable discussions.

---

31. 二三の土に於ける2種の粘性比とポアソン彈性比との關係

地震研究所 飯田汲事

本論文に於いては土の物理的性質特に彈性及び粘性に關係せる性質の實驗的研究の結果が述べてある.

土の彈性がそれが含有する水の量によつて大いに變化する事を已に屢々述べたが，今回は更に粘性に就いても研究し，且つ縱振動から求めた固體粘度と捩振動から求めた固體粘度との比に對する彈性 Poisson 比の關係を實驗的に檢べた. 又 λ,-μ に相當する固體粘度 λ', μ' 等を求めた.

以上の諸量の含水量に對する變化を檢べて見ると本鄉の赤土は含水率約 47〜48% 以上，丸の內の沈泥質粘土は含水率約 36% 以上に於て夫々粘性液體の樣な性質を示す事が判明した.

32. 支那震災の特異性と殘存する高塔より推定された其の震度に就て

地震研究所 齋田時太郎

（昭和13年1月18日發表——昭和13年3月20日受理）

内容梗概

支那が大震災國であるこさは専門家以外殆ご知つてゐない，英文梗概に引用してある通りダビソン氏の調査によれば，地震による死者の年平均は 13862 人さあつて第 1 位を示してゐる，本文には支那地震に就て其の活動さ地域，年代さの關係，最近の傾向，殘存してゐる高塔の構造より推定した震度及び地質より考へた支那震災の特性に關しては世界第 1 位の災度必ずしも第 1 位の震度を示してゐないこさ卽ち災度さ震度さは比例的でないこさを示し其の震度も我國のものさは大差ないさ考へられるこさ及び北支の方が南支の方より震度が高いさ考へてゐるのに對して北支の地質の關係により著しく災度の高く現はれるこさを注意し震度は北南何れも大差ないさ考へられるこさ等考察の結果を述べてある.

支那には屢々大洪水大旱魃の襲來することは周知のことであるが，大地震も亦頻發したとは一般に知られてゐない，實に支那は自然の暴威に對して全く無抵抗である．今や新政權の治下に資源の開發，産業の發展及文化の振興の緒に就かんとするに當りその先驅たるべき土木建築工作の遂行のために，支那に於ける地震活動の消長と其の震度とを考察することは，震災を研究し耐震構造を論ずる吾人の責務であると考へたので，支那の山河を踏査した經驗なく且つ支那の文献に暗い筆者にとりては誠に隔靴掻痒の憾があるが詳細な論證は後日に期し，こゝには極めて概說的であるが筆者の所信の解說を試みた次第である．

支那の大地震の年代は理科年表* によると西紀前 193 年漢惠帝 2 年甘肅省隴西に起つて家屋 400 餘を破損したのを初とし現今までに 151 回の大震災が記錄されてゐる．その內數百人以上の死者を生ぜしめた大地震を取り出すと下の通りである．

漢

年號	年	月	日	西	暦年	月	日		
高後	2	I	27	前	186	II	22	甘肅省武都	
本始	4	IV	29	〃	70	VI	1	關中（西安附近）	死 6000
綏和	2	IX	21	〃	7	XI	11	京師ヨリ北邊ニ至ル	

---

* 理科年表昭和 12 年，東京天文臺發行

南北朝

延昌	1	IV	20	後	512	V	23	京師他	死 5310

唐

開元	22	II	10		734	III	23	甘肅省秦州	死 4000 餘

宋

景祐	4	XII	17		1038	I	30	山西省代并忻三州	死 22391

金

大安	1	XI	8		1209	XII	13	山西省浮山縣	死 2(3)000
興定	3	IV	18		1919	VI	9	甘肅省平凉德順	死數千

元

大德	7	VIII	6		1303	IX	25	山西省太原平陽	家屋 10 萬破損
〃	9	IV	10		1305	V	11	山西省大同路懷仁縣	死 1400 餘
〃	11	VIII	10		1307	IX	15	甘肅省開城路	壓死 5000 餘

明

成化	13	IV	1		1477	V	22	甘肅省凉州寧夏	
弘治	12	冬			1499			雲南省大理宣頁	死數萬
〃	14	I	1		1501	I	29	陝西省咸陽長安	
正德	10	V	6		1515	VI	27	雲南省趙州	
嘉靖	34	XII	72		1556	II	2	山西，陝西，河南省＝亘ル	死 83 萬
〃	40	VI	24		1561	VIII	14	山西省太原大同，寧夏，固原	死無數
萬暦	34				1606			雲南省建水	
〃	37	VI	12		1609	VII	12	省甘肅省紅崖	
天啓	2	IX	21		1622	X	25	甘肅省平凉	死 12000

清

順治	9				1652			雲南省蒙化	死 3000
〃	11	VI	8		1654	VII	21	陝西省	死 10000
康熙	7	VI			1668			山東莒縣諸城	死 22700
〃	19	秋			1680			雲南省楚雄	死 1000 餘
〃	34	IV	6		1695	V	18	山省平陽	死 10000 餘
〃	48	IX	12		1709	X	14	甘肅省凉州，固原，寧夏	死 2000
〃	57	V	12		1718	VI	10	甘肅省莊浪	死 4000
乾隆	3	XI	25		1739	I	4	寧夏	死 50000
嘉慶	4	VII			1799			雲南省石屏	翌日再震死傷 3000
道光	13				1833			雲南路南徵江	死 6700
〃	30	VIII	7		1850	IX	12	四川西昌會理	死 20000
同治	10				1871			四川省西部	死 2298
光緒	5	V	10～12		1879	VI	29	甘肅省階州通渭	死 20710
〃	13				1887			雲南省石屏	死 2000

中華民國

	9				1920	XII	16	甘肅省六盤山	死 10 萬
	14				1925	III	16	雲南省大理府	死 6500
	16				1927	V	23	甘肅省凉州	死數萬
	20				1931	VIII	10	新疆省內	死 1 萬
	21				1932	XII	25	甘肅省高臺	死多數

以上 39 回の大震災の發起年代を顧みるに，西紀前 186 年以來上代に於ては 百年乃至數百年毎に點々と起り明末より清初の約百年間に約 10 回及前世紀後半期より現代までに亦 10 回の大地震が續發した活動の盛な時代が 2 回あるのが解る． これ等 39 回の大地震を地域別に見ると，30 回は北支の甘粛，陝西，山西，河南地方に，9 回は雲南，貴州の地方に起つてゐるから斷然北支の方が活動が盛んであると言へる．上記のやうな大規模のものは近年主として甘粛以西の奥地に起る傾向があるが，大正 12 年 11 月 15 日に山西省大同の西南約 50 里の岢嵐縣と言ふ炭坑所在地に死傷 1500 を生じた地震が發生したことがあるから注意を要する．なほ輕微な被害を與へる程度のものは山東泰山を中心とする一帶と福建の海岸に沿ふて起つてゐる．

支那の震災には極めて大なるものがあつて，我國の震災と比較すると其の震度の偉大なること想像も及ばぬものがある，例へば上記の嘉靖 34 年 12 月 12 日（西紀 1556 年）の山西，陝西，河南の三省に亘る大地震では死者 83 萬と記錄され，大正 9 年 12 月 16 日（西紀 1920 年）甘粛省六盤山附近の地震では 10 萬の死者が報ぜられてゐる，其の他數千の死者を出した程度のものならば 10 回を下らない．これを我國のものと比較するに明治 24 年 10 月 28 日（西紀 1891 年）の濃美大地震は近年の大地震で仙臺以北を除き日本中震動を感じ死者 7,273，全潰家屋 8 萬，非住家を合せば 14 萬餘，且餘震は十數年間續いてゐたと言ふ大規模のもので名古屋，岐阜其の他の市街に建築された洋風煉瓦造の官衙，工場等が徹底的に破壞され，其の後この種の建築構造に耐震的注意が喚起されるやうになつた，かゝる大地震にあつても我國傳來の木造建築なる名古屋城，大垣城，犬山城の天主閣は輕微な震害を受けたるに過ぎず，岐阜縣武儀郡關町新長谷寺及び同縣安八郡神戸町日吉神社の三重塔の如きは最激震地にありながら震害を免れたと言ふ狀態であつた．關東大地震では家屋全潰 12 萬餘，死者 14 萬餘であつたが其の大部分は火災によるもので直接家屋の倒潰によるものは 2 萬以下であつたと推定される．彼我災度の比較によると如何にも彼の大規模で戰慄するものがあり，其の震度の强烈なることが想像され一度この種の地震に襲はれゝば，如何なる施設と雖も震害を免れることは不可能であると感ぜられる．

支那人は古來よく文献を殘した國民で啻に政治上の事變ばかりでなく自然現象の方面にまで及んでゐるが，その誇張文飾も亦著しいことで有名である，從て文献の學術的價値極めて低く災度を表はす數字に信を置き難いが，文献に見える地震に伴ふ地鳴山崩，餘震等の記錄から考へると何れも大規模の地震であつたことは確である．

筆者の既往の震災調査によると震災は勿論地震々度の大小によるが，家屋構造と地

盤の性質と發震時刻並に人口密度とによることが大きいもので，地震の大小と震災の大小とは必ずしも比例しない，例へば昭和5年11月の伊豆北部地震では全潰住家2142，死者259人で昭和10年4月の臺灣中部地震は伊豆地震より震度小なるに關はらず全潰住家17000餘，死者3276を出してゐる，これは主として家屋構造の相違によることで常に臺灣震災[1]は内地の同程度地震に比べて數倍以上に及んでゐる．

支那の地震の震度を科學的に知るには直接觀測によるべきであらうが，それは將來のことであつて既往の大地震の震度は數多の文献を通して震災の情況を知ると同時に現地に於て地形地質構造及び住家の構造並に地震に襲はれて今なほ殘存する建築物とによつて認識を深めることである，從て其の震度は數字を以て精確に決定することは不可能である，たゞ其の規模を推察し得るに過ぎない．筆者未だ支那の山河を踏査した經驗はないが，現地を調査した地質學者の言と，殘存する高塔の耐震性と支那人の著した甘肅地震考[2]及び雲南地震考[3]の二書によつて其の震度を考察して見ようと思ふ．

北支那は森林に乏しく家屋を構造する木材の供給は極めて不足してゐるから，家屋は泥，土埆，煉瓦造のもの多く極めて粗造である，なほ山西及黃河沿岸は厚き黃土層

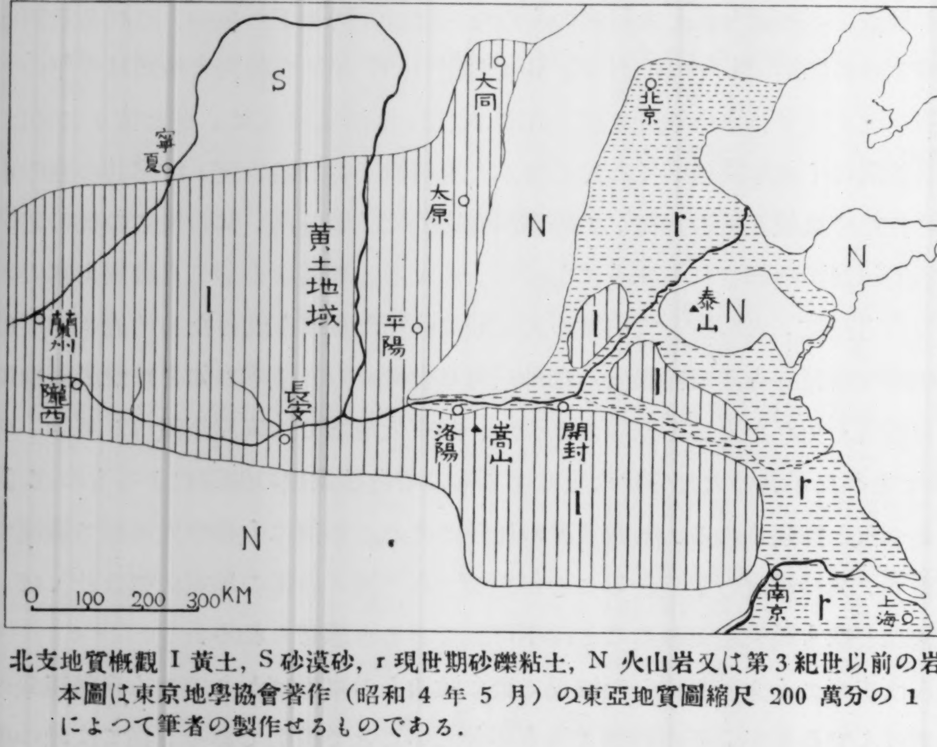

北支地質概觀 I 黃土，S 砂漠砂，r 現世期砂礫粘土，N 火山岩又は第3紀世以前の岩石
本圖は東京地學協會著作（昭和4年5月）の東亞地質圖縮尺200萬分の1によつて筆者の製作せるものである．

---

[1] 筆者「臺灣に於ける震害さ地盤に就て」地震研究所彙報別册第3號（昭和11年）
[2] 翁文灝「甘肅地震老」摘印地質彙報第3號（民國10年10月）
[3]「雲南地震考」雲南省公署樞要處第4課刊（民國15年11月）

より構成され垂直に近い斷崖が造られてゐるので木材に乏しく且つ空氣の常に乾燥してゐる此の地方には古來黃土の斷崖に横穴を穿つて穴居するもの多く今なほ全村穴居の部落もあると言ふことである（寫眞第 1 參照）．これに對して雲南貴州方面は玉石積及木造家屋である．

地盤は山西，陝西，甘肅，河南方面は厚い黃土の層で覆はれ農家はそこに階段狀に耕地を開き斜面に横穴を穿つて住居や倉庫や家畜小屋としてゐる，黃土は加里，燐酸石灰分に富み且細粒で乾燥すれば東京山手の赤土より堅いが極めて脆弱で振動には特に弱い，水を含むと殆ど凝集力がなく，其の崩壞するや常に垂直の面を造る性質がある，黃土の侵蝕地形は普通の谷のやうに V 字形とならず，殆ど垂直に近い谷をつくる，有名な函谷關の狹隘も黃土の特性によつて出來たものである．雲南貴州方面は山嶽地帶で岩質は火山岩又は第三紀世以前の古いもので堅硬である．（北支地質概觀參照）．

以上述べた地盤の特質が震災文献によく現はれてゐる，即ち北支の地震には常に山崩山津浪が伴ふ，例へば甘肅地震考に

> 宣和六年春三月蘭州地震諸山草木盡沒山下麥苗反在山上．
>
> 清世祖順治十一年六月秦州地震一年餘聲如雷官署民房均毀死萬餘人羅寺堡二山移合爲．

と言ふやうな全山移動の山崩を始とし其の他大小無數の山崩が地震毎に記錄されてゐる．これに對して雲南貴州方面では山崩の記錄は更にないが家屋の全潰數の著しく大なるものが多い．

要するに北支の震災の特色は家屋の脆弱なると，山崩山津浪に伴ふ住居の埋沒によるもので雲南貴州方面は家屋の全潰によるものと考へて誤りでない．なほ北支に死者の著しく多いのは本震に續く餘震によつて起り易い山崩れで積算されてゐるのではないかと疑はれる．と言ふのは文献* の各所に山崩續發の記事が多いので判る，文献では本震と餘震とによる震災を區別してゐない．前記 83 萬の死者を出した嘉靖 34 年の大地震も其の規模は大きくはあつたらうが本震 1 回による死者とは考へられない，これを我國の震災の發生機構と同様に考へたら誤であらう．

雲南貴州方面では山崩れがないから本震で家屋を失ひ餘震續發中は粗末な假小屋にゐさへすれば餘震の大なるものと雖も死者を生ずることはない．

かく地形地質と家屋構造とを考へると，北支も南支も同じ程度の地震に對し北支に著しく震災が大きく現はれるのが當然と言へる．筆者はこの見地からして支那の地震

---

* 甘肅地震考及び雲南地震考．

は北支も南支も其の震度に於て著しき差はないものと信ずる．

震度を推定する資料となるものに殘存する高塔がある，隋の文帝（推古天皇時代）は佛教の信心厚く天下に詔して佛塔を建立しその數 111[4] に及んだと云はれてゐる，筆者の知れるもので地震區域で，しかも大地震に遭遇したもの[5] を擧げると

名稱	位置	創建年代
文風塔 8 角 13 層塔	四川省綿陽縣	宋代
嵩山嵩岳寺 12 角 15 層塔	河南省登封縣	西紀 523
嵩山會善寺淨藏禪師塔	同上	746
齊雲塔（東白馬寺塔）13 層高 160 尺	洛陽	1175
孫八娘墓塔石造 7 層	同上	唐代
法王寺塼塔 15 層	嵩山	同上
永泰寺塼塔 11 層	同上	同上
永泰寺塼塔 7 層	同上	同上
慈恩寺大雁塔 4 角 7 層高 65 米	陝西省安	652
薦福寺小雁塔 4 角 13 層塔	同上	707
香積寺 4 角 11 層塔	同上	681
興教寺玄奘塔 5 層	同上	669
常樂寺（東）4 角 13 層塔	雲南縣	976
慧光寺（西）4 角 13 層塔	同上	1667
佛宮寺 8 角 5 層木塔	山西省應縣	1056
慈相寺 8 角 7 層塔	山西省平遙	1046
壽寧寺 6 角 3 層塔	山西省文水縣	1094
永祚寺雙塔	山西省太原	1611
淨明寺舍利塔	同上	1385
臺中大塔院大塔	山西省五臺山	1579
扶風縣內 8 角 9 層塔	陝西省扶風縣	宋代

等である，しかも屢々大震災地であつた長安（西安），洛陽（河南），嵩山，登封にかく多數が崩壞を免れて殘存してゐる（寫眞第 2～第 20 參照）． この種の高塔破壞記錄は清の道光 13 年雲南地震で昆明南門外東塔震倒[6] と同咸豐 5 年大通縣西十里塔破山崩[7] とあるものと大正 14 年浙江省杭縣に在る雷峰塔[8] 8 角 7 層塼塔（西紀 975年創建）が自然崩壞をしたと云ふ僅少な例があるのみで，一見我國の五重塔と同樣に耐震的であるやうに見えるが，上記の殘存する塔は何れも瓦に類する磚（塼又は甎ともかく）で築造されたもので，高さ 200 尺位あるものもあり其の耐震性は煉瓦，石造の煙突と同樣に極めて薄弱で，五重塔の如き木造と比較にならないと考へられる．因て支那の高塔が耐震的であると考へるよりも，地震の方が大きくないと考へるのが妥當

4）伊藤清造氏「支那建築」．

5）主として世界建築集成「支那建築上卷」によれるも鮑鼎氏の「唐宋塔之初步分析」中國營造學社彙栞第 6 卷，第 4 期による若干補つた．

6）前記ノ雲南地震考．

7）前記ノ甘肅地震考．

8）世界建築集成「支那建築上卷」．

である．かく殘存する高塔の耐震性を考へると支那の地震は災害記錄の示すほど大きくなく我國既往の地震より優勢とは考へられない．從て震災防止の策を講ずるならば震動に對しては我國と同程度でよいが山崩山津浪には特別な注意を拂ふ必要があると言ふことになる．なほ支那地震について興味あることは地震時には屢々現はれると言ふ發光現象である．この眞相は未だ解明されてゐないが我國の文献には奈良朝時代より記錄されてゐるのに，支那地震では鳴動を聞いたことは著しく記錄されてゐるが發光現象のことが絕無であるのは不思議と言ふべきである．

支那の古代文化の卓絕してゐたことは周知のことであるが，地震文化について言ふならば今より 1800 年以前に張衡が候風地動儀を創作して地震觀測を始めてゐる，この器械の構造の詳細は解らないが洛陽に据えつけて觀測中その西 200 里の隴西に起つた大地震を洛陽では人體に無感であつたにも關はらず，其の器械には感じたと言ふから精巧なものであつたと考へられる．其の後明の末期には伊太利人の宣教師ロンゴバルヂ Nicalao Longobardi をして地震解* なる書を作らしてゐる等特筆すべき功績を擧げながら現今に於ては其の見るべきものなく嘗北京，南京，上海（佛人によつて），香港（英人によつて），廣東等で地震觀測をなしてゐる程度に過ぎない． 今や皇國の指導援助のもとに支那が開發されんとするに當つて支那地震學及び其の應用も振興されなければならないと信ずる．筆者も機を得て現地に地形地質を調査し或は高塔の構造及び其の耐震性に就ても更に研究を進めてみたいと願つてゐる．

筆を擱くにあたり，黃土の性質について御教示を賜はつた東京帝國大學文學教授脇水鐵五郎博士及び支那塔に關する文献，磚の閲覽及び寫眞原板の借用等に御多忙中度々御手數を煩はした東京帝國大學工學部建築學教室の木村貞吉氏並に地震史料蒐集の方針について御教示を賜はつた東京帝國大學文學部教授池內宏博士に深甚の謝意を表する次第である．

---

* 高桑氏「支那文化史講話」.

32. *The Peculiarity of Chinese Earthquake Disasters and the Seismic Intensities as Deduced from Remaining Pagodas.*

By Tokitaro SAITA (SAIDA),

Earthquake Research Institute.

According to the investigation of C. Davison,* the mean annual loss of life caused by earthquakes in important earthquake districts is as follows:

13 862	in China
7980	in Colombia and Ecuador
2240	in Japan
1006	in Italy
991	in India
586	in Asia Minor
99	in Greece
35	in the Philippines
29	in Formosa
6	in the United States of America

China is therefore the greatest earthquake-devastated country in the world. In past great earthquakes, for example, the loss of life was reported as 830,000 in the earthquake which occurred in Shan-si, Shen-si and Ho-nan provinces in 1556 and 100,000 in the Kan-su earthquake in 1920.

There are in China not only a great many earthquakes but also great floods and severe drought. The people of that country make scarcely an effort to control natural calamities, but let them have their own way.

At this time the great attempts are being made to develop the natural resources and industries of China and also to diffuse calture by the cooperation of Japan and China. It may be significant to investigate the seismic activity and its intensity in that country. From some investigation carried out, the writer has made the following conclusions:

(1) It is generally believed that Chinese earthquakes in the northern districts (Shan-si, Shen-si and Kan-su provinces) have been much severer than in the southern districts (Yun-nan and Kueichou provinces). This opinion is based on the false conclusion that seismic intensity is proportionate to the disaster caused. The writer believes that seismic intensity in these two districts is almost the same.

(2) The seismic intensity has not been so great as the loss of life resulting would appear to indicate. This is seen in the earthquake resistance of the remaining numerous pagodas in Shan-si, Shen-si and Ho-nan provinces, which were the gratest earthquake-devastated districts in the past. These pagodas were built of Chinese tile in the dynasty of T'ang and Sung.

(3) The seismic intensity in China is of the same character and intensity as on the mainland of Japan and Formosa at least.

(4) The magnitude of north China earthquake disasters is due to numerous landslides during earthquakes.

(5) The frequent occurrence of landslides is due to the peculiar nature of the soil.

---

* Dr. C. DAVISON, *Nature, April* **11**, 1936.

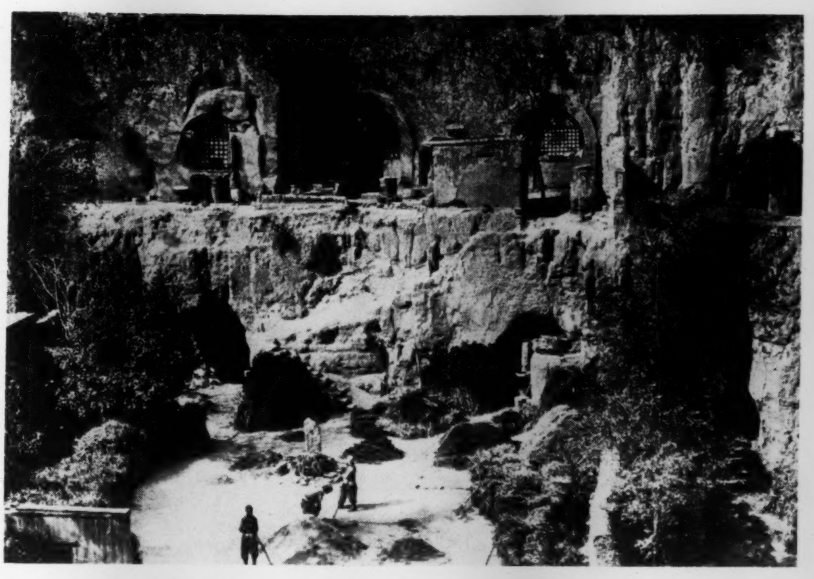

寫眞第 1. 山西省太原に於ける穴居の一例

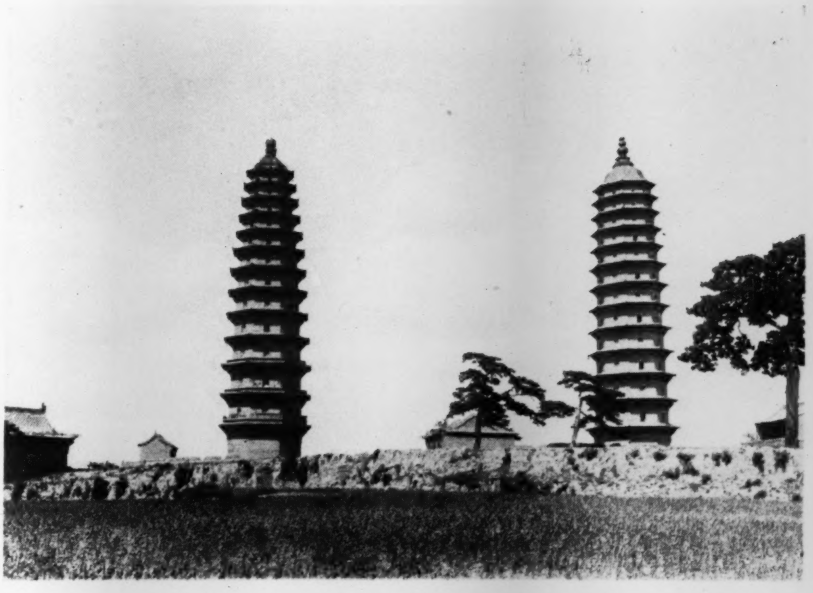

寫眞第 2. 永祚寺雙塔 關野博士撮影
高さ約 22(3) 丈と稱す

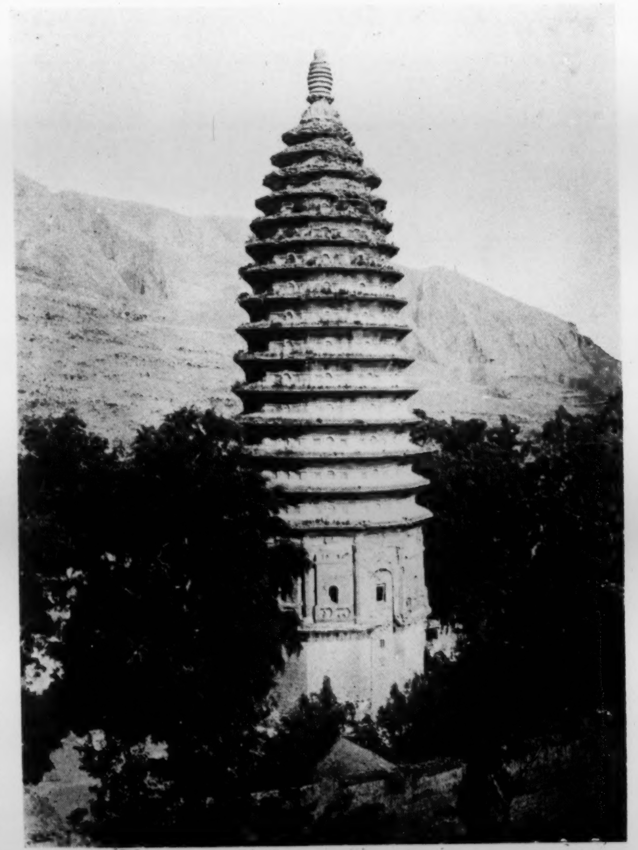

寫眞第 3. 嵩丘寺磚塔 關野博士撮影
支那最古の磚造建築と稱す

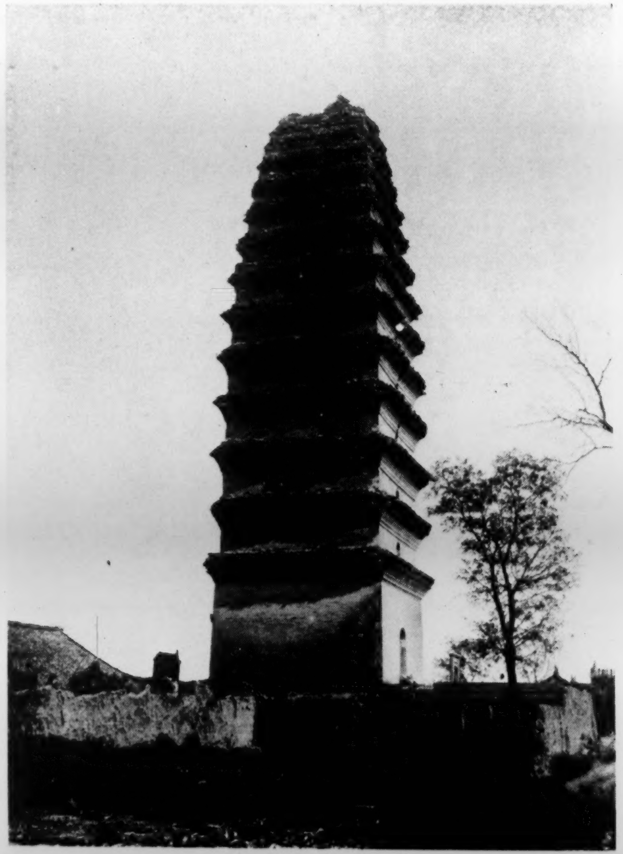

寫眞第 4. 薦福寺小雁塔 關野博士撮影

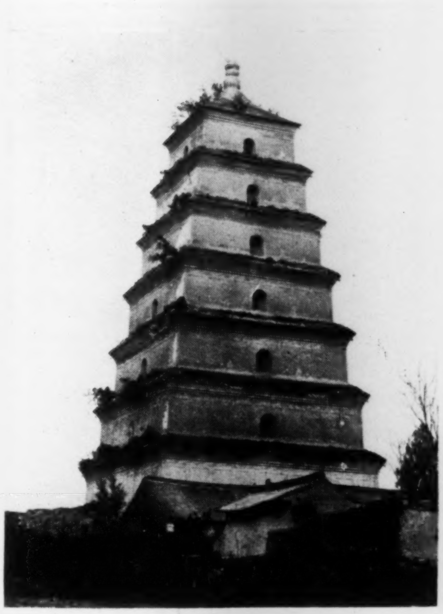

寫眞第 5.　慈恩寺大雁塔　關野博士撮影
高さ 60 米と稱す

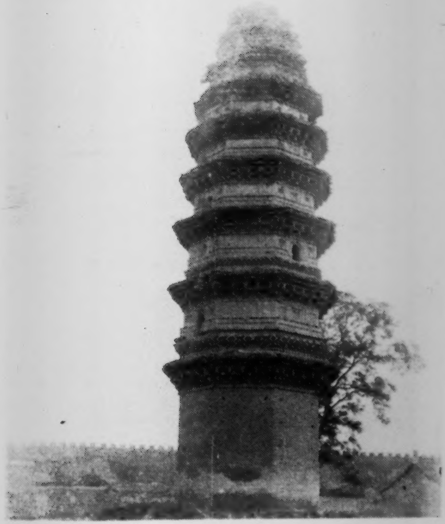

寫眞第 6.　扶風縣內磚塔　伊東博士撮影

（震研彙報　第十六號　圖版　齊田）

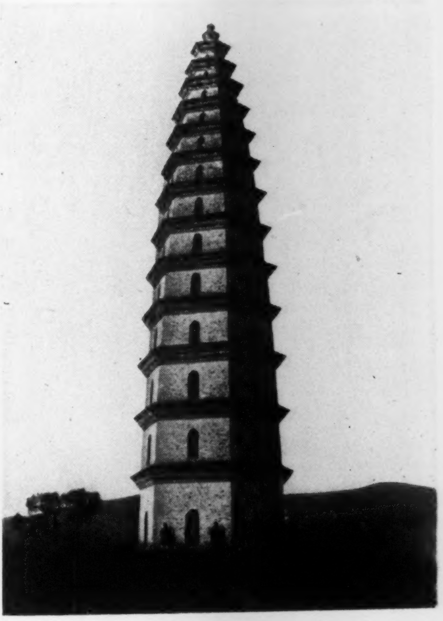

寫眞第 7.　四川省綿陽縣文風塔
伊東博士撮影

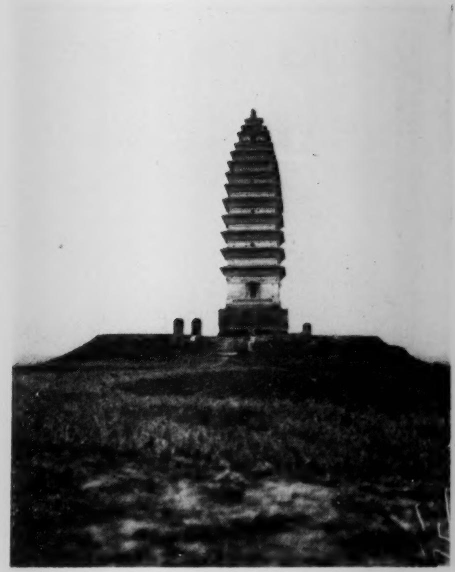

寫眞第 8.　齊雲塔（東白馬寺塔又は金塔）
高さ 160 尺と稱す　塚本博士撮影

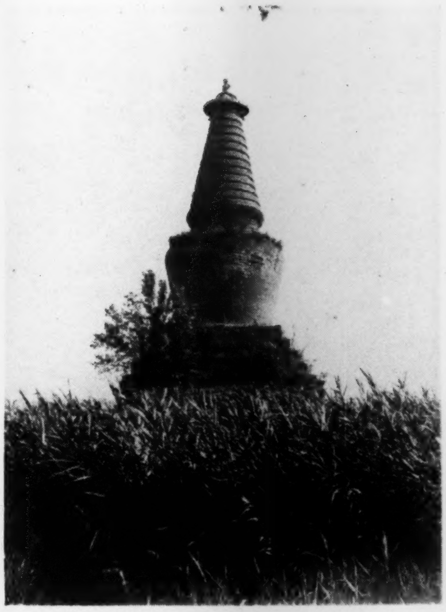

寫眞第 9. 淨明寺磚塔 關野博士撮影

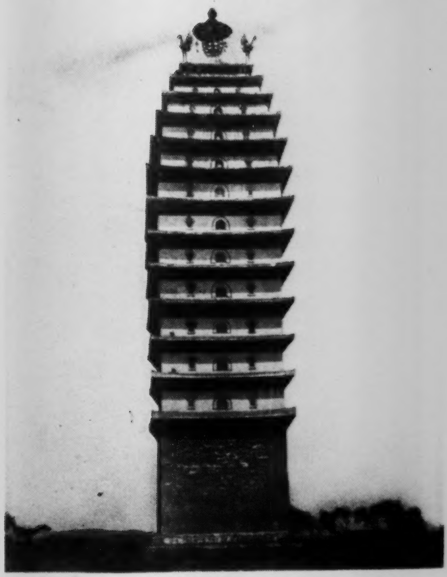

寫眞第 10. 常樂寺（東寺）磚塔
伊東博士撮影

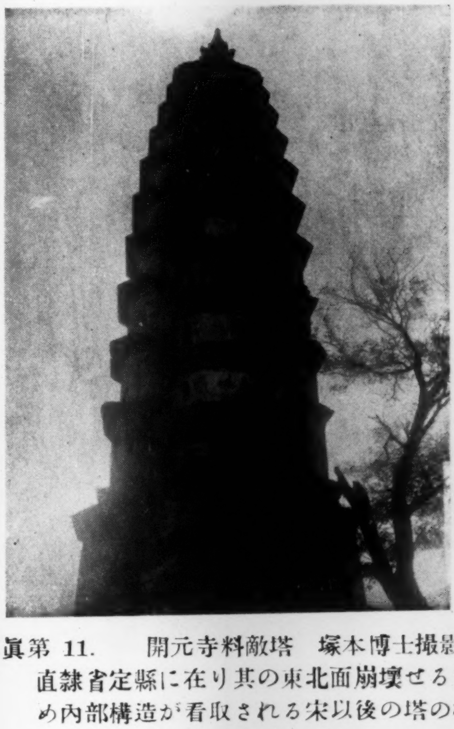

寫眞第 11. 開元寺料敵塔 塚本博士撮影
直隸省定縣に在り其の東北面崩壞せるため內部構造が看取される宋以後の塔の構造はこの型に準と言はれてゐる

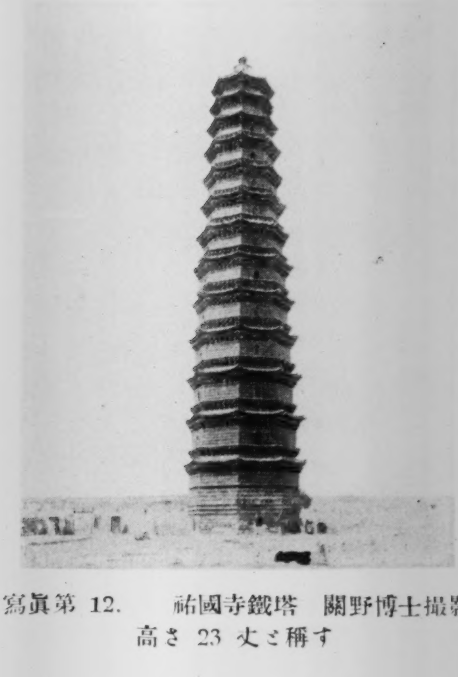

寫眞第 12. 祐國寺鐵塔 關野博士撮影
高さ 23 丈と稱す

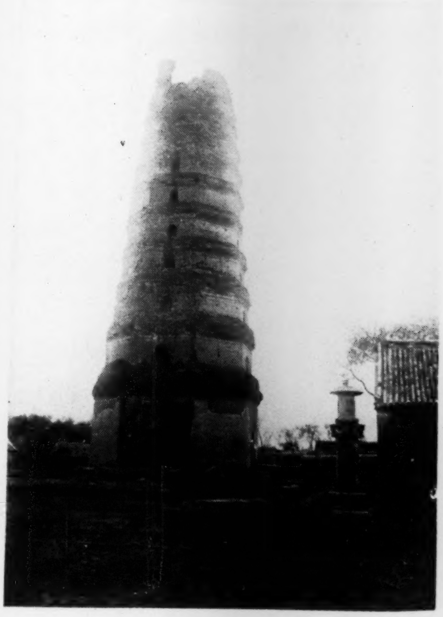

寫眞第 13.　開元寺磚塔　塚本博士撮影

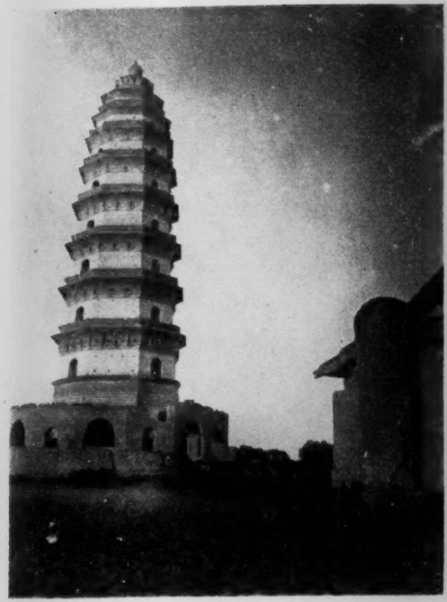

寫眞第 14.　慈相寺磚塔　塚本博士撮影
高さ 10 丈と稱す

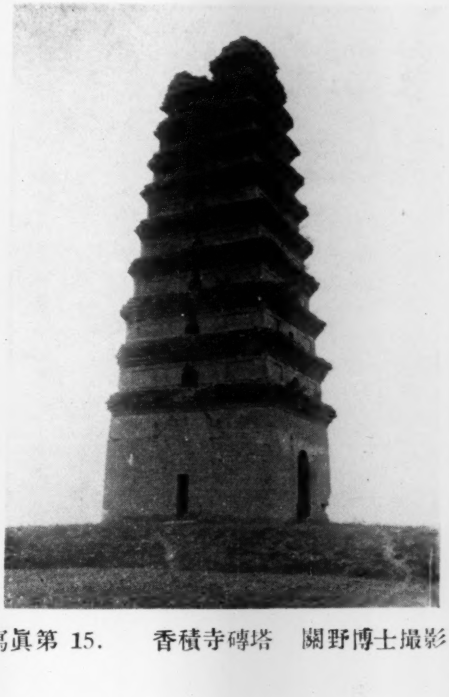

寫眞第 15.　香積寺磚塔　關野博士撮影

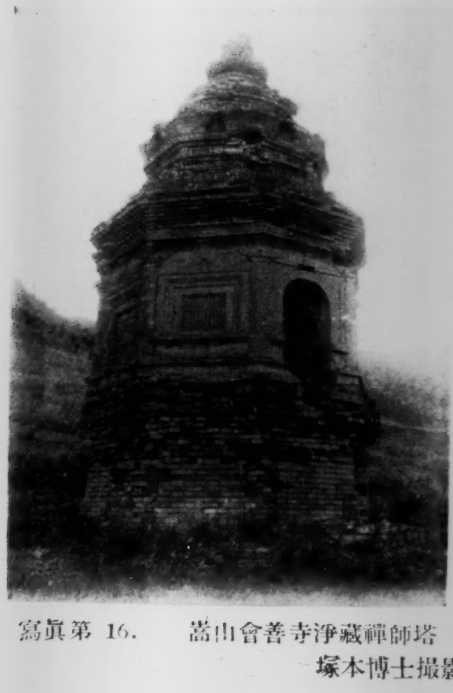

寫眞第 16.　嵩山會善寺淨藏禪師塔
塚本博士撮影

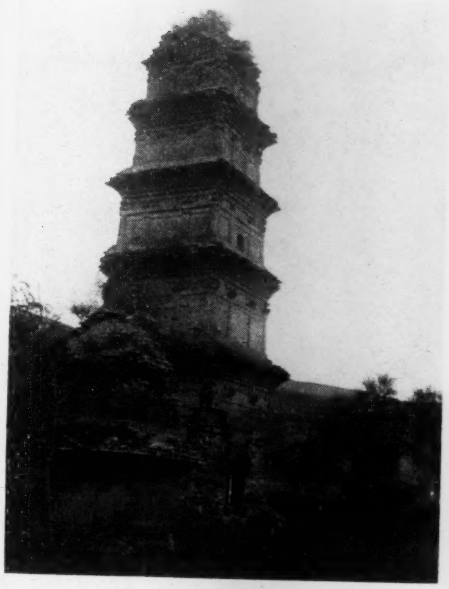

寫眞第 17. 興敎寺玄奘塔（5 層）
慈恩塔（3 層）圓測塔（3 層）
關野博士撮影

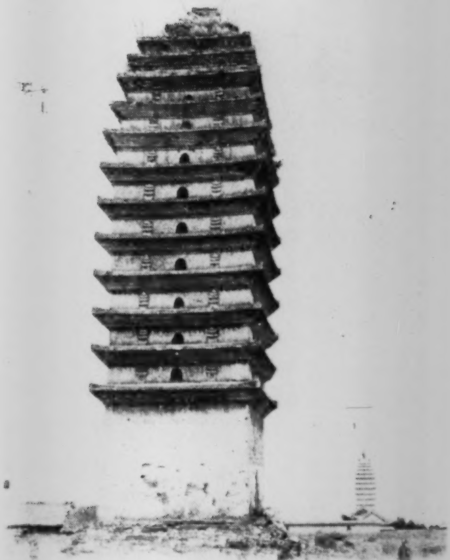

寫眞第 18. 慧光寺（西寺）磚塔
高さ 13 丈と稱す
伊東博士撮影

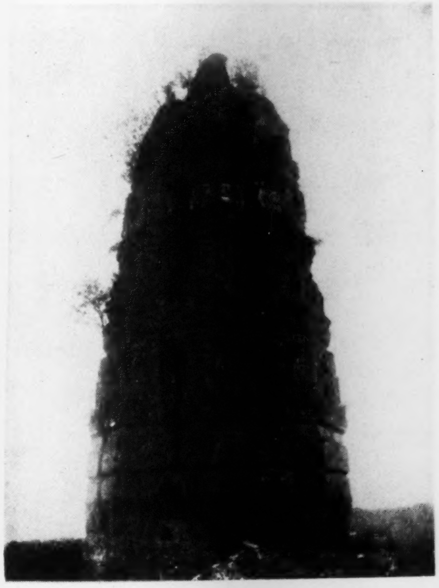

寫眞第 19. 雷峰塔 關野博士撮影
大正 14 年卒然崩壞

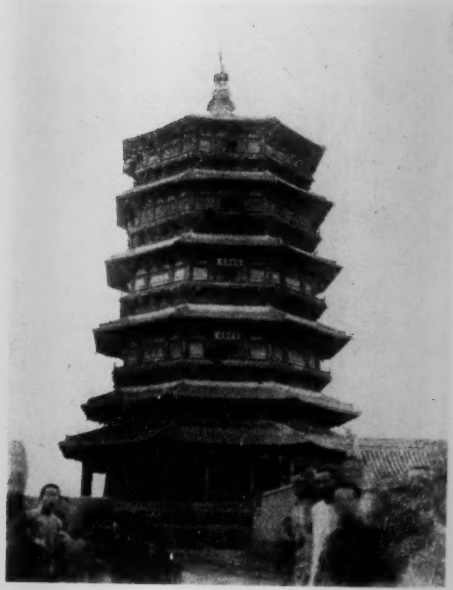

寫眞第 20. 佛宮寺木塔 伊東博士撮影
山西省應縣に在り高さ 360 尺と稱す

33.　靜岡縣庵原郡東部の地質構造*, **

地震研究所　大塚彌之助

（昭和8年6月20日發表——昭和13年3月20日受理）

目次

緒論
地形概要
層序
冲積統
　遷急點の問題
沼久保富士熔岩
洪積世段丘礫層
鷺ノ田礫層附足ヶ久保含植物化石
　砂泥層
岩淵安山岩體
城山安山岩體及び堰澤岩脈群
蒲原礫岩層
濱石岳層
小河內泥岩層
城山砂岩層
地質構造
入山逆斷層
水沼斷層
月代斷層
中山斷層
善幅寺斷層
城山斷層
斷層構造概說
撓曲及び皺曲
入山撓曲
松野撓曲
皺曲構造
地質構造から推定できる地殼運動
“Fossa Magna” 南部の地質構造一
　考察

緒論

東海道富士川の鐵橋を西へ向つて渡るとその西方に不規則な山形を示した一山地が急に聳え，我々は暫くこの山地をよけて狹い海岸平地を步まねばならない．こゝに記述し樣とするのはこの山地の地質構造發達史である．

本地域は NAUMANN 氏の “Fossa Magna” 地帶の南西隅にあるので，その地質構造の成立史を知ることは本地帶の構造地質學的意義やその地殼運動史を知る上から極めて重要なことである．

この地方は既に鈴木敏博士[1]が地質調査をされた事があり，第三紀層・安山岩・洪積世礫層等が發達することがわかつてゐた．特にこの附近の安山岩に就いて「安山岩ハ由比及富士兩河ノ間＝起伏スル小山岳ヲ占メ又更＝富士川ヲ經テ高原及萬野ノ地＝

---

* 本論文を東京帝國大學に於ける門弟の一人さして德永重康博士に捧ぐ．

** 本研究の一部は日本學術振興會の援助，補助を受けて達成したものである．こゝに筆者は同會に深謝する．

[1] 鈴木敏，1/200000 富士圖幅地質說明書（1888）．

伸張シ第三紀（下部ニ屬スル）岩層ヲ被覆ス．之ヲ構成セル輝石安山岩ハ黑灰若クハ暗褐色ノ石基ヲ有シ長石及輝石ヲ碁散ス．……」とあり，輝石安山岩が基盤の第三紀層を不整合に被覆することも知られてゐた．併しながら鈴木博士の調査はその目的上本地域の地質構造上の特性に迄言及されなかつたので，筆者は，こゝに新に本地域の地質構造に就いて補足したいと思ふ．

更に 1898 年故平林武博士2) は富士・愛鷹火山地質調査報文中に於いて富士川河口の西のこの山地を岩淵群火山と呼ばれ複輝石安山岩の集塊泥流と之を貫く含橄欖石輝石安山岩の存在を認められ，由比山・尻ノ池・高山・妙見山等の線狀に排列する圓錐丘（lineal cone）を古期火山と解され，之等の圓錐丘列中に火口の跡が存在する事をも指摘されてゐる．併しながら故平林博士の御研究もその目的が富士・愛鷹火山にあつたために，今こゝに述べやうとするが如き地質構造の問題を詳しく述べてをられない．筆者は兩博士の研究を基礎とし更にこの地方の地質構造を詳く述べてみたい．

筆者は本報告の概略を既に 1933年 4月日本地質學會總會で公にし，その摘要は同年 7 月の地質學雜誌3) に掲載された．併しその後研究の進捗と共に二，三の誤謬を發見し訂正しやうと欲してゐる時他方にはその年及び翌年井上春雄學士4) が「富士川下流々域の地形」及び「富士川下流流域の地質概觀.」と言ふ題で詳しい地形及地質學的記載を發表され，筆者は大いに啓發された．然れども井上氏の記事の中に筆者の觀察・解釋と異る點もあり，又井上氏の言ひ足りなかつた點もあり，筆者は之等に就いて彼の氣付いた點を補足しやうとも思つて，こゝに重複を顧ず新に本地域の地質構造の記載を試みた．この地方に興味を持たれる先輩諸兄の御批評を得れば幸と思ふ．本報告作製に當り靜岡高等學校教授今野圓藏學士に野外調査・植物化石鑑定の御援助を得たことを深く感謝する．

地　形　概　要

（地名は主として 1/25000 の地形圖　大宮・蒲原による.）

本地域は略ぼ海拔 500 m 前後以下の高度を有し，比高 1 km^2 で約 400 m の起伏の山地からなる．その中心部には北から雨乞山・嵐山・金丸山・571·4 m 山・444·8 m 山等の山巓を持つ所謂故平林武博士の岩淵群火山山稜が略ぼ N 45° E の走向に走り，この山稜の西北側と東南側とには海拔約 300〜400 m 前後の高度の多くの緩い傾斜の背面を持つ尾根（井上氏の第一段丘）が發達し，東南側の之等の尾根は東南方へ向つ

---

2) 平林武，震災豫防調査會報告 **24** 號（1898），pp. 69〜70.
3) 今野圓藏，大塚彌之助，地質學雜誌 第 **40** 卷（1933），第 477 號 408〜411 頁.
4) 井上春雄，地學雜誌 第 **46** 年（1934），539 號 18〜34頁.

て急に低まり海拔 160～120 m の高度の緩い傾斜の尾根（井上氏の第五段丘蒲原丘陵)* となり，更に急斜面によつて海岸低地と境してゐる．北西側のものは徐々に北へ向つて低まり，松野盆地を作り富士川溪谷に終はる．西は由比川・廻澤の上流の一直線狀の對頂谷によつて區切られ，その西には南北の走向を持つ山稜の群からなる濱石岳山地がある．

地形上特異な點の一つは由比川及び大晦日附近の廻澤の如く直線狀に並び，谷頭を互に反對側に向けてゐる流路で斷層を暗示する地形であるが，之は後に述べる樣にその大部は入山衝上斷層線と一致した谷である．

又，松野村鷺ノ田の山背面は海拔 410 m 前後の平夷な起伏面であるが，この平坦面のよく保存されてゐる地域の基礎は洪積統の殆ど水平な礫層から成り立つてゐるので，この礫層の堆積面がその後侵蝕作用・地殼變動のために變形され，その堆積面の面影が僅に鷺ノ田附近の山背面に殘されてゐるやうに見える．この平夷起伏の山稜は金丸山附近の N 45° E に走る山稜に比較して低く，之等兩者の境界は中山部落附近から略ぼ S 45° W の走向で南西へ向つてゐる．後に述べるやうにこの境界線の一部は衝上斷層と一致してゐる．

松野村南松野附近には東南西を急斜面で圍まれた矩形をした盆地があり，富士川がこの盆地を排水してゐる．この盆地を松野盆地と呼ぶがその周圍の急斜面には地質構造上撓曲及び斷層の證左が見出された．

富士川溪流は芝川附近で濱石岳山地を横谷として西から東へ流れ，南松野の東端で金丸山山稜を横切り，南へ曲つて海に注いでゐる．

この地方の地形はその地質構造の判明と共にそれと互に極めて密接な關係にあることが明にされる．地形とその解釋に就いては後章に再び地質學的記述に伴つて述べられる筈である．

層　　序

本地域に發達する地質系統・火山岩の層序を次の如く決定し得た．

a　冲積統

～～～～～～～～～～（不整合）～～～～～

a_1　沼久保富士基底熔岩

～～～～～～～～～～（不整合）～～～～～

du_2　岩淵段丘礫層及び蒲原段丘礫層

～～～～～～～～～～（不整合）～～～～～

$du_1 \sim dl_2$　鷺ノ田礫層（足ケ久保植物化石層）

～～～～～～～～～～（不整合）～～～～～

---

* この段丘に就いては後章遷急點の考察をした際に論及してゐる．

dl_2　岩淵安山岩體（金丸山安山岩・岩淵集塊岩）
（不整合）
城山安山岩體；堰澤岩脈.
$pd \sim dl_1$　蒲原礫岩層
（不整合）
$pl.$　濱石岳礫岩層
（不整合）
$m.$　小河内泥岩層
（層序關係不明）
$m.$　城山砂岩層

次に各層の分布・層位を記さう.

沖積統

沖積統は主として富士川沿岸及河口，蒲原海岸及び由比川河口に厚く堆積してゐる.

富士川河口は粗砂及び細礫の互層からなり，一部は沼久保富士基底熔岩の一部を不整合に被ふ.〔この不整合の露頭は Loc. 1* 庵原郡内房村瀬戸島；Loc. 2 岩淵町東海道鐵橋東端（鐵道橋にあらず)〕. 富士川の氾濫原の幅は平均 325 m で，沖積統はこの部分に薄く分布する.〔この平均値は芝川の北，長貫部落から岩淵鐵橋北部迄の約 250 m 間隔に 40 個の河幅を測定して得た値である.〕 河底礫の厚さは芝川の東南松野方面へ至る橋梁附近で約 3~4 m で，基盤には富士熔岩がない. 芝川の西北，橋上附近でその厚さ 8~20 m である.（何れも試錐で知つた事實）.〕

河口附近の堆積面は一扇狀地形に類似した表面を有し，駿河灣へ向つて三角洲狀に突出してゐる.

蒲原海岸も同樣な砂礫からなる海岸で，主として北の岩淵群火山・蒲原丘陵から由來した砂礫からなる. この北の山地からの供給量が過大なためこの山地からの溪底はこの海岸平野で一般にその兩側より高まり天上河道をなしてゐる.〔天上河道は Loc. 3 蒲原町小學校附近；Loc. 4 蒲原町堰澤の附近に見られる.〕

由比川河口のものは 20 cm 內外の大型な礫を含んでゐる. この沖積層は上流では入山部落附近，鍵穴附近に見られるが前述のもの等に比して餘り廣いものではない.

由比川流域に於ける遷急點と蒲原丘陵との地形學的關係.

由比川の流路は福澤（第 1 圖 M)・椚野（第 1 圖 L）に遷急點がある. 鍵穴部落附近の沖積層堆積面（Loc. 5）はその高度からみて舟場附近（Loc. 6）の段丘礫層の表面と同じ侵蝕基準で發達した樣に見られる. 鍵穴の沖積面は福澤の遷急點(Loc. 7)

---

* この Loc. の番號は地質圖內の番號の位置を示す.

を經て下位の冲積面に移つてゐる．この基準面の高度は大體鍵穴で 200 m，舟場の段丘で 200～180 m，その北の大代（Loc. 8）で 250～200 m を示してゐる．

由比川の中流入山から西へ入る渓谷には檜野の東（Loc. 9）に 1 つの大きな遷急點が瀧の形式で作られてゐる．この遷急點の上流の河底は 180～210 m の高度を有してゐて，舟場の段丘面と略ぼ類似の高度を有してゐる．

この遷急點の上端はその高度からみて，由比町の西北白井澤の附近（Loc. 10, 11）の 180～100 m 前後の段丘及び蒲原——由比町の北側の山地の尾根で代表される 160 120 mの段丘等と同一な侵蝕基準面であつたと思はれる．

第 1 a 圖 はこれらの河底の高度を流路に沿つて測定し，由比・蒲原の北にある山稜線の輪廓と共に南北の垂直面に投影したもので，河流も，山稜線も大體南北の走向に走るので，鍵穴・舟場・大代・檜野の各遷急點の位置及びその上流の河底の高度と由比・蒲原・北側山地の段丘との高度關係を一目に見ることができる．即ち第 1 a 圖 で 1, 2, 3, 4, 5 は第 1 b 圖 に示した様に各山稜線の輪廓を南北垂直面に投影したもので，SA, B, C は由比川の各流路の河底線の高度分布，qtr は由比川上流の鍵穴・大代附近の各河底と舟場段丘（t）の表面と蒲原丘陵の一般表面とを連續させる様に結

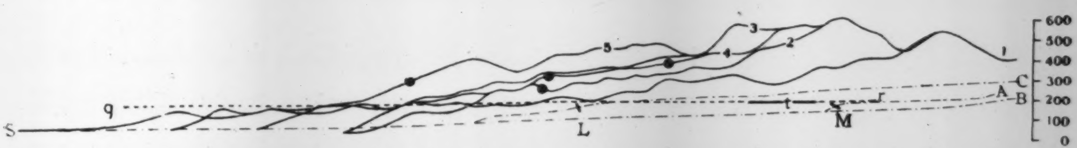

第 1a 圖　岩淵群火山（金丸山）山稜から南へ派出する尾根筋の高度さ由比川河底の高度さを南北の垂直面に投影した圖.

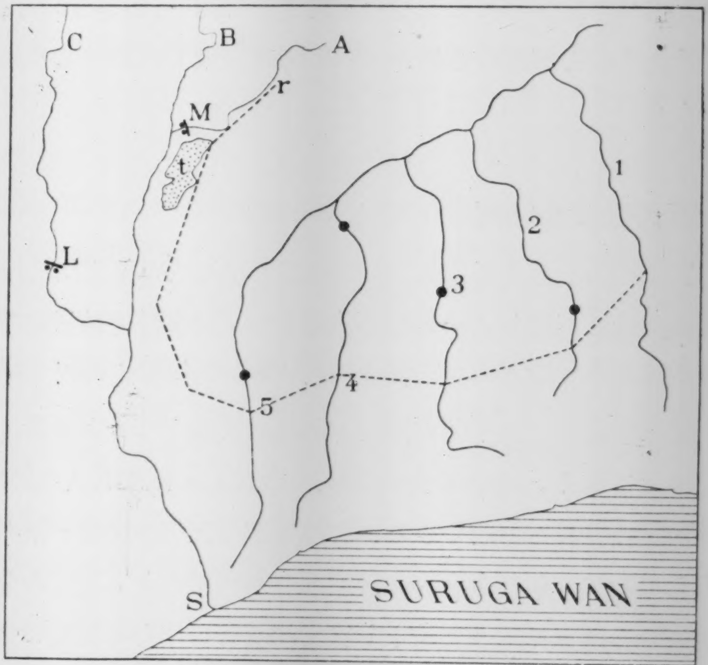

第 1b 圖　a 圖の平面圖．Plan of Fig. 1 a.
L and M=knick points of the Yui.
Dash line r=topographic boundary line of the Kanbara terrace.
SABC=the Yui river.

んだ傾斜した直線で，之等の三面が或る時代に同じ侵蝕基準で殆ど平衡狀態に達してゐたことを暗示してゐる.〔然るに槍野の遷急點より上流の河底 C のみは qtr 線より約 20 m 高位置にあるかの如く見えるが，之は作圖上室野附近の東西の流路が短縮されて投影されたために生じた差で，この短縮を補ふと SC の上流部も殆ど qtr 線に接してしまふ. 故にこの qtr 侵蝕基準地形が形成されて以來由比川の東西には著しい高度差を起す樣な個々別々な地殼變動があつた樣に見えない.〕 qtr 線の傾斜は約 2·3% である.

南松野・北松野の冲積統は沼久保富士基底熔岩が流下した後その南側の山地から由來した堆積物で作られたものであるが，有無瀨川の下流路は富士川のために清水でその流路を奪はれてゐる.

有無瀨川の上流部は海拔約 150～200 m 附近に比較的急湍部を有してゐる. 又松野盆地の東端を劃する血流川の上流は足ケ久保と平淸水附近に瀧の形式の遷急點を有し足ケ久保より上流部は高度約 200～250 m に達してゐる. このやうに岩淵山地から發する各溪谷には略ぼ類似の位置に遷急點を有し，之等の分布からみて多田助教授⁵⁾ が鈴鹿山地に試みられた如く岩淵山地が 100～150 m 程の比較的急な隆起性地殼運動を受けたものと解釋できる. 蒲原町附近の天上河道は斯の如き考へに都合のよい事實であらう.

沼久保富士熔岩

富士火山の基底熔岩流⁶⁾ の一部は本地域内の富士川沿岸，主として芝川・沼久保・岩淵附近に發達し，一部は冲積層下に，一部は冲積層の下から露出してかなりの高度にも分布してゐる. この富士熔岩⁷⁾ を沼久保富士熔岩と呼ぶ.

鈴木敏博士・故平林武博士・加藤武夫博士⁸⁾・伊原敬之助學士・井上春雄學士等の記述ある如く，本熔岩流の岩石は含輝石・橄欖石玄武岩熔岩で多孔質石板色 (slate color) の特異な熔岩である. その分布は芝川の溪谷・沼久保の溪谷・富士川沿岸に分布してゐて，何れも之等の河底及び兩岸にあり，之等の分布から本熔岩流が沼久保・芝川の各溪谷に沿うて流下し富士川溪谷に出たと推定でき，岩淵附近に露出する富士熔岩を前述したものゝ連續と假定すれば岩淵方面へも流れたものと推定される. 芝川

---

5) 多田文男，地震研究所彙報 7 號 (1928) 3 册，531～553 頁，

6) 故平林博士は本熔岩を三島一大宮熔岩の一部と考へられてゐる. 松野附近ではこの熔岩を俵石と呼んでゐる.

7) 以下便宜上富士熔岩と呼ぶものは本熔岩を指すこととする.

8) 加藤武夫，伊原敬之助，汎太平洋學術會議旅行案内書，C.～4 1926.

に沿うて流下した此の熔岩流の一部は芝川部落附近から富士川の溪に沿うて瀬戸島方面へ逆流した形跡も認められる.

この熔岩流の厚さは芝川附近で測定した値によれば平均約 11～10 m* で，その下半は美しい柱狀節理を示してゐる.

次に各地の露出に就いて記せば

身延電鐵芝川停車場に富士熔岩さ新第三紀層（濱石岳層）さの不整合をみる. Loc. 12 は富士熔岩の柱狀節理を示す露頭が兩岸に見られ，この上流 250 m で再び熔岩の基底の不整合が見られる. Loc. 1 で同樣な不整合が見られる. 橋場部落の一部は富士熔岩上にある，上述の各露出地の富士熔岩の表面の高度は橋場 110 m, 芝川 80～90 m である.

芝川の東の月代には富士川溪谷壁の途中に富士熔岩の殘片が侵蝕作用から取殘されて露出してゐるが，この熔岩の西部は海拔 50～60 m の高度にあるに反して，その東部は 100 m 以上の海拔高度にあり，兩者の間に略ぼ走向南北の西落ち斷層が存在してゐる. 寫眞 2 圖は之を示す. Loc. 13 はこの斷層の露出地・月代の東 身延線沿線でもよく觀察できる. 月代の東南（古田部落の對岸 Loc. 14）の富士川溪谷壁の途中にも富士熔岩流が見られる. この熔岩流の表面の海拔高度は 120～130 m, その基底面は 110～120 m に及び約 1000 m の間河岸段丘狀に續く. この熔岩流と基盤との間には礫層が薄く分布してゐるので富士熔岩流が過去の富士川河底に流れたと言ふ推定に對して都合がよい. 然るに沼久保（Loc. 15 and 16）及び北松野に露出する沼久保富士熔岩は海拔 60 m 前後の高度に低まり，前に擧げた高位置にある富士熔岩との間で撓曲して切斷されてゐる. この撓曲部の下（Loc. 15 の下）には水沼斷層が走つてゐてその周圍の撓曲運動のために斯の如き高度變化を生じたものと考へられる.

北松野の富士熔岩は更に東へ延びて俵石（Loc. 17）附近に迄延びてゐる.

この富士熔岩は沼久保の澤の上流にも分布してゐて，その一部はこの澤をも經て富士川河底に流下したことを示してゐる.**

富士川町岩淵の北端東海道鐵橋の東端（Loc. 2）に露出する多孔質石板色玄武岩は同樣富士熔岩である. その表面の海拔高度は約 25 m.

故に熔岩流の表面の高度と現河底の高度とを選ぶと第 2 圖の如くになり，假に富士熔岩の表面を原の河底の表面と平行であつたと定めると，兩者の高度分布の間に面白い關係が見られる. 即ち上流へ行く程高度差が大きくなり地盤隆起量が河口附近に少

---

* 芝川――岩淵間を厚さ 10 m で充たしたさするさ富士川溪谷に流下したものだけで約 4×10^7 m^3 以上の容積さなる.

** 津屋博士は芝川のものさ沼久保のものさを別々に流れたものさ解した方がよいさ言ふ考への樣である.

く芝川附近に大きいことを暗示し，又北松野——芝川間には地壘的地殼運動が存在したことを示す局部的高度變位が見られる．

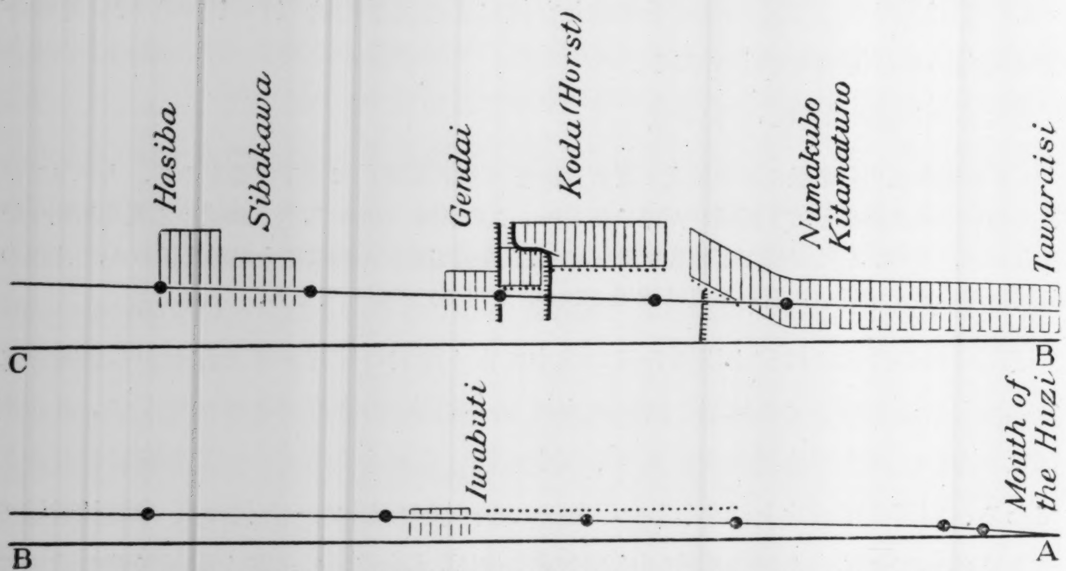
Hasiba
Sibakawa
Gendai
Kodu (Horst)
Numakubo
Kitamatuno
Tawaraisi
C
B
Iwabuti
Mouth of the Huzi
B
A

第 2 圖　富士川河底に於ける富士熔岩の高度分布．(Schematic profile of Huzi-lava flow along the river Huzi)　A B C は海水面．黑丸のある實線は富士川河底．縱線影の部分は富士熔岩．(Shaded area＝Huzi-lava.)

洪積世段丘礫層

段丘礫層はその分布區域によつて岩淵段丘礫層，蒲原段丘礫層等に分たれる．

岩淵段丘礫層は岩淵の背後に分布する段丘（寫眞 1 圖 a）を構成してゐる礫層で，段丘上には中の郷・富士川町の山手・籔下・小池等の部落が發達してゐる．段丘の表面の高度は海拔約 30～40 m で北の方が高く南へ向つて低まり，主として砂礫層からなり，礫は大型で徑 30 cm を超えるものも屢々あるが富士熔岩の礫を含んでゐない．他は現在の富士川の礫と類似のものからなる．之等の事實から岩淵段丘を過去の富士川氾濫原に類似した面が隆起して，僅に岩淵町背後に保存されたものとし，他は侵蝕し去られたと解釋した．堆積面の表面は平坦に近くよく保存されてゐるので新しい時代に成生されたことを示してゐる．表面に關東地方に見られる樣な關東ロームは見られなかつた．

由比川の上流舟場附近の段丘は既に沖積層遷急點の項で述べた樣に由比川の東岸に分布し，遷急點その他の研究から蒲原・由比町の北にある蒲原丘陵と略ぼ同じ侵蝕基準で形成されたかの如くに見える．故に鍵穴附近の溪底・舟場段丘の表面・蒲原丘陵の表面に點々と分布する礫層は略ぼ同時時代であらう．蒲原段丘の高度は岩淵段丘より高いので地形學的に後者の方が新しい時代に形成されたものであらうと推定できる．

蒲原町小金の東北部も段丘礫層を見るが，高度は低く海抜 25～50 m 程度で小範圍に分布してゐる．(Loc. 18, 19.)

之等の段丘礫層は何れも富士基底熔岩流出後の成生となす證左に缺き，富士川町岩淵町附近で富士基底熔岩に被はれぬことから，その流出前に堆積されて隆起し，段丘礫層となつたものと認めることができる．富士基底熔岩の流出の時代は種々の層序學的事實〔富士山の噴出物であると言ふ關東ロームの地質時代は洪積世末期と考へられてゐる．〕から洪積世末期か冲積世最初期と考へ得るから，富士基底熔岩の流下した時代より以前にあつた之等の段丘礫層の堆積した時代は勿論洪積世であらう．次に述べる鷺ノ田礫層は之等の段丘礫層より古いが植物化石からみてその地質時代を洪積世前半と考へ得るから，岩淵段丘礫層は洪積層としても新しいものであらう．

鷺ノ田礫層

靜岡縣庵原郡松野村鷺ノ田附近の地盤を作る厚さ約 150～250 m 以內の圓礫層を呼ぶ．(井上春雄氏の久保山礫層と同じものである．久保山部落は鷺ノ田礫層の上になく，濱石岳層の礫岩の上にあるのでなるべく筆者の既に提唱した“鷺ノ田”の名稱を用ひたい．) 鷺ノ田礫層を構成する礫は主として砂岩・珪岩・硬砂岩及び閃綠岩を主とし，安山岩質の礫をも多數に含んでゐる．之等の礫の大きさは拳大で往々徑 30 cm に達するものも少くない．この礫層中には砂層が介在する部分もあり，その層理は遠望すれば識別できる．この礫層の凝固程度は極めて弱く，地形圖にも見られる樣に，この礫層の露出してゐる崖には多數の崩壞が見られる．

第 I 表 足ケ久保化石植物群 (今野學士鑑定)

Abies firma Sieb. et Zucc. (現生モミ)	—	—	—	—	—
Chmae yparis obtusa Endl. (現生ヒノキ)	—	—	—	—	5
Finus sp. (アカマツ又はクロマツ)	—	—	—	—	5
Alnus japonica Sieb. et Zucc. (現生ハンノキ)	1	—	—	—	5
Carpinus laxiflora Bl. (現生アカシデ)	—	—	3?	—	5
Fagus nathorsti Konno. (新種・絕滅) (極めて豐富)	1	2	3	—	—
Quercus stenophylla Makino. (現生ウラジロガシ)	—	2?	—	—	5
Zelkowa Keaki L. *foss*. Nathorst. (現生ケヤキ化石種)	1	2	3	—	5
Ceratophyllum demersum? L. (現生キンギヨモ?)	—	—	—	—	5
Tetradenia foliosa Nees (現生イヌガシ)	1	—	—	—	5
Leguminoseites sp. (マメ科の一種) (豐富)	—	—	3?	—	—
Acer pictum Thunberg. (現生イタヤカヘデ)	1	2	3	4	5
Traxa natans L. var. *bispinosa* Makino. (現生ヒシ 但し葉は大形) (豐富)	—	—	—	—	5
Eurya sp. (サカキ屬の一種)	—	—	—	—	—

1＝麻積植物群 (長野)； 2＝茂木・天草植物群 (長崎)； 3＝屛風ケ浦植物群 (横濱市)；
4＝鹽原植物群 (栃木)； 5＝現生日本本州植物群.

この礫層の下部は泥層を介在し，その泥層中には屢々陸棲植物化石〔第1表〕を含んでゐる．特に *Fagus Nathorsti* KONNO（ナトルストブナ）と *Trapa natans* var. *bispinosa* MAKINO（ヒシ）の果實の化石とは饒産する種類である．未だ海棲の動植物化石を見出してゐないから本礫層は陸上堆積物であると考ふるべきものであらう．

鷺ノ田礫層の堆積狀態は殆ど水平に近いがその分布の東西兩縁は撓曲されて一部は斷層で切られ，その北部は松野盆地との間に撓曲・斷層構造を示してゐる．この礫層の堆積區域の表面は完全な平坦面でなく緩い起伏を有し，前に述べた岩淵段丘礫層の堆積面とは異る．鷺ノ田礫層は不整合に岩淵安山岩體の上に横はる．

分布

Loc. 20 松野村足ケ久保．足ケ久保の澤の東岸に新しく道が開鑿されて美しい露頭が見られる．薄い礫層を基底にその上に約 30～10 cm を單位とした薄層理を以て板狀泥層が殆ど水平に横はつてゐる．この板狀泥層は約 15 m の厚さで堆積し，その上に礫層が横はつてゐる．兩者の關係は井上氏の論文中の寫眞に示されてゐる．この泥層中から多數の植物化石〔第 I 表〕が產してゐる．

Loc. 21, 22, 23. には赤土を伴ふ殆ご水平に近い層位のこの礫層がみられる．Loc. 23 ではこの礫層が岩淵安山岩體上に横はり，こゝでは含植物化石泥層を含んでゐない．

Loc. 24. 足ケ久保から漆野への路にも不整合の關係が見られる．この礫層の層位は水平に近い．

Loc. 25. 粒良野の東斜面．岩淵安山岩體さの不整合を見る．

Loc. 26. 小溪谷底に上述の不整合關係がよく露はれてゐる．最上部に礫岩層を有し稍ゝ西斜し薄き泥層を介在し，次に明黄色の集塊岩を横へ，一枚の熔岩流を横へてゐる．泥層迄が鷺ノ田層である．

Loc. 27. 岩淵安山岩體の集塊岩さこの礫層さの接觸．

Loc. 28. 有無瀨川中流東岸に不整合をみる．

Loc. 29. 鷺ノ田礫層 崩れに露出する．

Loc. 30. 有無瀨川中流下平．この附近では實際の不整合の露頭を確めるこさはできなかつたが礫層の分布から推して Loc. 30 の位置を經て層向 N 80° W：傾斜 S 10° の礫層が存在する．

Loc. 31, 32, 33. は何れも鷺ノ田礫層の露頭．それらの內 Loc 32 は大晦日の澤東岸に見られる岩淵安山岩體に該當する火山岩層に對する不整合關係を示す．

Loc. 34, 35. も前さ同様．鷺ノ田礫層は東へ傾く．Loc. 33 から大晦日の澤への下り路でこの鷺ノ田礫層は不整合に岩淵集塊岩・安山岩の地質系統の上に横はる．

Loc. 36. 大代の南に不整合の露頭がある．この附近では不整合線は略ぼ等しい高度を保ち鍵穴の西側に達してゐる．鷺ノ田礫層は殆ご水平か稍ゝ東へ緩斜する．

Loc. 37. 香木穴の東南の澤．上から下へ觀察して行くさ上部に鷺ノ田礫層があり，次に不整合の面を境にして，岩淵安山岩體の熔岩流が横はつてゐる．この下に紅樺色か又は紅海老茶色の凝灰質沙層が横はり，再び安山岩の熔岩流があり次に集塊岩が横はつてゐる．

Loc. 38. 鍵穴の奧では不整合直上の鷺ノ田層は半凝固の泥層と礫層との互層で，岩淵安山岩體上に横はつてゐる． この互層の層位は稍ゝ西へ傾く．

舟場より東へ向つて登る山路は海拔約 300 m 附近から礫層となつてゐるが，その境界線の正確な位置は明でない． 松野村中山部落から S 30° W に向つて鷺ノ田礫層は井上氏の記せし如く後述の中山斷層線によつて境されてゐる．

大晦日の澤の附近及び久保山では入山逆斷層で切られて南北の境界線を示してゐる．

鍵穴の北側斜面の上端の崖崩は何れも鷺ノ田礫層のものである． 礫層は殆ど水平．

上記の外，鷺ノ田礫層の分布地は漆野・平清水等の地域である．

Loc. 39. 30°～20° 程で北へ傾く礫層と泥層との互層の露出． この互層は岩淵安山岩體を不整合に被うてゐる． その不整合面近くに西北へ 40° 前後に傾く正斷層をみるし，その下位には安山岩の大角礫が含有され，又一部には極めて薄層理（—薄層理の厚さ約 0·5 mm）の凝灰岩層がある． この薄層理凝灰岩中の層面を檢すると微細な植物質破片及び植物化石が含まれてゐる． その層位から判斷して鷺ノ田礫層はこの附近で撓曲し下つてゐるものと考へられる． この露頭の北の平清水では N 20° W : 50°～60° SW の層位のものが多く Loc. 39 との間に一向斜又は小斷層がある樣である．

Loc. 40. Loc. 39 と似た關係を確め得る．

Loc. 41, 42, 43, 44. 各露出地は何れも半凝固砂層．

鷺ノ田礫層は矢所・十字金・鐙田・新井の線に沿うても撓曲構造を示してゐるが，その東側の岩淵安山岩體との接觸の性質は確め得られなかつた． 併し兩岩層の最も接近した地點を結ぶと地質圖に示した樣になる． 鷺田礫層の層向はこの線と斜交する方向を示してゐる．

Loc. 45. 鷺ノ田礫層　層向 N 30° E : 傾斜 W 25°.

Loc. 46. 鷺ノ田礫層　層向 NS : 傾斜 W. 10°.

Loc. 47. 鷺ノ田礫層中の半凝固泥層． 殆ど水平．

Loc. 48. 鷺ノ田礫層　層向 N 70° E : 傾斜 W 20～15°.

Loc. 49. 鷺ノ田礫層　東へ緩斜する．

Loc. 50, 51. 嵐山・雨乞山附近に N 20° E に走る山稜があるが，矢所から室野への峠の近くから山稜線に沿うて，高度約 300～350 m 程の間に礫層が水平に分布してゐる． 筆者はその高度から判斷して鷺ノ田附近の礫層の高度と類似なので鷺ノ田礫層と見做した．

上述の各露頭から判斷して鷺ノ田礫層は松野村鷺ノ田附近， 松野村三十坂， 漆野平・清水附近，雨乞山山稜の三ケ所に分布し，それらの內三十坂・漆野・平清水附近は堆積後矩形に陷沒したと解釋できる．併しながらこの陷沒區域の周緣の東・南・西は主として撓曲構造で，その一部には小規模な正斷層が有る．

礫層の厚さは鷺ノ田附近が最も厚く約 250 m に達するが，雨乞山山稜のものは數 10 m 以內である．

鷺ノ田礫層中に含まれる化石は第 1 表の如く，Loc. 20 から植物化石が産するのみである．その概略は今野圓藏教授の御鑑定を得て次の樣な結果を得た．

“種名を決定し得たものは 11 乃至 10 種，絕滅種は僅に 1 種で全體の 1 割に過ぎない．中新統・鮮新統に普通な *Sequoia*, *Taxodium*, *Liquidambar* 等の如き現生に於ける內地以外の要

> 素を含まない．故に之は中新世•鮮新世の植物群ではなく，より新しい時代のものに違ひない．併し最も普通に産するブナの一種[9]は日本には現生しないものである． それはアメリカブナでもない． 又之と同一種のブナは嘗て Nathorst 氏が横濱化石植物群[10]中から *Fagus sylvatica*（歐州現生）の誤名の下に發表したもので，*F. sylvatica* とは側脈數が異り，從て別種であるが長葉柄で，葉身は卵狀形，長尾頭，廣底で，最下位脈長く，波狀葉緣には常に狹三角形の單鋸歯を有する點で，麻積化石植物群中に最も普通に產する種（今野が前にアメリカブナとして誤報したもの）と同系統のものらしい． 又茂木•天草化石植物群中にアメリカブナとして報ぜられてゐるものの内にも同系統のものがあるらしい． 本植物群のブナは側脈の數に於いて，又小形な點に於てはホンブナと似てゐるが，葉形と特に葉緣とに於いては全く異る． 本種は鹽原植物群及び信州荒船山附近產中には見られない． 之等の事實を綜合すると，本植物群の時代は洪積世と見做してもよく，植物群からは橫濱植物群に近いが， 絕滅種の率が少いから橫濱植物群より或ひは若いかも知れぬ，而も鹽原化石植物群より古いものと言へる． 又ヒシやキンギョモを除けば多くは山地性樹種からなり，ウラジロガシ，イヌガシ，乃至サカキ屬のやうな常綠濶葉樹が多く，暖帶的氣候を指示するものが含まれてゐることは注意を要する.”

上に擧げたやうに今野教授の植物化石の御研究結果から鷺ノ田礫層の地質時代は洪積世下半で橫濱植物化石に近似で鹽原植物化石群より古いものであることが推定できる．

岩淵安山岩體 （金丸山安山岩び岩淵集塊岩）

富士川町・金丸山附近に發達する安山岩・集塊岩よりなる一安山岩體を呼ぶ．含橄欖石・輝石・紫蘇輝石・安山岩・紫蘇輝石・輝石安山岩等の岩種よりなり，含橄欖石複輝石・安山岩は岩脈として複輝石安山岩を貫いてゐる場合がみられる．故平林武博士[11]が岩淵群火山と呼べるものは本安山岩體である．層序上本安山岩體は鷺ノ田礫層に覆はれ，蒲原礫岩層上に橫はるを以て兩層間に介在する．

此の安山岩體の安山岩質熔岩流間に赤色又は紅樺色の凝灰質火山砂層が屢々介在してゐる．斯の如き赤色又は紅樺色の凝灰質火山砂層は富士川町（岩淵町）の西の雨乞山東南麓，嵐山東麓，由比川上流香木穴澤の南斜面，廻澤の上流大晦日附近等に露出してゐる．

下位の蒲原礫岩層とこの安山岩體との境界は蒲原町北側丘陵内の溪谷底で觀察できる．岩淵安山岩體の鼠色の細粒凝灰角礫岩が不整合關係で蒲原礫岩層及び堰澤岩脈群を被せて分布してゐる．この凝灰角礫岩の層位は殆ど水平か又は北へ緩く傾いてゐる併しながら蒲原町以東では粗粒凝灰角礫質に變化してゐる．この粗粒凝灰角礫質岩中

---

9) 今野圓藏，大塚彌之助，前揭（1933）に於いて *Fagus Nathorsti* の新種名が與へられてゐる．

10) 筆者の長沼統屏風ケ浦層に含まれるもの． 地震研究所彙報第 **15** 號（1937）4 册．

11) 平林武，前揭（1898），pp. 69.

には小豆茶色（Ocher red）色の複輝石安山岩角礫を含んでゐるので，この角礫によつてこの地方の他層の凝灰角礫岩と區別できる．

富士川町西側の丘陵を作る岩淵安山岩體は主としてこの凝灰角礫岩である．故平林武博士が“岩淵集塊質泥流”とされたものの一部は之に該當する．

富士川町木島の北部ではこの凝灰角礫岩が圓礫層を介在して露出してゐる．この凝灰角礫岩の一部には前に述べた小豆茶色の複輝石安山岩角礫を含んでゐる．

由比川東岸では上に述べたやうな鼠色の凝灰角礫岩がなく，小豆茶色の複輝石安山岩角礫を持つ粗粒凝灰角礫岩が直に蒲原礫岩層上に不整合に載つてゐる．

入山部落の東 444·8 m の山稜もその岩種から岩淵安山岩體に含めたが，Loc. 8 で蒲原礫岩を不整合に被ふ露出が見られる．

廻澤の上流大晦日の東部では第3圖に示す様に蒲原礫岩を最下に赤色又は紅樺色の凝灰質砂岩を介在して岩淵安山岩流が横はり，最上部に鷺ノ田礫層が横はつてゐる．この安山岩體は大晦日部落の東北では薄く僅に 100 m 以内の厚さしか持たぬが，その東南では厚くなり，508·9 m の山巓を作つてゐる．この附近には入山衝上線が走つてゐるために，この安山岩體は濱石礫層とこの衝上線で接してゐるが，安山岩體の崖堆の一部は衝上線を被うてゐる．平林武博士[12]が“又此一連ノ群火山＝離レ西北＝二个小丘ヲナシテ同一岩石ノ露セルモノアリ．……”と記されてゐるものは恐らくこの 508·9 m の山巓に露出する岩淵安山岩體を指されたのであらう．

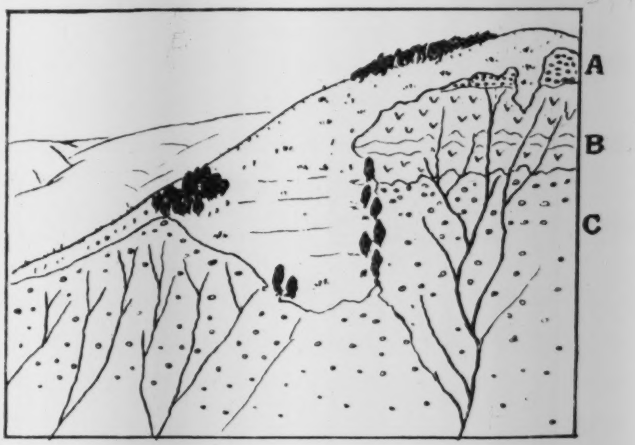

第 3 圖　大晦日澤東側．谷壁の露出面
A＝鷺ノ田礫層 (Saginota gravel.)
B＝岩淵安山岩體 (Iwabuti andesite mass)
C＝蒲原礫岩層 (Kanbara conglomerate bed.)

松野村北松野附近ではこの安山岩體は富士川を超えて水沼・沼久保の西側の丘陵方面へと延びてゐる．

本安山岩體の構造は比較的露頭が多いので，精査することによつてかなり復元できるが，本研究の目的から稍々離れるので後の調査に譲ることとした．

---

[12] 平林武，前掲 (1898)，p. 70.

城山安山岩體及び堰澤岩脈群

城山安山岩體は蒲原町城山の西北麓溪谷底に露出する安山岩體を言ふ．主として紫蘇輝石・輝石・角閃石安山岩よりなり，外見淡褐色又は灰白色にして石英安山岩質岩相を呈し斜長石・角閃石の斑晶を肉眼で識別できる．この安山岩體は蒲原礫岩層中に逆入してゐるがその逆入岩體の一部は堰澤岩脈群として蒲原町堰澤附近及びその北部に分布してゐる．

入山部落の東南 390·0 m の山嶺は同じく角閃石を含む安山岩からなる逆入岩體で，その北部で岩淵安山岩體に被はれてゐる．

城山逆入岩體中には後に述べる城山砂岩層と呼ぶ大きな沈積岩の包裏物を有してゐて，又その安山岩は堰澤岩脈群のものに比して石英安山岩質岩相を呈し，その組織は稍々破壞されてゐる部分があり，砂岩の xenolith も發見されてゐる．蒲原礫岩との境界は西へ 30°～45° に傾き下る接觸面をなし，逆入體が下方に擴がつてゐることを示してゐる．この安山岩體の構造の研究は火山體下の構造研究に極めて必要なことがわかつてきた．他日本安山岩體の組織排列を研究してみたい．

堰澤岩脈群は城山安山岩體と同時に同じ系統の地下熔融岩體から逆入した角閃石を含む安山岩岩脈で，その分布は地質圖に示す様に走向 N 30°～40° E，傾斜は西へ急斜するものが多い．この岩脈中の岩石の組織は城山安山岩より堅緻であり，石英安山岩質岩相を呈してゐないで且つ比較的擾亂を受けてゐない．

これらの角閃石を含む輝石安山岩體は所謂岩頸の露頭をなしその逆出部を缺き岩淵安山岩體地域には未だ發見されず一部は直接に被覆されてゐるので，城山安山岩體及び堰澤岩脈等からなる火山體成生後侵蝕期を經てこの火山體はかなり削剝された．然る後岩淵安山岩體の噴出があつたものと解し得られる．地質圖 Loc. 52～75 は主として角閃石を含む安山岩を採集した地點である．

本安山岩の地質時代* はそれの逆入後の侵蝕期の存在とそれが蒲原礫岩を貫くことから鮮新世中頃以後 ──洪積世初期以前と言ふことができるのみである．

蒲原礫岩層

蒲原礫岩層は東海道線蒲原驛の北にある高度 200 m 前後の丘陵を造る稍々凝固し

---

* 角閃石を含む複輝石安山岩又は石英安山岩類は下丹那層・大磯地塊の土澤層・津屋博士の冷川層・久野學士の天正山層等に凝灰輕石及び熔岩流として報告されてゐるし，又最近には鈴木好一學士が房總半島の朝生原層から輕石として報告されてゐる． 之等は何れもこの地方の鮮新世中頃以後──洪積世中初期以前に推積した地層と言ひ得る．參考に迄附記する．

た礫岩層である．それを構成する礫の性質は井上春雄氏が記した如き珪岩・白色珪岩・綠色砂岩・閃綠岩質岩石等の外，玢岩・角閃石安山岩・次に述べる濱石岳層の礫岩・砂岩等であつて。礫の徑は 5 cm 内外のものが多く，礫の大きさは比較的揃ひ，礫間には胡麻白狀の砂粒が存在して礫を凝固せしめ，且つ中部には白色細粒砂礫の部分があり，上部は岩淵安山岩體の集塊岩に不整合に被はれ，下部はその周圍が何れも斷層か若い岩層で被はれるため如何なる岩石に接するか明でない．次の濱石岳礫岩の礫を含むことは重要な事實で下部鮮新統濱石岳礫岩より新期のものであることを示してゐる．故に地質時代は鮮新世中期かそれより新しく城山安山岩體より古い．

本層の化石產地は殆ど報告されてゐない．

この礫層は主として由比川溪谷以東蒲原町附近に露出し，一部は庵原郡內房村廻澤の上流に分布する．

蒲原礫岩層の層位は上述した樣な礫層中に見られる層理から層向・傾斜を測定した結果によると，由比――蒲原附近に露出する蒲原礫層は蒲原町堰澤附近を南北に走り北へ傾き下る背斜軸を持つ背斜構造をなす．地質圖附圖斷面圖にその狀が示してある層向・傾斜の分布は附圖に示した如くで，東部で層向 N 40°～60° W： 傾斜 NE 30°～40° で西へ行く程緩傾斜となり，西部では由比川・東山寺で層向 N 20° E――N 60°～70° E で傾斜 NW 40°～50° の層位を有する．

廻り澤上流に露出する蒲原礫岩層は入山衙上斷層に接するため層向略ぼ南北： 東へ急斜するか，又は垂直・逆轉して西へ急斜（70°～90°）してゐる．

蒲原礫岩層は多數の小斷層及び角閃石安山岩々脈によつて截られてゐる．前者は斷層の項に述べるであらう．後者は既に堰澤岩脈群として述べた．併しながら之等の斷層・岩脈等によつては蒲原礫層の層位は殆ど變形されてゐない．

濱石岳層

濱石岳層は由比川溪谷以西の濱石岳山稜を作る礫岩層その他粗粒砂岩の一群を言ふ．この礫岩は黑褐色又は暗綠色の堅く凝固したもので，礫は珪岩・閃綠岩・安山岩等で黑褐色又は暗綠色の凝灰質物で膠結されてゐる． 礫は不齊で或る者は徑 10 cm を超えるが或者は數 cm 以內である．濱石岳層の砂岩層は稍々灰色を呈し，海棲貝化石を含むことがある．その他薄き泥岩層，凝灰岩層等を有し，安山岩を伴ふことがある．井上氏の富士川層の一部は之に屬する．屢々小區域に輝石安山岩の迸入があり，その一部は後述する入山衙上斷層の成生初期か又はそれ以前に迸入したかの如くに見えるものもある，後の調査に讓る．

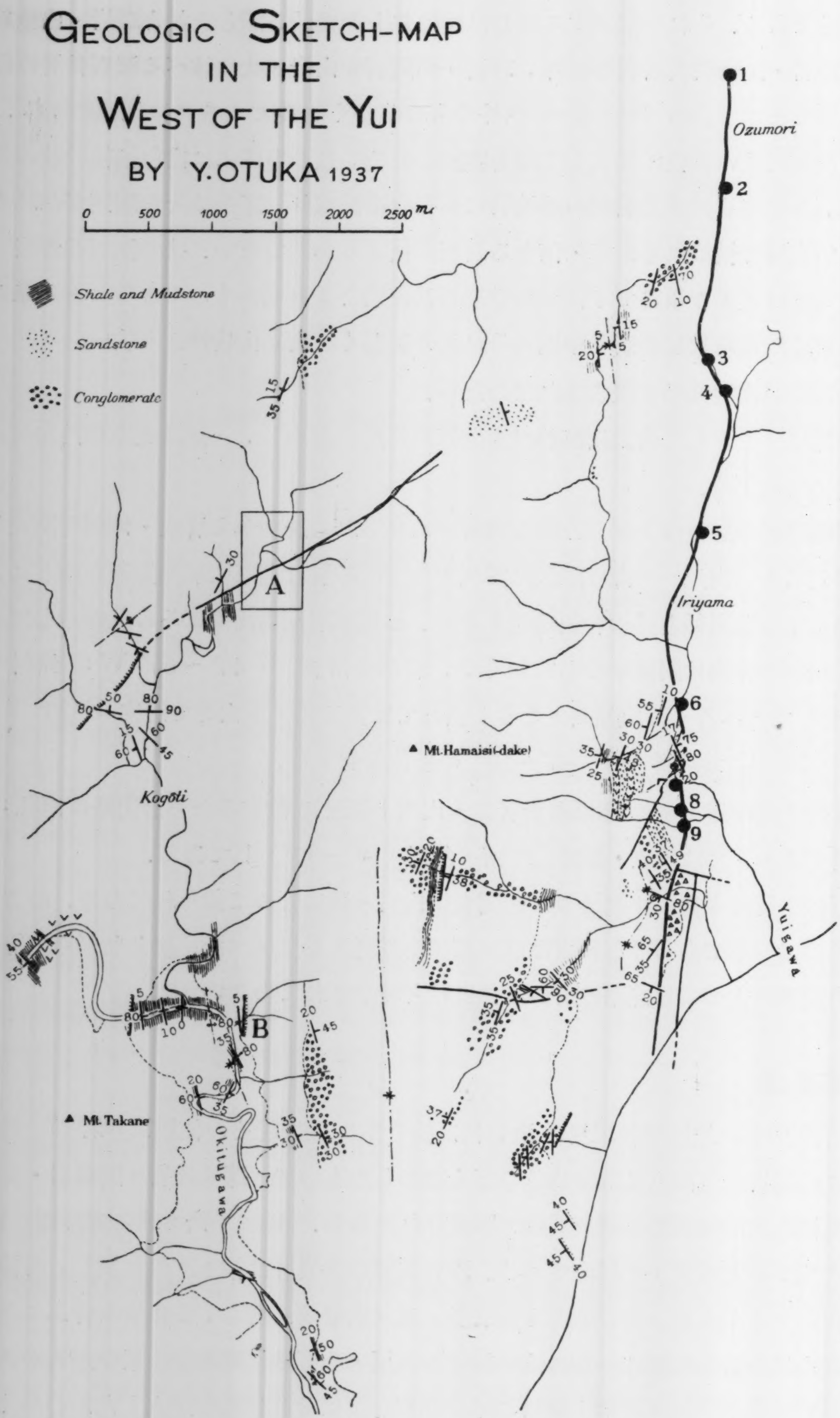
GEOLOGIC SKETCH-MAP
IN THE
WEST OF THE YUI
BY Y. OTUKA 1937
0 500 1000 1500 2000 2500 m
Shale and Mudstone
Sandstone
Conglomerate
Ozumori
Iriyama
Mt. Hamaisi(-dake)
Kogôti
Mt. Takane
Okitugawa
Yuigawa
A
B
1
2
3
4
5
6
7
8
9

第４圖　濱石岳山地の野稿圖.

この地層の上位の地層は問題にしてゐる地域では露出してゐない．この地層の下位の地層は問題にしてゐる地域の西では廣く東では狹く露出してゐて，濱石岳礫岩層に對して基底礫岩を伴はぬ不整合の層序關係を示してゐる．この下位の地層を小河内層と呼んだ．第4圖は濱石岳層とその下に横はる地層との露出の野稿圖であるが，之を見ると濱石岳層は濱石岳の山稜に沿うて略ぼ南北に走る向斜軸を有つ向斜構造をなしてゐる．この山地の地質調査完了の曉には後述する入山衝上斷層に對する構造關係も更に明になると思ふ．

化石は第 4 圖に示した様に由比川沿岸室野の南方の河底に露出する礫岩（第 4 圖 Loc.7）；西山寺の東の渓谷底等から産してゐる．

前産地* からは *Venericardia panda*（YOKOYAMA）ネコゼフミカヒ（新稱），*Cardium*（*Trachycardium*）sp., *Chlamys vesiculosus*（DUNKER）（ナデシコガヒ），*Chlamys* sp., *Amussiopecten praesignis*（YOKOYAMA）ナミウチツキヒガヒ（新稱），*Glycymeris* sp., *Ostrea* aff. *musashiana*（YOKOYAMA）ムサシガキ（新稱），*Conus* aff. *tuberculosus* TOMLIN ミウライモガヒ（瀧），*Lemintina muronoensis* OTUKA ムロノオホヘビガヒ（新稱）等を産し； 後の産地からは *Glycymeris* sp., *Chlamys* sp., 等で，*Glycymeris* sp., は兩産地共通な種である．

標本不完全なため鑑定できたのは僅に *Venericardia panda*, *Chlamys vesiculosus*, *Conus tuberculosus*, *Ostrea musashiana*, *Lemintina muronoensis*, *Amussiopecten praesignis* 等の 6 種にしか過ぎないが，*V. panda* は靜岡縣掛川統下部，13)・宮崎縣高鍋層群，14)・丹那隧道内の新第三系15)・二宮統の基底16)・田中學士の身延山北麓の靜川層17) 等に産してゐる．特に靜川層の礫質砂岩の特徴は濱石岳層の礫岩と類似してゐる．靜川層の遲澤化石動物群に就いては嘗て筆者は言及して，鮮新統下半なるべしと推定した．*Amussiopecten praesignis* は宮崎縣高鍋層群18)・靜岡縣掛川統下半19)・高知縣唐ノ濱層群20)・琉球の島尻層群21) 等に産する外，伊豆の鮮新統22) からも産し，下部鮮新統の特徴化石種と考へてゐる． *Conus tuberculosus* その他の化石は鮮新統乃至現生として報

---

* 之等の化石類に就いては東京帝大理科紀要に詳しい記載を發表した．

13) J. MAKIYAMA, *Mem. Coll. Sci. Kyoto Imp. Univ., Ser.* B. **7**, 1 (1931), pp. 6～8.

14) Y. OTUKA, *Geogr. Rev. Japan*, **6**. (1930), 7, pp. 1062～1064.

15) Y. OTUKA, *Bull. Earthq. Res. Inst.*, **11**, (1933), pt. 3, p. 548.

16) Y. OTUKA, 地質學雜誌 **38** 卷，(1931) 45 號，p. 178.

17) Y. OTUKA, 地質學雜誌 **41** 卷，(1934) 492 號，p. 568.

18) M. YOKOYAMA, *Jour. Fac. Sci. Imp. Univ. Tokyo*, (2) **2** (1928), 7; Y. OTUKA, 地理學評論，**4** 卷，7 號，p. 507～8.

19) J. MAKIYAMA, 前掲 (1931).

20) S. NOMURA, *Jap. Jour. Geol. Geogr.*, **14**, (1937) 3 and 4, p. 71.

21) S. NOMURA, *Sci. Rep. Tohoku Imp. Univ., Ser.* **2**, **1**, p. 60.

22) S. NOMURA and NIINO, *Sci. Rep. Tohoku Imp. Univ., Ser.* 2, **15**, 3, p. 180.

告されてゐる．故に濱石岳層は鮮新統の下半を代表する島尻層群・高鍋層群・唐ノ濱層群・掛川統・靜川層・丹那隧道の新第三系・伊豆の新第三系等と同時代と考へ得るが鮮新統以前又は以後と考へ得る資料は少ない．

小河內泥岩層

興津川の支流小河內川に沿うて發達する層理のよく見える泥岩層を主體とし，それに薄い砂岩・凝灰質砂岩層を介在する地質系統で，小型な有孔虫化石 *Pyrgo kogotensis* OTUKA MS を含んでゐる．

本層は濱石岳層の下に横はり，その地質構造極めて複雜である．

濱石岳層との境界は基底礫岩を伴はぬので一見整合狀を呈してゐるが．兩層の岩相及び地質構造の複雜さに相異が見られるので傾斜不整合的關係にあるかも知れぬ．本層が斯の如き層序關係で濱石岳層下に横はり，泥質である點は宛も掛川統下半と滿水層との層序關係，高鍋層群と妻層との層序關係に類似してゐる．幸にも濱石岳層中に含まれる貝化石類は下部掛川統に普通な種類からなるので，上の小河內層に關する類推が正しいとすれば小河內層は滿水・妻等の泥岩層と同層準のものと考へ得る．

小河內層を皺曲せしめてゐる皺曲の軸・及びこの層を截る斷層面の走向は一般に南北に近く斷層面は西へ傾斜するものが多い．第5圖及び第6圖はこの複雜な地質構造の一部を示したもので第5圖は小島村阪本附近の地質詳圖であり，第6圖は小島村但沼附近の東西斷面圖である．

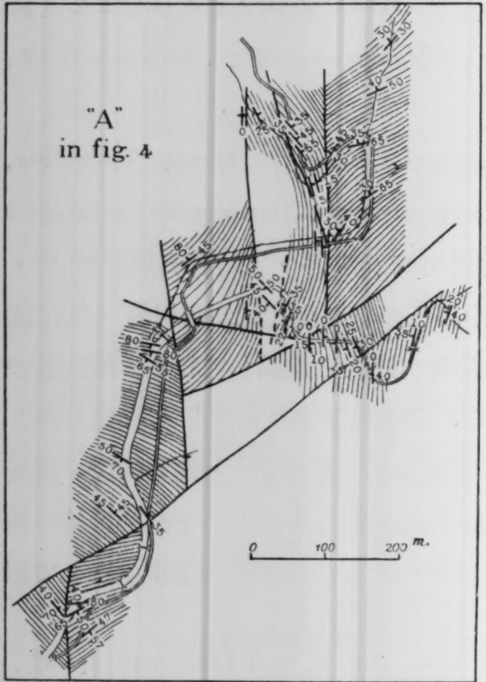

第 5 圖　小河內層の斷層構造の一露頭
Outcrop of faulted structure in the Kogôti bed.

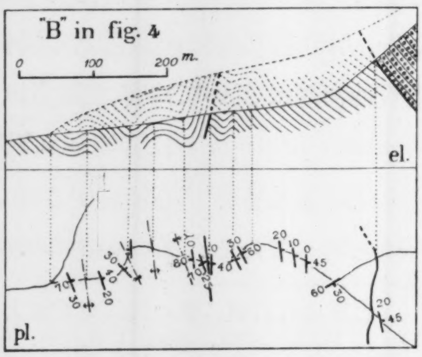

第 6 圖　小河內層の皺曲の一露頭.
Outcrop of folded structure in the Kogôti bed.

本層に該當する地層はこの地方の北部では身延山の西斜面に分布してゐることが柴田秀賢學士の調査で知られた．小河内層と同様 *Pyrgo kogotensis* OTUKA MS. を普通に含んでゐる．

城山砂岩層

城山層は蒲原町北側の山，城山山頂附近に露出する砂岩層である．主として凝固した凝灰質粗粒砂岩層でその下半は極めて凝灰質である．上半は種々の海成動物化石を含んでゐる．砂岩の色は新鮮乾燥せる場合は山鳩色を呈し，風化乾燥した場合は灰色又は橄欖色を呈す．砂粒は凝灰質で主として安山岩質砂粒を含んでゐる．部分的には石灰質砂岩になつてゐる．

本層の分布範圍はその西北南を城山角閃石安山岩體に圍まれ，その東側は斷層で蒲原礫岩層に接してゐて全く獨立した徑 300 m 内外の岩塊で岩塊内の層位は東縁では大體 N 15° E: NW; 西縁では東へ傾き下つてゐる ．東側の斷層はその走向と蒲原礫岩層の分布からみて西へ急に傾き下る逆斷層の様に考へ得る．この斷層の北の延長上では露頭で確め得るが，こゝでは蒲原礫岩と城山安山岩との接觸部で城山砂岩はない．

上に記した様に特別な露出狀態を示す弧立岩塊であるに關らず，動物化石類を豐富に含むため他層との層序關係が古生物學上から推定できた．採集した化石は次の様なものである.*

第 II 表　蒲原城山砂岩層產化石表

Astriclypeus integer YOSHIWARA　ムカシスカシクワシパン（新稱）［中新世］
Laganum fudsiyama tokunagai OTUKA n. sp.　（新稱）
Acila sp.
Glycymeris sp. (*vestitus* type)
Mytilus sp.　［中新世］
Lima konnoi OTUKA n. sp.　コンノミノガヒ（新稱）
Ostrea gigas THUNBERG　マガキ［現生—中新世］
Amussiopecten sp.　ナミウチツキヒガヒの一種［中新世—鮮新世初期］
Patinopecten kanbaraensis OTUKA n. sp.　カンバラホタテ（新稱）［中新世］
Chlamys sp.
Cardium sp.
Felaniella sp.
Dosinia matumotoi OTUKA n. sp.　マツモトカガミ（新稱）
Paphia hirabayasii OTUKA n. sp.　ヒラハヤシスダレ（新稱）［中新世］
Clementia nakamurai OTUKA n. sp.　ナカムラフスマガヒ（新稱）［中新世］
Trivia sp.　コシラタマの一種
Xenophora? sp.　クマサカガヒの一種？

---

* 化石の詳しい記載は東京帝大・理科紀要に掲載される．

之等の化石[23]は何れも風化保存不良であるが，*Astriclypeus integer* YOSHIWARA, *Patinopecten kanbaraensis* OTUKA, *Paphia hirabayasii* OTUKA, 及び *Clementia nakamurai* OTUKA, は日本の中新統から産してゐる．即ち *Astriclypeus integer* YOSHIWARA は德永博士[24]が山梨縣都留郡瑞穗村から報告されたのを初めに臺灣・琉球・石川縣金澤市外觀[25]・岩手縣二戸郡仁佐平[26]等の中新統からも報告されてゐる．

Patinopecten kanbaraensis OTUKA は美濃月吉の中新統[27]から產してゐるものと區別できない．*Clementia nakamurai* OTUKA は中村正義學士が富士山の西北麓三峠山東南麓に於いて有孔虫化石 *Operculinella complanata Japonica* HANZAWA 等を含む西桂層から採集したもの，佐川學士が日向油津統から採集したものと同一種である．

Paphia hirabayasii OTUKA は同じく三峠山麓の *Operculinella* 砂岩から採集した．

Amussiopecten 屬は下部鮮新統から中新統に限られてゐる屬である．

上述した種類の他は新種か又は種の鑑定不能なものからなる．

今上に擧げた種類をみると城山砂岩の化石動物群は濱石岳礫岩層の化石動物群とはその組成を異にし，この地方で最も近似なものとしては中村學士・久野學士等の西桂層の化石動物群を擧げることができる．試みに共通な化石種を擧げれば *Astriclypeus integer* YOSHIWARA, *Paphia hirabayasii* OTUKA, *Mytilus* sp., *Clementia nakamurai* OTUKA 等で兩層間の方が濱石岳層の動物群より遙に共通した化石種が多い．且つ之等の化石の大部は未だ鮮新統からは見出してゐない．この様な古生物學的特長から城山砂岩層は西桂層と略ぼ同時代と見做すことゝした．

西桂層の地質時代に就いては種々な說があるが中新世中期或は中初期とする說が正しい樣に見える．即ち矢部博士・半澤學士の高等有孔虫の研究，中村學士等の地質學的報文，關武夫學士の研究（西桂層は同氏の廣義の御坂層の一部に該當する．）等があり，何れも西桂層を以て中新統とする說の樣に見える．西桂層と *Lepidocyclina* 類を含む石灰岩レンズを含む御坂層との間には不整合が發見されてゐる．故に蒲原の城山砂岩層は *Lepidocyclina* を含む地層より若い．而して本砂岩層は濱石岳礫岩層及び蒲原礫岩層より古い地層であると言へる．

---

[23] 横山博士は上に揭げたものとは別に *Pecten yessoensis* (=*P. kanbaraensis*?), *Patella* sp., *Dentalium* sp., *Scutella* sp., (=*L. fudsiyama tokunagai*), *Corals*. を報告されてゐる．（震災豫防調査會報告 24 號，p. 68.）

[24] S. YOSHIWARA, *Jour. Geol. Soc. Tokyo*, **6**, 65 (1899)

[25] 鈴木敏, 1/200000 福井地質圖幅說明書, (1893), p. 34; H. YABE, *Sci. Rep. Tôhoku-Imp. Univ., Geol.* **4**, 3 (1918)

[26] *Bull. Earthq. Res. Inst.*, **12**, 3 (1934), p. 597〜8.

[27] M. YOKOYAMA, *Jour. Fac. Sci. Imp. Univ. Tokyo, Sec.* 2, **1**, pt. 7, p. 225. (as *jessoensis*.)

城山砂岩層の露出狀態は周圍三方を城山安山岩に圍まれ，他の一方東側は逆斷層で境され，城山安山岩との境は緩く東斜する暗葡萄色凝灰質砂岩・角礫凝灰岩を介在して接觸するので，地下で城山安山岩體を圍んでゐた城山砂岩がその安山岩體中に捕獲されて安山岩體の流動上昇と共に押し上げられ，若い地層中に弧立露出するに至つたものとしか考へられない．然るに城山砂岩層に該當する地層は筆者の調査區域内には知られなかつたし，又之より古い地質系統も本地域には知られなかつたから，若し假に蒲原礫岩中に迸入する前の溜の天井を作つてゐた岩層の破片であるとしてもかなり深處（少くとも 1km 以上の深さ）から分離移動し上つたと解さねばならぬ．

地質構造

地質構造の大體は既に層序の項の所々で言及してゐるが，次に斷層・撓曲・皺曲等に就いて詳細を述べやう．

斷層

入山逆斷層　本調査區域で最も著しい斷層は由比川溪谷から富士川方面へと本地域を南北に縱斷する入山逆斷層である．入山逆斷層は略ぼ由比川溪谷に沿ひ久保山部落を經て廻澤大晦日の澤に出て，大晦日の東北部から東北へ彎曲して，芝川古田の東に達する斷層である．この内入山部落附近に最もよくこの斷層が露出してゐるので，この部落の名稱をとつて入山斷層と既に命名しておいた．井上學士の室野阿僧線はその南半を代表し，KO 線の南部はその北半の一部を代表してゐる．

入山部落以南の露出

第 4 圖，Loc. 6：　入山衝上斷層の露出面は由比から入山への道路と由比川との交叉點に見られる．斷層の東側の蒲原礫層は傾斜が急となり，層向が斷層の走向と平行し，斷層に接した部分の蒲原礫層は著しく壓縮され，幅約 5 m 以内の帶の礫は壓碎されてゐる．西側は濱石岳礫岩層の砂岩で層向 N 35° E，傾斜 NW 60° 位の層位を示してゐる．

第 4 圖，Loc. 7：　この露頭は東山寺の南東にあり，井上春雄氏の詳しい記述がある．この露頭附近では，入山逆斷層の東側にある蒲原礫層がこの逆斷層に近付くに從つて層位を變へ撓曲してゐる樣が解る．この斷層面に近接した部分の礫は壓碎されてゐる．この斷層面に直角な方向の壓力が西からこの斷層面に對して加へられて礫が壓碎したかの如くに見える．

この逆の斷層面の露頭は河底によく露出し，斷層面の走向は N 5° W：傾斜約 70°

～60° W の衝上斷層* である．井上春雄氏論文第 4 圖は北岸に露出してゐる斷層面をよく示してゐる．寫眞第3圖も北岸に露出するものを示してある．

この衝上斷層線の西の濱石岳礫岩層中にこの斷層面から幅約 3 m の間に尙平行して數個の衝上斷層面を識別でき，斷層ネバの厚さも 30 cm 程の厚さがある．之等の衝上 斷層の各斷層鏡面に生じた平行條線は平面圖では西北から S 30° E の方向へ向き，鉛直線に對して下方から上方へ向つて約30° の角をなしてゐる．故にこの衝上斷層に沿うてその兩側は垂直變位を主要なものとして，水平的には西側の地域が相對的に東側に對して南へ移動したことを示してゐる．

この衝上斷層面の西側の濱石岳層の砂岩・凝灰岩は層向 N 17°～30° W：傾斜 E 75°～80° の層位で露出してゐる．略ぼ走向 N 60°～70° E の北へ急斜する斷層群によつて截られてゐる．この N 60°～70° E の走向の斷層群は入山衝上斷層には影響を與へてゐぬ．この群中の斷層線の分布から考察すると，入山衝上斷層の東西兩側が互に壓し合ひつゝその東側が相對的に西北下方へ，その西側が南東上方へ移動した際に生ずる二次的剪力斷層と解した．この剪力斷層の兩側の移動の方向は第4圖の如くで入山衝上斷層の兩側の移動方向に對して反對の性質を示してゐる．この様に主斷層の兩側の變位に對して一見反對の性質を示してゐる從屬的斷層は Cloos の可塑性物質を使用した斷層形成運動の實驗に見られる "antithetischer Verwerfung に類似した現象の様に見える．卽ちこの様な二次的剪力斷層で切られた各斷片は入山衝上線の兩側が水平方向にも移動したゝめに北のものから順次轉回してそのために二次的剪力斷層の兩側で北のものが東へ，南のものが西へ移動したかの如き狀を呈したと解し得る．

第 4 圖，Loc. 8, 9 は何れも上に述べた濱石岳礫岩層の砂岩と蒲原礫岩との分布によつて推定される斷層の露出である．

第 4 圖，Loc. 9 の南では入山逆斷層の延長上には上の様な特徴が見られずに蒲原礫岩層が約 250 m 東へ移動して分布してゐる．第 4 圖でもわかる様に，東へ移動した蒲原礫岩層の西端の性質が斷層であるか，不整合であるかは知られない．唯だ蒲原礫岩層の層位からみると斷層とした方が適當であらう．併しながら入山衝上斷層の延長上にある濱石岳層中には著しく層位の壓碎擾亂された帶があり，その東側には複輝石安山岩の集塊岩質礫岩が分布し，その西側には集塊岩質礫岩の薄層を挾む砂質泥岩層が横はつてゐる．故に入山衝上斷層はその儘この擾亂された帶に續け，蒲原礫岩層の東への移動は横斷層によつて移動されたものと解した．

---

* 衝上斷層は逆斷層中斷層面 45° 以上のものを呼び，thrust fault の邦譯である．upthrust downthrust の區別はあるが相對的な問題であるから暫く何れの意味をも含める．

入山部落以北の露出

第 4 圖，Loc. 5.　由比川河底に蒲原礫岩層と帶綠色の凝灰岩質砂岩層との境が略ぼ走向 N 20°～15° E：傾斜垂直或ひは W 80° 程度で露出してゐる．

第 4 圖，Loc. 4.　この露出面では斷層の東側の蒲原礫岩層は地表下に隱されて，蒲原礫岩層の上部に横はる岩淵集塊岩・安山岩の岩層が濱石岳礫岩層と斷層面で接してゐる．この露出は寫眞 4 圖に示した様に由比川の支流久保山澤の河底に露出してゐる．走向 N 5° E，傾斜 W 6 5°．

第 4 圖，Loc. 3　では岩淵安山岩體も地表下に沒してゐるために，鷺ノ田礫層が略ぼ垂直或ひは西へ急斜する斷層面で接してゐる．鷺ノ田礫層はこの部分で層位を層向南北：傾斜垂直にしてゐる．

久保山部落は入山衝上線の東側濱石岳層上にあり，部落東端の南北に走る一侵蝕谷に沿へる入山衝上斷層線によつて鷺ノ田礫層と接してゐる．斷層面の傾斜は西へ急斜してゐる．

大晦日の東の南北に走る澤は略ぼこの衝上斷層線を代表してゐるが一般には澤底より東側にある．

第 4 圖，Loc. 1　で斷層面は走向 NS：傾斜西へ 60°～55° 或は更に緩で，その東側には蒲原礫層が逆轉西へ急斜して露出してゐる．

Loc. 77, 78 （地質圖）で入山衝上斷層が東北へ彎曲してゐることは確め得たが，之から富士川北岸古田へ續く途中の露頭が確め得られなかつた．

Loc. 79 （地質圖）の身延電鐵線沿道で，濱石岳層と岩淵安山岩體の續きとその境の斷層とが明に見られるが，その北方が如何に分布するかは未調査である．

入山衝上線は地形學的にみると芝川方面へ續くかの如くに見えるが，仔細に地質調査をして露頭を確めて行くと，地質圖に示した様に東北へ向つて彎曲し，古

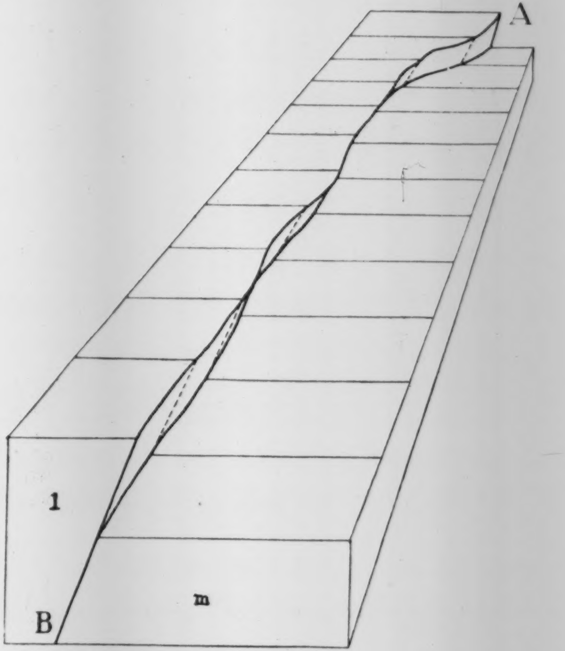

第 7 圖　入山衝上推し被せ斷層の立體圖.
Fig. shows the schematic block diagram of the reverse fault plane (AB) of the Iriyama thrust and overthrust fault.
l=Hamaisidake bed. m=the Kanbara bed the Iwabuti andesite mass, and the Saginota gravel bed.

田に露出する衝上斷層に續く．第7圖は入山衝上斷層面の變化を立體圖式で示したもので，衝上面が色々の角度に傾いてゐることを示してゐる．Bは阿僧．Aは沼久保の西．

入山衝上斷層は蒲原段丘と由比川遷急點との關係から知つたやうに段丘礫層を著しく變位せしめてゐないし，又芝川・松野間でも段丘礫層が變位されてゐないので，その主要な變位運動を鷺ノ田礫層堆積後蒲原段丘礫層堆積前に行ひ，その後比較的靜穩に經過し，却て之に平行した次に述べるやうな斷層線のみがその後も變位運動を行つたものと解し得る．卽ち水沼斷層と月代斷層とである．

水沼斷層 松野村北松野の對岸水沼の沼久保富士熔岩の下に露出してゐる．Loc. 80（地質圖）の富士川沿岸の河崖に層向南北：傾斜垂直乃至 30° の層位をして鷺ノ田礫層が横はり，その西端は垂直に近い斷層で岩淵安山岩體と接してゐる．この斷層を水沼斷層と呼ぶ．この斷層を不整合に被ふ沼久保富士熔岩は約 5° の角度で東へ傾き下り，水沼斷層で切斷されずに撓曲の構造を呈してゐる．

水沼斷層の北の延長は地形學的類推を許すならば安居山・大中里・青見・新道の方面へと續く樣に見え撓曲した鷺田礫層も之に沿うて分布してゐる．この南の延長は松野村大北で富士熔岩に變位を與へてゐるが，それより南では地質學的には確め得られなかつた．

地形の高度はこの斷層線の南の延長上にある有無瀨川溪谷の兩岸で著しく異るが，この兩岸にある鷺ノ田礫層の基底の高度は斷層の存在を否定する樣に見える．地形の高度差は入山衝上斷層の成生の際にその附近の鷺ノ田礫層が撓曲されて，その堆積面が變形したものと解することができる．

大北の南，又は北松野部落の西端から南45°西へ向つて走る一溪谷地形は水沼斷層の南の一延長線を思はせるが，露出が惡く後の調査に俟つこととした．入山衝上斷層がこの附近でその走向を變へることからみて，水沼斷層の走向もこの谷に沿うて變つてゐると疑ふことも可能の樣である．

月代斷層 は沼久保富士熔岩の項で述べた樣に沼久保富士熔岩を變位せしめた斷層で芝川溪谷の東側に沿うて月代附近にでて富士川を横つてゐる．その南方の延長ははつきりしない．沼久保富士熔岩はこの斷層によつてその東側が約 20 m 前後高められてゐる．故に入山衝上線に平行接近したこれらの二斷層は洪積世末期以後にも運動を起してゐる．

中山斷層 松野村中山部落の南から略ぼ N 40° E の走向を以て入山部落方面へと延びる斷層である．

Loc. 81（地質圖）に於いて觀察した露頭によると岩淵安山岩體と鷺ノ田礫層とが約 1 m の厚さの斷層ネバ帶を挾んで接してゐる．斷層の傾斜は東南 70°～80° で，岩淵安山岩體はこの斷層に接して角礫狀を呈し，西北側の鷺ノ田礫層中には中山斷層に平行して小斷層が見られる第 8 圖は上の露頭を示すスケツチ．

中山斷層の直接の露頭は他では確め得なかつたが Loc. 82, 83（地質圖）に於いて夫々鷺ノ田礫層と岩淵安山岩體との相接近した分布局限を確めることによつて，その位置を決定した．

鷺ノ田礫層と岩淵安山岩體とは後者の方が時代の古いものであるから，この斷層も衝上斷層である．入山衝上斷層と異り，中山衝上斷層面の傾斜は東へ急斜してゐる．故に入山衝上斷層と中山衝上斷層とによつて挾まれた地域は壓縮地溝（ramp）の地溝底部に該當する．

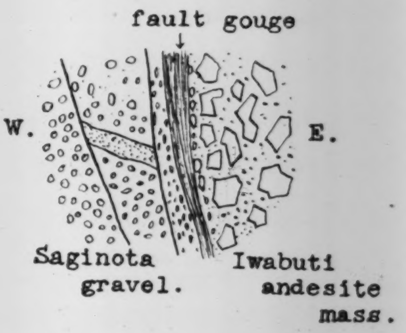

第 8 圖　中山衝上斷層の一露頭.
Fig. shows the outcrop of the Nakayama thrust. (Loc. 81 in geol map.)

中山斷層の東北延長は中山部落附近で消え，西南延長は舟場部落の東南 1 km 附近でその跡を消す．その活動の地質時代は鷺ノ田礫層堆積後と決定できるが沼久保富士熔岩に影響を與へてゐない．岩淵安山岩體の一部は崖錐として鷺ノ田礫層上に載るので中山斷層その他の地質時代に就て誤解を招き易い．

善福寺斷層　蒲原町々役場附近から善福寺の溪谷へ向つて東へ凸面を向け略ぼ南北に走る斷層である．

Loc. 84（地質圖）善福寺部落の北部河底に岩淵安山岩體の集塊岩と蒲原礫岩層とが走向 N 20° W：傾斜 60° W の斷層で接してゐる．

Loc. 85（地質圖）では同じく走向 N 10°～15° W：傾斜 60°～70° W の斷層で岩淵安山岩と蒲原礫岩層とが接してゐる．

Loc. 86（地質圖）では上の斷層は N 20° E：60° W の面で蒲原礫岩と岩淵安山岩體とを區別してゐる．

善福寺斷層の成生の時代は岩淵安山岩體成生後と推定できる．

上の三露頭を除いて斷層の露頭は中々發見できなかつたが，蒲原礫岩と岩淵安山岩體の集塊岩の分布から地質圖に示す樣な分布をなすことが明となつた．

蒲原礫岩層は岩淵安山岩體より古い地層であるから，善福寺斷層は一つの衝上斷層と解し得る．

城山斷層 蒲原町城山の東緣を區切る斷層であるがその露頭は僅に一ヶ所にしか知られない．即ち Loc. 87（地質圖）で，城山角閃石安山岩體と蒲原礫岩層とは垂直又は 80° W に近い傾斜の面で接してゐて，それは平面圖では東へ凸面を向けた弧狀形をなして城山層と蒲原礫岩層との境界に續いてゐる．この斷層面に接した礫岩層の或ものは壓縮のために壓碎されてゐる．この斷層の成生の時代は善福寺斷層と略ぼ同時代である．

斷層構造概說

上に述べた諸斷層系は何れも蒲原礫岩層堆積以後に成生されたもので，その性質は皆その走向南北に近く，東西方向に收縮したことを示す衝上斷層である．之等衝上斷層の面に接する各層中の砂礫は壓碎されてゐるので，この事實はこの地方にこの斷層成生の時代に東西方向の壓縮が行はれたと考へるに都合好い資料であらう．然るに之等の衝上斷層に挾まれた地域内の地層が壓縮の影響をみないことは，上の樣な壓縮が行はれても各地域内は變形されずに運動し，壓縮による變形は斷層の兩側の動きで代表される一方，斷層面に接近した僅な部分が變形壓碎されることによつても代表されてゐると解することができる．（之によつても地殼構造が單なる"側壓"と言ふ言葉を用ふることによつて萬事說明されたかの如く思ふ事は出來ない．） 上述した各斷層の成生は大部分が驚

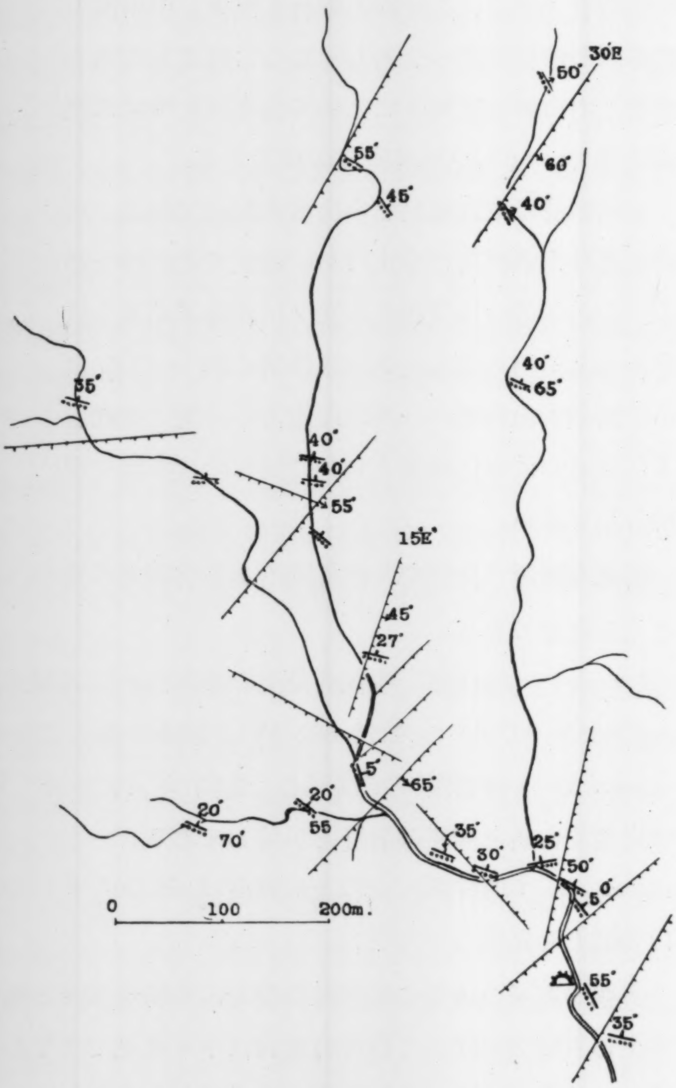

第 9 圖 蒲原礫岩層を切る斜斷層の分布.
Diagonal faults cut the Kanbara conglomerate.

ノ田礫層堆積直後までに完了してゐる．

第2圖に示した様に段丘礫層及び沼久保富士熔岩形成後にも多少の斷層成生運動があつたことは沼久保富士熔岩の高度分布からも確められる．この運動した部分は入山衝上斷層・水沼斷層等の發達する地帶であつて，之は大きな地域に及ぼす大規模な地殼運動が唯一の斷層面によらず或る破碎帶の中の色々な部分に於いて色々な形式の斷層で表はされると解するに都合がよい．

上に述べた斷層系とは別に小規模な斷層系を蒲原礫岩層の分布區域の東部に屢々觀察できる．第9圖は蒲原城山の西部附近でなるべくこの斷層系の斷層の走向・傾斜を測定記入したものであるが，勿論實際は第9圖に示されるものより遙に多い．第9圖によつて見られる通り岩石の分布には關係なく層向を斜斷して分布してゐて，壓碎による裂罅を暗示する様な斜斷層系である．未だ充分な調査をしたのではないし調査範圍が局部的であるから此の斷層系の成生機巧は斷言できないが，この地方に普通に見られる東西方向の壓縮を起す様な地殼運動の結果生じた裂罅としても說明できる．少くとも城山角閃石安山岩體や 390·0 m 山の角閃石安山岩體の迸入のために生じたとするには餘にその分布が東部に局部的に發達するのみであるし，類似な系統の斷層が堰澤岩脈を變位してゐる場合もあるのでそれらの安山岩體の迸入には關係ないとした方がよい．城山安山岩の岩石組織の結晶に顯微鏡的に後成破壞作用の證左があることをこゝに參考迄に附記しておく．

撓曲及び皺曲

入山撓曲　入山衝上斷層線の東側に沿うて發達する撓曲帶で，地層はこの部分でマクレ返つて西斜する．

第 7 圖は阿僧附近の入山衝上斷層の東側に於ける蒲原礫層の撓曲構造を示してゐる．

松野撓曲　は松野盆地の東・西・南の壁を作つてゐるもので，鷺ノ田礫層の堆積後矩形をなした松野盆地が形成される周圍に對する相對的陷沒運動が起り，東南西にこの撓曲構造が作られたと解し得る．

松野村三十坂の西，粒良野・漆野間，足ケ久保・平清水間，鎧田・十字金等は何れもこの撓曲構造を知ることができる場所である．この撓曲構造の一部は寫眞5圖に示す様に明な正斷層形式を示す斷層に移過する場合もあり，この盆地の成生機巧を示唆するものがある．

皺曲構造　には濱石岳層の向斜構造と蒲原礫岩層の背斜構造とがある．何れもその軸の走向は略ぼ南北で濱石岳層の方が皺曲度は大である．

濱石岳層下の小河內層の皺曲に就いては第 5, 6 圖に示した様に小皺曲構造及び斷層の集合で，濱石岳層の構造に比して複雜である．

地質構造から推定できる地殼運動

沖積世中の地殼運動はこの地方では確實な資料が得られない．富士川河口の沖積原は稍々沈降した地形を暗示せしめるのみである．

沖積世最初期か洪積世末期に流下した沼久保富士熔岩流は現在の富士川河底より高くその表面の富士川に沿う勾配は現在の富士川河底のものより稍々急であるから，沼久保富士熔岩が流下してから現在に至る迄に富士川は尙その河底を深めてゐることを示す一方，地盤は北が高まり南が低まる卽ち駿河灣へ向つて傾斜を增す様な運動が起つたと考へられる．この地盤運動が一様でなかつたことは第2圖の富士熔岩の高度分布の異常から推定できる様に芝富村月代附近の地壘的隆起となつて示される．

既に述べた如く蒲原背後の地形から推定できる地殼運動は香木穴・舟場・槍野の遷急點から示されるものと同じく隆起を意味してゐる．これらの遷急點段丘地形から推定できる隆起量は 150 m を超えてゐる．

鷺ノ田礫層の堆積面は著しく開析を受けて，その堆積當時の面影を僅にしか殘してゐないが，假にその面影が鷺ノ田の南方 410 m 前後の廣い平坦な山背面で代表されるとするならば，この堆積面も現在の海岸線の距離から判斷して前と同様に隆起した結果と推定できる．この礫層の厚さは最厚 250 m に達してゐて，その基底部には淡水湖底堆積物を示す足ケ久保含植物化石泥層があるので，少くとも 250 m の堆積物を堆積せしめるだけの沈降的現象の存在又は堆積量の增大が推定される．この礫層の分布とその西・東の境の衝上斷層系とはこの鷺ノ田區域が收縮地溝（ランプ）的構造のため堆積時代から周圍に比して相對的に沈降しつゝあつたと解する方が都合がよい．入山衝上斷層・中山衝上斷層等は鷺ノ田礫層の堆積時代及びその直後に迄繼續し，入山斷層の如きは鷺ノ田礫層の堆積面を變形せしめてゐる．この變形は鷺ノ田礫層が凝固してゐない礫層なので入山斷層の西側が宮部博士の砂の實驗に見られる壓し板の役をなし，同實驗の “slip line” の生ずる範圍內の地域宮部氏論文[29]（第 59 圖 A B 間の高まり）と解することができる．（A 部に見られる）この slip line の地上に於ける表現が野外に於いて期待されるが，この地形の變形と水沼衝上斷層との外には未だ野外に於いて確め得た衝上斷層・撓曲構造はない．

岩淵安山岩體の迸出は比較的廣範圍に亙つたが，その分布は入山衝上斷層線以東に

28） 宮部直巳，地震研究所彙報 **12** (1934) 2, p. 200.

限られ，以西に見出し得ないので，岩淵安山岩體噴出當時から入山衝上斷層線以東の地域は以西の地域に對して沈降してゐたのであらう．この分布上の特長は侵蝕作用でも說明されるが，卽ち入山斷層の西に分布した岩淵安山岩體が侵蝕し去られたとも考へられるが，入山衝上斷層線に接する蒲原礫層の擾亂程度はそれに接する岩淵安山岩體のそれより大きいことはこの衝上斷層が既に岩淵火山噴出前に存在してゐたことを示す．岩淵安山岩體迸出の直前の地表は岩淵安山岩體下の不整合線の分布から蒲原礫岩層及び城山安山岩體の露出する侵蝕面で城山安山岩體は岩頸として陸上に露はれて，稍々侵蝕を受け緩い起伏を待つてゐたかの如くに見える。この侵蝕面は Dl 面か或ひはそれより古期の地表であらう.（この侵蝕面と蒲原丘陵面とは一致してゐない.）

蒲原礫岩層と岩淵安山岩體との間に見られる衝上斷層系の成生は岩淵安山岩の迸出運動と關係附けても差支えない．

城山安山岩及び堰澤岩脈群は蒲原礫岩層の皺曲構造成生と同時か直後に迸入し，一部は迸入體とし，一部は斜斷層系岩脈として迸入したもので，城山砂岩層を捕獲してゐる事實をみると，城山（中新）層がこの城山角閃石安山岩體を由來した岩漿溜から地表に達する途中に（而も蒲原礫岩層より下であるから若しくは濱石岳層より下にあるかも知れぬから約 1 km は確實に下方に）發達してゐることを示してゐる．又その途中の迸入通路は少くとも城山砂岩層の包裹物が通過できる程で，此の砂岩の分布區域より大きいことを示してゐる．この時代の角閃石安山岩の分布からみると，それの由來した岩漿溜は蒲原礫岩層の下或る深さに廣く分布してゐると推定できるが之は上に述べた迸入通路の大きさに對する推論には都合がよい．

蒲原礫岩層の堆積はその礫の大きさの一定なことから海底で行はれたのではあるまいかと言ふ暗示を受けるが未だ海底であると言ふ充分な證左は得られなかつた．この礫岩層堆積後の皺曲運動は緩い背斜をなすが，入山衝上斷層，善福寺衝上斷層に接した部分は層位が急で壓縮變位の跡を示してゐる．併し蒲原層は城山安山岩體及び堰澤岩脈群の迸入のためには著しく層位を變へてゐない．

濱石岳層の向斜構造は第 4 圖に見られる樣に全體的に見て確められるもので，胴切斷層，層向斷層，斜斷層等が多數にあり，蒲原礫岩層の構造に比して複雜である．

濱石岳層下の小河內泥岩層は濱石岳層より更に複雜なことは既に記した如く，第 5 圖，第 6 圖によつて示される通であるが，濱石岳層との境界は筆者の觀察した限では著しい傾斜式不整合とは思はれない．この構造の複雜性は小河內層の岩種が極めて軟質變形され易いため大きな皺曲構造成生の際に層間に於いてこの樣な小皺曲構造を作つた疑がある．第 III 表は本地域の地質構造發達史を表示したものである．

第 III 表 由比川―富士川間の地質構造發達史を示す表

地質時代		古地理	斷層	皺曲	地殼運動	火山活動	地盤垂直運
中新世	城山層時代	暖流系淺海動物群の堆積	？	？	？	凝灰岩の噴出	→
中新世後半	小河內層時代	比較的深く泥帶					→
			小斷層系	興津川皺曲	收縮運動	？	⟵
鮮新世前半	濱石岳礫時代	暖流系淺海動物群の堆積				凝灰岩の噴出	→
		陸化・侵蝕作用	多くの構造線成生開始	濱石岳向斜等	收縮運動		⟵
鮮新世後半か又は洪積世初期	蒲原礫岩層時代	海成？礫の堆積					→
	城山角閃石安山岩層時代	城山安山岩よりなる火山體の成生	入山斷層の成生，岩脈を生ぜる裂罅	蒲原背斜，入山撓曲の成生	展開運動？	城山角閃石安山岩の迸入，岩脈群の成生	←
		侵蝕時代					←
洪積世前半	岩淵安山岩時代	岩淵群火山の成生	入山斷層の活動，善福寺斷層成生	入山撓曲の成生	展開運動及び收縮運動？	岩淵安山岩の迸出	
	鷺ノ田礫層時代	足ケ久保湖の成生礫層堆積				？	→
		礫層堆積面の變形；浸蝕作用	入山斷層の活動，水沼・中山斷層の成生	入山撓曲・水沼撓曲等の成生	收縮運動	？	←
洪積世後半	蒲原・岩淵段丘時代	侵蝕段丘成生；富士川流路の決定（現流路）	松野盆地形成		遷急點から見られる隆起		←
沖積世	沼久保富士熔岩の噴出時代	富士基底熔岩の流下			展開運動？	富士熔岩の流下	→
	現世	古田附近の地壘運動	水沼・月代斷層の活動		收縮運動		←

"Fossa Magna" 南部の地質構造一考察

上に述べた様に由比川——富士川間の地質構造は中新世からあだかも東西方向に壓縮されて皺曲・衝上せられつゝ，その間新しい堆積物が絕えずこの地域を被うため之等の新しい地層をも壓縮・皺曲・衝上の運動に與らしめたかの如き體をなしてゐる．その運動は沖積世初期までも繼續したと考へ得る．而して一般に西に古い地層が橫はり，東に新しい地層が橫はり，南北に走る數個の逆斷層で境されて排列し，NAUMANN 氏が "Fossa Magna" と呼んだ如く此の地方は，富士川河口附近に關する限り，中新世以來の地溝狀造構造帶の西緣部と認め得られる．併しながらその地溝狀構造は簡單な立體圖式で表はした教科書的な展開地溝ではないし，現在知られた各斷層は壓縮形式のものであるから假に地溝としても壓縮地溝として考へ得るもので展開地溝とは考へられない．又この構造の東部の境界の性質が今日尙明にされてゐないので，Fossa Magna を完全な地溝の概念で表はし得るか否かは明でないが，後述する樣に，少くともその南部ではその東境は地溝の性質を具へてゐない．

小川博士等が述べられた如くこの地域の中新統以上の地層は豐富な火山物質が認められるから，この地域に中新世頃から火山活動が激しかつたことが推定できる．

又原田豐吉博士が述べた御坂山地の山稜の走向から推定される對曲 (syntaxis) の構造の有無も檢討する必要がある．卽ち從來地質學的に明にされた Fossa・Magna 南部地域の新第三紀以後に形成された大規模な斷層線を考へると，その內故加藤鐵之助學士の神繩衝上及び推し被せ斷層の走向が略ぼ東西でありその斷層面は北へ傾き下りその東の延長は山北町の東北から松田町の東北に連り大磯地塊に達するが，宛もその東の延長上にあるかの如くに三浦半島に武山衝上斷層・房總半島に佐久間衝上・推し被せ斷層があり，之等は何れもその走向を東西又は北 70°～80° 西に向け，斷層面を北へ傾けてゐる．神繩衝上線の西の延長は富士山下に隱れてゐるがそれより西北方へ延びてゐる證左はない．三土技師[29]が決定した樣に小佛層の南緣を劃する逆斷層は中津附近から上野原・岩殿山・初狩方面へ走り，關武夫氏の論文で推察される樣に一部は三峠山の南東麓に達してゐる．この上野原——初狩衝上斷層線は西南日本外帶に類似した構造を持つ關東山地が北から丹澤山地を構成する新第三系の上へ衝き上げたかの如き狀を呈してゐて，矢部博士によつて詳しく論ぜられたフオツサ・マグナの西緣卽ち糸魚川——靜岡地質構造線と類似な地質構造上の意義を持つものと考へらる．故にこの斷層を糸魚川——靜岡地質構造線に對應し且つ Fossa Magna の東緣を代表す

---

[29] 三土知芳，1/75000．八王子地質圖幅及び說明書．(1932)．

る斷層であると考へることもできるが，その走向は寧ろ東西に近いので之を以て直ちに“Fossa Magna”なる壓縮地溝の東縁と考へる事はできない．

然るに富士川河口の各衝上斷層が走向南北であり，その大部分の斷層面は西へ傾き下り，それらの北部延長は甲府盆地地方に迄延びてゐる證左もないことからみて，少くとも“Fossa Magna”南部にはヒマラヤ山地の北西 Punjab, Kashmir. 地方に見られる對曲構造を想起させる様な斷層分布が不完全ながら見られる．併しながら“Fossa Magna”南部に於いてはこの構造に更に新生代末期の火山活動の結果が加つてゐるためにWADIA氏[30]が確めた様な對曲構造の兩翼の連續性は勿論その前山地方(foreland)の古い岩層からなる地塊構造も未だ確められてゐない．

今野圓藏教授によれば矢部博士の糸魚川——靜岡地質構造線の南部に於ける位置に就いて調査された結果，同構造線に平行な斷層線は千谷技師[31]の瀨戸川統の東端と高草——龍爪玄武岩及び粗面玄武岩の東縁に確認できる見込みがあり，安倍川の東側龍爪山地を略ぼ南北に走る平行した——壓縮斷層破碎帶で代表されてゐるから“Fossa Magna”西縁の南部は明に大きな壓縮型の斷層帶で西南日本外帶と境されてゐる*．

この様に“Fossa Magna”西南部の由比川・富士川間の地質構造はそれに關する先輩の種々な解釋の何れにも適合するかの如き構造様式を備へてゐて，之等の解釋を更に具體的に決定するためには尙大なる範圍の調査を敢行しなければならぬ．然れども“Fossa Magna”南部に於いては壓縮地溝と言ふよりは寧ろ不完全な對曲構造と考ふるべき地質構造上の性質を示してゐる．

本研究に於いて“Fossa Magna”地方が沖積世初期の地層に迄大なる擾亂を與へてゐるのに西南日本又は關東地方中部に於いては殆どその事實の認められぬ事，“Fossa Magna”地域内に於いて尙壓縮性の南北走向の衝上斷層が存在し，而も之等が沖積世初期迄も繼續運動した事を知り得た事は次に述べる推論に對して都合のよい資料となつた．卽ち關東地震の際の地殼の動きはその周圍に對して南方へ移動したことを示したが，この運動方向は上野原——初狩・神縄・武山・佐久間等の各逆斷層が示すものと同一形式である．然るに伊豆地震の丹那地震斷層地域の地形・地質學的研究は，筆者及び久野學士によつて確められた様に，由比・入山衝上斷層と類似の特徴を持つてゐる．故に丹那地震斷層の兩側の變位は“Fossa Magna”西南部の地質構造を作つた地殼運動と類似な運動が行はれつゝあることが暗示されると同時に關東地震の際に成

---

30) WADIA, *Rec. Geol. Sur. India*, **65** (1932), pt. 2, pp. 189〜220.

31) 千谷好之助，七萬五千分之一靜岡地質圖幅及び說明書．(1928〜9).

* この破碎帶の斷層鏡面條線は水平方向に近いものが大多數に發見されてゐる．

生された諸地震斷層（延命寺・下浦地震斷層）と地殼變動とは “Fossa Magna” の東南部の新第三紀以來の地質構造を作つた地殼運動と類似な運動が行はれつゝあることも暗示される.

故に今假に關東地震の地殼變動と伊豆地震の丹那斷層の兩側の地殼變動とを前述した樣に新第三紀以來の地殼運動の一表現と解するならば，兩地震の際の地殼運動は上に述べた對曲類似の構造成生運動中の兩翼の一運動と見做すことができる. Wadia 氏流の考へ方をすれば相模灣及びその灣口の深部以東南には西及び北よりの對曲類似の構造の前山地方（foreland）に該當する古き見えざる陸塊が存在するのではあるまいかとも解釋できやう.

---

33. *Geologic Structure of the Eastern Ibara District, Sizuoka Prefecture, Japan.*

By Yanosuke Otuka,

Earthquake Research Institute.

In this paper the writer describes the stratigraphy and structural geology of the Ibara district, which lies west of the mouth of the Huzi river. Since it occupies the southwestern corner of Naumann's 'Fossa Magna', to grasp the geologic developement of this district it is necessary to understand the geologic nature of this great tectonic zone.

Stratigraphically this district consists, in descending order, of Alluvial deposits, the Numakubo Huzi lava flow, the Iwabuti and Kanbara terrace deposits, the Saginota gravel bed, the Iwabuti andesite mass, the Siroyama andesite mass and the Sekizawa dykes, the Kanbara conglomerate bed, the Hamaisidake conglomerate bed, the Kogôti mud bed, and the Siroyama sandstone bed.

The Alluvial deposits mainly consist of unconsolidated fluviatile gravel and sand that were deposited on the shore of Suruga bay and the floor of the Huzi river.

The Numakubo Huzi lava flow, which is a basal lava flow extending from Volc. Huzi to the floor of the Huzi river through the valleys of the Sibakawa and the Numakubo, is overlain by Alluvial deposits.

The Iwabuti and the Kanbara terrace deposits consist of river gravels, mainly derived from the surrounding mountains. The Iwabuti terrace deposits form a terrace surface, above 30~20 m above sea-level, behind the town of Huzikawa-mati. The Kanbara terrace surface, which is 180~200 m high, and which consists of Kanbara terrace gravels, is well developed along the river Yui. From the topographical point of view, these terrace deposits may be Late Pleistocene, seeing that they are considered older than the Numakubo Huzi lava flow.

Terrace deposits similar to the foregoing may be seen exposed on the southern slope of Mt. Kanamaru, behind the town of Kanbara (-mati), and in the Matuno basin south of Numakubo. The geologic age of these deposits, which is uncertain owing to lack of fossils, may be almost contemporaneous with that of the Iwabuti and Kanbara terrace deposits, judging from its topograpnic relations.

The thick Saginota gravel bed exposed near Ságinota, in Matuno-mura consists of unconsolidated coarse gravels, the lower part of which intercalates with a mud bed containing fossil plants which E. KONNO and the writer call the Asigakubo flora. (see p. 423.).

According to E. KONNO, the Asigakubo flora, judging from its flora, may be Lower Pleistocene or Uppermost Pliocene. It is older than the Siobara flora, and the younger than the Japanese early Pliocene Flora.

The Iwabuti andesite mass consists of agglomerate (or lapilli) and lavas of two pyroxene andesite extruded by olivine pyroxene andesite. It is overlain by the Saginota gravel bed with paraunconformity. This andesite mass extruded and unconformably overlaid the erosional surface of the Kanbara conglomerate bed, the Siroyama andesite mass, and the Sekizawa dykes.

The Siroyama andesite mass and the Sekizawa dykes, both consisting of hypersthene bearing hornblende andesite, (or dacite) intruded the Kanbara conglomerate bed.

The Kanbara conglomerate bed is subconsolidated conglomerates which consist of pebbles of quartzite, white quartzite, green sandstone, conglomerate of the underlying Hamaisidake beds, diorite, andesite, and porphyry. These regular sized pebbles are overlain by the Iwabuti andesite mass with unconformity, and intruded by the Siroyama andesite mass and the Sekizawa dykes. They are bare of fossils.

The Hamaisidake conglomerate bed consists of greenish sandstone and conglomerate containing some fossil mollusca. The following fossil mollusca were collected from the Hamaisidake conglomerate bed exposed at Loc. 7 in Fig. 4.

Venericardia panda (YOKOYAMA), *Cardium* (*Trachycardium*) sp., *Chlamys vesiculosa* (DUNKER), *Amussiopecten praesignis* (YOKOYAMA), *Glycymeris* sp., *Ostrea* aff. *musashiana* YOKOYAMA, *Conus tuberculosus* TOMLIN. *Lemintina murcnoensis* OTUKA.

From the above listed the writer, although he determined only two Pliocene fossils, believes the Hamaisidake bed to be Lower Pliocene.

The Kogôti bed is an alternation of fine mud and sand beds exposed on the river Kogôti, a tributary of the Okitu. *Pyrgo kogotensis* OTUKA (MS.) frequently occurs in this bed. It is paraunconformity overlain by the Hamaisidake beds. What underlies this alternation is unknown.

The unconformity between the Hamaisidake bed and the Kogôti bed is not accompanied by the basal conglomerate of the former, which characteristic feature of the unconformity reminds the writer of similar features in the unconformity between the Lower Kakegawa series and the Tamari mud bed in the Kakegawa region, and the Takanabe group and the Tuma group in Miyasaki prefecture. While the Hamaisidake beds, the Lower Kakegawa series, and the Takanabe group are almost contemporaneous with one another as judged from their molluscan fauna, the Kogôti beds may be almost contemporaneous with the Tamari and the Tuma mud groups.

The Siroyama sandstone, which is a calcareous sandstone exposed on the top of Mt. Siroyama, north of the town of Kanbara, is a sedimentary xenolith or a sedimentary inclusion surrounded by the Siroyama hornblende andesite mass on its north, west, and south, and by a thrust fault on its east side. It consists of tuffaceous and calcareous sandstone that is andover green. The tuffacous sandstone which is in contact with the Siroyama andesite occupies the lowest horizon. The following marine fossils were collected from the calcareous sandstone at Loc. 88 in Geol. Map. (Fig. 10).

Astriclypeus integer YOSHIWARA (very frequent)	Miocene.
Laganum fudsiyama tokunagai OTUKA n. subsp.	
Glycymeris sp. (*retitus* type) (very frequnet)	?
Acila sp.	?
Mytilus sp.	Miocene.
Lima konnoi OTUKA n. sp.	
Ostrea gigas THUNBERG	Miocene-Recent.

Amussiopecten sp. (very frequnet)	Miocene-Pliocene.
Patinopecten kanbaraensis OTUKA n. sp.	Miocene.
Chlamys sp.	?
Cardium sp.	?
Flaniella sp.	?
Dosinia matumotoi OTUKA n. sp.	?
Paphia hirabayasii OTUKA n. sp.	Miocene.
Clementia nakamurai OTUKA n. sp.	Miocene.
Trivia sp.	?
Xenophora sp.	?

Of these fossils mentioned above, *Astriclypeus integer* YOSHIWARA, *Mytilus* sp., *Clementia nakamurai* OTUKA, and *Paphia hirabayasii* OTUKA are the same as those of the Miocene exposed near Kureti, NE of Volc. Huzi, from which *Operculinella complanata Japonica* HANZAWA was reported. *Patinopecten kanbaraensis* OTUKA was reported from the Miocene of Mino. Since the faunal character of the Siroyama sandstone bed is not related to that of the Hamaisidake bed, it is not improbable that the former bed is contemporaneous with these Miocene formations. From its faunal character, at all events, the writer believes that the former formation is decidedly older than the latter, although only five fossil species of them have been found in other Miocene formations.

Summarising the above written the following succession of strata and igneous rocks is inferable in this district (Table I).

Table I. Succession of strata in the Ibara district, Sizuoka pref.

Holocene	*a*	Alluvial deposits
		(unconformity)
	a_1	Numakubo Huzi basal lava flow
		(unconformity)
Pleistocene	du_2	Iwabuti and Kanbara terrace gravel beds
		(unconformity)
	dl	Saginota gravel bed (with Asigakubo flora)
		(unconformity)
		Iwabuti andesite mass
		(extensive unconformity)
Pliopleistocene	$pd \sim dl_1$	Siroyama andesite and Sekizawa dykes
		(intrusion)
		Kanbara conglomerate bed
		(unconformity)
Pow. Plio.	*pl*	Hamaisidake conglomerate bed
		(unconformity)
Miocene	*mu?*	Kogôti mud and sand altenation
		(stratigraphic relation unknown)
	m	Siroyama sandstone bed

Tectonic. There are six principal faults in this district. The Iriyama thrust fault runs along the Yui valley from the mouth of the Yui river to Numakubo through Iriyama and Ozumori. It trends NS∼N 5° E and dips westward about 70°∼40°. The fault plane and slickedside of this fault show that its west side moved upward and southeastward relatively to opposite side. Phot. 3 & 4 show the exposure of this thrust fault. The Saginota gravel bed is the youngest formation that was cut and flexed by this fault.

The Mizunuma fault, which is exposed on the valley wall of the Huzi river, at Numakubo and Mizunuma, east of Sibakawa, displaced the Saginota gravel and the Iwabuti andesite mass and flexed the Numakubo Huzi lava flow.

Table II. Geologic development of the Ibara district.

Geologic age		Palaeogeography	Faulting	Folding	Crustal movement	Volcanic activity
Miocene	Siroyama sandstone age.	Deposition of littoral fauna affected by warm current.	?	?	?	Eruption of tuff.
Later half of Miocene	Kogôti age.	Deposition of mud (deep mud zone deposits.)			Subsidence ?	?
			Minor fault system	Folding in Kogôti bed.	Upheavals. Contraction or compression.	?
Earlier half of Pliocene	Hamaisidake age.	Deposition of littoral fauna affected by warm current.				Eruption of tuff.
		Regression; formation of dry land; subaerial erosion.	Formation of many tectonic lines.	Formation of Hamaisidake syncline.	Contraction or compression.	
Later half of Pliocene or Early Pleistocene	Kanbara conglo. age.	Deposition of gravel.				
	Siroyama hornblende andeites age.	Formation of volcano which consists of Siroyama andesite.	Formation of dykes and Iriyama thrust.	Formation of Kanbara anticline and Iriyama flexure.	?	Intrusion of Siroyama andesite and dykes.
		Extensive denudation.				
Earlier half of Pleistocene	Iwabuti andesite age.	Formation of Iwabuti volcanic group.	Activity of Iriyama thrust. Formation of Zenpukuzi thrust etc.	Formation of Iriyama flexure.	Tension and compression.	Extrusion of Iwabuti andesite mass.
	Saginota gravel age.	Formation of Asigakubo lake. Deposition of terrestrial gravels.			?	?
		Deformation of depositional surface of the gravels; Erosion.	Activity of Iriyama fault; formation of Mizunuma and Nakayama thrust.	Formation of Iriyama and Mizunuma flexure.	Contraction or compression.	?
Later half of Pleistocene	Kanbara, Iwabuti terrace age.	Formation of erosion terrace; Settling of the Huzi river course.			Upheaval inferred from cusp point of the river floor.	
Holocene	Early Holocene.	Flow of the Huzi lava.			Tension ?	Extrusion of Numakubo Huzi basal lava.
	Recent.	Formation of Horst near Kota.	Activity of Mizunuma and Gendai fault.		Contraction or compression.	

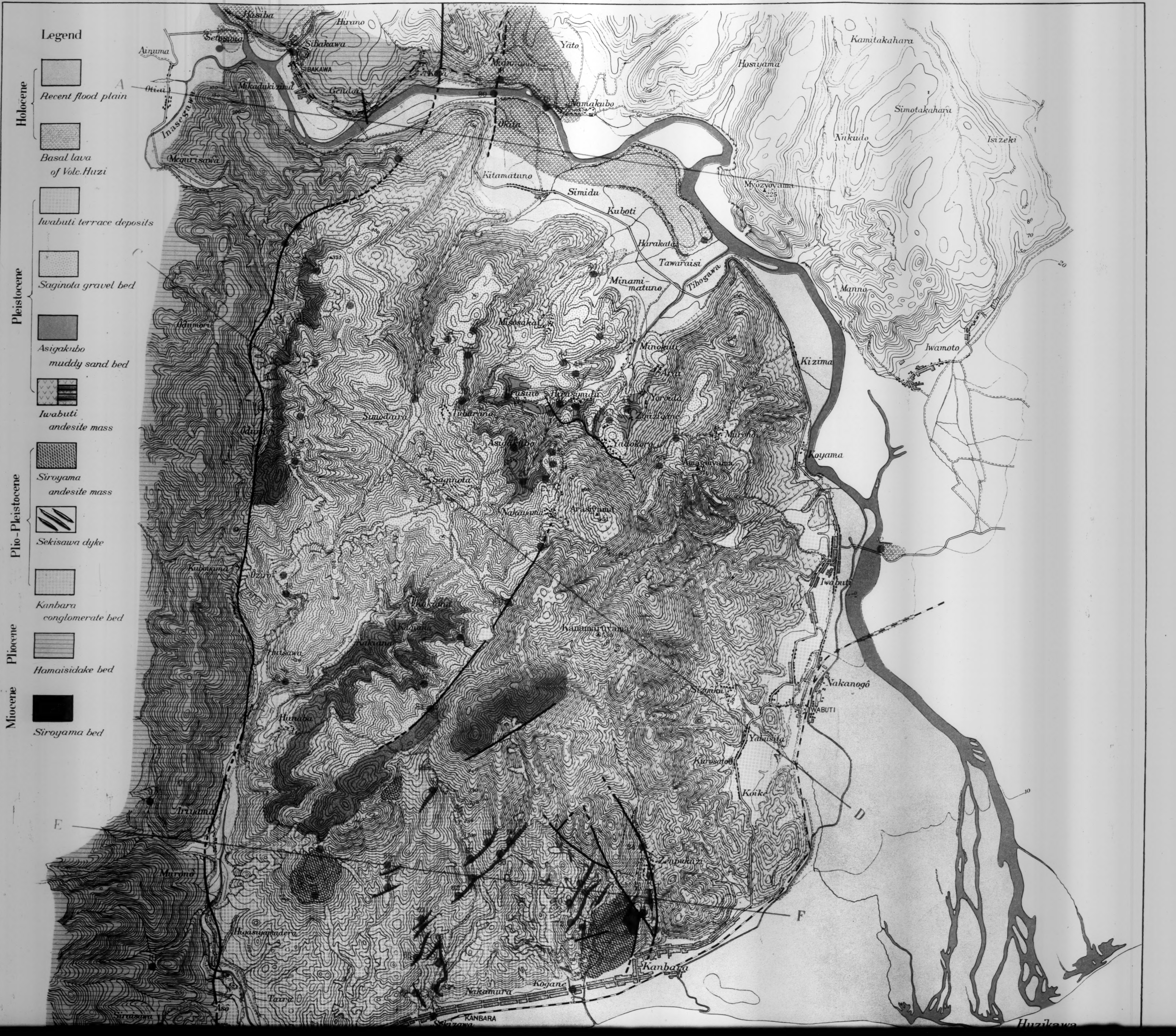
Legend
Holocene
Recent flood plain
Basal lava of Volc. Huzi
Pleistocene
Iwabuti terrace deposits
Saginota gravel bed
Asigakubo muddy sand bed
Iwabuti andesite mass
Plio-Pleistocene
Siroyama andesite mass
Sekisawa dyke
Kanbara conglomerate bed
Pliocene
Hamaisidake bed
Miocene
Siroyama bed
A
B
C
D
E
F
Hasiba
Hirano
Setusima
Sibakawa
SIBAKAWA
Ainuma
Otia
Inasegawa
Mikadukizima
Genda
Megurisawa
Yato
Midono
Namakubo
Okita
Kitamatuno
Simidu
Kuboti
Harakata
Tawaraisi
Tihogawa
Minami-matuno
Kamitakahara
Hosiyama
Simotakahara
Nukudo
Isizeki
Myozyoyama
Manno
Iwamoto
Odumori
Misosaka
Minokuti
Kizima
Arai
Simodairi
Inbaruma
Asigakubo
Saginota
Nakayama
Arasiyama
Yadokari
Koyama
Iwabuti
Kubayama
Ozaki
Hutisawa
Kakinoki
Iwanamaruyama
Nakanogô
IWABUTI
Sizuku
Yabasita
Kurosawa
Koike
Hunaba
Iriyama
Marono
Zenpukuzi
Hyasyonodera
Kanbara
KANBARA
Nakamura
Kogane
Taira
Sirasawa
Sekisawa
Huzikawa

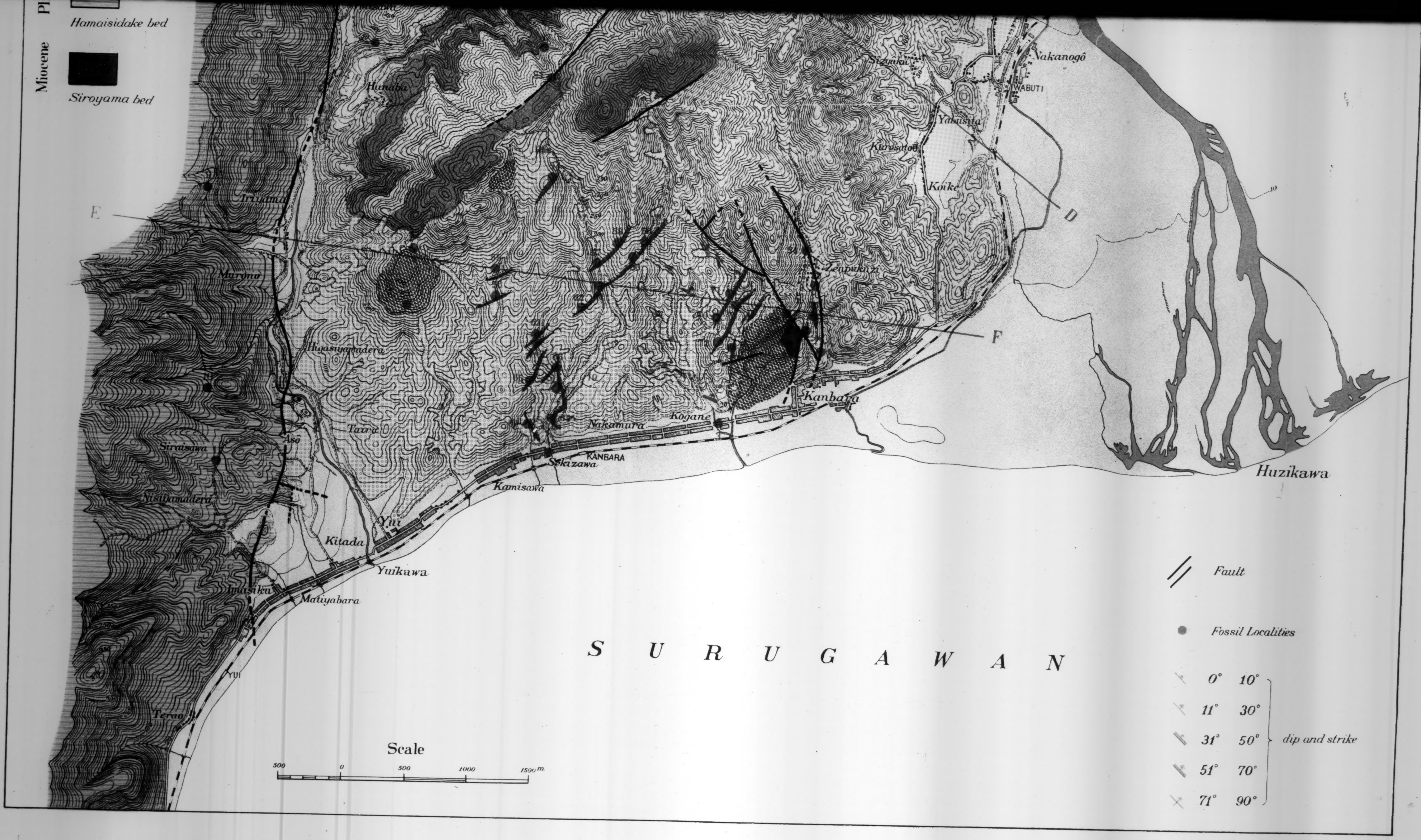
Pl
Hamaisidake bed
Miocene
Siroyama bed
Hanaba
Iriyama
E
Marono
Higasiyamadera
Taira
Aso
Siraisawa
Nisiyamadera
Yui
Kitada
Yuikawa
Imasiku
Matiyabara
YUI
Terao
Nakamura
Kogane
Kanbara
KANBARA
Sekizawa
Kamisawa
Sizuku
Nakanogô
IWABUTI
Yabusita
Kurosato
Koike
D
Zenpukuzi
F
Huzikawa
S U R U G A W A N
Fault
Fossil Localities
0° 10°
11° 30°
31° 50°
51° 70°
71° 90°
dip and strike
Scale
500 0 500 1000 1500 m.

Geologic Section

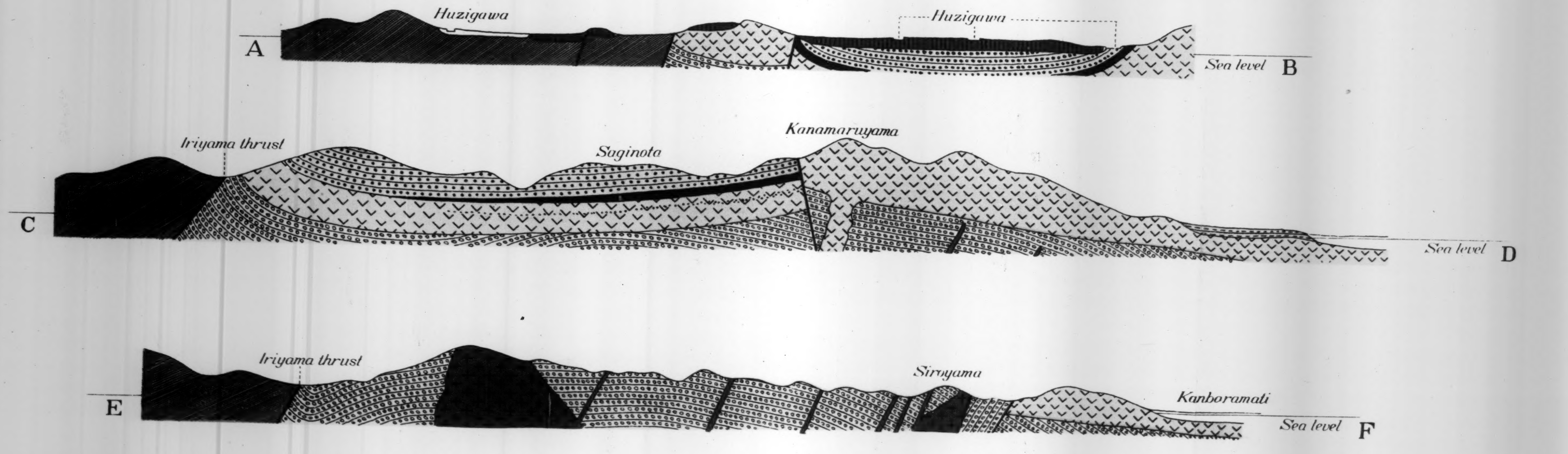
A
Huzigawa
Huzigawa
Sea level
B
C
Iriyama thrust
Saginota
Kanamaruyama
Sea level
D
E
Iriyama thrust
Siroyama
Kanboramati
Sea level
F

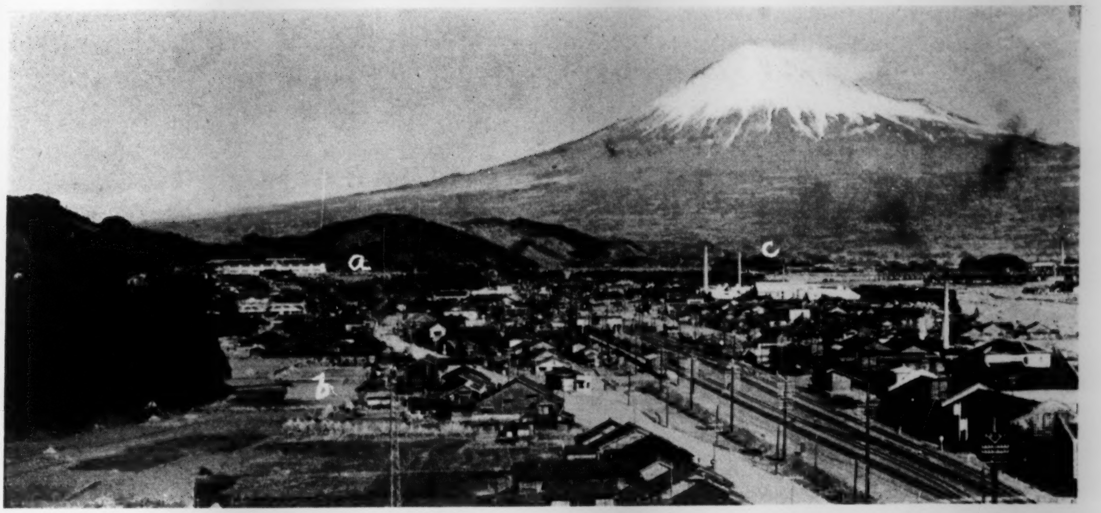

寫眞 1　富士川町岩淵. (Town of Huzikawa at Iwabuti.

a＝岩淵段丘 (Iwabuti terrace).
b＝沖積氾濫原 (Alluvial flood plain).
c＝富士基底熔岩露出地 (Outcrop of Huzi basal lava flow).

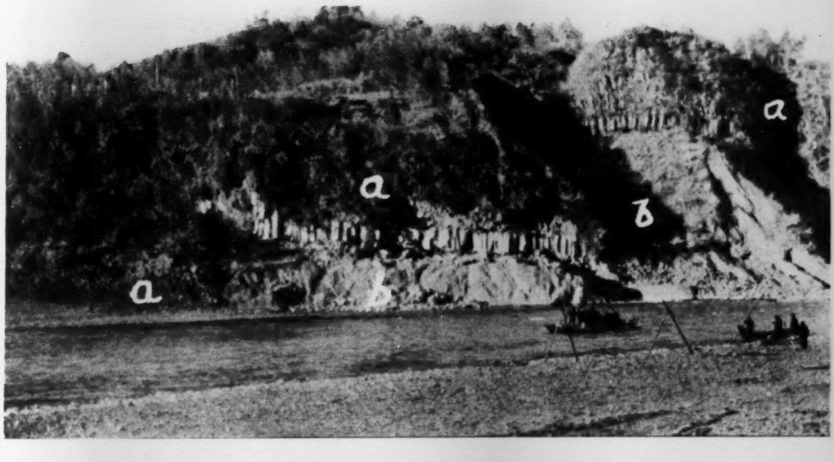

寫眞 2　芝川東部月代斷層 (Gendai fault, east of Sibakawa).

a＝沼久保富士基底熔岩 (Numakubo Huzi basal lava).
b＝濱石岳礫岩層 (Hamaisidake conglomerate bed).

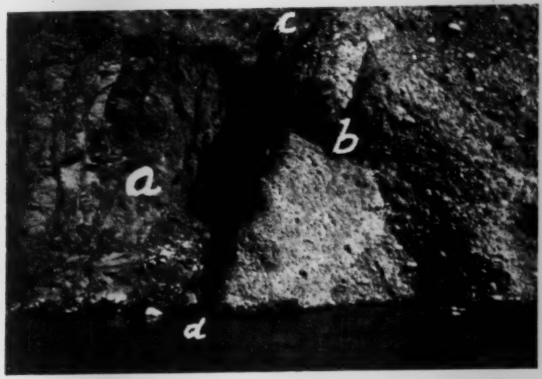

寫眞 3 （右，right）.

入山衝上斷層 東山寺西南 (Iriyama thrust 〔*cd*〕 at southeast of Higasiyamadera).

a＝濱石岳層 (Hamaisidake bed).

b＝蒲原礫岩層 (Kanbara conglomerate bed).

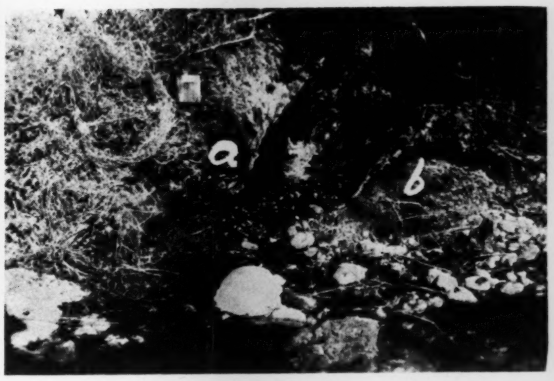

寫眞 4 （左，left）.

入山衝上斷層，福澤の西部 (Iriyama thrust at west of Hussawa).

a＝濱石岳層 (Hamaisidake bed).

b＝岩淵安山岩體 (Iwabuti andesite mass).

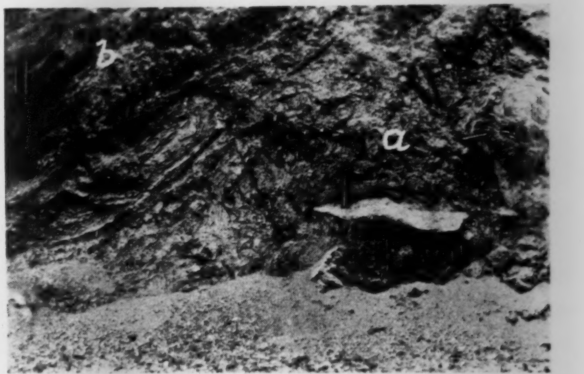

寫眞 5 （右，right）.

松野撓曲から移化した正斷層 (Normal fault in the Matuno flexure).

平清水の南 (South of Hirasimizu).

（震研彙報 第十六號 圖版 大塚）

The Gendai fault is a young fault that displaced the Numakubo Huzi lava flow as shown in Photo. 2

The Nakayama thrust fault runs from Nakayama village along the western foot of Mt. Kanamaru, trending N 30° E. The fault plane of this thrust, exposed at Loc. 81 in geol. map. as shown in Fig. 8, dips steeply eastward (about 70°~80°). The Iwabuti andesite mass was thrusted on the Saginota gravel bed by the fault plane.

The Zenpukuzi thrust fault runs from Zenpukuzi to Kanbara, east of Mt. Siroyama, trending N 10° W~N 10° E. It dips 60° westward, the Kanbara conglomerate having been thrusted on the Iwabuti andesite mass by this fault.

The Siroyama thrust fault which trends N 10° W and dips 70°~60° westward, limits the eastern extension of the Siroyama sandstone at Siroyama.

Most all the faults just described are of the thrust type, running in a nearly N~S trend. Most of them were active, and are as young as the post-Saginota gravel. Consequently during early Pleistocene, compression or contraction was the outstanding phenomenon connected with the fault system of the southern part of the "Fossa Magna". Generally speaking, since the strata in the western part of this district the extensions of which are limited by thrusts, is older than those in the eastern, the fault system may be regarded as evidence of structural habits in the compressive graben structure, or in the west wing of a syntaxis which diverges southeastward.

The flexed structure is observed along the principal fault planes. The Iriyama flexure is observed in the Kanbara conglomerate bed, in the Iwabuti andesite mass and in the Saginota gravel bed along the Iriyama thrust fault. Degree of the disturbances in the flexure is greater as the formation becomes to older.

The Matuno flexure forms boundaries on the eastern, southern, and western sides of the Matuno basin. It frequently changes into minor normal faults.

Folded structure is exposed in the Kanbara conglomerate bed, the Hamaisidake conglomerate bed, and in the Kogôti mud bed.

The folded structure in the Kanbara conglomerate bed which is very simple, shows an anticlinal fold, the axis of which runs with a trend N 30° E from the southern foot of Mt. Kanamaru to Sekizawa, in the town of Kanbara.

The folded structure in the Hamaisidake conglomerate bed is a syncline, the axis of which runs with a trend N~S. The trend of Hamaisidake ridge almost coinsides with the axis of this syncline.

The folding in the Kogôti mud bed is very complicated, and more minor than those just mentioned. Figures 5 and 6 show these minor foldings in the mud bed. The folding axis of these minor foldings runs with a N~S trend.

Judging from the folding structures mentioned above, the compression or contraction seems to have occurred since late Miocene or early Pliocene in this district.

The following table (II) shows the tectonic developement of this region.

From the foregoing remarks, we find that Naumann's 'Fossa Magna', at least in its southwestern part, is evidence of a compressive graben, or a syntaxial structure which branches off southeastward, but in order to decide which one of these structures it is, it behooves us make a more detailed geological survey of a much wider area that has been done so far. It is however clear that Naumann's Fossa Magna is not a simple tensional graben, as shown by the block diagram in text books of geology, but rather the result of a complicated and compressive operation of forces. It is, more over a tectogenetic zone that has been active since the Miocene to Recent.

34. 富士火山の地質學的並びに岩石學的研究 (I).

1. 小御嶽の構造

地震研究所　津屋弘逵

（昭和13年3月16日發表——昭和13年3月20日受理）

緒言

昭和2年以來，筆者は富士火山の局部的地質調査を屢々試み，昭和10年に至つて其數種の熔岩の岩石學的性質に就いて研究した結果を發表[1]した．然るに同年以後，幸にも日本學術振興會の補助に依つて，同火山の地質學的並びに岩石學的研究を系統的に實行し得る樣になり，現在も尙夫に從事してゐる．現在では，同火山全地域の約半分の地質調査を終つてゐて，今後其殘部を引續き調査するつもりである．既に調査の終了した地域のみに就いても，同火山の地質に關し從來誤解され，或は全然知られなかつた種々の事實が判明してゐるので，其中で局部的地質調査の結果の說明で略理解され得る事項から取敢へず順次發表し，地質調査の完了を俟つて富士火山全般に關する事項を發表する豫定である．茲に此研究の遂行に對し多大の補助を與へられた日本學術振興會並びに深き理解を與へられた石本所長に感謝の意を表する．

富士山の北麓船津，吉田方面から富士山を眺めると，同山の略正北面の中腹に在る寄生火山丸山（海抜 1700·3 m）の南々東側に接し，此寄生火山より更に一段と高く聳ゆる一の特異な地形を示す山體が認められる（圖版第1圖）．又，山中湖附近から見ると，富士山北面の山側線が此山體の處で著しい脹みを見せてゐる（圖版第2圖）．此山體は小御嶽と呼ばれ，吉田登山道六合目から所謂御中道に沿つて北西方向に約2 km 距たり，又，精進登山道五合目に當たる所の小御嶽神社の境內を最高部（海抜2300·1 m）とし，此地點から北方に數條の尾根を張り，周圍約6 km，東西及び南北の直徑約2 km の地域を占めてゐる。

故平林博士[2]は小御嶽に就いて何等言及せず，地質圖には其地域を富士山本體の一部として塗色してゐるが，小御嶽が富士山本體の少くとも現在見られる圓錐體の一部

---

[1] H. TSUYA, *Bull. Earthq. Res. Inst.*, **13** (1935), 645.

[2] 平林武，震災豫防調査會報告，**24** (1899).

でないことは單に兩者の地形が著しく不連續である事實からのみでも直ちに氣付かれる．故石原學士[3]は此事實に氣付き，小御嶽に就いて次の様に述べてゐる．

“全山小礫から成り，……火口の尋ぬべきものが無いのと，附近の富士山本體を構成すると同様のスコリアから成るを以て，側火山として稍々疑あれど，富士山腹の側線はこゝ程其整調を破られたる箇所は他に無く，吉田方面から望見する時は明瞭なる一大山瘤をなし，以て著るしく對數曲線を亂さる．もし此の小御嶽が側火山に非ずとせば，此の山瘤の成因は一に侵蝕に歸せざるべからず，而して此處にのみかゝる著るしき侵蝕作用が行はるべき理由はない．故に側噴出に歸因するものとする外說明は出來ない．憶ふに古き岩滓火山で，其の火口は崩壞し，周圍には輻射谷をさへ生じたるものであらう”．

以上の様に，石原學士は小御嶽を火山礫のみから構成される古い寄生火山が著るしい浸蝕を受けて殘つてゐるものと見てゐる．然し精進登山道或は吉田登山道を登つて小御嶽の頂上に至り，小御嶽神社の境內附近を觀察したのみでは，小御嶽の構造は全く分らないのであつて，其附近には富士山頂上から噴出した熔岩及び火山砂礫があるが，石原學士が述べてゐる様な小御嶽自體を構成する火山砂礫を識別する事は出來ない．

石原學士は多少の疑問を抱きながらも，尙小御嶽を富士山本體の一寄生火山と見做してゐるのであるが，神原博士[4]は之と全く別の興味ある一說を發表してゐる．卽，同博士は小御嶽が富士山北面中腹の著しい突出部で，しかも富士山腹に見られる幾多の寄生火山に比較して隔段の浸蝕地形を示してゐる事に注目して次の様に述べてゐる．

“富士山は單式火山の如く見ゆれども實は複式火山の一なる二重火山ならんと思はる．同火山發育の過程に於て一度は大火口を有したる事，夫の箱根山や阿蘇山と異なる事無かるべし．然るに其後同一火山に於て一個の中央火口丘大に發達し遂に其外輪山を殆ど埋沒して其斜面上に再び成層を形作り中央火口丘の頂上より舊外輪山の裾野まで單一なる傾斜面を形成せり．然れども外輪山の峰頭の尙埋もれ殘りたる箇處若干あり，其を小御嶽，高鉢山，小富士等となす”．

以上の様に，神原博士は小御嶽を，富士山東面の中腹及び南面の中腹に夫々突出する小富士（海拔 1970 m）及び高鉢山（海拔 1649.2 m）と共に，現在の富士山本體より古い山體で，二重火山の外輪山の一部に相當する突起であると考へてゐる．尙，同

---

3) 石原初太郎，富士の地理と地質，(1928)，168.
4) 神原信一郎，富士山の地質と水理，(1912)，147.

博士は小御嶽の北麓土合（丸山寄生火山の東方地域）附近から小御嶽の山腹を望見した結果次の様に述べてゐる．

“小御嶽の山腹は頗る急峻にして樹木蓊鬱し道路を通ぜざれば未だ踏査せざるも其崩壊箇處を眺むるに灰砂の表土厚きが如く其一谿谷に當りて多數の熔岩塊の崩落あり其岩塊流れて連續する事一里丸山の東土合の谷を埋め鳥居木前に至る．其岩質黑灰色の石基に白色の斑晶を有す．未だ此のものゝ噴出時期を確むる能はざるも岩質は夫の芝川熔岩に善く似たるを以て或は同時代のものかと思はる．其にしても此熔岩の同岳に於ける存在の狀態を確むるの要あり．尙此の土合の堀の傾斜緩なるにも拘らず直徑一二間にも及ぶ大塊の如何にして長距離を流轉せしものか不審なり．或は大噴火に依りて此の岩塊の崩壞するや小御嶽の西側を廻つて流れ來りし泥流に押し流されたるものか”．

神原博士が觀察した小御嶽山腹の熔岩塊は，後に述べる樣に，小御嶽自體を構成する熔岩の崩れたものであつて，富士山頂から流れて來た熔岩でなく，所謂芝川熔岩とは全く異なるものである．

要するに，小御嶽の突起の成因に關する從來の考へは主として小御嶽を遠望した地形的觀察に基づいてゐるのであつて，小御嶽の構造を直接に觀察した結果でない．小御嶽の構造を明かにするには同山の北側の急傾斜の山腹を調査しなければならないのであるが，同處は各登山道から距たり，人跡稀な原始林に蔽はれ，吉田方面から往復するにも不便であるため，從來實地に就いて踏査せられなかつたと思はれる．近來，小御嶽北腹の樹林が次第に伐採せられ，其材木が運搬される自動車道路が船津登山道の旭平，山ノ神の中間から劍丸尾を橫切り，小御嶽の北麓に通じたから，小御嶽の調査は容易に行はれる樣になつた．

筆者の調査した結果に依ると，神原博士の指摘した樣に，小御嶽が現在の富士山本體より古い山體である事は疑ひない事實であるが，現在の富士山本體の外輪山の一部に相當するといふ見方は妥當でない．神原博士が小御嶽と共に所謂富士山外輪山の一部と見做した小富士と高鉢山との中，小富士に就いては未だ一度も調査してゐないが，高鉢山に就いては筆者は現在の所富士山の一寄生火山と考へてゐる．之等の山に就いては更に今後調査を進めるつもりであるが，少くとも小御嶽自體は富士山本體の下に埋もれてゐる一の舊火山體で，其構造に關する限り，富士山本體と直接の關係を持つてゐない．卽，小御嶽と富士山とは丁度愛鷹山と富士山との關係と同樣の關係に在るものと考へられる．次に小御嶽の地形及び地質に就いて筆者の觀察した結果を述べ，夫に基づいて同山の構造を考察する．

小御嶽の地形

既に述べた様に，小御嶽は富士山本體の中腹の一般的地形及び同火山の數多の寄生

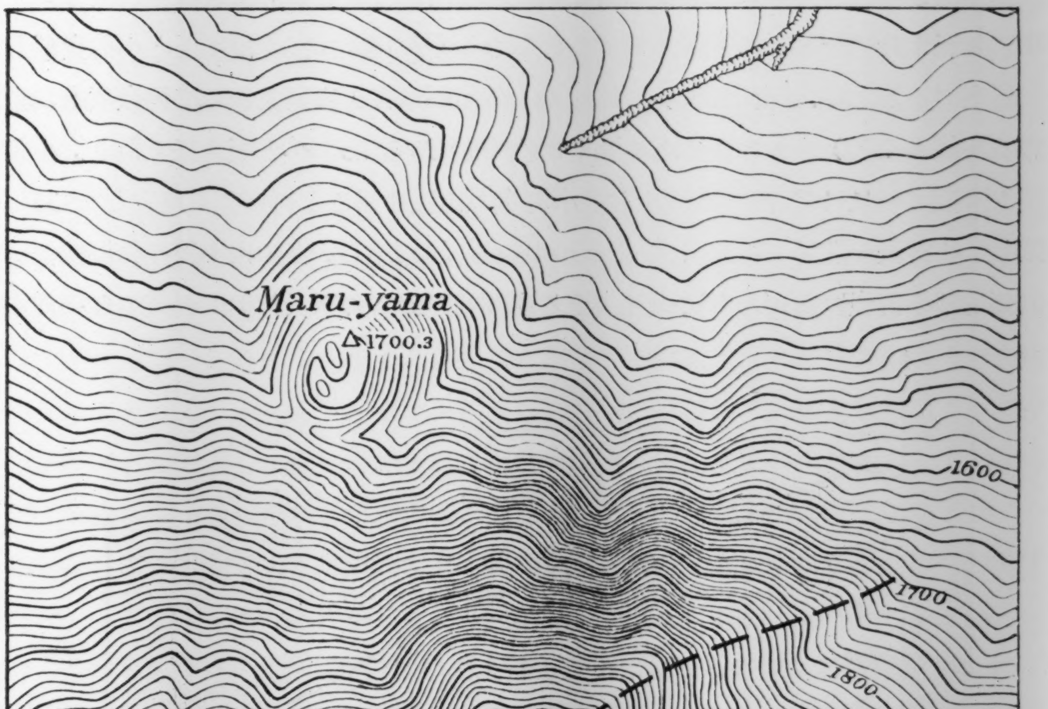
Maru-yama
△1700.3
1600
1700
1800
1900
2000
Komi-take
2100
2200
2300
2400
2500
2600
0
1000
2000 m

第１圖　富士山北腹の小御嶽及び附近の地形圖.
破線は小御嶽火山の噴火口壁の推定位置を示す.

火山の地形と著しく異なる地形を示してゐる．先づ小御嶽を其周圍の富士山本體の中腹と比較して見ると，前者は後者より一段と急傾斜の山腹を形成し，且つ一層甚しい浸蝕作用を受けてゐる．此事實は實地を見れば明かであるが，地形圖（五萬分ノ一或は二萬五千分ノ一）上にも明かに示されてゐる（第1圖）．富士山頂上と小御嶽頂上とを通過する南北の山側線を畫いて見ると，其傾斜は富士山頂上から小御嶽頂上の稍南方の海拔約 2400 m の山腹に至る間では約 35° から 25° へと順次緩くなり，小御嶽頂上附近で一旦 10° 内外に減少し，小御嶽の山腹に掛ると再び急に増大して 35° に達し，小御嶽の北麓では約 10° となつてゐる（第2圖）．富士山本體の山側線の一般的傾向は小御嶽の山頂から其山麓に至る海拔 2300 m 乃至 1300 m の高さに相當する山腹では 15° 内外である．從つて，斯樣な一般的山側線に比較して，小御嶽の頂上から山麓に至る山側線は著しく脹み，小御嶽の山麓附近の夫は反つて凹みを見せてゐる．

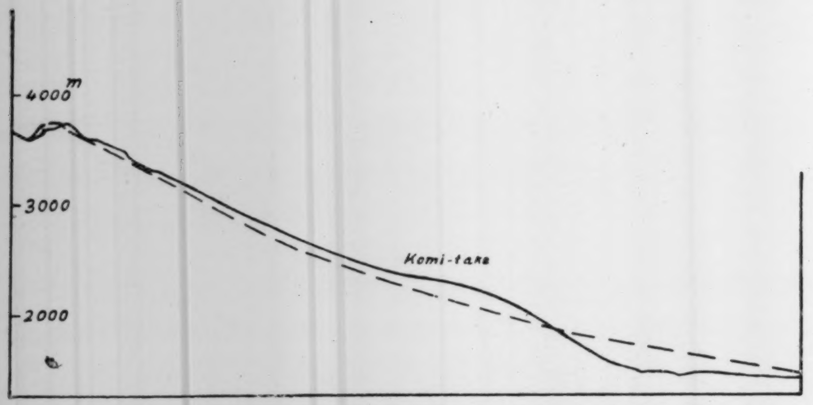

第2圖　富士山北面の山側線（實線）．
破線は富士山一般の正常の山側線．

小御嶽は其周圍の富士山本體と異なり著しい浸蝕地形を示してゐる（圖版第3圖）．卽小御嶽の山腹は幾多の深い谷に刻まれ，愛鷹山或は箱根山外輪山の山腹に極めてよく類似する一種の壯年期の浸蝕地形を示してゐる．其長さ，深さ，廣さ等に於いて小御嶽山腹の谷に優るものは富士山本體の他の部分に少くないが，之等は何れも富士山本體の山頂附近或は中腹附近に源を有する輻射谷である．小御嶽の谷系は之等と異なり，其谷系の下流は合一して富士山麓の輻射谷の一に續いてゐるが，上流は小御嶽山內に止まるのであつて，富士山本體上部の輻射谷の何れにも續いてゐない．後に述べる樣に，小御嶽は隣接する富士山本體と比較して遙かに不浸透性の，浸蝕され難い熔岩層から成つてゐるにも拘らず，常時の地表流水は其何處にも見られない．小御嶽のみに雪或は雪代水による浸蝕が特に激しいといふ事は其地質から考へて到底考へら

れない事である．從つて，小御嶽の浸蝕地形の大部分は現在の富士山本體に行はれてゐる浸蝕作用とは別の舊期の浸蝕作用に依つて形成されたと考へなければならない．卽，現在の富士山本體の出現する以前に，其處に一の舊火山體が少くとも海拔 2300 m 以上の高さを以つて聳え，小御嶽は其一部分として盛に浸蝕作用を受けてゐたのであるが，富士山本體が出現するに及んで，此舊火山體の大部分は其下に埋まつてしまつたものと考へられる．小御嶽が此舊火山體の如何なる部分を代表してゐるかは後に述べる．

小御嶽と富士山本體の寄生火山との地形的相違は明瞭である．富士山の寄生火山の中，單なる寄生噴火孔[5]及び少數の例外的寄生火山を除いて，大多數は形の大小に拘らず富士山本體の斜面から突起する圓錐丘を形成し，其頂上部には夫々其噴火口の跡たる凹地を有する．而して，斯様な寄生火山の外斜面は極めて圓滑な圓錐面で，多少の小溝以外には浸蝕谷に依つて刻まれてゐない．たゞ寄生火山の火口壁の一方が缺潰して，其處に發する一條の谷が圓錐面を深く刻んでゐる事があるのみである．[6]

小御嶽は斯る寄生火山と地形的に全く異なつて，其山頂部は小御嶽の全山體の南端に偏在し，富士山本體の斜面から著しく突出せず，噴火口の跡と考へられる凹地形を何處にも示してゐない．卽，小御嶽の頂上部と富士山本體との間には鞍部が存在せず，前者は後者の急傾斜の山腹に續く緩傾斜の山肩で，南北に伸びる幅の狹い一の尾根を形成してゐる．小御嶽の山腹は其山頂部から北方に派生する幾多の尾根と之を分かつ谷とから成つてゐる．尾根の中で最も主要なるものは小御嶽頂上部を代表する南北の尾根から北東方向に弓形に連なつてゐるものである．此弓形の尾根の凹面，卽，東面は約 30° の急傾斜をなして東方に比高約 250 m 下り，其麓に至つて小御嶽の東側を圍む富士山本體の比較的緩かな斜面に續いてゐる．弓形の尾根の凸面，卽，北西面は

---

[5] 富士山の山頂に近い部分の寄生火山は著しい圓錐丘を形成せず，單なる寄生噴火孔であり，山麓近くの寄生火山は，小さい圓錐丘も勿論あるが，比較的大形の圓錐丘である事が多い．例へば，富士山北西面の寄生火山列に見られる様に，山頂に最も近い御庭上方の寄生火山は單なる寄生噴火孔であり，山麓に最も近い大室山は此列中にて最も大きい圓錐丘であり，其間大體に於いて上方のものから下方のものに至るに從ひ大いさ及び比高を増してゐる．此傾向は山麓から山頂に近付くに從つて富士山本體の斜面の傾斜が大さなり，從つて寄生火孔から噴出した熔岩が噴出孔附近に止まらずして下方に流れ去り，又同處から噴出した火山砂礫が噴出當時の風に吹き飛ばされ，或は其後の風雨に洗ひ去られ易いためであろう．

[6] 斯様な谷には，完全な圓錐丘が出來上つて後に浸蝕作用のみに依つて生じた後生的の浸蝕谷ではなくて，圓錐丘が形成されつゝある間に其噴火作用に依つて生じたさ考へられるものがあり，噴出した熔岩が此谷に沿つて流下してゐる事がある．然し，富士山の寄生火山では多くの場合に於いて，先づ熔岩が噴して富士山本體の山麓方面に流下し，次に火山砂礫が噴出して，熔岩流の上に圓錐丘を形成してゐる．尙，富士山の北西及び南東側面には富士山成立時代の比較的新期に屬する寄生火山が數多くあるが，其他の方面の寄生火山の多くは富士山成立時代の中期或は夫以前に屬する．

東面と異なり，此尾根の各部から分岐して北西方及び北方に伸びる幾多の尾根に分たれてゐるのであつて，小御嶽の西端の尾根は夫に接する富士山本體の斜面に對して，弓形の尾根の東面に見られる様な著しい傾斜面をなして聳えてゐない．小御嶽の北麓部は，既に述べた様に，約10°の緩斜面をなして北方に下り，西方の丸山と東方の富士山本體の山腹との間に挾まれて，一の凹地を形成してゐる．

以上述べた様な小御嶽自體の地形及び小御嶽と富士山本體との地形的關係から判斷すると，小御嶽は富士山本體の寄生火山でなく，富士山本體の下に埋まつた一の舊火山體の一部であり，而も此舊火山の山頂部の一部を代表するものと考へられる．卽，小御嶽の頂上から北東に連なる弓形に彎曲した尾根の東側の急斜面は此舊火山體の火口壁北西部を代表し，弓形の尾根の西側及び北側の多數の尾根に分たれた斜面は此舊火山體の噴火口の北西外側斜面の一部を代表するものであつて，壯年期の浸蝕を受けた火山の噴火口或は爆裂火口の火口壁と夫に接續する外側斜面とに普通に見られる地形である．地形觀察に基いた以上の推定は，次に述べる様に，小御嶽の地質を調査し更に小御嶽の東方の燕澤の東側に小御嶽と全く同一の地質から成る小地域の見出される事に依つて益々確められた．

小御嶽の地質

小御嶽の地質は至つて簡單であつて，肉眼的にも顯微鏡的にも變化の少ない幾多の熔岩層と其間に介在する集塊岩層及び火山砂礫層とから成つてゐる．小御嶽の一部殊に其山頂附近と山麓一帶とは富士山本體の噴出物に厚く蔽はれてゐるが，其他の大部分には小御嶽自體を構成する之等の岩石が至る處に露出してゐるのであつて，小御嶽の北麓から其山腹の各谷に入つて急斜面を南方に登つて行くと，谷壁には小御嶽を構成する熔岩及び火山砂礫の累層がよく見られる．たゞ丸山の南麓に開く一の谷に於いては，谷の東壁に小御嶽の熔岩とは全く別種の熔岩（第3圖中のA）の厚層（厚さ20m以上）が露出してゐるが，此熔岩は富士山本體を構成する熔岩類の一種で，富士山本體の或時代の噴火口から噴出し，小御嶽の頂上を經て其北腹の急斜面を北方に流下したものである．

小御嶽の北腹及び北西腹に露出する同山の熔岩，集塊岩，及び火山砂礫の累層は北方及び北西方に35°内外の急傾斜を以つて下り，同地域の一般の尾根の傾斜と全く一致する傾斜を示してゐる．從つて，小御嶽の北腹及び北西腹の尾根の急傾斜面は浸蝕面ではなくて，小御嶽を以つて代表される一舊火山の山腹の原傾斜面の一部に相當する（第4圖）．而して，富士山本體に見られる様に，斯る急傾斜面は一般に圓錐形成

層火山に於いては其頂上部の外側斜面に形成されるのみであるから，小御嶽の北腹及

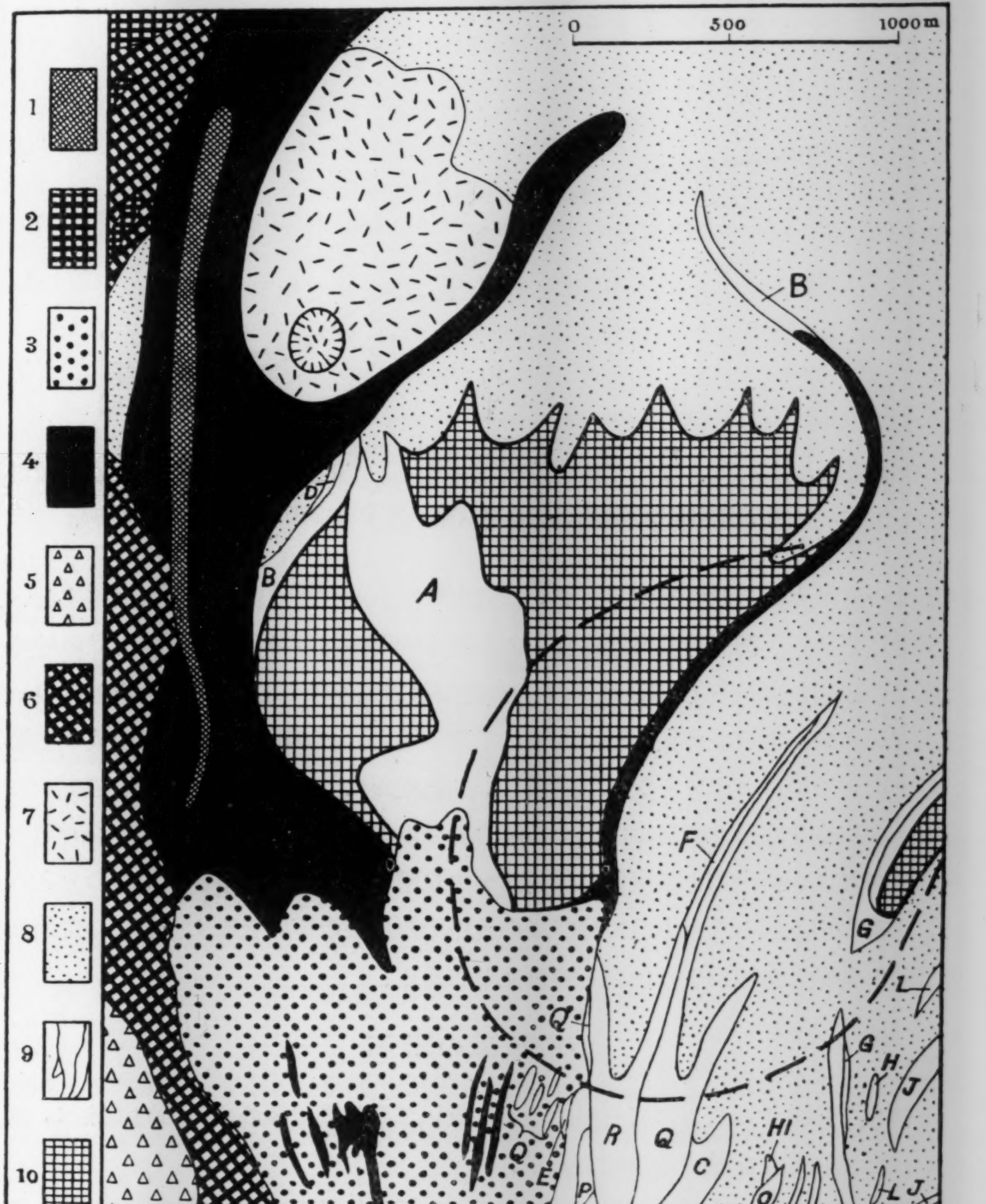
1
2
3
4
5
6
7
8
9
10
0
500
1000m
A
B
B
D
F
G
G
H
H
HI
I
J
J
L
L
M
O
P
Q
Q
Q
Q
R
R
C
E

第 3 圖　富士山小御嶽及び附近の地質圖.
1 小御嶽風穴熔岩.　2 ガラン熔岩.　3 牛ケ窪熔岩砂礫.　4 牛ケ窪熔岩.　5 劍丸尾熔岩砂礫.　6 劍丸尾熔岩.　7 丸山寄生火山砂礫.　8 火山灰一般.　9 火山灰に蔽はれる富士山舊期熔岩類（A～R）.　10 小御嶽火山噴出物（熔岩，集塊岩，及び火山砂礫）.

び北西腹の原傾斜面は一の圓錐形成層火山の頂上近くの外側斜面の一部を代表するも

のと考へられる．此原傾斜面の傾斜方向及び夫に一致する熔岩，集塊岩，火山砂礫等の累層の傾斜方向から判斷すると，既に地形から推定した樣に，小御嶽の北腹及び北西側は一圓錐火山の北西側傾斜面で，其噴火口は小御嶽の南東側に在るに相違ない．

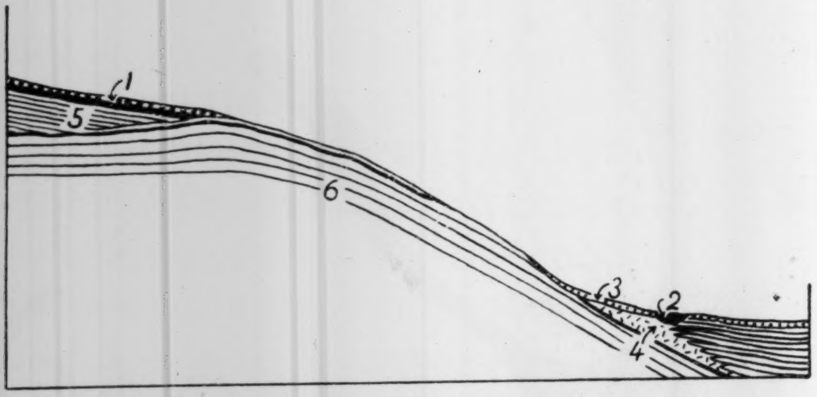

第 4 圖　富士山小御嶽の南北斷面圖.
1 牛ヶ窪熔岩砂礫. 2 牛ヶ窪熔岩（丸山東側の支流. 第 3 圖參照). 3 火山灰一般. 4 小御嶽北麓の崖錐及扇狀地堆積物. 5 富士山舊期熔岩類. 6 小御嶽火山噴出物.

小御嶽頂上の小御嶽神社附近は富士山本體の噴出物のみであるが，同神社の神苑内を通つて社祠の裏から小御嶽東側の急傾斜面を二三十米下ると，富士山本體の一熔岩（卽，丸山南方の小御嶽山腹に流下してゐる熔岩）の下に，小御嶽を構成する熔岩が殆ど直立の絕壁に累層をなして露出し，其絕壁面にては略水平に近い層理を示してゐる．小御嶽北腹及北西腹に露出する熔岩累層の傾斜の大いさ及び方向と合せ考へると，此事實は小御嶽頂上の東側の急斜面が火口壁の一部である事を示すものと考へられ，小御嶽頂上から北東方向に伸びてゐる弓形の尾根の東側をなす一續きの急斜面を火口壁と見做した地形上の推定を裏書きしてゐる．

小御嶽の岩石

小御嶽を構成する岩石の岩石學的性質に就いては玆では極めて概括的に述べ，更に他の機會に詳しく記載する豫定である．

小御嶽を構成する主要なる岩石は熔岩層で，集塊岩及び火山砂礫は夫に比較して極めて少量に過ぎず，熔岩層の間に一般に 1 m 或は夫以下の薄層をなして介在するのみである．熔岩は 1 m 內外から 10 m 內外に及ぶ厚さの層をなし，集塊岩或は火山砂礫の層に距てられて幾重にも重なり合つてゐるのであつて，30 層以上の熔岩層の數へられる露出が少くない．此多數の熔岩層の一々を詳しく檢べると，各層の熔岩相互の間に多少の岩石學的性質の變化が認められるが，概して何れもよく似た熔岩で，殊

に肉眼的には殆ど同一である．

小御嶽の熔岩は外觀何れも淡灰色緻密質で，直徑約 3 mm 或は夫以下の斜長石の白色斑晶を極めて多量に有する．尙，同程度の大いさの輝石の肉眼的斑晶が含まれてゐるが，其量は熔岩層に依つて異なり，或熔岩層には斜長石斑晶の間に點々と可成り多量に認められ，時としては殆ど認められない．

顯微鏡下で觀察すると，小御嶽の熔岩は一般に結晶度の非常に高い熔岩で，多量の斑晶と其間を埋める結晶質の石基とから成つてゐる．斑晶の中では斜長石（累帶構造が著しい）が勿論最も多く，輝石（單斜輝石及び斜方輝石）は熔岩に依つては一薄片中に殆ど一も入つて來ない程度に少ない事もある．之等の他に，橄欖石の斑晶が見出されるが，一般に直後 0·5 m 以下の微粒で，常に輝石粒に依つて圍まれてゐる．石基は短矩形乃至正方形の斜長石，柱狀のピジョン石，粒狀の磁鐵鑛，及び少量の珪酸鑛物（主として鱗石英）から成り，玻璃を殆ど含んでゐない．然し，1 m 内外の厚さの熔岩或は夫以上の厚さの熔岩の上面及び底面に近い多孔質の部分の石基には多少の玻璃質部が殘つてゐる．熔岩層の間に介在する集塊岩及び火山砂礫は岩石學的には上述の熔岩の性質と同樣の性質を有するものである．從つて，小御嶽の岩石は一般に斜長石の斑晶を多量に含み，結晶度の高い含橄欖石・複輝石安山岩である．

後に述べる樣に，小御嶽の熔岩と同一の熔岩は燕澤の小地域に見出されるが，之を除けば，現在迄に調査した限りに於いては，富士山の地域内の何處にも露出してゐない[7]．小御嶽の熔岩が富士山本體及び其寄生火山を構成する熔岩類と著しく異なつてゐる事は，兩者を比較すれば一見して明かである．後者は肉眼的及び顯微鏡的に多種多樣の岩質を示すが，何れも玄武岩[8]である．小御嶽の熔岩は富士山本體及び其寄生火山の熔岩類よりも寧ろ愛鷹山の或種の熔岩に極めてよく似てゐるのであつて，此事實は之等の火山の熔岩の化學成分を比較すれば直ちに了解される．

第 1 表の I は小御嶽熔岩の一の化學成分であつて，後に述べる燕澤から採集した一標本の分析結果であるが，小御嶽自體の熔岩の化學成分をも代表する事は疑ひない．之を II に示す愛鷹山の一熔岩の化學成分に比較すると，兩者の各成分の量及び割合ひがよく似てゐる．兩者共にアルミナの量が非常に多いが，之は分析した標本の何れもが灰長石成分に富む斜長石斑晶を多量に含む事に因る．富士山本體及び其寄生火山の熔岩類は既發表及び未發表のものを合せて十數個分析されてゐるが，其結果は何れ

---

[7] 筆者はさきに小御嶽熔岩が富士山南麓の最舊期熔岩類と同一であると考へたが，此考へは正しくないので茲で訂正する． H. TSUYA, *Bull. Earthq. Res. Inst.*, **15** (1937), 305.

[8] 富士山南東側の寶永山の下方に於いて見出される無斑晶黑曜石質の熔岩塊は中性安山岩質の化學成分 (SiO_2 63·94%) を有するが，此岩石の成因に就いては尙疑問が殘されてゐる． H. TSUYA, *Bull. Earthq. Res. Inst.*, **15** (1937), 307.

第　1　表

	I	II	III	IV	V
SiO_2	53·00	54·70	51·05	52·35	55·06
Al_2O_3	21·50	20·18	18·35	18·86	21·13
Fe_2O_3	2·10	2·40	2·76	3·68	2·28
FeO	5·60	5·10	7·72	5·29	5·61
MgO	2·63	2·67	4·63	4·42	2·15
CaO	9·96	8·33	9·90	8·32	7·55
Na_2O	3·19	3·65	2·81	3·62	2·27
K_2O	0·56	0·77	0·81	0·97	0·99
$H_2O(+)$	0·25	0·75	0·40	1·03	1·15
$H_2O(-)$	0.08	0·40	0·11	0·75	0·74
TiO_2	0·90	0·93	1·41	1·05	0·70
P_2O_5	0·10	0·20	0·24	0·27	0·24
MnO	0·15	0·14	0·18	0·10	0·15
Total	100·02	100·22	100·37	100·71	100·02

I.　含橄欖石・複輝石安山岩 (Olivine-bearing two-pyroxene-andesite). 富士山北東側，燕澤東壁 (海拔約 2050 m), 熔岩. 田中分析.

II.　紫蘇輝石安山岩 (Hypersthene-andesite). 愛鷹山東側，熔岩. H. Tsuya, *Bull. Earthq. Res. Inst.*, **15** (1937), 277.

III.　紫蘇輝石・普通輝石・橄欖石玄武岩 (Hypersthene-augite-olivine-basalt). 富士山南東側，熔岩. H. Tsuya, *Bull. Earthq. Res. Inst.*, **13** (1935), 645.

IV.　含橄欖石・普通輝石安山岩 (Olivine-bearing augite-andesite). 茅ヶ嶽. 市來政兼，地震研究所彙報，**7** (1929), 335.

V.　含橄欖石・複輝石安山岩 (Olivine-bearing two-pyroxene-andesite). 飯綱山. 山田節三，地震研究所彙報，**12** (1933), 96.

も小御嶽の熔岩の化學成分より基性で，玄武岩の成分を示してゐる．第1表の III は其中の一で，富士山本體の熔岩類の中で斜長石斑晶を比較的多量に含んでゐる熔岩の化學成分の一例である．小御嶽熔岩のアルカリ含有量は富士，愛鷹，茅ヶ嶽，飯綱山等の熔岩類の夫と同様に，箱根以南の伊豆及び南方諸島に產する類似熔岩類のアルカリ含有量に比較して大である（第 1 表の IV 及び V は夫々茅ヶ嶽火山9) 及び飯綱山火山10) の熔岩の化學成分を示す）．從つて，所謂廣義の富士火山帶を熔岩の化學成分上の特徴から箱根以南の“大島火山帶”と夫以北の狹義の“富士火山帶”とに分けて考へた筆者の論據が小御嶽熔岩の分析に依つて一層强められた次第である．11)

燕澤の小御嶽熔岩露出地域

燕澤は富士山頂上近くの北東側に發し，吉田登山道の西側に沿つて北東方に下つて

---

9)　市來政兼，地震研究所彙報，**7** (1929), 335.

10)　山田節三，前同，**12** (1933), 96.

11)　H. Tsuya, *Bull. Earthq. Res. Inst.*, **15** (1937), 340.

ゐる大きい澤である．小御嶽の熔岩と同一の熔岩が露出するのは吉田登山道三合目から小御嶽頂上の小御嶽神社に通ずる捷徑が此澤を横切る地點で，小御嶽頂上から東方に約 1500 m，吉田三合目から約 500 m 距たり，海拔約 1950 m で，小御嶽頂上より約 350 m 低位置に在る．同處に於いて，燕澤は約 150 m の幅と約 50 m の深さとを有し，澤の兩側の上半部は澤底に向つて殆ど絶壁をなし，澤を横切る道は此絶壁の僅かに崩れた處を上下してゐる．澤の西側の絶壁は厚さ 2〜5 m 内外の一枚の熔岩から成り，其上下には火山砂礫の厚い累層が在る．此熔岩は灰色緻密質の橄欖石玄武岩で富士山本體を構成する熔岩類の一である．澤の東側の絶壁は之と全く異なり，小御嶽自體を構成する熔岩と同一の熔岩と集塊岩及び火山砂礫との累層から成つてゐる．此累層は澤の東壁を下る道に沿つても見られるが，澤底に下りて上流に溯ると，約 300 m の間の澤底及び東壁に一層明瞭に露出してゐる．即，同處には厚さ 0·3〜1·0 m の熔岩が集塊岩及び火山砂礫の薄層を挾んで 21 枚以上重なり，東方に 10〜20° の傾斜を以て下つてゐる．此 21 層の熔岩を採集して比較して見ると，何れも殆ど同樣で小御嶽自體の熔岩に同じく，斜長石の多量の肉眼的斑晶を有する灰色緻密質の含橄欖石・複輝石安山岩である．第 1 表に掲げた小御嶽熔岩の化學成分は此處の露出に於いて上から二枚目の熔岩を分析した結果を示す．

燕澤西壁の玄武岩熔岩は澤に沿つて溯ると其西壁に續いて露出し，道から約 300 m の上流では 10 m 以上の厚さを示し，其附近で澤の東壁の小御嶽熔岩の累層を不整合的に蔽ひ，又此累層の絶壁に不整合的に接してゐる．從つて，燕澤東壁の小御嶽熔岩の絶壁は西壁の玄武岩熔岩が未だ噴出しない前から存在してゐたと考へなければならぬ．即，小御嶽熔岩の絶壁の西側には以前から低地或は一の澤が存在し，後に富士山の噴火口から噴出した玄武岩熔岩は此低地或は澤に沿つて流下し，小御嶽熔岩の絶壁に接して之を埋めたが，其後の浸蝕作用に依つて兩熔岩の境に沿つて燕澤の流路が生じ，其一方には小御嶽熔岩の絶壁が再び現れ，他方には玄武岩熔岩の絶壁が形成されたと考へられる．

小御嶽熔岩の露出してゐる燕澤東壁の外側の山腹，即，吉田登山道三合目から五合目に至る地域には小御嶽熔岩は露出せず，一帶に富士山本體の熔岩類及び火山砂礫層が分布してゐる．然し，此地域の山腹は富士山本體の中腹として異常に急な傾斜を示し，火山砂礫層は小御嶽熔岩の露出する燕澤東壁の崖緣に沿つた山腹を蔽つてゐるが，富士山噴出の熔岩類は此山腹を避けて吉田登山道五合目或は夫より上方から北々東に流れるか，或は燕澤西側の山腹を流下してゐる．從つて，三合目から五合目附近に至る間の富士山噴出物の下には舊山體が埋まり，其一部が燕澤の東壁に露出する小

御嶽熔岩の累層であると考へられる.

小御嶽本體と燕澤の小御嶽支體との構造的關係

燕澤東壁の小御嶽熔岩累層が富士山本體の熔岩類と岩石學的に明かに異なる事は小御嶽本體の熔岩に就いて述べたと同様であるが，更に同熔岩累層が 20° 内外の傾斜を以て南東方に下つてゐる事實は此累層の噴出中心が富士山本體の中心ではなくて，西方の小御嶽本體の方向に在る事を示すものである．然るに，小御嶽本體の構造は其熔岩の噴出中心が同體の南東方に在る事を示してゐる．從つて，小御嶽熔岩の噴出中心は小御嶽本體と燕澤の同支體との中間の位置を占めてゐるに相違ない．而して，小御嶽本體の頂上から北東方向に伸びる弓形の尾根の東側は火口壁の一部と考へられるから，小御嶽熔岩の噴出中心と推定される地域を距てゝ之に相對し，小御嶽熔岩に依つて構成されてゐる燕澤東壁は同一火口壁の他の一部を代表するものと考へられる．此燕澤東壁の現在の地形は勿論浸蝕作用の結果であつて，火口壁其ものではないが，火口壁の一部が其近くにあつた事は事實である．故に，小御嶽本體の弓形の尾根の峰線を延長し，燕澤東壁を通過する一の曲線を畫くと，其曲線は小御嶽熔岩の噴火口の周壁の上縁を代表する事になる．かくして得られる噴火口の外郭は略楕圓形で，北東—南西及び北西—南東に夫々約 130 m 及び 200 m の直徑を有する．此噴火口の北東壁は恐らく缺けてゐて，富士山本體の熔岩は其處を通つて自由に流下したに相違ない．又，南西壁は富士山の噴出物に全く蔽はれてゐるが，其地形は小御嶽頂上から吉田登山道六合目に通ずる道路に沿つた通稱“横ブキ”附近の急斜面に依つて表されてゐる．從つて，小御嶽熔岩の噴火口は北東方向に開いた一の馬蹄形噴火口であると考へられる．此噴火口が小御嶽に依つて代表される火山の唯一の主火口であるか否かは明かでないが，兎に角此火口を中心とし，小御嶽自體と燕澤東壁の同支體とに依つて形成される火山を玆に“小御嶽火山”と呼ぶことゝする．

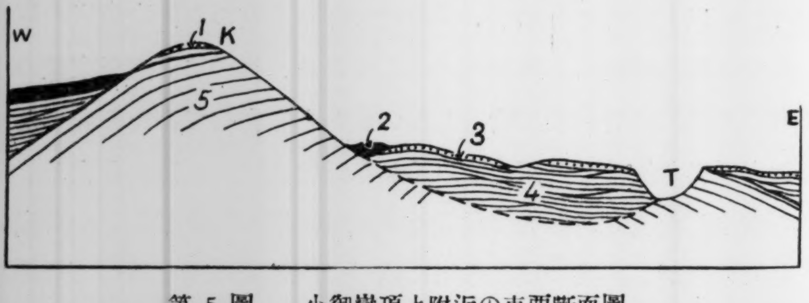

第 5 圖　小御嶽頂上附近の東西斷面圖.
1 牛ケ窪熔岩砂礫.　2 牛ケ窪熔岩.　3 火山灰一般.　4 富士山熔岩類.　5 小御嶽火山噴出物.　K 小御嶽.　T 燕澤.

小御嶽火山と富士火山本體との構造的關係

小御嶽は上に述べた様な構造を有する一の截頭圓錐形成層火山であるから，富士山本體より舊いが，後者の所謂外輪山であるとは考へられない．兩火山は，少くとも各自體の內部構造のみから見れば，夫々獨立無關係で，愛鷹山に對する富士山と同樣の位置的關係に在る．たゞ愛鷹山は富士山の噴出物に依つて其裾野の一部を蔽はれてゐるに過ぎないが，小御嶽火山は其頂上部の一部を殘して大部分を富士山の噴出物に依つて蔽はれてゐる．

小御嶽火山が完全な圓錐形火山であつたとすると，其南西斜面は現在の富士山の山頂部の直下に潛在するはずである．從つて，小御嶽火山の外斜面が現在の富士山の外斜面と略同樣の傾斜を有すると假定すると，富士山頂上の噴火口底の直下約 3000 m 卽，海拔 700 m 內外の高さの位置に小御嶽火山の南西斜面の中腹が潛在し，其裾野は富士山南西斜面の中腹（海拔 2500 m 內外）の直下にて現在の海水面の下に入つてゐるものと推定される．此推定が正しいとすると，富士山の南西面に於いては，其斜面が餘程深く浸蝕されない限り，小御嶽火山の山體は地表に露出するに至らない．小御嶽火山の他の方面の斜面も，其山頂に近い部分は現在の小御嶽に露出してゐるが，中腹以下の裾野の部分は同方面の富士山々腹の現地表面から少くとも數百米の地下に潛在してゐるものと推定される．

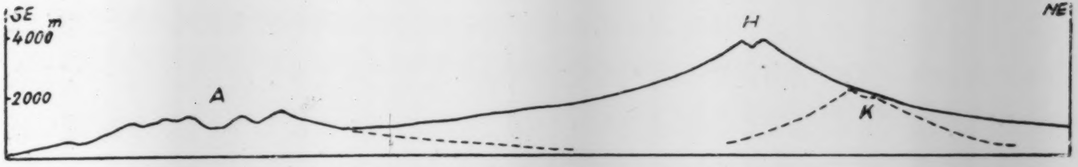

第 6 圖　　富士山，小御嶽，及び愛鷹山の構造的關係を示す．
H 富士火山．K 小御嶽火山．A 愛鷹火山．

以上の推定は小御嶽火山の基底の地形が略平坦であつたとして行はれたのであるが實際に於いては，富士山の周圍には南側を除いて第三紀層の山地があり，特に其東方山地は籠坂峠西大鶴から西方に富士山下に深く潛入してゐるから，小御嶽火山が之等の山地に接して如何なる擴がりを有するか明かでない．又，愛鷹山の北西斜面が圓滑な傾斜を以て富士山の下に潛入してゐると假定すると，同斜面の山麓部は小御嶽火山の南斜面に接してゐることになるが，此兩火山の噴出の前後關係は全く不明である．

要するに，小御嶽は一の圓錐形火山の頂上部を代表してゐるから，其基底が特殊の地形でない限り，同火山の南西斜面は富士山の頂上直下より更に南西方向に擴がつてゐると考へなければならぬ．換言すれば，富士山は小御嶽火山の南西斜面上の一地點

から噴火を初めたのであつて，少くとも位置的には，後者の寄生火山が主體より大きく成長したかの如き關係に在る．然し，富士火山が最初の噴火を初めたのは小御嶽火山が既に著しく浸蝕された後であるから，火山活動の輪廻から見れば，兩者は夫々獨立した火山と考へられる．

小御嶽火山の存在は富士山から噴火した熔岩類の分布狀態に影響を與へてゐる．富士山が，平林博士の考へた樣に，既に活動の初期に多量の所謂集塊質泥流の噴出に依つて巨大な山體を形成してゐたか，或は石原學士の考へた樣に，最初に熔岩を噴出したかは尙今後の調査の上でないと何れとも斷定出來ないが，少くとも現在地表に露出してゐる富士熔岩類の中，最舊期に屬するものは平林博士の所謂三島大宮熔岩で，富士山南麓の三島から大宮方面に亘つて分布する數種の熔岩類である．之に該當する熔岩類は，現在までの調査の結果では，富士山の北麓の吉田方面には，全く見出されない．富士山北麓方面に露出してゐる最舊期の熔岩類は主として富士山中腹の谷に露出してゐる熔岩累層中の下部の熔岩層に相當するもので，富士山の全熔岩類中の略中期熔岩類を代表してゐる．斯樣に富士山の最舊期の熔岩類が其南麓方面にのみ分布してゐるのは此熔岩類の噴出當時の地表が噴出地點の北方に高まり，南方に低まつてゐた事に因る．富士山の基底の北部は之を圍む第三紀層の山々に接して，駿河灣に近い南部より元々高まつてゐたと思はれるが，小御嶽火山の噴出に依つて一層高まつてゐたに相違ない．從つて，同火山の南西斜面上の一地點を中心として活動を始めた富士山が假りに最初に多量の所謂集塊質泥流を噴出し，次いで最舊期の熔岩類を噴出したとしても，之等の噴出物は主として南方山麓に向つて最も遠く流下し，小御嶽火山の蔭に當る北方山麓方向には達し得なかつたと考へられる．卽，此時代の富士山は小御嶽火山よりも餘程低い火山であつたに相違ない．然るに，富士山の中期の熔岩類は南麓方面のみならず，小御嶽火山の頂上部を越へ，或は之を廻つて北方山麓にも流下してゐる．其數種の熔岩類が小御嶽火山の馬蹄形噴火口の中に流れ落ち，其北東部の缺處を經て北東麓に達してゐる狀態は地形にもよく表されてゐる．從つて，此時代には富士山は小御嶽火山より高く，前者の噴出物は後者の大部分を埋めてゐたと考へられる．富士山の新期の熔岩類が小御嶽火山の山體を廻つて流下してゐる狀態は更に明瞭で，其一熔岩の如きは（地質圖に黑く塗られてゐるもの）小御嶽の頂上附近に於いて東西に分岐し，東方の熔岩流は小御嶽の東麓を狹い谷に沿つて流下してゐる．西方の熔岩流は小御嶽の西側を北方に流下し，丸山の頂上附近に於いて更に分岐し其一は丸山の西側を北流して所謂劍丸尾熔岩流の一部となつてゐるが，他は丸山と小御嶽との間を北東に流下し，小御嶽の北麓の低地に達して止まつてゐる．

總　括

富士山の北側の中腹に一の急斜面を成して突起する小御嶽は現在の富士山本體及び其寄生火山と異なつて，著しい浸蝕地形を示し，富士山頂上からの噴出物に依つて多少蔽はれてゐるが，其大部分は之と異なる含橄欖石・複輝石安山岩の多數の熔岩層及び其間に挾まる集塊岩，火山砂礫層等に依つて構成されてゐる．小御嶽の頂上から東方に約 1·5 km 距たり，燕澤中流の東側に，小御嶽の累層と全く同岩質の累層から成る小地域がある．小御嶽本體の累層は其北方及び北西方の山側傾斜と一致して，北方及び北西方に 35° 内外の傾斜を以て下つてゐるのに對し，燕澤支體の同累層は南東方に 20° 内外の傾斜を以て下つてゐる．從つて，小御嶽本體と燕澤支體とは共に現在の富士山本體の一部ではなく，一の成層火山の頂上附近の一部を代表するもので，茲に小御嶽火山と呼ばれる火山に屬する．而して，此火山の噴火口は小御嶽本體と燕澤支體との中間地域に在つて，北東壁を缺く馬蹄形（直徑約 1·5 km）の火口壁に依つて圍まれるものと推定され，小御嶽の頂上から北々東に連なる弓形の尾根の東側の急斜面は其北西壁を代表し，燕澤支體の燕澤に臨む絶壁は其南東壁の一部を代表する．

小御嶽本體及び燕澤支體は夫等に接する富士山の凡ての新舊噴出物より舊期に屬する　即，富士山から噴出した數多の熔岩流は之等の舊山體を取り卷いて埋め，推定された小御嶽火山の馬蹄形火口の中に流れ込み，更に其北東壁の缺處を通つて北東方に流下してゐる．

要するに，小御嶽は構造上から見て現在の富士山本體の一部でない事は勿論，其寄生火山でもなく，又所謂外輪山の一部でもない．小御嶽火山と富士山の初期の噴出物との地質關係は確められないから，前者が舊い富士山の寄生火山であると考へる事も全く不可能ではない．然し，若し斯樣な關係の舊富士山がありとすれば，小御嶽の位置及び地形から考へると，少くとも其山體の一部が小御嶽と同程度或は夫以上の高さの位置に露れてゐなければならないが，斯樣な山體は何處にも見出されない．又，普通に寄生火山と呼ばれるものは小御嶽の如く多數の熔岩の累層に依つて構成されてゐない．從つて，小御嶽火山は構造上富士山とは全く別個の圓錐形成層火山であると考へるのが最もよく凡ての事實を說明する．富士山が，少くとも現在見得る限り，玄武岩類に依つて構成されてゐるのに對し，小御嶽火山は寧ろ愛鷹山に產する或種の熔岩に類似する安山岩に依つて構成されてゐる．小御嶽火山は恐らく愛鷹山火山と略同時代で（洪積期の初期乃至中期），富士山の出現する前に既に壯年期の浸蝕作用を受けた火山として存在し，其後に至つて其南西側に出現した富士火山の噴出物に依つて

次第に埋沒せられ，現在僅かに其山頂附近の一部を小御嶽及び燕澤東側の小地域に露出してゐるものと考へられる．換言すれば，富士火山は小御嶽火山の寄生火山と見られる樣な位置に在る．然し，兩火山の活動期には著しい距たりがあるから，富士火山は偶々小御嶽火山の山側から噴出したのみであつて，通常の寄生火山の概念に從へば後者の寄生火山ではない．

34. *Geological and Petrological Studies of Volcano Huzi (Fuji), I.*

1. *Geological structure of Komitake.*

By Hiromichi Tsuya.

Earthquake Research Institute.

Komitake, situated 2300 m above sea level and about 1500 m below the summit of Volcano Huzi, is a prominent shoulder projecting from the northern flank of the volcano. The projection which, morphologically and structurally, differs considerably from any of the parasitic cones on the volcano, is a ruin of an old volcanic body that underlies the present cone of Huzi. Its northern side which slopes about 35° toward the northern foot of Huzi, is badly dissected by ravines radiating from the crest of an arcuate ridge that runs north-northeastwards from the top of Komitake. The east side (concave side) of the arcuate ridge, which represents the eastern margin of the projection, is a short, steep slope having the appearance so usual to walls of former craters on dissected conical volcanoes

Although Komitake is thinly covered by ejecta from Huzi, its main lower mass is composed of both lava-flows and pyroclastic beds which, petrographically, differ from any of the Huzi ejecta that are exposed in the area about the mass. The strata of these lava-flows and pyroclastic beds are well exposed in the ravines on the northern side of Komitake, where they show a steep northward dip (about 35°) that coincides with the surface slope on that side. They are also exposed on the eastern scarp of the arcuate ridge, their strata ending abruptly with the cliff.

About 2 km east of the top of Komitake and close to the third stage of the Yosida route leading to the summit of Huzi, lies a small outlier that belongs geologically to Komitake. The outlier is composed of both lava-flows and pyroclastic bed which, petrographically, are very similar to the lavas of Komitake itself. They are exposed on the cliff running in a southwest-northeast direction for a distance of about 1000 m along the west margin of the outlier and forming the east wall of the middle course of the Tubakuro-zawa, the largest gully on the northeast side of Huzi. The lava-flows which, together with the pyroclastic beds interposed between them, are formed in layers numbering more than twenty five, show a dip of about 20° southeast.

The Komitake lavas which may be called olivine-bearing two-pyroxene-andesite, differ petrographically from any of the Huzi basalts, so far the latter are represented by the lavas now exposed on the volcano. The Komitake lavas are pale-gray, compact, and strongly porphyritic with numerous phenocrysts of basic plagioclase and a few pyroxenes (rhombic and monoclinic). Microscopically, a few small phenocrysts of olivine are also found, besides the plagioclase and the

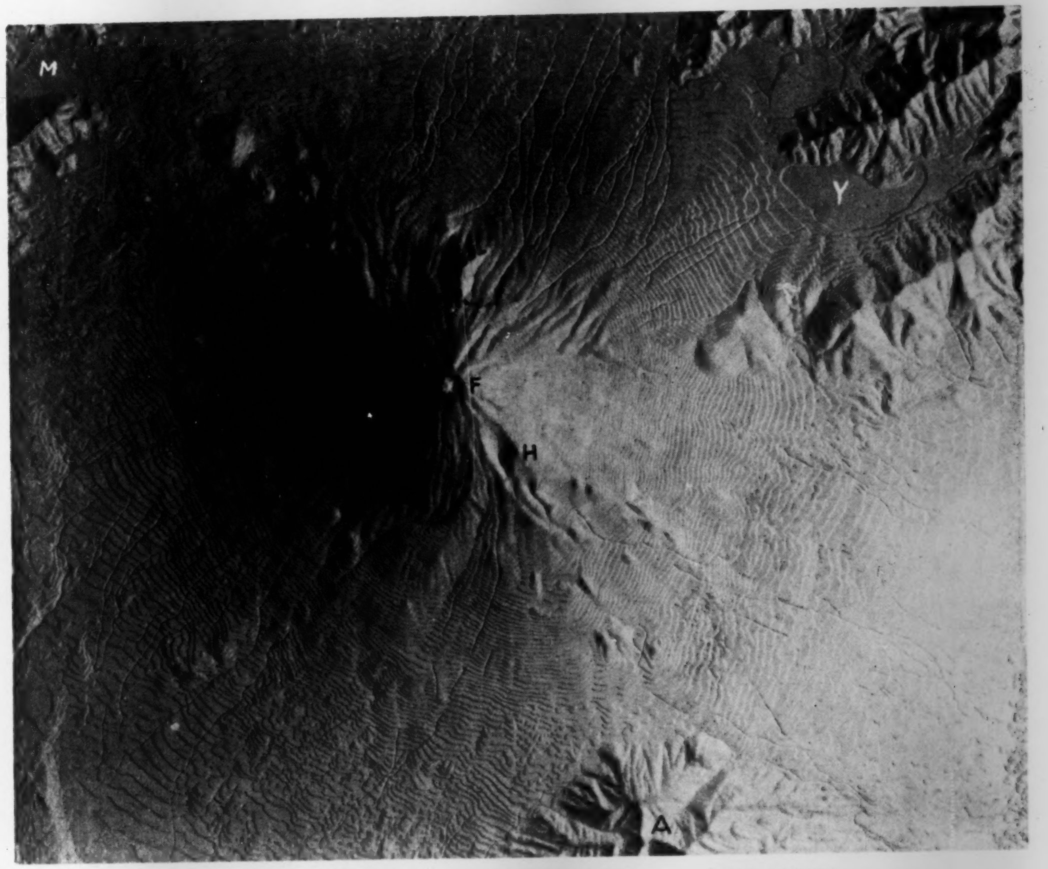

第 1 圖　富士山の地形模型圖（五萬分ノ一模型の縮寫）.
F, 富士山頂　H, 寳永山.　K, 小御嶽.　A, 愛鷹山.　M, 本栖湖.　Y, 山中湖.

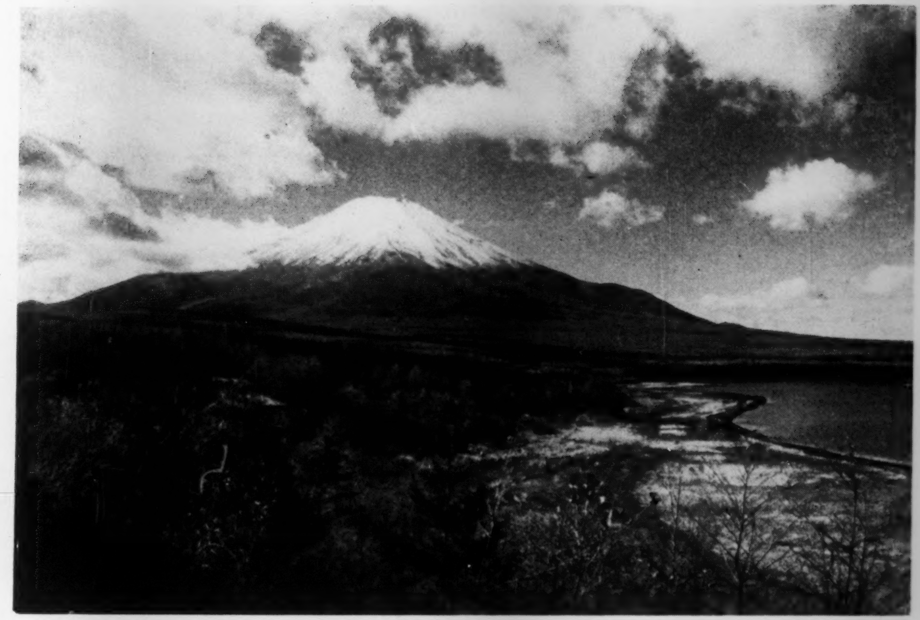

第 2 圖　山中湖岸より富士山を望む. 富士山右肩の膨みは小御嶽.

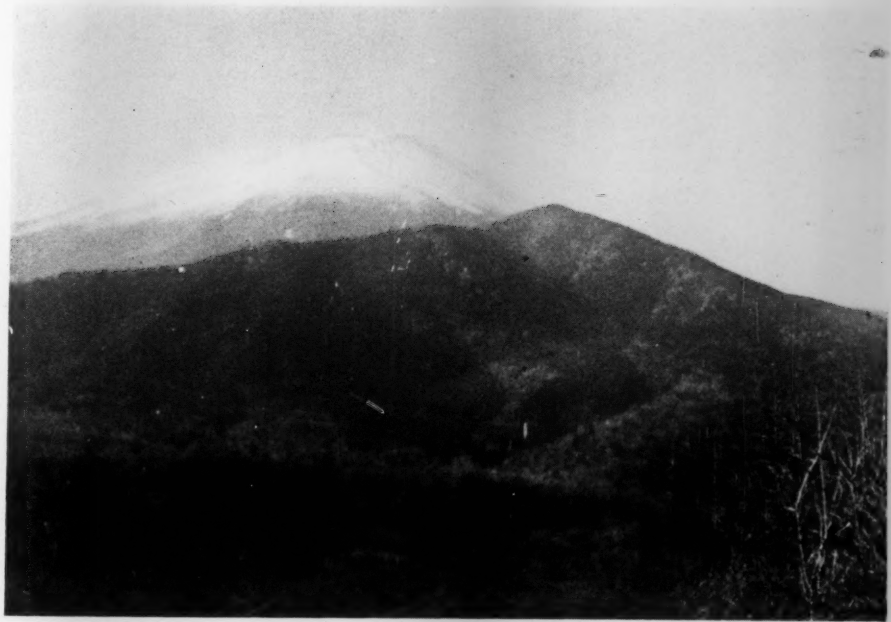

第 3 圖　小御嶽北麓より南方に小御嶽及び富士山頂部を望む.

pyroxenes, in a groundmass consisting of plagioclase laths, pigeonite prisms, magnetite cubes, and interstitial tridymite. As will be seen from Table I (I, Komitake lava. II, Asitaka-yama lava. III, Huzi lava. IV, Kayaga-take lava. V, Iizuna-yama lava.), the Komitake lavas show chemically a closer resemblance to certain lavas from Volcano Asitaka-yama adjoining the southeastern foot of Huzi than to the Huzi lavas.

Komitake and its outlier on the Tubakuro-zawa may therefore be interpreted as ruins of the top of a conical strato-volcano, the old centre of which is located midway between them, the greater part of the volcano having buried underneath the main body of Huzi. It seems best to refer to this andesitic volcano as the Komitake volcano. The Komitake volcano which, on the evidence of erosion alone, is supposed to be contemporaneous with the Asitaka-yama volcano, may be probably of lower-Pleistocene age.

35. 昭和13年1月12日，日ノ御崎沖
地震調査報告

地震研究所 水上 武

(昭和13年2月15日發表—昭和13年3月20日受理)

昭和13年1月12日0時12分頃和歌山縣日ノ御崎南方約15粁沖合に起つた地震は，和歌山縣及び德島縣に於いて，近年稀に見る震度の大なる地震であつた．その有感區域は，九州の福岡，宮崎より，四國，中國及び關東地方の一部，長野縣の一部(本所淺間山支所に於いて有感)亘る廣範圍の有感覺地震であつた．然しながら，幸ひに震央が陸地への最短距離15粁の海中にあつた爲に，家屋其の他構造物の被害は極めて輕微に過ぎず，全壞家屋一戸も無く，半壞程度の小屋2，3戸の損害に留り，一方斷層或は土地の隆起，沈下等著しい地學現象は全く現はれなかつた．海底に震央を有する強震として，津浪の襲來に就いて海岸各地に於いて警戒されたのであつたが，これまた大阪府，和歌山縣の各測候所の檢潮記錄は津浪の痕跡すら示して居ない．

然しながら和歌山縣及び德島縣各地踏査の結果を綜合するに，兩縣下並に奈良縣，大阪府の一部に亘り，家屋の壁，人造石に生じたる龜裂，道路，堤防の龜裂，小規模の山崩れ，落岩，井戸水，溫泉の混濁等の現象が至る處で認められた．

各地の被害概況

和歌山縣

震央に最も近い町，村は，御坊町，印南町，次いで南部町，田邊町及び白濱湯崎町に當り，縣下の被害狀況も上記の諸町村が他に較べてやゝ目立つて居る事が認められる．

田邊町

大濱港岸壁のコンクリート構造物に多數の龜裂が見られる．(第8,(c)及び10,(b)圖を見よ)．是等の龜裂は構造物に平行して，長さ約50米に及ぶ．縣道，町村道の至る處に小龜裂あり．家屋の壁に多數の龜裂及び土塀の倒壞2ヶ所，飾窓の破損多數あり．家屋の一部約5糎—10糎移動せるものあり．墓石約20°廻轉せるもの(第9圖を見よ)又廻轉せずに約10糎移動せるものあり，廻轉並に移動の方向は互に共通せ

ず．墓石の轉倒せるもの殆んど見當らず．井戸水の濁れるもの全町井戸の約 80% に達す．水量の增減は明瞭ならず．

地震前後に於ける田邊灣附近の漁獲の狀況には何等變化を認められず．

發光現象を認めたとの報告多數あるも，方向，色，は勿論，發見時間も一致せず．

南部町

土塀，家屋の龜裂，土藏の壁脫落多數あり．佛壇の點火せるローソクが地震の際倒れたるため，四棟全焼家屋を出す．南部川堤防に延長約200米，巾最大3糎の龜裂あり．井戸水の濁れるもの多數あり．

御坊町

震央に最も近い町であるが，被害狀況は田邊町，南部町と同程度にして，特に著しからず．飾窓硝子の破壞，壁の龜裂等多數あり．道路の龜裂，小規模の山崩れあり．井戸水の濁れるもの多數あれど增減は明かならず．

日高中學校校舍は今回の地震に於いて最も損害を受けた構造物の一つである．校舍は第8,(a),(b)圖の如く，鐵筋コンクリートの外側を煉瓦で補裝し，その上に厚さ約1糎のモルタルを蔽へる構造を有す．今回の地震で柱，壁，天井の境界の至る處に龜裂が入りモルタルの脫落あり，崩壞の危險に瀕する箇所あり．

發光現象を認めたりと報ずる者あれど現象明瞭ならず．

鉛山村（白濱湯崎溫泉）

白濱湯崎溫泉の2溫泉井戸，地震のため湧出を中止した事は關西各地に於いて極めて注目されたのであつたが間もなく復舊した．溫泉に就いては後にやゝ詳述する事にする．

京都帝國大學附屬臨海研究所の實驗室の屋根瓦の一部破壞し，落下したが，尙煙突等の建物附屬物の破損がやゝ著しい．水族館內の生物標本瓶の倒壞破壞せるもの 200 本以上に及ぶ．然しながら實驗室以外の水族館，官舍等の建築物には殆んど損害を受けず．當研究所の井戸水地震の 2，3 日前より約 10 糎增加し，地震の爲め濁るも地震後1日にして水位並に濁りは舊に復す．當研究所附近に於いて地震の際日ノ御崎方向よりの鳴動及び發光現象に氣付いたとの報告あり．

白濱溫泉街に於いては飾窓の破損，壁，コンクリート塀，人造石等に多數の龜裂を生じ，特に水田の埋立地に建設されたる白濱ホテル始め，附近の地盤約 10 糎低下しホテルの壁に大なる龜裂を生じたり．

串本町及び潮岬

土藏の一部崩壞せるものあり．井戸水の濁れるものもあり．潮岬測候所員によれば

地震の襲來と共に，震央方向より音響を聽きたれど發光現象は全く氣付かずとの事なり．

周参見町及び附近の町村

井戸水の濁り，道路，壁の龜裂あり．各戸の四周に防風設備として，自然石（徑約20糎—50糎）を積上げて造られたる石垣の崩壊せるもの所々に散見する．

新宮市

土塀，壁の龜裂，石垣の一部崩壊せる程度で他の被害無く，道路の龜裂，那智の瀧附近に岩石の落下せる所多少あり．

徳島縣

和歌山縣に次いで震央に接近せる徳島市，富岡町附近に多少の被害があつたが，全體として，和歌山縣下と同程度又はそれ以下の輕微のものに過ぎない．

徳島市

壁，土塀，コンクリート構造物，道路等に多數の龜裂あり，飾窓，硝子戸の破壊多數にのぼり，特に市内通町附近が顯著であつた．被害程度，田邊町，御坊町と同程度と認められる．

富岡町及びその附近

壁，土塀，道路の龜裂あり，屋根瓦落下せるものあり．同町殆んど井戸水濁り，2日間使用不能となりたるものあり．

富岡町の北林崎に於いて新築の鳥井倒壊，石垣の崩壊せるものあり．

富岡町の北東，出來町に於いて屋根8坪及び軒が崩壊して一名負傷す．

撫養町

製鹽工場の煙突が倒壊す．硝子戸の破壊，道路の龜裂を生ず．

里浦海岸の埋立地約5町歩に亘り，30糎乃至50糎に達する沈下を生ず．

徳島縣下に於いては今回の地震は大正12年9月1日の關東大地震及び丹後地震より，震度大きく，明治43年1月7日當地の地震以來の震度大なるものであつた．

地動に伴つた鳴動

踏査中和歌山，徳島兩縣下の各地で地震と共に鳴動を聽取されたとの報告が多數に及んだので，ポストカードの方法で，上記兩縣下は勿論，大阪府，奈良縣，兵庫縣及び三重縣の各中，小學校に調査を依頼した．その結果に基き鳴動聽域圖を示すと次の様になる．

即ち震央より約50粁以内の陸地では大概鳴動を聽取した様であるが，徳島縣吉野

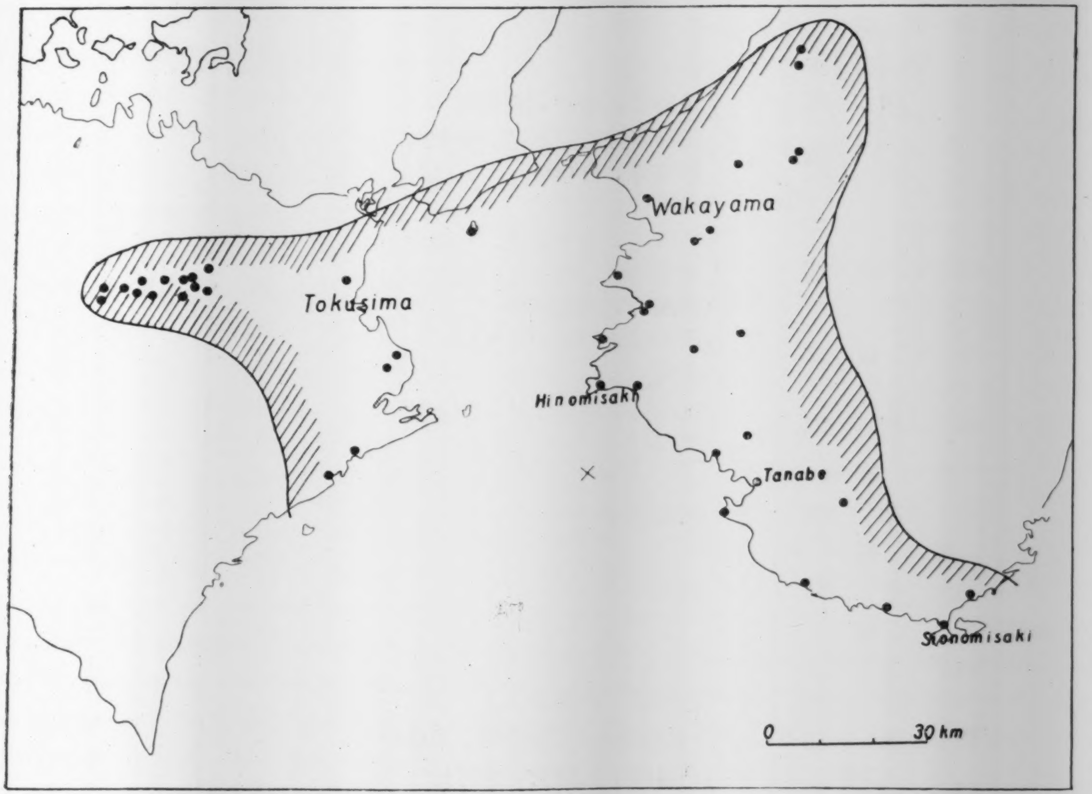

第1圖　地鳴の聽取された地域.
×震央

川流域の穴吹，脇，貞光，市場の各町に鳴動聽取域が擴がつて居る．又和歌山縣では紀の川の中流域笠田，上名手方面で鳴動を聽いたと報告して居る.

和歌山縣並に德島縣の大部分は中世紀の古い地層より成り，一般に地震に對して，堅固の地盤であると考へられてゐる． 各地の地震の被害を見るにコンクリート構造物，壁等の龜裂が著しく且廣範圍に亘つてゐるに反し，墓石等の轉倒，建築物の移動の極めて少い事は，各地に於ける地震動の主要動が短週期の地動より成つて居た事を暗示するものであるが，この事實は更に同地方が古い且堅固な地層より成ると言ふ地質學的事實に對して好都合であり，且又廣範圍に亘る鳴動聽域を生じた事の說明に對しても都合が良い．吉野川，紀ノ川流域に聽域が延長してゐるが，斯る沖積層の地層の地域に延長せる事は多少意外であるが，鳴動はとにかく地震波として傳幡し，地表にて空氣波の振動を誘發したものと考へられるが，空氣振動は適當の振動數と振幅とを有すれば常に鳴動として聽取される．且又一旦空氣波となれば地形の著しい影響を受ける事は爆音調查等に於いて常に認められる所である.

ポストカードの方法に依り知り得た，地震動襲來に際して音響聽域は次の如くである.

和歌山縣		
	和歌山市	
	有田郡	箕島町，廣村，湯淺町
	日高郡	三百瀬村，三尾村，南部町 御坊町，白崎村 川上村，船着村
	西牟婁郡	三川村，上芳養村，和深村 周参見町，新庄村，瀬戸鉛山 田邊町，白濱湯崎
	東牟婁郡	串本町，潮岬，三里村 古座町
	那賀郡	池田村，南野上村，野上村 笠田町
大阪府		
	泉北郡	北池田村
兵庫縣		
	三原郡	沼島村
德島縣		
	德島市	
	那賀郡	富岡町，平野村
	海部郡	三岐田町，日和佐町，牟岐町
	阿波郡	市場町，久勝村，伊澤村 久勝村
	麻植郡	山瀬町，學島村，川田村
	美馬郡	穴吹町，脇町，貞光町，三島村 岩倉村，郡里村
香川縣		
	高松市	
	小豆郡	草壁町

溫泉の異常

1. 白濱湯崎溫泉.

白濱湯崎溫泉中の2溫泉が地震後湧出の停止した事は各方面より注目されたが，湧出鐵管に高壓力を加へ，管內の洗滌により間も無く復舊した．現在溫泉井戶は總數約25本に及び，毎年その數を增すため各溫泉の湧出量は次第に減少の傾向にある事が認められる．主な溫泉井戶に就いて，湧出量，湧出溫度の測定が昭和9年以來定期に行はれた結果を第1表に表示す．尙地震後1月 15 日には白濱溫泉土地會社の助力を得て，2，3の溫泉の再測を行ふ事が出來た．第1表の中水晶湯並に垣谷湯は地震後湧出を停止したものであるが，復舊後の再測によれば前測定に比し，湧出溫度に變化無く，湧出量は毎時夫夫20石及び10石の增加となつた．これに反し，地震後湧出の停止を見なかつた生絹湯は，地震後の再測の結果は，湧出溫度は2·5°Cの低下を來たした．

第　一　表

白濱溫泉，湧出溫度，湧出量（石數ハ毎時湧出量）　（白濱溫泉土地會社測定）

測定年月日 溫泉井戸名	昭和9年3月2日	昭和9年4月3日	昭和9年10月17日	昭和10年4月3日	昭和10年10月10日	昭和11年4月3日	昭和11年6月29日	昭和11年10月17日	昭和12年1月7日	昭和12年2月23日	昭和12年4月3日	昭和12年5月14日	昭和12年6月5日	昭和12年6月18日	昭和12年10月31日	昭和13年1月15日
第二走リ湯			75°C 191·3石	77°C 148·5石	78°C 167·4石	77°C 154·7石	80°C 75·3石	78°C 198·5石			77·5°C 145·5石				80°C 187·7石	
衝（ツク）幹（モト）湯			80°C 157·8石		81°C 330·5石	81°C 130·9石	81°C 213·3石	79·5°C 163·1石			78°C 73·4石				80°C 157·8石	
やまさ湯				80°C 279·1石		87°C 104·5石										
水晶ノ湯					58°C 232·7石	58°C 202·1石	58·5°C 193·5石	58°C 217·1石			58°C 178·9石				57°C 191·3石	57°C 213·2石
生（スズ）絹（シ）湯	98·5石	56°C 117·3石	55°C 117·3石	56°C 117·3石	56°C 102·0石	56°C 97·3石	56·5°C 99·7石	56°C 104·5石	53·5°C 87·8石	54°C 87·8石	55·5°C 104·5石				55·5°C 114·7石	53°C 32·0石
垣谷湯	156·3石	50°C 187·8石	50°C 167·4石	50°C 157·8石	50·3°C 133.8石	50·5°C 142·5石	50·9°C 130·9石	50°C 145·5石				49°C 160·9石	49·8°C 176·3石	49·1°C 128·0石	50°C 151·5石	50°C 161·0石
小澤湯	12·3石	50.7°C 32·0石	50°C 32·0石	52°C 29·6石	46°C 17·6石											

又湧出量は毎時75石の減少を來たし，前回測定の約 1/3 となり著しく減少を示した．

水晶ノ湯及び垣谷ノ湯が地震後一時湧出を停止したのは，地震動のため湧出孔道に土砂及び NaCl，$MgCl_2$ 等の沈澱物が浸入し，管內の一部を閉鎖し，一時的に湧出を停止したものと考へられる．生絹湯が地震後湧出量が著しく減少せる事も同じ理由による事と考へられるが，更に同じ系統に屬すると考へられて居る垣谷，水晶の二湯の湧出量が增加した事にも關係を有すると考へられる．第2圖 a，b，c は上記三溫泉井戸の湧出量，湧出溫度の昭和9年以來の測定並に地震後の結果とを圖示したものである．

第2圖 (a)，(b)，(c) 白濱湯崎溫泉の 3 溫泉井戸の湧出量，
湧出溫度の變化圖． Qは每時湧出量， Tは湧出溫度．

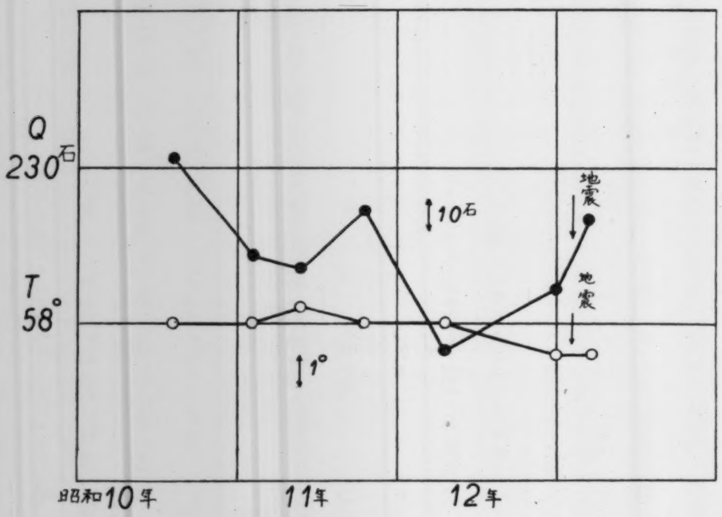

第2圖 (a) 水晶の湯

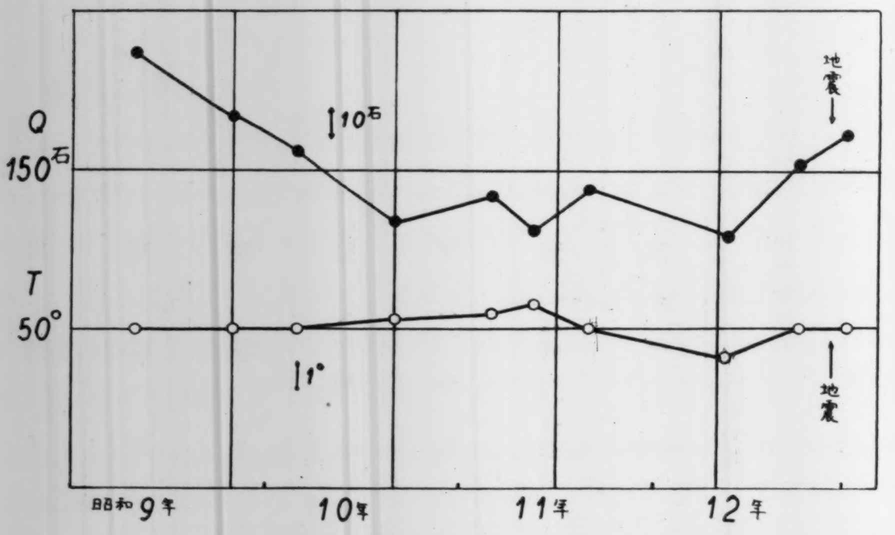

第2圖 (b) 垣谷の湯

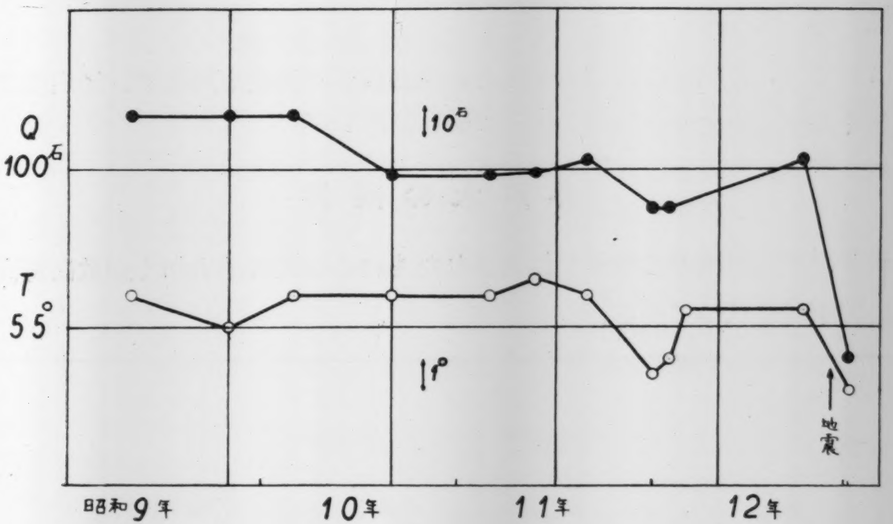

第2圖 (c) 生 絹 の 湯

尙，白濱溫泉に屬する黎明ノ湯は地震前後を通じて行はれた每日7時の湧出溫度測定結果を見ると，本回の地震に直接關係ありと認められる變化は何等現はれて居ない．然し，湯崎海岸に天然に湧出せる瓦斯が地震後噴出勢力の增大が認められる由である．尙溫泉は地震後總べて濁つたが2日後舊に復した．

當溫泉は昭和2年の丹後地震に際し，今回と同様に湧出量の1時的の變化を來たし，或る溫泉井戶は湧出を停止したのであるが，今回と同様に地震動のために生じた管内への土砂浸入に基づくもので，地球物理學的に特別に意義を有する現象とは考へられない．

2. 椿 溫 泉

湧出溫度に變化無く，湧出量多少增加の傾向あり．地震後溫泉白濁す．

3. 串 本 鑛 泉

串本驛前に湧出せる低溫鑛泉の湧出量，地震後約2倍となり，湧出溫度數度上昇せりと報ぜられて居る．

4. 勝浦の諸溫泉

越の湯は湧出量溫度共に異常なく，地震後白濁す．又現在掘穿中の井戶（湧出溫度44·3°C）も同様白濁すると共に瓦斯の噴出一時的に盛んとなる．

貴司，浦島，中ノ島の諸湯何れも濁るも，湧出溫度，量に異變を認めず，唯外ノ湯のみ多少湧出量の增加を認められる．

5. 湯 川 溫 泉

溫泉井戶總數7個の中總べて湧出量の增加を來した．その中松本市藏氏所有の井戶は地震前に比して湧出露頭約 15 糎上昇した．(第10圖，(a) を見よ)

6. 龍神溫泉

昭和 12 年 11 月以來湧出停止せる井戸地震後再び湧出を開始す．湧出溫度，量共に變化無く濁りも生ぜず．

井戸水の異常

地震後井戸水の增減並に濁りを報告されたものは次表に示す如く和歌山縣海岸地方並に德島縣東部に亘つて居る．

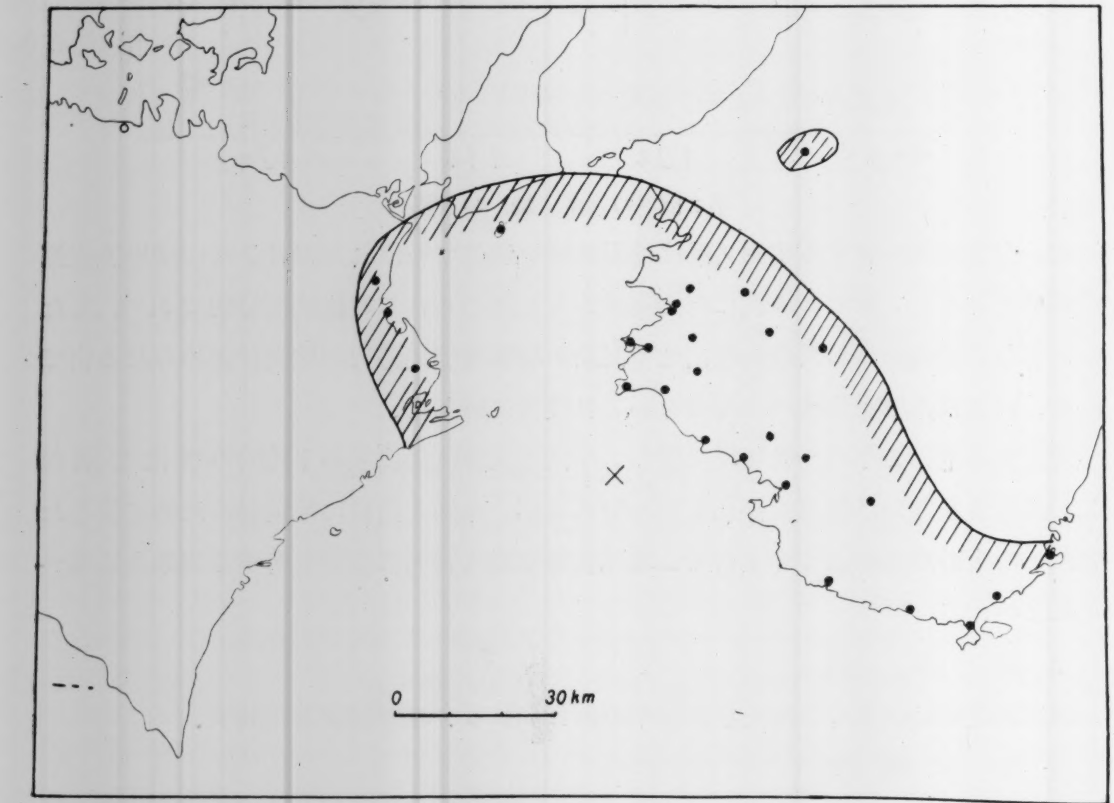

第3圖 井戸水の異變を生じた地域 × 震央

下記の町村の井戸何れも地震後濁る．其の中水位の變化ありたるもの ●增 ○減 ⊙增減

和歌山縣
　有田郡　岩倉村，⊙湯淺町，○廣村，○津木村，●藤並村
　日高郡　○由良町，⊙寒川村，○三百瀬村，●川上村，
　　　　　⊙三尾，南部町，御坊町，⊙白崎，⊙印南町
　西牟婁郡　新庄村，●周參見町，⊙和深村，上芳養村，⊙長野村，三川村
　東牟婁郡　串本町，古座町
　那賀郡　上名手村
兵庫縣　三原郡　沼島村
德島縣　德島市
　那賀郡　富岡町，○小松島町

地震に原因せる火災

倒壊家屋の發生を見なかつたので倒壊に原因する火災は起らなかつたが南部町に於いて點火せるローソクの轉倒より發火して四軒を燒失した以外に次の和歌山縣の各地に於いて炭燒の竈の破損より山火事を發し，山林の燒失が數ケ所にあつた．

1．西牟婁郡	周參見町字上戸川地積	數町歩山林燒失
2．西牟婁郡	周參見町字泥田谷	約5町歩山林燒失
3．西牟婁郡	長野村	雜木林4反歩燒失
4．南牟婁郡	御船村太字成川	雜木林約1町歩燒失

和歌山地震群

和歌山縣有田川流城，湯淺町附近，紀ノ川流域和歌山市附近及び日高川下流域御坊町附近は，現今我國に於いて，最も局部的地震の多い地方として，此等は和歌山地震群の名を以つて知られて居る．然しながら最近數十年に亘り，和歌山地方に破壞的大地震の發生を見る事無く經過したのであるが，今回の1月12日の地震は震央は海中にあつた爲め甚だしい損害を受けなかつたとは云へ，近來同地方に於ける注目すべき地震であつた．

和歌山地震群發生の狀態を知るため同地震群中有感地震の大正15年以來，昭和12年12月に至る每月の發生數を示したのが第4圖である．以上の期間中に於いて1ケ月總數の最大は57回，最小3回，平均26·7回の有感地震の發生を見て居る．地震群發生の狀態を時間的に見ると地震活動の消長の著しい事が特に注目される．卽ち大正15年2月の僅か3回の有感地震より次第に地震回數が增加し昭和3年1月には，49回の地震發生を見た．それ以後，地震回數の減少を來たし，一時昭和5年2月はに54回の多數地震の發生を見たが，一般に地震活動の衰へを見せ，昭和7年5月には僅か5回の地震發生を見たに過ぎなかつた．然るにそれ以來再び活動を示し，次第に地震回數の增加の傾向にあり，昭和10年12月には57回に達した以後今日に至る迄地震回數の漸減の傾向にある事が知られる．過去12年間に和歌山地震群の震央附近に起つた主な地震としては，氣象要覽のやゝ顯著地震と名づけられるもの次の5回の地震である．

	震　央
1．昭和2年4月20日	有田川中流域
2．昭和3年7月7日	紀伊水道中部
3．昭和4年7月4日	有田川流域
4．昭和4年11月20日	有田川河口附近
5．昭和5年12月6日	淡路島
6．昭和8年7月29日	紀伊水道

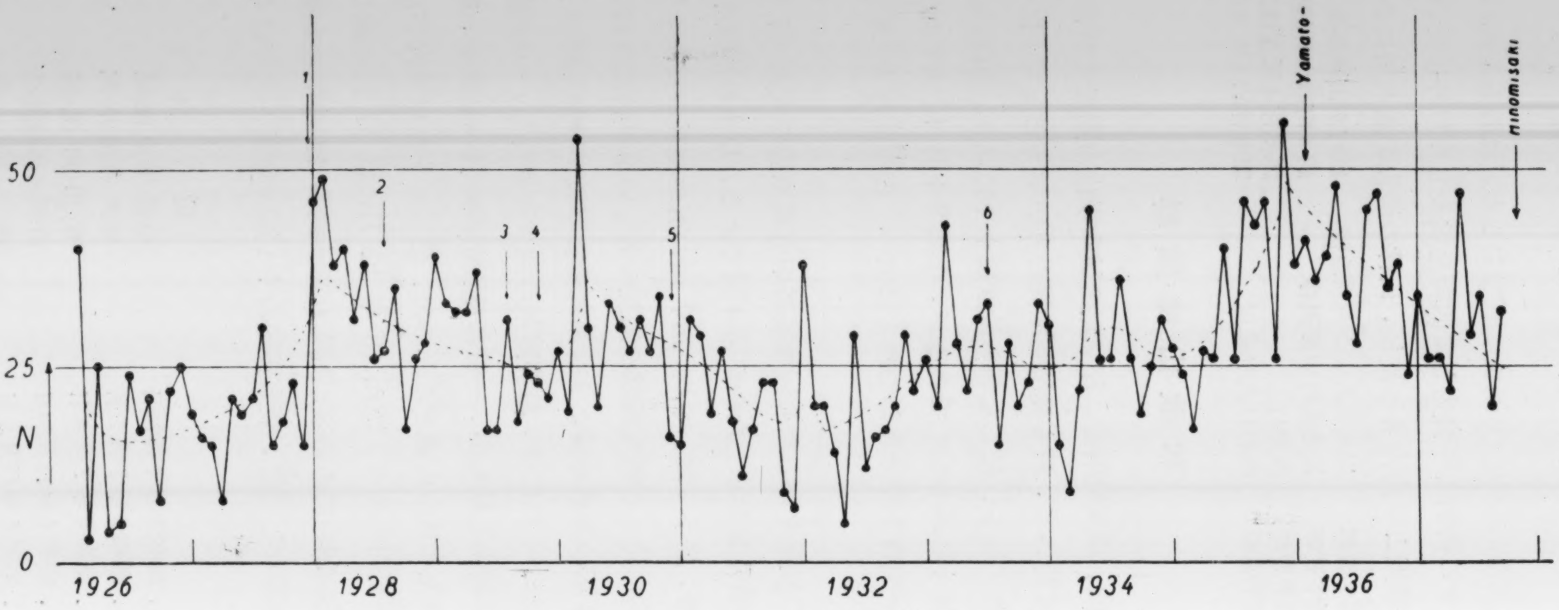

第 4 圖 和歌山地震群の消長

N; 和歌山地震群中有感地震の各月の和 1, 2, 3, 4, 5, 6 同地方に發生せるやゝ著しい地震.

1, 有田川中流域 2. 紀井水道中部 3. 有田川流域 4. 有田川河口 5. 淡路島 6. 紀井水道

この中昭和4年 11 月の地震は有田郡箕島，保田，湯淺町等に於いて多少の被害を生じた．

尙和歌山地震群震央より，多少遠隔の地ではあるが昭和 11 年2月 21 日には大和河內强震が起り，當時和歌山地震群は昭和10年12月の最も著しい活動の直後に起つた事が注目される．又上記の稍顯著地震の震央は總べて北緯 34° 以北に存在し，而も昭和8年8月以前に起つたものである．卽ち昭和8年8月以來和歌山地震群中には稍顯著地震及びそれ以上の地震の發生を見てゐない．今回の地震の震央附近は和歌山地震群の震央に極めて接近せる地域であるが，過去拾數年以來著しい地震の發生を見なかつた地域である．

結　　語

以上記述せる如く，今回の地震に伴つた地學現象として特に著しいものは何等現は

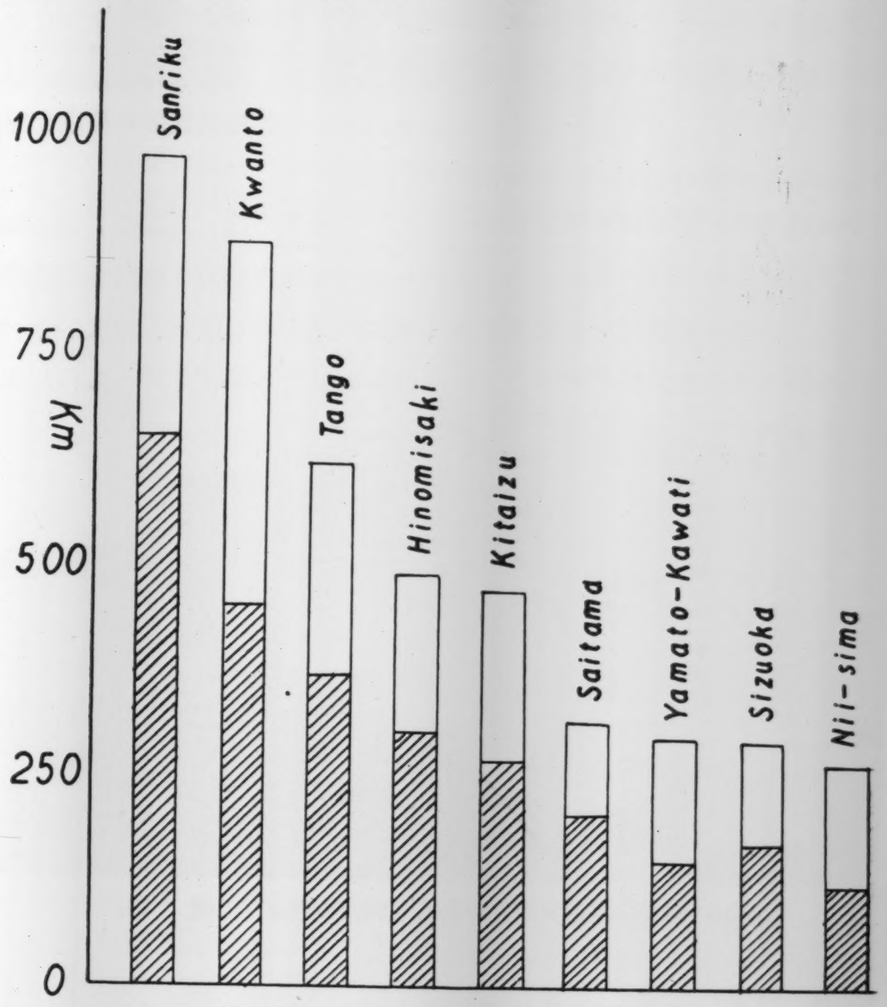

第5圖　最近本邦に發生せる顯著な地震の震度分布の比較

□ 有感區域震央距離　▨ 震度3以上の區域震央距離

れなかつたが，その有感覺區域が極めて廣範圍に亘れる事が，注目に値する．今回の地震を最近十數年間に發生せる顯著な地震の有感覺並に弱震（震度 III）地域面積の大小を比較するために第5圖を示す．有感覺地域並に弱震地域共に日ノ御崎地震は丹後地震よりやゝ小さく北伊豆地震より稍大きい．尙最近著名な，靜岡地震，大和河內地震より廣範圍に亘れる震域を有する地震であつた．萩原理學士が調査せる靜岡，大和河內地震の全潰家屋其の他著しく被害の生じた地域は略震央より5粁以內の地域內に限られて居る．今上記地震と今回の地震との有感地域，弱震地域が裂震地域に於いても略比例すると考へると今回の地震の裂震地域は約 10 粁の範圍內に推定される，從つて推定裂震地域は總べて海底に存在する事となる．

今回の踏査に於いて發光現象を確かむべく種々調査を行つたのであるが和歌山縣田邊町を中心として地震前後に發光を觀察したとの報告が多數あるが，是等報告に於いて互の一致點を見出し難く，今回の地震に於いても發光現象が發現したか否かに就いて尙疑問の點多く，何れかに斷定する事が困難である．

海底に發せる地震として津浪の發生に注目されたが，各地測候所の檢潮記錄は何等その痕跡を示してゐない．

最後に今回の調査に當り種々便宜を與へられたる和歌山縣，大阪府，德島縣の各府縣，市町村當局，各地測候所並にポスト・カードの方法に助力されたる德島縣美馬高等女學校始め，各地中等學校，小學校に厚く感謝の意を表し度い．尙又，今村博士の和歌山，德島縣各地の地震觀測所の方々から種々有益なる助言を與へられた事を附記して感謝の意を表し度い．

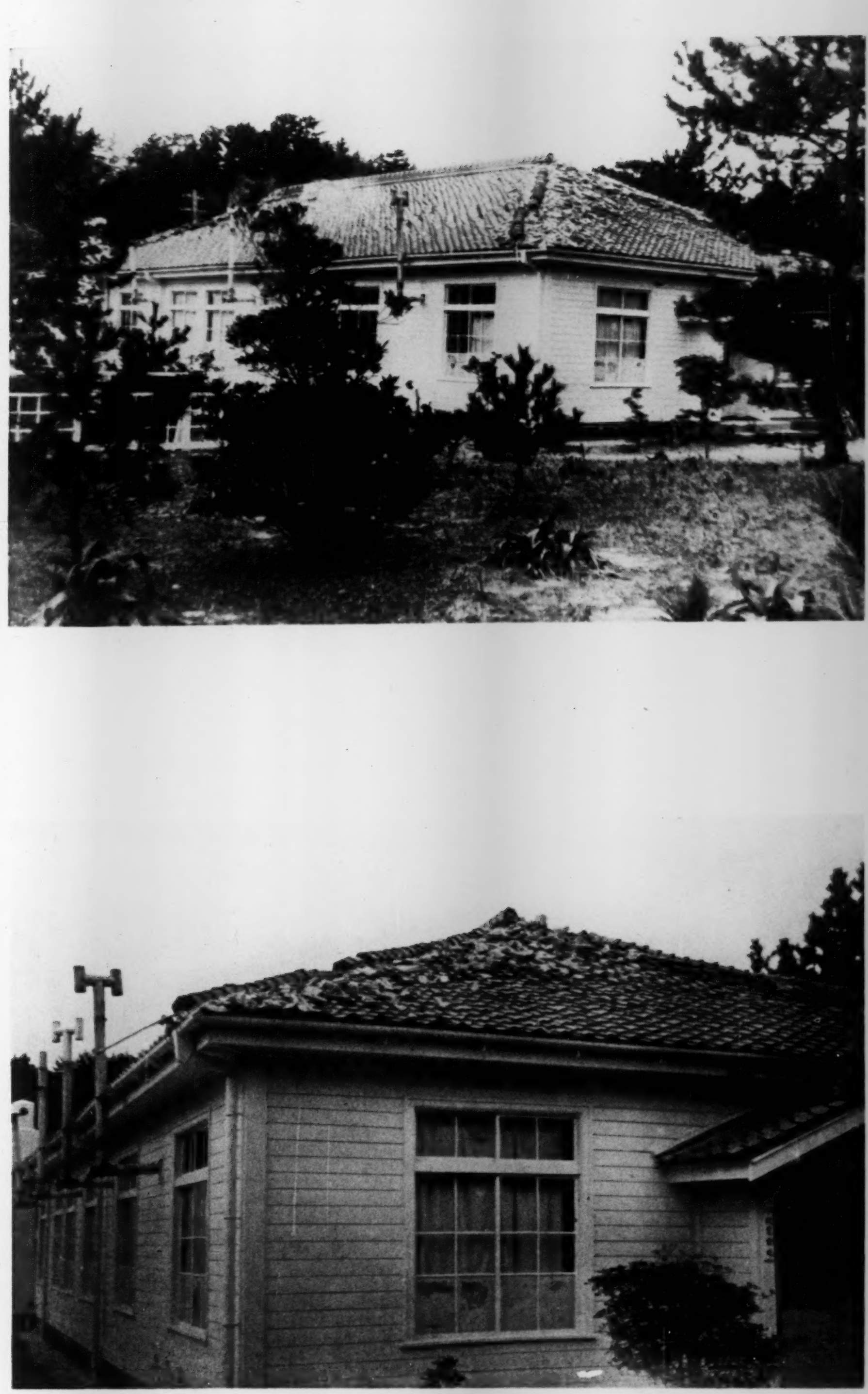

第 7 圖　京都帝大瀬戸臨海研究所實驗室の屋根の破損

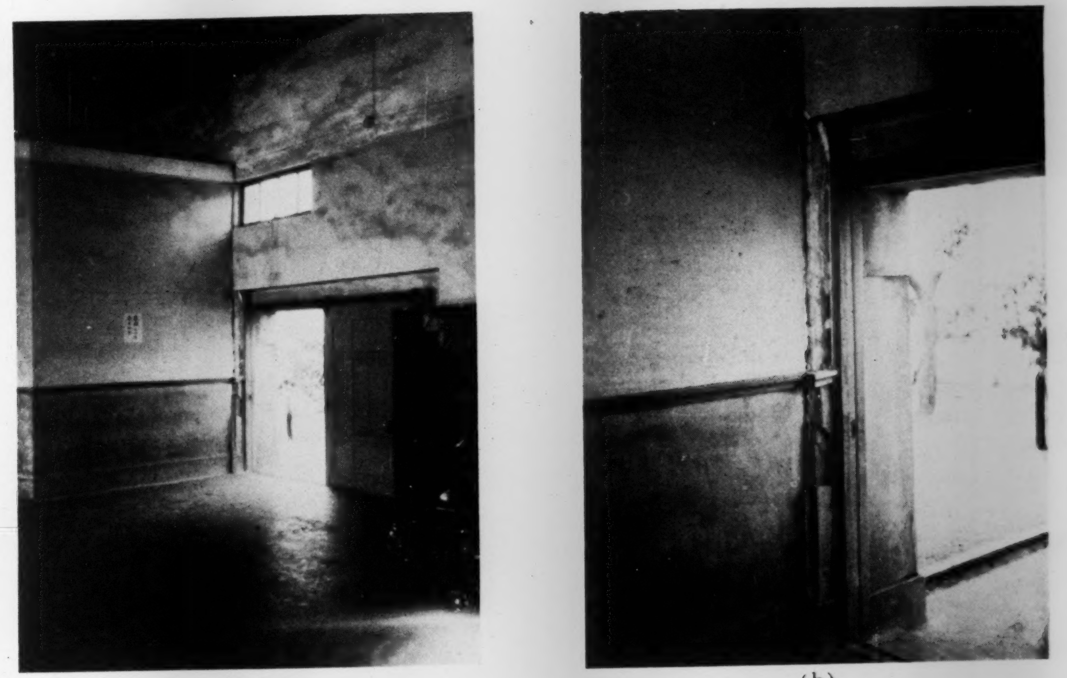

(a) (b)

(a) (b) 日高中學校舍の壁亀裂, 脫落.

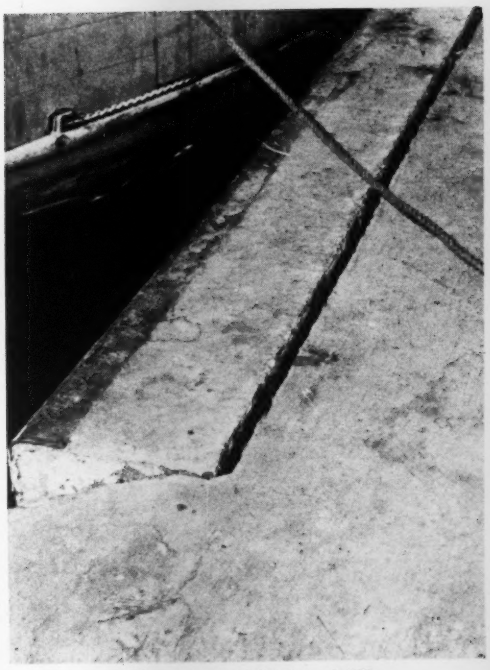

(c) 田邊町岩壁の亀裂

(d) 白濱湯崎溫泉
白濱ホテルのコンクリート構造物
に入りたる亀裂

第 8 圖

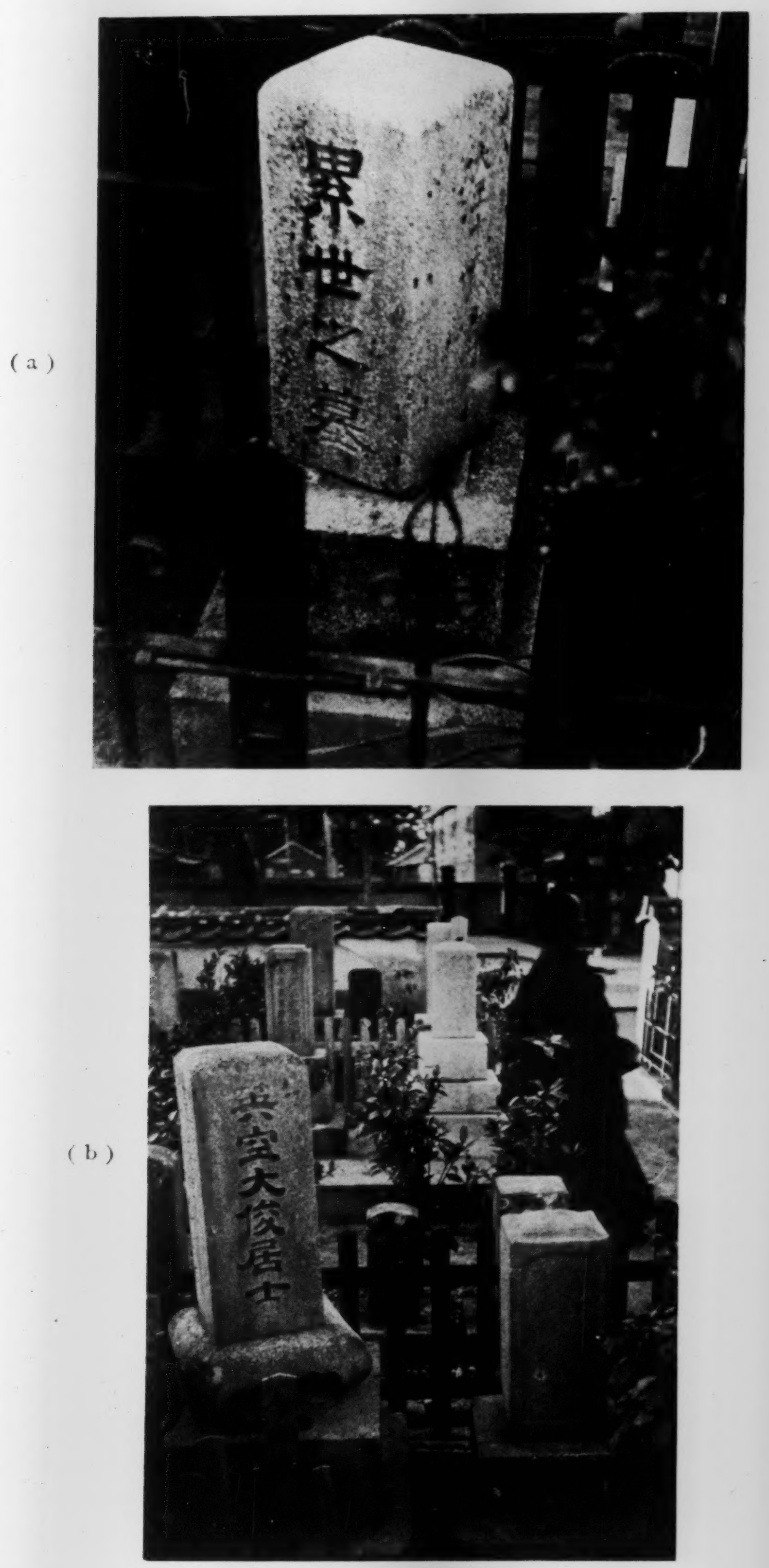

第 9 圖　(a) (b) 田邊町の墓石の回轉

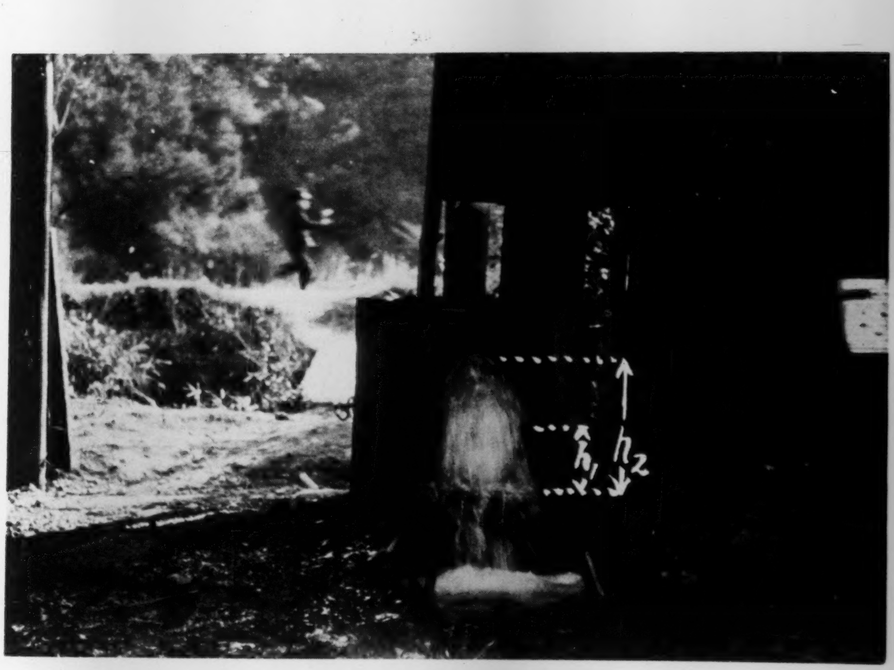

第10圖 (a)

湯川溫泉湧出露頭の變化

地震前 $h_1 = 15$ 糎

地震後 $h_2 = 30$ 糎

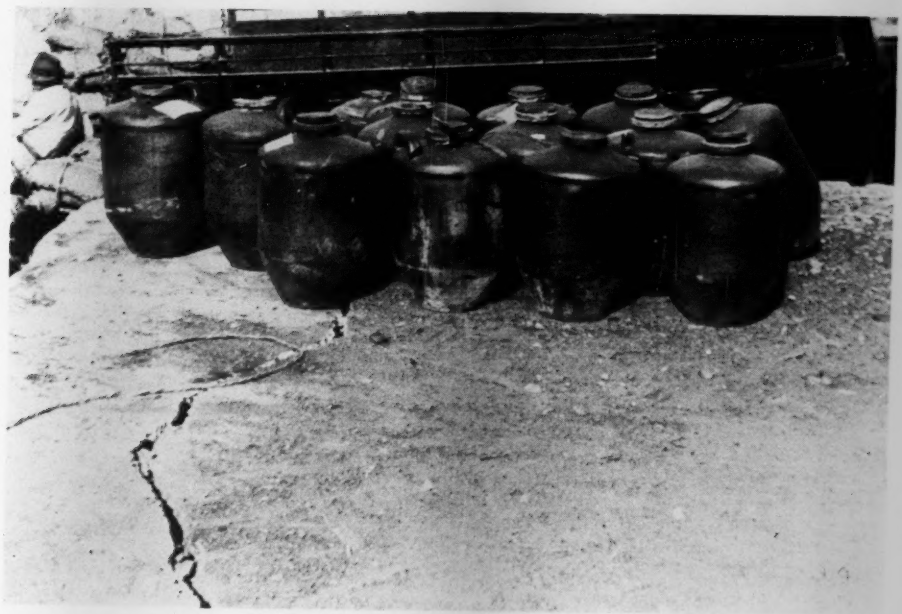

(b)

田邊町岸壁に入つた亀裂

35. *The Hinomisaki-Oki Earthquake of January 12, 1938.*

By Takeshi MINAKAMI,

Earthquake Research Institute.

An earthquake occurred in the neighbourhood of Hinomisaki, Wakayama prefecture, at 0 h 12 m, January 12, 1938. As the epicentre ($\varphi = 33°44{\cdot}'4$, $\lambda = 135°3{\cdot}'7$) was in the sea, about 15 km from the land, no serious damage resulted, but the area over which it was sensible to man was very wide. It was felt at our Asama Volcano Observatory, distant about 750 km from the epicentre.

After this earthquake changes were noticed in the orifice temperature and the rate of flow in some of the hot springs, like Sirahama-Yuzaki, Yukawa, and others in the shaken region.

Earth-sounds were heared in certain parts of Wakayama and Tokusima prefectures simultaneously with the earth-shock. These earth-sounds might have been due to sound waves in air caused by their vertical component of rapid vibration of the earth's surface. From field investigations made by the writer in the shaken region, it seems that the earthquake motions in areas where the sound was heared had the characteristics of rapid vibrations. It might be added that the geological character of these region does not preclude the possibility of rapid motions of the ground.

36. 岡山—厚狹間並に小松島—八幡濱間の水準改測結果

昭和 12 年度に於いて，本所の委託により，陸地測量部の改測を施行せる水準線路は，

（ i ） 岡山——厚狹間（尾道，廣島，德山，山口を經て）

（ ii ） 立江（小松島）——八幡濱間（德島，高松，丸龜，今治，松山，大洲を經て）

にして，その改測の結果知られたる沿線水準點の垂直變動量（mm）は，各水準點の分布圖と共に附圖に示せり．

尙この測量に關する要項次の如し．

（ i ） 各水準線路に於ける新舊測量時期は次の表に示す．

水準線區間	舊測量時期	新測量時期
岡山——厚狹	明治22年9月—明治23年3月	昭和12年10月—12月
立江——堀江 (B. M. 5079—5066)	明治28年12月—明治29年12月	昭和12年10月—11月
堀江—坂出 (B. M. 5066—J-354)	明治19年12月—明治20年3月	昭和12年11月—12月
坂出—杉山 (B. M. J-354—J-3440)	明治26年5月—12月	昭和12年10月—12月
杉山——八幡濱 (B.M.J-3440—4568)	明治28年2月— 7月	昭和12年10月—12月

（ ii ） 岡山—厚狹間に於ける水準點の變動量は岡山に在る水準點 379 號の變動を 0 とし，立江—八幡濱間に於ける水準點の變動量は小松島に在る水準點 5074 號の變動を 0 として各々算出せられたるものなり．

本改測は，原田積善會より本所に寄せられたる研究資金を以て遂行せられたるものにして，玆に，同會に對し深甚なる謝意を表す．

昭和 13 年3月

地震研究所

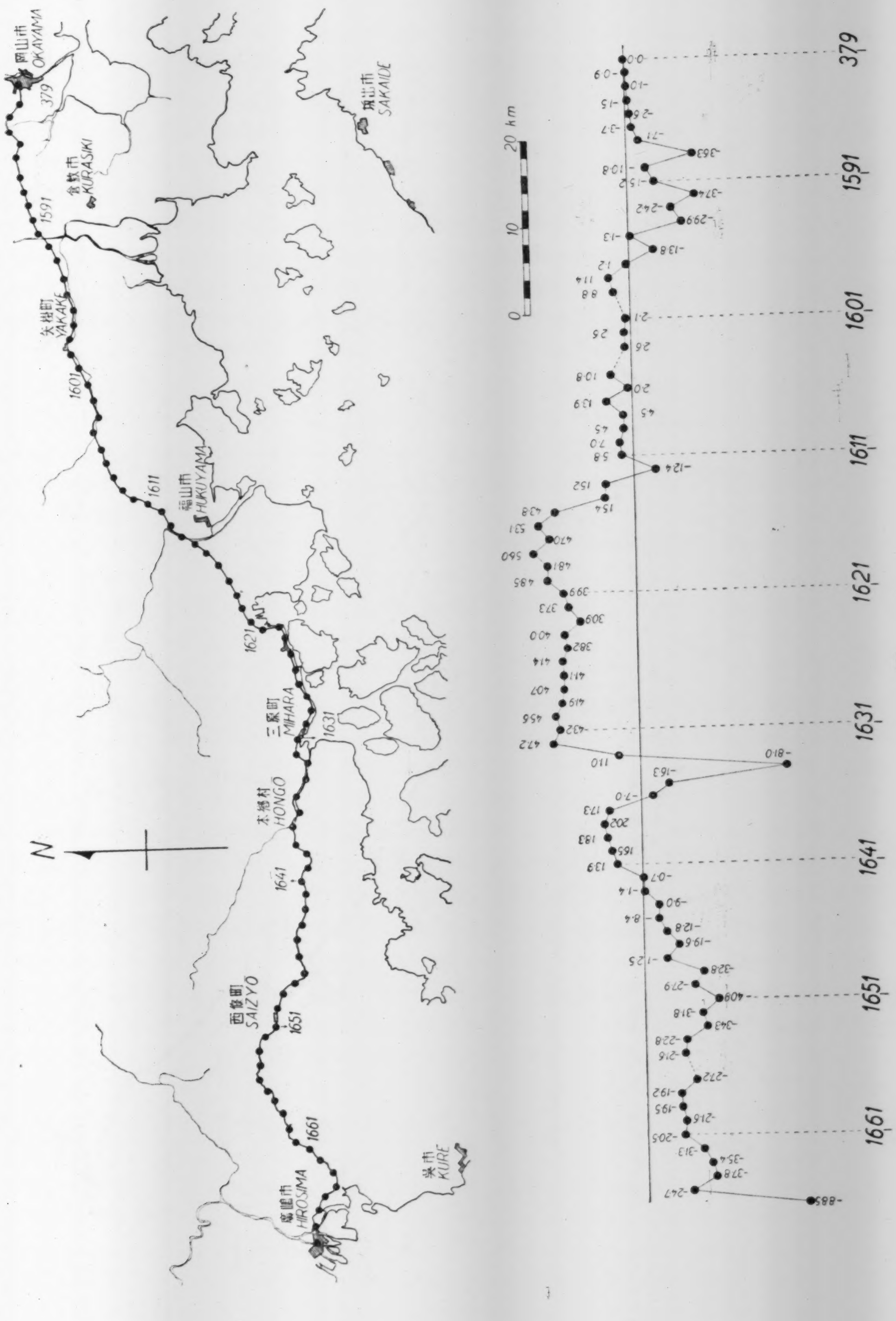
岡山市 OKAYAMA
379
倉敷市 KURASIKI
坂出市 SAKAIDE
1591
矢掛町 YAKAKE
1601
福山市 HUKUYAMA
1611
1621
三原町 MIHARA
1631
本郷村 HONGO
1641
西條町 SAIZYO
1651
1661
廣島市 HIROSIMA
呉市 KURE
N
0
10
20 km
379
1591
1601
1611
1621
1631
1641
1651
1661

Fig. 1.

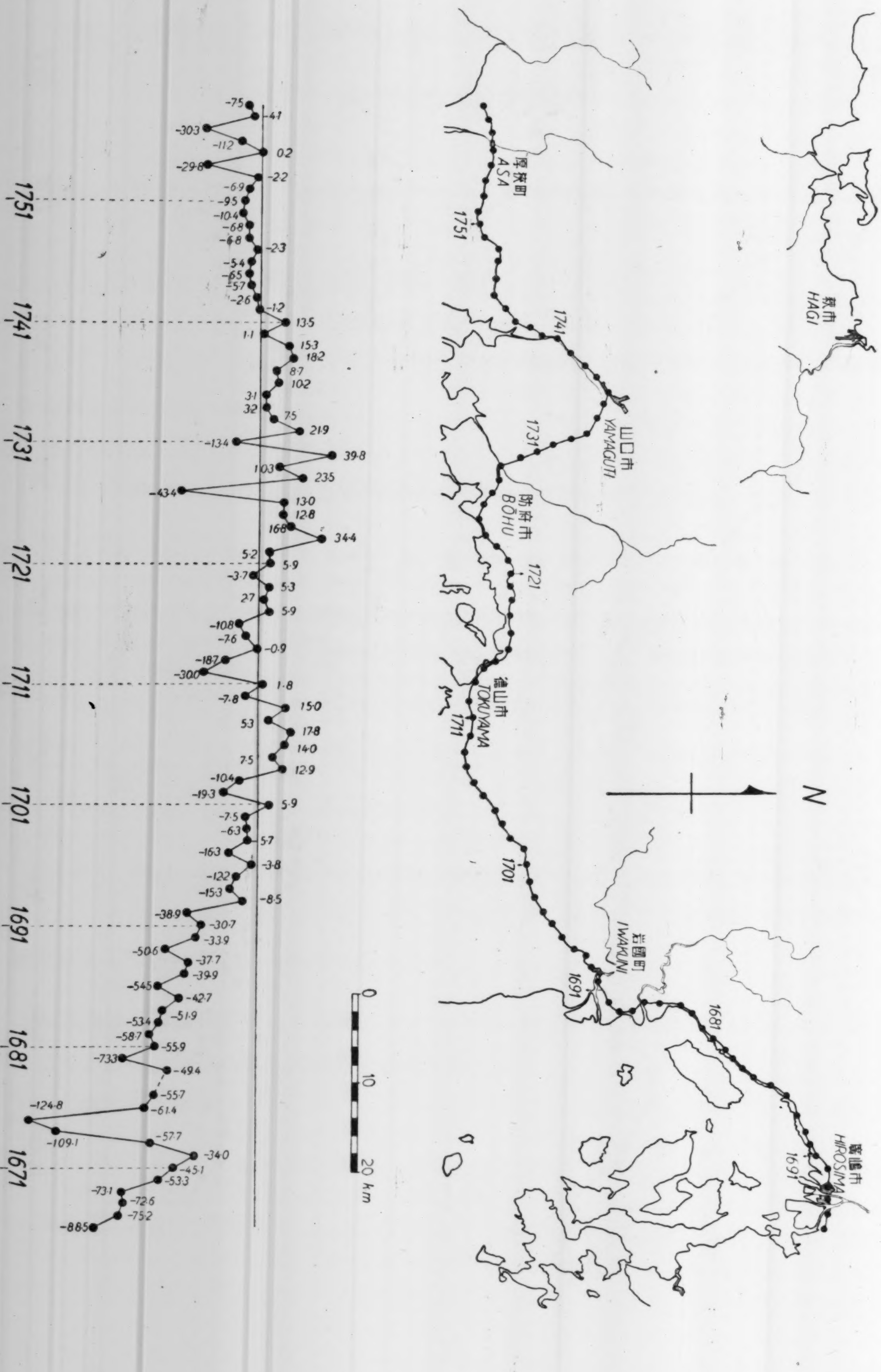
1751
1741
1731
1721
1711
1701
1691
1681
1671
厚狭町
ASA
山口市
YAMAGUTI
防府市
BŌHU
徳山市
TOKUYAMA
岩國町
IWAKUNI
廣島市
HIROSIMA
萩市
HAGI
N
0
10
20 km
-7.5
-4.1
-30.3
-11.2
0.2
-29.8
-2.2
-6.9
-9.5
-10.4
-6.8
-6.8
-2.3
-5.4
-6.5
-5.7
-2.6
-1.2
13.5
1.1
15.3
18.2
8.7
10.2
3.1
3.2
7.5
21.9
-13.4
39.8
10.3
23.5
-43.4
13.0
12.8
16.8
34.4
5.2
5.9
-3.7
5.3
2.7
5.9
-10.8
-7.6
-0.9
-18.7
-30.0
1.8
-7.8
15.0
5.3
17.8
14.0
7.5
12.9
-10.4
-19.3
5.9
-7.5
-6.3
5.7
-16.3
-3.8
-12.2
-15.3
-8.5
-38.9
-30.7
-33.9
-50.6
-37.7
-39.9
-54.5
-42.7
-53.4
-51.9
-58.7
-55.9
-73.3
-49.4
-55.7
-61.4
-124.8
-109.1
-57.7
-34.0
-45.1
-53.3
-73.1
-72.6
-75.2
-88.5

Fig. 2

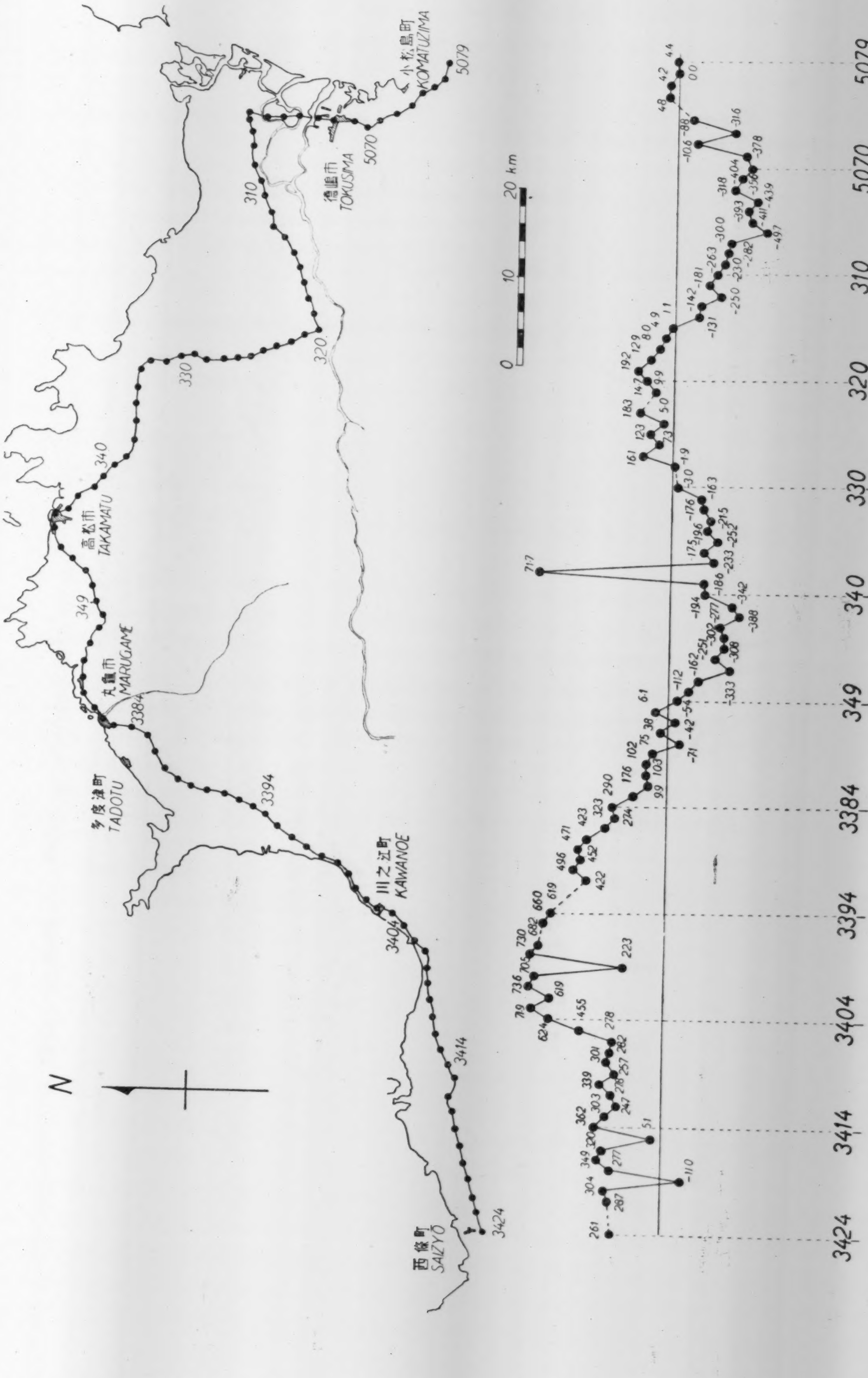
小松島町 KOMATUZIMA
徳島市 TOKUSIMA
高松市 TAKAMATU
丸亀市 MARUGAME
多度津町 TADOTU
川之江町 KAWANOE
西條町 SAIZYO
N
0 10 20 km
5079
5070
310
320
330
340
349
3384
3394
3404
3414
3424

Fig. 3.

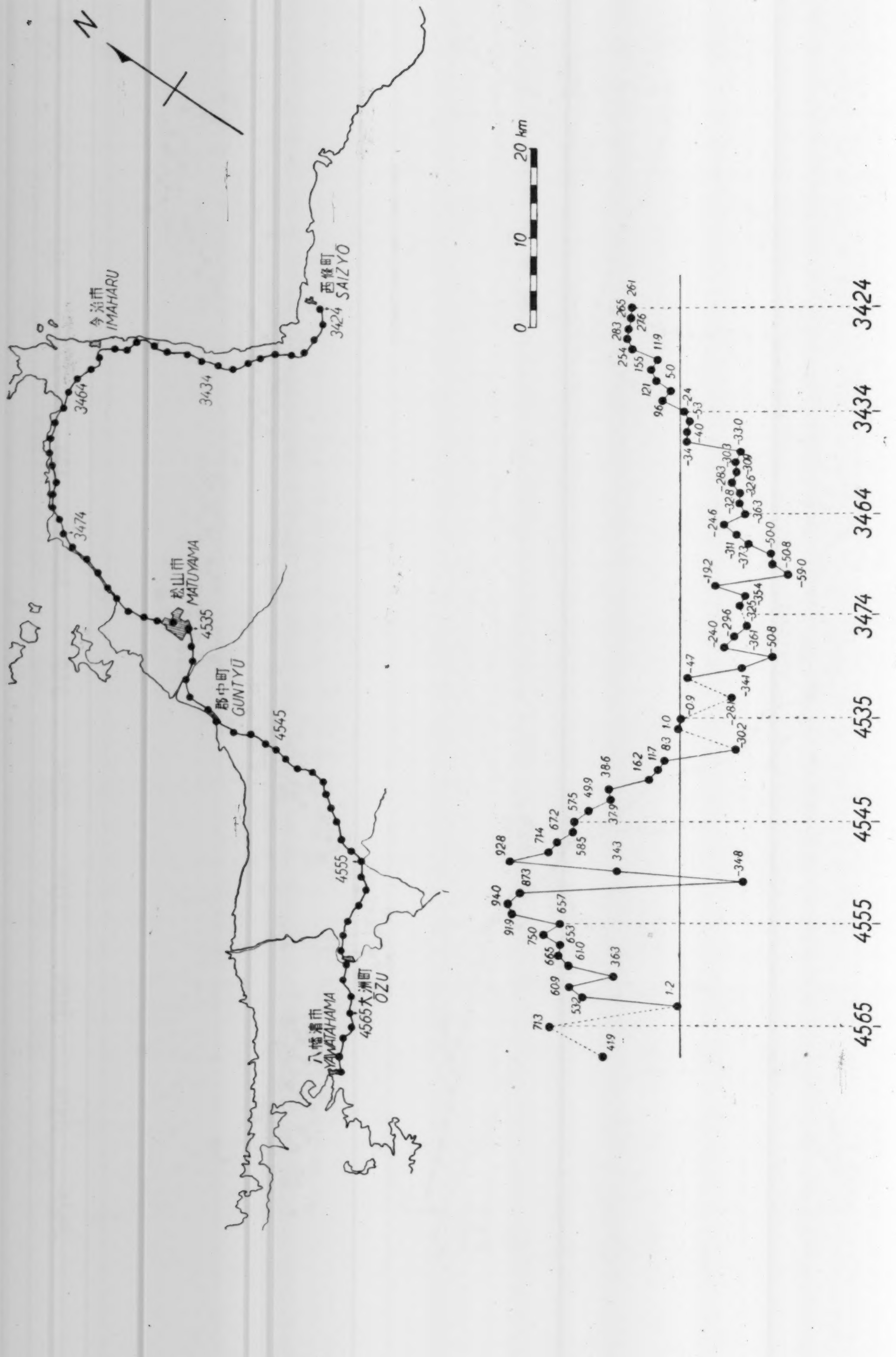
N
0
10
20 km
今治市
IMAHARU
西條町
SAIZYO
3424
3434
3464
3474
松山市
MATUYAMA
4535
郡中町
GUNTYU
4545
4555
大洲町
OZU
4565
八幡濱市
YAWATAHAMA
261
265
276
283
254
155
119
121
5.0
96
-2.4
-5.3
-4.0
-3.4
-33.0
-30.3
-28.3
-32.8
-30.9
-32.6
-36.3
-24.6
-31.1
-37.3
-50.0
-50.8
-59.0
-19.2
-29.6
-35.4
-32.5
-24.0
-36.1
-50.8
-4.7
-34.1
-0.9
-28.1
1.0
-30.2
8.3
11.7
16.2
38.6
37.9
49.9
57.5
58.5
67.2
71.4
92.8
34.3
-34.8
87.3
94.0
91.9
75.0
65.7
65.3
66.5
61.0
60.9
36.3
53.2
1.2
71.3
41.9

Fig. 4.

36. *Results of Recent Precise Levelling along the lines; Okayama —Asa, and Komatuzima (or Tatue)— Yawatahama.*

Precise levels were recently revised, at our request, by the Military Land Survey along the two lines, the one Okayama - Asa, via Onomiti, Hirosima, Tokuyama and Yamaguti, and the other, Komatuzima (Tatue) - Yawatahama, via Tokusima, Takamatu, Marugame, Imabari, Matuyama, and Ozu. The relative vertical displacements of the bench-marks along these lines of levels obtained by comparing the recent measurements with earlier ones are shawn in Figs. 1—4 together with maps showing the geographical distributions of the lines of levels. The amounts of vertical displacements denoted by numerals against the points in graphs of Figs. 1—4 are given in mm.

The dates of the field works for the different sections of the lines of leoels are as as follows:

Lines of levels	Former survey	Receet survey
Okayama-Asa	Sept., 1889—March, 1890	Oct.-Dec., 1937
Tatue-Horie B. M. 5079—J-5066	Dec., 1895—Oct., 1896	Oct.-Nov., 1937
Horie-Sakaide B. M. J-5066—J-354	Dec., 1886—March, 1887	Nov.-Dec., 1937
Sakaide-Matuyama B.M. J-354—J-3440	May -Dec., 1893	Oct.-Dec., 1937
Matuyama-Yawatahama B.M. J-3440—4568	Feb. -July, 1896	Oct.-Dec., 1937

Tne vertical displacements of the bench-marks of the lines Okayama-Asa are referred to B. M. 379, situated at Okayrma, and those of the line Komatuzima-Yawatahama are referred to B. M. 5074, situated at Komatuzima. The heights of these bench-marks of reference are regarded as unchanged during the period between the old and new surveys.

The present re-levellings were carried out by the aid of the research fund granted by the Harada-Sekizenkwai, to the council of which we wish to express our best thanks.

March, 1938.

The Earthuake Research Institute.

37. *Damping of Periodic Visco-Elastic Waves with Increase in Focal Distance.*

By Katsutada SEZAWA and Kiyoshi KANAI,

Earthquake Research Institute.

(Read May 17, 1938.—Received June 20, 1938.)

1. *Introduction.*

It is evident that the problem of the decay of visco-elastic waves has been receiving the attention of investigators. In the solution that we previously obtained,[1), 2)] particularly, with a view to ascertaining the manner of deformation of a given initial pulse, the elementary part of the solution was of the kind to show the condition of the damping of waves with time increase. The solutions of the problem obtained since then by other authors were also of the kind just mentioned, at any rate with regard to the condition of the damping of elementary waves. On the other hand, notwithstanding that the behaviour in transmission of a periodic visco-elastic wave whose amplitude at its source is constant, is also important, no one has so far discussed it, excepting such a special case as that of waves transmitted along a bar in the form of flexural waves, the expression for which we were the first to formulate.[3)] We shall now solve the general cases of bodily waves as well as those of surface waves, by means of which, such parts of the previous solutions as were treated approximately can now be represented in their exact forms with little complexity. Although in the previous paper, in seeking the solution for the transmission of Rayleigh-waves we assumed that $\lambda/\mu=\lambda'/\mu'$, in the present paper it is shown that it is possible to obtain solutions for waves of the same type for any ratios of λ/μ, λ'/μ', μ/μ'.[4)]

---

1) K. SEZAWA, "On the Decay of Waves in Visco-Elastic Solid Bodies", *Bull. Earthq. Res. Inst.*, **3** (1927), 43~50.

2) *Ditto*, "On the Diffusion of Tremors on the Surface of a Semi-infinite Solid Body", *Bull. Earthq. Res. Inst.*, **5** (1928), 71~83.

3) *Ibid.* 1), 50~53; and some other papers.

4) J. H. C. THOMPSON, citing our result, *loc. cit.* 1), discussed several conditions of λ'/μ', *Phil. Trans. Roy. Soc.*, **231** (1933), 347~350. Our previous assumption on this condition was made merely for the sake of mathematical simplicity. K. IIDA also dealt with a problem similar to Thompson's from his experimental result for soil, etc., *Bull. Earthq. Res. Inst.*, **16** (1938), 391~406.

Jeffreys[5] considered two kinds of damping in waves, namely, firmo-viscosity (similar to Voigt's viscous condition) and elastico-viscosity (similar to Maxwell's relaxation condition). Gutenberg and Schlechtweg[6] also studied Jeffreys's case. Here, however, we shall take the former condition of the two, namely, the firmo-viscous state of a solid body, calling it a visco-elastic body.

We shall first discuss the Rayleigh-type waves and Love-type waves, and then the plane and radial bodily waves, all of which are transmitted through visco-elastic bodies.

2. *Rayleigh-waves.*

Let λ, μ be Lamé's elastic constants and λ', μ' the dilatational and tangential coefficients of solid viscosities. The equations of motion of a visco-elastic body are then expressed by

$$\left.\begin{aligned} &\left\{(\lambda+2\mu)+(\lambda'+2\mu')\frac{\partial}{\partial t}\right\}\left(\frac{\partial^2\Delta}{\partial x^2}+\frac{\partial^2\Delta}{\partial y^2}\right)=\rho\frac{\partial^2\Delta}{\partial t^2}, \\ &\left\{\mu+\mu'\frac{\partial}{\partial t}\right\}\left(\frac{\partial^2\varpi}{\partial x^2}+\frac{\partial^2\varpi}{\partial y^2}\right)=\rho\frac{\partial^2\varpi}{\partial t^2}, \end{aligned}\right\} \tag{1}$$

where

$$\Delta=\frac{\partial u_1}{\partial x}+\frac{\partial v_1}{\partial y}, \qquad 2\varpi=\frac{\partial v_2}{\partial x}-\frac{\partial u_2}{\partial y}. \tag{2}$$

The solutions of (1) are

$$\left.\begin{aligned} \Delta &= Ae^{-ry+i(pt-fx)}, \\ 2\varpi &= Be^{-sy+i(pt-fx)}, \end{aligned}\right\} \tag{3}$$

in which

$$\left.\begin{aligned} &r^2=f^2-h^2, \quad s^2=f^2-k^2, \\ &h^2=\frac{\rho p^2}{(\lambda+2\mu)+ip(\lambda'+2\mu')}, \quad k^2=\frac{\rho p^2}{\mu+ip\mu'}. \end{aligned}\right\} \tag{4}$$

The solutions for u_1, v_1 and u_2, v_2 corresponding to Δ and ϖ are

$$\left.\begin{aligned} &u_1=\frac{if}{h^2}Ae^{-ry+i(pt-fx)}, \quad v_1=\frac{r}{h^2}Ae^{-ry+i(pt-fx)}, \\ &u_2=-\frac{s}{k^2}Be^{-sy+i(pt-fx)}, \quad v_2=\frac{if}{k^2}Be^{-sy+i(pt-fx)}. \end{aligned}\right\} \tag{5}$$

---

5) H. JEFFREYS, *M.N.R.A.S.*, **77** (1917), 449~456; *The Earth* (1929), 263.

6) B. GUTENBERG and H. SCHLECHTWEG, *Phys. ZS.*, **31** (1930), 745~752.

The boundary conditions are

$$\left.\begin{aligned} &\lambda\Delta+2\mu\frac{\partial v}{\partial y}+\frac{\partial}{\partial t}\left(\lambda'\Delta+2\mu'\frac{\partial v}{\partial y}\right)=0,\\ &\mu\left(\frac{\partial u}{\partial y}+\frac{\partial v}{\partial x}\right)+\mu'\frac{\partial}{\partial t}\left(\frac{\partial u}{\partial y}+\frac{\partial v}{\partial x}\right)=0, \end{aligned}\right\} \tag{6}$$

in which $u=u_1+u_2$, $v=v_1+v_2$.

Substituting (5) in (6), we get

$$\left\{\left(\frac{k}{f}\right)^2-2\right\}^2-\frac{4rs}{f^2}=0, \tag{7}$$

which is of the same form as the usual velocity equation for Rayleigh-waves, the condition being that the symbols k, r, s shall be written in the forms given in (4).

We write

$$\frac{k^2}{f^2}=\frac{\rho p^2}{f^2\mu\left(1+\dfrac{ip\mu'}{\mu}\right)}=a+ib, \tag{8}$$

whence

$$\frac{r^2}{f^2}=1-(a+ib)(P+iQ),\quad \frac{s^2}{f^2}=1-(a+ib), \tag{9}$$

where

$$P=\frac{\left(\dfrac{\lambda}{\mu}+2\right)+\left(\dfrac{p\mu'}{\mu}\right)^2\left(\dfrac{\lambda'}{\mu'}+2\right)}{\left(\dfrac{\lambda}{\mu}+2\right)^2+\left(\dfrac{p\mu'}{\mu}\right)^2\left(\dfrac{\lambda'}{\mu'}+2\right)^2},\quad Q=\frac{\dfrac{p\mu'}{\mu}\left(\dfrac{\lambda}{\mu}-\dfrac{\lambda'}{\mu'}\right)}{\left(\dfrac{\lambda}{\mu}+2\right)^2+\left(\dfrac{p\mu'}{\mu}\right)^2\left(\dfrac{\lambda'}{\mu'}+2\right)^2}, \tag{10}$$

from which the velocity equation (7) is transformed into the two expressions

$$\left.\begin{aligned} &(a-2)^2-b^2-4\left\{(1-aP+bQ)^2+(aQ+bP)^2\right\}^{\frac{1}{4}}\left\{(1-a)^2+b^2\right\}^{\frac{1}{4}}\\ &\qquad\cdot\cos\frac{1}{2}\left(\tan^{-1}\frac{aQ+bP}{1-aP+bQ}+\tan^{-1}\frac{b}{1-a}\right)=0, \end{aligned}\right\} \tag{11}$$

$$b(a-2)+2\left\{(1-aP+bQ)^2+(aQ+bP)^2\right\}^{\frac{1}{4}}\left\{(1-a)^2+b^2\right\}^{\frac{1}{4}} \cdot \sin\frac{1}{2}\left(\tan^{-1}\frac{aQ+bP}{1-aP+bQ}+\tan^{-1}\frac{b}{1-a}\right)=0.$$

From (8), (10) and (11) it is possible to get the velocity and damping coefficient (with increase in focal distance) of the periodic visco-elastic Rayleigh-waves for any ratios of λ/μ, λ'/μ', $p\mu'/\mu$.

Since, generally speaking, the f-value that defines the wave length assumes the form

$$f=f_1+if_2, \tag{12}$$

it follows that the actual wave length is $2\pi/f_1$ and that the damping coefficient of waves with increase in focal distance is f_2. The coefficients r, s showing the decay in amplitude with depth, are no longer aperiodic, but of the types $r=r_1+ir_2$, $s=s_1+is_2$, which indicate oscillatory decrease in wave amplitudes with depth. It should however be borne in mind that, in this case, the integral of the wave energy through the whole depth is not infinite.

The results of calculating the various ratios of $p\mu'/\mu$ in the case $\lambda/\mu=1$, $\lambda'/\mu'=100\,(\lambda'\eqslantgtr\mu')$ are shown in the formulae below and in Fig. 1.

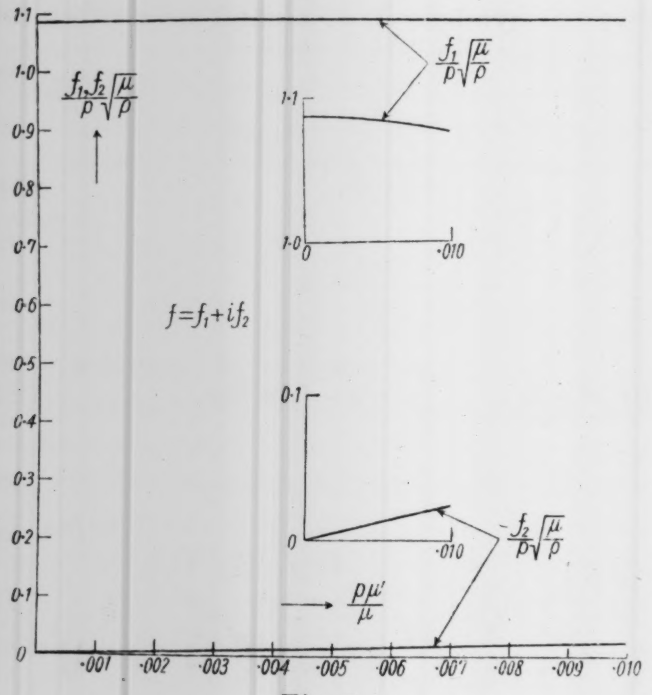

Fig. 1.

$$\frac{p\mu'}{\mu}=0; \qquad f=1{\cdot}08766p\sqrt{\frac{\rho}{\mu}},$$

$$\frac{p\mu'}{\mu}=\frac{1}{1000}; \qquad f=(1{\cdot}0875-i0{\cdot}002987)p\sqrt{\frac{\rho}{\mu}},$$

$$\frac{p\mu'}{\mu}=\frac{1}{200}; \qquad f=(1{\cdot}0843-i0{\cdot}01367)p\sqrt{\frac{\rho}{\mu}},$$

$$\frac{p\mu'}{\mu}=\frac{1}{100}; \qquad f=(1{\cdot}0764-i0{\cdot}02411)p\sqrt{\frac{\rho}{\mu}}.$$

Since $(f_1/p)\sqrt{\mu/\rho}$ and $(f_2/p)\sqrt{\mu/\rho}$ correspond to the first and second terms of

$$\frac{f}{p}\sqrt{\frac{\mu}{\rho}}\left\{=(f_1+if_2)\frac{1}{p}\sqrt{\frac{\mu}{\rho}}\right\} \tag{13}$$

in the solution of the velocity equation, curves A and B are proportional to the coefficient for wave length and to the coefficient for damping with increase in focal distance respectively.

It will be seen from Fig. 1 that whereas the increase in the damping coefficient with increase in $p\mu'/\mu$ is very marked, the increase in wave length (that is, decrease of f) with increase in the same $p\mu'/\mu$ is rather gradual. A similar condition will probably hold for any ratio of λ/μ as well as for any ratio of λ'/μ'. At all events, the respective expressions for the dilatational and distortional components assume the forms

$$\left.\begin{aligned} \Delta &= Ae^{-(r_1+ir_2)y+i(pt-f_1x)-f_2x}, \\ 2\varpi &= Be^{-(s_1+is_2)y+i(pt-f_1x)-f_2x}, \end{aligned}\right\} \tag{14}$$

f_1, f_2, r_1, r_2, s_1, s_2 being real. These expressions show that even should the damping of pure dilatational waves differ from that of pure distortional waves, the damping coefficients of both components (dilatational and distortional) in Rayleigh-waves are the same.

Although every feature of damping in Rayleigh-waves is involved implicitly in the curves in Fig. 1, since it is not an easy matter to compare the nature of the damping in Rayleigh-waves with that in bodily waves, we shall now show the expressions for the Rayleigh-waves in a special case. The condition of the case is such that

$$\frac{\lambda+2\mu}{\mu}=\frac{p(\lambda'+2\mu')}{p\mu'}=n. \tag{15}$$

Solving the problem as in the general case, we have

$$f=\sqrt{\frac{\rho p^2}{q\mu\sqrt{1+\left(\frac{p\mu'}{\mu}\right)^2}}}\left\{\cos\frac{1}{2}\tan^{-1}\frac{p\mu'}{\mu}-i\sin\frac{1}{2}\tan^{-1}\frac{p\mu'}{\mu}\right\}, \tag{16}$$

$$\left.\begin{aligned} r &= \sqrt{\frac{\left(1-\dfrac{q\mu}{\lambda+2\mu}\right)\rho p^2}{q\mu\sqrt{1+\left(\dfrac{p\mu'}{\mu}\right)^2}}}\left\{\cos\frac{1}{2}\tan^{-1}\frac{p\mu'}{\mu}-i\sin\frac{1}{2}\tan^{-1}\frac{p\mu'}{\mu}\right\}, \\ s &= \sqrt{\frac{(1-q)\rho p^2}{q\mu\sqrt{1+\left(\dfrac{p\mu'}{\mu}\right)^2}}}\left\{\cos\frac{1}{2}\tan^{-1}\frac{p\mu'}{\mu}-i\sin\frac{1}{2}\tan^{-1}\frac{p\mu'}{\mu}\right\}, \end{aligned}\right\} \quad (17)$$

where $q=0{\cdot}8453$ for $\lambda=\mu$ and $q=0{\cdot}9126$ for $\lambda/\mu=\infty$. The expressions for the dilatational and distortional components of Rayleigh-waves are the same as those in (14). These results are virtually the same as those that we obtained in the previous paper.7) Comparing (16) with the damping coefficients of bodily waves, the expressions for which will appear presently, it will be seen that under the condition (15), Rayleigh-waves, bodily distortional waves, and bodily dilatational waves have successively smaller damping coefficients with reference to increase in focal distance. If, on the other hand, the damping coefficient as referred to increase in time, that is to say, g in e^{-gt}, were considered, it would be found that the coefficients under consideration for the present particular case are the same for the three kinds of waves. Speaking generally, it seems that the damping coefficient of Rayleigh-waves as referred to time increase is intermediate between the coefficient of dilatational waves and that of distortional waves.8) As an example, we shall take the case, $\lambda/\mu=1$, $\lambda'/\mu'=100$ (which differs from the condition (15), and arrange the damping coefficients of the three kinds of waves as follows.

Table I. Damping coefficient $f(\div p\sqrt{\rho/\mu})$ as referred to increase in focal distance.

$p\mu'/\mu$	0	1/1000	1/200	1/100
Dilatational waves	0	0·00954	0·0476	0·0954
Rayleigh-waves	0	0·002987	0·01367	0·02411
Distortional waves	0	0·00050	0·0025	0·0050

Table II. Damping coefficient $g(\div p)$ as referred to time increase.

$p\mu'/\mu$	0	1/1000	1/200	1/100
Dilatational waves	0	0·0165	0·0805	0·165
Rayleigh-waves	0	0·002745	0·01256	0·02218
Distortional waves	0	0·00050	0·0025	0·0050

---

7) *loc. cit.* 1).

8) *loc. cit. poste.* § 4.

The condition that the damping coefficient of Rayleigh-waves as referred to increase in focal distance is intermediate between those of both bodily waves, is not very important. Since, nevertheless, Rayleigh-waves are in the condition of dilatational waves coupled with distortional waves, it is likely that the damping coefficient of Rayleigh-waves as referred to increase in time is generally intermediate between the damping coefficients of the two kinds of bodily waves.

3. *Love-waves.*

The equations of motion in this case are written

$$\left.\begin{aligned} \left(\mu_1+\mu_1'\frac{\partial}{\partial t}\right)\left(\frac{\partial^2 v_1}{\partial x^2}+\frac{\partial^2 v_1}{\partial z^2}\right) &= \rho_1\frac{\partial^2 v_1}{\partial t^2}, \\ \left(\mu_2+\mu_2'\frac{\partial}{\partial t}\right)\left(\frac{\partial^2 v_2}{\partial x^2}+\frac{\partial^2 v_2}{\partial z^2}\right) &= \rho_2\frac{\partial^2 v_2}{\partial t^2}, \end{aligned}\right\} \tag{18}$$

where μ_1, μ_1', ρ_1, v_1 refer to the surface layer and μ_2, μ_2', ρ_2, v_2 to the subjacent medium. The solutions of (18) are

$$\left.\begin{aligned} v_1 &= (A\cos s_1 z + B\sin s_1 z)e^{i(pt-fx)}, \\ v_2 &= Ce^{s_2 z}e^{i(pt-fx)}, \end{aligned}\right\} \tag{19}$$

where

$$s_1^2 = \frac{\rho_1 p^2}{\mu_1+i\mu_1'}-f^2, \quad s_2^2 = f^2-\frac{\rho_2 p^2}{\mu_2+i\mu_2'}. \tag{20}$$

Substituting (19) in the boundary conditions

$$\left.\begin{aligned} z=H; &\qquad \left(\mu_1+\mu_1'\frac{\partial}{\partial t}\right)\frac{\partial v_1}{\partial z}=0, \\ z=0; &\qquad v_1=v_2, \quad \left(\mu_1+\mu_1'\frac{\partial}{\partial t}\right)\frac{\partial v_1}{\partial z}=\left(\mu_2+\mu_2'\frac{\partial}{\partial t}\right)\frac{\partial v_2}{\partial z}=0, \end{aligned}\right\} \tag{21}$$

we get

$$\tan s_1 H = \frac{(\mu_2+ip\mu_2')s_2}{(\mu_1+ip\mu_1')s_1}. \tag{22}$$

Writing

$$\rho_1 p^2/\mu_1 f^2 = a+ib, \tag{23}$$

the expression (22) transforms into two equations

$$\left.\begin{aligned}
&\frac{\tan\left\{pH\sqrt{\dfrac{\rho_1}{\mu_1}}\zeta\sqrt{\dfrac{1+\cos\theta}{2}}\right\}\operatorname{sech}^2\left\{pH\sqrt{\dfrac{\rho_1}{\mu_1}}\zeta\sqrt{\dfrac{1-\cos\theta}{2}}\right\}}{1+\tan^2\left\{pH\sqrt{\dfrac{\rho_1}{\mu_1}}\zeta\sqrt{\dfrac{1+\cos\theta}{2}}\right\}\tanh^2\left\{pH\sqrt{\dfrac{\rho_1}{\mu_1}}\zeta\sqrt{\dfrac{1-\cos\theta}{2}}\right\}}\\
&\qquad-\frac{\mu_2}{\mu_1}\sqrt{\frac{\dfrac{1}{2}(1+\cos\varphi)\sqrt{\eta^2+\vartheta^2}}{\left\{(a-1)+\dfrac{p\mu_1'}{\mu_1}\left(-b+\dfrac{p\mu_1'}{\mu_1}\right)\right\}^2+\left\{b+\dfrac{p\mu_1'}{\mu_1}(a-2)\right\}^2}}=0,\\
&\frac{\sec^2\left\{pH\sqrt{\dfrac{\rho_1}{\mu_1}}\zeta\sqrt{\dfrac{1+\cos\theta}{2}}\right\}\tanh\left\{pH\sqrt{\dfrac{\rho_1}{\mu_1}}\zeta\sqrt{\dfrac{1-\cos\theta}{2}}\right\}}{1+\tan^2\left\{pH\sqrt{\dfrac{\rho_1}{\mu_1}}\zeta\sqrt{\dfrac{1+\cos\theta}{2}}\right\}\tanh^2\left\{pH\sqrt{\dfrac{\rho_1}{\mu_1}}\zeta\sqrt{\dfrac{1-\cos\theta}{2}}\right\}}\\
&\qquad-\frac{\mu_2}{\mu_1}\sqrt{\frac{\dfrac{1}{2}(1-\cos\varphi)\sqrt{\eta^2+\vartheta^2}}{\left\{(a-1)+\dfrac{p\mu_1'}{\mu_1}\left(-b+\dfrac{p\mu_1'}{\mu_1}\right)\right\}^2+\left\{b+\dfrac{p\mu_1'}{\mu_1}(a-2)\right\}^2}}=0,
\end{aligned}\right\}\qquad(24)$$

where

$$\zeta=\sqrt{\frac{\left\{(a^2+b^2)-a\left(1+\dfrac{p^2\mu_1'^2}{\mu_1^2}\right)\right\}^2+\left\{\dfrac{p\mu_1'}{\mu_1}(a^2+b^2)-b\left(1+\dfrac{p^2\mu_1'^2}{\mu_1^2}\right)\right\}^2}{(a^2+b^2)\left(1+\dfrac{p^2\mu_1'^2}{\mu_1^2}\right)}},$$

$$\cos\theta=\frac{(a^2+b^2)-a\left(1+\dfrac{p^2\mu_1'^2}{\mu_1^2}\right)}{\sqrt{\left\{(a^2+b^2)-a\left(1+\dfrac{p^2\mu_1'^2}{\mu_1^2}\right)\right\}^2+\left\{\dfrac{p\mu_1'}{\mu_1}(a^2+b^2)-b\left(1+\dfrac{p^2\mu_1'^3}{\mu_1^2}\right)\right\}^2}},$$

$$\begin{aligned}
\eta=&\left\{1-\frac{p^2\mu_2'^2}{\mu_2^2}+\frac{\rho_2\mu_1}{\rho_1\mu_2}\left(b\frac{p\mu_2'}{\mu_2}-a\right)\right\}\left\{(a-1)+\frac{p\mu_1'}{\mu_1}\left(-b+\frac{\mu_1'}{\mu_1}\right)\right\}\\
&+\left\{2\frac{\rho\mu_2'}{\mu_2}-\frac{\rho_2\mu_1}{\rho_1\mu_2}\left(b+a\frac{p\mu_2'}{\mu_2}\right)\right\}\left\{b+\frac{p\mu_1'}{\mu_1}(a-2)\right\},
\end{aligned}$$

$$\begin{aligned}
\vartheta=&-\left\{1-\frac{p^2\mu_2'^2}{\mu_2^2}+\frac{\rho_2\mu_1}{\rho_1\mu_2}\left(b\frac{p\mu_2'}{\mu_2}-a\right)\right\}\left\{b+\frac{p\mu_1'}{\mu_1}(a-2)\right\}\\
&+\left\{2\frac{p\mu_2'}{\mu_2}-\frac{\rho_2\mu_1}{\rho_1\mu_2}\left(b+a\frac{p\mu_2'}{\mu_2}\right)\right\}\left\{(a-1)+\frac{p\mu_1'}{\mu_1}\left(-b+\frac{p\mu_1'}{\mu_1}\right)\right\},
\end{aligned}$$

$$\cos\varphi=\frac{\eta}{\sqrt{\eta^2+\vartheta^2}},\qquad(25)$$

every quantity in (24) being real. If a, b were determined from (24), the value f_1 defining the actual wave length, and damping coefficient f_2 for increase in focal distance x, is expressed by

$$f(=f_1+if_2)=\frac{p\sqrt{\dfrac{\rho_1}{\mu_1}}\left\{\sqrt{\dfrac{1}{2}\left(1+\dfrac{a}{\sqrt{a^2+b^2}}\right)}-i\sqrt{\dfrac{1}{2}\left(1-\dfrac{a}{\sqrt{a^2+b^2}}\right)}\right\}}{(a^2+b^2)^{\frac{1}{4}}}. \tag{26}$$

Since in the present case there are a number of quantities, such as $p\mu_1'/\mu_1$, μ_2'/μ_1', μ_2/μ_1, ρ_2/ρ_1, $pH\sqrt{\rho_1/\mu_1}$, for determining the coefficient, $f(=f_1+if_2)$, the numerical treatment of the problem is extremely complex. We shall therefore complete this section by merely concluding that Love-waves probably damp in much the same way as do Rayleigh-waves.

4. *Plane dilatational waves and plane distortional waves.*

The problem here is very simple. The equation of motion and its solution for dilatational waves are

$$\left\{(\lambda+2\mu)+(\lambda'+2\mu')\frac{\partial}{\partial t}\right\}\frac{\partial^2 v}{\partial x^2}=\rho\frac{\partial^2 v}{\partial t^2}, \tag{27}$$

$$v=A\,exp.\left[ipt-x\frac{\sqrt{\rho}\,p}{\{(\lambda+2\mu)^2+p^2(\lambda'+2\mu')^2\}^{\frac{1}{4}}}\right.$$
$$\left.\cdot\left\{i\cos\frac{1}{2}\tan^{-1}\frac{p(\lambda'+2\mu')}{\lambda+2\mu}+\sin\frac{1}{2}\tan^{-1}\frac{p(\lambda'+2\mu')}{\lambda+2\mu}\right\}\right], \tag{28}$$

and those for distortional waves are

$$\left(\mu+\mu'\frac{\partial}{\partial t}\right)\frac{\partial^2 v}{\partial x^2}=\rho\frac{\partial^2 v}{\partial t^2}, \tag{29}$$

$$v=A\,exp.\left[ipt-x\frac{\sqrt{\rho}\,p}{\{\mu^2+p^2\mu'^2\}^{\frac{1}{4}}}\left\{i\cos\frac{1}{2}\tan^{-1}\frac{p\mu'}{\mu}+\sin\frac{1}{2}\tan^{-1}\frac{p\mu'}{\mu}\right\}\right]. \tag{30}$$

The second coefficient of x in every expression of v in (28), (30) corresponds to the damping coefficient under consideration. Particularly, when the solid viscosities are not large, the approximate values of damping coefficients as referred to increase in focal distance for both kinds of waves are

$$p^2\sqrt{\frac{\rho}{\lambda+2\mu}}\,\frac{(\lambda'+2\mu')}{2(\lambda+2\mu)}, \qquad p^2\sqrt{\frac{\rho}{\mu}}\,\frac{\mu'}{2\mu} \tag{31}$$

respectively, from which the numerical values for bodily waves shown in Tables I, II were calculated. It appears, at all events, that whereas the damping coefficients referred to distance, even approximately, are as those shown by (31), the damping coefficients referred to time are nearly

$$\frac{p^2(\lambda'+2\mu')}{2(\lambda+2\mu)}, \qquad \frac{p^2\mu'}{2\mu}. \tag{32}$$

5. *Spherical dilatational waves and spherical distortional waves.*

The general solutions of spherical waves transmitted in a pure elastic body have already been obtained.[9] Here we shall modify the solutions by writing

$$h^2=\frac{\rho p^2}{(\lambda+2\mu)+ip(\lambda'+2\mu')}, \quad k^2=\frac{\rho p^2}{\mu+ip\mu'}, \tag{33}$$

that is to say

$$h=\left(\frac{\rho p^2}{\mu}\right)^{\frac{1}{2}}\left\{\left(\frac{\lambda}{\mu}+2\right)^2+\left(\frac{p\mu'}{\mu}\right)^2\left(\frac{\lambda'}{\mu'}+2\right)^2\right\}^{-\frac{1}{4}}e^{-\frac{i\theta_1}{2}},$$

$$k=\left(\frac{\rho p^2}{\mu}\right)^{\frac{1}{2}}\left\{1+\left(\frac{p\mu'}{\mu}\right)^2\right\}^{-\frac{1}{4}}e^{-\frac{i\theta_2}{2}}, \tag{33'}$$

where

$$\theta_1=\tan^{-1}\frac{\frac{p\mu'}{\mu}\left(\frac{\lambda'}{\mu'}+2\right)}{\frac{\lambda}{\mu}+2}, \qquad \theta_2=\tan^{-1}\frac{p\mu'}{\mu}. \tag{34}$$

The expressions of spherical dilatational waves at a relatively large distance then assume the forms

$$\left.\begin{aligned}
u_1&=A_{mn}\sqrt{\frac{2}{\pi}}\left\{\frac{1}{r^2}\vartheta^{-\frac{5}{2}}e^{i\left(\frac{n+1}{2}\pi+\frac{5}{4}\theta_1\right)}\right.\\
&\qquad\left.-\frac{1}{r}\vartheta^{-\frac{3}{2}}e^{i\left(\frac{n}{2}\pi+\frac{3}{4}\theta_1\right)}\right\}e^{-r(h_1+ih_2)}P_n^m(\cos\theta)\cos m\phi e^{ipt},\\
v_1&=-A_{mn}\sqrt{\frac{2}{\pi}}\frac{1}{r^2}\vartheta^{-\frac{5}{2}}e^{-r(h_1+ih_2)+i\left(\frac{n+1}{2}\pi+\frac{5}{4}\theta_1\right)}\frac{dP_n^m(\cos\theta)}{d\theta}\cos m\phi e^{ipt},\\
w_1&=mA_{mn}\sqrt{\frac{2}{\pi}}\frac{1}{r^2}\vartheta^{-\frac{5}{2}}e^{-r(h_1+ih_2)+i\left(\frac{n+1}{2}\pi+\frac{5}{4}\theta_1\right)}\frac{P_n^m(\cos\theta)}{\sin\theta}\sin m\phi e^{ipt}.
\end{aligned}\right\} \tag{35}$$

---

[9] K. SEZAWA, *Bull. Earthq. Res. Inst.*, **6** (1929), 12; K. SEZAWA and K. KANAI, *ibid.*, **10** (1932), 299.

The distortional waves of the second and the first kinds have respectively the forms

$$\left.\begin{aligned} u_2 &= 0, \\ v_2 &= \frac{mB_{mn}}{n(n+1)}\sqrt{\frac{2}{\pi}\frac{1}{r}}\,\zeta^{-\frac{1}{2}}e^{-r(k_1+ik_2)+i\left(\frac{n+1}{2}\pi+\frac{1}{4}\theta_2\right)}\frac{P_n^m(\cos\theta)}{\sin\theta}\cos m\phi e^{ipt}, \\ w_2 &= -\frac{B_{mn}}{n(n+1)}\sqrt{\frac{2}{\pi}\frac{1}{r}}\,\zeta^{-\frac{1}{2}}e^{-r(k_1+ik_2)+i\left(\frac{n+1}{2}\pi+\frac{1}{4}\theta_2\right)}\frac{dP_n^m(\cos\theta)}{d\theta}\sin m\phi e^{ipt}, \end{aligned}\right\} \tag{36}$$

$$\left.\begin{aligned} u_3 &= -\frac{n(n+1)C_{mn}}{m}\sqrt{\frac{2}{\pi}\frac{1}{r^2}}\,\zeta^{-\frac{5}{2}}e^{-r(k_1+ik_2)+i\left(\frac{n+1}{2}\pi+\frac{5}{4}\theta_2\right)}P_n^m(\cos\theta)\cos m\phi e^{ipt}, \\ v_3 &= \frac{C_{mn}}{m}\sqrt{\frac{2}{\pi}\frac{1}{r}}\,\zeta^{-\frac{3}{2}}e^{-r(k_1+ik_2)+i\left(\frac{n+2}{2}\pi+\frac{3}{4}\theta_2\right)}\frac{dP_n^m(\cos\theta)}{d\theta}\cos m\phi e^{ipt}, \\ w_3 &= C_{mn}\sqrt{\frac{2}{\pi}\frac{1}{r}}\,\zeta^{-\frac{3}{2}}e^{-r(k_1+ik_2)+i\left(\frac{n}{2}\pi+\frac{3}{4}\theta_2\right)}\frac{P_n^m(\cos\theta)}{\sin\theta}\sin m\phi e^{ipt}. \end{aligned}\right\} \tag{37}$$

The symbols ϑ, ζ, h_1, h_2, k_1, k_2 in (35), (36), (37) are such that

$$\left.\begin{aligned} &\vartheta = \left(\frac{\rho p^2}{\mu}\right)^{\frac{1}{2}}\left\{\left(\frac{\lambda}{\mu}+2\right)^2+\left(\frac{p\mu'}{\mu}\right)^2\left(\frac{\lambda'}{\mu'}+2\right)^2\right\}^{-\frac{1}{4}}, \quad \zeta = \left(\frac{\rho p^2}{\mu}\right)^{\frac{1}{2}}\left\{1+\left(\frac{p\mu'}{\mu}\right)^2\right\}^{-\frac{1}{4}}, \\ &h_1 = \vartheta\sqrt{\frac{1-\cos\theta_1}{2}}, \qquad h_2 = \vartheta\sqrt{\frac{1+\cos\theta_1}{2}}, \\ &k_1 = \zeta\sqrt{\frac{1-\cos\theta_2}{2}}, \qquad k_2 = \zeta\sqrt{\frac{1+\cos\theta_2}{2}}. \end{aligned}\right\} \tag{38}$$

The damping coefficients here are the same as those in the case of plane bodily waves, at any rate in the case of relatively large focal distances from the origin of the waves.

6. *Concluding remarks.*

By treating the behaviour of transmission of a periodic visco-elastic wave whose amplitude at its source is constant, it was possible for us to get accurate expressions for the damping condition of that wave for any ratio in every one of λ/μ, λ'/μ', $p\mu'/\mu$. The cases discussed in this paper cover Rayleigh-waves, Love-waves, and plane and radial bodily waves (dilatational as well as distortional).

In the case of Rayleigh-waves, even should the damping of pure dilatational waves in the medium of transmission differ from that of pure distortional waves in the same medium, the damping coefficients of both (dilatational and distortional) the components in Rayleigh-waves are the same. It also appears that the coefficients r, s showing the decay in amplitude with depth, are never aperiodic but are of the types $r = r_1 + ir_2$, $s = s_1 + is_2$, which point to oscillatory decrease in wave amplitudes with depth. The integral of the wave energy throughout the whole depth is, in this case, finite. Since Rayleigh-waves are in the condition of dilatational waves coupled with distortional waves, it is probable that the damping coefficient of Rayleigh-waves as referred to time increase is usually intermediate between the damping coefficients of the two kinds of bodily waves.

Although, in the case of Love-waves, there are a number of quantities, such as $p\mu_1'/\mu$, μ_2'/μ_1', μ_2/μ_1, ρ_2/ρ_1, $pH\sqrt{\rho_1/\mu_1}$ for determining the wave length and damping coefficient, the problem being then extremely complex, it is likely that a condition quite similar to that of Rayleigh-waves holds.

The problems in plane dilatational waves and plane distortional waves are very simple. When, in particular, the solid viscosities are not large, the approximate values of the damping coefficients as referred to increase in focal distance for both kinds of waves are $p^2(\lambda' + 2\mu')\sqrt{\rho/(\lambda+2\mu)}/2(\lambda+2\mu)$, $p^2\mu'\sqrt{\rho\mu}/2\mu$ respectively, whereas the damping coefficients as referred to time increase are nearly $p^2(\lambda'+2\mu')/2(\lambda+2\mu)$, $p^2\mu'/2\mu$ for the respective kinds of waves.

The damping coefficients in the case of spherical bodily waves are somewhat complex, but when the focal distance is relatively large, the coefficients under consideration assume the same values as those in the case of plane bodily waves.

37. 周期的粘彈性波の走波距離についての減衰

地震研究所 {妹澤克惟
金井清

粘彈性波の減衰といふ問題は絶えず研究家の注意を惹いて來たやうである．我々が以前に試みた研究では，與へられた初變形が時間的に如何に變化するかを見るために，解の基礎部分を時間的に減衰する型にして置いたのである．其後の他の研究家の試みた解法もやはり同様な型を用ひたやうである．然るに一方では原點の振動振幅が一定で走波距離について振幅が減少する問題も大切であるのに拘らず，棒に傳播する減衰屈曲波（我々が最初に形を作つた）の場合以外は誰も之に就て議論する人がなかつたのである．そこで一般の彈性波について（固體波にも，表面波にも），この方針で問題を解くことにした．之によつて表面波の場合に便宜上用ひた粘性の特定條件をも取除くことができたのである．

レーレー波の場合にはそれを構成する縱波の粘性と橫波の粘性とが違つてをつても，レーレー波の波動方向に從つての縱波振動の減衰係數と橫波振動の減衰係數とが同じになる．之を時間的の減衰係數に換算すると，レーレー波の減衰係數は縱波の減衰係數と橫波の減衰係數との中間の値を取る．之はレーレー波は縱波と橫波の聯成する振動であるからである．尙，レーレー波の地中に於ける振幅は，粘性のないときのやうに無周期的でなく，周期的減幅性を表はす．しかし振動勢力をすべての深さを通して積分しても無限大にならぬから好都合である．

ラブ波の場合は問題が複雜であるけれども，レーレー波の場合と似た性質のあることが確められた．

平面固體波については，縱波でも橫波でもその減衰性が極めて簡單な形で表される．球面固體波の場合でも震原距離が少しく大きくなると平面固體波と同じ減衰係數を取るものである．

38. The Formation of Boundary Waves at the Surface of a Discontinuity within the Earth's Crust. I.

By Katsutada SEZAWA and Kiyoshi KANAI,

Earthquake Research Institute.

(Read June 21, 1938.—Received June 20, 1938.)

I. *Introduction.*

1. Stoneley,[1] in a recent paper, showed that, although it is possible for Rayleigh-type waves to be transmitted along the surface of separation of two solids (for some conditions of two solids), it is impossible for Love-type waves to be so transmitted. It appears that Stoneley's result just mentioned has an important bearing on the fact that the horizontal amplitudes of distortional waves are much larger than vertical amplitudes of the same distortional waves as well as amplitudes of dilatational waves. In the case of dilatational waves, or distortional waves with amplitudes orientated in a vertical plane, the energy of the waves is partly converted into that of boundary waves in passing through every discontinuous surface within the earth's crust, whereas in the case of distortional waves with amplitudes orientated horizontally, no boundary wave is formed at the said discontinuous surface so that the conditions of the problem for the two cases are quite different.

In the present paper we shall show, mathematically, how bodily waves generated from a point source in the solid excite boundary waves at any discontinuous surface in the same solid, the problem being two-dimensional. The method of calculation is somewhat similar to that which Sommerfeld[2] used in his paper on the transmission of electromagnetic waves, by means of which it was possible for us to get the solutions even in the case of some difficult conditions of the problem. We shall first deal with the behaviour of waves in the case of dilatational primary waves. The case of distortional primary waves, which will next be discussed, will be divided into two subcases, namely, the one in which the amplitudes of the primary waves are orientated in a vertical plane and the other in which the amplitudes in question are orientated horizontally.

---

[1] R. STONELEY, "Elastic Waves at the Surface of Separation of Two Solids", *Proc. Roy. Soc., London,* **106** (1924), 416～428.

[2] A. SOMMERFELD, "Über die Ausbreitung der Wellen in der drahtlosen Telegraphie", *Ann. Phys.,* [4], **28** (1909), 665～738.

II. *The Case of Dilatational Primary Waves.*

2. Let the axes of x and y be drawn in coincidence with and perpendicular to the surface of discontinuity, the densities and elastic constants in the media on the positive and negative sides of y being ρ, λ, μ; ρ', λ', μ' respectively. In the case of plane primary waves

$$\phi_0 = \mathfrak{A} e^{ry+ifx-ipt}, \tag{1}$$

where $\tan^{-1}(f/ir)$ is the angle of incidence, the reflected and refracted dilatational and distortional waves assume the forms

$$\left.\begin{aligned} \phi &= Ae^{-ry+ifx-ipt}, & \psi &= Be^{-sy+ifx-ipt}, \\ \phi' &= Ce^{r'y+ifx-ipt}, & \psi' &= De^{s'y+ifx-ipt}, \end{aligned}\right\} \tag{2}$$

where

$$\left.\begin{aligned} r^2 &= f^2 - h^2, & s^2 &= f^2 - k^2, & r'^2 &= f^2 - h'^2, & s^{2} &= f^2 - k'^2, \\ h^2 &= \frac{\rho p^2}{\lambda + 2\mu}, & k^2 &= \frac{\rho p^2}{\mu}, & h'^2 &= \frac{\rho' p^2}{\lambda' + 2\mu'}, & k'^2 &= \frac{\rho' p^2}{\mu'}. \end{aligned}\right\} \tag{3}$$

The displacements in both media are then expressed by

$$\left.\begin{aligned} u &= \frac{\partial}{\partial x}(\phi_0 + \phi) + \frac{\partial \psi}{\partial y}, & v &= \frac{\partial}{\partial y}(\phi_0 + \phi) - \frac{\partial \psi}{\partial x}, \\ u' &= \frac{\partial \phi'}{\partial x} + \frac{\partial \psi'}{\partial y}, & v' &= \frac{\partial \phi'}{\partial y} - \frac{\partial \psi'}{\partial x}. \end{aligned}\right\} \tag{4}$$

Since the two media are continuous, the conditions at the boundary $y=0$, are such that

$$\left.\begin{aligned} u = u', \qquad & v = v', \\ \lambda\left(\frac{\partial u}{\partial x} + \frac{\partial v}{\partial y}\right) + 2\mu\frac{\partial v}{\partial y} &= \lambda'\left(\frac{\partial u'}{\partial x} + \frac{\partial v'}{\partial y}\right) + 2\mu'\frac{\partial v'}{\partial y}, \\ \mu\left(\frac{\partial v}{\partial x} + \frac{\partial u}{\partial y}\right) &= \mu'\left(\frac{\partial v'}{\partial x} + \frac{\partial u'}{\partial y}\right). \end{aligned}\right\} \tag{5}$$

Substituting (1), (2) in (5), we get

$$\left.\begin{aligned}
\frac{A\Phi}{\mathfrak{A}} &= \mu'^2\left(f^2+\sqrt{f^2-h^2}\sqrt{f^2-k^2}\right)\left\{4f^2\sqrt{f^2-h'^2}\sqrt{f^2-k'^2}-(2f^2-k'^2)^2\right\}\\
&\quad +\mu\mu' k^2k'^2\left(\sqrt{f^2-k^2}\sqrt{f^2-h'^2}-\sqrt{f^2-h^2}\sqrt{f^2-k'^2}\right)\\
&\quad +2\mu\mu' f^2\left(2f^2-k^2+2\sqrt{f^2-h^2}\sqrt{f^2-k^2}\right)\\
&\quad .\left(2f^2-k'^2-2\sqrt{f^2-h'^2}\sqrt{f^2-k'^2}\right)\\
&\quad +\mu^2\left(\sqrt{f^2-h'^2}\sqrt{f^2-k'^2}-f^2\right)\left\{4f^2\sqrt{f^2-h^2}\sqrt{f^2-k^2}-(2f^2-k^2)^2\right\},\\
\frac{B\Phi}{\mathfrak{A}} &= 2if\sqrt{f^2-h^2}\Big[\mu'^2\left\{4f^2\sqrt{f^2-h'^2}\sqrt{f^2-k'^2}-(2f^2-k'^2)^2\right\}\\
&\quad +\mu\mu'(4f^2-k^2)\left(2f^2-k'^2-2\sqrt{f^2-h'^2}\sqrt{f^2-k'^2}\right)\\
&\qquad\qquad +2\mu^2(2f^2-k^2)\left(\sqrt{f^2-h'^2}\sqrt{f^2-k'^2}-f^2\right)\Big],\\
\frac{C\Phi}{\mathfrak{A}} &= 2\mu k^2\sqrt{f^2-h^2}\Big[\mu'\left\{(2f^2-k'^2)\sqrt{f^2-k^2}-2f^2\sqrt{f^2-k'^2}\right\}\\
&\qquad\qquad +\mu\left\{(2f^2-k^2)\sqrt{f^2-k'^2}-2f^2\sqrt{f^2-k^2}\right\}\Big],\\
\frac{D\Phi}{\mathfrak{A}} &= 2i\mu fk^2\sqrt{f^2-h^2}\Big\{\mu'\left(2f^2-k'^2-2\sqrt{f^2-k^2}\sqrt{f^2-h'^2}\right)\\
&\qquad\qquad +\mu\left(2\sqrt{f^2-k^2}\sqrt{f^2-h'^2}+k^2-2f^2\right)\Big],
\end{aligned}\right\}\quad (6)$$

where

$$\begin{aligned}
\Phi &= \mu'^2\left(f^2-\sqrt{f^2-h^2}\sqrt{f^2-k^2}\right)\left\{(2f^2-k'^2)^2-4f^2\sqrt{f^2-h'^2}\sqrt{f^2-k'^2}\right\}\\
&\quad -\mu\mu' k^2k'^2\left(\sqrt{f^2-h^2}\sqrt{f^2-k'^2}+\sqrt{f^2-k^2}\sqrt{f^2-h'^2}\right)\\
&\quad +2\mu\mu' f^2\left(2\sqrt{f^2-h^2}\sqrt{f^2-k^2}+k^2-2f^2\right)\left(2f^2-k'^2-2\sqrt{f^2-h'^2}\sqrt{f^2-k'^2}\right)\\
&\quad +\mu^2\left(f^2-\sqrt{f^2-h'^2}\sqrt{f^2-k'^2}\right)\left\{(2f^2-k^2)^2-4f^2\sqrt{f^2-h^2}\sqrt{f^2-k^2}\right\}. \quad (7)
\end{aligned}$$

Although we have discussed the problem of reflection and refraction of waves at a plane boundary, yet owing to the type of the expressions in (1), (2), the disturbances may be assumed to be a kind of boundary waves near $y=0$. The condition that $\Phi=0$, exactly corresponds to the equation for determining the velocity of the waves that are possibly transmitted along the boundary under consideration. The velocity equation obtained by Stoneley[3] is

$$\begin{aligned}
&c^4\left\{(\rho_1-\rho_2)^2-(\rho_1A_2+\rho_2A_1)(\rho_1B_2+\rho_2B_1)\right\}\\
&\quad +2Kc^2\left\{\rho_1A_2B_2-\rho_2A_1B_1-\rho_1+\rho_2\right\}+K^2(A_1B_1-1)(A_2B_2-1)=0. \quad (8)
\end{aligned}$$

---

[3] *loc. cit.* 1).

If the symbols used by Stoneley are replaced by the corresponding ones in the present case, such that

$$\left.\begin{aligned} &c^2\equiv\frac{p^2}{f^2},\quad \alpha_1^2=\frac{\lambda_1+2\mu_1}{\rho_1}\equiv\frac{1}{p^2h^2},\quad \beta_1^2=\frac{\mu_1}{\rho_1}\equiv\frac{1}{p^2k^2},\quad \rho_1\equiv\rho,\quad \lambda_1\equiv\lambda,\quad \mu_1\equiv\mu,\\ &\qquad\quad \alpha_2^2=\frac{\lambda_2+2\mu_2}{\rho_2}=\frac{1}{p^2h'^2},\quad \beta_2^2=\frac{\mu_2}{\rho_2}\equiv\frac{1}{p^2k'^2},\quad \rho_2\equiv\rho',\quad \lambda_2\equiv\lambda',\quad \mu_2\equiv\mu',\\ &A_1=\left(1-\frac{c^2}{\alpha_1^2}\right)^{\frac{1}{2}},\quad A_2=\left(1-\frac{c^2}{\alpha_2^2}\right)^{\frac{1}{2}},\quad B_1=\left(1-\frac{c^2}{\beta_1^2}\right)^{\frac{1}{2}},\quad B_2=\left(1-\frac{c^2}{\beta_2^2}\right)^{\frac{1}{2}},\\ &\qquad\qquad\qquad K=2\,(\rho_1\beta_1^2-\rho_2\beta_2^2), \end{aligned}\right\}\quad (9)$$

the form of the expression in (8) reduces to that in (7).

Let us next consider the condition in which the primary dilatational waves are radiated from a point source at $x=0$, $y=\xi$. Then

$$\left.\begin{aligned} \phi_0&=\mathfrak{A}e^{-ipt}H_0^{(1)}(hR)\\ &=\frac{\mathfrak{A}e^{-ipt}}{\pi}\int_{-\infty}^{\infty}\frac{e^{r(y-\xi)+ifx}}{r}\,df,\quad [y<\xi]\\ &=\frac{\mathfrak{A}e^{-ipt}}{\pi}\int_{-\infty}^{\infty}\frac{e^{-r(y-\xi)+ifx}}{r}\,df.\quad [y>\xi] \end{aligned}\right\}\quad (10)$$

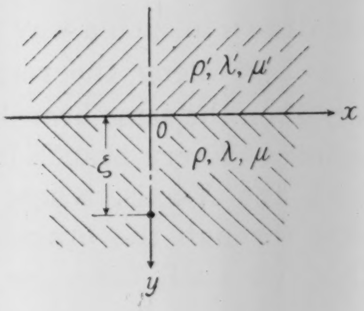

Fig. 1.

From (1), (2) it follows that the reflected and refracted waves assume the forms

$$\left.\begin{aligned} \phi&=\frac{e^{-ipt}}{\pi}\int_{-\infty}^{\infty}\frac{Ae^{-r(y+\xi)+ifx}}{r}\,df,\quad &\psi&=\frac{e^{-ipt}}{\pi}\int_{-\infty}^{\infty}\frac{Be^{-sy-r\xi+ifx}}{r}\,df,\\ \phi'&=\frac{e^{-ipt}}{\pi}\int_{-\infty}^{\infty}\frac{Ce^{r'y-r\xi+ifx}}{r}\,df,\quad &\psi'&=\frac{e^{-ipt}}{\pi}\int_{-\infty}^{\infty}\frac{De^{s'y-r\xi+ifx}}{r}\,df. \end{aligned}\right\}\quad (11)$$

The displacements at any point are obtained by using (10), (11), (4).

3. To evaluate the integral expressions of displacements, we consider such integrals in which the f-value in (10), (11) is replaced by a complex quantity $Z=X+iY$. The paths of integration are: (i) the real axis in the Z plane from $-\infty$ to ∞, (ii) a circular arc of infinite radius in the first and second quadrants in the same plane, (iii) an arc around the pole $Z=\kappa$, which satisfies the condition $\Phi(\kappa)=0$, (iv) four branch lines connecting the respective branch points with $Z=i\infty$. The sum of the four kinds of contour integrals vanishes, from which it is possible to obtain the integrals performed along the real axis from $-\infty$ to ∞. The integral performed along the semi-circular arc vanishes owing to the factor $e^{-Rx\sin\theta}$, whereas the integral of

$$\int \frac{\chi(Z)}{\Phi(Z)}\,dZ \tag{12}$$

around the pole $Z=\kappa$, is merely written

$$-2\pi i\frac{\chi(\kappa)}{\Phi'(\kappa)}. \tag{13}$$

There remains the integral along every branch line.

The branch lines assumed here are similar to those used by Sommerfeld. Let $Z=h,\ k,\ h',\ k'$ be four branch points. Four branch lines are drawn in such a way that the values of $\sqrt{Z^2-h^2}$, $\sqrt{Z^2-k^2}$, $\sqrt{Z^2-h'^2}$, $\sqrt{Z^2-k'^2}$ along the respective branch lines are purely imaginary for any Z on the same branch lines. $Z=i\infty$ satisfies this condition, at least at infinity. Every branch line near its branch point makes angle $\theta\,(=\pi-\varphi)$ with the X-axis, where φ is the angle of inclination of the line passing through the branch point and the origin $X=0$, $Y=0$. To prove this, we shall take, for example, the line through $Z=h$. Then $Z-h=\zeta_h=|\zeta_h|e^{i\theta}$, $h=|h|e^{i\varphi}$, so that $\sqrt{Z^2-h^2}=\sqrt{2|h|\zeta_h|}\,e^{\frac{i(\varphi+\theta)}{2}}$. In order that the value of $\sqrt{Z^2-h^2}$ shall be purely imaginary, $\varphi+\theta$ should be π, the problem being thus proved. Although the condition of $\sqrt{Z^2-h^2}$ being purely imaginary for intermediate points is not verified, the existence of such special points, arranged in a certain line, is quite possible. It should also be borne in mind that the two values of $\sqrt{Z^2-h^2}$ on both sides of the branch line have opposite signs. The conditions here given are valid for every branch line in the Z-plane.

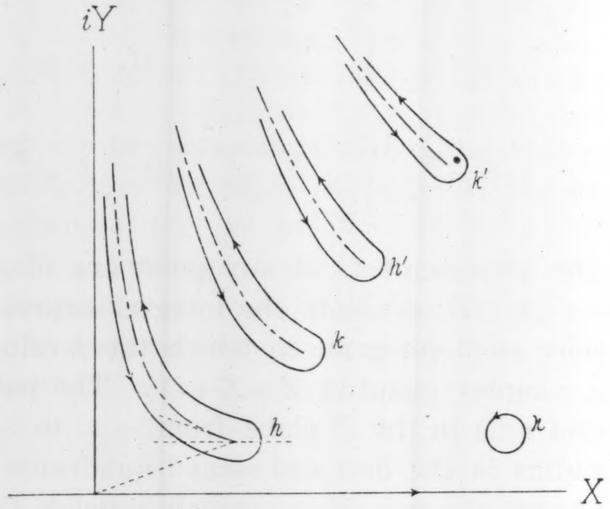

Fig. 2.

4. In the present paper there are six cases of representative integrations along branch lines, the respective ones of which will be shown successively.

In every case the sense of the integration along the contour is opposite to that along the X-axis.

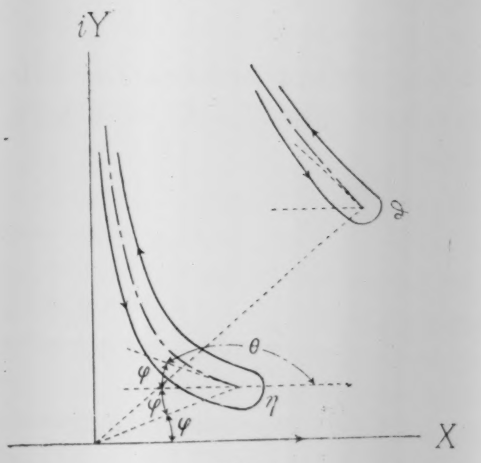

Fig. 3.

$$\text{(i)} \quad \int_{i\infty}^{\eta} \frac{U_1 e^{\sqrt{Z^2-\eta^2}y+iZx}}{-\sqrt{Z^2-\eta^2}}\, dZ + \int_{\eta}^{i\infty} \frac{U_2 e^{-\sqrt{Z^2-\eta^2}y+iZx}}{\sqrt{Z^2-\eta^2}}\, dZ \qquad (14)$$

along the branch line through $Z=\eta$. We change the variable, such that

$$\pm\sqrt{Z^2-\eta^2}=\pm i\tau, \quad Z=i\sqrt{\tau^2-\eta^2},$$

$$dZ=\frac{i\tau d\tau}{\sqrt{\tau^2-\eta^2}}, \qquad (15)$$

with the condition that $y \gtrless 0$, $x \gtrless 0$.

The limits of integration $i\infty$, η, in Z-plane become ∞ and 0 in the τ-plane. The integrals (14) then assume the forms

$$\int_{\infty}^{0} \frac{U_1' e^{i\tau y-\sqrt{\tau^2-\eta^2}x}}{-i\tau} \frac{i\tau d\tau}{\sqrt{\tau^2-\eta^2}} + \int_{0}^{\infty} \frac{U_2' e^{-i\tau y-\sqrt{\tau^2-\eta^2}x}}{i\tau} \frac{i\tau d\tau}{\sqrt{\tau^2-\eta^2}}. \qquad (14')$$

If we write $\tau=-\tau'$ in the first integral, the integrals transform to

$$\int_{-\infty}^{0} \frac{U_1'' e^{-i\tau' y-\sqrt{\tau'^2-\eta^2}x}\, d\tau'}{\sqrt{\tau'^2-\eta^2}} + \int_{0}^{\infty} \frac{U_2'' e^{-i\tau y-\sqrt{\tau^2-\eta^2}x}\, d\tau}{\sqrt{\tau^2-\eta^2}}, \qquad (14'')$$

U_1'' being equal to U_2'' for $\tau=0$. If U_1'' is important merely in the vicinity of the branch point $\tau=0$, the integral (14″) is evidently

$$\pi U_1'' H_0^{(1)}(\eta R), \qquad (16)$$

where $R^2=x^2+y^2$, $y \gtrless 0$, $x \gtrless 0$.

$$\text{(ii)} \quad \int_{i\infty}^{\kappa} \frac{U_1 e^{\sqrt{Z^2-\eta^2}y+iZx}}{-\sqrt{Z^2-\eta^2}}\, dz + \int_{\kappa}^{i\infty} \frac{U_2 e^{-\sqrt{Z^2-\eta^2}y+iZx}}{\sqrt{Z^2-\eta^2}}\, dZ \qquad (17)$$

along the branch line through $Z=\kappa$. In this case, we write

$$\pm\sqrt{Z^2-\kappa^2}=\pm i\tau, \quad Z=i\sqrt{\tau^2-\kappa^2}, \quad dZ=\frac{i\tau d\tau}{\sqrt{\tau^2-\kappa^2}}, \qquad (18)$$

so that the limits of integration $i\infty$, κ in the Z-plane become ∞ and 0 in the τ-plane. The integrals (17) transform to

$$\int_{\infty}^{0} \frac{U_1' e^{-i\sqrt{\tau^2-\kappa^2+\eta^2}\,y-\sqrt{\tau^2-\kappa^2}\,x}}{\sqrt{\tau^2-\kappa^2+\eta^2}} \frac{\tau d\tau}{\sqrt{\tau^2-\kappa^2}} + \int_{0}^{\infty} \frac{U_2' e^{-i\sqrt{\tau^2-\kappa^2+\eta^2}\,y-\sqrt{\tau^2-\kappa^2}\,x}}{\sqrt{\tau^2-\kappa^2+\eta^2}} \frac{\tau d\tau}{\sqrt{\tau^2-\kappa^2}}. \tag{17'}$$

In the present problem the values of U_1', U_2' are important near $\tau=0$, in which case $U_1'=U_2'$, and both the integrals in (17′) then cancel each other.

(iii)
$$\int_{i\infty}^{\kappa} U_1 e^{\sqrt{Z^2-\kappa^2}\,y+iZx} dZ + \int_{\kappa}^{i\infty} U_2 e^{-\sqrt{Z^2-\kappa^2}\,y+iZx} dZ. \tag{19}$$

Writing $\pm\sqrt{Z^2-\kappa^2}=\pm i\tau$, this reduces to

$$\int_{\infty}^{0} U_1' e^{i\tau y-\sqrt{\tau^2-\kappa^2}\,x} \frac{i\tau d\tau}{\sqrt{\tau^2-\kappa^2}} + \int_{0}^{\infty} U_2' e^{-i\tau y-\sqrt{\tau^2-\kappa^2}\,x} \frac{i\tau d\tau}{\sqrt{\tau^2-\kappa^2}}. \tag{19'}$$

If we put $\tau=-\tau'$ in the first integral of (19′) and put $\tau=0$ in U_1', U_2', then (19′) becomes

$$\int_{-\infty}^{\infty} U_1' e^{-i\tau y-\sqrt{\tau^2-\kappa^2}\,x} \frac{i\tau d\tau}{\sqrt{\tau^2-\kappa^2}}. \tag{19''}$$

Since U_1' is a constant and

$$-\int_{-\infty}^{\infty} \frac{e^{-i\tau y-\sqrt{\tau^2-\kappa^2}\,x}}{\sqrt{\tau^2-\kappa^2}} i\tau d\tau = \pi \frac{\partial H_0^{(1)}(\kappa R)}{\partial y}, \tag{20}$$

(19″) reduces to

$$\pi U_1' \kappa H_1^{(1)}(\kappa R) \frac{y}{R}, \tag{21}$$

where $R^2=x^2+y^2, x\neq 0,\ y\neq 0$.

(iv)
$$\int_{i\infty}^{\eta} \frac{U_1 e^{\sqrt{Z^2-\eta^2}\,y+iZx}}{-\sqrt{Z^2-\eta^2}} ZdZ + \int_{\eta}^{i\infty} \frac{U_2 e^{-\sqrt{Z^2-\eta^2}\,y+iZx}}{\sqrt{Z^2-\eta^2}} ZdZ. \tag{22}$$

In the same way as in the preceding case, the integral transforms to

$$i\int_{-\infty}^{\infty} U_1' e^{-i\tau y-\sqrt{\tau^2-\eta^2}\,x}\, d\tau. \tag{22'}$$

By means of the condition

$$-\frac{1}{\pi}\int_{-\infty}^{\infty} e^{i\tau y-\sqrt{\tau^2-\eta^2}\,x}\, d\tau = \frac{\partial H_0^{(1)}(\eta R)}{\partial x}, \tag{23}$$

the integral finally assumes the form

$$i\pi U_1'\gamma_1 H_1^{(1)}(\gamma_1 R)\frac{x}{R}\,. \qquad [x\neq 0, \quad y\neq 0] \tag{24}$$

(v)
$$\int_{i\infty}^{\varkappa}\frac{U_1 e^{\sqrt{Z^2-\gamma_1^2}y+iZx}}{-\sqrt{Z^2-\gamma_1^2}}ZdZ+\int_{\varkappa}^{i\infty}\frac{U_2 e^{-\sqrt{Z^2-\gamma_1^2}y+iZx}}{\sqrt{Z^2-\gamma_1^2}}ZdZ\,. \tag{25}$$

In this case the integrals transform to

$$-\int_{\infty}^{0}\frac{U_1' e^{-i\sqrt{\tau^2-\varkappa^2+\gamma_1^2}y-\sqrt{\tau^2-\varkappa^2}x}}{i\sqrt{\tau^2-\kappa^2+\gamma_1^2}}\tau d\tau-\int_{0}^{\infty}\frac{U_2' e^{-i\sqrt{\tau^2-\varkappa^2+\gamma_1^2}y-\sqrt{\tau^2-\varkappa^2}x}}{\sqrt{\tau^2-\kappa^2+\gamma_1^2}}\tau d\tau. \tag{25}$$

Thus, when $U_1'=U_2'$ for $\tau=0$, both the integrals cancel each other.

(vi)
$$\int_{i\infty}^{\varkappa}U_1 e^{\sqrt{Z^2-\varkappa^2}y+iZx}ZdZ+\int_{\varkappa}^{i\infty}U_2 e^{-\sqrt{Z^2-\varkappa^2}y+iZx}\,ZdZ\,. \tag{26}$$

Proceeding in the same way as before, the integrals reduce to

$$-\int_{-\infty}^{0}U_1' e^{-i\tau' y-\sqrt{\tau'^2-\varkappa^2}x}\,\tau' d\tau'-\int_{0}^{\infty}U_2' e^{-i\tau y-\sqrt{\tau^2-\varkappa^2}x}\,\tau d\tau. \tag{26'}$$

When $U_1'=U_2'$ for $\tau=0$, the integrals transform to

$$-\int_{-\infty}^{\infty}U_1' e^{-i\tau y-\sqrt{\tau^2-\varkappa^2}x}\tau d\tau. \tag{26''}$$

Using the relation

$$\frac{i}{\pi}\int_{-\infty}^{\infty}e^{-i\tau y-\sqrt{\tau^2-\varkappa^2}x}\tau d\tau=\frac{\partial^2}{\partial x\partial y}H_0^{(1)}(\kappa R)=-\kappa^2\frac{xy}{R^2}\left\{H_0^{(1)}(\kappa R)-\frac{1}{\kappa R}H_1^{(1)}(\kappa R)\right\}, \tag{27}$$

the integral (26″) is approximately

$$-i\pi U_1'\kappa^2\frac{xy}{R^2}H_0^{(1)}(\kappa R). \qquad [x\neq 0, \quad y\neq 0] \tag{28}$$

5. Although in the condition of boundary waves any one among ϕ_0, ϕ, ψ, ϕ_1' ψ_1' by itself, would indicate no wave, in the condition of bodily waves, on the other hand, the respective ones of such quantities represent separate waves. Besides physically, the displacements corresponding to ϕ_0 and ϕ are inseparable, in consequence of which it would be advisable to get such expression of $\phi_0+\phi$ as has the form

$$\begin{aligned}\phi_0+\phi&=e^{ifx-ipt}\left\{\mathfrak{A}e^{ry}+Ae^{-ry}\right\}\\&=\frac{\mathfrak{A}}{\Phi}e^{ifx-ipt}\left\{P\cosh ry+Q\sinh ry\right\},\end{aligned}\tag{29}$$

where

$$\left.\begin{aligned}\frac{\Phi P}{\mathfrak{A}}&=\mu'^2\sqrt{f^2-k^2}\left\{4f^2\sqrt{f^2-h'^2}\sqrt{f^2-k'^2}-(2f^2-k'^2)^2\right\}\\&\quad-\mu\mu'k^2k'^2\sqrt{f^2-k'^2}+4\mu\mu'f^2\sqrt{f^2-k^2}(2f^2-k'^2-2\sqrt{f^2-h'^2}\sqrt{f^2-k'^2})\\&\qquad+4\mu^2f^2\sqrt{f^2-k^2}(\sqrt{f^2-h'^2}\sqrt{f^2-k'^2}-f^2),\\\frac{\Phi Q}{\mathfrak{A}}&=\mu'^2f^2\left\{(2f^2-k'^2)^2-4f^2\sqrt{f^2-h'^2}\sqrt{f^2-k'^2}\right\}\\&\quad-\mu\mu'k^2k'^2\sqrt{f^2-k^2}\sqrt{f^2-h'^2}\\&\quad+2\mu\mu'f^2(k^2-2f^2)(2f^2-k'^2-2\sqrt{f^2-h'^2}\sqrt{f^2-k'^2})\\&\qquad+\mu^2(2f^2-k^2)^2(f^2-\sqrt{f^2-h'^2}\sqrt{f^2-k'^2}).\end{aligned}\right\}\tag{30}$$

The expressions of $\phi_0+\phi$ in the case of a point source thus assume the forms

$$\left.\begin{aligned}\phi_0+\phi&=\frac{2e^{-ipt}}{\pi}\int_{-\infty}^{\infty}\frac{e^{-ry+ifx}}{r}\left\{P\sqrt{f^2-h^2}\cosh r\xi+Q\sinh r\xi\right\}df,\quad[y>\xi]\\\phi_0+\phi&=\frac{e^{-ipt}}{\pi}\int_{-\infty}^{\infty}\left\{\frac{\mathfrak{A}e^{ry-r\xi+ifx}}{r}+\frac{Ae^{-ry-r\xi+ifx}}{r}\right\}df.\qquad[y<\xi]\end{aligned}\right\}\tag{31}$$

6. From the results shown in Sections 3, 4, 5, it is now possible to get the general expressions of waves at relatively large values of x, y as follows:

$$\left.\begin{aligned}&\phi_0=\mathfrak{A}e^{-ipt}H_0^{(1)}(hR),\qquad\qquad[R^2=x^2+(y-\xi)^2]\\&\phi_0+\phi=e^{-ipt}\left[\frac{2i\beta\alpha'\beta'}{\kappa}A_1e^{\alpha y-\alpha\xi+i\kappa x}+\mathfrak{A}H_0^{(1)}(hR_1)+A_2H_0^{(1)}(hR_2)\right],\\&\qquad[y<\xi,\quad x\neq 0,\quad y\neq 0,\quad R_1^2=x^2+(y-\xi)^2,\quad R_2^2=x^2+(y+\xi)^2]\\&\phi_0+\phi=2e^{-ipt}\left[\frac{2i\beta\alpha'\beta'}{\kappa}e^{-\alpha y+i\kappa x}(P_1\alpha\cosh\alpha\xi+Q_1\sinh\alpha\xi)\right.\\&\qquad\qquad\left.+hP_2\frac{y}{R}H_1^{(1)}(hR)\right],\quad[y>\xi,\quad R^2=x^2+y^2]\end{aligned}\right\}\tag{32}$$

$$\left.\begin{aligned}
\psi &= 2e^{-ipt}\left[-2\alpha\beta\alpha'\beta' B_1 e^{-\alpha\xi-\beta y+i\kappa x}+k^2 e^{-\sqrt{k^2-h^2}\,\xi} B_2 \frac{xy}{R^2} H_0^{(1)}(kR)\right],\\
&\qquad\qquad [y>0,\quad x\neq 0,\quad y\neq 0,\quad R^2=x^2+y^2]\\
\phi' &= 2\mu k^2 e^{-ipt}\left[\frac{2i\alpha\beta\alpha'\beta'}{\kappa} C_1 e^{-\alpha\xi+\alpha' y+i\kappa x}+h' e^{-\sqrt{h'^2-h^2}\,\xi} C_2 \frac{y}{R} H_1^{(1)}(h'R)\right],\\
\psi' &= 2\mu k^2 e^{-ipt}\left[-2\alpha\beta\alpha'\beta' D_1 e^{-\alpha\xi+\beta' y+i\kappa x}+k'^2 e^{-\sqrt{k'^2-h^2}\,\xi} D_2 \frac{xy}{R^2} H_0^{(1)}(k'R)\right],\\
&\qquad\qquad [y<0,\quad x\neq 0,\quad y\neq 0,\quad R^2=x^2+y^2]
\end{aligned}\right\}\tag{33}$$

where κ is the root of $\Phi(\kappa)=0$ shown in (7) and

$$\begin{gathered}
R^2=x^2+y^2,\quad \alpha=\sqrt{\kappa^2-h^2},\quad \beta=\sqrt{\kappa^2-k^2},\\
\alpha'=\sqrt{\kappa^2-h'^2},\quad \beta'=\sqrt{\kappa^2-k'^2},
\end{gathered}\tag{34}$$

$$\begin{aligned}
\frac{A_1\Phi_1}{\mathfrak{A}} &= \mu'^2(\kappa^2+\alpha\beta)\left\{4\kappa^2\alpha'\beta'-(2\kappa^2-k'^2)^2\right\}+\mu\mu' k^2k'^2(\beta\alpha'-\alpha\beta')\\
&\quad +2\mu\mu'\kappa^2(2\kappa^2-k^2+2\alpha\beta)(2\kappa^2-k'^2-2\alpha'\beta')\\
&\quad +\mu^2(\alpha'\beta'-\kappa^2)\left\{4\kappa^2\alpha\beta+(2\kappa^2-k^2)^2\right\},\\
\frac{P_1\Phi_1}{\mathfrak{A}} &= \mu'^2\beta\left\{4\kappa^2\alpha'\beta'-(2\kappa^2-k'^2)^2\right\}-\mu\mu' k^2k'^2\beta'\\
&\quad +4\mu\mu'\kappa^2\beta(2\kappa^2-k'^2-2\alpha'\beta')+4\mu^2\kappa^2\beta(\alpha'\beta'-\kappa^2),\\
\frac{Q_1\Phi_1}{\mathfrak{A}} &= \mu'^2\kappa^2\left\{(2\kappa^2-k'^2)^2-4\kappa^2\alpha'\beta'\right\}-\mu\mu' k^2k'^2\beta\alpha'\\
&\quad +2\mu\mu'\kappa^2(k^2-2\kappa^2)(2\kappa^2-k'^2-2\alpha'\beta')+\mu^2(2\kappa^2-k^2)^2(\kappa^2-\alpha'\beta'),\\
\frac{B_1\Phi_1}{\mathfrak{A}} &= \mu'^2\left\{4\kappa^2\alpha'\beta'-(2\kappa^2-k'^2)^2\right\}+\mu\mu'(4\kappa^2-k^2)(2\kappa^2-k'^2-2\alpha'\beta')\\
&\quad +2\mu^2(2\kappa^2-k^2)(\alpha'\beta'-\kappa^2),\\
\frac{C_1\Phi_1}{\mathfrak{A}} &= \mu'\left\{(2\kappa^2-k'^2)\beta-2\kappa^2\beta'\right\}+\mu\left\{(2\kappa^2-k^2)\beta'-2\kappa^2\beta\right\},\\
\frac{D_1\Phi_1}{\mathfrak{A}} &= \mu'(2\kappa^2-k'^2-2\beta\alpha')+\mu(2\beta\alpha'+k^2-2\kappa^2),
\end{aligned}\tag{35}$$

$$\begin{aligned}
\Phi_1 &= 4\mu'^2\alpha\beta(\kappa^2-\alpha\beta)\left\{2(2\kappa^2-k'^2)\alpha'\beta'-2\alpha'^2\beta'^2-\kappa^2\beta'^2-\kappa^2\alpha'^2\right\}\\
&\quad +\mu'^2\alpha'\beta'(\alpha-\beta)^2\left\{4\kappa^2\alpha'\beta'-(2\kappa^2-k'^2)^2\right\}\\
&\quad -\mu\mu' k^2k'^2(\beta\alpha'\beta'+\alpha\beta\alpha'+\alpha\alpha'\beta'+\alpha\beta\beta')\\
&\quad +4\mu\mu'\alpha\beta\alpha'\beta'(2\alpha\beta+k^2-2\kappa^2)(2\kappa^2-k'^2-2\alpha'\beta')\\
&\quad +2\mu\mu'\kappa\alpha'\beta'(2\kappa\beta^2+2\kappa\alpha^2+k^2\alpha\beta-4\kappa\alpha\beta)(2\kappa^2-k'^2-2\alpha'\beta')
\end{aligned}$$

$$
\begin{aligned}
&+2\mu\mu'\kappa\alpha\beta(2\alpha\beta+k^2-2\kappa^2)(4\kappa\alpha'\beta'-k'^2\alpha'\beta'-2\kappa\beta'^2-2\kappa\alpha'^2)\\
&+\mu^2\alpha\beta(\alpha'-\beta')^2\left\{4\kappa^2\alpha\beta-(2\kappa^2-k^2)^2\right\}\\
&\qquad+4\mu^2\alpha'\beta'(\kappa^2-\alpha'\beta')\left\{2(2\kappa^2-k^2)\alpha\beta-2\alpha^2\beta^2-\kappa^2\beta^2-\kappa^2\alpha^2\right\},
\end{aligned}
\tag{36}
$$

$$
\left.
\begin{aligned}
\frac{A_2\Phi_{A_2}}{\mathfrak{A}}&=\mu'^2h^2\left\{4h^2\sqrt{h^2-h'^2}\sqrt{h^2-k'^2}-(2h^2-k'^2)^2\right\}\\
&\quad+\mu\mu'k^2k'^2\sqrt{h^2-k^2}\sqrt{h^2-h'^2}\\
&\quad+2\mu\mu'h^2(2h^2-k^2)(2h^2-k'^2-2\sqrt{h^2-h'^2}\sqrt{h^2-k'^2})\\
&\qquad\qquad+\mu^2(\sqrt{h^2-h'^2}\sqrt{h^2-k'^2}-h^2)(2h^2-k^2)^2,\\
\frac{P_2\Phi_{P_2}}{\mathfrak{A}}&=\mu'^2\sqrt{h^2-k^2}\left\{4h^2\sqrt{h^2-h'^2}\sqrt{h^2-k^2}-(2h^2-k'^2)^2\right\}\\
&\quad-\mu\mu'k^2k'^2\sqrt{h^2-k'^2}+4\mu^2h^2\sqrt{h^2-k^2}(\sqrt{h^2-h'^2}\sqrt{h^2-k'^2}-h^2)\\
&\qquad\qquad+4\mu\mu'h^2\sqrt{h^2-k^2}(2h^2-k'^2-2\sqrt{h^2-h'^2}\sqrt{h^2-k'^2}),
\end{aligned}
\right\}
\tag{37}
$$

$$
\begin{aligned}
\Phi_{A_2}=\Phi_{P_2}&=\mu'^2h^2\left\{(2h^2-k'^2)^2-4h^2\sqrt{h^2-h'^2}\sqrt{h^2-k'^2}\right\}\\
&\quad-\mu\mu'k^2k'^2\sqrt{h^2-k^2}\sqrt{h^2-h'^2}\\
&\quad+2\mu\mu'h^2(k^2-2h^2)(2h^2-k'^2-2\sqrt{h^2-h'^2}\sqrt{h^2-k'^2})\\
&\qquad\qquad+\mu^2(h^2-\sqrt{h^2-h'^2}\sqrt{h^2-k'^2})(2h^2-k^2)^2.
\end{aligned}
\tag{38}
$$

$$
\left.
\begin{aligned}
\frac{B_2\Phi_{B_2}}{\mathfrak{A}}&=\mu'^2\left\{4k^2\sqrt{k^2-h'^2}\sqrt{k^2-k'^2}-(2k^2-k'^2)^2\right\}\\
&\quad+3\mu\mu'k^2(2k^2-k'^2-2\sqrt{k^2-h'^2}\sqrt{k^2-k'^2})\\
&\qquad\qquad+2\mu^2k^2(\sqrt{k^2-h'^2}\sqrt{k^2-k'^2}-k^2),\\
\Phi_{B_2}&=\mu'^2k^2\left\{(2k^2-k'^2)^2-4k^2\sqrt{k^2-h'^2}\sqrt{k^2-k'^2}\right\}\\
&\quad-\mu\mu'k^2k'^2\sqrt{k^2-h^2}\sqrt{k^2-k'^2}+\mu^2k^4(k^2-\sqrt{k^2-h'^2}\sqrt{k^2-k'^2})\\
&\qquad\qquad+2\mu\mu'k^4(2\sqrt{k^2-h'^2}\sqrt{k^2-k'^2}+k'^2-2f^2),
\end{aligned}
\right\}
\tag{39}
$$

$$
\left.
\begin{aligned}
\frac{C_2\Phi_{C_2}}{\mathfrak{A}}&=\mu'\left\{(2h'^2-k'^2)\sqrt{h'^2-k^2}-2h'^2\sqrt{h'^2-k'^2}\right\}\\
&\qquad\qquad+\mu\left\{(2h'^2-k^2)\sqrt{h'^2-k'^2}-2h'^2\sqrt{h'^2-k^2}\right\},\\
\Phi_{C_2}&=\mu'^2(h'^2-\sqrt{h'^2-h^2}\sqrt{h'^2-k^2})(2h'^2-k'^2)^2\\
&\quad-\mu\mu'k^2k'^2\sqrt{h'^2-h^2}\sqrt{h'^2-k'^2}\\
&\quad+2\mu\mu'h'^2(2\sqrt{h'^2-h^2}\sqrt{h'^2-k^2}+k^2-2h'^2)(2h'^2-k'^2)\\
&\qquad\qquad+\mu^2h'^2\left\{(2h'^2-k^2)^2-4h'^2\sqrt{h'^2-h^2}\sqrt{h'^2-k^2}\right\},
\end{aligned}
\right\}
\tag{40}
$$

$$\left.\begin{aligned}
\frac{D_2\Phi_{D_2}}{\mathfrak{A}} &= \mu'\,(k'^2-2\sqrt{k'^2-k^2}\sqrt{k'^2-h'^2}) \\
&\qquad +\mu(2\sqrt{k'^2-k^2}\sqrt{k'^2-h'^2}+k^2-2k'^2), \\
\Phi_{D_2} &= \mu'^2(k'^2-\sqrt{k'^2-h^2}\sqrt{k'^2-k^2})k'^4 \\
&\quad -\mu\mu'k^2k'^2\sqrt{k'^2-k^2}\sqrt{k'^2-h'^2} \\
&\quad +2\mu\mu'k'^4(2\sqrt{k'^2-h^2}\sqrt{k'^2-k^2}+k^2-2k'^2) \\
&\qquad +\mu^2k'^2\left\{(2k'^2-k^2)^2-4k'^2\sqrt{k'^2-h^2}\sqrt{k'^2-k^2}\right\}.
\end{aligned}\right\} \quad (41)$$

The expressions of displacements are as follows:

$$\left.\begin{aligned}
u_1 &= \frac{\partial}{\partial x}(\phi_0+\phi) = e^{-ipt}\Big[-2\beta\alpha'\beta'A_1e^{\alpha-y-\alpha\xi+i\kappa x} \\
&\qquad -h\mathfrak{A}\frac{x}{R}H_1^{(1)}(hR_1)\;-hA_2\frac{x}{R}H_1^{(1)}(hR_2)\Big], \\
v_1 &= \frac{\partial}{\partial y}(\phi_0+\phi) = e^{-ipt}\Big[-\frac{2i\alpha\beta\alpha'\beta'}{\kappa}A_1e^{-\alpha y-\alpha\xi+i\kappa x} \\
&\qquad -h\mathfrak{A}\frac{y}{R}H_1^{(1)}(hR_1)-hA_2\frac{y}{R}H_1^{(1)}(hR_2)\Big], \\
&[R_1^2=x^2+(y-\xi)^2,\quad R_2^2=x^2+(y+\xi)^2,\quad x\neq 0,\quad y\neq 0,\quad y<\xi]
\end{aligned}\right\} \quad (42)$$

$$\left.\begin{aligned}
u_1 &= \frac{\partial}{\partial x}\,(\phi_0+\phi) = 2e^{-ipt}\Big[-2\beta\alpha'\beta'\,e^{-\alpha y+i\kappa x}\left\{P_1\alpha\cosh\alpha\xi+Q_1\sinh\alpha\xi\right\} \\
&\qquad -h^2P_2\frac{xy}{R^2}H_0^{(1)}(hR)\Big], \\
v_1 &= \frac{\partial}{\partial y}\,(\phi_0+\phi) = 2e^{-ipt}\Big[\frac{2i\alpha\beta\alpha'\beta'}{\kappa}e^{-\alpha y+i\kappa x}\left\{P_1\alpha\sinh\alpha\xi+Q_1\cosh\alpha\xi\right\} \\
&\qquad -h^2P_2\frac{y^2}{R^2}H_0^{(1)}(hR)\Big], \\
&[R^2=x^2+y^2,\quad x\neq 0,\quad y>\xi]
\end{aligned}\right\} \quad (42')$$

$$\left.\begin{aligned}
u_2 &= \frac{\partial\psi}{\partial y} = 2e^{-ipt}\Big[2\alpha\beta^2\alpha'\beta'B_1e^{-\alpha\xi-\beta y+i\kappa x} \\
&\qquad -k^3e^{-\sqrt{k^2-h^2}\xi}B_2\frac{xy^2}{R^3}H_1^{(1)}(kR)\Big], \\
v_2 &= -\frac{\partial\psi}{\partial x} = 2e^{-ipt}\Big[2i\kappa\alpha\beta\alpha'\beta'B_1e^{-\alpha\xi-\beta y+i\kappa x} \\
&\qquad +k^3e^{-\sqrt{k^2-h^2}\xi}B_2\frac{x^2y}{R^3}H_1^{(1)}(kR)\Big], \\
&[R^2=x^2+y^2,\quad x\neq 0,\quad y\neq 0,\quad y>0]
\end{aligned}\right\} \quad (43)$$

$$\left.\begin{aligned}
u_1' &= \frac{\partial\phi'}{\partial x} = 2\mu k^2 e^{-ipt}\Big[-2\alpha\beta\alpha'\beta' C_1 e^{-\alpha\xi+\alpha' y+i\gamma x} \\
&\qquad - h'^2 e^{-\sqrt{h'^2-h^2}\,\xi} C_2 \frac{xy}{R^2} H_0^{(1)}(h'R)\Big], \\
v_1' &= \frac{\partial\phi'}{\partial y} = 2\mu k^2 e^{-ipt}\Big[\frac{2i\alpha\beta\alpha'^2\beta'}{\kappa} C_1 e^{\alpha\xi+\alpha' y+i\gamma x} \\
&\qquad - h'^2 e^{-\sqrt{h'^2-h^2}\,\xi} C_2 \frac{y^2}{R^2} H_0^{(1)}(h'R)\Big], \\
u_2' &= \frac{\partial\psi'}{\partial y} = 2\mu k^2 e^{-ipt}\Big[-2\alpha\beta\alpha'\beta'^2 D_1 e^{-\alpha\xi+\beta' y+i\gamma x} \\
&\qquad - k'^3 e^{-\sqrt{k'^2-h^2}\,\xi} D_2 \frac{xy^2}{R^3} H_1^{(1)}(k'R)\Big], \\
v_2' &= -\frac{\partial\psi'}{\partial x} = 2\mu k^2 e^{-ipt}\Big[2i\kappa\alpha\beta\alpha'\beta' D_1 e^{-\alpha\xi+\beta' y+i\gamma x} \\
&\qquad + k'^3 e^{-\sqrt{k'^2-h^2}\,\xi} D_2 \frac{x^2 y}{R^3} H_1^{(1)}(k'R)\Big]. \\
&[R^2 = x^2+y^2, \quad x \mathrel{\neq} 0, \quad y \mathrel{\neq} 0, \quad y<0]
\end{aligned}\right\} \qquad (44)$$

The first term within every pair of brackets represents the boundary surface waves (for some conditions of two media) and the second one the bodily waves. It will be seen that, whereas the amplitudes of boundary surface waves do not vary with changes in the epicentral distance, those of bodily waves decrease rapidly with increase in horizontal distance and, furthermore, the horizontal components of the same bodily waves also decrease fairly rapidly with increase in vertical distance. The law of decrease in the amplitudes of bodily waves for a given $y(=Y)$ and for a given $x(=X)$ is shown below.

Table I. Amplitudes of bodily waves/$H^{(1)}$.

	u_1	v_1	u_2	v_2	u_1'	v_1'	u_2'	v_2'
At Y	$\frac{xY}{R^2}$	$\frac{Y^2}{R^2}$	$\frac{xY^2}{R^3}$	$\frac{x^2Y}{R^3}$	$\frac{xY}{R^2}$	$\frac{Y^2}{R^2}$	$\frac{xY^2}{R^3}$	$\frac{x^2Y}{R^3}$
At X	$\frac{Xy}{R^2}$	$\frac{y^2}{R^2}$	$\frac{Xy^2}{R^3}$	$\frac{X^2y}{R^3}$	$\frac{Xy}{R^2}$	$\frac{y^2}{R^2}$	$\frac{Xy^2}{R^3}$	$\frac{X^2y}{R^3}$

At a relatively large x for a given Y, the values of u_1, v_2, u_1', v_2' are proportional to $R^{-3/2}$, and the values of v_1, u_2, v_1', u_2' are proportional to $R^{-5/2}$. At a relatively large y for a given X, the values of u_1, u_2, u_1', u_2' are proportional to $R^{-3/2}$ and the values of v_2, v^2 are proportional to $R^{-5/2}$, the exception being that at these values of y, X; v_1, v_1' are proportional to $R^{-1/2}$.

It should be borne in mind that the decrease in amplitudes with increase in radial distance R is always proportional to $R^{-1/2}$. More detailed feature will be discussed in Chapter V.

III. *The Case of Distortional Primary Waves with Amplitudes Orientated in a Vertical Plane.*

7. Using the same axes of x, y and ρ, λ, μ; ρ', λ', μ', as in the preceding section, it is possible to solve the present problem. Even in the case of plane primary waves

$$\psi_0 = Be^{sy+ifx-ipt}, \tag{45}$$

where $\tan^{-1}(f/is)$ is the angle of incidence, the reflected and refracted dilatational and distortional waves are of the same expressions as those in (2). Proceeding in the same way as in Chapter II, and remembering that the expressions for the displacements are

$$\left.\begin{aligned} u &= \frac{\partial\phi}{\partial x} + \frac{\partial(\psi_0+\psi)}{\partial y}, \qquad & v &= \frac{\partial\phi}{\partial y} - \frac{\partial(\psi_0+\psi)}{\partial x}, \\ u' &= \frac{\partial\phi'}{\partial x} + \frac{\partial\psi'}{\partial y}, \qquad & v' &= \frac{\partial\phi'}{\partial y} - \frac{\partial\psi}{\partial x}, \end{aligned}\right\} \tag{46}$$

it is possible to determine the constants A, B, C, D. The result is given below.

$$\begin{aligned} A\Phi = 2if\sqrt{f^2-k^2}\Big[& 2\mu^2(2f^2-k^2)(f^2-\sqrt{f^2-h'^2}\sqrt{f^2-k'^2}) \\ & +\mu\mu'(2f^2-k'^2-2\sqrt{f^2-h'^2}\sqrt{f^2-k'^2})(k^2-4f^2) \\ & \qquad +\mu'^2\left\{(2f^2-k'^2)^2-4f^2\sqrt{f^2-h'^2}\sqrt{f^2-k'^2}\right\}\Big], \end{aligned}$$

$$\begin{aligned} B\Phi = {} & \mu'^2(f^2+\sqrt{f^2-h^2}\sqrt{f^2-k^2})\left\{4f^2\sqrt{f^2-h'^2}\sqrt{f^2-k'^2}-(2f^2-k'^2)^2\right\} \\ & +\mu\mu' k^2k'^2(\sqrt{f^2-h^2}\sqrt{f^2-k'^2}-\sqrt{f^2-k^2}\sqrt{f^2-h'^2}) \\ & +2\mu\mu' f^2(2f^2-k^2+2\sqrt{f^2-h^2}\sqrt{f^2-k^2})(2f^2-k'^2-2\sqrt{f^2-h'^2}\sqrt{f^2-k'^2}) \\ & +\mu^2(\sqrt{f^2-h'^2}\sqrt{f^2-k'^2}-f^2)\left\{(2f^2-k^2)^2+4f^2\sqrt{f^2-h^2}\sqrt{f^2-k^2}\right\}\Big], \end{aligned}$$

$$\begin{aligned} C\Phi = 2i\mu fk^2\sqrt{f^2-k^2}\Big\{ & \mu(2f^2-k^2-2\sqrt{f^2-h^2}\sqrt{f^2-k'^2}) \\ & \qquad +\mu'(2\sqrt{f^2-h^2}\sqrt{f^2-k'^2}+k'^2-2f^2)\Big\}, \end{aligned}$$

$$D\Phi=2\rho k^2\sqrt{f^2-k^2}\Big[\mu\Big\{(2f^2-k^2)\sqrt{f^2-h'^2}-2f^2\sqrt{f^2-h^2}\Big\}$$
$$+\mu'\Big\{(2f^2-k'^2)\sqrt{f^2-h^2}-2f^2\sqrt{f^2-h'^2}\Big\}\Big], \tag{47}$$

where Φ is of the same form as (7), i. e. the velocity equation of the boundary waves.

8. If primary distortional waves are radiated from a point source at $x=0$, $y=\xi$, then

$$\left.\begin{aligned} \psi_0&=\frac{\mathfrak{B}e^{-ipt}}{\pi}\int_{-\infty}^{\infty}\frac{e^{s(y-\xi)+ifx}}{s}\,df, && [y<\xi]\\ \psi_0&=\frac{\mathfrak{B}e^{-ipt}}{\pi}\int_{-\infty}^{\infty}\frac{e^{-s(y-\xi)+ifx}}{s}\,df, && [y>\xi] \end{aligned}\right\} \tag{48}$$

so that the reflected and refracted waves assume the forms

$$\left.\begin{aligned} \psi&=\frac{e^{-ipt}}{\pi}\int_{-\infty}^{\infty}\frac{Be^{-s(y+\xi)+ifx}}{s}\,df, & \phi&=\frac{e^{-ipt}}{\pi}\int_{-\infty}^{\infty}\frac{Ae^{-ry-s\xi+ifx}}{s}\,df, && [y>0]\\ \phi'&=\frac{e^{-ipt}}{\pi}\int_{-\infty}^{\infty}\frac{Ce^{r'y-s\xi+ifx}}{s}\,df, & \psi'&=\frac{e^{-ipt}}{\pi}\int_{-\infty}^{\infty}\frac{De^{s'y-s\xi+ifx}}{s}\,df, && [y<0] \end{aligned}\right\} \tag{50}$$

and the superposed values of $\psi_0+\psi$ are

$$\left.\begin{aligned} \psi_0+\psi&=\frac{e^{-ipt}}{\pi}\int_{-\infty}^{\infty}\frac{e^{-s\xi+ifx}}{s}(\mathfrak{B}e^{sy}+Be^{-sy})\,df, && [y<\xi]\\ \psi_0+\psi&=\frac{e^{-ipt}}{\pi}\int_{-\infty}^{\infty}\frac{e^{-sy+ifx}}{s}(\mathfrak{B}e^{s\xi}+Be^{-s\xi})\,df. && [y>\xi] \end{aligned}\right\} \tag{50}$$

After calculating as in the preceding chapter, we get

$$\left.\begin{aligned} &\psi_0=\mathfrak{B}e^{-ipt}H_0^{(1)}(kR), \qquad [R^2=x^2+(y-\xi)^2]\\ &\psi_0+\psi=e^{-ipt}\Big[\frac{2i\alpha\alpha'\beta'}{\kappa}B_1e^{-\beta y-\beta\xi+i\gamma x}+\mathfrak{B}H_0^{(1)}(kR_1)+B_2H_0^{(1)}(kR_2)\Big],\\ &\qquad [y<\xi,\quad x\neq0,\quad y\neq0,\quad R_1^2=x^2+(y-\xi)^2,\quad R_2^2=x^2+(y+\xi)^2]\\ &\psi_0+\psi=2e^{-ipt}\Big[\frac{2i\alpha\alpha'\beta'}{\kappa}e^{-\beta y+i\gamma x}(P_1\beta\cosh\beta\xi+Q_1\sinh\beta\xi)+kP_2\frac{y}{R}H_1^{(1)}(kR)\Big],\\ &\qquad [y>\xi,\quad x\neq0,\quad R^2=x^2+y^2] \end{aligned}\right\} \tag{51}$$

$$\left.\begin{aligned}
\phi &= 2e^{-ipt}\left[-2\alpha\beta\alpha'\beta' A_1 e^{-\alpha y-\beta\xi+i\kappa x} + h^2 e^{-\sqrt{h^2-k^2}\,\xi} A_2 \frac{xy}{R^2} H_0^{(1)}(hR)\right], \\
&\qquad\qquad [y>0,\quad x\neq 0,\quad y\neq 0,\quad R^2=x^2+y^2] \\
\phi' &= 2\mu k^2 e^{-ipt}\left[-2\alpha\beta\alpha'\beta' C_1 e^{\alpha' y-\beta\xi+i\kappa x} + h'^2 e^{-\sqrt{h'^2-k^2}\,\xi} C_2 \frac{xy}{R^2} H_0^{(1)}(h'R)\right], \\
&\qquad\qquad [y>0,\quad R^2=x^2+y^2] \\
\psi' &= 2\mu k^2 e^{-ipt}\left[\frac{2i\alpha\beta\alpha'\beta'}{\kappa} D_1 e^{\beta' y-\beta\xi+i\kappa x} + k' e^{\sqrt{k'^2-k^2}\,\xi} D_2 \frac{y}{R} H_1^{(1)}(k'R)\right], \\
&\qquad\qquad [y<0,\quad x\neq 0,\quad y\neq 0,\quad R^2=x^2+y^2]
\end{aligned}\right\} \quad (52)$$

where κ is the root of $\Phi(\kappa)=0$ shown in (7) and

$$\alpha=\sqrt{\kappa^2-h^2},\quad \beta=\sqrt{\kappa^2-k^2},\quad \alpha'=\sqrt{\kappa^2-h'^2},\quad \beta'=\sqrt{\kappa^2-k'^2},$$

$$\left.\begin{aligned}
\frac{B_1\Phi_1}{\mathfrak{B}} &= \mu'^2(\kappa^2+\alpha\beta)\left\{4\kappa^2\alpha'\beta'-(2\kappa^2-k'^2)^2\right\}+\mu\mu' k^2k'^2(\alpha\beta'-\beta\alpha') \\
&\quad +2\mu\mu'\kappa^2(2\kappa^2-k^2+2\alpha\beta)(2\kappa^2-k'^2-2\alpha'\beta') \\
&\quad +\mu^2(\alpha'\beta'-\kappa^2)\left\{(2\kappa^2-k^2)^2+4\kappa^2\alpha\beta\right\}, \\
\frac{P_1\Phi_1}{\mathfrak{B}} &= \mu'^2\alpha\left\{4\kappa^2\alpha'\beta'-(2\kappa^2-k'^2)^2\right\}-\mu\mu' k^2k'^2\alpha' \\
&\quad +4\mu\mu'\kappa^2\alpha(2\kappa^2-k'^2-2\alpha'\beta')+4\mu^2\kappa^2\alpha(\alpha'\beta'-\kappa^2), \\
\frac{Q_1\Phi_1}{\mathfrak{B}} &= \mu'^2\kappa^2\left\{(2\kappa^2-k'^2)^2-4\kappa^2\alpha'\beta'\right\}-\mu\mu' k^2k'^2\alpha\beta' \\
&\quad +2\mu\mu'\kappa^2(2\kappa^2-k^2-2\alpha'\beta')(k^2-2\kappa^2)+\mu^2(\kappa^2-\alpha'\beta')(2\kappa^2-k^2)^2, \\
\frac{A_1\Phi_1}{\mathfrak{B}} &= 2\mu^2(2\kappa^2-k^2)(\kappa^2-\alpha'\beta')+\mu\mu'(2\kappa^2-k'^2-2\alpha'\beta')(k^2-4\kappa^2) \\
&\quad +\mu'^2\left\{(2\kappa^2-k'^2)^2-4\kappa^2\alpha'\beta'\right\}, \\
\frac{C_1\Phi_1}{\mathfrak{B}} &= \mu(2\kappa^2-k^2-2\alpha\beta)+\mu'(2\alpha\beta'+k'^2-2\kappa^2), \\
\frac{D_1\Phi_1}{\mathfrak{B}} &= \mu\left\{(2\kappa^2-k^2)\alpha'-2\kappa^2\alpha\right\}+\mu'\left\{(2\kappa^2-k'^2)\alpha-2\kappa^2\alpha'\right\},
\end{aligned}\right\} \quad (53)$$

$$\begin{aligned}
\Phi_1 &= \mu'^2(\kappa^2-\alpha\beta)\left\{(2\kappa^2-k'^2)^2-4\kappa^2\alpha'\beta'\right\}-\mu\mu' k^2k'^2(\alpha\beta'+\beta\alpha') \\
&\quad +2\mu\mu'\kappa^2(2\alpha\beta+k^2-2\kappa^2)(2\kappa^2-k'^2-2\alpha'\beta') \\
&\quad +\mu^2(\kappa^2-\alpha'\beta')\left\{(2\kappa^2-k^2)^2-4\kappa^2\alpha\beta\right\}, \quad (54)
\end{aligned}$$

$$
\left.\begin{aligned}
\frac{B_2\Phi_{B_2}}{\mathfrak{B}} &= \mu'^2k^2\left\{4k^2\sqrt{k^2-h'^2}\sqrt{k^2-k'^2}-(2k^2-k'^2)^2\right\} \\
&\quad +\mu\mu'k^2k'^2\sqrt{k^2-h^2}\sqrt{k^2-k'^2}+\mu^2(\sqrt{k^2-h'^2}\sqrt{k^2-k'^2}-k^2)k^4 \\
&\qquad +2\mu\mu'k^4(2k^2-k'^2-2\sqrt{k^2-h'^2}\sqrt{k^2-k'^2}), \\
\frac{P_2\Phi_{P_2}}{\mathfrak{B}} &= \mu'^2\left\{4k^2\sqrt{k^2-h'^2}\sqrt{k^2-k'^2}-(2k^2-k'^2)^2\sqrt{k^2-h^2}\right. \\
&\quad +4\mu\mu'k^2\sqrt{k^2-h^2}(2k^2-k'^2-2\sqrt{k^2-h'^2}\sqrt{k^2-k'^2}) \\
&\quad -\mu\mu'k^2k'^2\sqrt{k^2-h'^2}+4\mu^2k^2\sqrt{k^2-h^2}(\sqrt{k^2-h'^2}\sqrt{k^2-k'^2}-k^2),
\end{aligned}\right\} \tag{55}
$$

$$
\begin{aligned}
\Phi_{B_2}=\Phi_{P_2} &= \mu'^2k^2\left\{(2k^2-k'^2)^2-4k^2\sqrt{k^2-h'^2}\sqrt{k^2-k'^2}\right\} \\
&\quad -2\mu\mu'k^4(2k^2-k'^2-2\sqrt{k^2-h'^2}\sqrt{k^2-k'^2}) \\
&\quad -\mu\mu'k^2k'^2\sqrt{k^2-h^2}\sqrt{k^2-k'^2}+\mu^2k^4(k^2-\sqrt{k^2-h'^2}\sqrt{k^2-k'^2}),
\end{aligned} \tag{56}
$$

$$
\left.\begin{aligned}
\frac{A_2\Phi_{A_2}}{\mathfrak{B}} &= 2\mu^2(2h^2-k^2)(h^2-\sqrt{h^2-h'^2}\sqrt{h^2-k'^2}) \\
&\quad +\mu\mu'(2h^2-k'^2-2\sqrt{h^2-h'^2}\sqrt{h^2-k'^2})(k^2-4h^2) \\
&\qquad +\mu'^2\left\{(2h^2-k'^2)^2-4h^2\sqrt{h^2-h'^2}\sqrt{h^2-k'^2}\right\}, \\
\Phi_{A_2} &= \mu'^2h^2\left\{(2h^2-k'^2)^2-4h^2\sqrt{h^2-h'^2}\sqrt{h^2-k'^2}\right\} \\
&\quad -\mu\mu'k^2k'^2\sqrt{h^2-k^2}\sqrt{h^2-h'^2} \\
&\quad +2\mu\mu'h^2(k^2-2h^2)(2h^2-k'^2-2\sqrt{h^2-h'^2}\sqrt{h^2-k'^2}) \\
&\qquad +\mu^2(h^2-\sqrt{h^2-h'^2}\sqrt{h^2-k'^2})(2h^2-k^2)^2,
\end{aligned}\right\} \tag{57}
$$

$$
\left.\begin{aligned}
\frac{C_2\Phi_{C_2}}{\mathfrak{B}} &= \mu(2h'^2-k^2-2\sqrt{h'^2-h^2}\sqrt{h'^2-k'^2}) \\
&\qquad +\mu'(2\sqrt{h'^2-h^2}\sqrt{h'^2-k'^2}-k'^2), \\
\Phi_{C_2} &= \mu'^2(h'^2-\sqrt{h'^2-h^2}\sqrt{h'^2-k^2})(2h'^2-k'^2)^2 \\
&\quad -\mu\mu'k^2k'^2\sqrt{h'^2-h^2}\sqrt{h'^2-k'^2} \\
&\quad +2\mu\mu'h'^2(2\sqrt{h'^2-h^2}\sqrt{h'^2-k^2}+k^2-2h'^2)(2h'^2-k'^2) \\
&\qquad +\mu^2h'^2\left\{(2h'^2-k^2)^2-4h'^2\sqrt{h'^2-h^2}\sqrt{h'^2-k^2}\right\},
\end{aligned}\right\} \tag{58}
$$

$$
\left.\begin{aligned}
\frac{D_2\Phi_{D_2}}{\mathfrak{B}} &= \mu\left\{(2k'^2-k^2)\sqrt{k'^2-h'^2}-2k'^2\sqrt{k'^2-h^2}\right\} \\
&\qquad +\mu'k'^2\left\{\sqrt{k'^2-h^2}-2\sqrt{k'^2-h'^2}\right\}, \\
\Phi_{D_2} &= \mu'^2k'^4(k'^2-\sqrt{k'^2-h^2}\sqrt{k'^2-k^2})-\mu\mu'k^2k'^2\sqrt{k'^2-k^2}\sqrt{k'^2-h'^2} \\
&\quad +2\mu\mu'k'^4(2\sqrt{k'^2-h^2}\sqrt{k'^2-k^2}+k^2-2k'^2) \\
&\qquad +\mu^2k'^2\left\{(2k'^2-k^2)^2-4k'^2\sqrt{k'^2-h^2}\sqrt{k'^2-k^2}\right\}.
\end{aligned}\right\} \tag{59}
$$

The expressions for the displacements are shown below.

$$\left.\begin{aligned}
u_1 &= \frac{\partial\phi}{\partial x} = 2e^{-ipt}\left[-2i\kappa\alpha\beta\alpha'\beta' A_1 e^{-\alpha y-\beta\xi+i\kappa x} - h^3 e^{-\sqrt{h^2-k^2}\,\xi} A_2 \frac{x^2 y}{R^3} H_1^{(1)}\, hR)\right],\\
v_1 &= \frac{\partial\phi}{\partial y} = 2e^{-ipt}\left[2\alpha^2\beta\alpha'\beta' A_1 e^{-\alpha y-\beta\xi+i\kappa x} - h^3 e^{-\sqrt{h^2-k^2}\,\xi} A_2 \frac{x y^2}{R^3} H_1^{(1)}(hR)\right],\\
&\qquad [R^2 = x^2+y^2,\quad x\neq 0,\quad y\neq 0,\quad y>0]
\end{aligned}\right\}\quad(60)$$

$$\left.\begin{aligned}
u_2 &= \frac{\partial(\psi_0+\psi)}{\partial y} = e^{-ipt}\left[-\frac{2i\alpha\beta\alpha'\beta'}{\kappa} B_1 e^{-\beta y-\beta\xi+i\kappa x}\right.\\
&\qquad\left. -k\mathfrak{B}\frac{y}{R} H_1^{(1)}(kR_1) - kB_2\frac{y}{R} H_1^{(1)}(kR_2)\right],\\
v_2 &= \frac{-\partial(\psi_0+\psi)}{\partial x}\, e^{-ipt}\left[2\alpha\alpha'\beta' B_1 e^{-\beta y-\beta\xi+i\kappa x}\right.\\
&\qquad\left. +k\mathfrak{B}\frac{x}{R} H_1^{(1)}(kR_1) + kB_2\frac{x}{R} H_1^{(1)}(kR_2)\right],\\
&[y<\xi,\quad x\neq 0,\quad y\neq 0,\quad R_1^2 = x^2+(y-\xi)^2,\quad R_2^2 = x^2+(y+\xi)^2]
\end{aligned}\right\}\quad(61)$$

$$\left.\begin{aligned}
u_2 &= \frac{\partial(\psi_0+\psi)}{\partial y} = 2e^{-ipt}\left[-\frac{2i\alpha\beta\alpha'\beta'}{\kappa} e^{-\beta y+i\kappa x}\,(P_1\beta\cosh\beta\xi + Q_1\sinh\beta\xi)\right.\\
&\qquad\left. -k^2 P_2\frac{y^2}{R^2} H_0^{(1)}(kR)\right],\\
v_2 &= \frac{-\partial(\psi_0+\psi)}{\partial x} = 2e^{-ipt}\left[2\alpha\alpha'\beta' e^{-\beta y+i\kappa x}(P_1\beta\cosh\beta\xi + Q_1\sinh\beta\xi)\right.\\
&\qquad\left. +k^2 P_2\frac{xy}{R^2} H_0^{(1)}(kR)\right],\\
&\qquad [y>\xi,\quad x\neq 0,\quad R^2 = x^2+y^2].
\end{aligned}\right\}\quad(61')$$

$$\left.\begin{aligned}
u_1' &= \frac{\partial\phi'}{\partial x} = 2\mu k^2 e^{-ipt}\left[-2i\kappa\alpha\beta\alpha'\beta' C_1 e^{\alpha' y-\beta\xi+i\kappa x}\right.\\
&\qquad\left. -h'^3 e^{-\sqrt{h'^2-k^2}\,\xi} C_2\frac{x^2 y}{R^3} H_1^{(1)}(h'R)\right],\\
v_1' &= \frac{\partial\phi'}{\partial y} = 2\mu k^2 e^{-ipt}\left[-2\alpha\beta\alpha'^2\beta' C_1 e^{\alpha' y-\beta\xi+i\kappa x}\right.\\
&\qquad\left. -h'^3 e^{-\sqrt{h'^2-k^2}\,\xi} C_2\frac{x y^2}{R^3} H_1^{(1)}(h'R)\right],\\
u_2' &= \frac{\partial\psi'}{\partial y} = 2\mu k^2 e^{-ipt}\left[\frac{2i\alpha\beta\alpha'\beta'^2}{\kappa} D_1 e^{\beta' y-\beta\xi+i\kappa x}\right.\\
&\qquad\left. -k'^2 e^{-\sqrt{k'^2-k^2}\,\xi} D_2\frac{y^2}{R^2} H_0^{(1)}(k'R)\right],
\end{aligned}\right\}\quad(62)$$

$$\left.\begin{aligned} v_2' = -\frac{\partial\psi'}{\partial x} = 2\mu k^2 e^{-ipt}\Big[& 2\alpha\beta\alpha'\beta' D_1 e^{\beta' y+-\beta\xi+i\kappa x} \\ & + k'^2 e^{-\sqrt{k'^2-k^2}\xi} D_2 \frac{xy}{R^2} H_0^{(1)}(k'R)\Big]. \\ [y<0, \quad x \neq 0, \quad y \neq 0, \quad & R^2 = x^2+y^2] \end{aligned}\right\}$$

In the present case, too, the first term within every pair of brackets indicates the boundary surface waves (for some conditions of two media) and the second one the bodily waves.

Although the amplitudes of the boundary waves do not decrease with epicentral distance, those of bodily waves decay in some manner; the law of decrease of amplitudes of the same waves for a given $y(=Y)$ and for a given $x(=X)$ is shown below.

Table II. Amplitudes of bodily waves/$H_0^{(1)}$

	u_1	v_1	u_2	v_2	u_1'	v_1'	u_2'	v_2'
At Y	$\frac{x^2Y}{R^3}$	$\frac{xY^2}{R^3}$	$\frac{Y^2}{R^2}$	$\frac{xY}{R^2}$	$\frac{x^2Y}{R^3}$	$\frac{xY^2}{R^3}$	$\frac{Y^2}{R^2}$	$\frac{xY}{R^2}$
At X	$\frac{X^2y}{R^3}$	$\frac{Xy^2}{R^3}$	$\frac{y^2}{R^2}$	$\frac{Xy}{R^3}$	$\frac{X^2y}{R^3}$	$\frac{Xy^2}{R^3}$	$\frac{y^2}{R^2}$	$\frac{Xy}{R^2}$

At a relatively large x for a given Y, the values of u_1, v_2, u_1', v_2' are proportional to $R^{-3/2}$, while the values of v_1, u_2, v_1', u_2' are proportional to $R^{-5/2}$. At a relatively large y for a given X, the values of v_1, v_2, v_1', v_2' are proportional to $R^{-3/2}$, while the values of u_1, u_1' are proportional to $R^{-5/2}$, the exception being that, at these values of y, X; u_2, u_2' are proportional to $R^{-1/2}$. More detailed feature will be discussed in chapter V.

The amplitudes distribution at a relatively large x for a given Y in the present case is quite similar to that in the case in which the primary waves are dilatational, whereas the amplitude distribution at a relatively large y for a given X in the present case would become similar to that of the last one, provided the letters u's are replaced by v's, the letters v_2, v_2' by u_1, u_1', and the letters v_1, v_1' by u_2, u_2'.

IV. *Primary Distortional Waves with Amplitudes Orientated Horizontally.*

9. In the present case λ, λ' do not participate in the problem. The expressions of incident, reflected, and refracted plane waves assume the forms

$$\left.\begin{aligned} v_0 &= \mathfrak{B}e^{sy+ifx-ipt}, \\ v &= Be^{-sy+ifx-ipt}, \qquad v' = B'e^{s'y+ifx-ipt}, \end{aligned}\right\} \tag{63}$$

where

$$B = \frac{\mu s - \mu' s'}{\mu s + \mu' s'}\,\mathfrak{B}, \quad B' = \frac{2\mu s}{\mu s + \mu' s'}\,\mathfrak{B}. \tag{64}$$

When the primary waves are radiated from a point source $x=0$, $y=\xi$, the displacements of the three kinds of waves assume the forms

$$\left.\begin{aligned} v_0 &= \mathfrak{B}e^{-ipt}H_0^{(1)}(kR) = \frac{\mathfrak{B}e^{-ipt}}{\pi}\int_{-\infty}^{\infty}\frac{e^{s(y-\xi)+ifx}}{s}\,df, \qquad [y<\xi], \\ &= \frac{\mathfrak{B}e^{-ipt}}{\pi}\int_{-\infty}^{\infty}\frac{e^{-s(y-\xi)+ifx}}{s}\,df, \qquad [y>\xi], \\ v &= \frac{e^{-ipt}}{\pi}\int_{-\infty}^{\infty}\frac{Be^{-s(y+\xi)+ifx}}{s}\,df, \qquad [y>0] \\ v' &= \frac{e^{-ipt}}{\pi}\int_{-\infty}^{\infty}\frac{B'e^{s'y-s\xi+ifx}}{s}\,df. \qquad [y<0] \end{aligned}\right\} \tag{65}$$

Since in every integral of the present case no principal value of the integrand exists, it is impossible for boundary waves to exist. The superposition of v_0+v gives

$$\left.\begin{aligned} v_1 = v_0 + v &= \frac{e^{-ipt}}{\pi}\int_{-\infty}^{\infty}\left[\frac{\mathfrak{B}e^{s(y-\xi)+ifx}}{s} + \frac{Be^{-s(y+\xi)+ifx}}{s}\right]df, \qquad [y<\xi] \\ &= \frac{2\mathfrak{B}e^{-ipt}}{\pi}\int_{-\infty}^{\infty}e^{-sy+ifx}\left[\frac{\mu}{\mu s+\mu' s'}\cosh s\xi + \frac{\mu' s'}{s(\mu s + \mu' s')}\sinh s\xi\right]df. \quad [y>\xi] \end{aligned}\right\} \tag{66}$$

Integrating (67) for $x \neq 0$, $y \neq 0$ in the same way as in the preceding cases, we finally obtain

$$\left.\begin{aligned} v_1 &= e^{-ipt}\left[\mathfrak{B}H_0^{(1)}(kR_1) - BH_0^{(1)}(kR_2)\right], \\ &\qquad [R_1^2 = x^2 + (y-\xi)^2, \quad R_2^2 = x^2 + (y+\xi)^2, \quad y \neq 0, \quad y<\xi] \\ v_1 &= 2\mathfrak{B}e^{-ipt}\frac{k\mu}{\mu'\sqrt{k^2-k'^2}}\frac{y}{R}H_1^{(1)}(kR), \qquad [R^2 = x^2+y^2, \quad y>\xi] \\ v' &= 2\mathfrak{B}e^{-ipt}\frac{k'}{\sqrt{k'^2-k^2}}\frac{y}{R}H_1^{(1)}(kR). \quad [R^2 = x^2+y^2, \quad y \neq 0, \quad y>0] \end{aligned}\right\} \tag{67}$$

Since the calculation is rather approximate, the result in (67) is only qualitatively correct. It will be seen that the distribution of the amplitudes for v_1, v' are such that at a relatively large x for a given Y, they vary as Y/R, while at a relatively large y for a given X, they vary as y/R.

V. *Comparison of the Three Cases.*

10. In the cases of dilatational primary waves and distortional primary waves with amplitudes orientated in a vertical plane, the amplitudes in the epicentral region that decay the least with distance are proportional to $R^{-1/2}(y/R)^2$, whereas in the case of distortional primary waves with amplitudes orientated horizontally, the amplitudes that decay the least are proportional to $R^{-1/2}\,y/R$, from which it is possible to conclude that in the former condition of the two, the region (epicentral) in which large amplitudes of the waves appear is much narrower than that in the latter condition.

Similar conditions exist in the region of large epicentral distance, that is to say, at a relatively large x for a given Y. In the cases of dilatational primary waves and distortional primary waves with amplitudes orientated in a vertical plane, the amplitudes that decay the least with distance are proportional to $R^{-1/2}(x/R)(Y/R)$, whereas in the case of distortional primary waves with amplitudes orientated horizontally, the amplitudes that decay the least are proportional to $R^{-1/2}\,Y/R$. Thus, even from this feature, in the former condition of the two the region of a large horizontal focal distance in which the amplitudes decay the least, is much narrower than that in the latter condition.

In the actual condition, the phenomena just given occur repeatedly in passing through successive discontinuities, from which it is possible to expect that the regions (the epicentral region as well as the region of large horizontal focal distance) in which large amplitudes of the horizontal distortional waves appear, become increasingly greater than similar regions for dilatational waves and distortional waves with amplitudes orientated in a vertical plane.

Aside from the above condition, there is the feature that, in the case of dilatational primary waves and in the case of distortional primary waves with amplitudes orientated in a vertical plane, the energy of the bodily waves is converted, in a majority of cases, into that of boundary waves in passing through or reflected from a discontinuity, whereas in the case of distortional primary waves with amplitudes orientated horizontally, no boundary wave is formed even in passing through or reflected from any discontinuity. There is no doubt that there are a number of nearly horizontal discontinuous surfaces in the crust, so that the energy of bodily waves other than horizontal distortional waves are successively converted into that of boundary waves at such discontinuous surfaces. It is therefore obvious that the amplitudes of bodily waves, excepting those of horizontal distortional waves, become smaller and smaller in passing through or reflected from discontinuous surfaces.

Dynamically, it is possible to conclude that the condition that the region in which the large amplitudes of horizontal distortional waves appear, is broader than the similar regions for other kinds of waves, is equivalent to the condition whether energy of bodily waves is unchanged or changed into that of boundary waves.

It also appears that the reason for *ScS* waves being of relatively large amplitudes, is possibly explained to a certain extent by the present theory.

From the present investigation it has also been ascertained that Lamb's and Nakano's (and also our) mathematical condition that the amplitudes of bodily waves accompanying Rayleigh-waves on a semi-infinite body shall decay very rapidly, is nothing more than the condition on an azimuth difference in a spherical wave front.

In the present paper we have given only an approximate discussion of the two-dimensional case of the problem from the standpoint of the formation of Stoneley's boundary waves, the case of the three dimensional condition being now under investigation in a more rigorous manner.

Note on the paper No. 19 entitled "Anormolous Dispersion of Elastic Surface Waves" *Bull. Earthq. Res. Inst.*, **16** (1938), 225~233.

When the paper in printing had already been revised, some one asked us as to whether or not there is any part of dispersion curve within the range between $L/H=0$ and 4·635 in Fig. 3, p. 230. It was theoretically proved in the same paper that dispersion curve with ordinate higher than $p_1\sqrt{\rho/\mu}/f=1$ is impossible to exist at that range. Since, furthermore, the functions contained in the velocity equation (10) are all hyperbolic and not sinusoidal, the curve in thick line is the only dispersion curve lying below the ordinate $p_1\sqrt{\rho/\mu}/f=1$. The dotted line extending from thick curve is nothing more than the indication that the thick curve near its end (not the very point of the end) inclines in that sense.

Although in the case of very small ratio of L/H, Stoneley's boundary waves are possibly transmitted along the surface between two media, since in the present case the velocity of distortional waves in one of the media much differs from that in the other, Stoneley's waves are scarcely transmitted as has been proved by Stoneley. Thus, there is no evidence of transmission of waves of surface type at such range of L/H as less than 4·635. It should, however, be borne in mind that when $L/H=0$, Rayleigh-waves of such velocity as $0{\cdot}9194\sqrt{\mu'/\rho'}$ are physically possible to exist at the free surface, but since, in the present case, the conditions as to $(r/f)^2 \gtrless 1$, $(s/f)^2 \gtrless 0$ are restricted, the waves under consideration does not concern the problem.

Since, furthermore, we discussed the possible existence of waves of permanent type, the consideration of waves that shall decay with time in consequence of the boundary conditions is out of question. (This note was read by K. SEZAWA, June 21, 1938.)

---

38. 地殼內の不連續面に於ける境界波の生成 (第1報)

地震研究所 {妹澤克惟
　　　　　 {金井清

2 種の固體が平面で密着連續してをるとき，この境界層に沿うて Rayleigh 型の彈性波が傳播し得るけれども Love 型の彈性波は傳播し得ぬ事を Stoneley が述べてゐる．この論文では最初に傳はる固體波が夫々縱波，鉛直横波，水平横波である場合について前述の境界波が如何にして生成するか，又，反射，屈折の固體波は如何なるものであるかを數理的に取扱つて見たのである．

地殼の中には水平な不連續面が幾つもある事は極く明かであるが，その結果として，水平横波が最初に傳はるときには結局境界波が現れ得ぬことになるのである．之に反して縱波や鉛直横波が最初に傳はるときは，境界波が生成するから，多くの不連續面に於て通過し反射する毎に固體波の波動勢力が境界波のそれに變化するのである．從て水平横波の振幅が比較的に減衰しない事實と一致する物理的性質をあらはす．

直接數理的に示される振幅に就ては，水平横波の場合の卓越せる振幅のある地殼區域が，他の波の場合のその區域に比して著しく廣いといふ事である．尙，Lamb 其他が論じたやうに表面波に伴ふ固體波が，距離と共に著しく減少するのは寧ろ，走波面の方向性の結果に過ぎぬ事もわかつた．

39. *The Effect of Cooling on a Plastic Earth under Gravitational Forces. II.*

By Katsutada SEZAWA and Kiyoshi KANAI,

Earthquake Research Institute.

(Read April 19, 1938.—Received June 20, 1938.)

1. *Preliminary notes.*

In our previous paper1) we ascertained that the horizontal compression exceeding the vertical in the surface crust of the Earth is the result of the usual gravitational forces, the effect of temperature fall of the substratum being negligible compared with the action of gravity. Whereas in the previous paper we discussed the case in which a layer of uniform thickness is cooled uniformly, in the present paper we shall deal with the case in which the cooling is of any distribution with depth in the earth's crust.

Although we shall deal with the problem as in the case of plasticity as well as in that of elasticity, since our aim is to find the maximum shear stress and not the normal stress, the condition that the materials forming the earth's crust shall be compressible, even in the statical state, is particularly important. If, on the other hand, the Earth is incompressible in the statical state, the shear stresses at any part of the Earth are zero, so that there is no plastic stress; the manner of treatment, whether as for plasticity or for elasticity, being therefore immaterial.

As already mentioned in the previous paper, the equation of equilibrium in the case of a pure plasticity problem is

$$\rho\frac{\partial V}{\partial r}+\frac{\partial\widehat{rr}}{\partial r}+\frac{2}{r}(\widehat{rr}-\widehat{\theta\theta})-\beta\frac{\partial\theta}{\partial r}=0\,, \tag{1}$$

with a plastic condition

$$\widehat{rr}-\widehat{\theta\theta}=\pm 2k\,.$$

Although the solutions of the above two equations in the case of uniform ρ and k, for example, are merely written

---

1) K. SEZAWA and K. KANAI, "The Effect of Cooling on a Plastic Earth under Gravitational Forces", *Bull. Earthq. Res. Inst.*, **16** (1938), 244~255.

$$\left.\begin{aligned}\widehat{rr}&=4k\log\frac{a}{r}-\frac{\eta}{2}(a^2-r^2)+\beta\{\theta_{r=a}-\theta\},\\ \widehat{\theta\theta}&=4k\log\frac{a}{r}-\frac{\eta}{2}(a^2-r^2)+\beta\{\theta_{r=a}-\theta\}-2k,\end{aligned}\right\}\tag{2}$$

since these normal stresses are not so significant as the plastic stress $(\widehat{rr}-\widehat{\theta\theta})/2$, namely k, it is possible to conclude that were the Earth purely plastic, the effect of cooling has no place in the problem. All plasticity problems in the present paper will be so treated as in the manner of elasticity.

It should be borne in mind that we are to ascertain the stress state of a solid Earth with reference to the state of a liquid Earth, the gravitational conditions for both cases being the same.

2. *General theory, the problem being treated in the manner of elasticity.*

Let us assume that both density and temperature fall vary with the radius of the Earth. The equation of equilibrium is written

$$\rho\frac{\partial V}{\partial r}+(\lambda+2\mu)\left(\frac{\partial^2 u}{\partial r^2}+\frac{2}{r}\frac{\partial u}{\partial r}-\frac{2u}{r^2}\right)-\beta\frac{\partial\theta}{\partial r}=0,\tag{3}$$

where $\rho\partial V/\partial r$ is the rate of change of bodily force with radius, λ, μ are elastic constants, and $\beta=(\lambda+2\mu/3)q$; $\lambda+2\mu/3$, q being the modulus of compression and the expansion coefficient respectively.

The term $\rho(\partial V/\partial r)$ in (3) is determined from the conditions

$$\rho\frac{\partial V}{\partial r}=-\frac{\gamma M}{r^2}\rho,\quad M=\frac{4}{3}\pi\int_0^r\rho dr^3.\tag{4}$$

Let us assume that the displacement u in (3) is of the form

$$u=u_1+u_2,\tag{5}$$

where u_1, u_2 satisfy the equations

$$\left.\begin{aligned}(\lambda+2\mu)\left(\frac{\partial^2 u_1}{\partial r^2}+\frac{2}{r}\frac{\partial u_1}{\partial r}-\frac{2u_1}{r^2}\right)-\beta\frac{\partial\theta}{\partial r}&=0,\\ (\lambda+2\mu)\left(\frac{\partial^2 u_2}{\partial r^2}+\frac{2}{r}\frac{\partial u_2}{\partial r}-\frac{2u_2}{r^2}\right)+\rho\frac{\partial V}{\partial r}&=0.\end{aligned}\right\}\tag{6}$$

The superposition of u_1 and u_2 obviously satisfies the equation (3). Since it is now possible to get the solutions u_1, u_2 separately, treatment of the problem is greatly simplified.

3. *The determination of u_1 in the case of irregular distribution of temperature fall.*

Let us assume that the distribution of temperature (rise) is

$$\theta = f(r) = \alpha \sum_{n=0}^{\infty} A_n r^n. \tag{7}$$

To solve the first equation of (6), we write

$$u_1 = \sum_{n=0}^{\infty} a_n r^n. \tag{8}$$

From (5), (6), (7), (8) we find the relation

$$a_n = \frac{\alpha A_{n-1}}{n+2}, \quad (n = 2,\ 3, \cdots \infty) \tag{9}$$

so that the expressions for displacement and the stresses are

$$u_1 = B'r + \frac{\beta\alpha}{\lambda+2\mu} \sum_{n=2}^{\infty} \frac{A^{n-1}}{n+2} r^n, \tag{10}$$

$$\widehat{rr}_1 = (3\lambda+2\mu)B' + \frac{\beta\alpha}{\lambda+2\mu} \sum_{n=2}^{\infty} \left[\frac{r^{n-1}A_{n-1}}{n+2} \left\{ 2\lambda + n(\lambda+2\mu) \right\} - A_n r^n (\lambda+2\mu) \right], \tag{11}$$

$$\widehat{\theta\theta}_1 = \widehat{\phi\phi}_1 = (3\lambda+2\mu)B'$$
$$+ \frac{\beta\alpha}{\lambda+2\mu} \sum_{n=2}^{\infty} \left[\frac{r^{n-1}A_{n-1}}{n+2} \left\{ 2(\lambda+\mu) + n\lambda \right\} - A_n r^n (\lambda+2\mu) \right]. \tag{12}$$

Since the free surface has no normal stress, that is,

$$r = a; \qquad \widehat{rr}_1 = 0, \tag{13}$$

we find that

$$(3\lambda+2\mu)B' = -\frac{\beta\alpha}{\lambda+2\mu} \sum_{n=2}^{\infty} \left[\frac{a^{n-1}A_{n-1}}{n+2} \left\{ 2\mu m + \lambda(n+2) \right\} - A_n a^n (\lambda+2\mu) \right]. \tag{14}$$

The plastic stress is

$$\frac{\widehat{rr}_1 - \widehat{\theta\theta}_1}{2} = \frac{\beta\alpha\mu}{\lambda+2\mu} \sum_{n=2}^{\infty} \frac{(n-1) r^{n-1} A_{n-1}}{n+2}. \tag{15}$$

From the expression (15) it will be seen that, were the rigidity of the earth's crust very small, that is, $\mu \to 0$, the plastic stress would then be zero for any distribution of temperature in the crust.

4. *The determination of u_2 in the case of irregular distribution of mass density.*

Let the distribution of mass density be of the form

$$\rho = F(r) = \varepsilon \sum_{n=0}^{\infty} B_n r^n, \tag{16}$$

then, by means of (4),

$$\rho \frac{\partial V}{\partial r} = -4\pi\gamma \sum_{n=0}^{\infty} \frac{1}{n+3} B_n^2 r^{2n+1}. \tag{17}$$

Writing

$$u_2 = \sum_{n=0}^{\infty} b_n r^n, \tag{18}$$

and substituting it in the second equation of (6), we get

$$b_{2n+3} = \frac{1}{2(n+1)(2n+5)} \frac{4\pi\gamma\varepsilon^2}{n+3} B_n^2 \frac{1}{\lambda+2\mu}. \quad (n=0,\ 1,\ 2, \cdots \infty) \tag{19}$$

The expressions for displacement and the stresses are

$$u_2 = B''r + \sum_{n=0}^{\infty} \frac{r^{2n+3} 4\pi\gamma\varepsilon^2 B_n^2}{2(\lambda+2\mu)(n+1)(n+3)(2n+5)}, \tag{20}$$

$$\begin{aligned} \widehat{rr}_2 = {} & (\lambda+2\mu)B'' \\ & + 4\pi\gamma\varepsilon^2 \sum_{n=0}^{\infty} \frac{r^{2n+2} B_n^2}{2(n+1)(n+3)(2n+5)} \left\{ \frac{\lambda(2n+5) + 2\mu(2n+3)}{\lambda+2\mu} \right\}, \end{aligned} \tag{21}$$

$$\begin{aligned} \widehat{\theta\theta}_2 = \widehat{\phi\phi}_2 = {} & (\lambda+2\mu)B'' \\ & + 4\pi\gamma\varepsilon^2 \sum_{n=0}^{\infty} \frac{r^{2n+2} B_n^2}{2(n+1)(n+3)(2n+5)} \frac{\lambda(2n+5) + 2\mu}{\lambda+2\mu}. \end{aligned} \tag{22}$$

The value of B'' can be determined from the condition

$$r = a; \qquad \widehat{rr}_2 = 0, \tag{23}$$

the result being

$$(3\lambda+2\mu)B'' = -4\pi\gamma\varepsilon^2 \sum_{n=0}^{\infty} \frac{a^{2n+2} B_n^2}{2(n+1)(n+3)(2n+5)} \frac{\{\lambda(2n+5) + 2\mu(2n+3)\}}{\lambda+2\mu}. \tag{24}$$

The plastic stress is

$$\frac{\widehat{rr}_2-\widehat{\theta\theta}_2}{2}=\frac{4\pi\gamma\varepsilon^2\mu}{\lambda+2\mu}\sum_{n=0}^{\infty}\frac{r^{2n+2}B_n^2}{(n+3)(2n+5)}\,, \tag{25}$$

which shows that if the rigidity of the crust is very small, the plastic stress assumes zero value, as in the preceding case.

5. *General solution for the case in which distribution of temperature and that of mass density are both given.*

When the distribution of temperature as well as that of density are both specified in such forms as (7) and (16), the solutions for displacement and the stresses are obtained by merely algebraically superposing the corresponding expressions in two cases, namely,

$$u=u_1+u_2,\quad \widehat{rr}=\widehat{rr}_1+\widehat{rr}_2,\cdots\cdots\cdots\cdots,\frac{\widehat{rr}-\widehat{\theta\theta}}{2}=\frac{\widehat{rr}_1-\widehat{\theta\theta}_1}{2}+\frac{\widehat{rr}_2-\widehat{\theta\theta}_2}{2}\,. \tag{26}$$

The resultants u, $rr,\cdots$, $(\widehat{rr}-\widehat{\theta\theta})/2$ obviously satisfy the equation (3) and the boundary condition

$$r=a;\qquad \widehat{rr}=0\,. \tag{27}$$

The ratio of plastic stress due to temperature distribution to that due to gravitational forces is obtained from (15) and (25) in the form

$$\frac{\beta\alpha}{4\pi\gamma\varepsilon^2}\left\{\sum_{n=2}^{\infty}\frac{(n-1)r^{n-1}A_{n-1}}{n+2}\Big/\sum_{n=0}^{\infty}\frac{r^{2n+2}B_n^2}{(n+3)\,(2n+5)}\right\}, \tag{28}$$

which shows that, provided the values of $\beta\alpha$ and $\gamma\varepsilon^2$ were specified in addition to the distributions of temperature and density, the ratio under consideration would invariably be the same for any value of μ — a satisfactory condition for concluding that the smallness of μ never increases that part of the plastic stress that is due to temperature change in the total plastic stress.

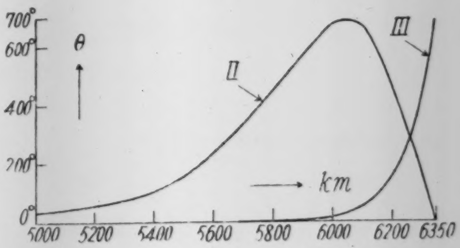

Fig. 1. Distributions of temperature fall.

6. *Numerical examples in the case of uniform mass density.*

(i) We shall first consider the case in which a part of the earth's crust, corresponding to a substratum of it, is cooled in a distribution such as that shown by curve II in Fig. 1, in which case the expression for θ is empirically of the form

$$\theta \; in \, C^{0} = f(r) = -14.10^{4}\left\{\left(\frac{r}{6350}\right)^{32}\left(1-\frac{r}{6150}\right)+\frac{200}{6150}\left(\frac{r}{6350}\right)^{64}\right\}, \tag{29}$$

r being in km. The maximum temperature change occurs at a depth 300 km from the earth's surface and assumes the value −700°C. The temperature changes at depths 900 km and 1300 km from the earth's surface are only about −100°C and −30°C respectively. Let us assume that

$$\left.\begin{aligned} \beta &= \left(\lambda+\frac{2}{3}\mu\right)q = (10^{12}.3).(0\cdot08.10^{-4}) = 24.10^{6}, \\ \mu/\lambda &= 1, \quad \rho = 5\cdot52, \quad \gamma = 648.10^{-10}. \end{aligned}\right\} \tag{30}$$

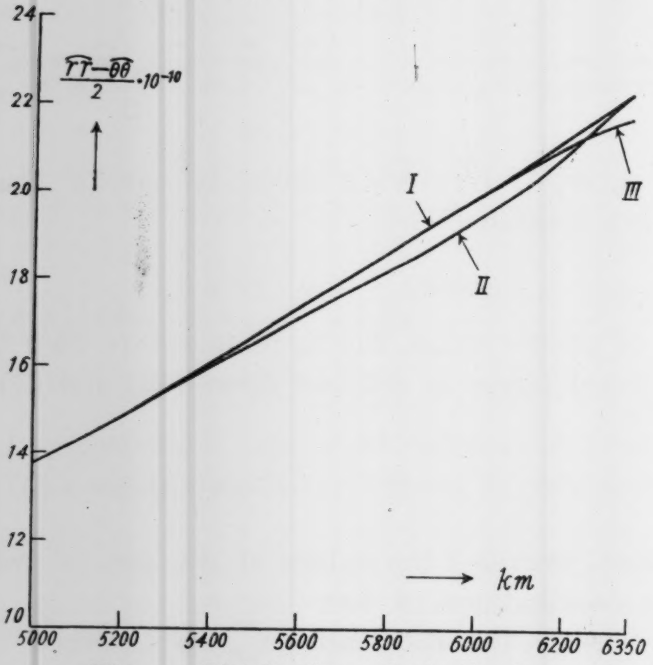

Fig. 2. Distributions of plastic stress.

Then, since from (29)

$$\alpha = -14.10^{4}, \quad A_{32} = \frac{1}{6350^{32}}, \quad A_{33} = \frac{1}{6350^{32}.6150}, \quad A_{64} = \frac{200}{6350^{64}.6150}, \tag{31}$$

we get the plastic stress and radial stress due to both temperature change and the gravitational forces

$$\widehat{rr}-\widehat{\theta\theta} = 10^{10}\left[1\cdot103r'^{2} + 224\left(\frac{r'}{6\cdot35}\right)^{32}\left\{-0\cdot9146+0\cdot9160\frac{r'}{6\cdot15}-0\cdot03104\left(\frac{r'}{6\cdot35}\right)^{32}\right\}\right], \tag{32}$$

$$\widehat{rr} = 10^{10}\Bigg[-122{\cdot}2 + 3{\cdot}033 r'^2 - 0{\cdot}1684$$

$$+ 336\Big(\frac{r'}{6{\cdot}35}\Big)^{32}\Big\{0{\cdot}038095 - 0{\cdot}037037\Big(\frac{r'}{6{\cdot}15}\Big) + 0{\cdot}000647\Big(\frac{r'}{6{\cdot}35}\Big)^{32}\Big\}\Bigg], \quad (33)$$

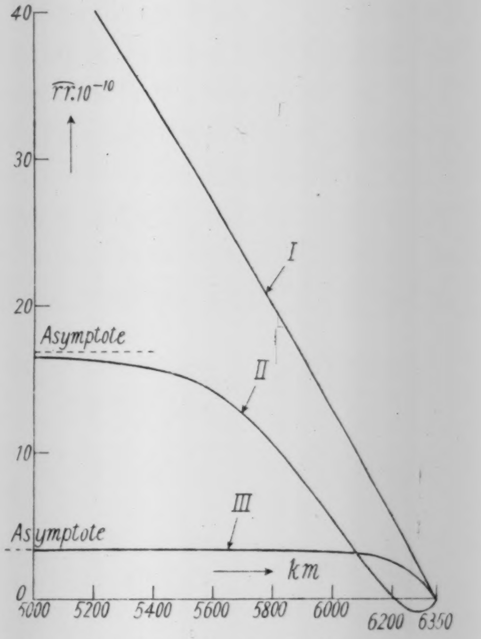

Fig. 3. Distributions of radial stress. Curves II and III represent 100 $\widehat{rr}.10^{-10}$ due to temperature fall only.

$(1000 r')$ being in km. The result of calculation for plastic and radial stresses are shown by curve II both in Fig. 2 and 3 (actual radial stress = ordinate I in Fig. 3 + ordinate II/100 in Fig. 3). With a view to ascertaining the correction due to temperature change, we calculated the gravitational plastic stress for the case of no temperature change, and plotted the results by curve I in Figs. 2 and 3. It will be seen that the effect of cooling on plastic stress and on radial stress under gravitational forces is negligible.

(ii) We shall next consider the case in which a superficial part of the earth's crust is cooled in such distribution as that shown by curve III in Fig. 1. In this case the empirical expression for it is extremely simple, namely,

$$\theta \; in \; C^{\circ} = f(r) = -700\Big(\frac{r}{6350}\Big)^{64}, \quad (34)$$

so that

$$a = -700, \quad A_{64} = \frac{1}{6350^{64}}, \quad (35)$$

the values of β, μ/λ, ρ, γ being assumed the same as those in (30). The expressions for plastic and radial stresses due to both temperature change and gravitational forces are

$$\widehat{rr} - \widehat{\theta\theta} = 10^{10}\Big[1{\cdot}103 r'^2 - 1{\cdot}07\Big(\frac{r'}{6{\cdot}35}\Big)^{64}\Big], \quad (36)$$

$$\widehat{rr} = 10^{10}\Big[-122{\cdot}2 + 3{\cdot}033 r'^2 + 0{\cdot}0334\Big\{-1 + \Big(\frac{r'}{6{\cdot}35}\Big)^{64}\Big\}\Big]. \quad (37)$$

The results of calculation for both stresses are shown by curve III in

Figs. 2 and 3 (actual radial stress = ordinate I in Fig. 3 + ordinate III/100 in Fig. 3). In this case, too, the effect of cooling on both plastic and radial stresses under gravitational forces are negligible.

7. *A numerical example in the case of varying mass density.*

It has been shown in Section 2 that, in the case of varying temperature and varying density, the general solutions of the problem can be obtained by merely superposing the two solutions, namely, the solution corresponding to the condition of thermal stress and that corresponding to the condition of stress under gravitational forces. We shall therefore discuss here the problem of mass density varying only with the radius of the Earth, regardless of thermal conditions. The empirical expressions for continuous distribution of mass density in the Earth differ with their authors, examples of some of them being[2]

Legendre: $\rho=\rho_0 \sin nr/nr$, $\rho_0=$ density at the centre $=11\cdot0$, $nR=2\cdot487$.

Roche: $\rho=\rho_0\left\{1-\beta\left(\frac{r}{R}\right)^2\right\}$, $\rho_0=10\cdot1$, $\beta=0\cdot764$.

Lipschitz: $\rho=\rho_0\left\{1-\beta\left(\frac{r}{R}\right)^\lambda\right\}$, $\rho_0=9\cdot453$, $\lambda=2\cdot39$, $\beta=0\cdot736$.

Helmert: $\rho=\rho_0\left\{1-\beta_1\left(\frac{r}{R}\right)^2+\beta_2\left(\frac{r}{R}\right)^4\right\}$, $\rho_0=11\cdot3$, $\beta_1=1\cdot04$, $\beta_2=0\cdot275$.

Oekinghaus: $\rho=\rho_0 e^{-\alpha\left(\frac{r}{R}\right)^2}$, $\rho_0=13\cdot78\sim10\cdot375$, $\alpha=1\cdot707\sim1\cdot4$,

Williamson and Adams (from the condition of compression of material):

$$\log\frac{\rho}{\rho_m}=-\int_R^r\frac{k^2M\rho}{r^2\kappa}dr,$$

where κ is the modulus of compression. More reasonable expressions were obtained by Wiechert, Klussmann, Gutenberg, and Haalck, who took into account of the discontinuities in mass density in the Earth,[3] every one of which is too well known to require any description here.

From Jeffreys's recent investigation, the distribution of mass den-

---

2), 3) The expressions for mass density without discontinuity, or with discontinuity, will be found in the papers of the respective authors; the data here given are from H. SCHMEHL u. K. JUNG, Massenverteilung der Erde, *Handbuch d. Exp. Physik*, **25**, 2, 353.

sity has been greatly modified; two discontinuities exist at depths of 400 km and 2900 km from the Earth's surface. Although the following formula gives no discontinuity at any radius, it still appears that the curve corresponding to the formula somewhat resembles that due to Jeffreys's distribution (See Fig. 4).[4]

$$\rho = F(r) = 12{\cdot}09 - 8{\cdot}8\left(\frac{r}{6350}\right)^2 - 50\left(\frac{r}{6350}\right)^4\left\{1-\left(\frac{r}{6350}\right)\right\}\left\{1-\left(\frac{r}{6350}\right)^4\right\}. \quad (36)$$

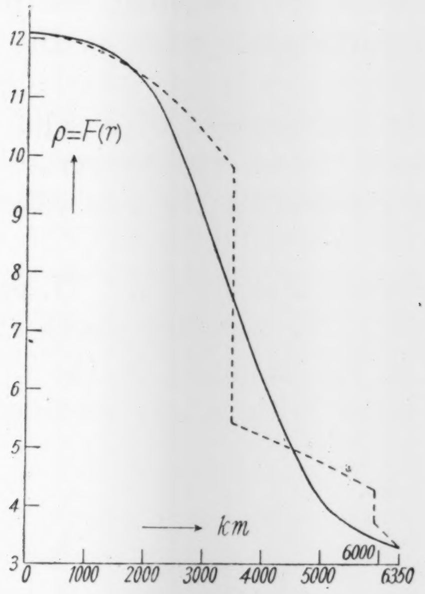

Fig. 4. Density distribution. Broken line: Jeffrey's, full line: ours.

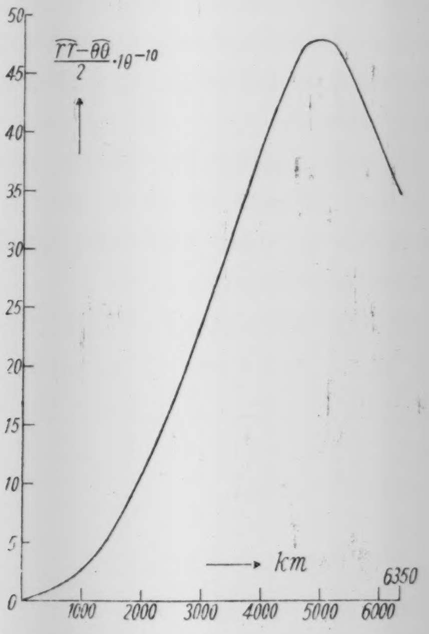

Fig. 5. Distribution of plastic stress due to our density distribution.

Using (16), (25), we have obtained the distribution of plastic stress, with the result as shown in Fig. 5. The distribution of plastic stress for the case in which both temperature and the gravitational forces are effective, is readily obtained by superposing result in this figure and that in Fig. 2.

8. *Concluding remarks.*

It has been ascertained that even in the case of irregular distributions of temperature and mass density, the effect of cooling of any part of the Earth on its plastic deformation is very slight compared with that of the gravitational forces on the same deformation. A very important condition is that the rigidity of the crust shall not be zero, regardless of whether the problem is treated in the manner of plasticity or in that of elasticity. The present problem, particularly, has another condition that the state of the solid Earth under consideration differs from that of a liquid Earth of nearly equal radius, notwithstanding that the gravitational condition is the same for both cases.

---

[4] H. JEFFREYS, *M. N. R. A. S. Geophys. Suppl.*, **3** (1937), 53~59.

It has been shown that, were the values of βa and $\gamma\varepsilon^2$ specified in addition to the distributions of temperature and density, the ratio of plastic stress due to temperature distribution to that due to gravitational forces would invariably be the same for any value of μ, from which it follows that, even should the value of μ be small, the plastic stress due to temperature change never participates much in the total plastic stress.

In calculating the stress condition or displacement of a solid body under the effects of both the gravitational forces and temperature, it is possible to deal with the problem by considering the two effects in question separately.

In the numerical calculation we assumed that $\mu/\lambda=1$. If, on the other hand, we were to assume that $\mu/\lambda \ll 1$, the resulting plastic stresses would be much smaller than those in the examples in the present paper, although it would fit in rather better with actual conditions in the earth's crust.

---

39. 地球の冷却が重力の下にあるその
プラスチック狀態に及ぼす影響 II

地震研究所 {妹澤克惟
{金井清

この前の論文で地球が固體化してからのプラスチック應力の狀態は主として重力から來るものとして差支なく，熱冷却の影響は大したものでないことを述べて置いた．この論文では更に進んで熱冷却の分布や質量分布が不規則な場合をしらべて見たのであるが，プラスチック應力の一般的傾向は依然として同じ事がわかつた．

プラスチック應力があるためには，地殼の剛性がなにがしかなければならぬ．之は地殼を彈性體として取扱つてもプラスチック體として取扱つても同樣である．又，只今の問題では特に，固形の地球の狀態が液狀のそれと如何に異なるかを論じたものである．之は重力の狀態が殆ど同じとして取扱ふからである．

$\beta\gamma$，$\gamma\epsilon^2$，溫度の分布，質量密度の分布が一定であれば，溫度分布によるプラスチック應力と重力によるプラスチック應力との比が一定であり，μ 自身の値の大小に關しない事がわかつた．從て溫度によるプラスチック應力は常に重要でない事がわかつた．

應力の計算をなすには，重力による應力の計算と溫度による應力の計算とを別々にやつてその結果を代數的に加へ合せればよいことがわかつた．

只今の計算の例では $\mu/\lambda=1$ と置いた．若し $\mu/\lambda\ll1$ とすると，その結果として出るプラスチック應力は只今のそれよりも遙かに小くなる．しかし之は寧ろ地殼の實際の狀態に近いものであらう．

40. *Three-dimensional Vibrations of a Framed Structure. I.*

By Kiyoshi KANAI,

Earthquake Research Institute.

(Read May 17, and June 21, 1938.—Received June 20, 1938.)

1. *Introduction.*

In the previous paper[1] the aseismic properties of a 'daikokubasira' (extra-thick column) in a Japanese style building was discussed mathematically, in certain parts of which it was necessary to consider the three-dimensional vibration of a framed structure. Although in the same paper the solution of a space-latticed framed structure for a special case was obtained, no general feature of the problem had yet been ascertained. In the present paper, besides discussing the general feature under consideration, we give the general solution for such a different case as concerns the three-dimensional vibration of a structure, which in itself is apparently in a two-dimensional condition. The mathematical results just mentioned were furthermore confirmed by means of model experiments, from which it was possible to show that, notwithstanding the extremely complex forms of the mathematical solutions, there was little error even in the numerical constants of the solutions.

2. *The solutions of the problem of a space-latticed framed structure.*

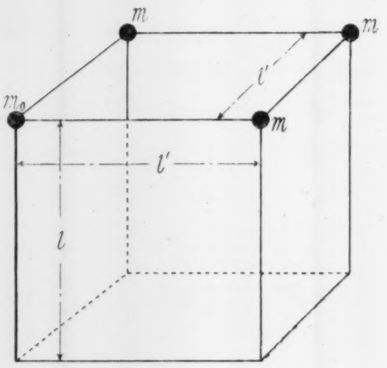

Fig. 1.

The method of dealing with the problem of a space-latticed framed structure with four columns and four horizontal members (beams) (so as to form a framed structure of the type of a parallelopiped) was shown in the previous paper.[2] When $m_0=m$, $l=l'$, $E'I'=EI=G'J'=GJ$, $E_0I_0=G_0J_0$, where E_0I_0, G_0J_0 are the bending and torsional stiffnesses of the extra thick column, EI, GJ those of ordinary columns, and $E'I'$, $G'J'$ those of horizontal members,

---

1), 2) K. KANAI, "Aseismic Properties of a Daikoku-basira (Principal Column) or Similar Column in a Japanese Style House", *Bull. Earthq. Res. Inst.*, **16** (1938), 256～272.

we get a pair of frequency equations for the free or resonance vibrations of the structure as follows:

$$\left.\begin{aligned}
&\gamma^2(5548\,\gamma_0^2+45044\,\gamma_0+43008)\\
&\qquad-\gamma(8322\,\gamma_0^3+310072\,\gamma_0^2+1988902\,\gamma_0+1567744)\\
&\qquad+(172353\,\gamma_0^3+3175014\,\gamma_0^2+14889369\,\gamma_0+7709184)=0,\\
&\gamma^2(5548\,\gamma_0^2+45044\,\gamma_0+43008)\\
&\qquad-\gamma(8322\gamma_0^3+206104\gamma_0^2+992998\gamma_0+594016)\\
&\qquad+(94377\,\gamma_0^3+1455438\,\gamma_0^2+5215377\,\gamma_0+1762488)=0,
\end{aligned}\right\} \quad (1)$$

where $\gamma=\frac{mp^2l^3}{EI}$, $\gamma_0=\frac{E_0I_0}{EI}$.

Solving the above equations for six cases of E_0I_0/EI we get[3]

(i) $E_0I_0/EI=0$; $\gamma=$ 4·322, 5·865, 9·5, 30·63,

(ii) $E_0I_0/EI=1$; $\gamma=$ 8·4, 8·4, 10·846, 33·0,

(iii) $E_0I_0/EI=3$; $\gamma=$ 9·5, 10·5, 15·3, 35·77,

(iv) $E_0I_0/EI=10$; $\gamma=$10·19, 14·03, 27·45, 43·8,

(v) $E_0I_0/EI=20$; $\gamma=$10·63, 16·46, 42·97, 56·9,

(vi) $E_0I_0/EI=100$; $\gamma=$12·58, 22·13, 161·1, 170·5,

these numerical values being plotted in Fig. 2. Since the masses are concentrated at the panel points there are four vibrational frequencies I, II, III, IV.

Although, because every vibrational mode is in a coupled condition, it is scarcely possible to indicate accurately the type of vibration that corresponds to each vibrational frequency, the frequency curves in Fig. 2 enable us to know that the type of vibration IV is, roughly, that of a shear of the square formed by four horizontal members (beams), while

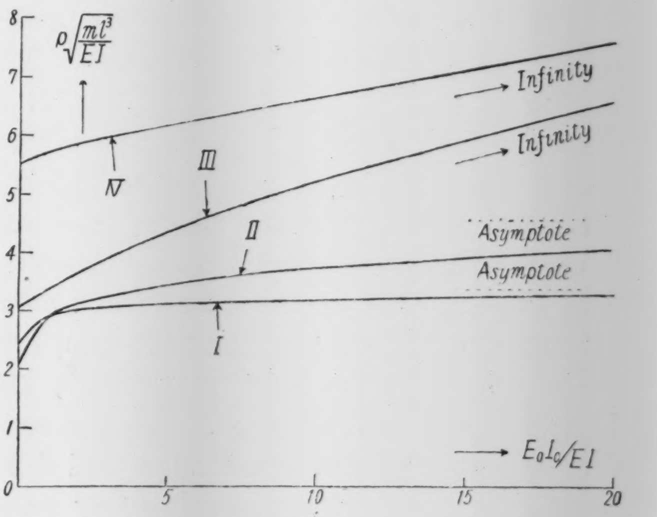

Fig. 2.

---

[3] These numerical values were also shown in the preceding paper, *loc. cit.* 1).

the type of vibration III is that of rotation, about a vertical axis of the same square. Vibrations II and I are somewhat complex. At a smaller value of E_0I_0/EI, the type of vibration II is that of translation of the square just mentioned in the direction of the diagonal line between the panel point at the extra thick column and the opposite panel point, whereas the type of vibration I is that of translation in the direction of another diagonal of the same square. At a larger value of E_0I_0/EI, from the nature of things, the type of vibration I is that of rotation, whereas the type of vibration II is that of shear.

Notwithstanding that at a larger value of E_0I_0/EI, vibrations I and III are both of rotational type, and vibrations II and IV are both of shear type, the vibrational frequencies for III and IV increase with increase in the value of E_0I_0/EI, whereas the vibrational frequencies for I and II remain approximately constant, even with increase in E_0I_0/EI. Interpreted physically, although in vibrations I and II the movements of the extra thick column are much smaller than those of the remaining columns, in vibrations III and IV the movements of the extra thick column are comparable to those of the remaining columns. It should also be borne in mind that in the condition $E_0I_0/EI=1$, the vibrational frequency of case I is the same as that of case II,—an obvious fact from the nature of the problem.

3. *Model experiment confirming the preceding mathematical results.*

With a view to confirming the preceding mathematical results, we conducted simple model experiments. The form of the model was quite similar to that in the sketch in Fig. 1. The column height and beam span are both 40 cm. The members corresponding to the columns and beams were made of steel wire and the concentrated masses were at the panel points, of brass blocks, the mass of every block being 13 gr. Whereas the diameters of the ordinary columns and that of every beam was 1·5 mm, that of the extra thick column differed, namely, (i) 1 mm, (ii) 1·5 mm, (iii) 2 mm, (iv) 2·5 mm, and (v) 3 mm. The masses of the respective wires were (i) 2·63 gr, (ii) 5·58 gr, (iii) 10·01 gr, (iv) 15·23 gr, and (v) 22·08 gr. In the numerical calculation we assumed that the sum of the brass mass and 3/2 the mass of the 1·5 mm wire is effective as inertia mass at every panel point. Whence, in the case of a larger value of E_0I_0/EI, the calculated vibrational frequency is liable to be somewhat higher than the observed frequency.

For comparing the calculated and the observed values, we made two preliminary experiments, such that a single wire with an end mass oscillated freely in the sense of torsion on the one hand and in the sense of bending on the other, from which we found the values of the elastic constants of every wire, their values being $E=19{\cdot}48.10^{11}$ dyne/cm², $G=7{\cdot}84.10^{11}$ dyne/cm².

The model just mentioned was clamped to the vibration table that was used for experiments in connexion with the vibration damper. The direction of the diagonal was set in various ways. By observing the resonance conditions of the model on the vibration table, we found four vibrational periods in every case, the results being shown with thick lines in Fig. 3.

On the other hand, from the numerical data in the preliminary experiments and the relations in Fig. 2, we calculated the theoretical vibrational periods and plotted the results with broken lines in Fig. 3. It will be seen that the mathematical results fairly agree with the experimental results. Notwithstanding that, as a matter of fact, there is the theoretical relation $E=2(1+\sigma)G$, we calculated a special case in which $EI=GJ$, that is to say, $J=2I$, $E=2G$, from which it appears that the torsional rigidity in every calculation is likely to be overestimated. Furthermore, as already mentioned, at higher values of E_0I_0/EI, the m values in the calculation are underestimated. For these two reasons, the calculated vibrational periods are invariably less than the observed vibrational periods.[4]

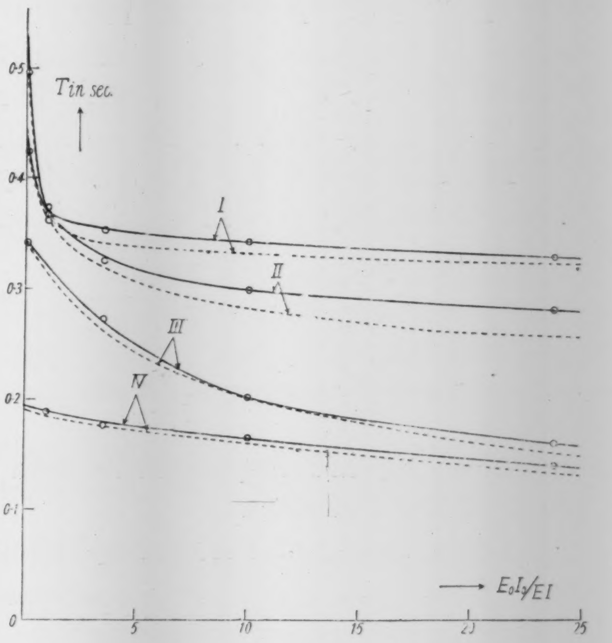

Fig. 3.

From these considerations, there does not seem to be any error in the mathematical result in the preceding section.

4. *Solution of the problem of a plane framed structure oscillating in the direction normal to the plane of the same structure.*

---

[4] It appears now evident that the smaller vibrational periods in mathematical side did not result from such dynamical condition that approximate calculation shall always give vibrational periods that are somewhat less than the actual periods.

When the framed structure shown in Fig. 4 oscillates in the direction normal to the plane of that structure, the vibration becomes a three-dimensional one for certain conditions of the columns and beams.

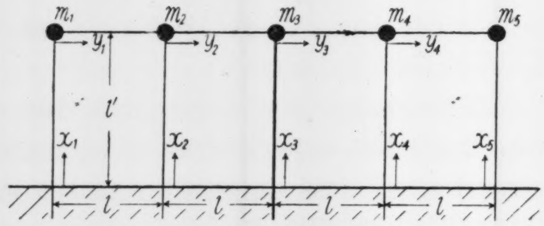

Fig. 4.

Let the bending and torsional stiffnesses of the respective columns be E_1I_1, E_2I_2, ... , E_5I_5; G_1J_1, G_2J_2, ... , G_5J_5, and those of the respective beams be $E'_1I'_1$, $E'_2I'_2$, $E'_3I'_3$, $E'_4I'_4$; $G'_1J'_1$, $G'_2J'_2$, $G'_3J'_3$, $G'_4J'_4$. Let also the inertia masses at the panel points corresponding to the tops of the respective columns be m_1, m_2, ... , m_5. The heights of the columns and the lengths of every span are shown in the sketch.

The expressions for the vibratory motion of the columns and the beams in bending as well as in torsion are of the types

$$\left.\begin{aligned} &\frac{\partial^4 u_s}{\partial x_s^4}=0, \quad \frac{\partial^2 \theta_s}{\partial x_s^2}=0, \quad [s=1,\ 2,\ \ldots\ldots,\ 5] \\ &\frac{\partial^4 w_s}{\partial y_s^4}=0, \quad \frac{\partial^2 \varphi_s}{\partial y_s^2}=0, \quad [s=1,\ 2,\ \ldots\ldots,\ 4] \end{aligned}\right\} \tag{2}$$

where u_s, w_s are displacements both in the direction normal to the plane of the structure.

The solutions of the corresponding equations have the forms

$$\left.\begin{aligned} u_s&=(A_s+B_sx_s+C_sx_s^2+D_sx_s^3)e^{ipt}, \\ \theta_s&=(\alpha_s+\beta_sx_s)e^{ipt}, \end{aligned}\right\} \quad [s=1,\ 2,\ \ldots\ldots,\ 5] \tag{3}$$

$$\left.\begin{aligned} w_s&=(P_s+Q_sy_s+R_sy_s^2+S_sy_s^3)e^{ipt}, \\ \varphi_s&=(\lambda_s+\mu_sy_s)e^{ipt}. \end{aligned}\right\} \quad [s=1,\ 2,\ \ldots\ldots,\ 4] \tag{4}$$

The boundary conditions are such that

$$x_s=0; \quad u_s=0, \quad \frac{\partial u_s}{\partial x_s}=0, \quad \theta_s=0, \quad [s=1,\ 2,\ \ldots\ldots,\ 5] \qquad (5),\ (6),\ (7)$$

$$x_1=l,\ y_1=0; \qquad u_1=w_1, \quad \frac{\partial u_1}{\partial x_1}=\varphi_1, \quad \frac{\partial w_1}{\partial y_1}=-\theta_1, \qquad (8),\ (9),\ (10)$$

$$-E_1I_1\frac{\partial^2 u_1}{\partial x_1^2}+G'_1J'_1\frac{\partial \varphi_1}{\partial y_1}=0, \quad E'_1I'_1\frac{\partial^2 w_1}{\partial y_1^2}+G_1J_1\frac{\partial \theta_1}{\partial x_1}=0, \qquad (11),\ (12)$$

$$-E_1I_1\frac{\partial^3 u_1}{\partial x_1^3}+E'_1I'_1\frac{\partial^3 w_1}{\partial y_1^3}=m_1p^2u_1, \tag{13}$$

$x_{s+1}=l,\ y_s=l',\ y_{s+1}=0;$

$$u_{s+1}=w_s=w_{s+1},\ \frac{\partial u_{s+1}}{\partial x_{s+1}}=\varphi_s=\varphi_{s+1},\ \frac{\partial w_s}{\partial y_s}=\frac{\partial w_{s+1}}{\partial y_{s+1}}=-\theta_{s+1}, \quad (14), (15), (16)$$

$$-E_{s+1}I_{s+1}\frac{\partial^2 u_{s+1}}{\partial x_{s+1}^2}-G'_sJ'_s\frac{\partial \varphi_s}{\partial y_s}+G'_{s+1}J'_{s+1}\frac{\partial \varphi_{s+1}}{\partial y_{s+1}}=0, \quad (17)$$

$$-E'_sI'_s\frac{\partial^2 w_s}{\partial y_s^2}+E'_{s+1}I'_{s+1}\frac{\partial^2 w_{s+1}}{\partial y_{s+1}^2}+G_{s+1}J_{s+1}\frac{\partial \theta_{s+1}}{\partial x_{s+1}}=0, \quad (18)$$

$$-E_{s+1}I_{s+1}\frac{\partial^3 u_{s+1}}{\partial x_{s+1}^3}-E'_sI'_s\frac{\partial^3 w_s}{\partial y_s^3}+E'_{s+1}I'_{s+1}\frac{\partial^3 w_{s+1}}{\partial y_{s+1}^3}=m_{s+1}p^2u_{s+1}, \quad (19)$$

$[s=1, 2, 3]$

$$x_5=l,\ y_4=l';\quad u_5=w_4,\quad \frac{\partial u_5}{\partial x_5}=\varphi_4,\quad \frac{\partial w_4}{\partial y_4}=-\theta_5, \quad (20), (21), (22)$$

$$-E_5I_5\frac{\partial^2 u_5}{\partial x_5^2}-G'_4J'_4\frac{\partial \varphi_4}{\partial y_4}=0,\quad -E'_4I'_4\frac{\partial^2 w_4}{\partial y_4^2}+G_5J_5\frac{\partial \theta_5}{\partial x_5}=0, \quad (23), (24)$$

$$-E_5I_5\frac{\partial^3 u_5}{\partial x_5^3}-E'_4I'_4\frac{\partial^3 w_4}{\partial y_4^3}=m_5p^2u_5. \quad (25)$$

Substituting (3), (4), in (5) ~ (25) and eliminating constants, it is possible to get the frequency equations. We now write

$$\left.\begin{array}{l}\dfrac{E_sI_s}{E_{s+1}I_{s+1}}=\varphi_s,\ \dfrac{E'_sI'_s}{E_sI_s}=\eta_s,\ \dfrac{G'_sJ'_s}{E_sI_s}=\vartheta_s,\ [s=1, 2, 3, 4]\\ \dfrac{G_sJ_s}{E_sI_s}=\zeta_s,\ \dfrac{m_sp^2l^3}{E_sI_s}=\gamma_s,\ [s=1,\ 2,\ \ldots\ldots,\ 5]\ \dfrac{l'}{l}=\xi.\end{array}\right\} \quad (26)$$

After careful calculations we obtain the set of equations

$$2(\vartheta_1+\xi)C_1+3(\vartheta_1+2\xi)lD_1-2\vartheta_1C_2-3\vartheta_1lD_2=0, \quad (27)$$

$$\begin{aligned}&\xi^3\left\{(4\eta_1+\xi\zeta_1)(2\eta_2+\xi\zeta_2)+8\varphi_1\eta_1(2\eta_1+\xi\zeta_1)-2\xi\varphi_1\zeta_1\eta_1\right\}\left\{\gamma_1C_1+(\gamma_1+6)lD_1\right\}\\&-12\eta_1\left\{(\eta_1+\xi\zeta_1)(2\eta_2+\xi\zeta_2)+\xi\varphi_1\zeta_1\eta_1\right\}(C_1+lD_1)\\&+2\xi^3\eta_1(2\eta_1+\xi\zeta_1)\left\{\gamma_2C_2+(\gamma_2+6)lD_2\right\}\\&+12\eta_1\left\{\eta_2(2\eta_1+\xi\zeta_1)+(\eta_1+\xi\zeta_1)(2\eta_2+\xi\zeta_2)+\xi\varphi_1\zeta_1\eta_1\right\}(C_2+lD_2)\\&-12\eta_1\eta_2(2\eta_1+\xi\zeta_1)(C_3+lD_3)=0, \quad (28)\end{aligned}$$

$$2\xi\varphi_1C_1+6\xi\varphi_1lD_1+2(\vartheta_2+\xi)C_2+3(\vartheta_2+2\xi)lD_2-2\vartheta_2C_3-3\vartheta_2lD_3=0, \quad (29)$$

$$\begin{aligned}
&\xi^3\Big[(2\eta_3+\xi\zeta_3)\Big\{(4\eta_1+\xi\zeta_1)(\eta_2+\xi\zeta_2)+9\varphi_1\eta_1(2\eta_1+\xi\zeta_1)-2\xi\zeta_1\varphi_1\eta_1\Big\}\\
&\quad+\varphi_2\eta_2\Big\{14\varphi_1\eta_1(2\eta_1+\xi\zeta_1)+\xi\zeta_2(4\eta_1+\xi\zeta_1)-2\xi\zeta_1\varphi_1\eta_1\Big\}\Big]\Big\{\gamma_1C_1+(\gamma_1+6)lD_1\Big\}\\
&\quad+12\eta_1\Big[(2\eta_3+\xi\zeta_3)\Big\{(\eta_1+\xi\zeta_1)(\eta_2+\xi\zeta_2)+\xi\zeta_1\varphi_1\eta_1\Big\}\\
&\quad+\xi\varphi_2\eta_2\Big\{\zeta_1\varphi_1\eta_1+\zeta_2(\eta_1+\xi\zeta_1)\Big\}\Big]\Big\{(C_2+lD_2)-(C_1+lD_1)\Big\}\\
&\quad+\xi^3\eta_1(2\eta_1+\xi\zeta_1)\Big\{3(2\eta_3+\xi\zeta_3)+8\varphi_2\eta_2\Big\}\Big\{\gamma_2C_2+(\gamma_2+6)lD_2\Big\}\\
&\quad+2\xi^3\eta_1\eta_2(2\eta_1+\xi\zeta_1)\Big\{\gamma_3C_3+(\gamma_3+6)lD_3\Big\}\\
&\qquad\qquad\qquad+12\eta_1\eta_2\eta_3(2\eta_1+\xi\zeta_1)\Big\{(C_3+lD_3)-(C_4+lD_4)\Big\}=0\,, \quad (30)
\end{aligned}$$

$$\begin{aligned}
&2\xi\varphi_1\varphi_2(C_1+3lD_1)+2\xi\varphi_2(C_2+3lD_2)+2(\vartheta_3+\xi)C_3\\
&\qquad\qquad\qquad+3(\vartheta_3+2\xi)lD_3-2\vartheta_3C_4-3\vartheta_3lD_4=0\,, \quad (31)
\end{aligned}$$

$$\begin{aligned}
&\xi^3\Big\{(\eta_2X_1+\xi\zeta_2X_2)(4\eta_1+\xi\zeta_1)+\varphi_1\eta_1(6X_2+X_3)(2\eta_1+\xi\zeta_1)\\
&\quad-2\xi\zeta_1\varphi_1\eta_1X_2\Big\}\Big\{\gamma_1C_1+(\gamma_1+6)lD_1\Big\}+12\eta_1\Big\{(\eta_2X_1+\xi\zeta_2X_2)(\eta_1+\xi\zeta_1)\\
&\quad+\xi\zeta_1\varphi_1\eta_1X_2\Big\}\Big\{(C_2+lD_2)-(C_1+lD_1)\Big\}\\
&\quad+\eta_1(2\eta_1+\xi\zeta_1)\Big[\xi^3X_3\Big\{\gamma_2C_2+(\gamma_2+6)lD_2\Big\}+2\xi^3\eta_2\eta_3\Big\{\gamma_4C_4+(\gamma_4+6)lD_4\Big\}\\
&\quad+\xi^3\eta_2\Big\{3(2\eta_4+\xi\zeta_4)+8\varphi_3\eta_3\Big\}\Big\{r_3C_3+(r_3+6)lD_3\Big\}\\
&\qquad\qquad\qquad+12\eta_2\eta_3\eta_4(C_4+lD_4)-12\eta_2\eta_3\eta_4(C_5+lD_5)\Big]=0\,, \quad (32)
\end{aligned}$$

$$\begin{aligned}
&3\xi^2(2\eta_1+\xi\zeta_1)\Big\{\xi\eta_2Y_1+(2\varphi_1\eta_1+\xi\zeta_2)Y_2+\varphi_1\eta_1Y_3\Big\}\Big\{\gamma_1C_1+(\gamma_1+6)lD_1\Big\}\\
&\quad-2\Big[\eta_1(\eta_2Y_1+\zeta_2Y_2)+\zeta_1\Big\{\xi\eta_2Y_1+(\varphi_1\eta_1+\xi\zeta_2)Y_2\Big\}\Big]\\
&\quad\cdot\Big[\xi^3\Big\{\gamma_1C_1+(\gamma_1+6)lD_1\Big\}+6\eta_1(C_1+lD_1)-6\eta_1(C_2+lD_2)\Big]\\
&\quad+3\xi\eta_1(2\eta_1+\xi\zeta_1)\Big[\xi\eta_2\eta_3(2\varphi_4\eta_4+\xi\zeta_5)\Big\{\gamma_4C_4+(\gamma_4+6)lD_4\Big\}\\
&\quad+\xi\eta_2\Big\{\xi\zeta_5\eta_4+(\varphi_4\eta_4+\xi\zeta_5)(2\varphi_3\eta_3+\xi\zeta_4)+\varphi_3\eta_3(2\varphi_4\eta_4+\xi\zeta_5)\Big\}\\
&\qquad\qquad\cdot\Big\{\gamma_3C_3+(\gamma_3+6)lD_3\Big\}+\xi Y_3\Big\{\gamma_2C_2+(\gamma_2+6)lD_2\Big\}\Big]=0\,, \quad (33)
\end{aligned}$$

$$\begin{aligned}&2\xi\varphi_1\varphi_2\varphi_3(C_1+3lD_1)+2\xi\varphi_2\varphi_3(C_2+3lD_2)+2\xi\varphi_3(C_3+3lD_3)\\&\qquad+2(\vartheta_4+\xi)C_4+3(\vartheta_4+2\xi)lD_4-\vartheta_4(2\mathrm{C}_5+3lD_5)=0\,,\end{aligned}\tag{34}$$

$$\begin{aligned}&\varphi_1\varphi_2\varphi_3\varphi_4(C_1+3lD_1)+\varphi_2\varphi_3\varphi_4(C_2+3lD_2)+\varphi_3\varphi_4(C_3+3lD_3)\\&\qquad+\varphi_4(C_4+3lD_4)+(C_5+3lD_5)=0\,,\end{aligned}\tag{35}$$

$$\begin{aligned}&\varphi_1\varphi_2\varphi_3\varphi_4\left\{\gamma_1C_1+(\gamma_1+6)lD_1\right\}+\varphi_2\varphi_3\varphi_4\left\{\gamma_2C_2+(\gamma_2+6)lD_2\right\}\\&\quad+\varphi_3\varphi_4\left\{\gamma_3C_3+(\gamma_3+6)lD_3\right\}+\varphi_4\left\{\gamma_4C_4+(\gamma_4+6)lD_4\right\}\\&\qquad+\left\{\gamma_5C_5+(\gamma_5+6)lD_5\right\}=0\,,\end{aligned}\tag{36}$$

where

$$\begin{aligned}X_1&=(2\eta_4+\xi\zeta_4)(\eta_3+\xi\zeta_3)+\xi\zeta_3\varphi_3\eta_3\,,\\X_2&=\eta_3(2\eta_4+\xi\zeta_4)+(\varphi_2\eta_2+\xi\zeta_3)(2\eta_4+\xi\zeta_4+\varphi_3\eta_3),\\X_3&=3(2\eta_4+\xi\zeta_4)(\eta_3+3\varphi_2\eta_2+\xi\zeta_3)+\varphi_3\eta_3(3\xi\zeta_3+14\varphi_2\eta_2),\\Y_1&=\eta_3\left\{\zeta_5\eta_4+\zeta_4(\varphi_4\eta_4+\xi\zeta_5)\right\}+\zeta_3\left\{\xi\zeta_5\eta_4+(\varphi_4\eta_4+\xi\zeta_5)(\varphi_3\eta_3+\xi\zeta_4)\right\},\\Y_2&=\xi\eta_3\left\{\zeta_5\eta_4+\zeta_4(\varphi_4\eta_4+\xi\zeta_5)\right\}\\&\qquad+(\varphi_2\eta_2+\xi\zeta_3)\left\{\xi\zeta_5\eta_4+(\varphi_4\eta_4+\xi\zeta_5)(\varphi_3\eta_3+\xi\zeta_4)\right\},\\Y_3&=\xi\eta_3\left\{\zeta_5\eta_4+\zeta_4(\varphi_4\eta_4+\xi\zeta_5)\right\}\\&\quad+(2\varphi_2\eta_2+\xi\zeta_3)\left\{\xi\zeta_5\eta_4+(\varphi_4\eta_4+\xi\zeta_5)(\varphi_3\eta_3+\xi\zeta_4)\right\}\\&\quad+\varphi_2\eta_2\left\{\xi\zeta_5\eta_4+(\varphi_4\eta_4+\xi\zeta_5)(2\varphi_3\eta_3+\xi\zeta_4)+\varphi_3\eta_3(2\varphi_4\eta_4+\xi\zeta_5)\right\}.\end{aligned}\tag{37}$$

We shall take the special case $l'=l$, $m_s\equiv m$ $[s=1, 2, \ldots\ldots, 5]$, $E_3I_3=G_3J_3\equiv E_0I_0$, $E_sI_s=G_sJ_s\equiv EI$ $[s=1, 2, 4, 5]$, $E'_sI'_s=G'_sJ'_s\equiv EI$ $[s=1, 2, 3, 4]$, that is to say, the stiffnesses of the middle column differ from those of the remaining columns and the beams. In this case we get a pair of frequency equations of such simple forms as

$$\begin{aligned}&(3\gamma-16)(a_2c_1-a_1c_2)+(4\gamma-12)(a_1b_2-\mathrm{b}_1a_2)+(2\gamma+96)(b_1c_2-c_1b_2)=0\,,\\&(715\gamma-4392)\left\{(517\kappa+1736)\gamma-(2760\kappa+8508)\right\}\\&\qquad-(536\gamma-3036)\left\{(683\kappa+2269)\gamma-(3852\kappa+11736)\right\}=0\,,\end{aligned}\tag{38}$$

where

$$\left.\begin{aligned}
a_1&=(4\kappa+35)\gamma-(84\kappa+336), & a_2&=(12\kappa+39)\gamma-(90\kappa+360),\\
b_1&=(6\kappa+32)\gamma+(76\kappa+32), & b_2&=(18\kappa+38)\gamma+(348\kappa+108),\\
c_1&=-(21\kappa+35)\gamma+(72\kappa+96), & c_2&=-(63\kappa+51)\gamma+(198\kappa+144),\\
&\kappa=\frac{E_0I_0}{EI}, & \gamma&=\frac{mp^2l^3}{EI}.
\end{aligned}\right\}\qquad(39)$$

Solving these equations for the five cases of E_0I_0/EI, we get

$$\begin{array}{lllllll}
\text{(i)} & E_0I_0/EI=0; & \gamma=2{\cdot}186, & 4{\cdot}071, & 6{\cdot}335, & 16{\cdot}72, & 38{\cdot}703,\\
\text{(ii)} & E_0I_0/EI=1; & \gamma=3{\cdot}00, & 4{\cdot}21, & 8{\cdot}09, & 17{\cdot}95, & 39{\cdot}03,\\
\text{(iii)} & E_0I_0/EI=10; & \gamma=4{\cdot}444, & 4{\cdot}596, & 16{\cdot}523, & 21{\cdot}53, & 57{\cdot}45,\\
\text{(iv)} & E_0I_0/EI=30; & \gamma=4{\cdot}692, & 4{\cdot}727, & 21{\cdot}675, & 23{\cdot}31, & 112{\cdot}2,\\
\text{(v)} & E_0I_0/EI=\infty; & \gamma=4{\cdot}823, & 4{\cdot}823, & 24{\cdot}84, & 24{\cdot}84, & \infty,
\end{array}$$

these numerical values being plotted in Fig. 5. Since the masses are concentrated at five panel points, there are five vibrational frequencies, namely, I, II, III, IV, V.

In this case, too, since every vibrational frequency is in a coupled condition, it is scarcely possible to determine the accurate type of vibration that corresponds to each vibrational frequency. In this case, however, to estimate the respective types of vibrations is a simple matter. Since the masses are arranged in a straight line and the movements are only in the direction normal to the said straight line, the vibrational modes would be somewhat similar to those of flexural vibrations of a bar with free ends. Consequently the modes of the vibrations I, II, III, IV, V in the present case are similar to those of no-nodal, one-nodal, two-nodal, three-nodal, and quasi-four-nodal[5] vibrations in the case of the flexural

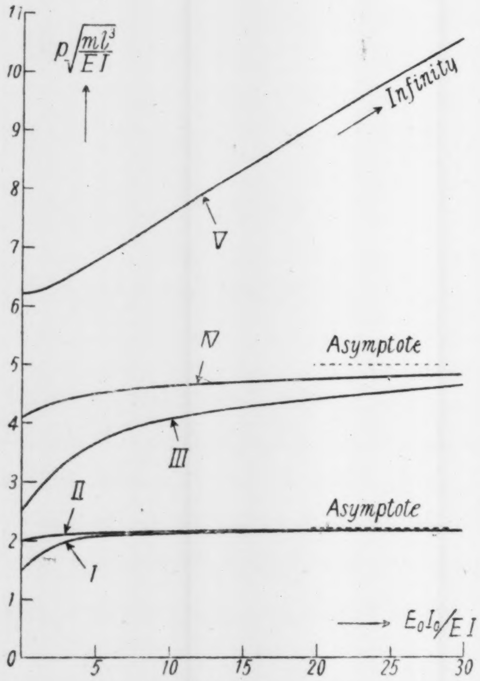

Fig. 5.

---

[5] Case V is of somewhat different nature. In the case of five masses four nodal vibration is scarcely possible. In this case the middle thick column alone participates in the vibrational energy.

vibrations of a bar. When the vibration is observed from the top, namely, in the lengthwise direction of the columns, modes I, III, V represent the vibrations that are symmetrical with respect to the middle column, while modes II, IV correspond to the vibrations that are asymmetrical with respect to the middle column.

With increase in E_0I_0/EI, the vibrational frequency for I and that for II tend to approach a common asymptotic line of no inclination and the vibrational frequency for III and that for IV also tend to approach another common asymptotic line of no inclination. This fact shows that at such a high value of E_0I_0, every set of ordinary columns on any one side of the middle thick column vibrates with little effect on the columns on the other side of the middle thick column under consideration. The reason that the asymptotes of these cases have no inclination is that, at such a high value of E_0I_0, the middle thick column merely serves as the fixed edge of a flexible framed structure. The condition in the case of V is somewhat special: the vibration is not a simple four-nodal vibration, but in this condition the vibrational amplitudes of the middle thick column is comparable to the remaining one, that is to say, the principal vibration is that of the middle thick column.

It must be remembered that the vibrational frequency of mode I at $E_0I_0/EI=1$ is nearly $p\sqrt{ml^3/EI}=\sqrt{3}$, which corresponds to the vibrational frequency of a canti-lever beam with a concentrated mass at its free end.

5. *Model experimental confirmation of the preceding mathematical result.*

In this case, too, for confirming the mathematical result, model experiments were conducted. The model tested was similar in form to that shown in the sketch in Fig. 4. The column height and beam span were both 23 cm. The brass mass at every panel point weighed 13 gr. The usual columns and the beams were 1·5 mm in diameter, whereas the extra thick middle column was (i) 1 mm, (ii) 1·5 mm, (iii) 2 mm, (iv) 2·5 mm, and (v) 3 mm, the masses of the respective columns being (i) 2·00 gr, (ii) 3·84 gr, (iii) 6·25 gr, (iv) 9·39 gr, and (v) 13·40 gr. In the numerical calculation we assumed that the sum of the brass mass and $(1/2+4/5)$ of the mass of the 1·5 mm wire, is effective as an inertia mass at every panel point. The inertia mass in this case, too, is likely to be underestimated. The values of E and G are the same as those shown in Section 3. For the same reason shown in Section

3, the value of G in the numerical calculation is an overestimate.

The model just mentioned was clamped to the vibration table with the lengthwise direction of the model at right angles to the direction of the vibratory motion of the table. By observing the resonance conditions of the forced vibrations, we found five vibrational periods in every case, the results being plotted with thick lines in Fig. 6.

At the same time, we calculated the theoretical vibrational periods, and plotted the results with broken lines in the same figure. It will be seen that both results, mathematical and experimental, fairly agree, not exactly. The reason for the calculated periods being somewhat smaller than the experimented ones is explained in Section 3.[6]

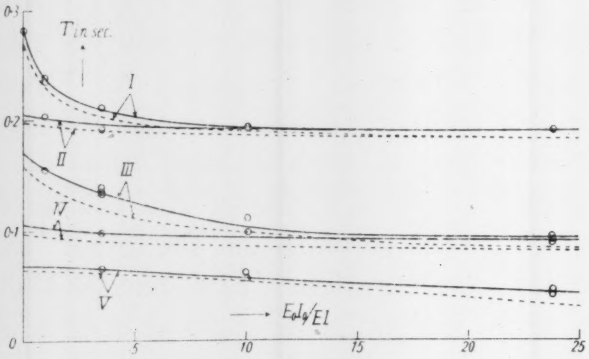

Fig. 6.

6. *Concluding remarks.*

From mathematical calculation and model experiments we ascertained certain cases of three-dimensional vibrations of a framed structure. Even should the framed structure be apparently of two-dimentional form, the vibration is liable to be three-dimensional according to certain conditions of the structure as well as the direction of the movements of the seismic vibrations. When a horizontally long house is subjected to seismic disturbance with amplitudes orientated in the direction normal to the length of the house, there would probably be bending vibrations of various modes of the house, even should there be no asymmetrical relations between the structural conditions and the seismic movements. The occurrence of asymmetrical vibrations in the case of a three-dimensional framed structure is too evident to call for remarks here.

The detailed nature of the vibrations for different cases has been dealt with in their respective parts in the paper.

The present investigation was made at Professor Sezawa's suggestion in connection with his research work as member of the Investigation Commitee for Earthquake-proof Construction, of the Japan Society of the Promotion of Scientific Research, to whom I wish to express my sincerest thank for his many kind advices.

---

[6] As explained in Section 3, the condition never resulted from such error that might be involved in numerical calculation.

Note. Notwithstanding that the problem of a three-dimensional vibration is very important in earthquake-proof construction, the problem has received rather scant attention probably owing to mathematical difficulties. Dr. Kanai, in my opinion, being the person most fitted for attacking the problem, I requested him to make the investigation. This problem, in future, will be extended, I hope, to the problem of decay of the vibrational energy in the seismic vibration of a structure and also to the dynamic damper of the seismic vibration of the same structure.

Finally, I wish to express my warmest thanks to the Council of the Japan Society for the Promotion of Scientific Research for aid given to a series of investigations of which this is a part. (K. Sezawa)

---

40. 架構の立體的振動

地震研究所　金井　清

この前論じた大黑柱の問題に關聯して立體的架構又は平面的架構の立體的振動を研究して見たのである.

立體的架構の最も簡單なる例として四本柱の一本の柱の剛度が種々變化する場合を取ると質量が4點に分布する場合には4種の振動數が出るが，その型は角點を結ぶ2つの斜線の方向の移動的振動，梁線で作られる正方形が菱形になる振動，鉛直軸の周圍の回轉的振動とになる．しかし1本の柱の剛度が著しく高くなると，始めの2つの振動も後の2つの各の型の振動に變化する．但し，型は同じでも周期は著しく高いものが現れる．以上の數理的結果を振動臺の上で共振れする模型の實驗で確めると可なりよく一致する性質を示す．卽ち困難なる計算結果が先づ正確な事が證明されたのである.

平面的架構が架構面に直角な方向に振動するときには，對稱的構造であつてもその振動が立體的となる．之も數理的と實驗的とに研究して見たがよく一致する事がわかつた．架構を上から見ると兩端自由なる棒の振動と似てをる．しかし（中央にある）1本の柱の剛度が高くなると互に別の型に屬する一對宛の振動型の振動周期が近づくやうになる．尙，特に剛い柱特有の自己振動數に相當する振動のあることもわかつた.

41. *Magnetic Anomalies and the Corresponding Subterranean Mass Distribution.*

By Takesi NAGATA.

Earthquake Research Institute.

(Read Mar. 15, Apr. 19 and May 17, 1938.—Received June 22, 1938)

Introduction.

One of the most interesting studies in geophysics, probably, is to ascertain the relation between local magnetic anomalies on the earth's surface and the corresponding subterranean geological structures. The relation, if it could be found, could be applied not only to magnetic prospecting of geological structures, but also to studies of the variations that accompany earthquakes and volcanic activities.

Methods have been proposed by a number of authors[1] for finding the subterranean mass distribution to which the magnetic anomalies on the earth's surface are due. The principle of these methods consists in selecting a suitable one out of many schematic models that explain the observed magnetic anomalies; in other words, in adjusting the mode of distribution of the subterranean mass and its magnetic properties so that the magnetic field, due to the properly adjusted mass distribution with appropriate magnetic properties, coincides with the observed magnetic field.

Strictly speaking, it is not possible to determine uniquely the subterranean mass distribution from the intensity distribution of the magnetic field on the earth's surface alone, as has been proved in "potential theory". It is not impossible, however, to find a satisfactory solution of the "inverse problem of potential" mentioned above, provided we make several assumptions which geologically are not improbable.

C. Tsuboi[2] recently proposed a method of finding the density distribution concentrated on a subterranean plane directly from the gravity values observed on the earth's surface, which is believed to be due to the subterranean distribution of mass. This method was proved to be applicable to a number of cases of actual distributions of gravity anomalies.

---

[1] For instnace, R. THALÉN, *Berg. u. Hütt. Z. S.*, (1875.)
A. NIPPOLDT, Verwertung magnetischer Messungen zur Mutung. (1930), Berlin.
J. KOENIGSBERGER, *Gerl. Beitr.* **19** (1928), 241.
H. HAALCK, *Z. S. Geophys.* **2** (1926), 1.

[2] C. TSUBOI, *Bull. Earthq. Res. Inst.*, **15** (1937), 636; **16** (1938), 273.

In this paper, the writer gives the results of his studies on the relations between magnetic anomalies and subterranean mass distribution, which were made by applying a method similar to that used in Tsuboi's study.

CHAPTER I. Magnetic Anomalies and the Corresponding Subterranean Magnetized Plane.

§ 1. *Magnetic field due to subterranean magnetized layer (a two-dimensional case).*

We take AA in Fig. 1 as the plane of the earth's surface, and BB, CC as the planes at depths d and $d+D$ respectively from the earth's surface, on which are distributed intensities of magnetization that do not change in the direction perpendicular to the paper. It is also assumed that the distributions of magnetic intensities on planes BB and CC are not arbitrary, but are related to each other so that the intensity at any point $P'(\xi, d+D)$ on CC is determined by J, provided it is $-J$ at P $(\xi - D\cot\theta, d)$ on BB, i. e. a horizontal layer of thickness D is magnetized uniformly in the direction dipping θ to the horizon and the intensity distribution is a function of merely the horizontal coordinate ξ.

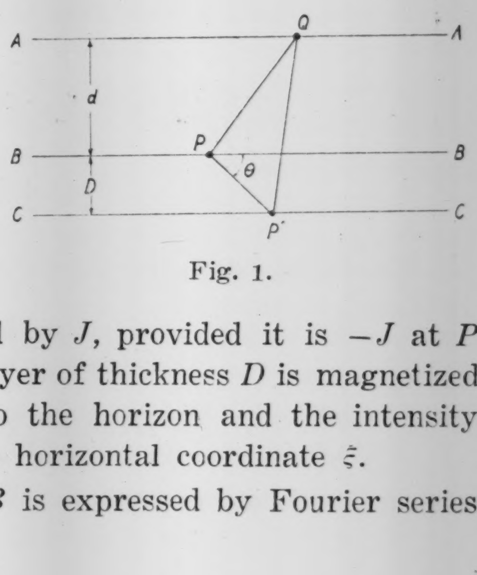

Fig. 1.

If the intensity distribution on BB is expressed by Fourier series as

$$m_-(\xi) = -\sum_n A_n \cos n\xi - \sum_n B_n \sin n\xi \tag{1}$$

then that on CC becomes

$$m_+(\xi) = \sum_n A_n \cos n(\xi - D\cot\theta) + \sum_n B_n \sin n(\xi - D\cot\theta) \tag{1'}$$

The vertical component $Z(x)$ and the horizontal component $H(x)$ of the magnetic force at a point $Q(x, 0)$ on plane AA due to these intensity distributions are expressed by

$$\left.\begin{aligned}
Z(x)&=2d\int_{-\infty}^{\infty}\frac{m_-(\xi)}{d^2+(x-\xi)^2}d\xi+2(d+D)\int_{-\infty}^{\infty}\frac{m_+(\xi)}{(d+D)^2+(x-\xi)^2}d\xi\\
H(x)&=2\int_{-\infty}^{\infty}\frac{m_-(\xi)(x-\xi)}{d^2+(x-\xi)^2}d\xi+2\int_{-\infty}^{\infty}\frac{m_+(\xi)(x-\xi)}{(d+D)^2+(x-\xi)^2}d\xi
\end{aligned}\right\}\quad(2).$$

Substituting the relations (1) and (1′) in eq. (2), we get

$$\left.\begin{aligned}
Z(x)=2\pi\sum_n\Big[&A_ne^{-nd}-A_ne^{-n(d+D)}\cos(nD\cot\theta)\\
&+B_ne^{-n(d+D)}\sin(nD\cot\theta)\Big]\cos nx\\
+2\pi\sum_n\Big[&B_ne^{-nd}-B_ne^{-n(d+D)}\cos(nD\cot\theta)\\
&-A_ne^{-n(d+D)}\sin(nD\cot\theta)\Big]\sin nx\\
H(x)=2\pi\sum_n\Big[&B_ne^{-nd}-B_ne^{-n(d+D)}\cos(nD\cot\theta)\\
&-A_ne^{-n(d+D)}\sin(nD\cot\theta)\Big]\cos nx\\
-2\pi\sum_n\Big[&A_ne^{-nd}-A_ne^{-n(d+D)}\cos(nD\cot\theta)\\
&+B_ne^{-n(d+D)}\sin(nD\cot\theta)\Big]\sin nx
\end{aligned}\right\}\quad(3).$$

On the other hand, the observed values of $Z(x)$ and $H(x)$ are expanded in Fourier series

$$\left.\begin{aligned}
Z(x)&=\sum_n\alpha_n\cos nx+\sum_n\beta_n\sin nx\\
H(x)&=\sum_n\alpha'_n\cos nx+\sum_n\beta'_n\sin nx
\end{aligned}\right\}\quad(4).$$

Since the series expressed in these two different ways of eq. (3) and (4) must be identical, the following relations are established,

$$\left.\begin{aligned}
\alpha_n&=2\pi\Big[A_ne^{-nd}\Big\{1-e^{-nD}\cos(nD\cot\theta)\Big\}+B_ne^{-n(d+D)}\sin(nD\cot\theta)\Big]\\
\beta_n&=2\pi\Big[B_ne^{-nd}\Big\{1-e^{-nD}\cos(nD\cot\theta)\Big\}-A_ne^{-n(d+D)}\sin(nD\cot\theta)\Big]\\
\alpha'_n&=2\pi\Big[B_ne^{-nd}\Big\{1-e^{-nD}\cos(nD\cot\theta)\Big\}-A_ne^{-n(d+D)}\sin(nD\cot\theta)\Big]\\
\beta'_n&=2\pi\Big[A_ne^{-nd}\Big\{1-e^{-nD}\cos(nD\cot\theta)\Big\}+B_ne^{-n(d+D)}\sin(nD\cot\theta)\Big]
\end{aligned}\right\}\quad(5).$$

From eq. (5) we get the relations

$$\alpha_n = -\beta'_n, \quad \beta_n = \alpha'_n \quad (n \geq 1) \tag{6}$$

Conversely, if the Fourier's expression for $Z(x)$ or $H(x)$ is given from actual observed data, the Fourier coefficients of the distribution of magnetic intensity of the corresponding subterranean magnetized layer are given by

$$\left.\begin{aligned} A_n &= \frac{1}{2\pi}\cdot\frac{\alpha_n e^{-nd}(1-e^{-nD}\cos n\omega) - \beta_n e^{-n(d+D)}\sin n\omega}{e^{-2nd}(1-e^{-nD}\cos n\omega)^2 + e^{-2n(d+D)}\sin^2 n\omega} \\ B_n &= \frac{1}{2\pi}\cdot\frac{\beta_n e^{-nd}(1-e^{-nD}\cos n\omega) + \alpha_n e^{-n(d+D)}\sin n\omega}{e^{-2nd}(1-e^{-nD}\cos n\omega)^2 + e^{-2n(d+D)}\sin^2 n\omega} \end{aligned}\right\} \tag{7},$$

where

$$\omega = D\cot\theta.$$

Substituting these values in eq. (1) or (1′), we get the distribution of the magnetic intensity, provided d, D, and θ are known from either other data or assumed.

§ 2. *Magnetic field due to subterranean magnetized plane (a two-dimensional case).*

In a special case in which the thickness D of the magnetized layer is infinitely small, the magnetic moment $\dfrac{mD}{\sin\theta}$ being preserved in finite value, α_n, β_n, α'_n and β'_n are given by

$$\left.\begin{aligned} \alpha_n &= -\beta'_n = 2\pi n e^{-nd}(a_n\sin\theta + b_n\cos\theta) \\ \beta_n &= \alpha'_n = 2\pi n e^{-nd}(b_n\sin\theta - a_n\cos\theta) \end{aligned}\right\} \tag{8},$$

where

$$\frac{A_n D}{\sin\theta} = a_n, \qquad \frac{B_n D}{\sin\theta} = b_n.$$

In this limiting case, the intensity of magnetization is concentrated on a plane at depth d from the earth's surface, and the distribution of magnetic moments on the plane is given by

$$J(\xi) = \sum_n a_n \cos n\xi + \sum_n b_n \sin n\xi \tag{9}.$$

Constants a_n and b_n are Fourier coefficients of the distribution of the magnetic moments of the magnetized layer, as shown in Fig. 2.

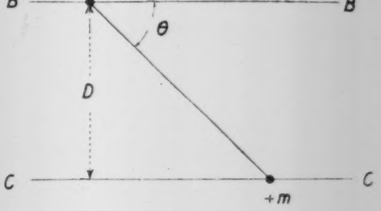

Fig. 2.

Conversely, if (α_n, β_n) or (α'_n, β'_n) are given from observed data, the distribution of intensity of magnetization on the subterranean plane, to which the observed anomalies are due, is expressed by Fourier series of the type of eq. (9), the coefficients a_n, b_n of which are given by

$$\left.\begin{aligned} a_n &= \frac{e^{nd}}{2\pi n}(\alpha_n \sin\theta - \beta_n \cos\theta) \\ b_n &= \frac{e^{nd}}{2\pi n}(\alpha_n \cos\theta + \beta_n \sin\theta) \end{aligned}\right\} \tag{10}$$

Thus, if θ and d are given, a_n and b_n, and consequently $J(\xi)$, can be calculated with the aid of equations (10) and (9). The Fourier series (9) is not always convergent, even if eq. (4) are convergent series, for $\frac{e^{nd}}{n}$ becomes a large value when n becomes large. The magnitude of d is therefore limited so that the series (9) does not diverge. Actually, however, there is no need to be concerned about the convergency, for, in most cases, the higher terms of α_n and β_n become zero.

Relation (10) can be obtained directly by calculating the magnetic potential due to the subterranean magnetized plane. In Fig. 3, magnetic potential $d\psi$ at $P(x, z)$, due to the magnetic dipole dipping θ at depth d, is given by

$$d\psi = 2J\cos\theta \frac{(x-\xi)}{(x-\xi)^2+(d-z)^2} - 2J\sin\theta \frac{(d-z)}{(x-\xi)^2+(d-z)^2} \tag{11}$$

where J denotes the magnetic moment of the dipole.

If we assume that dipoles magnetized in the same direction are distributed continuously on plane BB, and that the distribution of the moment of dipoles is expressed by

$$J(\xi) = \sum_n a_n \cos n\xi + \sum b_n \sin n\xi \quad (9),$$

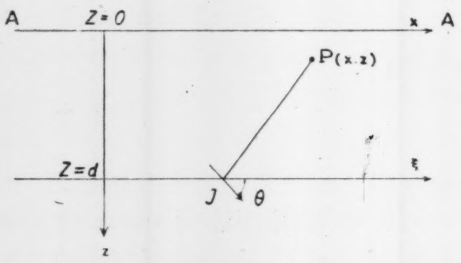

Fig. 3.

then the potential at any point above plane BB is given by

$$\psi(x) = 2\pi\cos\theta\left[\sum_n a_n \int_{-\infty}^{\infty} \frac{(x-\xi)\cos n\xi}{(x-\xi)^2+(d-z)^2}d\xi + \sum_n b_n \int_{-\infty}^{\infty} \frac{(x-\xi)\sin n\xi}{(x-\xi)^2+(d-z)^2}d\xi\right]$$

$$-2\pi\sin\theta(d-z)\left[\sum_n a_n \int_{-\infty}^{\infty} \frac{\cos n\xi}{(x-\xi)^2+(d-z)^2}d\xi + \sum_n b_n \int_{-\infty}^{\infty} \frac{\sin n\xi}{(x-\xi)^2+(d-z)^2}d\xi\right]$$

$$
\begin{aligned}
&= -2\pi\sum_{n} e^{-n(d-z)}(a_n \sin\theta + b_n \cos\theta)\cos nx \\
&\qquad\qquad + 2\pi\sum_{n} e^{-n(d-z)}(a_n \cos\theta - b_n \sin\theta)\sin nx \qquad (12).
\end{aligned}
$$

Since, on the other hand, the vertical and horizontal components, $Z(x)$ and $H(x)$, of the magnetic force on the earth's surface AA (in Fig. 3) are

$$
Z(x) = -\left(\frac{\partial\psi}{\partial z}\right)_{z=0} \qquad H(x) = -\left(\frac{\partial\psi}{\partial x}\right)_{z=0} \qquad (13),
$$

they can be obtained by differentiating the right-hand side of eq. (12) with respcet to x and z, provided the series are uniformly convergent. The values of $Z(x)$ and $H(x)$, expressed by eqs. (4) and (13), must be exactly equal, whence we have

$$
\left.
\begin{aligned}
\alpha_n &= -\beta'_n = 2\pi n e^{-nd}(a_n \sin\theta + b_n \cos\theta) \\
\beta_n &= \alpha'_n = 2\pi n e^{-nd}(b_n \sin\theta - a_n \cos\theta)
\end{aligned}
\right\} \qquad (8)
$$

Thus relation (8) is directly obtained.

§ 3. *Actual examples.*

(1) For demonstrating the feasibility of the present method, we take the schematic model given by R. v. Eötvös.[3] The smoothed curves of $Z(x)$ and $H(x)$, as calculated by him, are shown in Fig. 4 (a).

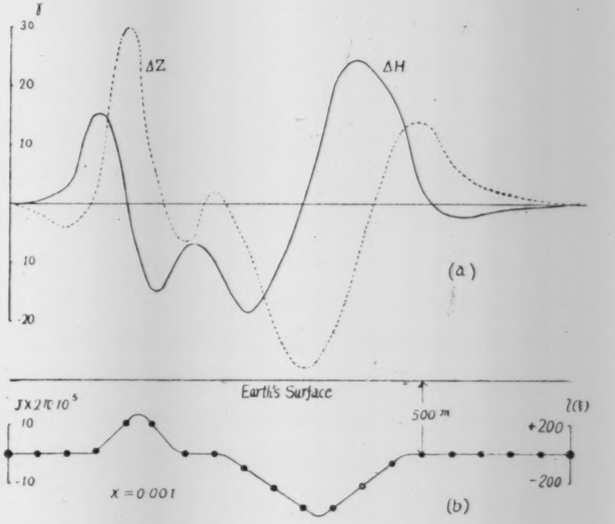

Fig. 4.

With the aid of the method above described, the Fourier coefficients (α_0, α_1, …… α_{12}) (β_1, β_2, …… β_{11}), (α'_0, α'_1, …… α'_{12}) and (β'_1, β'_2, …… β'_{11}) of these curves are determined. If the magnetic field has a potential, and the curves shown by Eötvös are sufficiently accurate, the conditions given by eq. (6) must be satisfied, barring errors in calculations and analyses, which are inevitable. The conditions are satisfied as shown in Fig. 5. Substituting these values of α_n and β_n in eq. (10), and assuming that $d=0{\cdot}5$ km and $\tan\theta=2{\cdot}00$, the Fourier coefficients a_n and b_n of the distribution of magnetization are calculated. We then obtain the distribution of the intensity of magnetization on the subterranean plane by applying these values of a_n and b_n to eq. (9). The result is shown in Table I and in Fig. 4 (b) where the calculated values are shown by black circles. We may proceed on the interpretation that the intensity distribution thus obtained is proportional to the undulatory form of the boundary between the two strata, the magnetizations of which differ. If we assume that the magnetization is induced by the normal magnetic force of the earth, we can take

---

[3] R. v. Eötvös, Verh. XVI. allg. Konfer. intern. Erdruessung in London u. Cambridge (1909), 335.

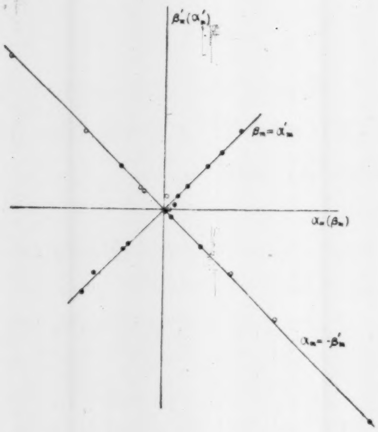

Fig. 5.

Table I.

x	$J\times2\pi\cdot10^5$	x	$J\times2\pi\cdot10^5$	x	$J\times2\pi\cdot10^5$	x	$J\times2\pi\cdot10^5$
$\frac{\pi}{12}\times0$	$+2{\cdot}1$	$\frac{\pi}{12}\times7$	$+11{\cdot}0$	$\frac{\pi}{12}\times14$	$-15{\cdot}4$	$\frac{\pi}{12}\times21$	$+2{\cdot}1$
1	$+2{\cdot}0$	8	$+8{\cdot}9$	15	$-10{\cdot}4$	22	$+1{\cdot}7$
2	$+2{\cdot}3$	9	$+1{\cdot}0$	16	$-2{\cdot}5$	23	$+2{\cdot}2$
3	$+1{\cdot}9$	10	$+2{\cdot}4$	17	$+2{\cdot}1$	24	$+2{\cdot}1$
4	$+2{\cdot}0$	11	$-2{\cdot}7$	18	$+2{\cdot}4$		
5	$+1{\cdot}8$	12	$-9{\cdot}5$	19	$+2{\cdot}0$		
6	$+3{\cdot}2$	13	$-14{\cdot}8$	20	$+1{\cdot}9$		

$$J(\xi)=F_0\kappa l(\xi),$$

where κ denotes the difference in the magnetic susceptibility of the material of the lower stratum from that of the upper, F_0 the intensity of the normal magnetic force, and $l(\xi)$ the undulation of the boundary between the upper and lower strata which is measured from the plane at $d=0{\cdot}5$ km.

The values of $l(\xi)$, calculated by taking $F_0=0{\cdot}447\Gamma$ and $\kappa=0{\cdot}001$, exactly agree with those given by Eötvös as a model in showing the calculation of magnetic surface anomalies. This agreement shows that the subterranean mass distribution estimated by the present method, namely, by assuming the excess mass to be concetrated on a certain plane situated at a certain depth, deviates slightly from the actual mass distribution, even when the amplitude of its undulation exceeds a half or more of depth d, as shown in the present case.

(2) Substituting the values of α_n and β_n obtained in the beginning of the present example in eq. (7), and assuming that $d=0{\cdot}25$ km and $D=0{\cdot}5$ km, we get the distribution of magnetic intensity $m(\xi)$ on plane $z=d$, as shown in Fig. 6. The distribution of intensity $m(\xi')$ on plane $z=d+D$ is then given by

$$m(\xi')=-m(\xi-D\tan\theta)$$

as mentioned in §2, where the moment of the magnetized layer is given by

$$J(\xi)=D\ m(\xi)\operatorname{cosec}\theta.$$

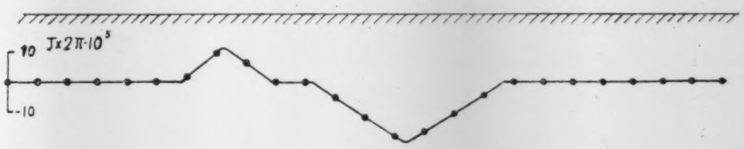

Fig. 6.

The distribution of the magnetic moment thus calculated agrees with that as calculated with reference to the model of magnetization condensed on a plane, as shown in Table II, no difference being found between the two. It may, therefore, be concluded that the assumption that the magnetized mass is concentrated on a plane at mean depth, is satisfactory in estimating the undulatory form of the boundary between the upper and lower strata, which mass is responsible for the actual magnetic anomalies on the earth's surface.

Table II.

x	$J\times2\pi\cdot10^5$	x	$J\times2\pi\cdot10^5$	x	$J\times2\pi\cdot10^5$	x	$J\times2\pi\cdot10^5$
$\frac{\pi}{12}\times 0$	+ 2·1	$\frac{\pi}{12}\times 7$	+11·1	$\frac{\pi}{12}\times 14$	−14·9	$\frac{\pi}{12}\times 21$	+ 2·0
1	+ 1·9	8	+ 8·2	15	− 9·1	22	+ 2·0
2	+ 2·1	9	+ 1·8	16	− 2·6	23	+ 2·3
3	+ 2·1	10	+ 2·1	17	+ 2·4	24	+ 2·1
4	+ 2·5	11	− 3·1	18	+ 2·3		
5	+ 1·5	12	− 9·7	19	+ 2·3		
6	+ 3·8	13	−15·3	20	+ 2·3		

(3) Another example is given in Fig. 7, in which (a) shows the distribution of vertical intensity along the east-west line, crossing per-

pendicularly the basalt flow in Gulgong, Australia,[4] where θ would be taken as 90°. The result of calculation on the assumption that $d=70$ ft is shown in Fig. 7 (b). Since it is known from geological data that the basalt flows fill up valleys on the surface of the diorite that forms the bedrock, the thickness of the alluvial deposit often reaching 70~100 ft, we may accept the distribution of J to be as that shown in Fig. 7 (c), where the black part represents the magnetic intensity of the basalt mass, and the hatched part that due to the undulatory form of the surface of the diorite-bed. The geological structure derived from the result of calculation is shown in Fig. 7 (d), where the magnetic susceptibilities of basalt and diorite are taken as 0·0065 and 0·0012 c. g. s. respectively. This structure agrees well with the results of borings.

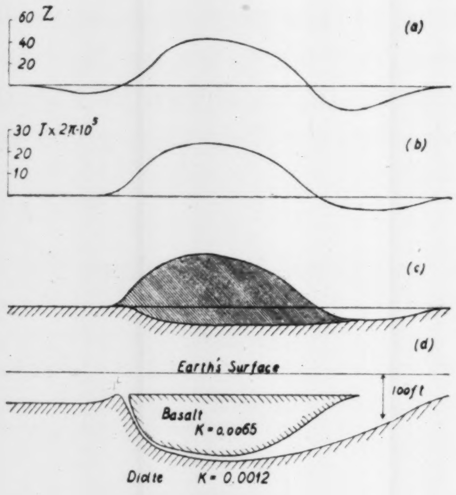

Fig. 7.
Magnetic Anomaly and Subterranean Structure in Gulgong.

§ **4.** *Magnetic anomalies due to the magnetized subterranean mass being distributed on a plane (a three-dimensional case).*

In this paragraph, the method that was used in the preceding case of the two-dimensional problem is modified so that it shall apply also to the case of a three-dimensional problem.

Let A, in Fig. 8, be the plane exposing the earth's surface along which the magnetic anomalies are known from point to point, and B another plane at depth d from the earth's surface, on which are distributed intensities of magnetization $J(\xi, \eta)$ which are responsible for these magnetic anomalies on the surface.

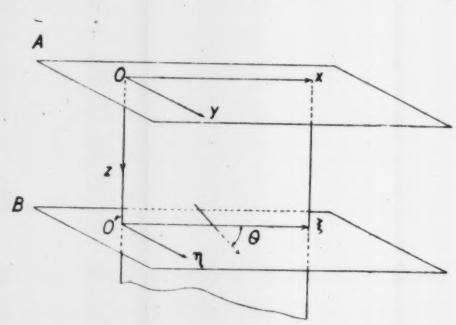

Fig. 8.

Take the surface A, regarded as the xy-plane as before, and the positive direction of z, downward, as shown in Fig. 8, the density $\rho(\xi\eta)$ being distributed on plane B. The gravitational potential U, due to $\rho(\xi\eta)$, is then a solution of the Laplace equation

---

[4] Internationl Geophysical Experimental Survey (1931), Cambridge. pp. 188.

$$\nabla^2 U = 0 \qquad (14),$$

which satisfies

$$-\left(\frac{\partial U}{\partial z}\right)_{z=d} = 2\pi k^2 \rho(\xi,\ \eta) \qquad (15),$$

where k^2 is the gravitation constant.

Hence U assumes the form

$$U = -\sum_m \sum_n A_{mn} \begin{matrix}\cos\\ \sin\end{matrix} mx \begin{matrix}\cos\\ \sin\end{matrix} ny \ e^{-\sqrt{m^2+n^2}(d-z)} \qquad (16)$$

in the space above the plane B.

If $\rho(\xi\eta)$ is capable of being expanded in double Fourier series

$$\rho(\xi\eta) = \sum_m \sum_n B_{mn} \begin{matrix}\cos\\ \sin\end{matrix} m\xi \begin{matrix}\cos\\ \sin\end{matrix} n\eta \qquad (17),$$

then, from the boundary condition at $z=d$, it follows that

$$A_{mn} = \frac{2\pi k^2 B_{mn}}{\sqrt{m^2+n^2}} \qquad (18),$$

whence U becomes

$$U = -2\pi k^2 \sum_m \sum_n \frac{e^{-\sqrt{m^2+n^2}(d-z)}}{\sqrt{m^2+n^2}} B_{mn} \begin{matrix}\cos\\ \sin\end{matrix} mx \begin{matrix}\cos\\ \sin\end{matrix} ny. \qquad (19).$$

On the other hand, if we assume that the same mass is magnetized in the direction that dips θ, and that the intensity of magnetization at any point of the mass is proportional to the density at that point, then the magnetic potential ψ is connected with the gravitational potential U by the well-known Poisson's law, i.e.,

$$\psi = \frac{J}{k^2 \rho} \frac{\partial U}{\partial r} \qquad (20),$$

where J and r denote the intensity of magnetization and the unit vector in the direction of magnetization respectively. Taking the rectangular coordinate with its xz-plane parallel to the direction of magnetization, we have

$$\psi = \frac{J}{k^2 \rho}\left(\cos\theta \frac{\partial}{\partial x} + \sin\theta \frac{\partial}{\partial z}\right) U \qquad (21).$$

Putting

$$\rho(\xi\eta)=\sum_m\sum_n(p_{mn}\cos m\xi\cos n\eta+q_{mn}\sin m\xi\cos n\eta$$
$$+r_{mn}\cos m\xi\sin n\eta+s_{mn}\sin m\xi\sin n\eta) \qquad (22)$$

and

$$J(\xi\eta)=\sum_m\sum_n(a_{mn}\cos m\xi\cos n\eta+b_{mn}\sin m\xi\cos n\eta$$
$$+c_{mn}\cos m\xi\sin n\eta+d_{mn}\sin m\xi\sin n\eta) \qquad (23),$$

we have from equations (19), (21), (22) and (23)

$$\psi(xy)=2\pi\sum\sum e^{-\sqrt{m^2+n^2}(d-z)}\Bigg[\left(a_{mn}\sin\theta+b_{mn}\cos\theta\frac{m}{\sqrt{m^2+n^2}}\right)\cos mx\cos ny$$
$$+\left(b_{mn}\sin\theta-a_{mn}\cos\theta\frac{m}{\sqrt{m^2+n^2}}\right)\sin mx\cos ny$$
$$+\left(c_{mn}\sin\theta+d_{mn}\cos\theta\frac{m}{\sqrt{m^2+n^2}}\right)\cos mx\sin ny$$
$$+\left(d_{mn}\sin\theta-c_{mn}\cos\theta\frac{m}{\sqrt{m^2+n^2}}\right)\sin mx\sin ny\Bigg]$$
$$(24),$$

in which

$$\frac{J}{k^2\rho}=\frac{a_{mn}}{k^2p_{mn}}=\frac{b_{mn}}{k^2q_{mn}}=\frac{c_{mn}}{k^2r_{mn}}=\frac{d_{mn}}{k^2s_{mn}} \qquad (25).$$

Let X, Y and Z denote respectively the northward, eastward, and downward components of the magnetic force on the earth's surface due to the magnetized subterranean mass. They can be expressed by double Fourier series, namely,

$$\left.\begin{aligned}
X=\sum_m\sum_n(\alpha'_{mn}\cos mx\cos ny+\beta'_{mn}\sin mx\cos ny&\\
+\gamma''_{mn}\cos mx\sin ny+\delta'_{mn}\sin mx\sin ny)&\\
Y=\sum_m\sum_n(\alpha''_{mn}\cos mx\cos ny+\beta''_{mn}\sin mx\cos ny&\\
+\gamma''_{mn}\cos mx\sin ny+\delta''_{mn}\sin mx\sin ny)&\\
Z=\sum_m\sum_n(\alpha_{mn}\cos mx\cos ny+\beta_{mn}\sin mx\cos ny&\\
+\gamma_{mn}\cos mx\sin ny+\delta_{mn}\sin mx\sin ny)&
\end{aligned}\right\} \qquad (26).$$

The values of X, Y, Z are also obtainable from the relations

$$X=-\left(\frac{\partial\psi}{\partial x}\right)_{z=0},\quad Y=-\left(\frac{\partial\psi}{\partial y}\right)_{z=0},\quad Z=-\left(\frac{\partial\psi}{\partial z}\right)_{z=0} \qquad (27),$$

by differentiating the right-had side of eq. (24) with respect to x, y and z, provided the series are uniformly convergent. The expressions for X, Y and Z given in these two different ways must be identical, whence we have the relations

$$\left.\begin{aligned}
\alpha_{mn}&=2\pi\sqrt{m^2+n^2}e^{-\sqrt{m^2+n^2}d}\left(a_{mn}\sin\theta+\frac{m}{\sqrt{m^2+n^2}}b_{mn}\cos\theta\right)\\
\beta_{mn}&=2\pi\sqrt{m^2+n^2}e^{-\sqrt{m^2+n^2}d}\left(b_{mn}\sin\theta-\frac{m}{\sqrt{m^2+n^2}}a_{mn}\cos\theta\right)\\
\gamma_{mn}&=2\pi\sqrt{m^2+n^2}e^{-\sqrt{m^2+n^2}d}\left(c_{mn}\sin\theta+\frac{m}{\sqrt{m^2+n^2}}d_{mn}\cos\theta\right)\\
\delta_{mn}&=2\pi\sqrt{m^2+n^2}e^{-\sqrt{m^2+n^2}d}\left(d_{mn}\sin\theta-\frac{m}{\sqrt{m^2+n^2}}c_{mn}\cos\theta\right)
\end{aligned}\right\}\quad(28),$$

$$(m^2+n^2\geqq1)$$

and

$$\left.\begin{aligned}
&\frac{\alpha_{mn}}{\sqrt{m^2+n^2}}=-\frac{\beta_{mn}}{m}=-\frac{\gamma''_{mn}}{n},\quad \frac{\beta_{mn}}{\sqrt{m^2+n^2}}=\frac{\alpha'_{mn}}{m}=-\frac{\delta''_{mn}}{n}\\
&\frac{\gamma_{mn}}{\sqrt{m^2+n^2}}=-\frac{\delta'_{mn}}{m}=\frac{\alpha''_{mn}}{n},\quad \frac{\delta_{mn}}{\sqrt{m^2+n^2}}=\frac{\gamma'_{mn}}{m}=\frac{\beta''_{mn}}{n}
\end{aligned}\right\}\quad(29).$$

Conversely, if α_{mn}, β_{mn}, γ_{mn} and δ_{mn} are obtained from the observed values with the aid of double Fourier analysis, the coefficients of the Fourier series for the intensity distribution on the subterranean plane are given by

$$\left.\begin{aligned}
a_{mn}&=\frac{e^{\sqrt{m^2+n^2}d}}{2\pi\sqrt{m^2+n^2}}\cdot\frac{(m^2+n^2)\alpha_{mn}\sin\theta-m\sqrt{m^2+n^2}\beta_{mn}\cos\theta}{m^2+n^2\sin^2\theta}\\
b_{mn}&=\frac{e^{\sqrt{m^2+n^2}d}}{2\pi\sqrt{m^2+n^2}}\cdot\frac{m\sqrt{m^2+n^2}\alpha_{mn}\cos\theta+(m^2+n^2)\beta_{mn}\sin\theta}{m^2+n^2\sin^2\theta}\\
c_{mn}&=\frac{e^{\sqrt{m^2+n^2}d}}{2\pi\sqrt{m^2+n^2}}\cdot\frac{(m^2+n^2)\gamma_{mn}\sin\theta-m\sqrt{m^2+n^2}\delta_{mn}\cos\theta}{m^2+n^2\sin^2\theta}\\
d_{mn}&=\frac{e^{\sqrt{m^2+n^2}d}}{2\pi\sqrt{m^2+n^2}}\cdot\frac{m\sqrt{m^2+n^2}\gamma_{mn}\cos\theta+(m^2+n^2)\delta_{mn}\sin\theta}{m^2+n^2\sin^2\theta}
\end{aligned}\right\}\quad(30).$$

$$(m^2+n^2\geqq1)$$

Substituting $(\alpha'_{mn}, \beta'_{mn}, \gamma'_{mn}, \delta'_{mn})$ or $(\alpha''_{mn}, \beta''_{mn}, \gamma''_{mn}, \delta''_{mn})$ for $(\alpha_{mn}, \beta_{mn}, \gamma_{mn}, \delta_{mn})$, which are connected with each other by the relations (29), we get the similar relations of $(a_{mn}, b_{mn}, c_{mn}, d_{mn})$ to $(\alpha'_{mn}, \beta'_{mn}, \gamma'_{mn}, \delta'_{mn})$ and to $(\alpha''_{mn}, \beta''_{mn}, \gamma''_{mn}, \delta''_{mn})$.

We, therefore, obtain the distribution of the intensity of magnetization $J(\xi\eta)$ on the subterranean plane of depth d from the earth's surface, substituting the calculated values of a_{mn}, b_{mn}, c_{mn} and d_{mn} in eq. (23).

In a special case in which the intensity of magnetization, and consequently the magnetic anomalies on the earth's surface, are invariable in the direction of the y-axis, then n in equations (23) and (30) would be taken as zero, whence they reduce to

$$J(\xi) = \sum_m a_m \cos m\xi + \sum_m b_m \sin m\xi \qquad (31),$$

and

$$\left.\begin{aligned} a_m &= \frac{e^{md}}{2\pi m}(\alpha_m \sin\theta - \beta_m \cos\theta) \\ b_m &= \frac{e^{md}}{2\pi m}(\alpha_m \cos\theta + \beta_m \sin\theta) \end{aligned}\right\} \qquad (32).$$

$$(m \geqq 1)$$

These relations are the same as in equations (9) and (8) in the two-dimensional case studied in §2.

CHAPTER II. Magnetic Anomalies and the Corresponding Magnetized Dykes.

§ 1. *Magnetic field due to the inclined magnetized dyke (a two dimensional case).*

The foregoing method, in which the subterranean distribution of masses is obtained by assuming that the mass is concentrated on a certain subterranean plane, is satisfactory for studying the magnetic anomalies due to the undulatory form of the boundary between the upper and lower strata or of the mass distribution of a small thickness. It would not be applicable, however, to an analysis of the magnetic anomalies due to dykes, batholiths, etc.

Another simple model must be resorted to for cases in which the mass distribution is like that in dykes, etc., as will now be shown.

We shall deal only with two-dimensional problems in this chapter. Let AA in Fig. 10 be the plane of the earth's surface, and XX an elementary plane on which are distributed the surface intensities of magnetization. We assume further that the distribution of intensity does not vary in the direction of OO', which makes an angle φ with the vertical, as shown in Fig. 10, and that the mass lies between depths d and d'.

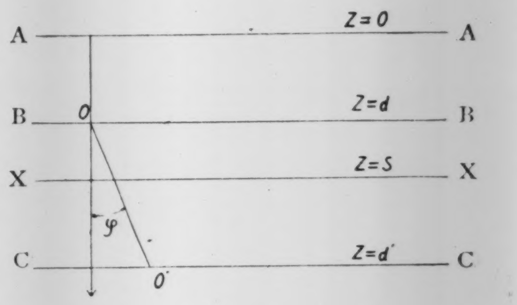

Fig. 9.

If we assume that the intensity distribution on plane BB at depth d is

$$J(\xi) = \sum_n a_n \cos n\xi + \sum_n b_n \sin n\xi \quad (1),$$

then the intensity distribution on an elementary plane at depth ζ is given by

$$J\left\{\xi - (\zeta - d)\tan\varphi\right\} = \sum_n a_n \cos n\left\{\xi - (\zeta - d)\tan\varphi\right\}$$
$$+ \sum_n b_n \sin n\left\{\xi - (\zeta - d)\tan\varphi\right\} \quad (2).$$

The magnetic potential at any point above plane BB due to the intensity distribution on this elementary plane of thickness $d\zeta$ is given by

$$d\psi = -2\pi\sum_n e^{-n(\zeta - z)}(a_n \sin\theta + b_n \cos\theta)\cos n\left\{x - (\zeta - d)\tan\varphi\right\}d\zeta$$
$$+ 2\pi\sum_n e^{-n(\zeta - z)}(a_n \cos\theta - b_n \sin\theta)\sin n\left\{x - (\zeta - d)\tan\varphi\right\}d\zeta \quad (3).$$

As already proved in §3, the potential due to the whole mass is

$$\psi(x) = -2\pi\sum_n \int_d^{d'} e^{-n(\zeta - z)}(a_n \sin\theta + b_n \cos\theta \cos n\left\{x - (\zeta - d)\tan\varphi\right\}d\zeta$$
$$+ 2\sum_n \int_d^{d'} e^{-n(\zeta - z)}(a_n \cos\theta - b_n \sin\theta)\sin n\left\{x - (\zeta - d)\tan\varphi\right\}d\zeta$$
$$= -2\pi\sum_n \left[\frac{e^{-n(d - z)}}{n}\cos\varphi\left\{a_n \sin(\theta + \varphi) + b_n \cos(\theta + \varphi)\right\}\right.$$
$$- \frac{e^{-n(d' - z)}}{n}\cos\varphi\left\{a_n \sin(\theta + \varphi + nD\tan\varphi)\right.$$
$$\left.\left. + b_n \cos(\theta + \varphi + nD\tan\varphi)\right\}\right]\cos nx$$

$$+2\pi\sum_{n}\Bigg[\frac{e^{-n(d-z)}}{n}\cos\varphi\Big\{a_n\cos(\theta+\varphi)-b_n\sin(\theta+\varphi)\Big\}$$
$$-\frac{e^{-n(d'-z)}}{n}\cos\varphi\Big\{a_n\cos(\theta+\varphi+nD\tan\varphi)$$
$$-b_n\sin(\theta+\varphi+nD\tan\varphi)\Big\}\Bigg]\sin nx \qquad (4),$$

where

$$D=d'-d\,.$$

Utilizing the same notations as in the foregoing chapter, we get

$$\left.\begin{aligned}
\alpha=-\beta'_n=&2\pi e^{-nd}\cos\varphi\Big\{a_n\sin(\theta+\varphi)+b_n\cos(\theta+\varphi)\Big\}\\
&-2\pi e^{-nd'}\cos\varphi\Big\{a_n\sin(\theta+\varphi+nD\tan\varphi)\\
&\qquad+b_n\cos(\theta+\varphi+nD\tan\varphi)\Big\}\\
\beta_n=\alpha'_n=&-2\pi e^{-nd}\cos\varphi\Big\{a_n\cos(\theta+\varphi)-b_n\sin(\theta+\varphi)\Big\}\\
&+2\pi e^{-nd'}\cos\varphi\Big\{a_n\cos(\theta+\varphi+nD\tan\varphi)\\
&\qquad-b_n\sin(\theta+\varphi+nD\tan\varphi)\Big\}
\end{aligned}\right\}\qquad(5).$$

Conversely, if α_n and β_n are deduced from the observed magnetic anomalies, the coefficients of the Fourier series for the intensity distribution on plane BB are given by

$$\left.\begin{aligned}
a_n=&\frac{e^{nd}}{2\pi\cos\varphi[1+e^{-2nD}-2e^{-nD}\cos(nD\tan\varphi)]}\Bigg[\alpha_n\Big\{\sin(\theta+\varphi)\\
&\qquad-e^{-nD}\sin(\theta+\varphi+nD\tan\varphi)\Big\}\\
&\qquad-\beta_n\Big\{\cos(\theta+\varphi)-e^{-nD}\cos(\theta+\varphi+nD\tan\varphi)\Big\}\Bigg]\\
b_n=&\frac{e^{nd}}{2\pi\cos\varphi[1+e^{-2nD}-2e^{-Dn}\cos(nD\tan\varphi)}\Bigg[\alpha_n\Big\{\cos(\theta+\varphi)\\
&\qquad-e^{-nD}\cos(\theta+\varphi+nD\tan\varphi)\Big\}\\
&\qquad+\beta_n\Big\{\sin(\theta+\varphi)-e^{-nD}\sin(\theta+\varphi+nD\tan\varphi)\Big\}\Bigg]
\end{aligned}\right\}\qquad(6).$$

With the aid of eq. (6), the intensity $J(\xi)$ can be calculated from the values of $Z(x)$ or $H(x)$ observed on the earth's surface, if either θ,

φ, d and d' are given from the other data or they are correctly assumed.

If d' were so large that the terms involving the factor e^{-nD} on the right-hand side of eq. (6) are negligible, matters will be greatly simplified, the coefficients a_n and b_n in this case being give by

$$\left.\begin{aligned} a_n &= \frac{e^{nd}}{2\pi\cos\varphi}\left\{\alpha_n\sin(\theta+\varphi)-\beta_n\cos(\theta+\varphi)\right\} \\ b_n &= \frac{e^{nd}}{2\pi\cos\varphi}\left\{\alpha_n\cos(\theta+\varphi)+\beta_n\sin(\theta+\varphi)\right\} \end{aligned}\right\} \qquad (7).$$

§ 2. *The Special case.*

In a number of actual cases, however, the value of φ, because it is unknown, is sought from the observed data. If $J(\xi)$ were a symmetric function with respect to ξ, it will be possible to determine the value of φ in terms of α_n and β_n. The origin of ξ in this case may not necessarily be in agreement with that of x.

If we assume that

$$J(\xi)=\sum_n a_n\cos n\xi,\quad b_n=0,\quad \xi=x+x_0 \qquad (8)$$

and

$$\left.\begin{aligned} Z(x) &= \sum_n \alpha_n\cos nx+\sum_n \beta_n\sin nx \\ H(x) &= \sum_n \alpha'_n\cos nx+\sum_n \beta'_n\sin nx \end{aligned}\right\} \qquad (9),$$

then the magnetic potential ψ is expressed by

$$\begin{aligned} \psi(x) = &-2\pi\sum_n \frac{e^{-n(d-z)}}{n}a_n\cos\varphi\Big\{\sin(\theta+\varphi) \\ &\qquad -e^{-nD}\sin(\theta+\varphi+nD\tan\varphi)\Big\}\cos n(x+x_0) \\ &+2\pi\sum_n \frac{e^{-n(d-z)}}{n}a_n\cos\varphi\Big\{\cos(\theta+\varphi) \\ &\qquad -e^{-nD}\cos(\theta+\varphi+nD\tan\varphi)\Big\}\sin n(x+x_0) \end{aligned} \qquad (10),$$

whence the Fourier coefficients of $Z(x)$ and $H(x)$ on the earth's surface are given by

$$\left.\begin{aligned}\alpha_n=-\beta'_n&=2\pi a_n e^{-nd}\cos\varphi\Big\{\sin(\theta+\varphi-nx_0)\\&\qquad-e^{-nD}\sin(\theta+\varphi+nD\tan\varphi-nx_0)\Big\}\\\beta_n=\alpha'_n&=2\pi a_n e^{-nd}\cos\varphi\Big\{-\cos(\theta+\varphi-ux_0)\\&\qquad+e^{-nD}\cos(\theta+\varphi+nD\tan\varphi-nx_0)\Big\}\end{aligned}\right\}\quad(11).$$

Conversely, if α_n and β_n are given, then

$$\left.\begin{aligned}a_n&=\frac{\alpha_n e^{nd}}{2\pi\cos\varphi\{\sin(\theta+\varphi-nx_0)-e^{-nD}\sin(\theta+\varphi+nD\tan\varphi-nx_0)\}}\\&\text{or}\\&=\frac{-\beta_n e^{nd}}{2\pi\cos\varphi\{\cos(\theta+\varphi-nx_0)-e^{-nD}\cos(\theta+\varphi+nD\tan\varphi-nx_0)\}}\\&\qquad\qquad(n\geqq1)\end{aligned}\right\}\quad(12),$$

and from eq. (12), we get

$$\begin{aligned}\alpha_n\cos(\theta+\varphi-nx_0)&+\beta_n\sin(\theta+\varphi-nx_0)\\&=e^{-nD}\Big\{\alpha_n\cos(\theta+\varphi+nD\tan\varphi-nx_0)\\&\qquad+\beta_n\sin(\theta+\varphi+nD\tan\varphi-nx_0)\Big\}\end{aligned}\quad(13).$$

Although it is theoretically possible to find the values of φ and x_0 through eq. (13), it is difficult to actually solve this equation. If, however, d' is so large that e^{-nD} becomes actually 0, we obtain

$$\left.\begin{aligned}a_n&=\frac{\alpha_n e^{nd}}{2\pi\cos\varphi\sin(\theta+\varphi-nx_0)}\\&\text{or}\\&=\frac{-\beta_n e^{nd}}{2\pi\cos\varphi\cos(\theta+\varphi-nx_0)}\end{aligned}\right\}\quad(14)$$

$$\tan(\theta+\varphi-nx_0)=-\frac{\alpha_n}{\beta_n}\quad(15).$$

Equation (15) gives the relation between n and $\tan(\theta+\varphi-nx_0)$. Taking the former as abscissa and plotting $-\frac{\alpha_n}{\beta_n}$ as ordinate, the relation is expressed by a straight line, the inclination of which gives the value of x_0, and the value of the ordinate at $n=0$ gives $\theta+\varphi$. Hence, if θ is given, φ can be determined. Substituting these values of x_0 and φ in eq. (14), we can determine the values of a_n, and consequently the distribution of $J(\xi)$.

§ 3. *Actual example.*

As an example, we give here a method of studing the magnetic anomalies, as found by the magnetic survey made by P. Lasareff[5] in Kursk. The smoothed curve of the observed valus is reproduced in Fig. 10 (a).

Table III.

n	α_n	β_n	α_n/β_n
1	$-0{\cdot}324$	$-0{\cdot}143$	$-2{\cdot}27$
2	$+0{\cdot}162$	$+0{\cdot}158$	$-1{\cdot}03$
3	$-0{\cdot}061$	$-0{\cdot}140$	$-0{\cdot}44$
4	$+0{\cdot}014$	$+0{\cdot}123$	$-0{\cdot}11$
5	$+0{\cdot}017$	$-0{\cdot}095$	$+0{\cdot}18$
6	$-0{\cdot}030$	$+0{\cdot}068$	$+0{\cdot}44$
7	$+0{\cdot}036$	$-0{\cdot}044$	$+0{\cdot}82$
8	$-0{\cdot}034$	$+0{\cdot}030$	$+1{\cdot}13$
9	$+0{\cdot}032$	$-0{\cdot}019$	$+1{\cdot}68$
10	$-0{\cdot}029$	$+0{\cdot}011$	$+2{\cdot}64$
11	$+0{\cdot}027$	$-0{\cdot}005$	$+5{\cdot}40$
12	$-0{\cdot}014$	—	—

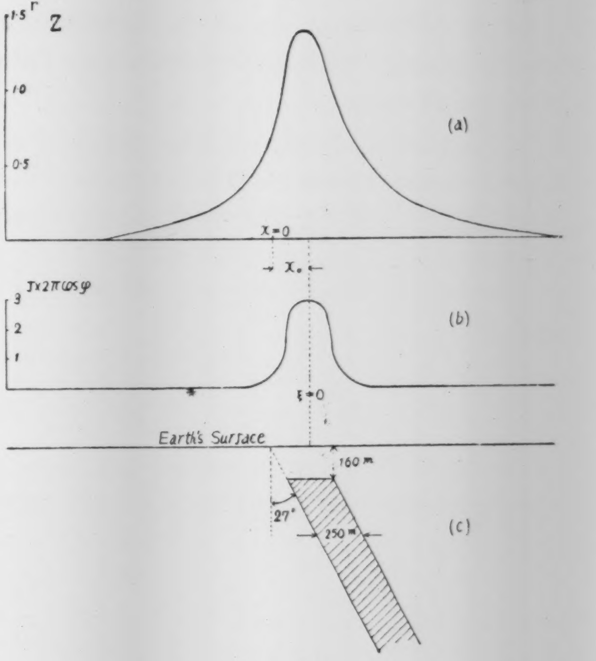

Fig. 10.
Magnetic Anomaly and Subterranean Structure in Kursk.

The curve is subjected to Fourier analysis. From the Fourier coefficients α_n and β_n thus obtained, we get Table III, together with the values of α_n/β_n.

By plotting these values of α_n/β_n, as in Fig. 11, against n which are taken as ordinates, x_0 and $\theta+\varphi$ are found to be

$$x_0 = -16°$$

$$\theta+\varphi = 105°.$$

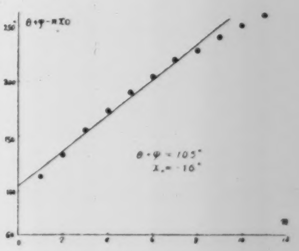

Fig. 11.

Since the total intensity and the dip angle of the normal magnetic field in Kursk are $0{\cdot}475\,\Gamma$ and 65° respectively, and since the direction in which the distribution of magnetization is considered invariant deviates by angle 26° west from the normal magnetic meridian in this district, the value of θ in the present case may be taken as 78°, whence φ becomes 27°.

---

[5] P. Lasareff, *Gerl. Beitr.*, **15** (1926), 71.

Substituting these values of x_0 and φ in eq. (14) with the assumption that $d=160$ m, we get the values of a_n, which give the distribution of intensity of magnetization $J(\xi)$ on the plane at depth d as shown in Fig. 10 (b). The subterranean mass distribution is derived from these results as shown in Fig. 10 (c). For the case in which the intensities of magnetization on the plane $z=d$ are regarded as being either 0 or a constant, I_0, it is possible to determine more accurately the width along which the constant intensity of I_0 is distributed, as will now be shown.

Assuming that, on the plane $Z=d$,

$$J(\xi)=O \qquad \text{at} \qquad \pi\geqq\xi>S, \quad -S>\xi\geqq-\pi$$

$$J(\xi)=I_0 \qquad \text{at} \qquad S>\xi>-S,$$

and

$$J(\xi)=\frac{I_0}{2} \qquad \text{at} \qquad \xi=S, \ \text{and} \ \xi=-S,$$

the intensity distribution $J(\xi)$ is expressed by the Fourier series

$$J(\xi)=\frac{SI_0}{\pi}+\frac{2I_0}{\pi}\sum_{n=1}^{\infty}\frac{\cos n\xi\sin nS}{n} \qquad (16).$$

In comparing eq. (16) with eq. (14), we get

$$a_n=\frac{2I_0\sin nS}{n\pi} \qquad (n\geqq1) \qquad (17),$$

whence we have

$$\frac{2I_0\sin nS}{n\pi}=\frac{e^{d}\alpha_n}{2\pi\cos\varphi\sin(\theta+\varphi-nx_0)}=\frac{-e^{d}\beta_n}{2\pi\,\mathrm{ccs}\,\varphi\cos(\theta+\varphi-nx_0)}$$

$$(n\geqq1) \qquad (18)$$

From this relation, we obtain the values of I_0 and S, and consequently the width of the mass. In the case of the magnetic anomalies at Kursk, the relation expressed by eq. (18) is as shown in Fig. 12, from which we have $I_0=0{\cdot}57$ and $S=130$ m.

These results agree well with the results of borings made by A. D, Archgelski,[6] as well as with the results of studies made by[7] H. Haalck, G. A. Gamburzeff and M. Polikaepoff,[8] P. Lasareff,[9] and others, as will be seen from Fig. 13.

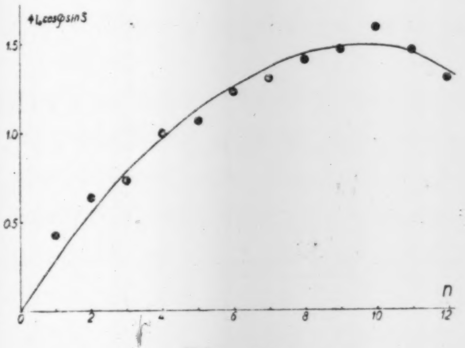

Fig. 12.

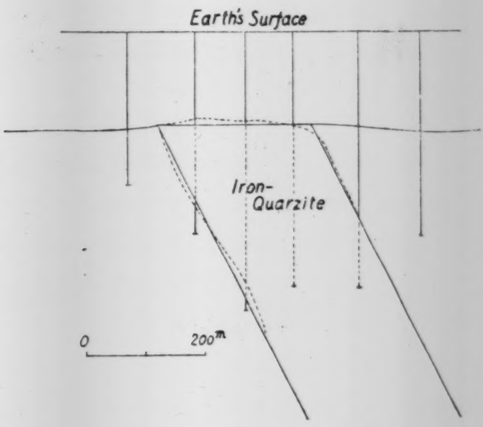

Fig. 13. Subterranean Structure in Kursk. Full lines; Calculated. Dotted lines. Results of Borings.

§ 4. *Magnetic field due to an inclined magnetized dyke* (*a three dimensional case*).

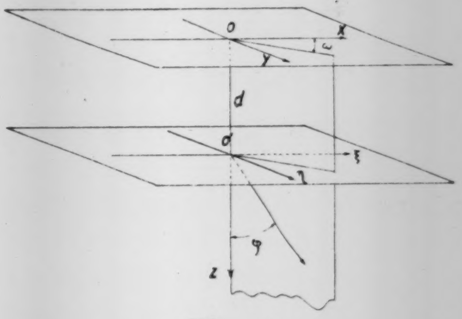

Fig. 14.

The problem studied in the foregoing paragraphs of this chapter, concerning the two-dimensional case will be extenped to the case of three dimensions. We assume that the intensity distribution on an elementary plane does not vary in the direction that is denoted by φ and ω in Fig. 14, and also that d' is infinitely large.

Although, the relations between the coefficients of the Fourier series representing the intensity disribution on the plane $z=d$ and those of the magnetic anomalies on the earth's surface should easily be found, theoretically, the actual calculations in this case are very laborious. The final relations alone are shown below, where α_{mn}, β_{mn}, γ_{mn}, ∂_{mn}, a_{mn}, b_{mn}, c_{mn} and d_{mn} denote the same quantities as those given in §4 in chapter I.

---

6) A. D. **Archagelski**, Transact. of the Special Comm. for the Study of the Kursk mag. Anomaly, vol. **7** (1926).

7) H. **Haalck**, *Gerl., Beitr.*, **22** (1929), 241, 219.

8) G. A. **Gamburzeff** u. M. **Polikaepoff**, *Gerl. Beitr.*, **19** (1928), 210, 219.

9) P. **Lasareff**, *Gerl. Beitr.*, **15** (1926), 91.

$$\left.\begin{aligned}
a_{mn}&=\frac{e^{-\sqrt{m^2+n^2}d}}{\pi}\,\frac{\alpha_{mn}\lambda_{mn}+\beta_{mn}\mu_{mn}+\gamma_{mn}\nu_{mn}-\delta_{mn}\chi_{mn}}{\sigma}\\
b_{mn}&=\frac{e^{-\sqrt{m^2+n^2}d}}{\pi}\,\frac{-\alpha_{mn}\mu_{mn}+\beta_{mn}\lambda_{mn}+\gamma_{mn}\chi_{mn}+\delta_{mn}\nu_{mn}}{\sigma}\\
c_{mn}&=\frac{e^{-\sqrt{m^2+n^2}d}}{\pi}\,\frac{-\alpha_{mn}\nu_{mn}+\beta_{mn}\chi_{mn}+\gamma_{mn}\lambda_{mn}+\delta_{mn}\mu_{mn}}{\sigma}\\
d_{mn}&=\frac{e^{-\sqrt{m^2+n^2}d}}{\pi}\,\frac{\alpha_{mn}\chi_{mn}+\beta_{mn}\nu_{mn}+\gamma_{mn}\mu_{mn}-\delta_{mn}\lambda_{mn}}{\sigma}
\end{aligned}\right\}\quad(19),$$

where

$$\left.\begin{aligned}
\lambda_{mn}&\equiv p_{mn}(p^2_{mn}+q^2_{mn}+r^2_{mn}-s^2_{mn})-2q_{mn}r_{mn}s_{mn},\\
\mu_{mn}&\equiv q_{mn}(p^2_{mn}+q^2_{mn}-r^2_{mn}+s^2_{mn})-2p_{mn}r_{mn}s_{mn},\\
\nu_{mn}&\equiv r_{mn}(p^2_{mn}-q^2_{mn}+r^2_{mn}+s^2_{mn})-2p_{mn}q_{mn}s_{mn},\\
\chi_{mn}&=s_{mn}(-p^2_{mn}+q^2_{mn}+r^2_{mn}+s^2_{mn})-2p_{mn}q_{mn}r_{mn},
\end{aligned}\right\}\quad(20),$$

where

$$\left.\begin{aligned}
p_{mn}&\equiv\sqrt{m^2+n^2}\sin\theta(P_{mn}+R_{mn})+m\cos\theta(Q_{mn}+S_{mn})\\
q_{mn}&\equiv\sqrt{m^2+n^2}\sin\theta(Q_{mn}+S_{mn})-m\cos\theta(P_{mn}+R_{mn})\\
r_{mn}&\equiv\sqrt{m^2+n^2}\sin\theta(Q_{mn}-S_{mn})-m\cos\theta(P_{mn}-R_{mn})\\
s_{mn}&\equiv\sqrt{m^2+n^2}\sin\theta(P_{mn}-R_{mn})+m\cos\theta(Q_{mn}-S_{mn})
\end{aligned}\right\}\quad(21),$$

where

$$\left.\begin{aligned}
P_{mn}&\equiv\frac{\sqrt{m^2+n^2}}{(m^2+n^2)+(m\cos\omega+n\sin\omega)^2\tan^2\varphi}\\
Q_{mn}&\equiv\frac{(m\cos\omega+n\sin\omega)\tan\varphi}{(m^2+n^2)+(m\cos\omega+n\sin\omega)^2\tan^2\varphi}\\
R_{mn}&\equiv\frac{\sqrt{m^2+n^2}}{(m^2+n^2)+(m\cos\omega-n\sin\omega)^2\tan^2\varphi}\\
S_{mn}&\equiv\frac{(m\cos\omega-n\sin\omega)\tan\varphi}{(m^2+n^2)+(m\cos\omega-n\sin\omega)^2\tan^2\varphi}\\
&\qquad\qquad(m^2+n^2\geqq1)
\end{aligned}\right\}\quad(22).$$

CHAPTER III. Magnetic Anomalies in Dip and Declination, and the Corresponding Subterranean Magnetized Plane.

§ 1. *The dip and the subterranean magnetized plane.*

In the foregoing chapters, the relations between the intensities of the magnetic force and the subterranean mass distribution to which the former are due, were studied. Although it is most desirable in magnetic surveys to observe either the vertical or horizontal components of the magnetic force in order to obtain accurate results, observations of dip by the dip-circle or by the earth-inductor are sometimes made, seeing that its absolute measurement is comparatively simple and easy.

The variations in the earth's magnetism both before and after the occurrence of earthquakes or volcanic eruptions, which have been studied by the geophysists in Japan, S. T. Nakamura and Y. Kato,[10] T. Minakami,[11] and the writer,[12] were measured in most cases with either a dip-circle or an earth-inductor. Since, in these cases, the maximum values of the variations are smaller than 30′, we may take the relation, approximately, to be

$$\tan(\theta_0+\Delta\theta)=\frac{Z_0+\Delta Z}{H_0+\Delta H}\fallingdotseq\tan\theta_0+\tan\theta_0\left(\frac{\Delta Z}{Z_0}-\frac{\Delta H}{H_0}\right)$$

$$\fallingdotseq\tan\theta_0+\tan\theta_0\left(\frac{\Delta Z}{Z_0}-\frac{\Delta X}{H_0}\right) \qquad (1),$$

where H_0, X_0 and Z_0 denote respectively the horizontal, northward, and downward components of the normal magnetic force, θ_0 the normal values of dip, ΔH, ΔX and $\Delta\theta$ denote their changes.

Then, by putting

$$f(\Delta\theta)=\frac{\tan(\theta_0+\Delta\theta)-\tan\theta_0}{\tan\theta_0} \qquad (2),$$

we have the relation

$$f(\Delta\theta)=\frac{\Delta Z}{Z_0}-\frac{\Delta X}{H_0} \qquad (3).$$

On the other hand, the following conditions are known regarding the magnetic field due to the subterranean mass distribution concentrated on a plane, as studied in Chapter I;

---

[10] S. T. Nakamura and Y. Kato, *Proc. Jmp. Acad. Japan*, **10** (1935) 456; **12** (1936), 64.

[11] T. Minakami, *Bull. Earthq. Res. Inst.*, **16** (1938), 100; 117.

[12] T. Nagata, *Bull. Earthq. Res. Inst.*, **15** (1937), 497.

If

$$\left.\begin{aligned}\varDelta Z&=\sum_m\sum_n(\alpha_{mn}\cos mx\cos ny+\beta_{mn}\sin mx\cos ny\\&\qquad+\gamma_{mn}\cos mx\sin ny+\delta_{mn}\sin mx\sin ny)\\\varDelta X&=\sum_m\sum_n(\alpha'_{mn}\cos mx\cos ny+\beta'_{mn}\sin mx\cos ny\\&\qquad+\gamma'_{mn}\cos mx\sin ny+\delta'_{mn}\sin mx\sin ny)\end{aligned}\right\}\quad(4),$$

then

$$\left.\begin{aligned}\frac{\alpha_{mn}}{\sqrt{m^2+n^2}}&=-\frac{\beta'_{mn}}{m},\qquad\frac{\beta_{mn}}{\sqrt{m^2+n^2}}=\frac{\alpha'_{mn}}{m}\\\frac{\gamma_{mn}}{\sqrt{m^2+n^2}}&=-\frac{\delta'_{mn}}{m},\qquad\frac{\delta_{mn}}{\sqrt{m^2+n^2}}=\frac{\gamma'_{mn}}{m}\end{aligned}\right\}\quad(5),$$

where

$$\left.\begin{aligned}\alpha_{mn}&=2\pi\sqrt{m^2+n^2}e^{-\sqrt{m^2+n^2}d}\left(a_{mn}\sin\theta_0+\frac{m}{\sqrt{m^2+n^2}}b_{mn}\cos\theta_0\right)\\\beta_{mn}&=2\pi\sqrt{m^2+n^2}e^{-\sqrt{m^2+n^2}d}\left(b_{mn}\sin\theta_0-\frac{m}{\sqrt{m^2+n^2}}a_{mn}\cos\theta_0\right)\\\gamma_{mn}&=2\pi\sqrt{m^2+n^2}e^{-\sqrt{m^2+n^2}d}\left(c_{mn}\sin\theta_0+\frac{m}{\sqrt{m^2+n^2}}d_{mn}\cos\theta_0\right)\\\delta_{mn}&=2\pi\sqrt{m^2+n^2}e^{-\sqrt{m^2+n^2}d}\left(d_{mn}\sin\theta_0-\frac{m}{\sqrt{m^2+n^2}}c_{mn}\cos\theta_0\right)\end{aligned}\right\}\quad(6).$$

Hence, from equations (3), (4) and (5) we get

$$\begin{aligned}f(\varDelta\theta)=\sum_m\sum_n\Bigg[&\left(\frac{\alpha_{mn}}{Z_0}-\frac{m}{H_0\sqrt{m^2+n^2}}\beta_{mn}\right)\cos mx\cos ny\\&+\left(\frac{\beta_{mn}}{Z_0}+\frac{m}{H_0\sqrt{m^2+n^2}}\alpha_{mn}\right)\sin mx\cos ny\\&+\left(\frac{\gamma_{mn}}{Z_0}-\frac{m}{H_0\sqrt{m^2+n^2}}\delta_{mn}\right)\cos mx\sin ny\\&+\left(\frac{\delta_{mn}}{Z_0}+\frac{m}{H_0\sqrt{m^2+n^2}}\gamma_{mn}\right)\sin mx\sin ny\Bigg]\end{aligned}\quad(7).$$

If we assume that $f(\varDelta\theta)$ is expressed by double Fourier series as

$$f(\varDelta\theta)=\sum_m\sum_n A_{mn}\cos mx\cos ny+\sum_m\sum_n B_{mn}\sin mx\cos ny$$
$$+\sum_m\sum_n C_{mn}\cos mx\sin ny+\sum_m\sum_n D_{mn}\sin mx\sin ny \qquad (8),$$

then the Fourier coefficients of this series are given by

$$\left.\begin{aligned}
A_{mn}&=2\pi e^{-\sqrt{m^2+n^2}d}\sqrt{m^2+n^2}\,(\lambda_{mn}a_{mn}+\mu_{mn}b_{mn})\\
B_{mn}&=2\pi e^{-\sqrt{m^2+n^2}d}\sqrt{m^2+n^2}\,(-\mu_{mn}a_{mn}+\lambda_{mn}b_{mn})\\
C_{mn}&=2\pi e^{-\sqrt{m^2+n^2}d}\sqrt{m^2+n^2}\,(\lambda_{mn}c_{mn}+\mu_{mn}d_{mn})\\
D_{mn}&=2\pi e^{-\sqrt{m^2+n^2}d}\sqrt{m^2+n^2}\,(-\mu_{mn}c_{mn}+\lambda_{mn}d_{mn})
\end{aligned}\right\}\qquad (9),$$

where

$$\left.\begin{aligned}
\lambda_{mn}&\equiv\left(\frac{1}{Z_0}\sin\theta_0+\frac{1}{H_0}\frac{m^2}{m^2+n^2}\cos\theta_0\right)\\
\mu_{mn}&\equiv\frac{m}{\sqrt{m^2+n^2}}\left(\frac{\cos\theta_0}{Z_0}-\frac{\sin\theta_0}{H_0}\right)
\end{aligned}\right\}\qquad (10).$$

If the direction of magnetization of the subterranean mass coincides with the direction of the dip angle of the normal magnetic field, i.e. $Z_0=F_0\sin\theta$, $H_0=F_0\cos\theta$, where F_0 is the total magnetic intensity, then

$$\left.\begin{aligned}
\lambda_{mn}&=\frac{1}{F_0}\left(1+\frac{m^2}{m^2+n^2}\right)\\
\mu_{mn}&=\frac{1}{F_0}\,\frac{m}{\sqrt{m^2+n^2}}\left(\cot\theta_0-\tan\theta_0\right)
\end{aligned}\right\}\qquad (11).$$

Conversely, if A_{mn}, B_{mn}, C_{mn} and D_{mn} are given from observed data, then

$$\left.\begin{aligned}
a_{mn}&=\frac{e^{\sqrt{m^2+n^2}d}}{2\pi\sqrt{m^2+n^2}}\cdot\frac{\lambda_{mn}A_{mn}-\mu_{mn}B_{mn}}{\lambda_{mn}^2+\mu_{mn}^2}\\
b_{mn}&=\frac{e^{\sqrt{m^2+n^2}d}}{2\pi\sqrt{m^2+n^2}}\cdot\frac{\mu_{mn}A_{mn}+\lambda_{mn}B_{mn}}{\lambda_{mn}^2+\mu_{mn}^2}\\
c_{mn}&=\frac{e^{\sqrt{m^2+n^2}d}}{2\pi\sqrt{m^2+n^2}}\cdot\frac{\lambda_{mn}C_{mn}-\mu_{mn}D_{mn}}{\lambda_{mn}^2+\mu_{mn}^2}\\
d_{mn}&=\frac{e^{\sqrt{m^2+n^2}d}}{2\pi\sqrt{m^2+n^2}}\cdot\frac{\mu_{mn}C_{mn}+\lambda_{mn}D_{mn}}{\lambda_{mn}^2+\mu_{mn}^2}
\end{aligned}\right\}\qquad (12).$$

Substituting these values in

$$J(\xi\eta)=\sum_m\sum_n a_{mn}\cos m\xi\cos n\eta+\sum_m\sum_n b_{mn}\sin m\xi\cos n\eta+\sum_m\sum_n c_{mn}\cos m\xi\sin n\eta+\sum_m\sum_n d\sin m\xi\sin n\eta \quad (13),$$

we get the intensity distribution on a subterranean plane at depth d from the earth's surface.

These relations will be used not only in the analysis of the variations in the magnetic field, but also in that of local magnetic anomalies, where the largest value of deviations from the mean value of dip does not exceed a few degrees.

§ 2. *Actual example.*

Soon after the great earthquake of North Idu, in 1930, S. T. Nakamura13) observed the dip angles of the earth's magnetism at 20 stations on both sides of the Tanna fault. From re-observations carried out at these stations in 1934, the secular variations during this period were found to be systematically distributed as shown in Fig. 15. The anomalous variations in dip were subjected to double Fourier analysis. Substituting coefficients A_{mn}, B_{mn}, C_{mn} and D_{mn} thus obtained in eq. (12) with the assumption that $d=250$ m and $\theta_0=48°$, we obtained the values

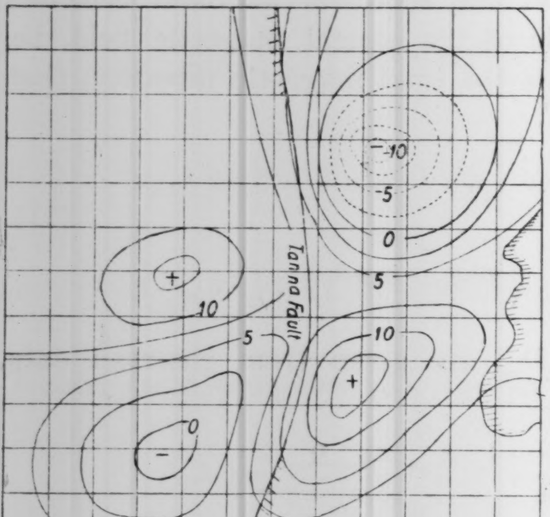

Fig. 15. Secular Variation in Magnetic Dip during the Period of from 1930 to 1934, in North Idu. (From the results of Nakamura's Survey)

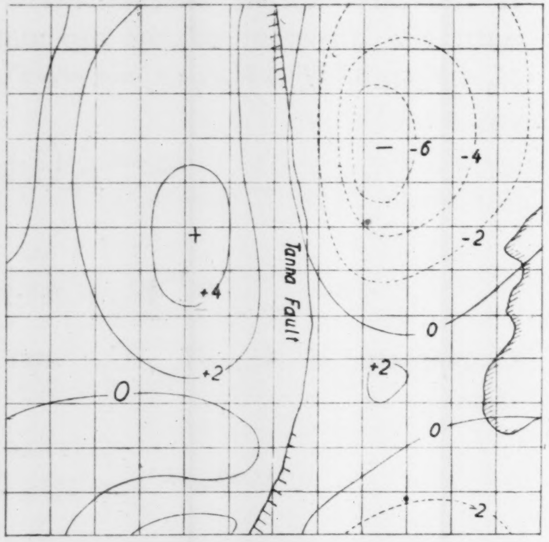

Fig. 16. Changes in the Intensity of Magnetization on the assumed Subterranean plane. Numerals denote $J\times 3{\cdot}3\times10^4$.

---

13) S. T. NAKAMURA, *Proc. Imp. Acad. Japan*, **10** (1934), 456.

of a_{mn}, b_{mn}, c_{mn} and d_{mn}. Substituting these value in eq. (13), we obtained the result shown in Fig. 16.

In Fig. 16, it will be noticed that the distribution of intensity is positive on the west side of the fault and negative on the east side. If this variation in magnetic intensity is due to the rising or sinking of the subterranean stratum, the intensity of magnetization of which exceeds that of the upper layer of soil, we may conclude that the upper boundary of the subterranean stratum rose on the west side and sank in the east side during the period from 1930 to 1934.

According to the result of Yamaguti's study(14) on the deformation of the earth's crust associated with the earthquake, the vertical displacements were positive (upward) on the eastern side of the fault and negative (downward) on the western side. The areal dilatation was also positive on the eastern side and negative on the western side. These facts show that, on the eastern side of the fault the earth's crust was elevated as well as expanded, whereas on the western side, it was sunk as well as contracted by a certain force that associated the earthquake. From the fact that the mode of post-seismic crustal deformation, as estimated from our analysis is, however, contrary to the mode of deformation as deduced from the results of geodetic triangulations, it may be concluded that the deformation of the earth's crust associated with the 1930 earthquake has been restored to some extent during the period 1930∼1934.

§ 3. *Declination and the subterranean magnetized plane.*

If the distribution of anomalies in declination is given instead of that of dip, the intensity distribution on an assumed plane is also obtainable, provided the anomalies are small.

We assume that

$$\begin{aligned}\tan\delta=&\sum_m\sum_n A_{mn}\cos mx\cos ny+\sum_m\sum_n B_{mn}\sin mx\cos ny\\&+\sum_m\sum_n C_{mn}\cos mx\sin ny+\sum_m\sum_n D_{mn}\sin mx\sin ny\qquad(14),\end{aligned}$$

where δ denotes the anomaly in the declination on the earth's surface.(14) We then get

$$a_{mn}=-\frac{X_0e^{\sqrt{m^2+n^2}\,d}}{2\pi n}\cdot\frac{(m^2+n^2)C_{mn}\sin\theta-m\sqrt{m^2+n^2}D_{mn}\cos\theta}{m^2+n^2\sin^2\theta}$$

---

14) S. YAMAGUTI, *Bull. Earthq. Res. Inst.*, **15** (1937), 899.

$$\left.\begin{aligned} b_{mn} &= -\frac{X_0 e^{\sqrt{m^2+n^2}\,d}}{2\pi n}\cdot\frac{m\sqrt{m^2+n^2}C_{mn}\cos\theta + m\sqrt{m^2+n^2}D_{mn}\sin\theta}{m^2+n^2\sin^2\theta} \\ c_{mn} &= -\frac{X_0 e^{\sqrt{m^2+n^2}\,d}}{2\pi n}\cdot\frac{(m^2+n^2)A_{mn}\sin\theta - m\sqrt{m^2+n^2}B_{mn}\cos\theta}{m^2+n^2\sin^2\theta} \\ d_{mn} &= -\frac{X_0 e^{\sqrt{m^2+n^2}\,d}}{2\pi n}\cdot\frac{m\sqrt{m^2+n^2}A_{mn}\cos\theta + (m^2+n^2)B_{mn}\sin\theta}{m^2+n^2\sin^2\theta} \end{aligned}\right\} \quad (15)$$

where X_0 denotes the northward component of the earth's normal magnetic force, since

$$\tan\delta = \frac{Y}{X_0} \quad .$$

Eq. (15) can then be applied with little error to the case in which the maximum value of δ does not exceed a few degrees.

Conclusion.

The foregoing methods of finding the subterranean mass distribution directly from the observed magnetic anomalies on the earth's surface may be applied to a number of actual cases. If, however, the undulation of the earth's surface is so large that the surface connot be taken as a horizontal plane, it may not be possible to apply the foregoing methods directly to the results of observation on the surface. In such cases, the observed values must be reduced to those on a horizontal plane with the aid of suitable correction formulae, for instance, Tanakadate's correction formula. This problem is now receiving the attention of the writer.

In conclusion, the writer wishes to express his sincerest thanks to Dr. C. Tsuboi for his valuable advices and suggestions throughout the course of this study. His hearty thanks are also due to Dr. R. Takahasi and Dr. N. Miyabe for their kind advices in the present work.

41. 地磁氣異常と地下構造

地震研究所 永田 武

地磁氣の局部異常の原因として，地下に帶磁物質の存在を考へて，其の分布を求めるのに，從來の方法は專ら適當な模型を考へて，之に因る磁力場が實際に測定された値に一致するかどうかを檢するといふ方針である．然し與へられた觀測値から直接に地下の物質の分布狀態を求める事が最も望ましい．現在の磁氣測定に於ける如く，地表での磁力の分布のみが與へられてゐる場合に一義的に問題の解を求める事は不可能であるが，適當な假定を與へれば之を近似的に求める事が出來る．

第 1 章．

地下の異常物質の鉛直方向への擴りがあまり大きくない場合や，帶磁の强さの異る二層があまり凹凸の量が大きくない曲面で境されてゐる場合等には，之等を地下適當な深さ d にある水平面，又は厚さ D の水平層の帶磁の强さの分布に置き換へる事が出來る．地表の磁氣異常の分布を一つの調和級數で表はす時，その係數と求める地下平面又は水平層の帶磁の强さの分布を同じ調和級數で表はす場合の相對應する係數との間に一義的の關係が成立するから，本論文の (7)，(10)，(30) 式等によつて，前者から後者を決定する事が出來る．Eötvös の有名な例，其の他の實際例に應用した結果，地下の異常物質が鉛直方向へ相當大きな擴りを持つ場合 (d と同程度) や，二層の境界面の凹凸の大きさが d に近い樣な場合にも，上記の假定による方法を適用して，實際問題としては充分な精度で問題を解決出來る事を知つた．

第 2 章．

Dyke や Batholith の樣に，鉛直方向への擴りが非常に大きい場合には，第一章の關係は適用出來ない．此の場合に物質の分布狀態が鉛直線とある角を爲す一定方向へは全く一樣に續いてゐるといふ假定が宥される場合には，やはり比較的簡單に問題の解を求める事が出來る．實例として，Kursk の磁氣測定の結果に之を應用して諸家の研究やボーリングの結果と非常に良く一致する事を示す．

第 3 章．

觀測値が伏角又は偏角で與へられてゐる場合にも，其の異常量が數度の範圍內にあれば，簡單な關係式で近似的の解が求められる．之を北伊豆地震後の丹那斷層兩側に於ける伏角の永年異常變化の分布に適用して，興味ある結果を得た．

42. Crustal Deformations in Central Taiwan. Part 2.

By Naomi MIYABE, Mituo HUKUNAGA and
Mitunosuke SATO,

Earthquake Research Institute.

(Read May 20, 1938. Received June 20, 1938.)

1. In their preceding paper, two of the present writers, Hukunaga and Sato, dealt with the crustal deformations in Central Taiwan based on the data of horizontal displacements of primary triangulation points and the vertical displacements of bench-marks on the lines of levels traversing the region under consideration.[1]

Since then a re-triangulation of the secondary and tertiary triangulation points distributed in the same region has been done, as a result of which the horizontal and vertical displacements of the secondary and tertiary triangulation points were measured.[2]

In the present paper, the writers discuss, in greater detail than in the last, the modes of crustal deformations in the regions that were most disturbed by the destructive earthquake of 1935, with the data of the horizontal and vertical displacements of the secondary and tertiary triangulation points as reference.

Since, in determining the positions of tertiary triangulation points, the Military Land Survey measured them with reference to the primary triangulation points, the horizontal displacements of the tertiary triangulation points are affected considerably by displacements of the surrounding primary triangulation points, with the result that the general mode of crustal deformation as studied by using the data of displacements of the secondary and tertiary triangulation points is not likely to differ much from that obtained by a study of the displacements of the primary triangulation points, as given in the preceding paper (Part 1).

In this paper, the crustal deformations are discussed in greater detail, particularly in connection with the active faults that appeared at the time of the destructive earthquake, based on the data of displacements of the secondary and tertiary triangulation points,[3] as will now be shown.

---

[1] M. SATO and M. HUKUNAGA, *Bull. Earthq. Res. Inst.*, **16** (1938), 300—316.

[2] Report of the Military Land Survey issued in 1936.

[3] The distribution of horizontal displacements of the triangulation points, which were used as data in the present study, is shown reproduced in Fig. 1.

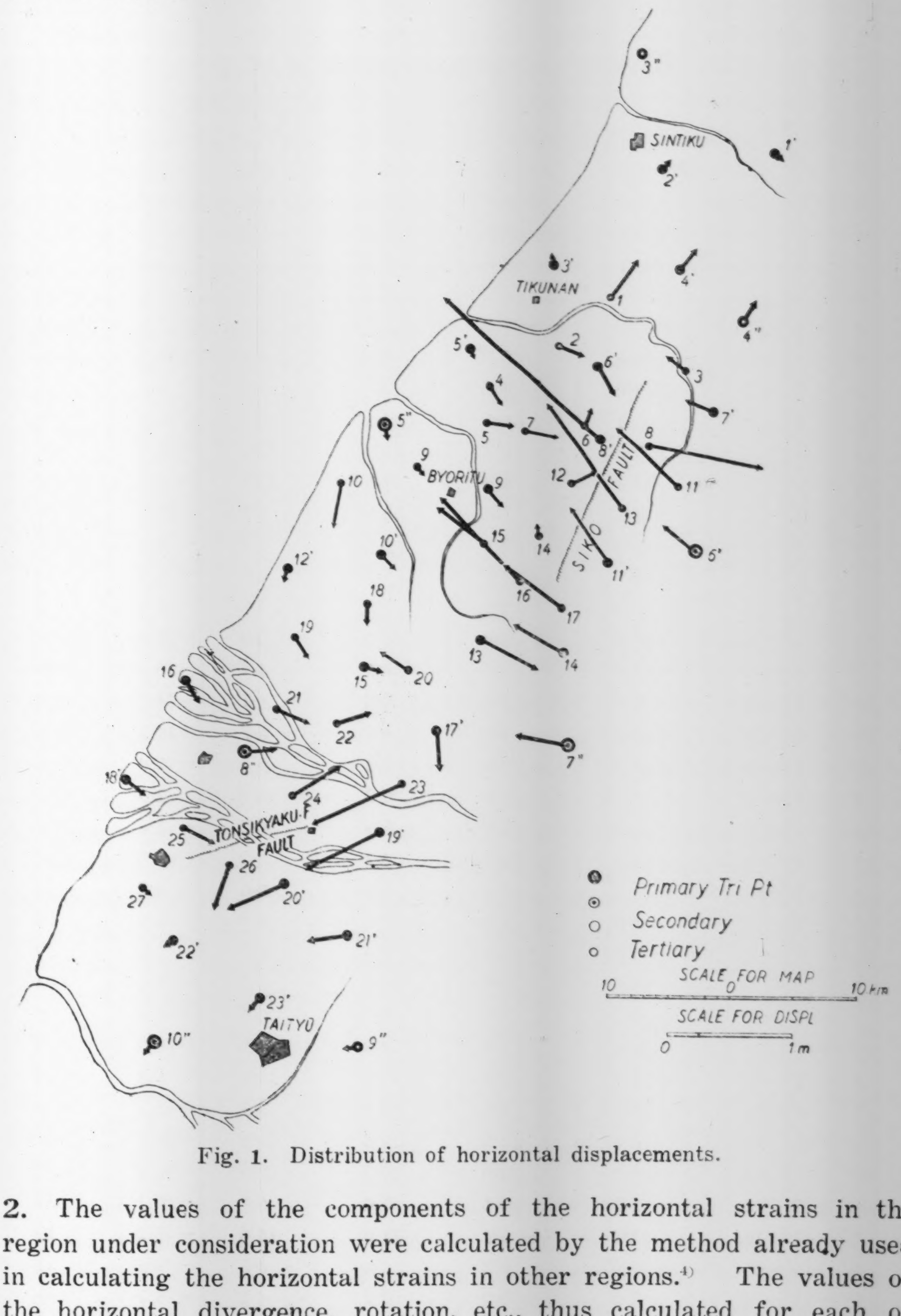
3"
SINTIKU
1'
2'
3'
TIKUNAN
1
4'
4"
5'
2
6'
3
7'
4
5"
5
7
6
8'
8
9
BYORITU
9
12
11
FAULT
SIKO
13
10
6"
15
14
10'
11'
12'
16
17
18
19
13
14
16'
15
20
21
22
17'
7"
8"
18'
23
24
TONSIKYAKU-F FAULT
19'
25
26
20'
27
22'
21'
Primary Tri Pt
Secondary
Tertiary
SCALE FOR MAP
10
0
10 km
SCALE FOR DISPL
0
1 m
23'
TAITYŪ
10"
9"

Fig. 1. Distribution of horizontal displacements.

2. The values of the components of the horizontal strains in the region under consideration were calculated by the method already used in calculating the horizontal strains in other regions.[4] The values of the horizontal divergence, rotation, etc., thus calculated for each of

---

[4] T. TERADA and N. MIYABE, *Bull. Earthq. Res. Inst.*, 7 (1929), 233∼240.

the triangular areas, with the triangulation points at their vertices, are given in Table I.

Table I. Horizontal strains in 10^{-6}.

Triangle	Δ	ω	S_m	γ_1	γ_2	θ_1
3″ — 1′ — 2′	+ 0·5	− 0·2	2·2	1·7	− 2·7	−34°
3″ — 2′ — 2′	1·0	0·5	2·0	3·0	− 1·0	− 5
1′ — 2′ — 4′	− 0·9	0·1	2·8	1·9	− 3·7	−31
2′ — 3′ — 4′	1·1	0·8	2·5	3·6	− 1·4	− 5
4″ — 1′ — 4′	− 2·4	− 0·1	1·1	− 1·3	− 3·5	−30
4″ — 4′ — 1	− 4·2	− 0·8	3·2	− 1·0	− 7·4	−21
4′ — 3′ — 1	− 4·8	2·5	9·2	4·4	−14·0	−11
3′ — 1 — 2	6·6	4·4	3·3	9·9	3·3	58
3′ — 5′ — 2	5·1	1·6	3·1	8·2	2·0	−46
1 — 2 — 6′	9·4	− 0·7	12·8	22·2	− 3·4	85
4′ — 1 — 6′	10·4	− 1·3	11·6	22·0	− 1·2	88
4″ — 3 — 6′	− 7·2	− 3·2	16·0	8·8	−23·2	48
4″ — 3′ — 7′	3·5	− 2·1	4·6	8·1	− 1·1	36
7′ — 3 — 11	− 1·3	− 4·5	5·3	4·0	− 6·0	−12
3 — 11 — 13	− 2·5	− 7·5	5·5	3·0	− 8·0	− 8
3 — 6 — 13	−15·8	− 0·8	13·0	− 2·8	−28·8	40
3 — 6 — 6′	−12·5	1·3	8·1	− 4·4	−20·6	30
6′ — 2 — 6	− 7·9	− 4·6	6·8	− 1·1	−14·7	− 9
2 — 6 — 7	− 7·4	1·9	6·7	− 0·7	−14·1	55
2 — 4 — 7	1·7	2·0	4·1	5·8	− 2·4	− 5
2 — 4 — 5′	4·2	0·6	2·3	6·5	1·9	−35
5″ — 5′ — 5	2·3	2·2	3·9	6·2	− 1·6	−11
5″ — 5 — 9	2·1	0·3	4·1	6·2	− 2·0	20
5″ — 9 — 10	3·7	1·8	4·9	8·6	− 1·2	46
5 — 9 — 9′	4·2	− 1·3	1·2	5·4	3·0	64
5 — 7 — 9′	3·9	− 1·4	2·3	6·2	1·6	59
7 — 12 — 9′	0·7	0·5	6·8	7·5	− 6·1	41
6 — 7 — 12	− 4·1	3·2	4·7	0·6	− 8·8	76
6 — 12 — 13	−24·0	− 8·4	28·2	4·2	−52·2	63
6″ — 11 — 13	5·1	− 3·4	13·5	18·6	− 8·4	−40
6″ — 11′ — 13	12·2	0·0	15·5	27·7	− 3·3	−60
11′ — 13 — 14	0·0	12·5	20·6	20·6	−20·6	67
12 — 13 — 14	−26·7	0·0	29·3	2·6	−56·0	52
9′ — 12 — 14	− 1·7	− 0·1	8·4	6·7	−10·1	34
9′ — 14 — 15	3·8	− 6·7	11·0	14·8	− 7·2	19
9′ — 10′ — 15	− 4·9	0·2	4·6	− 0·3	− 9·5	31
9′ — 10′ — 9	2·0	0·2	2·2	4·2	− 0·2	−48

(to be continued.)

Table I. (*continued.*)

Triangle	Δ	ω	S_m	γ_1	γ_2	θ_1
10′—9—10	0·9	3·4	4·4	5·3	−3·5	19°
10′—12′—10	−0·8	1·4	6·6	5·8	−7·4	−3
10′—12′—18	−1·9	−1·8	5·0	3·1	−6·9	75
10′—14—18	−0·5	−0·8	5·5	5·0	−6·0	57
14—16—18	−26·7	−5·0	31·8	5·1	−58·5	39
14—15—16	−7·6	−8·4	23·9	16·3	−31·5	15
14—16—11′	−20·4	−7·1	24·0	3·6	−44·4	18
11′—16—17	12·6	−3·1	6·9	19·5	5·7	−63
14′—16—17	5·6	−8·9	22·2	27·8	−16·6	−46
14′—13′—16	0·0	7·3	25·4	25·4	−25·4	−84
13′—16—18	18·6	18·7	36·4	55·0	−17·8	−63
10′—13′—18	6·8	−1·2	4·6	11·4	2·2	10
12′—18—19	4·0	1·0	3·3	7·3	0·7	−31
12′—16′—19	2·1	1·0	3·0	5·1	−0·9	−48
15′—18—19	−2·8	2·2	3·2	0·4	−6·0	−22
13′—15′—18	1·7	1·0	8·0	9·7	−6·3	−18
13′—17′—20	18·8	−4·8	10·6	29·4	8·2	−28
13′—15′—17′	3·8	−3·8	2·4	6·2	1·4	50
13′—14′—17′	−11·7	−1·7	18·6	6·9	−30·3	58
7′—14′—17′	−2·0	2·2	7·8	5·8	−9·8	77
15′—17′—22	−3·7	−2·1	6·3	2·6	−10·0	−55
15′—19—22	−3·2	1·5	3·6	0·4	−6·8	−12
19—21—92	−2·4	3·1	1·4	1·0	−3·8	23
16′—19—21	0·1	1·8	3·4	3·5	−3·3	−26
8″—16′—21	−1·2	0·1	5·4	4·2	−6·6	−5
8″—16′—18′	0·0	1·6	2·9	2·9	−2·9	9
8″—21—22	−4·9	1·0	5·9	1·0	−10·8	15
17′—22—23	−1·2	−12·5	16·6	15·4	−17·8	58
19′—22—23	−14·5	−4·5	18·8	4·3	−33·3	−87
19′—22—24	−9·6	−5·9	12·5	2·9	−22·1	−86
8″—22—24	−3·2	2·6	5·2	2·0	−8·4	−1
8″—24—25	0·7	3·1	4·9	5·6	−4·2	22
8″—18′—25	2·6	1·2	0·4	3·0	2·2	31
18′—25—27	2·5	−1·6	4·3	6·8	−1·8	4
24—25—26	8·0	−4·6	16·0	24·0	−8·0	69
20′—24—26	3·8	−3·5	20·5	24·3	−16·7	59
19′—20′—24	−3·3	−8·8	18·2	14·9	−21·5	78
19′—20′—21′	−3·2	−1·8	4·2	1·0	−7·4	−19
25—26—27	−3·0	−6·3	7·0	4·0	−10·0	87
22′—26—27	−5·1	−2·8	3·0	−2·1	−8·1	−56

(*to be continued.*)

Table I. (*continued.*)

Triangle	Δ	ω	S_m	γ_1	γ_2	θ_1
20′ −22′−26	−10·9	−0·8	4·3	−6·6	−15·2	47°
20′ −22′−23′	−3·2	1·0	4·9	1·7	−8·1	−55
20′ −21′−23′	−2·1	2·8	1·9	−0·2	−4·0	−34
9″−21′−23′	−1·8	1·8	2·1	0·3	−3·9	−66
10″−22′−23	0·1	−0·2	1·1	1·8	−0·4	−85

The geographical distributions of these horizontal strains, i. e. divergence Δ, rotation ω, maximum shear S_m, and the principal strains γ_1, γ_2, are shown in Figs. 2∼5, respectively.

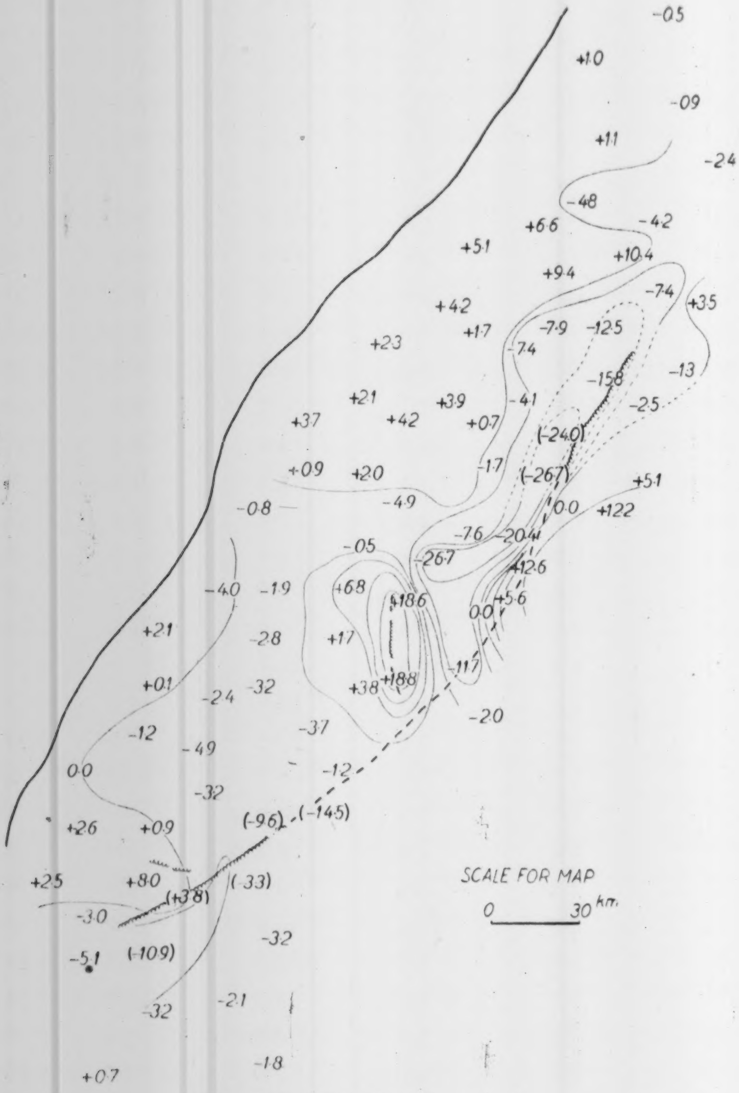
-05
+1.0
-09
+11
-24
-48
+6.6
-42
+5.1
+10.4
+9.4
-7.4
+35
+4.2
+1.7
-7.9
-12.5
+23
-7.4
-15.8
-13
+2.1
+3.9
-4.1
-25
+3.7
+4.2
+0.7
(-24.0)
+0.9
+2.0
-1.7
(-26.7)
+5.1
-0.8
-4.9
0.0
+12.2
-0.5
-7.6
-20.4
-26.7
+12.6
-4.0
-1.9
+6.8
+18.6
+5.6
0.0
+2.1
-2.8
+1.7
+0.1
-2.4
-3.2
+3.8
+18.8
-11.7
-20
-1.2
-3.7
-4.9
0.0
-1.2
-3.2
(-9.6)
(-14.5)
+2.6
+0.9
+2.5
+8.0
(+3.8)
(3.3)
SCALE FOR MAP
0
30 km.
-3.0
-3.2
-5.1
(-10.9)
-3.2
-2.1
-1.8
+0.7

Fig. 2. Distribution of Δ.

In drawing the lines of iso-Δ, and iso-S_m, as in Figs. 2 and

4, the values of the strains in areas traversed by active faults are neglected.

As to the distributions of these horizontal strains, shown in Figs. 2~5, the following points will be noticed.

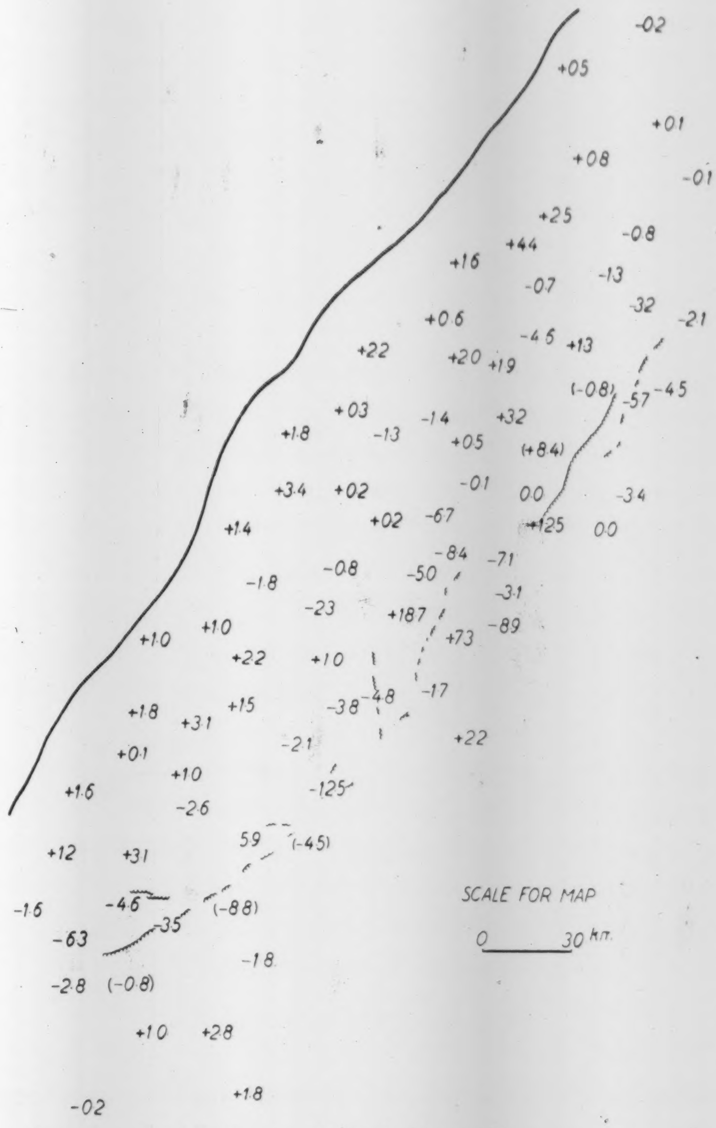
-02
+05
+01
+08
-01
+25
-08
+44
+16
-07
-13
-32
-21
+0.6
-4.5
+13
+22
+20
+19
(-0.8)
-57
-4.5
+03
-1.4
+32
+1.8
-13
+05
(+8.4)
+3.4
+02
-01
0.0
-3.4
+02
-67
+125
0.0
+1.4
-8.4
-71
-0.8
-50
-1.8
-3.1
-23
+187
+73
-89
+1.0
+1.0
+2.2
+1.0
-17
-3.8
-4.8
+1.8
+3.1
+15
-2.1
+22
+0.1
+1.0
-125
+1.6
-2.6
5.9
(-4.5)
+12
+31
-1.6
-4.6
(-8.8)
-35
-63
-1.8
-2.8
(-0.8)
+1.0
+2.8
+1.8
-02
SCALE FOR MAP
0
30 km.

Fig. 3. Distribution of ω.

(i) In the distribution of horizontal divergence, and of maximum shear, a zone of maximum disturbances was found on the western side of the Siko fault, parallel to the trend of the fault and close to it.

(ii) Upon extending the line that represents the trend of the active Siko fault southward to connect with the northeastern end of the line of the Tonsikyaku fault, the existence of which was also found at the time of the destructive earthquake of 1935, it was noticed that the

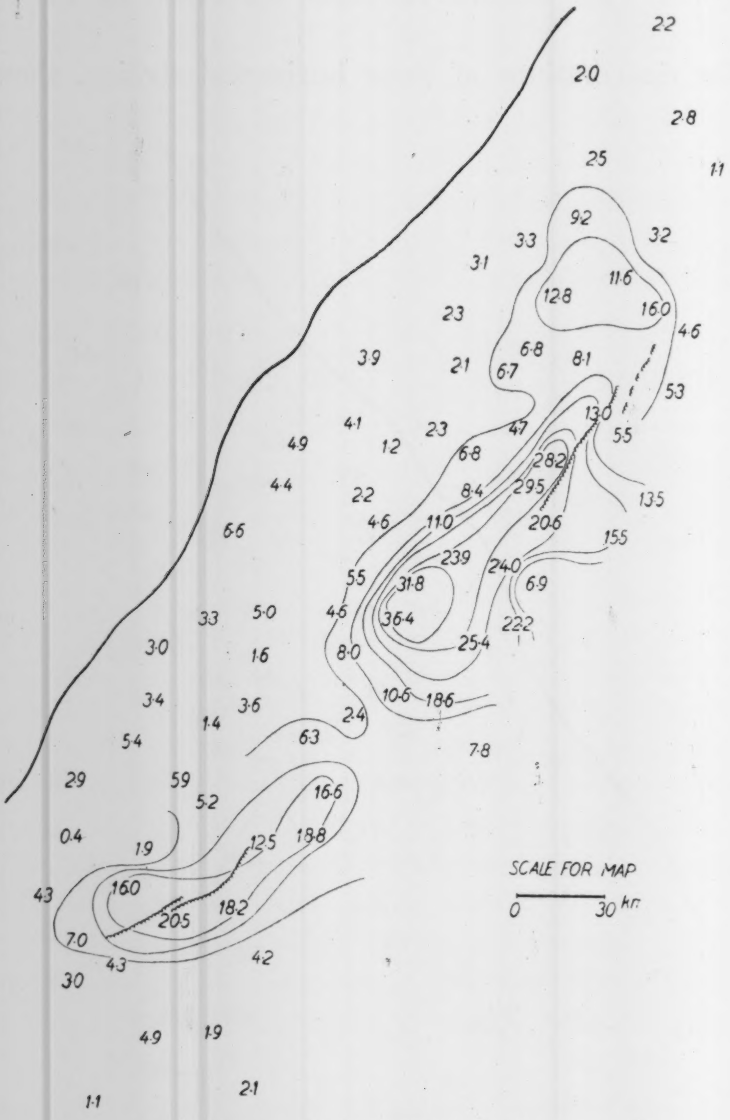
22
2·0
2·8
25
1·1
9·2
3·3
3·2
3·1
11·6
12·8
16·0
23
4·6
6·8
8·1
3·9
2·1
6·7
53
13·0
4·1
2·3
47
5·5
4·9
1·2
6·8
28·2
4·4
2·2
8·4
29·5
13·5
4·6
11·0
20·6
6·6
15·5
23·9
24·0
5·5
31·8
6·9
33
5·0
4·6
36·4
22·2
3·0
1·6
8·0
25·4
3·4
3·6
10·6
18·6
1·4
2·4
5·4
6·3
7·8
29
59
5·2
16·6
0.4
1·9
12·5
18·8
SCALE FOR MAP
43
16·0
0
30 km
18·2
20·5
7·0
4·3
4·2
30
4·9
1·9
2·1
1·1

Fig. 4. Distribution of S_m.

zone of maximum disturbance is situated on the western side of the line that represents the estimated trend of the fault line, as shown by the dotted lines in Fig. 2.

(iii) The principal strain, especially compression, was greater in the region traversed by the dotted line, namely, the estimated southward extension of the Siko fault, where there are many traces of landslides that might have occurred at the time of the 1935 destructive earthquake.

The horizontal strain was also greater in the zone that includes the Tonsikyaku fault. This zone however extends symmetrically on both sides of the fault. Elsewhere in the region, the horizontal strain is

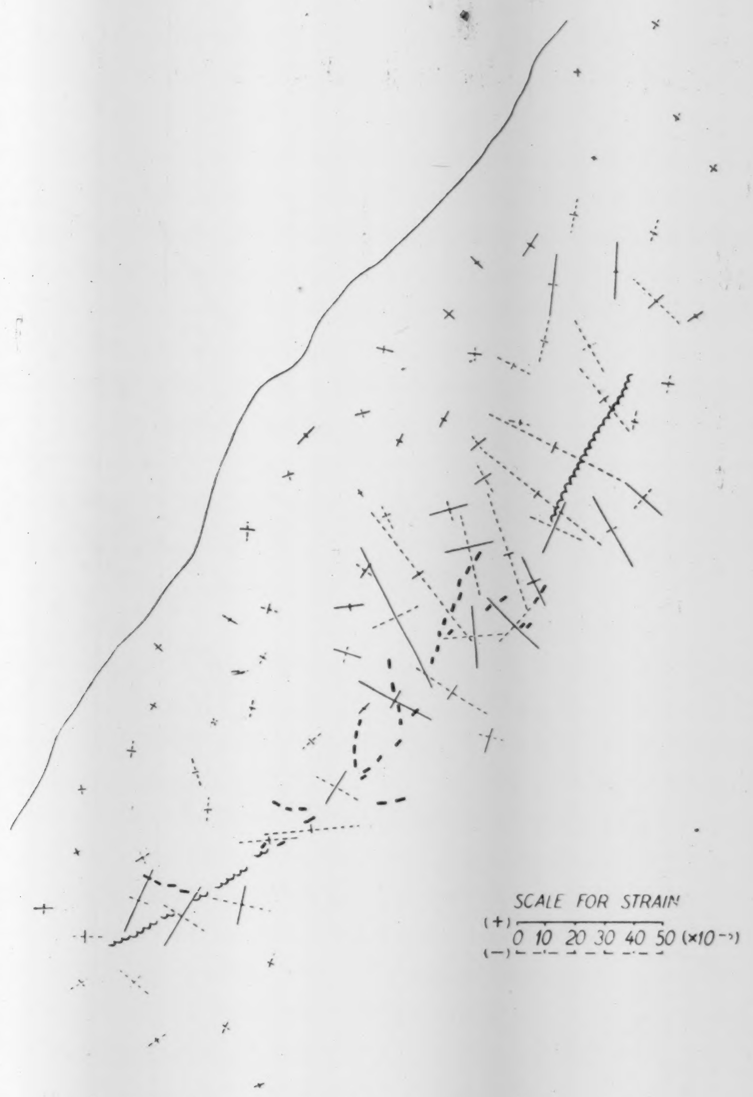

Fig. 5. Distribution of principal strain.

generally smaller, being of the order of 10^{-5} or less. In short, the crustal deformations, which are believed to have occurred in association with the destructive 1935 earthquake, were concentrated in a narrow zone on the western side of the Siko fault and on both sides of the Tonsikyaku fault.

3. In order to compare the horizontal crustal deformation with the vertical deformation, we have reproduced in Fig. 6 the distribution of the vertical displacements of the secondary and tertiary triangulation points.

In comparing this figure with Fig. 2, which latter shows the distribution of the horizontal divergence, it was found that the region of remarkable contraction situated west of the line of the Siko fault was

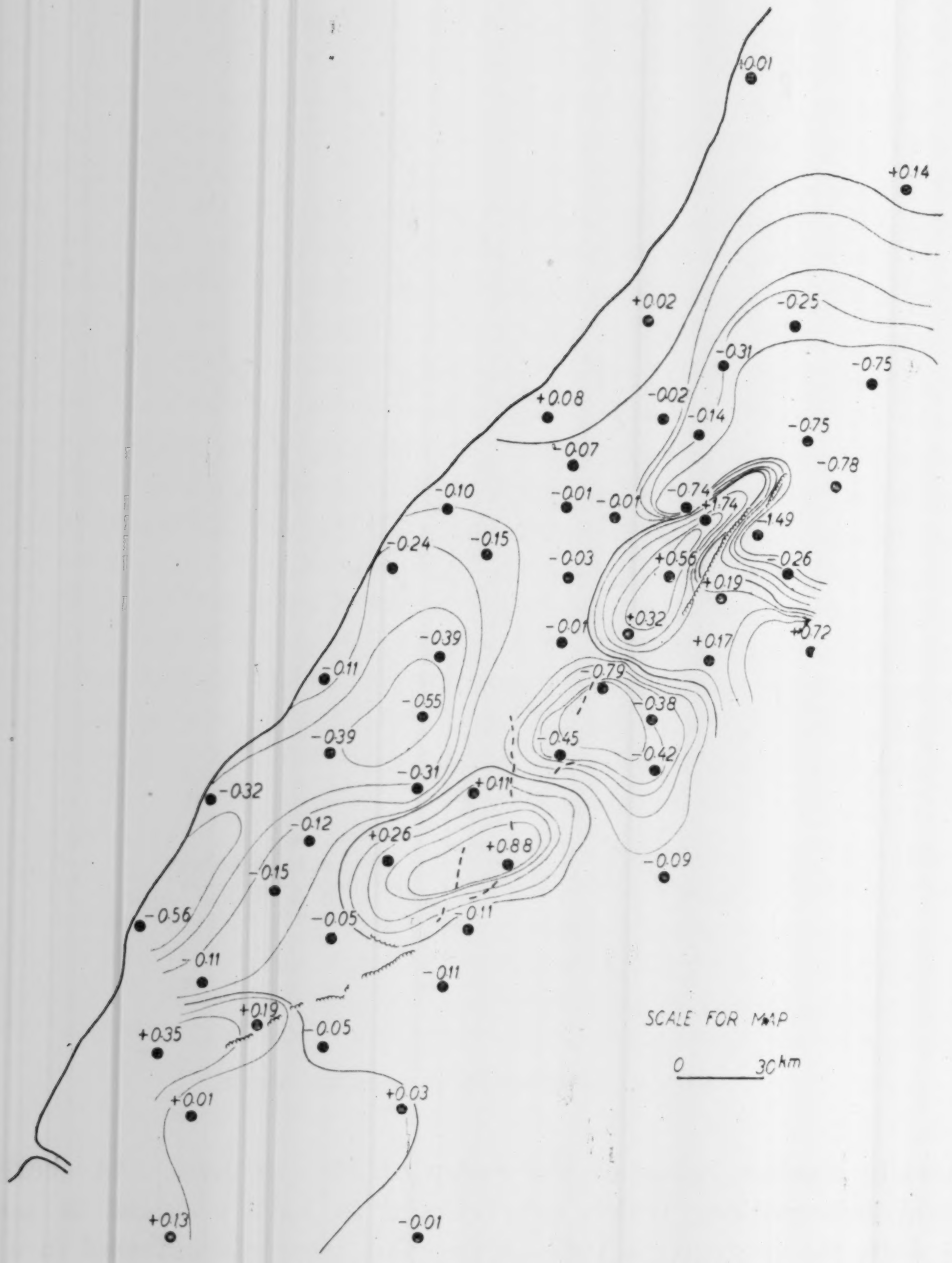
+0.01
+0.14
+0.02
-0.25
-0.31
-0.75
+0.08
-0.02
-0.14
-0.75
-0.07
-0.78
-0.10
-0.01
-0.01
-0.74
+1.74
-1.49
-0.24
-0.15
-0.03
+0.56
-0.26
+0.19
-0.01
+0.32
+0.17
+0.72
-0.39
-0.11
-0.79
-0.55
-0.38
-0.39
-0.45
-0.42
-0.31
+0.11
-0.32
-0.12
+0.26
+0.88
-0.09
-0.15
-0.56
-0.05
-0.11
-0.11
-0.11
+0.19
-0.05
+0.35
SCALE FOR MAP
0 30km
+0.01
+0.03
+0.13
-0.01

Fig. 6. Distribution of vertical displacements.

relatively elevated. It may be added that most of the epicentres of the after-shocks were found to be in this elevated and compressed zone.

Although the southern part of this compressed zone was not elevated appreciably, many landslides occurred there in association with the destructive earthquake.

To study such relation in greater detail, profiles of the horizontal divergence and those of the vertical earth movements along several lines crossing, perpendicularly, the line representing the Siko fault, were taken as shown in Figs. 7 a~d.

It will be seen from these figures that, in the northern part, as in Fig. 7 a~b, the horizontal divergence and the upward movements of the earth's crust are in positive correlation, whereas, in the southern part, as in Fig 7 c, these two quantities are in negative correlation.

This difference in correlation between the vertical earth movements and the horizontal divergence in the zone that includes the Siko fault may be regarded as indicating that, in the northern part, the after-shocks were frequent, while in the southern part, landslides were frequent, although the causal relation of these two phenomena and their corresponding correlation cannot easily be explained.

4. To ascertain the nature of the active faults that appeared at the time of the destructive earthquake, the distribution of horizontal displacements was studied.

The components of the horizontal displacements of the triangulation points, both parallel and perpendicular to the line representing the general trend of the Siko fault, were calculated, their distributions being shown in Figs. 8~9.

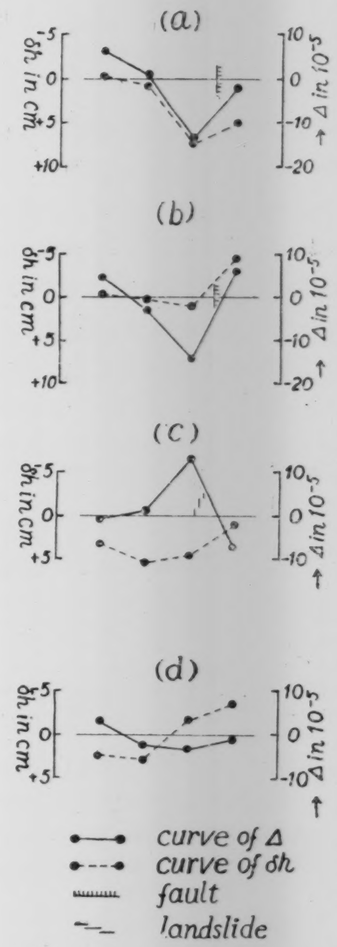

Fig. 7. δh and Δ along the W—E sections.

As to the distribution of the parallel components of the horizontal displacements, nothing remarkable was noticed. The distribution of the perpendicular components, however, shows that the two parts of the earth's crust dissevered by the Siko fault will be seen to have moved as if the one compressed the other. As the result of such a crustal deformation, the western part of the earth's crust overthrusted the eastern part, as reported by Otuka.[5]

There are, however, several exceptions, in a number of triangulation points, the horizontal displacements deviated from such a general tendency as mentioned above, i. e. the points on the western side of the

---

5) Y. OTUKA, *Bull. Earthq. Res. Inst.*, Suppl. Vol. **3** (1936), 22~74. This fact was also referred to in the preceding report. *loc. cit.* 1).

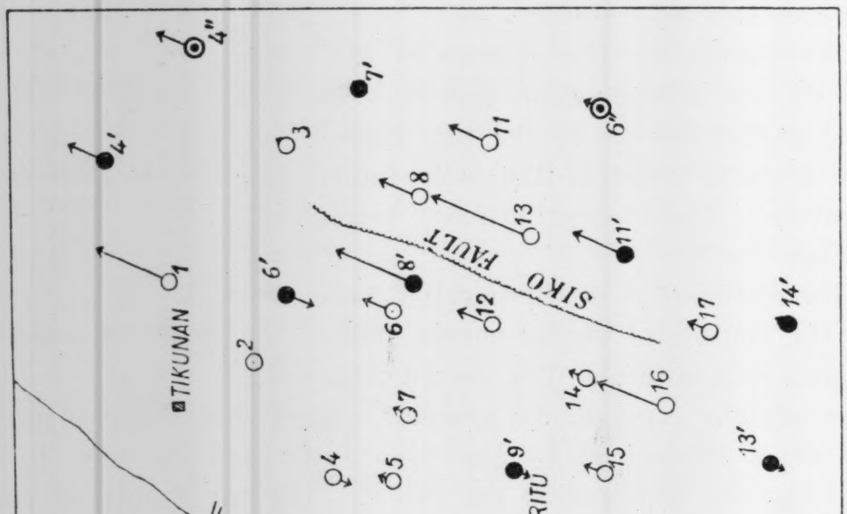
TIKUNAN
BYŌRITU
SIKO FAULT
1
2
3
4
5
6
7
8
9
11
12
13
14
15
16
17
18
20
4'
6'
7'
8'
9'
10'
11'
13'
14'
4"
6"

Fig. 8. Distribution of components of hor. displ. parallel to the Siko fault.

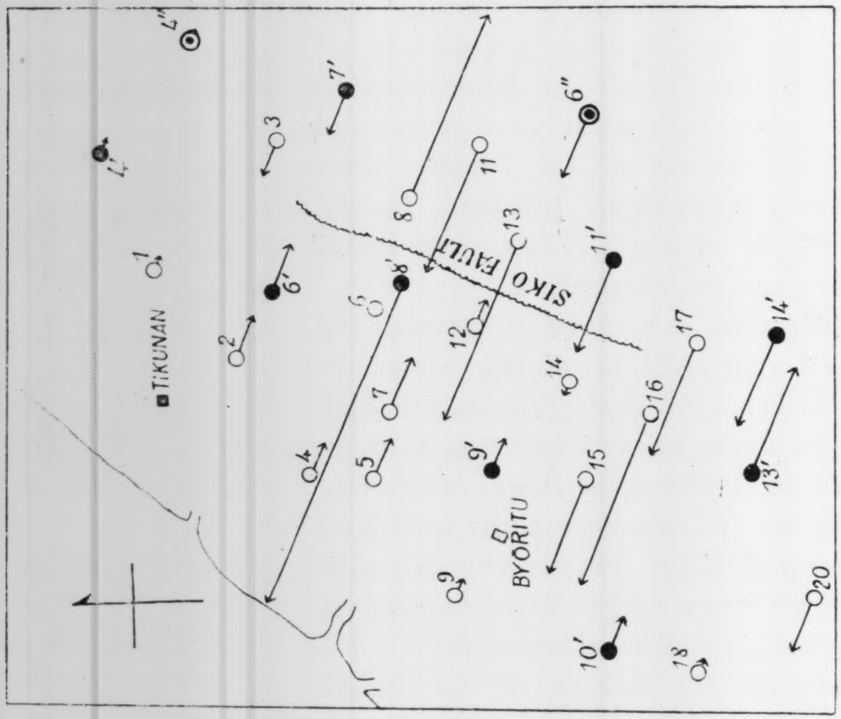
TIKUNAN
BYŌRITU
SIKO FAULT
1
2
3
4
5
6
7
8
9
11
12
13
14
15
16
17
18
20
4'
6'
7'
8'
9'
10'
11'
13'
14'
4"
6"

Fig. 9. Distribution of components of hor. displ. perpendicular to the Siko fault.

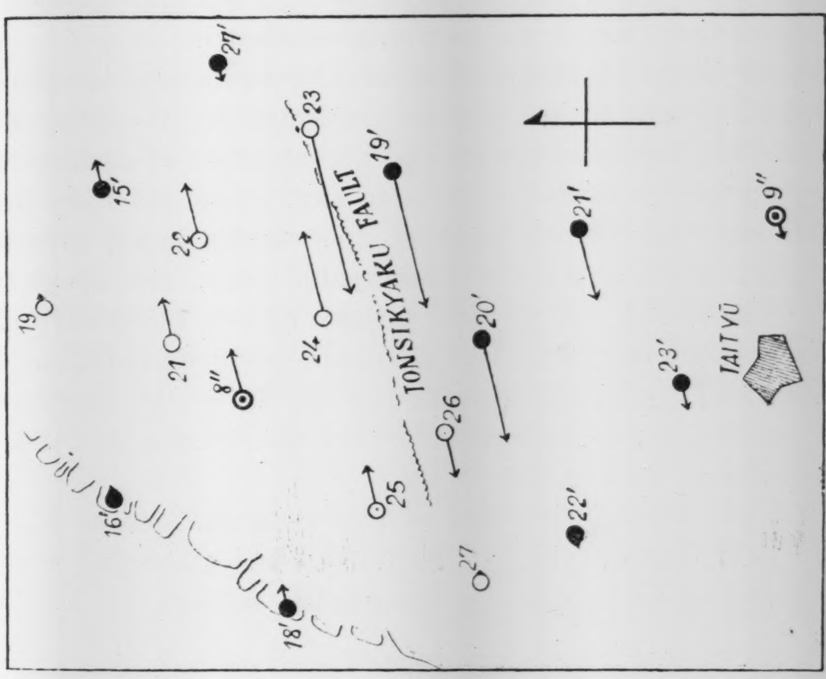
19
15'
27'
22
23
21
8''
24
19'
TONSIKYAKU FAULT
26
20'
21'
9''
25
16'
22'
23'
TAITYŪ
27
18'

Fig. 10. Distribution of components of hor. displ. parallel to the Tonsikyaku fault.

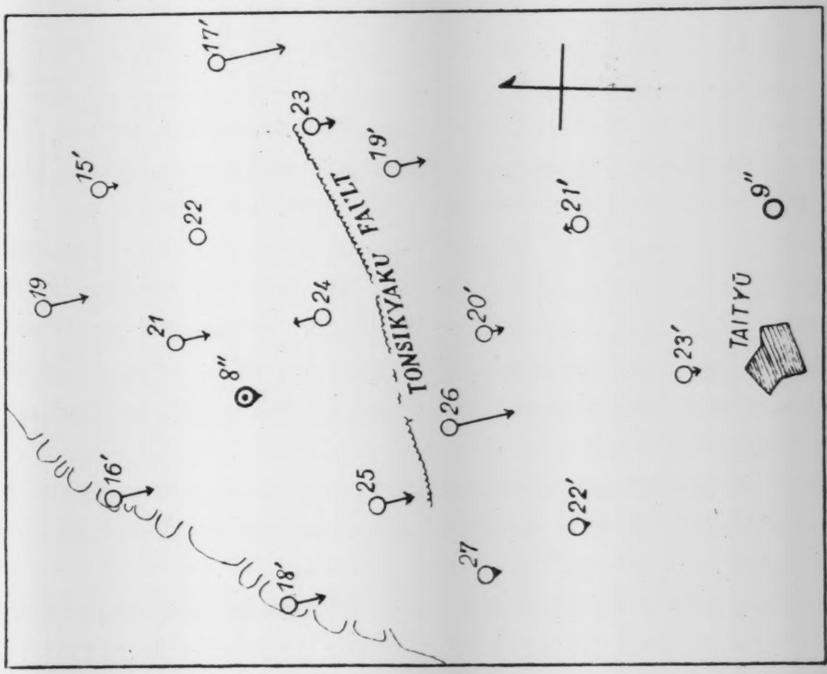
19
15'
17'
21
22
23
8''
24
19'
TONSIKYAKU FAULT
16'
26
20'
21'
25
23'
9''
TAITYŪ
22'
27
18'

Fig. 11. Distribution of components of hor. displ. perpendicular to the Tonsikyaku fault.

Siko fault moved westward, while those on the eastern side moved westward, while those on the eastern side moved westward.. For example, triangulation point 8, situated eastof the Siko fault, was displaced 0·95 m eastwards, while triangulation point 8′, situated west of the fault, was displaced 1·70 m westwards. In that region north of the apparent northern end of the Siko fault, triangulation points 1, 4′, 4″ were displaced northeastwards, i. e. approximately parallel to the direction of the line representing the general trend of the fault.

The triangulation points in the region where many landslides occurred, triangulation points 14′, 15, 16, 20 were displaced northwestward, although they are situated west of the estimated southward extension of the Siko fault, while, the displacement of triangulation point 13′ is directed southeast, which however is regarded as being on the east side of the Siko fault.

The distribution of parallel and perpendicular components of horizontal displacements of the triangulation points on both sides of the Tonsikyaku fault are shown in Figs. 10～11.

In this case, the distribution of the perpendicular components does not show any marked characteristics, while that of the parallel components is distributed similarly to those observed in the Tango earthquake of 1927,[6] and the Idu earthquake of 1930,[7] i. e. the triangulation points situated north of the fault were displaced eastward and those in the southern part were displaced westward.

The general mode of distribution of the horizontal displacements of triangulation points in the region traversed by the Siko and the Tonsikyaku faults, agree well with the actual mode of dislocations observed along the active faults; that is to say, along the Siko fault, as already mentioned, the western part of the earth's crust overthrusted the eastern part, while along the Tonsikyaku fault, the shear-type of dislocation predominated, the vertical dislocation not being very marked.

5. It was reported[8] that a series of cracks are distributed in succession in a approximate line along the valley, from the north of Mt. Kwantôzan[9] northward to Rôkeiryû.[10] The distribution of these cracks is shown reproduced in Fig. 12.

As to the geophysical meaning of this series of cracks in connection with the 1935 earthquake, so far no one has attempted to explain it. It was supposed to be a mere topographic feature.

---

[6] N. MIYABE, *Bull. Earthq. Res. Inst.*, **15** (1937), 654～662.

[7] S. YAMAGUTI, *Bull. Earthq. Res. Inst.*, **15** (1937), 899～934.

[8] *cf. Bull. Earthq. Res. Inst.*, Suppl. Vol. 3 (1936).

[9] 關刀山. [10] 老雞隆.

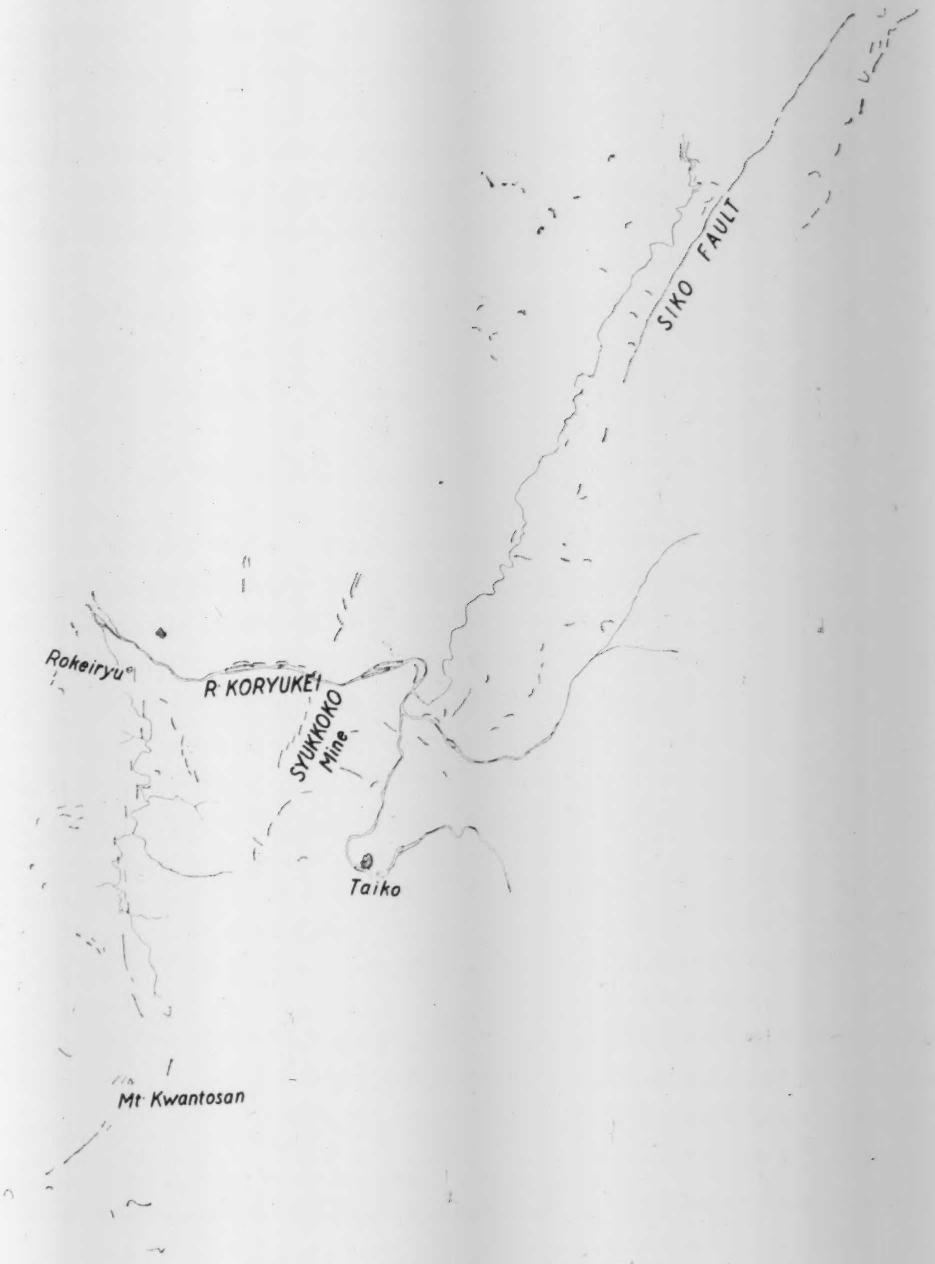
SIKO FAULT
Rokeiryu
R KORYUKEI
SYUKKOKO Mine
Taiko
Mt Kwantosan

Fig. 12. Distribution of cracks.

In our present study, this series of succession of cracks was found to coincide approximately with the western boundary of the zone of marked horizontal compression, already referred to in the preceding paragraph. It is also notable that this zone of remarkable compression, situated west of the Siko fault, approximately coincides with the zone of the Syukkôkô anticline. In the Syukkôkô mine and neighbourhood, there are many traces of landslides and cracks that occurred at the time of the destructive 1935 earthquake.

The following is our explanation of the foregoing phenomena.

The zone of the Syukkôkô anticline suffered marked disturbance in association with the 1935 earthquake, especially in its northern part, where the earth's crust was elevated more or less. The result of this marked disturbance in the Siko fault on the eastern boundary; and the Kwantôzan-Rôkeiryû line on the western boundary of which we find a succession of cracks.

That part of the earth's between the Siko fault and the Kwantôzan-Rôkeiryû line of succession of cracks, together with their southward and northward extensions, very severely disturbed at the time of the 1935 earthquake.

6. The distribution of horizontal displacements of the triangulation points in the neighbourhood of the Tonsikyaku fault deserves further study.

The distribution of horizontal displacements of triangulation points in the neighbourhood of the Tonsikyaku fault is shown in Fig. 13. If we draw a pair of nodal lines (thick lines) in Fig. 13, intersecting with each other near Tonsikyaku we find that there is some sort of system in the directions of the horizontal displacements of triangulation points distributed in each quadrant divided by the nodal lines.

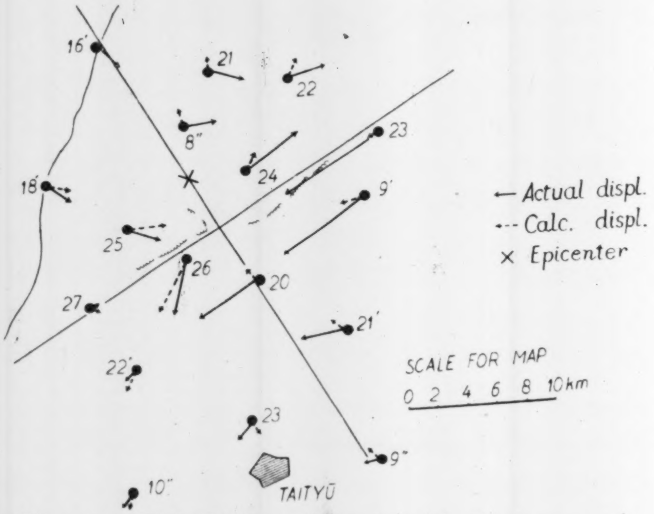

Fig. 13. Distribution of horizontal displacements in the neghbourhood of Tonsikyaku fault.

On the other hand, the directions of the horizontal components of the initial motions at various stations due to the destructive earthquake of April 21, 1935, reproduced in Table II,[11] are distributed systematically in the following manner.

The direction of the initial motion of the earthquake at Taihoku[12] was NE. Taihoku being situated in the 1st quadrant, as shown in Fig. 13, the direction of the initial motion of the earthquake agrees with the

---

[11] Taken from Kensin-Zihō, **9** (1935), 3–9.

[12] 臺北.

Table II.
Components of amplitudes of first motion of the 1935 earthquake.

station	N—S	E—W	U—D
Taityu	-210μ	-120μ	60μ
Arisan	−100	5	300
Kwarenkô	205	−412	− 27
Taihoku	N	E	11
Tainan	S	W	U
Taitô	− 36	23	77
Takao	1·9	0·5	—
Kôsyun	− 30	10	12

directions of the horizontal displacements of the triangulation points in the same quadrant and also near the point of intersection of the nodal lines.

The initial motion at Kwarenkô[13] was toward SW, so that its direction is approximately the same as those of the horizontal displacements of the triangulation points in the 4th quadrant, in which Kwarenkô is situated.

The directions of the initial motions of the earthquake that occurred at Taityû[14] and other stations situated in the southern part of Taiwan are south and southwest, the same as the directions of the horizontal displacements of triangulation points in the 3rd quadrant.

The coincidence in distribution of the directions of the horizontal displacements and that of the directions of the initial motions of the seismic waves observed at various stations has already been discussed by Ishimoto in connection with the mechanism of earthquakes, as also for the case of other earthquakes. According to Ishimato's theory,[15] the horizontal displacement at a point (r, θ) is expressed by

$$\frac{1}{4}\psi+\psi'$$

when the seismic waves originate from a quadrupple source, where ψ and ψ' are given, for simplest case, by

$$\psi=\frac{e^{iht}}{r}P_0,$$

and

$$\psi'=\frac{e^{iht}}{r}P_2(\cos\theta).$$

With the aid of the above expression, the horizontal displacement of a number of triangulation points were estimated as shown by the dotted arrows in Fig. 13. The magnitudes of the calculated displacements are obviously arbitrary. They have been adjusted so that one of the calculated displacements shall coincide in magnitude with the corresponding actual displacements. The discordance, as seen in Fig. 13, between the calculated and the actual displacements may be due partly to the assumption from which the actual displacements have been deduced, namely, that the displacements of two triangulation points situated far from the region disturbed by the earhquake are zero, and partly to the fact that the actual displacements consisted, as a rule, of acute movements caused by the crustal deformation associated with the earthquake and the cumulative movements that had been going on in the time interval between the old and new surveys.

---

[13] 花蓮港. [14] 臺中.
[15] M. Ishimoto, *Bull. Earthq. Res. Inst.*, **11** (1933), 254.

It is also interesting that the point of intersection of the two nodal lines is situated very near the epicentre of the earthquake as determined by Kawasumi and Honma,[16] denoted by × in Fig. 13.

7. Lastly, the magnitude of the disturbance of the earth's crust in the region under consideration was studied.

First, we plotted a frequency curve of the triangular areas, the horizontal strains for each of which were calculated, assuming that the deformations in each of the triangular areas was uniform. In Fig. 14, the frequency curve of the horizontal divergence thus plotted is shown by filled circles.

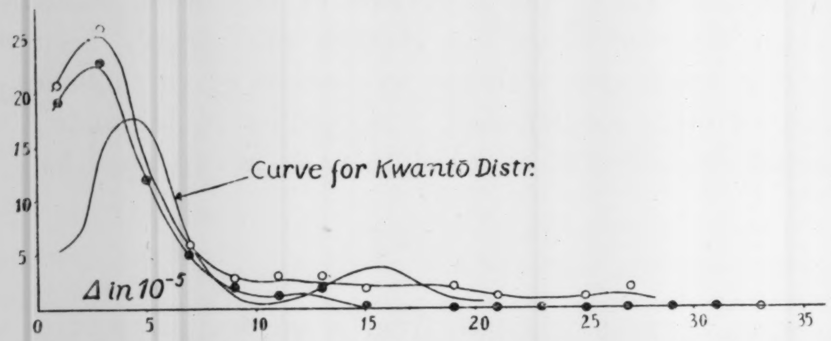

Fig. 14. Frequency of triangles plotted against Δ.

Second, the whole region under consideration was divided into a mesh of 5 km, and the mean values of certain strain components were calculated for each unit mesh, after which the frequency curves for the meshes were plotted against one of the strain components. As an example, the frequency curve of the divergence thus plotted is shown in Fig. 14 by the circles.

For comparison, a similar curve for the crustal deformations associated with the Kwanto earthquake of 1923[17] was plotted, as shown in the same figure. The frequency maximum occur at $\Delta=4\times10^{-5}$, the second maximum does not appear in the frequency curve of divergence for the crustal deformation in Central Taiwan, whereas, in the case of crustal deformation in the Kwanto district, it occurs at $\Delta=6\times10^{-5}$. This however may be no more than an indication of the fact that the region of marked disturbance is limited to a narrow zone, as already mentioned.

---

[16] H. KAWASUMI and S. HONMA, *Bull. Earthq. Res. Inst.*, Suppl. Vol. **3** (1936), 10~21.

[17] N. MIYABE, *Bull. Earthq. Res. Inst.*, **11** (1933), 637~691.

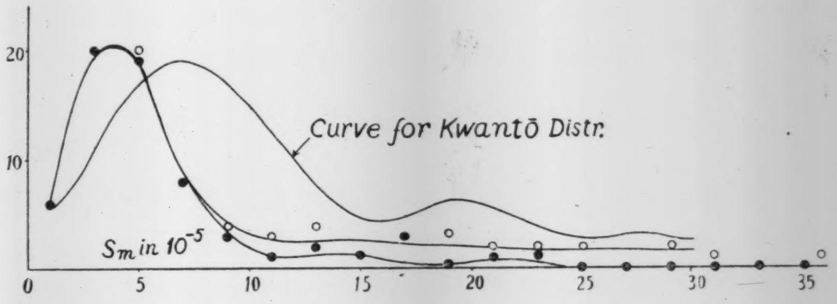

Fig. 15. Frequency of triangles plotted against S_m.

The same thing was also noticed in the frequency curves of S_m, as shown in Fig. 15.

8. Summary. In the present paper, the writers studied the modes of crustal deformation that was associated with the destructive earthquake of April 21, 1935, that occurred in Central Taiwan (Formosa), by using the data of horizontal and vertical displacements of triangulation points. The following are the outstanding results of our study;

(i) A narrow zone of remarkable disturbance was found, extending in a N—S direction, and bounded by the Siko active fault on the east and by the Kwantôzan-Rôkeiryû line of succession of cracks on the west. This zone of remarkable disturbance approximately coincides with the zone of the Syukkôkô anticline.

(ii) The distribution of the horizontal displacements of triangulation points in the neighbourhood of the Tonsikyaku fault suggests its coincidence with the distribution of initial motions that began at the various stations from the earthquake. A pair of nodal lines, estimated from the distribution of the horizontal displacements, was found to coincide with those deduced from the distribution of initial motions that began at various stations, within, of course, the allowable limit of errors. The point of intersection of the two nodal lines lies very close to the epicentre of the earthquake.

42. 臺灣中部の地殼變形 第2報

地震研究所
宮部直巳
福永三郎
佐藤光之助

昭和10年4月の地震の際に災害を被つた臺灣中部地方の地殼變形に關しては，既にその概略を，該地域に在る一等三角點の移動並に水準點の高さの變化の資料に基いて研究し，之を第1報として報告した.

その後，同一地域内の二等及び三等三角點の水平移動並に高さの變化が測量されたので，本報告では，是等の資料に基き，前號より稍々詳細に地殼變形の模樣を調べた.

研究の結果の主要なる點を擧げれば，次の通りである.

(i) 紙湖斷層の西側に於いて，この斷層に沿ひ水平方向の變形の著しい地帶がある．換言すれば，水平方向變形の著しい狹長なる地帶が南北に延びて居り，その東緣の一部が紙湖斷層となつてゐる．而してその西緣の一部は，關刀山—老雞隆間に顯れた一連の割目列に一致する．又，この變形地帶は，大體に於いて，所謂，出鑛坑の背斜軸を中心とする地帶に一致する.

(ii) 屯子脚斷層の方向を一つの節線とし，之と之に直角な節線とで4地域を分けるとその各地域における水平移動ヴエクトルの分布は，嘗て，石本博士が指摘したやうに，震源における適當な發震機巧から期待される初動の分布と稍々似てゐる．而して，これ等の2節線の交點は河角博士等の決定したこの地震の震央の位置に非常に接近してゐる.

43. *Notes on the Origin of Earthquakes.* (*Sixth paper.*)

By Win INOUYE,

Earthquake Research Institute.

(Read March 16, 1938.—Received June 20, 1938.)

1. *Introduction.*

In his previous papers,[1] the writer endevoured to show the importance of taking into consideration the dimensions of the seismic origins in dealing with the generation of seismic waves form such origins, and suggested the propriety of assuming that elastic waves are sent out form the origins, the lengths of which waves are comparable (several times the radius) with the dimension of the origins.

Recently, Dr. H. Honda and Mr. T. Miura,[2] after examining the observed amplitudes in the "p" and "s" phases of several deep-focus earthquakes, concluded that the writer's idea might be correct.

Assuming a spherical cavity at the seismic focus, they made a theoretical study of the elastic waves generated upon application of normal pressure periodically to the surface of the cavity.

They further assumed the forces on the sphere $r=a$ to be

$$F_r = F \sin 2\theta \cos\varphi e^{ipt}, \quad F_\theta = 0, \text{ and } F_\varphi = 0,$$

where r, θ, φ are the spherical coordinates and F is a constant.

At a point distant form the origin the radial component of the displacement of the dilatational wave can be expressed by

$$u_r = \mathfrak{A}_p \frac{1}{r} \sin 2\theta \cos\varphi\, e^{i(pt-hr)+i\varepsilon_1},$$

and the co-latitudinal and the longitudinal components of the displacement of the distortional wave can be expressed respectively by

$$u_\theta = \mathfrak{A}_s \frac{1}{r} \cos 2\theta \cos\varphi\, e^{i(pt-kr)+i\varepsilon_2},$$

$$u_\varphi = -\mathfrak{A}_s \frac{1}{r} \cos\theta \sin\varphi\, e^{i(pt-kr)+i\varepsilon_2},$$

---

[1] W. INOUYE, *Bull. Earthq. Res. Inst.*, **14** (1936), 582: **15** (1937), 90; 956.

[2] H. HONDA and T. MIURA, *Kensindihô*, **10** (1938), 1.

where

$$h=\sqrt{\frac{\rho}{\lambda+2\mu}}\,p=\frac{2\pi}{l_p},\quad k=\sqrt{\frac{\rho}{\mu}}\,p=\frac{2\pi}{l_s},$$

l_p and l_s are respectively the wave lengths of the dilatational and the distortional waves.

Then,

$$\frac{\mathfrak{A}_s}{\mathfrak{A}_p}=\left(\frac{k}{h}\right)^3 R=5{\cdot}20R \text{ (if we assume } \lambda=\mu),$$

where

$$R=\sqrt{\frac{D^2+E^2}{F^2+G^2}},$$

$$D=-24(ha)+2(ha)^3,\quad E=24-10(ha)^2,$$

$$F=-24(ka)+2{\cdot}5(ka)^3 \text{ and } G=24-10{\cdot}5(ka)^2+0{\cdot}5(ka)^4.$$

Upon examining the amplitudes $\mathfrak{A}_p$ and $\mathfrak{A}_s$ of several deep-focus earthquakes, they found that R takes a certain value between 0·13 and 0·81, showing that the wave lengths of seismic waves are comparable with the dimensions of the seismic origins.

In what follows, the writer studies the case where either the normal or the tangential stress, or both, have changed with different rapidities on the surface of a spherical cavity.

It is shown that in actual earthquakes these stresses attain almost their final values in that period during which the distortional wave travels a distance comparable with the radius of the cavity, suggesting that the stress changes proceed while plastic yielding goes on throughout the seismic focus.

It is also shown that it may be in order to suppose that waves might be generated having wave lengths comparable with the size of the origin, and, further, that it may also be preferable to suppose that the normal and the tangential stresses about the seismic focus may both change simultaneously than to suppose that they change alone.

2. *Periodic force of quadrant type.*

We shall first study the case in which the normal stress on the surface of the spherical cavity as measured at the seismic focus undergoes a periodic variation in time.

The solution of the equation of motion in spherical coordinates assumes the forms

$$\Delta = A_{mn}\frac{H^{(2)}_{n+\frac{1}{2}}(hr)}{\sqrt{r}}P^m_n(\cos\theta)\cos m\varphi e^{ipt},$$

$$\left.\begin{aligned}
u_1 &= -\frac{A_{mn}}{h^2}\frac{d}{dr}\frac{H^{(2)}_{n+\frac{1}{2}}(hr)}{\sqrt{r}}P^m_n(\cos\theta)\cos m\varphi e^{ipt},\\
v_1 &= -\frac{A_{mn}}{h^2}\frac{H^{(2)}_{n+\frac{1}{2}}(hr)}{r^{3/2}}\frac{dP^m_n(\cos\theta)}{d\theta}\cos m\varphi e^{ipt},\\
w_1 &= \frac{mA_{mn}}{h^2}\frac{H^{(2)}_{n+\frac{1}{2}}(hr)}{r^{3/2}}\frac{P^m_n(\cos\theta)}{\sin\theta}\sin m\varphi e^{ipt},
\end{aligned}\right\}$$

$$\left.\begin{aligned}
u_2 &= 0,\\
v_2 &= \frac{mB_{mn}}{n(n+1)}\frac{H^{(2)}_{n+\frac{1}{2}}(kr)}{\sqrt{r}}\frac{P^n_n(\cos\theta)}{\sin\theta}\cos m\varphi e^{ipt},\\
w_2 &= -\frac{B_{mn}}{n(n+1)}\frac{H^{(2)}_{n+\frac{1}{2}}(kr)}{\sqrt{r}}\frac{dP^m_n(\cos\theta)}{d\theta}\sin m\varphi e^{ipt},
\end{aligned}\right\}$$

$$\left.\begin{aligned}
u_3 &= -\frac{n(n+1)C_{mn}}{mk^2}\frac{H^{(2)}_{n+\frac{1}{2}}(kr)}{r^{3/2}}P^m_n(\cos\theta)\cos m\varphi e^{ipt},\\
v_3 &= -\frac{C_{mn}}{mk^2}\frac{1}{r}\frac{d}{dr}\left\{\sqrt{r}\,H^{(2)}_{n+\frac{1}{2}}(kr)\right\}\frac{dP^n_n(\cos\theta)}{d\theta}\cos m\varphi e^{ipt},\\
w_3 &= \frac{C_{mn}}{k^2}\frac{1}{r}\frac{d}{dr}\left\{\sqrt{r}\,H^{(2)}_{n+\frac{1}{2}}(kr)\right\}\frac{P^m_n(\cos\theta)}{\sin\theta}\sin m\varphi e^{ipt},
\end{aligned}\right\}$$

where

u_1, v_1, w_1 = radial, co-latitudinal, and longitudinal components of the displacement of the dilatational wave respectively,

u_2, v_2, w_2 = radial, co-latitudinal, and longitudinal components of the displacement of a distortional wave of the second kind (after Prof. K. Sezawa) respectively,

u_3, v_3, w_3 = radial, co-latitudinal, and longitudinal components of the displecement of a distortional wave of the first kind (after Prof. K. Sezawa) respectively.

We shall take a special case in which it is assumed that the surface is free from tangential stress and is under normal stress

$$NP^m_n(\cos\theta)\cos m\varphi e^{ipt}.$$

The boundary conditions are such that the equations

$$\widehat{rr}=\lambda\Delta+2\mu\frac{\partial u}{\partial r}=NP_n^m(\cos\theta)\cos m\varphi e^{ipt},$$

$$\widehat{r\theta}=\mu\left(\frac{\partial v}{\partial r}-\frac{v}{r}+\frac{1}{r}\frac{\partial u}{\partial\theta}\right)=0,$$

$$\widehat{r\phi}=\mu\left(\frac{1}{r\sin\theta}\frac{\partial u}{\partial\varphi}+\frac{\partial w}{\partial r}-\frac{w}{r}\right)=0,$$

where

$$u=u_1+u_3,\quad v=v_1+v_2+v_3,\quad w=w_1+w_2+w_3,$$

must hold on that surface.

Satisfying these conditions, we have

$$B_{mn}=0,$$

$$2A_{mn}\left\{-\frac{(n-1)}{h^2r^2}H^{(2)}_{n+\frac{1}{2}}(hr)+\frac{1}{hr}H^{(2)}_{n+\frac{3}{2}}(hr)\right.$$

$$+\frac{C_{mn}}{m}\left\{-\frac{2(n^2-1)}{k^2r^2}H^{(2)}_{n+\frac{1}{2}}(kr)+\frac{2n+1}{kr}H^{(2)}_{n+\frac{3}{2}}(kr)-H^{(2)}_{n+\frac{5}{2}}(kr)\right\}=0,$$

$$A_{mn}\left\{\left(\frac{\lambda}{\mu}-\frac{2n(n-1)}{h^2r^2}\right)H^{(2)}_{n+\frac{1}{2}}(hr)+2\left(\frac{2n+1}{hr}H^{(2)}_{n+\frac{3}{2}}(hr)-H^{(2)}_{n+\frac{5}{2}}(hr)\right\}\right.$$

$$+2\frac{C_{mn}}{m}n(n+1)\left\{-\frac{n-1}{k^2r^2}H^{(2)}_{n+\frac{1}{2}}(kr)+\frac{1}{kr}H^{(2)}_{n+\frac{3}{2}}(kr)\right\}=\frac{N\sqrt{r}}{\mu}$$

at $r=a$.

If $m=1$, these equations are exactly the same as those obtained in the previous paper,[3] where the normal pressure on the spherical surface was assumed to be expressed by one of the zonal harmonics.

Therefore, the value of $\frac{\mathfrak{A}_s}{\mathfrak{A}_p}$ in Dr. H. Honda's paper just mentioned can be obtained by doubling the value of $\frac{v_{2,2}}{u_{1,2}}$ in Fig. 2, in the writer's previous paper, which is the proportion of the displacement of the distortional to that of the dilatational wave, ignoring the azimuthal terms.

The value $R=\frac{1}{5{\cdot}20}\frac{\mathfrak{A}_s}{\mathfrak{A}_p}$ is given in Table I.

---

3) W. INOUYE, *Bull. Earthq. Res. Inst.*, **15** (1937), 956.

Table I.

ha	R	ha	R	ha	R	ha	R
0·1	1·00	1·0	0·91	2·0	0·97	4·0	0·15
0·2	0·99	1·2	0·90	2·4	0·57	5·0	0·11
0·4	0·97	1·4	0·94	2·8	0·34	6·0	0·08
0·6	0·96	1·6	1·04	3·0	0·24	7·0	0·07
0·8	0·93	1·8	1·08	3·4	0·20	8·0	0·06

3. *Aperiodic force of quadrant type.*

We shall next investigate the case in which the stresses on the surface of the spherical cavity change with different rapidities.

The general case has been treated in the previous paper.4)

(a) We shall first take the case in which the tangential stresses $\widehat{r\theta}=0$, $\widehat{r\varphi}=0$, and the change in the normal stress at $r=a$ are

$$\left.\begin{aligned}\widehat{rr}&=0, & (r=a,\ t<0)\\ \widehat{rr}&=Ne^{-ct}(1-e^{-qt})P_2^1(\cos\theta)\cos\varphi, & (r=a,\ t>0)\end{aligned}\right\}$$

in which $c\to 0$.

We shall consider now only that case in which Poisson's ratio $\sigma=\dfrac{1}{4}$, that is $\lambda=\mu$.

The solutions are exactly the same as for the case that was considered in the previous paper in which the azimuthal distribution of the normal stress was assumed to be expressed by $P_2(\cos\theta)$, excepting the azimuthal terms.

But as there were some errors in the numerical calculation in the previous paper, we shall repeat the expressions of the solution as follows.

The normal component of displacement of the dilatational wave at a point distant from the origin as compared with the wave length is given by

$$u_1=\frac{1}{2\pi}\int_{-\infty}^{\infty}\frac{\Delta_1}{\Delta}\frac{d}{dr}\frac{H_{\frac{5}{2}}^{(2)}(hr)}{\sqrt{r}}e^{ipt}dp\int_{-\infty}^{\infty}\varphi(\omega)e^{-ip\omega}d\omega P_2^1(\cos\theta)\cos\varphi$$

$$=\frac{1}{2\pi}\frac{N\mathfrak{v}^4}{\mu a r^2}P_2^1(\cos\theta)\cos\varphi\, i\left[\int_{-\infty}^{\infty}\frac{f(p)e^{ip\left(t-\frac{r-a}{v}\right)}}{(p-ic)g(p)}dp-\int_{-\infty}^{\infty}\frac{f(p)e^{ip\left(t-\frac{r-a}{v}\right)}}{(p-iq)g(p)}dp\right],$$

---

4) W. INOUYE, *Bull. Earthq. Res. Inst.*, **15** (1937), 90.

where

$$\Delta=-\mu^2\left\{h^2\frac{H^{(2)}_{\frac{5}{2}}(ha)}{\sqrt{a}}-2\frac{d^2}{da^2}\frac{H^{(2)}_{\frac{5}{2}}(ha)}{\sqrt{a}}\right\}$$

$$\times\left[\frac{d}{da}\left(\frac{1}{a}\frac{d}{da}\left\{\sqrt{a}\,H^{(2)}_{\frac{5}{2}}(ka)\right\}\right)-\frac{1}{a^2}\frac{d}{da}\left\{\sqrt{a}\,H^{(2)}_{\frac{5}{2}}(ka)\right\}\right.$$

$$\left.+6\frac{H^{(2)}_{\frac{5}{2}}(ka)}{a^{5/2}}\right]-12\mu^2\left\{\frac{d}{da}\frac{H^{(2)}_{\frac{5}{2}}(ha)}{a^{3/2}}-\frac{H^{(2)}_{\frac{5}{2}}(ha)}{a^{5/2}}\right.$$

$$\left.+\frac{1}{a}\frac{d}{da}\frac{H^{(2)}_{\frac{5}{2}}(ha)}{\sqrt{a}}\right\}\frac{d}{da}\frac{H^{(2)}_{\frac{5}{2}}(ka)}{a^{3/2}},$$

$$\Delta_1=-N\mu\left[\frac{d}{da}\left(\frac{1}{a}\frac{d}{da}\left\{\sqrt{a}\,H^{(2)}_{\frac{5}{2}}(ka)\right\}\right)\right.$$

$$\left.-\frac{1}{a^2}\frac{d}{da}\left\{\sqrt{a}\,H^{(2)}_{\frac{5}{2}}(ka)\right\}+6\frac{H^{(2)}_{\frac{5}{2}}(ka)}{a^{5/2}}\right],$$

$\varphi(\omega)=e^{-c\omega}(1-e^{-q\omega})$ in which $c\to0$,

$$f(p)=\left[5\frac{a}{\mathfrak{v}}p^2-48\frac{\mathfrak{v}}{a}+i\left\{\frac{a^2}{\mathfrak{v}^2}p^3-21p+48\frac{\mathfrak{v}^2}{a^2p}\right\}\right]$$

$$\times\left[-\frac{1}{\sqrt{3}}\frac{r}{\mathfrak{v}}p^2+9\sqrt{3}\frac{\mathfrak{v}}{r}+i\left\{4p-27\frac{\mathfrak{v}^2}{r^2p}\right\}\right]$$

$$\fallingdotseq\frac{r}{\sqrt{3}}\left(-i\frac{a^2}{\mathfrak{v}^3}p^5-5\frac{a}{\mathfrak{v}^2}p^4+i21\frac{1}{\mathfrak{v}}p^3+48\frac{1}{a}p^2-i48\frac{\mathfrak{v}}{a^2}p\right)$$

$$-i4\left(-i\frac{a^2}{\mathfrak{v}^2}p^4-5\frac{a}{\mathfrak{v}}p^3+i21p^2+48\frac{\mathfrak{v}}{a}p-i48\frac{\mathfrak{v}^2}{a^2}\right),$$

$$g(p)=p^6-i\,12{\cdot}506\frac{\mathfrak{v}}{a}p^5-81{\cdot}672\frac{\mathfrak{v}^2}{a^2}p^4+i326{\cdot}05\frac{\mathfrak{v}^3}{a^3}p^3$$

$$+759{\cdot}7\frac{\mathfrak{v}^4}{a^4}p^2-i870{\cdot}7\frac{\mathfrak{v}^5}{a^5}p-552\frac{\mathfrak{v}^6}{a^6}$$

$$\fallingdotseq\left\{p-(i1{\cdot}8014+4{\cdot}1855)\frac{\mathfrak{v}}{a}\right\}\left\{p-(i1{\cdot}8014-4{\cdot}1855)\frac{\mathfrak{v}}{a}\right\}$$

$$\times\left\{p-(i3{\cdot}6486+1{\cdot}4400)\frac{\mathfrak{v}}{a}\right\}\left\{p-(i3{\cdot}6486-1{\cdot}4400)\frac{\mathfrak{v}}{a}\right\}$$

$$\times\left\{p-(i0{\cdot}8032+1{\cdot}0407)\frac{\mathfrak{v}}{a}\right\}\left\{p-(i0{\cdot}8032-1{\cdot}0407)\frac{\mathfrak{v}}{a}\right\},$$

and $\mathfrak{v}$ is the velocity of the distortional wave.

Upon evaluating the integration by applying the theory of residues, the normal component of displacement of the dilatational wave at a point distant from the origin is given by

$$u_1 = -0{\cdot}3478\frac{Na^3}{\mu r^2}P_2^1(\cos\theta)\cos\varphi + \frac{Na^2}{\sqrt{3}\,\mu r}P_2^1(\cos\theta)\cos\varphi$$

$$\times\Bigg[\bigg[(\Omega^5 - 5\Omega^4 + 21\Omega^3 - 48\Omega^2 + 48\Omega)e^{-\Omega\tau}$$

$$\div(-\Omega^6 + 12{\cdot}506\Omega^5 - 81{\cdot}672\Omega^4 + 326{\cdot}05\Omega^3 - 759{\cdot}7\Omega^2$$

$$+ 870{\cdot}7\Omega - 552)\bigg]$$

$$+ 2\,\frac{e^{-1{\cdot}801\tau}}{8{\cdot}370}\bigg[\Big\{(1{\cdot}2273\times10^6 - 8{\cdot}595\times10^4\Omega)\cos(4{\cdot}185\tau)$$

$$+ (1{\cdot}0182\times10^5 - 2{\cdot}5627\times10^5\Omega)\sin(4{\cdot}185\tau)\Big\}$$

$$\div\Big\{(1566{\cdot}7 - 138{\cdot}29\Omega)^2 + (11{\cdot}73 + 314{\cdot}83\Omega)^2\Big\}$$

$$-\Big\{1\ 2273\times10^6\cos(4{\cdot}185\tau) + 1{\cdot}0182\times10^5\sin(4{\cdot}185\tau)\Big\}$$

$$\div(2{\cdot}4546\times10^6)\bigg]$$

$$+ 2\,\frac{e^{-3{\cdot}649\tau}}{2{\cdot}880}\bigg[\Big\{(-1{\cdot}7387\times10^5 + 7{\cdot}2545\times10^4\Omega)\cos(1{\cdot}440\tau)$$

$$+ (3{\cdot}3466\times10^5 - 6{\cdot}3085\times10^4\Omega)\sin(1{\cdot}440\tau)\Big\}$$

$$\div\Big\{(832{\cdot}26 -- 192{\cdot}39\Omega)^2 + (52{\cdot}98 - 90{\cdot}44\Omega)^2\Big\}$$

$$-\Big\{-1{\cdot}7387\times10^5\cos(1{\cdot}440\tau) + 3{\cdot}3466\times10^5\sin(1{\cdot}440\tau)\Big\}$$

$$\div(6{\cdot}9547\times10^5)\bigg]$$

$$+ 2\,\frac{e^{-0{\cdot}863\tau}}{2{\cdot}082}\bigg[\Big\{(3{\cdot}5305\times10^3 + 2{\cdot}2310\times10^3\Omega)\cos(1{\cdot}041\tau)$$

$$+ (6{\cdot}4278\times10^3 - 5{\cdot}1124\times10^3\Omega)\sin(1{\cdot}041\tau)\Big\}$$

$$\div\Big\{(53{\cdot}99 + 122{\cdot}15\Omega)^2 + (244{\cdot}47 - 146{\cdot}09\Omega)^2\Big\}$$

$$-\left\{3{\cdot}5305\times 10^{3}\cos(1{\cdot}041\tau)+6{\cdot}4278\times 10^{3}\sin(1{\cdot}041\tau)\right\}$$

$$\div(6{\cdot}2681\times 10^{4})\Big]\Big],$$

where

$$\Omega=\frac{aq}{\mathfrak{v}},\quad \tau=\frac{\mathfrak{v}}{a}\left(t-\frac{r-a}{v}\right).$$

Next, the co-latitudinal and the longitudinal components of the displacement of the distortional wave at $kr\gg 1$ are expressed respectively by

$$v_3=\frac{1}{2\pi}\int_{-\infty}^{\infty}\frac{\Delta_2}{\Delta}\frac{1}{r}\frac{d}{dr}\left\{\sqrt{r}\,H^{(2)}_{\frac{5}{2}}(kr)\right\}e^{ipt}dp$$

$$\times\int_{-\infty}^{\infty}\varphi(\omega)e^{-ip\omega}d\omega\frac{dP^1_2(\cos\theta)}{d\theta}\cos\varphi$$

$$=-\frac{1}{2\pi}\frac{2N\mathfrak{v}^4}{\mu a r^2}\frac{dP^1_2(\cos\theta)}{d\theta}\cos\varphi\, i\left[\int_{-\infty}^{\infty}\frac{f'(p)e^{ip\left(t-\frac{r-a}{\mathfrak{v}}\right)}}{(p-ic)g(p)}dp\right.$$

$$\left.-\int_{-\infty}^{\infty}\frac{f'(p)e^{ip\left(t-\frac{r-a}{\mathfrak{v}}\right)}}{(p-iq)g(p)}dp\right],$$

$$w_3=-\frac{1}{2\pi}\int_{-\infty}^{\infty}\frac{\Delta_2}{\Delta}\frac{1}{r}\frac{d}{dr}\left\{\sqrt{r}\,H^{(2)}_{\frac{5}{2}}(kr)\right\}e^{ipt}dp$$

$$\times\int_{-\infty}^{\infty}\varphi(\omega)e^{-ip\omega}d\omega\frac{P^1_2(\cos\theta)}{\sin\theta}\sin\varphi$$

$$=\frac{1}{2\pi}\frac{2N\mathfrak{v}^4}{\mu a r^2}\frac{P^1_2(\cos\theta)}{\sin\theta}\sin\varphi\, i\left[\int_{-\infty}^{\infty}\frac{f'(p)e^{ip\left(t-\frac{r-a}{\mathfrak{v}}\right)}}{(p-ic)g(p)}dp\right.$$

$$\left.-\int_{-\infty}^{\infty}\frac{f'(p)e^{ip\left(t-\frac{r-a}{\mathfrak{v}}\right)}}{(p-iq)g(p)}dp\right],$$

where

$$\Delta_2=+N\mu\left\{\frac{d}{da}\frac{H^{(2)}_{\frac{5}{2}}(ha)}{a^{3/2}}-\frac{H^{(2)}_{\frac{5}{2}}(ha)}{a^{5/2}}+\frac{1}{a}\frac{d}{da}\frac{H^{(2)}_{\frac{5}{2}}(ha)}{\sqrt{a}}\right\},$$

$$f'(p)=\left[\frac{12v}{a}-\frac{ap^2}{v}+i\left(-\frac{12v^2}{a^2p}+5p\right)\right]$$

$$\times\left[\frac{6\mathfrak{v}}{r}-\frac{rp^2}{\mathfrak{v}}+i\left(-\frac{6\mathfrak{v}^2}{r^2p}+3p\right)\right]$$

$$\fallingdotseq r\left(0{\cdot}57735\frac{a}{\mathfrak{v}^2}p^4-i5\frac{1}{\mathfrak{v}}p^3-20{\cdot}785\frac{1}{a}p^2+i36\frac{\mathfrak{v}}{a^2}p\right)$$

$$+3\left(-i0{\cdot}57735\frac{a}{\mathfrak{v}}p^3-5p^2+i20{\cdot}785\frac{\mathfrak{v}}{a}p+36\frac{\mathfrak{v}^2}{a^2}\right),$$

and v is the velocity of the dilatational wave.

Evaluating the integration, we get as the final results

$$v_3=-0{\cdot}3912\frac{Na^3}{\mu r^2}\,\frac{dP_2^1(\cos\theta)}{d\theta}\cos\varphi-\frac{2Na^2}{\mu r}\Psi\,\frac{dP_2^1(\cos\theta)}{d\theta}\cos\varphi,$$

$$w_3=0{\cdot}3912\frac{Na^3}{\mu r^2}\,\frac{P_2^1(\cos\theta)}{\sin\theta}\sin\varphi+\frac{2Na^2}{\mu r}\Psi\,\frac{P_2^1(\cos\theta)}{\sin\theta}\sin\varphi,$$

where

$$\Psi=(0{\cdot}57735\Omega^4-5\Omega^3+20{\cdot}785\Omega^2-36\Omega)e^{-\Omega\tau'}$$

$$\div(-\Omega^6+12{\cdot}506\Omega^5-81{\cdot}672\Omega^4+326{\cdot}05\Omega^3$$

$$-759{\cdot}7\Omega^2+870{\cdot}7\Omega-552)$$

$$+2\frac{e^{-1{\cdot}801\tau'}}{8{\cdot}370}\biggl[\biggl\{(1{\cdot}0880\times10^5+1{\cdot}4759\times10^4\Omega)\cos(4{\cdot}185\tau')$$

$$+(1{\cdot}2003\times10^5-3{\cdot}2348\times10^4\Omega)\sin(4{\cdot}185\tau')\biggr\}$$

$$\div\Bigl\{(1566{\cdot}7-138{\cdot}29\Omega)^2+(11{\cdot}73+314{\cdot}38\Omega)^2\Bigr\}$$

$$-\Bigl\{1{\cdot}0880\times10^5\cos(4{\cdot}185\tau')+1{\cdot}2003\times10^5\sin(4{\cdot}185\tau')\Bigr\}$$

$$\div(2{\cdot}4546\times10^6)\biggr]$$

$$+2\frac{e^{-3{\cdot}649\tau'}}{2{\cdot}880}\biggl[\biggl\{(-1{\cdot}6538\times10^4+6{\cdot}1945\times10^3\Omega)\cos(1{\cdot}440\tau')$$

$$
\begin{aligned}
&+(2{\cdot}4292\times10^{4}-4{\cdot}2127\times10^{3}\Omega)\sin(1{\cdot}440\tau')\Big\}\\
&\div\Big\{(832{\cdot}26-192{\cdot}39\Omega)^{2}+(52{\cdot}98-90{\cdot}44\Omega)^{2}\Big\}\\
&-\Big\{-1{\cdot}6538\times10^{4}\cos(1{\cdot}440\tau')+2{\cdot}4292\times10^{4}\sin(1{\cdot}440\tau')\Big\}\\
&\div(6{\cdot}9547\times10^{5})\Big]\\
&+2\frac{e^{-0{\cdot}803\tau'}}{2{\cdot}082}\Big[\Big\{(3{\cdot}868\times10^{2}-4{\cdot}7198\times10^{3}\Omega)\cos(1{\cdot}041\tau')\\
&+(-7{\cdot}5385\times10^{3}+3{\cdot}2693\times10^{3}\Omega)\sin(1{\cdot}041\tau')\Big\}\\
&\div\Big\{(53{\cdot}99+122{\cdot}15\Omega)^{2}(244{\cdot}47-146{\cdot}09\Omega)^{2}\Big\}\\
&-\Big\{3{\cdot}868\times10^{2}\cos(1{\cdot}041\tau')-7{\cdot}5385\times10^{3}\sin(1{\cdot}041\tau')\Big\}\\
&\qquad\qquad\qquad\qquad\div(6{\cdot}2681\times10^{4})\Big],
\end{aligned}
$$

and

$$\tau'=\frac{\mathfrak{v}}{a}\left(t-\frac{r-a}{\mathfrak{v}}\right).$$

As to the displacements u_1 (P phase) and v_3, w_3 (S phase) in a number of cases, Ω in every one of them assumes a certain definite value, as graphically represented in Figs. 1∼7, where, for simplicity, the azimuthal terms, that is $P_2^1(\cos\theta)\cos\varphi$ in the case of u_1, $\dfrac{dP_2^1(\cos\theta)}{d\theta}\cos\varphi$ in the case of v_3 and $-\dfrac{P_2^1(\cos\theta)}{\sin\theta}\sin\varphi$ in the case of w_3, are taken as unity.

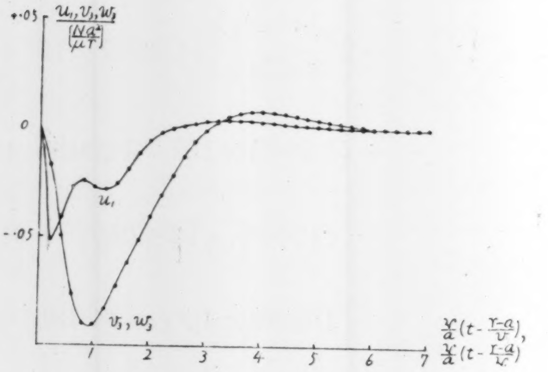

Fig. 1. Normal stress: $\Omega=\infty$.

The quantity $\Omega=\dfrac{aq}{\mathfrak{v}}$ gives the rapidity of the changes in the stress on the surface of the spherical cavity.

To show the rate of change in the stresses, the function $N(1-e^{-\gamma t})$ is shown in Fig. 8, assuming several different values for Ω.

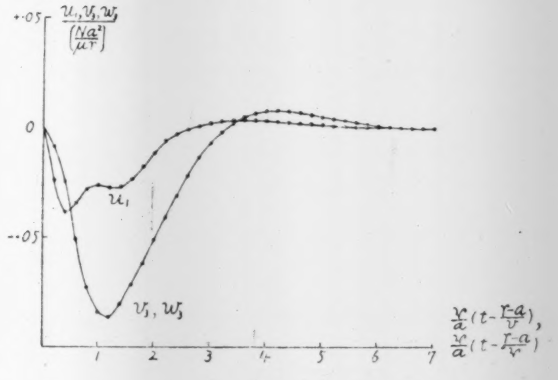

Fig. 2. Normal stress: $\Omega=5$.

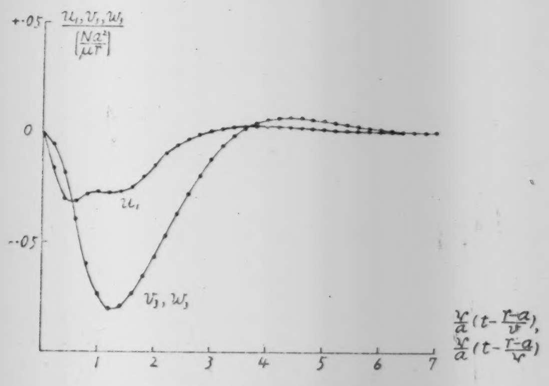

Fig. 3. Normal stress: $\Omega=4$.

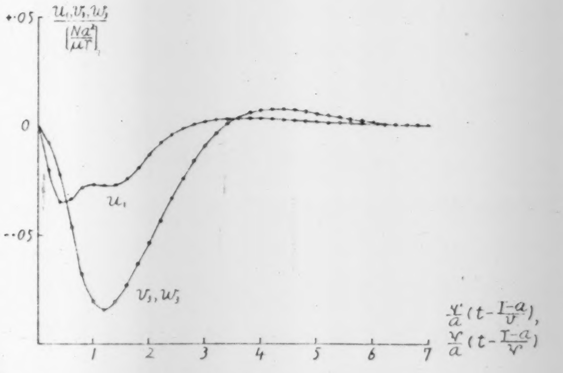

Fig. 4. Normal stress: $\Omega=3$.

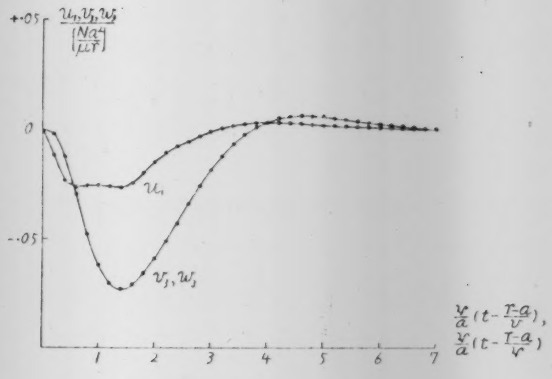

Fig. 5. Normal stress: $\Omega=2$.

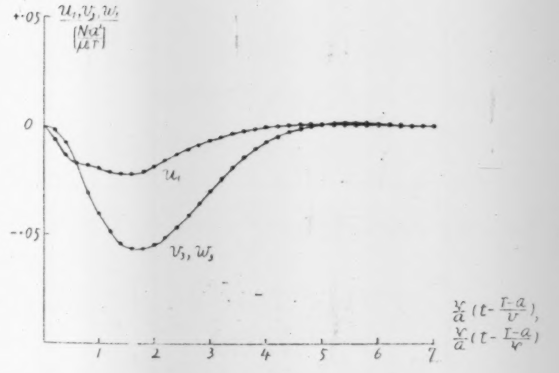

Fig. 6. Normal stress: $\Omega=1$.

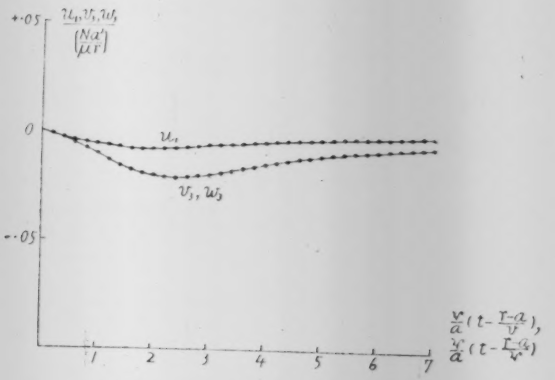

Fig. 7. Normal stress: $\Omega=0{\cdot}2$

As will be seen from the figure, the stress change almost attains its final value in the period during which the distortional wave travels

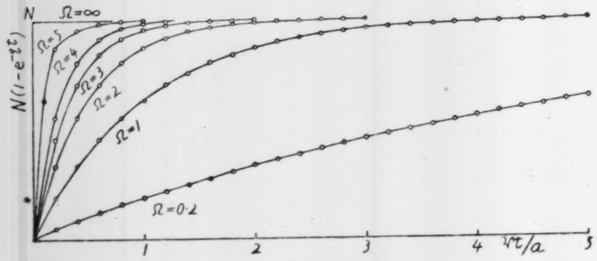

Fig. 8.

a distance that is nearly equal to the radius or the diameter of the sphere $r=a$, for the case in which $\Omega=5$ or 3 respectively.

(b) We shall next consider the case in which normal stress $\widehat{rr}=0$, and the change in the tangential stresses at $r=a$ are

$$\widehat{r\theta}=\widehat{r\varphi}=0, \qquad (r=a,\ t<0)$$

$$\left.\begin{aligned} \widehat{r\theta}&=Te^{-ct}(1-e^{-qt})\frac{dP_2^1(\cos\theta)}{d\theta}\cos\varphi \\ \widehat{r\varphi}&=-Te^{-ct}(1-e^{-qt})\frac{P_2^1(\cos\theta)}{\sin\theta}\sin\varphi \end{aligned}\right\},\ (r=a,\ t>0)$$

in which $c\to 0$.

As done previously, we shall consider only the case in which Poisson's ratio $\sigma=\dfrac{1}{4}$.

The normal component of displacement of the dilatational wave at a great focal distance is given by

$$\begin{aligned} u_1&=\frac{1}{2\pi}\int_{-\infty}^{\infty}\frac{\Delta_1'}{\Delta}\frac{d}{dr}\frac{H_{\frac{5}{2}}^{(2)}(hr)}{\sqrt{r}}e^{ipt}dp\int_{-\infty}^{\infty}\varphi(\omega)e^{-ip\omega}d\omega P_2^1(\cos\theta)\cos\varphi \\ &=\frac{1}{2\pi}\frac{12T\mathfrak{v}^4}{\mu ar^2}P_2^1(\cos\theta)\cos\varphi\, i\left[\int_{-\infty}^{\infty}\frac{f''(p)e^{ip\left(t-\frac{r-a}{v}\right)}}{(p-ic)g(p)}dp\right. \\ &\qquad\left.-\int_{-\infty}^{\infty}\frac{f''(p)e^{ip\left(t-\frac{r-a}{v}\right)}}{(p-iq)g(p)}dp\right], \end{aligned}$$

where

$$\Delta_1'=-12T\mu\frac{d}{da}\frac{H_{\frac{5}{2}}^{(2)}(ka)}{a^{3/2}},$$

$$\begin{aligned}
f''(p) = & \Big[-\frac{a}{\mathfrak{v}}p^2 + 12\frac{\mathfrak{v}}{a} + i\Big(5p - 12\frac{\mathfrak{v}^2}{a^2 p}\Big)\Big] \\
& \times\Big[-\frac{1}{\sqrt{3}}\frac{r}{\mathfrak{v}}p^2 + 9\sqrt{3}\frac{\mathfrak{v}}{r} + i\Big(4p - 27\frac{\mathfrak{v}^2}{r^2 p}\Big)\Big] \\
& \div\frac{r}{\sqrt{3}}\Big(\frac{a}{\mathfrak{v}^2}p^4 - i5\frac{1}{\mathfrak{v}}p^3 - 12\frac{1}{a}p^2 + i12\frac{\mathfrak{v}}{a^2}p\Big) \\
& \qquad\qquad - i4\Big(\frac{a}{\mathfrak{v}}p^3 - i5p^2 - 12\frac{\mathfrak{v}}{a}p + i12\frac{\mathfrak{v}^2}{a^2}\Big).
\end{aligned}$$

Evaluating the integration, we have

$$\begin{aligned}
u_1 = & 1\cdot044\frac{Ta^3}{\rho r^2}P_2^1(\cos\theta)\cos\varphi + \frac{12Ta^2}{\sqrt{3}\rho r}P_2^1(\cos\theta)\cos\varphi \\
& \times\Bigg[\Big[(\Omega^4 - 5\Omega^3 + 12\Omega^2 + 12\Omega)e^{-\Omega\tau} \div (-\Omega^6 + 12\cdot506\Omega^5 - 81\cdot672\Omega^4 \\
& + 326\cdot05\Omega^2 - 759\cdot7\Omega^2 + 870\cdot7\Omega - 552)\Big] \\
& + 2\frac{e^{-1\cdot801\tau}}{8\cdot370}\Big[\Big\{(3\cdot5481\times10^5 - 7\cdot4500\times10^4\Omega)\cos(4\cdot185\tau) \\
& + (-2\cdot1685\times10^5 - 5\cdot2715\times10^4\Omega)\sin(4\cdot185\tau)\Big\} \\
& \div\Big\{(1566\cdot7 - 138\cdot29\Omega)^2 + (11\cdot73 + 314\cdot83\Omega)^2\Big\} \\
& - \Big\{3\cdot5481\times10^5\cos(4\cdot185\tau) - 2\cdot1685\times10^5\sin(4\cdot185\tau)\Big\} \\
& \div(2\cdot4546\times10^6)\Big] \\
& + 2\frac{e^{-3\cdot649\tau}}{2\cdot880}\Big[\Big\{(-2\cdot2475\times10^4 + 1\cdot0859\times10^4\Omega)\cos(1\cdot440\tau) \\
& + (5\cdot9094\times10^4 - 1\cdot1910\times10^4\Omega)\sin(1\cdot440\tau)\Big\} \\
& \div\Big\{(832\cdot26 - 192\cdot39\Omega)^2 + (52\cdot98 - 90\cdot44\Omega)^2\Big\} \\
& - \Big\{-2\cdot2475\times10^4\cos(1\cdot440\tau) + 5\cdot9094\times10^4\sin(1\cdot440\tau)\Big\} \\
& \div(6\cdot9547\times10^5)\Big]
\end{aligned}$$

$$+2\frac{e^{-0.803\tau}}{2{\cdot}082}\Bigg[\Bigg\{(-7{\cdot}8938\times10^2-6{\cdot}1551\times10^2\Omega)\cos(1{\cdot}041\tau)$$

$$+(-1{\cdot}6309\times10^3+1{\cdot}2331\times10^3\Omega)\sin(1{\cdot}041\tau)\Bigg\}$$

$$\div\Big\{(53{\cdot}99+122{\cdot}15\Omega)^2+(244{\cdot}47-146{\cdot}09\Omega)^2\Big\}$$

$$-\Big\{-7{\cdot}8938\times10^2\cos(1{\cdot}041\tau)-1{\cdot}6309\times10^3\sin(1{\cdot}041\tau)$$

$$\div(6{\cdot}2681\times10^4)\Big\}\Bigg]\Bigg].$$

Next, the co-latitudinal and the longitudinal components of the distortional wave at a distant point is expressed respectively by

$$v_3=\frac{1}{2\pi}\int_{-\infty}^{\infty}\frac{\Delta_2'}{\Delta}\frac{1}{r}\frac{d}{dr}\Big\{\sqrt{r}\,H_{\frac{5}{2}}^{(2)}(kr)\Big\}e^{ipt}dp$$

$$\times\int_{-\infty}^{\infty}\varphi(\omega)e^{-ip\omega}d\omega\,\frac{dP_2^1(\cos\theta)}{d\theta}\cos\varphi$$

$$=\frac{1}{2\pi}\frac{T\mathfrak{v}^4}{\mu a r^2}\frac{dP_2^1(\cos\theta)}{d\theta}\cos\varphi\, i\Bigg[\int_{-\infty}^{\infty}\frac{f'''(p)e^{ip\left(t-\frac{r-a}{\mathfrak{v}}\right)}}{(p-ic)g(p)}dp$$

$$-\int_{-\infty}^{\infty}\frac{f'''(p)e^{ip\left(t-\frac{r-a}{\mathfrak{v}}\right)}}{(p-iq)g(p)}dp\Bigg],$$

$$w_3=-\frac{1}{2\pi}\int_{-\infty}^{\infty}\frac{\Delta_2'}{\Delta}\frac{1}{r}\frac{d}{dr}\Big\{\sqrt{r}\,H_{\frac{5}{2}}^{(2)}(kr)\Big\}e^{ipt}dp$$

$$\times\int_{-\infty}^{\infty}\varphi(\omega)e^{-ip\omega}d\omega\,\frac{P_2^1(\cos\theta)}{\sin\theta}\sin\varphi$$

$$=-\frac{1}{2\pi}\frac{T\mathfrak{v}^4}{\mu a r^2}\frac{P_2^1(\cos\theta)}{\sin\theta}\sin\varphi\, i\Bigg[\int_{-\infty}^{\infty}\frac{f'''(p)e^{ip\left(t-\frac{r-a}{\mathfrak{v}}\right)}}{(p-ic)g(p)}dp$$

$$-\int_{-\infty}^{\infty}\frac{f'''(p)e^{ip\left(t-\frac{r-a}{\mathfrak{v}}\right)}}{(p-iq)g(p)}dp\Bigg],$$

where

$$\Delta_2'=-T\mu\Big\{h^2\frac{H_{\frac{5}{2}}^{(2)}(ha)}{\sqrt{a}}-2\frac{d^2}{da^2}\frac{H_{\frac{5}{2}}^{(2)}(ha)}{\sqrt{a}}\Big\},$$

$$f'''(p)=\left[72\sqrt{3}\,\frac{\mathfrak{v}}{a}-\frac{13}{\sqrt{3}}\,\frac{a}{\mathfrak{v}}p^2-i\left\{-216\,\frac{\mathfrak{v}^2}{a^2p}+37p-\frac{a^2}{\mathfrak{v}^2}p^3\right\}\right]$$

$$\times\left[6\,\frac{\mathfrak{v}}{r}-\frac{r}{\mathfrak{v}}p^2+i\left(-\frac{6\mathfrak{v}^2}{r^2p}+3p\right)\right]$$

$$=r\left(-i\frac{a^2}{\mathfrak{v}^3}p^5+\frac{13}{\sqrt{3}}\,\frac{a}{\mathfrak{v}^2}p^4+i37\frac{1}{\mathfrak{v}}\,p^3-72\sqrt{3}\,\frac{1}{a}\,p^2-i216\,\frac{\mathfrak{v}}{a^2}p\right)$$

$$-i3\left(-i\frac{a^2}{\mathfrak{v}^2}p^4+\frac{13}{\sqrt{3}}\,\frac{a}{\mathfrak{v}}\,p^3+i37p^2-72\sqrt{3}\,\frac{\mathfrak{v}}{a}\,p-i216\,\frac{\mathfrak{v}^2}{a^2}\right).$$

Evaluating the integration, we get

$$v_3=-1{\cdot}1739\,\frac{Ta^3}{\mu r^2}\,\frac{dP_2^1(\cos\theta)}{d\theta}\cos\varphi+\frac{Ta^2}{\mu r}\,\Psi'\,\frac{dP_2^1(\cos\theta)}{d\theta}\cos\varphi,$$

$$w_3=+1{\cdot}1739\,\frac{Ta^3}{\mu r^2}\,\frac{P_2^1(\cos\theta)}{\sin\theta}\sin\varphi-\frac{Ta^2}{\mu r}\,\Psi'\,\frac{P_2^1(\cos\theta)}{\sin\theta}\sin\varphi,$$

where

$$\Psi'=(\Omega^5+7{\cdot}5056\Omega^4+37\Omega^3+124{\cdot}71\Omega^2+216\Omega)\,e^{-\Omega\tau'}$$

$$\div(-\Omega^6+12{\cdot}506\Omega^5-81.672\Omega^4+326{\cdot}05\Omega^3-759{\cdot}7\Omega^2$$

$$+870{\cdot}7\Omega-552)$$

$$+2\,\frac{e^{-1{\cdot}8014\tau'}}{8{\cdot}3710}\Big[\Big\{(-4{\cdot}8800\times10^6-3{\cdot}6785\times10^5\Omega)\cos(4{\cdot}1855\tau')$$

$$+(-3{\cdot}9252\times10^6+1{\cdot}3243\times10^6\Omega)\sin(4{\cdot}1855\tau')\Big\}$$

$$\div\Big\{(1567{\cdot}3-138{\cdot}18\Omega)^2+(10.93+314{\cdot}99\Omega)^2\Big\}$$

$$-\Big\{-4{\cdot}8800\times10^6\cos(4{\cdot}1855\tau')-3{\cdot}9252\times10^6\sin(4{\cdot}1855\tau')\Big\}$$

$$\div(2{\cdot}4565\times10^6)\Big]$$

$$+2\,\frac{e^{-3{\cdot}6486\tau'}}{2{\cdot}8800}\Big[\Big\{(2{\cdot}1499\times10^6-4{\cdot}82\times10^3\Omega)\cos(1{\cdot}4400\tau')$$

$$+(5{\cdot}3957\times10^6-1{\cdot}4807\times10^6\Omega)\sin(1{\cdot}4400\tau')\Big\}$$

$$\div\Big\{(831{\cdot}90-192{\cdot}33\Omega)^2+(52{\cdot}84-90{\cdot}39\Omega)^2\Big\}$$

$$-\left\{2{\cdot}1499\times10^{6}\cos(1.4400\tau')+5{\cdot}3957\times10^{6}\sin(1{\cdot}4400\tau')\right\}$$

$$\div(6.9485\times10^{5})\Big]$$

$$+2\frac{e^{-0{\cdot}8032\tau'}}{2{\cdot}0814}\Big[\left\{(-1{\cdot}0913\times10^{5}+6{\cdot}8525\times10^{4}\Omega)\cos(1{\cdot}0407\tau')\right.$$

$$\left.+(2{\cdot}9569\times10^{4}+5{\cdot}1975\times10^{4}\Omega)\sin(1{\cdot}0407\tau')\right\}$$

$$\div\left\{(53{\cdot}95+122{\cdot}11\Omega)^{2}+(244{\cdot}41-146{\cdot}08\Omega)^{2}\right\}$$

$$-\left\{-1{\cdot}0913\times10^{5}\cos(1{\cdot}0407\tau')+2{\cdot}9569\times10^{4}\sin(1{\cdot}0407\tau')\right\}$$

$$\div(6{\cdot}2647\times10^{4})\Big].$$

In regard to the displacements u_1 (P phase) and v_3, w_3 (S phase) in a number of cases, Ω in every one of them assumes values differing from one another, as shown in Figs. 9∼15.

It will be remembered that the azimuthal terms $P_2^1(\cos\theta)\cos\varphi$, $\frac{dP_2^1(\cos\theta)}{d\theta}\cos\varphi$ and $-\frac{P_2^1(\cos\theta)}{\sin\theta}\sin\varphi$ in the cases respectively of u_1, v_3, and w_3 are taken as unity.

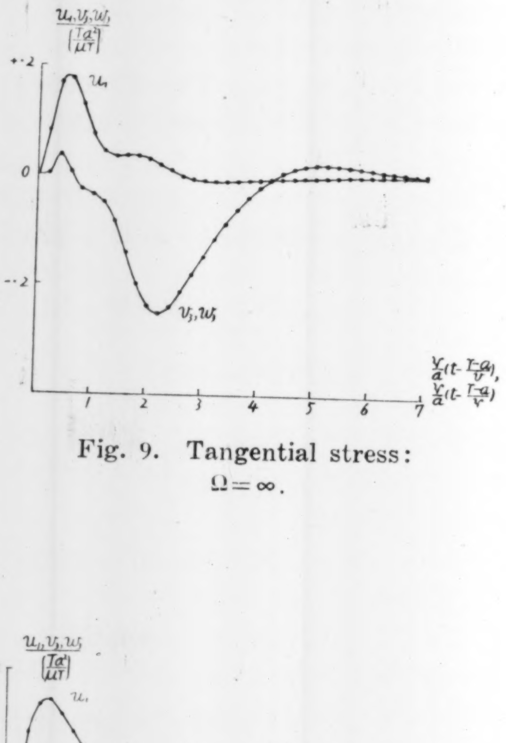

Fig. 9. Tangential stress: $\Omega=\infty$.

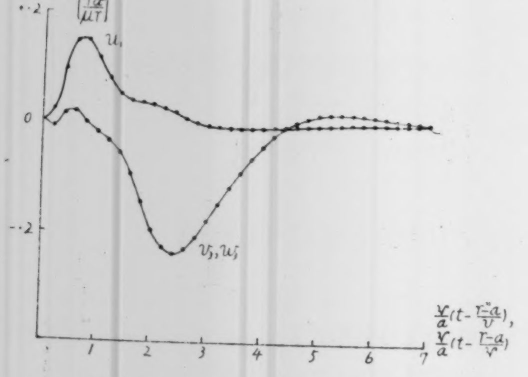

Fig. 10. Tangential stress: $\Omega=5$.

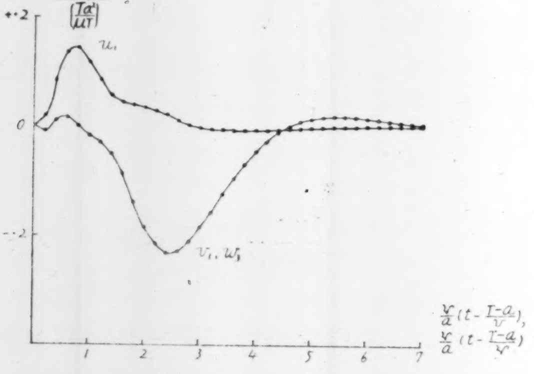

Fig. 11. Tangential stress: $\Omega=4$.

(c) We shall next consider the case in which both the normal and the tangential stresses on the surface of a spherical cavity undergo changes with different rapidities.

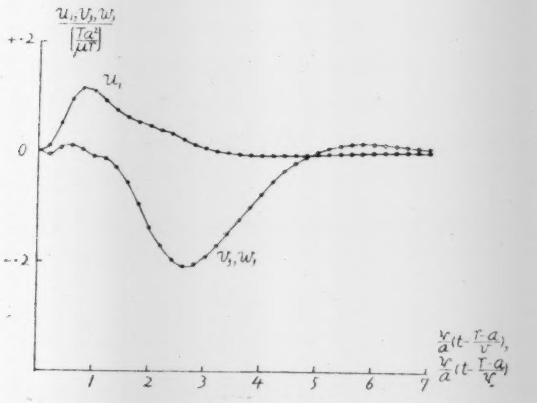

Fig. 12. Tangential stress: $\Omega=3$.

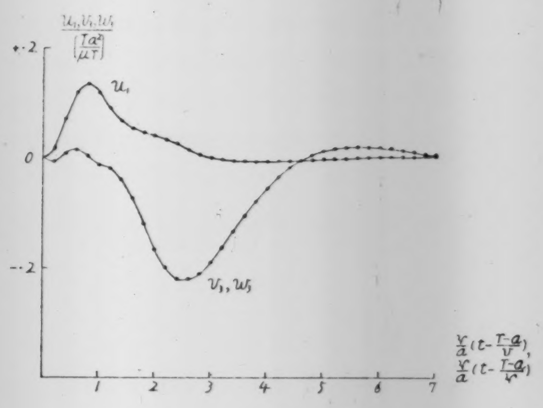

Fig. 13. Tangential stress: $\Omega=2$.

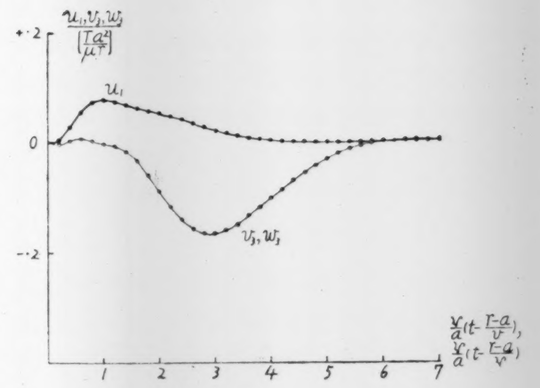

Fig. 14. Tangential stress: $\Omega=1$.

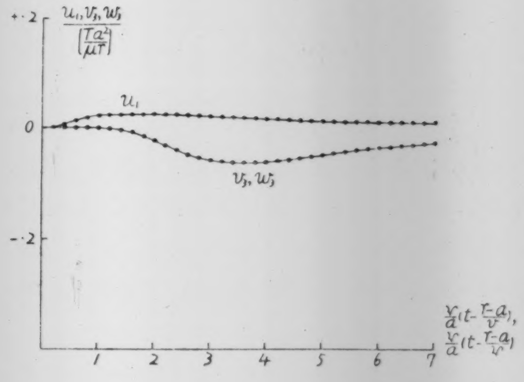

Fig. 15. Tangential stress: $\Omega=0{\cdot}2$

The boundary conditions are

$$\widehat{rr}=\widehat{r\theta}=\widehat{r\varphi}=0, \qquad (r=a,\ t<0)$$

$$\left.\begin{aligned}
\widehat{rr}&=Ne^{-ct}(1-e^{-qt})P_2^1(\cos\theta)\cos\varphi,\\
\widehat{r\theta}&=Te^{-ct}(1-e^{-qt})\frac{dP_2^1(\cos\theta)}{d\theta}\cos\varphi,\\
\widehat{r\varphi}&=-Te^{-ct}(1-e^{-qt})\frac{P_2^1(\cos\theta)}{\sin\theta}\sin\varphi,
\end{aligned}\right\}\quad (r=a,\ t>0)$$

in which $c\to 0$.

Here, we have cases in which

$$T=-N,\ -\frac{1}{2}N,\ -\frac{1}{3}N,\ -\frac{1}{5}N,$$

$$-\frac{1}{10}N,\ +\frac{1}{10}N,\ +\frac{1}{5}N,\ +\frac{1}{3}N,\ +\frac{1}{2}N.$$

The displacements u_1 and v_3, w_3 in these cases are plotted in Figs. 16~28.

4.

In article 1, the writer mentioned that Dr. H. Honda, after examining the amplitudes at the initial phases of the dilatational and the distortional waves, had concluded that the wave lengths of the seismic waves might be comparable with the dimensions of the seismic origins.

As just stated, however, the assumption was that only the normal stress had changed periodically on the surface of the sphere, the tangential stress remaining zero.

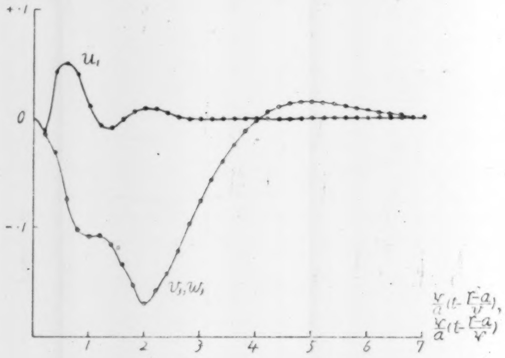

Fig. 16. $\frac{T}{N}=+\frac{1}{2}$: $\Omega=\infty$.

To the writer it seems more appropriate to consider the two stresses, normal and tangential, as having changed with a certain rapidity on the surface of the sphere at the seismic focus, than to assume simple periodic forces.

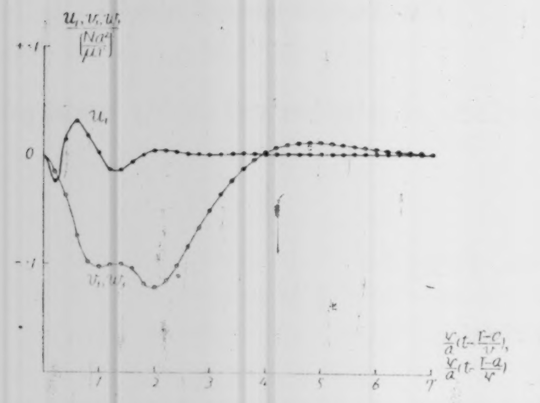

Fig. 17. $\frac{T}{N}=+\frac{1}{3}$: $\Omega=\infty$.

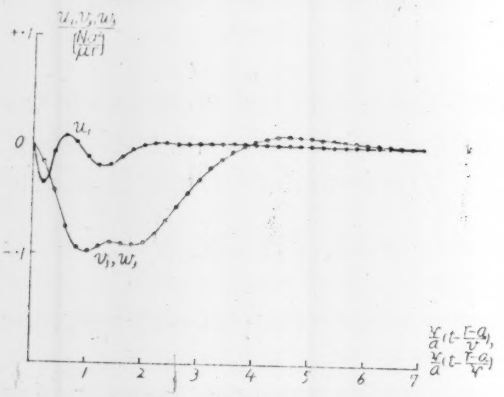

Fig. 18. $\frac{T}{N}=+\frac{1}{5}$: $\Omega=\infty$.

We shall next consider the quantity $R = \frac{1}{5\cdot20}\frac{\mathfrak{A}_s}{\mathfrak{A}_p}$, which concerns

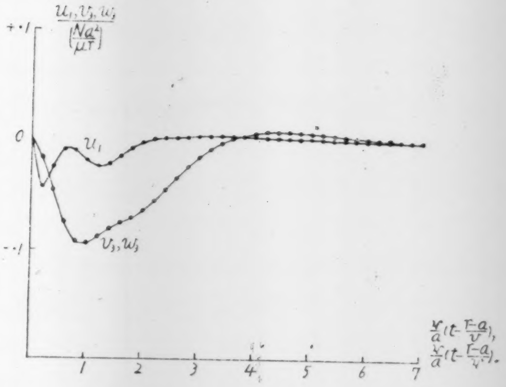

Fig. 19. $\frac{T}{N} = +\frac{1}{10}$: $\Omega = \infty$.

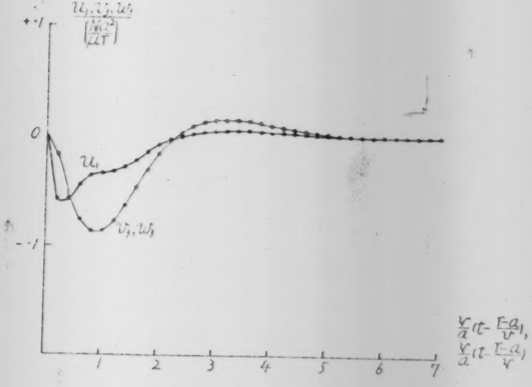

Fig. 20. $\frac{T}{N} = -\frac{1}{10}$: $\Omega = \infty$.

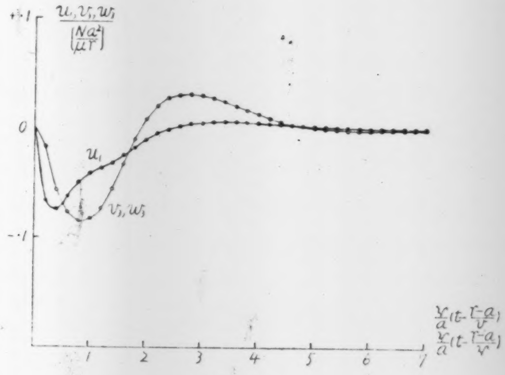

Fig. 21. $\frac{T}{N} = -\frac{1}{5}$: $\Omega = \infty$.

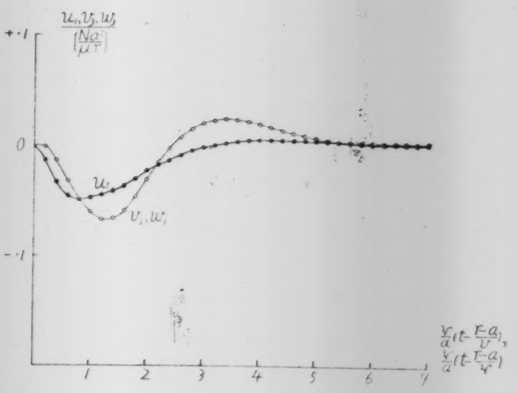

Fig. 22. $\frac{T}{N} = -\frac{1}{5}$: $\Omega = 2$.

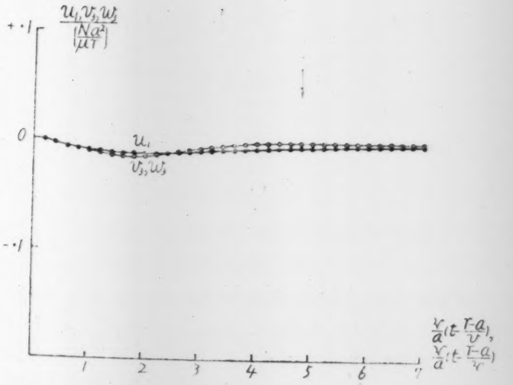

Fig. 23. $\frac{T}{N} = -\frac{1}{5}$: $\Omega = 0\cdot2$.

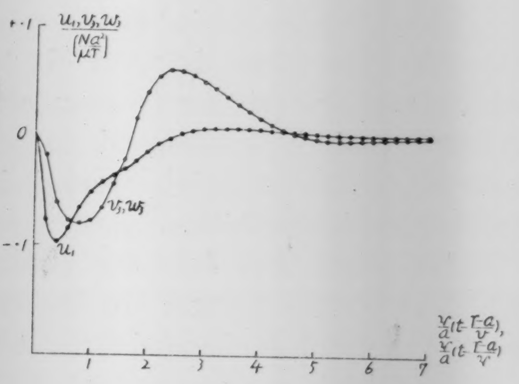

Fig. 24. $\frac{T}{N} = -\frac{1}{3}$: $\Omega = \infty$.

the proportion in the amplitudes of the *P* and *S* phases, and the periods of the two waves in our cases that have been treated mathematically in the preceding articles.

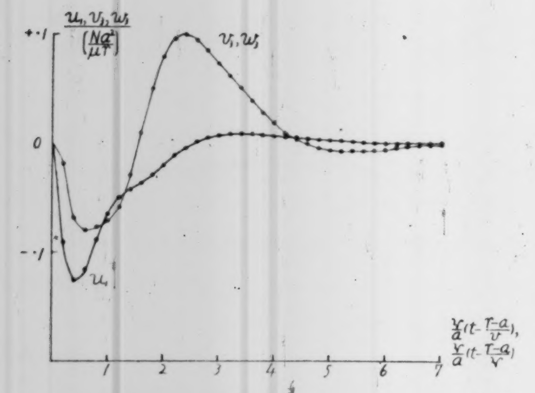

Fig. 25. $\frac{T}{N}=-\frac{1}{2}$: $\Omega=\infty$.

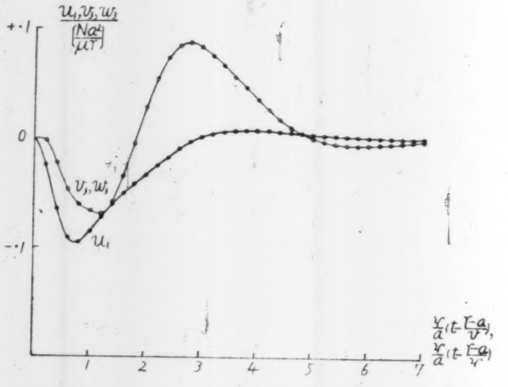

Fig. 26. $\frac{T}{N}=-\frac{1}{2}$: $\Omega=3$.

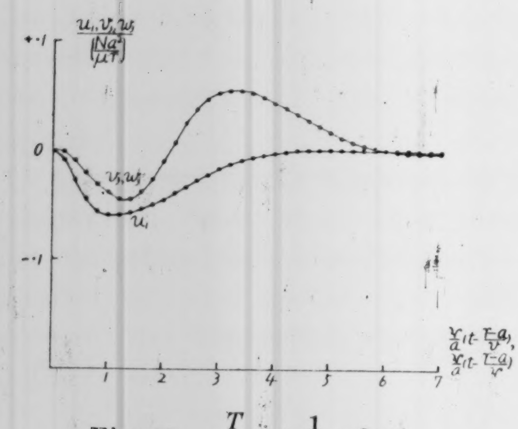

Fig. 27. $\frac{T}{N}=-\frac{1}{2}$: $\Omega=1$.

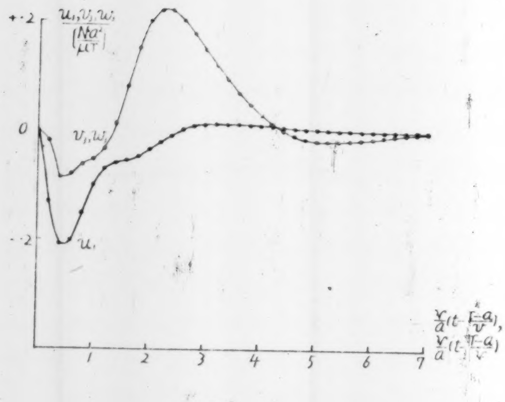

Fig. 28. $\frac{T}{N}=-1$: $\Omega=\infty$.

Since, for the period of the wave, we take the time interval during which the first stroke is completed, it may roughly correspond to one-quarter of the complete period in the harmonic oscillation.

We shall first take the case in which either the normal or the tangential stress has changed separately.

In the latter case we neglect the minor fluctuating displacement at the very initial part of the distortional waves.

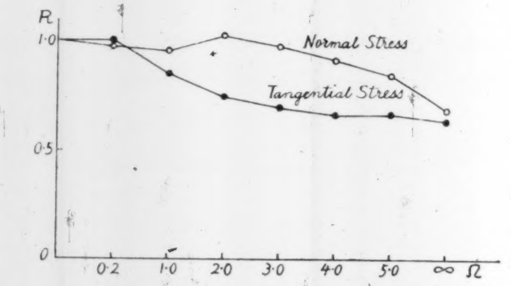

Fig. 29. The quantity R in the case in which either the normal or the tangential stress changes separately with a certain rapidity Ω.

The values of R and the periods of the waves will be found in

Table II, R being plotted in Fig. 29.

We shall next take the case in which both the normal and the tangential stresses change simultaneously with a certain rapidity.

The proportion between the two ranges of the stress change is taken as

$$\frac{T}{N}=-1,\ -\frac{1}{2},\ -\frac{1}{3},\ -\frac{1}{5},\ -\frac{1}{10},\ +\frac{1}{10},\ +\frac{1}{5},\ +\frac{1}{3},\ +\frac{1}{2}.$$

The values of R and the periods of the waves in these cases are shown in Table II.

The quantity R and the ratio γ between the two periods of the distortional (T_2) and the dilatational (T_1) waves are plotted in Fig. 30.

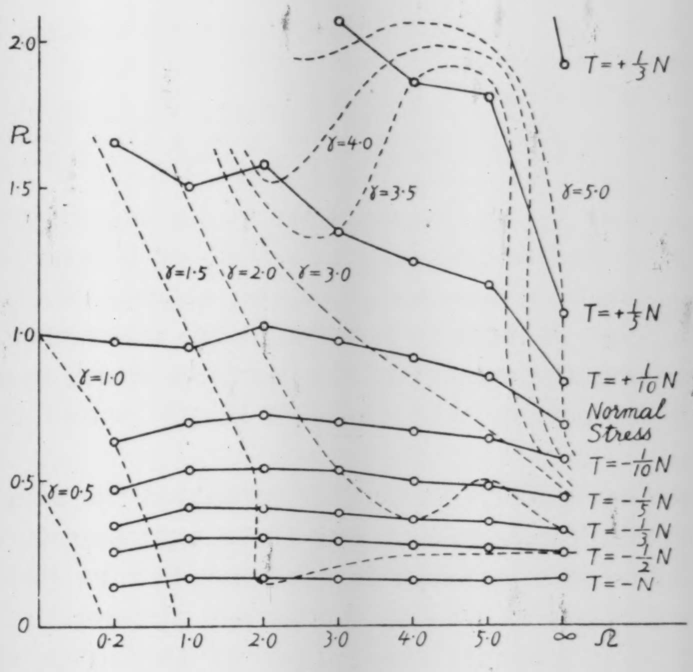

Fig. 30. The quantity R and the ratio γ betweeen the two periods of the distortional and the dilatational waves in the case in which both the normal and the tangential stresses change simultaneously with a certain rapidity Ω.

As just stated, in some deep-focus earthquakes, R assumes a value between 0·13 and 0·81. According to Mr. T. Ishikawa, in the deep-focus earthquake of Feb. 20, 1931, the observed periods of the S phases were in the mean, 1·77 times greater than those of the P phases. The writer estimated the quantities γ in some deep-focus earthquakes from the seismograms obtained by Omori type long period seismometers (proper period = 30 ~ 60 sec.) installed at Hongô, Tokyo.

They are shown in the following Table.

Table III.

Date of Occurrence	Epicenter		Depth	T_1	$\gamma = \frac{T_2}{T_1}$
	λ	φ			
June 30, 1931	136·5	34·2	360 km	1·5 sec	1·5
Nov. 13, 1932	137·25	43·57	320	3·0	1·5
Dec. 5, 1933	144·3	46·4	350	2·4	1·2

As will be seen from Fig. 30, we may conclude that in these deep-focus earthquakes, the normal and the tangential stresses cooporated at the same time on the spherical surface in certain proportions ranging from $\frac{T}{N} = 0$ to $\frac{T}{N} = -1$, and, further, that these stresses changed with rapidities ranging from $\Omega = 1$ to $\Omega = \infty$.

As stated above, the stresses attain almost their final value during the period in which the distortional wave travels a distance nearly equal to the radius or to the diameter of the sphere, as measured at the seismic focus, in the case in which $\Omega = 5$ or 3 respectively.

We may therefore conclude that the stresses about the seismic focus might change in magnitude through the occurrence of something like slippings along the numerous slip surfaces which might take place with velocities comparable with those of elastic waves throughout the seismic focus.

In his previous paper,[5] the writer estimated the range of pressure changes in certain earthquakes,* but these examples turned out to be unsuitable for the reason that it is necessary to take into consideration the tangential stresses as well as the normal stresses.

We shall next consider the ranges of the stress change at the origins, taking into consideration the tangential stresses as well as the

---

5) W. INOUYE, *Bull. Earthq. Res. Inst.*, **15** (1937), 90.

* The writer erred in his calculation, in that N should have been multiplied by $\frac{2}{3}$, the amended result being

$$N = -\frac{2}{3} \times 273 = -182 \text{ atms. in the first example}$$

and

$$N = -\frac{2}{3} \times 228 = -152 \text{ atms. in the second example.}$$

normal stresses.

According to Dr. H. Honda,[6] the normal component of the dilatational wave when r is large is expressed by

$$u_r = \mathfrak{A}_p \frac{1}{r} \sin 2\theta \cos\varphi \, e^{i(pt-hr)+i\varepsilon_1}$$

$$= \frac{2}{3} \mathfrak{A}_p \frac{1}{r} P_2^1(\cos\theta) \cos\varphi \, e^{i(pt-hr)+i\varepsilon_1}.$$

In the deep-focus earthquakes of June 30, 1931 (epicenter; $\lambda = 136{\cdot}5°$, $\varphi = 34{\cdot}2°$: focal depth $= 360$ km), the observed amplitudes in the P phases are well given by assuming that

$$\mathfrak{A}_p = 1{\cdot}54 \times 10^5 \mathrm{cm}^2.$$

Moreover, it has been reported by Dr. H. Honda that $R = \frac{1}{5{\cdot}20} \times \frac{\mathfrak{A}_s}{\mathfrak{A}_p} = 0{\cdot}47$. The writer estimated $T_1 = 1{\cdot}5$ sec and $\frac{T_2}{T_1} = 1{\cdot}5$ from the seismograms obtained at Hongô, Tokyo.

We may assume that this case corresponds to that in which $\frac{T}{N} = -\frac{1}{5}$ and $\Omega = 2$.

We then have

$$\mathfrak{A}_p = -\frac{3}{2} \times 0{\cdot}0490 \frac{Na^2}{\mu}.$$

Assuming

$$v = 8{\cdot}8 \text{ km/sec},$$

we obtain

$$l_p = vT_1 = 8{\cdot}8 \times 1{\cdot}5 = 13 \text{ km},$$

while

$$l_p = \frac{v}{\mathfrak{v}} aT_1 = \sqrt{3}\, a \times 0{\cdot}8 = 1{\cdot}4a,$$

whence

$$a = \frac{13}{1{\cdot}4} = 9{\cdot}3 \text{ km}.$$

Assuming

---

[6] *loc. cit.*

$\mu = 8{\cdot}4 \times 10^{11}$ dyne/cm^2 (ρ is assumed to be 3·0),

$$N = -\frac{2}{3}\,\frac{1{\cdot}54 \times 10^5 \times 8{\cdot}4 \times 10^{11}}{4{\cdot}90 \times 10^{-2}(9{\cdot}3 \times 10^5)^2} = -1{\cdot}9 \times 10^6 \text{ dyne/cm}^2.$$

Therefore,

$$T = \frac{1}{5} \times 1{\cdot}9 \times 10^6 \text{ dyne/cm}^2.$$

In the deep-focus earthquake of June 3, 1929 (epicenter; $\lambda = 137{\cdot}2^\circ$, $\varphi = 34{\cdot}3^\circ$: focal depth$=$320 km), the observed amplitudes in the P phases are well expressed by assuming that

$$\mathfrak{A}_p = 4{\cdot}94 \times 10^5 \text{ cm}^2.$$

Dr. H. Honda has reported that $R = 0{\cdot}55$. The writer estimated the period $T_1 = 1{\cdot}5$ sec from the record obtained at Tokyo.

We may assume that this case corresponds to the one in which $\dfrac{T}{N} = -\dfrac{1}{5}$ and $\Omega = 3$.

We then have

$$\mathfrak{A}_p = -\frac{3}{2} \times 0{\cdot}0555 \frac{Na^2}{\mu}.$$

Assuming

$$v = 8{\cdot}6 \text{ km/sec},$$

we obtain

$$l_p = 8{\cdot}6 \times 1{\cdot}5 = 1{\cdot}29 \text{ km},$$

while

$$l_p = \frac{v}{\mathfrak{v}} a T_1 = \sqrt{3}\, a \times 0{\cdot}6 = 1{\cdot}04a,$$

whence

$$a = \frac{12{\cdot}9}{1{\cdot}04} = 12{\cdot}4 \text{ km}.$$

Assuming

$\mu = 8{\cdot}0 \times 10^{11}$ dyne/cm^2,

$$N = -\frac{2}{3}\,\frac{4{\cdot}94 \times 10^5 \times 8{\cdot}0 \times 10^{11}}{5{\cdot}55 \times 10^{-2}(12{\cdot}4 \times 10^5)^2} = -3{\cdot}08 \times 10^6 \text{ dyne/cm}^2.$$

Therefore,

$$T = \frac{1}{5} \times 3{\cdot}08 \times 10^6 \text{ dyne/cm}^2.$$

Since, according to Dr. H. Jeffreys'[7] estimate, the strength of a substance at a depth of 300 km in the earth's crust is about $9{\cdot}2\times 10^7$ dyne/cm^2, the range of the stress changs at the moment of the occurrence of an earthquake is a fraction that of the strength of the substance just mentioned.

5. *Discussion.*

(a) In the foregoing articles, it is assumed that the stresses at the seismic origin, starting from no stress, attained to certain final values with certain rapidities.

But in the case in which the existing stresses become zero with various rapidities, the boundary conditions are expressed by

$$\left.\begin{aligned}\widehat{rr}&=NP_2^1(\cos\theta)\cos\varphi\\ \widehat{r\theta}&=T\frac{dP_2^1(\cos\theta)}{d\theta}\cos\varphi\\ \widehat{r\varphi}&=-T\frac{P_2^1(\cos\theta)}{\sin\theta}\sin\varphi\end{aligned}\right\}\;,\quad (r=a,\ t<0)$$

$$\left.\begin{aligned}\widehat{rr}&=Ne^{-ct}P_2^1(\cos\theta)\cos\varphi\\ \widehat{r\theta}&=Te^{-ct}\frac{dP_2^1(\cos\theta)}{d\theta}\cos\varphi\\ \widehat{r\varphi}&=-Te^{-ct}\frac{P_2^1(\cos\theta)}{\sin\theta}\sin\varphi\end{aligned}\right\}\;.\quad (r=a,\ t>0)$$

The displacements in this case can be obtained by merely changing the signs of those given in the foregoing articles.

(b) In the preceding articles, in order to explain the actual earthquakes, we had to consider the tangential stresses as well as the normal stresses. Moreover, the signs of the two kinds of stresses differed in the deep-focus earthquakes.

We shall next consider the case in which the two stresses around the seismic focus take different signs, taking the case in which the elastic body that contains a spherical inclusion is subjected to a uniform simple shear.

This problem has already been treated in the previous paper.[8]

Let a be the radius of the spherical inclusion, λ', μ' Lame's elastic constants, u', v', w' the components of displacement, and $\widehat{rr}'$, $\widehat{\theta\theta}'$, $\widehat{\varphi\varphi}'$, $\widehat{r\theta}'$, $\widehat{r\varphi}'$, $\widehat{\theta\varphi}'$ the components of stress in the inclusion, and let the unaccented symbols represent those in the outer medium.

---

[7] H. Jeffreys, *Phil. Mag.*, **19** (1935), 840.

[8] W. Inouye, *Bull. Earthq. Res. Inst.*, **16** (1938), 125.

The boundary conditions are then as follows.

At $r=a$,

$$u=u', \quad v=v', \quad w=w',$$

$$\widehat{rr}=\widehat{rr}', \quad \widehat{r\theta}=\widehat{r\theta}', \quad \widehat{r\varphi}=\widehat{r\varphi}',$$

and at $r=\infty$,

$$\widehat{rr}=S\sin^2\theta\sin 2\varphi, \quad \widehat{r\theta}=\frac{S}{2}\sin 2\theta\sin 2\varphi,$$

$$\widehat{\theta\theta}=S\cos^2\theta\sin 2\varphi, \quad \widehat{r\varphi}=S\sin\theta\cos 2\varphi,$$

$$\widehat{\varphi\varphi}=-S\sin 2\varphi, \quad \widehat{\theta\varphi}=S\cos\theta\cos 2\varphi,$$

where S is the shearing stress applied to the elastic body.

The stresses in the spherical inclusion are given by

$r\leq a$:—

$$\widehat{rr}'=12\mu'E\sin^2\theta\sin 2\varphi, \quad \widehat{r\theta}'=6\mu'E\sin 2\theta\sin 2\varphi,$$

$$\widehat{\theta\theta}'=12\mu'E\cos^2\theta\sin 2\varphi, \quad \widehat{r\varphi}'=12\mu'E\sin\theta\cos 2\varphi,$$

$$\widehat{\varphi\varphi}'=-12\mu'E\sin 2\varphi, \quad \widehat{\theta\varphi}'=12\mu'E\cos\theta\cos 2\varphi,$$

where

$$E=\frac{5}{4}\,\frac{(\lambda+2\mu)S}{\{\mu(9\lambda+14\mu)+2\mu'(3\lambda+8\mu)\}}\,.$$

The stresses in the outer medium are given by

$r\geq a$:—

$$\widehat{rr}=\left\{\frac{9\lambda+10\mu}{3}\,\frac{A'}{r^3}+4\mu C+\frac{24\mu C'}{r^5}\right\}P_2^2(\cos\theta)\sin 2\varphi,$$

$$\widehat{\theta\theta}=\left\{-\frac{5}{3}\mu A'\frac{1}{r^3}+4\mu C-\frac{6\mu C'}{r^5}\right\}P_2^2(\cos\theta)\sin 2\varphi$$

$$+\left\{-\frac{\mu}{3}A'\frac{1}{r^3}+2\mu C+\frac{2\mu}{r^5}C'\right\}\frac{d^2P_2^2(\cos\theta)}{d\theta^2}\sin 2\varphi,$$

$$\widehat{\varphi\varphi}=\left\{-\frac{5\mu}{3}A'\frac{1}{r^3}+4\mu C-\frac{6\mu C'}{r^5}\right\}P_2^2(\cos\theta)\sin 2\varphi$$

$$+\left\{\frac{4\mu}{3}\,\frac{A'}{r^3}-8\mu C-8\mu\frac{C'}{r^5}\right\}\frac{P_2^2(\cos\theta)}{\sin^2\theta}\sin 2\varphi$$

$$+\left\{-\frac{\mu}{3}\frac{A'}{r^3}+2\mu C+\frac{2\mu C'}{r^5}\right\}\cot\theta\frac{dP_2^2(\cos\theta)}{d\theta}\sin 2\varphi,$$

$$\widehat{r\theta}=\left\{-\frac{3\lambda+2\mu}{6}\frac{A'}{r^3}+2\mu C-8\mu\frac{C'}{r^5}\right\}\frac{dP_2^2(\cos\theta)}{d\theta}\sin 2\varphi,$$

$$\widehat{r\varphi}=\left\{-\frac{3\lambda+2\mu}{3}\frac{A'}{r^3}+4\mu C-16\mu\frac{C'}{r^5}\right\}\frac{P_2^2(\cos\theta)}{\sin\theta}\cos 2\varphi,$$

$$\widehat{\theta\varphi}=\left\{-\frac{\mu}{3}\frac{A'}{r^3}+2\mu C+\frac{2\mu C'}{r^5}\right\}\frac{d}{d\theta}\left(\frac{P_2^2(\cos\theta)}{\sin\theta}\right)\cos 2\varphi$$

$$-\left\{\frac{\mu}{3}\frac{A'}{r^3}-2\mu C-\frac{2\mu C'}{r^5}\right\}\frac{\cot\theta}{\sin\theta}P_2^2(\cos\theta)\cos 2\varphi$$

$$+\left\{-\frac{\mu}{3}\frac{A'}{r^3}+2\mu C+\frac{2\mu C'}{r^5}\right\}\frac{1}{\sin\theta}\frac{dP_2^2(\cos\theta)}{d\theta}\cos 2\varphi,$$

where

$$\left.\begin{aligned} C&=\frac{S}{12\mu},\\ A'&=-\frac{5(\mu-\mu')a^3S}{\{\mu(9\lambda+14\mu)+2\mu'(3\lambda+8\mu)\}},\\ C'&=\frac{(\mu-\mu')(\lambda+\mu)a^5S}{2\mu\{\mu(9\lambda+14\mu)+2\mu'(3\lambda+8\mu)\}}.\end{aligned}\right\}$$

The stresses in the spherical inclusion are independent of r, and might be in a plastic state, provided S were sufficiently large; moreover, the normal stress $\widehat{rr}$ and the two tangential stresses $\widehat{r\theta}$, $\widehat{r\varphi}$ have the same sign, ignoring the azimuthal terms.

We shall then consider the stresses in the outer medium in the neighbourhood of the nucleus.

For simplicity, we put $\lambda=\mu$,
whence

$$\left.\begin{aligned} C&=\frac{S}{12\mu},\\ A'&=\frac{-5(\mu-\mu')a^3S}{23\mu^2+22\mu\mu'},\end{aligned}\right\}$$

$$C' = \frac{(\mu-\mu')a^5 S}{23\mu^2+22\mu\mu'}, \Bigg\}$$

and

$$\widehat{rr} = \frac{1}{3}S\left[1-\frac{95a^3}{r^3}D+\frac{72a^5}{r^5}D\right]P_2^2(\cos\theta)\sin 2\varphi,$$

$$\widehat{r\theta} = \frac{1}{6}S\left[1+\frac{25a^3}{r^3}D-\frac{48a^5}{r^5}D\right]\frac{dP_2^2(\cos\theta)}{d\theta}\sin 2\varphi,$$

$$\widehat{r\varphi} = \frac{1}{3}S\left[1+\frac{25a^3}{r^3}D-\frac{48a^5}{r^5}D\right]\frac{P_2^2(\cos\theta)}{\sin\theta}\cos 2\varphi,$$

where

$$D = \frac{\mu-\mu'}{23\mu+22\mu'}.$$

If μ' is comparabie with μ, the normal stress and the tangential stresses have the same sign independent of r.

But if μ' is very small compared with μ, the normal stress has a different sign from, or the same sign as, the tangential stresses according to the distance from the nucleus.

Some of the numerical calculations are tabulated below.

Table IV.

r	$\mu'=0$		$\mu'=0{\cdot}01\mu$	
	$\widehat{rr}$ * $\left(\times\frac{1}{3}S\right)$	$\widehat{r\theta},\ \widehat{r\varphi}$ * $\left(\times\frac{1}{6}S,\ \times\frac{1}{3}S\right)$	$\widehat{rr}$ * $\left(\times\frac{1}{3}S\right)$	$\widehat{r\theta},\ \widehat{r\varphi}$ * $\left(\times\frac{1}{6}S,\ \times\frac{1}{3}S\right)$
1·05a	−0·115	+0·304	−0·094	+0·317
1·1 a	−0·159	+0·521	−0·137	+0·530
1·2 a	−0·132	+0·790	−0·110	+0·794
1·5 a	+0·188	+1·047	+0·204	+1·046
2·0 a	+0·582	+1·071	+0·590	+1·069

* The azimuthal terms are omitted.

Since, as will be seen from the table, at the margin of the nucleus the normal stress and the tangential stresses in the outer medium have different signs, it seems to the writer that seismic waves may be generated as the result of changes in the stresses in the elastic medium at the extreme margin of the seismic focus as the result of plastic yielding within the said focus, rigidity in the focus very small compared with that in the outer medium.

(c) Several authors have already discussed on the dimension of the seismic focus. Mr. T. Hirano[9] remarked on the area of the seismic origin of the Kwantô earthquake of Sept. 1, 1923.

Examining the time-distance curves of some earthquakes, Prof. T. Matuzawa[10] said, "The author is inclined to believe that the accumulation of energy producing the $\bar{P}$ movement takes place in the superficial layer mainly in the form of strain energy and that producing the P movement will do in the lower layer."

Dr. H. Kawasumi,[11] after examining the stress near the hypocenter of the deep-focus earthquake of June 2, 1931, concluded that the magnitude of the hypocentral region might not be smaller than the sphere $r=2$ km.

Prof. S. Fujiwhara[12] discussed about the magnitude of the seismic focus, assuming a very high velocity in the formation of fissures at the said focus.

Recently, Mr. M. Morita[13] treated theoretically the time-distance curves of the waves from the seismic focus of finite dimension.

6. *Summary.*

In the present paper, the writer has compared the data of a number of deep-focus earthquakes obtained by Dr. H. Honda with the results from elastic waves treated theoretically on the assumption that both the normal and the tangential stresses had changed with a certain rapidity on the surface of a spherical cavity as measured at the seismic focus.

We must remember that in these earthquakes the geographical distributions of "pull" and "push" waves at the initial phase of earthquake waves belong to the quadrant type.

The main results are as follows.

(1) Seismic waves may be generated at the result of changes in the stresses in the elastic medium at the extreme margin of the seismic focus as the result of plastic yielding within the said focus, rigidity in the focus being very slight compared with that in the outer medium.

---

9) T. Hirano, *Journ. Meteor. Soc. Japan*, [ii] **2** (1924), 116.

10) T. Matuzawa, *Bull. Earthq. Res. Inst.*, **5** (1928), 1.

11) H. Kawasumi, *Bull. Earthq. Res. Inst.*, **11** (1933), 403.

12) S. Fujiwhara, *Kagaku*, **5** (1935), 506.

13) M. Morita, *Kensindihô*, **10** (1938), 43.

(2) We may conclude that in these deep-focus earthquakes both the normal and the tangential stresses had changed simultaneously at the seismic focuses in certain proportions ranging from $\frac{T}{N}=0$ to $\frac{T}{N}=1$.

(3) In these earthquakes these stresses almost attain their final values in the length of time during which the elastic waves travel a distance comparable with the radius of the seismic origins.

(4) The wave lengths of seismic waves may probably be comparable (several times the radius) with the dimensions of the origins.

(5) The range of stress changes in the seismic origins may be of the order of 10^6 dyne/cm^2.

7. *General Summary.*

In a series of his papers titled "Notes on the Origin of Earthquakes"[14] and "Experiments on Artificial Earthquakes",[15] the writer has dealt with the following subjects.

(a) What are the dimension of the seismic origins compared with the seismic waves that issue from them,

(b) what are the conditions prevailing within the seismic origins?

(c) In what length of time do the stresses change at the seismic origins at the moment of occurrence of the earthquake?

(d) What is the explanation of the fact that the periods of the distortional waves usually exceed those of the dilatational waves?

(e) Is it possible to imitate the distribution of the "push" and "pull" waves at the initial phases of an earthquake waves by an artificial earthquakes or not?

The main results are as follows.

(1) In the majority of earthquakes, we observe two types of distributions of push and pull waves at the initial phase of earthquake waves, namely, conical and quadrant. We cannot yet represent any of these types by means of artificial earthquakes. The case of a weight being allowed to fall on the earth's surface or into a pit dug in the earth corresponds to the doublet source. When the weight falls into the pit, we observe pull waves in the neighbourhood of the pit and push waves at a distance from it. When explosives are fired underground, the initial motions are all push waves.

---

[14] W. INOUYE, *Bull. Earthq. Res. Inst.*, **14** (1936), 582: **15** (1937), 90; 674; 686; 956: **16** (1938), 125.

[15] W. INOUYE and H. KIMURA, *Bull. Earthq. Res. Inst.* **13** (1935), 194.

(2) Our conclusion is that the maximum shear stresses might be constant within the seismic focus, reaching the limit of the ultimate strength of the material immediately preceding an earthquake.

These conditions are fulfilled, for example, within a nuclear mass that is included in an elastic medium that is stressed in one direction or subjected to a uniform simple shear.

(3) In the cases in which conical types are observed, we have to consider the single source $P_0(\cos\theta)$ as well as the quadruple source $P_2(\cos\theta)$ to explain the azimuthal distributions of "pull" and "push" waves. So long as the wave length is greater than the radius of the seismic origin, the component due to the term $P_0(\cos\theta)$ is greater than that due to the term $P_2(\cos\theta)$. Should the wave length become comparable with the dimension of the seismic origin, we find that the azimuthal distribution of the displacement of the dilatational wave becomes quite similar to the azimuthal distribution in the normal stress at the seismic origin.

Next, the following conclusions are mainly deduced from the investigation of the deep-focus earthquakes in which the quadrant types were observed.

(4) Seismic waves may be generated as the result of changes in stress in the elastic medium at the extreme margin of the seismic focus as the result of plastic yielding within the said focus, rigidity in the focus being very slight compared with that in the outer medium.

(5) We may conclude that in deep-focus earthquakes, both the normal and the tangential stresses had changed simultaneously at the seismic origins.

(6) In deep-focus earthquakes these stresses almost attain their final values in that period of time during which the elastic waves travel a distance that is comparable with the radius of the seismic origins.

(7) It is in order to assume that the wave lengths of the seismic waves may be comparable (several times the radius) with the dimensions of the origins.

(8) The range of stress changes in the seismic origins may be of the order of 10^6 dyne/cm^2.

(9) In the case in which the stress on the surface of a spherical cavity changes with different rapidities, the periods of the distortional waves are usually longer than those of dilatational waves.

In concluding this note, the writer wishes to thank Prof. Katsutada Sezawa, Prof. Chuji Tsuboi, Prof. Fuyuhiko Kishinouye, and Dr. Genorkuro Nishimura for their kind interest and valuable advices.

Table. II.

Normal Stress:

Ω	$\frac{u}{\left(\frac{Na^2}{\mu r}\right)}$	$\frac{T_1}{\left[\frac{\mathfrak{v}}{a}\left(t-\frac{r-a}{v}\right)\right]}$	$\frac{v}{\left(\frac{Na^2}{\mu r}\right)}$	$\frac{T_2}{\left[\frac{\mathfrak{v}}{a}\left(t-\frac{r-a}{\mathfrak{v}}\right)\right]}$	R	$\gamma=\frac{T_2}{T_1}$
∞	−0·0513	0·2	−0·0906	1·0	0·68	5·0
5	−0·0390	0·4	−0·0860	1·2	0·85	3·0
4	−0·0356	0·4	−0·0845	1·2	0·91	3·0
3	−0·0318	0·6	−0·0803	1·2	0·97	2·0
2	−0·0270	0·6	−0·0731	1·4	1·04	2·3
1	−0·0227	1·4	−0·0567	1·8	0·95	1·3
0·2	−0·00856	2·0	−0·0215	2·4	0·97	1·2

u: The maximum displacement of the first stroke of the dilatational wave.

v: The maximum displacement of the first stroke of the distortional wave.

T_1: The period of the dilatational wave.

T_2: The period of the distortional wave.

Tangential Stress:

Ω	$\frac{u}{\left(\frac{Ta^2}{\mu r}\right)}$	$\frac{T_1}{\left[\frac{\mathfrak{v}}{a}\left(t-\frac{r-a}{v}\right)\right]}$	$\frac{v}{\left(\frac{Ta^2}{\mu r}\right)}$	$\frac{T_2}{\left[\frac{\mathfrak{v}}{a}\left(t-\frac{r-a}{\mathfrak{v}}\right)\right]}$	R	$\gamma=\frac{T_2}{T_1}$
∞	+0·1758	0·6	−0·2896	1·8	0·63	3·0
5	+0·1505	0·8	−0·2595	1·8	0·66	2·3
4	+0·1446	0·8	−0·2497	1·8	0·66	2·3
3	+0·1338	0·8	−0·2402	2·0	0·69	2·5
2	+0·1135	0·8	−0·2195	2·0	0·74	2·5
1	+0·0782	1·0	−0·1717	2·4	0·85	2·4
0·2	+0·0249	2·0	−0·0647	3·0	1·00	1·5

$T=-N$:

Ω	$\frac{u}{\left(\frac{Na^2}{\mu r}\right)}$	$\frac{T_1}{\left[\frac{\mathfrak{v}}{a}\left(t-\frac{r-a}{v}\right)\right]}$	$\frac{v}{\left(\frac{Na^2}{\mu r}\right)}$	$\frac{T_2}{\left[\frac{\mathfrak{v}}{a}\left(t-\frac{r-a}{\mathfrak{v}}\right)\right]}$	R	$\gamma=\frac{T_2}{T_1}$
∞	−0·2094	0·4	−0·0876	0·4	0·16	1·0
5	−0·1837	0·6	−0·0707	0·8	0·15	1·3
4	−0·1736	0·8	−0·0690	0·8	0·15	1·0
3	−0·1625	0·8	−0·0608	0·8	0·14	1·0
2	−0·1398	0·8	−0·0574	1·2	0·16	1·5
1	−0·0983	1·0	−0·0416	1·2	0·16	1·2
0·2	−0·0335	2·0	−0·0116	1·4	0·13	0·7

(to be continued.)

Table II. (*continued.*)

$T=-\frac{1}{2}N$:

Ω	u	T_1	v	T_2	R	γ
∞	−0·1255	0·4	−0·0795	0·6	0·24	1·5
5	−0·1094	0·6	−0·0733	1·0	0·26	1·7
4	−0·1021	0·6	−0·0716	1·0	0·27	1·7
3	−0·0956	0·8	−0·0704	1·2	0·28	1·5
2	−0·0831	0·8	−0·0641	1·2	0·30	1·5
1	−0·0592	1·0	−0·0453	1·4	0·29	1·4
0·2	−0·0211	2·0	−0·0138	1·4	0·25	0·7

$T=-\frac{1}{3}N$:

Ω	u	T_1	v	T_2	R	γ
∞	−0·0975	0·4	−0·0815	0·8	0·32	2·0
5	−0·0846	0·6	−0·0769	1·0	0·35	1·7
4	−0·0794	0·6	−0·0747	1·2	0·36	2·0
3	−0·0733	0·8	−0·0737	1·2	0·39	1·5
2	−0·0641	0·8	−0·0663	1·2	0·40	1·5
1	−0·0462	1·0	−0·0484	1·4	0·40	1·4
0·2	−0·0169	2·0	−0·0150	1·6	0·34	0·8

$T=-\frac{1}{5}N$:

Ω	u	T_1	v	T_2	R	γ
∞	−0·0752	0·4	−0·0850	0·8	0·43	2·0
5	−0·0647	0·6	−0·0797	1·0	0·47	1·7
4	−0·0613	0·6	−0·0786	1·2	0·49	2·0
3	−0·0555	0·6	−0·0764	1·2	0·53	2·0
2	−0·0490	0·8	−0·0681	1·2	0·54	1·5
1	−0·0365	1·2	−0·0508	1·4	0·53	1·2
0·2	−0·0136	2·0	−0·0164	1·8	0·46	0·9

$T=-\frac{1}{10}N$:

Ω	u	T_1	v	T_2	R	γ
∞	−0·0593	0·2	−0·0875	0·8	0·57	4·0
5	−0·0499	0·6	−0·0824	1·2	0·64	2·0
4	−0·0477	0·6	−0·0816	1·2	0·66	2·0
3	−0·0437	0·6	−0·0783	1·2	0·69	2·0
2	−0·0377	0·8	−0·0700	1·4	0·72	1·8
1	−0·0295	1·4	−0·0532	1·6	0·69	1·1
0·2	−0·0111	2·0	−0·0181	2·0	0·63	1·0

(*to be continued.*)

Table II. (*continued.*)

$T=+\frac{1}{10}N$:

Ω	u	T_1	v	T_2	R	γ
∞	−0·0433	0·2	−0·0942	1·0	0·84	5·0
5	−0·0295	0·4	−0·0896	1·2	1·16	3·0
4	−0·0272	0·4	−0·0874	1·2	1·24	3·0
3	−0·0239	0·4	−0·0833	1·4	1·34	3·5
2	−0·0188	0·4	−0·0770	1·6	1·57	4·0
1	−0·0164	1·6	−0·0638	2·0	1·50	1·2
0·2	−0·0061	1·8	−0·0262	2·8	1·65	1·6

$T=+\frac{1}{5}N$:

Ω	u	T_1	v	T_2	R	γ
∞	−0·0353	0·2	−0·0979	1·0	1·06	5·0
5	−0·0199	0·4	−0·0931	1·2	1·80	3·0
4	−0·0189	0·4	−0·0909	1·4	1·85	3·5
3	−0·0170	0·4	−0·0906	2·0	2·05	5·0
2	−0·0136	0·4	−0·0877	2·0	2·48	5·0
1	−0·0085	0·4	−0·0755	2·4	3·42	6·0
0·2	−0·0020	0·4	−0·0320	3·0	6·15	7·5

$T=+\frac{1}{3}N$:

Ω	u	T_1	v	T_2	R	γ
∞	−0·0246	0·2	−0·1218	2·0	1·9	10
5	−0·0105	0·2	−0·1176	2·0	2·7	10
4	−0·0139	0·2	−0·1160	2·0	3·2	10
3	−0·0116	0·2	−0·1140	2·2	3·8	11
2	−0·0083	0·2	−0·1095	2·2	5·1	11
1	−0·0051	0·2	−0·0945	2·4	7·1	12
0·2	−0·0012	0·4	−0·0399	3·2	13	8

$T=+\frac{1}{2}N$:

Ω	u	T_1	v	T_2	R	γ
∞	−0·0112	0·2	−0·1621	2·0	5·6	10
5	−0·0125	0·2	−0·1551	2·2	4·8	11
4	−0·0105	0·2	−0·1506	2·2	5·5	11
3	−0·0090	0·2	−0·1488	2·4	6·4	12
2	−0·0065	0·2	−0·1425	2·4	8·4	12
1	−0·0043	0·2	−0·1207	2·6	11	13
0·2	−0·00087	0·2	−0·0501	3·2	22	16

43. 發震機構に就いて

地震研究所　井上宇胤

初動の“壓し波”“引き波”の分布が象限型を示す場合の深發地震の數理的研究は數年前から中央氣象臺に於て本多博士を初め多數の有爲の地震學者に依つてなされて幾多の報告となつて居るが，最近に至り本多博士に依つて其等の總括的報告が爲された．其れに依ると震源の大きさは其處から送り出された地震波の波長と同程度のものであると考へられると云ふ事であつて筆者の主張と全く一致するものである．

但し此の場合は球形震源の表面に於て垂直應力が週期的に變化する場合を取扱はれて居るが，もし應力が或る早さを以て變化したとした場合にはどう云ふ事になるかと思ひ蛇足の樣ではあるが此處に問題として見たのである．

其の結果に依ると，

（イ）　此の場合には震源に於ては垂直應力だけでなく切線應力も同時に變化したとしなければならない．

（ロ）　此等の應力變化は彈性波が震源の一端から他端に達する時間と同程度の時間内に終結するものと考へられる．

（ハ）　從つて震源から出る地震波の波長は震源の大きさと同程度のものとなる．

（ニ）　此の事からも震源に於ては割目の樣なものが出來て，其の割目の進行と共に應力が變化するものと考へられる．

（ホ）　結局震源の一つの模型として，外界よりも遙に剛性の小さい震源内に於て急激な塑性變形が起つて其れに接した彈性部分に於て應力變化が生じ地震波を發生する場合が考へられる．

（ヘ）　此等の應力變化は 10^6 dyne/cm^2 の程度のものと思はれる．

以上の議論は始め無かつた應力が急に發生した場合にも或は又始め存在した應力が或る早さを以て消失した場合にも當てはまるものであるが筆者は後者の方を考へたいと思つて居る．

最後に今迄に筆者の發表した數篇の震源に關する論文の總括的結論を簡單に述べてある．

44. 東京帝國大學構内に於ける地震動加速度の比較觀測（其の一）

地震研究所 萩原尊禮
表俊一郎

（昭和13年6月21日發表——昭和13年6月22日受理）

地震動の卓越週期は夫々土地により一定して居り，所謂大地震時に於ける構造物の災害の大小と密接な關係があることは既に知られて居るところである．石本教授[1]は東京市及其附近の10餘個所に加速度地震計を設置して地震を觀測し，各土地に於いて固有の地震動卓越週期のあることを指示せられて居る．例へば東京本郷の地震研究所地下室に於て觀測せられる卓越週期は 0·3 秒前後であるが，東京丸の内工業クラブ前の空地に於ては其の卓越週期は 0·6 秒である．斯様に僅か數 km を隔てた土地に於て全く異つた性質の地震動が存在することが明かになつたが，比較的近距離例へば數十米乃至數百米の距離に於ては地震動はどの程度に異るものであらうか．此の問題は地震動の性質を明かにする上に於て重要な事柄である．著者等は此の問題に對する研究の手始めとして東京帝國大學構内の地震研究所附近に加速度地震計を設置して其の觀測結果と地震研究所地下室に於ける觀測結果とを比較することを試みた．今回加速度地震計を設置した場所は，一つは地震研究所の東側空地に建てられて居るミルン小屋と稱する小木造建築物内であり，他の一つは地震學教室機械室（木造）内である．何れも表土の上に作られたコンクリートの實驗臺上に機械を設置した．

使用した地震計は石本加速度地震計であつて，1 臺は地震研究所地下室に設置した儘とし，他の1臺を始めミルン小屋に設置し，後之を地震學教室内に移した．地震計の要素は次の如くである．2臺共要素は全く等しく，始め2臺を地震研究所地下室に相並べて觀測し，兩者の記錄が全く相等しいことを確めてから後1臺を他の場所へ移した．

振子の重錘	15 kg.
成分	水平2成分.
感度	記錄紙上 1 mm が 1·7 gal に相當す.
制振器	空氣制振器により振子を極限制振狀態に置く，
起動機	シンクロナスモートル.
ドラム（直徑20 cm）回轉速度	10分に1回轉，記錄紙の進行速度 1 sec に約 1 mm.

---

[1] 石本巳四雄，地震研究所彙報 **10** (1932)，171；**12** (1934)，234；**13** (1935)，592；**14** (1936)，240.

觀測せられた地震の中主なものは第1表に示す通りである.

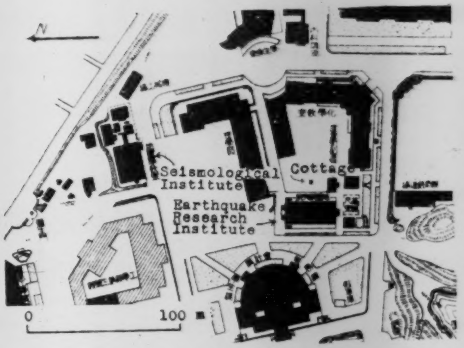

第 1 圖

地震記象は第9～15圖に示す通りである. 地震記象を見て第一に氣付くことはミルン小屋及び地震學教室に於ては 0·2 秒程度の比較的小週間の振動が初期微動及び主要動の部分に於て著しく卓越して居り，其の加速度も地震研究所地下室の其れに比較して著しく大きいことである. 此の小週期の振動は主要動を過ぎると速かに減衰して尾部に於ては地震研究所，地震學教室，ミルン小屋共に全く同一の振動を示して居る. 此の間の模様は第14圖及び第15圖に掲げた記録の擴大圖を見れば明かである. 週期の頻度曲線を從來の方法に依り作り第 2～8 圖に示してある. 即ち記象上に平衡線 (Zero line) を引き，此の線を各波動が同一方向に通過する點に着目し，相隣る是等2點間の距離を讀み取り之に相當する時間を以て其の時の週期と定めた. 此の頻度曲線から見られる樣にミルン小屋及地震學教室に於ては常に 0·2 秒の振動が卓越して居る. 地震研究所に於ては卓越週期が 0·3 秒より大又は小になることがあり，又地震によつては頻度曲線に判然と極大が認められない場合があるが，此の時に於ても地表の觀測に於いては常に 0·2 秒の卓越週期が存在する.

Table I

Date	Epicenter	Epicentral distance (& depth) (km)	Earthquake Research Institute		Seismological Institute		
			Maximum acceleration (gal)	Predominating period (sec)	Maximum acceleration (gal)	Predominating period (sec)	Ratio of max. acceleration
Mar. 28, 6 h 10 m, 1937	Near Haneda	18 (35)	23·0(N) 15·6(W)	0·3(N–S) 0·3(E–W)	*41·8(N) *35·7(W)	0·2(N–S) 0·2(E–W)	1·8 2·3
Oct. 17, 13 47, 1937	South East of the cape of Inubôsaki	117 (40)	14·9(N) 11·7(W)	0·4(N–S) 0·4(E–W)	23·3(N) 21·8(W)	0·3(N–S) 0·2(E–W)	1·6 1·9
Nov. 23, 2 39, 1937	Near Mt. Komagatake, Province of Kai	137 (20)	1·9(S) 1·7(E)	0·4(N–S)	2·9(N) 2·9(E)	0·2(N–S)	1·5 1·7
Dec. 6, 5 51, 1937	Simoduma, Ibaragi Prefecture	60 (30)	2·7(S) 2·4(W)	0·2(N–S)	6·5(S) 9·7(E)	0·2(N–S)	2·4 4·0
Jan. 10, 0 34, 1938	Near Matudo, Tiba Prefecture	22 (40)	6·0(S) 6·3(E)	0·3(N–S)	14·3(N) 10·9(W)	0·2(N–S)	2·4 1·8
May 23, 16 19, 1938	South East of Onahama	170 (70)	26·3(S) 34·0(W)	0·2(N–S)	66·2(S) 62·3(W)	0·2(N–S)	2·5 1·8
June 6, 1 30, 1938	Near the marsh of Teganuma	36 (60)	25·3(S)		27·6(S)	0·2(N–S)	1·1

* ミルン小屋觀測値 (Values obsereved in the cottage.)

地震學教室に於て比較のためは尙1臺（1成分）の加速度地震計を並置して，振子に極限制振の場合の約2倍の大きさの制振力を與へ比較的小週期の振動に對して著しく感度を遞下せしめた狀態に置いた．此の樣な狀態に置かれた地震計の記象は第12圖及び第13圖に示し，其の記象より得られた週期の頻度曲線は第7圖及び第8圖に示してある．

地震研究所地下室の床面は地表下約4mであつて相當深い基礎工事が施されてゐるのであるから，其の地下室に於ける觀測は地表下或る深さに於ける觀測と見做して差支へないであらう．地震研究所の建物は極めて剛構造であつて地震時に自己の振動を示さないことは地下室と2階とに於ける地震計の比較觀測から既に知られて居るのであるから，建物自身の影響は殆どないと考へられる．約0·2秒の振動が土地に於て卓越し地下數米に於てこれに相當するものが認められないと云ふ事實は，此の種の振動が極めて表面に起つて居る現象であることを示して居る．卽ち地表に近い軟弱な土層に起因するものであらう．而して此の種の小週期の減衰した地震動の尾部に於て何れの場所の振動も全く同一であることを示して居ることから，實際には同一の振動の上に地表に於ては小週期の振動の重疊して居るものと推定されるのである．此の地表に現れる小週期の振動は加速度が相當に大であることは構造物に對する耐震的見地から注目す可きことの樣に思はれる．卽ち極めて淺い基礎の上に立つ構造物は地震時に此の種の比較的小週期の極めて大きい加速度を受けることが想像される．此の樣に軟弱な土地に於て小週期の地震動の生ずることは曾て今村博士等が國會議事堂の工事中行はれた同所の基礎の上と附近の地表とに於ける變位地震計に依る比較觀測に於いても認められて居る．又齋田氏は丸の內に於て井上氏は東京駒場に於て地上と地下の地震動を比較されたことがある．然し兩氏の場合は地表と地下の地震動は振幅は大いに異るが，兩者の記錄上に於て相當する波動と波動とは互に符合せしめることが出來た．今回の場合は地震研究所地下室に於ては全く現れない振動が地表に於て現れてゐる．表面層の如何なる部分が0·3秒の卓越振動に關與し如何なる部分が0·2秒の卓越振動を起して居るかは表面層の彈性的性質と厚さ等を知らなければ斷定することは出來ない．此の問題は彈性波による地下探査の方法（Seismic prospesting）に依つて將來研究を進めて見る積りである．

2）今村明恒，地震研究所彙報 **1**（1926），7.
3）今村明恒，岸上冬彥，地震研究所彙報 **5**（1928），143.
4）齋田時太郎，鈴木正治，地震研究所彙報 **12**（1934），517.
5）井上宇胤，地震研究所彙報 **12**（1934），712.

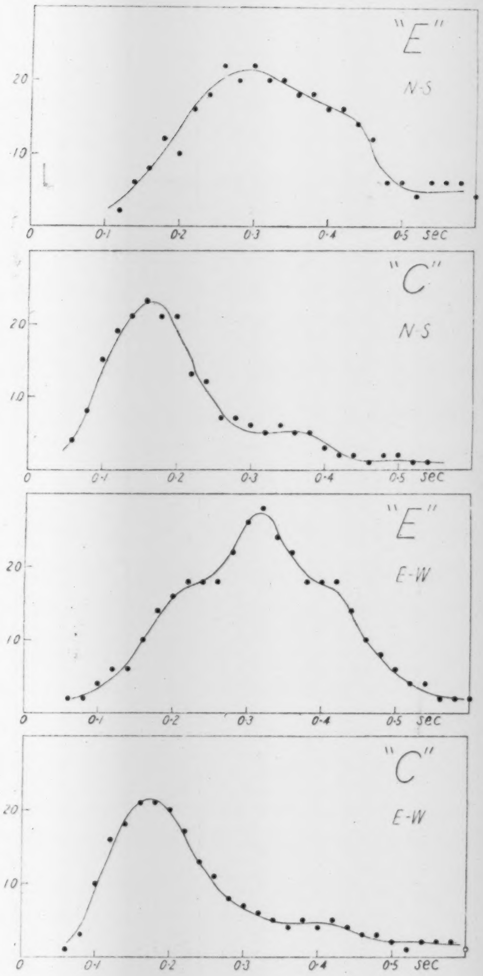

第2圖 震央 羽田附近 The earthquake of March 28, 1927. (E Earthquake Research Institute, C The cottage)

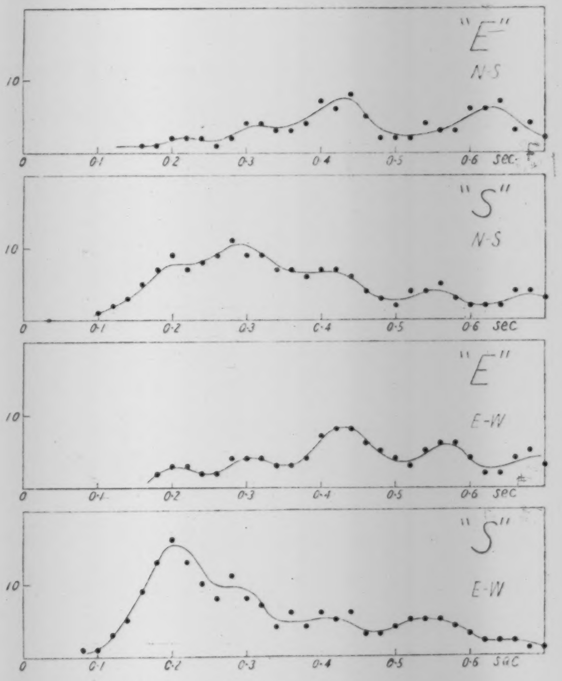

第3圖 震央 犬吠岬沖 The earthquake of October 17, 1937. (E Earthquake Research Institute, S Seismological Institute)

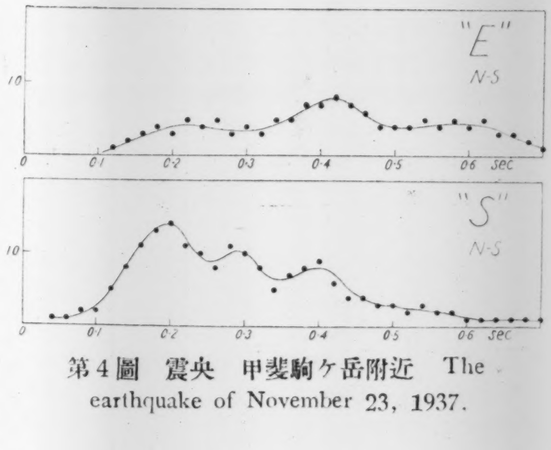

第4圖 震央 甲斐駒ヶ岳附近 The earthquake of November 23, 1937.

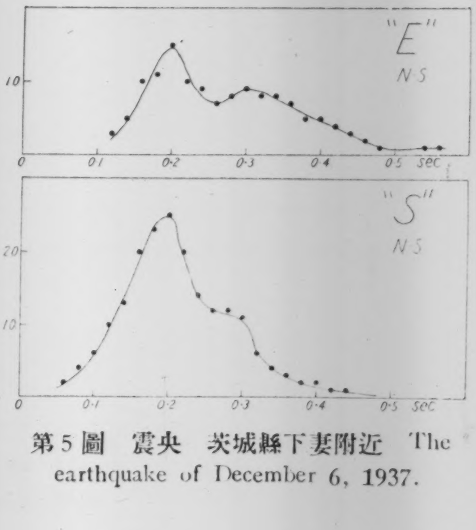

第5圖 震央 茨城縣下妻附近 The earthquake of December 6, 1937.

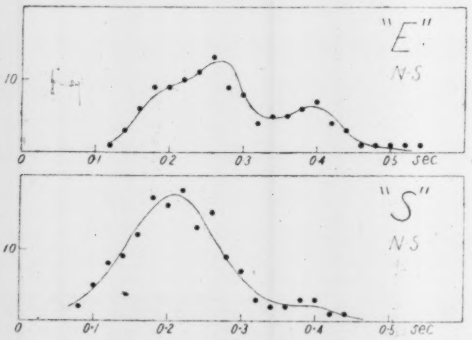

第6圖　震央　千葉縣松戸附近　The earthquake of January 10, 1938.

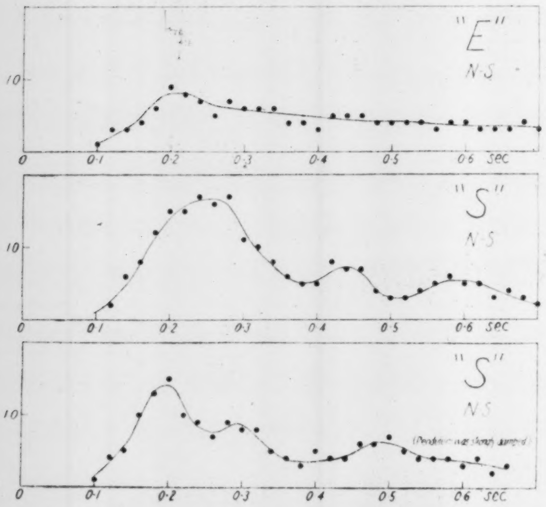

第7圖　震央　小名濱南東沖　The earthquake of March 23, 1938.

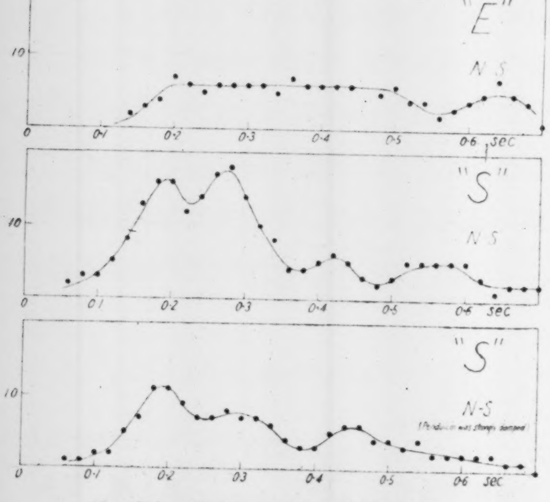

第8圖　震央　手賀沼附近　The earthquake of June 6, 1938.

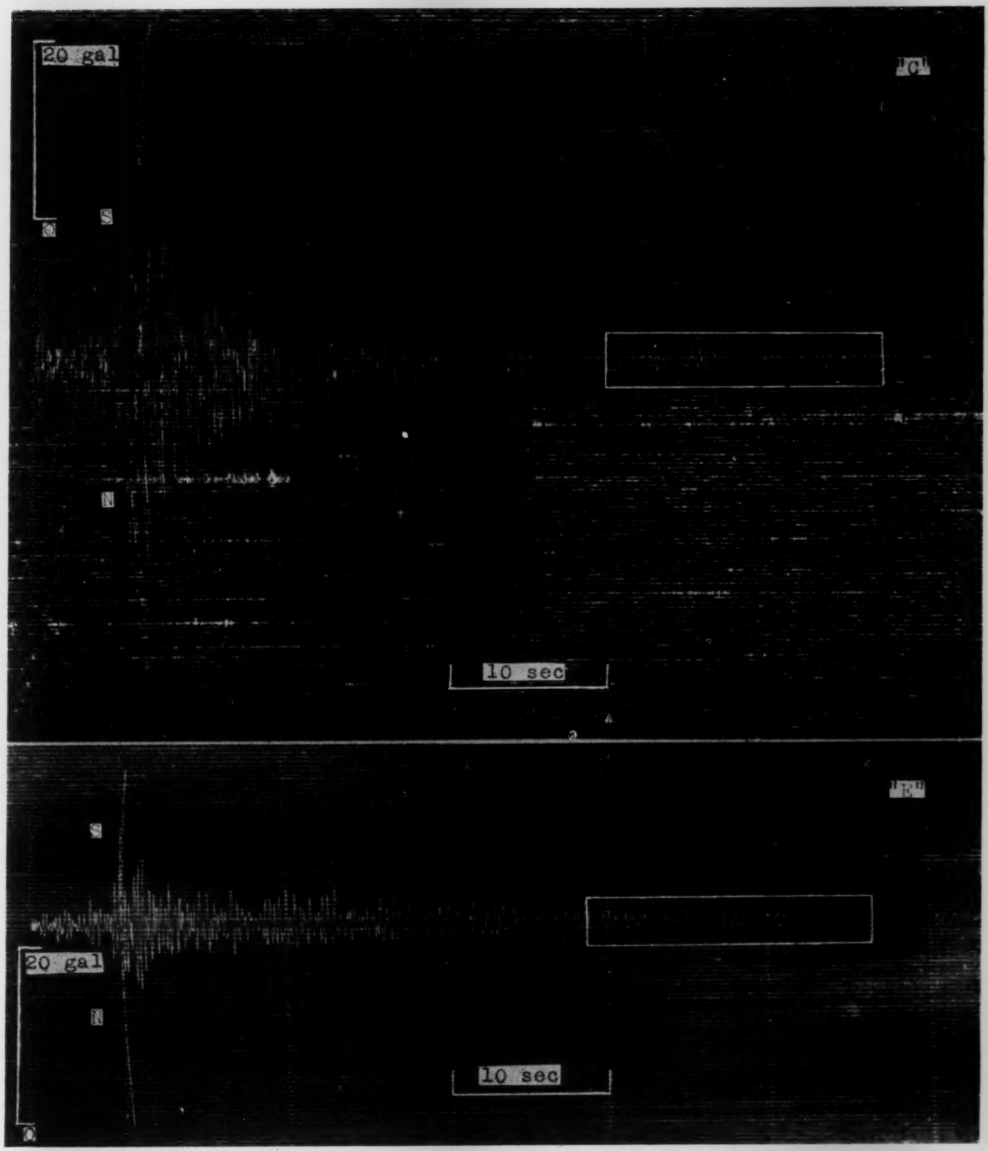

第9圖　震央　羽田附近　（白線にて區切りたる部分を第 10 圖に擴大示す）

The earthquake of March 28, 1937 (C the cottage, E Earthquake Research Institute)

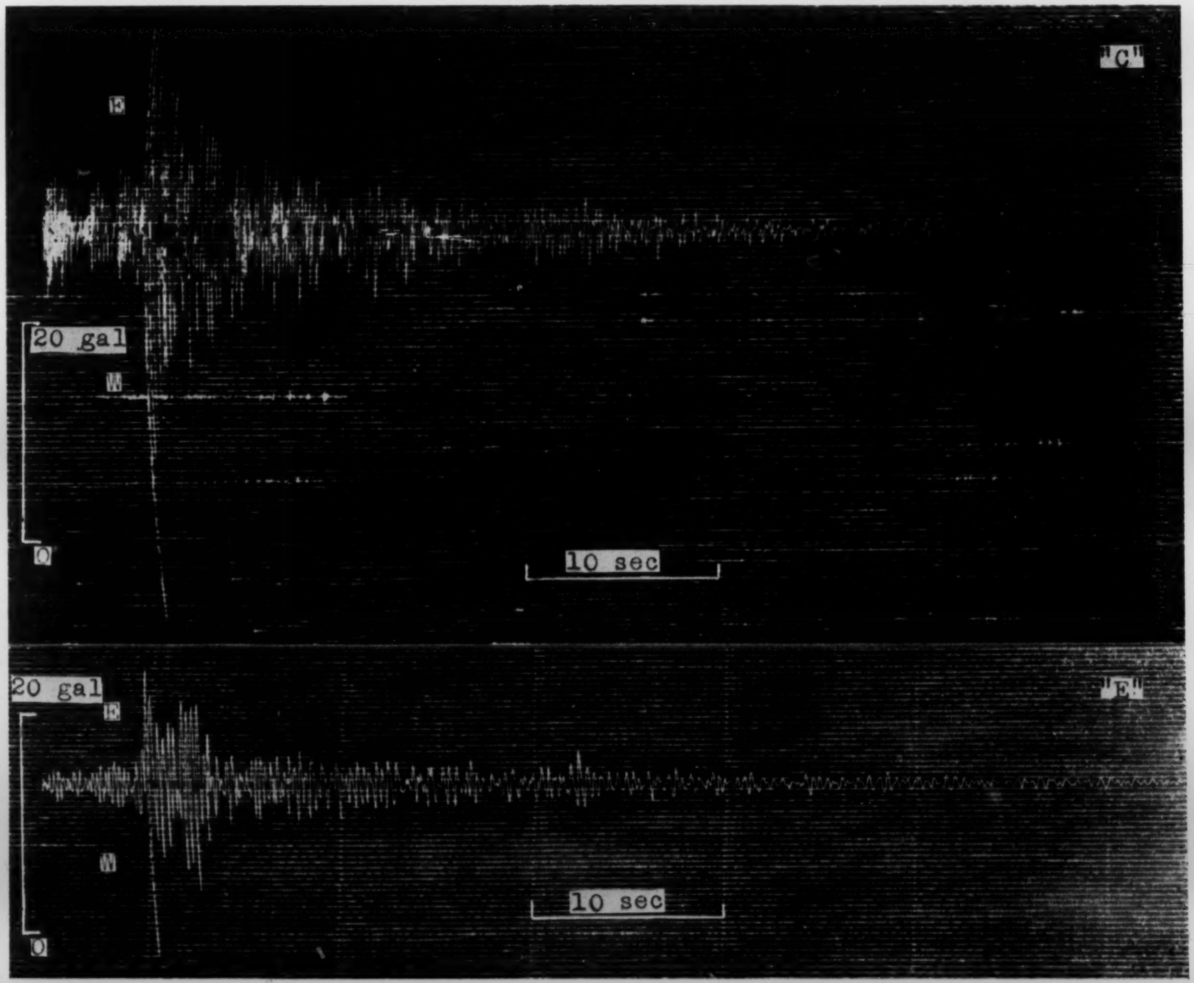

第 10 圖 震央 羽田附近 The earthquake of March 28, 1937 (C the cottage, E Earthquake Rearch Institute)

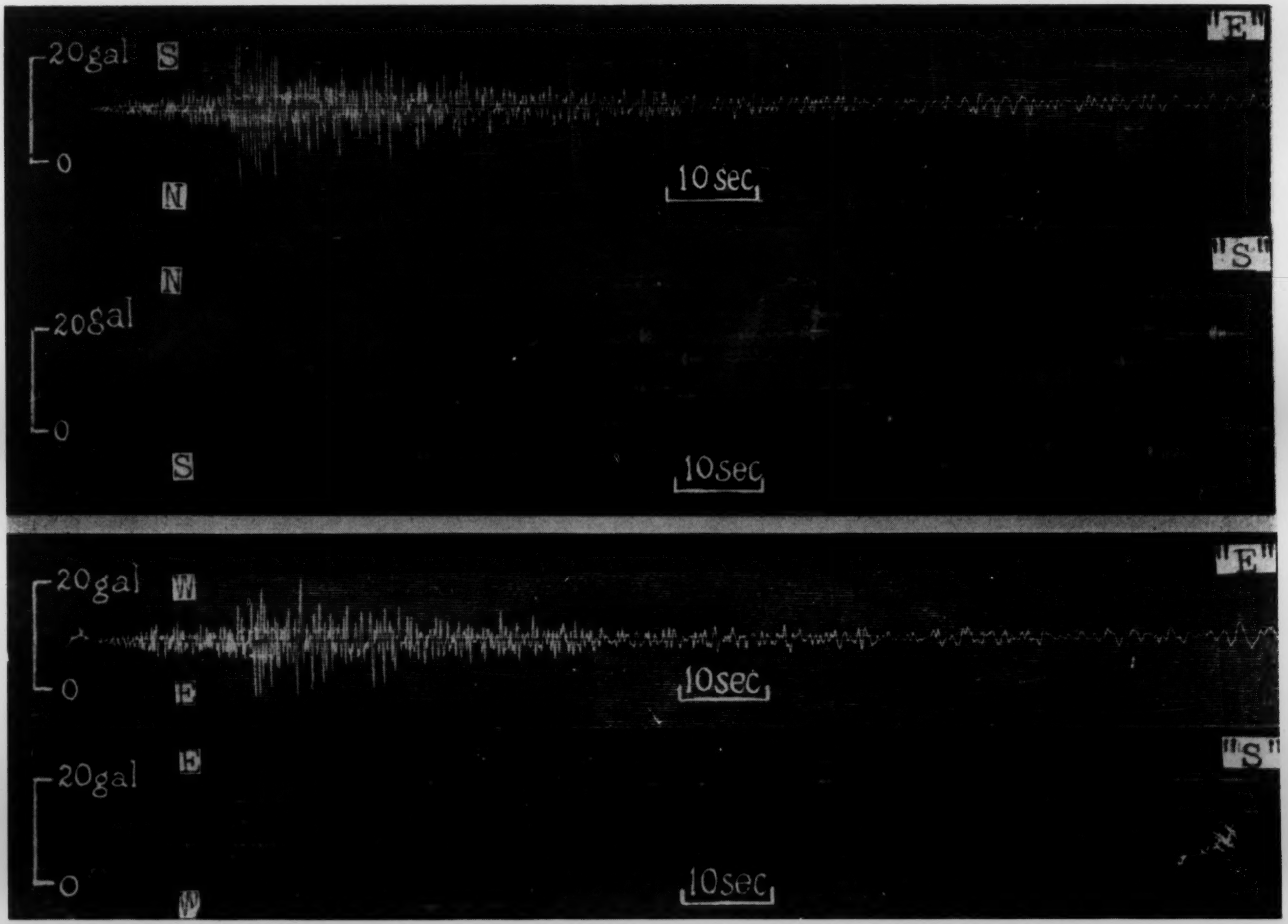

第 11 圖　震央　犬吠岬南東沖　The earthquake of October 17, 1937. (E Earthquake Research Institiute, Seismological Institute)

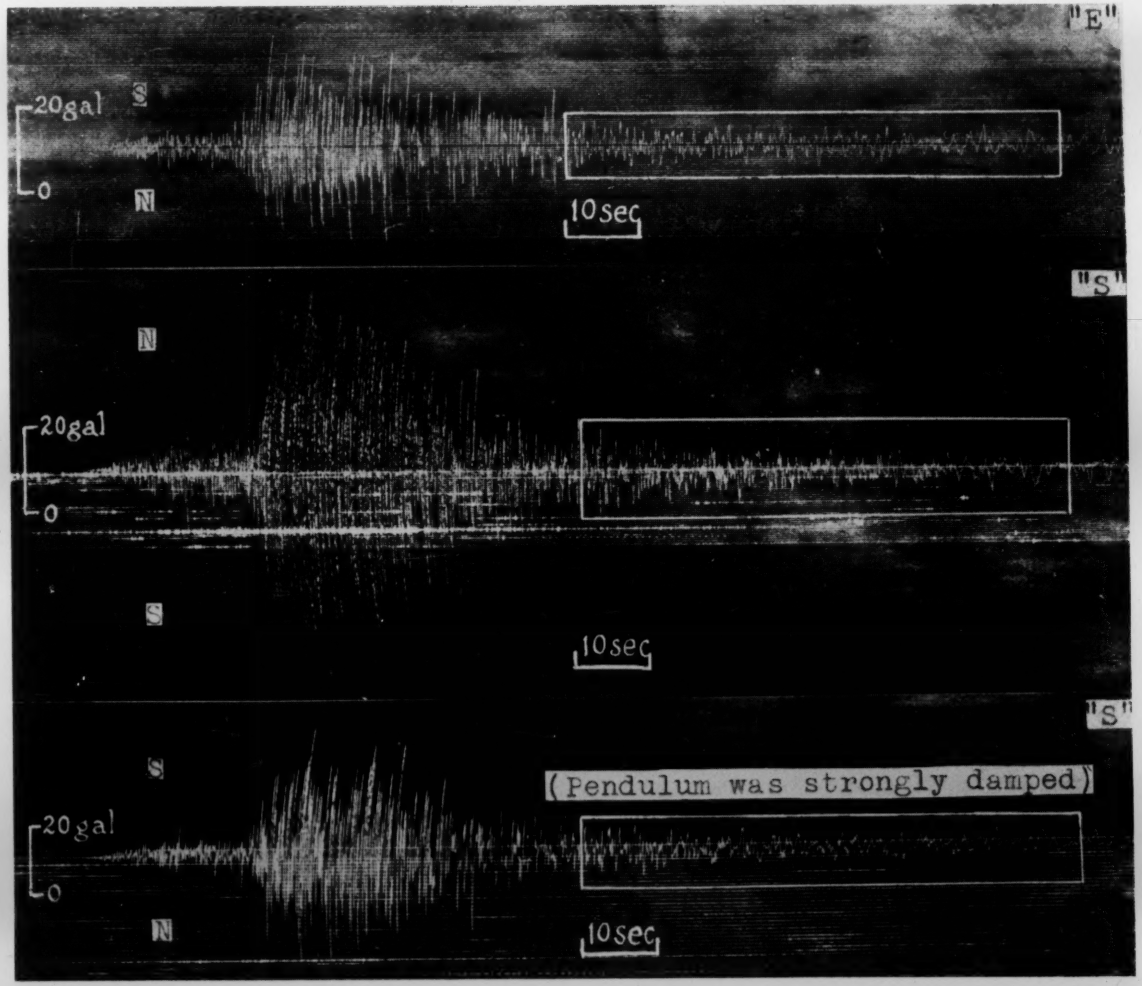

第 12 圖　震央　小名濱南東沖（白線にて區切りたる部分を第 14 圖に擴大示す） The earthquake of may 23, 1938. (E Earthquake Research Institute, Seismological Institute)

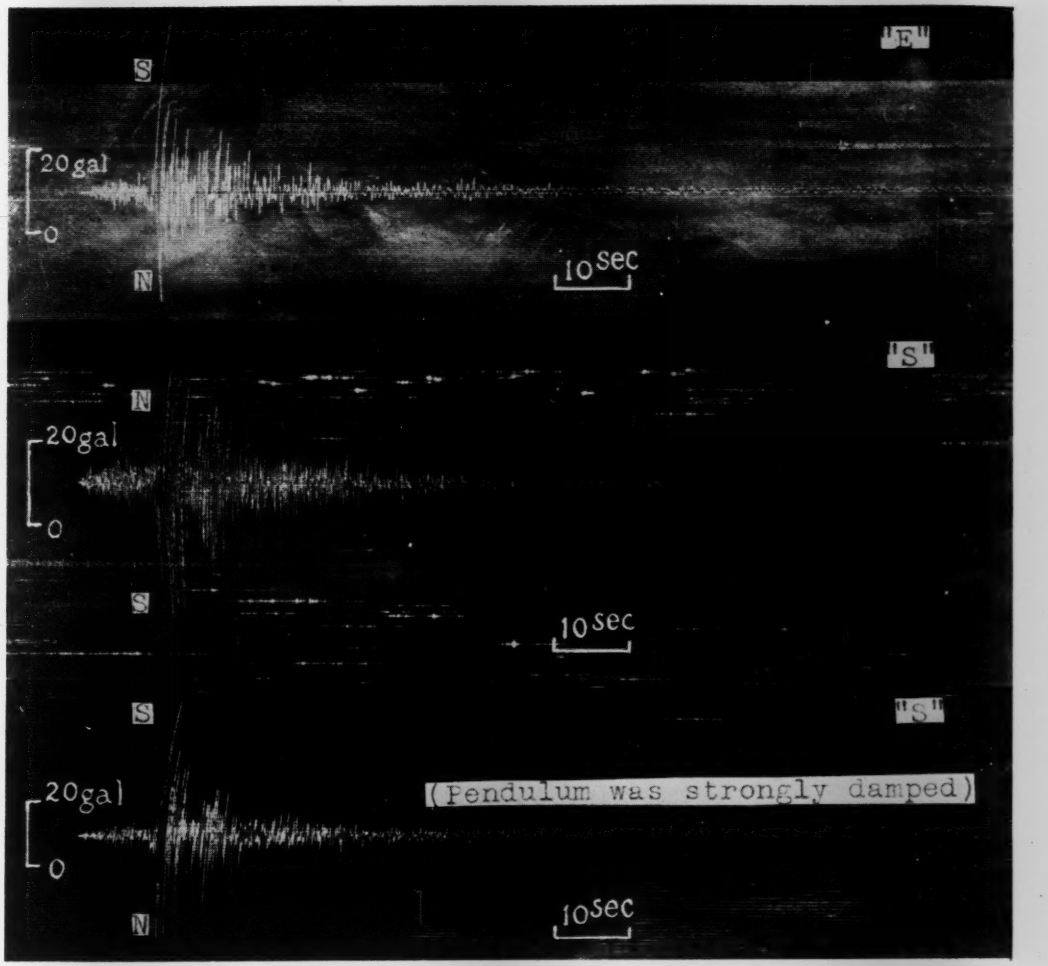

第 13 圖 震央 手賀沼附近 The earthquakr of June 6, 1938.

(E Earthbuake Research Institute, S Seismological Institute)

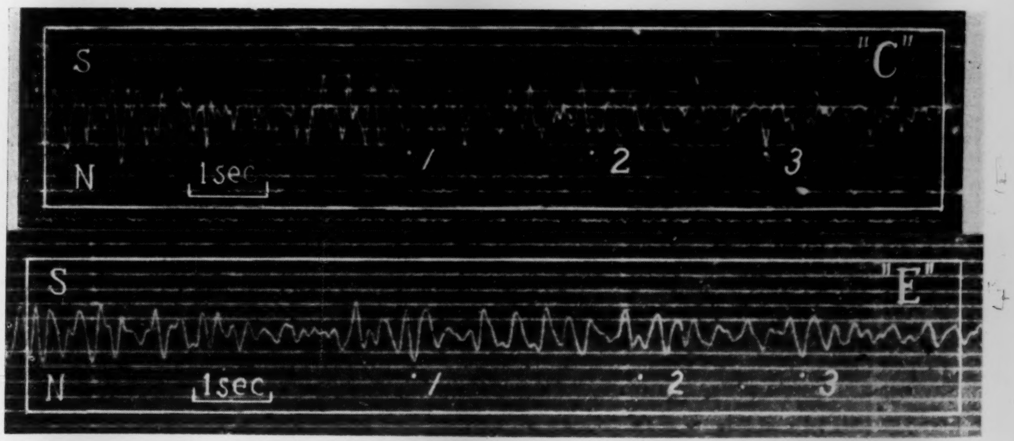

第 14 圖　第 9 圖の一部を擴大せるもの
Enlarged photo. of a part of Fig. 9.

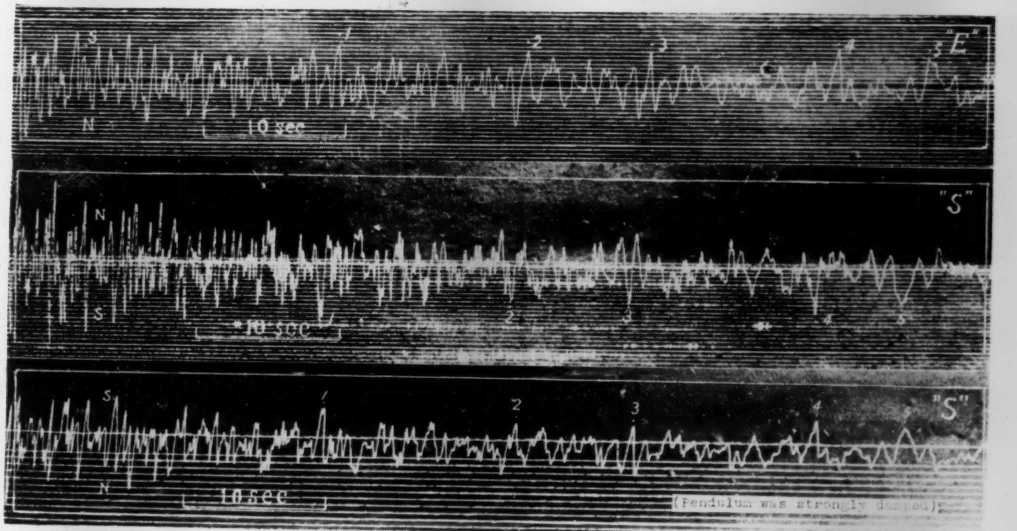

第 15 圖　第 12 圖の一部を擴大せるもの
Enlarged photo. of a part of Fig. 12.

44. *Comparative Observations of the Acceleration of Earthquake Motions in the compound of the Tokyo Imperial University.* (Part I)

By Takahiro HAGIWARA and Syun'itirô OMOTE.

Earthquake Research Institute.

The acceleration* seismograph was first installed in a wooden cottage near the Earthquake Research Institute and later in the Seismological Institute (wooden structure). The instrument was set on a concrete block in the structure. The elements of the instrument are as follows.

Mass of pendulum	15 kg
Component	Two horizontal components
Period of pendulum	0.115 sec
Sensibility	1 mm on the record corresponds to acceleration 1·7 gal
Damping of pendulum	Critical (Air damper)

The acceleration of earthquake motion in these two places were compared with that in the groundfloor of the Earthquake Research Institute, which is at a depth of 4 m from the surface of the ground. The frequency curves of the period of motion were made from the acceleration seismograms. The curves show that the motions with comparatively small period predominate on the surface of the ground.

45. 富士火山の地質學的並に岩石學的研究 (II)

2. 青木原熔岩の分布と噴出中心

地震研究所　津屋弘逵

(昭和12年11月16日發表——昭和13年6月20日受理)

緒言

富士山の北西山麓部の青木原，卽，寄生火山大室山の東麓附近から北方及び北西方に下つて西湖，精進湖，本栖湖等の湖岸に至る廣大な地域の大部分には富士山の新期噴出の丸尾[1] が分布してゐる．此丸尾は一般に青木原丸尾或は青木原熔岩と呼ばれ，富士山の貞觀6年(西暦864)噴火の際に噴出したと考へられてゐる一熔岩流である．

青木原熔岩の噴出地點は從來區々に考へられてゐた．平林博士[2] は青木原熔岩を富士山頂から北西側中腹（海拔 2400 m）の御庭附近に流下してゐる熔岩と同一視し，青木原熔岩の噴出地點を富士山頂に求めた．加藤博士及び伊原學士[3] も亦平林博士の考へに從つてゐる．之等に反して，石原學士[4] は青木原熔岩を側火山の噴出物と見做し，“青木原丸尾の噴出口が中道御庭の東側あたりであることは，下方から其分布を段々追跡して，此邊まで辿ぶことが出來るに依りて明かである．但し上方から落下せる砂礫に覆沒された爲め噴口を認むることは出來ない”と述べてゐる．石原學士は青木原熔岩と御庭及び奥庭から噴出した熔岩とを區別してゐるが，神原博士[5] は此兩者を同一と見做し，御庭及び奥庭を青木原熔岩の噴出地點と考へた．

以上の如く青木原熔岩の噴出地點に關する考へが一致しないのは，富士山の北西腹に數座の比較的新期の寄生火山が在り，其各々から噴出した熔岩が何れも略同樣に北西方向に流下し，相互に部分的に相連なつて一見一續きの熔岩流の如く分布してゐるので，之等の熔岩流が動もすれば混同され易いことに因るものと思はれる．卽，此方

---

[1] 富士山の山麓地方では火山灰其他の噴出物に蔽はれないで地表に露出し，塊狀をなして累々さ堆積してゐる新期噴出の熔岩流を一般に“丸尾”さ呼んでゐる．

[2] 平林武，震災豫防調査會報告，**24** (1899)，36.

[3] 石原初太郎，富士の地理さ地質．1928，195.

[4] T. KATO and K. IHARA, *Guide-book, C-4. Pan-Pacific Sci. Congr., Tokyo*, 1926, 44.

[5] 神原信一郎，富士山の地質．1929, 65.

面の寄生火山の中で，大室山，片蓋山，弓射塚，臼山，八軒山，幸助丸等は何れも比較的舊期に屬するが，長尾山，イガトノ山，天神山，氷池，白大龍王，氷穴，奥庭，御庭等は何れも比較的新期の寄生火山で，夫々の噴火口から噴出した熔岩流は所謂丸尾の狀態で地表に露出してゐる．筆者は青木原熔岩の噴出地點を最初には神原博士の調査結果に從つて御庭及び奥庭に置き[6]，其後此方面の豫察的調査の結果，之を氷池に在ると改めたが[7]，更に其後の詳細な調査及び各寄生火山熔岩の顯微鏡的比較觀察の結果，玆に述べる如く長尾山に在ることを確めるに至つた．

青木原熔岩の噴出地點が長尾山であることを了解するには，從來同熔岩と混同されてゐた熔岩類の前者と相違する點を知らなければならない．故に玆では次の熔岩類の岩質，噴出地點，分布等の概略を順次述べることとする．

（1） 御庭及び奥庭熔岩（橄欖石玄武岩）．
（2） 氷穴熔岩（含橄欖石複輝石・玄武岩）．
（3） 白大龍王熔岩（含斜方輝石・單斜輝石・橄欖石玄武岩）．
（4） 氷池熔岩（含單斜輝石・橄欖石玄武岩）．
（5） 天神山熔岩（複輝石・橄欖石玄武岩）．
（6） イガトノ山熔岩（複輝石・橄欖石玄武岩）．
（7） 長尾山熔岩—青木原熔岩（含複輝石・橄欖石玄武岩）．

以上の熔岩類の中，青木原熔岩に就いては筆者が既に岩石學的研究の一端を發表したが[8]，其他の熔岩類に就いても岩石學的研究の結果を他日發表する豫定であるから玆では之等の熔岩類を識別するに役立つ肉眼的及び顯微鏡的の性質の若干を述べるに止めて置く．

御庭及び奥庭熔岩

此熔岩は御庭及び奥庭（圖版第1圖）から噴出した熔岩の總稱である．御庭は富士山北西腹の海拔 2400 m の高さに在つて，富士山中道に沿つた一休泊處に當たり，小御嶽頂上から西方に約 3 km 距たつてゐる．奥庭は御庭の下方（北西方）約 500 m 距たり，御庭から精進登山道3合目に至る捷徑の中途に當たる．此兩地の一帶を蔽つてゐる塊狀熔岩が所謂御庭及び奥庭熔岩であつて，其噴出孔は少くも 10 個或は夫以上あり，北西—南東方向，卽，富士山頂に向ふ略2列の割目狀の溝の上に配列されてゐる．其1列は御庭の休泊小屋の東方に，他の1列は其西方に在り，相互に約 250 m

---

6) H. Tsuya, *Bull. Earthq. Res. Inst.*, **13** (1935), 645.
7) H. Tsuya, *Bull. Earthq. Res. Inst.*, **15** (1937), 303.
8) 前掲 (6 及び 7).

相距たつてゐる．此２列は共に富士山の山體を縱斷する放射狀の割目の中の北西に走るものを代表し，御庭及び奧庭熔岩は此割目に沿つて所謂裂罅噴出をなしたものと考へられるが，明瞭なる噴出孔は赭色の熔岩岩滓が其周圍に堆積してゐること，小形の圓錐丘に取圍まれてゐること等に依つて示されてゐる．

御庭の熔岩噴出孔は何れも十數米內外の深さ及び孔徑を有するに過ぎない．而して噴出した熔岩の大部分は噴出孔附近に堆積せず，急峻な山腹を下方に流れ去つてゐる．從つて，御庭全體としては際立つて突起した寄生火山の地形を示さずたゞ同熔岩の噴出地域の最上端（2428·6 m 三角點の上方）から御庭に亘る山腹の傾斜が一段と緩かになつてゐるに過ぎない．奧庭は下方から仰ぎ見ると，不完全ではあるが一の突起した寄生火山の地形を示し，頂上に直徑約 150 m，深さ約 30 m の皿狀噴火口を有する．尙，其附近には

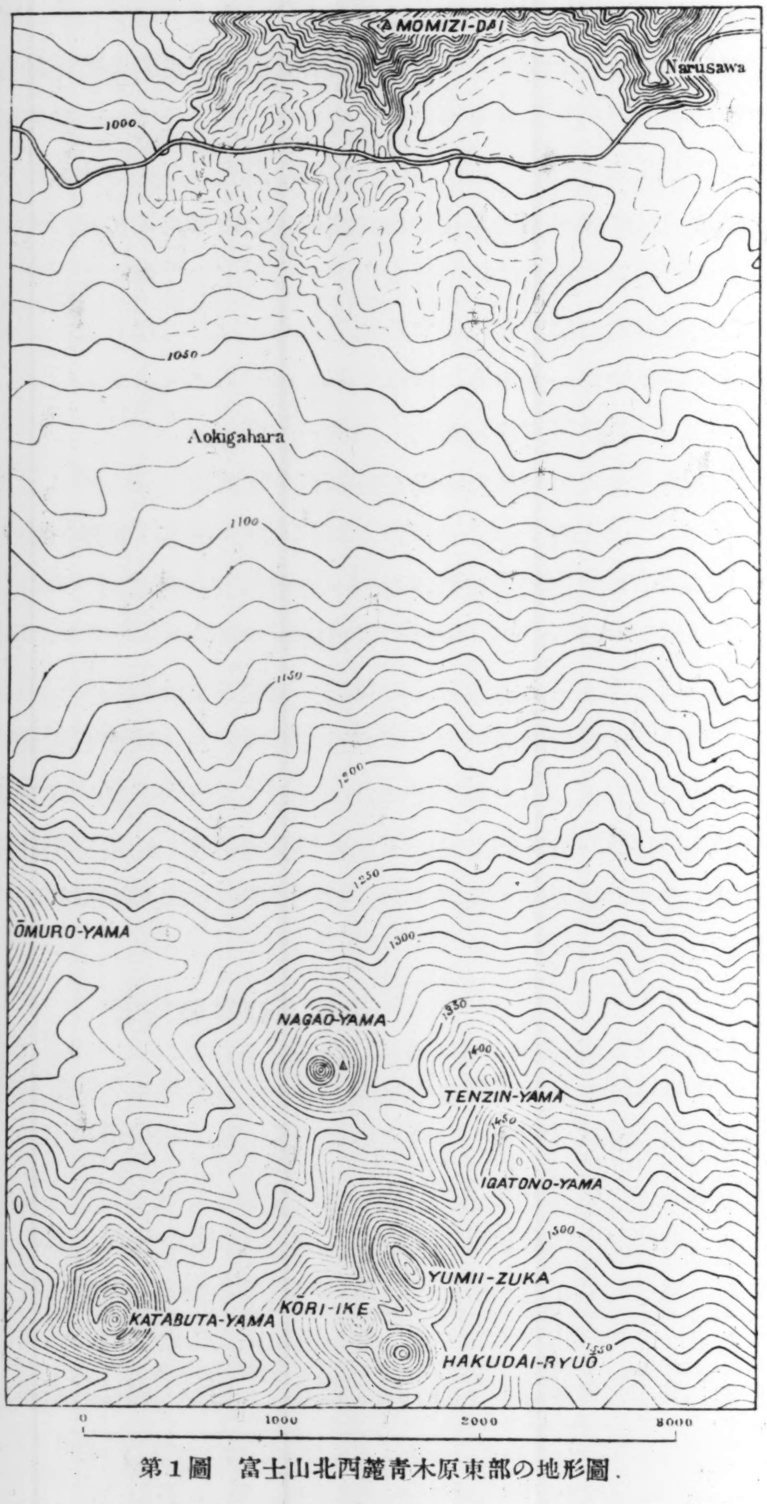
MOMIZI-DAI
Narusawa
1000
1050
Aokigahara
1100
1150
1200
1250
1300
ŌMURO-YAMA
NAGAO-YAMA
1350
1400
TENZIN-YAMA
1450
IGATONO-YAMA
1500
YUMII-ZUKA
KORI-IKE
KATABUTA-YAMA
HAKUDAI-RYUŌ
1550
0
1000
2000
3000

第１圖　富士山北西麓青木原東部の地形圖．

二三の火口狀窪地が在る．御庭奧庭共に，噴火口附近に多少の火山砂礫が堆積してゐるのみで，共他は大小の岩塊に分離した熔岩に依つて占められてゐる．

御庭及び奧庭熔岩は一の熔岩流でなく，多くの噴出孔から多少時を異にして噴出した幾つかの熔岩流の相重なつたものである．例へば，御庭の休泊處の前方に在る一噴出孔から噴出した熔岩は約 300 m 流下して止まり，一の舌狀熔岩流をなしてゐる．然し，御庭及び奧庭熔岩全體として殆ど同時期の噴火に依つて噴出したものと見做され，共中の各熔岩流は岩質上から區別して考へられねばならぬ何等の相違をも示さない．

御庭及び奧庭熔岩はたゞに此兩地の地表部を構成してゐるのみでなく，遠く北西方に流下して幾つかの所謂丸尾をなしてゐる．奧庭の北西方に流下した熔岩は分岐して三本の幅の狹い熔岩流となり，幸助丸の南方海拔 1800 m 內外の山腹に終る．奧庭の北方に流下した熔岩は先づ東西の 2 流に分岐し，共東流は精進登山道 3 合目から 2 合目に至る急坂の西側の谷に流下し，既に海拔 1650 m 附近で終つてゐるが，西流は一の尾根を距てて東流の西側を北方に遠く流下してゐる．此西流は御庭及び奧庭熔岩の最も著しい流れであつて，海拔 I650 m 附近に下つて臼山に衝突し，同山の南西側に一支流を出し，更に同山の北東側に至つて一支流を西方に出してゐる．此支流はゴンタク丸尾（上流）或はツジョウ丸尾（下流）と呼ばれ，片蓋山の南方の谷に沿つて海拔 1300 m 附近に至る迄追跡される．臼山の北東側を過ぎて北西方に流下した熔岩流は弓射塚の西側で大部分止まつたが，尙共一部は片蓋山の南麓を過ぎて西方に，他の一部は片蓋山の北東方に流下してゐる．

御庭及び奧庭熔岩は部分に依つて多孔質或は緻密質であるが，一般に暗灰色乃至黑色で少量の肉眼的斜長石斑晶を有する．此斜長石斑晶は一般に外觀暗灰色の色澤を帶び石基と殆ど同色である．從つて，同熔岩の斑狀構造は肉眼的に極めて不明瞭である．顯微鏡下では，斑晶としては少量の斜長石の他に稀に橄欖石が見出され，石基には斜長石と橄欖石との微晶が多量に認められる．卽，同熔岩は一種の橄欖石玄武岩である．

御庭及び奧庭熔岩には所謂熔岩樹型が見られ，特に臼山の北東方及び弓射塚の西方の同熔岩流上に多く發達してゐる．同熔岩と青木原熔岩とは岩石學的に見て全く別種であるのみでなく，兩者の熔岩流は直接に相接觸してゐない．既に述べた樣に，弓射塚の西方に達した御庭及び奧庭熔岩は更に北西方（長尾山と片蓋山との中間）に幅の狹い熔岩流となつて流下してゐるが，共先端は青木原熔岩流の南緣の手前で止まつてゐる．此事實は長尾山の西麓附近に，御庭及び奧庭熔岩と異なり，青木原熔岩とも異

なる氷穴熔岩及び氷池熔岩の存在することを知つて初めて了解されるのである．

氷穴熔岩

此熔岩は弓射塚とイガトノ山との中間の山腹から噴出し，北方及び北西方に流下してゐる．卽，精進登山道1合目から2合目に至る間の登山道及び其兩側に露出してゐる丸尾は此熔岩である．而して，同登山道の西側には熔岩上に割目狀の溝及び噴火口狀の窪み或は堅穴が大小十數個在つて，北西—南東方向に走る一線上に配列されてゐる．氷穴，長尾風穴等と呼ばれてゐるものは其例である．之等の溝及び孔の中の若干は所謂熔岩隧道の天井の落下して生じたもの，或は Daly[9] の “Blowholes” に相當するものであるかも知れないが，多くは玆に云ふ氷穴熔岩の噴出孔を代表するものと考へられる．特に上述の北西—南東方向の一線の南東端に當る處には疑ひの無い噴火口が見出される．其位置は精進登山道2合目から同1合目に向つて約 400 m 下り，西方の樹林内に約 100 m 入つた處で，海拔約 1500 m の高さに當たる．同處には4個の擂鉢狀の噴火口が相接して北西—南東方向に並んでゐる．其直徑は北西端のものから順次に約 10 m，50 m，5 m，及び 100 m であり，深さは南東端のものに於いて約 50 m で，其他に於いては遙かに淺い．各噴火口の內壁には氷穴熔岩が露出し，火口外には熔岩の他に赭色岩滓狀の火山砂礫及び火山彈が堆積してゐる．更に北西端の噴火口の北西側には幅約 10 m，深さ約 5 m の溝狀噴火口が同方向に走つてゐる．氷穴熔岩は之等の噴火口附近から初まつて北西方に分布してゐるのであつて，南東方には全く見られない．精進登山道2合から約 200 m 下つて，弓射塚に至る小徑の入口近く，或は同2合目から西方の白山に至る小徑附近に，一見氷穴熔岩に類似の熔岩の露出があるが，此熔岩は厚さ3 m 內外の火山灰層に蔽はれてゐて，氷穴熔岩とは明かに異なり，精進登山道2合目より遙か南方の山腹から流下し，天神山及びイガトノ山の東方の山腹に擴がり，鳴澤部落附近に迄達してゐる舊い一熔岩流の一部である．

以上に述べた事實から，氷穴熔岩は精進登山道1合，2合間の道路の西側に當たる山腹（海拔 1400～1500 m）に於いて，北西—南東方向に走る一裂線上に各處から噴出したものと考へられる．噴出した熔岩は弓射塚の東麓を巡り，北西方及び北方に數條の熔岩流に分岐して下つてゐる．然し，之等の熔岩流は大部分長尾山，氷池，イガトノ山，天神山等の噴出物に蔽はれ，一部分地表に露出するのみである．卽，北西方向に流下した氷穴熔岩は長尾山圓錐丘，同山から噴出した青木原熔岩，氷池から噴出し

---

9) R. A. DALY, *Igneous Rocks and the Depths of the Earth.* 1933, 161.

た氷池熔岩等に蔽はれ，僅かに長尾山の南西麓及び大室山東麓の神座山附近に一部分露出してゐる．長尾山の南西麓に於いては氷穴熔岩上に多くの樹型が見出される．北方に流下した氷穴熔岩は中途に於いて天神山及びイガトノ山から噴出して同方向に流下した熔岩流に依つて蔽はれ，たゞ其下流のみが 4 條の熔岩流として見出される．鳴澤部落から南西に向つて大室山に至る山道を約 2 km 登つた處（海拔 1010 m）で，道の南側に露出してゐる丸尾（幅約 100 m）は氷穴熔岩の最も東に位する一支流の末端である．此地點から更に約 1 km 南西に進むと，同熔岩の第二の支流（幅約 200 m）をを横切る．同支流及び其西側に約 500 m 距たる第三の支流は共に其末端附近に於いて鳴澤部落に向つて流下した青木原熔岩に依つて蔽はれてゐる．氷穴熔岩の第四の支流は長尾山北麓の北方山腹を約 100 m の幅を以て北方に下り，海拔約 1160 m 附近の山腹に終つてゐる様である．氷穴熔岩と御庭及び奥庭熔岩とは長尾山の西麓に於いて僅かに相重なつてゐる様であつて，共に氷池熔岩に蔽はれてゐるが，其分布狀態から判斷すれば，恐らく氷穴熔岩は御庭及び奥庭熔岩の下位に在るものと考へられる．

氷穴熔岩と御庭及び奥庭熔岩とは肉眼的に既に著しい相違を示し明かに區別せられるが，前者と青木原熔岩，イガトノ山熔岩，天神山熔岩等とは肉眼的には一見殆ど區別せられない程度によく似てゐるのであつて，石原學士は氷穴熔岩と青木原熔岩とを神原博士は前者と天神山熔岩（天神峠式熔岩）とを夫々同一視してゐる．然し，顯微鏡下に於いては，之等の熔岩は夫々明かに區別せられ，氷穴熔岩は上に述べた様な噴出地點と分布とを有する獨自の熔岩である．同熔岩は其熔岩流の表面部に於いては多孔質，岩滓狀の塊狀熔岩で，暗灰色乃至黑色を呈し，內部に於いては，其噴出孔の內壁の露出に見られる樣に，灰色を帶びた緻密質熔岩である．肉眼的には，斜長石の白色斑晶が多量に認められる他に，輝石の黑色斑晶が屢々見出される．顯微鏡下で認められる斑晶は斜長石，單斜輝石，及び斜方輝石を主とし，極めて稀に直徑 0·5 mm 以下の橄欖石を含み，石基は斜長石及び單斜輝石の柱狀微晶，橄欖石及び磁鐵鑛の粒狀微晶，及び玻璃に依つて構成されてゐる．從つて，氷穴熔岩は含橄欖石・複輝石玄武岩である．

白大龍王熔岩

精進登山道 2 合目から西方に約 2 km 距たり，弓射塚の南西隣に，2 個の臼狀の寄生火山が相接して北西一南東方向に並び，一の双子火山を形成してゐる．其北西側及び南東側に在るものは夫々氷池及び白大龍王と呼ばれ，玆に述べる白大龍王熔岩は後者から噴出した一熔岩である．

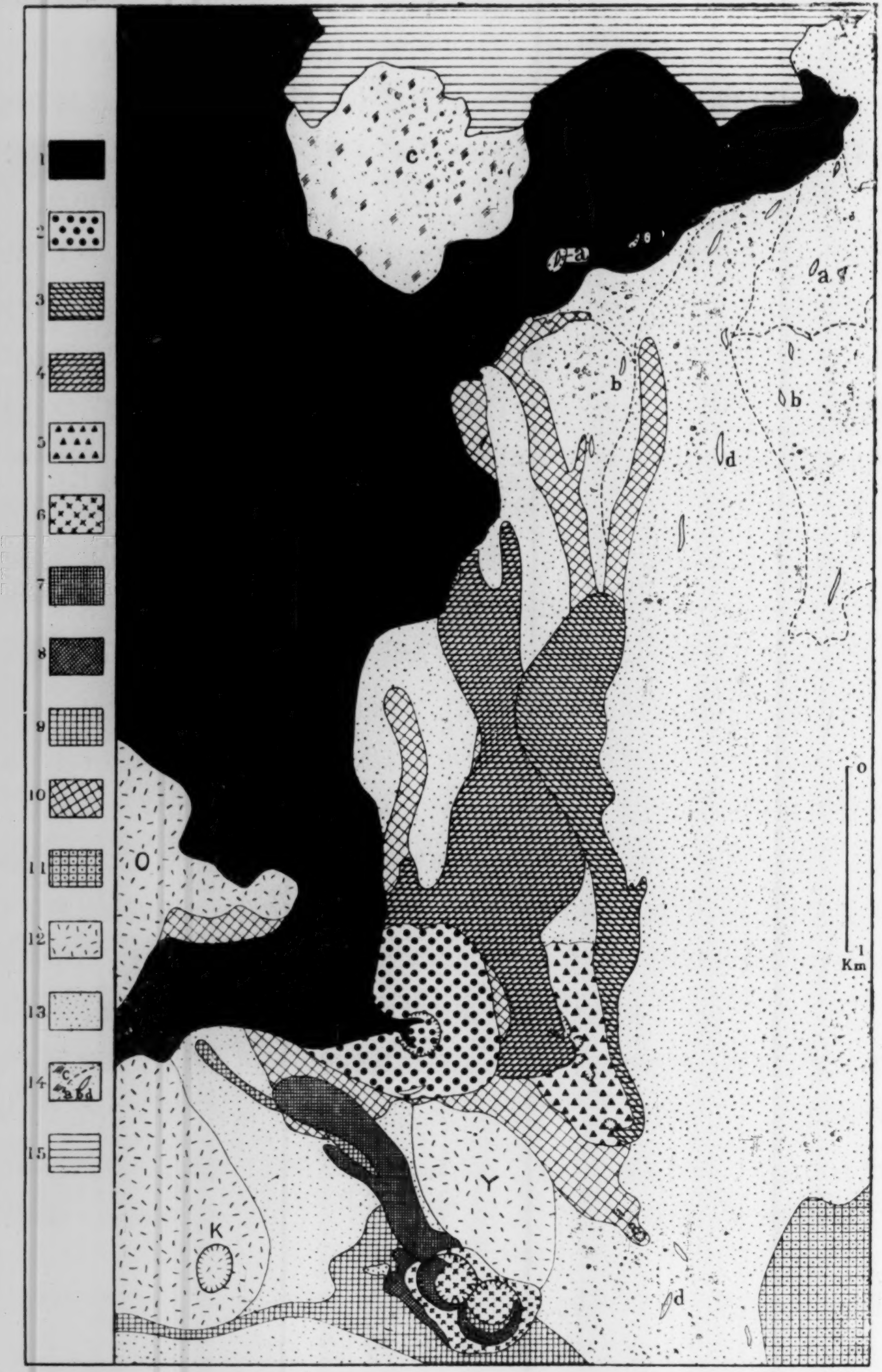
1
2
3
4
5
6
7
8
9
10
11
12
13
14
c
a b d
15
c
a
a
b
b
d
O
Y
K
d
0
1
Km

第２圖　富士山北西麓，青木原東部の地質圖，

1，青木原熔岩（長尾山熔岩）．2，長尾山火山砂礫．3，イガトノ山熔岩．4，天神山熔岩　5，イガトノ山及び天神山火山砂礫．6，氷池及び白大龍王火山砂礫．7，氷池熔岩　8，白大龍王熔岩．9，御庭及び奥庭熔岩．10，氷穴熔岩．11，大平山及び棧數山熔岩．12，寄生火山噴出物一般（K片蓋山，O大室山，Y弓射塚）．13．火山灰一般．14，火山灰下の熔岩一般．15，第三紀層．

白大龍王は比高 20～50 m，基底の直徑約 600 m に過ぎない小寄生火山で，其中央に直徑約 300 m，深さ約 60 m に達する摺鉢形の噴火口を有する．同山の東西兩側は 30° 内外の傾斜の斜面を形造つてゐるが，南東側は御庭及び奧庭熔岩に蔽はれてゐる南方山腹から僅かに高まつてゐるに過ぎず，北東側は弓射塚に妨げられて殆ど發達してゐない．又，其北西側は氷池火山と結合して全く缺けてゐる．噴火口の上緣（海拔 1520 m 内外）は南東部に最も高く，北西方に次第に低まり，同火口と氷池火口との隔壁上に於いて最も低い．

白大龍王の火口壁及び火口底の大部分は崖錐に依つて蔽はれ，たゞ前者の處々に熔岩が絶壁を形造つてゐる．同火口壁の上位，中位，下位に露出するものは夫々氷池熔岩，白大龍王熔岩，御庭及び奧庭熔岩で，之等は集塊岩及び火山砂礫層に依つて距てられて上下に相重なる．此關係は氷池火山の北西麓に於いても確められる．卽，同處には樹型に富む御庭及び奧庭熔岩の上に，土堤狀をなして白大龍王熔岩の短かい Coulée が載り，更に此兩者の上に氷池熔岩が載つてゐる．從つて御庭及び奧庭熔岩が流下した後に，之を破つて先づ白大龍王熔岩が噴出し，次いで氷池熔岩が氷池及び白大龍王の兩火口から噴出したと考へられる．

白大龍王熔岩は肉眼的並に顯微鏡的に御庭及び奧庭熔岩と著しく相違し，氷池熔岩青木原熔岩，氷穴熔岩等とは肉眼的に類似してゐるが，顯微鏡下では之等とも明かに區別される．卽，同熔岩は多孔質，岩滓狀で，暗灰色乃至黑色を呈し，斜長石の肉眼的白色斑晶を多量に含む．顯微鏡下では，同斑晶の他に橄欖石及び單斜輝石の小斑晶が多量に認められ，尙斜方輝石の比較的大きい斑晶が極めて稀に見出される．石基は半玻璃質で，短柱狀の斜長石，粒狀の單斜輝石及び橄欖石，微粒狀或は樹枝狀の磁鐵鑛及び褐色玻璃に依つて構成されてゐる．卽，此熔岩は含斜方輝石・單斜輝石・橄欖石玄武岩である．

氷 池 熔 岩

此熔岩は上述の白大龍王熔岩に次いで，之と同じ噴火口から噴出すると共に，其北西側に接する氷池から噴出した熔岩である．氷池火山は白大龍王火山より稍小さく，比高 30～50 m，基部の直徑約 500 m で，中央に直徑約 250 m，深さ約 50 m の摺鉢形火口を有する．同山の外斜面は，南東側の白大龍王に接する部分を除いて，完全な圓錐面をなし，約 30° の傾斜を示してゐる．氷池の火口壁の上緣は南東から北西に向つて次第に低まり，北西隅に於いて一の銚子口を形造つてゐる．氷池の南東火口壁と白大龍王の北西火口壁とは兩火口の隔壁をなし，相迫つて鋭い稜を挾み，隔壁の最

低部に於ける幅は僅かに 2〜3 m である.

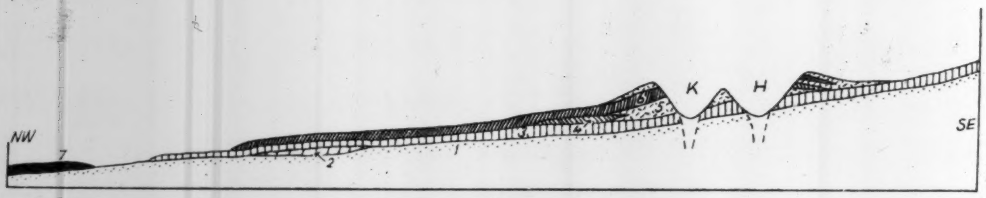

第3圖 富士山北腹の氷池及び白大龍王附近の地質斷面圖.
1，火山灰一般．2，氷穴熔岩．3，御庭及び奥庭熔岩．4，白大龍王熔岩．
5，氷池及び白大龍王火山砂礫．6，氷池熔岩．7，青木原熔岩．

氷池熔岩は氷池の火口壁の上半部，特に其西側の火口壁に絶壁をなして露出する．東側火口壁は同一熔岩の岩滓，岩塊等に依つて蔽はれてゐる．又，火口壁の下部及び火口底は崖錐に依つて蔽はれてゐるが，白大龍王の火口壁に見られる様に，氷池熔岩の下には白大龍王熔岩，御庭及び奥庭熔岩等が存在するに相違ない．氷池熔岩の砂礫及び岩滓狀熔岩塊は氷池及び白大龍王の外斜面一帶を蔽ひ，更に同熔岩は氷池火口の北西側銚子口から外側に流出し，幅約 250 m の熔岩流となつて御庭及び奥庭熔岩流の上及び其東側の山腹を北西方に約 1·2 km 下り，長尾山の南西麓に於いて氷穴熔岩流の上に止まつてゐる．

精進登山道 2 合目から片蓋山の南麓を經て二ツ山方面に通ずる道路は弓射塚の西麓に於いて氷池熔岩流の東縁に達し，此處から約 250 m 西方に進めば，同熔岩流を横切つて其西縁に出る．此西縁近くの路傍の氷池熔岩に標式的の横臥樹型（直徑 0.5 m 内外，長さ約 3 m）が見られる．若し此樹型が氷池熔岩の噴出前に御庭及び奥庭熔岩流の上に生じてゐた樹木に由來するものであるとすると，兩熔岩の噴出時代には少くとも此樹木の生長に要した期間だけの距たりがあつたと考へなければならない．然し，氷池熔岩は御庭及び奥庭熔岩に蔽はれなかつた地域をも流れて居り，兩熔岩が明かに相重なつてゐる處に於いて氷池熔岩中に直立樹型の存在する事は未だ確められてゐないから，上述の横臥樹型の存在を以て直ちに氷池熔岩と御庭及び奥庭熔岩流との噴出年代の距たりは判定されない．

氷池熔岩の熔岩流をなす部分は多孔質，岩滓狀で，暗灰色乃至黑色を呈し，斜長石の多量の肉眼的白色斑晶を含み，一見白大龍王熔岩，氷穴熔岩，青木原熔岩等に似てゐる．然し，前者は肉眼的には斜長石斑晶の他に橄欖石斑晶を含み，顯微鏡的には之等の斑晶及び極めて稀に見出される單斜輝石の小斑晶と多玻璃質で柱狀の斜長石，粒狀の單斜輝石，磁鐵鑛等を含む石基とに依つて構成される含單斜輝石・橄欖石玄武岩である．氷池の火口壁に露出する氷池熔岩は灰色，緻密質で，熔岩流をなす部分と同

様に斜長石，橄欖石，及び極めて少量の單斜輝石の斑晶を含んでゐるが，其石基は遙かに結晶質で，柱狀斜長石，粒狀單斜輝石，磁鐵鑛，鱗石英，及び少量の間隙玻璃に依つて構成されてゐる．

天神山熔岩

此熔岩は精進登山道1合目の東方に突起する天神山から噴出したものである．天神山（海抜 1430 m）は其東南側のイガトノ山に接して，不完全な圓錐形をなし，比高約 100 m，基部の直徑約 600 m を有する小寄生火山である．其北西斜面は東西兩斜面より緩傾斜で，前者は約 15°，後者は約 25° である．其南斜面はイガトノ山の北斜面に對し，兩者の合する處は一の鞍部となつてゐる．此鞍部から天神山の頂上までの高さは十數米に過ぎない．天神山の頂上，北西斜面，同山とイガトノ山との間の鞍部等に亘つて，少くとも4個の噴火口が略北西南東方向に並ぶ．之等は何れも2萬分の1地形圖にも現れてゐない程小さいもののみである．

天神山の北東及び東方斜面は主として天神山熔岩の砂礫のみから成つてゐるが，其北西斜面は大部分同熔岩に蔽はれてゐる．同熔岩は天神山の北西麓から更に北方に，幅 100～600 m の熔岩流をなして分布し，海抜約 1100 m の山腹（天神山の頂上から北方に約 3 km）まで追跡される．又，同熔岩は長尾山の下を青木原の方面にも流下したと想像されるが，青木原熔岩に蔽はれてゐるので，其分布は明かでない．

天神山熔岩は肉眼的に青木原熔岩，イガトノ山熔岩，氷穴熔岩等と極めてよく類似し，且つ之等と相接する部分に於いて著しい地形的差違を示さないので，兩者の分布の境界は甚だ紛はしい．地質圖上に示されてゐる天神山熔岩と之に接する他の熔岩との境界線は實地に於いて兩者の境界附近の熔岩を細かく採集し，夫を一々顯微鏡的に觀察した結果から設定されたものである．從つて，天神山熔岩と之に接する他の熔岩との上下關係は實地に於いては十分確められないが，地質圖上に現れてゐる各熔岩の分布の狀態，長尾山が天神山熔岩上に載つてゐる事實，イガトノ山熔岩が天神山の東麓を巡つて流れてゐる事實等から考へると，天神山熔岩は氷穴熔岩上に載り，青木原熔岩及びイガトノ山熔岩に蔽はれてゐるに相違ない．天神山熔岩と氷池，白大龍王，御庭及び奥庭等の熔岩との噴出の前後關係は不明である．

天神山熔岩は岩滓質，塊狀で，暗灰色を呈し，多量の白色斜長石斑晶の他に，橄欖石及び輝石の肉眼的斑晶を含む．顯微鏡的には，其斑晶は斜長石，橄欖石，單斜輝石及び斜方輝石であり，石基は柱狀の斜長石，微粒狀の單斜輝石，磁鐵鑛，及び少量の褐色玻璃に依つて構成されてゐる．即，同熔岩は複輝石・橄欖石玄武岩の一種である．

イガトノ山（五十殿山）熔岩

此熔岩は天神山の南東側に接するイガトノ山（海抜 1490 m）から噴出した熔岩である．同山は基部の直徑約 500 m，比高 90 m 以下で，不完全な圓錐丘をなし，其中央より南東寄りに山頂を有する．其山腹は北西方向に最も長く延びて 15° 内外傾斜し，東西兩方向には之より短くて 25° 内外傾斜してゐるが，南東方向には殆ど發達してゐない．卽，イガトノ山は天神山との間の鞍部から約 75 m 高まり，南東側の富士山山腹との間の鞍部からは僅かに約 15 m 高まつてゐるに過ぎない．同山の噴火口は頂上及び北西斜面に數個あるらしく，石原學士に依れば，天神山及びイガトノ山に合せて 8 個の噴火口が並んでゐると云ふ．

イガトノ山自體は大部分火山砂礫及び熔岩塊に蔽はれてゐるが，其山頂火口から噴出したイガトノ山熔岩は東側斜面を下り，東麓の谷の中に流込み，幅約 50 m の熔岩流をなして天神山の東麓に沿つて北流し，同山の北東山麓に隣接する緩傾斜地に出でて約 250 m の幅を有する熔岩流となり，天神山熔岩流の東緣部に接しつゝ更に北方に流下し，海抜約 1120 m 附近の山腹に於いて氷穴熔岩の北方支流の上に止まつてゐる．

イガトノ山熔岩は暗灰色，多孔質の塊狀熔岩で，多量の白色斜長石の他に，橄欖石及び輝石の肉眼的斑晶を含む．顯微鏡的には輝石斑晶は單斜輝石と斜方輝石とに區別される．石基は柱狀の斜長石，粒狀の單斜輝石及び磁鐵鑛，及び少量の間隙玻璃に依つて構成されてゐる．卽，同熔岩は複輝石・橄欖石・玄武岩である．

イガトノ山熔岩と天神山熔岩とは肉眼的及び顯微鏡的に最もよく類似し，たゞ顯微鏡下で認められる石基の構造の相違に依つてのみ區別される．イガトノ山と天神山とは恐らく殆ど同時の噴火に依つて形成された寄生火山で，後者の熔岩流出後間もなく前者の熔岩流出が行はれたものと考へられる．

長尾山熔岩（青木原熔岩）

青木原熔岩の分布地域近くに在つて，從來之と同一視されてゐた熔岩が 6 種に分たれ，之等が夫々別個の寄生火山から噴出し，各自に別個の熔岩流として分布してゐるものである事は以上に述べた通りであるが，次に青木原熔岩が之等 6 種の熔岩の何れとも異なり，長尾山から噴出して所謂青木原一帶に擴がつたものである事を述べる．

岩石學的性質． 青木原熔岩を肉眼的に觀察すると，其熔岩流の表面部は暗灰色乃至黑色を呈し，多孔質，岩滓狀であるが，內部は灰色を帶び，殆ど緻密堅實で，比較

的大形の氣孔を稀に有するに過ぎない．肉眼的斑晶は多量の斜長石と少量の橄欖石及び輝石とである．既に發表した青木原熔岩の岩石學的研究の結果の中で，其顯微鏡的性質に關する部分を摘錄すれば次の如くである．

斑晶：　亞灰長石（1～2 mm）$Ab_{25}An_{75}$～$Ab_{29}An_{71}$；25·15%（容量 100 分比）；橄欖石（0.5 mm）$2V=(-)86°$，2.84%；單斜輝石（0.5～1 mm）$n_1=1·6979$，0·07%；斜方輝石（0·5～1 mm）$n_1=1·6983$，$n_2=1·7076$，微量．

石基：　曹灰長石（0·2 mm 以下），單斜輝石，磁鐵鑛，暗褐色玻瑠．

他の熔岩類との比較．　上述の 6 種の熔岩に含まれてゐる鑛物の光學的性質を檢べて青木原熔岩の夫に比較すれば，兩者の相違は一層明瞭になるものと豫想されるが，單に肉眼的及び顯微的に觀察される兩者の組織，成分鑛物の種類及び量等のみに就いても，兩者の相違は明瞭に認められる．其主なる相違點は次の如くである．

青木原熔岩――イガトノ山熔岩及び天神山熔岩．　前者の含む斑晶輝石は後者の夫に比較して明かに少量である．又，前者の石基は後者の夫より著しく粗粒で，其結晶度の高い部分は多少粗粒玄武岩狀の構造を示す．

青木原熔岩――氷池熔岩．　前者に比較して，後者は斜長石斑晶の量に於いて劣つてゐるのみでなく，單斜輝石の少斑晶を極めて稀に含むが，斜方輝石斑晶を全く缺いてゐる．

青木原熔岩――白大龍王熔岩．　前者と異なつて，後者は波動消光を示す單斜輝石の小斑晶を多量に有する．

青木原熔岩――氷穴熔岩．　後者は前者に比較して單斜輝石及び斜方輝石の斑晶を著しく多く有するが，橄欖石斑晶を殆ど含まない．

青木原熔岩――御庭及び奥庭熔岩．　後者は斑晶の少ない黑色熔岩であるから，肉眼的に一見して前者と區別されるが，顯微鏡的には橄欖石及び輝石の斑晶を含まない事に於いて前者と著しく異なる．

分布．　青木原熔岩は長尾山の北西側から大室山を巡つて北方及び西方に擴がり，所謂青木原の大部分に丸尾として露出してゐる．

吉田から本栖方面に至る縣道に沿つて觀察すると，青木原熔岩は先づ鳴澤部落の人家附近に露出し，同處から西方の燒間ヶ原（雲雀ヶ岳）に至る約 2 km の間續いてゐる．此區間の青木原熔岩は燒間ヶ原の南方に於いて北東方に分岐した一支流で，足和田山（第三紀層）の南麓に沿つて鳴澤の低地に流込んだものである．燒間ヶ原は舊期噴出の富士熔岩の一が足和田山の西端部なる紅葉臺の山麓に停滯した結果生じた高まりで，一帶に火山灰に依つて蔽はれてゐるが，同熔岩の一部を其地表に點々と露出せ

しめてゐる．東西の幅約 1 km の燒間ヶ原を過ぎると，其西端から御殿庭を經て赤池附近に至る約 5 km の區間に亘つて，青木原熔岩が間斷なく露出してゐる．西湖の湖岸，根場附近，及び王ヶ嶽の南麓の一帶に分布してゐる青木原熔岩は此區間を通つて北方に流下してゐるものである．赤池附近から精進湖岸に至る約 1 km の間，道路は第三紀層の山地の中を通じてゐるが，青木原熔岩は赤池の低地を距てて其南側に一の段崖を形成し，赤池の低地一帶をも蔽つてゐる．精進湖岸から烏帽子岳（第三紀層）の東麓（精進部落に通ずる道路の分岐點）に至る約 1 km の間には青木原熔岩が見られるが，同熔岩は北西に續いて精進湖中に沒する．烏帽子岳及び其南東部の城山の東麓を巡る約 1 km の間に於いては，青木原熔岩が此山地に接して停滯してゐるのが見られる．城山の南東端を迂回して本栖部落の北端に至る約 1 km の間には，2 ヶ處に舊期噴出の富士熔岩（本栖部落內に露出するものに同じ）の島を殘して，青木原熔岩が分布し，烏帽子岳の南麓に沿つて本栖湖岸迄續いてゐる．同熔岩の縣道上に於ける露出は本栖部落の北端で終り，夫以南には見られない．

以上に述べた樣に，青木原熔岩の主要部の分布は山麓地方に於いては外郭の第三紀層山地に圍まれ，鳴澤及び本栖を夫々東西兩翼の限界とし，其間約 12km の幅の地域一帶に及んでゐるが，南方に至るに從つて次第に狹まる．（圖版第 1 圖）即，其東翼の限界は鳴澤から先づ南西方に向ひ，燒間ヶ原の南方に於いて南々西の方向に轉じ，長尾山の北麓に至り，西翼の限界は本栖から南東方に向ひ，大室山の北麓及び北東麓に沿つて長尾山北西麓附近に至つてゐるのであつて，大室山東麓に於いて青木原熔岩の分布地域は東西に約 1 km の幅を有するに過ぎない．

本栖から縣道を南方に約 2·5 km 進み，龍ヶ嶽（第三紀層）東麓の舊期富士熔岩流の臺地上に出ると，道路から東方に約 50 m 入つた處に青木原熔岩が露出し，約 150 m 內外の幅を以て南東方に續いてゐるのが見られる．又，同縣道を更に南方に進み根原から東方に約 1 km 登ると，山梨，靜岡兩縣の境界附近に，青木原熔岩が露出し約 150 m 內外の幅を以て北東方向に續いてゐる．此兩者は根原の北東約 1·5 km の山腹に於いて合し，約 500～700 m の幅を以て東方に續き，大室山の南麓に沿つて長尾山の北西麓に達する．

青木原熔岩の分布地域の中には火山灰に蔽はれた舊期富士熔岩類が處々に島となつて露出してゐる．其小さいものは本栖附近及び鳴澤附近に見出され，大室山北西麓近くに在つて，大室山熔岩及び舊期の富士熔岩から成る島が最も大きい．尙，青木原には氷穴熔岩及び天神山熔岩が同樣に島となつて露出してゐるかも知れないが，之等は野外に於いては青木原熔岩と殆ど同一の外觀を有する丸尾であるから，斯樣な島があ

つたとしても，夫を見出す事は仲々容易でない．神原博士は精進湖中に2層の熔岩流の在る事を認め，其上層を青木原熔岩，下層を赤池の底面に露出する熔岩と共に天神山熔岩（同博士の天神峠式熔岩）と考へてゐる．精進湖中の下層の熔岩は未だ確められてゐないが，赤池の底面に露出する熔岩は青木原熔岩であつて，天神山熔岩ではない．

噴出中心（長尾山）． 青木原熔岩は長尾山の北西麓から更に同山の北西斜面を上り，遂に其山頂に達する迄間斷なく追跡される．而して，其分布は長尾山の北西麓に於いては約800m の幅を有し，同山の斜面を上るに從つて次第に狹まり，山頂附近では僅かに 30 m 内外に過ぎない．長尾山の北麓及び西麓に於ける限界は細心の注意を以て觀察しないと見逃される恐れがある．卽，北麓に於いては，青木原熔岩は天神山熔岩及び氷穴熔岩と境を接し，西麓に於いては，前者は氷穴熔岩と境を接するのみならず，氷池熔岩及び御庭及び奧庭熔岩の各熔岩流の末端近くに達してゐる．而して，之等は何れも殆ど丸尾の狀態で露出してゐるから，若し此點のみに着眼して觀察されると，青木原熔岩は一方に於いて長尾山の北東麓を巡つて天神山及び氷穴の方向に續き，他方に於いては長尾山の西麓を過ぎて氷池方面に續いてゐるかの如く見誤られる．從來青木原熔岩が長尾山の山麓を過ぎて更に南東方に續くものと考へられたのは恐らく斯る觀察に基づくもので，其誤りである事は旣に述べた諸事實に依つて明かである．神原博士は青木原熔岩と御庭及び奧庭熔岩とを臼山と弓射塚との中間地域に於いて岩質の漸移する同一熔岩流と考へてゐるが，此地域に見出される一見青木原熔岩に似た斜長石斑晶の多い熔岩は氷池或は白大龍王火口から噴出し，御庭及び奧庭熔岩流の上に堆積してゐる熔岩塊に過ぎないのであつて，御庭及び奧庭熔岩自身が此地域で斜長石斑晶を增して青木原熔岩に移化するのではない．一つの熔岩流の上流と下流とが岩質を異にする事は有り得る現象であるが，青木原熔岩は斯る現象を示さず，青木原一帶から長尾山の頂上に至る迄殆ど同樣の岩質（成分鑛物の種類，分量等に就いて）を以て續いてゐる．

以上に述べた樣に，青木原熔岩は長尾山の北西麓から其山頂に續き，これに反し同山の南西及び北東麓に露出する熔岩は之と明かに異なる氷穴熔岩及び天神山熔岩で，長尾山の火山砂礫を被つてゐる．從つて，青木原熔岩の噴出中心が長尾山である事には疑ふ餘地が少しも存しない．

長尾山（海拔 1424·1 m）は比高約 70～150 m，基部の直徑約 1 km に達し，其頂上に直徑約 200 m，深さ約 60 m の擂鉢形火口を有する完全な圓錐形の寄生火山である（圖版第 2，3 圖）．旣に述べた樣に，其北西斜面は青木原熔岩に蔽はれてゐるの

であつて，頂上から約20°以下の傾斜を以て北西麓に下り，地形的に著しい不連續的傾斜を示さずして青木原の熔岩地表面に續いてゐる．其他の方面の斜面は大部分同火山から噴出した火山砂礫，火山彈，熔岩塊等に蔽はれ，山頂から山麓迄殆ど一様に約25° の傾斜を示し，外郭の緩かな地表面（氷穴熔岩及び天神山熔岩の地表面）から急に聳え立つてゐる．山頂火口の火口壁は東部に於いて最も高く，北西方に次第に低まつてゐて，火口底に向つて約20° 内外の傾斜を有する．但し同火口の北西側は火口壁を缺き，一の銚子口をなして外方斜面に通じてゐる．火口底は火山砂礫及び熔岩塊に埋められ，略平坦で，銚子口から僅かに數米低まつてゐるに過ぎない．銚子口の處には直徑 10 m 内外，深さ數米の皿狀火口が在る．此火口の附近及び主火口の北，西兩壁附近には熔岩（一部分は集塊熔岩）が露出し，同熔岩は青木原熔岩と全く同一である．

長尾山の噴出物は其周圍の山麓に於いて氷穴熔岩及び天神山熔岩を明かに蔽つてゐる．從つて，前者は後者より新期の噴出物であるが，兩者は共に類似の岩石學的性質を有し，新鮮な地形を形造つてゐるから，其噴出の時代的間隔は大して長くないと想像される．長尾山の噴出物と氷池，白大龍王，御庭及び奥庭等の熔岩類とは直接相接せず，兩者の前後關係は明かでないが，若し前者を代表する青木原熔岩が貞觀6年に噴出し，富士山に於ける有史時代の最新の熔岩流であるとすれば，後者は何れも夫以前の噴出物であるに相違ない．

要するに，長尾山は氷穴及び天神山の熔岩の流出した後に，之等熔岩流の地表面上に現れた火山で，此火山は先づ活動の初期に主として火山砂礫，火山彈，熔岩塊等を噴出して圓錐丘の大部分を形成し，末期に至つて多量の熔岩を噴出した．而して，此熔岩は同圓錐丘の頂上火口から噴出し，火口壁の北西部の缺處を經て北西麓に流下し其大部分は更に大室山の東及び北麓を巡り，鳴澤と本栖との間の山麓地域に擴がつて所謂青木原熔岩となり，他の一部分は大室山の南麓に沿つて西方に流下し，根原東方の山腹に達したのである．

噴出時代． 確實なる歴史的記録に殘されてゐる有史時代の富士山噴火は天應1年（西暦 781）に始まり寶永 5 年（1708）に至る迄の間に十數回[10]起つてゐる．其中で最新の寶永年間の噴火を除けば，青木原熔岩を噴出したと考へられてゐる貞觀 6 年（864）の噴火は延暦 19 年（800）の噴火と共に多少詳しく記録されてゐて，有史時代の富士山の比較的著しい火山活動であつたと想像される．此貞觀6年の噴火に關する

---

[10] 大森房吉，震災豫防調査會報告，86 (1918), 90．平林博士の報告（前掲）には天應 6 年以前に起つたと思はれる 6 回の噴火（?）の記録が擧げられてゐるが，之等は大森博士の報告中には採用されてゐない．

記錄の一部を摘錄すれば次の如くである．

“5 月 25 日庚戌霖雨，……，駿河國言，富士郡正三位淺間大神大山火，其勢甚熾，燒山方 1. 2 許里，光炎高 20 許丈，有雷地震 3 度，歴 10 餘日火猶不滅，焦巖崩嶺，沙石如雨，煙雲鬱蒸，人不得近，大山西北有本栖水海，所燒巖石流埋海中，遠 30 許里，廣 3，4 許里，高 2，3 許丈，火焰遂屬甲斐國界”．(三代實錄)．

“貞觀 6 年秋 7 月 17 日辛丑，甲斐國言，駿河國言，富士大山忽有暴火，燒碎崗巒，草木焦，熱土礫石流埋八代郡本栖並剗兩水道，水熱如湯魚鼈皆死，百姓居宅與海共埋，或有宅無人，其數難記，兩海以東亦有水海，名曰河口海，火焰赴向河口海，本栖剗等海未燒埋之前，地大震動，雷電暴雨，雲霧晦冥，山野難辨，然後有此災異焉”．(前同)．

“貞觀 7 年 12 月 9 日丙辰，……，先之彼國司言，往年八代郡暴風大雨雷電地震雲霧，杳冥難辨山野，駿河國富士大山西峯，忽有熾火燒碎巖谷，……，雖然異火之變于今未止，遣使者檢察，埋剗海千許町……”．(前同)．

以上の記錄に依つて，貞觀 6 年には富士山の山麓地方に先づ暴風雨及び地震があり，次いで富士山の噴火が起り，其際噴出した熔岩流が本栖湖及び剗ノ海を埋め，附近の住民，家屋等に災害を及ぼした有樣が略想像される．剗ノ海は嘗て富士山の北西麓に在つた湖水で，此噴火の噴出物に依つて大部分埋められて失つたと想像されるが，現在の精進湖及び西湖が其殘部に相當するものと考へられてゐる．本栖湖が此噴火以前既に剗ノ海から獨立した別個の湖水であつた事は本栖部落から其北方の城山山麓に至る間に舊期の富士熔岩が在り，同熔岩の上に何等の湖底堆積物と考へられる地層が無くて，青木原熔岩が載つてゐる事實に依つて明かである．

精進湖と西湖とを距ててゐる熔岩は青木原熔岩であり，本栖湖に流込んでゐる最新の熔岩も同熔岩である．而して，貞觀 6 年以後の富士山噴火の記錄には之等の湖岸地域に熔岩が流下したと想像される記事は見られない．從つて，上記の記錄が正しいとすれば，青木原熔岩が貞觀 6 年に噴出したといふ推定には誤りが無いものと考へられる．

上記の記錄中には貞觀 6 年の噴火の中心は明示されてゐないが，長尾山が少くとも其一中心である事は青木原熔岩が同山から噴出してゐる事實から明かである．上記の記錄中，“富士大山西峯……”とある西峯は或は長尾山を指した語であるかも知れない．又，平林博士に依ると，某舊記に“噴火の前劇烈の地震ありたり．又山巓を繞て空際を燒くこと 20 丁四方，煙焰の昇騰すること 72 尺，之れに伴ふに雷鳴を以てす．又 3 回の地震ありて噴焰 10 日に涉り，山脚終に破裂して灰石を雨らし，其一部西北の湖中に墜落し，湖水爲めに沸騰す……”とある．此記錄が正しいとすれば，“山脚終に破裂して……”の語は富士山の山麓に噴火が起つた事を意味するもので，長尾山の噴火を指すものと解して矛盾しない．“山巓を繞て……”の語に據つて，平林博

士は青木原熔岩の噴出中心が富士山頂に在ると考へたのであるが，同熔岩の噴出中心が長尾山に求められた現在では，此語は別の意味に解釋されなければならない．即，貞觀6年には長尾山が噴火して青木原熔岩を噴出したのみでなく，富士山頂其他にも噴火が起つたと解釋するのが其一である．若し之が事實であるとすれば，青木原熔岩の他にも貞觀6年の噴出物が存在する筈である．其存在を確める事は尚今後の問題として殘されてゐるが，所謂劍丸尾が青木原熔岩と共に從來貞觀6年の噴出物と考へられてゐるので，次に此兩者の噴出時代の關係を吟味する．

青木原熔岩と劍丸尾との噴出時代關係． 從來劍丸尾と呼ばれてゐるものは富士山の北側中腹の寄生火山丸山と東劍との間を通り，約 1km の幅を以て南々西から北々東の方向に下り吉田の西側を經て柱川の谷に沿つて小沼附近に至る迄，一見一熔岩流であるかの如き地形を以て帶狀に連なつてゐる丸尾である．此丸尾が貞觀6年の噴出物であると考へられたのは前記の三大實錄の噴火記錄中に見られる“兩海以東亦有水海，名曰河口海，火焰赴向河口海……”の語に據つてゐるのであつて，河口海が現在の河口湖であり，劍丸尾が略此湖の方向に流れたと解釋された結果である．即，平林博士は貞觀6年に富士山頂から噴出した熔岩の一流は北西山麓に下つて青木原熔岩となり，他の一流は中腹に於いて前者から分岐し，北東山麓に下つて劍丸尾となつたと考へた．神原博士も亦劍丸尾を貞觀6年の噴出物とし，其噴出地點を精進登山道3合目上に在る寄生火山太平山の南隣“押ツ立テ”附近に在ると推定した．石原學士は劍丸尾を精進登山道4合目附近に噴出中心を有し，青木原熔岩より多少舊期の噴出物であると考へた．

筆者の詳細な野外調査と顯微鏡的觀察の結果に依れば，從來の所謂劍丸尾は單一の熔岩流ではなく，夫々明かに噴出地點，噴出時代，岩石學的性質等を異にする5種類の熔岩流11)を包含してゐるのであつて，之等熔岩流は中途以下に於いて上下に相重なり或は左右に相接觸し，宛も一續きの丸尾であるが如く連なつてゐる．此5種類の熔岩を古いものから時代順に擧げれば次頁の表の如くである．

從來の所謂劍丸尾は小沼から溯り，吉田の西方を經て吉田胎內附近（海拔約 1080 m）の山腹に間に於いては此表中に定義されてゐる劍丸尾熔岩のみであるが，吉田胎內附近から山ノ神附近に至る間に於いては同熔岩と牛ケ窪熔岩とに分たれ，山ノ神から更に上方に於いては上記の5種の熔岩に分たれるのである．之等熔岩の分布，地質

---

11) 尚，精進登山道3合目の南方に在る寄生火山大平山附近に，之等の熔岩流より舊く，富士山頂から流下してゐる2種類の熔岩流が丸尾として見出される．大平山自體は同3合目附近の幾數山と共に之等の熔岩流より更に舊い寄生火山で，其噴出物（無斑晶玄武岩）は精進登山道2合目の東方山腹（西劍，東劍附近）に分布してゐる．

熔岩名	岩種	噴出地點	熔岩流末端所在
1. 劍丸尾熔岩	橄欖石玄武岩	富士山頂附近	桂川谷の小沼附近
2. ガラン熔岩	單斜輝石・橄欖石玄武岩	精進登山道3合目・4合目間中途の南方山腹ガラン附近（海拔約 2200 m）.	船津登山道山ノ神北東方の海拔 1350 m 附近.
3. 牛ヶ窪熔岩	含複輝石・橄欖石玄武岩	富士山頂	吉田胎內（北口胎內）附近海拔約 1030 m.
4. 小御嶽風穴熔岩	橄欖石玄武岩	小御嶽風穴（精進登山道 4 合目，海拔約 2120 m）.	寄生火山丸山の北西麓近く海拔 1500 m 附近.
5. 劍ノ出丸尾熔岩	含普通輝石・橄欖石玄武岩	大流レの丸山（御庭の北東方山腹，海拔 2250 m 附近）	寄生火山東劍の北東方，劍ノ出丸尾及び山ノ神附近，海拔 1370 m.

的相互關係，岩石學的性質等に就いては別に詳細に發表するはずであるから玆には省略する.

青木原熔岩と上記の5種の熔岩とは岩石學的性質を明かに異にしてゐる. 然し，同一火山に於いて相距たつた地點から夫々岩石學的性質の異なる熔岩が殆ど同時に噴出する事は有り得る現象であるから，青木原熔岩と同一の岩石學的性質を有する丸尾が富士山の他の部分に見出されない事實のみを以て必ずしも青木原熔岩のみが貞觀6年の噴出物であると斷定することは出來ない. 青木原熔岩と從來の所謂劍丸尾とは共に新鮮な丸尾であり，相互に相距たつて分布し，其噴出の前後關係は地形並に地質の上からは直接的にも間接的にも未だ不明である. 三代實錄中の“火焰赴向河口海”の語を，熔岩が現在の河口湖の方向に流れたといふ意に解すれば，所謂劍丸尾に包含されてゐる上記の5種の熔岩の中で，之に最も適合する劍丸尾熔岩が貞觀6年に富士山頂から噴出したと考へられなければならない. 而して，若し之が事實であるとすれば貞觀6年以後に於いて更に何回か富士山頂及び北腹に噴火が起り，ガラン熔岩，牛ヶ窪熔岩，小御嶽風穴熔岩，劍ノ出丸尾熔岩等を流出せしめたことになる[12]. 最近の噴火（寶永 4〜5 年）を除き，貞觀6年以後の噴火の記錄は何れも極めて簡略で，熔岩流出の有無を判斷するに足る內容を含んでゐない. 從つて，現在では劍丸尾熔岩を青木原熔岩と同樣に貞觀6年の噴出物であると斷定することは出來ないのであつて，反つて若し貞觀6年以後に熔岩流出が全く行はれなかつたと假定すれば，地質學的事實から劍丸尾熔岩は貞觀6年以前の噴出物であると斷定されるのである. 三代實錄中の“火焰赴向河口海”が現在の河口湖の方向に熔岩の流下した事を意味するとしても，其熔岩は必ずしも劍丸尾熔岩であると考へる必要はないのであつて，鳴澤方面に向つて流下した青木原熔岩であると考へることも出來る.

---

[12] 御庭及び奧庭熔岩，白大龍王熔岩，氷池熔岩等も劍丸尾熔岩より新しい噴出物であり富士山頂附近にも後者より新しい熔岩類が存在する.

總 括

青木原熔岩は富士山の貞觀6年の噴火に際して噴火した熔岩で，從來同火山の頂上或は北西側の御庭附近から噴火したと考へられてゐたが，今回の調査の結果，御庭より遙かに下方の一寄生火山長尾山から噴出してゐる事が明かにせられた．卽，同熔岩は長尾山の頂上から其北西斜面を下り，大室山を取圍んで北方には鳴澤及び本栖を夫々東西の限界とする廣大なる山麓地域一帶に分布し，西方には幅狹い帶狀をなして根原の東方山腹に達してゐる．長尾山より上方の山腹には天神山熔岩，イガトノ山熔岩氷穴熔岩，白大龍王熔岩，氷池熔岩，御庭及び奧庭熔岩等が何れも殆ど丸尾の狀態で分布してゐるが，之等は夫々の噴出中心を有する別の熔岩流を形成し，岩石學的にも青木原熔岩とは明かに區別されるものである．

所謂劒丸尾は青木原熔岩と同様に貞觀6年の噴火に際して小御嶽と御庭との間の山腹から噴出した熔岩であると從來考へられてゐた．然るに今回の調査の結果，所謂劒丸尾は單一の熔岩流ではなくて，岩石學的性質を異にする少くとも5種の熔岩が何れも殆ど丸尾の狀態で覆瓦狀に相重なり合つてゐるものである事が確められた．卽，吉田と船津との中間に位する鐘懸松附近を經て柱川谷の上暮地附近に達してゐる丸尾が從來の如く劍丸尾熔岩と名付けられるとすれば，吉田胎内から上方の山腹に於いて此熔岩の上にガラン熔岩，牛ケ窪熔岩，小御嶽風穴熔岩，及び劍ノ出丸尾熔岩と名付けられる夫々別種の熔岩流が重なり合つてゐる．劍丸尾熔岩は岩石學的に青木原熔岩と全く異なり，恐らく富士山頂から噴出したものである．從つて，噴火の歴史的記錄のみから前者が貞觀6年の噴出物であると斷定するには尙疑問があるのであつて，現在の所筆者は之を後者より多少舊期の噴出物であらうと考へてゐるが，今後尙此疑問の解決に努めるつもりである．

---

45. *Geological and Petrological Studies of Volcano Huzi (Fuji), II.*

2. Distribution of the Aokiga-hara lava and its vent.

By Hiromichi TSUYA.

Earthquake Research Institute.

Of a number of the so-called "marubi" (recent bare lava-flows not covered by any pyro-

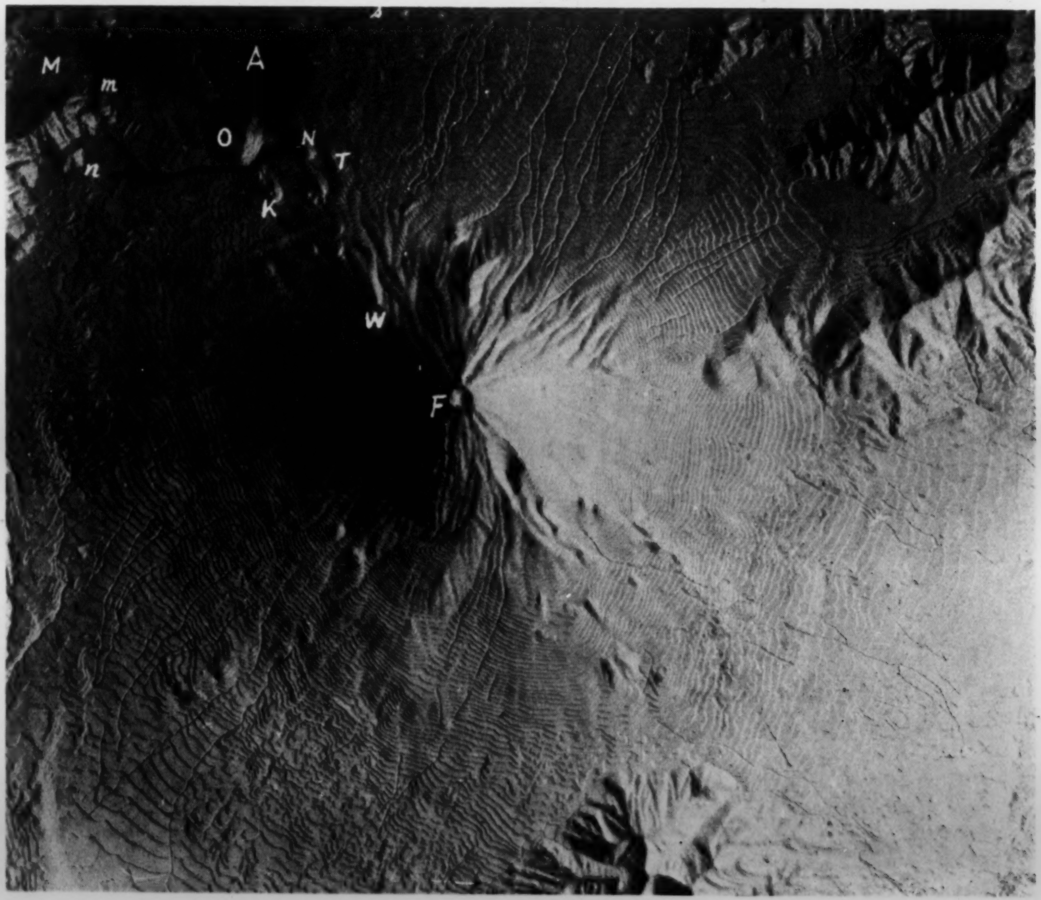

第1圖　富士山模型圖．　A，青木原熔岩分布地域．F，富士山頂．M，本栖湖．N，長尾山．K，片蓋山．O，大室山．T，天神山．W，御庭．m，本栖．n，根原．s，鳴澤．

第２圖　富士山麓大田和より南西方に長尾山を望む（圖の中央）.

（震研彙報・第十六號・圖版・津屋）

第３圖　弓射塚北麓より東方に長尾山を望む.

clastic ejecta) on the outer slopes of Huzi, the Aokiga-hara marubi is the most conspicuous, covering an area of about 32 sq. km on the northwestern skirt of the volcano. Although history tells the lava to be a product of the 864 A.D. eruption, it does not record the exact lot wherein the lava originated. Some of the previous authors believe that the vent of the lava is the summit-crater of the volcano, while the others consider that the former is represented by some of the openings that lie in the vicinity of Oniwa (about 2300 m above sea level) half-way down the northwest flank of the volcano. As a result of extensive field work and microscopical studies, the writer offers here an account of the facts indicating that the Aokiga-hara lava issued from the crater of Nagao-yama, a parasitic cone, 1424 m above sea level, on the lower part of the northwest flank.

46. 昭和13年5月9日及び15日の磐梯山麓川上溫泉附近に於ける山津浪並びに流下せる火山灰質土砂の二三の物理的性質

地震研究所　飯田汲事

(昭和13年6月21日發表—昭和13年6月22日受理)

1. 緒　　言

昭和13年5月9日及び15日の兩日に於いて磐梯山噴火口壁の東北端をなす燕岩附近の山腹に山崩れがあり，其れによつて福島縣耶麻郡猪苗代町字山ノ神原地內川上溫泉地帶に山津浪襲來し，死者2名負傷者數名を出し，家屋を流失，破壞或ひは埋沒し川上溫泉をして殆ど全滅に瀕せしめたのである．該地方に於いて斯樣な慘事を惹起せしは明治21年7月15日に於けるかの有名な磐梯山の大破裂の際にもあつたが，其の後今日迄約50年間幸ひ無事に經過して來た事とて，今回の事件は土地の人をして再度の磐梯破裂或ひは其の前兆に非ずやとの想像を抱かしめたのであつた．

5月15日の山津浪發生後約1週間を經過してはゐたが，筆者は該地方に於ける山津浪調査を命ぜられしにより，該地方に至り5月21日より約5日間に亙り山津浪による被害及びその原因等について實地調査をしたのである．本文に於いてはそれ等の結果及び該地方より採取せる泥流物質なる火山灰質土砂に就いて測定したる2~3の物理的性質を述べ山崩れ，山津浪等の本性を究明する手段としたい考へである．

2. 崩壞地の位置及び其の附近の地形

山崩れ及び山津浪の發生したる位置及び其の附近の地形は第1圖に於て示した如くである．川上溫泉は猪苗代町の北方9 kmの處にあり，又崩壞地は川上溫泉の西南約3 kmの處にあつて磐梯山火口壁の東北端なる燕岩（土地の人は斯く呼ぶ）崖下である．川上溫泉附近は海拔約700 mであり，崩壞せる現場附近の最高所は海拔約1100 mである．從つて此れから傾斜角を出して見ると約7~8° となる．又崩壞箇所は磐梯登山道の沿線であり，噴火口跡には崩壞現場の最高所を越えて至るのである．從つて崩

壞地は火口周壁をなす小山の北側斜面で，此の崩壞により生じた泥流が山津浪となつて川上溫泉を襲つたのである．

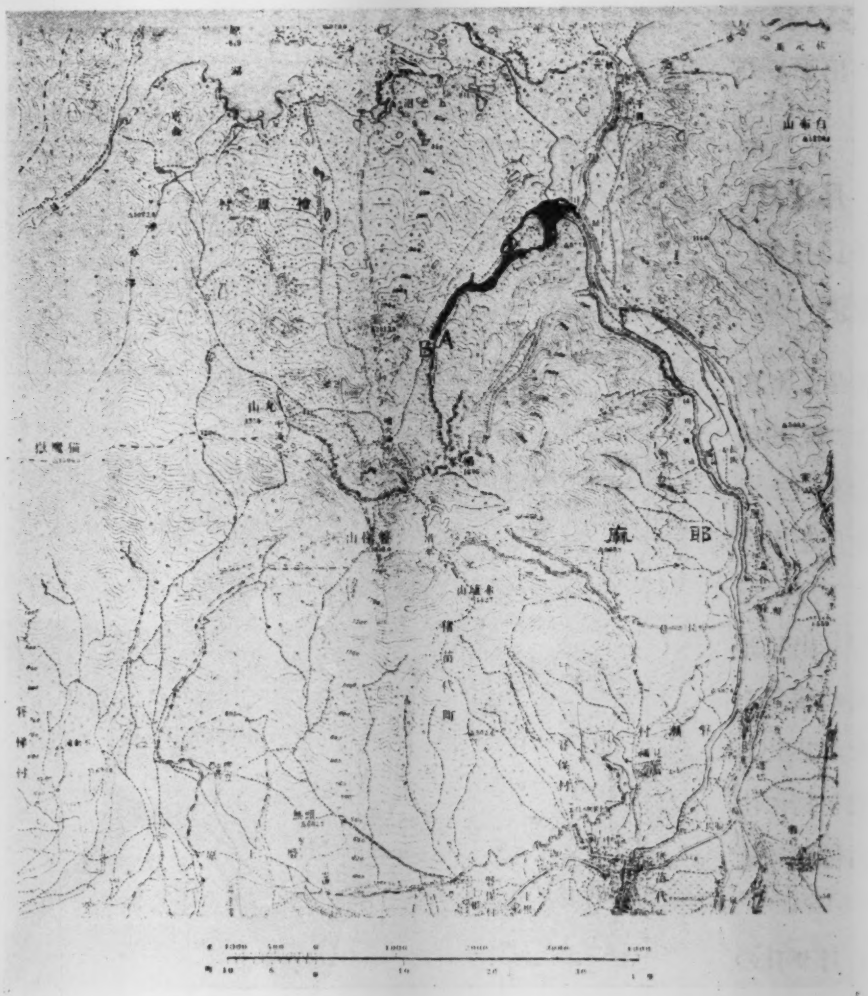

第1圖　山津浪發生地附近の地形圖

A，燕岩．B，崩壞地より噴火湯に至る途中の窪地

Fig. 1.　Topographical map in the neighbourhood of the landslide.

現在の磐梯山爆裂火口北側附近の山は明治 21 年に於ける大爆發の際に生じた泥流によつて形成されたもので，火山灰，火山礫等からなつてゐる．從つて只今の崩壞地も同樣に火山灰，火山礫等から形成されてゐるであらう事は容易に想像される事であるが，實地踏査によつて一層明確に認められた次第である．倘火山灰質物質は如何なる程度に散布してゐるかを示すために第2圖を揭げて置く．

此の第2圖[1]は故關谷教授，菊地助教授によつて磐梯の大破裂直後調査され製作さ

1）　關谷清景　東洋學藝雜誌　5（1888），493．

れたもので磐梯山破裂の際に於ける土石散布の有樣を示した圖である.

此の圖から今回の慘狀を惹起した地方は明治 21 年に於ける磐梯山の大破裂後に其の火山灰質土砂によつて生成されたものである事が判り，此の附近の地質の大略をも知る事が出來るであらう.

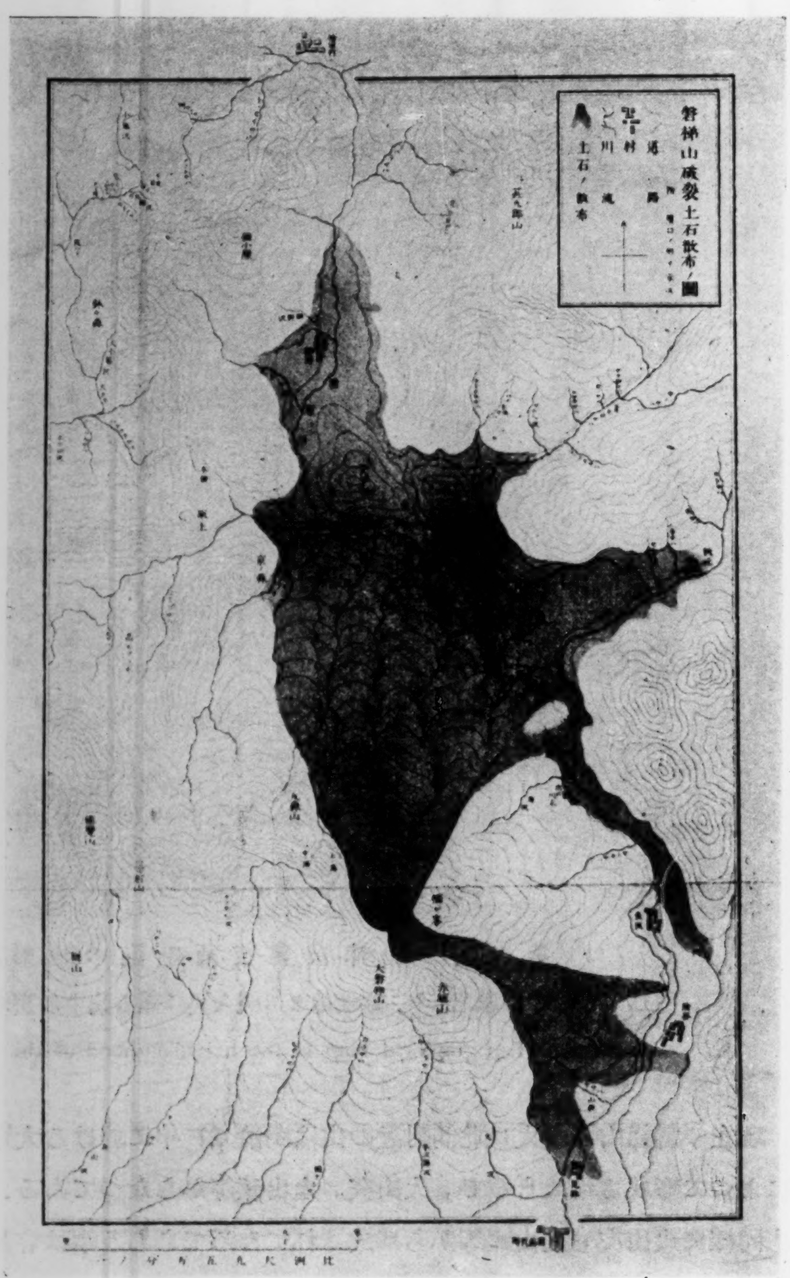

第2圖　山津浪發生地附近に於ける明治 21 年磐梯破裂の際の火山灰質土石分布圖（關谷，菊地兩博士による）

Fig. 2. The shaded area shows the distribution of volcanic sands, ash, etc. by the great eruption of Mt. Bandai on July 15, 1888. (By Sekiya and Kikuchi.)

3. 5月9日及び15日の山津浪

今回發生した山崩れによつて崩壊せる火山灰質土砂が水の作用を十分に受けて下流には泥流を押し出し結局山津浪の現象を表はしたため此の自然現象を特に山津浪と名付けて置く.

1) 5月9日の山津浪　川上溫泉にては5月9日午前1時頃磐梯山の方向より自動車の疾走する時或ひは檜原湖の水門を拔く時の如き“ゴオ”と云ふ音響が聞え其の後約1時間足らずにして土砂或ひは土石流の

襲來を受けたのである．此の時の崩壞箇所は燕岩より北東約 800 m の距離を隔てたる處にして第3圖中蔭影を附した處である．而して土砂の流出せる跡は第3圖に於いて示してある如く川上溫泉附近に於ては一つの谷間中ノ澤に沿うて居り，縣道（檜原猪苗代線）に於ては 1 m 程度の高さを以て押し出して來たと云ふ事で，火山灰と云ふよりは寧ろ土砂石などが大部分を占めてゐたとの事である．

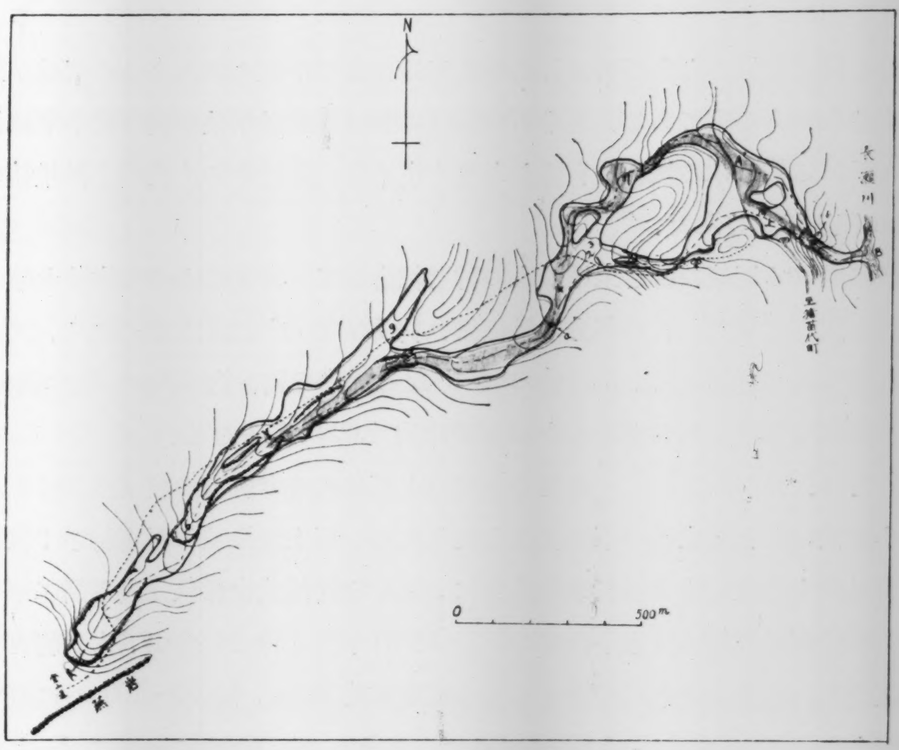

第3圖　5 月 15 日の泥流の跡（測量による）
〔1～9 涌水或ひは河水の採取場所，等高線は 10 m 毎に示してある．赤く蔭影を附した部分は5月9日の泥流の跡．A B は5月9日の崩壞部分，A C は5月 15 日の崩壞部分である．〕

Fig. 3. Outline of the present mud flow (May 15, 1938). The shaded area shows the trace of the mud flow on May 9, 1938. Contour lines drawn every 10 m. Areas of A B and A C: the upper parts of the landslide on May 9 and 15, 1938, respectively. Water samples were taken from the places of Nos. 1～9.

此の日の被害の有様は次の如くである．

縣道	約 200 m 破壞
死者	1 名（4 歲の女兒）
川上小學校其の他 2～3 軒	床上浸土
山林，畑，宅地等の崩壞及び埋沒	數町步

川上小學校に於ては床上約 1m 土砂が堆積した由である．此等の被害の有様は寫眞に示してある（第4圖～第7圖）．筆者の調査は 5 月 21 日からであつた爲以上の被害の狀況が見られなかつたのであつたが，幸ひ猪苗代町長谷川及び清水の兩寫眞店の撮影せる寫眞があつた爲，それらによつて當時の土石流出の有様を知る事が出來た．此等の寫眞を見ると先づ目に付く事は泥流に混じて種々の大きさの岩塊が遠方に迄運び出されてゐる事である．又小學校附近に於ける土砂堆積の高さは小學校校舎及び校庭に於ける柳の木の埋れた有様から推定出來る．前述の如く此の土砂堆積の高さは約 1m 程と推定された．

此の日に於ける泥流の跡を土地の人の言を綜合して，測量によつて求めた第3圖の上に蔭影を附して見た．此の部分の總面積は約 72,000 m² 程度と思はれる．又此の日の山崩れ現場地は蔭影を附した部分の A B なる部分で長さ約 250m，幅は廣い所で約 50 m 程度であり，此の部分のみの面積は約 9,000 m² となる．

2） 5 月 15 日の山津浪　　前述の9日の土石流により縣道の破壞或ひは埋沒又は人家，小學校の床上浸土等の事故發生したるため，川上溫泉並に吾妻村字干貫部落民約 40 名は川上分教場土砂岩石取除作業に，東京電燈株式會社秋元發電所工事飛島組人夫 19 名は縣道發掘に從事中の處，5 月 15 日午後2時 20 分頃，大音響と共に 9 日の崩壞箇所の後方より燕岩の崖下に至る迄距離約 800m，幅 50～100 m に亘る再度の崩壞があり，（第3圖赤字 A C にて示せる部分），此のために泥流は 2～3 の支流を作り本流は中ノ澤，山ノ神澤の2流に分岐し川上溫泉地帶に押し出し合流したが，縣道發掘に從事中の人夫が音響を聞くと共に逃亡せしも數人の人は間に合はず負傷し共の中1人は泥流にのまれ遂に長瀬川の本流に落ちて死亡した．共の他家屋等にも相當の被害を生ぜしめた．又七曲澤にも流出しかゝつてゐたが此の方面は途中で止り多量の泥水を 200 m も下方に迄押し流した痕跡が認められた．此の場合には縣道に於ける泥流の高さは約 3m であり，流出せる物質は5月9日とは異り火山灰の水に溶解せるものが大部分であつたと云はれて居る．而して流出繼續時間は約2時間であつて5月9日の場合と殆ど同じであつたと云ふ．尙泥流の本流は漸く長瀬川に達する程度であつた．

此の場合に於ける被害狀況は猪苗代警察署の調査によれば次の如くである．

a）	流　失戸數	7	
	棟數	11	（住家，流失 4 半流 3；非住家，流失 2 半流 2）
b）	床上浸土戸數	5	
	棟數	6	（住家 5　非住家 1）

c) 埋沒箇所

i) 縣道猪苗代—檜原線 270 m

最高 15 m

ii) 畑 8反 宅地 4反

iii) 山林，杉松等植林地 1町4反

以上損害は1萬圓程度であるとの事である．

d) 死者 1， 傷者 5

e) 崩壞箇所

猪苗代町共有山林 156 町歩

杉，松，雜木の倒壞による樹木損害見積は調査中

次に崩壞箇所の面積及び體積を測量（第3圖）によつて求めると，

面積 約 55,400 m²

體積 約 1,108,000 m³（高さ約 20 m）

となる．

5月15日に於ける川上溫泉附近の被害及び崩壞箇所原狀の有樣は第7圖 b）より第17圖の間に於て示してある．第7圖 b）より第9圖迄は川上溫泉附近に於ける山津浪襲來直後の寫眞である．又第10~17圖は其の後約1週間經過せる後の寫眞である．何れも去る9日の被害よりも大きく，9日に殘つてゐた小學校等も15日に於ては流失し校庭の柳の木のみ前よりは尙一層泥土に埋つて存在してゐるのが目立つであらう．又第10圖に於て見られる如く，周圍12m，高さ2·6m 地下埋沒3m 程度とも思はれる大石塊が縣道上に押し出されてゐる．第13圖，第14圖及び第15圖は何れも燕岩附近に於ける山崩れ現場地の寫眞である．第14圖は燕岩崖下に於ける殘雪面に現はれた割れ目を示してゐる．雪塊の寫生を第14圖 b）に示した如く，崩壞面附近では小雪塊に分れて居り，崩壞面を離れるに從つて大雪塊に分れて居る．第16圖は川上溫泉より約500mの距離にある場所の泥流の跡をうつしたものであつて，此の附近より泥流が三方面に分岐して川上溫泉へ流下したのである．

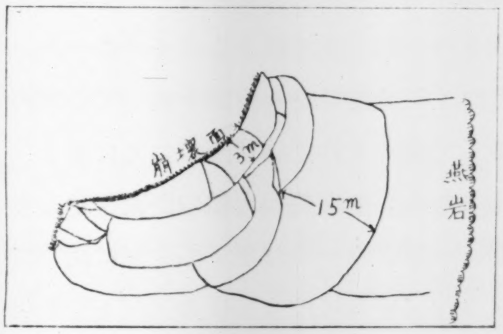

第14圖 b） 燕岩崖下に於ける殘雪の割れ目

Fig. 14. b) Sketch of the cracks of snow.

川上溫泉附近の家屋の被害狀況を申すならば，滿足な家は2~3軒程度であるが此等の家も殆ど空家同樣の狀態であつて，老

人婦女子が全部猪苗代町に避難して居る有樣であつた．人家の約半分は流失し，流失しない家には土砂が見舞つて，破壞し或ひは大損害を與へ大慘狀を呈した．川上には小學校があるがそれは分教場であつて，生徒は約 50 人，先生が1人と云ふやうな狀態で小學校の大さは 6×12 m 及び 8×3 m 程度の2棟からなり一方は藁屋根であり，一方は小板屋根であつて何れも平屋作りのものであつた．此の附近に於ける家屋は槪ね藁ぶきの平屋作りの家が多いのであつた．家屋の被害及び流れた方向を示す有樣は第 19 圖に示してある．此等は次節に於て再び述べる事にする．

4. 土砂流出跡の測量

山津浪の跡の稍々詳しい地形圖及び面積等を調査するために測量を行つたのであるが，此の測量にはポケットコンパスを使用し猪苗代町組合役場芳賀武氏の應援を得て測定したものである．測定は土砂流出後新たに出來た河に沿うて行ひ，且つ測點は約 40 m ごとに求めたのである．測定を河に沿うて行つたのは現在の河或ひは泥流の流れの方向を知るための目的による外，河水の溫度測定，土砂の採取等種々なるものの測定上の便宜があつたからである．此の測定は場所によつては膝はおろか腰迄もぬかり込み，歩行困難な不便をも凌いで遂行したものである．出來上つた圖面は第3圖の如くである．此の測定に於いては一巡後卽ちぐるりと廻つて始めの測點に達した場合に水平距離にして約 15 m 程の誤差を生じた．

第3圖に於ける等高線は 10 m 毎に入れてあり，又今回新たに出來た崖が入れてある．泥流の跡の全體の長さは約 3 km，幅は川上溫泉附近に於いては縣道に沿うて約 300 m，其の他の部分に於いては廣い所で 130 m 程度である．プラニメエタアを使用して第3圖より面積を求めると總面積は 248,500 m^2 となる（泥流の先端は漸く長瀨川に達する程度であつたので長瀨川河岸迄測つた）．崩壞箇所は噴火口壁の外側斜面一帶にして稍々東北に向いて居り，出來た崩壞面は相當急傾斜をなしてゐたが，流出せる泥流は流路の途中に於いても處々を崩壞し崖を作つたと思はれる處が多々あつた．

次に今回新たに出來た河の流れが圖に示す如く泥流跡の略々中間を通つてゐるので，此の河に沿うて谷の斷面を縣道を標準に取つて圖示すれば第18圖の如くになる．實線で示したのが今回の斷面であるが點線で示したのが崩壞前の大體の斷面を示してゐる．第 18 圖には2本の實線が示してあるが，a 點より一つは中ノ澤を河に沿うて下つた場合のものであり，他の一つは a 點より山ノ神澤に沿うて長瀨川迄下つた場合のものである．此の山ノ神澤に沿うて測つた場合の方が中ノ澤に沿うて測つたものに比して距離が短い關係上，何れも長瀨川迄測つたのであるが最後の點は一致してゐ

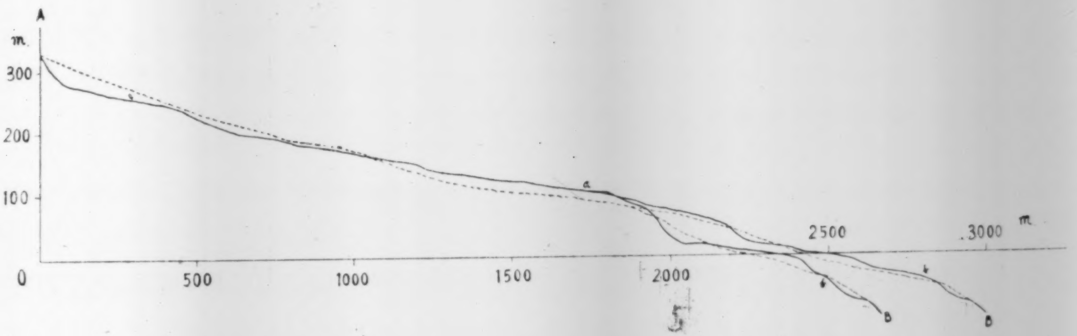

第 18 圖　泥流の跡に出來た谷に沿うて切った斷面圖

（第3圖に於ける AaA′bB 及び AabB の斷面圖．切斷箇所は第3圖中 —·— にて示す．點線は舊の谷のプロフィルを示す）

Fig. 18. Profile of the section of AaA′bB and AabB of Fig. 3. (Dotted line; profile of the valley before the mud flow.)

ないのである．此等の切斷面の位置は第3圖に破線で示してある．

第 19 圖は川上溫泉附近を擴大して畫いたもので，家屋の被害及び流れた方向等を示したものである．圖中黑くなつてゐる家屋は今回の山津浪のために流失，破壞されたものは勿論，床上浸土砂のために使用に耐へなくなつて壞したものをも含んでゐ

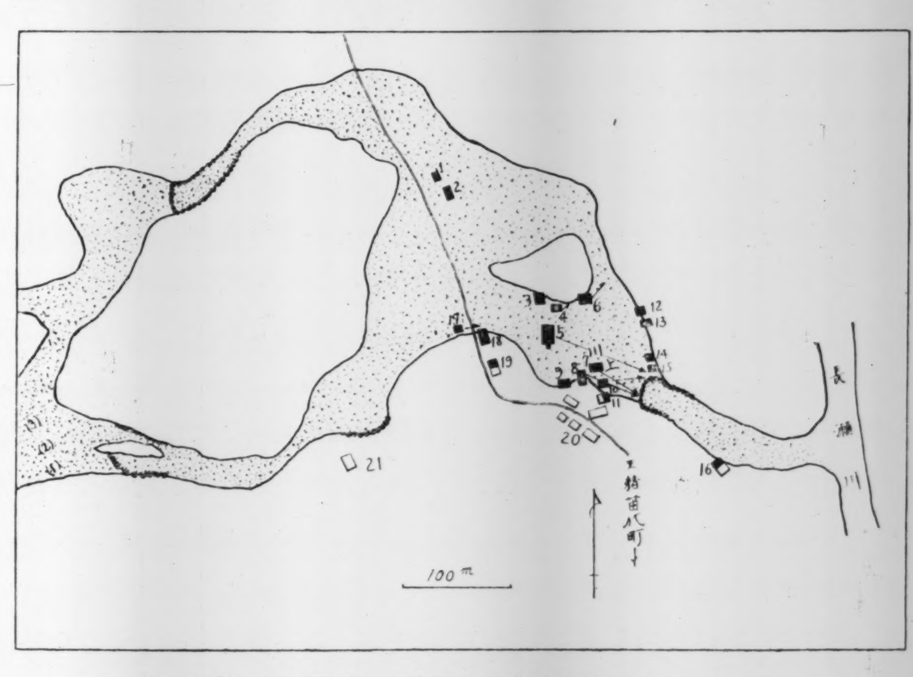

第 19 圖　山津浪による家屋の破害分布及び流された方向

1，2，3，4，5 は5月9日の山津浪の際に 1 m 以上の土砂が床上に浸入した家屋．1～19 は5月15日の山津浪により流失，半流失，破壞された家屋，20～21 は被害を免れた家屋．5 は川上小學校（(1), (2), (3) は水を採取せる位置を示す）．

Fig. 19. Distribution of houses that were demolished by the mud flow.

る．泥流路の中央に位置してゐた川上分教場は約 100 m 下流に流されたが，其の他の人家でも 50 m 程度流されたものは 2～3あつた．此等は何れも圖の如く長瀬川に至る流路に於ける崖の上にて食ひ止められたのであつた．

5. 山崩れ前後の狀況

5 月 9 日の場合は 8 日午後には相當烈しい降雨があり，山の方に於いてはみぞれをも混じた程度で可なり荒れた天候であつたとの事であるが， 15 日には非常によい天氣であつて 9 日の山崩れ後はあまり雨にも見舞はれない有樣であつた．川上溫泉附近に於いては山崩れ前に於いて溫泉の溫度の變化，澤の水の溷濁，井戶水の變化，微動の存在等の如き異常が殆ど認められなかつたとの事であるが，前兆と云ふが如きものを後になつて考へて見ると七曲澤に出口を有してゐた水が多小減じたやうに思はれるとの事であつた．次に動物に就いてである．明治 21 年の磐梯山破裂の時には蛇や野兎が多數移動した由であつて，破裂前の地變をよく動物が感知した由であるが，今回は斯樣な事實もないとの事であつた．只噴火湯に食量などを運搬する役をなす牛が 8 日にも 15 日にも相當鳴き叫んだ（通常餘り鳴き叫んだ事がない由である）との事であつたが，此れも後になつての思ひ出であつて當時は何の前兆であるかを知る由もなかつたものと思はれる．

次に崩壞現場地に於いてもその當時は何も變つた事が認められなかつたのであつた．噴火口內に於ては何等の異常が認められなかつた由であり，噴火湯に於ては崩壞時に於ける岩石落下の音さへも聞えなかつたと云ふ．又地變として考へなければならない事は噴火口北方の崖壁をなす燕岩の前側が現在 1 m 程度の食違ひを生じて下つてゐるが，此れは數年前から年々沈下が認められ現在の如くになつたのだとの事である．斯樣な事實があつたとすれば燕岩附近の地下に堆積してゐると思はれる火山灰，砂礫の如きものが地下水などに影響されて其の緻密度を異にした爲か或ひは又他の作用によつて變化を生じ斷層面に沿うて沈下したものと考へられる．斯樣な事實は崩壞の原因の一つに數へられるであらうが，何れにしてもその崩壞直前の前兆は殆どないと云つてもよい位のものである．

泥土砂の流出後に於ける川上溫泉附近の狀況を述べると溪谷を流下する水量が增加した外溫泉，井戶水等には何等の變化も認められなかつた程度である．

崩壞現場地に於いては頂上崖下より 150 m 下方の崩壞岩石の間からゴンゴン水が流出してゐる．斯樣な事實を綜合すると此の附近の地下には相當の水が溜められてあつたもののやうに思はれる．又燕岩崖下の崩壞せざりし部分に殘存せる約 3 m の積

雪には大なる幾多の割れ目が生じて居り（第14圖），尙15日崩壞せる山の頂上には崩壞崖より約20m噴火湯寄りの所に帶狀をなして約40mの長さの龜裂が生じてゐた．

又噴火口附近に於ける山崩れ後の狀況を調べて見ると次の如くである．

噴火湯に於ては溫泉の涌出量の減少及び溫度の降下等が認められた．涌出量の變化を測る尺度になるものを考へると，平年に於いては湯をたたへて置く湯元の小池があふれて居る程度であつた由であるが，調査當時に於てはあふれる所ではなく却つて淵より約5cmも下つて居る狀態であつた．今年は積雪量も平年よりは遙に多かつた故涌出量も平年よりは尙多い筈であるが事實は却つて逆の現象を示してゐた．從つて相當減少してゐるものと思はれた．溫度は70°C內外の由であるが今回は59°C（氣溫10.6°C）と測定された．溫泉の溫度は氣溫により變化するのであるが，此の低下は氣溫の低下よりやゝ著しいやうに思はれた．次に噴氣孔から出てゐる水蒸氣の勢力であるが，此れは多少勢力が弱くなつたやうに見受けられるとの事である．水蒸氣の出てゐる箇所は大小合計6位であつて，明治21年の大破裂當時は相當烈しく數も多かつたが其の後は凋落の一途を辿り現在の樣に微々たるものになつてしまつた由である．

6. 泥流の速度

1） 5月9日の泥流の速度を川上溫泉の人々によつて聞いた資料から求めて見よう．

5月9日の山津浪發生は丁度眞夜中の事であつた爲，流出物を認めるが如き事は出來ず殊に此の地方には電燈が無い關係もあつたであらうが，兎に角人々は磐梯山の方向から檜原湖の水門を拔くやうな音或ひは自動車の疾走する時の如き音を聞いたとの事である．此れが唯一の速度決定の手掛りとなるのみである．丁度眞夜中の事故相當遠方の音迄聞えたものと思はれるし又人々が感づく程であつたから可なり大きな音であつたものと思はれる．從つて此の音は崩壞箇所附近から發生したものと考へてもよいであらう．

川上溫泉の人々が音を聞いてから約30分程經過して土砂の流れが來たとの事であつて，此の時間も人によつては相當に色々で1時間と云ひ或ひは20分と云ひ或ひは1時間以上だと云ひ判然とはしないが，約30～50分程度の時間と推定される．川上溫泉より崩壞現場迄は約1700mである．從つて土砂が流れ出すと同時に音が出たものとすれば音は約330m/secの速度を持つて傳播するから音が川上溫泉迄到達する時間は約5～6分である．從つて土砂流の要した時間は約40分程度となる．故に此の場合の平均速度Vは

$$V=\frac{1700}{40\times 60}\approx 0{\cdot}7\ (\mathrm{m/sec})$$

となり最初の土砂流の平均速度は毎秒 1 m 未滿のものと推定される．

5月9日のは土砂流であつた上その土砂流が松の木や白樺，山毛欅などを倒して押し出した爲，途中に於ては相當の摩擦があつたものと思はれる．從つて崩壊現場附近の速度は相當大なるものであつたらうと想像される．

2）　5月 15 日の泥流の速度を求めて見よう．此の場合には惨事が晝間でもあり，又規模が9日の場合に比して相當に大きかつた關係上，よく物の流れる有樣や色々なものが速度測定の手掛りとなつた．

先づ川上溫泉附近の泥流速度を家屋の流れた距離と時間，人夫が縣道から逃げた時間や距離と崩壊の音を聞いた時間等から求めて見る．

i）　川上小學校が 100 m を約5秒位で流失したと云ふからその速度は

$$V=20\ \mathrm{m/sec}$$

となる．此の5秒位と云ふのはアツト云ふ間に流失したと云ふ事であるから斯樣に取つたのである．人によつては 2～3 秒で流失したと云ふ人もある．從つて此の場合の速度は多く見積つて 30 m/sec，少く見積つて 20 m/sec であらうと思はれるから平均 25 m/sec の速度位と考へてよい．

ii）　縣道にゐた人夫が約 400 m 上方の崖を流下する泥流の音を聞いて約 50 m の距離を辛じて逃げた人もあり，逃げ遲れて泥に埋つた人もあるが，之等から泥流の速度を出して見ると次の如くになる．

音を聞いてから其の方向を見てそれから走り出すために 50 m を逃げのびるに多く見積つて 15 秒位と考へられる．驚きの餘り却つて足が出ない場合もあらうが 100m を相當遲くかけても 20 秒位と思はれるから，以上の如く取つたのである．從つて此の場合の 15 秒は最大に過ぎるかも知れないが斯く取るときは泥流の速度 V は

$$V=\frac{400}{15}=26\ (\mathrm{m/sec})$$

となる．大體此の程度のものと思はれる．

iii）　次に泥流の跡から判斷する方法である．即ち泥流が流下する場合に彎曲した流路を取る時には，その外側が高くなつてゐると云ふ事を利用して求めた．此の方法は中村(左)博士2) が十勝岳泥流の速さを求められた時にも用ひられて居る方法であつて，今泥流は重力と摩擦とにより等速運動をなすものとし，その外側の高くなるのは

2）　中村左衞門太郎　地球 **6** (1926)，79～82．

その彎曲による遠心力の作用と考へれば

$$\frac{F}{g} = \frac{V^2}{\rho g} = \tan\theta$$

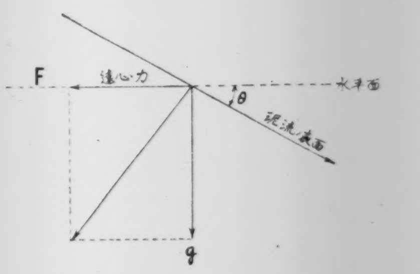

第20圖　泥流に作用する力

Fig. 20. Centrifugal force (F) and g.

となる．茲に F は遠心力 V は泥流の速度，ρ は曲率半徑，g は重力加速度，θ は泥流表面の傾斜である（第 20 圖）．θ, ρ は實地に求められるから V が測定出來る．從つて速度 V は

$$V = \sqrt{\rho g \tan\theta}$$

であり，今 $\rho = 100$ m，$\theta = 15°$ の測定値を入れて計算すれば，　$V = 13$ m/sec

となり稍々小さな値となつたが，此の速度は泥流の底部の速度を與へるものと思はれる．從つて川上溫泉附近に於ける泥流の表面部分の速度は約 25 m/sec 程度と考へられるが，泥流下部の速度は約 10 m/sec 程度であつたのであらう．

次に縣道より 600 m 上流に於ける速度を上述の iii) の方法により求めると

$$\theta = 20°, \qquad \rho = 63 \text{ m}$$

故に　$V = 15$ m/sec

となり縣道より 1500 m/sec 上流に於ける速度は

$$\theta = 30°, \qquad \rho = 55 \text{ m}$$

なるにより　$V = 18$ m/sec

等となる．之等の値は何れも川上溫泉の縣道附近に於いて同樣にして求めた値より稍々大きく，上流に行くに從つて增大して居る．又處々の松の木や白樺の木の 2～3 m の高さの所に泥流の跳ね上つた跡が見られたが，是等から速度を推定すると相當速く，やはり每秒 30 m 前後と思はれる．此の速度は明治 21 年の磐梯大破裂に際して生じた泥流の 21 m/sec なる速度[3] と殆ど同じ程度のものであらう．從つて明治 21 年に於いても今回と同程度の速度を持つた山津浪が襲來したものと思はれる．

十勝岳泥流[4] は山頂から約 2·5 km の距離の處では約 30 m/sec の速度を有して居り，山頂より 24 km の距離にある上富良野では約 10 m/sec の速度を有してゐた．今回の泥流の速度も之等のものと殆ど同じ大きさのものの樣に考へられる．

---

[3] S. Sekiya and Y. Kikuchi, "The Eruption of Bandai-san," *Trans. Seism. Soc. Japan*, **13** (1890), 139～222.

[4] 中村左衞門太郎　前揭.

7. 火山灰質土砂の二三の物理的性質

被害地から採取して來た火山灰質土砂の 2~3 の物理的性質特に粘性係數，凝集强度，摩擦角，ヤング率等を調べて見た．之等は山崩れや泥流を支配する有力な要素であると考へられる．

1) 粘性係數

泥土の流れを支配する一つの要素として泥土の粘性が大切であると考へられるがその粘性係數が如何なる値を有するかを知り度いと考へ採取せるものを實驗室に於いて以下に述べる如き方法によつて調べた．

崩壞地に於ける土砂の含水量は可なり多く 40~60% の程度と推定されるにより，此の火山灰及び土砂等は殆ど流體と考へられる．流體の粘性係數測定法として Stokes の方法があるが，今回は水分の多量な所の値を知るのが目的である爲，Stokes の方法を用ひて行つた．然しながら泥土の場合にはその中を落下する球の運動を直接觀測出來ないので細い針金（直徑 0·2 mm）にてボオルベアリング用の鋼鐵球を吊し第 21 圖に示せる如き裝置によつて A なる硝子容器に入れた土砂 (B) 中を落下する球 (S) の速度を測定した．鋼鐵球 (S) に附した針金 (W) の先端 E が細き硝子管を落下する距離を硝子管に附した目盛 (L) にて測定し，且落下に要した時間をストップウオッチにて測り，鋼鐵球の落下速度を求めた．泥土の粘性係數 η は

$$\eta = \frac{2}{9} \frac{(\rho - \rho')r^2 g}{V}$$

から求められる．玆に r は鋼鐵球の半徑，ρ はその密度，ρ' は土砂の密度，V は鋼鐵球の落下する速度である．用ひた球の密度は 7·77~7·80 である．

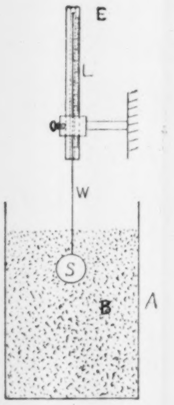

第 21 圖 粘性係數測定實驗裝置
A ガラス製圓筒（高さ 40 cm，直徑 10 cm）(Vessel)
B 火山灰質土砂 (Volcanic mud)
E ガラス管 (Glass tube)
L 尺 度 (Scale)
W 細い針金 (Steel wire)
S 鋼鐵球 (Steel ball)

Fig. 21. Apparatus for the measurement of the viscosity coefficient of volcanic mud.

粘性係數の含水量に對する變化を求めるために水を加へて含水量を變じ以上の測定を繰り返した．水分が增加すると球の落下速度も增すので球の半徑の異なるものを適當に變じて測定した．此等の値は第 I 表に示した如くである．

第I表　土砂の粘性係數

含水量 Water cont. %	土砂の密度 ρ'	球の直徑 d (cm) Dia. of ball	粘性係數 η (c.g.s.) Viscosity coeff.	落下速度 V cm/sec
22·0	1·80	3·50	902	4·41
22·8	1·84	2·85	1050	2·52
24·2	1·85	2·55	1140	1·84
27·9	1·85	2·06	700	1·97
29·2	1·90	1·68	590	1·53
30·6	1·91	1·26	525	0·97
32·0	1·89	1·03	435	0·78
32·7	1·88	1·03	300	1·14
34·5	1·87	0·79	115	1·75
36·5	1·86	0·79	63	3·20
38·2	1·86	0·65	35	3·91
40·0	1·84	0·50	15	5·42
42·0	1·80	0·47	8	9·03
43·9	1·79	0·32	6	5·54

又粘性係數の含水量に對する變化は第 22 圖に示せる如くであつて，含水量の增加と共に急激に小となつて居り，含水量 32～33% に至ると不連續的に小となる傾向が見られる．尙水分の減少と共に急激に泥土が硬くなる關係上測定には誤差が含まれる許りでなく土砂も流體の性質を失ふやうになるので，此の方法によつて求めた値は實際の粘性係數とは異つた破壞强度の如きものであるかも知れない．

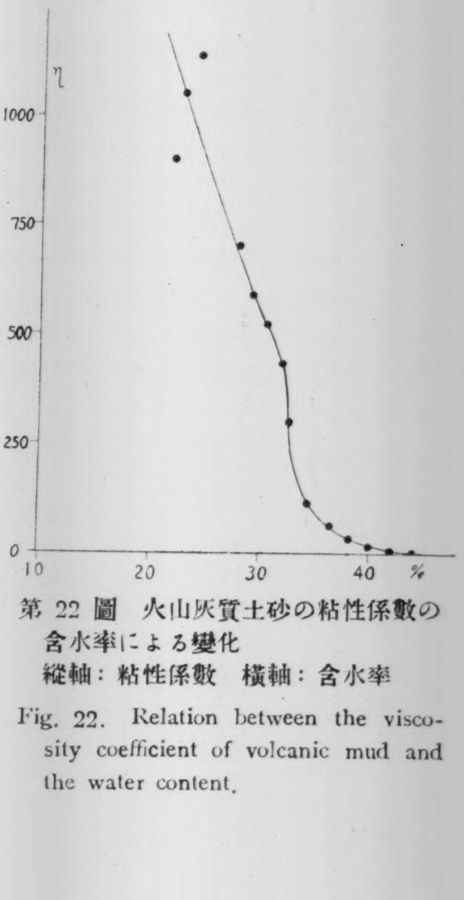

第 22 圖　火山灰質土砂の粘性係數の含水率による變化
縱軸：粘性係數　橫軸：含水率

Fig. 22. Relation between the viscosity coefficient of volcanic mud and the water content.

今以上とは異つた方法によつて泥流の粘性係數を求めて見よう．但し土砂の流が 2 平行平面にて限られたみぞの中を定狀狀態で流れてゐると假定する．泥流の粘性係數を μ, 速度を u, y 軸を泥流と直角方向に，x 軸を泥流の方向に z 軸を深さの方向にとる（第23圖）．d はみぞの幅である．又 α は xy 面が水平面となす角である．然るときは次の運動方程式を得る．

$$\left.\begin{aligned}&\mu\Delta u+\rho g\sin\alpha=0,\\&\frac{\partial p}{\partial y}=0,\\&\frac{\partial p}{\partial z}=\rho g\ \cos\alpha.\end{aligned}\right\}$$

上式から u 及び p を求めれば

$$u=\frac{1}{2}\Big[\varphi(y+iz)+\Phi\,(y-iz)\Big]-\frac{\rho g}{2\mu}z^2\sin\alpha,\ p=\rho gz\cos\alpha+p_0$$

となる5)．

今川上小學校の附近に於ける泥流の粘性係數を求めて見ると次の如くになる．

$u=25\,\mathrm{m/sec}$, $d=40\mathrm{m}$, $\alpha=14°$, $z=2\sim3\mathrm{m}$, $\rho=1{\cdot}8$

とすれば

$$\mu\approx10^3\sim10^4(\mathrm{c.g.s.})$$

となり，前述の實驗室に於いて求めた値に比して大となつてゐる．採取せる土砂は自然狀態のものであるから大小の石片があるため實驗室に於いてはそれ等を適當に取除いて測定したのである．從つて實際のは實驗室に於ける値のよりも稍々大となる可きであると考へられる．實驗に用ひた火山灰質土砂の mechanical ratio は 70% の砂（粒徑 1·1～0·2 mm）と粒徑 0·07 mm のもの 20%，粒徑 0·005 mm のもの約 10% であつた．又眞の密度は 2·50 である．

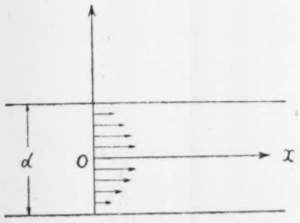

第 23 圖 泥流の表面

Fig. 23. Surface of mud flow.

次に縣道などに於いて泥流によつて運搬されて來た相當大なる石塊が止つて土砂に埋沒或ひは頭を出してゐるがそれについてその石塊を靜止せしめるために作用する力 F を計算して見よう．

今一様な流體の流れの中に自由に動き得る球がありとし，その密度を ρ，球の半徑を a，泥流の速さを V とすれば球を靜止せしめるに要する力 F は

$$F=\frac{4\pi a^3}{3}(\rho-\rho')g+6\pi\mu aV$$

となる．玆に μ は粘性係數であり，ρ' ρ は泥流及び岩石の密度である．μ, ρ', V 等には前述の値を代入し岩石塊を大體球と假定して F の値を求めれば

---

5) M. Lagally, *Gerl. Beit. z. Geophys. Suppl.*, **2** (1933), 14.
此等については次の機會に詳しく述べる考へである．

$$F \fallingdotseq 7 \times 10^4 \text{ dyne/cm}^2$$

となる．從つて實際には此の値より大なる力が作用したものであらうと考へられる．茲に於ける岩石の値には高さ 4m 周圍 12m の略球形をなした岩石で密度が 2·65 のものを採用した．而して之は寫眞に示した縣道上に流出せるものである．此等の値も泥流の性質を知る上に多少手掛りとなるものと思はれる．

2）弾性係數

弾性係數を求める爲に採取して來た土砂を適當に水分を蒸發せしめ柱狀體となし，之を振動盤の上に乘せて其の共鳴する周期を測定し，それより土柱を傳る縱波及び捩波の速度を求めた．而して結局從來の方法⁶⁾によつて，E, μ, σ 等の弾性係數を測定した．その値は次の如くである．

第II表　土砂の弾性係數

含水率 Water cont. %	密度 ρ	縱波の速度 V_l (m/sec)	橫波の速度 V_t (m/sec)	ヤング率 E (c.g.s.)	剛性率 μ (c.g.s.)	Poisson's ratio σ
				$\times 10^8$	$\times 10^8$	
0	1·86	200·0	115·0	7·13	2·46	0·46
4·5	1·89	170·0	104·0	5·46	2·04	0·34
5·0	1·91	130·0	78·8	3·23	1·18	0·36
7·2	1·94	95·1	56·8	1·75	0·62	0·40
10·0	1·93	80·0	46·6	1·23	0·42	0·47

上表より知られる如く含水量の增加と共に急激にその弾性係數が小となつて居り，之等は土に於いて屢々求めたものと同一の傾向を示して居る．

3）凝集力及び摩擦角

山崩れ地辷り等の場合には辷り面が假定されるが，その辷り面に沿うて一部の表土層が滑り落ちるのであつて，その滑落を惹起する主なる力は土層に働く重力である．又これを止めようとする主なる力は辷り面に沿へる摩擦と土粒の凝集力とである．即ち辷り落ちるか起らないかと云ふ所では重力による力と摩擦等による力とが釣合にあるのである．此等を式にて表はせば

$$F = \mu N + AC$$

となる．茲に F は重力により辷り面に沿うて土砂を落下させようとする力，N は辷り面に直角に働く力で A は辷り面の面積，μ, C は摩擦係數と單位面積に於ける凝集力を示すものである．從つて山崩れを考へる場合に於いては μ, C 等の諸種の値が必

---

6) M. ISHIMOTO and K. IIDA, *Bull. Earthq. Res. Inst.*, **14** (1936), 632; **15** (1937), 67.

要である．今回に於ける之等の値は如何程であらうかを求めるために剪斷抵抗器を用ひて測定した．卽ち土砂を上中下三重になつてゐる枠に塡め，上から 10，20，30 kg 等の壓力を加へて，中央の枠を水平に横に引抜く時の力を測定したのである．剪斷抵抗器は $4^2\times6$ cm の容積を有する小型のものを鐵道省大臣官房研究所から借用して測定した．それらの測定値を含水量に對する變化として求めたのを圖示すれば第 24 圖第 25 圖の如くになる．第 24 圖は凝集力の變化を示し，第 25 圖は摩擦角の變化を示してゐる．凝集力は含水量のある値に於いて卽ち 10％ 程度にて maximum となり尚水量を增加すると凝集力は減少してくる．又摩擦角も含水量のある値に於いて增加する傾向を有してゐるが，土砂の種類によつて異つてゐる．然しながら含水量 30％以後に於いては凝集力も，摩擦角も減少の程度を高め，結局今回の如き泥流に於いては非常に小なるものである事が容易に推定される所である．卽ち實驗によつて含水量と共に凝集力，摩擦角の急激に減少する有樣をたしかめ得た次第で，今回の如き水分の過飽和狀態に於ける土砂に於いては凝集力，摩擦角の急激な減少を來し重力による力との安定が破れて流出したものと考へられる．

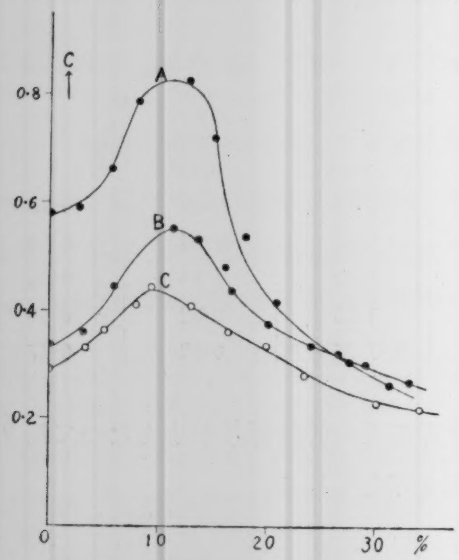

第 24 圖　凝集力の含水率による變化
縱軸：凝集力　横軸：含水率
A No. 1. B No. 2. C No. 3.

Fig. 24. Relation between the cohesional force of volcanic mud and the water content.

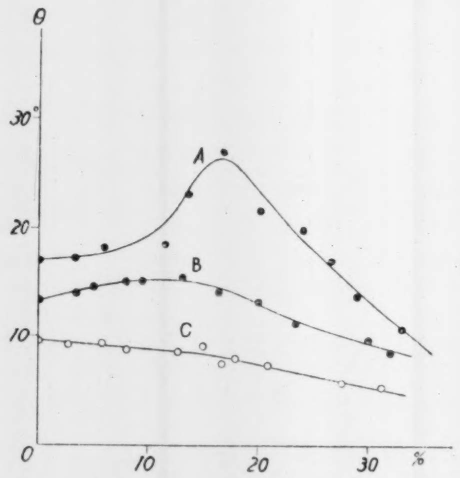

第 25 圖　摩擦角の含水率による變化
縱軸：摩擦角　横軸：含水率
A No. 1. B No. 2. C No. 3.

Fig. 25. Relation between the frictional angle of volcanic mud and the water content.

A, B, C in these figures correspond to those in Table III (showing different grain sizes).

又土砂に於いても比較的あらひ粒子を含んだものはある含水率に於いて大なる凝集

力及び摩擦角を有してゐる事が第 24〜25 圖から判るのである．圖中 A，B，C 等の記號は粒子の比較的大なるものから小なるものに至る順序を示せるもので，第 III 表中の土砂の種類の分類記號と一致してゐる．

測定せる土砂の機械的分析の結果は第 III 表に示してある．

第 III 表　機械的分析表

土砂の種類	篩目（Tyler の標準篩目）						silt	clay
	8	14	28	48	100	200		
A	6·58	10·44	14·32	15·36	16·92	12·44	15·18	8·76
B	0	10·80	23·68	19·38	14·74	9·28	13·14	8·98
C	3·58	2·20	4·70	10·60	10·30	20·50	28·27	30·15

4） 涌水の pH

火山灰質土砂は酸性であるとの事である[7]が，採取して來た澤からの涌水を化學教室野口學士の援助を受けて pH を測定して見た．その結果によると川上溫泉の湯は 7·1〜7·0 であり他は上表の如くである．測定は6月2日で採取後約1週間である．

No.	1	2	3	4	5	6	7	8	9
pH	7·6	5·9	7·4	5·0	6·9	5·9	7·2	6·5	5·6

此の表（表中の番號は第3圖に示してある）にて見られる如く相當に酸性の強いものも見受けられた次第である．之等から水の酸性強度の地理的分布が求められる筈であるが，以上の材料では未だ不十分だし相當複雜してゐるやうにも思はれるので只測定値を示す程度に止める．尙參考迄に示すが，吉村信吉氏[8]による長瀨川の pH は 2·8 であつて相當に酸性が強いやうである．

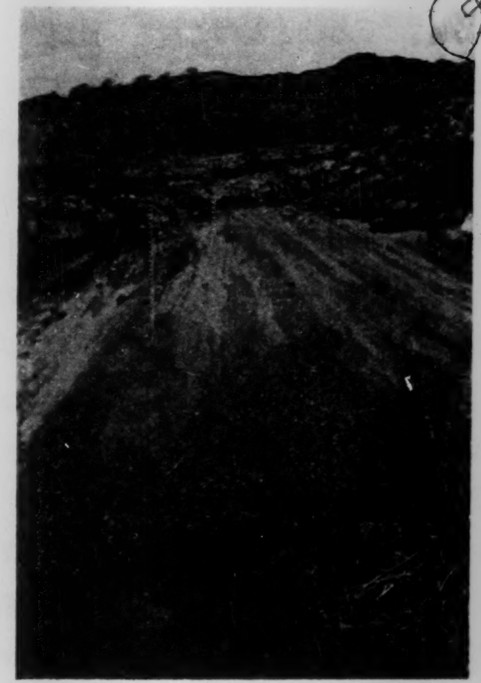

第 26 圖　磐梯山噴火口東側壁の崩壞

Fig. 26.　Landslide of the crater-wall of Mt. Bandai.

8. 山津浪の原因

7）　地學雜誌　1 (1889), 19.

8）　吉村信吉　地理學評論　14 (1938), 68〜69.

今回の山津浪の原因と考へられる點の一二を述べて見る．

現在の磐梯山爆裂火口北側附近の山は明治21年の大破裂の際に出來たものである事はよく知られて居り，本文に於いても既に述べた所であるが，今回の崩壊附近の山を形成してゐる火山灰質の物質が，過飽和狀態の地下水によつて崩壊し今回の山津浪を惹起したもののやうに考へられる．即ち地下水の作用が最も主要な役割をなしてゐるやうに考へられた．

明治21年に出來た火口壁の崩壊が其の後引き續いて行はれ噴火口內に落ち込んで居る．火口壁の崩壊は寫眞第26圖によつてもその有樣の大略が伺はれるであらう．昭和6年6月26日長雨の爲櫛ケ峰中腹に當る一帶が大音響と共に崩壊したが如きは，其の規模の大なるものなるため地元民をして磐梯鳴動の前兆に非ずやとの不安を起させた程であつて，火口壁の風化，浸蝕等による破壊作用は絶えず全壁に亙つて行はれてゐる．燕岩に於ても寫眞第12圖の如く鉛直方向に平行せる割れ目が多數出來て居り，崖下には岩石がかけ落ちて堆積して居る．5月15日崩壊せし現場の頂上（第1圖A）と燕岩との間には川上溫泉口より磐梯登山への登山道がある．此の登山道は相當谷間にあつたものであるが，岩石崩壊と共に徐々に高められて現在の如き有樣となり火口內に至る峠となつて居る．此處より火口內に入るのであるが，此の邊には岩塊の下に小さな沼の如き水溜りの存在するのが氣づかれるのである（第1圖Bの邊）．此の水溜りが噴火湯附近より流出して來たる水によつて出來てゐるのであるが，此の水が今回崩壊せる部分の地下に多年に亙つて浸透してゐたものと思はれる．それは此の水溜りから漏れて出る水の川上側への出口が數十年來判然として居らず疑問の一つとなつてゐた事にも據るが，尙此の水の地下に浸透してゐたと思はれる燕岩の前側には數年來斷層面さへ發達し土地沈下の傾向も認められる程度になつてゐた事にもよる．

斯樣に明治21年以來水が火山灰に浸透し飽和狀態に達してゐると思はれる程度になつてゐた所へ偶々今年の大雪があり，その雪解けの水量の增加により急に過飽和に達したものと思はれる．

試みに今年の積雪狀態を示すと第27圖の如くである．此の圖は福島縣會津測候所の調査によるもので猪苗代町に於ける積雪量である．圖に於ける平年の値は13年間の平均を示し，積雪量は毎日午前10時5日毎の平均の値である．本年の積雪は平年に比して多く殊に2月20日前後に於いては平年の3倍もあり，測候所開所以來の216cmなる記錄をも示してゐる．尙今年の雪は平年のとは異り水分を多く含有し密度の大なる雪であつたと云はれてゐる．然も平年に比して著しく早く消えてゐる事が目立つてゐるのである．即ち本年は非常に澤山の雪が降りその割合に早く消えて水とな

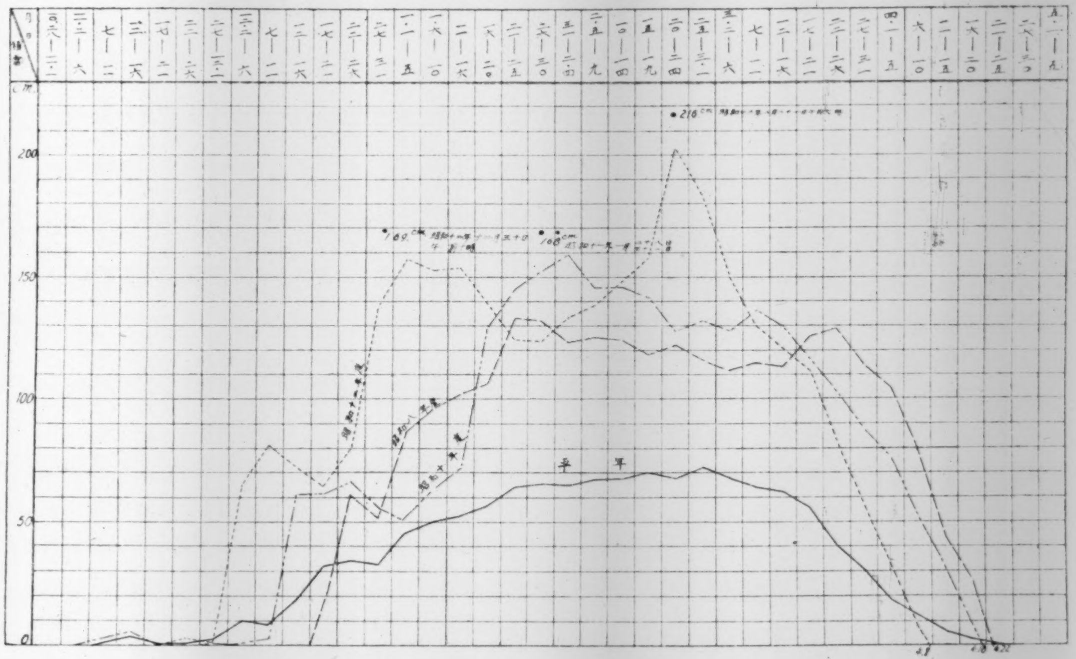

第 27 圖　昭和 12〜13 年と平年とに於ける積雪量の比較
（昭和 8〜9 年及び10〜11 年の兩年に於いても平年より其の積雪量は大であつた.）

Fig. 27. Time variation in the amount of snowfall (comparison of 1937〜1938 and annual year).

つたのである．以上は今回の崩壊現場とは約 9 km の距離を隔てた猪苗代町に於いての觀測であるが，崩壊現場地附近に於いては尙一層の積雪を蒙つたものと思はれる．筆者が調査を行つた 5 月下旬に於いても尙約 3 m の殘雪を有してゐた程であり，その殘雪の丁度中間部分が 5 月 15 日の崩壊によつて取り去られたのである．

又崩壊せる當時の 5 月前後に於ける降水量を示したのが第 IV 表及び第 V 表である．但し此れは猪苗代町に於ける値である．之等の表から知られる如く 1 月から 4 月迄は降雪による降水量が大部分であつて，之等の量の相當に大なる事は既に述べた．尙 5 月に於いては降水量も減じて居り，殊に 5 月 15 日前後に於いては快晴であつた．從つて山の殘雪も相當に消失したものと考へられる．又 5 月 9 日の場合には前日來雨も降つてゐたのであつて，此の場合には雨によつて山の殘雪が消失したのであらう．何れにしも烈しい雨か或ひは快晴の後に崩壊が起つてゐるやうである．但しとけた水がすぐ土砂の中深く迄滲透して崩壊の端緒となつたかは不明であり，又 15 日に崩壊せる部分が 9 日の崩壊に續いてすぐ崩壊せずして約 1 週間もの間隔があつたのは如何なる原因によるか判明しない．

此の地方の火山灰質土砂は著しい吸濕性を有し，而も實驗上から知られた如く水の

第IV表 1月より4月迄の降水量 (Precipitation) (會津測候所調査による)

月 日	1	2	3	4
1	1·7 mm	14·1	—	—
2	17·2	0·3	4·2	—
3	18.9	0·1	5·5	1·1
4	8·8	0·0	1·3	5.5
5	6·0	1·2	0·0	18·1
6	0·0	1·0	2·8	0·9
7	0·6	4·4	2·4	0·2
8	22·9	1·1	0·2	5·4
9	5·5	4·0	0·1	1·0
10	1·2	1·0	4·3	0·1
11	0·4	11·0	0·1	14·4
12	15·5	3·9	1·2	0·3
13	9·3	0·2	0·1	1·1
14	0·1	16·6	—	—
15	—	17·0	0·1	13·2
16	1·7	—	—	9·1
17	1·7	28·8	—	—
18	—	40·7	0·3	6·7
19	0·8	54·3	0·6	0·0
20	12·5	37·4	—	—
21	1·3	17·5	—	—
22	0·9	0·3	6·6	—
23	1·6	0·7	23·8	11·7
24	2·7	0·2	13·1	3·2
25	0·0	1·7	0·8	17·0
26	4·7	0·1	2·6	—
27	3·9	1·1	—	0·1
28	0·3	0·4	7·2	0·1
29	1·4		0·9	9·9
30	5·1		—	—
31	—		—	

第V表 5月1日より20日迄の降水量 (會津測候所調査による)

時 日	22—2^{h}	2—6^{h}	6—10^{h}	10—14^{h}	14—18^{h}	18—22^{h}	sum
1	— mm	—	—	—	—	—	—
2	—	—	—	—	0·9	4·1	5·0
3	1·3	3·2	9·8	0·8	0·3	—	15·4
4	—	—	—	—	—	—	—
5	—	—	—	—	—	—	—
6	—	—	—	—	0·4	1·1	1·5
7	0·3	0·2	0·1	—	—	—	0·6
8	—	—	0·0	8·8	1·9	1·1	11·8
9	4·3	5·2	1·5	0·3	0·5	0·6	12·4
10	5·1	—	0·1	—	—	—	5·2
11	—	—	—	—	0·0	—	0·0
12	—	—	—	0·0	3·1	0·5	3·6
13	3·7	3·3	—	—	—	—	7·0
14	—	—	—	—	—	—	—
15	—	—	—	—	—	—	—
16	—	—	—	—	—	—	—
17	—	—	—	—	0·0	7·0	7·0
18	0·2	0·0	0·1	0·7	3·0	1·1	5·1
19	—	—	—	—	—	1·8	1·8
20	0·0	—	0·1	0·0	0·0	—	0·1

增加と共に著しく其の性質を異にするのである．水の滲透した土砂は其の表面が日光などに當つて乾くと急に硬くなる．其の爲に土砂の中の部分は軟く恰も鷄卵の殼と中味の如き狀態となつてゐる．從つて中味に相當する土砂の部分に餘分な水などが加はり殼の部分に相當する土砂が其の壓力に耐へきれなくなると，今迄保たれてゐた釣合が破られ中味に相當する土砂流が押し出すのである．

尙崩壞發生現場は活火山なる磐梯山の噴火口壁北側の斜面にあつた事故，今回の事件は火山活動による地變と密接なる關係にあるであらうと考へられるが，此れに關しては判然と確める事が出來なかつた．

9. 結　語

以上述べた如く，今回發生した山崩れによる地變は相當に大規模であつたが，其の割合に人畜の被害は少なかつたのは幸ひであつた．それは最初比較的小規模なる山津浪が5月9日に發生し，此れにより人々は多少不安の念を抱いて警戒して居た爲であつた．其處へ15日に至り再度の大規模なる山津浪が襲來して來たので人々は素早く避難した次第である．

崩壞せる現場附近を見ると，地下に貯へられた水溜りの水が恰も堤防を缺潰するが如く火山灰質土砂の堆積せる弱い部分を破つて押し出したと云ふが如き感が深い．

又火山灰質土砂の物理的性質の2～3を述べたが水に對する影響は顯著であつて，山津浪の現象を說明するのに有力のやうに思はれる．

原因に就いては尙考究を要する事であり，地下水丈を取り上げる事は當を得て居ない事は勿論であり，他にも種々な原因があつてそれ等の原因が結合して今回の慘事を惹起したのであらう事は容易に想像される所であるが，其の中でも地下水の過飽和による原因が有力な役割をなしてゐるものと考へられる．尙地下水の火山灰に對する化學的の作用も考慮しなければならぬ問題であると考へられる．

明治21年の磐梯大破裂の際の火山灰質土砂の下に埋沒されたと思はれる山毛櫸の大木片（長さ1·6 m 直徑1·5 m）が今回の泥流と共に燕岩附近より距離約2 km もある下流の地點迄運び出されてゐるのが2～3見られたのである．從つて今回の崩壞せる土砂は全く明治21年の磐梯大破裂の際に積つた火山灰質土砂にして，それが長年の間地下水によつて浸透され飽和狀態となり，今年の大雪解を待つて5月9日の崩壞の先驅部分を出しその後方が安定を失つて續いて5月15日の再度の崩壞となり，上流に於いては明治21年の磐梯大破裂前の谷間に沿ひ又下流に於いては現在存在せる谷に沿うて流下したものと考へられる次第である．今後も多少の崩壞があらうが現在見

られる今回新らしく出來た谷川の排水口が閉塞されない限りは餘り大なる慘事を引き起すものとも考へられない.

猪苗代附近に最近 2～3 の局發地震があり，卽ち昭和 10 年 3 月の中川流域の局發地震（磐梯山より 50 km の距離で西南の方向）あり，昭和 11 年 11 月會津若松附近の局發地震（磐梯山より 10 km の距離で西南方向）があり何れも弱震程度で數日にして止み，主に上下動を伴つた地震である．此等は今回の山崩れと何等かの關係がありはしないかとの懸念を抱く人もあるが直接の關係はないと思はれる．然しながら磐梯山附近に於いて斯樣な局發地震が存在する事は別の意味に於いて注目に價する事だと思はれる.

末筆乍ら今回の山津浪調査に當り種々調査上の便宜を與へて下さつた福島縣猪苗代町猪苗代警察橋本署長並びに猪苗代町長青木常吉氏，同組合役場助役原田小平氏，猪苗代町壽田直吉壽田勇兩氏，川上溫泉區長小板橋久三郎氏の諸氏に對し深く感謝の意を表する．猶被害地の測量に助力せられた福島縣農林技手芳賀武氏並びに氣象學的の材料を與へて下さつた會津測候所長佐藤煌氏に厚く御禮申し上げる次第である.

倘土砂の力學的性質を求めるために剪斷抵抗測定器を御貸し下さつた鐵道省土質調査委員會に對し，又涌水の pH 測定に御便宜を與へて下さつた東大化學教室の野口喜三雄學士に對し深く感謝の意を表する.

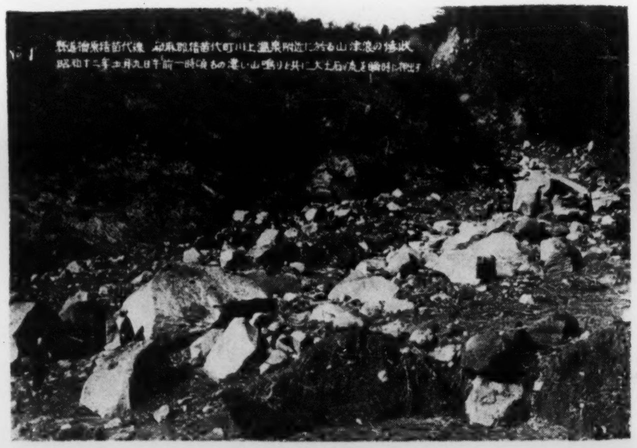

第４圖 a)　５月９日縣道檜原猪苗代線に押し出した土石

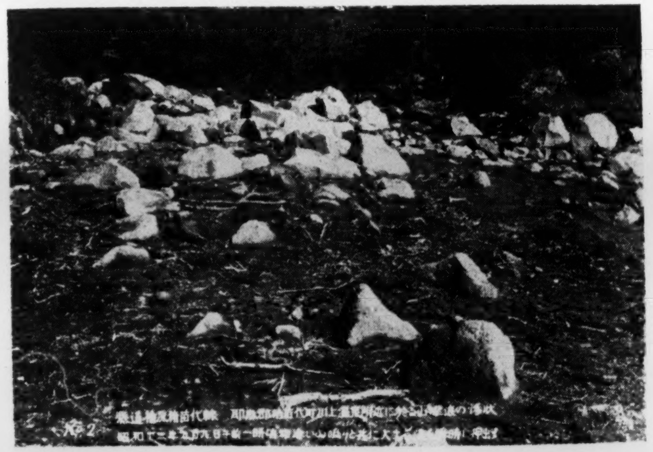

第４圖 b)　５月９日縣道に押し出した土石及び泥

第５圖 a)　５月９日の山津浪による縣道の破壞

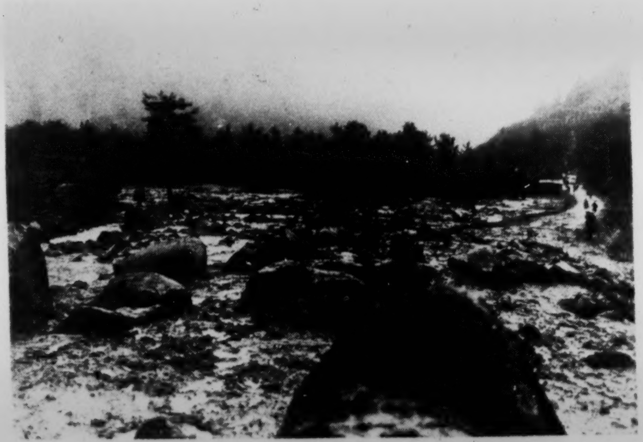

第５圖 b)　５月９日の山津浪に襲はれ死者を出した人家

Figs. 4～5.　A mud flow invaded the Kawakami Hot Springs (May 9, 1938).

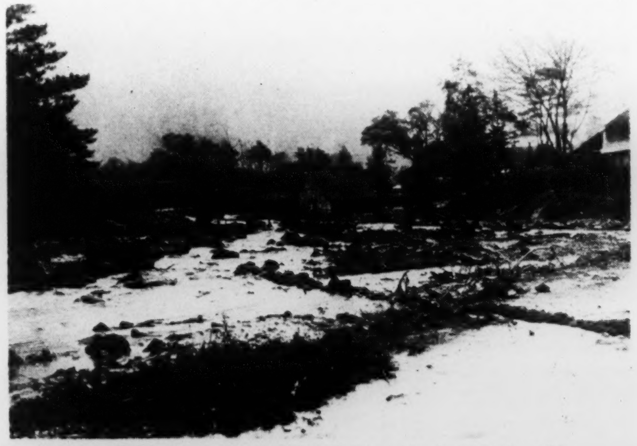

第６圖 a） 川上小學校附近に於ける泥流の跡
（５月９日の山津浪による）

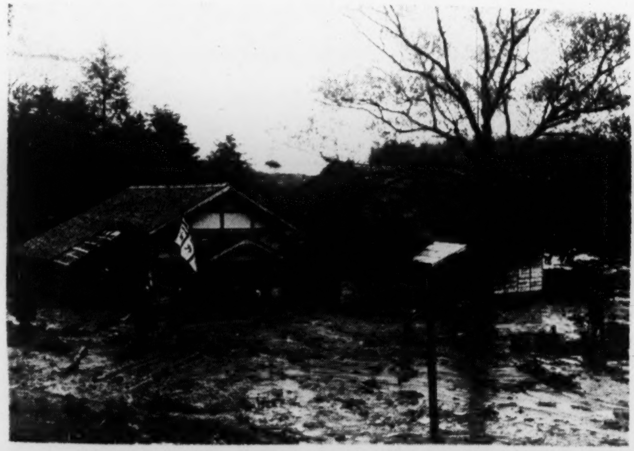

第６圖 b） ５月９日の山津浪に襲はれた川上小學校
（床上浸土約 1 m）

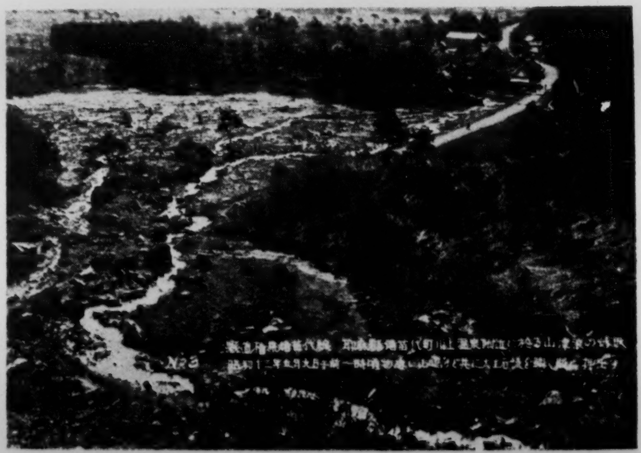

第７圖 a） ５月９日の山津浪に襲はれた川上溫泉

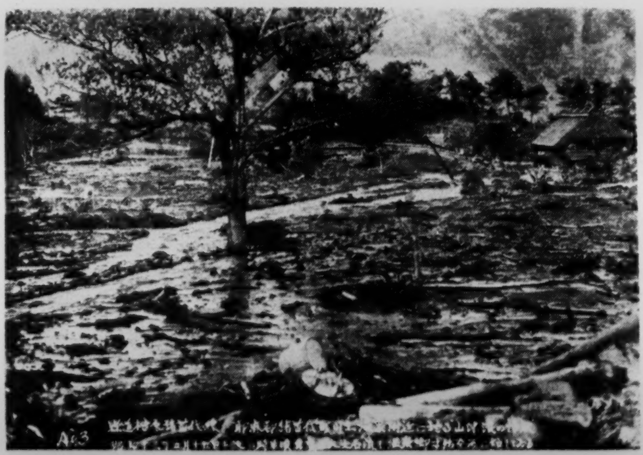

第７圖 b） ５月15日の山津浪に襲はれ流失した川上小學校，校庭に殘存せる柳の木

Figs. 6～7.a) General view of the Kawakami Hot Springs.

Fig. 7. b) The primary school was demolished by the mud flow (May 15).

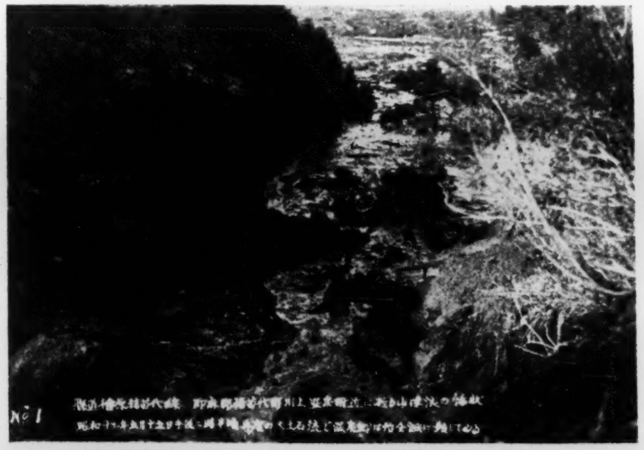

第8圖 a） 5 月 15 日縣道に押し出した土砂

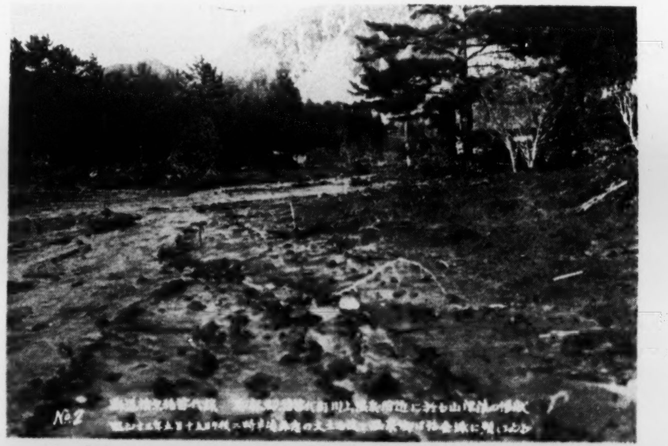

第8圖 b） 5 月 15 日の山津浪に襲はれた川上溫泉
家屋の多くは流失埋沒す

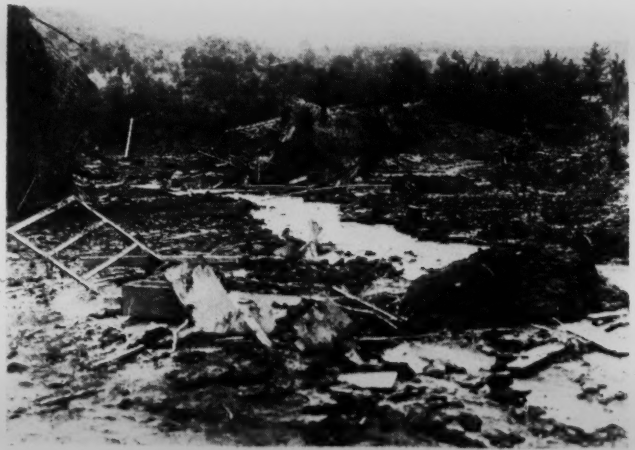

第9圖 a） 5 月 15 日の山津浪による家屋の被害

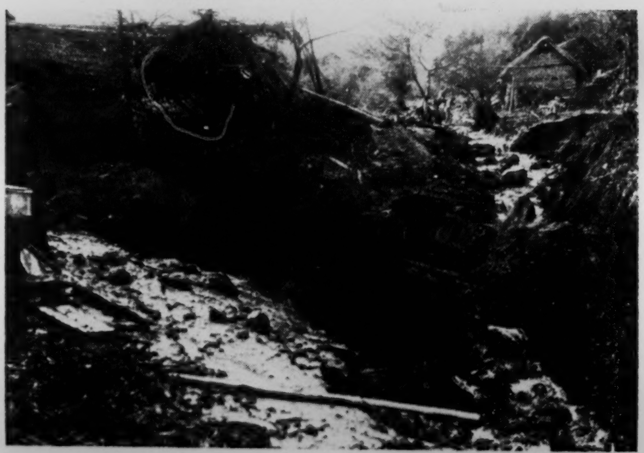

第9圖 b） 5 月 15 日の山津浪により流された家屋

Figs. 8～9. General view of the mud flow (May 15).

（震研彙報 第十六號 圖版 飯田）

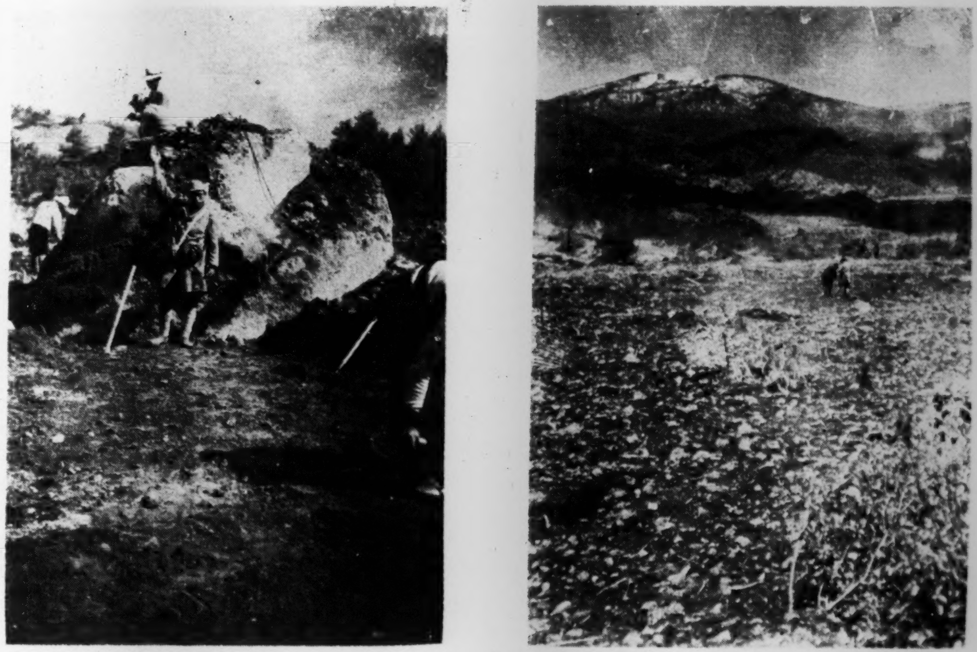

第 10 圖 a) 5 月 15 日の泥流により運搬された縣道上の大石塊

第 10 圖 b) 5 月 15 日の泥流跡の測量

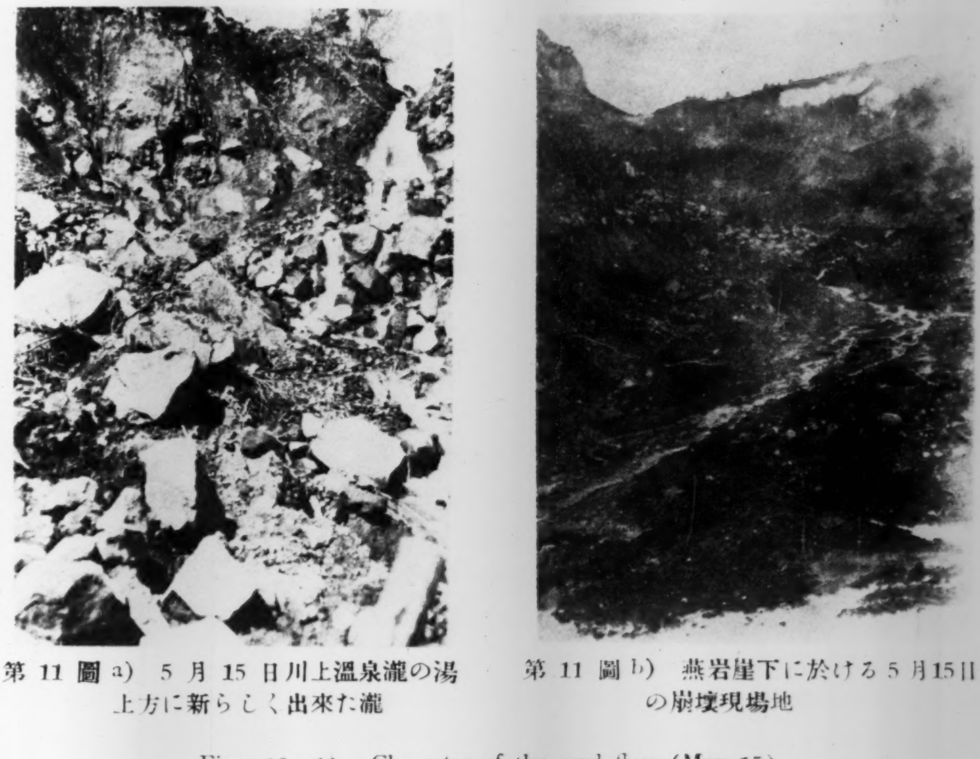

第 11 圖 a) 5 月 15 日川上溫泉瀧の湯上方に新らしく出來た瀧

第 11 圖 b) 燕岩崖下に於ける 5 月15日の崩壊現場地

Figs. 10～11. Character of the mud flow (May 15).

（震研彙報 第十六號 圖版 飯田）

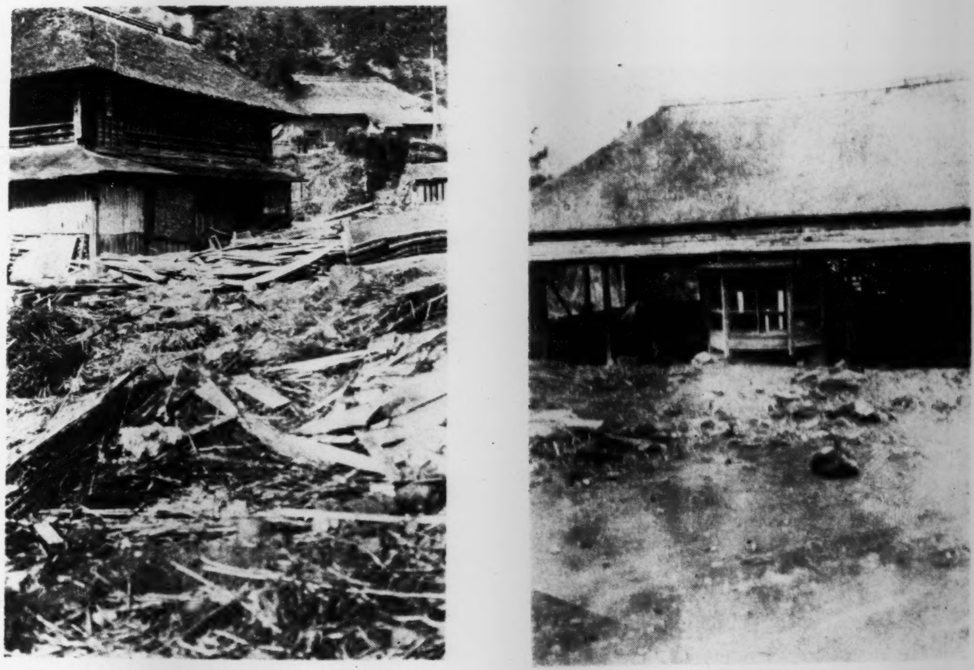

第 12 圖 a) 5 月 15 日の山津浪による家屋の被害

第 12 圖 b) 5 月 15 日の山津浪による家屋の被害(床上浸土)

Fig. 12. a), b) Destruction of houses due to the mud flow (May 15).

（震研彙報 第十六號 圖版 飯田）

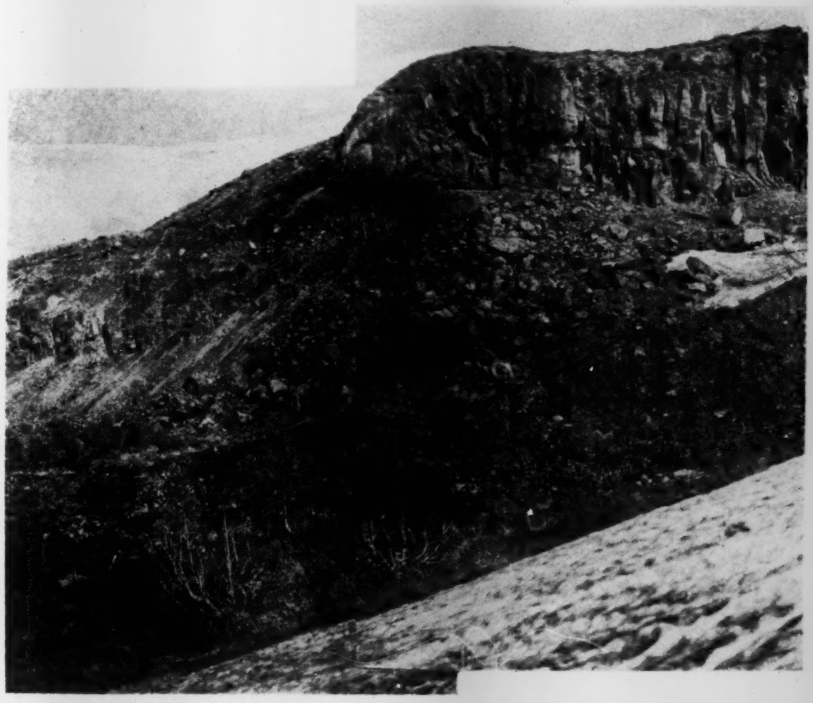

第 13 圖 a) 燕岩屋下の崩壊現場地.

Fig. 13. a) The upper part of the landslide.

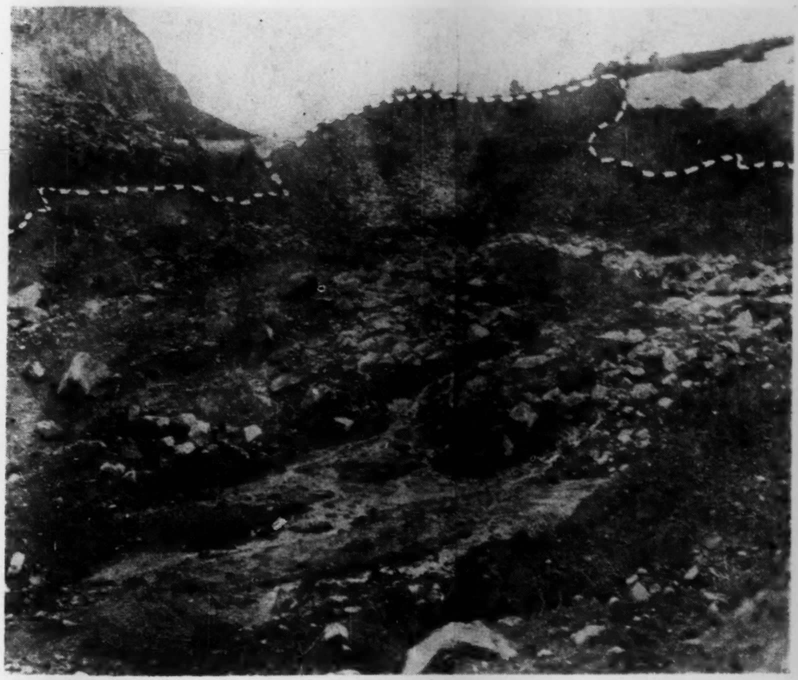

第 13 圖 b） 崩壞現場地の最上部分

Fig. 13. b) The upper part of the landslide.

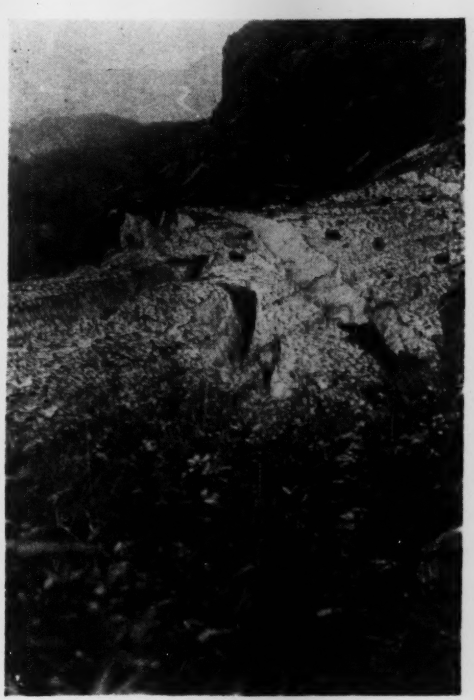

第 14 圖 a） 燕岩崖下の殘雪の割れ目

Fig. 14. a) Cracks of Snow at the upper part of the landslide.

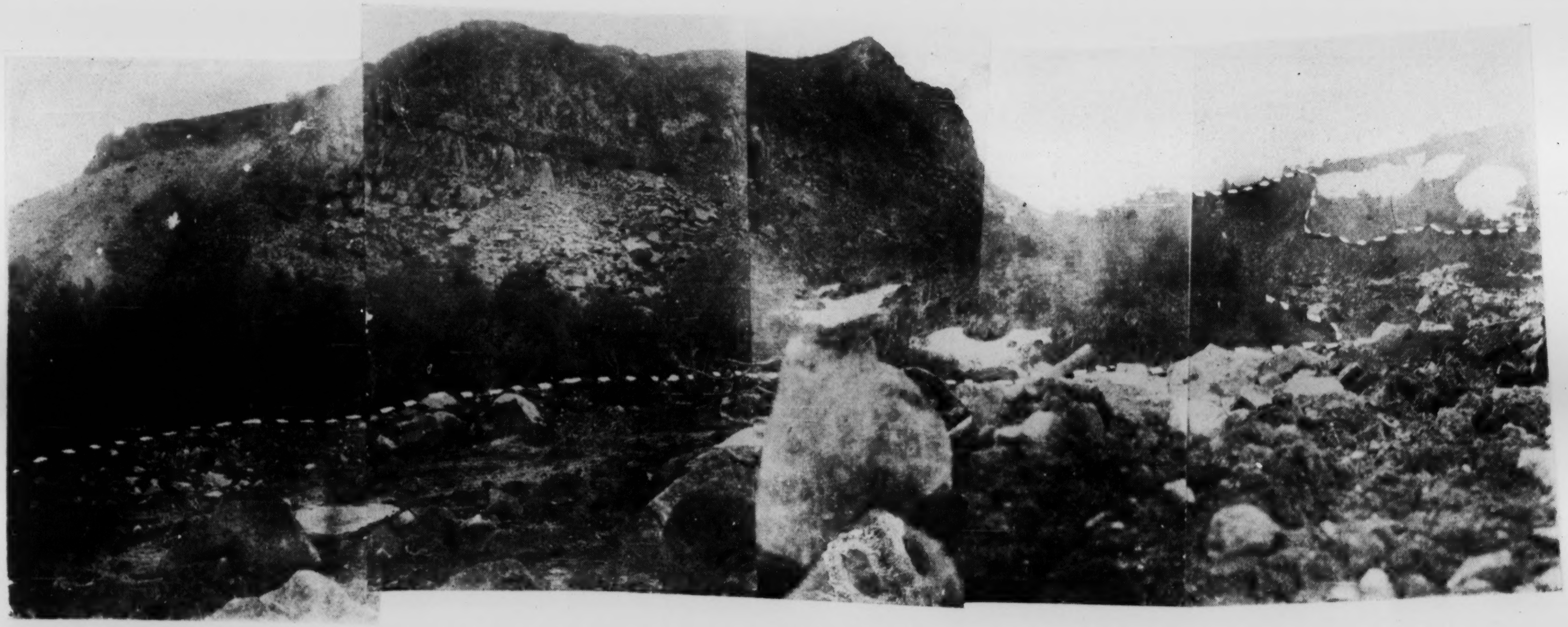

第 15 圖　燕岩附近に於ける崩壞地（崩壞現場地を隔たる 300 m の地點より望む）

Fig. 15. The upper part of the mud flow.

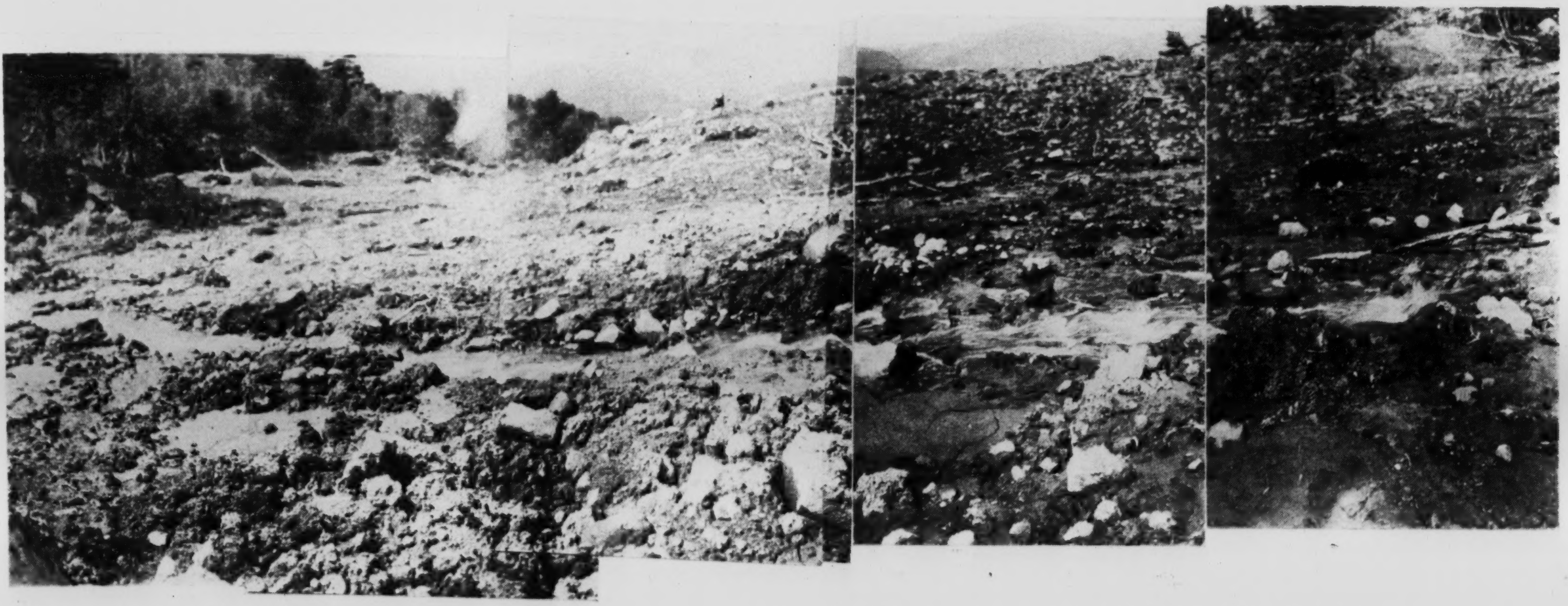

第 16 圖　土砂流の跡（川上溫泉より 500 m の山腹，此の邊より 3 方に分岐して川上溫泉に押し出した）

Fig. 16. The middle part of the mud flow.

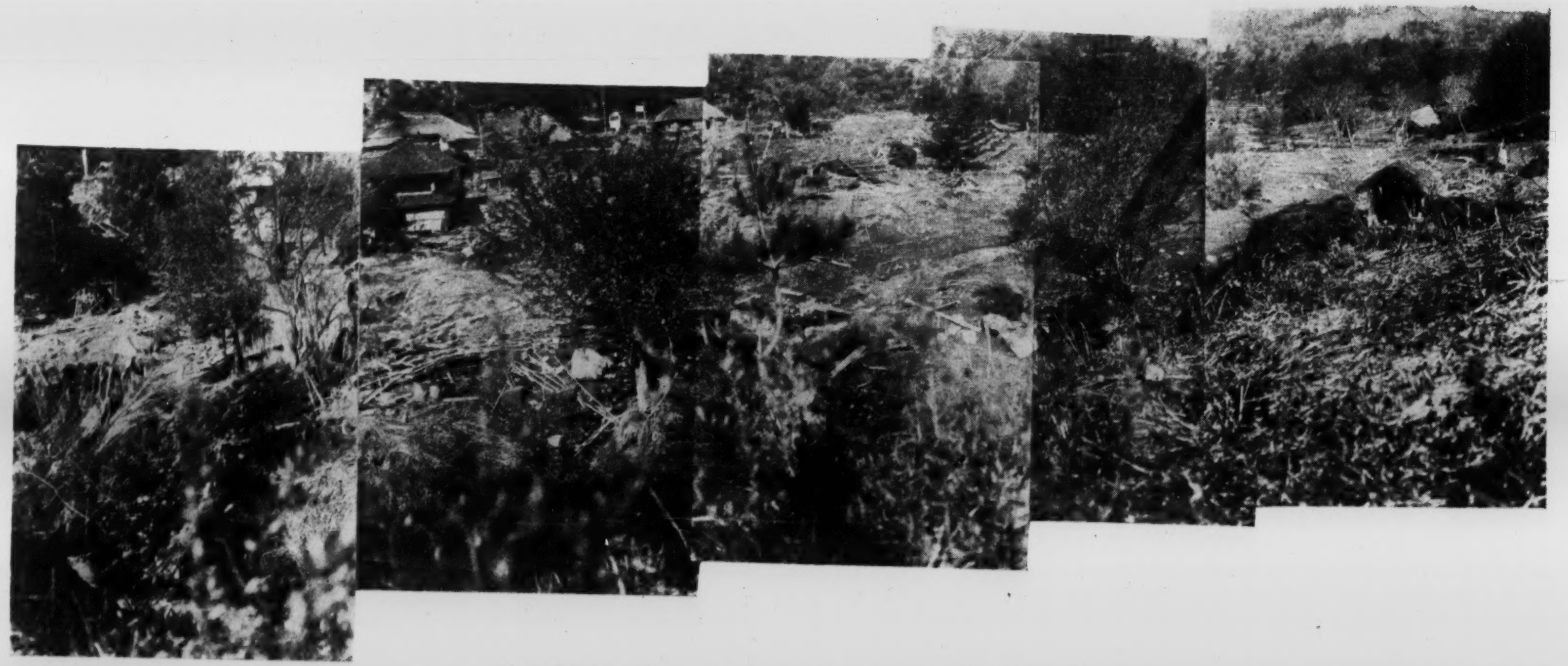

第17圖　川上溫泉に於ける山津浪の跡

Fig. 17. View of the destruction of houses at the Kawakami Hot Springs.

46. *The Mud Flow that occurred near the Explosion-crater of Mt. Bandai on May 9 and 15, 1938, and some Physical Properties of Volcanic Mud.*

By Kumizi IIDA,

Earthquake Research Institute.

On May 9 and 15, 1938, a mud flow invaded the Kawakami Hot Springs, a resort about 3 km from the explosion-crater of Mt. Bandai, Hukusima Prefecture, and besides demolishing ten houses, killed and wounded a few people.

This paper gives a general description of the mud flow and its phenomena, namely, certain physical properties such as the coefficient of viscosity, modulus of elasticity, cohesional force, and the frictional angle of the mud. In the present case the velocity of the mud flow was estimated about 25 m/sec, the coefficient of viscosity of the mud taken from Kawakami arrived at by experiment is of the order of 10 (c.g.s.) with 40 per cent water content, and 10^3 (c.g.s.) with a 23 per cent water content. This coefficient decreases somewhat rapidly with increase of water content. The modulus of elasticity decreases also with the water content, but its cohesive strength suddenly increases between 5~15 per cent water content, the maximum value being reached at 10 per cent. The frictional angle of certain kind of mud increases also between 10~20 per cent water content. The frictional angle and the cohesive strength of the mud as it flowed on May 9 and 15 must have been smaller than the foregoing values, as, according to estimate, the water content of the mud at that time was about 40~60 per cent.

The action of the underground water that penetrated the volcanic ash remaining in the explosion-crater since the great eruption of Mt. Bandai in 1888, seems to be one of the most important causes of the present disaster. It is worth noting in this connexion that more snow fell this year in that district than at any time during the last ten years. Owing to the water from the melting of these snows, the volcanic ash became super-saturated with water, thus disturbing the stability of the volcanic sands, resulting in the present mud flow.

47. *Anomalous Dispersion of Elastic Surface Waves. II.*[1]

By Katsutada SEZAWA and Kiyoshi KANAI,

Earthquake Research Institute.

(Read July 5, 1938.—Received Sept. 20, 1938.)

1. *Introduction.*

In a previous paper[2] we showed that even should the velocity of bodily waves in the surface layer be higher than that in the subjacent medium, it is possible for Rayleigh-type waves of certain ranges of wave-length to be transmitted, the propagational velocity of the waves then diminishing with increase in wave-length. Under the condition of the problem particularly selected in the last case, namely, the condition that $\rho'/\rho=1/2$, $\mu'/\mu=1$, the dispersion curve beginning discontinuously with ordinate $V/\sqrt{\mu/\rho}=1{\cdot}000$ and abscissa $L/H=4{\cdot}650$, existed only in the range, $L/H=4{\cdot}650\sim\infty$, tending to assume the asymptotic value $0{\cdot}9194$ at $L/H\rightarrow\infty$. If any part of the dispersion curve were within the range $L/H=4{\cdot}650\sim0$, the value of $V/\sqrt{\mu/\rho}$ would be greater than 1, in which case the mathematical conditions prevent the waves from assuming a surface type or even a permanent type.

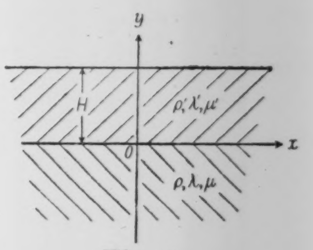

Fig. 1.

Although in the condition just mentioned, the dispersion curve incidentally meets the line $V/\sqrt{\mu/\rho}=1$, with the result that the same curve ends at an intermediate value of L/H, it is however possible to expect another case in which the curve does not meet the line $V/\sqrt{\mu/\rho}=1$, the end of the curve probably intersecting with the abscissa $L/H=0$. With a view to ascertaining the general feature of the problem for widely different cases of the dispersion curves, the calculation is now extended to the cases $\mu'/\mu=0{\cdot}8$, $0{\cdot}58$, $0{\cdot}50$, $0{\cdot}44$, $0{\cdot}40$ ($\lambda=\mu$, $\lambda'=\mu'$), ρ'/ρ being kept at $0{\cdot}5$; at the same time the nature of the velocity equation that we obtained in a very simplified form a few years ago, is now rediscussed from a more analytical point of view.

---

[1] Preliminary report published in the *Proc. Imp. Acad.*, **14** (1938), 246~249.

[2] K. SEZAWA, "Anomalous Dispersion of Elastic Surface Waves," *Bull. Earthq. Res. Inst.*, **16** (1938), 225~233.

2. *Velocity equation of dispersive Rayleigh-waves.*

Let the thickness of the surface layer be H and the wave-length L, and let also densities and elastic constants of the layer and the subjacent medium be ρ', λ', μ'; ρ, λ, μ respectively. Then, the equation that is necessary for obtaining the velocity of transmission of the dispersive Rayleigh-waves of frequency p is expressed by[3]

$$\begin{aligned}\frac{4r's'}{f^2}\left(2-\frac{k'^2}{f^2}\right)\eta-\frac{r's'}{f^2}\left\{4\vartheta+\left(2-\frac{k'^2}{f^2}\right)^2\zeta\right\}\cosh r'H\cos s'H\\+\frac{r'}{f}\varphi\left\{\frac{4rs'^2}{f^3}+\frac{s}{f}\left(2-\frac{k'^2}{f^2}\right)^2\right\}\cosh r'H\sin s'H\\+\frac{s'}{f}\varphi\left\{-\frac{4sr'^2}{f^3}+\frac{r}{f}\left(2-\frac{k'^2}{f^2}\right)^2\right\}\sinh r'H\cos s'H\\+\left\{-\frac{4r'^2s'^2}{f^4}\zeta+\left(2-\frac{k'^2}{f^2}\right)^2\vartheta\right\}\sinh r'H\sin s'H=0\,,\end{aligned}\qquad(1)$$

where

$$\left.\begin{aligned}&\varphi=\frac{\mu'k^2k'^2}{\mu f^4},\quad \zeta=\frac{4rs}{f^2}\left(\frac{\mu'}{\mu}-1\right)^2-\alpha^2,\quad \eta=\frac{2rs}{f^2}\left(\frac{\mu'}{\mu}-1\right)\beta-\alpha\gamma,\\&\vartheta=\frac{rs}{f^2}\beta^2-\gamma^2,\quad \alpha=\frac{2\mu'}{\mu}-\left(2-\frac{k^2}{f^2}\right),\quad \beta=\frac{\mu'}{\mu}\left(2-\frac{k'^2}{f^2}\right)-2,\\&\gamma=\frac{\mu'}{\mu}\left(2-\frac{k'^2}{f^2}\right)-\left(2-\frac{k^2}{f^2}\right),\quad f=\frac{2\pi}{L},\\&r^2=f^2-h^3,\quad s^2=f^2-k^2,\quad r'^2=f^2-h'^2,\quad s'^2=k'^2-f^2,\\&h^2=\rho p^2/(\lambda+2\mu),\quad h'^2=\rho'p^2/(\lambda'+2\mu'),\quad k^2=\rho p^2/\mu,\quad k'^2=\rho'p^2/\mu'.\end{aligned}\right\}\qquad(2)$$

When $fH\rightarrow 0$, that is, $L/H\rightarrow\infty$, the equation (1) reduces to

$$\frac{r's'k'^4}{f^6}\left\{\left(2-\frac{k^2}{f^2}\right)^2-\frac{4rs}{f^2}\right\}=0\,,\qquad(3)$$

which is of the same form as the velocity equation of Rayleigh-waves for a semi-infinite body. This shows that even should the velocity of bodily waves in the surface layer be much higher than that in the subjacent medium, the behaviour of Rayleigh-waves of great length in passing through the stratified body does not differ from that of the

---

3) *loc. cit.*

same waves in the case of a semi-infinite body which is of the material as the subjacent medium just mentioned.

When $fH \to \infty$, that is $L/H \to 0$, the equation (1) reduces to a pair of factors, as follows,

$$\left\{\left(2-\frac{k'^2}{f^2}\right)^2-\frac{4r's'}{f^2}\right\}\left[\frac{rs}{f^2}\left\{\frac{\mu'}{\mu}\left(2-\frac{k'^2}{f^2}\right)-2\right\}^2-\left\{\frac{\mu'}{\mu}\left(2-\frac{k'^2}{f^2}\right)-\left(2-\frac{k^2}{f^2}\right)\right\}^2\right.$$

$$\left.-\frac{4r's'rs}{f^4}\left(\frac{\mu'}{\mu}-1\right)^2+\frac{r's'}{f^2}\left\{\frac{2\mu'}{\mu}-\left(2-\frac{k^2}{f^2}\right)\right\}^2+\frac{\mu'k^2k'^2sr'}{\mu f^6}+\frac{\mu'k^2k'^2rs'}{\mu f^6}\right]=0\,. \quad (4)$$

The first factor represents the velocity equation of Rayleigh-waves that are transmitted through a semi-infinite body composed of the same material as that in the surface layer, and the second one the velocity equation of the waves that are transmitted along the boundary between the surface and the subjacent media. The latter kind of waves corresponds to the one that Stoneley[4] already found, the type of expression in (4) being formulated by us for other purposes.[5] As a matter of fact, the decomposition of the velocity equation was shown by Love[6] for the case of incompressible materials, and also by Lee[7] for a more general case in Love's type of expression. Although it appears possible for two kinds of waves to exist for any value of ρ'/ρ, or μ'/μ, Stoneley wave only exists in the case wherein the densities and elasticities of the media are likely to satisfy Wiechert's condition, namely, $\rho'/\rho=\mu'/\mu=\lambda'/\lambda$.

One of the important conditions for the present kind of waves that the same waves should be of surface or boundary type, would be $V/\sqrt{\mu/\rho}<1$; otherwise, the amplitude distribution of the waves in the subjacent medium would be sinusoidal, from which the total energy of the waves, integrated through the whole depth, would assume an infinitely large value even should the amplitude at any depth in the subjacent medium be very small.

In the present problem, so far as the nature of the waves differed from that of surface or boundary waves, the waves under consideration would not be of permanent type at the same time, whence follows the importance with respect to two different conditions of the relation $V/\sqrt{\mu/\rho}<1$.

---

4) R. STONELEY, "Elastic Waves at the Surface of Separation of Two Solids", *Proc. Roy. Soc.*, **106** (1924), 416~428.

5) K. SEZAWA and K. KANAI, *Bull. Earthq. Res. Inst.*, **16** (1938), 504~526.

6) A. E. H. LOVE, *Some Problems of Geodynamics*, 1911, 168.

7) A. W. LEE, *M. N. R. A. S. Geophys. Suppl.*, **3** (1934), 252.

3. *Numerical examples and interpretation of their results.*

As mentioned in the introductory part, we calculated the cases (I) $\mu'/\mu=1$, (II) $\mu'/\mu=0{\cdot}8$, (III) $\mu'/\mu=0{\cdot}58$, (IV) $\mu'/\mu=0{\cdot}5$, (V) $\mu'/\mu=0{\cdot}44$, (VI) $\mu'/\mu=0{\cdot}40$; $\rho'/\rho=0{\cdot}5$, $\lambda=\mu$, $\lambda'=\mu'$ being kept constant. The results of the calculation are shown in the annexed tables.

Table I. $\mu'/\mu=1$.

$V/\sqrt{\mu/\rho}$	1·000	0·980	0·950	0·930	0·9194
L/H	4·650	8·240	18·91	58·50	∞

Table II. $\mu'/\mu=0{\cdot}8$.

$V/\sqrt{\mu/\rho}$	1·000	0·9798	0·9644	0·9194
L/H	3·217	6·042	8·760	∞

Table III. $\mu'/\mu=0{\cdot}58$.

$V/\sqrt{\mu/\rho}$	0·9902	0·9798	0·9487	0·9194
L/H	0	2·565	7·604	∞

Table IV. Case IV. $\mu'/\mu=0{\cdot}5$.

$V/\sqrt{\mu/\rho}$	0·9194	0.9327		0·9534		0·9487		0·9194
L/H	0	1·359	10·13	2·303	3·736	1·946	4·862	∞

Table IV(S). Case IV(S). $\mu'/\mu=0{\cdot}5$.

$V/\sqrt{\mu/\rho}$	0·9951	0·9960	0·9970	0·9975	0·9995	0·9999	1·000
L/H	0	0·6000	0·7950	0·8748	1·1575	1·267	1·282

Table V. $\mu'/\mu=0{\cdot}44$.

$V/\sqrt{\mu/\rho}$	0·8625	0·9000	0·9165	0·9247		0·9298		0·9194
L/H	0	1·751	2·112	2·363	11·256	2·574	7·868	∞

Table VI. $\mu'/\mu=0{\cdot}4$.

$V/\sqrt{\mu/\rho}$	0·8223	0·8944	0·9165	0·9195		0·9194
L/H	0	2·235	2·881	3·046	12·738	∞

The same results are also shown in Fig. 2. The dispersion curve in case I is reproduced from our preceding result.

It will be seen that, as in case I, the dispersion curve in case II beginning discontinuously at such an abscissa of L/H as not zero with ordinate $V/\sqrt{\mu/\rho}=1{\cdot}000$, tends to touch the asymptotic line $V/\sqrt{\mu/\rho}=0{\cdot}9194$ at $L/H\to\infty$, the curve thus lying within a limited range of abscissa. In cases III, IV, V, VI, on the other hand, the respective dispersion curves extend through the whole range of L/H.

There are two dispersion curves in case IV, where Wiechert's condition, namely $\rho'/\rho=\mu'/\mu$, is satisfied. In this case the dispersion curve passing through the ordinate corresponding to Stoneley wave is indicated by IV(S). The question may arise whether or not dispersion curves analogous to IV(S) can exist in the respective remaining cases, namely, I, II, III, V, VI. The answer is relatively simple. It was confirmed that in cases I, II, III, no point, excepting those shown in the sketch, on the line $V/\sqrt{\mu/\rho}=1$, can represent real propagational velocity. Since, on the other hand, the curve analogous to IV(S) should be so inclined as to meet the line $V/\sqrt{\mu/\rho}=1$, it is scarcely possible for the curve in question to exist. In case V, there is no point analogous to IV(S) on the line, $V/\sqrt{\mu/\rho}=0{\cdot}938$, beyond which ordinate the value of s' becomes imaginary, that is to say, the amplitude distribution in the surface layer becomes of sinusoidal type. For the same reason as that given in cases I, II, III, it is impossible for the second dispersion curves to exist. It is also obvious that in case VI no second dispersion curve exists. At all events, ordinate of every dispersion curve tends to assume the asymptotic value $V/\sqrt{\mu/\rho}=0{\cdot}9194$ at $L/H\to\infty$.

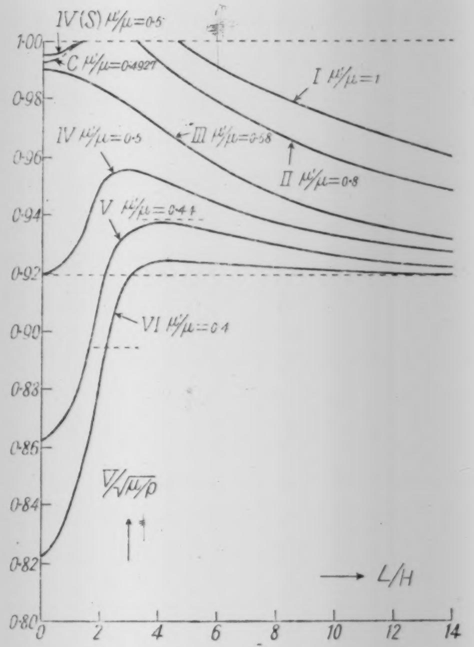

Fig. 2. Dispersion curves.

If the ratio of μ'/μ be somewhat less than 0·495, the amplitude distribution, of the waves similar to IV(S), within the surface layer becomes of sinusoidal type for a relatively large wave-length, say $L/H>0{\cdot}5$. In the limiting case, where the ratio of μ'/μ is 0·4927, the amplitude distribution, of the waves also similar to IV(S), in the surface layer is sinusoidal for any wave-length. Such a limiting case is shown by curve C in Fig. 2, its ordinate at $L/H=0$ being 0·9926. Although it is possible to consider dispersion curves, of the waves similar to IV(S), below the curve C for such cases that the elastic constants satisfy the condition $\mu'/\mu<0{\cdot}4927$, since the amplitude distribution within the surface layer in any one of such cases is sinusoidal, it is improbable for the waves under consideration to be of boundary type. Thus, Stoneley waves are possible to exist only for the range between $\mu'/\mu=0{\cdot}4926\sim0{\cdot}563$, the velocities corresponding to these limits then being $0{\cdot}9926\sim1$.

The dispersion curve in case IV has an odd form. Notwithstanding that the velocity of longitudinal waves or transverse waves in the surface layer is the same as that in the subjacent medium, the velocity of Rayleigh-waves is considerably greater than that of usual Rayleigh-waves, namely $V=0{\cdot}9194\sqrt{\mu/\rho}=0{\cdot}9194\sqrt{\mu'/\rho'}$, excepting for the condition $L/H=0$ and $L/H=\infty$. The dispersion curve in case V resembles that in case IV; after reaching a maximum it is slowly depressed, and approaches the asymptote $V/\sqrt{\mu/\rho}=0{\cdot}9194$. In the dispersion curve in case VI, no appreciable maximum of ordinate exists for intermediate value of L/H. It appears that for a smaller value of μ'/μ, the dispersion curve is similar to that in the case of the normal dispersion of Rayleigh-waves.

The values of μ'/μ, for which the ordinate of the dispersion curve is exactly $V/\sqrt{\mu/\rho}=1$ at $L/H=0$, is $\mu'/\mu=0{\cdot}592$. It follows then that so long as $\mu'/\mu>0{\cdot}592$ in the case $\rho'/\rho=1/2(\lambda=\mu,\ \lambda'=\mu')$, there should exist a certain range of L/H within which no surface wave (permanent type) can exist.

4. *Concluding remarks.*

From mathematical calculations we found that in certain elasticity and density conditions, the dispersion of Rayleigh-waves is anomalous. When the stratification nearly satisfies Wiechert's condition, the velocity of Rayleigh-waves for an intermediate ratio of L/H is considerably higher than that of the usual Rayleigh-waves. In this case there is a second dispersion curve that passes through the point corresponding to the velocity of Stoneley waves. When the stratification is nearly in the usual condition rather than Wiechert's condition, the dispersion curve tends to assume the normal dispersion type. Should, on the other hand, the condition of stratification be the reverse of that in the usual meaning even beyond Wiechert's condition, the dispersion curve becomes quite anomalous and, beyond a certain critical condition, there should exist a range of L/H within which no surface wave (permanent type) can exist. Particularly, in the present problem, the condition that prevents the existence of surface waves also prevents the waves from being of permanent type.

The condition of stratification just given, that is to say, the condition that the increase of density is more rapid than that of elasticity, both with increase in depth, is more likely to be actual than merely ideal in the surface crust of the Earth. The fact that the vibration of Rayleigh-waves in some case is limited to certain periods, may result from the condition of the waves possibly existing for a certain range of wave-lengths. The evidence that the group velocity of surface waves is greater than their phase velocity, is also likely to be connected with the problem in the present paper.

---

47. 彈性表面波の異常分散(第2報)

地震研究所 {妹澤克惟
{金井清

前回の研究に於て，地殼の深い所程その物質の密度が大きい場合に，分散性レーリー波が異常分散になり得る事を説明して置いた．今回はそれに關係のある問題を一層廣い範圍に涉つてしらべて見たのである．

地殼の層がウイーヘルトの條件を滿足する場合には，中間位の波長に限つて普通のレーリー波から想像できる速度よりも高い傳播速度があり得るのである．しかしウイーヘルトの條件よりも普通の層狀に近い場合，卽ち表面程固體波の速度が遲い場合には，普通の場合の型の分散曲線が出るものである．又普通の層狀とは逆になり，而もウイーヘルトの條件を越してをる狀態になると，波長が長い程速度が遲くなるといふ場合があり得る．その場合には，ある範圍の波長については實在の波の存在し得ぬものである．

ウイーヘルトの條件を滿足するやうな場合に近い狀態では固體と固體との間の境界を傳播するレーリー型の波が存在することもわかつた．

只今のやうな波の出る場合は，よく考へるとむしろ大いに可能な狀態である．又，地震波から見ても，表面波が或る範圍の波長にしか涉つてをらぬ場合や，波の群速度がその位相速度よりも速い場合などが只今の問題と大いに關係のあることもわかつた．

48. *The Effect of Viscosity on the Gravitational Stability of the Earth at its Liquid Cooling Stage.*

By Katsutada SEZAWA and Kiyoshi KANAI,

Earthquake Research Institute.

(Read Sept. 20, 1938.—Received Sept. 20, 1938.)

1. *Introduction.*

In the previous paper[1] we discussed the gravitational stability of the earth at its liquid cooling stage without taking into account the liquid viscosity. Since, as a matter of fact, stability is a statical problem, not dynamical, we thought that the viscosity of the liquid would have no effect on stability. On the other hand, Lord Rayleigh[2] and Jeffreys[3] found that the stability of a layer of fluid that is heated below it is affected by its viscosity, which has raised the question whether or not viscosity also affects our problem. Since, however, the problems treated by Lord Rayleigh and Jeffreys are restricted to that case in which a liquid is bounded between two parallel rigid planes, and therefore not immediately available for our use, we have treated our case independently of that due to the authors just mentioned, although it is quite similar to that used in our previous paper.[4] The condition in our present problem which differs from that in our previous one is that, for simplicity, we deal with a two-dimensional problem of the earth's crust without regard to the surface curvature of the earth.

We shall first discuss the problem of the stability of a plane boundary between two liquids extending upward and downward to infinity and next treat the problem of the case in which there is a superficial layer of liquid on another liquid extending downwards to infinity.

The criterion of stability is such that, after discussing the vibratory motion of a boundary between two different liquids, the neutral state of the vibrational stability is specially examined. Since the physical conception of instability is that the vibratory deformation at every boundary between different liquids never assumes its original state, the criterion of the problem just mentioned is quite reasonable.

---

[1] K. SEZAWA and K. KANAI, "Gravitational Stability of the Earth at its Liquid Cooling Stage", *Bull. Earthq. Res. Inst.*, **16** (1938), 234～243.

[2] LORD RAYLEIGH, "On Convection Currents in a Horizontal Layer of Fluid, when Higher Temperature is on the Under Side", *Phil. Mag.*, **32** (1916), 529～546.

[3] H. JEFFREYS, "The Stability of a Layer of Fluid heated below", *Phil. Mag.*, [7] **2** (1926), 833～844.

[4] *loc. cit.* 1).

Our investigations show that viscosity affects gravitational stability, though not very much. Instability without viscosity would be changed to stability were the liquid viscous. Furthermore, for the stable condition in question to be realized, it is not necessary that the whole of the liquid shall be viscous. It is possible for the liquid to be in a stable condition provided a certain part of the same liquid near the boundary under consideration is viscous.

2. *Mathematical solutions for the case in which the two liquids extend to infinity.*

Let x, y be drawn in coincidence with and upward normal to the boundary between two liquids, and let u', v', u, v be the x- and y-components of the velocities of the upper and lower layers respectively. The equations of motion and continuity for the upper and the lower layer are

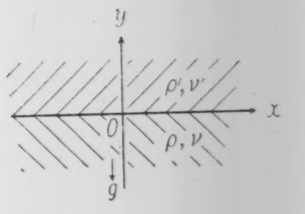

Fig. 1.

$$\left.\begin{aligned}\frac{\partial u'}{\partial t}=-\frac{1}{\rho'}\frac{\partial p'}{\partial x}+\nu'\nabla^2 u',\quad \frac{\partial v'}{\partial t}=-\frac{1}{\rho'}\frac{\partial p'}{\partial y}+\nu'\nabla^2 v',\\ \frac{\partial u'}{\partial x}+\frac{\partial v'}{\partial y}=0,\end{aligned}\right\}\quad(1)$$

$$\left.\begin{aligned}\frac{\partial u}{\partial t}=-\frac{1}{\rho}\frac{\partial p}{\partial x}+\nu\nabla^2 u,\quad \frac{\partial v}{\partial t}=-\frac{1}{\rho}\frac{\partial p}{\partial y}+\nu\nabla^2 v,\\ \frac{\partial u}{\partial x}+\frac{\partial v}{\partial y}=0,\end{aligned}\right\}\quad(2)$$

where ρ', ρ; $\nu'=\mu'/\rho'$, $\nu=\mu/\rho$ are densities and the kinematic coefficients of the viscosities in the respective media. These equations are satisfied by

$$u'=-\frac{\partial\phi'}{\partial x}-\frac{\partial\psi'}{\partial y},\quad v'=-\frac{\partial\phi'}{\partial y}+\frac{\partial\psi'}{\partial x},\quad \frac{p'}{\rho'}=\frac{\partial\phi'}{\partial t}-g\eta',\qquad(3)$$

$$u=-\frac{\partial\phi}{\partial x}-\frac{\partial\psi}{\partial y},\quad v=-\frac{\partial\phi}{\partial y}+\frac{\partial\psi}{\partial x},\quad \frac{p}{\rho}=\frac{\partial\phi}{\partial t}-g\eta,\qquad(4)$$

under the condition that

$$\nabla^2\phi'=0\,,\quad \frac{\partial\psi'}{\partial t}=\nu'\nabla^2\psi', \tag{5}$$

$$\nabla^2\phi=0\,,\quad \frac{\partial\psi}{\partial t}=\nu\nabla^2\psi. \tag{6}$$

Solving (5), (6), we have

$$\phi'=Be^{-ky+ikx+nt},\quad \psi'=De^{-m'y+ikx+nt}, \tag{7}$$

$$\phi=Ae^{ky+ikx+nt},\quad \psi=Ce^{my+ikx+nt}, \tag{8}$$

where $m'^2=k^2+n/\nu'$, $m^2=k^2+n/\nu$.

The normal displacements at the surface and the corresponding normal pressures are such that

$$\left.\begin{aligned} \eta'&=\frac{k}{n}(B+iD)e^{ikx+nt},\\ \frac{p'}{\rho'}&=\frac{\partial\phi'}{\partial t}-g\eta'=\left\{\frac{n^2-gk}{n}B-\frac{igk}{n}D\right\}e^{ikx+nt}, \end{aligned}\right\} \tag{9}$$

$$\left.\begin{aligned} \eta&=-\frac{k}{n}(A-iC)e^{ikx+nt},\\ \frac{p}{\rho}&=\frac{\partial\phi}{\partial t}-g\eta=\left\{\frac{n^2+gk}{n}A-\frac{igk}{n}C\right\}e^{ikx+nt}. \end{aligned}\right\} \tag{10}$$

The velocity components in both media are

$$\left.\begin{aligned} u'&=-\frac{\partial\phi'}{\partial x}-\frac{\partial\psi'}{\partial y}=-\left\{ikBe^{-ky}-m'De^{-m'y}\right\}e^{ikx+nt},\\ v'&=-\frac{\partial\phi'}{\partial y}+\frac{\partial\psi'}{\partial x}=-\left\{-kBe^{-ky}-ikDe^{-m'y}\right\}e^{ikx+nt}, \end{aligned}\right\} \tag{11}$$

$$\left.\begin{aligned} u&=-\frac{\partial\phi}{\partial x}-\frac{\partial\psi}{\partial y}=-\left\{ikAe^{ky}+mCe^{my}\right\}e^{ikx+nt},\\ v&=-\frac{\partial\phi}{\partial y}+\frac{\partial\psi}{\partial x}=-\left\{kAe^{ky}-ikCe^{my}\right\}e^{ikx+nt}, \end{aligned}\right\} \tag{12}$$

The boundary conditions at $y=0$ are

$$\eta'=\eta\,,\quad -p'+2\mu'\frac{\partial v'}{\partial y}=-p+2\mu\frac{\partial v}{\partial y}\,,\quad \mu'\left(\frac{\partial v'}{\partial x}+\frac{\partial u'}{\partial y}\right)=\mu\left(\frac{\partial v}{\partial x}+\frac{\partial u}{\partial y}\right)=0\,. \tag{13}$$

These relations imply the conditions that although all stresses and normal velocities are continuous respectively, there is a relative tangential motion at the boundary, that is to say, both media are slidable at the same boundary. If one of the media is inviscid, this condition is obviously satisfied.

Substituting (9), (10), (11), (12) in the boundary conditions (13), we get an equation in n as follows

$$n^2(1+\alpha)+4nk^2(\nu+\alpha\nu')+\left\{4k^4(\nu^2+\alpha\nu'^2)+gk(1-\alpha)\right\}-4k^3(\nu^2 m+\alpha\nu'^2 m')=0, \tag{14}$$

where $\alpha=\rho'/\rho$. Since $m'^2=k^2+n/\nu'$, $m^2=k^2+n/\nu$, the accurate treatment of this equation is, generally, fairly difficult.

In the special case, $\mu'\rightarrow 0$, $\mu\rightarrow 0$, we have

$$n^2(\rho+\rho')+gk(\rho-\rho')=0, \tag{15}$$

which is the same as that shown by Lamb.[5]

In the special case, $\alpha=0$, we have

$$(n+2\nu k^2)^2+gk=4\nu^2k^3m\,, \tag{16}$$

which is of the same form as that shown by Lamb[6] for the case of a semi-infinite fluid.

3. *Approximate solution of the above case.*

Although it is possible to solve (14) in elimination of m, m' by using the relations $m^2=k^2+n/\nu$, $m'^2=k^2+n/\nu'$, since the equation thus obtained is of the eighth degree in n, we solve (14) by omitting m, m'.

Even in such a solution the correction due to m, m' is of the second order in $\nu k^2/n$.

Now, the approximate solution of (14) is

$$n=-\xi\pm i\sigma \tag{17}$$

where

$$\xi=\frac{2k^2(\nu+\alpha\nu')}{1+\alpha},\quad \sigma=\frac{1}{1+\alpha}\sqrt{4k^4\alpha(\nu-\nu')^2+gk(1-\alpha^2)}. \tag{18}$$

If

$$\left\{4k^4(\nu^2+\alpha\nu'^2)+gk(1-\alpha)\right\}>0\,, \tag{19}$$

the oscillation of the boundary is stable, whereas if

$$\left\{4k^4(\nu^2+\alpha\nu'^2)+gk(1-\alpha)\right\}<0\,, \tag{19'}$$

---

[5] H. LAMB, *Hydrodynamics*, § 267.

[6] H. LAMB, *ibid.*, § 349.

the same oscillation is unstable.

If we put, specially, $\nu=\nu'$, the criterion of stability becomes

$$a=\frac{\rho'}{\rho}<\frac{gk+4k^4\nu^2}{gk-4k^4\nu'^2}\approx 1+\frac{8\nu^2k^3}{g}. \tag{20}$$

On the other hand, Lord Rayleigh⁷⁾ has given the criterion of stability for a fluid contained between two parallel plates, the result being that in the disturbed condition of density of fluid due to its temperature change, the condition of stability is defined by

$$a=\frac{\rho'}{\rho}<1+\frac{27\pi^4\kappa\nu}{4g\zeta^3}, \tag{21}$$

where $\kappa=$diffusibility for temperature$=5\nu/2$ for air from Maxwell's theory and ζ is the distance between parallel plates. Since, furthermore, the case of maximum instability in a two-dimensional problem is given by the condition, $2\pi/k=2\zeta$, where $2\pi/k$ is the wave length corresponding to the disturbed state of the fluid taken along the lengths of the plates, the relation (21) reduces to

$$a<1+\frac{135\pi}{8g}\nu^2k^3 \tag{21'}$$

for air,which is nearly four times as great as that which we obtained for the fluid extending in both vertical directions to infinity.

It will be seen that, if either one or both of the liquids be viscous, the critical condition of stability is raised somewhat beyond that for the case of non-viscous fluids. The greater the kinematic viscosities or the smaller the wave length of the disturbance, the greater the increase in the critical condition of the stability.

Finally, the components of the disturbed velocities can be derived from

$$\left.\begin{aligned}\phi&=Ae^{-\xi t+ky+i(kx\pm\sigma t)}, & \psi&=Ce^{-\xi t+my+i(kx\pm\sigma t)},\\ \phi'&=Be^{-\xi t-ky+i(kx\pm\sigma t)}, & \psi'&=De^{-\xi t-m'y+i(kx\pm\sigma t)},\end{aligned}\right\} \tag{22}$$

where

$$\frac{C}{A}\simeq\frac{-2i\nu k^2}{n+2\nu k^2},\quad \frac{B}{A}\simeq\frac{-(n+2\nu'k^2)}{n+2\nu k^2},\quad \frac{D}{A}\simeq\frac{-2i\nu'k^2}{n+2\nu k^2}, \tag{23}$$

so that the velocity components corresponding to the viscous state of

---

7) LORD RAYLEIGH, *loc. cit.* 2).

the fluids are very small compared with those corresponding to the inviscid state of the same fluids.

4. *Mathematical solutions for the case in which an inviscid liquid layer is on a viscous liquid extending to infinity.*

In this case the equations and the solutions for the fluid in the subjacent liquid are the same as those shown in Section 2, whereas the solutions for the superficial layer are

$$\phi' = \left\{A'e^{ky} + B'e^{-ky}\right\} e^{ikx+nt}, \qquad \psi' = 0\,, \tag{24}$$

$$u' = -\frac{\partial\phi'}{\partial x}, \quad v' = -\frac{\partial\phi'}{\partial y}, \quad \frac{p'}{\rho'} = \frac{\partial\phi'}{\partial t} - g\eta', \quad p'_{yy} = -p'. \tag{25}$$

The boundary conditions are

$$y = H; \qquad p'_{yy} = 0\,, \tag{26}$$

$$y = 0; \qquad p'_{yy} = p_{yy}, \quad p_{xy} = 0\,, \quad v = v'. \tag{27}$$

Substituting (9), (10), (12), (25) in (26), (27), we get the frequency equation

$$\begin{aligned} n^4(1+\alpha\,\mathrm{th}\,kH) + n^3(4\nu k^2) + n^2\left\{gk(1+\mathrm{th}\,kH) + 4\nu^2k^4\right\} \\ + n\left\{4\nu k^2 gk\,\mathrm{th}\,kH\right\} + gk\left\{gk(1-\alpha) + 4\nu^2k^4\right\}\mathrm{th}\,kH \\ = 4\nu^2k^3m\left\{n^2 + gk\,\mathrm{th}\,kH\right\}, \end{aligned} \tag{28}$$

where H is the thickness of the surface layer, $\alpha = \rho'/\rho$, and ν the kinematic coefficient of viscosity of the subjacent medium. Since, in the present case, too, the effect of m is negligible, we shall solve equation (28), omitting the term on the right-hand side of the same equation. Even in such a simplified condition of the problem, since the solution of a linear equation of fourth degree is somewhat difficult, we shall use the following approximation. Let

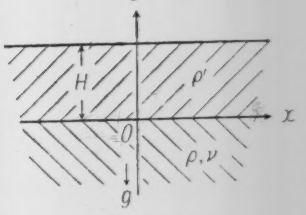

Fig. 2.

$$n_1 = -\xi_1 \pm i\sigma_1, \quad n_2 = -\xi_2 \pm i\sigma_2, \tag{29}$$

then, there are such relations as

$$2(\xi_1 + \xi_2) = \frac{-4\nu k^2}{1+\alpha\,\mathrm{th}\,kH}, \tag{30}$$

$$\xi_1^2+\sigma_1^2+4\xi_1\xi_2+\xi_2^2+\sigma_2^2=\frac{gk(1+\mathrm{th}\,kH)+4\nu^2k^4}{1+\alpha\,\mathrm{th}\,kH}, \tag{31}$$

$$2\xi_1(\xi_2^2+\sigma_2^2)+2\xi_2(\xi_1^2+\sigma_1^2)=\frac{-4\nu k^2gk\,\mathrm{th}\,kH}{1+\alpha\,\mathrm{th}\,kH}, \tag{32}$$

$$(\xi_1^2+\sigma_1^2)(\xi_2^2+\sigma_2^2)=\frac{gk\{gk(1-\sigma)+4\nu^2k^4\}\,\mathrm{th}\,kH}{1+\alpha\,\mathrm{th}\,kH}. \tag{33}$$

From these conditions we shall first solve

$$n^4+n^2\frac{gk(1+\mathrm{th}\,kH)+4\nu^2k^4}{1+\alpha\,\mathrm{th}\,kH}+\frac{gk\{gk(1-\alpha)+4\nu^2k^4\}\,\mathrm{th}\,kH}{1+\alpha\,\mathrm{th}\,kH}=0, \tag{34}$$

under the assumption that νk^2 is small, that is to say, $\xi_1=0$, $\xi_2=0$. Solving (34), we get

$$\sigma_1^2,\ \sigma_2^2=\frac{gk(1+\mathrm{th}\,kH)+4\nu^2k^4}{2(1+\alpha\,\mathrm{th}\,kH)}$$
$$\mp\sqrt{\left\{\frac{gk(1+\mathrm{th}\,kH)+4\nu^2k^4}{2(1+\alpha\,\mathrm{th}\,kH)}\right\}^2-\frac{\{gk(1-\alpha)+4\nu^2k^4\}\,gk\,\mathrm{th}\,kH}{1+\alpha\,\mathrm{th}\,kH}} \tag{35}$$

approximately. Substituting these values of σ_1, σ_2 in (32), and solving (30) and (32), we get

$$\left.\begin{aligned}\xi_1&=\frac{\nu k^2}{1+\alpha\,\mathrm{th}\,kH}\left[1-\frac{1}{\sqrt{M^2-N}}\left\{M-2(1+\alpha\,\mathrm{th}\,kH)\,\mathrm{th}\,kH\right\}\right],\\ \xi_2&=\frac{\nu k^2}{1+\alpha\,\mathrm{th}\,kH}\left[1+\frac{1}{\sqrt{M^2-N}}\left\{M-2(1+\alpha\,\mathrm{th}\,kH)\,\mathrm{th}\,kH\right\}\right],\end{aligned}\right\} \tag{36}$$

where

$$M=1+\mathrm{th}\,kH,\quad N=4(1-\alpha)(1+\alpha\,\mathrm{th}\,kH)\,\mathrm{th}\,kH. \tag{37}$$

Again, substituting the values of ξ_1, ξ_2 in (36) in those of (31), (33), we get more accurate values of σ_1, σ_2 as follows

$$\left.\begin{aligned}\sigma_1&=\sqrt{\frac{1}{2}\left\{P_1-\sqrt{P_1^2-4Q_1}\right\}},\\ \sigma_2&=\sqrt{\frac{1}{2}\left\{P_2+\sqrt{P_2^2-4Q_2}\right\}},\end{aligned}\right\} \tag{38}$$

where

$$P_1=\frac{gkM+4\nu^2k^4}{1+\alpha\,\mathrm{th}\,kH}-\frac{\nu^2k^4}{(1+\alpha\,\mathrm{th}\,kH)^2}\left[3-\frac{1}{\sqrt{M^2-N}}\left\{M-2(1+\alpha\,\mathrm{th}kH)\,\mathrm{th}\,kH\right\}\right]\left[1-\frac{1}{\sqrt{M^2-N}}\left\{M-2(1+\alpha\,\mathrm{th}\,kH)\,\mathrm{th}\,kH\right\}\right],$$

$$Q_1=\frac{\{gk(1-\alpha)+4\nu^2k^4\}\,gk\,\mathrm{th}\,kH}{1+\alpha\,\mathrm{th}kH}-\frac{gk\nu^2k^4M}{(1+\alpha\,\mathrm{th}\,kH)^2}\left[1-\frac{1}{\sqrt{M^2-N}}\left\{M-2(1+\alpha\,\mathrm{th}\,kH)\,\mathrm{th}\,kH\right\}\right]^2,$$

$$P_2=\frac{gkM+4\nu^2k^4}{1+\alpha\,\mathrm{th}\,kH}-\frac{\nu^2k^4}{(1+\alpha\,\mathrm{th}\,kH)^2}\left[3+\frac{1}{\sqrt{M^2-N}}\left\{M-2(1+\alpha\,\mathrm{th}kH)\,\mathrm{th}\,kH\right\}\right]\left[1+\frac{1}{\sqrt{M^2-N}}\left\{M-2(1+\alpha\,\mathrm{th}\,kH)\,\mathrm{th}\,kH\right\}\right],$$

$$Q_2=\frac{\{gk(1-\alpha)+4\nu^2k^4\}\,gk\,\mathrm{th}\,kH}{1+\alpha\,\mathrm{th}\,kH}-\frac{gk\nu^2k^4M}{(1+\alpha\,\mathrm{th}\,kH)^2}\left[1+\frac{1}{\sqrt{M^2-N}}\left\{M-2(1+\alpha\,\mathrm{th}\,kH)\,\mathrm{th}\,kH\right\}\right]^2. \quad (39)$$

From the expressions of σ_1, σ_2 in (38), it is obvious that the vibration corresponding to $n_2=-\xi_2\pm i\sigma_2$ does not participate in the problem of stability. Thus, $n_1=-\xi_1\pm i\sigma_1$ only concerns the stability problem, its condition being

$$\left.\begin{aligned}&P_1-\sqrt{P_1^2-4Q_1}+2\xi_1^2>0 \text{ for stable condition,}\\&P_1-\sqrt{P_1^2-4Q_1}+2\xi_1^2<0 \text{ for unstable condition.}\end{aligned}\right\} \quad (40)$$

The deformations or velocities of the fluids are determined from

$$\left.\begin{aligned}&\phi=Ae^{-\xi t+ky+i(kx\pm\sigma t)}, \qquad \psi=Ce^{-\xi t+my+i(kx\pm\sigma t)},\\&\phi'=A'e^{-\xi t+ky+i(kx\pm\sigma t)}+B'e^{-\xi t-ky+i(kx\pm\sigma t)},\end{aligned}\right\} \quad (41)$$

where

$$\left.\begin{aligned}&\frac{C}{A}=\frac{-2i\nu k^2}{n+2\nu k^2},\\&\frac{A'}{A}=\frac{n(n^2-gk)e^{-kH}}{2(n+2\nu k^2)(n^2\,\mathrm{ch}\,kH+gk\,\mathrm{sh}\,kH)},\\&\frac{B'}{A}=\frac{-n(n^2+gk)e^{kH}}{2(n+2\nu k^2)(n^2\,\mathrm{ch}\,kH+gk\,\mathrm{sh}\,kH)}.\end{aligned}\right\} \quad (42)$$

It will be seen that in this case too, the component of velocity corresponding to the viscous state of the fluid is very small compared with that due to the inviscid state of the same fluid.

5. *Interpretation of the two kinds of vibrations in the above case.*

It has already been ascertained that the vibration corresponding to expression $n_1=-\xi_1\pm i\sigma_1$ only concerns the problem of stability. We shall now examine the kinds of disturbances that the vibrations $n_1=-\xi_1\pm i\sigma_1$, $n_2=-\xi_2\pm i\sigma_2$ represent.

Let us take the case $kH\rightarrow 0$, then

$$\left.\begin{array}{lll}\xi_1=0\,, & \sigma_1^2=gk+4\nu^2k^4, & 0\,, \\ \xi_2=2\nu k^2, & \sigma_2^2=gk\,, & -4\nu^2k^4.\end{array}\right\} \qquad (43)$$

so that $n_2=-\xi_2\pm i\sigma_2=-2\nu k^2\pm i\sqrt{gk}$ represents the gravitational waves on a semi-infinite viscous fluid as already shown by Lamb.[8] In other words, the vibration $n_2=-\xi_2\pm i\sigma_2$ corresponds to the vibration of the free surface of the case of a very thin layer, the vibration being stable even in the present special case.

Let us next take the case $kH\rightarrow\infty$, then

$$\xi_1=\frac{2\nu k^2}{1+\alpha}\,,\quad \xi_2=0\,,\quad \sigma_2^2=gk\,, \qquad (44)$$

the expression of σ_1 being rather complex. Since vibration $n_2=-\xi_2\pm i\sigma_2$ in the present case represents the gravitational waves that are transmitted over the surface of an inviscid fluid, the vibration in question corresponds to the one on the free surface and has no place in the problem of stability.

It is now established that vibration $n_1=-\xi_1\pm i\sigma_1$ concerns the condition at the boundary between the two fluids and contributes much to gravitational stability, whereas vibration $n_2=-\xi_2\pm i\sigma_2$ represents the waves on the free surface and is outside the problem of stability.

6. *The calculation for the case in which there is an inviscid surface layer.*

Using the equations shown in Section 4, we have calculated the ratio of ρ'/ρ, namely α, corresponding to the critical condition of stability for different ratios of L/H, $(L=2\pi/k)$, and gk(and νk^2). The values of gk taken here are $gk\ =0{\cdot}06$ and $0{\cdot}02$, both of which correspond to the waves of lengths, 1 km and 1/3 km respectively. The values of ν, on the other hand, roughly corresponds to the viscosity of rocks or of soils. It should be borne in mind that νk^2 should change in agreement with the change in gk.

---

[8] H. LAMB, *loc. cit.*, 6).

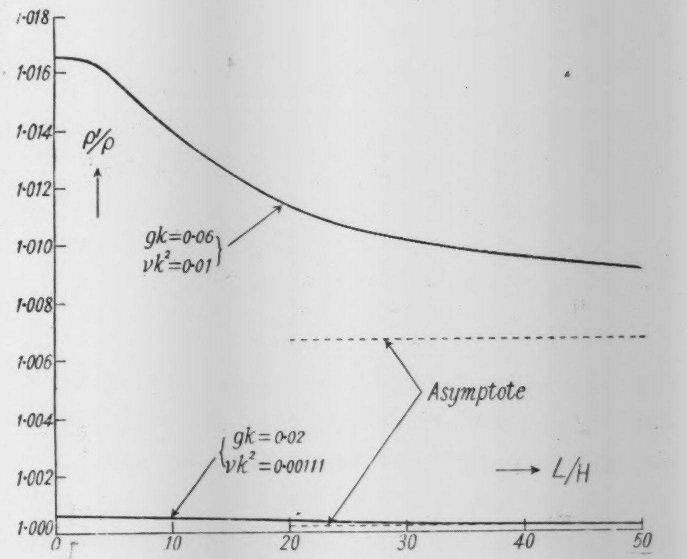

Fig. 3. Critical conditions of stability for two cases.

The calculation for the two conditions (I) $gk=0{\cdot}06$, $\nu k^2=0{\cdot}01$ and (II) $gk=0{\cdot}02$, $\nu k^2=0{\cdot}00111$ are shown in Tables I, II and Fig. 3. It will be seen that the value of ρ'/ρ corresponding to the critical stability decreases as the ratio of L/H increases, that is to say, as the thickness of the surface layer decreases, tending to approach the asymptotic value:

$$\alpha = 1 + 4\nu^2k^3/g \tag{45}$$

for $L/H \to \infty$. This asymptotic value incidentally coincides with the value of α for $\nu'=0$ that has been obtained in using equation (19) in Section 3. The value of α for $L/H=0$ does not agree with that obtained in the manner in Section 2. This results from the assumption in neglecting higher orders of νk^2 in both the cases.

In any case, if the liquid viscosity is not zero, the value of ρ'/ρ corresponding to the critical stability is greater than 1.

Table I. Case I. $gk=0{\cdot}06$, $\nu k^2=0{\cdot}01$.

kH	0	0·1	0·2	0·5	1·0	2·1	π	∞
L/H	∞	62·832	31·416	12·566	6·283	2·994	2·000	0
ρ'/ρ	1·0067	1·0087	1·0100	1·0132	1·0152	1·0164	1·0165	1·0165

Table II. Case II. $gk=0{\cdot}02$, $\nu k^2=0{\cdot}00111$.

kH	0	0·1	0·2	1	2	∞
L/H	∞	62·832	31·416	6·283	3·142	0
ρ'/ρ	1·00025	1·00026	1·00027	1·00057	1·00059	1·00065

7. *Concluding remarks.*

From the mathematical calculation it is shown that in stratified liquids, even should the upper liquid be denser than the lower liquid, the dynamical condition may be stablilized to a certain extent by means of the viscosity of one or both liquids. It was also found that although the disturbance at the boundary between the liquids contributes only to the problem of stability under consideration, disturbance at the free surface, on the other hand, does not participate in the same problem.

In the liquid stage of the earth, as soon as the part near the free surface, as the result of cooling, becomes slightly denser than the subjacent medium, the same part becomes gravitationally unstable and sinks. But, since at such a stage, the liquids were perhaps fairly viscous, stability is likely to have been maintained to a certain extent even if the density relation in the liquid layers was in unstable condition.

The general feature of equilibrium seen in the present state of the earth's crust, is probably a continuation of the stage just mentioned. Some local changes in the gravitational forces may at times result from the unstable displacements of layers in the earth's crust. If that is the case, it ought not to be hopeless to attempt to examine the origin of earthquakes by means of careful observations of crustal deformation, or of changes in the gravitational forces, or even of changes in terrestrial magnetism.

48. 粘性が地球の液狀冷却時代に於ける重力的安定に及ぼす影響

地震研究所 妹澤克惟
金井清

地球が液狀をなして冷却した時代は相當長く續いたものと見てよろしく，その場合に表面から冷却する結果として種々の重力的安定の問題があり得るのである．大體に於ては上層の物質が內部層のそれよりも重くなると，重力的不安定が起る譯であるが，粘性が働く場合には上部の層が少し位重くても安定の狀態が保たれ得るのである．この問題は Rayleigh や Jeffreys も取扱つた事があるけれども，二つの層が接し且つ兩方の層の一方又は兩方が無限に續いてをる場合や自由面のある場合，卽ち地球の問題に直接關係のありそうな場合は未だ手がつけられてをらなかつたので，茲にこの問題を研究して見たのである．

表面層のある場合を理論的に研究して見ると，表面層の自由面の振動と兩方の層の境界に起る振動とになる．表面の振動は如何なる場合にも安定であるけれども境界の振動は兩方の層の比重と粘性とによつて不安定になるのである．

無限に厚い層が接する場合には，勿論兩方の境界面の振動の安定不安定が問題となるのである．

粘性はいつでも安定狀態を助けることになる．而も液體の全部が粘性をもつ必要がなく，その一方だけに粘性があつても不安定の狀態が安定の狀態になり得るのである 之は表面の層が薄い場合にも無限に厚い場合にもあり得るものである．

現在の地殼は液體の狀態からは殆ど脫してをるとはいへ，極めて遲い運動については可なり液狀の運動があるものと見てもよい譯である．又，冷却して行く狀態も既になくなつてをるとはいへ，地殼の水平壓力のため輕い層が重い層の下に入り込むこともあり得る譯である．大陸の邊緣等にはこのやうな狀態があるであらう．その場合の重力的不安定の問題はたしかに地震の原因と結びつけられるものと思はれる．又，下層の物質に於ける熱力學的又は放射能的變化の結果として密度の變化が起ることも考へられる．茲にも重力的の不安定の問題があり得るのである．地殼の變形乃至は地球上の重力，地磁氣，地電流等の時間的變化を測定する事は以上の點に於て大いに意味があるものと考へられる．但し粘性の影響も大いにある事をも記憶して問題を取扱ふ必要があるのである．

49. *Theory of the Aseismic Properties of the Brace Struts (Sudikai) in a Japanese-style Building.*
(Preliminary Notes)

By Katsutada SEZAWA and Kiyoshi KANAI,

Earthquake Research Institute.

(Read Sept. 20, 1938.—Received Sept. 20, 1938)

1. *Aseismic properties of the brace struts* (*sudikai*) *in Japanese-style buildings.*

Brace struts (sudikai) have been used as structural members in almost every Japanese-style building that has been newly erected or reconstructed since the Great Kwantô Earthquake of 1923.[1] Although it is well known that these brace struts show excellent aseismic properties, no theoretical examination of these properties has yet been made. Miura[2] has given a solution of the problem in which a framed structure with inclined columns is subjected to horizontal forces, but his results cannot be applied to the present case. Obviously, it is of practical importance to know what sort of brace strut possesses the aseimic properties necessary for a particular kind of building, which subject we shall now investigate from the mathematical point of view.

We shall first deal with the case in which both ends of the brace strut are hinged, and then treat the case in which the two ends are clamped. As to the kind of building, we shall restrict ourselves to a one-storied building, the floor being endless horizontally, reserving the more complicated cases for treatment by one of us (Kanai) later.

2. *The case in which both ends of a brace strut are hinged.*

For simplicity, it is assumed that the masses are concentrated at the panel points, in consequence of which the mass for horizontal movement will differ from that for vertical movement, the respective masses in question thus being m_1, m_2. Let l_1, l_2, l_3 be the length of a column, beam span, and length of a brace strut respectively; let also E_1I_1, E_2I_2, E_3I_3; E_1a_1,

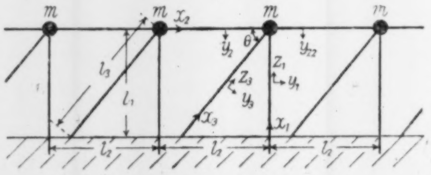

Fig. 1.

---

[1] The Earthquake Investigation Committe has been encouraging the use of brace struts ever since the Tokyo Earthquakes of 1894.

[2] A. MIURA, *Journ. Soc. Arch., Japan*, **43** (1929), 409~417.

E_2a_2, E_3a_3 be the bending and longitudinal stiffnesses of the respective members just mentioned. The lateral displacements y_1, y_2, y_3 and the longitudinal displacements z_1, z_2, z_3 of the respective members satisfy differential equations of the types

$$\partial^4 y/\partial x^4 = 0\,, \quad \partial^2 z/\partial x^2 = 0\,. \tag{1}$$

The solutions of the above equations are

$$\left.\begin{aligned} y_1 &= A_1 + B_1 x + C_1 x^2 + D_1 x^3, & z_1 &= \alpha_1 + \beta_1 x_1, \\ y_2 &= A_2 + B_2 x + C_2 x^2 + D_2 x^3, & z_2 &= \alpha_2 + \beta_2 x_2, \\ y_3 &= A_3 + B_3 x + C_3 x^2 + D_3 x^3, & z_3 &= \alpha_3 + \beta_3 x_3, \end{aligned}\right\} \qquad (2),\ (3)$$

in which y_3 is unnecessary in the present case.

Taking the senses of the coordinates in the respective members as shown in Fig. 1, the boundary conditions are such that

$$x_1 = 0; \qquad y_1 = 0, \quad \frac{dy_1}{dx_1} = 0\,, \quad z_1 = 0\,, \qquad (4),\ (5),\ (6)$$

$$x_3 = 0; \qquad z_3 = 0\,, \qquad (7)$$

$$x_1 = l_1, \quad x_2 = l_2, \quad x_{22} = 0\,, \quad x_3 = l_3; \qquad y_2 = y_{22} = -z_1, \qquad (8),\ (9)$$

$$z_3 = z_1 \sin\theta + y_1 \cos\theta\,, \quad \frac{dy_1}{dx_1} = \frac{dy_2}{dx_2} = \frac{dy_{22}}{dx_{22}}\,, \qquad (10),\ (11),\ (12)$$

$$-E_1I_1 \frac{d^2y_1}{dx_1^2} - E_2I_2\left(\frac{d^2y_2}{dx_2^2} - \frac{d^2y_{22}}{dx_{22}^2}\right) = 0\,, \tag{13}$$

$$-E_1I_1 \frac{d^3y_1}{dx_1^3} + E_3a_3 \frac{dz_3}{dx_3} \cos\theta = m_1p^2y_1, \tag{14}$$

$$E_2I_2\left(\frac{d^3y_{22}}{dx_{22}^3} - \frac{d^3y_2}{dx_2^3}\right) - E_3a_3 \frac{dz_3}{dx_3} \sin\theta - E_1a_1 \frac{dz_1}{dx_1} = m_2p^2y_2. \tag{15}$$

Substituting (2), (3) in (4) ~ (15), we get the frequency equation for free vibrations of the frame as follows:

$$\begin{aligned} &\gamma_1\gamma_2(1+3\zeta_1\beta) - \gamma_1\xi_1(1+3\zeta_1\beta)(1+\vartheta_1\alpha\sin^2\theta) \\ &\quad - \gamma_2\left\{3(1+12\zeta_1\beta) + \vartheta_1\xi_1\alpha(1+3\zeta_1\beta)\cos^2\theta\right\} \\ &\quad + \xi_1\left\{3(1+12\zeta_1\beta)(1+\vartheta_1\alpha\sin^2\theta) + \vartheta_1\xi_1\alpha(1+3\zeta_1\beta)\cos^2\theta\right\} = 0\,, \end{aligned} \tag{16}$$

where

$$\gamma_1=\frac{m_1p^2l_1^3}{E_1I_1}, \quad \gamma_2=\frac{m_2p^2l_1^3}{E_1I_1}, \quad \vartheta_1=\frac{E_3a_3}{E_1a_1},$$

$$\zeta_1=\frac{E_2I_2}{E_1I_1}, \quad \xi_1=\frac{a_1l_1^2}{I_1}, \quad \alpha=\frac{l_1}{l_3}, \quad \beta=\frac{l_1}{l_2}. \tag{17}$$

The equation (16) gives two vibrational frequencies, the one corresponding to motion of horizontal type and the other to that of vertical type. It must be borne in mind that the terms 'horizontal type' and 'vertical type' do not mean pure horizontal motion and pure vertical motion; they are nothing more than the conditions that whereas in the first case there is a relatively large horizontal component of displacement, in the second there is a relatively large vertical component of displacement.

If we assume as usually done, that, the inertia mass for the movement in vertical sense is the same as that for the movement in horizontal sense, it is possible to put $\gamma_1=\gamma_2$, from which the frequency equation reduces to

$$\gamma=\frac{Q\pm\sqrt{Q^2-4PR}}{2P}, \tag{18}$$

where

$$\left.\begin{aligned} P&=1+3\zeta_1\beta,\\ Q&=3(1+12\zeta_1\beta)+\xi_1(1+3\zeta_1\beta)(1+\vartheta_1\alpha),\\ R&=\xi_1\Big\{3(1+12\zeta_1\beta)(1+\vartheta_1\alpha\sin^2\theta)+\vartheta_1\xi_1\alpha(1+3\zeta_1\beta)\cos^2\theta\Big\}. \end{aligned}\right\} \tag{19}$$

This equation will be used in the numerical calculations, the results of which will be found in the next section.

(i) In the special case in which the inertia force that is directed in vertical sense is neglected, the frequency equation assumes the form

$$\gamma_1=\frac{3(1+12\zeta_1\beta)(1+\vartheta_1\alpha\sin^2\theta)+\vartheta_1\xi_1\alpha(1+3\zeta_1\beta)\cos^2\theta}{(1+3\zeta_1\beta)(1+\vartheta_1\alpha\sin^2\theta)}, \tag{20}$$

which may be used for obtaining the resonance condition in the case of horizontal earthquake motion.

(ii) In the case in which the inertia force that is directed in horizontal sense is neglected, the frequency equation assumes the form

$$\gamma_2=\frac{\xi_1\{3(1+12\zeta_1\beta)(1+\vartheta_1\alpha\sin^2\theta)+\vartheta_1\xi_1\alpha(1+3\zeta_1\beta)\cos^2\theta\}}{3(1+12\zeta_1\beta)+\vartheta_1\xi_1\alpha(1+3\zeta_1\beta)\cos^2\theta}, \tag{21}$$

which may be used for determining the resonance condition in the case of vertical earthquake motion.

(iii) In the special case $\vartheta=E_3a_3/E_1a_1=0$, that is to say, in which there is no brace strut, the frequency equation (18) reduces to two equations

$$\gamma=3(1+12\zeta\beta)/(1+3\zeta\beta),\quad \gamma=\xi, \tag{18$'$}$$

the first representing the pure horizontal oscillation of a braceless framed structure and the second the purely vertical oscillation of the same structure. The two equations in (18′) can also be obtained by putting $\vartheta=0$ in the respective equations (20), (21).

3. *Numerical examples of the above case and their interpretation.*

With a view to ascertaining the aseismic properties of brace struts, we have selected some cases of numerical conditions.

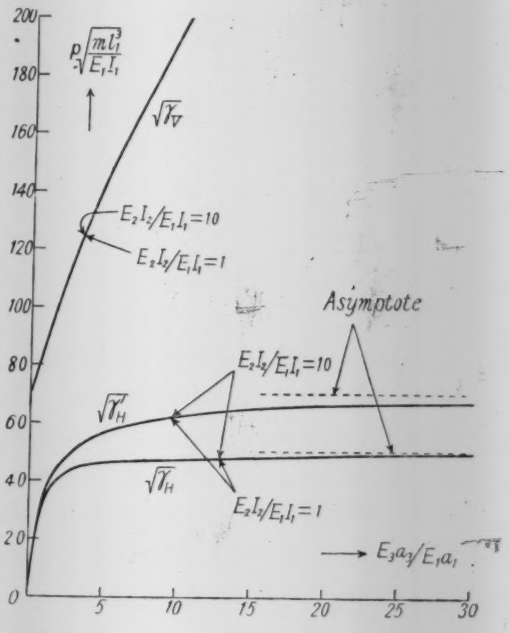

Fig. 2. $\theta=45°$, $\frac{l_1}{l_2}=1$, $\frac{a_1l_1^2}{I_1}=5000$.

(i) First, let $\theta=45°$, $l_2/l_1=1$, $a_1l_1^2/I_1=5000$[3] be the given lower end of the brace strut at the foot of the column. The vibrational frequences of horizontal type $\sqrt{\gamma_H}$ and those of vertical type $\sqrt{\gamma_V}$ for the two cases $\zeta=E_2I_2/E_1I_1=1$, 10, as accurately calculated by means of the equation (19), are shown by $\sqrt{\gamma_H}$, $\sqrt{\gamma_V}$ respectively in Fig. 2. The respective curves $\sqrt{\gamma_H}$, $\sqrt{\gamma_V}$ assume the same values irrespective of that of $\zeta=E_2I_2/E_1I_1$, which shows that the effect of stiffness of the beam is negligible compared with that of the brace strut. It will also be seen that the vibrational frequency in the horizontal type increases very rapidly with increase in the ratio of $\vartheta=E_3a_3/E_1a_1$, particularly in the range $E_3a_3/E_1a_1=0\sim5$. Beyond a certain ratio of E_3a_3/E_1a_1, namely $E_3a_3/E_1a_1>5$ in the present case, the frequency assumes an asymptotic value, at which the vibration of horizontal type changes to rotational vibration of the brace strut about its lower hinge. The vibration of vertical type increases more rapidly with increase in the ratio of $\vartheta = E_3a_3/E_1a_1$ through the whole range of the same ratio. It appears that at a very large ratio of E_3a_3/E_1a_1, say, larger than $E_3a_3/E_1a_1 > 5$, to the vibration of vertical type changes to the longitudinal vibration of the brace strut.

---

[3] When the diameter of a circular column is 1/2 foot and its height 10 feet, the values of $a_1l_1^2/I_1$ becomes 6400, so that $a_1l_1^2/I_1=5000$ is rather near that in practice.

The approximate values of $\sqrt{\gamma'_H}$ for the horizontal vibration can be obtained by means of the equation (20), the results of which are shown by the curve $\sqrt{\gamma'_H}$ in Fig. 2. It will be seen that for a small ratio of E_3a_3/E_1a_1, say, less than $E_3a_3/E_1a_1 \doteqdot 1$, the approximate results in question agree well with those obtained with accurateness. For a relatively large value of E_3a_3/E_1a_1, say, larger than $E_3a_3/E_1a_1 = 1$, the approximate values of the frequency are larger than the accurate ones, which is obvious from Rayleigh's dynamical principle. In this case, too, there is an asymptotic value of the frequency for a very large value of E_3a_3/E_1a_1.

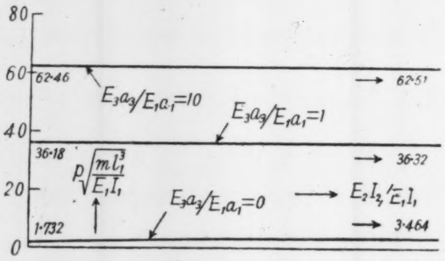

Fig. 3. The value γ'_H. $\theta = 45°$, $\frac{l_1}{l_2} = 1$, $\frac{a_1l_1^2}{I_1} = 5000$.

As a matter of fact, it has been known that increase in the longitudinal stiffness of a brace strut is enormously effective in raising the vibrational frequency of the framed structure.

(ii) The above results may be shown in another way. The change in vibrational frequency of horizontal type (approximate value) with change in E_2I_2/E_1I_1 for three cases $E_3a_3/E_1a_1 = 0$, 1, 10 are shown in Fig. 3. It will be seen that the change in E_2I_2/E_1I_1 is almost ineffective compared with that in E_3a_3/E_1a_1.

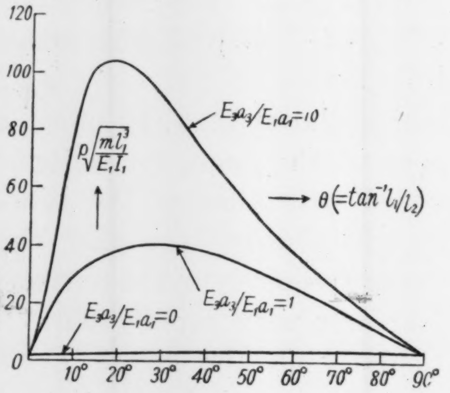

Fig. 4. $\frac{E_2I_2}{E_1I_1} = 10$, $\tan\theta = \frac{l_1}{l_2}$, $\frac{a_1l_1^2}{I_1} = 5000$.

(iii) We shall next consider the effect of change in beam span, for three cases $E_3a_3/E_1a_1 = 0$, 1, 10 (the bottom hinge of the brace strut is at the foot of the column); the ratios of $E_2I_2/E_1I_1 = 10$ and $a_1l_1^2/I_1 = 5000$ being kept constant. There is a maximum of vibrational frequency at a certain angle $\theta = \tan^{-1}(l_1/l_2)$ for every ratio of E_3a_3/E_1a_1, which is also apparent from the fact that a brace strut that is excessively inclined or almost upright does not much participate in the resistance to vibration. When the pin-joint brace strut is upright, the position of the brace strut in question coincides with that of the column, the bending moments of the strut at its both ends then being zero, and also the beam span becomes zero, in consequence of which the vibrational frequency of horizontal vibration becomes $\gamma_{\prime\prime}=12m_1p^2l^3/E_1I_1$, that is, the frequency assumed by the braceless framed structure of the extremely rigid floor. When the pin-joint brace strut inclines almost horizontally, the vibrational frequency, as a matter of fact, assumes the value for the case of a braceless framed structure of the infinitely flexible floor. With increase in the ratio of E_3a_3/E_1a_1, the angle at which the vibrational frequency is maximum, decreases, from which it is possible to conclude that in the case of a thin brace strut, the inclination θ of the same strut to horizontal should be fairly large for getting an efficient aseismic condition.

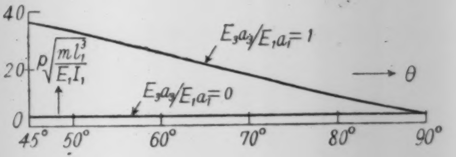

Fig. 5. $\frac{E_2I_2}{E_1I_1}=10$, $\frac{a_1l_1^2}{I_1}=5000$, $\frac{l_1}{l_2}=1$.

(iv) Finally, we shall take the case in which, column height l_1 and beam span l_2 being the same, the inclination of the brace strut alone is changed (the bottom hinge of the brace strut is not at the foot of the column). The vibrational frequencies for various inclinations of the brace strut (the ratios $E_2I_2/E_1I_1=10$, $a_1l_1^2/I_1=5000$, $l_1/l_2=1$ being kept constant) for two cases of E_3a_3/E_1a_1, i. e. $E_3a_3/E_1a_1=0$, 1, are shown in Fig. 5. In the nature of things, the most effective condition is given by $\theta=45°$.

4. *The solutions for the case in which both ends of the brace strut are clamped.*

The equations and solutions for the present case are shown in (1), (2), (3) in Section 2. The boundary conditions are such that

$$x_1=0; \qquad y_1=0, \quad \frac{dy_1}{dx_1}=0, \quad z_1=0, \qquad (22),\ (23),\ (24)$$

$$x_3=0; \qquad y_3=0, \quad \frac{dy_3}{dx_3}=0, \quad z_3=0, \qquad (25),\ (26),\ (27)$$

$$x_1=l_1, \quad x_2=l_2, \quad x_{22}=0, \quad x_3=l_3; \qquad y_3=y_1\sin\theta+y_2\cos\theta, \qquad (28)$$

$$z_3=z_1\sin\theta+y_1\cos\theta, \quad y_2=y_{22}=-z_1, \qquad (29),\ (30),\ (31)$$

$$\frac{dy_1}{dx_1}=\frac{dy_2}{dx_2}=\frac{dy_{22}}{dx_{22}}=\frac{dy_3}{dx_3}, \qquad (32),\ (33),\ (34)$$

$$-E_1I_1\frac{d^2y_1}{dx_1^2}-E_2I_2\left(\frac{d^2y_2}{dx_2^2}-\frac{d^2y_{22}}{dx_{22}^2}\right)-E_3I_3\frac{d^2y_3}{dx_3^2}=0\,, \tag{35}$$

$$-E_1I_1\frac{d^3y_1}{dx_1^3}-E_3I_3\frac{d^3y_3}{dx_3^3}\sin\theta+E_3a_3\frac{dz_3}{dx_3}\cos\theta=m_1p^2y_1, \tag{36}$$

$$E_2I_2\left(\frac{d^3y_{22}}{dx_{22}^3}-\frac{d^3y_2}{dx_2^3}\right)-E_3I_3\frac{d^3y_3}{dx_3^3}\cos\theta-E_3a_3\frac{dz_3}{dx_3}\sin\theta-E_1a_1\frac{dz_1}{dx_1}=m_2p^2y_2. \tag{37}$$

Here too, the inertia mass for horizontal vibration and that for vertical vibration are assumed to differ. Substituting (2), (3) in (22) ~ (37), we obtain the frequency equation for natural vibrations, namely,

$$\begin{aligned}
&\gamma_1\gamma_2(1+3\zeta_1\beta+\zeta_2\alpha)\\
&\quad-\gamma_1\left\{(1+3\zeta_1\beta+\zeta_2\alpha)(12\zeta_2\alpha^3\cos^2\theta+\xi_1+\vartheta_1\xi_1\alpha\sin^2\theta)-9\zeta_2^2\alpha^4\cos^2\theta\right\}\\
&\quad-\gamma_2\left\{3(1+12\zeta_1\beta+4\zeta_2\alpha)+3\zeta_2\alpha^2(4\alpha-6\operatorname{cosec}\theta+12\zeta_1\alpha\beta+\zeta_2\alpha^2)\sin^2\theta\right.\\
&\qquad\qquad\left.+\vartheta_1\xi_1\alpha(1+3\zeta_1\beta+\zeta_2\alpha)\cos^2\theta\right\}\\
&\quad+\Big[36\zeta_2\alpha^3(1+12\zeta_1\beta+\zeta_2\alpha)\cos^2\theta+3\xi_1\left\{(1+12\zeta_1\beta+4\zeta_2\alpha)\right.\\
&\qquad\qquad\left.+\zeta_2\alpha^2(4\alpha-6\operatorname{cosec}\theta+12\zeta_1\alpha\beta+\zeta_2\alpha^2)\sin^2\theta\right\}\\
&\quad+3\xi_1\vartheta_1\alpha\left\{(1+12\zeta_1\beta+4\zeta_2\alpha)\sin^2\theta+\zeta_2\alpha^2(4\alpha-6\sin\theta+12\zeta_1\alpha\beta+\zeta_2\alpha^2)\right\}\\
&\qquad\qquad+\xi_1^2\vartheta_1\alpha(1+3\zeta_1\beta+\zeta_2\alpha)\cos^2\theta\Big].
\end{aligned} \tag{38}$$

where

$$\gamma_1=\frac{m_1p^2l_1^3}{E_1I_1}\,,\quad \gamma_2=\frac{m_2p^2l_1^3}{E_1I_1}\,,\quad \vartheta_1=\frac{E_3a_3}{E_1a_1}\,,\quad \zeta_1=\frac{E_2I_2}{E_1I_1}\,,$$

$$\zeta_2=\frac{E_3I_3}{E_1I_1}\,,\quad \xi_1=\frac{a_1l_1^2}{I_1}\,,\quad \alpha=\frac{l_1}{l_3}\,,\quad \beta=\frac{l_1}{l_2}\,, \tag{39}$$

one of the frequencies corresponding to vibration of horizontal type and the other to vibration of vertical type.

If we assume, as usually done, that the inertia mass for movement in the horizontal sense is the same as that for movement in the vertical sense, it is possible to put $\gamma_1=\gamma_2$, from which the frequency equation (38) reduces to

$$\gamma=\frac{Q\pm\sqrt{Q^2-4PR}}{2P}, \tag{40}$$

where

$$\begin{aligned} P &= 1+3\zeta_1\beta+\zeta_2\alpha, \\ Q &= 3\left\{(1+12\zeta_1\beta+4\zeta_2\alpha)+\zeta_2\alpha^2(4\alpha-6\sin\theta+12\zeta_1\alpha\beta+\zeta_2\alpha^2)\right\} \\ &\qquad +\xi_1(1+3\zeta_1\beta+\zeta_2\alpha)(1+\vartheta_1\alpha), \\ R &= 36\zeta_2\alpha^3(1+12\zeta_1\beta+\zeta_2\alpha)\cos^2\theta \\ &\quad +3\xi_1\left\{(1+12\zeta_1\beta+4\zeta_2\alpha)+\zeta_2\alpha^2(4\alpha-6\operatorname{cosec}\theta+12\zeta_1\alpha\beta+\zeta_2\alpha^2)\sin^2\theta\right\} \\ &\quad +3\xi_1\vartheta_1\alpha\left\{(1+12\zeta_1\beta+4\zeta_2\alpha)\sin^2\theta+\zeta_2\alpha^2(4\alpha-6\sin\theta+12\zeta_1\alpha\beta+\zeta_2\alpha^2)\right\} \\ &\qquad +\xi_1^2\vartheta_1\alpha(1+3\zeta_1\beta+\zeta_2\alpha)\cos^2\theta. \qquad (41) \end{aligned}$$

(i) If the effect of inertia mass in vertical sense were neglected, the expression for the approximate frequency equation would then assume the form

$$\begin{aligned} \gamma_1\Phi &= 36\zeta_2\alpha^3(1+12\zeta_1\beta+\zeta_2\alpha)\cos^2\theta \\ &\quad +3\xi_1\left\{(1+12\zeta_1\beta+4\zeta_2\alpha)+\zeta_2\alpha^2(4\alpha-6\operatorname{cosec}\theta+12\zeta_1\alpha\beta+\zeta_2\alpha^2)\sin^2\theta\right\} \\ &\quad +3\xi_1\vartheta_1\alpha\left\{(1+12\zeta_1\beta+4\zeta_2\alpha)\sin^2\theta+\zeta_2\alpha^2(4\alpha-6\sin\theta+12\zeta_1\alpha\beta+\zeta_2\alpha^2)\right\} \\ &\qquad +\xi_1^2\vartheta_1\alpha(1+3\zeta_1\beta+\zeta_2\alpha)\cos^2\theta, \qquad (42) \end{aligned}$$

where

$$\Phi=(1+3\zeta_1\beta+\zeta_2\alpha)(12\zeta_2\alpha^3\cos^2\theta+\xi_1+\vartheta_1\xi_1\alpha\sin^2\theta)-9\zeta_2^2\alpha^4\cos^2\theta, \quad (43)$$

which can be used to find the resonance condition in the case of horizontal seismic vibration.

(ii) If the effect of inertia mass in horizontal sense were neglected, the approximate frequency equation would then become

$$\begin{aligned} \gamma_2\Phi &= 36\zeta_2\alpha^3(1+12\zeta_1\beta+\zeta_2\alpha)\cos^2\theta \\ &\quad +3\xi_1\left\{(1+12\zeta_1\beta+4\zeta_2\alpha)+\zeta_2\alpha^2(4\alpha-6\operatorname{cosec}\theta+12\zeta_1\alpha\beta+\zeta_2\alpha^2)\sin^2\theta\right\} \\ &\quad +3\xi_1\vartheta_1\alpha\left\{(1+12\zeta_1\beta+4\zeta_2\alpha)\sin^2\theta+\zeta_2\alpha^2(4\alpha-6\sin\theta+12\zeta_1\alpha\beta+\zeta_2\alpha^2)\right\} \\ &\qquad +\xi_1^2\vartheta_1\alpha(1+3\zeta_1\beta+\zeta_2\alpha)\cos^2\theta, \qquad (44) \end{aligned}$$

where

$$\begin{aligned} \Phi &= 3(1+12\zeta_1\beta+4\zeta_2\alpha)+3\zeta_2\alpha^2(4\alpha-6\operatorname{cosec}\theta+12\zeta_1\alpha\beta+\zeta_2\alpha^2)\sin^2\theta \\ &\qquad +\vartheta_1\xi_1\alpha(1+3\zeta_1\beta+\zeta_2\alpha)\cos^2\theta. \qquad (45) \end{aligned}$$

(iii) In the special case, if we put $\vartheta_1=E_3a_3/E_1a_1=0$, $\zeta_2=E_3I_3/E_1I_1=0$ in (40), we get two frequency equations

$$\gamma=3(1+12\zeta_1\beta)/(1+3\zeta_1\beta), \quad \gamma=\xi, \tag{40'}$$

the former corresponding to the frequency equation of purely horizontal vibration of a braceless framed structure and the latter to that of purely vertical vibration of the same structure. Two equations in (40′) can also be obtained by putting $\vartheta_1=E_3a_3/E_1a_1=0$, $\zeta_2=E_3I_3/E_1I_1=0$ in (42), (44).

(iv) In the special case, if we put $\theta=90°$ in (40), we have two frequency equations

$$\gamma=\frac{3(1+\zeta_2)\{(1+\zeta_2)+12\zeta_1\beta\}}{(1+\zeta_2)+3\zeta_1\beta}, \quad \gamma=\xi_1(1+\vartheta_1), \tag{40''}$$

the former and the latter of which correspond to the frequency equations of uncoupled vibrations of the braceless framed structure in horizontal and in vertical senses respectively. In this case, the longitudinal or bending stiffness corresponding to that of the column is equal to the sum of the longitudinal (or bending) stiffness in the column and that in the brace strut. In the nature of things, the two equations in (40″) can also be obtained by putting $\theta=90°$ in (42), (44) respectively.

(v) In the special case, if $\vartheta_1=E_3a_3/E_1a_1=\infty$, $\zeta_2=E_3I_3/E_1I_1=\infty$, we have two vibrational frequencies

$$\gamma=\alpha\vartheta_1\xi_1, \quad \gamma=3\zeta_2\alpha^3. \tag{40'''}$$

The former corresponds to the frequency equation of the flexural vibration of the brace strut with its lower end in clamped condition, whereas the latter represents the frequency equation of longitudinal vibration of the brace strut under consideration. These features of the problem are quite similar to those shown in the preceding broblem.

5. *Numerical examples of the above case and their interpretation.*

(i) We shall now show the nature of the above case more quantitatively in performing the numerical calculation. Assuming that $l_1/l_2=1$, $\tan\theta=1$, $a_1l_1^2/I_1=5000$, $E_3a_3/E_1a_1=E_3I_3/E_1I_1$ (for simplicity) and using the equation (40), we have calculated the vibrational frequencies for various ratios of E_3a_3/E_1a_1 in the two conditions $E_2I_2/E_1I_1=1$, 10; the vibration of horizontal type and that of vertical type being $\sqrt{\gamma_H}$, $\sqrt{\gamma_V}$ respectively in Fig. 6. The approximate values of $\sqrt{\gamma_H}$ for the horizontal vibration can be obtained by means of equation (42), the results of which are shown by curve $\sqrt{\gamma'_H}$ in Fig. 6.[4]

It will be seen that the frequency curves are quite similar to those shown in the case of the brace strut being hinged at its two ends. The condition that the frequencies are almost independent of the ratio of E_2I_2/E_1I_1, resembles that in the previous case. Another remarkable similarity between the present and the previous cases is that, whereas for a smaller ratio of E_3a/E_1a_1 the frequency increases very rapidly with increase in E_3a_3/E_1a_1, for a larger ratio of E_3a_3/E_1a_1 the increase in frequency with increase in the same ratio, E_3a_3/E_1a_1, is very gradual, the exception being that in the present case, since $\sqrt{\gamma_H}$ increases indefinitely as $E_3a_3/E_1a_1 \rightarrow \infty$, no asymptotic value in the $\sqrt{\gamma_H}$ curve exists when the ratio of E_3a_3/E_1a_1 is very large.

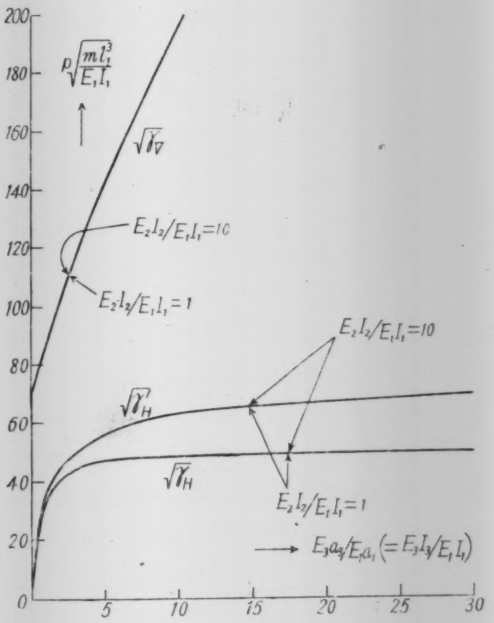

Fig. 6. $\dfrac{l_1}{l_2}=\tan\theta$, $\theta=45°$, $\dfrac{a_1l_1^2}{I_1}=5000$.

(ii) We shall next consider the effect of change in beam span for three cases $E_3I_3/E_1I_1=E_3a_3/E_1a_1=0$, 1, 10 (the bottom hinge of the brace strut is at the foot of the column); the ratio of $E_2I_2/E_1I_1=10$ and $a_1l_1^2/I_1=5000$ being kept constant. The results are shown in Fig. 7. Since we have used the exact formula, there are two frequencies of vibrations, one for horizontal type and one for vertical type. In this case the angle θ at which the frequency of vibration of horizontal type is maximum, is fairly large, say, $\theta=10°$ in the case $E_3a_3/E_1a_1=10$ and $\theta=30°$ in the case $E_3a_3/E_1a_1=1$. Speaking generally, in this case too, the angle θ at which the frequency of vibration of horizontal type is maximum, decreases with increase in E_3I_3/E_1I_1. The angle at which the frequency of vibration of vertical type is maximum is $\theta=90°$ in any case. When the brace strut is upright, the frequency of vibration of horizontal type is expressed by $\gamma_H=12m_1p^2l_1^3/(E_1I_1+E_3I_3)$, which represents the condition that, the beam span being extremely small, the brace strut takes part in the resistance of the column for the case of extremely rigid floor.

---

[4] In the present case the lower end of the brace strut is at the foot of the column.

(iii) As another example of the present calculation, the vibrational frequencies for various ratios of l_3/l_1 in the case $E_3a_3/E_1a_1=E_3I_3/E_1I_1=0,\ 10$, $E_2I_2/E_1I_1=10$, $a_1l_1^2/I_1=5000$, $l_1/l_3=\sin\theta$, have been examined, the result of which is plotted in Fig. 8.[5] In this case, too, the general feature of the problem is the same as that in the preceding section.

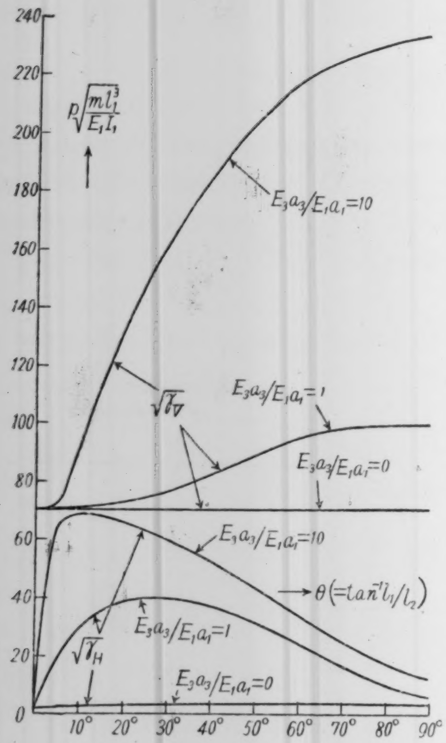

Fig. 7. $\frac{E_2I_2}{E_1I_1}=10$, $\frac{a_1l_1^2}{I_1}=5000$, $\tan\theta=\frac{l_1}{l_2}$.

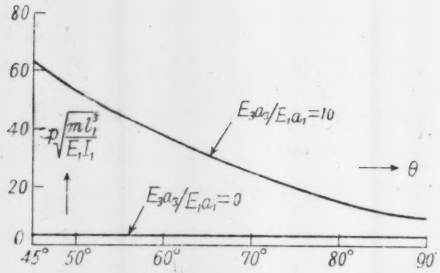

Fig. 8. $\frac{E_2I_2}{E_1I_1}=10$, $\frac{a_1l_1^2}{I_1}=5000$, $\frac{l_1}{l_2}=1$.

6. *General summary and concluding remarks.*

By mathematical investigations, we have ascertained the dynamical condition of the aseismic properties of the brace strut. There are two vibrational frequencies, the one corresponding to vibrations of horizontal type and the other to vibrations of vertical type, both of which are more or less in coupled condition in the case of the brace strut being fitted to a framed structure. In the case of no brace strut, the two vibrations just mentioned are in uncoupled condition.

In the case in which the longitudinal stiffness of the brace strut is small, a small increase in the same stiffness enormously increases the vibrational frequency of the framed structure, whereas in the case of the longitudinal stiffness being fairly large, even increase in the same stiffness can scarcely increase the vibrational frequency in question. It is also noteworthy that when there is a brace strut, the flexural stiffness of the beam has little to do with the aseismic properties of the framed structure.

---

[5] In the present case, the lower end of the brace strut is not necessarily at the foot of the column.

Although in this paper the aseismic properties of only a singled-storied framed structure with endless floor have been investigated, there are a number of other cases to be discussed, the results of investigation of which will be published later.

In conclusion we wish to express our thanks to Mr. Unoki, whose aid in the present investigation was of great value. Finally, we wish to express our warmest thanks to the Council of the Japan Society for the Promotion of Scientific Research for aid received in a series of investigation, of which this is a part.

49. 筋違の耐震効果の理論（序報）

地震研究所 妹澤克惟
金井清

筋違が家屋の耐震上に特に効果のある事はあまりにもよく知られてをる．しかし如何なる程度の寸法のものが必要かさいふ段になるさ必しもわかり切つた問題でないのである．然るに筋違に關する耐震の理論は今迄不思議に殆ご誰によつても研究されてをらぬやうである．以上の點からこの問題を一度充分に而も理論的にしらべて見る事にしたのである．但しこの論文はそのいさぐちに過ぎないのであつて，種々の場合又は一般的の本論は著者の一人によつて近いうちに報告できる積りである．この論文からわかつた要點を述べるさ次の如くである．

一階建で而も床が横に無限に長い場合に，各張間毎に筋違のある場合を考へる．その自己振動數には卓越水平振動のものさ卓越上下振動のものさがあるが，しかし振動型は筋違のためにこの兩者の型が聯成してをるのである．又，筋違の長さの方向の剛度が低い間はこの剛度を少しく增すさ，架構の振動數が著しく高くなり，同じ剛度が相當に大きくなつてる場合にはそれ以上この剛度を增しても架構の振動數は一定以上に高くならぬこさがわかつた．尙又，筋違が有效な狀態では梁の屈曲剛度は殆ご役に立たぬこさもわかつたのである．

以上の外に筋違がある場合の張間さ柱高さの間の耐震的有效比や筋違の脚部の位置さ柱の脚部の位置さの關係等をも研究して置いた．

50. Geophysical Studies of Mihara Volcano, Oosima Island. IV.

A Minor Activity of Volcano Mihara, August 11, 1938.

By Takesi NAGATA,

Earthquake Research Institute.

(Read Sept. 21, 1938.—Received Sept. 21, 1938.)

1. Mihara Volcano has been calm since the great eruption during the period of 1911～1914, as already reported by the writer[1]. Minor activities of the volcano, however, observed several times after the great eruption, the most recent being a succession of miniature eruptions that occurred on August 11, 1938, which was the severest since the outburst of September 1934. Before the volcano became active, its crater bottom was covered with a solidified lava-sheet pierced with several openings. From the midnight of August 10, new incandescent lava-flows began to spread over the bottom, until in the early morning of 11 th, the surface of the lave-flow rose to a height of 35 *m* from the bottom. Throughout this activity, gas was emitted violently once or twice every minute, simultaneously with which fragments of incandescent or solidified lava were projected. This activity reached maximum at about 6 *h* of the 11 th, which from 8 *h* began to cease down with decrease of lava-flow. At 11 *h*, the incandescent lava-flow settled down to its usual depth below the crater-bottom, solidified lava sheets still adhering to the pit-wall. The maximum height of the lava that welled up could therefore be estimated by measuring the height of the lava-sheet.

2. Although no fragments of incandescent lava that was projected during the recent activity reached as far as the pit-mouth, those of the solidified lava were thrown out of the pit and fell around the pit-mouth. The fragments are porous, black basalt of diameters from 2·5 to 6·0 *cm*. These projected fragments are "Miharaite" as determined petrologically by S. Tsuboi[2]. They were in an amorphous state and very porous, the mean density being 0·5～0·7. Several of these specimens are shown in Fig. 1, and the distribution of the projected fragments in Fig. 2

---

[1] R. TAKAHASI and T. NAGATA, *Bull. Earthq. Res. Inst.*, **15** (1937), 441.

[2] S. TSUBOI, *Journ. Sci. Coll. Tokyo Imp. Univ.*, **43**.

(plate). It will be seen from the figure that more fragments were projected on the S–W side of the pit than on the other sides, which fact is probably due to the effect of the N–E wind that had a velocity of 10 m/sec. throughout the period of activity. Hence, the outer-boundary of the area on which the fragments were distributed, were there no wind, would have been as that shown with dotted line in Fig. 2.

From the distribution of these fragments it is possible to estimate the initial velocity of the projection and the gas-pressure of the present eruption. The relation between bomb–distribution and their initial velocities that have been studied by a number of investigator³⁾ do not seem to apply to the present case unless with certain modifications. In the present case, both the effects of air-viscosity and of the shape of the pit must be taken into account. We shall now calculate this relation, taking the two effects into account.

For simplicity of mathematical treatment, we take the mean shape of the fragment as a sphere. If the x–axis be drawn horizontally, and the z–axis upward, the equation of motion would be approximately

$$\left.\begin{aligned} &M\frac{d^2x}{dt^2}+K\rho_0 d^2\left(\frac{dx}{dt}\right)^2=0,\\ &M\frac{d^2z}{dt^2}+\delta K\rho_0 d^2\left(\frac{dz}{dt}\right)^2+Mg=0,\end{aligned}\right\}\qquad (1)$$

where $\quad \delta=1$ when $\dfrac{dz}{dt}\geqq 0$ and $\delta=-1$ when $\dfrac{dz}{dt}\leqq 0$,

M = Mass of the fragment,
d = Mean diameter of the fragment,
g = Gravity,
ρ_0 = Density of air,
ρ' = Mean density of the fragment,
K = Coefficient of air-resistance determined empirically.

As mentioned in Matuzawa's⁴⁾ paper, K is a constant, 0·12, provided Reynolds's number is $10^3\sim10^5$.

The solutions of the equation which satisfy the initial conditions

$$\left.\begin{aligned} &x=z=0,\\ &\frac{dx}{dt}=V_0\cos\theta,\qquad \frac{dz}{dt}=V_0\sin\theta,\end{aligned}\right\}\ \text{when } t=0,$$

and the condition of continuity

---

3) T. Matuzawa, *Bull. Earthq. Res. Inst.*, **11** (1933), 329.
T. Fukutomi, *Zisin. (in Japanese.)*, **1** (1929), 852.
T. Nomitsu and M. Namba, *Mem. Col. Sci., Kyoto Imp. Univ., A.* **15** (1932), 215.

4) T. Matuzawa, *loc. cit.*

$$z_{+}=z_{-} \quad \text{when} \quad \frac{dz_{+}}{dt}=\frac{dz_{-}}{dt}=0,$$

are

$$\left.\begin{aligned} x&=\frac{1}{\lambda}\log\left(\lambda t+\frac{1}{V_0\cos\theta}\right)+\frac{1}{\lambda}\log V_0\cos\theta,\\ z_{-}&=-\frac{1}{\lambda}\log\cosh\left\{\sqrt{\lambda g}\,t+\cot^{-1}\left(\sqrt{\frac{\lambda}{g}}V_0\sin\theta\right)-\frac{\pi}{2}\right\}\\ &\quad+\frac{1}{\lambda}\log\sqrt{1+\frac{\lambda}{g}V_0^2\sin^2\theta},\\ z_{+}&=\frac{1}{\lambda}\log\,\sin\left\{\sqrt{\lambda g}\,t+\cot^{-1}\left(\sqrt{\frac{\lambda}{g}}V_0\sin\theta\right)\right\}\\ &\quad+\frac{1}{\lambda}\log\sqrt{1+\frac{\lambda}{g}V_0^2\sin^2\theta},\end{aligned}\right\} \tag{2}$$

where

$$\lambda=\frac{K\rho_0 d^2}{M}=\frac{6K\rho_0}{\pi d\rho'},$$

and z_{+}, z_{-} denote respectively the value of the z–ordinate of the locus in the upward and downward courses of the projectile.

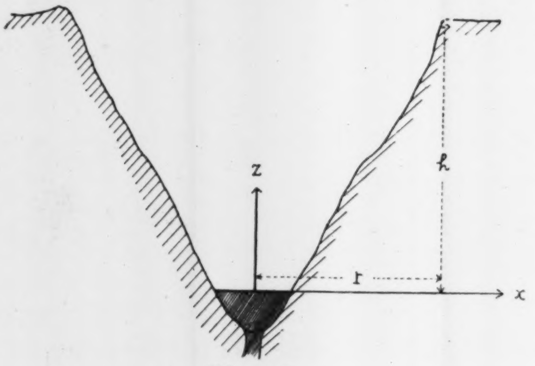

Fig. 3.

If the pit is assumed to be of the shape shown in vertical section in Fig. 3, the fragments that were projected on the old-crater bottom must have had the initial velocity and the angle of projection as determined by the relation

$$\left.\begin{aligned} z_{+}&\geqq h \quad \text{when } x=r, \quad \text{if } x_0\geqq r,\\ z_{-}&\geqq h \quad \text{when } x=r, \quad \text{if } x_0\leqq r,\end{aligned}\right\} \tag{3}$$

where x_0 is the value of x when $\frac{dz}{dt}=0$. These relations are expressed in our case as follows:

$$\left.\begin{aligned} &\sqrt{1+\frac{\lambda}{g}V_0^2\sin^2\theta}\geqq e^{\lambda h}\operatorname{cosec}\left\{\sqrt{\frac{g}{\lambda}}\frac{e^{\lambda}-1}{V_0\cos\theta}+\cot^{-1}\left(\sqrt{\frac{\lambda}{g}}V_0\sin\theta\right)\right\}\\ &\qquad\text{if}\quad \sqrt{\frac{\lambda}{g}}V_0\cos\theta\left\{\frac{\pi}{2}-\cot^{-1}\left(\sqrt{\frac{\lambda}{g}}V_0\sin\theta\right)\right\}\geqq e^{\lambda r}-1,\\ &\sqrt{1+\frac{\lambda}{g}V_0^2\sin^2\theta}\geqq e^{\lambda h}\cosh\left\{\sqrt{\frac{g}{\lambda}}\frac{e^{\lambda r}-1}{V_0\cos\theta}+\cot^{-1}\left(\sqrt{\frac{\lambda}{g}}V_0\sin\theta\right)-\frac{\pi}{2}\right\}\\ &\qquad\text{if}\quad \sqrt{\frac{\lambda}{g}}V_0\cos\theta\left\{\frac{\pi}{2}-\cot^{-1}\left(\sqrt{\frac{\lambda}{g}}V_0\sin\theta\right)\right\}\leqq e^{\lambda}-1.\end{aligned}\right\} \tag{4}$$

In the case of the present eruption, we may take

$$\rho_0 = 0{\cdot}00120, \qquad \rho' = 0{\cdot}64, \qquad d = 0{\cdot}035\ \mathrm{m}$$

and

$$r = 160\ \mathrm{m}, \qquad h = 220\ \mathrm{m},$$

whence we have the actual relations

$$\left.\begin{aligned} \sqrt{1+0{\cdot}0127\,\xi^2} &\geqq 15{\cdot}3\ \operatorname{cosec}\left\{\frac{56{\cdot}0}{\xi}\tan\theta + \cot^{-1}(0{\cdot}113\,\xi)\right\}, \\ \sqrt{1+0{\cdot}0127\,\xi^2} &\geqq 15{\cdot}3\ \cosh\left\{\frac{56{\cdot}0}{\xi}\tan\theta + \cot^{-}(0{\cdot}113\,\xi) - 1{\cdot}571\right\}, \end{aligned}\right\} \qquad (5)$$

each of which corresponds respectively to the cases

$$\left.\begin{aligned} 0{\cdot}113\xi\ \cot\theta\left\{1{\cdot}571 - \cot^{-1}(0{\cdot}113\xi)\right\} &\geqq 6{\cdot}32, \\ 0{\cdot}113\xi\ \cot\theta\left\{1{\cdot}571 - \cot^{-1}(0{\cdot}113\xi)\right\} &\leqq 6{\cdot}32, \end{aligned}\right\} \qquad (6)$$

where $\xi \equiv V_0 \sin\theta$.

These relations are shown by the graphs in Fig. 4. From this figure, we may conclude that the minimum velocity and the angle of projection with which the fragments can be thrown out on the old-crater bottom is about 135 m/sec. and 75° respectively. Moreover, if we assume that the gas-pressure p, by which the fragments were projected is given by

$$p = \frac{1}{2}\rho' V_0^2,$$

the least pressure by which the fragment can just be ejected from the pit is

$$p = 58\ \mathrm{atm}.$$

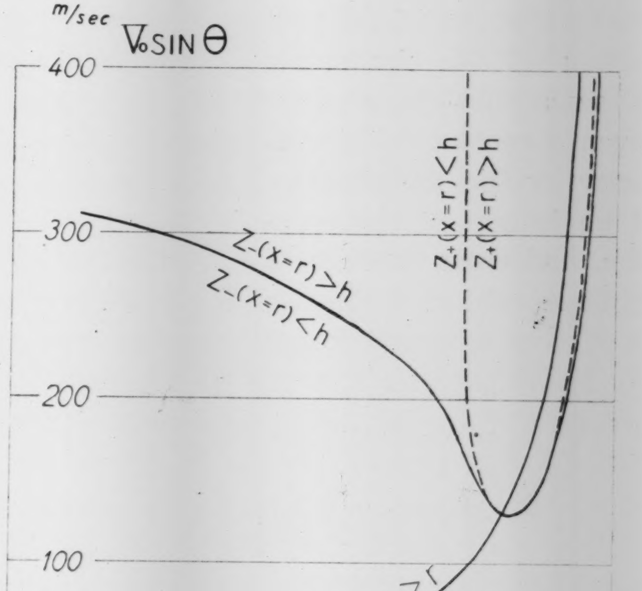

Fig. 4.

On the other hand, if we assume that the initial velocity of the projection is uniform in all directions, i.e. independent of θ, the direction of projection, the maximum horizontal distance x_0, of the fragment on plane $z=h$ (old-crater bottom) is a function of V_0 alone. Conversely, if we know the largest value of x_m, we can estimate the maximum initial velocity, that is, on the above assumption. The value of x in the case of $z_{-}=h$ was calculated from eq. (2), V_0 and θ in which satisfy the condition of eq. (4). The largest value of x thus obtained corresponding to each of the various values of V_0 was selected, and denoted x_m. Then the relation between V_0 and x_m in our case is expressed by the curve shown in Fig. 5. As the distance between the centre of eruption and the outer-boundary of the area where the fragments were distributed (i.e. the largest value of x_m), is about 200 m, as shown in Fig. 2, the maximum velocity in the present case is 170 m/sec., while the corresponding gas pressure is 92 atm. This value of gas-pressure is much smaller compared with those estimated by T. Matuzawa[5] for the cases of the eruption of Volcano Asama and other volcanoes in Japan, where $p=230\sim550$ atm.

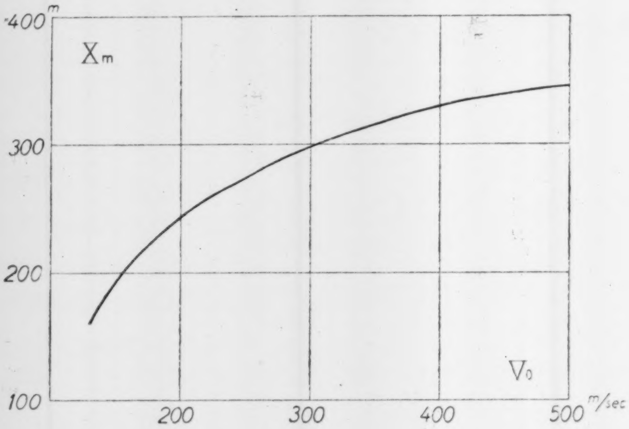

Fig. 5.

In the above calculations it was assumed that the mechanism of the projection of the fragments is such that they were given a certain initial velocity by the gas-pressure at an instant of the eruption, and their subsequent motions subjected only to the forces of gravity and the resistance of air, which is standstill. Other forces, such as the pressure of the ascending gas emitted from the crater-bottom and the convective motion of the air in the pit etc might also affect the motion of the fragments. While in the present case, these effects would not be negligibly small, they may be not so large as to change the order of the initial velocity of the projection obtained by the above calculations. In the case of violent eruptions of Volcano Asama that these forces extremely affect the motion of the fragments is conceivable. Seeing that in the present eruption of Volcano Mihara the emitted gas began to diffuse in all directions soon after the emission and began to make a convective motion before the gas-front reached the height of only 50 m from the bottom, while in the cases of violent eruptions of Volcano

---

5) T. MATUZAWA, *loc. cit.*

Asama the emitted gas ascends to the height of several thousand meters making a shape of a column, we may conclude that the pressure of the ascending gas would be large in the latter but very small in the former.

3. The temperature in the fumaroles on the old-crater bottom has been measured once or twice a week since September 1937. R. Takahasi and the writer6) reported that when gas is emitted more or less violently, the temperature varies by two or three degrees, that is, when the volcano is comparatively active, it fluctuates in the range between 66°C and 69°C, whereas on calm days it is constantly 67°C. The observed values of the temperature both before and after the recent eruption are shown in Fig. 6, where we notice that the temperature has changed in association with the present activity, that is, it started to fall at the beginning of the activity until it reached 58°C, a minimum, after which it is now rising back to its normal value. The mechanism responsible for the temperature-change is not at present clear, although several can be assumed.

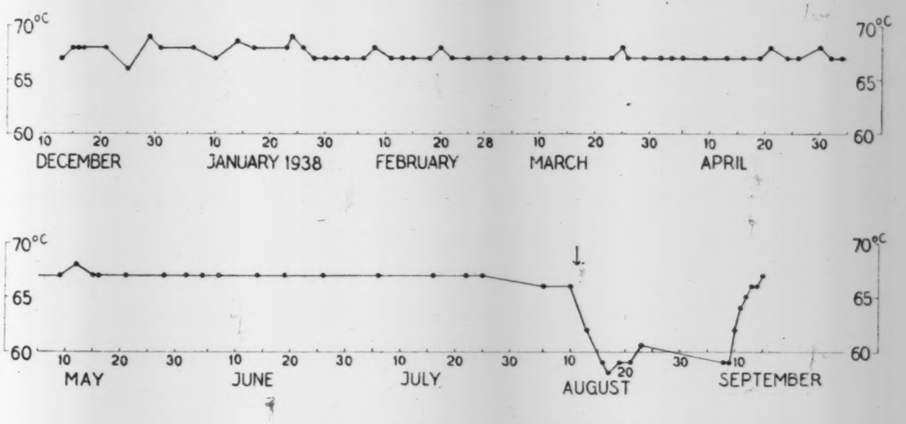

Fig. 6. Change in Temperature of Humarole.

4. The present activity not being violent, there were no marked change in volcanic tremors, earth–tilts, or earth-currents, notwithstanding the continuous observations that were being made at the foot of Mt. Mihara and on its somma.

In short the activity of August 11 was the severest during the last four years, yet it was very quiet compared with the frequeut eruptions of Volcano Asama and other volcanoes in Japan.

In conclusion, the writer wishes to record his indebtedness to Prof. M. Ishimoto, the director of the Institute, for his encouragement, and

---

6) R. TAKAHASI and T. NAGATA, *Read at the annual meeting of Physico Math. Soc. Japan* (Apr. 1938).

to Dr. C. Tsuboi, Dr. N. Miyabe, and Dr. K. Kanai for their valuable advices. His hearty thanks are also due to the Hattori-Hôkô-Kai, by the aid of whose grant these geophysical studies of Volcano Mihara were carried out.

50. 三原火山の地球物理學的研究

昭和13年8月11日の小活動

地震研究所 永田 武

1. 昭和13年8月10日深更より翌11日早朝にかけて三原火山は小活動を爲した． その間直徑數糎の熔岩片を多數に噴出したがその分布から爆發の壓力を推定した結果 60〜90 氣壓程度と思はれる．

2. 噴氣孔の蒸氣溫度が今度の噴火前後から著しい低下を示した他には，火山微動，傾斜，地電流，火山地震の發生等には著しい變化が見られなかつた．

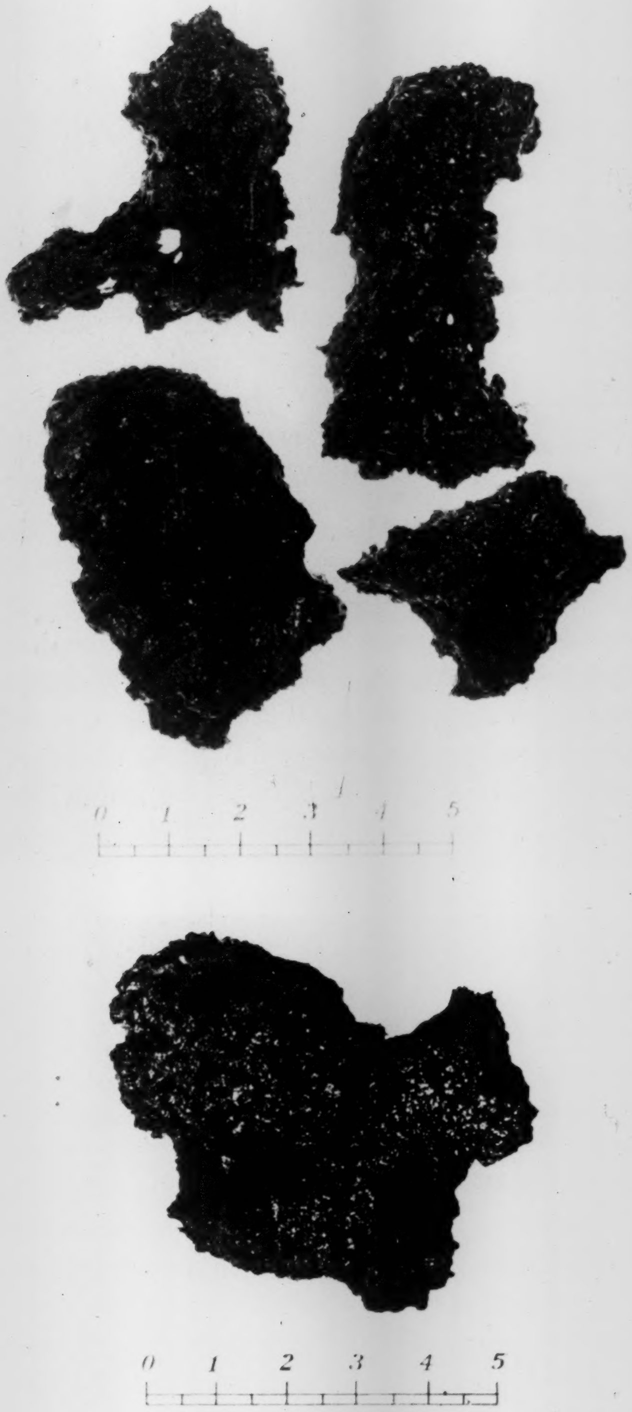
0 1 2 3 4 5
0 1 2 3 4 5

Fig. 1. The Fragments of Lava, projected Aug. 11, 1938.

（震研彙報 第十六號 圖版 永田）

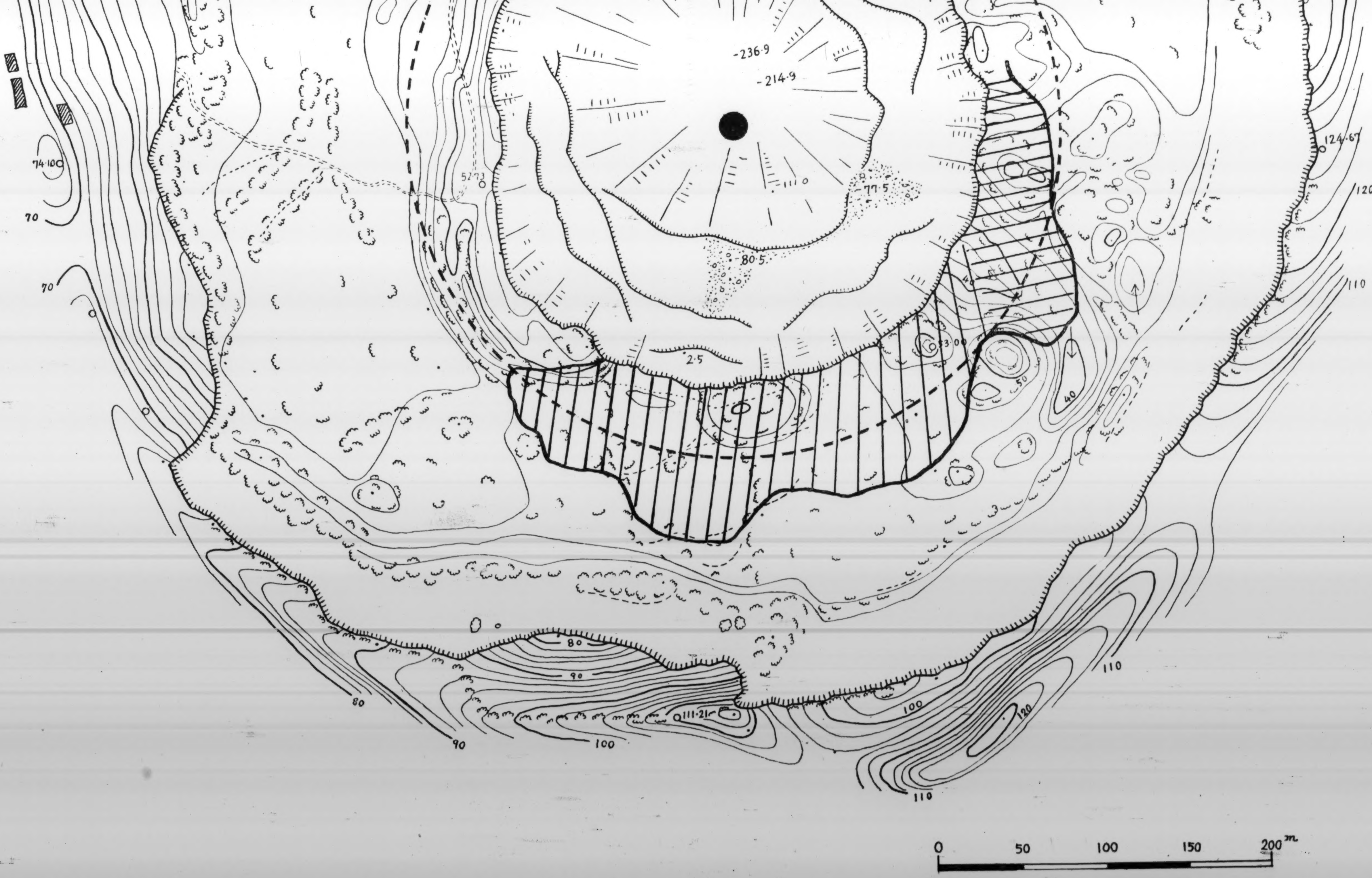
-236·9
-214·9
74·10
70
70
52·73
77·5
80·5
2·5
53·00
50
40
40
124·67
120
110
80
90
80
90
100
111·21
100
120
110
110
0
50
100
150
200 m.

Fig. 2. The distribution of the projected fragments in the minor eruptions of Volcano Mihara, August 11, 1938.

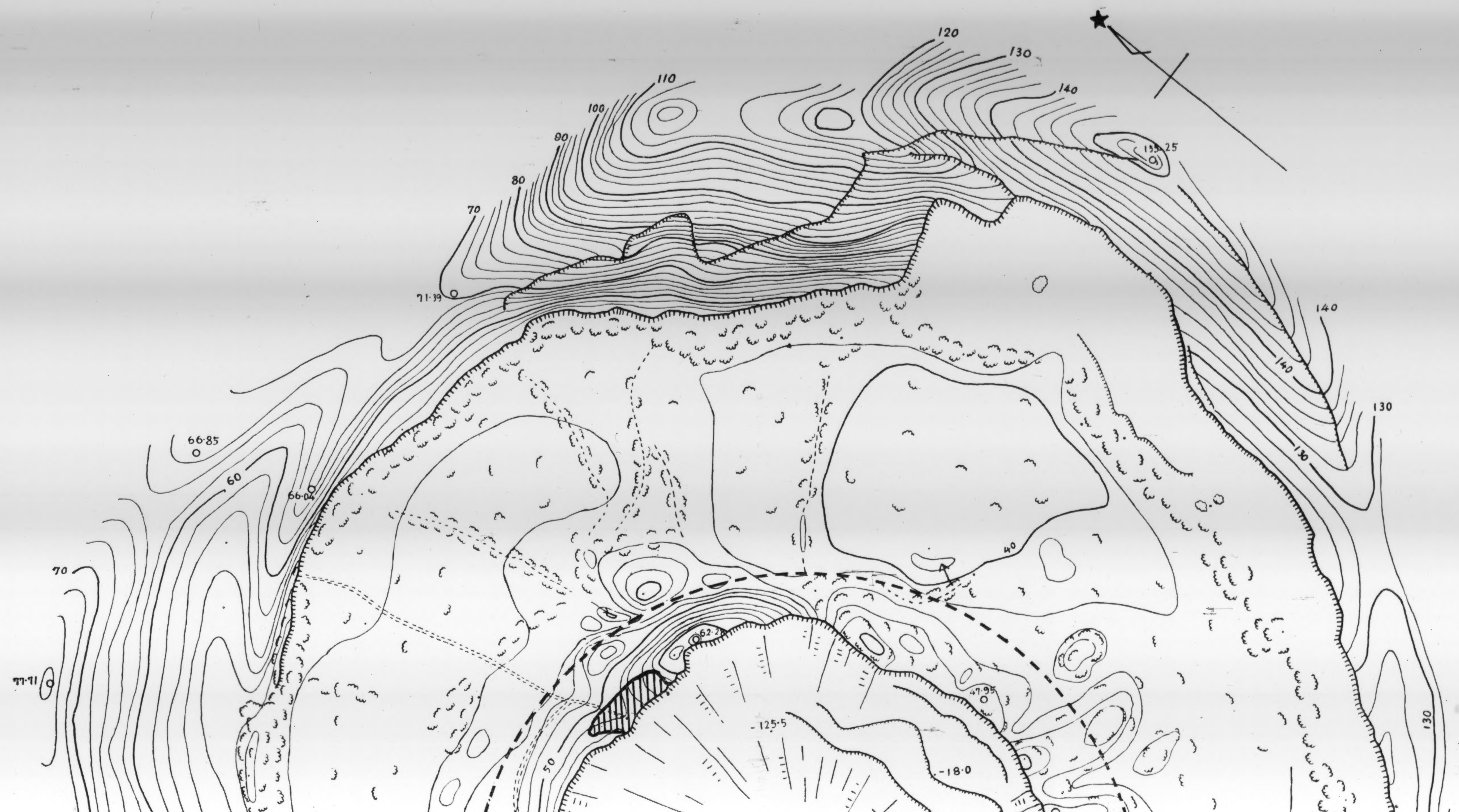
120
130
140
110
100
90
80
70
71·39
135·25
140
140
130
130
66·85
60
66·04
70
77·71
62·2
40
47·95
-125·5
-18·0
50
130

51. 江東地域に於ける地盤沈下に就て II.

地震研究所 宮部直巳

（昭和13年9月21日發表—昭和13年9月20日受理）

1. 前報告に於いて,[1]東京市内の江東その他の地域の地盤沈下の現象は，主として，地表面に在る軟土層の收縮によつて生ずるものであると推定し得る事を明かにした．

そこで，斯様な軟土層が如何にして收縮し，沈下現象を顯はすかといふ事が，次の問題である．それには，先づ軟土の物理的性質に關して知る所がなければならない．

前報告[2]に示した本所及び深川に設けた特種の水準點に於けるボーリングの際に得た土の試料に就き，若干の物理的性質を調べ,[3]尚，1~2 の補足的實驗をも行つたので，先づ是等の結果について報告しやうと思ふ．

2. 土の物理的性質として測定された量は，含水量 (Water conteut), 空隙率 (Porosity, P), Mechanical ratio (即ち，大いさの異る粒子成分の混合の割合), 凝集力 (Cohesion. c,) 彈性率(Young's modulus, E), プラステイツク限界 (Plastic limit), 流動限界 (Flow limit) 等で，第 1~第 2 表に掲げてある．この中，Youngs modulus と稱するものは，靜力學的に求められた見掛上の値である．又，Plastic limit 及びFlow limit は共に含水比 (Moisture ratio) を以て與へてある．

是等の表に與へられた量の中で，先づ問題となるのは，Porosity であらう．

土が，その自重によつて沈着したとすれば，Porosity と深さとの間にある簡單な關係が先づ豫想される．併し，實際は，さ程簡單ではない．第 1~2 表によれば，Porosity と深さとは寧ろ無關係であるかのやうである．これは，自重によつて沈著するといふ現象が全然ないことを意味するのではなく，その影響が，吾々の得た 30 乃至 35 m 程度の深さの間では著しくないことと，Porosity の差異が，土の組成分たる土粒子の大いさ，換言すれば，Mechanical ratio の如何によつて著しく左右され，深さ

---

1) N. Miyabe, *Bull. Earthq. Res. Inst.*, **15** (1937), 102~108.

2) N. Miyabe, *ibid.*

3) 土の物理的性質に關する測定は，鐵道省官房研究所土質調査委員會に委托して行つた．

第 II 表　本所茅場町小學校々庭試錐土質試驗成績

I.

番號	採取場所 深さ (m)	自然含水量		機械分析 (%)							
		含水率 (%)	含水比	8 目 2·36 mm	14 目 1·17 mm	28 目 0·59 mm	48 目 0·30 mm	100 目 0·15 mm	200 目 0·07 mm	Silt 0·07〜0·005 mm	Clay 0·005 mm 〜0
1	3·7〜 4·4	26·50	0·361	0·90	0·60	2·18	12·82	48·14	24·28	7·34	3·74
2	4·4〜 5·1	24·80	0·330	8·38	2·70	0·86	2·90	14·66	22·06	20·80	27·66
3	5·1〜 5·8	24·28	0·321	15·40	1·48	0·90	4·14	33·82	23·30	9·32	11·64
4	6·1〜 6·4	46·50	0·866	19·00	4·64	2·60	6·36	29·04	22·42	7·56	8·38
5	6·5〜 7·2	24·05	0·351	2·28	1·46	0·76	1·06	8·36	43·16	34·28	8·64
6	7·2〜 7·9	34·50	0·526	0	0·18	0·84	1·32	0·80	7·34	57·70	31·82
7	8·6〜 9·3	43·66	0·774	0·08	0·34	0·26	0·32	0·44	0·54	28·60	51·60
8	9·3〜11·0	37·29	0·594	1·12	1·26	1·52	1·46	1·60	6·00	43·50	43·54
9	10·0〜10·7	39·20	0·646	0·84	0·54	0·46	0·34	0·48	5·02	41·94	50·38
10	12·1〜12·8	38·92	0·638	7·72	1·00	0·76	1·00	1·24	4·10	36·06	48·12
11	12·5〜14·2	42·65	0·775	1·32	1·08	0·64	0·42	0·38	2·38	34·96	58·82
12	15·6〜16·3	39·31	0·648	0·22	0·12	0·32	0·32	0·32	6·68	43·44	48·56
13	17·0〜18·4	40·90	0·692	1·02	0·40	0·52	0·32	0·36	4·26	47·22	45·90
14	19·1〜20·5	43·80	0·779	0·26	0·30	0·22	0·12	0·18	4·50	35·68	58·74
15	21·9〜23·3	41·13	0·699	0·40	0·36	0·30	0·18	0·26	5·68	43·92	48·90
16	25·4〜26·1	41·92	0·721	0	0·42	0·82	1·84	3·00	8·40	35·20	50·32
17	26·1〜26·8	37·69	0·639	0·40	0·62	0·62	0·90	1·02	9·72	45·54	41·18
18	28·8〜29·6	37·80	0·608	0·16	1·38	3·84	5·62	7·40	8·34	17·88	55·38
19	29·6〜30·0	47·20	0·895	0·10	1·32	10·84	18·60	14·72	8·44	10·76	35·22
20	30·0〜31·0	37·98	0·612	1·16	2·20	3·12	4·20	7·66	9·14	23·68	48·84
21	31·0〜31·7	42·63	0·743	0·64	2·10	6·36	14·62	21·22	12·32	15·14	27·60
22	31·7〜32·0	12·64	0·145	32·12	5·40	3·80	6·62	3·88	7·22	17·36	19·60
23	32·0〜32·0$_5$	21·66	0·277	0	0·08	3·14	18·74	23·04	31·94	18·70	4·36
24	32·0$_5$〜32·6	5·70	0·065	37·70	20·08	19·70	14·12	5·10	1·50	1·30	0·50
25	32·6〜34·0	7·91	0·086	39·22	16·16	17·08	14·24	6·80	2·46	2·70	1·34

第 I 表 II.

番號	凝集强度 c. kg/cm²	摩擦角 φ.	彈性係數 E. kg/cm²	最大應壓力 kg/cm²	比重		間隙率 (%)	間隙比	流動限界 (含水比)	プラスティシティ限界 (含水比)
					見掛	眞				
1	0·366	2°30′	—	—	1·806	2·618	51·40	1·057	0·411	0·344
2	0·219	14 00	10·53	0·421	1·735	2·577	55·02	1·224	0·578	0·493
3	0·075	12 30	4·91	0·204	1·512	2·564	66·90	2·021	0·944	0·372
4	0·354	4 30	12·00	0·535	1·493	2·551	68·35	2·160	1·214	0·492
5	0·372	14 00	16·16	0·634	1·594	2·604	61·75	1·614	0·802	0·407
6	0·031	21 00	12·92	0·535	1·700	2·577	57·70	1·364	0·711	0·311
7	0·344	16 00	18·50	0·714	1·669	2·564	58·53	1·412	0·762	0·335
8	0·181	15 00	15·18	0·280	1·669	2·564	57·72	1·366	0·755	0·398
9	0·262	13 40	23·50	0·764	1·618	2·551	58·05	1·384	0·727	0·377
10	0·453	21 30	12·83	0·602	1·638	2·577	58·08	1·386	0·700	0·351
11	0·350	25 40	24·05	0·815	1·625	2·591	58·76	1·424	0·747	0·369
12	0·594	16 30	27·20	0·871	1·638	2·564	57·50	1·353	0·753	0·409
13	0·653	20 00	37·10	0·624	1·544	2·551	73·37	2·75	1·774	1·178
14	0·378	28 50	24·70	1·172	1·594	2·591	55·40	1·242	0·470	0·379
15	0·514	33 00	16·43	0·306	1·888	2·103	48·65	0·947	0·379	—
16	0·001	40 40	—	—	1·919	2·688	38·40	0·620	—	—

第 I 表　深川數矢小學校々庭試錐土質試驗成績

I.

番號	採取場所 深さ (m)	自然含水量		機械分析 (%)							
		含水率 (%)	含水比	8 目 2·36 mm	14 目 1·17 mm	28 目 0·59 mm	48 目 0·30 mm	100 目 0·15 mm	200 目 0·07 mm	Silt 0·07～0·005 mm	Clay 0·005 mm～0
1	5·0 ～ 6·97	29·60	0·420	19·33	0·22	0·24	0·64	6·10	17·26	32·78	23·38
2	6·97～ 8·37	33·35	0·500	0·50	0·48	0·46	0·44	0·86	18·86	45·72	32·68
3	11·3～11·83	43·88	0·782	2·88	0·98	0·92	0·82	0·80	4·98	40·98	47·64
4	13·0～13·7	45·95	0·850	0·08	0·54	0·98	0·82	0·46	2·80	37·80	56·52
5	14·8～15·1	37·45	0·599	3·54	0·08	0·34	1·83	5·02	25·56	36·72	25·86
6	15·1～15·8	35·91	0·560	0·52	0·32	0·28	0·32	1·06	14·10	52·50	30·90
7	16·6～17·2	36·31	0·5[illegible]1	0·08	0·44	0·34	0·24	0·64	7·68	58·72	31·68
8	19·3～20·0	35·02	0·541	0·14	0·22	0·26	0·16	0·42	9·90	57·86	31·34
9	20·7～22·1	33·90	0·513	0	0·20	0·24	0·18	0·38	12·18	54·52	31·60
10	24·9～26·3	34·13	0·519	0	0·28	0·28	0·18	0·74	20·46	42·58	35·48
11	26·3～27·7	34·25	0·525	0	0·26	0·38	0·24	0·24	7·58	47·24	44·06
12	29·1～29·8	33·50	0·504	0	0·60	2·20	5·88	7·14	11·14	32·64	40·40
13	29·8～30·0	56·00	1·273	0	0·36	1·06	1·94	2·18	2·04	9·22	83·20
14	31·4～32·1	27·45	0·379	0·06	0·26	0·20	0·93	8·28	27·04	40·82	22·36
15	32·1～33·7	26·43	0·359	0·20	0·40	1·06	3·76	19·78	32·36	35·16	7·23
16	33·7～35·0	13·72	0·159	26·62	13·78	13·80	15·98	13·82	8·54	5·34	2·12

第 II 表 II.

番號	凝集强度 c. kg/cm²	摩擦角 φ.	彈性係數 E. kg/cm²	最大應壓力 kg/cm²	比重 見掛	比重 眞	間隙率 (%)	間隙比	流動限界 (含水比)	プラスティシティ限界 (含水比)
1	0·141	27°10′	—	—	1·533	2·688	58·10	1·386	—	—
2	0·594	26 00	28·85	0·407	1·867	2·717	48·30	0·935	0·434	—
3	0·250	26 00	—	—	1·842	2·646	47·30	0·898	0·368	—
4	0·187	24 00	—	—	1·821	2·618	62·78	1·686	0·926	—
5	0·178	20 40	14·80	0·239	1·742	2·632	49·78	0·988	0·391	0·213
6	0·375	13 30	29·60	0·407	1·654	2·564	57·75	1·366	0·582	0·324
7	0·303	1 30	13·32	0·216	1·547	2·577	66·15	1·955	0·950	0·420
8	0·250	8 20	16·87	0·407	1·579	2·618	62·15	1·643	0·723	0·375
9	0·250	8 20	22·18	0·255	1·575	2·591	63·05	1·706	0·842	0·375
10	0·313	3 00	—	—	1·533	2·732	65·70	1·915	0·772	0·407
11	0·422	4 10	30·20	0·752	1·504	2·551	66·85	2·018	1·006	0·457
12	0·218	6 00	21·60	0·382	1·529	2·538	64·05	1·735	0·845	0·360
13	0·250	6 10	14·80	0·356	1·558	2·538	63·70	1·755	0·926	0·489
14	0·531	2 30	29·60	0·853	1·496	2·500	66·35	1·973	1·132	0·539
15	0·344	11 20	56·25	1·222	1·525	2·538	64·62	1·827	1·020	0·419
16	0·400	10 00	47·40	1·055	1·529	2·475	64·10	1·785	1·014	0·522
17	0·006	13 30	53·30	1·163	1·567	2·525	61·33	1·585	0·888	0·382
18	1·193	4 30	97·70	1·157	1·563	2·778	64·98	1·855	1·068	0·453
19	1·000	18 00	106·60	1·054	1·354	2·392	70·10	2·345	1·235	0·701
20	0·890	23 00	—	—	1·296	2·488	67·68	2·094	0·951	0·432
21	0·938	13 40	48·60	1·304	1·283	2·513	70·70	2·415	1·040	0·590
22	0·162	26 00	—	—	1·584	2·632	47·40	0 902	—	—
23	—	—	82·80	2·545	1·432	2·660	57·80	1·370	0·571	0·116
24	—	—	—	—	1·683	2·778	42·75	0·747	—	—
25	—	—	—	—	1·953	2·762	34·80	0·534	—	—

の影響が覆はれてしまつてゐることに因るものと思はれる.

Porosity と, Mechanical ratio, 特に Clay の含有量との關係は, 比較的簡單のやうである. 第1圖は, Porosity と Clay content との關係を示した圖である. この圖から知れる樣に Porosity は, Clay content が大きくなればなる程大となる.

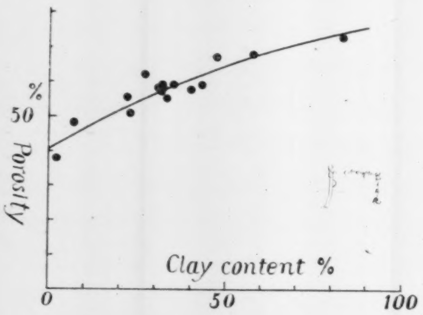

第1圖　空隙率と Clay 含有量の關係.

併し乍ら, "Clay content が大きくなればなる程 Porosity も亦大となる" といふ事自體は, 決して自明の事ではない. 何故ならば, 若しも, 粒子の大いさの齊しい球形粒子の集合體について言ふならば, その土を構成する個々の粒子の大いさ如何に拘らず, Closest packing の狀態では, Porosity は一定でなければならないからである. 其故, 特別な事情, 例へば, "粒子の小さいものの集合體は, 全體一樣に Closest packing の狀態に到達することは出來難い" とか, "微粒子の集合體の安定狀態における Porosity は, 粒子の徑が小さい程大である" とかいふ事を既知のこととして前提しない以上, 上述の事實は簡單には諒解されないであらう. 而も, その樣なことは, 之を實驗的に確かめる事すら却々容易ではないと思はれる. この問題は地盤沈下の現象とは現在のところ直接關係はないのであるから, 玆にはこれ以上觸れる事をやめ, 單に注意を促がす程度に止めておかう.

土の含水量が, 流動限界より小さく, プラスティツク限界より大であれば, その土は Plastic, 若しくは Visco-elastic な固態として存する.

實際の土の含水量はこの中間にあるのであるが, 問題は, 含水量の變化に伴つて土の力學的性質が如何に變化するかといふことである. 略々豫想されることは流動限界に於いては勿論であるが Plastic limit に於いても, 凝集力 c は o 若しくは o に近いと考へられることである.

併し, 玆に少し考慮すべきことがある. それは含水量は勿論, 空隙率に關係がある4)

---

4) 空隙を滿した時の含水量と, 流動限界の含水量とは一般に一致せず, 後者の方が大である. 後者と前者との比は次の別表の如く一般に1より大である.

別表　M_f（流動限界の含水量）と M（自然含水量）との比.

深さ (m)	6·97 ~8·37	11·3 ~11·83	13·0 ~13·7	14·8 ~15·1	15·1 ~15·8	16·6 ~17·2	19·3 ~20·0	20·7 ~22·1	24·9 ~26·3	26·3 ~27·7	29·1 ~29·8	29·8 ~30·9	31·4 ~32·1	32·1 ~33·1
M_f/M	1·156	1·206	1·428	1·342	1·270	1·338	1·399	1·414	1·345	1·431	1,498	4·945	1·240	1·058

から，空隙率の大なる土と，それの小なる土とは，自然狀態に於ける含水量が同等であつても，その含水量が力學的性質に及ぼす效果まで同等であるとは限らない．

そこで，今，例へば，凝集力と含水量との關係を全般的に調べやうとする場合に，含水量をそのまゝ用ひることは不適當であるから，その代りに

$$q=\frac{Q_f-Q}{Q_f-Q_p}$$

で與へられる q を用ひる．玆に，Q は實際の含水量，Q_f，Q_p，は夫々流動限界，並びに Plastic limit に相當する含水量である．斯うして，新らしい Parameter q と凝集力　c，及び彈性率 E，との關係を示したものが，第 2〜3 圖である．是等の圖の上の點を，その圖にある如き曲線で連ねる事には多少の異論があるかもしれないが，大體の傾向はこの曲線によつて示されると思はれる．5) この曲線が，含水量の變化に伴ふ c（凝集力）の變化を示すものとすれば，次の樣な考察も亦，多少の可能性はあらうと思はれる．

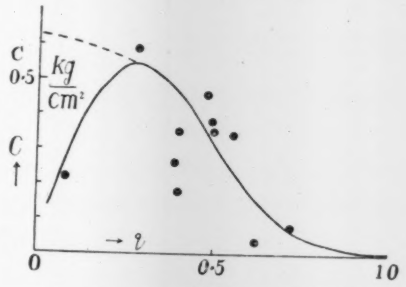

第 2 圖　土の凝集力と含水量．

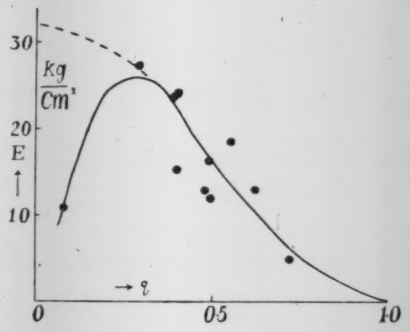

第 3 圖　土の彈性率と含水量．

今，土の中に水が浸込んでゐる狀態を考へてみると，土粒の中間を滿し，土粒と土粒とを連絡してゐるとすることが出來る．この水の連絡によつて，土粒間が結び付けられ，之を破る爲めにある力を要する所から，例へば，凝集力 c 6) が生ずると考へる．一方に於いて，流動限界のあることをより水分が過剩にあれば，その水分は，却つて，土粒間の滑劑の如き役目をするであらうと考へられ，從つて過大の含水量は凝集力 c の減少する原因ともなる．

又，土に水が浸込む時，その浸込み方は，一樣とするよりは，寧ろ不均一と考へた

---

5)　一度水に浸した土を乾してゆく場合，含水量が小さくなつても c は小さくならない場合も考へられる．それで，第 2〜3 圖における點線の如き部分も考へられる．これは，土の c を支配する土の中の Gel の性質に關聯したものと思はれるが，これ等の點に關しては未だ研究が充分進んでゐない．

6)　凝集强度といふ名稱が適當であるかもしれない．

方が適當であらう．勿論，水分が增加するに從つて，水の浸潤狀態は均一に近づくとすることが出來るであらう．さうすれば，土全體としての强さ，或は，換言すれば，凝集力 c は浸み込んだ水が均一に配分されてゐる方が大であると考へられる．何故ならば，浸込み方が不均一であれば，その Capilary water の表面張力による土の試片內部の Stress 分布狀態も亦不均一であるから，比較的小さい外力によつても破壞され易い狀態にあると思はれるからである．

そこで今，土の試片につき，之を多數の小部分に分けたと考へ，各小部分における含水量を n，とすれば，n の Fluctuation は

$$\delta=\frac{n-\nu}{\nu}$$

で表はすことが出來る．但し，ν は n の平均値である．それ故，ν は又土全體の含水量をあらはす量とすることが出來る．こゝで，前述の2條件，即ち，

（i）含水量（全體としての）の增加と共に凝集力 c は減少する．

（ii）凝集力 c は，浸込んだ水が土の中に一樣に配布されてゐる時に最も大となる．

といふことを考慮して，上述の量を用ひて c を，試みに

$$c=k\frac{e^{-a\nu}}{\overline{\delta^2}}$$

と置いてみる．玆に，k，a はある常數である．

又，$\overline{\delta^2}$ は，土中に浸込んだ水の分布の均一さをあらはす量である．この場合は，a も ν も比較的大きく，$n-\nu=\nu\delta \gg 1$，であるから，

$$\overline{\delta^2}=\frac{q}{\nu}=\frac{1}{N}\cdot\frac{N-\nu}{\nu}$$

とすることが出來る．

故に

$$c=kN\cdot e^{-a\nu}\frac{\nu}{N-\nu}$$

となる．この c を ν に關して plot すれば曲線は，大體，第2圖の如きものとなる．

彈性率 E は，物理的には凝集力 c と異るものであるが，この土の場合には，大體同樣に考へることが出來るであらう．

玆で，一寸注意されることは，從來，Colloid Gel の彈性率 E について，

$$E=AC^2,$$

といふ式が認められてゐる.[7] C は濃度である．これは，丁度，第2又は第3圖の曲線の右半に相當する部分と略々一致するであらう．

粘土を Colloid Gel と同一視することには多少の異論があるかもしれないが，この事實は注意されてもよい事であらうと思はれる．

3．次の問題は，土の收縮である．土の見掛け上の體積が收縮する現象には2様の方式が考へられる．その1は，適當な振動を與へることにより Loose な狀態にあつた土が Settle down して Compact な狀態になる爲に見掛の體積が小さくなる．この點に關しては旣に飯田氏の研究がある.[8] その2は，土が水分を失ふことによつて，その見掛けの體積を減ずる．この種の收縮は Colloid Gel の縮化の現象と略々同様に考へることが出來るであらう．筆者も亦，同様の考への下に，2 種の試料に就いてその乾燥による土の收縮を觀察した．2種の實驗中一方は普通の水の中に沈積した土で，他は，鹽化マグネシウム 0·5 g を 130 cc の水に溶かした溶液中に沈積した土である．それは，Colloid ならば，その凝固に際して鹽類の影響を受けることが大であるからである．鹽類の影響は，土を沈積させる場合に先づ認められる．鹽化マグネシウム溶液の中で土を沈積させる場合は，上部に溜る液體が數分の中に，澄んでしまふが，之に反して普通の水中で沈積させる場合は，長時間濁つてゐる．微小粒子は鹽化マグネシウムの混入によつて直に Flocculation を起して容易に沈積するものと解される．

實驗は斯様な2種の土を別々に Meter glass に入れて上部の水を取り去り，放置して土の表面が次第に沈下してゆく有様を記錄し[9]，同時に，重さをはかるのである．重さは普通の天秤で測る．その結果は第 3，4 表に示す通りである．

第 III 表 土の收縮
(水中に沈積した土)

經過日數(日)	土の重さ (g)	重さの減少 (g)	土の體積 (cc)	體積の減少 (cc)
0	252	0	162	0·0
2	252·5	0·5	161	1·0
3	252	1·0	160	2·0
4	251	2·0	160	2·0
7	250	3·0	158	4·0
9	250	3·0	158	4·0
11	249	4·0	157	5·0
16	247·5	5·5	155·8	6·2
18	246·5	6·5	154·5	7·5
30	244·5	8·5	152	10·2
37	243	10·0	150·8	11·2
42	241	12·0	150	12·0

---

7) 例へば，簑作新六 膠質化學 232 頁參照．
8) 飯田汲事 震研彙報 **15** (1937)，544〜558．
9) 收縮に際しては，少くとも後に Crack を生ずるまで，土柱の高さの方向にのみ收縮し，Meter glass と土柱との間に目に見える程の間隙を生ずることがない．

第IV表 土の收縮

（3·8% $MgCl_2$ 溶液中に沈積した土）

經過日數(日)	土の重さ (g)	重さの減少 (g)	土の體積 (cc)	體積の減少 (cc)
0	234	0·0	152	0·0
2	233	1·0	151·5	0·5
3	232·5	1·5	151	1·0
4	232·3	1·7	150·5	1·5
7	231	3·0	149·8	2·2
9	230·5	3·5	149	3·0
11	230	4·0	148	4·0
16	229	5·0	146·8	5·2
18	228·5	5·5	146·1	5·9
30	226	8·0	144	8·0
37	225	9·0	142·5	9·5
42	223·5	10·5	140·7	11·3
56	218·5	15·5	136·5	15·5

この結果は第4乃至第6の3様の圖に示してある．第4圖は，時と共に重さの減少する有様をⅠ（普通の水中で沈積させた土）及びⅡ（鹽化マグネシウム溶液中で沈積させた土）につき夫々∘及び•で示してある．（以下この一節では ∘，•，は何れも同様の意味を有する）．Ⅰの土は，43日目に割目が生じたので，その後のデータはとれなかつた．この圖に見られる様に，重さの減少する量は，多少の差異こそあれ，殆ど同一である．

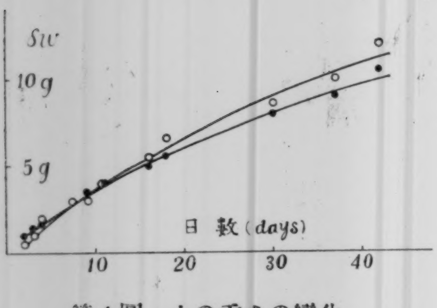

第4圖　土の重さの變化
∘：普通の水中で沈積した土．
•：MgCl 溶液中で沈積した土．

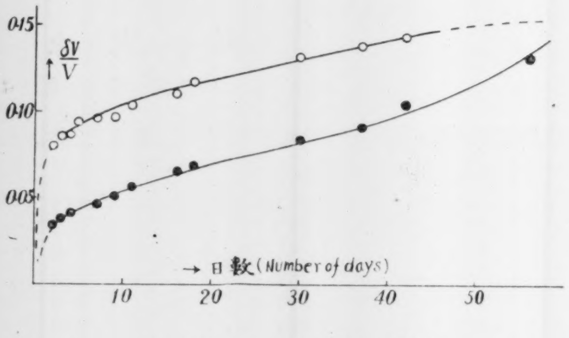

第5圖　土の收縮度の變化

この重さの減少は殆ど全部が，水分の蒸發によるものであるから，叙上の様なことは別に注意すべきことではないかもしれない．併し，之に對して，土の體積が時日の經過とともに減少する有様は必ずしも同じではない．卽ち，第5圖においては，體積

減少の割合（＝收縮の割合），dv/v. を時に對し（經過日數に對し）て Plott してあるが，この圖から見られる樣に I の土の方が，dv/v が幾分大きくなつてゐる．II の土の試料については，40日以後に於いて，dv/v が遽かに增大する傾向が見えるけれど，之に對應すべき I の土に關するデータが無いから，比較することが出來ない．若し，42日以後に於ける dv/v の變化の傾向が，それ以前の變化の有樣の延長で示されるとすれば（第5圖には點線で示してある），長い時日の後には，II の土の方がよけいに收縮する樣になると言へる．

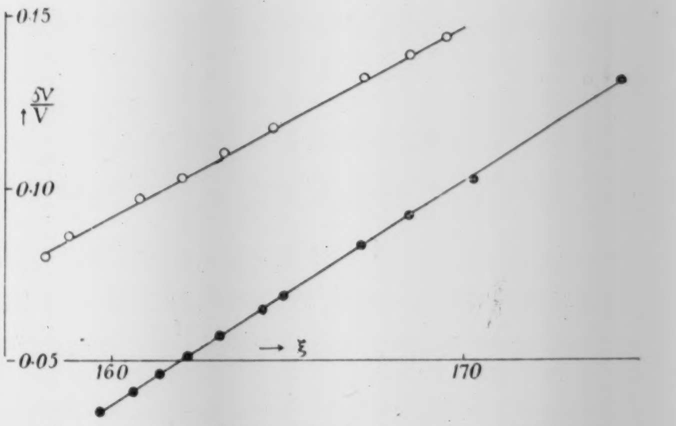

第6圖　土の收縮度と土膠質 1000 cc 中の固體の量．

I，及び II の收縮する有樣の差異は，更に，第6圖によつても示される．この圖では，體積縮少度 dv/v_0 を ξ に對して Plott してある．ξ は，水を含む土 100 cc 中の土の質量（gr）を示す數字である．この圖で ξ が增加するといふことは含水量の減少を意味するのであるが，II の土においては，ξ と $\frac{\delta v}{v_0}$ との比の値が I の土のそれよりも稍大であることが認められる．

上述の如き，土の收縮する經過における鹽化マグネシウムの影響は，次の如く考へることも出來るであらう．鹽化マグネシウム溶液中で沈積した土は，沈積が早く行はれたのであるから，普通の水中で沈積した土に比較して，その構成が比較的 Loose である．とすれば，結局において，II の土の方が dv/v が大きくなると考へる事は，他に特別な事情がない限り，寧ろ自然であらうと思はれる．10)

土の收縮が Colloid Gel の收縮と同樣に考へられるとすれば，Colloid Gel に關して知り得てゐることは大體そのまゝ土の問題にも適用できる．

水分の喪失に伴ふ土の收縮の場合も，Gel の場合と同じく，土の內部の Capilary pressure の變化によつて收縮すると考へることが出來るならば，かゝる Capilay pressure は外壓に置き換へて考へることも出來るから11)，ある程度まで，收縮の機構に關する考察を進めることも出來る．又，かゝる Capilary pressure P は，Gel 1000 cc 中

---

10)　このことは次の樣な事實とも一致する．I，及び II の土の見掛けの密度は沈積の初に於いて夫々 1·539 及び 1·539 であつたが，42日經過後には夫々 1·607，1·601．となつた．卽ちこの間に見かけの密度の增加は I では 0·045 であるに對して II の土では 0·062 となつてゐる．

11)　君島八郎　地下水　110 頁參照．

の分散體の瓦數 ξ と，

$$P=P_0\xi^k.$$

で結ばれてゐるから，ξ と，dv/v_0 との關係を求めれば，從つて，P と dv/v との關係も亦，求められることになる．第6圖に示した例を見ると，I, II の何れの土でも ξ と dv/v_0 とが大體比例してゐる．從つて，これから，$\left(\frac{dv}{v}\right)^k$ が P に比例すると考へられる．K の値は，通常の Gel では，2~3 位であるが，土についても，大體その程度であると見られるかもしれない．P の時と時と共に變化する割合は，何れ，dw, 即ち水分の減少と關係があるのであらうが，第 4，5 圖に見られる樣に dv/v と dw との時と共に變化する樣が，大體平行してゐる事から推して，その關係は，少くとも實驗的には，$P\propto(dw)^k$ の如きものではなからうかと思はれる．P を別な方法で，獨立に測るか，ある模型を考へてそれから理論的に求めるかすることが出來れば幸である．

dv/v，又は，dv/dt, が時と共に變る有樣，(第7圖には，dv/dt の變化を示してある)，は，後に，述べる樣に地盤の，窮極の沈下量を推定する場合に幾分か參考になる．

もう一つ注意されることは，P と ξ との上述の關係が土の場合には成り立つとすれば，第 6 圖から認められる樣に II の場合の方が P の値が大となる．このことは，別の見方からすれば，II の方が收縮し易い傾向を持つことであり，II の土の構成が I の土よりも Loose であらうとの想像の一根據となり得る．

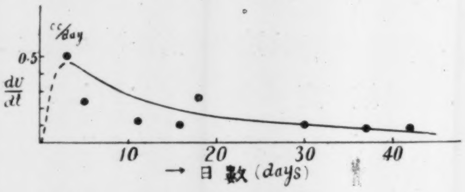

第7圖　日數の經過に伴ふ土の收縮率の變化．

4. 前報告に略述した樣に，深川に建設した 35 m 鐵管製水準點頂部と，附近地表面との間の比高の變化を，昭和 12 年 3 月以來自記してゐる．茲には，今日迄に得たその結果について略述しやう．

先づ，自記紙上に記錄された比高の變化を 1 日 3 回讀みとり，之を平均して每日の平均の高さを算出し，それを 時に對して Plott したものが，第 8 圖に示されてゐる．この曲線に示されて居る樣に，地表面は絕えず不規則な昇降を繰返してゐる．是等の不規則な昇降に混つて，略 1 日週期の變化がある．これは，鐵管が氣溫の變化に應じて膨脹～收縮する爲に生ずるとしても一應は解釋できる．即ち，鐵管の底部が固定されてゐるとすれば，その頂部の上昇高は，鐵管全體が一樣の溫度 T となつた時，

$$\delta l=\alpha\cdot T\cdot l.$$

で與へられる．α は鐵の線膨脹係數で，約 $0{\cdot}1\times10^{-4}$, l は鐵管の長さで，約 30 m で

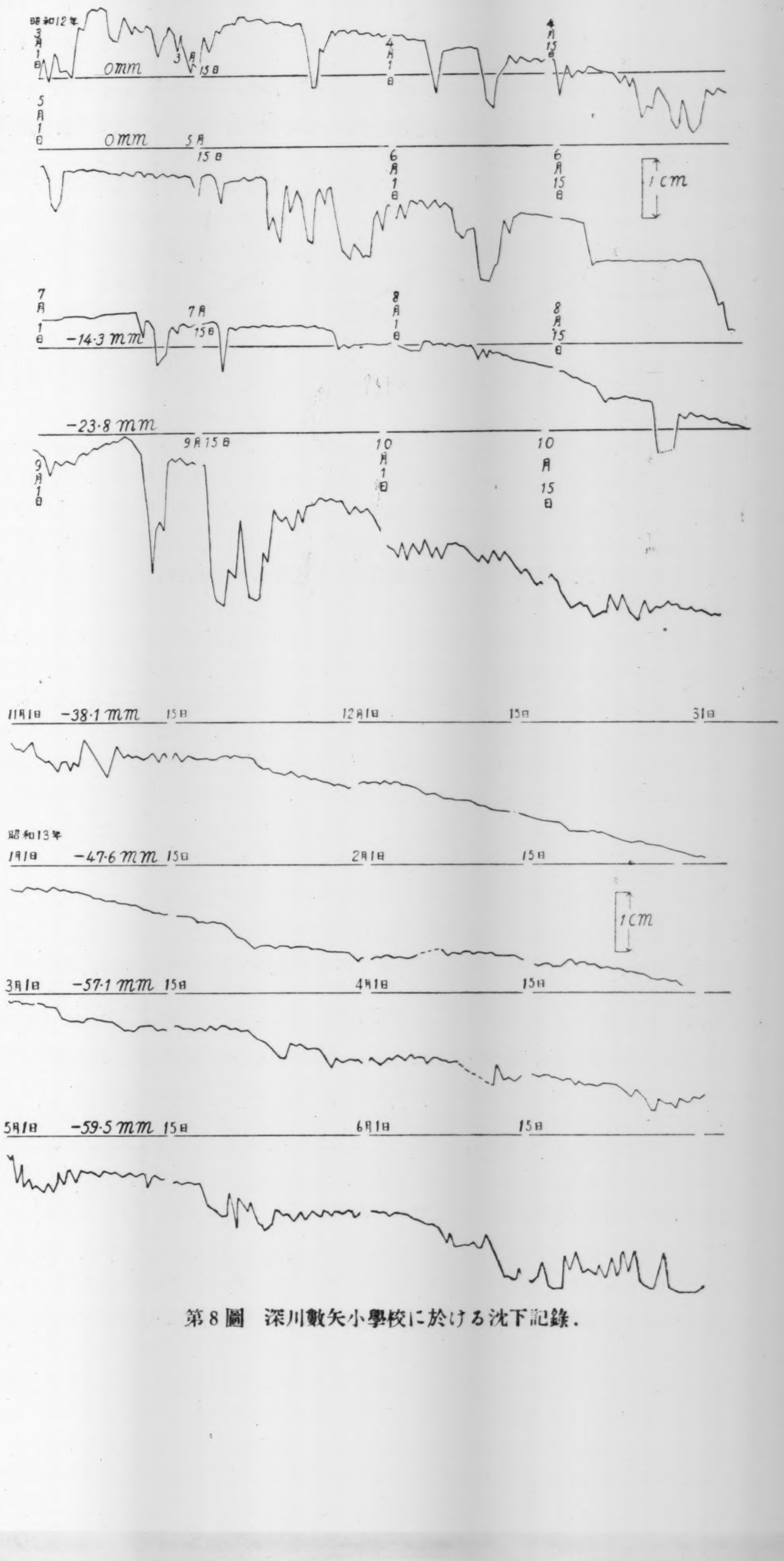

第8圖 深川數矢小學校に於ける沈下記錄.

あるから，Tが 10°C の時 $\delta l = 3{\cdot}0$ mm となる．併し，實際の場合は，鐵管全部が一樣な溫度にはならないであらうし[12]，底部を固定するといふ條件も滿足されてゐるかどうか分らないから，$\delta l = 3{\cdot}0$ mm といふ値は，寧ろ上限値を與へるものと考へるべきであらう．實際の沈下曲線（第8圖の曲線を假にかく名づける）における日週的變化は事柄が更に複雜である．それは，第9～10圖に示す樣に，ある期間の沈下曲線に於

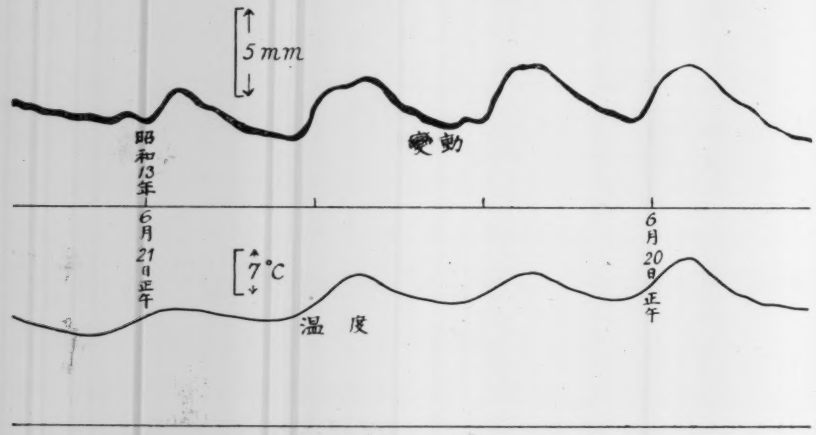

第9圖　溫度の變化と變動曲線とが略平行する場合．

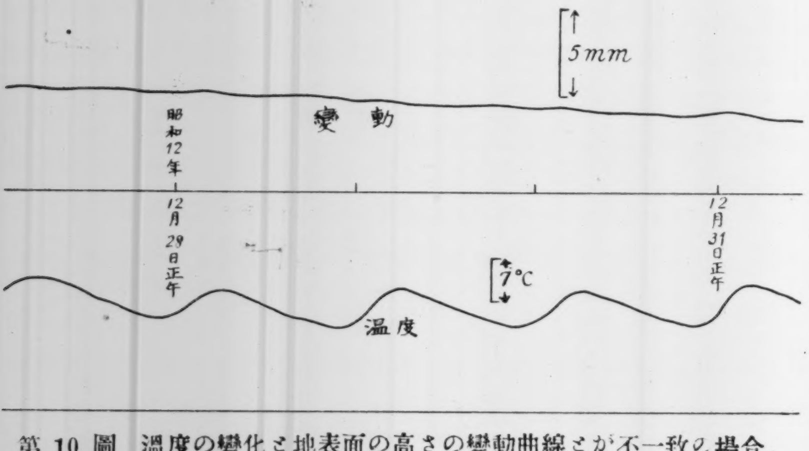

第 10 圖　溫度の變化と地表面の高さの變動曲線とが不一致の場合．

ける氣溫と曲線との關係と，他の期間の同じ關係とは，量的に必ずしも等しくない．これは，更に第三の事情が，關聯してゐることを示すものであらう．その第三の事情については未だ何も考へられてゐない．併し，さ樣な事情の存在如何にかゝはらず，沈下曲線の長期變化卽ち，地盤が，全體としては徐々に低下しつゝあるといふ傾向は

---

[12] 半無限體の表面に溫度を與へれば地下 z の深さでは　$T = T_0 e^{-z\sqrt{\frac{\pi c\rho}{k\tau}}} \sin\left(2\pi\frac{t}{\tau} - z\cdot\sqrt{\frac{\pi c\rho}{k\tau}}\right)$ であるから之に應ずる鐵管の延びは　$\delta l_1 = \alpha T_0 \int_0 e^{-z\sqrt{\frac{\pi c\rho}{k\tau}}} \sin\left(2\pi\frac{t}{\tau} - z\sqrt{\frac{\pi c\rho}{k\tau}}\right) dz$ で與へられる．かくして算出した δl_1 は勿論上述の $\alpha T{\cdot}l$ よりは小さい．

氣溫によつて殆ど影響されてゐないと言へるであらう.

沈下曲線における日週變化以外の不規則な變化は雨量と關係あるらしく見える. 第11圖は, 雨量と, 沈下曲線から沈下の一般的傾向を除いた Fluctuation とを比較した圖である.

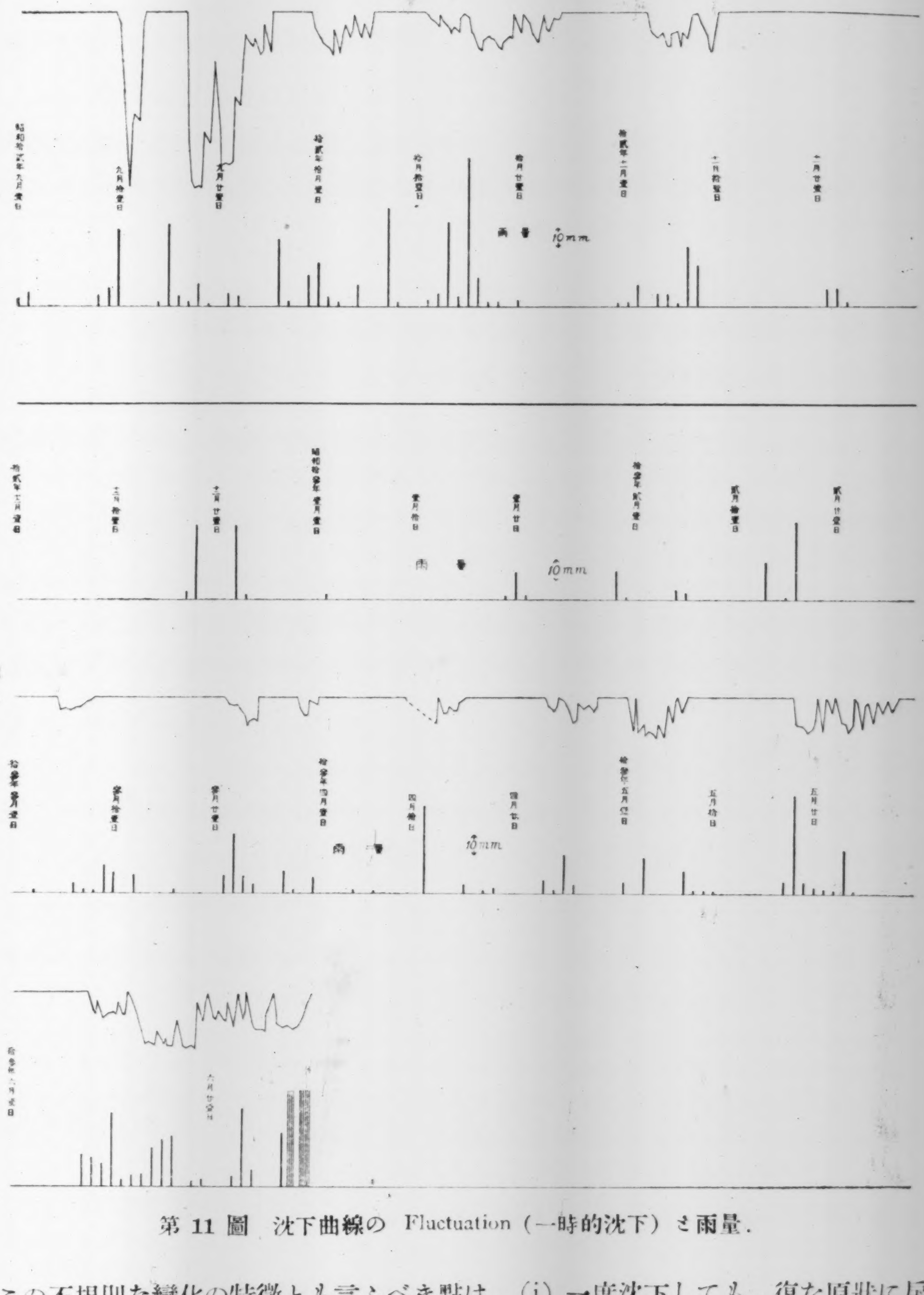

第 11 圖　沈下曲線の Fluctuation (一時的沈下) と雨量.

この不規則な變化の特徴とも言ふべき點は, (i) 一度沈下しても, 復た原狀に戻る

ことと，(ii) 單に沈下して，それが回復するといふだけで，隆起して回復するといふ場合は殆どない，といふことである．

普通の沈泥又は粘土に於いては，水分が增加すると共に膨脹し，乾くと共に收縮するのが常であるから，上述の様な不規則な一時的沈下は，雨の水分が，一時的に土中に浸み込んだ爲に生じたと考へることは困難である．

雨水の一部が表面土層中に淺く浸み込んで，それが荷重として作用し，表面土層を變形せしめると考へることは可能である．併し，雨水の幾パーセントが荷重として作用し得るかといふ問題もあり，その荷重による表面土層の見掛上の彈性變形（原狀に戻るといふ意味で）が，實際記錄された變形と同程度になる樣に安排することは出來るが，實際現在の樣に，鋪裝，排水の設備がよくなつてゐる時に，充分水分が浸み込んで，荷重の作用をするかどうか疑問でもある．

尙，雨量と，一時的沈下の量との間の關係も，量的には必ずしも單純でない．第11圖に示す樣に，同樣の雨量に對しての一時的沈下の樣式は多樣である．

以上に述べたのは，沈下曲線中に現はれる一時的な變化についてゞあつて，其等に對しても未だ明確な解答は與へられないわけである．

以上に述べた樣な Fluctuation を除いた後，沈下曲線は Smooth な曲線となる．この曲線の形は，地盤沈下の趨勢を示すものであるから，充分長期に亘つて觀測した後に於いて，はじめて沈下現象が，若しそれが眞に表面的な現象であるならば，如何に終局に近づくかを知ることが出來る．併し，現在では，未だ1年餘のデータがあるのみであるから，その樣なことを論ずるわけにはゆかない．たゞ，季節的に沈下の割合が如何に變化したかについては述べることが出來る．

每1週間の沈下量を第8圖の沈下曲線から求め，之を1個月につき平均する．每1週間の沈下量は，前述の樣な降雨に伴ふ Fluctuation の爲めに，かなり Fluctuate するが，之を1個月につき平均すれば，大體，著しい Fluctuation は Smooth される．月平均の每週沈下量は，第 V 表に示した通りであつて，大略1年を週期とする變化がある樣にみえる．卽ち，昭和 12 年の3月，4 月の値は，昭和 13 年の3月，4 月

第 V 表 月平均每週沈下量 (mm/week)

月次	1937 3	4	5	6	7	8	9	10	11	12
每週沈下量 (mm)	1·63	1·37	1·07	2·48	2·52	2·48	2·33	2·18	1·22	2·15
月次	1938 1	2	3	4						
每週沈下量 (mm)	2·04	1·00	1·63	1·41						

の値に略々等しい．そこで，昭和 12 年 5 月から一昭和 13 年 4 月までの毎週沈下量について調和分析を試みた．その結は次の表の通りである（第 VI 表）．

第 VI 表　調和分析の結果

Order	0	1	2	3	4
Amplitude	-1·87(mm/Week)	-0·53(mm/Week)	-0·34(mm/Week)	-0·04(mm/Week)	-0·46(mm/Week)
Phase	—	−1·4 month	+2·9 month	−2·9 month	−0·9 month

分析の結果はもつと高次の項も出るが，あまり高次のものは，實際 Amplitude も小さい上，誤差も大となり，且つ原の値に既に誤差があり，その誤差に基く Fluctuation があるのであるから，計算の結果としては出ても，物理的にはあまり意味がないであらうといふ意味で除いた．又，上表の如く，第 4 次の項と第 2 次の項とは Amplitude が大であつて，位相差もあるやうであるが，この両者の間の位相差は約 3 個月であつて，それは丁度 4 次の變化の週期に一致する故，第 2 次と 4 次の變化は略々同一位相であると稱してもよいのではないかと思はれる．

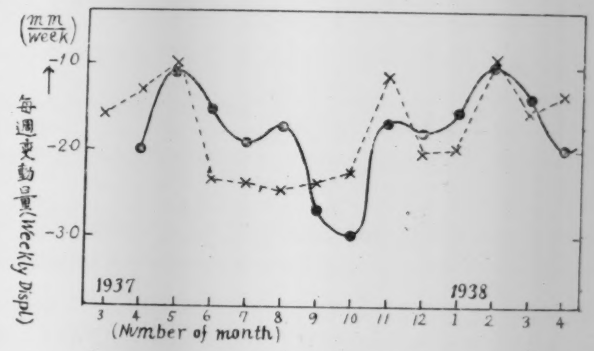

第 12 圖　月平均毎週變動量の變化．

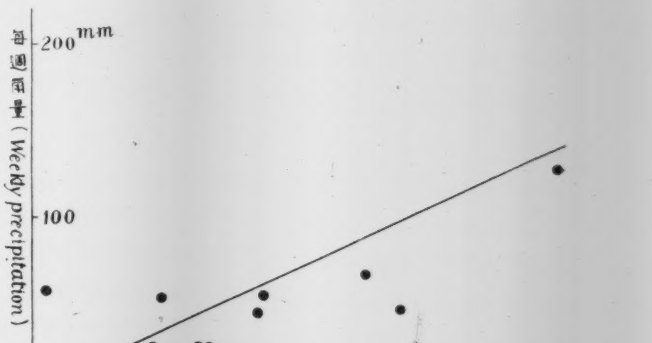

第 13 圖　毎週變動量と毎週雨量．

上の第 1，2，4 次の變化だけをとつて計算した．[13] 毎週沈下量の年變化の有様と，實際の毎週沈下量とは第 12 圖に比較してある．

とにかく，何によつて生ずるかは別として，今までに知られた所では，沈下の割合は，夏から秋の期間に大であり，冬から春の間に於いて小さいといふことになる．今後更に，數年間同様の記錄を得た後，もう少し深く現象を理解することが出來るやうになるであらう．

尙，雨量が Fluctuation に對しては比較的密接な關係にあることは既に示したが，General な沈下とは如何なる關係にある

---

[13] 3 次の項は他に較べて Amplitude が小さいから除いておいた．
第 12 圖で，×は實測値，●は計算値を示す．

かを見る爲に，第 13 圖を作つてみた．これは一週間の間の沈下量と，その間の全雨量との關係を示したものである．これによれば，″雨量が多い程沈下量も大になる傾向″ はあるが，沈下量が大なる時でも雨量は必ずしも大でない．この圖に於ける雨量と沈下量との比較關係は寧ろ，第 11 圖の傾向があらはれたものと解せられてよいのではないかと思はれる．

5. 前節に述べた鐵管製水準點における地盤沈下の記錄の Check とすると共に，その附近の地表面の移動が，鐵管の Relative movement によつて影響されるか否かを調べる目的で，鐵管から，夫々 0·3 m，1·0 m，3·0 m，13 m 離れた場所に，鐵のリベツトを埋め，之を臨時の水準點として，是等と，鐵管水準點との間の上下方向の變位を普通の水準測量の方法で測定した．その結果は第 VII 表の通りである．

第 VII 表

水準點	B_1	B_2	B_3	B_4	N·B.
鐵管からの距離	0·3m	1·0m	8·0m	13·0m	
1937·Aug 10 測定	−0·5067m	−0·5379m	−0·8831m	−0·9247m	U字管を用ふ
1937·Oct. 30. ″	−0·5208m	−0·5546m	−0·9112m	−0·9542m	″
1938·July. 11. ″	−0·5499m	−0·5850m	−0·9298m	−0·9651m	Zeisslevel.を用ふ
1938·Aug. 9. ″	−0·5568m	−0·5898m	−0·9332m	−0·9705m	″
1938·Sep. 9. ″	−0·5599m	−0·5925m	−0·9370m	−0·9751m	″

是等の測定結果から第 VII 表に掲げた所の，各水準點 B_1，B_2，B_3，B_4 の鐵管水準點震 1 號に對する各期間の上下方向の移動量が算出される．(第VIII表)

第 VIII 表

水準點 / 期間	B_1	B_2	B_3	B_4
1937 : 8月10日 1937 : 8月30日	−14·1mm	−16·7mm	−28·1mm	−29·5mm
1937 : 10月30日 1938 : 7月11日	−29·1mm	−30·4mm	−18·6mm	−10·9mm
1937 : 8月10日 1938 : 7月11日	−43·2mm	−47·1mm	−46·7mm	−40·2mm
1938 : 7月11日 1938 : 8月 9日	− 6·9mm	− 4·8mm	− 3·4mm	− 5·4mm
1937 : 8月10日 1938 : 7月 9日	−50·1mm	−51·9mm	−50·1mm	−45·6mm
1938 : 8月 9日 ″ : 9月 9日	− 3·1mm	− 2·7mm	− 3·8mm	− 4·6mm
1937 : 8月10日 1938 : 9月 9日	−53·2mm	−54·6mm	−53·9mm	−50·2mm

以上の結果によると，鐵管の見掛けの拔上りによつて附近の地表面が變形されるやうな傾向も見える．この測量では最初の2回はU字管を用ひた．このU字管による水準測量の場合には，U字管を連絡するゴム管中に空氣の混入しやすい傾向があつて，その成果は，充分信頼し得ない．大體の移動量の Order 位が信用し得る程度であらう．これに反して，精密水準測量用の Zeiss の Level と，標尺とを用ひて行つた昭和 13 年以後の測量成果は充分信用し得るやうである．例へば昭和 12 年7月 11 日から8月9日迄の記録紙上の讀みの差は 18·6 である．記録紙上の 1 目盛は 1·56mm にあるから，記録紙上には，29·02 mm の移動を描いたことになる．而して，記録裝置中の移動量の擴大裝置における槓杆の比は 4·3 であるから，[14] 29·02 mm をこれで割れば，$6{\cdot}7_5$ mm となり，記録裝置に近接してゐる水準點 B_1 の同一期間の移動量と殆ど相等しくなる．

この測定も，今後尙，數多く繰返へせば，更に深く沈下現象を理解する一助となり得るであらう．

丸の內及び日比谷附近にも，地盤の著しい沈下が認められる．それで，此にも同樣の設備を施して研究の資料を得たいといふ希望を持つてゐたところ，水準點を建築物に設置することが許されるに至つたので，之を利用することが出來やうになつた．既に北澤博士も[15]，日比谷附近で地表面の移動を不斷に測定して居られるが，方法も多少異るので，敢て，この測定を開始した．

建物に設置した水準點は，第 14 圖にその構造の大要を示してある．主要部分は鐵の鑄物で作られ；蓋は眞鍮製である．之を建物の外壁の一部に埋め込み，中心部にある標識の頂部の高さを精密水準測量の方式で測定する（第 14 圖參照）．

是等の水準點を設置した建物は，大體に於いて，基礎の堅固なものを選んだ．卽ち下記（第IX表）の諸建築物で，昭和 13 年5月中に測定した其等の水準點の高さも併記してある．

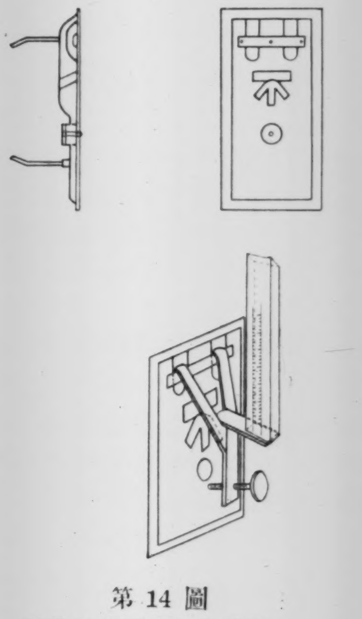

第 14 圖
建物に設置した水準點．

---

[14] 記録紙上の讀定値を實際の移動量に直す爲めの "直しの係數" は 0·36 となる．

[15] 北澤五郎　建築學會論文集 9 (1938)，187〜194.

第 IX 表

水準點名稱		所在	眞高（昭和13年5月測定）
海	W	海上ビル新館南側西	3·5786m
海	E	同　東	3·5879
21	E	三菱21號館東側玄關	4·0535
21	M	同　南側西寄玄關	4·0376
21	W	同　西側玄關	4·0204
寳	E	東寳劇場北側東	3·1863
寳	W	同　西	3·1814
大	W	大阪ビル舊館裏側西	3·7719
大	M	同　東	4·2326
大	E	同　新館東	2·9250
政	E	市政會館東側北寄玄關	5·1119
政上	W	同西側同上	5·1494
政下	W	同西側地階	0·9278

以上の中，東寳劇場に設置した水準點は，麴町3號の既設水準點に近接してゐるので，寳 W，寳 E，と麴3號との間の水準測量を毎月1回施行することにした．既に得た結果は次の第 X 表の通りである．各點の高さは，常に麴3號水準點を 2·2564m として算出してある．尙，念の爲に，途中に固定點を1點とり[16]（之をA點と假稱する）その高さをも測定しておく．

第 X 表

日附 / 水準點	昭和13年5月20日	同年7月11日	同年8月9日	同年9月9日
寳 W	3·1814	3·1836	3·1873	3·1885
寳 E	3·1863	3·1888	3·1919	3·1931
A	2·4466	2·4466	2·4461	2·4442
kd 3 號	2·2564	——	——	

斯くて是等諸點の變動量は次表（第XI表）に示される．

第 XI 表

期間 / 水準點	1938年5月20日 〜 〃 7月11日	1938年7月11日 〜 〃 8月9日	1938年5月20日 〜 〃 8月9日	1938年8月9日 〜 〃 9月9日	1938年5月20日 〜 〃 9月9日
寳 W	+2·2mm	+3·7mm	+5·9mm	+1·2mm	+7·1mm
寳 E	+2·5mm	+3·1mm	+5·6mm	+1·2mm	+6·8mm
A	0·0	−0·5mm	−0·5mm	−1·9mm	−2·4mm

この結果は，東寳劇場の建物が2個月餘の間に約6mm上昇したことになつてゐる

16）固定點Aは有樂座さ日比谷映畫劇場さの中間附近で道路の西側溝石．

が，それは，勿論，建物が上昇したとするよりも，地表面の方がそれだけ沈下したとした方が妥當である．又，固定點 A の移動量 −0·5 mm は，それだけ麴3號水準點より多く沈下した意味ではあるが，± 0·5 mm 程度の誤差は測定の誤差と同程度であるから，確かにそれだけよけいにA點が沈下したとすることは出來ない．

以上の結果も，今後更に多くのデータを蒐め得た後，沈下現象の考察を進める上に重要なる資料になるものと思はれる．

6. 昭和 13 年 3~4 月に，東京市内に散在する 298 個の水準點を含む路線につき改測を行つた．東京市内には，舊市内に東京市土木局所管 169 個の水準點と，復興局の設置した 16 個の水準點とがあり，昭和 4~5 年にその高さが測定されて居る．その後昭和7年に，その一部の改測を行ひ17)，更に，江東方面の新市域に 57 個の水準點を新設し，その第一回測量を昭和 8~9 年に完了した．それ故，今次の改測は，一部に關しては第2回，他の部分に對しては第1回の改測である．

その外，東京市内外には，陸地測量部所管の水準點も，56點在り，これ等の水準點に關しては，從來屢々改測されて居る．今回の改測の結果を，前回の測量成果と比較して算出された各水準點の垂直變動量は，第 XII 表に示されてゐる．又，これらの水準點の分布は第 15 圖に揭げられてゐる．

第 XII 表　昭和 13 年 3~4 月測定垂直變動量

水準點 (B.M.)	前測量	變動量	水準點 (B.M.)	前測量	變動量
	昭和	mm		昭和	mm
1	5年 2月	− 243·5	12	5年 6月	16·6
J—2	〃 〃	8·2	13	〃 〃	15·8
3	〃 〃	− 7·7	J-14	〃 〃	10·3
4	〃 〃	− 23·6	15	〃 〃	− 7·1
J—5	〃 〃	− 17·1	J-16	〃 〃	2·0
6	〃 〃	− 254·5	II	〃 〃	10·3
J—0	〃 6	− 12·6	J-17	〃 〃	− 136·4
J—7	〃 〃	− 15·5	18	〃 〃	10·1
8	〃 〃	3·0	19	〃 〃	6·4
J—9	5 12	2·9	20	〃 〃	− 2·3
10	5 6	− 206·9	21	〃 〃	− 9·4
I	〃 〃	9·9	III	〃 〃	− 9·9
11	〃 〃	16·5	J-22	〃 〃	− 14·2

（次頁へ續く）

---

17) N. MIYABE, *Bull. Earthq. Res. Inst.*, **10** (1932), 844~857; *Proc. Imp. Acd.*, **8** (1932), 417~420.

水準點 (B.M.)	前測量	變動量	水準點 (B.M.)	前測量	變動量
	昭和	mm		昭和	mm
23	5年 6月	− 20·7	R 21	5年 4月	− 17·5
24	〃 〃	− 19·2	R 23	5 3	− 327·3
J-25	8 7	− 249·1	R 26	〃 〃	− 50·3
26	5 3	− 214·6	R 27	〃 〃	− 19·3
IV	8 11	− 237·8	R 32	〃 8	− 422·0
2002	5 6	− 351·2	R 35	〃 〃	− 644·0
2003	〃 〃	− 26·0	Kd 1	〃 〃	− 45·6
2004	〃 〃	− 20·8	Kd 2	〃 〃	− 50·2
3365	8 10	− 206·4	Kd 3	〃 9	− 443·5
3366	〃 11	− 221·4	Kd 4	〃 〃	− 16·0
3367	9 3	− 185·2	Kd 5	〃 〃	− 10·0
3368	〃 4	− 175·8	Kd 6	〃 〃	− 256·0
0	〃 〃	− 177·8	Kd 7	〃 10	− 6·2
3369	〃 〃	− 59·7	Kd 8	〃 11	− 2·7
3370	〃 5	− 7·8	Kd 9	〃 〃	− 7·4
0	9 10	56·2	Kd 10	〃 〃	− 7·4
3374	〃 9	55·9	Kn 1	4 10	− 35·0
3375	〃 〃	− 192·5	Kn 2	〃 〃	− 21·5
3376	10 3	− 217·6	Kn 3	〃 〃	− 36·0
3377	〃 6	− 299·0	Kn 4	〃 〃	− 27·9
3378	5 3	− 709·1	Ni 1	〃 〃	− 109·5
3379	〃 〃	− 398·3	Ni 2	〃 〃	− 32·9
0	〃 〃	− 87·6	Ni 3	〃 9	− 35·4
9831	6 3	− 610·0	Ni 4	〃 〃	− 30·3
9832	5 6	− 906·8	Ni 5	〃 10	− 25·5
9833	10 7	− 202·7	Ni 6	〃 〃	− 477·1
9834	〃 6	− 301·3	Ky 1	〃 11	− 6·6
9835	〃 2	− 133·4	Ky 2	〃 〃	− 5·8
9836	9 12	− 50·5	Ky 3	〃 10	− 17·8
9837	10 10	7·1	Ky 4	〃 〃	− 15·7
R−1	4 8	− 14·6	Ky 5	5 3	− 130·3
R 2	〃 〃	− 3·3	Sb 1	8 5	− 30·5
R 3	〃 〃	− 161·2	Sb 2	〃 〃	− 13·3
R 8	4 10	− 21·5	Sb 3	〃 〃	− 5·3
R 12	〃 〃	− 32·2	Sb 4	5 4	0·2
R 13	4 9	− 4·1	Sb 5	5 3	1·8
R 15	〃 〃	− 17·8	Sb 6	〃 4	3·6
R 18	5 4	− 167·8	Sb 7	〃 〃	− 26·6
R 19	〃 〃	− 204·4	Sb 8	〃 〃	− 44·0
R 20	〃 〃	− 9·4	Sb 9	〃 〃	− 53·8

(次頁へ續く)

水準點 (B.M.)	前測量	變動量	水準點 (B.M.)	前測量	變動量
	昭和	mm		昭和	mm
Sb 10	5年 4月	2·4	Us 2	4年11月	− 6·4
Sb 11	〃 〃	8·1	Us 3	〃 〃	− 0·2
Sb 12	〃 〃	11·4	Us 4	〃 〃	− 10·8
Sb 13	〃 〃	7·4	Us 5	〃 〃	3·6
Sb 14	〃 〃	− 1·8	Us 6	〃 〃	− 0·6
Sb 15	〃 〃	7·6	Us 7	〃 〃	2·0
Sb 16	〃 〃	7·1	Us 8	〃 〃	1·4
Sb 17	5 4	3·1	Us 9	〃 〃	− 1·5
Sb 18	〃 〃	− 28·7	Us 10	〃 〃	0·4
Sb 19	〃 〃	− 34·7	Us 11	〃 〃	− 3·0
Sb 20	〃 〃	− 11·6	Us 12	〃 〃	3·5
Az 1	4 9	5·6	Ki 1	〃 12	− 807·1
Az 2	〃 〃	− 19·0	Ki 2	〃 〃	− 209·6
Az 3	〃 〃	0·8	Ki 3	〃 〃	− 20·5
Az 4	〃 〃	− 3·9	Ki 4	〃 10	2·6
Az 5	〃 〃	1·0	Ki 5	〃 〃	− 2·4
Az 6	〃 〃	7·5	Ki 6	〃 〃	—
Az 7	〃 〃	7·2	Ki 7	〃 〃	− 4·1
Az 8	〃 〃	8·4	Ki 8	〃 〃	—
Az 9	〃 〃	3·2	Ki 9	〃 〃	− 15·7
Az 10	〃 〃	6·6	Ki 10	〃 〃	− 19·5
Az 11	〃 〃	− 45·5	Ki 11	〃 〃	− 25·2
Ak 1	〃 10	− 632·9	Ki 12	〃 11	− 26·4
Ak 2	〃 〃	− 141·7	Ki 13	〃 〃	− 24·2
Ak 3	〃 〃	3·7	Ki 14	〃 〃	− 75·8
Ak 4	〃 〃	10·5	Ki 15	〃 〃	− 6·3
Ak 5	〃 〃	− 448·6	Ki 16	〃 〃	− 8·0
Ak 6	〃 〃	11·4	Ki 17	〃 〃	− 8·5
Ak 7	〃 〃	10·2	Ki 18	〃 〃	—
Ak 8	〃 〃	5·8	Ki 19	〃 〃	− 6·9
Yt 1	〃 〃	1·8	Ki 20	〃 〃	− 11·2
Yt 2	〃 〃	2·1	Ki 21	〃 〃	− 31·3
Yt 3	〃 〃	5·5	Hn 1	5 2	− 24·5
Yt 4	〃 〃	2·1	Hn 2	〃 〃	− 33·7
Yt 5	〃 〃	—	Hn 3	〃 〃	− 23·3
Yt 6	〃 11	—	Hn 4	〃 〃	− 30·1
Yt 7	〃 〃	4·0	Hn 5	〃 3	− 32·2
Yt 8	〃 〃	1·0	Hn 6	〃 〃	− 26·9
Yt 9	〃 〃	− 1·6	Hn 7	〃 〃	—
Us 1	〃 〃	− 304·1	Hn 8	〃 〃	− 40·4

（次頁へ續く）

水準點 (B.M.)	前測量	變動量	水準點 (B.M.)	前測量	變動量
	昭和	mm		昭和	mm
IIn 9	5年 3月	− 40·4	IIk 5	4年 8月	− 447·6
IIn 10	〃 〃	− 43·7	IIk 6	〃 〃	− 992·3
IIn 11	〃 〃	− 129·0	IIk 7	〃 〃	− 568·1
IIn 12	〃 〃	− 36·3	IIk 8	〃 9	− 780·7
St 1	〃 〃	− 15·4	IIk 9	〃 〃	− 949·9
St 2	〃 〃	− 20·9	IIk 10	〃 8	− 503·2
St 3	〃 〃	− 25·4	IIk 11	〃 11	− 585·4
St 4	〃 2	− 64·8	IIk 12	〃 9	− 676·6
St 5	〃 〃	− 24·3	IIk 13	〃 11	− 886·0
St 6	〃 〃	− 33·8	IIk 14	〃 9	− 498·7
St 7	〃 〃	− 34·3	IIk 15	〃 〃	− 774·4
St 8	〃 〃	− 259·5	IIk 16	〃 〃	− 508·7
St 9	〃 〃	− 203·9	IIk 17	4 9	− 708·9
St 10	〃 〃	− 33·7	IIk 18	〃 〃	− 246·9
As 1	〃 〃	− 20·9	IIk 19	——	——
As 2	〃 〃	− 55·1	Ad 1	8 10	− 223·0
As 3	〃 1	− 243·8	Ad 2	〃 11	− 234·4
As 4	〃 〃	− 411·5	Ad 3	〃 9	− 141·8
As 5	〃 〃	− 384·2	Ad 4	〃 11	− 172·1
As 6	〃 〃	− 103·9	Ad 5	〃 10	− 112·6
As 7	〃 3	− 29·9	Ad 6	〃 12	− 33·0
IIz 1	4 10	− 52·0	Ad 7	〃 〃	− 11·5
IIz 2	〃 〃	− 113·3	Ad 8	〃 〃	− 6·7
IIz 3	〃 11	− 237·5	Ad 9	〃 〃	− 4·1
IIz 4	〃 8	− 449·6	Ad 10	9 1	− 14·4
IIz 5	7 2	− 420·6	Ad 11	〃 〃	− 89·0
IIz 6	4 10	− 638·1	Ad 12	〃 〃	− 20·1
IIz 7	〃 9	− 647·6	Ad 13	〃 〃	− 18·8
IIz 8	7 1	− 249·2	Ad 14	〃 2	− 51·5
IIz 9	4 11	− 676·0	Ad 15	〃 3	− 145·3
IIz 10	4 8	− 454·3	Ad 16	11 11	− 114·8
IIz 11	〃 〃	− 420·6	Ar 1	8 10	
IIz 12	〃 〃	− 783·4	Ar 2	〃 〃	
IIz 13	〃 7	− 519·0	Ar 3	〃 〃	
IIz 14	〃 8	− 363·4	Ar 4	〃 〃	
IIz 15	〃 〃	− 250·7	Ar 5	〃 9	− 168·0
IIk 1	〃 10	− 316·6	Ar 6	〃 〃	− 280·5
IIk 2	〃 8	− 572·9	Kt 1	8 10	− 245·5
IIk 3	〃 〃	− 488·0	Kt 2	9 7	− 144·0
IIk 4	〃 〃	− 431·8	Kt 3	〃 〃	− 41·2

(次頁へ續く)

水準點 (B.M.)	前測量	變動量	水準點 (B.M.)	前測量	變動量
Kt 4	昭和 9年 6月	mm 38·0	Zt 2	昭和 10年 7月	mm − 330·5
Kt 5	〃 〃		Ed 1	〃 6	− 299·9
Kt 6	〃 7		Ed 2	〃 4	− 282·8
Kt 7	〃 〃		Ed 3	9 10	55·1
Kt 8	〃 6	52·9	Ed 4	〃 9	54·3
Kt 9	〃 9	− 64·2	Ed 5	〃 11	46·3
Kt 10	〃 8	− 137·5	Ed 6	〃 〃	− 25·0
Kt 11	〃 〃	− 190·6	Ed 7	〃 〃	− 15·9
Kt 12	〃 7	− 116·9	Ed 8	〃 〃	53·3
Kt 13	〃 〃	− 57·4	Ed 9	〃 10	54·1
Mk 1	10 5	− 72·7	Ed 10	〃 11	39·9
Mk 2	〃 〃	− 139·3	Ed 11	〃 12	8·1
Mk 3	〃 4	− 217·4	Ed 12	〃 〃	− 17·5
Mk 4	〃 5	− 200·2	Ed 13	10 1	− 20·3
Mk 5	〃 4	− 463·9	Ed 14	〃 〃	− 38·5
Zt 1	〃 6	− 292·4	Ed 15	〃 〃	− 296·2

[N.B.] 數字の前のローマ字は，交點 (J) 復興局水準點 (R) を意味する外，次表の如く各所屬區名を示す．

記號	區名	記號	區名
Kd	麴町	Hn	本郷
Kn	神田	St	下谷
Ni	日本橋	As	淺草
Ky	京橋	Hz	本所
Sb	芝	Hk	深川
Az	麻布	Ad	足立
Ak	赤阪	Ar	荒川
Yt	四谷	Kt	葛飾
Us	牛込	Mk	向島
Ki	小石川	Zt	城東
		Ed	江戸川

是等の變動量に相應する期間は場所によつて異るから，變動の分布狀況を研究する爲めには，これを年平均變動量に直さなければならない．そこで，上表の變動量をその變動を生じた期間（年數）で割り，年平均變動量を算出した．第 XIII 表に示したのがその數字である．

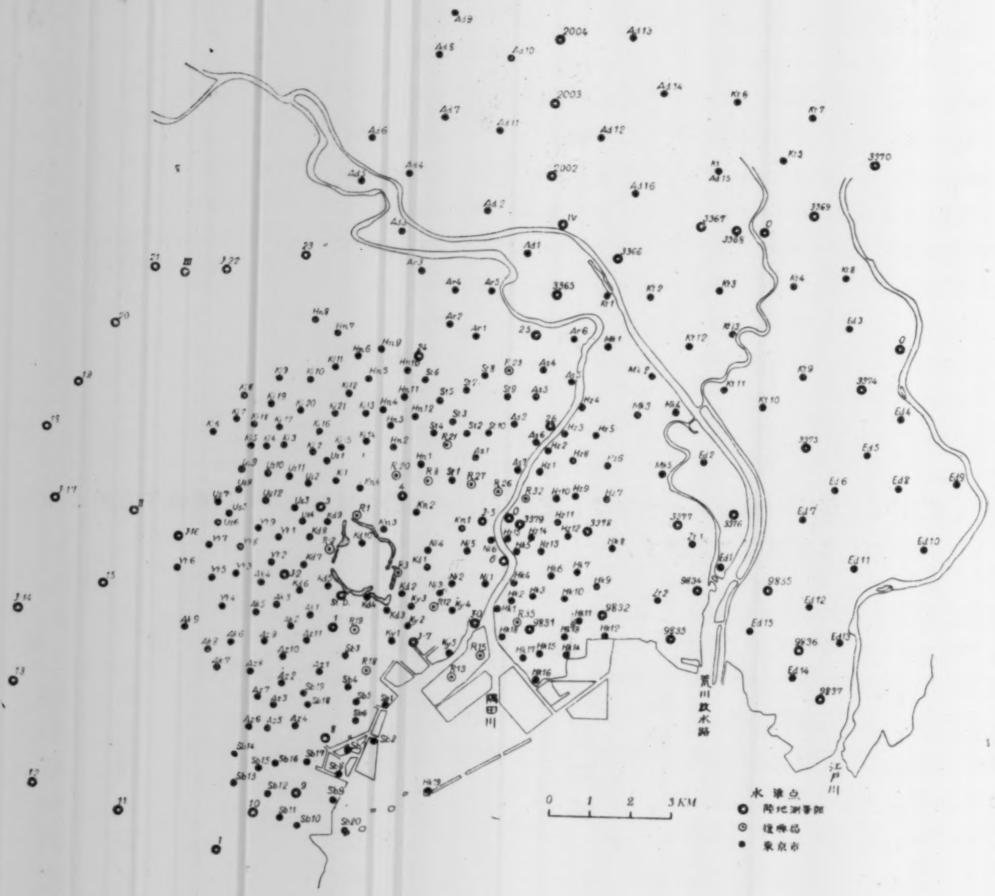
荒川放水路
隅田川
江戸川
0 1 2 3 KM
水準点
◎ 陸地測量部
⊙ 復興局
● 東京市

第 15 圖 東京市內の水準點の分布．

第 XIII 表 江東方面にある水準點の最近の沈下率.

（＋は沈下を示す）

水準點 (B.M.)	沈下率 (mm/year)	水準點 (B.M.)	沈下率 (mm/year)	水準點 (B.M.)	沈下率 (mm/year)
J—25	+ 53·0	3368	+ 44·0	9834	+ 107·6
Ar 5	+ 37·3	0	+ 44·5	Zt 1	+ 104·4
Ar 6	+ 62·3	3369	+ 14·9	Zt 2	+ 122·4
As 3	+ 26·5	3370	− 0·7	3378	+ 88·6
As 4	+ 50·2	Kt 2	+ 38·9	3379	+ 49·8
As 5	+ 46·9	Kt 3	+ 11·1	0	+ 11·0
26	+ 26·8	Kt 4	− 10·0	R 32	+ 49·1
As 6	+ 12·7	Kt 8	− 13·9	Hz 1	+ 6·1
As 7	+ 3·7	Kt 9	+ 18·3	Hz 2	+ 12·2
R 26	+ 6·1	Kt 10	+ 38·2	Hz 3	+ 28·3
R 27	+ 2·3	Kt 11	+ 52·9	Hz 4	+ 51·3
J—-5	+ 2·1	Kt 12	+ 31·6	Hz 5	+ 69·0
K n1	+ 4·2	Kt 13	+ 15·5	Hz 6	+ 75·1
Ni 1	+ 12·9	0	− 16·6	Hz 7	+ 76·2
Ni 2	+ 3·9	3374	− 16·0	Hz 8	+ 42·1
Ni 3	+ 4·2	3375	+ 55·0	Hz 9	+ 80·5
Ni 5	+ 3·0	3376	+ 72·5	Hz 10	+ 59·8
Ni 6	+ 51·7	9835	+ 43·0	Hz 11	+ 48·9
6	+ 31·4	9836	+ 15·3	Hz 12	+ 91·1
J—-0	+ 1·7	9837	− 3·0	Hz 13	+ 54·7
Ky 4	+ 1·9	Ed 1	+ 107·1	Hz 14	+ 42·8
Ky 5	+ 15·5	Ed 2	+ 94·3	Hz 15	+ 23·7
J—7	+ 2·0	Ed 3	− 15·7	9831	+ 87·1
R 13	+ 0·5	Ed 4	− 15·5	9832	+ 116·3
R 15	+ 2·1	Ed 5	− 13·6	R3·5	+ 74·8
R 18	+ 21·0	Ed 6	+ 7·4	Hk 1	+ 37·7
Sb 1	+ 3·8	Ed 7	+ 46·8	Hk 2	+ 66·6
Sb 2	+ 2·8	Ed 8	− 15·8	Hk 3	+ 56·7
Sb 6	− 0·5	Ed 9	− 15·9	Hk 4	+ 50·2
8	− 0·4	Ed 10	− 11·7	Hk 5	+ 52·0
Sb 7	+ 3·3	Ed 11	− 2·5	Hk 6	+ 80·5
Sb 8	+ 5·5	Ed 12	+ 5·3	Hk 8	+ 66·0
Sb 9	+ 6·7	Ed 13	+ 6·3	Hk 9	+ 90·9
Sb 20	+ 1·4	Ed 14	+ 12·0	Hk 10	+ 111·4
Sb 10	− 0·3	Ed 15	+ 92·6	Hk 11	+ 69·1
J—9	− 0·4	M k1	+ 72·1	Hk 12	+ 79·6
Sb 1	− 0·4	Mk 2	+ 49·8	Hk 13	+ 105·5
Ad 1	+ 49·5	Mk 3	+ 72·5	Hk 14	+ 58·7
3365	+ 45·9	Mk 4	+ 69·0	Hk 15	+ 90·0
J—IV	+ 54·0	Mk 5	+ 155·9	Hk 16	+ 59·8
Kt 17	+ 54·6	3377	+ 106·8	Hk 17	+ 83·0
3366	+ 50·3	6833	+ 75·1	Hk 18	+ 29·0
3367	+ 46·3				

これには江東方面の水準點の値のみを擧げてある．尙この分布は，第 16 圖に示してある．

併し，この數字が，各水準點の沈下率（年平均沈下量）を示すと見做す爲には，若干の假定を必要とする．

今，原點からn番目の水準點の高さを第1回測量において H^n_n と測定したとし，第2回測量の時の高さを H'^n_n とする．この高さは，その絕對値を直接に測るのではなくて，隣接の水準點との間の比高 h_n, h'_n を測り，これ等の比高を原點からn番目の

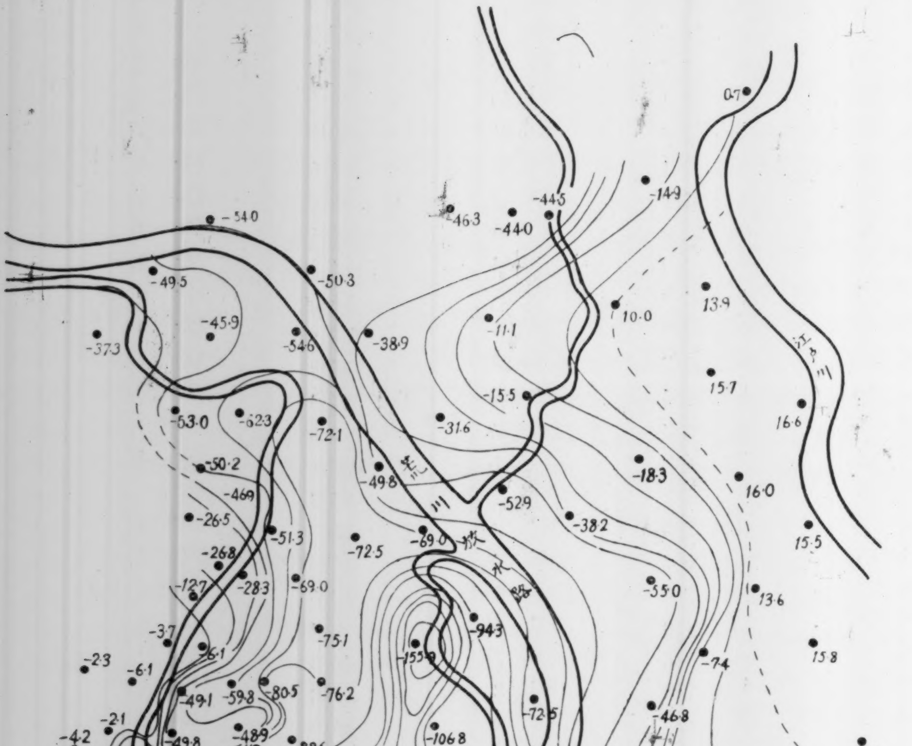
荒川
放水路
荒川放水路
隅田川
江戸川
東京湾
0.7
-14.9
-44.5
-46.3
-44.0
-54.0
-50.3
-49.5
-45.9
-37.3
-54.6
-38.9
-11.1
10.0
13.9
15.7
16.6
-15.5
-31.6
-53.0
-52.3
-72.1
-50.2
-46.9
-49.8
-52.9
-18.3
16.0
-38.2
15.5
-26.5
-51.3
-72.5
-69.0
-26.8
-28.3
-69.0
-12.7
-55.0
13.6
-3.7
-75.1
-94.3
-2.3
-6.1
-56.1
-155.9
-7.4
15.8
-49.1
-59.8
-80.5
-76.2
-72.5
-2.1
-46.8
-4.2
-49.8
-48.9
-88.6
-106.8
-23.7
-42.8
-91.1
11.7
-3.0
-51.7
-52.0
-54.7
-104.4
-107.1
2.5
-31.4
-129.1
-50.2
-111.4
-107.6
-43.0
-3.9
-56.7
-4.2
-66.6
-122.4
-5.3
-1.9
-1.7
-37.7
-69.1
-116.3
-92.6
-74.8
-87.1
-6.3
-29.0
-105.5
-79.6
-75.1
-15.3
-15.5
-58.7
-83.0
-12.0
-59.8
3.0

第 16 圖・江東地域に於ける水準點の沈下率の分布．

點まで，加へ合せるのであるから，

$$H^n_n - H^n_{n-1} = h_n,\quad H^{n-1}_{n-1} - H^{n-1}_{n-2} = h_{n-1},\ \text{etc.}$$

$$H'^n_n - H'^n_{n-1} = h'_n,\quad H'^{n-1}_{n-1} - H'^{n-1}_{n-2} = h'_{n-1},\ \text{etc.}$$

とおけば，

$$\sum h_n = H^n_n - H_0 - \left\{(H^n_{n-1} - H^{n-1}_{n-2}) + (H^{n-1}_{n-2} - H^{n-2}_{n-2}) + \cdots\cdots\right\}$$

$$\sum h'_n = H'^n_n - H'_0 - \left\{(H'^n_{n-1} - H'^{n-1}_{n-1}) + (H'^{n-1}_{n-2} - H'^{n-2}_{n-2}) + \cdots\right\}$$

となる．$(H^n_{n-1} - H^{n-1}_{n-1})$，$(H^{n-1}_{n-2} - H^{n-2}_{n-2})$ 等は，h_n，h_{n-1}，h_{n-2} 等の比高を測つた時期が夫々異つて居り，其等の僅かの期間に生じたと考へられる．高さの變化を無視し得ない時には當然殘るものである．其故，是等は，多くの場合は0とおいてゐるものである．是等の項は簡單に，$\sum\frac{\partial H^n_{n-1}}{\partial t}\partial\tau_{n-1}$，$\sum\frac{\partial H'^n_{n-1}}{\partial t}\partial\tau'_{n-1}$ 等と書き直せる．

第1回測量の時期と第2回測量の時期との間の期間も亦，場所によつて，多少異り n の函數であるから，之を τ_n とする．

尙，H_0，及 H'_0 は原點の高さであつて，これは前後2回の測量の間で變化はないと認めるのであるから

$$H'_0 - H_0 = 0$$

とおいて差支ない．

精密に言へば，H_n の變化の割合は，

$$\sum_n \frac{h_n - h'_n}{\tau_n}$$

で，計算されなければならない．τ_n は大體は同じ値で，$\tau_n = \tau(1+\varepsilon_n)$．とおきかへられ，$\varepsilon_n$ は，$1 \ll \varepsilon_n$ なる條件を滿足するとすれば，

$$\sum_n \frac{h_n - h'_n}{\tau_n} \approx \frac{1}{\tau}\sum_n (h_n - h'_n)(1-\varepsilon_n).$$

$$= \frac{1}{\tau}\left\{\sum_n (h_n - h'_n) - \sum_n \varepsilon_n (h_n - h'_n)\right\}$$

となる．卽ち，

$$\frac{1}{\tau}\sum\left\{H^n_n - H'^n_n) - (1-\varepsilon_n)\left[\frac{\partial H^n_{n-1}}{\partial t}\partial\tau_{n-1} - \frac{\partial H'^n_{n-1}}{\partial t}\partial\tau'_{n-1}\right]\right.$$

$$\left. - \sum \varepsilon_n (H^n_n - H^n_n)\right\}$$

となるから，

$$\frac{1}{\tau}\left\{\sum(1-\varepsilon_n)\left[\frac{\partial H^n_{n-1}}{\partial t}\delta\tau_{n-1}-\frac{\partial H'^n_{n-1}}{\partial t}\delta\tau'_{n-1}\right]-\sum\varepsilon_n(H^n_n-H'^n_n)\right\}$$

が 0 になるか，$\frac{1}{\tau}(H^n_n-H'^n_n)$ に對して充分小なる限り，前述の様に，高さの變動量を期間で割つた $\frac{1}{\tau}(H^n_n-H'^n_n)$ を以て各水準點の垂直變動率（玆では年平均變動量）と見做し，その分布を論ずることが出來る．

而して，その爲めには，各水準點の變動率（沈下率）が著しい變化を示さないことが必要である．

そこで，從來屢々測量されてゐる，陸地測量部の水準點につき，沈下率の變化する有様を調べてみると第 17 圖に示したやうなものとなり，多少の變動はあるけれども，前後 2 回の測量期間中で不連續的の變化はないから，期間が充分に長ければ上述の條件を滿足して居ると言へる．

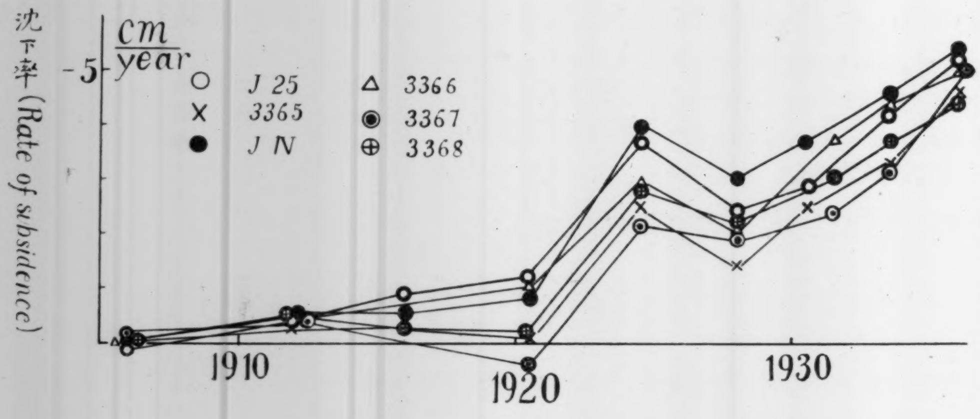

第 17 圖 I. 沈下率の變化.

下述の様な理由で，第 16 圖が沈下率（或は沈下速度）の分布少くともその大體の形勢を示すものである，といふことが認められるとすれば，最も著しく沈下する地帶の，深川區南部から東北に荒川放水路に沿うて北の方に延びてゐることが知られる．即ち，向島，城東の各區には，本所深川の兩區にも勝つて，沈下の著しい場所がある．

又，沈下の著しい地域の東緣は，大體，荒川放水路の東約 1 粁にひかれる放水路と略々平行な線であることが判る．更に，沈下の稍々著しい地域が，千住一松戸を結ぶ線より北の方へも延びてゐるらしい形跡も見える．

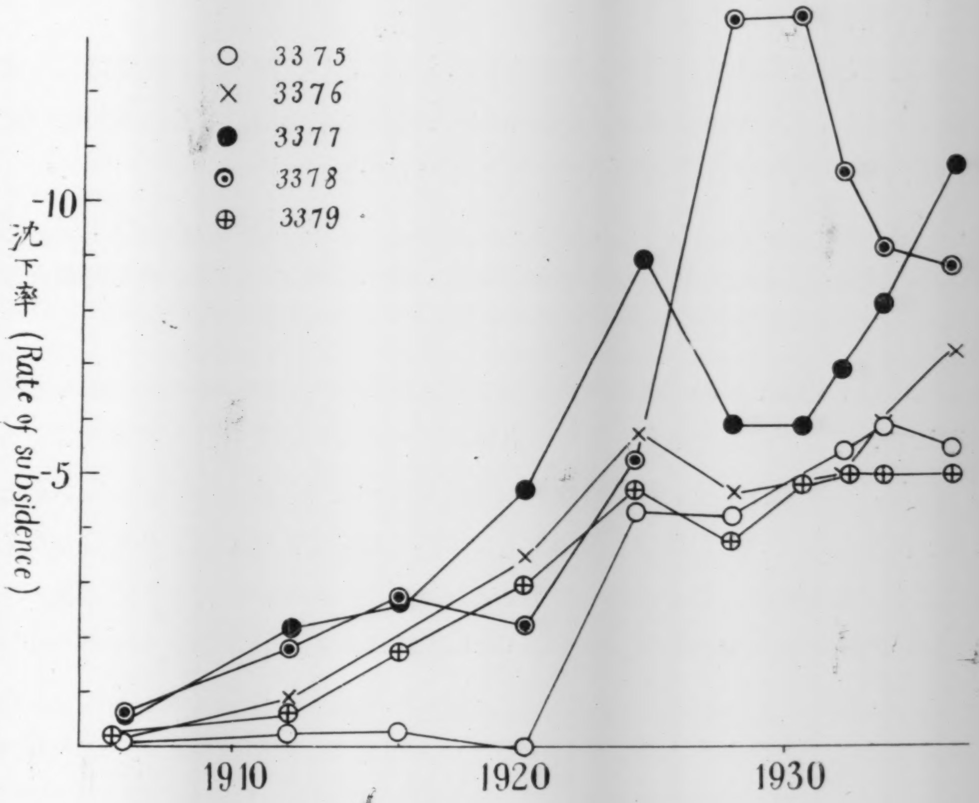

第17圖 II. 沈下率の變化,

この測量は今後更に何回か行ひ，その成果を待つて，更に考察を進め得る希望を持つものである．

7. 實際問題としては，沈下の現象の研究に關して次の點の解答を求めてゐる．

（i） 地盤の著しい沈下は，一時的の現象か？ 若し，さうならば，結局，幾何の沈下をするのであらうか．

（ii） 一時的の現象ならば，その終熄するまでに幾何の歳月を要するか？

是等の要求に對して，一部は解答されてゐる．卽に既に報じたやうに，江東その他の地域に於ける地盤沈下は，主として，表面にある厚さ 20～30 m 位の軟土層の收縮によるものと考へられるのである．已に，表面の軟土層の收縮である限りは，その收縮に限度がある筈であり．限りなく沈下を繼續するものとは考へられないであらう．

以上の如き考へに基いて，簡單な假定をおけば，最後の狀態に至る迄の全沈下量，或は又，年數等を推定することも出來る．たゞその結果は，あくまで推定量であることを注意する必要がある．何故ならば，その推定は，現在までに判明してゐる事實だけを基礎として，假定する方式のもとに沈下現象が進行し，中途で何等の障害なく最

後の狀態に到達することを前提としてゐるからである．

その推定の方法に關しては色々異見があるかもしれない．例へば，渡邊博士[18]は，軟土層の自重と，その表面荷重とが，沈下を生ずる原因であつて，その中特に"表面荷重"は，所謂"早期沈下"の原因であると考へてゐる．

今，問題となるのはこの所謂"早期沈下"であつて，土の自重による沈下は，渡邊氏の計算の結果によれば，實際の沈下量に比して遙かに少さいので，殆ど問題とはならない．

渡邊氏は，"早期沈下"が"表面荷重"による土の密化（Verdichtung）に基くと考へた．そして，その"表面荷重"として，具體的に地表面に建設された建築物等を考慮する．併し，この場合には，具體的な表面荷重を考へなくてもよいのではないかと思はれる．何故ならば，土が水分を失ふことによつて收縮する時には，外壓は加はらないけれども，水分を失ふことによつて生ずる Capilary pressure は外壓に置換へて考へることが出來るからである[19]．つまり Colloid Gel の狀態にある土が水分を失ふといふことは，それによる Capilary pressure の變化に相當する外壓を被るものと見做されるからである．水分を失ふ爲に收縮するといふ現象と，表面荷重によつて收縮沈下するといふこととは，その構想においては異るが，實質的には同等の効果を及ぼすと考へてよいのであらう．さうだとすれば，O. K. Fröhlich[20]氏の方式による渡邊氏の推定沈下量[21]を，そのまゝ，單に水分が失はれてゆく爲に生ずる沈下量と考へても大した差違はない．

併し，こゝで行はうとする沈下量の推定は，さういふ方法ではなく，實際の水準點の沈下率（每年の沈下量）の年と共に變化する有樣から，即ち v（沈下率）の時（年）の函數としての型を適當に假定し，結局幾何の沈下をなすべきかを推定しやうといふのである．

例として，本所にある B. M. 3378 號，及び，深川の B. M. 9832 號の 2 水準點をとり，是等の水準點の沈下率を示せば，第 13 表の如き數字となる．

是等の數字を圖に表はせば第 18 a, b 圖となる．この圖上の Graph 又は第 XIV 表で見られる樣に，沈下率は，こゝ數年間に稍々減少するかの如き趨勢を示してゐるものもある．そこで，是等の Graph から將來の沈下率の變化を推定しやうとするのである．

---

18) 渡邊貫　地震 **9** (1937)，143～158.
19) 君島八郎　地下水　前掲 11).
20) TERZAGHI-FRÖHLICH, *Theri: der Setzung von Tonschichten.*
21) 渡邊貫　地震　前掲 18).

第 XIV 表　垂直變動速度 (mm/year).

期　間	1002 ~1910	1910 ~1914	1914 ~1918	1918 ~1923	1923 ~1926	1926 ~1930	1930 ~1931	1930, Feb.~March ~1934, Feb.~March	1930, Feb.~March ~1937, Jan.~Feb
B.M.3378	− 5·8	−18·3	−27·1	−22·0	−52·5	−133·5	−134·0	−105·7	− 91·4
B.M.9832				−72·9	−93·8	− 91·2	−115·5	−102·3	−108·4

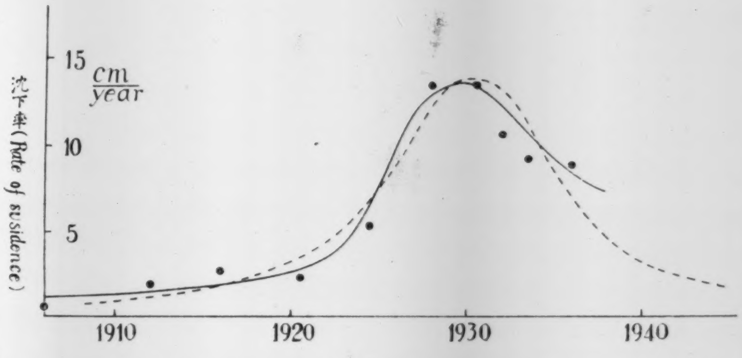

第 18 圖 I. B.M. 3378 號の沈下の率變化.

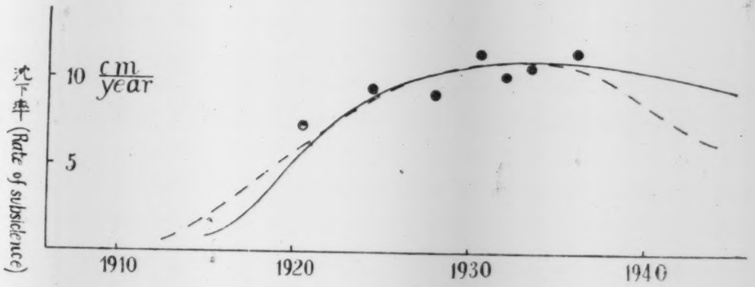

第 18 圖 B.M. 9832 號の沈下率の變化.

それで，是等ら，沈下率 v を，時の函數として如何なる形におくかといふことが問題である．一つの假定は，

$$v = v_0 e^{-k^2t^2}$$

とおき，結局の沈下量を

$$s_1 = v_0 \int_{-\infty}^{\infty} e^{-h^2t^2}\, dt.$$

で計算することである．この場合，v_0 は，v の max. に達した時の値であり，t は v が max. に達した時から計つた年數である．

尙，この場合，沈下現象の實際的に止むまでの年數を t_m とし，v が v_0 の 100 分の 1 になつた時を實際的に止んだ時とすれば，

$$\log\frac{v_0}{v}=h^2t^2,\ \text{であるから}\ t_m=\frac{1}{h}\sqrt{\log 100},$$

で計算される．實際に，第 18 圖の a の Graph では，vが上に述べた樣な變化をして居るやうに見えるので，之を應用し得るやうである．

他の一つの假定は，

$$v\doteq v_0te^{-kt}$$

とすることである．

この場合も全沈下量 s は

$$s_{\mathrm{II}}=v_0\int_0^\infty te^{-kt}\,dt$$

で求められる．この場合，t_m の方は簡單には求め難いが，前述の假定の場合よりは遙かに大となる．v が Max. になつてから後の v の減少率が前の場合より小さいからである．

以上の假定は，單に實際の v の變化になるべく近似せしめるといふ以外，理論的に充分根據のあるものとは言ひ難いが，ともかくもこれによつて，全沈下量を，B. M. 3378 號，及び B. M. 9332 號の兩水準點について求めてみると次の表の樣になる．

第 XV 表　B.M. 3378 及 B.M. 9832 の推定全沈下量.[22]

	B. M. 3378	B. M. 9832
s_{I}	243 cm	239 cm
t_m	8 years	26 years.
s_{II}	386 cm	247 cm

この表にある推定全沈下量は，偶然かもしれないが，既に，渡邊氏が推定した値に近い．

又 II の如き假定は，土を乾燥させてその收縮を測つた時その變化，dv/v，が略同樣に時と共に變化したことに基いてなされる假定ではある．併し，實際の沈下率の變化はこの I，II の中間をゆくやうになることと思はれる．

叙上の如き沈下量の推定値は，假定が妥當でなければあまり意味はないものである．又，その假定が，現在までの情勢に關しては妥當であつても，將來，沈下現象の終熄を見るまでは，現在までの情勢がそのまゝ持續されなければならぬといふことも含まれてゐる．

要するに，これは，沈下量推定の一案であつて，その數字が絕對に不動のものでは

---

[22] 現在までの沈下量は B.M. 3378 號については 1.5903 m，9832 號については 1.6579 m であるから今後尙，3378 號は 0.84 m～ 2.27 m，9832 號は 0.73 m～ 0.81 m 沈下するこさになる．

ない．

本稿を終るにあたり，この研究の爲に，多大の研究費を補助して下さつた服部報公會に對して，深甚なる謝意を表すると共に，種々の便宜を與へて下さつた，東京市土木局，陸地測量部，鐵道大臣官房研究所土質調査委員會の各當局に對しても亦，深謝の意を表する次第である．又，本研究の遂行に終始助力せられた，川島正治，猪俣眞三郎，武井柳吉及び實川顯の四君に對しても深く感謝するものである．

---

51. *Subsidence of the Earth's Surface in the Kōtō region, Tokyo II.*

By Naomi MIYABE,

Earthquake Research Institute.

In the preceding paper, the writer showed that the remarkable subsidence of the earth's surface in the Kōtō region, Tokyo, was mainly due to contraction of the soil layer over the region under consideration. It was then felt desirable to ascertain just how the soil layer contracts. For this purpose, contraction of the soil specimen taken from the region under consideration was first studied, with results as summarized below.

(i) For the reason that cracks developed in the soil specimen before it was thoroughly dessicated, total contraction was not measured, as the experiment could not be continued to the end. As far as it could be measured, the contraction was about 7% of volume. The total contraction would probably exceed 10% of the volume.

(ii) The rate of contraction, which was increasing rapidly at the begining of the experiment, attained a maximum, and then diminished very gradually to zero.

(iii) The effect of $MgCl_2$, although not very evident, was neverthless noticeable. The soil when deposited from a $MgCl_2$-solution seems to be less densely packed compared with that deposited from ordinary water. The change in apparent specific weight of the former soil by dessication was 0·062, i. e. from 1·539 to 1·601, whereas that of the latter was 0·045, i. e. from 1·562 to 1·607. It may be due to the effect of Mg-ion on the colloid sol: that is to cause quick deposition due to addition of a slight amount of Mg-salt causes flocculation of colloid sol.

Next, a continuous record of contraction of actual soil as measured in Hukagawa was studied with the following results:

(i) Irregular fluctuations in the curve showing the change in the height of the earth's surface was found to be closely correlated with precipitations (Fig. 11). Heavy rains were in most cases followed by greater changes in the height of the earth's surface, whereas great changes in the height were not always associated with heavy rains. (Fig. 12.)

(ii) A seasonal variation in the weekly amount of contraction was noticed. The monthly mean values of the weekly contractions were plotted, as in Fig. 13, and it seems to have varied with approximate annual period. This curve of variation in weekly contraction was expanded by Fourier series and the coefficients for several harmonics were determined (Table 5).

Lastly, the variation in rate of change in the heights of several bench-marks, measured by means of precise levels, were examined.

For several bench-marks, for instance, B.M. 3378, the rate of vertical displecement increased during **1918~1930**, since when, it has been tending to decrease. From these data, the rate of vertical displacement is assumed to vary with time as in the form of $v_0e^{-h^2t^2}$ or of a_0te^{-kt}.

The total amount of subsidence were calculated for cases of these assumptions. In both cases, the amount of total subsidence was estimated to be about 3 m, which is approximately the same as the value of **10%** for the thickness of the surface layer of soft soil, that covers the Kōtō region, which boring gave as about **30** m.

These results may be important in dealing with the cause of the subsidence or the contraction of the actual soil layer in the Kōtō region of Tokyo.

52. *Phenocryst distribution in the Siroyama hornblende andesite mass exposed near the town of Kanbara, Sizuoka prefecture, and its geologic interpretation.*

By Yanosuke OTUKA and Sinzaburo INOMATA,

Earthquake Research Institute.

(Read March 16, 1938.—Received Sept. 20, 1938.)

Mt. Siroyama, situated behind the town of Kanbara, Sizuoka prefecture, consists of hornblende andesite intruding the Kanbara Plio-Pleistocene conglomerate beds. On the summit of this mountain there is a small isolated patch of a Miocene fossil bearing sandstone, surrounded by the hornblende andesite on all sides except the east, on which last mentioned side there is a thrust fault. The Miocene sandstone, which is called the Siroyama sandstone beds, contacts with the hornblende andesite, intercalating at its boundary a thin layer of tuffaceous sandstone. The senior writer[1], therefore, concluded from these geologic facts that the sandstone might be a xenolith, derived from the roof of the magma reservoir of the hornblende andesite.

In order to obtain further details of the nature of the xenolith and the intrusive phenomena of this andesite mass, the writers examined the inner structure of the andesite mass.

As to the inner structure of an igneous body, H. CLOOS[2] has made a close study of this subject in connection with various igneous masses, the results obtained with a trachyte intrusive mass, the "Quellkuppe" of "Drachensfels" on the river "Rhein", being of particular interest.

In Japan, Prof. M. MORISITA,[3] following the the method of CLOOS, studied the structure of the quartz diorite mass in the Tanzawa mountainland. F. C. PHILLIPS, recently examined the orientation of minerals in some olivine-rich rocks by means of the polarisation microscope with universal stage.

Judging from the results of these studies just mentioned, it would seen that these igneous masses have a certain structures as inferred from the orientation of the crystals distributed. The writers, therefore, expecting to be able to ascertain the inner structure of any igneous mass by examining the orientation of its phenocryst distribution made a study of the Siroyama hornblende andesite mass in the manner to be described. In this study, the junior authour mainly occupied himself with determining the orientation of phenocryst distribution which is the most laborious part of the study.

---

[1] Y. OTUKA, *Bull. Earthq. Res. Inst.*, **16** (1938), 2, pp. 415~451.

[2] H. und E. CLOOS, *Zeitschr. f. Vulk.*, **11** (1927), p. 33.

[3] M. MORISITA, *Journ. Geol. Soc. Japan*, **40** (1933), pp. 325~327.

[4] F. C. PHILLIPS, *Geol. Mag.*, **75** (1938), 885, pp. 130~134.

Has the hornblende andesite a certein structural orientation in the distribution of its phenocrysts?

As the trachyte and the quartz diorite studied by H. CLOOS and M. MORISITA consisted of large crystals, it was an easy matter for them to examine the orientation of phenocryst distribution with the naked eye, but in the case of the phenocrysts in the Siroyama hornblende andesite mass, the crystals were so microscopically small that it was difficult to say whether there was any orientation at all of phenocryst distribution. The writers verified the existence of orientation in the hornblende andesite in the following way:

1. Collecting samples of the hornblende andesite from the field localities, which original situations are recorded, size about (5 cm)^3.
2. Preparing three thin sections from each sample, every plane of which sections must be perpendicular to one another e. g., the horizontal, the meridionally vertical, and the equatorially vertical.
3. Determining the orientation of the long axis of the phenocrysts scattered in these thin sections.
4. Calculating the frequency of occurrence of similarly orientated phenocrysts.

Fig. 1a, b, c show the frequency of these orientated phenocrysts in every three section. These figures show a certain orientation, according to which most all the phenocrysts are arranged, every thin section showing an orientation in the distribution of its phenocrysts. Should, however, orientation in these three sections be at random (haphazard) with respect to one another, a certain orientation would be lacking from one plane as determined by the remaining two of orientations. Although these three orientations shown in Figs. 1a, b, c are included in one plane, it is possible to find

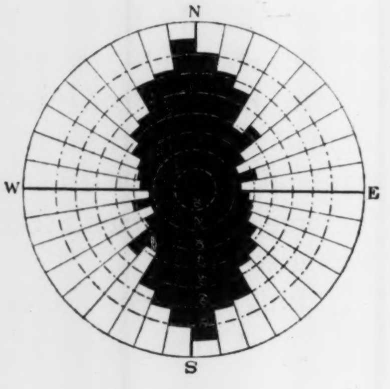

Fig. 1a.

a certain orientation in the phenocryst distribution also in the hornblende andesite mass.

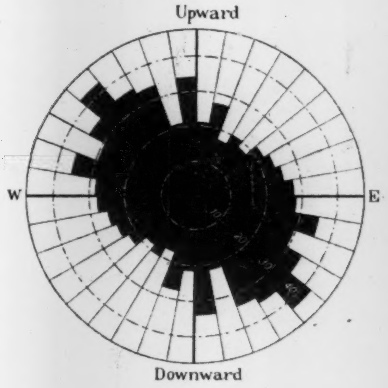

Fig. 1b.

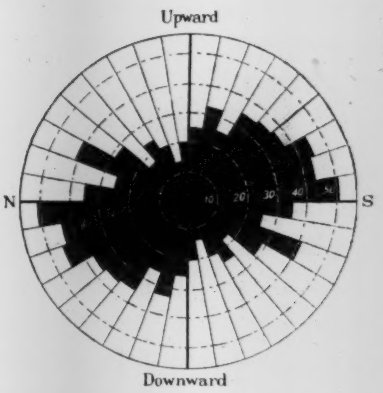

Fig. 1c.

Limits of area similarly orientated.

Since, as just mentioned, the orientated structure in the Siroyama hornblende andesite was ascertained only in one small fragment of rock (5 cm)[3], it was not yet known whether the orientation affects only that part whence the sample came, or whether it affects a larger area. In order to verify this point, the writers examined some specimens obtained a few meters away from the original locality. Examination of these samples showed orientated structure similar to those from the original locality, as shown in Figs. 2, 3, 4. From these facts, the writers conclude that the samples from the two localities seperated by a few meters from each other are similarly orientated, whence it is presumed that the inner structure of the Siroyama andesite mass may be

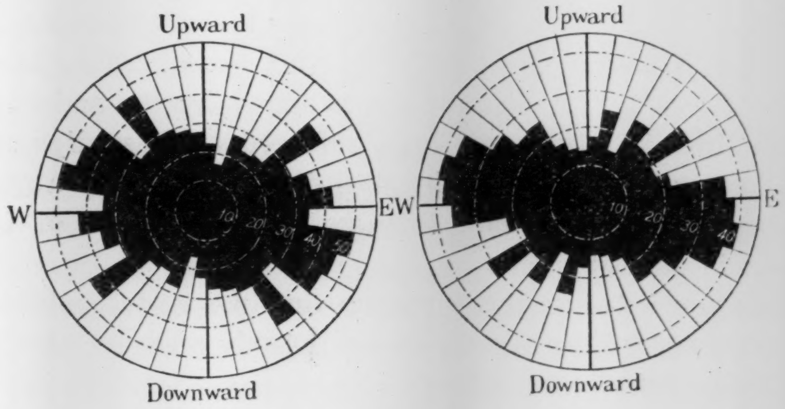

Fig. 2.

inferred from examinations of samples collected from localities seperated by suitable distances.

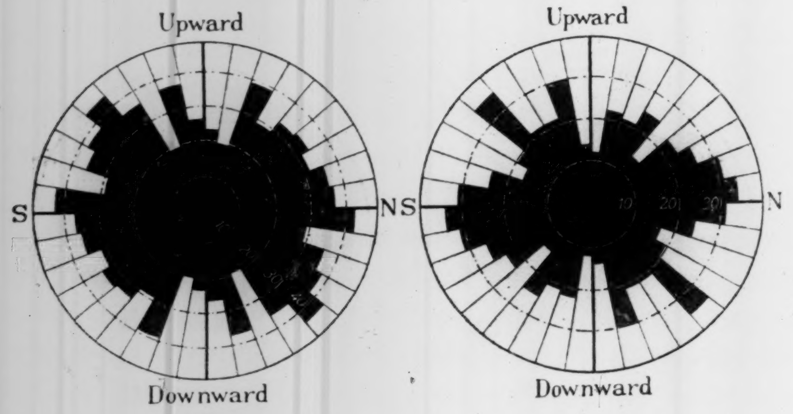

Fig. 3.

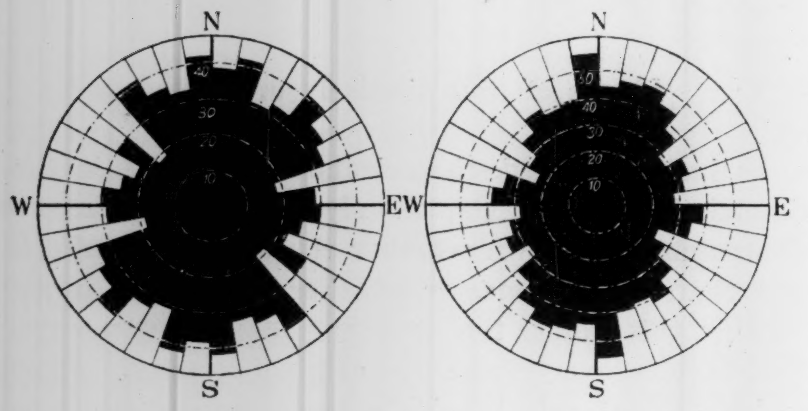

Fig. 4.

Orientation in the distribution of phenocrysts in the Siroyama hornblende andesite mass.

Using the foregoing method, the writers examined the orientation of phenocryst distribution in 12 samples of the Siroyama hornblende andesite. Fig. 5 shows the results of this examination, in which the orientation of phenocryst distribution is shown by dip-and-strike marks. The stream line-like structural lines referred to these dips and strikes, as shown in Fig. 5, are shown by dash-lines. Fig. 6 is a geologic section showing the inner stream line-like structural lines of the Siroyama hornblende andesite.

The relation between these stream line-like structural lines and the geologic boundary of the Siroyama hornblende andesite, reminds one of CLOOS's "Diskonform" contact.

If the writer be allowed to presume that, in an igneous mass that consolidates direct from the molten stage as it wells up from the magma reservoir, the orientation in the distribution of the phenocrysts in the igneous mass makes a "konform" contact with the boundary surface of the magma reservoir; then the Siroyama hornblende andesite mass, after consolidation of the inner structure in the upper part of the magma reservoir, must have been pushed upward by the ascentional force of the still unconsolidated molten part of the magma that lay underneath it. The reason is that it may not be possible for the consolidated inner structure of the upper part of the magma reservoir to conform with the new contact surface that was formed by the welling up of the upper part of the magma reservoir; that is the inner structure of the Siroyama andesite mass, was formed before the establishment of the contact relation now seen near Siroyama.

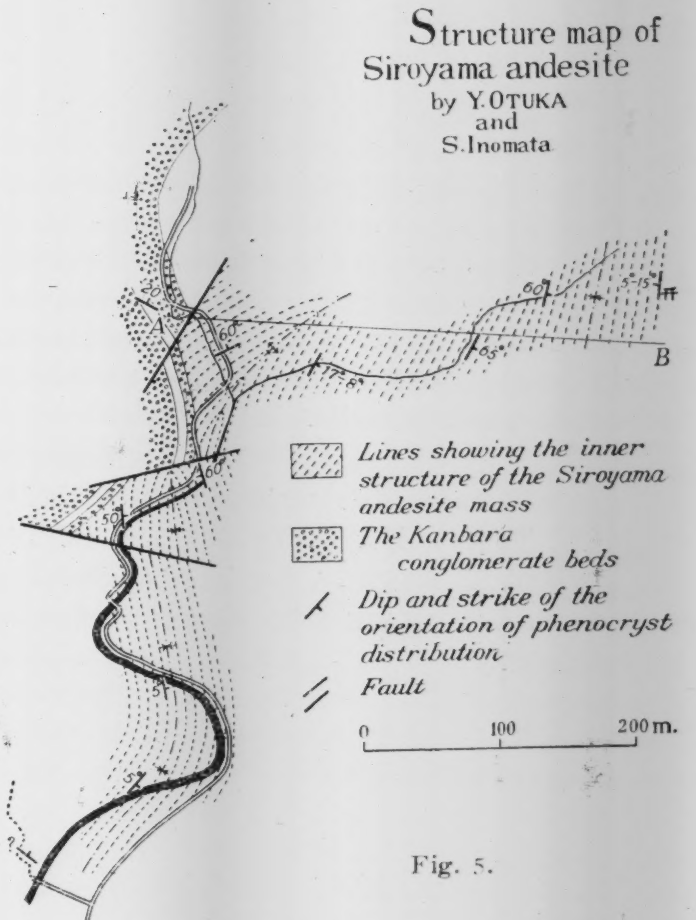
Structure map of
Siroyama andesite
by Y. OTUKA
and
S. Inomata
A
B
Lines showing the inner structure of the Siroyama andesite mass
The Kanbara conglomerate beds
Dip and strike of the orientation of phenocryst distribution
Fault
0
100
200 m.

Fig. 5.

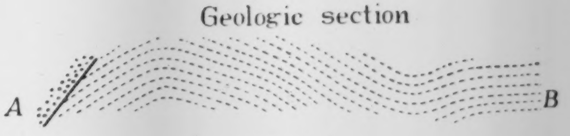
Geologic section
A
B

Fig. 6.

This interpretation would imply certain fault contacts between the Kanbara conglomerate beds and the Siroyama hornblende andesite mass, which implication field observations have confined, seeing that the boundary plane is very smooth with large curvature, and its environs are greatly compressed.

The contact relation between the Miocene Siroyama sandstone xenolith and the inner structure of the Siroyama hornblende andesite mass is rather a "konform" contact, which relation is advantageous to the senior authour's theory of the Siroyama xenolith.

Concluding Remarks.

To sum up,

1) There is a certain orientation in the distribution of the phenocrysts in the hornblende andesite.

2) The orientation not being at random (haphazard), the inner structure of the hornblende andesite mass may be inferred by examining the orientation of phenocryst distribution.

3) The inner structure of the Siroyama hornblende andesite it "diskonform" to its geologic boundary.

4) It seems that the inner structure of the Siroyama andesite mass conforms with the Siroyama sandstone xenolith.

5) The capture of the Siroyama sandstone xenolith occurred earlier than the contact between the Kanbara conglomerate beds and the Siroyama andesite mass.

In conclusion the writers return their thanks to Prof. H. YABE, Prof. S. TSUBOI, Dr. C. TSUBOI, Dr. H. TSUYA, Dr. R. TAKAHASI, H. KUNO, and T. FUCHIDA for kindly interest and criticism in this study, and to S. WATANABE who kindly made many orientated thin sections from them.

---

52. 靜岡縣蒲原町の城山角閃石安山岩體中の斑晶配列方位とその地質學的解釋

地震研究所 大塚彌之助
猪俣眞三郎

靜岡縣庵原郡蒲原町の城山角閃石安山岩體中の斑晶の長軸の方位を顯微鏡を用ひて決定し，此の安山岩體中の斑晶配列に就いて知つた．この結果によると城山角閃石安山岩體は地下にあつて熔融してゐた當時にその岩漿溜の外境に接した一部を既に冷却凝固せしめられてゐたし，その當時の岩漿溜の屋根と思はれる城山砂岩層を破壞捕獲して推し上げ現在の狀態に達したと言ふ解釋に都合のよい斑晶配列構造を示してゐることが解つた．この際この方法の吟味に就いても言及してゐる．

53. *A Note on the Daruma Volcano, Izu, Japan.*

By Hisashi KUNO,

Earthquake Research Institute.

(Read May 17, 1938.—Received Sept. 20, 1938.)

Introduction.

The Daruma volcano, which lies close to the western coast of north Izu (Fig. 1), has received but little attention from investigators, notwithstanding that many other volcanoes in the Fossa Magna region, especially those in Izu and adjacent areas, have been studied in detail during the last ten years. For the purpose of comparing the structure and petrology of this volcano with those of the volcanoes on the eastern coast of north Izu, on the latter of which the writer has been engaged in detailed study, a short trip was made across the area in the spring of 1938,[1] when the general outline of the geology and petrology of the volcano was brought out. The scope of this paper is to present the result of this preliminary investigation.

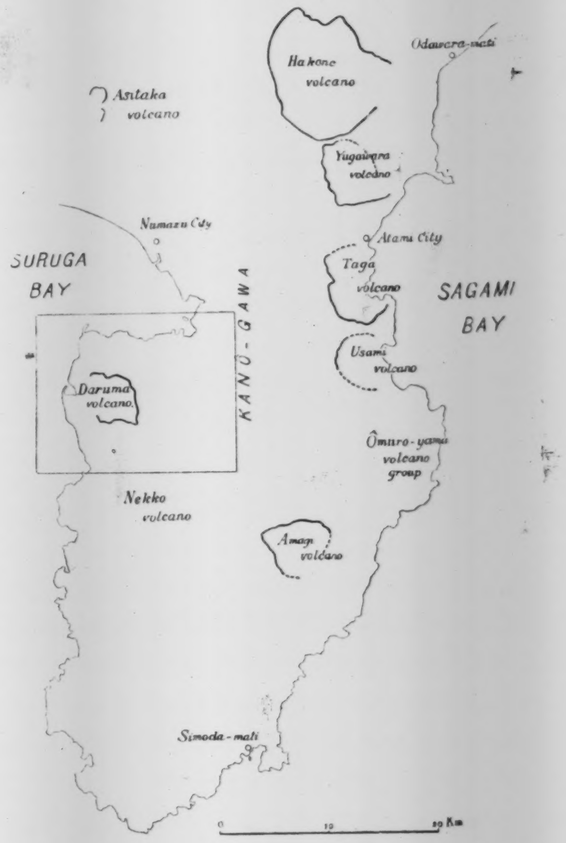
Hakone volcano
Odawara-mati
Asitaka volcano
Yugawara volcano
Numazu City
Atami City
SURUGA BAY
KANO-GAWA
Taga volcano
SAGAMI BAY
Usami volcano
Daruma volcano.
Ômuro-yama volcano group
Nekko volcano
Amagi volcano
Simoda-mati
0
10
20 Km

Fig. 1. Map showing the distribution of chief volcanoes in Izu peninsula.

As early as 1897, Hatutarô Isiwara, in his classical memoir on the volcanoes of Izu,[2] briefly referred to the geology of the Daruma volcano. He recognized a breached central crater, surrounded by a horseshoe-shaped ridge that stretches from Sanagi-yama, through Daruma-yama (981·9 meters), the highest peak of the area, to a point southeast of Heta, and also a side crater which now is represented by a small pond near the summit of Sanagi-yama. According to him, the volcano is underlain by Tertiary tuffs and agglomerates. From observations made on the eastern crater wall, he established the following succession of lavas: first a flow of pyroxene-andesite; second an agglomerate lava; and third a flow of two-pyroxene-andesite. Most of Isiwara's conclusions are confirmed by the present investigation, except that the present writer had no opportunity of visiting the Sanagi-yama crater pond.

---

[1] The trip took the routes from Ôhito, through Huruu, to Heta, thence to Hunayama, and from Heta again, to Syuzenzi-mati.

[2] H. ISIWARA, *Report of the Earthq. Invest. Committee*, **17** (1897).

Topography.

The Daruma volcano is bounded by Suruga Bay on the north and west, by the valley of Kanô-gawa on the east, and abuts against the Nekko volcano, which lies southward, and is presumably older than the former.

Although Daruma is deeply dissected, its eastern half still retains an elegant slope, for which reason, when looking from the north, say, a point near Numazu City, for some distance southward, one finds an even slope descending gently (at about 10°∼5°) from Daruma-yama to the Kanô-gawa valley, a marked contrast to the northerly lying Huzi and Asitaka volcanoes, the flanks of which dip at about 30° near the summits. This slope is bounded on the west by a ridge that extends horseshoe-shape, opening westward. The inner side of this ridge is a precipitous steep slope more than 700 meters high, overlooking the village of Nitta. As already noted by Isiwara, this topography is obviously the remnant of the former crater, although later erosion may have more or less modified the original form.

The western part of the volcano, where dissection is more pronounced, presents a rather complicated topography, scarcely any of the original surface of the volcano being preserved. Numerous spurs, reaching the sea from the western margin of the horseshoe-shaped ridge already referred to, are cut abruptly by a great cliff more than 100 meters high. This cliff extends continuously from north to south, suggesting a fault, along which the western part of the volcano was thrown down into Suruga Bay, although no geological evidence for it is to be found.

In order to give a general topographic outline of the volcano, the map Fig. 2 was constructed by drawing a tangent to each contour line at intervals of 100 meters, using the topographic maps "Numazu" and "Syuzenzi" published by the Land Survey Department. The contour lines in Fig. 2 indicate the most probable extension of the volcano as inferred from the topography.

The features mentioned in the foregoing are also shown in this map.

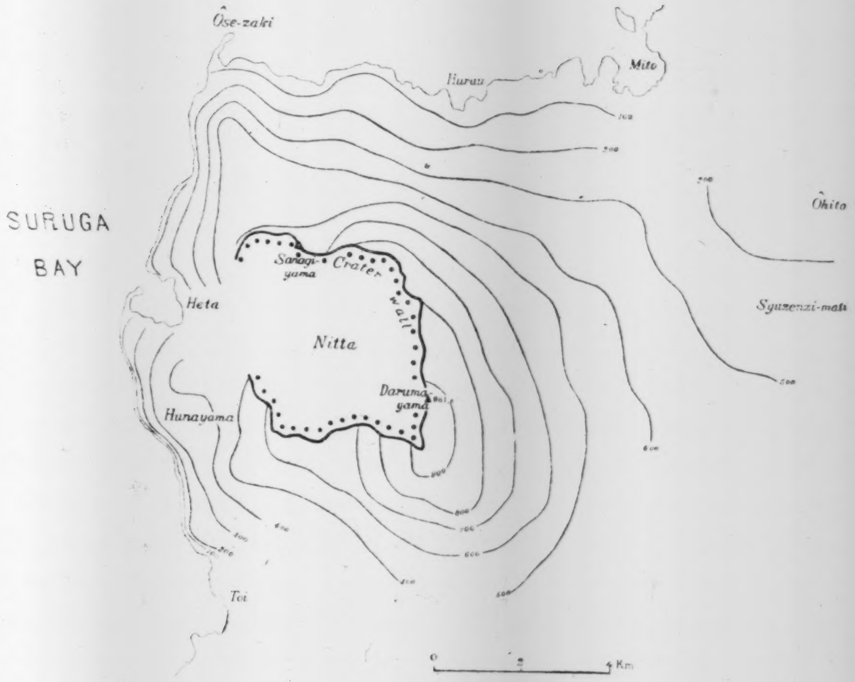
Ôse-zaki
Mito
Hurau
100
200
200
Ôhito
SURUGA
BAY
Sanagi-yama
Crater wall
Heta
Syuzenzi-mati
Nitta
500
Daruma-yama
Hunayama
600
900
800
700
600
400
300
200
400
500
Toi
0
2
4 Km

Fig. 2. Map showing the general topographic outline of the Daruma volcano. Heights are shown in meters.

Geology.

Basement. The bedrocks underlying the volcano are altered dark green andesites, propylite, and the associated pyroclastics, most of which belong to the Yugasima Series[3] (Older Miocene) that form the basement of the whole Izu region. These rocks appear along the numerous valleys around the volcano, namely, between Ôhito and Syuzenzi-mati, and further south; and also near Toi. Although no exposure of these rocks is to be found in the crater bottom around Nitta[4] or along the sea cliff near Heta, it is highly probable that they will be found also underneath the volcano. Some volcanic rocks younger than the Yugasima Series, which seem to form also a part of the basement of

---

3) R. Tayama, Report of the Saitô-Hôonkai, Sendai, **11** (1931).
R. Tayama and H. Niino, Report of the Saitô-Hôonkai, Sendai, **13** (1931).

4) Except some doubtful decomposed rocks that are exposed immediately east of Nitta.

the area, may be seen at several localities.

Structure of the volcano. The volcano is made up chiefly of lavas of hypersthene-augite-andesite, which dip periclinally from the central crater, usually conforming with the topography, although, in the area between Heta and Hunayama, they dip to the north or northwest.

The outstanding feature of this volcano is the remarkable paucity of true pyroclastic rocks, such as tuffs and tuff breccias, lying between the lavas.

On the other hand, each of the lavas is associated with scoriaceous blocky parts both above and below the solid interior, there being a complete gradation between these two parts. The blocks, which, in their lithologic characters, differ in no way from the associated solid parts, are cemented by means of comminuted fragments of the same material. Obviously, these blocky parts represent the auto-brecciated top and base of the lava flow, the interior part of which consolidated into a homogeneous solid mass. Rocks with similar brecciated appearance occur in greater bulk than the solid lavas, and are widely distributed throughout the area. Upon weathering, these rocks look like tuff breccia, and toward the lower part of the flank (between Mito and Huruu), pass into volcanic conglomerate. At any rate, most of these rocks may be classed as blocky lavas, provided that breccias of true explosive origin may not be entirely absent.

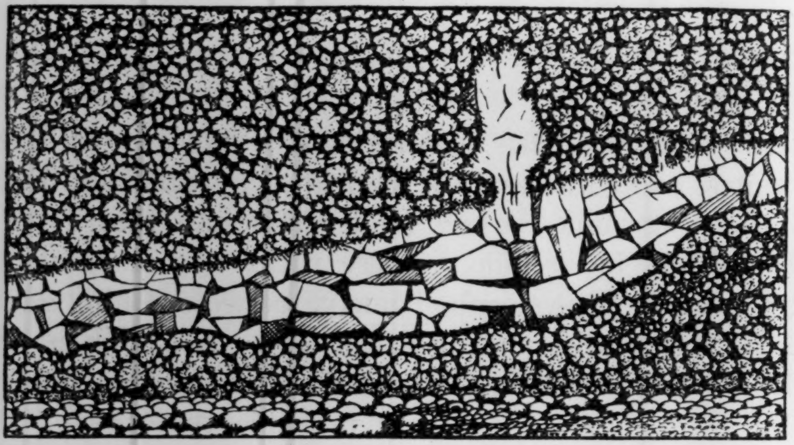

Fig. 3. Auto-intrusion in a lava flow (3~5 meters thick). Beach-gravel is shown in the lower part of the sketch.

An interesting example of an auto-intrusion is seen in one of the flows that are exposed along the sea cliff near Hunayama (Fig. 3). A small offshcot from the solid interior part of the flow, which seems to have been sufficiently fluid at the time of emplacement, is seen to cut the overlying blocky part that had already consolidated then.

The virtual absence in this volcano of layers of tuffs or tuff breccias, combined with the predominance of blocky lavas, gives rise to a peculiar landscape. In the other strato-volcanoes of Izu and Hakone, which are built of solid lavas regularly interbedded with nearly equal amounts of tuffs, the crater walls and the valley walls exhibit a characteristic step-like topography, the resistant lavas forming lines of cliffs that alternate with those of somewhat gentle slope formed of less resistant tuffs. Such a feature is rather an exception in the Daruma crater wall, the chief characteristics of which, however, is a uniformly craggy scarp.

So far as the writer's observations go, dikes are rare in this volcano; he saw one from the valley bottom, immediately south of Sanagi-yama, and another from the sea cliff immediately west of Heta, both trending from northwest to southeast.

Petrology and Succession of Lavas.

The majority of the rocks that were collected from various parts of the volcano are found to be of the same general petrographic type. They are hypersthene-augite-andesite, often with subordinate olivine. Rock types somewhat richer in olivine, and in composition, transitional to basalt, are also represented by a few specimens.

1) *Hypersthene-augite-andesite.* This wide-spread type shows, in fresh specimens, abundant phenocrysts (usually less than 2 mm) of white plagioclase and black pyroxene, occasionally with subordinate yellow olivine, scatterred uniformly through a greyish compact matrix.

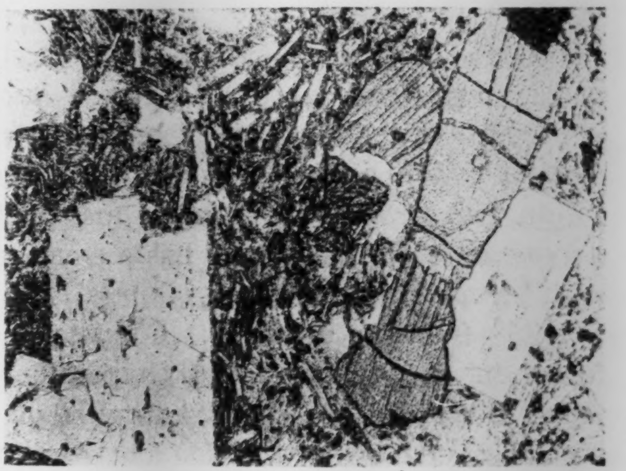

Fig. 4. Olivine-bearing hypersthene-augite andesite, showing phenocrysts of plagioclase, hypersthene, and magnetite. Northeast of Daruma-yama. ×41

Under the microscope (Fig. 4), it carries phenocrysts of zoned plagioclase, light-green augite, weakly pleochroic hypersthene, and magnetite, sometimes attended by a few olivine and apatite. Olivine is often resorbed with formation of corona of hypersthene grains, occasionally accompanied with vermicular magnetite. In a more advanced stage of resorption, it is completely replaced by dense stellate groupings of vermicular magnetite, which are again surrounded by corona of hypersthene (Fig. 5). Apatite is usually rich in inclusions of minute rods or needles of brownish pleochroic mineral (brownish black in the direction parallel to the elongation of the needle, and brownish in the direction perpendicular to the elongation).

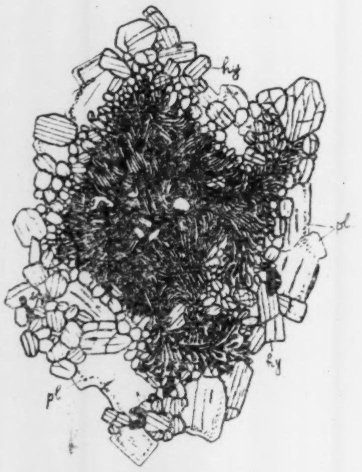

Fig. 5. Olivine phenocryst pseudomorphed with vermicular magnetite. *pl*-plagioclase. · *hy*-hypersthene.

The groundmass varies slightly in texture, ranging from an exceedingly fine-grained compact type to a medium-grained holocrystalline type. The constituent minerals are plagioclase, pyroxenes, magnetite, ilmenite, alkali-feldspar, quartz, tridymite, apatite, biotite, and pale brown glass. In most specimens, hypersthene and augite ((+) 2 V about 50°) occur side by side in the groundmass, while in only one example, quasi-uniaxial pigeonite is found instead of the two pyroxenes. Ilmenite (or an isomorphous mixture of ilmenite and hematite), which is fairly abundant in the relatively coarse-grained, crystalline types, occurs in irregular-shaped plates, and is subtransparent with chestnut-brown colour. Alkali-feldspar, quartz, and biotite, all closely associated with one another, tend to occur in holocrystalline groundmass or in coarsely crystalline patches. Biotite, which occurs in irregular flakes, and which sometimes forms a thin rim around porphyritic magnetite, is pale reddish brown with a weak greenish tinge, and has a small optic angle ((−) 2 V about 20°) with strong dispersion $\rho < v$.[5]

2) *Cognate inclusion.* Cognate inclusion of plutonic texture is found in one of the lavas (hypersthene-augite-andesite) that are exposed along the sea cliff 2 km west of Heta. In hand specimen, it is vesicular, somewhat friable, and equigranular with visible crystals of pyroxene and feldspar. In thin section, the rock consists of a hypidiomorphic aggregate of zoned plagioclase, weakly zoned, light-green au-

---

5) These groundmass minerals have many characters in common with those found in the rocks of the Hakone and the adjacent volcanoes. They will be described in detail in a later paper dealing with the general petrography of these volcanoes.

gite, pleochroic hypersthene, olivine, dark-brown hornblende which is mostly replaced with iron ore, and magnetite. The interstices of these crystals are filled with meshes of acicular crystals of plagioclase, which the latter is rimmed with alkali-feldspar, besides those of hypersthene and smoky apatite, together with patches of cristobalite and tridymite. In its mineral composition, the rock is gabbroic.

3) *Olivine-andesite and -basalt.* A specimen collected from a roadside 2 km northeast of Sanagi-yama, which represents one of the younger flows of the volcano, is an augite-bearing olivine-andesite, transitional to basalt in mineral composition. Megascopically, it carries phenocrysts of abundant white plagioclase (up to 5 mm), sporadic yellowish olivine, and a few dark-green augite. Microscopically (Fig. 6), there are phenocrysts of zoned calcic plagioclase (anorthite-bytownite) and olivine, the latter of which is rimmed with groundmass pigeonite, besides those of a few magnetite and augite; while the groundmass consists of plagioclase, pigeonite ((+) $2V \fallingdotseq 40° \sim 0°$), magnetite, and interstitial cristobalite and pale brown glass.

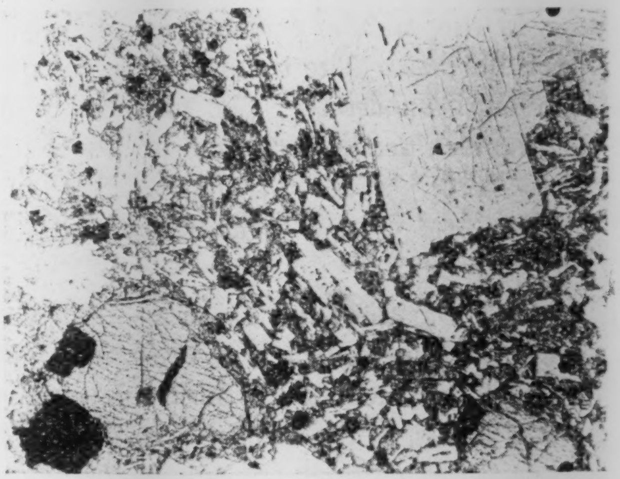

Fig. 6. Augite-bearing olivine-andesite, showing phenocrysts of plagioclase, olivine, and magnetite. Northeast of Sanagi-yama. ×41

Another specimen collected from the dike west of Heta, already referred to, may be classed as olivine-basalt, carrying, in hand specimen, large sporadic phenocrysts of anorthite (up to 1 cm) together with those of smaller plagioclase and olivine in a slightly vesicular dark-grey groundmass. In thin section, we find phenocrysts of calcic plagioclase (anorthite-bytownite) and olivine set in an intergranular basaltic groundmass consisting of plagioclase, pigeonite ((+) $2V \fallingdotseq 40° \sim 0°$), magnetite, and interstitial brown glass and cristobalite.

It was found that in the Daruma rocks, porphyritic hypersthene tends to decrease in amount in the more olivine-rich rocks until it finally disappears in the most olivine-rich basaltic types—a feature worthy of special mention in view of the fact that a similar tendency generally holds in the series of lavas that belong to the other volcanic complexes of north Izu.

On the other hand, the predominance, in the Daruma volcano, of the rock type with both hypersthene and augite in the groundmass, is a remarkable contrast to the volcanoes of the eastern coast (Taga, Yugawara, and Hakone), as most of the andesites of the latter volcanoes carry single pigeonite in the groundmass instead of the two pyroxenes.

The lava succession of the Daruma volcano can be observed almost from the base to the top in the eastern crater wall. In this craggy scarp, more than seven successive flows are exposed, each being accompanied with thick blocky parts. The lowest flow that is visible, appears immediately west of Nitta. It is a dark-green, very compact hypersthene-augite-andesite, showing a trace of deuteric or pneumatolytic alteration. As we go up the scarp along the shortcut between Nitta and the pass (735 meters high) north of Daruma-yama, traces of the alteration gradually disappear, while olivine phenocrysts, which first appear in the middle flows, progressively increase in amount toward the upper horizon. The topmost lava in this succession is an olivine-hypersthene-augite-andesite. The richness in olivine of the younger flows was verified also for other parts of the volcano (cf. p. 769).

Summary and Conclusion.

The Daruma volcano may best be classed as a shield volcano of Hawaiian type. It has a breached central crater and a gently sloped flank. The volcano was built up chiefly by repeated gentle outpowerings of lavas, and scarcely any violent explosive eruption seems to have occurred throughout the whole history of its activity. Each lava was accompanied with large masses of blocky parts above and below the solid interior,[6] which were formed by breaking down the already consolidated scoriaceous crusts. The compositions of these lavas did not change much during the successive effusions. They were mostly hypersthene-augite-andesite, which became slightly richer in olivine toward the later stage of activity. Augite-olivine-basaltic andesite and olivine-basalt were also erupted at some periods during the later stage.

Although no decisive conclusion can be drawn regarding the age of the volcano, a comparison of the extent to which dissection has proceeded in it with those of the other north Izu volcanoes, suggests that it is Older Pleistocene or slightly older.

---

6) Similar examples of shield volcanoes, which are made up essentially of blocky lavas, are described by Howel Williams from the Lassen Volcanic National Park, California, namely the Prospect Peak and Mount Harkness volcanoes. H. WILLIAMS: *Bull. Dep. Geol. Sci., Univ. California Publications*, **21** (1932).

In conclusion, the writer wishes to take this opportunity of offering his cordial thanks to Professor Seitarô Tsuboi for kindly reading the manuscript.

---

53. 伊豆達磨火山に就いて

地震研究所　久野　久

達磨火山は伊豆半島北部西海岸に存在する。本火山に就いては従來あまり詳細な研究が行はれて居なかつたが，筆者は北伊豆東海岸及び箱根等の諸火山との比較の爲，昭和 13 年春本地域の極く概察的な調査を試みた。其の結果本火山の構造・岩石等の大略を知り得たので玆に報告して置く。

達磨火山は所謂ハワイ式の楯狀火山に屬するもので，頂上には西方に向つて開いた解析火口（新田部落を中心とする）を有し，其の外側（特に東方）に緩かな斜面を引く。本火山は主として熔岩の靜かな流出がくり返し行はれて建設されて行つたもので，その間に烈しい爆發的な活動は殆んど行はれなかつたらしい。各熔岩の中層部は緻密に凝固して居るが，その上下層には厚い塊狀部 (Blocky part) を伴ふ。熔岩の成分は火山の活動中著しい變化を示さなかつた。其等は大部分紫蘇輝石-普通輝石-安山岩であるが，後期の熔岩程僅かながら橄欖石斑晶の量を増加して行つた。又普通輝石-橄欖石-玄武岩質安山岩及び橄欖石玄武岩等も少量ながら後期に噴出されて居る。

本火山の時代に就いては何等決定的な事は云ひ得ないが，其の解析程度から考へると下部洪積期或は稍々古期に屬するものではなからうかと思はれる。

達磨火山が北伊豆東海岸の諸火山（多賀・湯河原・箱根等を含める）に比較して著しく異る點は，其の構成物質が主として熔岩より成り，純粹の火山拋出物（凝灰岩・角礫凝灰岩等）が極めて僅少な事と，其等熔岩に塊狀熔岩 (Blocky lava) が多い事とである。又岩石學的には，達磨火山産安山岩には其の石基に紫蘇輝石並びに普通輝石の兩者を有する岩型が極めて優勢である點が特徵である。因に東海岸諸火山の安山岩の石基輝石は大抵の場合ピヂオン輝石一種で代表されて居る。

54. 昭和13年7月上旬の降雨による兵庫縣下の山崩

地震研究所　宮部直巳

（昭和13年9月21日發表――昭和13年9月20日受理）

1.　本年（昭和13年）7月初旬に，關西方面に多大の降雨があり，7月5日には各河川氾濫して，殊に神戸附近では，大小の礫並に土砂を流出し，慘憺たる災害を生じた．その被害の狀況，分布等に就いては，已に，災害科學研究所の調査報告[1]がある．

筆者は，8月初旬，その被害狀況を見る機會を與へられたので，山地の崩壞狀況とその被害に關して，些か見聞した所を玆に報告する．

2.　この度の，所謂水害の特質とも言ふべき點は，極めて多量の礫及び土砂が山地から水と共に流出したといふ點にある．その礫や土砂は，"山津浪" といふ概念で知られてゐる樣に，その流路に在つた構造物を破壞したり，洗ひ去つたりした樣な害よりは水の流れによつて，土砂が家屋等の中に運び込まれ，之を埋めたための害の方が一層大であつた樣に思はれる．

例として住吉川附近の狀況について述べる．第1～3圖は，阪神電鐵住吉驛附近及び，省線住吉驛附近において土砂に埋つた家の有樣を示したもので，甚しいものは，階下が殆ど土砂で埋め盡されてゐる．土砂の堆積狀態は，阪神電鐵住吉驛附近では最大1·0m乃至1·5m位であるが，省線住吉驛附近では2·0m以上に及ぶと思はれるものもあつた．

第4圖は，やはり，省線住吉驛の南約500mの住宅地内における被害狀況であつて，この場合は，土砂を含んだ水流の爲に家屋の一部が破壞され，電柱がやゝ押し枉げられてゐる．

阪神國道以南の地域は，傾斜も緩やかである．そして，土砂の流は省線の北側から2支流に分れ，住吉川の東側と西側とに堆積してゐる．この附近に見られる土砂の堆積狀態の特徵とも言ふべき點は，

（i）大部分が細砂であつて，礫と稱すべき程度の大きさのものは見あたらない．

（ii）家々の裏の空地，校庭等に，比較的厚く堆積してゐる．

等のことである．

1）災害科學研究所報告 1（1938）．

是等のことは，土砂を運んできた水流が比較的淺かつたか，その流速が比較的小さかつたか，或は又その兩方であつたかを意味するであらう．

土地の傾斜が緩やかなことや，浸水した地帶の幅が非常に廣くなつてゐたこと等は上記の何れにも符合する事實である．

住吉川附近の狀況に關して，一寸注意されることは，阪神國道より北側の地域に於いて礫が多いことである．第 5～6 圖は，阪急電鐵線附近の狀況を示すものであるが，この附近では，徑 10 cm 乃至 30 cm 位の礫が非常に多い．又，國道附近省線の陸橋（その上を住吉川が流れてゐる）附近には，徑 50～60 cm の大礫も多數にある．住吉川附近における礫の分布を示すと，大體において第7圖の樣になる．圖中點々は土砂の多い地域，小圓は礫の多い地域を略示するものである．是等のことは，この附近における氾濫當時の流の速さのある測度 (measure) を示すものではないかと思はれる.2)

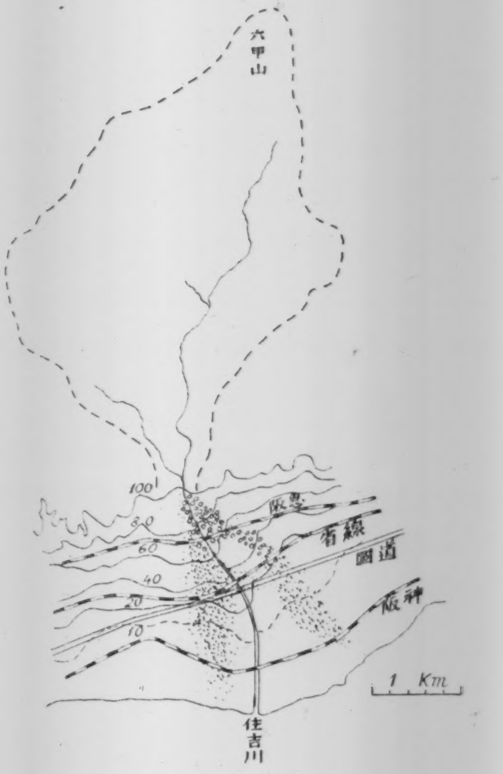

第7圖　住吉川沿岸地域の土砂及び礫の分布狀況略圖.

例へば Sainjon によれば，礫の直徑とその礫を運ぶに要する水流の速度との關係は次の通りである.3)

礫の直徑	水流の速度
0·25 cm	25 cm/sec
1·0 〃	50 〃
4·0 〃	100 〃
10·0 〃	150 〃
17·0 〃	200 〃
38·0 〃	300 〃
67·0 〃?	400 〃 ?

これは勿論礫が全體水中に浸る程度の水量がある場合の議論である．

この結果が直に現在の場合に適用出來るとすれば，阪神國道の北部における氾濫時の水流の速さは約 1·5 乃至 2·5 m/sec といふことになり，國道以南における，水流の速さは，0·25 m/sec 若しくはそれ以下であるといふことになる．

氾濫した水の流速の推定値を用ゐて，更に次の樣に流の斷面積及び單位時間の水の流出量をある程度まで推定することが出來る．理想的な場合を考へ，Gravelius の與

---

2) 大なる礫が遠くまで運び出されてゐるといふことは岩塊それ自身の質量が大である爲，斜面を轉落する時のその岩塊の運動量が大であつたことにもよるのではないかと思はれる．(第8圖寫眞參照).

3) Rudkzi, *Physik der Erde*, s. 474.

へた式

$$V_m = \frac{87}{1+\frac{\gamma}{\sqrt{L}}}\sqrt{L\cdot i},$$[4]

が成立つものと考へる．こゝに，L は hydraulic radius で，水が半徑 R の管の中を流れるとした時，$L=\frac{1}{2}R$ で與へられる．又 i は傾斜で，γ は，管底が普通の土の時に 1·30，不整形をなす場合に 1·75 といふ數で與へられる．

問題にしてゐる地域の傾斜を地圖上で讀み，大體 0·04 とし，$\gamma=1{\cdot}30$，$V_m=1{\cdot}5$ (m/sec) を入れれば

$$R=7{\cdot}8\,\mathrm{m}$$

となる．これは勿論，水流の有效半徑と言ふべきである．これで，V_m と R とが判つたから，住吉川が，山地から平地へ出る出口における毎時の流出量を推算してみると

$$\begin{aligned}流出量&=\pi\times(7{\cdot}8)^2\times1{\cdot}5\times3600\,(\mathrm{m^3}).\\&=1{\cdot}04\times10^6\,\mathrm{m^3}.\end{aligned}$$

となる．

一方において，7 月 3 日以來の降雨量の神戸における記錄は，5 日午前 8 時までに約 280 mm となり，その後 4 時間の間に 179 mm となつてゐる.[5] この最後の 4 時間の毎時の平均雨量は約 45 mm である．これだけの雨が，全部水流となつて，1 時間の間に住吉川に流出したとすれば，その容積は，住吉川に水を供給する地域の面積が約 $11{\cdot}6\times10^6\,\mathrm{m^2}$ であるから.[6]

$$\begin{aligned}&0{\cdot}045\times11{\cdot}6\times10^6\,(\mathrm{m^3})\\&=0{\cdot}52\times10^6\,(\mathrm{m^3})\end{aligned}$$

となり，前述の流出量の約 1/2 ではあるが，略々同等の容積となる．

六甲附近の様に急傾斜の山地では，雨が土中に浸透することも比較的少なく，又，降雨は 7 月 3 日以來のことであつて，山地には已に多量の水があるとすれば，流水量の最大時には，その時の雨量以上に上ることもあり得るかもしれない．他方，斯様に多くの假定と略算との結果得た數字としては，寧ろ一致してゐると言へる．

3.　7 月 5 日の "水害" の主要部分をなす流出土砂の源は，山地の崩壞によつて生じたものであることは言ふまでもない．山地の崩壞は必ずしも一時に起つたとは考へられないといふことは，土砂の流出は何回かに行はれ，全部の土砂が一時に市街地に流

---

[4] RUDZKI, *Physik der Erde*, s. 466.

[5] 災害科學研究所報告 1 前掲．

[6] 5 萬分の 1 の地形圖上で測る．

出して來たのではない様であるといふことから推定される．

又單に山腹の土砂が崩壞集積したのみではなく，例へば，神戸海洋氣象臺北側の谷に流出した土砂の如きは，再度谷奥の貯水池の土堰堤決潰によるものが主である．この谷の兩岸の傾斜面には崩壞の痕跡が無數にある．是等の崩壞によつて供給された土砂の量も勿論少なくないと思はれるが，また，谷の中に取殘されて谷の一部を埋めた土砂の量も少なくない．然るに，谷の奥にあたる一貯水池の決潰による土砂の量は，是等の多數の崩壞による土砂の量に匹敵するか，或はそれ以上かとも思はれる程である．第9圖は，その土堰堤決潰の跡を谷の下流から撮影したものである．堰堤の高さは約 20 m 表面における長さ 30～40 m，底面における幅も 20～30 位と推定される．この堰堤が全く形體を止めない許りでなく，この貯水池の底に沈澱してゐた土砂が，同時に流出したのである．沈澱してゐた土砂の流出した部分の Dimension は，面積約 100 m 平方卽ち 10^4 m^2 厚さ約 3 m である．第9圖中 L_1 は平常時の水面，L_2 は舊底面を示すものである．この堰堤の崩壞は，貯水池に水が增し，且つ排水口が流木等の爲にふさがれ，水が堰堤を越えて流れ出した爲めに生じたものであらうと推定されてゐる．海洋氣象臺での觀察によれば，7 月 5 日の 12 時頃多量の土砂流出があつたといふことである．この土砂が，貯水池の堰堤崩壞によるものと思はれる．

第 10 圖は，再度山附近の地形圖である．圖上で問題の貯水池に雨水を供給する地域の廣さを測ると約 3～4×10^5m^2 位になる．排水口の塞がつた時が不明であるけれども，これだけの地域に降つた雨が池の水位を 3～4 m 上昇させるには，相當の雨量，と，それ等が池に集つてくる爲に相當の時間とを要するであらう．

第 11 圖は，山地の崩壞狀況の一部を示したものである．場所は，再度山のドライヴウエイに沿つた，再度谷より一つ東側の谷である．

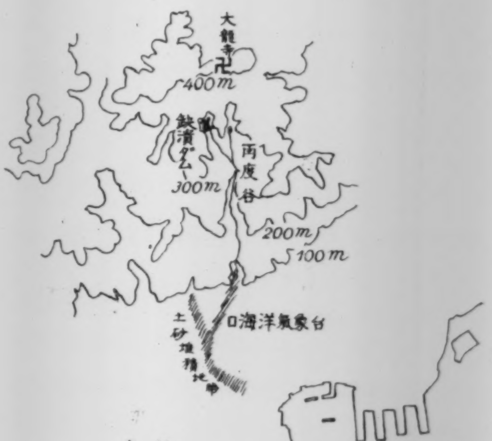

第 10 圖　再度山附近の地形．

斯様な崩壞が雨によつて生ずる場合について少し考へてみやう．

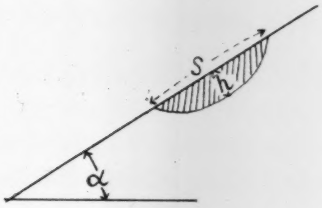

第 12 圖

第 12 圖の如き傾斜面があつた場合に，この傾斜面に

沿うて，第 12 圖の如く崩壊が生ずるとすれば，傾斜面の水平面となす角 α は，

$$\tan\alpha=\frac{1}{\frac{16}{9}\frac{s^4}{(s^2+4h^2)^2}-\frac{4c^2}{w^2h^2}}\left\{\frac{4}{3}\frac{s^2}{s^2+4h^2}\mu+\frac{2c}{wh}\sqrt{\frac{4c}{w^2h^2}+\frac{16}{9}\frac{s^4}{(s^2+4h^2)^2}-\mu^2}\right\},$$

によつて與へられる．

玆で，降雨の影響は，土中に浸潤した雨水が μ（砂粒間の摩擦）及び c（土の凝集强度）を變へることにある．更に，土に雨水が浸透する事により，土の有效質量が增加することも考へられるであらう．土の有效質量の增加は，上式の成立つ限り，c の影響を小にする．

問題の地域においては，Colloidal の土よりも細砂程度の砂が多い様であるから，c の値は元來小さいと思はれる． 從つて μ に對する水の影響が主要なものであらう．そこで，住吉川下流の氾濫地帶に沈積した土砂を採取し，その μ，c，の値の含水量による變化を調べた．その結果は第 13 圖に揭げてある．μ も c も含水量の增加と共に減少する傾向を示すから α の値も亦小さくなる傾向にある．α が小さくなるといふことは，斜面の傾度の定つた場所では崩れ易くなるといふことを意味するわけである．又，實驗に供した土砂は含水量が 22·8% 以上に達すれば流動する．卽ち容積比で水がその砂との割合が 3:4 になる程度含まれるか或はそれ以上の水が含まれるに至れば流動するに至るものと思つてよいことになる．

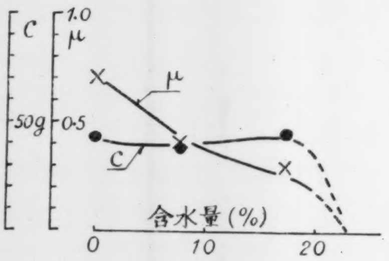

第 13 圖 含水量の變化に伴ふ c, μ の變化．

要するに，この場合の土砂の流れの，從來山津浪といふ概念の下に理解してゐた現象とやゝ異る點は，後者が，″水を含んだ土砂流″ と言ふべき性質のものであるに對し，前者が，″多量の土砂を含んだ水流″ といふ樣な性質を持つてゐたところに在るやうに思はれる．卽ち，土砂流によつて破壊し去られた家屋よりも土砂が詰め込まれた家屋の多いことが，よくその性質を示してゐるもののやうである．尙，山地の崩壊に對して所謂砂防工事が幾分か役立つてゐることの 1 例として第 14 圖を揭げた．斯樣な砂防工事が常に役立つとは言へないかもしれないが，附近に松林地帶があり，その松林地帶が滑落してゐるのに對して，この砂防工事を施した部分が殘つてゐるといふことは事實である．

併し，この 1 例を以て植林が，山地崩壊防止，並に下流の災害防止に有效であると

---

6) 山口昇 土の力學，110．

か無效であるといふことも一概には斷定し得ないであらう．山地を構成する地質，地形，並びに植林すべき樹種，植林の方法等の具體的な事情によつて定まることと思はれる．

以上は，兵庫縣下の降雨に伴ふ流出土砂の災害につき，1~2 見聞した所を報告し筆者の見解を略述したものである．今後の研究資料として記錄に止める次第である．

現地の見學に際し，海洋氣象臺の堀口博士及び棚橋氏より御示教を賜はつたことに對して深く感謝の意を表する．

54. *The Landslides in Hyôgo Prefecture that accompanied the Heavy Rain of July 5, 1938.*

By Naomi MIYABE,

Earthquake Research Institute.

In the early part of July, 1938, the Kwansai district was the scene of heavy and long-continued rains. The precipitation in Kobe during 8 h~12 h, on 5 th of July, was reported to be 179 mm, the total precipitation during July 3~July 5 being 440 mm. Many landslides occurred on the slopes of Mt. Rokkô and the debris washed down to the cities at the foot of the mountains, destroyed, buried, or inundated a large number of houses. As many as 1000 or more casualties were also reported.

The writer here first attempts to estimate roughly the velocity of the water that rushed down a valley in the mountains, carrying the debris down to the flat country at its foot. The estimation of the velocity is based on the distribution of deposites along the Sumiyosi-gawa (river).

The distribution of the debris along the Sumiyosi-gawa (river) is shown in Fig. 7. In the neighbourhood of the mouth of the valley in the upper course of the Sumiyosi-gawa, pebbles of large size abund, as shown in photograms of Figs. 5~6, the size of the pebbles being 10~30cm in diameter. By applying Sainjan's result, the velocity of the flow of water at the mouth of the valley on the upper course of the Sumiyosi-gawa was estimated from the size of the pebbles distributed there in great abundance, to be about 1.50 m/sec. By applying the effective radius of the flow, 7·8 m, deduced by using Gravelius's formula, the amount of water discharged per hour was then estimated to be 1.04×10^6 m^3.

On the other hand, the extent of the area, from which the precipitation would flow into the Sumiyosi-gawa was estimated from a topographic map to be 11.6×10^6 m^2, the rate of precipitation per hour in Kôbe during 8 h~12 h of July 5 being 45 mm. Although the rate of precipitation in Kôbe might not have been the same as that in the mountaneous region, the hourly precipitation in the area mentioned above was assumed to be the same as that of Kôbe, whence the volume of hourly precipitation in the entire area mentioned above works out to $0{\cdot}045\,(\mathrm{m})\times11{\cdot}6\times10^6(\mathrm{m}^2)\fallingdotseq0{\cdot}5\times10^6(\mathrm{m}^3)$, which apporximately equals to the quantity discharged estimated from the distribution of the debris.

Next, the writer measured the values of c (cohesion) and $\mu\,(=\tan\theta$, where θ is an angle of repose) of the soil deposited in the flooded area. The results show, as in Fig. 13, that an increase of the water content causes a decrease in the value of μ, and that the value of c is approximately constant over a wide range of the water content. At the flow–limit of the soil, the water content is 22·86%, at which the values of c and μ may become zero. The effect of rain on the physical properties of soil is chiefly to reduce the value of μ, though rain water cannot easily penetrate the soil when the latter forms a steep slope. It may also be noted that increase in water content also causes an increase in the apparent specific weight of the soil, which reduces the effect of cohesion c of the soil.

The critical angle for slide of the slope is given by

$$\tan\alpha = \frac{1}{\frac{16}{9}\frac{s^4}{(s^2+4h^2)^2} - \frac{4c^2}{w^2h^2}} \left\{ \frac{4}{3}\frac{s^2}{(s^2+4h^2)}\mu + \frac{2c}{wh}\sqrt{\frac{4c^2}{w^2h^2} + \frac{16}{9}\frac{s^4}{(s^2+4h^2)^2} - \mu^2} \right\},$$

where s, h, w are respectively the length of the sliding area, the maximum thickness of the sliding volume, and the apparent specific weight (see Fig. 12).

Since the effect of the rain is to reduce the value of μ, and to increase w, it also reduces the critical angle α of the slope for slide, whence it follows that heavy rain sometimes causes landslides.

Many of the landslides that occurred on July 5, 1938, in Hyōgo prefecture, might have been caused in this way.

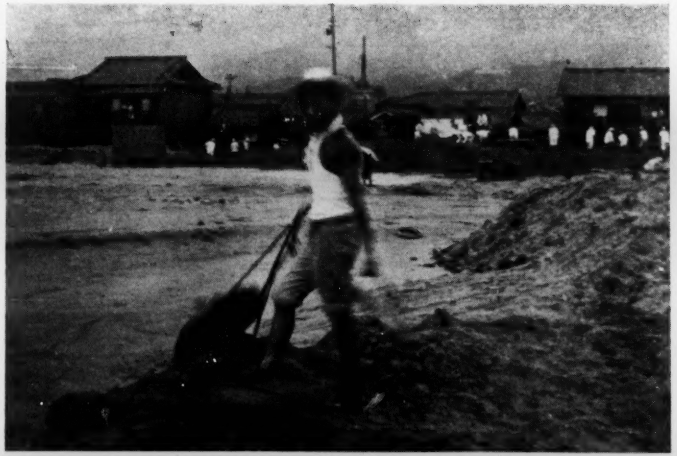

第１圖　阪神電鐵住吉驛附近の土砂堆積．

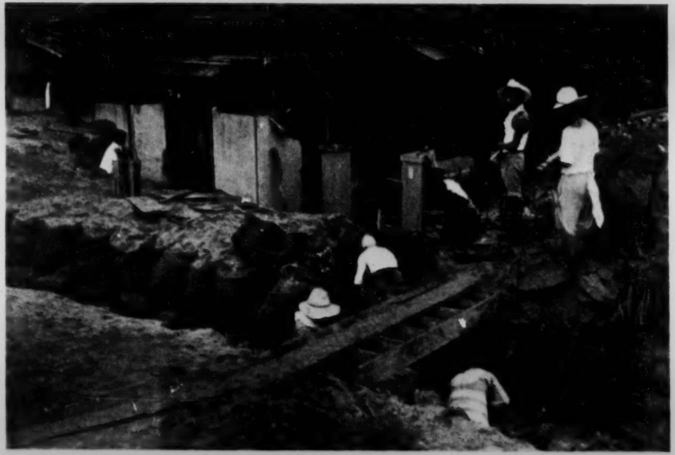

第　２　圖　　同　　上

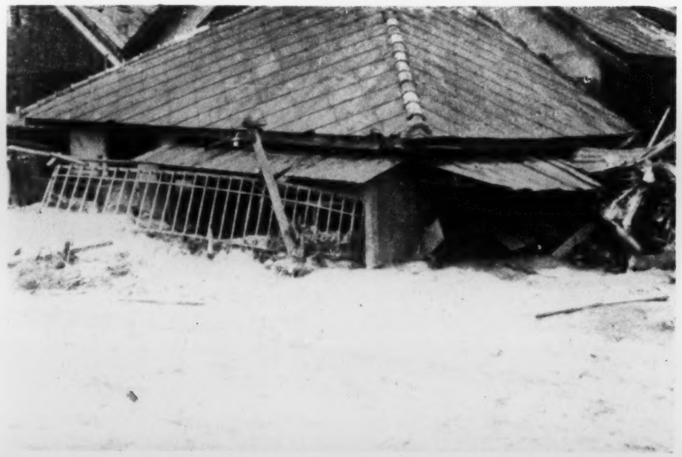

第３圖　阪神國道（住吉川西約 100 m）にある埋沒家屋．

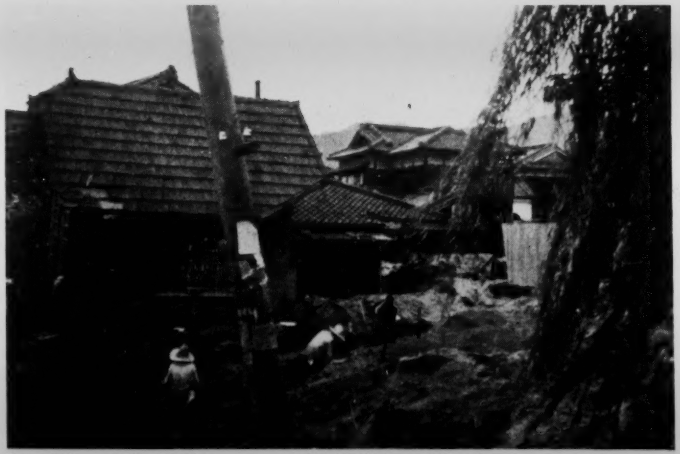

第４圖　住吉川西約 500m. 國道南側住宅地域内の土砂堆積．

[N. MIYABE.]

[Bull. Earthq. Res. Inst., Vol. XVI, Pl. LVIII.]

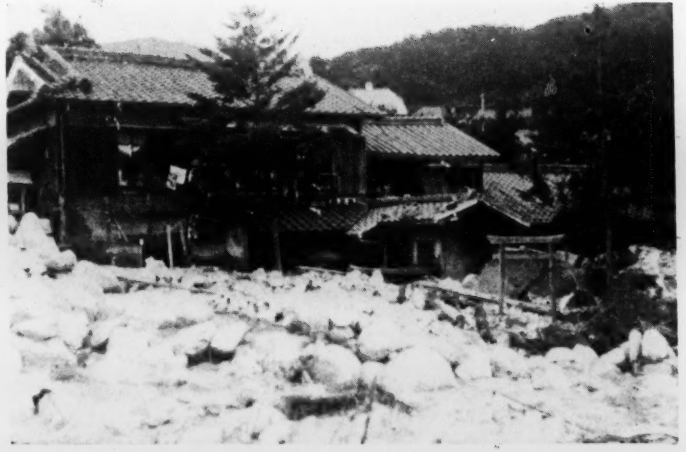

第５圖　住吉川上流阪急電鐵北側の礫の堆積.

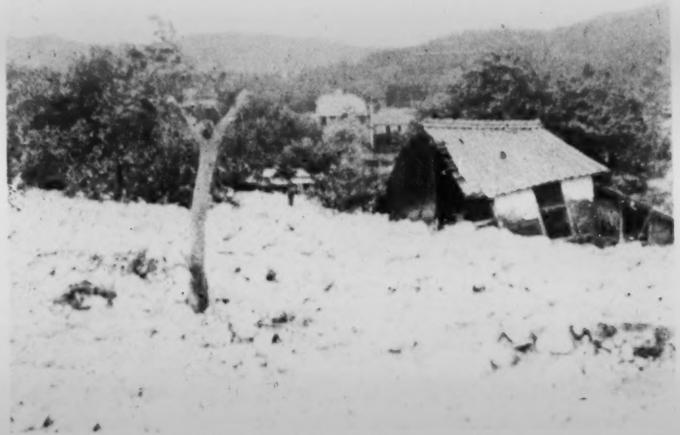

第　6　圖　同　　上

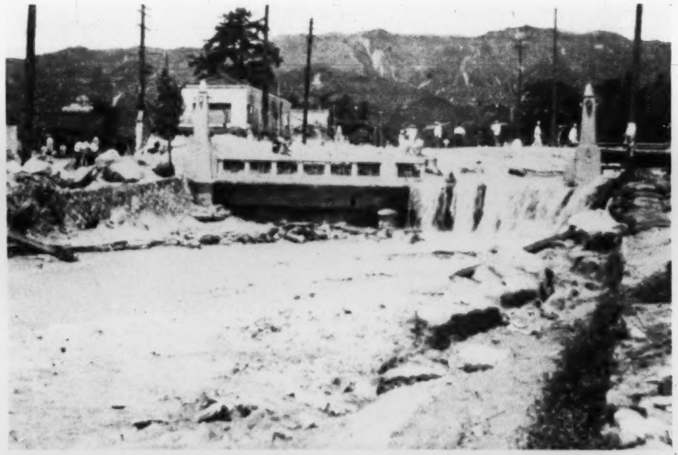

第８圖　阪神國道，住吉川附近（流は住吉川）.

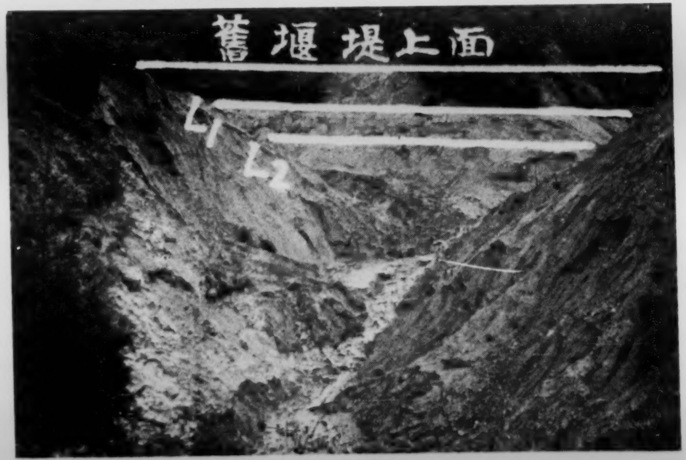

第９圖　神戸北側再度谷面の貯水池堰堤決潰の跡.

L_1：常時水面,

L_2：常時池底面.

（震研彙報　第十六號　圖版　宮部）

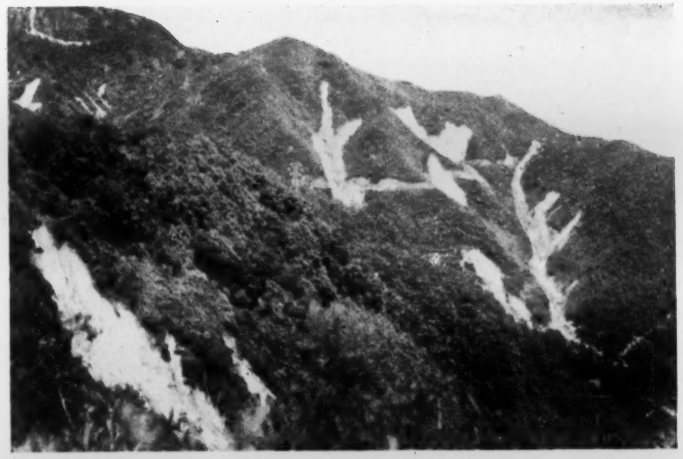

第11圖　山地崩壞の１例.

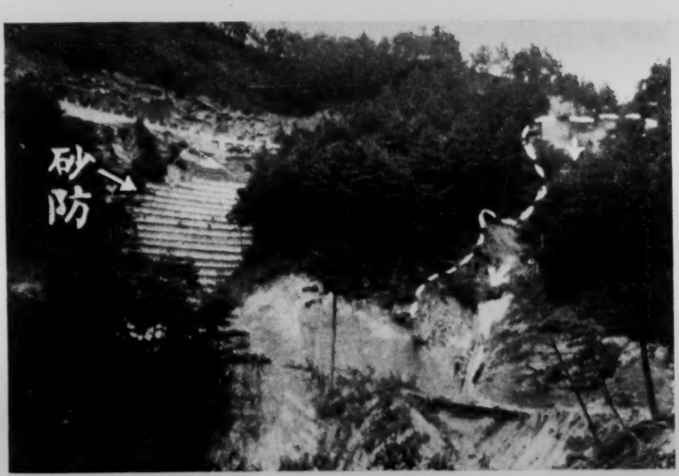

第14圖　砂防工事の１例.

55. 筑波山山津浪調査報告

地震研究所 萩原尊禮

(昭和13年9月22日發表——昭和13年9月20日受理)

昭和13年7月28日より同月30日にかけて關東地方に於ては豪雨が降り續いた．これが爲關東平野各地は河川の氾濫，堤防の決潰續出し其の被害は實に大なるものがあつた．筑波山に於ては7月3日筑波町を過ぎる千手澤に山津浪を生じ，此の澤沿岸に相當の災害を與へた．此の山津浪は山津浪其のものとしては左程規模の大きいものでは無いが，町の中央部を流れ然も幸にして其の部分に於ては澤は深い谷となつて居り氾濫の憂へが少なかつたため，多くの町民に依つて其の現象が比較的正確に觀察されたことが特色である．

筑波町東山地震研究所支所に於いて6月1日以向觀測せられた雨量は次表の如くである．

日	雨量	日	雨量	日	雨量
6月3日	2·2 mm	17日	22·8	29日	**198·6**
9	24·2	18	15·7	30	**239·0**
10	4·5	20	0·1	1	0
11	11·5	21	1·9	2	40·6
13	10·6	22	6·2	4	98·3
14	1·1	24	32·9	5	4·6
15	6·3	26	21·9	6	0
16	30·2	28	34·8	(毎10時觀測)	

7月2日17時豪雨も既に降り止んだ頃筑波町の町民は山頂方向に當つて低い地鳴樣の音を聞いた．未だ雲低きため展望きかず原因は確められなかつたが何處にか崩壞があつたことは誰にも察せられた．此の時鷺石入附近に於ける急斜面の崩壞が起つたものと推察される．崩壞した泥土は此の時は未だ泥流となるには含水量に乏しかつたが千手澤[1]を偃き止め此の水を吸收して次第に泥流となる性質を具備して行つたものであらう．かくして3日7時43分頃再び前日と同樣の地鳴樣の音響が今度は眞近かに聞かれた．此の音響は第2回目の崩壞が起つたためか或は泥流化した泥土が澤の途中迄下つて來たためかは不明であるが，恐らく後者によるものであつたらう．此頃漸

---

1) 此の澤は正確には大谷より上流を鷺石澤それより下流を千手澤と稱すると云ふが，一般には混同されて居る．此處では簡單のため何れの場合も千手澤とする．

く町民は千手澤上流に山崩れのあつたことを察し６名が探索のため澤に沿つて登つた．9 時頃一行が十一面岩の下に到達した時，恰も彼等の來るのを待つて居たかの樣に大音響と共に岩石，大木を混へた泥流が沿岸の杉，松，樅の立木を押倒し乍ら迫つて來た．一行にとつては全く突然であつて一行中 3 名は避難の暇無く泥流に呑まれて行方不明となり，翌々日此の中 1 名のみの屍體が大谷の下方 100 m 位の地點で發見された．此の時の泥流は大谷附近迄達し古通寺及び其れに隣接した賣店 1 軒を押倒して殆ど此處で止まつた．10 時 10 分頃に至り又大音響と共に倒壞した古通寺及び賣店を左岸に押付け泥流は岩石，大木を含んで下流へ流れ落ちた．此の時の音響は大谷附近では大砲をドンドン發砲する樣な音だつたと云ひ，町民は泥流そのものより寧ろ此の音響に恐怖を感じた．此の樣な泥流は

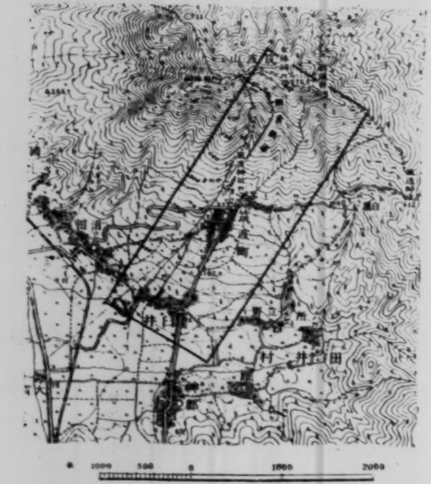
1000
500
0
1000
2000

第 1 圖

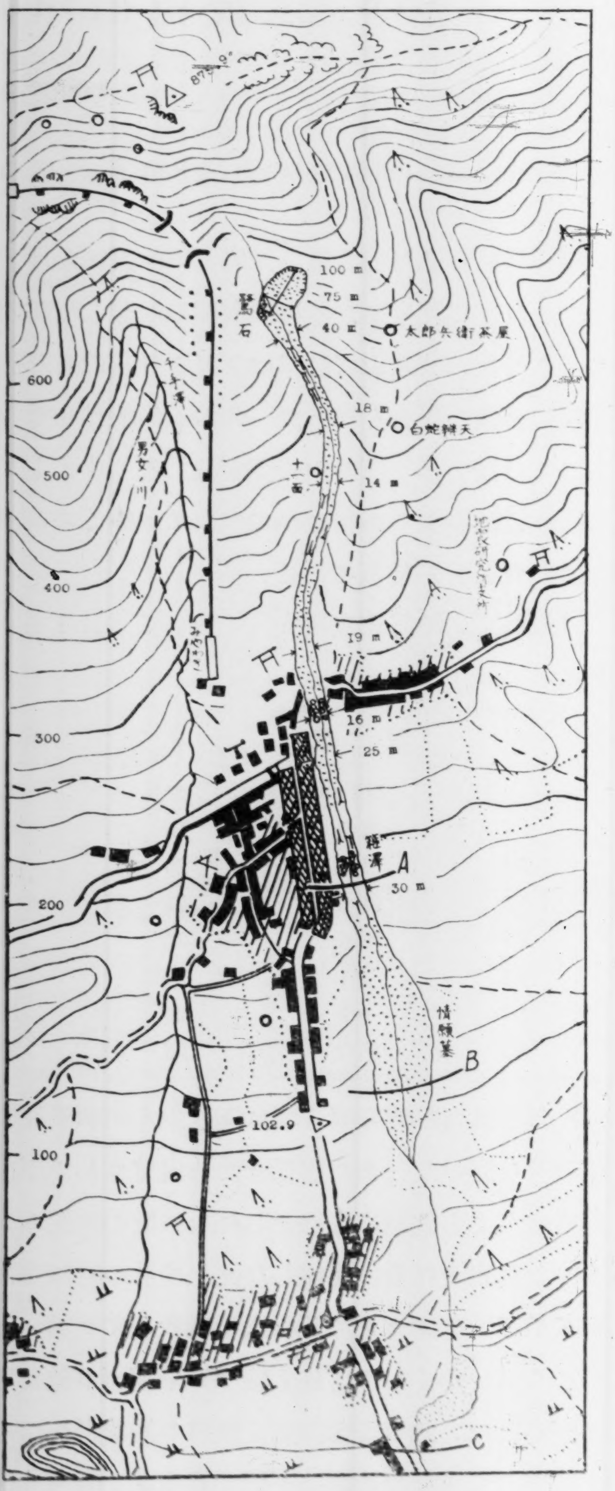
100 m
75 m
40 m
太郎兵衛茶屋
18 m
白蛇辨天
十一面
14 m
19 m
16 m
25 m
30 m
A
B
C
102.9
600
500
400
300
200
100
鷲石
千手澤
男女ノ川

第 2 圖

其後 4～5 回大谷邊を通過したが最初のものが最も大であつた．此の泥流の爲，筑波町東山へ至る道は破壊され電燈線，電話線は切斷され東山は孤立に陥つたが大谷邊は其の名の如く深い谷となつて居るため此の附近に於ては澤の外へ泥流は氾濫することなく附近の住家は難を免れた．此の日は之で終り翌 7 月 3 日 14 時 40 分頃より再び泥流あり 15 時 40 分頃に至る 1 時間の間約 14 回斷續して大谷を通過した．其の規模の大小は次の通である．

第 1 回	大	第 8 回	中
第 2 回	大	第 9 回	大（長し）
第 3 回	中	第10回	大
第 4 回	最大（前日と同程度）	第11回	中
第 5 回		第12回	小
第 6 回	中	第13回	大（長し）
第 7 回	中	第14回	大（長し）

此處に大と記したものは大木，岩石を含んだ泥流，中は岩石を含んだ泥流，小は泥水のみであつたことを示す．普通 1 回の繼續時間は 5 分乃至 10 分程度である．何れも大谷附近に於て觀察せられたものである．何れの場合も泥流の來る前には澤の水は減少し直前には殆ど止るのを例とし，上流にザー（或はゴーと形容しても良い）と云ふ瀧又は怒濤の様な音響を聞き之が次第に近付き，音響を聞き始めてから約 2 分位經過して大谷を泥流が通過した．泥流は其後 7 月 5 日 2 時 15 分頃より 4 時 45 分頃迄，數回小規模のものがあり以後は全く終熄した．

泥流の流速は左程早いものでは無く最初よりの觀察者たる筑波山測候所長沖住雄氏の談に依れば大谷附近に於いて毎秒 2 米程度であつたと云ふ．筆者も 7 月 5 日の最後の小規模の泥流は目撃した．其の少し隔つた所より見た其の感じは濃いしる粉の様である．粘着性は相當に強く，沈積箇所に於て約 20 cm の深さに足を踏入れたら拔くのに困難である．

山津浪の因をなした崩壊箇所は筑波山ケーブルカーの交換所の東方に當る海拔約 500 m の鷲石附近の地點で，千手澤左岸の急斜面である（第 3 圖）．崩壊面積は幅約70～80 m，奥行約 100 m であり崩壊以前は灌木の外に杉，樅，松等が密生して居た．崩壊箇所附近は平素から足で踏むと地表に水が浸み出る様な濕潤の場所であつたと云ふから常に相當の含水があつたものと思はれる．崩壊した部分は全部風化土であつて，始め崩壊が起つて千手澤を堰き此の澤及び周圍から注ぐ水を吸收して泥流化したものであらう．泥流中の岩石は崩壊の際對岸の轉石に富む鷲岩附近の崖を削つたためと途中澤にあつた轉石を運んだためである．7 月 5 日筆者等の踏査の際は崩壊に由つて生じた斷崖の上方 20～40 m 附近に尚數個所龜裂が存在して居るのが見られた．龜

裂の大きいものは約1m位斷崖側が低く段違ひとなつて居り長さは斷續的に 30～40m 程度であつた、然し其の後、崩壊は起らなかつた、

今回の山津浪の流出區域は第2圖に示す通りである、此の澤は平素水量は極めて少なく、大谷より上流の沿岸には樹木が密生して居たが、泥流のため谷は斷面がV字狀に刳られその幅は20m前後深さは6～7m程度に達した（第8圖）、大谷より下流に於ける沿岸は耕地であるが泥流は多少氾濫して之を洗ひ農作物に被害を與へた（第4圖）、岩石、樹木、木根流出は第2圖に示す如く、岩石は籠澤附近迄至り大は1噸乃至2噸のものがある、樹木は概ね情願墓附近にて止り大なるものは長さ 20m 直徑 1m 程度である、被害のあつた畑は7反5畝と云ふ、山麓の田井村に於ては泥水が田地に氾濫せんとしたが土嚢を積んで防いだ．

此の地の山津浪は慶應2年（1866年）にも起つたことが傳へられて居る．此の時は他の澤にも山津浪を生じたと云ふ．幸ひ筑波神社社掌塚本定吉氏の好意に由り當時の記錄を寫すことが出來たので次に記する．これを讀むに其の時の山津浪も全く今回のものと同樣な形態をとつたことが判る．

筑波山大津波の事

慶應二年丙寅七月三日此の九ツ半時分より大雨ふり出し男體山下峯大にぬけ大石大木をたおし○（缺字）又男女川大杉並にもみ數十本根よりぬけ出し一ゑんに大水にまじり大石を流す事土水一○（不明）にぶちあがり石波立つて麓に押し出しありさまはなんともたといがたく此の大山今くづれやぶらんかと人々魂お飛し後日のうれへおなげきあいけり次に白滝山右同樣なり，籠所をぬきみせをたほし土石をうち立てしんどうする事云ばかりなし籠の人々かながなにげ去り思石に書するところの男女の川下なだかふちより西澤に押出し右大木たといば棟の如しおゑんに一本松はかば寮を流し石とふ壹本も是無く押流るゝ事並に古通寺澤（註千手澤の別名）右同段大杉おぬき石を流し土水さか波立つて押流るゝありさまは八十餘歲の者あいて是を聞かずと云是卽ち天べんなるや地へんなるや大木さながら風もつよからずして折るゝ事など天神のわざならんかとしたおまき恐れおのゝきさはぎあいけり尤も七つ半時分に天氣あがり雨のみなりやみむ此の時の御代官は久保庄藏樣此の時米相場兩に一斗五升崩所は第一みなの川次に男體山の岩谷下よりぬけてとふ石に押出すその巾二十間餘次にその西の峯下崩れ出し沼田村へ押出す田畑大いにそじる．

沼田新田山不動尊の下にて人一人死す筑波山におつた米つきおじいと云ふ．次に行人塚稻荷○（缺字）東谷　次白瀧不動尊谷同籠所のゑんの下の石垣崩る古今まれなること共なり．

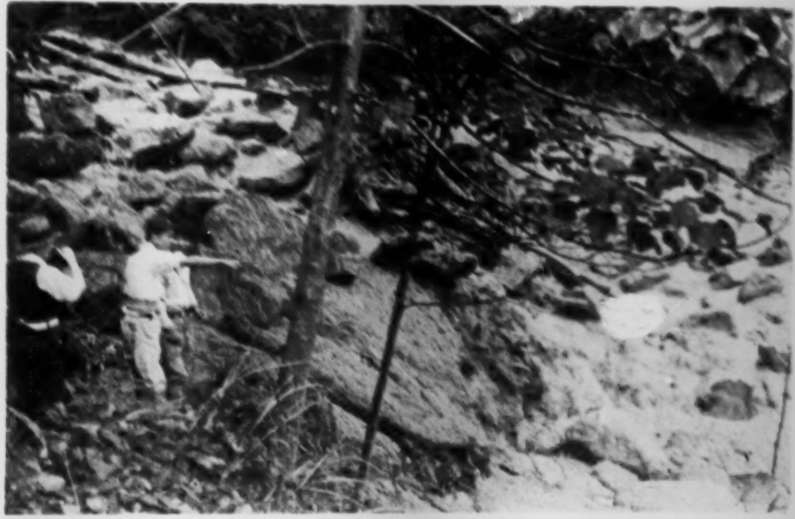

第3圖　崩壞箇所ヨリ 1,200 m 下流たがさわ附近.

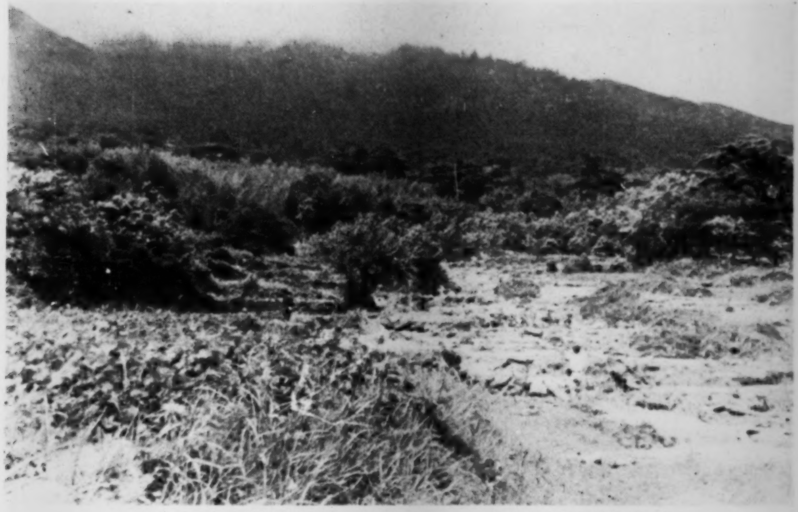

第4圖　崩壞箇所ヨリ 1,500 m 下流情願墓附近.

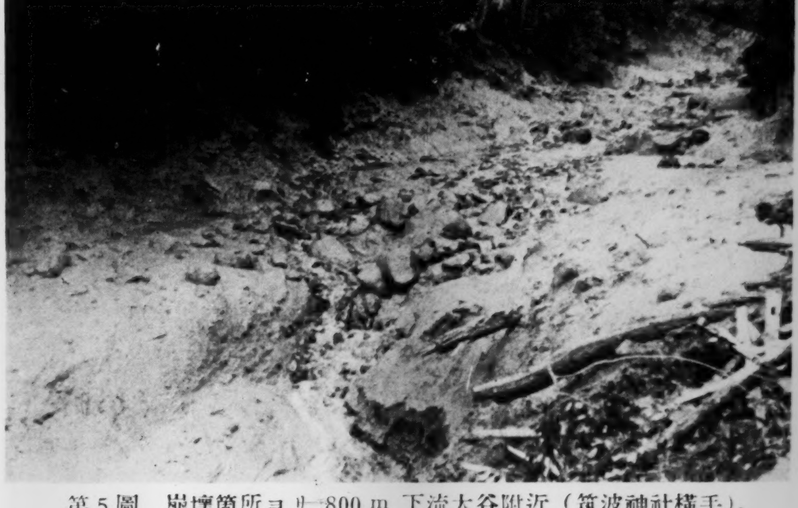

第5圖　崩壞箇所ヨリ 800 m 下流大谷附近（筑波神社横手）.

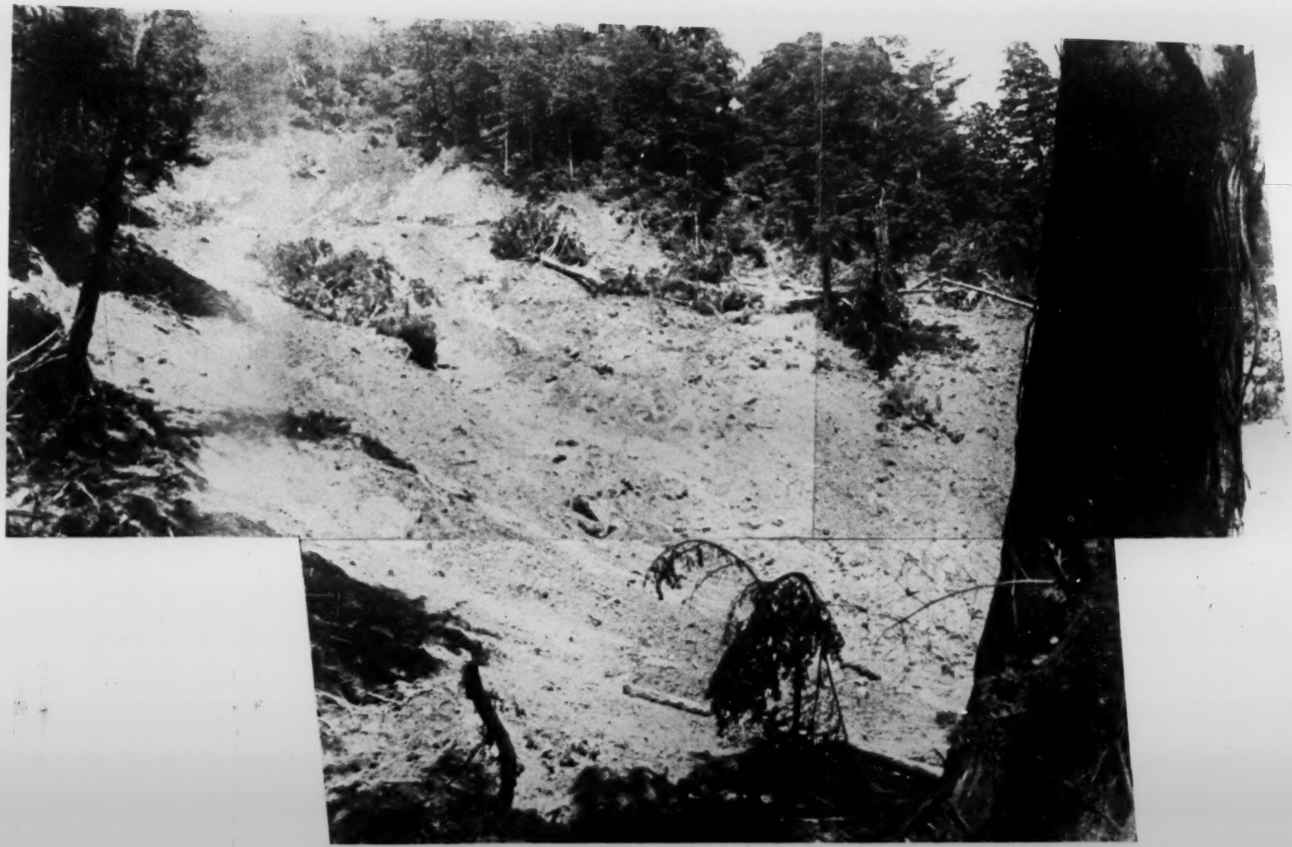

第6圖　鷲石附近崩壞現場（昭和13年7月6日撮影）.

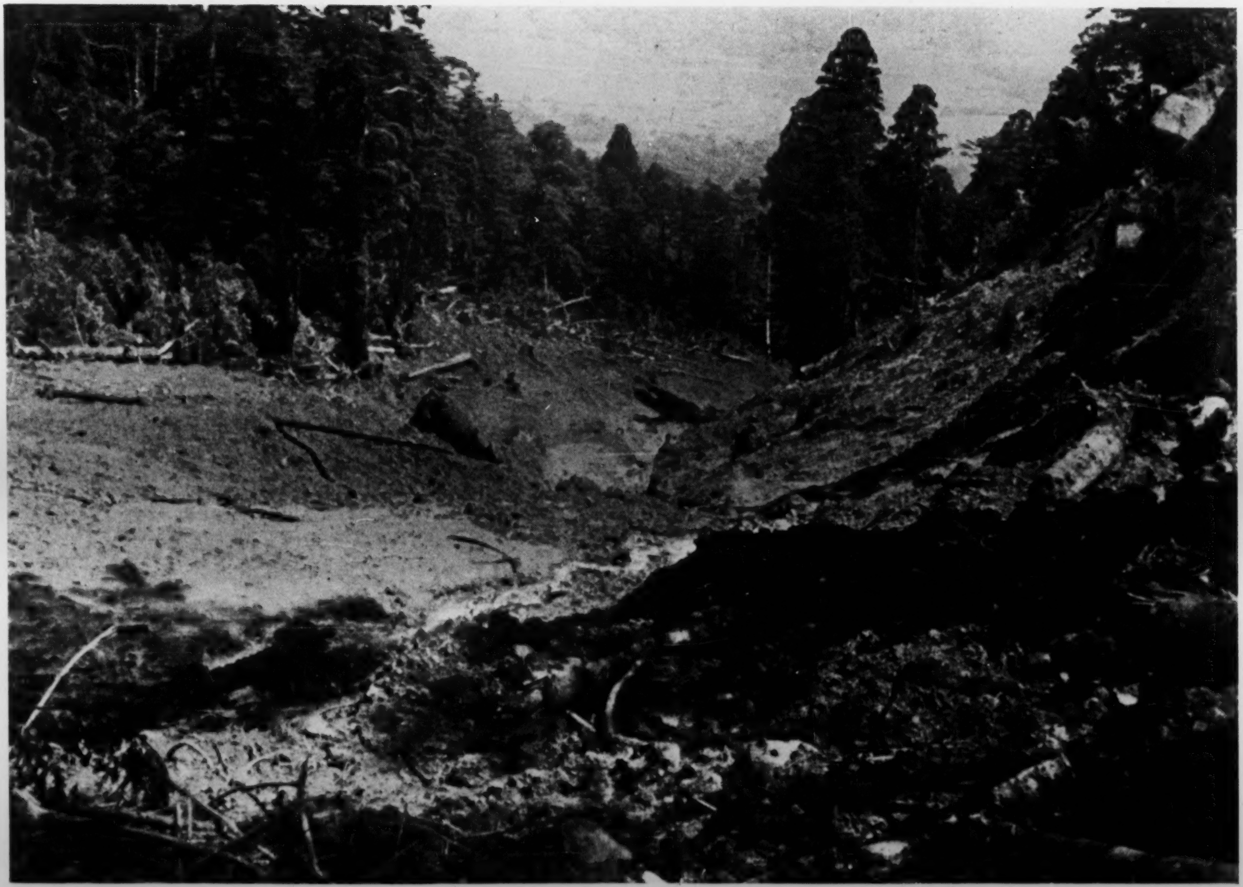

第 7 圖 崩壊現場より千手澤下流を望む。

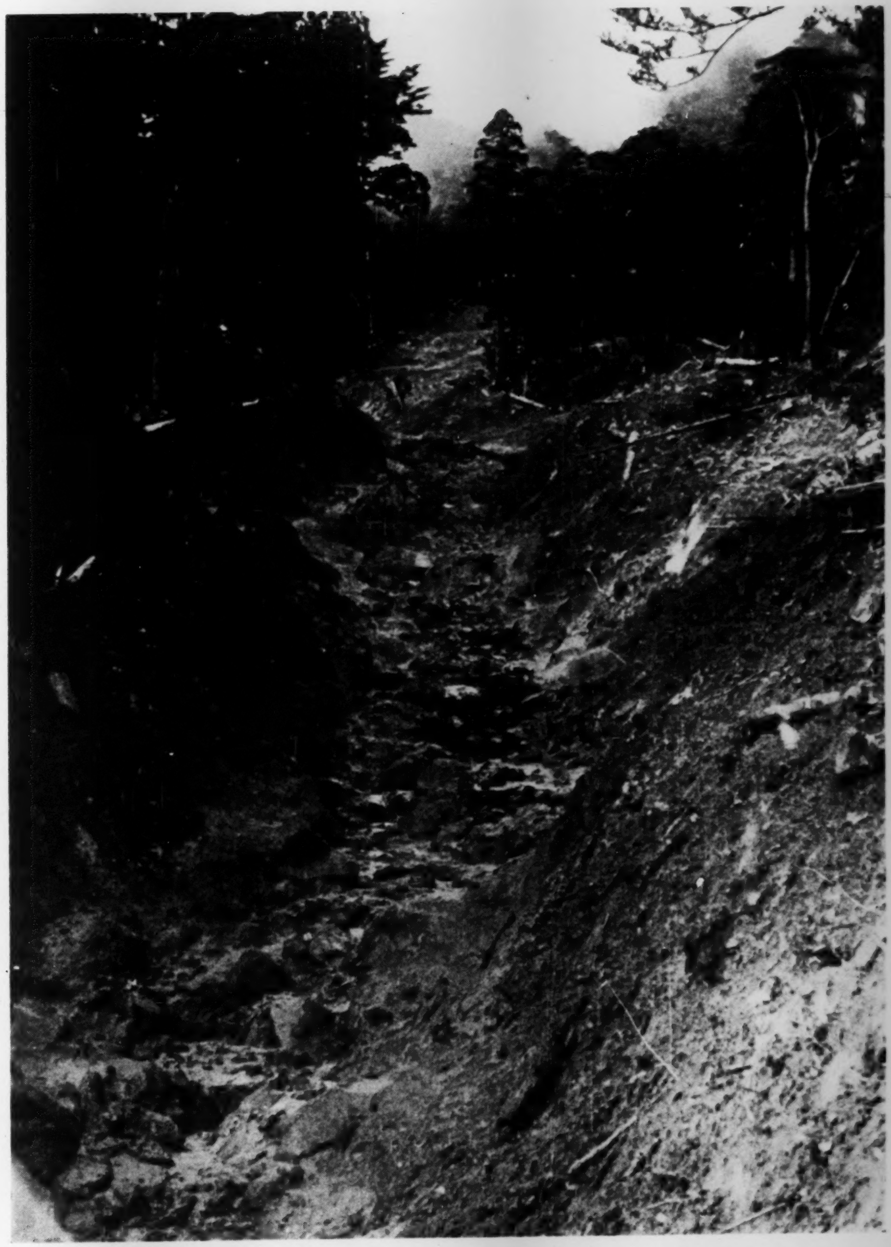

第8圖　百蛇辨天附近より上流を望む.

此の頃長州せいばつ相はじまりその消そくを知らず.

この午年の大水當年八十一年の事なり.

（筑波山神社々掌塚本定吉氏所藏同氏祖父塚本勇範氏記）

附記　龜裂箇所は其の後大雨のある毎に多少崩壊し小規模の泥流を起して居る.

---

55. *Mud Avalanche at Mt. Tukuba, Ibaraki Prefecture.*

By Takahiro HAGIWARA,

Earthquake Research Institute.

A mud avalanche occurred at Mt. Tukuba, Ibaraki prefecture, on July 3, 1938. In flowing down the valley it swept away two wooden buildings and killed three men. The avalanche was caused by collapse of soil in the upper waters of the valley as the result of heavy rains. The velocity of the flow was estimated to be less than 10 meters per second.

——所　報——

○談話會記事

第138回談話會（昭和13年6月21日）

1.	東京帝國大學構内三ケ所に於ける地震動加速度の比較	萩原尊禮 表俊一郎
2.	昭和13年5月9日及び15日の磐梯山麓に於ける山津浪調査概報	飯田汲事
3.	震源に就て	井上宇胤
4.	地震の水平横波の振幅は特に大きいか 附話　最近の二三報告の補遺	妹澤克惟 金井清
5.	屈斜路地震調査概報	津屋弘逵

第139回談話會（昭和13年7月5日）

1.	城山角閃石安山岩體の結晶排列に就て（其の2）	大塚彌之助 猪俣眞三郎
2.	振動方法による岩石の彈性學的研究（第1報） 附話　伊豆新島の抗石の彈性及び粘性	飯田汲事 岩下圓
3.	伊豆大島の重力測定	永田武 武井柳吉 實川顯 猪俣眞三郎
4.	南關東地方に於ける重力分布と地震活動	坪井忠二
5.	彈性表面波の異常分散（第2報）	妹澤克惟 金井清
6.	地殼の内部層に傳播する彈性波の異常分散	妹澤克惟 金井清
7.	淺間山の噴火に就て	長岡半太郎 白井俊明

第140回談話會第1日（昭和13年9月20日）

1.	淺間火山灰並に淺間火山地獄谷附近砂の浸出水の ph（續報）	野口喜三雄
2.	木造住家の振動及倒潰實驗	齊田時太郎
3.	微動計による地震觀測（1） （地震動の大さとその頻度）	石本巳四雄 飯田汲事
4.	粘性が地球の液狀冷却時代に於ける重力的安定に及ぼす影響	妹澤克惟 金井清
5.	筋違の耐震效果の理論（序論）	妹澤克惟 金井清
6.	噴火山の創成に關する一考案	長岡半太郎

第140回談話會第2日（昭和13年9月21日）

7.	横濱市鶴見にて採集せる「關東ローム」の鑛物成分と化學成分	津屋弘逵

8.	昭和13年8月11日三原火山の小活動に就て	永田武
9.	筑波山山津浪調査報告	萩原尊禮
10.	江東地域の地盤沈下に就て（續報）	宮部直巳
11.	大雨に伴つて生じた神戸附近の山崩	宮部直巳
12.	長野縣茶臼山地辷に就て	大塚彌之助
13.	陸羽地震川舟斷層の現況	大塚彌之助

第141回談話會（昭和13年10月18日）

1.	地下層面が平面でない場合の走時曲線解析法	萩原尊禮
2.	長野縣茶臼山地辷調査（彈性波法による辷面の決定）	萩原尊禮 表俊一郎
3.	長野縣蓼科山麓の溫泉並に天然瓦斯に就て	野口喜三雄
4.	淺間火山に於ける地磁氣偏角及び水平分力變化の觀測	水上武
5.	淺間火山に於ける磁氣測量（第2報）	水上武 內堀定市
6.	重力分布より見たる北アメリカ合衆國の地殼構造（其の1）	坪井忠二 金子徹一 宮村攝三 矢橋德太郎
7.	上下動成分三百五十倍微動計	石本巳四雄 飯田汲事
8.	ストンレー波の實在範圍及び之に關聯する問題	妹澤克惟 金井清

第16號索引

頁

淵田隆門；坪井忠二・淵田隆門　參照

萩原尊禮　(29) 筑波山に於ける土地傾斜變化の觀測 (英文)…………………………366

萩原尊禮・表俊一郎　(44) 東京帝國大學構內に於ける地震動加速度の比較觀測 (其の一) (邦文)……………………………………632

萩原尊禮　(55) 筑波山山津浪調査報告 (邦文)……………………………………779

平能金太郎；高橋龍太郎・永田武・平能金太郎　參照

佐藤光之助・福永三郎　(26) 臺灣中部の地殼變形 (第一報) (英文)……… ………300

福永三郎・宮部直巳・佐藤光之助；宮部直巳・福永三郎・佐藤光之助　參照

飯田汲事　(31) 砂の中を傳播する彈性波の速度 (英文)……………………………131

飯田汲事　(31) 二三の土に於ける2種の粘性化とポアソン彈性比との關係 (英文)…………………………………………………………………………391

飯田汲事　(46) 昭和13年5月9日及び15日の盤梯山麓川上溫泉附近に於ける山津浪並びに流下せる火山灰質土砂の二三の物理的性質(邦文)………658

猪俣眞三郎；大塚彌之助・猪俣眞三郎　參照

井上宇胤　(11) 發震機構に就いて (第5報) (英文)……………………………125

井上宇胤　(43) 發震機構に就いて (英文)…………………………………………597

金井清　(3) 構造物震動の力學的制振器の模型實驗 (不規則な振動) (英文)……　21

金井清　(22) 家屋の大黑柱又は類似部の耐震的效果 (英文)……………………256

金井清　(40) 架構の立體的振動 (英文)……………………………………………538

金井清・妹澤克惟；妹澤克惟・金井清　參照

久野久　(53) 伊豆達磨火山に就いて (英文)………………………………………763

水上武　(9) 淺間火山の磁氣測量 (其の1) (英文)…………………………………100

水上武　(10) 草津白根火山の磁氣測量 (其の1) (英文)…………………………117

水上武　(30) 淺間火山の活動と地表傾斜變化 (英文)……………………………372

水上武　(35) 昭和13年1月12日，日ノ御崎沖地震調査報告 (邦文)………470

水上武・高橋龍太郎；高橋龍太郎・水上武　參照

宮部直巳・福永三郎・佐藤光之助　(42) 臺灣中部の地殼變形 (第2報) (英文)…578

宮部直巳　(51) 江東地域に於ける地盤沈下に就て II. (邦文)……………………721

宮部直巳　（54）昭和 13 年 7 月上旬の降雨による兵庫縣下の山崩（邦文）…… 772
宮部直巳・武藤勝彦；武藤勝彦・宮部直巳　參照
武藤勝彦　（5）大島に於ける重力異常と鉛直線偏倚（英文）……………………… 39
武藤勝彦　（6）水準測量によるヂオイドの形の決定に就て（英文）………………… 60
武藤勝彦・宮部直巳　（7）年平均潮位のフラクチユエーシヨン（英文）………… 70
永田武　（25）火口周邊に於ける地磁氣偏角の異常分布（英文）…………………… 288
永田武　（41）地磁氣異常と地下構造（英文）………………………………………… 550
永田武　（50）三原火山の地球物理學的研究
昭和 13 年 8 月 11 日の小活動（英文）……………………………………………… 714
永田武・高橋龍太郎・平能金太郎；高橋龍太郎・永田武・平能金太郎　參照
西村源六郎・高山威雄　（27）彈性地殼內にある球狀震源より出る地震波
（英文）………………………………………………………………………………… 317
表俊一郎　（14）朝鮮大同江に於ける彈性波式地下探査實施と其の吟味（邦文）… 155
表俊一郎・萩原尊禮；萩原尊禮・表俊一郎　參照
大塚彌之助　（16）七島・マリアナ海嶺の地下構造に關する一解釋（英文）……… 201
大塚彌之助　（33）靜岡縣庵原郡東部の地質構造（邦文）…………………………… 415
大塚彌之助・猪俣眞三郎　（52）靜岡縣蒲原町の城山角閃石安山岩體中の
斑晶配列方位とその地質學的解釋（英文）………………………………………… 757
齊田時太郎　（13）名古屋城天守閣の耐震性に就て（邦文）………………………… 145
齊田時太郎　（32）支那震災の特異性と殘存する高塔より推定された
其の震度に就て（邦文）……………………………………………………………… 407
佐藤光之助；宮部直巳・福永三郎・佐藤光之助　參照
妹澤克惟　（1）不連續性分散曲線を有するレーレー波の振幅（英文）…………… 1
妹澤克惟・金井清　（2）重力を受ける天體のプラスチツク釣合（英文）………… 7
妹澤克惟・金井清　（4）五重塔の耐震性（第 3 報）（英文）………………………… 30
妹澤克惟　（19）彈性表面波の異常分散（英文）……………………………………… 225
妹澤克惟・金井清　（20）地球の液狀冷却時代に於ける重力的安定（英文）……… 234
妹澤克惟・金井清　（21）地球の冷却が重力の下にあるそのプラスチツク
狀態に及ぼす影響（英文）…………………………………………………………… 244
妹澤克惟・金井清　（37）周期的粘彈性波の走波距離についての減衰（英文）…… 491
妹澤克惟・金井清　（38）地殼內の不連續面に於ける境界波の生成（第 1 報）
（英文）………………………………………………………………………………… 504

妹澤克惟・金井清 （39）地球の冷却が重力の下にあるそのプラスチツク狀態に及ぼす影響（II）（英文）…… 527

妹澤克惟・金井清 （47）彈性表面波の異常分散に就て（第 2 報）（英文）…… 683

妹澤克惟・金井清 （48）粘性が地球の液狀冷却時代に於ける重力的安定に及ぼす影響（英文）…… 690

妹澤克惟・金井清 （49）筋違の耐震效果の理論（序報）（英文）…… 702

高橋龍太郎・永田武・平能金太郎 （8）大島三原火山の地球物理學的研究（第3報）（英文）…… 87

高橋龍太郎・水上武 （18）小串鑛山に於ける山崩の調査報告（英文）…… 218

高山威雄・西村源六郎；西村源六郎・高山威雄 参照

坪井忠二・淵田隆門 （23）重力と地下構造との關係（2）（英文）…… 273

坪井忠二 （24）地殼均衡說による地殼の厚さを求める簡單な方法（英文）…… 285

津屋弘逵 （15）伊豆七島新島の火山（邦文）…… 171

津屋弘逵 （34）富士火山の地質學的並びに岩石學的研究（I）1. 小御嶽の構造（邦文）…… 452

津屋弘逵 （45）富士火山の地質學的並に岩石學的研究（II）2. 青木原熔岩の分布と噴出中心（邦文）…… 638

山口生知 （28）世界地震の季節的分布（英文）…… 355

山本莊毅；吉村信吉・山本莊毅 参照

吉村信吉・山本莊毅 （17）千葉市西北郊登戸の地下水と震害（邦文）…… 212

（36）岡山—厚狹間並に小松島—八幡濱間の水準改測結果（邦文）…… 484

Index to Vol. XVI.

Pape

Fuchida, T., *See* Tsuboi, C. and Fuchida, T.

Hagiwara, T. (29) Observation of Changes in the Inclination on the Earth's Surface at Mt. Tukuba. (in English) 366

Hagiwara, T. and Omote, S. (44) Comparative Observations of the Acceleration of Earthquake Motions in the Tokyo Imperial University. (Part I) (in Japanese) 632

Hagiwara, T. (55) Mud Avalanche at Mt. Tukuba, Ibaraki Prefecture. (in Japanese) 779

Hirano, K., *See* Takahasi, R., Nagata, T. and Hirano, K.

Hukunaga, M. and Sato, M. (26) Crustal Deformations in Central Taiwan. (in English) 300

Hukunaga, M., Miyabe, N. and Sato, M., *See* Miyabe, N., Hukunaga, M. and Sato, M.

Iida, K. (12) The Velocity of Elastic Waves in Sand. (in English) 131

Iida, K. (31) Relation between the Normal-Tangential Viscosity Ratio and Poisson's Elasticity Ratio in Certain Soils. (in English) 391

Iida, K. (46) The Mud Flow that occurred near the Explosion-crater of Mt. Bandai on May 9 and 15, 1938, and some Physical Properties of Volcanic Mud. (in Japanese) 658

Inomata, S., *See* Otuka, Y. and Inomata, S.

Inouye, W. (11) Notes on the Origin of Earthquakes. (Fifth paper.) (in English) 125

Inouye, W. (43) Notes on the Origin of Earthqukes. (Sixth paper.) (in English) 597

Kanai, K. (3) Model Experiments of a Dynamic Damper for Seismic Structural Vibration. Irregular Vibration. (in English) ... 21

Kanai, K. (22) Aseismic Properties of a Daikoku-basira (Principal Column) or Similar Column in a Japanese Style House. (in English) 256

Kanai, K. (40) Three-dimensional Vibrations of a Framed Struc-

ture. I. (in English) 538
KANAI, K. and SEZAWA, K., *See* SEZAWA, K. and KANAI, K.
KUNO, H. (53) A Note on the Daruma Volcano, Izu, Japan. (in English).. 763
MINAKAMI, T. (9) Magnetic Surveys of Volcano Asama. (in English) 100
MINAKAMI, T. (10) Magnetic Surveys of Volcano Kusatu-Sirane. (in English) 117
MINAKAMI, T. (30) Explosive Activities of Volcano Asama and Tiltings of the Earth's Surface. (in English)........................ 372
MINAKAMI, T. (35) The Hinomisaki-Oki Earthquake of January 12, 1938. (in Japanese) 470
MINAKAMI, T. and TAKAHASI, R., *See* TAKAHASI, R. and MINAKAMI, T.
MIYABE, N., HUKUNAGA, M. and SATO, M. (42) Crustal Deformations in Central Taiwan. Part 2. (in English) 578
MIYABE, N. (51) Subsidence of the Earth's Surface in the Kôtô region, Tokyo II. (in Japanese) 721
MIYABE, N. (54) The Landslides in Hyôgo Prefecture that accompanied the Heavy Rain of July 5, 1938. (in Japanese) 772
MIYABE, N. and MUTO, K., *See* MUTO, K. and MIYABE, N.
MUTO, K. (5) Gravity Anomalies and Deviations of the Vertical in Izu-Osima. (in English) 39
MUTO, K. (6) The Possibility of Determining the Geoid by means of Levelling. (in English) 60
MUTO, K. and MIYABE, N. (7) Studies in Fluctuations in the Heights of Yearly Mean Sea-levels. (in English) 70
NAGATA, T. (25) Magnetic Anomalies around Volcanic Craters. (in English).. 288
NAGATA, T. (41) Magnetic Anomalies and the Corresponding Subterranean Mass Distribution. (in English) 550
NAGATA, T. (50) Geophysical Studies of Mihara Volcano, Oosima Island. IV. A Minor Activity of Volcano Mihara, August 11, 1938.

(in English) 714

NAGATA, T., TAKAHASI, R. and HIRANO, K., *See* TAKAHASI, R., NAGATA, T. and HIRANO, K.

NISHIMURA, G. and TAKAYAMA, T. (27) Seismic Waves due to Tractions Applied to the Inner Surface of a Spherical Cavity in an Elastic Earth. (in English) 317

OMOTE, S. (14) Results of Seismic Prospecting at the Daidôkô River, Korea. (in Japanese) 155

OMOTE, S. and HAGIWARA, T., *See* HAGIWARA, T. and OMOTE, S.

OTUKA, Y. (16) A Geologic Interpretation on the Underground Structure of the Sititô-Mariana Island Arc in the Pacific Ocean. (in English) 201

OTUKA, Y. and INOMATA, S. (52) Phenocryst distribution in the Siroyama hornblende andesite mass exposed near the Town of Kanbara, Sizuoka prefecture, and its geologic intepretation. (in English) 757

OTUKA, Y. (33) Geologic Structure of the Eastern Ibara District, Sizuoka Prefecture, Japan. (in Japanese) 415

SAITA, T. (13) Vibrations of the Keep of Nagoya Castle due to Earthquake and Wind Pressure. (in Japanese) 145

SAITA, T. (32) The Peculiarity of Chinese Earthquake Disasters and the Seismic Intensities as Deduced from Remaining Pagodas. (in Japanese) 407

SATO, M., *See* HUKUNAGA, M. and SATO, M. *See* MIYABE. N., HUKUNAGA, M. and SATO, M.

SEZAWA, K. (1) Amplitudes of Rayleigh-waves with Discontinuities in their Dispersion Curves. (in English) 1

SEZAWA, K. and KANAI, K. (2) The Plastic State of Certain Planets under Gravitational Forces. (in English) 7

SEZAWA, K. and KANAI, K. (4) Studies on the Seismic Vibration of a Gozyûnotô. III. (in English) 30

SEZAWA, K. (19) Anomalous Dispersion of Elastic Waves. (in English) 225

SEZAWA, K. and KANAI, K. (20) Gravitational Stability of the Earth at its Liquid Cooling Stage. (in English) 234

SEZAWA, K. and KANAI, K. (21) The Effect of Cooling on a Plastic Earth under Gravitational Forces. (in English) 244

SEZAWA, K. and KANAI, K. (37) Damping of Periodic Visco-Elastic Waves with Increase in Focal Distance. (in English)...... 491

SEZAWA, K. and KANAI, K. (38) The Formation of Boundary Waves at the Surface of a Discontinuity within the Earth's Crust. I. (in English).. 504

SEZAWA, K. and KANAI, K. (39) The Effect of Cooling on a Plastic Earth under Gravitational Forces. II. (in English) 527

SEZAWA, K. and KANAI, K. (47) Anomalous Dispersion of Elastic Waves. II. (in English).. 683

SEZAWA, K. and KANAI, K. (48) The Effect of Viscosity on the Gravitational Stability of the Earth at its Liquid Cooling Stage. (in English) 690

SEZAWA, K. and KANAI, K. (49) Theory of the Aseismic Properties of the Brace Struts (Sudikai) in a Japanese-style Building. (Preliminary Notes.) (in English).. 702

TAKAHASI, R., NAGATA, T. and HIRANO, K. (8) Geophysical Studies of Volcano Mihara, Oosima Island. III. Microtremor Measurements in Oosima. (in English).. 87

TAKAHASI, R. and MINAKAMI, T. (18) The Land-slide at the Ogusi Mine. (in English) 218

TAKAYAMA, T., *See* NISHIMURA, G. and TAKAYAMA, T.

TSUBOI, C. and FUCHIDA, T. (23) Relation between Gravity Anomalies and the Corresponding Subterranean Mass Distribution. (II.) (in English) 273

TSUBOI, C. (24) A Simple Method of Approximately Determining the Thickness of the Isostatic Earth's Crust. (in English)......... 285

TSUYA, H. (15) Volcanoes of Nii-sima, One of the Seven Izu Islands. (in Japanese) 171

TSUYA, H. (34) Geological and Petrological Studies of Volcano

Huzi (Fuji), I. 1. Geological structure of Komitake. (in Japanese) 452

TSUYA, H. (45) Geological and Petrological Studies of Volcano Huzi (Fuji), II. 2. Distribution of the Aokiga-hara lava and its vent. (in Japanese) 638

YAMAGUTI, S. (28) Seasonal Distributions of Earthquakes in the World. (in English) 355

YAMAMOTO, S., *See* YOSHIMURA, S. and YAMAMOTO, S.

YOSHIMURA, S. and YAMAMOTO, S. (17) The Underground Water in the Vicinity of Tiba City with Special Reference to Earthquake Damages. (in Japanese) 212

(36) Results of Recent Precise Levelling along the Lines; Okayama-Asa, and Komatuzima (or Tatue)-Yawatahama. (in Japanese) 484